Performance of Mechanically Stabilized Earth Structures When Subjected to Passive Forces

by

Richard Benjamin Jannett

A dissertation submitted to the Graduate Faculty of
Auburn University
in partial fulfillment of the
requirements for the Degree of
Doctor of Philosophy

Auburn, Alabama
August 3, 2019

Keywords: Passive Resistance, Geosynthetic, Stabilized Earth,
Retaining Structure, Abutment

Approved by

David J. Elton, Chair, Professor Emeritus of Civil Engineering
J. Brian Anderson, Professor of Civil Engineering
David H. Timm, Brasfield & Gorrie Professor of Civil Engineering
Lorraine W. Wolf, Professor of Geosciences

Abstract

Mechanically stabilized earth structures are increasing in popularity due to their relative ease of construction and favorable performance. Current mechanically stabilized earth designs consider only active pressures acting on the structure.

Previous research has been performed to model or measure the passive (laterally compressive) forces that are exerted on mechanically stabilized abutments due to thermal expansion of a bridge deck. While such research measures the magnitude of passive forces applied to mechanically stabilized earth structures, it fails to address the *performance* of the mechanically stabilized structure when subjected to these forces. As such, a knowledge gap exists.

This research fills this knowledge gap by providing insight into the performance of such structures when subjected to passive forces, allowing this technology to be implemented in a wider variety of applications that can now include passive forces in addition to active forces.

This research evaluates the performance of model mechanically stabilized earth structures through a laboratory testing program consisting of instrumented, scale tests where passive strain is applied to specimens with varying reinforcement schemes. Finite difference modeling was used to simulate the laboratory testing program.

The primary aspect of performance evaluated is the load-deformation response when presence, length, width, and vertical spacing of reinforcement are varied. The secondary aspect

of performance evaluated is the location of the passive failure surface in the soil with respect to the previously described reinforcement variances.

The load-deformation response is quantified by measuring the following four key elements: Peak Force, displacement where Peak Force occurred, Residual Force, and stiffness at 50% of the Peak Force (K_{50}). The addition of reinforcement to a soil structure causes a decrease in Peak Force values, an increase in K_{50} values, and a non-determinate effect on Peak Force Displacement and on Residual Force. Among reinforced specimens, increasing the reinforcement surface area results in increased Peak Force, Residual Force, and K_{50} values, as well as decreased Peak Force Displacement values.

Increased vertical spacing tended to produce longer failure surfaces.

Acknowledgments

I would like to thank my advisor, Dr. David Elton, for guidance on this project and what he has taught me about engineering as well as other aspects of life. I would also like to thank Dr. Anderson, Dr. Timm, and Dr. Wolf for serving on my committee and for their input and time invested in this project.

Contributions of knowledge, time, and testing equipment by Dr. Farag are much appreciated and were instrumental to the completion of this research.

Additionally, I would like to thank my parents, Suzette B. Jannett and Dr. Thomas Cottongim Jannett, for their continued support and advice during my pursuit of this degree as well as my other life pursuits.

Finally, I'd like to thank my Chocolate Labrador Retriever, Sir Red Jannett, for letting me duck hunt with him for the past 8 years. The most important things in life cannot be learned in a classroom or from a book, and many of these are only learned by spending time afield with a dog.

Table of Contents

List of Tables

List of Figures

Chapter I: Introduction

a. Statement of Need

The principle behind Mechanically Stabilized Earth (MSE) is the addition of a tensile element to soil, which is weak in tension, resulting in an increase in soil strength. MSE has been in use for thousands of years, with construction using MSE principles dating back to the 5th and 4th millennia BC (Jones 1996). The Agar-Quf ziggurat and the Great Wall of China are the earliest remaining structures using MSE. The Agar-Quf ziggurat used woven mats of reed to reinforce soil while the Great Wall of China reinforced mixtures of clay and gravel with tamarisk branches (Jones 1996). Today's MSE structures no longer use plants, but commonly use steel strips or geosynthetic sheets to add tensile strength and reinforce soil (Bell 2002). As reinforcement materials and design techniques have improved, the use of MSE structures has become widespread. Traditionally, MSE is used for earth retaining structures to resist the active earth pressure induced by a change in grade. However, as engineers gain confidence in this technology, it is being implemented in bridge abutments. The basic design of a bridge abutment is the same as that of a retaining wall, with the majority of the design devoted to resisting the active earth pressure forces generated by the backfill as well as the additional bridge deck loading. However, thermal expansion of the bridge deck during warmer months pushes the bridge deck into the MSE abutment, inducing passive forces on the abutment. While it is well known how to design for the active pressures in an MSE abutment, the effect of passive pressure is unknown. By determining the effect that reinforcing a soil mass has on its performance when subjected to passive forces, engineers can have greater confidence when using MSE technology in situations where passive resistance is induced on the reinforced soil mass. This allows the potential for MSE to be used in a wider variety of applications and may provide a better option than currently available.

b. Proposal of Work

The proposed research consists of a laboratory study using scale models in conjunction with finite difference modeling to determine the effect of horizontal sheet reinforcement on the soil's performance when loaded passively. The passive resistance will be determined for a variety of reinforcement configurations as well as non-reinforced soil for comparison.

The method for determining the passive resistance used a box with a movable plate and an electronically controlled ball screw jack piston to provide passive force. The test structures were prepared inside a box and failed by forcing the movable plate into the structure with the ball screw jack piston. Displacement and load data were collected as well as the location of the failure surface within the specimen. The system was modeled using finite difference software, with the intention of being able to predict the behavior of the reinforcement configurations that were tested in the laboratory.

c. Research Objective

The objective of this research was to determine how the addition of horizontal sheet reinforcement affects the engineering performance of soil subjected to passive loading and develop a model to predict the behavior of the passively loaded, reinforced soil structures that were tested in the laboratory. This research does not intend to create a design procedure for mechanically stabilized earth loaded passively. Rather, it provides the first step towards the development of such procedures.

d. Scope of Work

A program of laboratory testing and computer modeling was performed to determine the effect of horizontal sheet reinforcement on a soil structure's engineering performance. Scale test models with varying reinforcement geometry were built and failed with passive force. Quantitative data were gathered using GeoJac software during laboratory testing. FLAC3D™ software was used to model the laboratory testing and provide additional quantitative data. The results identified changes in engineering performance of horizontally reinforced structures with respect to addition of and varying reinforcement geometry when subjected to passive loading.

Chapter II: Background and Literature Review

a. Mechanically Stabilized Earth

Mechanically Stabilized Earth (MSE) is a composite of soil and reinforcement. The tensile strength of reinforcement is much greater than the tensile strength of soil. The addition of tensile elements to soil results in a significant increase in soil strength compared to soil without these elements. In addition to reinforcement and reinforced soil, MSE structures may have retained soil and facing to prevent erosion. Figure 1 shows the basic parts of an MSE structure.

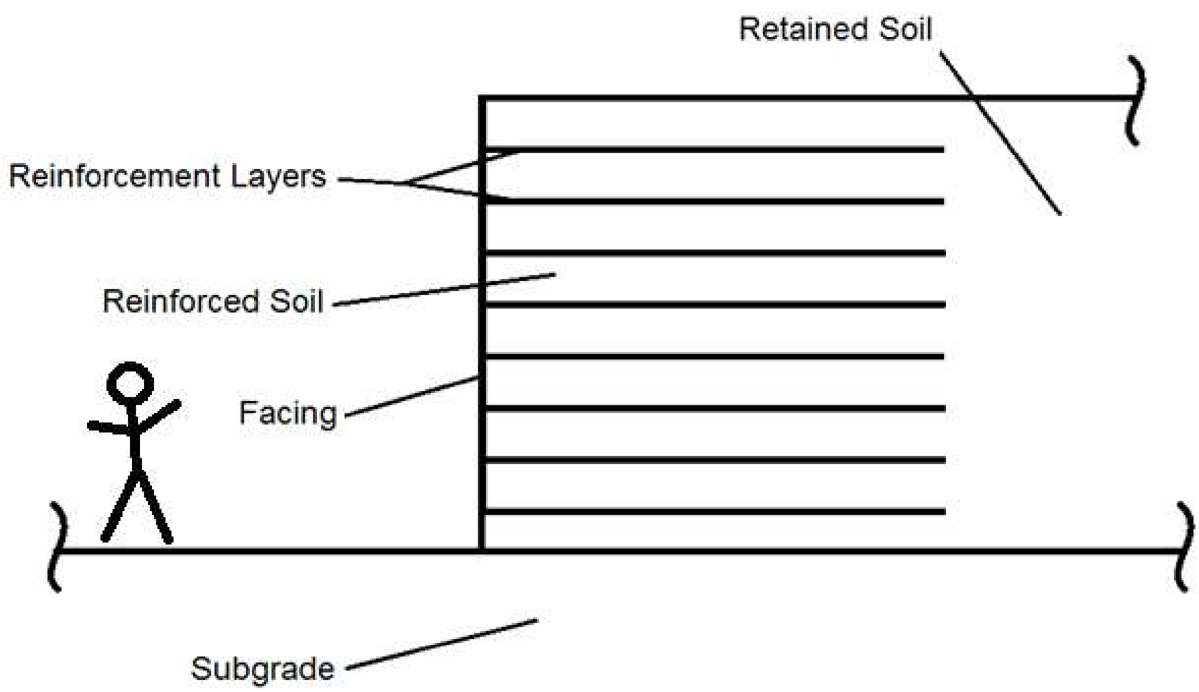

Figure 1: Schematic showing the basic parts of an MSE structure

i. Reinforcement Types

1. Strips

Strip reinforcement consists of strips that have a breadth greater than their thickness and a length greater than their breadth. Strips may be formed from a variety of materials including steel, aluminum, copper, plastic, and glass fiber reinforced plastic. Steel strips are often galvanized or coated to prevent corrosion. Metallic strips can be smooth, but often have a series of ribs, grooves, crimps, or other protrusions intended to increase the friction between the reinforcement and the fill. Strips are typically three to twenty millimeters (0.118 to 0.787 inches) in thickness, thirty to one hundred millimeters (1.18 to 3.94 inches) in breadth, and can be any length (Jones 1996). Figure 2 shows steel strips during installation.

Figure 2: A concrete panel faced, steel strip reinforced structure under construction (Reinforced Earth Company 2008)

2. Planks

Planks are similar to strips because their breadth is greater than their thickness and their length is greater than their breadth. However, planks are constructed of timber, reinforced concrete, or prestressed concrete, making them more rigid. Like strips, planks come in a variety of sizes, but typical planks are about one hundred millimeters (3.93 inches) in thickness and two hundred to three hundred millimeters (7.87 to 11.81 inches) in breadth (Jones 1996).

3. Geogrids

Geogrids are a sheet type reinforcement comprised of a mesh of transverse and longitudinal ribs. Geogrids may be formed from a variety of polymers as well as fiberglass and polypropylene coated polyester fibers. A key feature of geogrids is that they allow the soil covering to "strike through" the geogrid to the soil surrounding geogrid. Geogrids may be uniaxial, having strength in one direction, or biaxial with strength in two directions. (Koerner 2005). Although polymeric grids are the most widely used, grids may also be made of welded wire mesh or expanded metal (Jones 1996). Geogrids come in a variety of shapes and sizes. Figure 3 shows an example of high density polyethylene (HDPE) geogrid while Figure 4 and Figure 5 show uniaxial and biaxial polypropylene coated polyester geogrids, respectively.

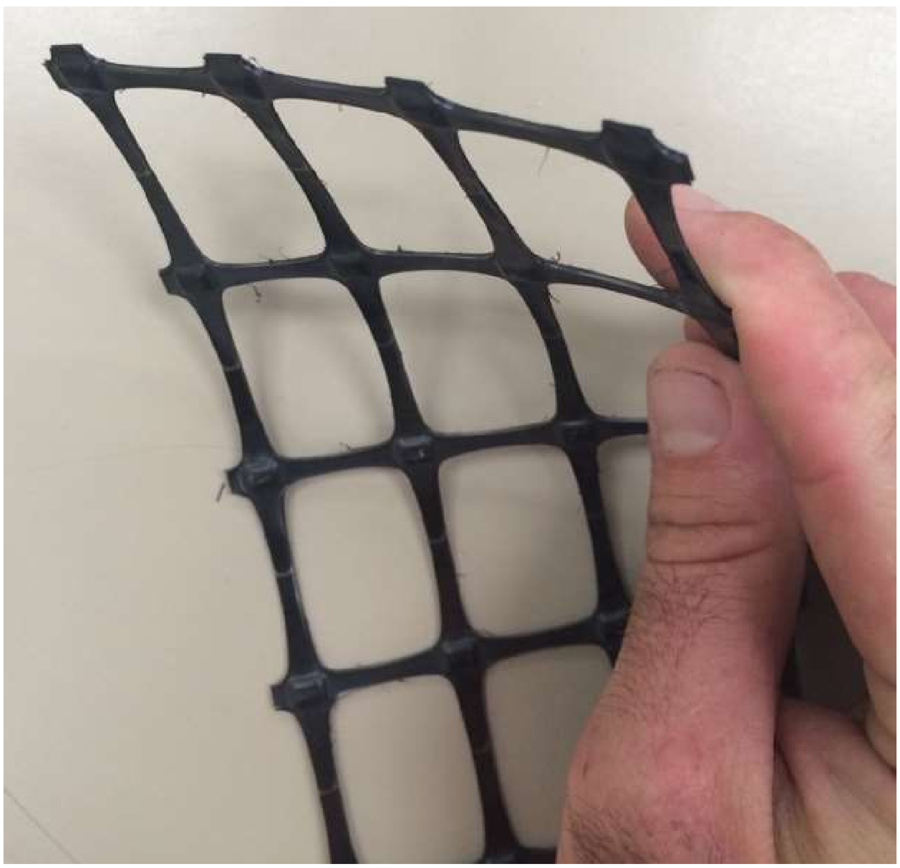

Figure 3: HDPE Geogrid

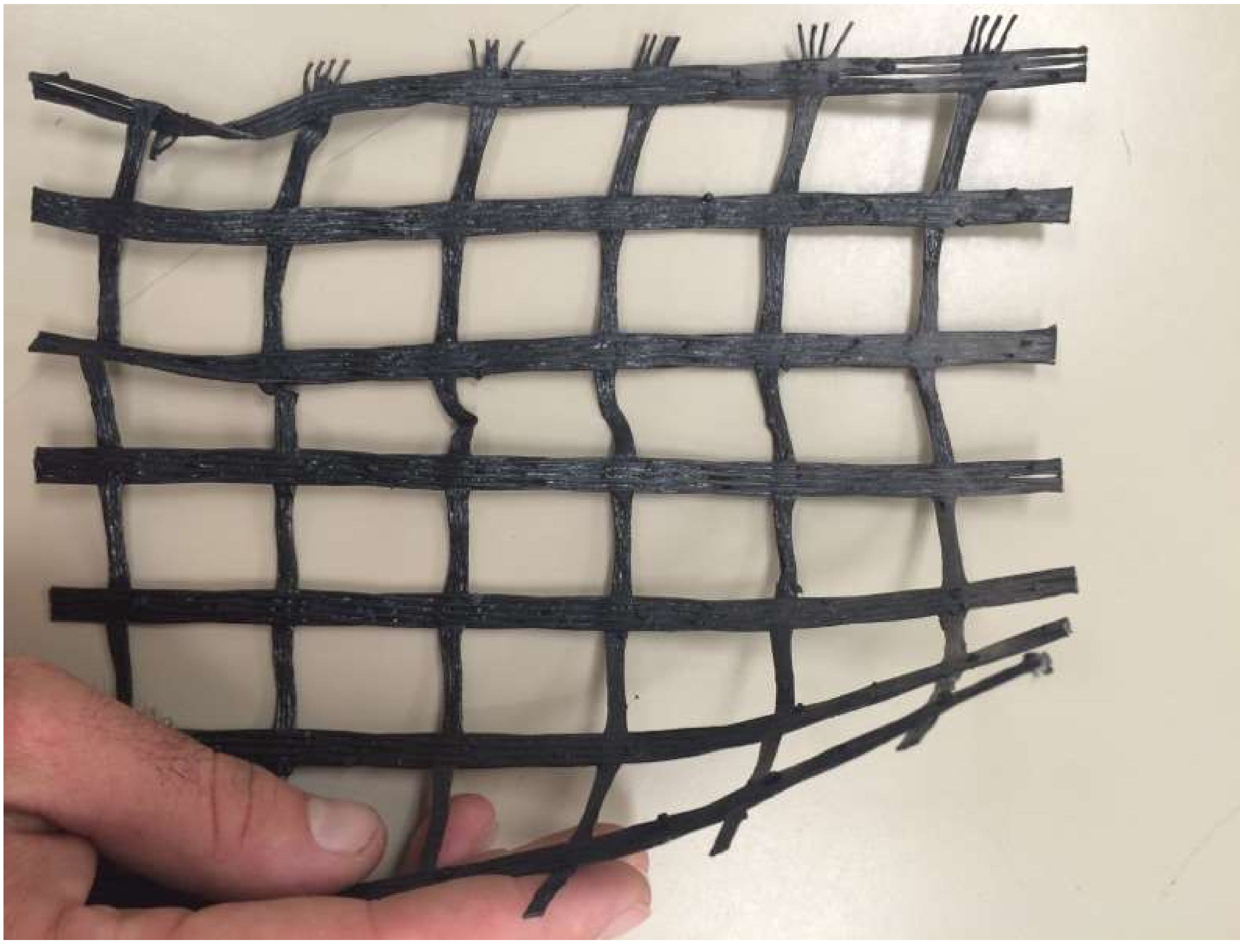

Figure 4: Polypropylene coated polyester uniaxial geogrid. Note transverse ribs have more fibers for greater strength in that direction.

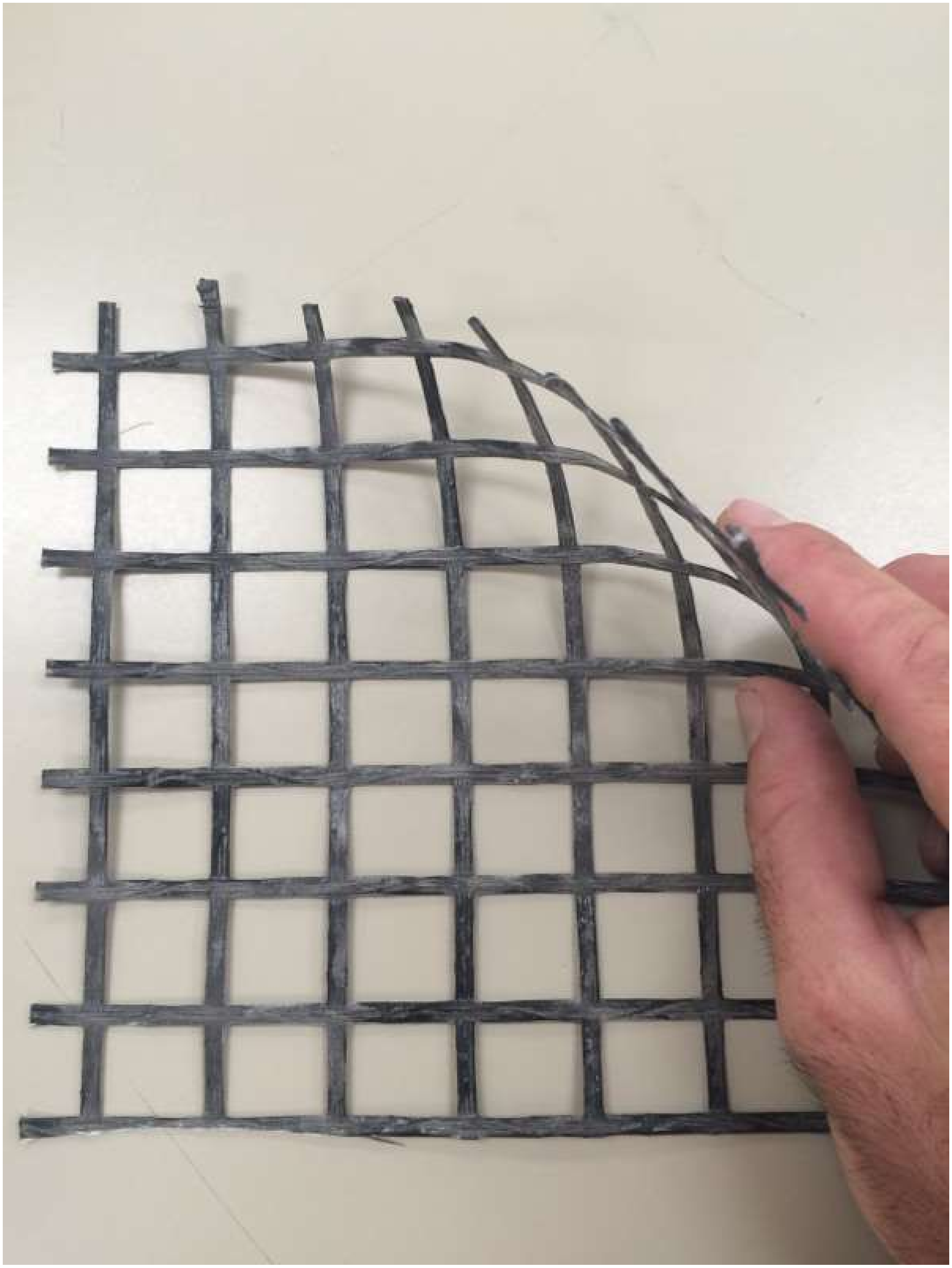

Figure 5: Biaxial polyester coated polypropylene geogrid.

4. Geotextile Sheet Reinforcement

Geotextiles are the most common sheet material used for reinforcement. Geotextile refers to sheet materials that are produced from polymers and may be woven, nonwoven, knitted, or stitch bonded. The most common geotextiles are woven and nonwoven. Figure 6 shows a geotextile being used to reinforce gravel fill to construct a GRS-IBS abutment. Figure 7 and Figure 8 show examples of nonwoven geotextile and woven geotextile, respectively.

Figure 6: Geotextile sheet reinforcement being used on a GRS-IBS abutment in Escambia County, Florida


Figure 7: Nonwoven geotextile

Figure 8: Woven geotextile

5. Composite Reinforcement

Composite reinforcement consists of combinations of different materials to meet a design goal. Composites may combine sheet reinforcement with strips, strips with grids, or strips with anchors (Jones 1996). Geocomposites are comprised strictly of polymeric materials and may provide other benefits in addition to reinforcement such as drainage, separation, filtration, and containment. Geocomposites are a combination of geotextiles, geogrids, geonets, and/or geomembranes (Koerner 2005). Figure 9 shows a geocomposite that takes advantage of the drainage capabilities of a geonet and the reinforcement and filtration capabilities of a nonwoven geotextile.

Figure 9: Geonet-nonwoven geotextile composite

ii. Applications of Mechanically Stabilized Earth

This section provides an overview of a variety of applications of mechanically stabilized earth and shows the flexibility and broad applications of mechanically stabilized earth technology. This section is not a comprehensive list of applications of mechanically stabilized earth; rather, it provides insight into the wide variety of applications of this technology.

1. Concrete Faced Mechanically Stabilized Bridge Abutments

The use of strip, grid, or anchor type reinforcement connected to concrete facing panels is a common way to construct bridge abutments (Jones 1996). After initial excavation, vertical abutment construction occurs by placing precast concrete elements with attached reinforcement, compacting horizontal soil layers behind the concrete elements, and placing the reinforcement at a specified vertical and horizontal spacing. This type of construction is beneficial because it is economical, may be used on poor subsoils, is able to accommodate compressive ground strains, and is a rapid construction technique (Jones 1996). A concrete faced, steel strip mechanically stabilized earth structure under construction is shown in Figure 2.

2. GRS-IBS Bridge Abutments

Geosynthetic Reinforced Soil-Integrated Bridge System (GRS-IBS) technology, promoted by the Federal Highway Administration, uses geosynthetic reinforced soil to construct a bridge support structure. The GRS-IBS system consists of a reinforced soil foundation, a GRS abutment, and a GRS integrated approach. Advantages associated with GRS-IBS technology include ease of design, economical construction, and that construction can occur in a variety of weather conditions without specialized labor, materials, or equipment (Adams et al., 2011).

After the project requirements have been established, the site evaluation has been performed, and the project has been deemed feasible, there are six main steps in GRS-IBS design. The first step is to determine the required geometry and layout. Following this step, loads are calculated including live loads, dead loads, impact loads, and earthquake loads. The third step is to conduct an external stability analysis which includes direct sliding, bearing capacity, and global stability. The fourth step is to conduct an internal stability analysis including capacity, deformations, and reinforcement strength. The fifth step includes design of the reinforced soil foundation, guardrails, drainage, and utilities. The sixth step is to finalize the design with final reinforcement and facing block layout and fill type (Adams et al., 2011).

Unique to the GRS-IBS design is the implementation of an integration zone which blends the soils of the approaching roadway with the abutment soils. The integration zone aims to provide a seamless transition between the roadway and the bridge (Adams et al., 2011). Figure 10 shows an illustration of a typical GRS-IBS cross section.

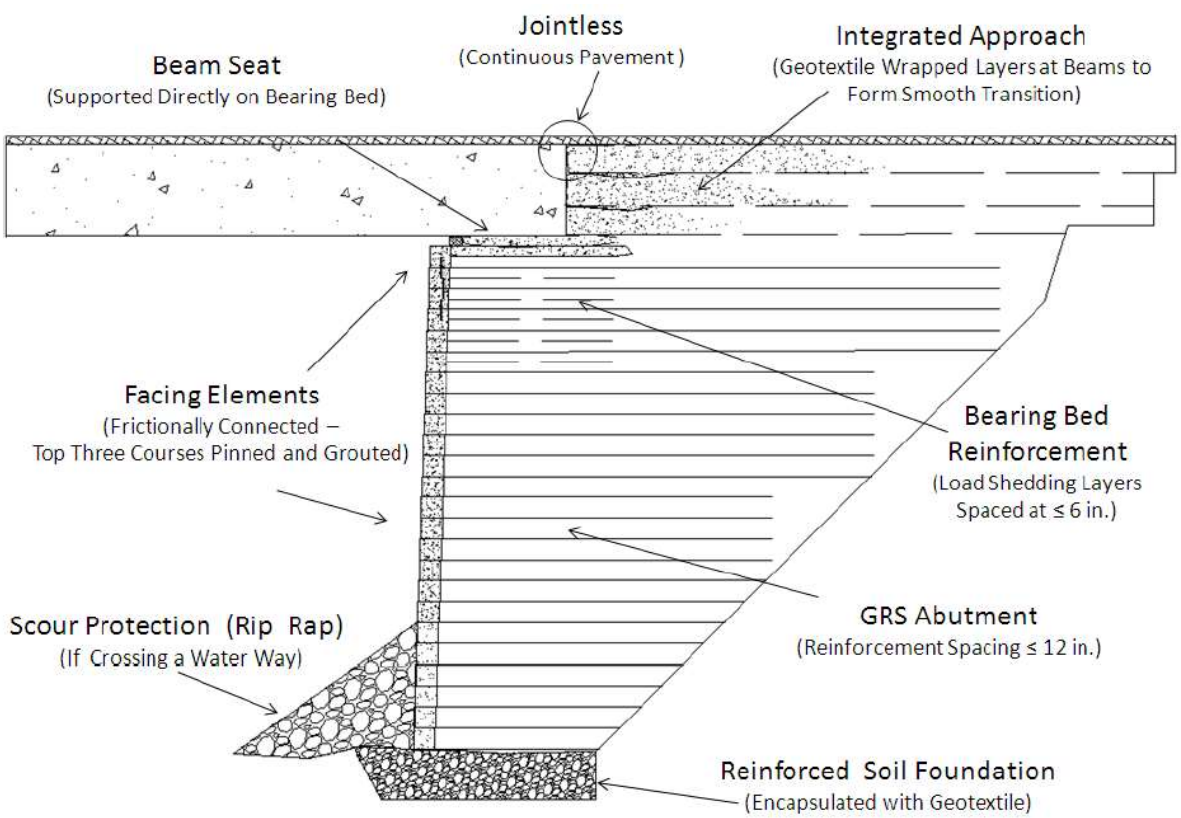

Figure 10: Illustration of a typical GRS-IBS cross section (Adams et al., 2011)

Figure 11 shows a GRS-IBS abutment under construction in Escambia County, Florida. Figure 12 shows the completed GRS-IBS abutments after construction but before the integration zone was constructed to bring the roadway up to grade with the precast prestressed bridge decking.

Figure 11: GRS-IBS abutment under construction in Escambia County, FL

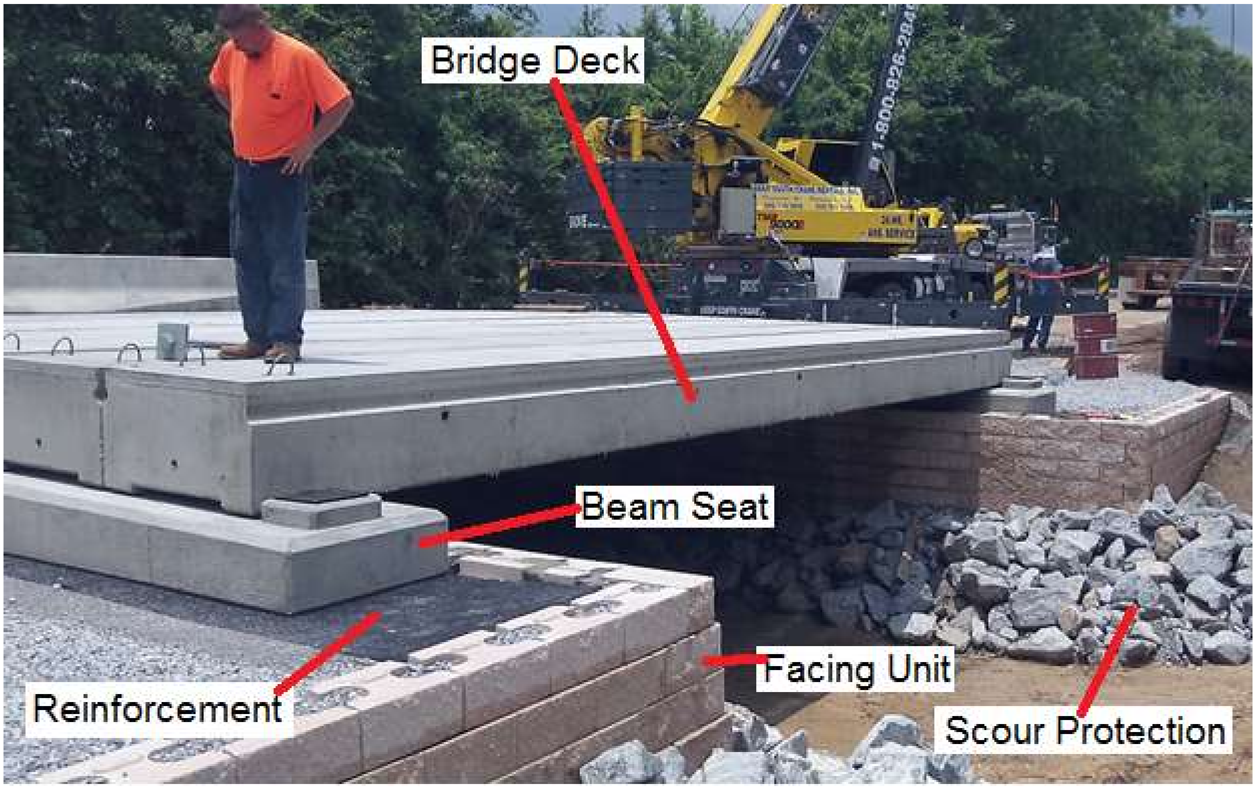

Figure 12: Two GRS-IBS abutments constructed in Escambia County, FL with precast prestressed concrete bridge decking in place, before placement of integration zone soils

3. Dams

Mechanically stabilized earth construction techniques can be applied to new construction of a dam or to raise the height of an existing dam. Earth fill dams may be constructed using reinforced concrete facing, anchor blocks, and tiebacks (Jones 1996). The dam is constructed vertically by compacting horizontal soil layers and reinforcement is added at specified horizontal and vertical spacing. Figure 13 shows a cross section of an earth fill dam.

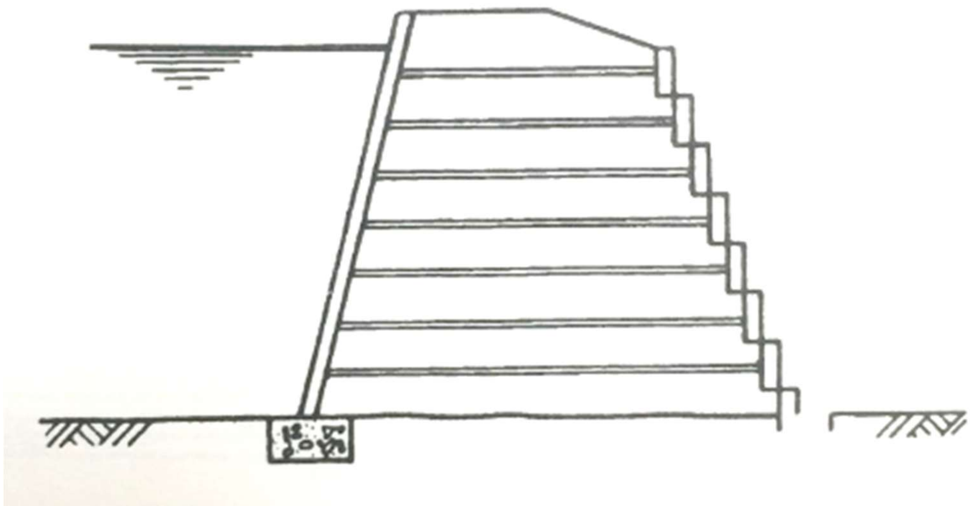

Figure 13: Earth fill dam cross section (Chabal et al., 1983)

A mechanically stabilized earth dam uses a reinforced concrete facing in conjunction with metal strip, grid, or anchor type reinforcement to provide slope stability to the earthen dam (Jones 1996). Figure 14 shows an illustration of a mechanically stabilized earth dam.

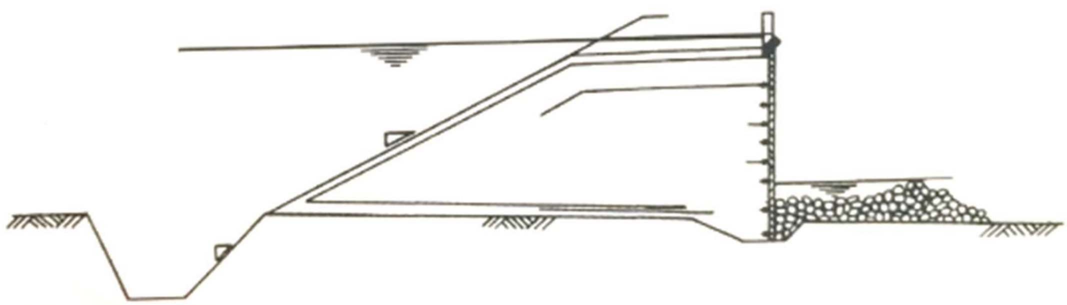

Figure 14: Mechanically stabilized earth dam cross section (Cassard et al., 1979)

In addition to new construction, mechanically stabilized soil can also be used to raise the height of an existing dam (Jones 1996). Figure 15 shows an illustration of how mechanically stabilized soil can be used to raise the height of an existing dam.

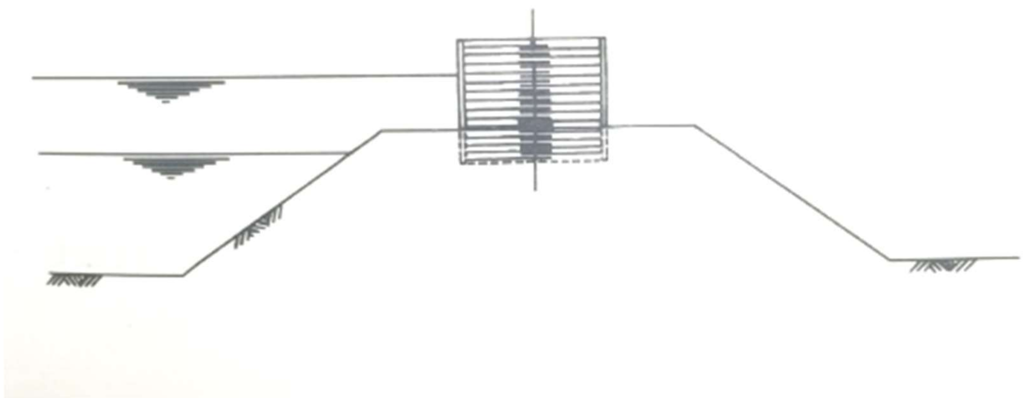

Figure 15: An illustration of one way mechanically stabilized earth can be used to raise the height of an existing dam (Engineering News Record 1983)

For small earth dams, spillways often represent a large fraction of the construction cost. Using geosynthetics to create a vertical downstream face, the Maraval Dam in France greatly reduced the size of the spillway and reduced cost (Shukla et al., 2002). Figure 16 shows an illustration of the Maraval Dam, and its vertical rear face.

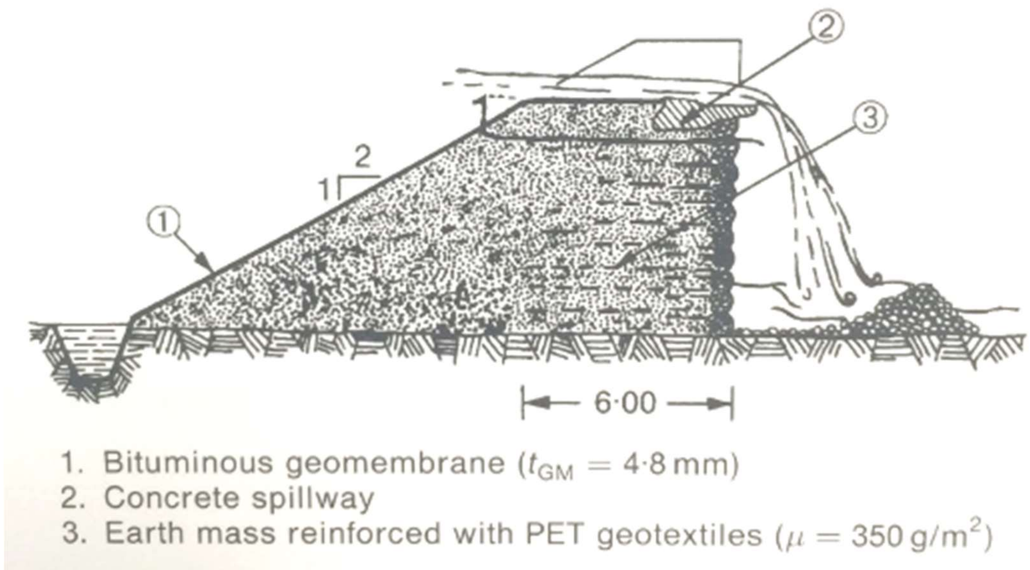

Figure 16: An illustration of the cross section of the Maraval Dam, France (Shukla et al., 2002)

4. Embankments

Geotextile or geogrid sheet reinforcement is often used in embankment construction to allow steeper side slopes, strengthen the embankments, or allow use of marginal fill (Jones 1996). Mechanically stabilized earth embankments are constructed vertically by compacting horizontal lifts of soil and installing the horizontal geogrid, geotextile sheet, or other reinforcement at specified vertical spacing. Vertical spacing and reinforcement length may be consistent throughout the embankment or vary depending on project requirements. Project requirements often include non-uniform stresses throughout an embankment, adding additional short layers of reinforcement at the edge of the embankment to stabilize this area of difficult compaction, and also adding additional short layers of reinforcement to eliminate sloughing failures between widely spaced reinforcement layers (Koerner 2005). Illustrations of reinforcement techniques using consistent vertical spacing and length as well as varying the spacing and length are shown in Figure 17 and Figure 18, respectively.

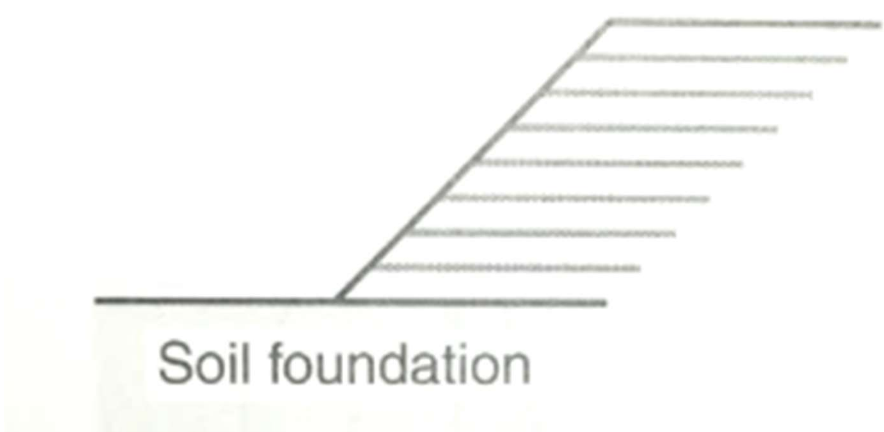

Figure 17: An example of consistent reinforcement length and vertical spacing used in a mechanically stabilized embankment (Koerner 2005)

Figure 18: An example of varying reinforcement length and vertical spacing used in a mechanically stabilized embankment (Koerner 2005).

Additionally, a layer of reinforcement may be added as a basal reinforcement in embankments. Installing a layer of reinforcement atop a weak soil layer before embankment construction occurs can significantly increase the factor of safety of the embankment with respect to a failure occurring through soft subgrade soils (Shukla et al., 2002). Figure 19 shows an illustration of how a geosynthetic layer can be used as basal reinforcement.

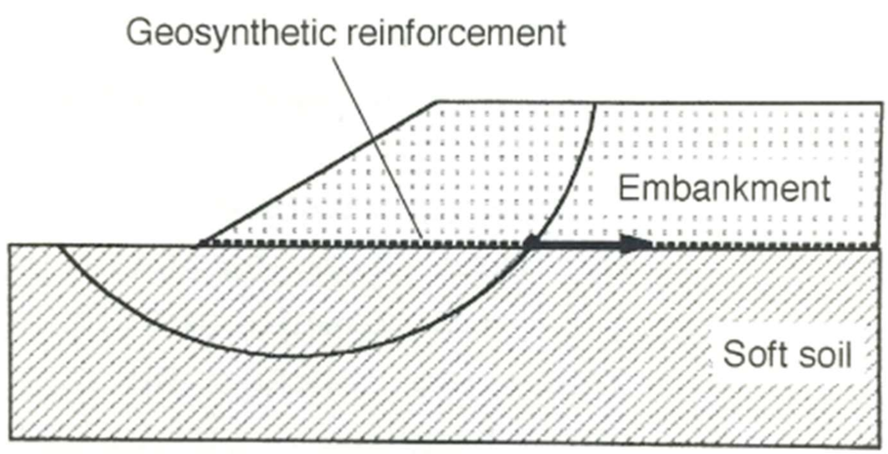

Figure 19: Geosynthetic layer used as basal reinforcement for an embankment over soft ground. Theoretical circular arc failure surface is also shown. (Shukla et al., 2002)

5. Foundations

The most common application for using reinforcement with foundations is to stabilize unsuitable or weak soils so that stable embankment soil or other structural loads may be placed above them (Koerner 2005). One such method involves surcharging the weak subgrade materials. A geotextile is placed over the weak existing soils followed by a sand drainage layer. Wick drains are then installed through the sand drainage layer to the bottom of the soft subgrade layer. A surcharge equivalent to or greater than the design load is placed above the drainage layer and settlement is allowed to occur, with wick drains increasing the time rate of settlement (Koerner 2005). The geotextile stabilizes the weak *in situ* soils, allowing the surcharge to be placed without causing a shear failure of the underlying soil.

Another application of mechanically stabilized earth uses horizontal layers of reinforcement beneath footings and structures. This technique involves the addition of alternating layers of geosynthetic reinforcement and granular fill to provide a composite material with improved performance (Shukla et al., 2002). When used beneath a footing, reinforcement can increase stability of the underlying soils and reduce settlement. When used beneath a structure such as a storage tank, reinforcement can reduce total settlement as well as differential settlement (Jones 1996). Figure 20 shows an illustration of how geosynthetic layers can be used to stabilize soils beneath a footing. Figure 21 shows an illustration of how geosynthetic layers can be used to decrease total and differential settlement under a structure.

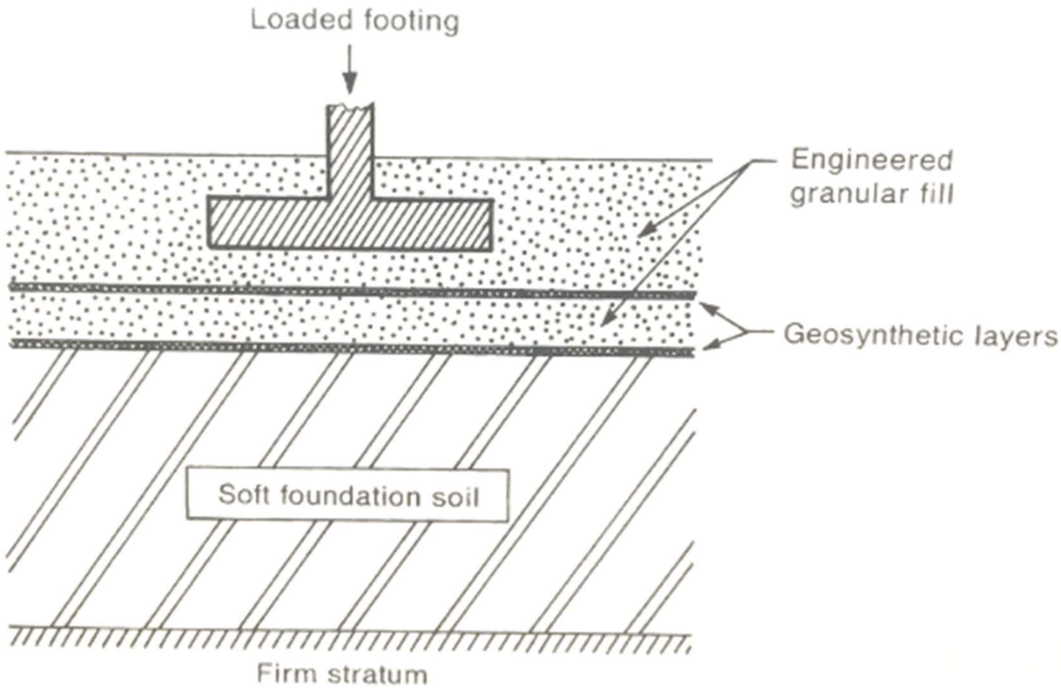

Figure 20: Geosynthetics used to reinforce soil beneath a footing (Shukla et al., 2002)

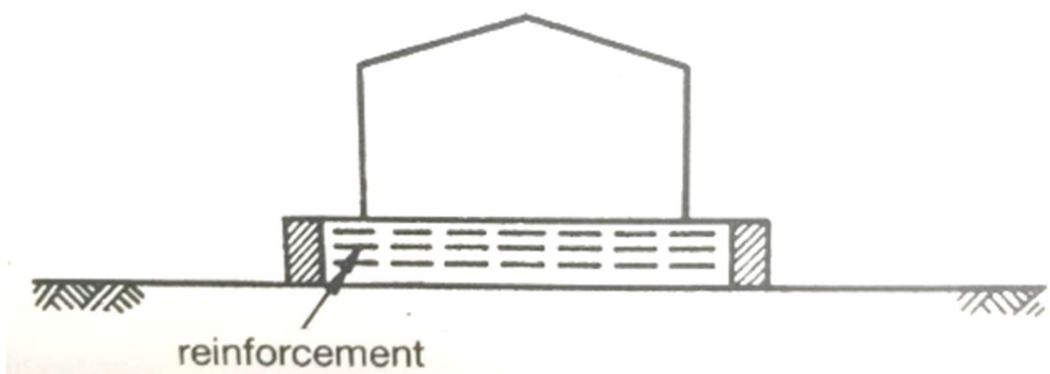

Figure 21: Horizontal layers of reinforcement used to reduce total and differential settlement under a structure (Chinese Report 1979)

6. Highways

Highways utilize a variety of mechanically stabilized soil structures including bridge abutments, mechanically stabilized embankments, and retaining walls. Since these types of structures are covered in other sections, this section will focus on reinforcing soils directly beneath the roadway that, if left untreated, would lead to significant pavement distress.

Often, roadway alignments require passage through areas of compressible or weak soils. If a roadway is placed on an excessively yielding soil subgrade, it will cause the subgrade to deform (Koerner 2005). Deformation of the subgrade will cause the asphalt concrete or Portland cement concrete surface layer to crack, leading to further and more rapid distress. The soft soil subgrade can be reinforced by placing a geotextile atop the subgrade and placing a coarse aggregate base course atop the geotextile. While deformation is required to mobilize the geotextile's strength, some believe that heavily rolling the aggregate base course will sufficiently mobilize the geotextile's strength (Koerner 2005). Others believe that the reinforcement acts as a lateral restraint at the bottom of the aggregate base course which increases the base course stiffness and decreases vertical deformation in the base layer (Shukla et al., 2002). Stabilizing the base course in this manner will allow a suitable base for roadway construction over soft subgrades.

7. Retaining Structures

Mechanically stabilized earth is commonly used in retaining structures. A variety of mechanically stabilized earth techniques are used to retain soil including facing panels with metal strip or wire mesh reinforcement, facing panels with tieback anchors, anchored gabion walls, anchored crib walls, geotextile reinforced walls, and geogrid reinforced walls (Koerner 2005). Typically, these reinforcement materials are used in conjunction with a free draining granular backfill (Shukla et al., 2002). Geotextile and geogrid reinforced walls use horizontal sheets of reinforcement at a required vertical spacing to provide reinforcement. Walls reinforced with geotextiles and geogrids are flexible compared to traditional reinforced concrete retaining walls (Shukla et al., 2002). Anchors, tiebacks, strips, and wire mesh reinforced walls use individual pieces of reinforcement at a required horizontal and vertical spacing to achieve reinforcement. All of the aforementioned retaining structure types utilize vertical construction where the wall is built from the subgrade upwards using compacted layers of soil and installing reinforcement at its required location. Mechanically stabilized earth retaining structures provide a simple solution where an abrupt change in grade is necessary that may be impossible with other forms of construction (Jones 1996). Figure 22 shows an illustration of a geogrid reinforced wall with gabion facing.

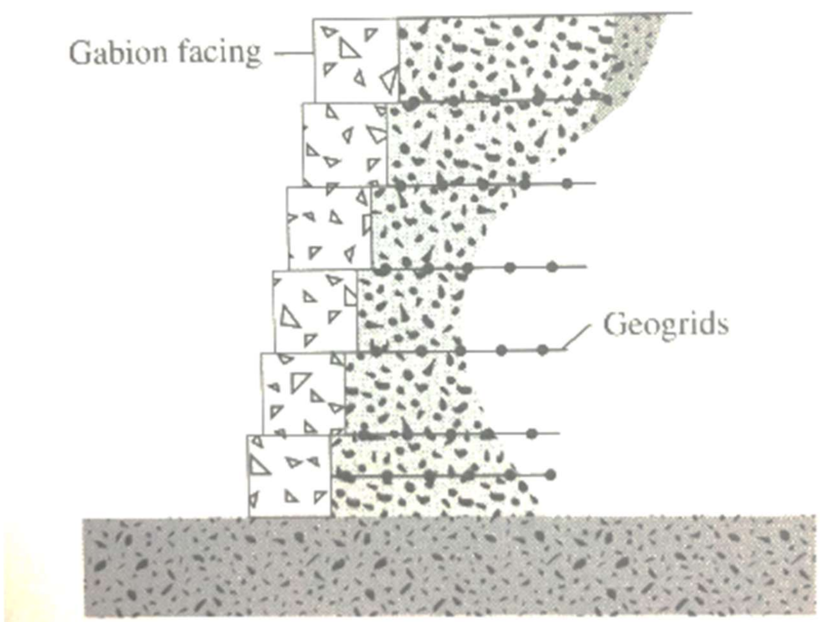

Figure 22: Geogrid reinforced wall with gabion facing (Das 2006)

8. Railways

Similar to highway embankments, mechanically stabilized earth technology is also used in the railroad industry. Railways utilize reinforcement in embankment construction to provide stability over poor subgrade and also to protect embankments from erosion. Geogrids as well as strip type reinforcements may be used to reinforce the embankments. These structures have been proven to adequately support heavy railway loadings on the edge of the embankments (Jones 1996).

In addition to mechanically stabilized abutments, geotextile layers are also used to reinforce ballast beneath railway track. Addition of a geotextile layer under the ballast adds confinement and subsequent reinforcement to the ballast. This layer of geotextile also reduces the shear stresses in the subgrade and may increase overall bearing capacity (Shukla et al., 2002). Figure 23 shows a crew retrofitting a geotextile under an existing railway.

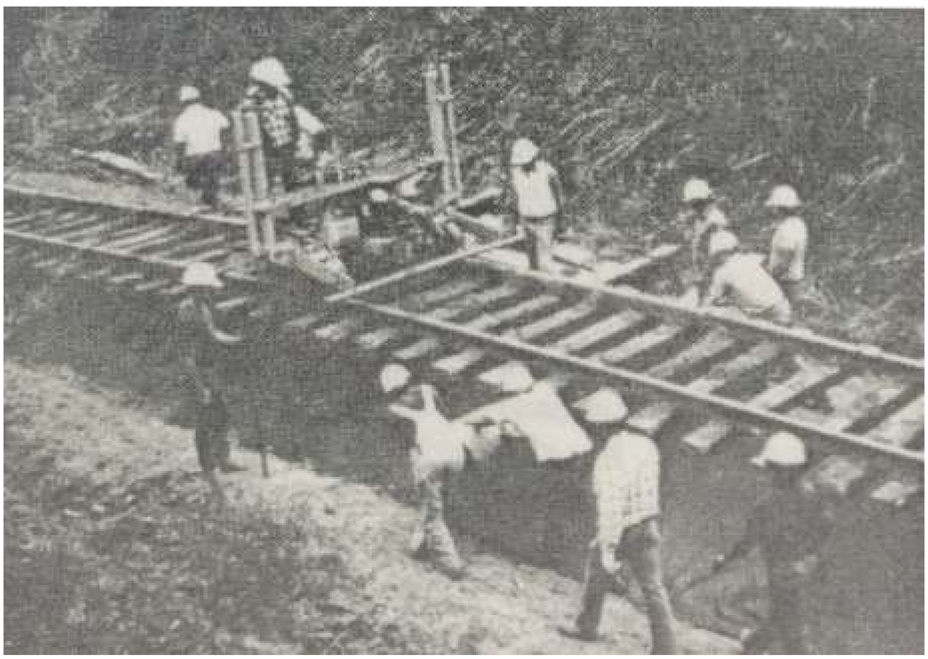

Figure 23: Retrofit installation of a geotextile in a railway application (Shukla et al., 2002)

iii. Geosynthetic Sheet Reinforcement Theory

The general theory of geosynthetic sheet reinforcement is that the geosynthetic sheet provides reduction or suppression of one normal strain rate (the interparticular tensile strain rate) (Jones 1996). In order to reduce one normal strain rate, the soil transfers tensile forces to the geosynthetic reinforcement frictionally between soil particles and geosynthetic reinforcement (Jones 1996). In essence, forces that would have previously resulted in tensile strain of the soil now result in tensile stress of geosynthetic reinforcement with very little tensile strain of the reinforcement or soil. Figure 24 depicts how soil particles interact with reinforcement.

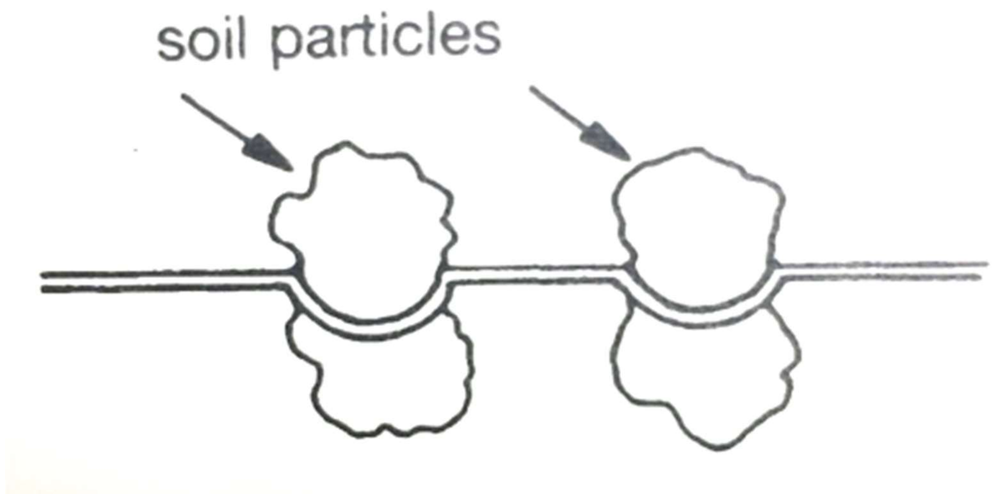

Figure 24: Depiction of soil particles with the addition of reinforcement acting as a tensile member (Jones 1996)

When a vertical load is applied to a non-reinforced soil, a vertical contraction and horizontal expansion occur. For horizontal expansion to occur, the soil must push against adjacent soil with a horizontal stress equal to the at-rest horizontal stress or active horizontal stress, dependent upon whether the soil is in the at-rest condition or the active condition (Jones 1996). Figure 25 shows an illustration of how a non-reinforced soil behaves when a vertical load is applied.

Theoretically, when a vertical load is applied to a reinforced soil, the reinforcing layers do not allow horizontal expansion. If no horizontal expansion is allowed, no additional horizontal stress is applied from the reinforced soil to anything adjacent to the soil (Samtani and Nowatzki 2006; Jones 1996). Also, since horizontal expansion cannot occur, mobilization of the soil into the active case cannot occur and the soil remains in the at-rest condition. For equilibrium, the force transferred from the soil to the reinforcement must equal the force caused by the at-rest lateral stress, $K_0\sigma'_v$, of the soil (Jones 1996). If the force in the reinforcement can be calculated in this manner, the resulting tensile stress and strain in the reinforcement for any depth of reinforcement can be calculated using Equations 1 and 2, respectively. Equation 3 can be used to calculate the lateral strain of the soil in the direction of reinforcement strain. The effective stiffness of the reinforcement, a_rE_r, is typically high, so the argument that significant lateral expansion of the soil does not occur holds (Jones 1996). An illustration of how reinforced soil behaves when a vertical load is applied is shown in Figure 26.

$$\boldsymbol{\sigma_{tensile}} = \frac{\boldsymbol{P_0}}{\boldsymbol{a_r}}$$ (Eq. 1) (modified from Jones 1996)

Where: $\sigma_{tensile}$ is the tensile stress in the reinforcement
P_0 is the resultant horizontal force of the at rest horizontal earth pressure distribution of the soil that is causing tensile forces to develop in the reinforcement
a_r is the unit cross-sectional area of the reinforcement

$$\boldsymbol{\delta_r} = \frac{\boldsymbol{P_0}}{\boldsymbol{a_r E_r}}$$ (Eq.2) (modified from Jones 1996)

Where: δ_r is the strain in the reinforcement
P_0 is the resultant horizontal force of the at rest horizontal earth pressure distribution of the soil that is causing tensile forces to develop in the reinforcement
a_r is the unit cross-sectional area of the reinforcement
E_r is the elastic modulus of the reinforcement

$$\boldsymbol{\in_r} = \boldsymbol{\delta_r} = \frac{\boldsymbol{P_0}}{\boldsymbol{a_r E_r}}$$ (Eq. 3) (modified from Jones 1996)

Where: ϵ_r is the lateral strain of the soil in the direction of reinforcement strain, assuming high soil-reinforcement interface friction.
δ_r is the strain in the reinforcement
P_0 is the resultant horizontal force of the at rest horizontal earth pressure distribution of the soil that is causing tensile forces to develop in the reinforcement
a_r is the unit cross-sectional area of the reinforcement
E_r is the elastic modulus of the reinforcement

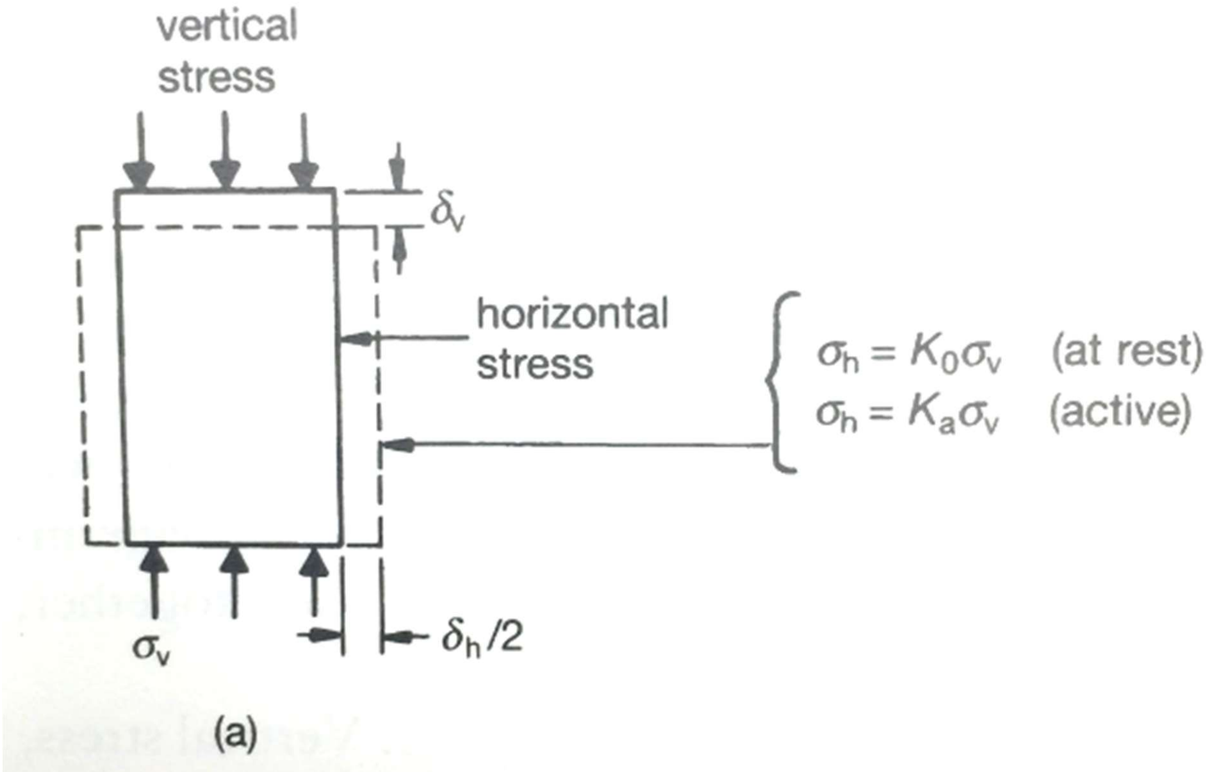

Figure 25: Theoretical stresses and strains of non-reinforced soil when a vertical stress is applied (Jones 1996)

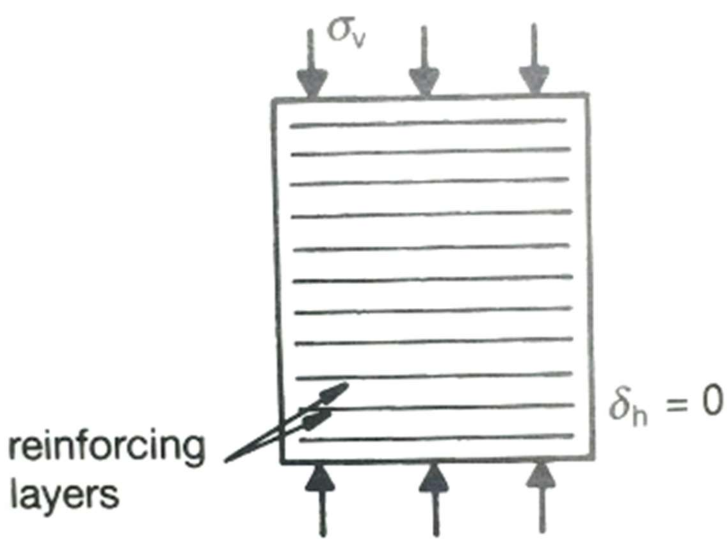

Figure 26: Theoretical stresses and strains of reinforced soil when a vertical stress is applied (Jones 1996)

If Equations 1, 2, and 3 hold, the reinforced soil mass will be in the at-rest lateral earth condition which always lies below the rupture curve defined by the active lateral earth pressure condition. Figure 27 shows a general active effective stress state, at-rest effective stress state, and rupture curve defined by the active effective stress state. For failure to occur, the reinforcement must either rupture or the soil-reinforcement interface friction must be weak (Jones 1996). If rupture occurs, the reinforcement is no longer able to carry the tensile stresses that are transferred to it by the soil. If the soil-reinforcement interface friction is weak, the soil cannot effectively transfer force to the reinforcement so only small tensile forces develop in the reinforcement.

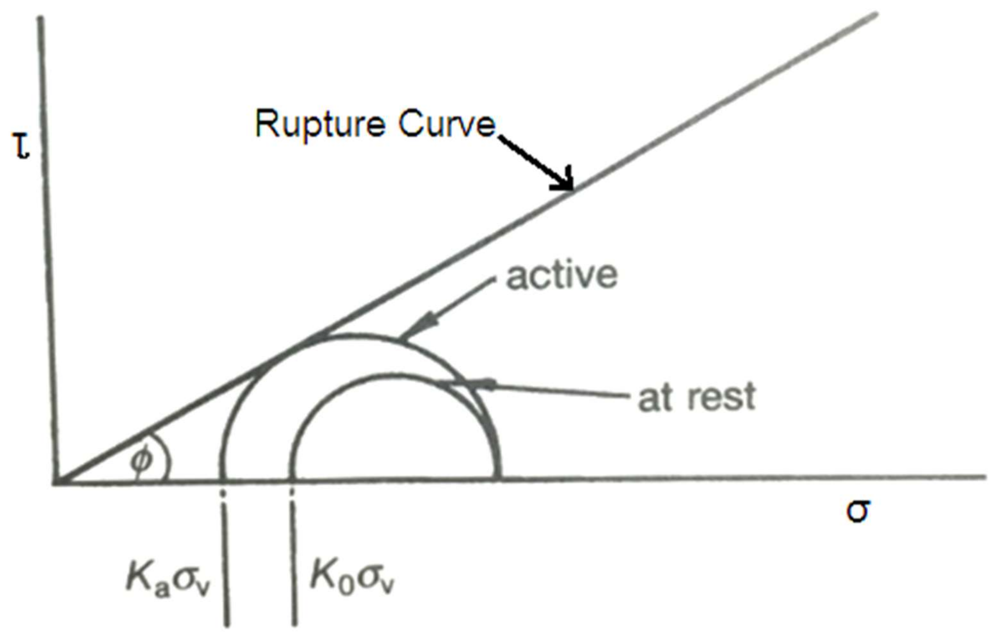

Figure 27: Active and at-rest effective stress state of soil with rupture curve (Jones 1996)

b. Soil Shear Strength Theory

i. Introduction

Shear strength is arguably the most important parameter in geotechnical engineering. The shear strength of soil is the maximum amount of shear stress that a soil can resist (Holtz and

Kovacs 1981). Shear strength has a high impact on a variety of geotechnical engineering applications including slope stability, bearing capacity, and lateral earth pressure (Das 2005). When a soil is sheared, particles roll and slide past each other or may be crushed (Bowles 1996). While fracturing of grains during shear is possible, it is uncommon as the individual soil grains typically have a relatively high resistance to compressive and shear forces (McCarthy 2007). If water is present in the soil, existing pore pressures or a change in pore pressure induced by shearing will also affect the shear strength of a soil (Bowles 1996). The shear strength of a soil is usually defined by the soil's cohesion (c) and angle of internal friction (ϕ) (Das 2005). Often, the shear strength parameters, c and ϕ, are taken as constants. However, this is a mistake as the shear strength of a soil is highly dependent on the current stress state of the soil, density of the soil, previous stress history, loading conditions, and other factors such as grain shape and mineral, and water content (Bowles 1996).

ii. Mohr-Coulomb Failure Criteria

There are many failure theories in geotechnical engineering. The most common failure theory, Mohr-Coulomb, is reviewed in this section. Mohr's theory for rupture in materials indicates that materials fail when subjected to a critical combination of normal stress and shear stress, and not solely normal stress or shear stress. Thus, the shear stress on the failure plane is a function of the normal stress applied to the failure plane (Das 2005). This relationship is shown in Equation 4.

$$\boldsymbol{\tau_f = f(\sigma)} \qquad \text{(Eq. 4) (Mohr 1900)}$$

Where: τ_f is the shear stress on the failure plane
σ is the normal stress on the failure plane

The relationship shown in Equation 4 represents a curved failure envelope (Das 2005). Coulomb discovered that for the majority of soils, the relationship between shear stress on the failure plane and normal stress is fairly linear and can be approximated as such (Coulomb 1776). Combining Mohr's theory of failure due to a combination of shear and normal stress and Coulomb's linear approximation for soils yields the Mohr-Coulomb failure criteria, Equation 5.

$$\boldsymbol{\tau_f = c + \sigma tan\varphi} \qquad \text{(Eq. 5) (Coulomb 1776)}$$

Where: τ_f is the shear stress on the failure plane
σ is the normal stress on the failure plane
c is the cohesion
ϕ is the angle of internal friction

However, in saturated soils, effective stress parameters govern soil behavior and must be used. Equation 6 is the Mohr-Coulomb failure criteria for saturated soils.

$$\boldsymbol{\tau_f = c' + \sigma' tan\varphi'} \qquad \text{(Eq. 6) (Coulomb 1776)}$$

Where: τ_f is the shear stress on the failure plane
σ' is the effective normal stress on the failure plane
c' is the effective cohesion
ϕ' is the effective angle of internal friction

The Mohr-Coulomb Failure Criteria is shown graphically in Figure 28. In Figure 28, the curved line labeled "Mohr's failure envelope" represents the actual failure envelope of a material. The straight line labeled "Mohr-Coulomb failure criteria" represents an approximated linear failure envelope that is generally accurate enough for most soils and easier to work with due to its linearity. τ, σ', c', and ϕ' are also shown graphically in Figure 28. Additionally, Figure 28 shows points A, B, and C to graphically illustrate Mohr's failure theory. Each point represents a combination of stresses on a particular plane in the soil mass. The state of stress represented by point A lies beneath Mohr's failure envelope, meaning that a shear failure will not occur along that plane. The combination of shear and normal stresses shown by point B lies on the failure envelope, indicating that shear failure will occur along that plane. The combination of shear and normal stresses defined by point C lies above the failure envelope, indicating that that this combination is unattainable as shear failure would have already occurred at point B (Das 2005).

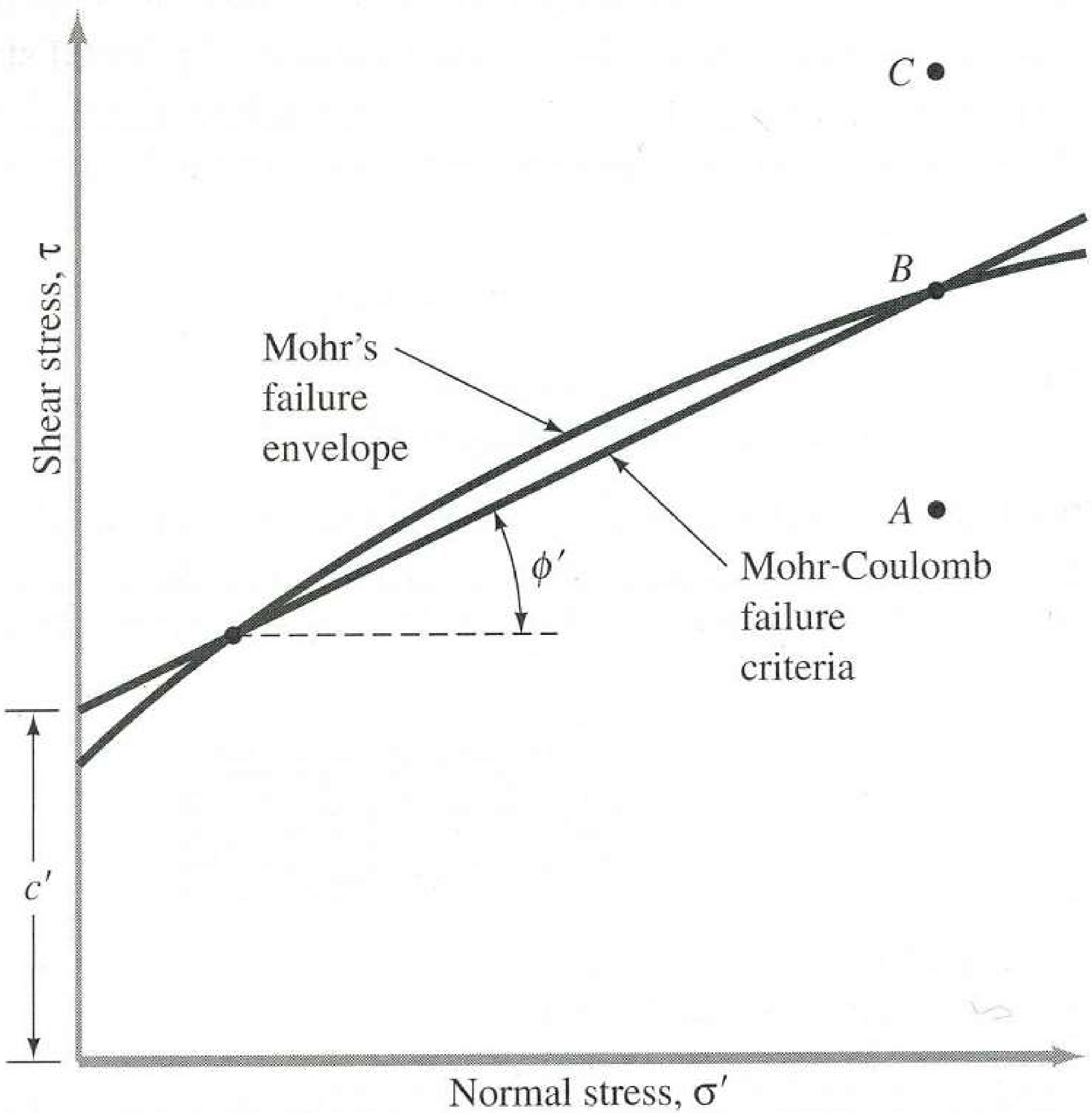

Figure 28: Theoretical Mohr's failure envelope and corresponding Mohr-Coulomb failure envelope (Das 2005)

iii. Tests for the Shear Strength of Soils

1. Overview

To determine the soil strength parameters and the Mohr-Coulomb failure envelope, a number of tests have been developed. Each test induces shear failure in soil and the state of stress at failure is recorded. Laboratory tests as well as field tests are available to determine the shear strength of soils.

2. Laboratory Tests

Laboratory tests require a field sample to be taken and returned to the laboratory, intact, or later reconstituted. Field sampling techniques cause sample disturbance that can provide misleading strength parameters in laboratory testing (DeGroot, Poirier, and Landon 2005). With this in mind, care should be taken during sampling as well as interpretation of laboratory test results. While this section is not comprehensive, it outlines the two most common laboratory tests to determine shear strength parameters: direct shear test and triaxial test. Both are described below.

a. Direct Shear Test (ASTM D3080/D3080M)

The direct shear test was first used by Coulomb in 1776, making it the oldest type of shear test (Day 2001). The test consists of a shear box, a soil specimen, a rigid loading cap, and means to determine shear load, horizontal deformation and vertical deformation (Holtz and Kovacs 1981). An illustration of the direct shear testing device is shown in Figure 29.

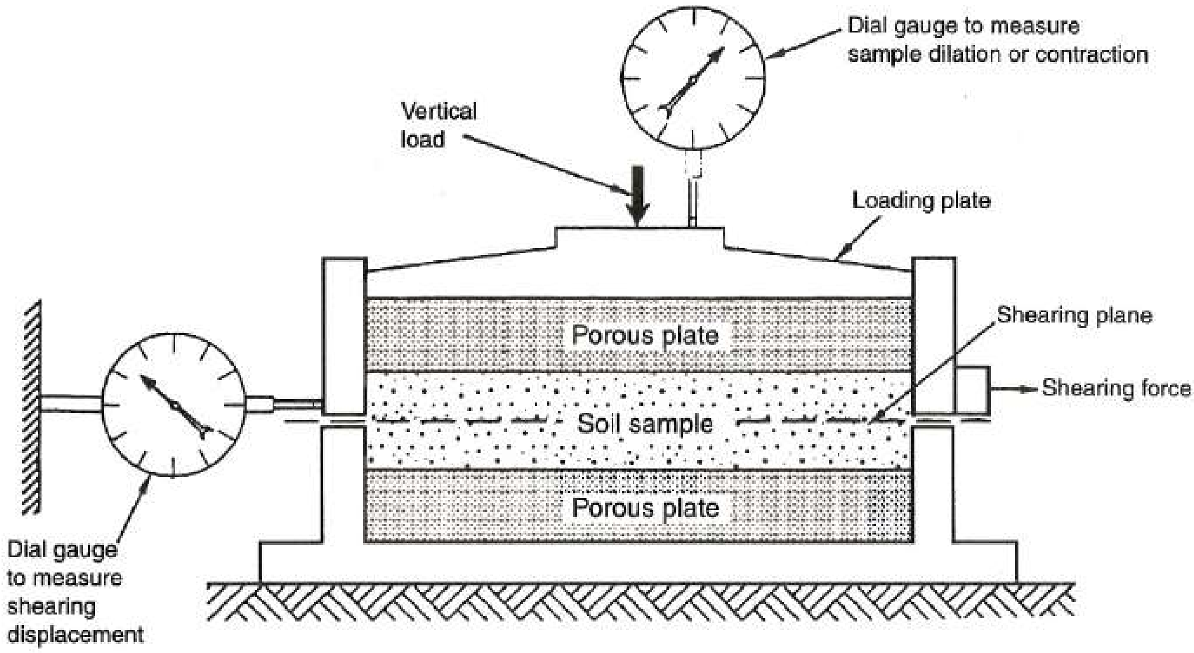

Figure 29: Illustration of an elevation view of Direct Shear Testing Device (Day 2001)

The procedure for performing a direct shear test is described according to ASTM D3080/D3080M and summarized according to Das (2002). The procedure for testing sands is:

1. Remove the shear box assembly. Back off the three vertical and two horizontal screws (not shown). Remove the loading plate. Insert the two vertical pins (not shown) to keep the two halves of the shear box together.
2. Weigh some dry sand in a large porcelain dish, *W*. Fill the shear box with sand in small layers. A tamper may be used to compact the sand layers. The top of the compacted soil sample should be about ¼ in. below the top of the shear box. Level the surface of the soil sample.
3. Determine the dimensions of the soil sample (Length, L; Width, B; Height, H).
4. Slip the loading plate down from the top of the shear box to rest on the soil sample.
5. Put the shear box assembly in place in the direct shear machine.

6. Apply the desired normal load, N, on the specimen. This can be done by hanging dead weights to the vertical load yoke (not shown). The top crossbars will rest on the loading plate of the specimen, which in turn, rests on the soil sample.
7. Remove the two vertical pins (not shown), allowing the two halves of the shear box to move independently of each other.
8. Advance the three vertical screws (not shown) that are located on the side walls of the top half of the shear box. This is done to separate the two halves of the box. The space between the two halves of the box should be slightly larger than the largest grain size of the soil sample.
9. Set the loading plate by tightening the two horizontal screws (not shown) located at the top half of the shear box. Now back off the three vertical screws (not shown). After doing this, there will be no connection between the two halves of the shear box except the soil.
10. Attach the horizontal and vertical dial gauges to the shear box to measure respective displacements during the test.
11. Apply horizontal load, *S*, to the top half of the shear box. The rate of shear displacement should be between 0.1 and 0.02 in./min (2.54 to 0.508 mm/min). For every tenth small division displacement in the horizontal dial gauge, record the readings of the vertical dial gauge and the horizontal load cell. Continue this until either the horizontal load cell reading reaches a maximum and then falls, or the horizontal load cell reading reaches a maximum and then remains constant.
12. Repeat the test at least two more times. For each test the dry unit weight of compaction of the sand specimen should be the same as that of the first specimen.

For each test, the dry unit weight of the specimen, the void ratio of the specimen, the normal stress on the specimen, and the shear stress applied to the specimen should be calculated. Equations 7-10 show how to calculate these values.

$$\gamma_d = \frac{W}{LBH} \qquad \text{(Eq. 7) (Das 2002)}$$

Where: γ_d is the dry unit weight of the specimen
W is the weight of dry sand
L is the length of the specimen
B is the width of the specimen
H is the height of the specimen

$$e = \frac{G_s \gamma_w}{\gamma_d} - 1 \qquad \text{(Eq. 8) (Das 2002)}$$

Where: e is the void ratio of the specimen
γ_d is the dry unit weight of the specimen
G_s is the specific gravity of soil solids
γ_w is the unit weight of water

$$\sigma' = \frac{N}{LB} \qquad \text{(Eq. 9) (Das 2002)}$$

Where: σ' is the normal effective stress on the specimen
N is the normal load applied to the specimen
L is the length of the specimen
B is the width of the specimen

$$\tau = \frac{S}{(L - \Delta L)B} \qquad \text{(Eq. 10) (from Das 2002)}$$

Where: τ is the shear stress on the sample
S is the shear force
L is the length of the specimen
ΔL is the horizontal displacement of the direct shear test
B is the width of the specimen

This test should be repeated at least three times using different normal stresses to determine the total stress strength parameters and total stress Mohr-Coulomb failure envelope. Figure 30 is a plot of shear stress vs. normal stress for three different applied normal stresses. The total stress Mohr-Coulomb failure envelope (bold line) is defined by the applied shear stress that caused failure for each of the three applied normal stresses. The total stress shear strength parameters, c and ϕ, can be determined from this plot. The cohesion, c, of the soil is the intersection of the total stress Mohr-Coulomb failure envelope with the ordinate, while the angle of internal friction is the angle defined by the total stress Mohr-Coulomb failure envelope and the horizontal measured on the plot, when the τ and σ scales are equal. It should be noted that for sands and gravels, no excess pore pressure is expected to build and the test is often run dry.

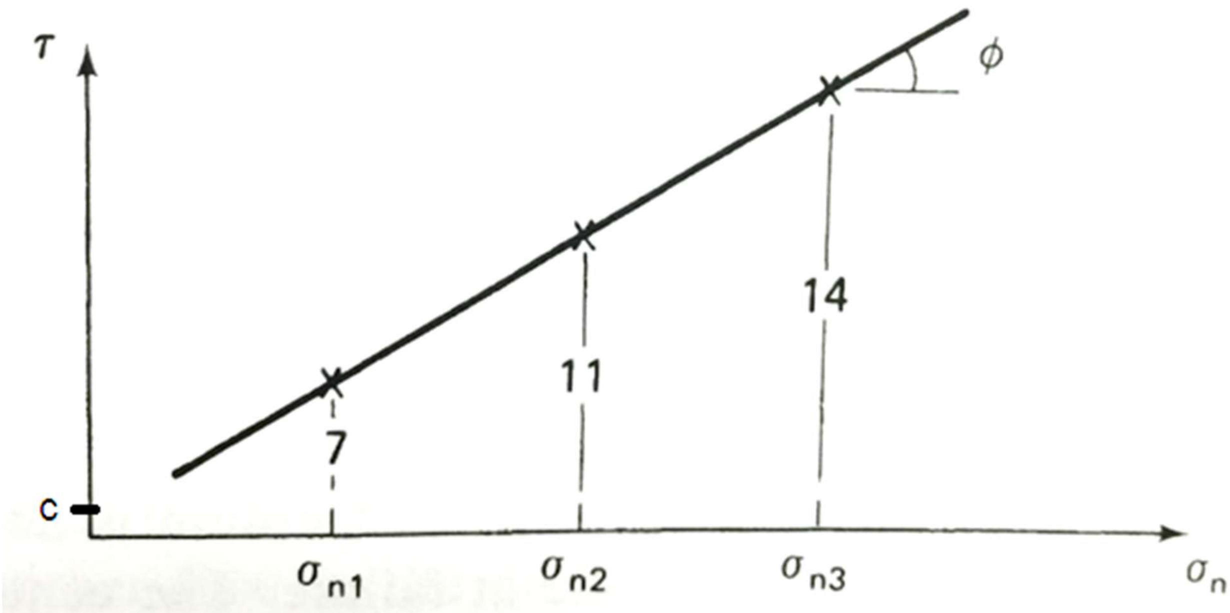

Figure 30: Mohr diagram of direct shear testing results to determine Mohr-Coulomb failure envelope and strength parameters (Holtz and Kovacs 1981)

There are advantages and disadvantages to the direct shear test. Advantages of the direct shear test include low cost, relatively short test durations, and simplicity (Holtz and Kovacs 1981). Disadvantages include not being able to calculate effective stress, high stress concentrations at the sample boundaries, forcing the failure to occur through a plane through the specimen which may or may not be the weakest/critical direction, and the fact that the principal planes rotate uncontrollably between the start of the test and failure (Holtz and Kovacs 1981).

The principal planes rotate during testing because, initially, the horizontal plane is a principal plane as there is no shear stress on it. During testing, a shear stress is forced through the horizontal plane meaning that it is no longer a principal plane and that the principal plane must exist elsewhere.

b. Triaxial Test (ASTM D4767)

The triaxial test was developed by Arthur Casagrande in 1930 (Holtz and Kovacs 1981). While the triaxial test is much more complicated than the direct shear test, it adds quite a bit of versatility and many advantages. Unlike the direct shear test, the triaxial test offers full control over specimen drainage, no rotation of principal planes, and significantly reduced stress concentrations. An added advantage of the triaxial test is that the stress paths to failure can be controlled fairly well, allowing field conditions to be modeled more accurately in the laboratory (Holtz and Kovacs 1981). An illustration of the cross-section of a triaxial test is shown in Figure 31.

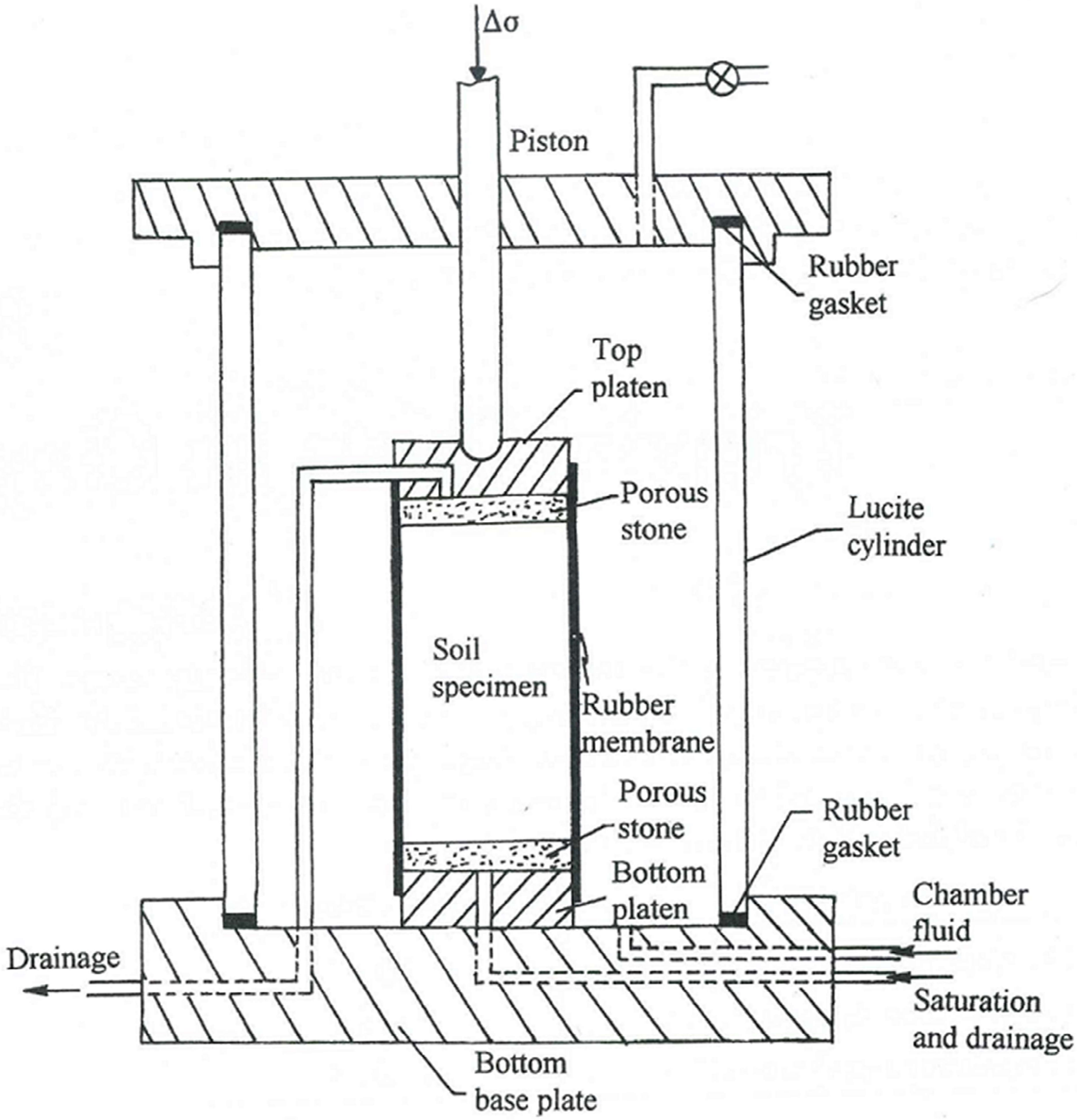

Figure 31: Triaxial cell elevation view cross-section schematic (Das 2002)

The basic principle of a triaxial test assumes that the stresses on the boundary of the specimen are principal stresses and that any combination of principal stresses may be applied to a soil specimen until failure occurs (Holtz and Kovacs 1981). To achieve this, the soil specimen is encased in a rubber membrane between two impervious platens. This specimen is placed inside the clear acrylic cylinder filled with liquid. The impervious platens and rubber membrane do not allow the liquid in the cell to enter the specimen. As the pressure of the liquid is changed, a pressure acting normal to the entire soil specimen with the magnitude of the change in liquid pressure is induced on the soil specimen. Initially, the cell pressure equals the major and minor principal stresses because the same stress is applied to the top of the specimen as the sides, which are principal planes at the start of the test. During the test, the top platen is pushed into the specimen by the piston, inducing an additional axial (vertical) stress. Thus, a difference in the major and minor principal stresses occurs (Holtz and Kovacs 1981). As this difference in principal stresses increases, it will eventually reach such a difference that failure occurs (Winterkorn and Fang 1975). Knowing the major and minor principal stresses at failure, a Mohr's Circle can be plotted. Performing multiple triaxial tests at different confining pressures allows multiple Mohr's Circles to be plotted and a Mohr-Coulomb failure envelope to be determined (Winterkorn and Fang 1975). Figure 32 shows how a Mohr-Coulomb failure envelope is defined by triaxial test failure circles resulting from tests at various cell pressures.

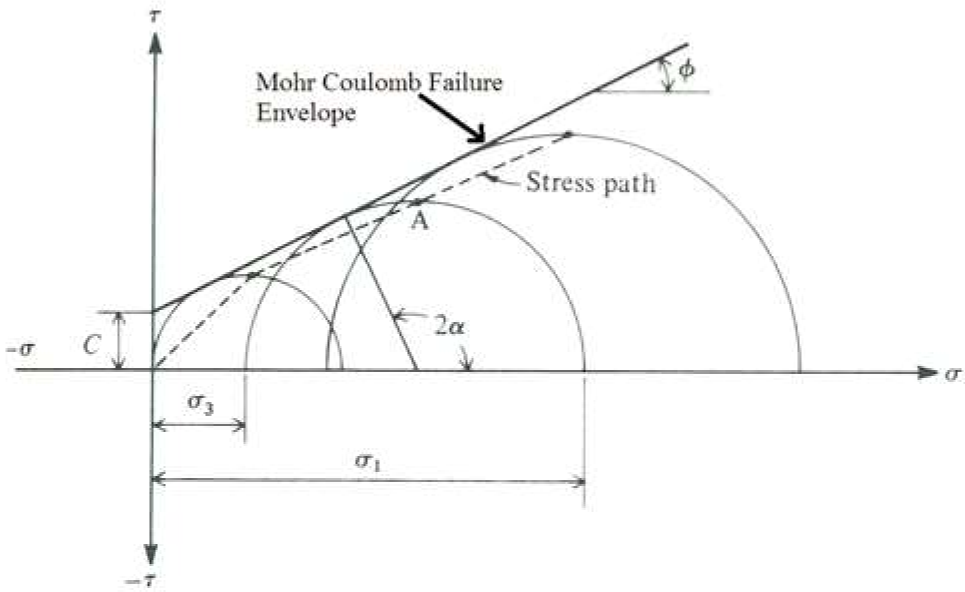

Figure 32: Mohr diagram showing three total stress triaxial test failure circles and the related Mohr-Coulomb Failure Envelope (Winterkorn and Fang 1975)

The ability to control drainage in a triaxial test allows a wide variety of tests to be performed. There are three types of triaxial shear tests based on differing sample drainage conditions before and during shear (Holtz and Kovacs 1981). The three types of triaxial tests are unconsolidated-undrained (UU), consolidated-drained (CD), and consolidated-undrained (CU) (Das 2002; Holtz and Kovacs 1981; Day 2001). To obtain these different test types, the drainage valves allowing drainage atop and below the specimen are opened and closed at strategic points during testing.

i. Unconsolidated-Undrained Test (UU)

In an unconsolidated-undrained test, the drainage valves are closed from the beginning of the test. Assuming sample saturation, no consolidation of the sample can occur, even with applied confining pressure (Holtz and Kovacs 1981). However, pore pressure within the sample will increase at the same rate of applied confining pressure. The drainage valves remain closed for the duration of the test as axial load is applied to the specimen and shear occurs. Typically, the unconsolidated-undrained test is performed as a total stress test and will produce a total stress Mohr-Coulomb failure envelope with zero slope. The zero slope failure envelope occurs because all samples have the same effective consolidation stress throughout the test. Assuming samples are at the same water content and density, they will have the same strength (Holtz and Kovacs 1981). Figure 33 shows the horizontal total stress failure envelope defined by three different UU tests where pore pressure was not measured. It should be noted that the slope of the total stress failure envelope is equal to zero and therefore the total stress internal friction angle is equal to zero (Holtz and Kovacs 1981). The UU test provides only one parameter, known as undrained shear strength, c (Holtz and Kovacs 1981; Das 2002). If the pore water pressures are measured in a UU test, the pore pressures increase at the same rate of increase as the confining pressure. This causes effective stresses at failure that are independent of the cell pressures applied to specimens in a test series, resulting in a single effective stress Mohr circle at failure (Holtz and Kovacs 1981).

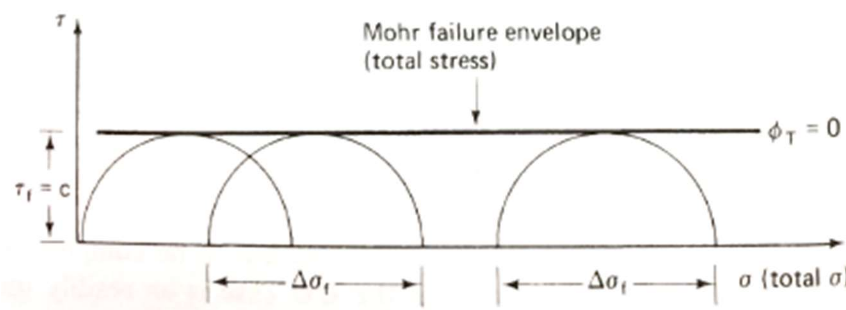

Figure 33: Mohr-Coulomb failure envelope defined by three UU tests (Holtz and Kovacs 1981)

The procedure to perform a UU test is described by Das (2002). The procedure is to place the triaxial cell (with specimen inside it) on the platform of the compression machine. Make proper adjustments so that the piston of the triaxial cell just rests on the top platen of the specimen. Fill the chamber of the triaxial cell with water. Apply a hydrostatic pressure, σ_3, to the specimen through the chamber fluid. All drainage valves to and from the specimen should be closed now so that drainage from the specimen does not occur. Check for proper contact between the piston and the top platen on the specimen. Zero the dial gauge of the proving ring and the gauge used for measurement of the vertical compression of the specimen. Set the compression machine for a strain rate of about 0.5% per minute, and begin compression. Take initial load readings for vertical compression intervals of 0.01 in. (0.254 mm). This interval can be increased to 0.02 in. (0.508 mm) or more, when the rate of increase of load on the specimen decreases. The load will increase to a peak value and then may decrease or remain approximately constant. During the test, the axial load and axial deformation are recorded allowing computation of axial stress and axial strain. After completion of the test, reverse the compression machine, lower the triaxial cell, and then turn off the machine. Release the chamber pressure and drain the water in the triaxial cell. Then remove the specimen and determine its moisture content.

ii. Consolidated-Drained Test (CD)

In a consolidated-drained test, the drainage valves are initially left open and as the cell pressure is increased. The sample is allowed to consolidate to a state of stress that appropriately models a field condition or design scenario. However, it should be noted that applied consolidation stresses may also be anisotropic as a stress difference may be applied axially (Holtz and Kovacs 1981). At the end of consolidation, the drainage valves remain open as the axial load is applied. In this test, the axial load must be applied very slowly to allow excess pore pressure to dissipate during the test (Holtz and Kovacs 1981). Figure 34 shows the results of a single consolidated-drained test performed on a normally consolidated clay and the resulting total and effective stress Mohr-Coulomb Failure envelope. Note that for CD testing for normally consolidated clays, both a cohesion intercept and angle of internal friction can be obtained (Das 2002).

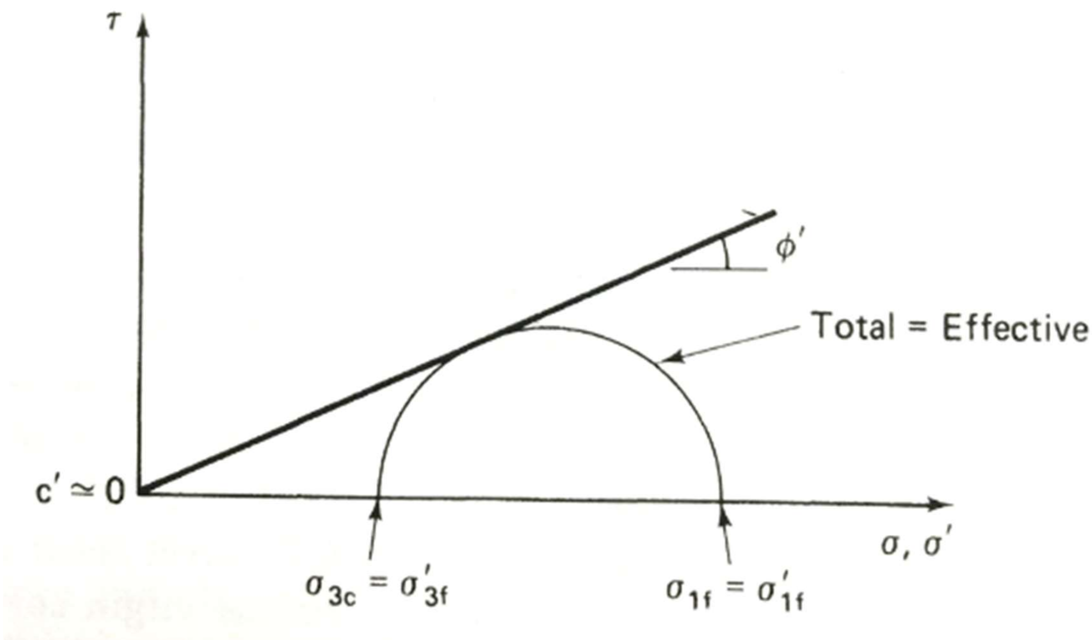

Figure 34: Total and effective stress Mohr-Coulomb failure envelope tested in CD triaxial testing for a normally consolidated clay (Holtz and Kovacs 1981)

iii. Consolidated-Undrained Test (CU)

Similar to the consolidated-drained test, the drainage valves are initially left open and as the cell pressure is increased, the sample is allowed to consolidate to a state of stress that appropriately models a field condition or design scenario. However, it should be noted that applied consolidation stresses may also be anisotropic as a stress difference may be applied axially (Holtz and Kovacs 1981). At the completion of consolidation, the drainage valves are closed and the specimen is loaded axially until shear failure occurs. It is common to measure pore water pressure during consolidated-undrained testing so that both total and effective stresses may be calculated (Holtz and Kovacs 1981). Figure 35 shows total and effective Mohr's circles and total and effective failure envelopes that were obtained through a single test on a normally consolidated clay to obtain effective strength parameters from total strength parameters, the pore pressure is subtracted from both the major and minor principal stress at failure (Holtz and Kovacs 1981). Similar to the consolidated-drained test, both total stress and effective stress cohesion intercepts and angle of internal friction can be obtained (Das 2002).

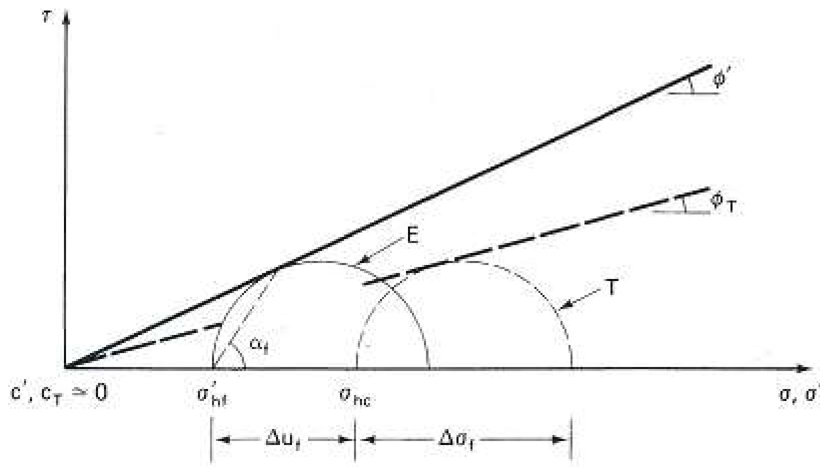

Figure 35: Effective (E) and total (T) stress Mohr's Circles and their respective failure envelopes for a consolidated-undrained test performed on a normally consolidated clay (Holtz and Kovacs 1981)

The procedure to perform a CU test is described by Das (2002). The procedure is:

1. Place the triaxial cell with the saturated specimen on the compression machine platform and make adjustments so that the piston of the cell makes contact with the top platen of the specimen.
2. Fill the chamber of the triaxial cell with water, and apply the hydrostatic pressure, σ_3, to the specimen through the chamber fluid.
3. The application of the chamber pressure, σ_3, will cause an increase in the pore water pressure in the specimen. For consolidation, connect the drainage lines from the specimen to a calibrated burette. When the water level in the burette becomes constant, it will indicate that consolidation is complete. For a saturated specimen, the

volume change due to consolidation is equal to the volume of water drained from the burette. Record the volume of the drainage (ΔV).

4. Now connect the drainage lines to the pore-pressure measuring device.
5. Check the contact between the piston and the top platen. Zero the load cell and the LVDT, which measures the axial deformation of the specimen.
6. Set the compression machine for a strain rate of about 0.5% per minute, and begin compression. When the axial load on the specimen is increased, the pore water pressure in the specimen will also increase. Record the load cell reading and the corresponding excess pore water pressure (Δu) in the specimen for every 0.01 in. (0.254 mm) or less of axial deformation. The load cell reading will increase to a maximum and then decrease or remain approximately constant.
7. At the completion of the test, reverse the compression machine and lower the triaxial cell. Shut off the machine. Release the chamber pressure, σ_3, and drain the water out of the triaxial cell.
8. Remove the tested specimen from the cell and determine its moisture content.
9. Repeat the test on one or two more similar specimens. Each specimen should be tested at a different value of σ_3.

3. Field Tests

Field tests are performed *in situ* and do not require a sample to be returned to the laboratory. This section is not comprehensive but outlines the most widely used and accepted field tests for shear strength.

a. Vane Shear Test (ASTM D2573)

The vane shear test allows geotechnical engineers to determine the shear strength and sensitivity of soft clays *in situ*. The ability to perform this test *in situ* reduces the effect of sampling disturbance, especially when dealing with highly sensitive clays (Clayton et al., 1995).

The first vane shear test was designed and used in 1919 by John Olsson during the construction of the Lidingoe Bridge in Stockholm, Sweden (Clayton et al., 1995). The vane shear test consists of pushing a four-bladed cruciform vane attached to a solid rod into the soil, rotating the rod, and measuring the torque required to rotate the vane. Figure 36 shows elevation and cross-sectional views of rectangular and tapered field vanes, respectively. Vane shear tests may be carried out in the laboratory or in the field. However, tests conducted in the laboratory may be subjected to additional disturbance caused by sampling or remolding. In the field, tests can be conducted at any depth allowed by the equipment (Clayton et al., 1995). The vane shear test is only suitable for soils with low shear strengths. According to BS 1377 (1990), the vane shear test is not appropriate for soils with undrained shear strengths greater than seventy five kPa (10.88 psi) (Clayton et al., 1995). Vane blades may be rectangular or tapered and are employed in one of four ways. The first and simplest way is an unprotected vane pushed from the bottom of a bore hole or from the ground surface. In the second way, a vane housing is pushed simultaneously with the fragile vane to protect it during penetration and, at the desired depth, the vane is pushed ahead of the vane housing before administering the test. The third way incorporates sleeved vane rods to minimize friction between the rods and adjacent soil. The fourth way incorporates a swivel above the blades, allowing nine hundred degrees of rod rotation before engagement of the vanes so that rod friction can be measured and taken into account (Clayton et al., 1995).

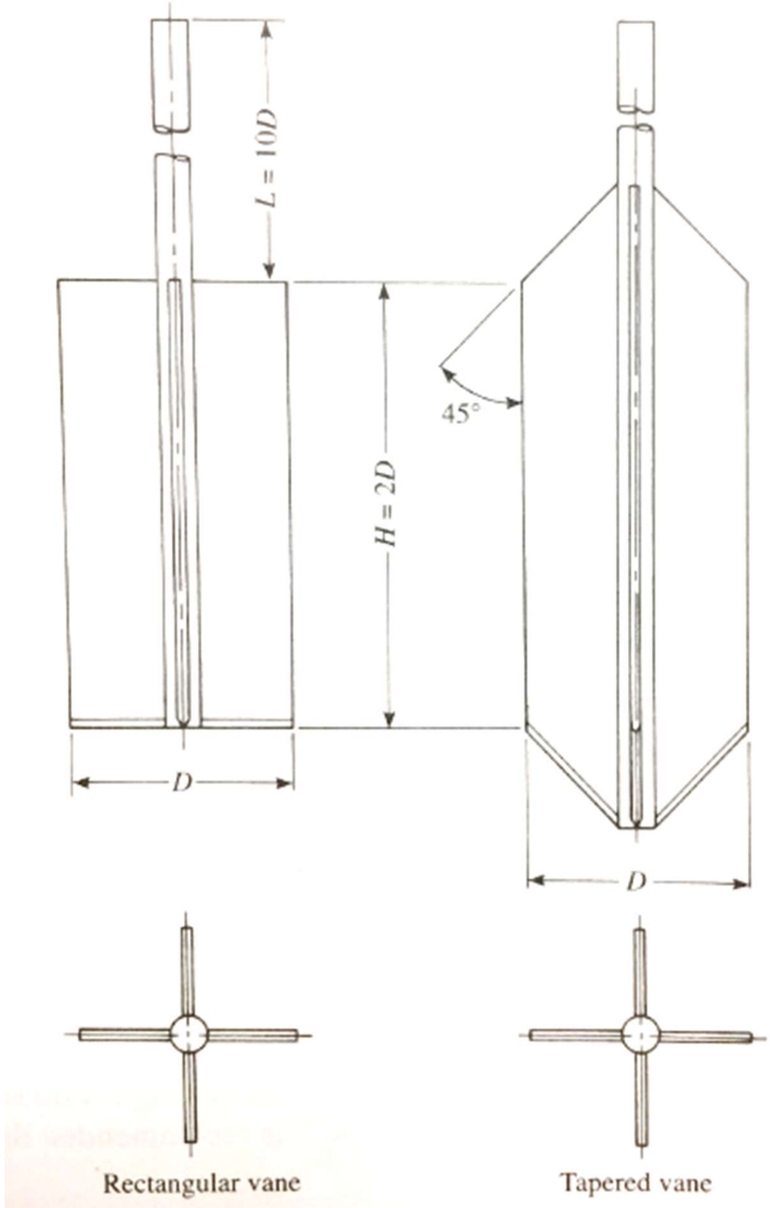

Figure 36: Elevation and cross-sectional views of rectangular and tapered field vanes, respectively (ASTM D2573)

The testing procedure described by Clayton et al. (1995) is as follows:

1. Push the vane slowly with a single thrust from the bottom of the bore hole or protected sleeve for the distance required to ensure that it penetrates undisturbed soil. Ensure that the vane is not rotated during this stage.

2. Attach a torque wrench, or preferably a purpose-built geared drive unit, to the top of the vane rods, and turn the rods at a slow but continuous rate. BS 1377:1990 specifies a rate of 6-12˚/min whilst ASTM D2573 specifies that the rate shall not exceed 6˚/min.
3. Record the relationship between rod rotation (at ground surface) and measured torque by taking readings of both at intervals of 15-30s. Once maximum torque is achieved, rotate the vane rapidly through a minimum of ten revolutions, and immediately (within 1 min- ASTM D2573) restart shearing at the previous slow rate, to determine the remoulded strength of the soil.

To provide accurate test results, it is important that a sleeved vane is pushed sufficiently ahead of disturbance caused by the vane housing or boring. ASTM D2573 specifies that the vane be pushed five vane housing diameters ahead of the vane housing or five bore hole diameters below the bottom of the bore hole depending on the method used to advance the vane to the test depth (Clayton et al., 1995).

The vane shear test is used to obtain undisturbed peak undrained shear strength and remoulded undrained shear strength (Clayton et al., 1995). Interpretation of test results is based on the following seven assumptions outlined by Clayton et al. (1995):

1. Vane penetration causes negligible disturbance, both in terms of changes in effective stress and shear distortion.
2. No drainage occurs before or during shear.
3. The soil is isotropic and homogenous.
4. The soil fails on a cylindrical shear surface.
5. The diameter of the shear surface is equal to the width of the vane blades.

6. At peak and remoulded strength, there is a uniform shear stress distribution across the shear surface.
7. There is no progressive failure, so that at maximum torque, the shear stress at all points on the shear surface is equal to the undrained shear strength, c.

The amount of torque that must be applied to the vane to fail the soil is a function of undrained shear strength and dimensions of the vane (Das 2004). Knowing the applied torque, Equations 11 and 12 are used to calculate undrained shear strength of a rectangular vane test.

$$\boldsymbol{c_u = \frac{T}{K}} \qquad \text{(Eq. 11) (Das 2004)}$$

Where: c_u is the undrained shear strength of the soil, N/m^2
T is the torque applied to the rod at the ground surface, N-m
K is a constant based on vane dimensions, m^3

$$\boldsymbol{K = (\pi)\left(\frac{D^2H}{2}\right)\left(1+\frac{D}{3H}\right)} \qquad \text{(Eq. 12) (Das 2004)}$$

Where: K is a constant based on vane dimensions, m^3
D is the diameter of the vane, m
H is the height of the vane, m

b. Cone Penetration Test (ASTM D5778/D3441)

The cone penetration test (CPT) is used to identify types of soil deposits and determine their *in situ* properties (Day 2001). The basic principle of the CPT is push a standard cone-shaped piece of metal into the ground and measure the resistance to penetration. Originally, a standard cone having a geometry of 60º tip with a base area of 10 cm^2 (1.55 in^2) was pushed into the ground and only the tip resistance was measured. Current cone penetrometers include a friction sleeve to measure side friction and a conical tip to measure tip resistance. The friction sleeve (friction jacket) and conical tip are shown in Figure 37. CPT soundings include cone (tip) resistance (q_c) and frictional resistance (f_c) (Das 2004). Cone resistance is defined as the vertical force applied to the cone divided by the cone's horizontally projected area. Frictional resistance is defined as the vertical force applied to the friction sleeve divided by the surface area of the friction sleeve (Das 2004). Two types of penetrometers are typically used to measure cone resistance and frictional resistance: the mechanical friction cone penetrometer and the electric friction cone penetrometer (Das 2004). The electric friction cone penetrometer is far more common than the mechanical friction cone. Figure 37 shows a mechanical friction cone penetrometer while Figure 38 shows an electric friction cone penetrometer.

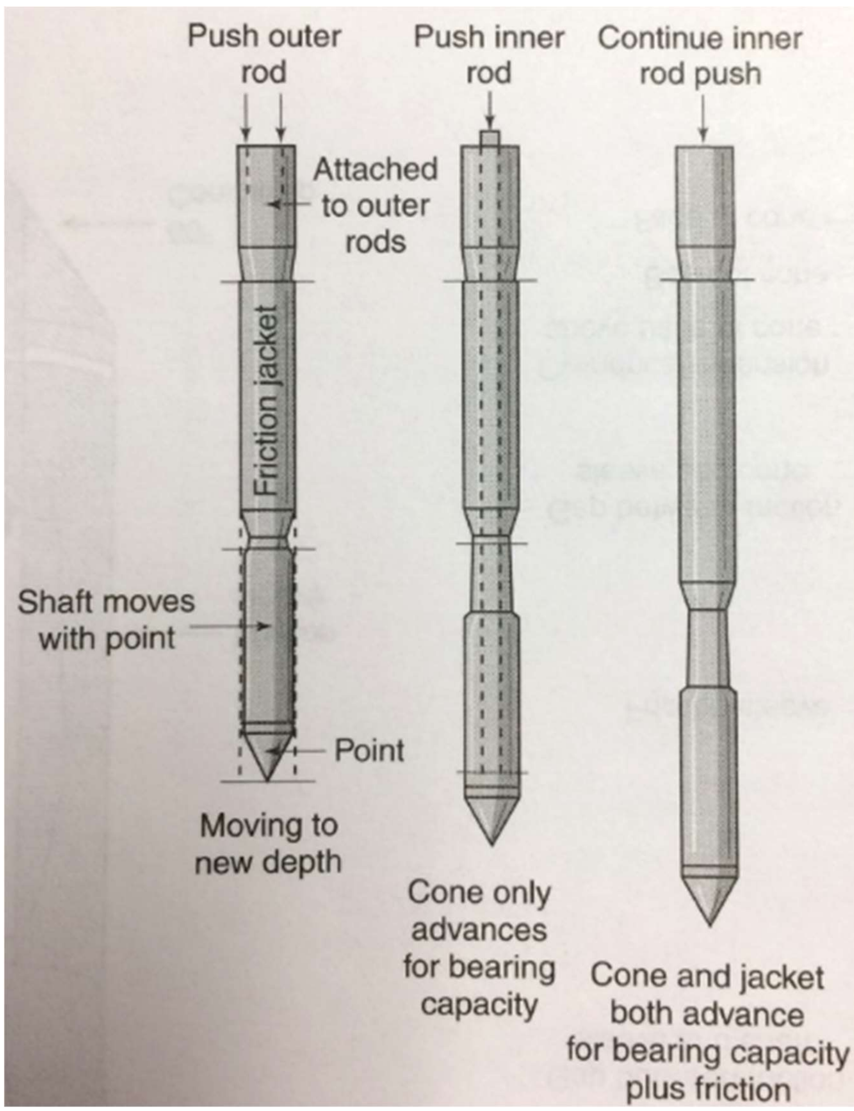

Figure 37: Depiction of the mechanical friction cone penetrometer and the rod push sequence used to obtain both cone and frictional resistance (McCarthy 2007)

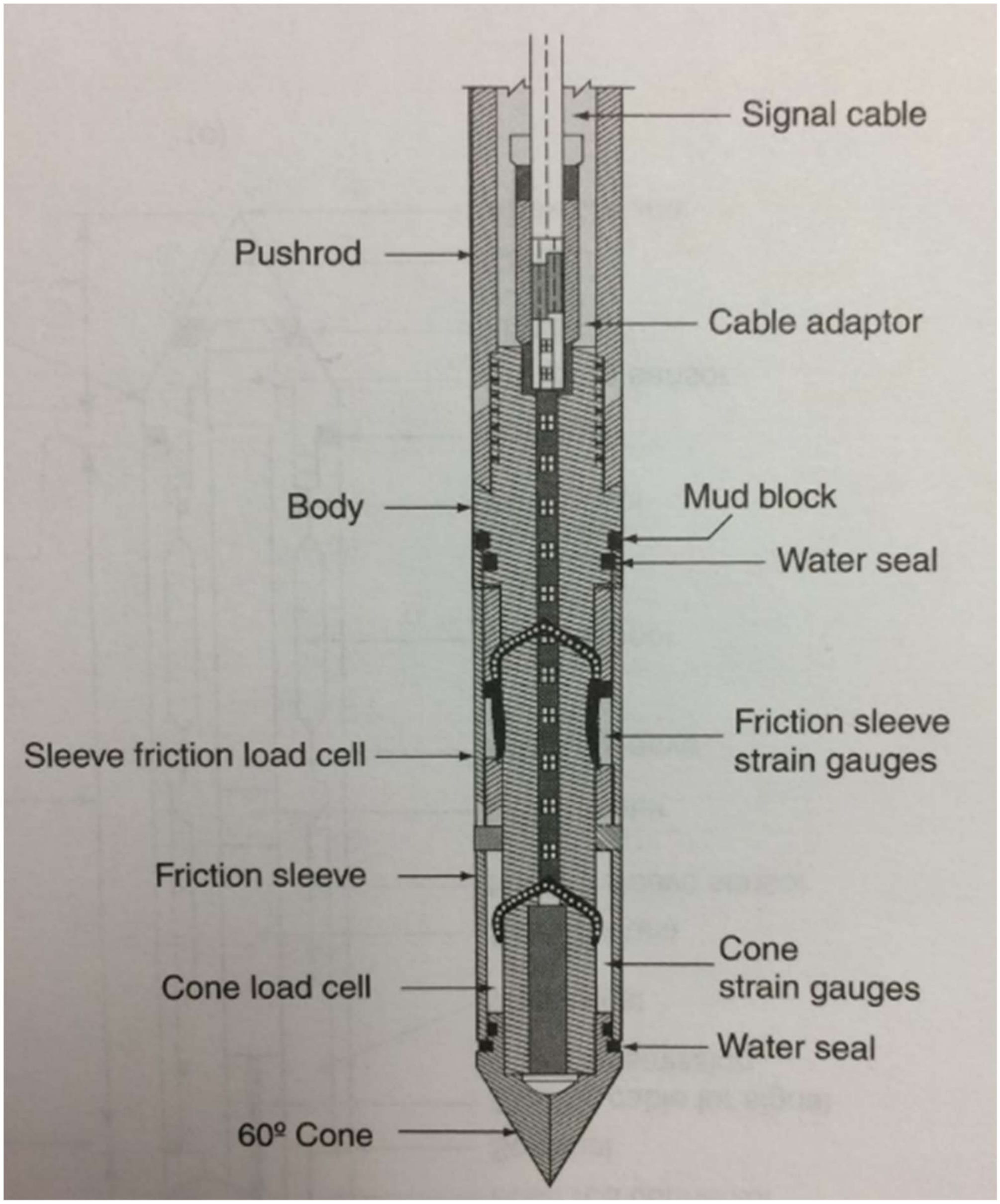

Figure 38: Electric friction cone penetrometer (McCarthy 2007)

The test procedure outlined in ASTM D3441-16 for mechanical friction cone penetrometer testing is as follows (2016):

1. Advance the penetrometer tip to the required test depth by applying sufficient thrust on the push rods.
2. Apply sufficient thrust on the inner rods to extend the penetrometer tip. Obtain the cone resistance at a specific point, Q_c, during the downward movement of the

inner rods relative to the stationary push rods. When the lower part of the tip engages and pulls down the friction sleeve, immediately obtain a second measurement of the total resistance of the cone plus the sleeve, Q_f. Do not stop the extension of the tip between the two resistance readings. Repeat Step 1. Apply sufficient thrust on the push rods to collapse the extended tip and advance it to a new test depth. Continual repetition of this two-step cycle cone resistance data and sleeve resistance data can be obtained at constant increments of depth that shall not ordinarily exceed 200 mm (7.87 in). Subtraction of the first reading (cone resistance) from the second reading (combined cone and friction sleeve resistance) provides the sleeve resistance.

The test procedure for the electric friction cone penetrometer as outlined by ASTM D5778-12 is as follows (2012):

1. The penetrometer is advanced through the soil at a constant rate of 20 mm/s (0.787 in/s). The force on the cone required to penetrate the soil is measured by electrical methods at least every 50 mm (1.97 in.) of penetration. Cone resistance, q_c, is obtained by dividing the measured force by the cone base area.
2. A friction sleeve is present on the penetrometer immediately behind the cone tip, and the force exerted on the friction sleeve is measured by electrical methods at least every 50 mm (1.97 in.) of penetration. Stress is calculated by dividing the measured axial force by the surface area of the friction sleeve to determine sleeve resistance, f_s.

Regardless of the type of penetrometer used to gather data, both q_c and f_s are obtained. The ratio of the frictional resistance to the cone resistance is called the friction ratio. Several correlations that are useful in estimating soil properties have been developed for the cone resistance and the friction ratio (Das 2004). The friction ratio is calculated using Equation 13

$$\boldsymbol{F_r} = \frac{\boldsymbol{f_c}}{\boldsymbol{q_c}} \qquad \text{(Eq. 13) (ASTM D5778)}$$

Where: F_r is the friction ratio
f_c is the friction sleeve resistance
q_c is the cone resistance

McCarthy offers the following general relationships between the friction ratio and tip resistance (2007):

1. Sandy soils typically have a high cone tip resistance and a low friction ratio.
2. Soft clays typically have a low cone tip resistance and a high friction ratio.
3. Organic soils typically have a very low cone tip resistance and a very high friction ratio.
4. Sensitive soils typically have low cone tip resistance and low friction ratio.
5. Soils with high over consolidation ratios typically have a high cone tip resistance and high friction ratio.

c. Standard Penetration Test (ASTM D1586-11)

The standard penetration test (SPT) is by far the most widely used *in situ* testing method in geotechnical exploration in the US. The SPT test is performed by simply driving a standard split-barrel sampler (tube) into soil and obtaining a disturbed soil sample as well as a measure of the resistance of the soil to penetration by the sampler (ASTM D1586-11 2011). Figure 39 shows the standard split spoon sampler used in the SPT. To advance the split spoon sampler, a 140 pound (63.5 kg) weight (hammer) is dropped 30 inches (762 mm), striking the anvil which transfers the energy to the drill rods and sampler, thus advancing the sampler. Each drop of the 140 pound (63.5 kg) weight is considered one hammer blow (ASTM D1586-11 2011). The SPT is an old test and during its tenure, has experienced quite a bit of change, especially in terms of hammers used to drive the sampler. In the past, pinweight hammers and donut hammers were used (McCarthy 2007). These hammer systems performed inconsistently. Safety hammers improved efficiency by about 30% over previous hammers, but often provide inconsistent results (McCarthy 2007). Current SPT testing utilizes the automatic hammer, which offers improved consistency over previous hammer systems (McCarthy 2007). Regardless, extreme care should be taken when analyzing SPT data due to its inherent inconsistency and how the test has changed over time.

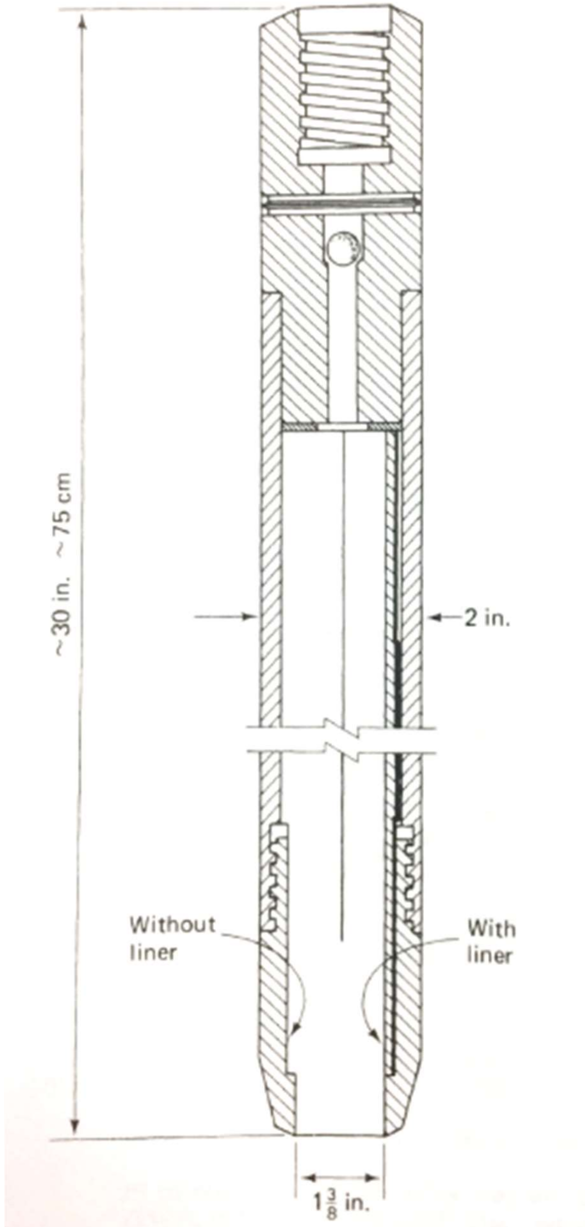

Figure 39: Standard penetration test split spoon sampler (Holtz and Kovacs 1981)

ASTM D1586-11 outlines the testing procedure for the SPT (2011):

1. After advancing the bore hole to the desired sampling depth and excessive cuttings have been removed, record the cleanout depth to the nearest 0.1 ft (3.05 cm).

2. Attach the split-barrel sampler to the sampling rods and lower into the bore hole. Do not allow the sampler to drop onto the soil to be sampled.
3. Position the hammer above and attach the anvil to the top of the sampling rods.
4. Rest the dead weight of the sampler, rods, anvil, and drive weight on the bottom of the bore hole. Record the sampling start depth to the nearest 0.1 ft (3.05 cm). Compare the sampling start depth to the cleanout depth recorded in step 1. If excessive cuttings are encountered at the bottom of the bore hole, remove the sampler and sampling rods from the bore hole and remove the cuttings.
5. Mark the drill rods in three successive 0.5 ft. (15.24 cm) increments so that the advance of the sampler under the impact of the hammer can be easily observed for each 0.5 ft (15.24 cm) increment.
6. Drive the sampler with blows from the 140 lbf (63.5 kg) hammer and count the number of blows applied in each 0.5 ft (15.24 cm) increment until one of the following occurs: A total of 50 blows have been applied during any of the three 0.5 ft (15.24 cm) increments, a total of 100 blows have been applied, there is no observed advance of the sampler during the application of 10 successive blows of the hammer, or the sampler is advanced the complete 1.5 ft (45.72 cm).
7. If the sampler sinks under the weight of the hammer, weight of rods, or both, record the length of travel to the nearest 0.1 ft (3.048), and drive the sampler through the remainder of the test interval. If the sampler sinks the complete interval, stop the penetration, remove the sampler and sampling rods from the bore hole, and advance the bore hole through the very soft or very loose materials

to the next desired sampling elevation. Record the N-value as either weight of hammer, weight of rods, or both.

8. Record the number of blows (N) required to advance the sampler each 0.5 ft. (15.24 cm) interval of penetration or fraction thereof. The first 0.5 ft. (15.24 cm) interval is considered to be a seating drive. The sum of the number of blows to penetrate the second and third intervals is termed the "standard penetration resistance" or "N-Value." If the test is terminated before the sampler is driven the full 1.5 ft. (45.72 cm), the number of blows per each complete 0.5 ft. (15.24 cm) increment and per each partial increment shall be recorded on the boring log. For partial increments, the depth of penetration shall be reported to the nearest 0.1 ft. (3.048 cm) in addition to the number of blows. If the sampler advances below the bottom of the bore hole under the static weight of the drill rods or the weight of the drill rods plus the static weight of the hammer, this information should be noted on the boring log.
9. The raising and dropping of the hammer shall be accomplished using either Method A or Method B, described below. Energy entering the drill rods can be measured according to procedures in ASTM D4633.
10. Method A involves using a trip, automatic, or semi-automatic hammer drop system that lifts the hammer and allows it to drop 30 inches (762 mm). Drop height adjustments for automatic and trip hammers should be checked daily and at first indication of variations in performance. Operation of automatic hammers shall be in strict accordance with operations manuals.

11. Method B involves using a cathead to pull a rope attached to the hammer. When the cathead and rope method is used the system and operation shall conform to the following: The cathead shall be essentially free of rust, oil, or grease and have a diameter in the range of 6-10 in. (152.4 to 254 mm). The cathead should be operated at a minimum speed of rotation of 100 RPM. The operator should generally use either 1-3/4 or 2-3/4 rope turns on the cathead, depending upon whether or not the rope comes off the top or the bottom of the cathead during the performance of the penetration test. The cathead rope should be stiff, relatively dry, clean, and should be replaced when it becomes excessively frayed, oily, limp, or burned. For each hammer blow, a 30 inch (762 mm) lift and drop shall be employed by the operator. The operation of pulling and throwing the rope shall be performed rhythmically without holding the rope at the top of the stroke.
12. Bring the sampler to the surface and open. Remove, label and store samples appropriately.

After testing, a variety of correlations are available to estimate soil parameters based on the observed N-value, including unconfined compressive strength, q_u. It should be noted that SPT correlations are highly approximate and should be treated as such (Das 2006). Equation 14 is one of many correlations to relate the SPT N-value to unconfined compressive strength.

$$\frac{q_u}{p_a} = 0.58{N_{60}}^{0.72}$$ (Eq. 14) (Kulhawy and Mayne 1990)

Where: N_{60} is the SPT N-value corrected to 60% energy
q_u is the unconfined compressive strength
p_a unit atmospheric pressure

d. Iowa Bore hole Shear Test

The Iowa Bore hole Shear Test is a shear test that is conducted against the sidewalls of a bore hole. The shear head of the device is lowered into the bore hole and expanded against the sidewalls at a known pressure. After the shear head has engaged the soil for a sufficient amount of time, it is pulled vertically and the load required to pull the shear head is measured. Additional testing stages should be performed by increasing the expansion pressure of the shear head and measuring the load required to pull the shear head at the new expansion pressure (Holtz and Kovacs 1981). Knowing the area of the shear head, expansion pressure, and force required to pull the shear head, a normal stress and a shear stress can be determined for each testing stage. Shear strength parameters can be determined by plotting these results on a Mohr diagram (Holtz and Kovacs 1981). Figure 40 shows the Iowa Bore hole Shear Test setup.

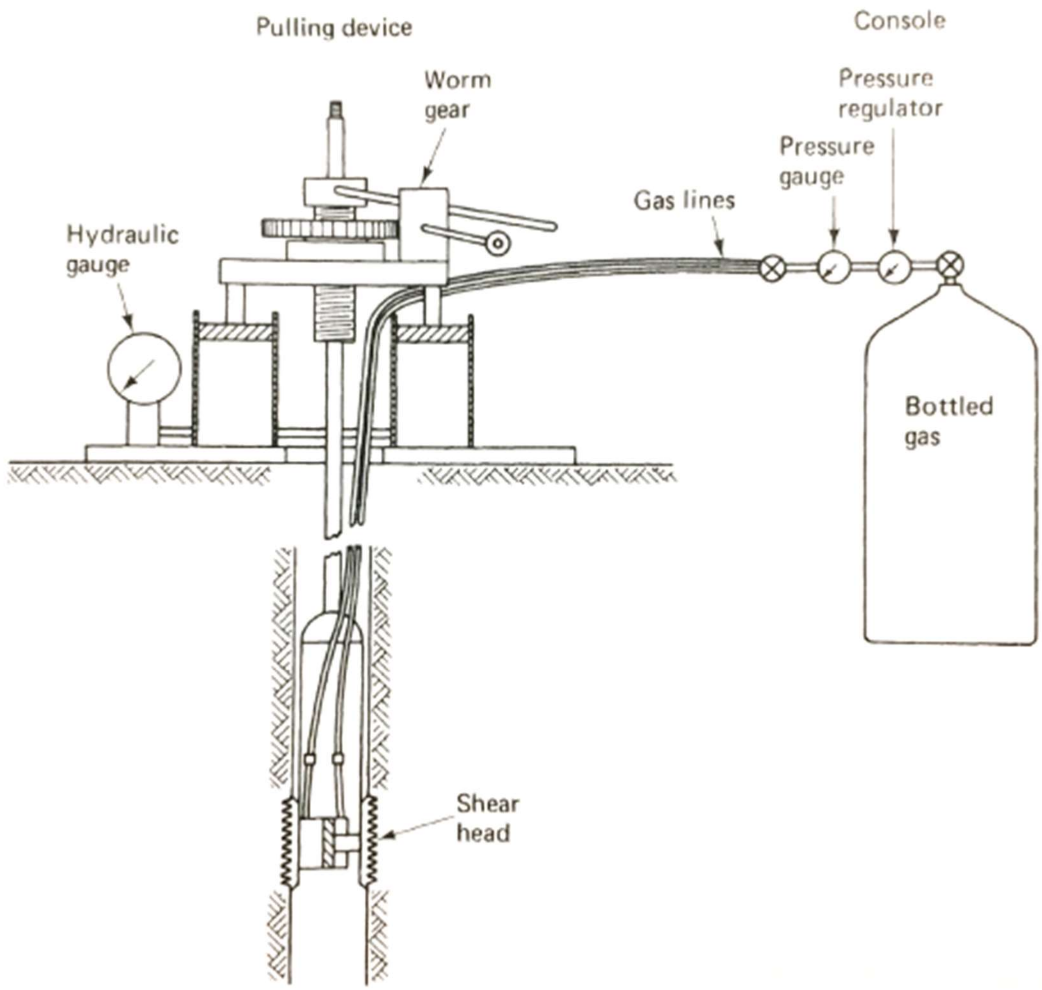

Figure 40: Iowa Bore hole Shear Test (Holtz and Kovacs 1981)

Before performing the test, it is important that the bore hole should have clean walls and disturbance to the bore hole wall should be kept to a minimum (Lutenegger 1987). There are two methods, multi-stage and single-stage, both outlined by Lutenegger (1987), and described below.

Procedure common to both multi-stage and single-stage testing (Lutenegger 1987):

1. Choose, examine, and attach appropriate shear plates for testing.
2. Record the initial gage reading on the reaction base shear gage.

3. Connect the pressure source and pneumatic lines from the shear head to the control console. Select the retract position on the control console and apply about 20 psi (138 kPa) of pressure to keep the shear head retracted while inserting into the bore hole.
4. Lower the shear head to the test depth, adding reaction rods in sections as the shear head is lowered.
5. Position the shear face reaction base over the bore hole. If necessary, level the ground before positioning the reaction base. The base must be level with the ground surface so that the transmitted shear force is applied perpendicular to the reaction base.
6. Attach the rod clamp to the reaction rods and allow the shear head and rods to rest on the base plate worm-gear mechanism, making sure that the splines in the worm-gear are aligned with the grooves in the rod clamp. Record the gage reading on the base plate shear force gage (hydraulic gauge in Figure 40). This reading represents the weight of the suspended shear head and reaction rods and is the initial shear gage reading, which must be subtracted from all test readings.
7. Record the gage reading on the control console pressure gage. This reading represents an initial gage reading that must be subtracted from all subsequent readings. Apply an initial normal pressure to the shear head by adjusting the control console regulator. A sufficient amount of time (minimum five minutes) should be allowed for consolidation of the soil to occur. The initial normal pressure and subsequent intervals should be selected before testing.

Shear phase: Multi-stage testing method (Lutenegger 1987):

1. At the end of consolidation, apply a shear force to the reaction rods by turning the worm-gear handle clockwise at a rate of two rps to apply a vertical translation of 0.05 mm/s (0.002 in/s). Observe the reaction base pressure gage reading and record the maximum value. Experience has shown that the maximum reading should be achieved before a shear displacement of about five millimeters (0.2 inches). Subtract the initial reaction base reading from the maximum value to obtain the corrected reaction base reading. Release the shear force by turning the worm-gear handle counterclockwise until the base plate reading returns to the initial reading.
2. Increase the control console regulator to the next value of normal pressure and repeat the consolidation phase.
3. The sequence of applying successively normal pressures and shear forces as described should be repeated to obtain a minimum of five data sets.

Shear phase: Single-Stage Testing

1. At the end of consolidation, apply a shear force to the reaction rods by turning the worm-gear handle clockwise at a rate of two rps to apply a vertical translation of 0.05 mm/s (0.002 in/s). Observe the reaction base pressure gage reading and record the maximum value. Experience has shown that the maximum reading should be achieved before a shear displacement of about five millimeters (0.2 inches). Subtract the initial reaction base reading from the maximum value to obtain the corrected reaction base reading. Release the shear force by turning the

worm-gear handle counterclockwise until the base plate reading returns to the initial reading.

2. Release the normal pressure by releasing the control console regulator and opening the vent. Apply a small amount of retract pressure to the shear head and remove it from the bore hole. Reinsert the shear head into the bore hole and either rotate it ninety degrees from the previous test position or move the shear plate either up or down one hundred millimeters from the previous position so that fresh material is engaged. Apply the next increment of normal pressure and proceed with the consolidation phase.
3. This procedure of applying normal pressures and measuring maximum shear force should be repeated to obtain a minimum of four data sets.

Plotting the normal stress and shear stress data points on a Mohr diagram allows the shear strength parameters to be determined.

e. Pressuremeter Test (ASTM D4719-07)

The pressuremeter test is an *in situ* stress-strain test performed by inserting a cylindrical probe into a bore hole and radially expanding it against the bore hole walls (ASTM D4719-07 2007, Day 2001). Similar to the Iowa Bore hole Shear Test, disturbance to the bore hole walls must be minimized to produce viable results (ASTM D4719-07 2007). The basic pressuremeter test setup is shown in Figure 41. The standard pressuremeter probe shown is a triple cell design which utilizes two guard cells to ensure radial expansion of the measuring cell (ASTM D4719-07 2007).

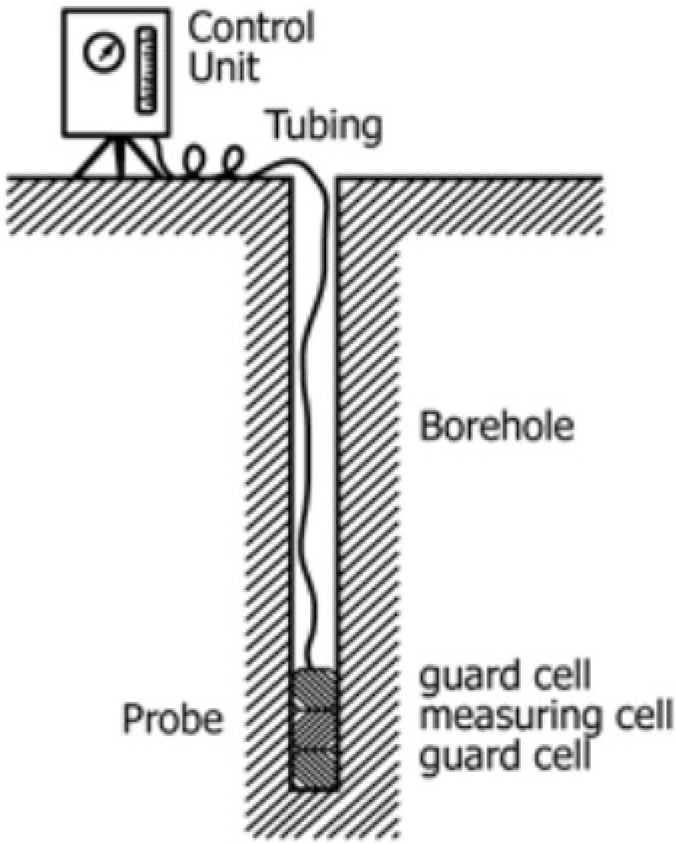

Figure 41: Basic pressuremeter test setup (ASTM D4719-07 2007)

Pressuremeter tests may be conducted by inflating the probe under equal pressure increments or equal volume increments. Termination of the test occurs when soil yielding becomes disproportionately large (ASTM D4719-07 2007). The test procedure for both equal pressure increment and equal volume increment pressuremeter tests follow (ASTM D4719-07 2007):

1. Drill the bore hole to the test level and clean debris and cuttings.
2. Before positioning the probe for testing, make an accurate determination of the zero volume reading, which is the volume of the measuring portion of the uninflated probe at atmospheric pressure. This is accomplished by deairing all

circuits and adjusting all gages of the instrument to zero while the probe is at atmospheric pressure. Close the volume circuit to prevent any further volume change of the measuring circuit. Lower the probe to the test depth in this condition. The test depth should be the depth of the probe's midpoint.

3. To perform equal pressure increment testing, place the probe in the test position and apply the pressure on the control unit in equal increments until the expansion of the probe during one load increment exceeds about ¼ of the zero volume reading. Generally, 25, 50, 100, or 200 kPa (3.62, 7.25, 14.5, or 29 psi) pressures are selected for testing soils. Too small steps will result in an excessively long test, too large steps may yield results with inadequate accuracy. The pressure steps should be determined in such a way that about 7 to 10 load increments are obtained.
4. To perform equal volume increment testing, increase the volume of the probe in volume increments of 0.05 to 0.1 times the zero volume reading until the limit of the equipment is reached.
5. For both procedures, take readings after 30s and 1 min after the pressure or volume increments have been applied. Volume readings should be recorded to an accuracy of 0.2% of the zero volume reading and pressure readings to an accuracy of 5% of the limit pressure.
6. Once the test has reached the maximum test step, terminate the test by deflating the probe to its original volume and removing it from the hole.
7. If desired, one or several load-unload cycles may be performed as long as they are performed within the material's elastic expansion range.

After testing, calculations should be performed according to ASTM D4719-07 to determine the pressuremeter modulus and the limit pressure. Figure 42 shows pressuremeter data with the limit pressure and the change in pressure (Δp) and change in volume (Δv) of the pseudo elastic section used to calculate pressuremeter modulus.

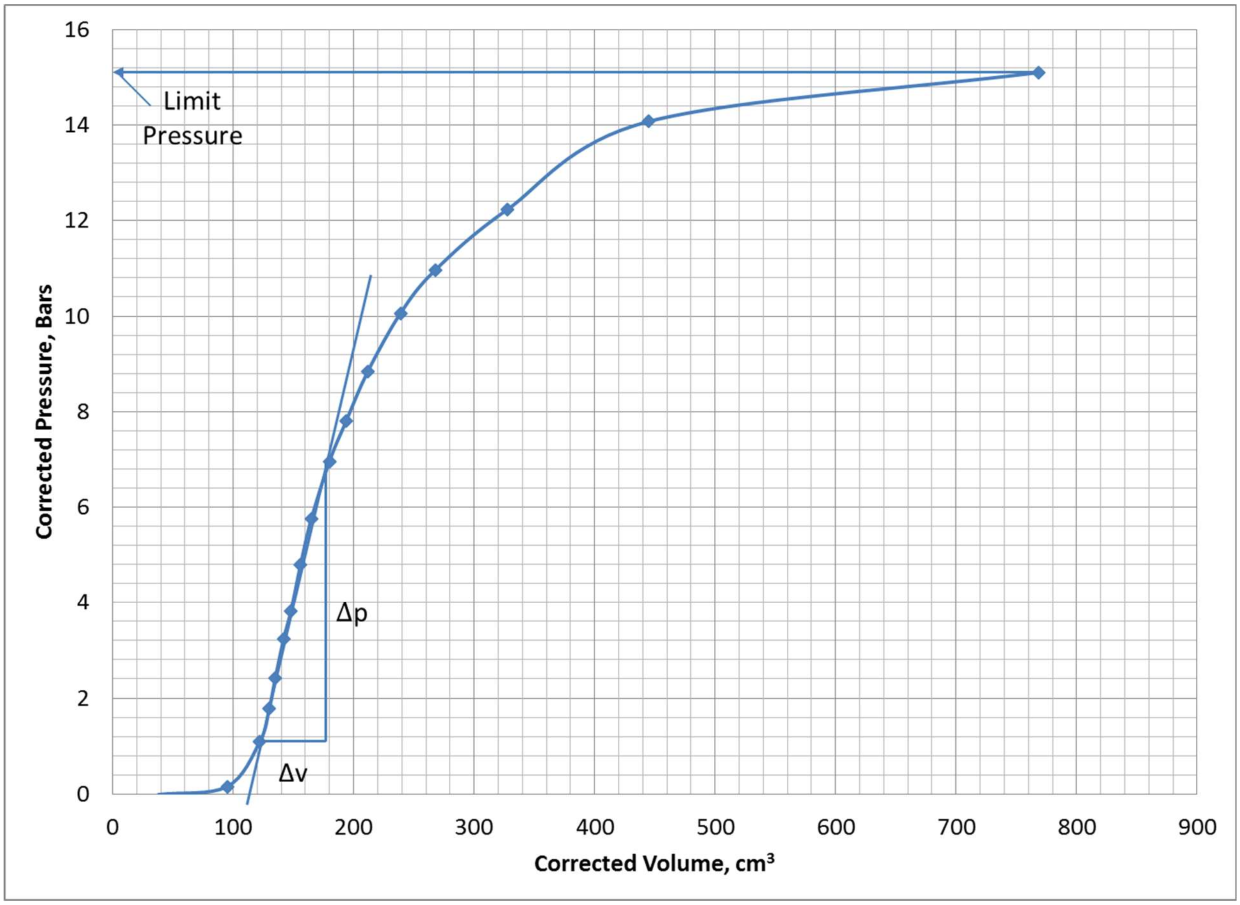

Figure 42: Sample pressuremeter data

iv. Behavior of Cohesionless Soil During Shear

As increasing shear force is applied to a cohesionless soil, a resulting shear stress is induced. According to Mohr-Coulomb failure theory, continual increase of the shear force will eventually induce a shear stress on a plane in the sample that is large enough to cause shear failure, assuming the normal stress on the plane is kept constant (Das 2006). While knowing the combinations of shear and normal stresses that can be applied to soil before it fails is important, changes in volume, stress-strain response, and pore pressure that occur during shear are also important to study.

1. Volumetric Changes and Stress-Strain Response

Factors that affect the shear strength of sands include void ratio, particle shape, grain size distribution, particle surface roughness, presence of water, intermediate principal stress, particle size, mineral type, and overconsolidation (Holtz and Kovacs 1981). The two factors that affect volumetric changes and the stress-strain response are void ratio and confining pressure (Holtz and Kovacs 1981).

Figure 43 shows theoretical stress-strain and volumetric response for both high void ratio soils and low void ratio soils subjected to direct shear. Figure 43 will be used to explain how soils are affected by void ratio, assuming a constant confining pressure for all cases. It should be noted that in this section examples refer to drained shear where excess pore pressures are not allowed to build. Excess pore pressures will be discussed in the next section. In terms of stress-strain response, the low void ratio sand initially has a higher modulus than the loose sand (high void ratio) and reaches a peak shear strength greater than the shear strength obtained by the higher void ratio sand. After the peak shear strength is reached, continual shear displacement reduces the shear stress until it reaches the ultimate shear strength. The loose sand gains strength continually and eventually stops gaining strength at its ultimate shear strength. Theoretically, the ultimate shear strength should be the same for both low and high void ratios, with all other factors held constant (Holtz and Kovacs 1981).

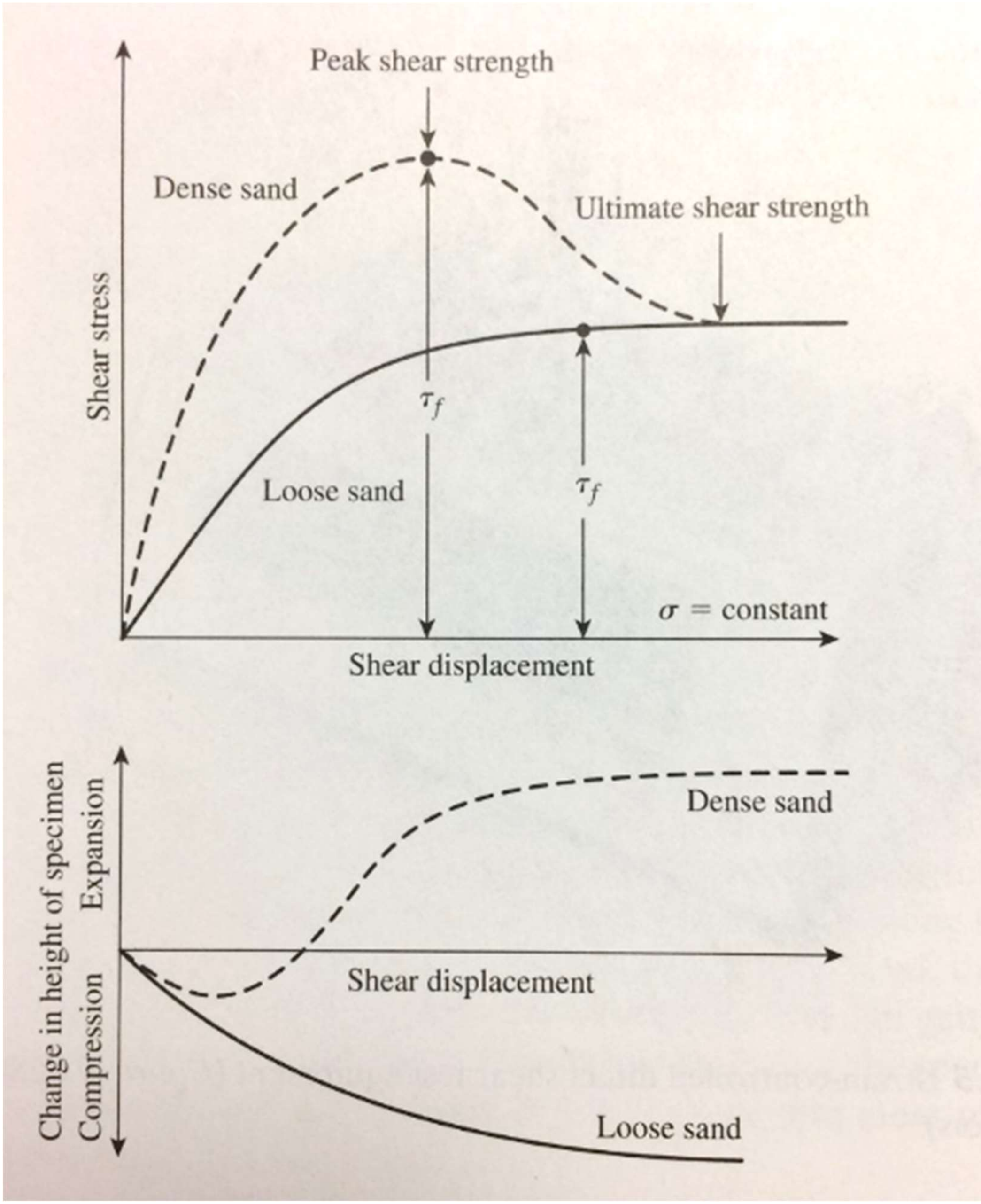

Figure 43: Theoretical plot of shear stress and change in height of specimen against shear displacement for loose (high void ratio) and dense (low void ratio) dry sand of a direct shear test (Das 2006)

The lower half of Figure 43 can be used to explain volumetric response of shearing soils with respect to void ratio. For the low void ratio test (dense sand), the particles are arranged densely. As particles roll past each other during shear, the configuration may briefly become a bit denser, resulting in a reduction in volume. With continued shear displacement, the densely configured particles rolling past each other open void spaces along the shearing plane. Additional void space causes the soil to dilate and results in an increase in volume. For the high void ratio specimen, the particles are loosely configured before shear and as shear occurs, the particles rearrange into a denser configuration resulting in a volume decrease (Das 2006).

Confining pressure also plays a role in the stress-strain and volumetric responses of sheared soils. Figure 43 had a constant confining pressure for both the low void ratio and high void ratio direct shear tests. However, changing the confining pressure has a noticeable effect on the behavior of soils during shear. As confining pressure increases, shear strength increases as long as all other factors are held constant (Holtz and Kovacs 1981). To examine the effects of confining pressure, Holtz and Kovacs suggest preparing several samples at the same void ratio and testing them in triaxial shear at varying confining pressures (1981). The first set of tests was performed with samples of relatively high void ratio (loose) and the second set was performed with samples of relatively low void ratio (dense). In Figure 44 (b), volumetric strain vs. axial strain is plotted for tests performed at different confining pressures for relatively loose samples. In most cases, loose samples usually compress when sheared, resulting in a volume reduction. However, when the confining pressure is low enough, even loose samples can dilate, resulting in a volume increase (Holtz and Kovacs 1981). In Figure 45 (b), volumetric strain vs. axial strain is plotted for tests performed at different confining pressures for relatively dense samples. In most cases, dense samples usually dilate when sheared, resulting in a volume increase. However, when the confining pressure is high enough, even dense samples can compress, resulting in a volume decrease (Holtz and Kovacs 1981).

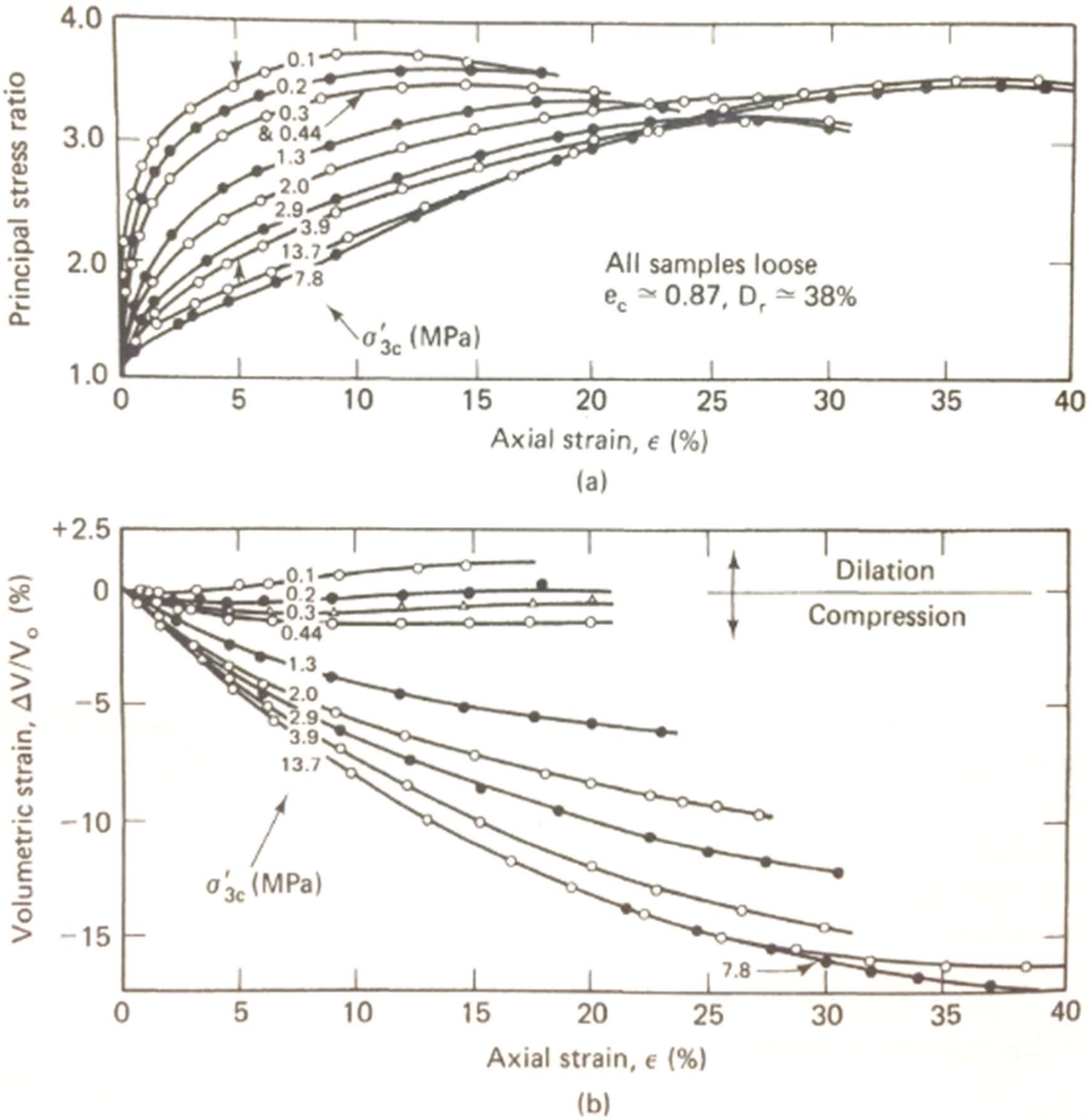

Figure 44: All samples were prepared at the same, loose, relative density and tested at various confining pressures (a) principal stress ratio vs. axial strain (b) volumetric strain vs. axial strain (Lee 1965)

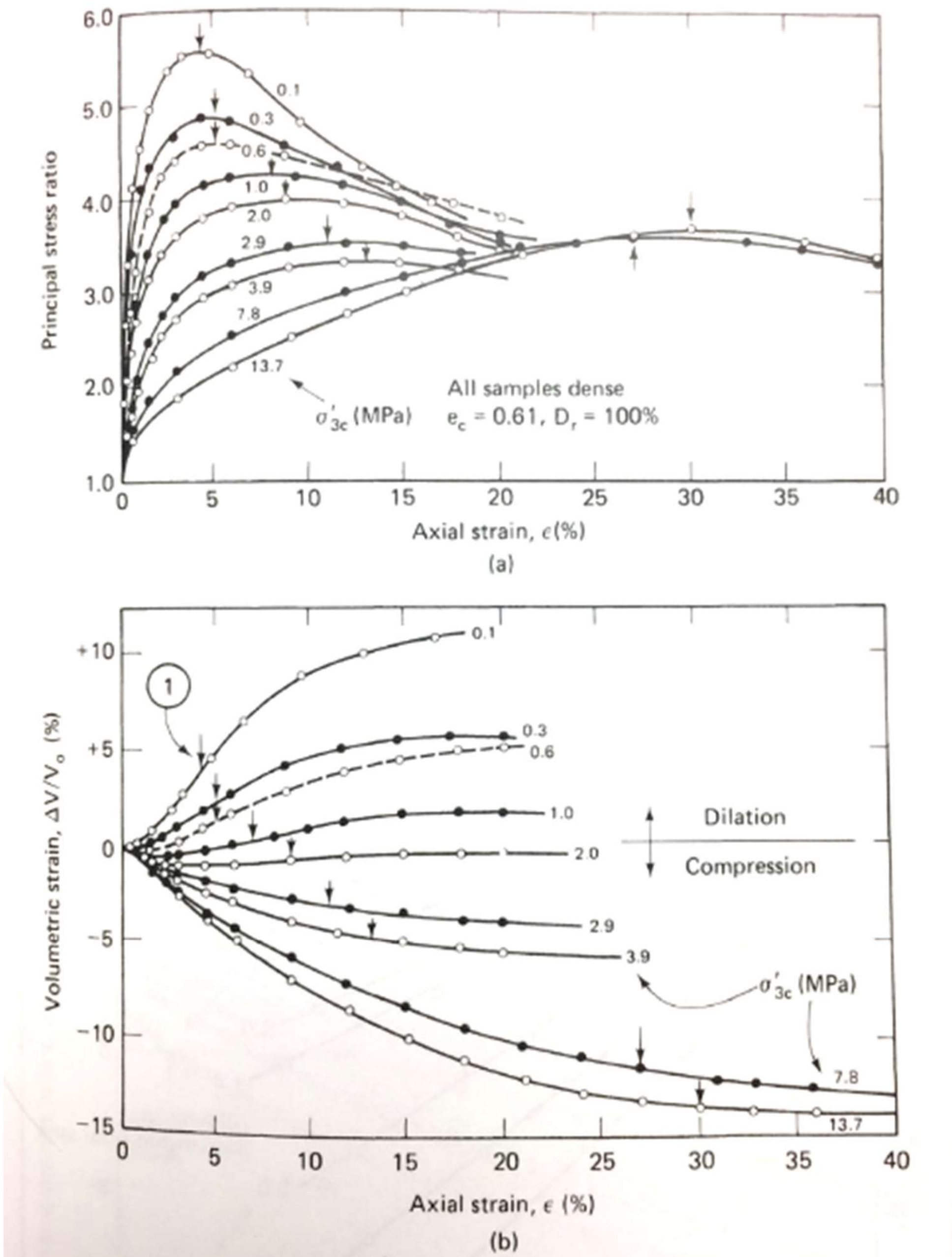

Figure 45: All samples were prepared at the same, dense, relative density and tested at various confining pressures (a) principal stress ratio vs. axial strain (b) volumetric strain vs. axial strain (Lee 1965)

For drained triaxial tests, failure is defined as either the maximum (σ_1-σ_3) or the maximum σ_1/ σ_3. For drained tests, these are equal (Holtz and Kovacs 1981). Plotting the volumetric strain at failure vs the void ratio at the end of consolidation yields Figure 46. It is evident from Figure 46 that for a given confining pressure, the volumetric strain increases with increasing density (Holtz and Kovacs 1981). The critical void ratio is the void ratio at failure when the volumetric strain is zero (Holtz and Kovacs 1981). Figure 46 also shows how the critical void ratio increases with decreasing confining pressure (Holtz and Kovacs 1981).

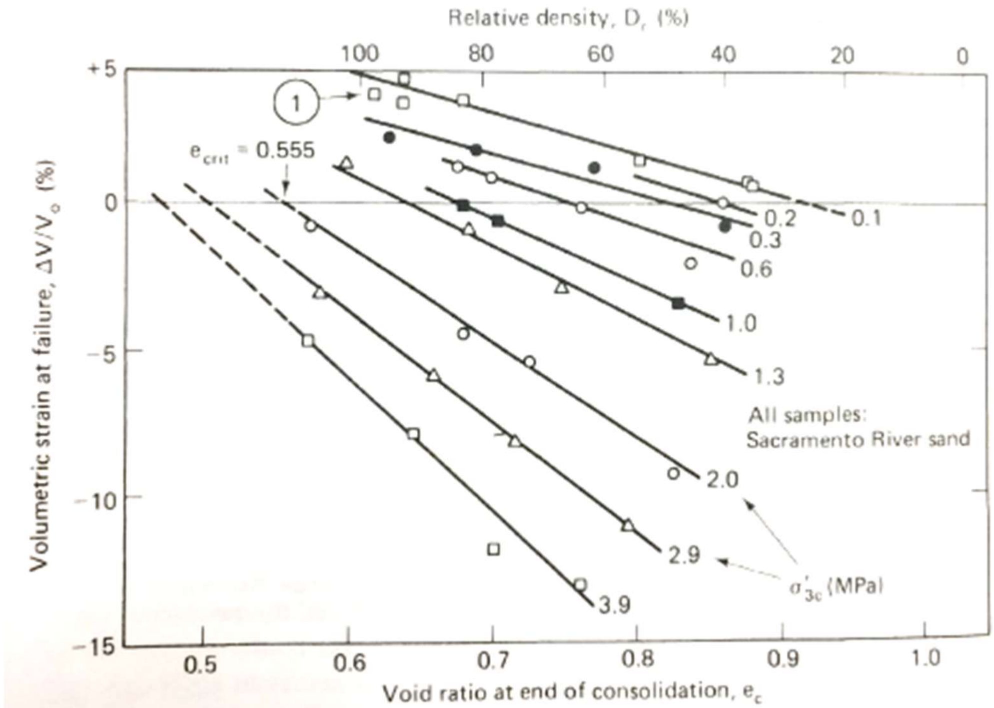

Figure 46: Volumetric strain at failure vs. void ratio at end of consolidation at various confining pressures (Lee 1965)

2. Pore Pressure Response

While drained tests exhibit volume change during shear, undrained tests are not allowed to change volume and either positive or negative pore pressures are induced unless the sample is at the critical void ratio and no pore pressure is induced (Holtz and Kovacs 1981). The concepts discussed above for drained tests apply to undrained tests in this manner: If a drained sample tends to dilate, a negative pore pressure response would tend to occur in a similar undrained sample and if a drained sample tends to compress, a positive pore pressure response would tend to occur in a similar undrained sample (Holtz and Kovacs 1981). Similarly, if the sample is at the critical void ratio and no tendency towards volume change occurs, no pore pressure change will be induced (Holtz and Kovacs 1981). Introducing changes in pore pressure results in changes in effective stress as shown in Equation 15.

$$\boldsymbol{\sigma' = \sigma - u} \qquad \text{(Eq. 15) (Terzaghi 1925)}$$

Where: σ' is the effective stress
σ is the total stress
u is the pore pressure

c. Lateral Earth Pressure Theory

i. Overview

Lateral earth pressure is exerted by soil, water, or both in the horizontal direction. The magnitude of this lateral earth pressure is dependent on the presence of water, and the strength and stress-strain properties of the soil as well as the deformations that result from lateral movement (McCarthy 2007). The most common way to evaluate lateral earth pressure is to determine the vertical pressure at a point and multiply this vertical pressure by a constant, K_{LEP}, which represents the ratio of effective lateral earth pressure to effective vertical earth pressure. This K_{LEP} value is dependent upon soil properties and lateral deformations of the soil. The effect of lateral deformation will be described in succeeding sections. The three types of lateral earth pressure are at-rest, active, and passive. The vertical earth pressure at a depth, z, is easily calculated using Equation 16. However, the effective vertical earth pressure is usually of greater concern, and may be calculated using Equation 17.

$$\boldsymbol{\sigma_{vertical} = \gamma_{soil} Z} \quad \text{(Eq. 16)}$$

$$\boldsymbol{\sigma'_{vertical} = \gamma_{soil} Z - \gamma_w Z_w} \quad \text{(Eq. 17)}$$

Where: $\sigma_{vertical}$ is the total vertical stress at a point at depth Z
$\sigma'_{vertical}$ is the effective vertical stress at a point at depth Z
γ_{soil} is the unit weight of soil
γ_w is the unit weight of water
Z is the depth to the point of interest
Z_w is the height of water above the point of interest

With the total and effective vertical pressures calculated, the total and effective lateral earth pressures can be simply calculated using Equations 18 and 19, respectively. It should be noted that for a given soil deposit, K can change due to a changing water table and is not constant. However, K_{LEP} is a coefficient of lateral earth pressure and is constant for a given soil mass because it expresses lateral earth pressure in terms of effective stresses (Holtz and Kovacs 1981).

$$\boldsymbol{\sigma_{horizontal} = K\sigma_{vertical}} \quad \text{(Eq. 18) (Holtz and Kovacs 1981)}$$

$$\boldsymbol{\sigma'_{horizontal} = K_{LEP}\sigma'_{vertical}} \quad \text{(Eq. 19) (Holtz and Kovacs 1981)}$$

Where: $\sigma_{horizontal}$ is the total lateral earth pressure
$\sigma_{vertical}$ is the total vertical stress at the depth in question
$\sigma'_{horizontal}$ is the effective lateral earth pressure at the depth in question
$\sigma'_{vertical}$ is the effective vertical lateral earth pressure at the depth in question
K is an earth pressure coefficient
K_{LEP} is the coefficient of lateral earth pressure

The lateral earth pressure coefficient can be calculated using Equation 20.

$$\boldsymbol{K_{LEP} = \frac{\sigma'_h}{\sigma'_v}} \quad \text{(Eq. 20) (McCarthy 2007)}$$

Where: K_{LEP} is the coefficient of lateral earth pressure
σ'_h is the effective lateral earth pressure
σ'_v is the effective vertical stress

ii. At-rest Lateral Earth Pressure Condition

The coefficient of lateral earth pressure at-rest, K_0, is the ratio of effective lateral earth pressure to effective vertical stress for the condition where no lateral soil deformation occurs. The at-rest earth lateral earth pressure condition may be used to determine the earth pressure on a rigid buried pipe for example, as the lateral deformation is negligible. Values for K_0 range from 0.4 to greater than 3.0 depending on the stress history of the soil deposit (Holtz and Kovacs 1981). Typically, K_0 is between 0.5 and 1.0. Figure 47 shows the stress state of soil in the at-rest stress condition. Notice that the semicircle representing the stress state does not contact the Mohr-Coulomb failure envelope. Contact with the Mohr-Coulomb failure envelope indicates shear failure, but because no lateral deformation occurs in the at-rest condition, shear failure cannot not occur.

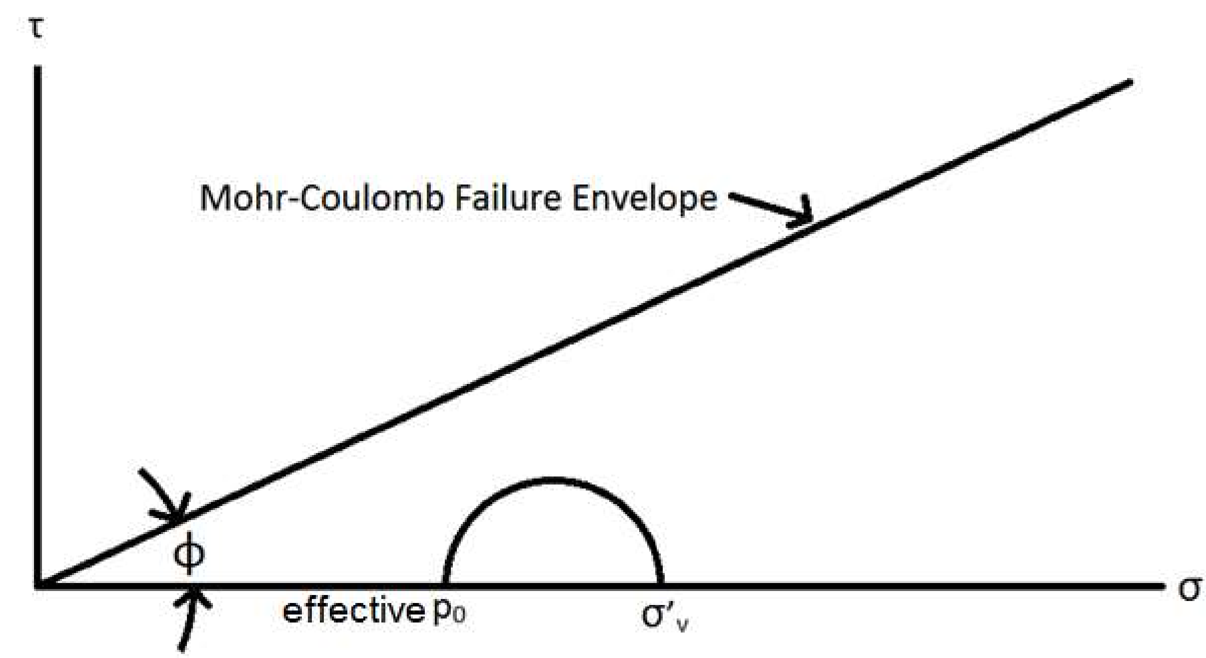

Figure 47: Stress state of soil in the at-rest condition

iii. Active Lateral Earth Pressure Condition

The active condition exists in soil deposits where lateral expansion occurs. The lateral expansion mobilizes shearing resistance in the soil mass which acts opposite of the direction of lateral expansion. The active lateral earth pressure condition may be used to determine the soil pressure being exerted on retaining wall by the retained fill. As the shearing resistance develops, lateral pressures in the direction of the lateral expansion are reduced. Figure 48 shows this phenomenon. The effective vertical stress does not change from Figure 47 to Figure 48. However, as the soil expands laterally the lateral earth pressure (p_a) decreases. If enough lateral expansion occurs shear failure occurs and is indicated by the Mohr's circle for the active condition touching the Mohr-Coulomb failure envelope making it a failure condition. Also note that as the lateral earth pressure decreases, the ratio of p_a to σ'_v also decreases when compared to the at-rest condition. Thus, for a given soil deposit K_a is always less than K_0.

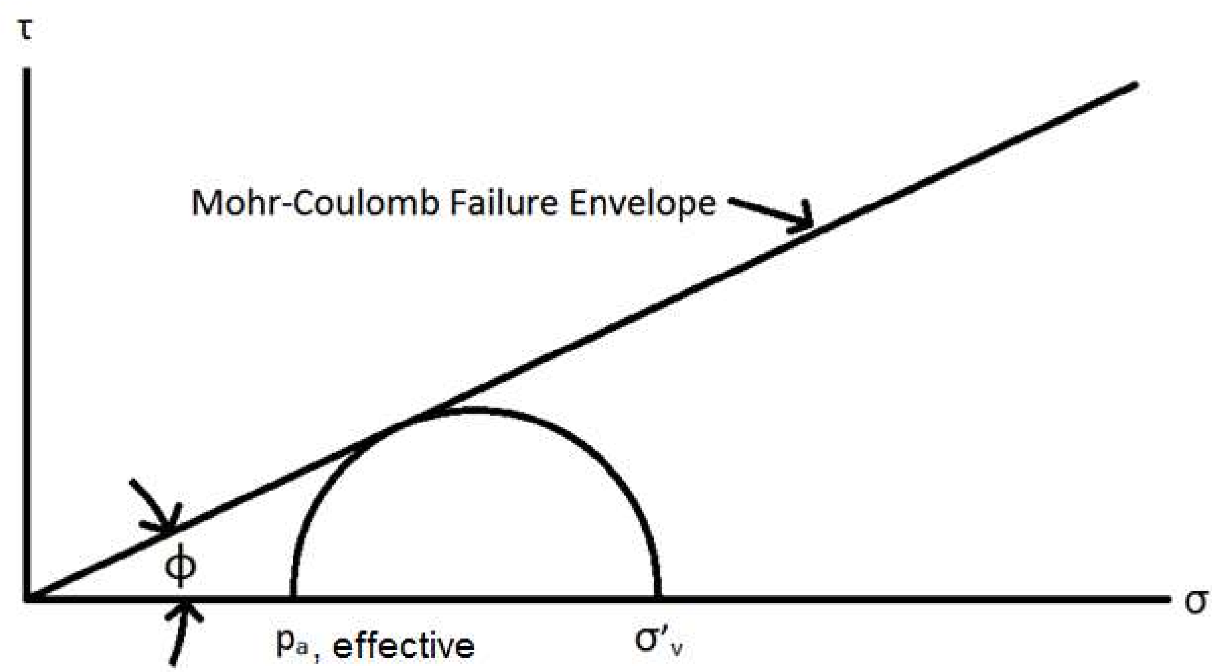

Figure 48: Stress state of soil in the active condition

iv. Passive Lateral Earth Pressure Condition

The passive condition occurs in soil deposits where lateral contraction occurs. The lateral contraction mobilizes shearing resistance in the soil mass which acts opposite of the direction of lateral contraction. The passive lateral earth pressure condition may be used to determine the pressure exerted on a soil mass by an adjacent bridge deck of a GRS-IBS as it undergoes thermal expansion. As the shearing resistance develops, lateral pressures in the direction of the lateral contraction are increased. Figure 49 shows this phenomenon. The effective stress remains the same as in Figure 47. However, as the soil is allowed to contract laterally, the lateral earth pressure (p_p) increases. As with the active condition, a large enough shearing of the soil in the passive condition leads to a failure state as evidenced by the passive state of stress Mohr's circle contacting the Mohr-Coulomb failure envelope. Also note that as p_p increases, the ratio of p_p to σ'_v becomes much larger than the ratio of the ratio of p_a to σ'_v and consequently larger than the ratio of p_o to σ'_v. Thus, for a given soil deposit, K_p is always larger than K_a, which is smaller than K_0.

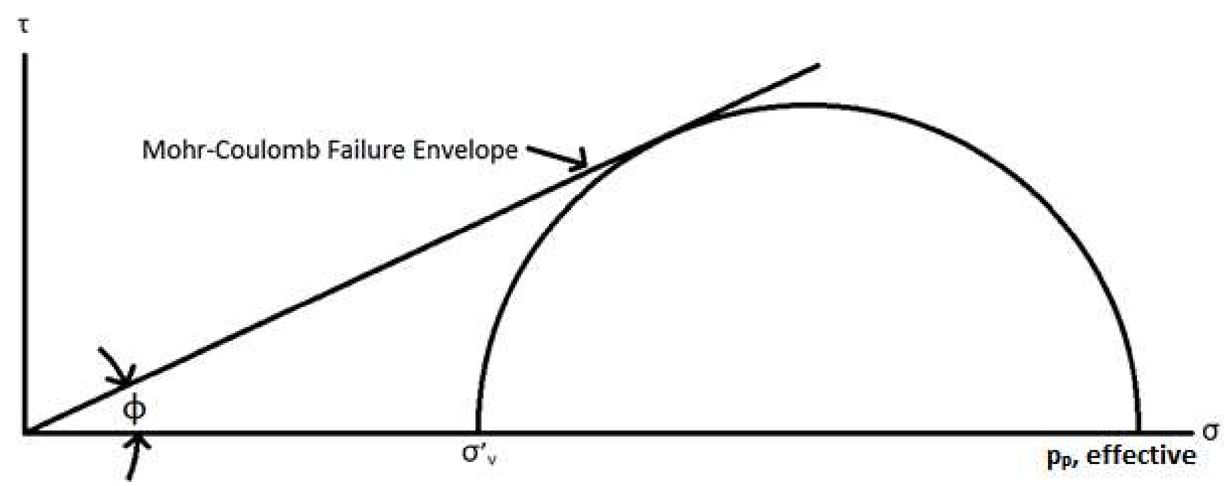

Figure 49: Stress state of soil in the passive condition

d. Research Related to the Passive Resistance of Mechanically Stabilized Earth Structures

While limited, some research related to the performance of mechanically stabilized earth structures subjected to passive forces exists.

Some finite-element analysis has been performed regarding the soil-structure interaction of integral-abutment bridges (IABs) (Horvath 2000). Horvath used two dimensional finite element analysis to model lateral earth pressure variations due to temperature change for three different design scenarios, including soil that has been reinforced with MSE behind a rigid abutment. Horvath's research included a non-reinforced backfill as well as one polymeric sheet and one steel strip reinforcement geometry. The facing was a one-piece concrete wall. The passive load was induced at the top of the wall, causing it to rotate into the reinforced fill. As expected with mechanically stabilized soil, Horvath found that reinforcement caused a reduction in lateral earth pressure (Figure 50).

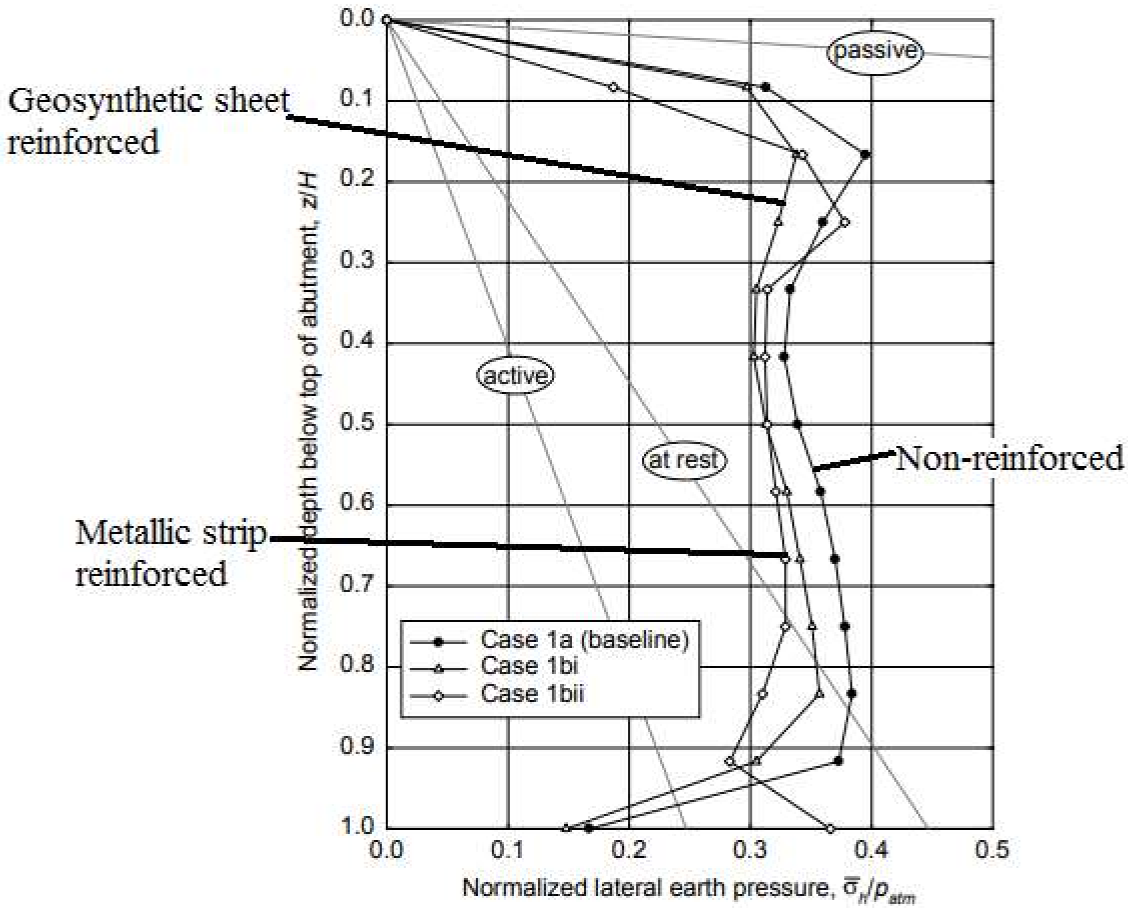

Figure 50: Plot of normalized depth below top of abutment vs. normalized lateral earth pressure for two reinforced structure types and one non-reinforced earth structure (Horvath 2000)

While Horvath induced passive loading on the structure, he did not provide enough displacement to mobilize passive shear failure in the soil, as the current research does. Horvath used a two dimensional finite element model which limited his research solely to reinforcement length and spacing geometry considerations. Additionally, Horvath's research did not involve laboratory testing and modeling, as is performed in the current research.

Field study research has been performed to determine the pressure exerted on geosynthetic reinforced backfill placed behind an integrated abutment (Abu-Hejleh 2006). This research used three pressure cells to determine the pressure exerted by the thermally expanding bridge deck on the geosynthetic reinforced backfill. In addition to the pressure cells, strain gauges were attached to one of the geogrids to measure tensile strain response. The design used polystyrene foam board as a compressible inclusion between the geosynthetic reinforced backfill and the concrete bridge seat in an attempt to decrease the passive pressure exerted on the backfill. Abu-Hejleh found that lateral earth pressure varied seasonally, due to thermal expansion and contraction (Figure 51).

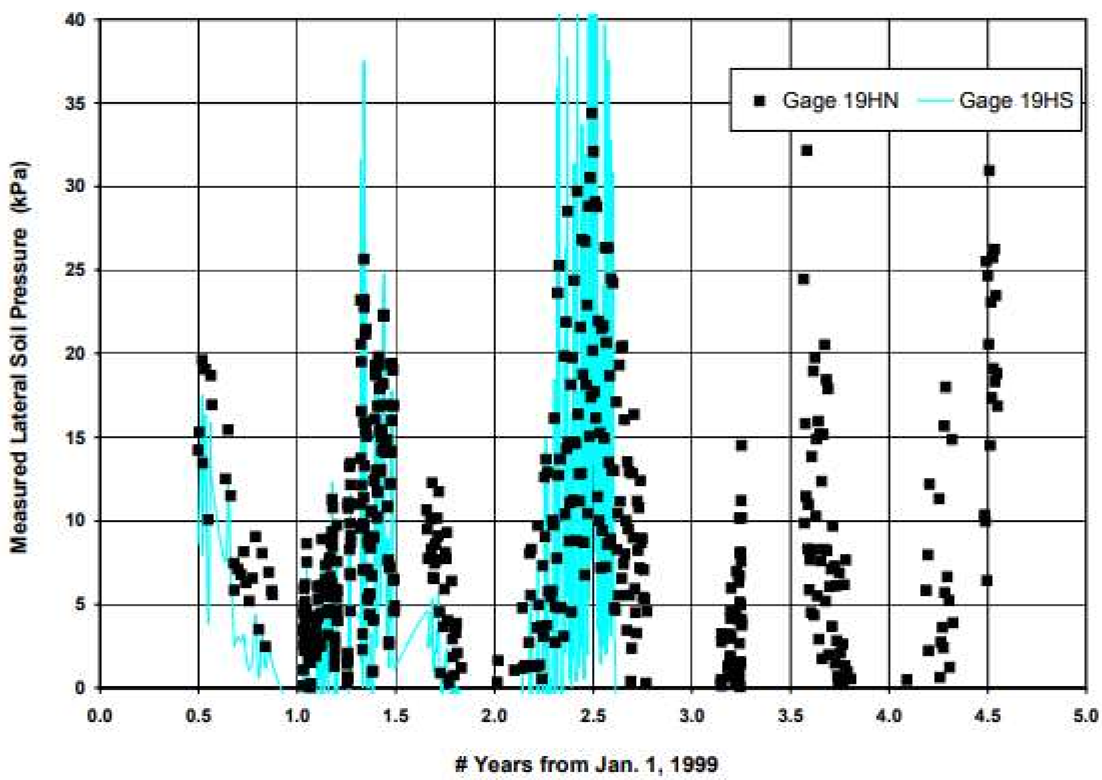

Figure 51: Measured lateral earth pressure against the top portion of the abutment wall (Abu-Hejleh 2006)

Strain gauge measurements indicated that strains in the geotextiles also varied seasonally, likely due to changes in the pressure exerted by the bridge deck. However, as shown in Figure

52, the geogrid is always in tension, indicating that the thermal expansion of the bridge deck did not provide enough displacement to fully mobilize the passive resistance of the reinforced backfill.

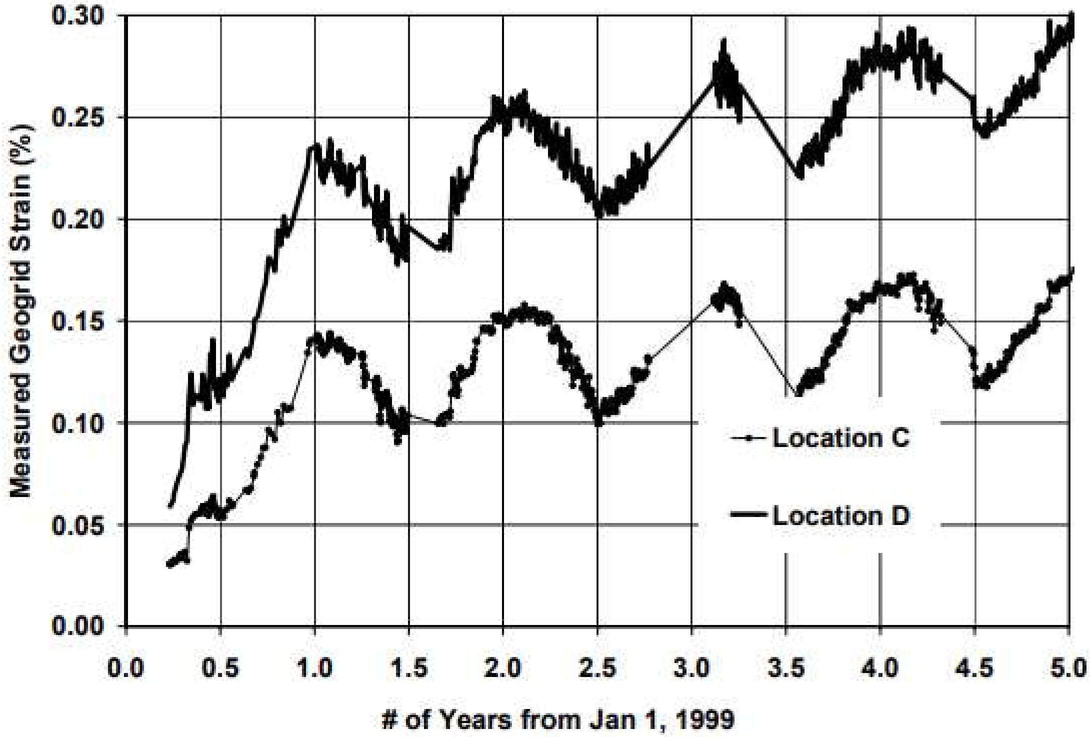

Figure 52: Measured geogrid tensile strains at various times from gages placed in the MSE abutment backfill (Abu-Hejleh 2006)

While the pressure exerted on the reinforced soil is measured, there is no measurement of pressure exerted on a non-reinforced soil for comparison. The current research generated information on both non-reinforced and reinforced model structures tested to failure.

Chapter III: Research Methodology

The research consists of a laboratory study to determine soil parameters, then testing models with varying reinforcement geometry in passive resistance. During testing, force and displacement are recorded and the location of the failure surface is determined. Additionally, a finite difference model is created using FLAC3D™ software to model the passive resistance tests performed in the laboratory, with the intention of predicting the results of other laboratory tests.

a. Laboratory Study

i. Description of Testing Apparatus

1. Overview

The benchtop testing apparatus consists of an open top rectangular wooden box, two steel channels, an aluminum pusher plate, polypropylene fibers, a soil placement device, an acrylic sheet with 1” grid, a plate compactor, a rod and bushing assembly with universal joint, a GeoJac load actuator, a 500 lb. load cell, and a laptop computer with GeoJac software. A plan view of the testing apparatus is shown in Figure 69.

2. Rectangular Wooden Box

The rectangular wooden box was constructed of pine lumber with cross sectional dimensions of 1.5” x 3.5”, a sheet of 0.5” thick pine plywood, and 3” long deck screws. The box was constructed by stacking six layers of 1.5” x 3.5” lumber with the short dimension vertical in an overlapping corner joint pattern and affixing each layer to the layer below with 3” deck screws. The overlapping corner joint pattern is shown in Figure 53. The internal box dimensions are 19.75” long x 20” wide x 9” high.

Figure 53: Overlapping corner joint pattern of the box

3. Aluminum Pusher Plate

The solid aluminum pusher plate has dimensions of 1” thick x 5.5” wide x 5.0” tall. The rear face of the pusher plate is drilled and tapped to receive a flange connection shown in Figure 54.

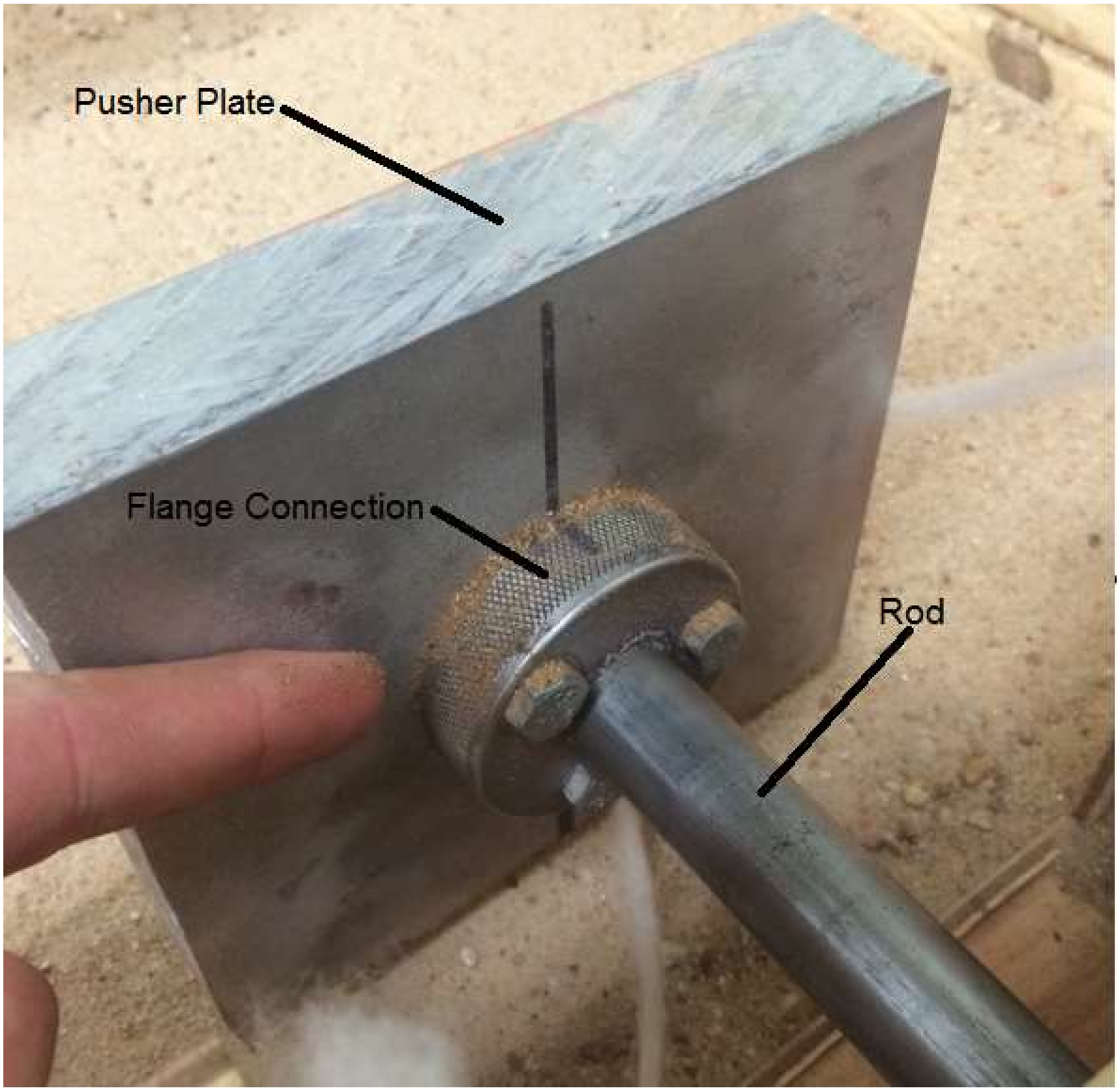

Figure 54: Drilled and tapped flange connection on the backside of the pusher plate between the rod and pusher plate

4. Rod and Bushing Assembly with Universal Joint

The rod and bushing assembly consists of the top cap and rod from a triaxial test. The design of the bushing allows the rod to move only along its long axis, through the bushing with minimal frictional losses. The triaxial top cap, bushing, and rod are shown in Figure 55.

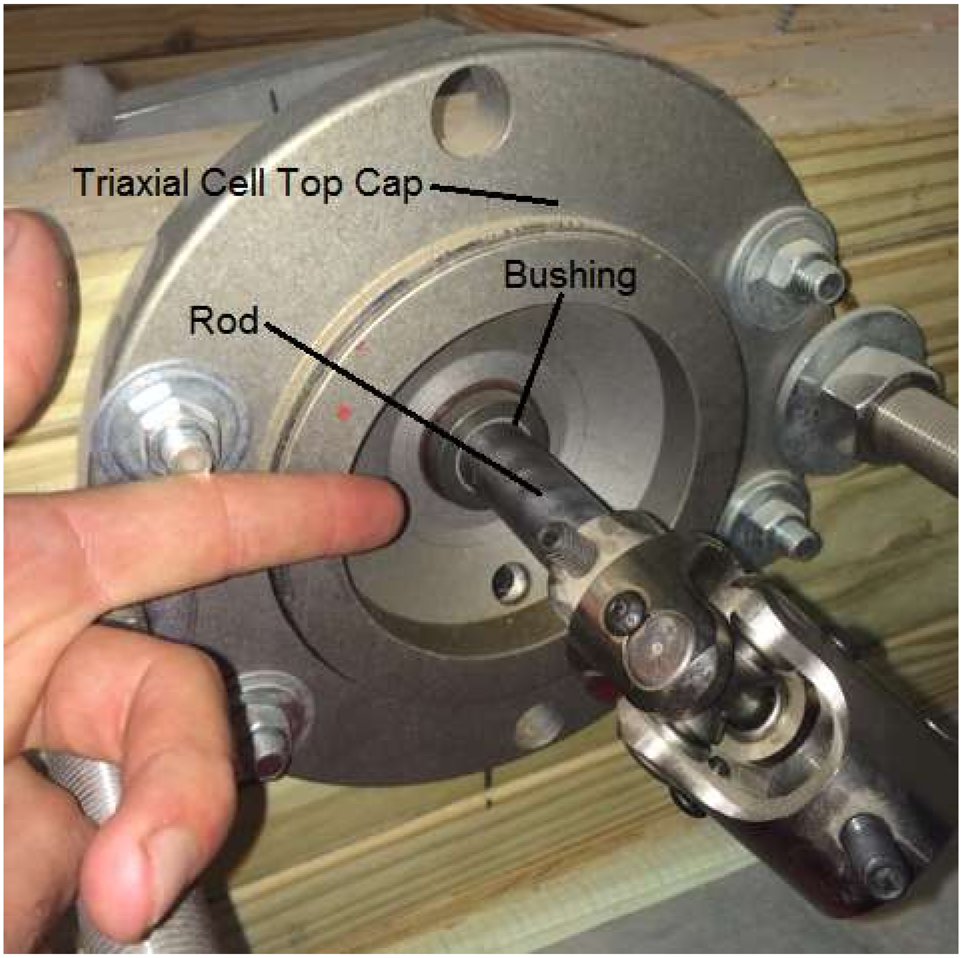

Figure 55: Triaxial cell top cap, bushing, and rod

A universal joint was installed at the end of the rod opposite the pusher plate to provide a connection to the GeoJac actuator. The universal joint allows bending in any direction to mitigate binding in the bushing, but does not allow rotation which ensures the plate does not rotate during testing. The universal joint is shown in Figure 56.

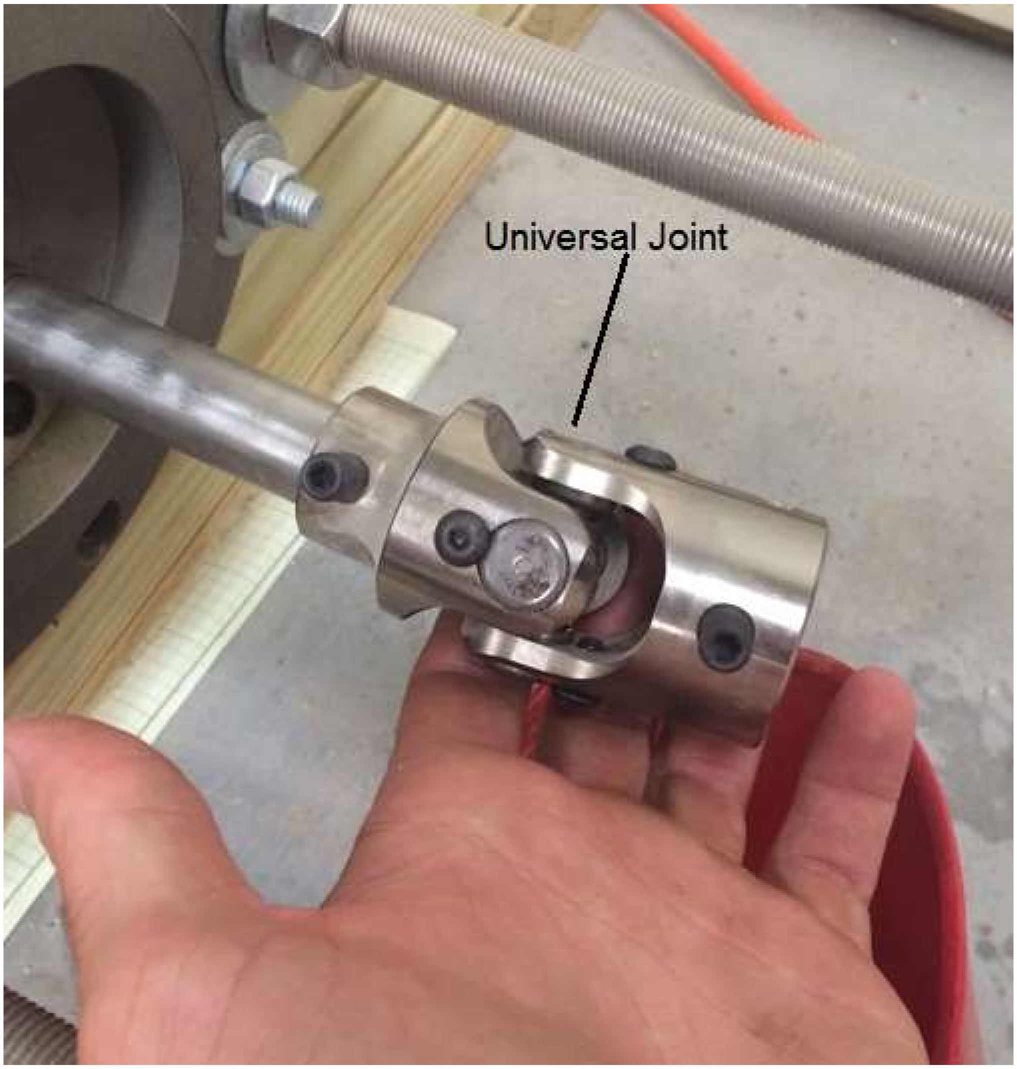

Figure 56: Universal joint connection

5. Plate Compactor

A compaction device was necessary to compact the soil to the appropriate density. A simple vibrating plate compactor was designed using a sheet of ¾" plywood, a 120 volt alternating current electric motor, and an asymmetric weight attached to the output shaft of the motor. When energized, motor spins the asymmetric weight causing the entire plate compactor to vibrate in a vertical plane. The plate compactor is shown in Figure 57.

Figure 57: The plate compactor atop a lift of soil, inside the testing box

6. Soil Placement Apparatus

The soil was placed in the test apparatus in lifts. To provide consistent lift thicknesses that are planar and horizontal, a scraper type soil placement apparatus was designed. Figure 58 shows an overview of the soil placement apparatus.

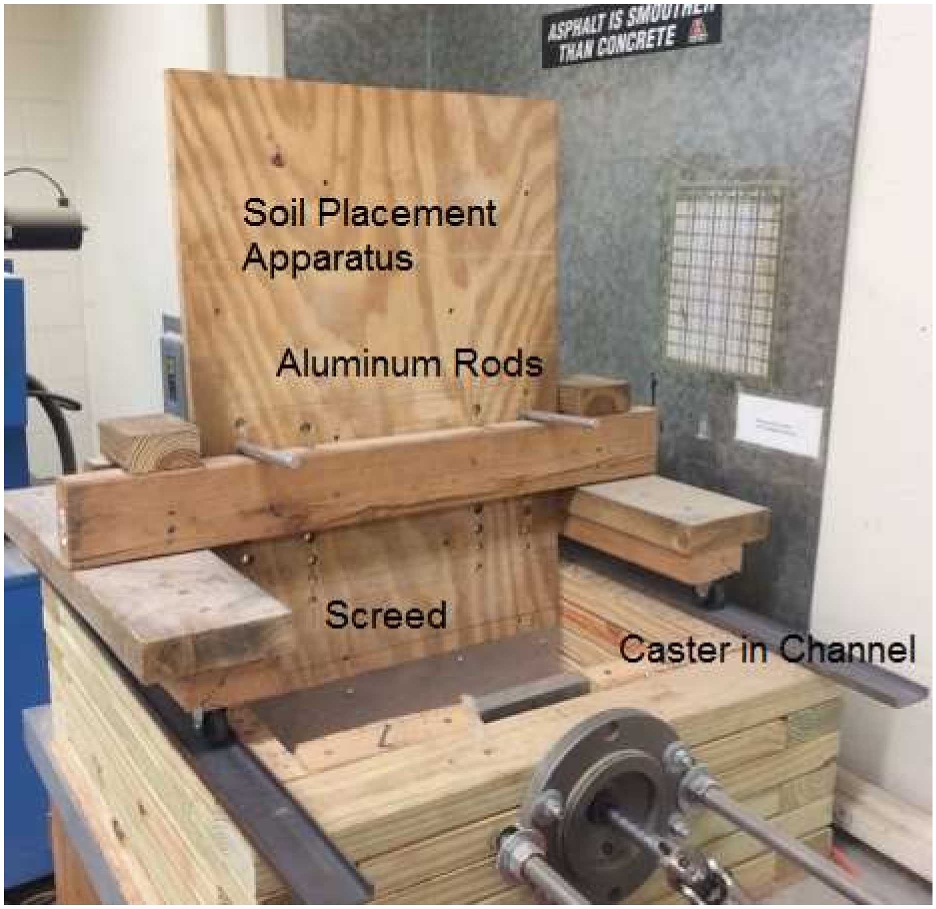

Figure 58: Soil placement apparatus

Using an extremely accurate woodworking jig and drill press, a series of holes on exact half inch spacing were drilled into a plywood plate. The holes accept ½" diameter aluminum rods, shown in Figure 59.

Figure 59: Aluminum rod fitted into a hole drilled in the plywood plate

The plywood plate was fitted vertically between two pieces of 2x4 (actual dimensions: 1.5”x3.5”) lumber. The aluminum rods do not allow the plate to move downward between the 2x4 lumber, providing precise height adjustment of the plate in ½” increments. Four casters attached to the 2x4 lumber ride in steel channels that are affixed to the top of the box and allow the plate to be moved horizontally along the soil surface. Figure 60 shows a caster in the steel channel.

Figure 60: Caster in steel channel

To ensure that the edge of the plate that contacts the soil is perfectly straight, an aluminum screed was screwed to the bottom of the plate, shown in Figure 61.

Figure 61: Aluminum straight edge affixed to the bottom of the plate

With this setup, the rods can be moved incrementally to the next vertical hole, changing the height of the aluminum plate that contacts the soil, in precise half inch increments. The entire apparatus is allowed to move horizontally along the steel channel which enables the aluminum straight edge to scrape the soil to a consistent lift thickness.

7. Instrumentation

One test per reinforcement geometry is instrumented using horizontal layers of paint to determine the approximate failure surface.

To determine the location of the failure surface, a thin layer of spray paint is applied atop certain compacted soil lifts. Soil layers are placed at precise half inch thicknesses using the soil placement apparatus shown in Figure 58. Every second horizontal layer beginning at the base of the pusher plate is painted (1” vertical spacing), as shown in Figure 62.

Figure 62: Painted horizontal soil layer

When the test is performed, the pusher plate is forced into the soil specimen. Some of the soil in the box does not move, while other soil moves in the direction of the plate and also upwards. The upward deformation of failed soil carries the planar horizontal paint layer upwards as well. After the test is performed, the soil is removed in layers, gently scraped off using the same soil placement device shown in Figure 63.

Figure 63: Soil placement device scraping away soil and paint that moved during a test

The soil and paint that moved upwards is scraped off, leaving the soil and paint that did not move behind, shown in Figure 64. The areas where paint was scraped away indicate that soil moved upwards. A piece of clear plexiglass with a grid of 1” squares is placed atop the scraped soil and paint and the horizontal coordinates of the outline of the soil layer that moved upwards is recorded, allowing three dimensional coordinates of the failure surface to be obtained. See Figure 65.

Figure 64: Scraped soil layer revealing failure location

Figure 65: Plexiglass with grid atop scraped soil and paint layer

8. GeoJac System

A GeoJac digital load actuator was used in conjunction with a 500 lb. load cell, GeoTAC's Sigma-1 software, and GeoTAC's Test Net data acquisition system. The GeoJac digital load actuator uses a ball screw jack piston that is controlled by a digital servo control motor to provide displacement to specimens. Integral to the GeoJac is a precision optical encoder that ultimately provides displacement data. The Sigma-1 software provides instruction to the digital servo control motor to control displacement for a variety of tests. The TestNet data acquisition system records output from the 500 lb. load cell and the precision encoder to provide load and displacement data, respectively. The collective system loads specimens and obtains load and displacement data.

ii. Development of Benchtop Test

1. Apparatus Shape

The plan view of the benchtop testing box in the initial research proposal is shown in Figure 66. The initial plan view consisted of a trapezoidal shaped box with wingwalls at a specified, but undetermined angle. Initially this was considered in an effort to use less soil per test. Due to the relatively small amount of soil needed per test and because the same soil was used for every test, soil usage was not an issue.

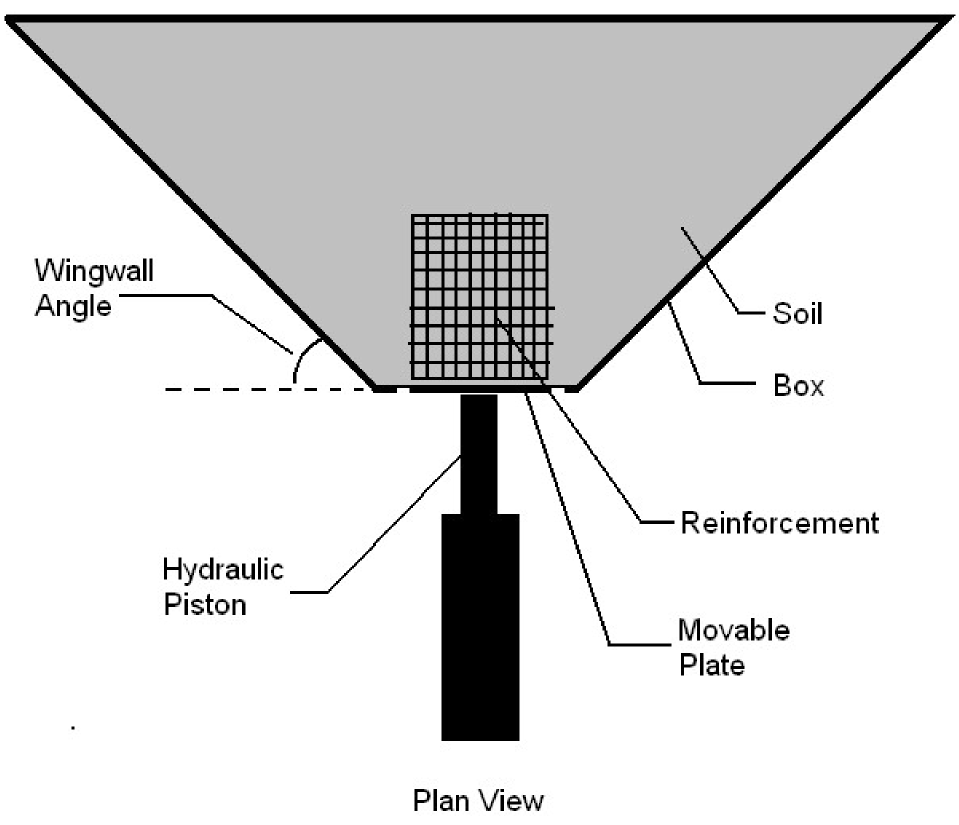

Figure 66: Plan view of passive resistance testing box from initial proposal

The expected shape of the passive failure surface at the soil's surface is round, terminating at the edges of the movable plate (Figure 67). This expected failure surface is somewhat similar to the Boussinesq distribution (0.02P line) for square footings shown in Figure 68. The lines on the Boussinesq distribution represent isobars of estimated stress associated with a load (P) applied to certain footing geometries. Figure 67 shows such a failure surface drawn on the initially proposed plan view of the testing box. As shown in Figure 67, the expected failure surface may come into contact or come very close to contacting the sidewalls of the box. To eliminate variability due to wingwall orientation, a rectangular plan view section was selected for testing to focus solely on variables related to reinforcement geometry. A depiction of the plan view of the test box used for this research is shown in Figure 69.

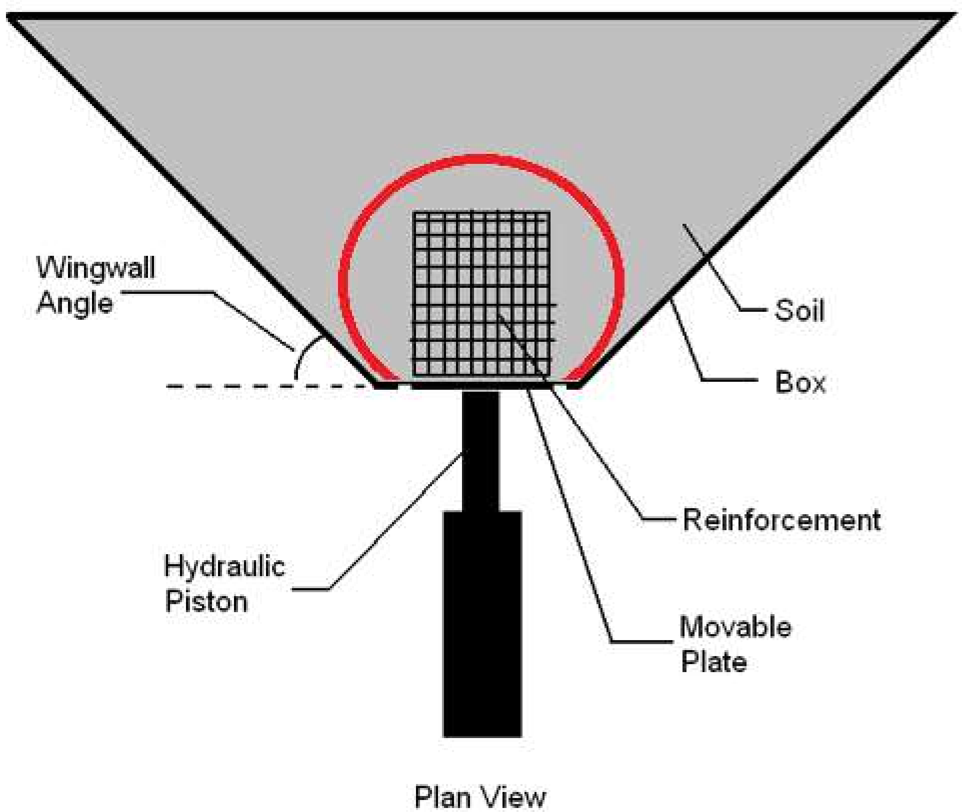

Figure 67: Plan view of passive resistance testing box from initial proposal with expected failure surface drawn in red

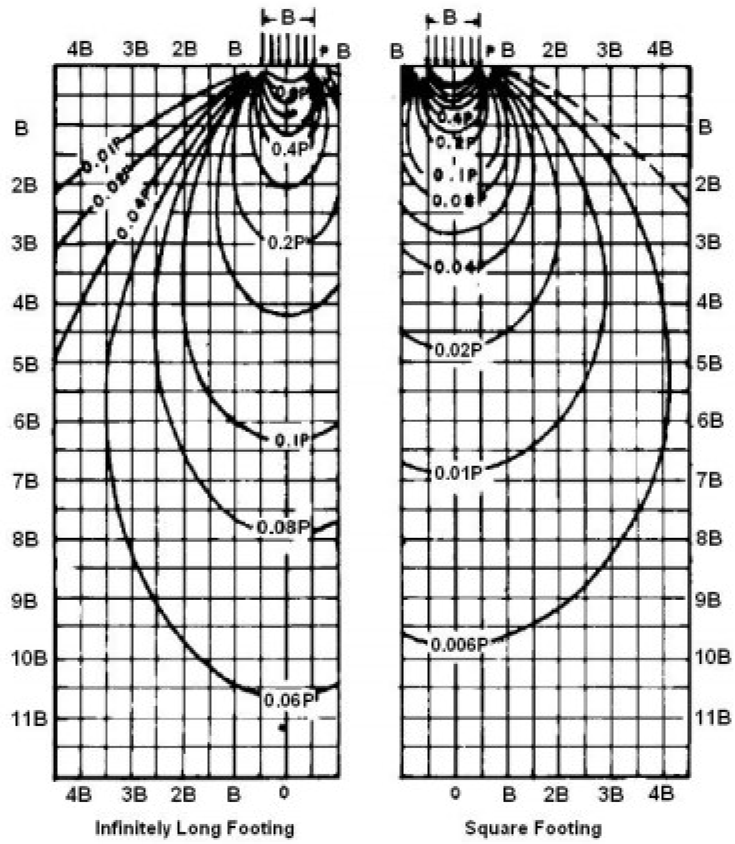

Figure 68: Boussinesq stress contours under infinitely long and square footings (NAVFAC 1986)

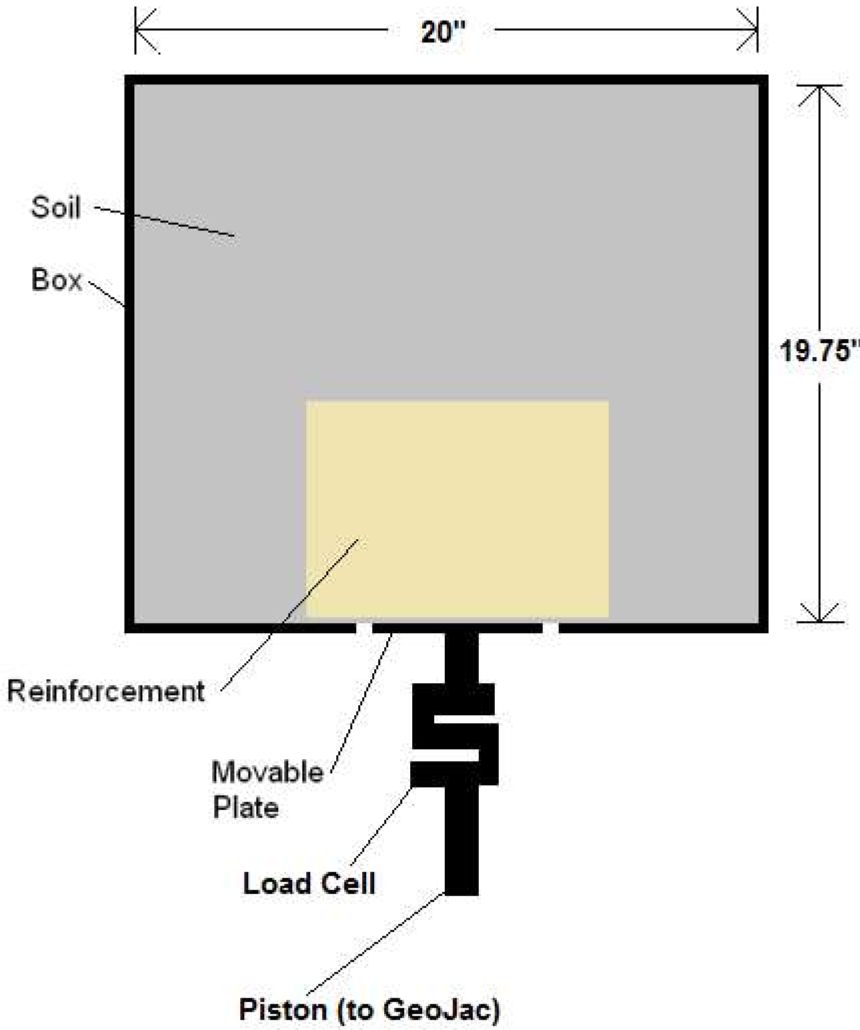

Figure 69: Plan view of current passive resistance testing box

2. Apparatus Size

The main concern with sizing the apparatus was the proximity of the failure surface to the sides and bottom of the box and the ensuing influence that this would have on the test results. To estimate the distance from the top of the pusher plate to the intersection of the rupture plane and the soil surface (Figure 70, Distance Y), the theoretical Rankine rupture plane shown in Figure 70 was used. Using an estimated angle of internal friction of 35º for sand, the distance from the top of the pusher plate to the intersection of the rupture plane and the soil surface is 9.6 inches.

It should also be noted that the actual rupture plane is a curved surface that extends somewhat below the theoretical rupture plane depicted in Figure 70.

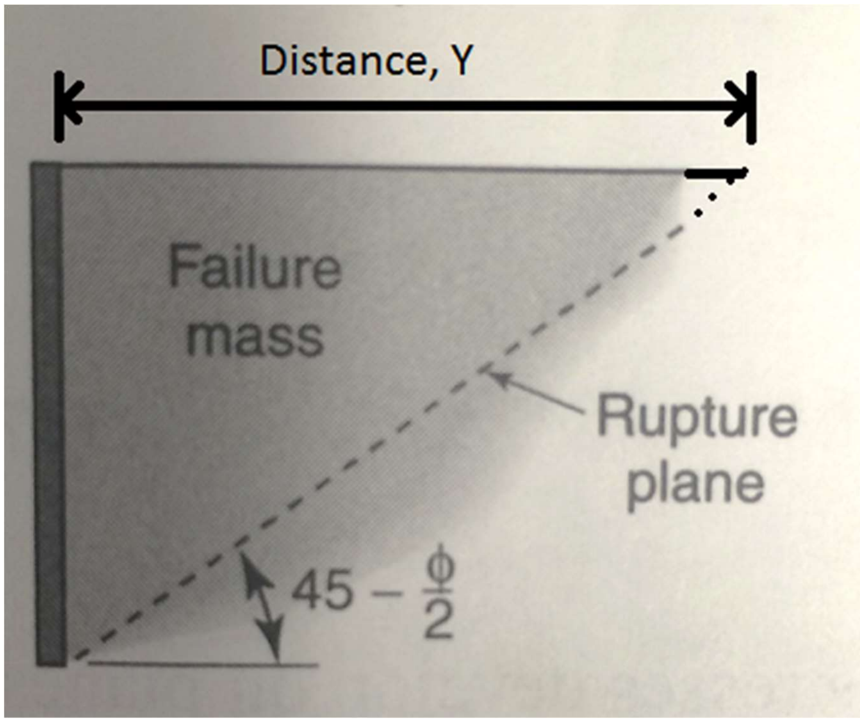

Figure 70: Elevation view of a theoretical Rankine rupture plane for the passive pressure condition behind a retaining wall (McCarthy 2007)

The theoretical rupture plane depicted in Figure 70 represents the case of an infinitely long wall subjected to passive forces, and therefore the maximum failure plane length, Y, that would be developed with a wall of finite length. The benchtop model, however, is not an infinitely long wall, which changes how far the failure surface would extend past the edges of the pusher plate (Y). To estimate where the failure surface would extend past the edges of the plate, a Boussinesq pressure distribution was used to determine when the stress increase caused by the plate would be negligible, and, thus, the soil would not move in this area. Note the situation of a plate pushing horizontally into a soil mass is not the same as a surface load pushing vertically. In addition to the difference in load direction, the test setup does not have soil past the top edge of the plate where the surface loading modeled by the Boussinesq distribution has soil extending in all directions from all edges of the plate. However, the Boussinesq distribution was used only as an estimation tool. No failure surface contacted the box for any test configuration and failure surfaces occurred at a minimum of 2" from the box edges, indicating that the box size likely had little effect on results. Figure 68 shows the stress contours under strip and square footings on the ground surface. At a distance of 2B (twice the width of the footing) from the center of the plate the stress is only 2% of the applied stress.

Taking all of these factors into consideration, the box was made 19.75" long, 20" wide, and 9" deep. The 19.75" length allows more than double the length of the estimated rupture plane of (9.6"). The width places the walls of the box nearly twice the plate width away from the center of the plate. The depth allows 4" of soil (0.73 plate widths) to be below the bottom of the pusher plate. Although the actual passive rupture surface is curved and extends below the straight line rupture surface seen in Figure 70, it is felt that 4" provides an adequate buffer zone between the actual rupture plane and the bottom of the box.

3. Soil compaction Technique

Soil specimens in all tests must have the same strength. To achieve this, a compaction technique was designed to provide consistent compaction from test to test and within the soil specimen of each individual test. The results of the test rely heavily on the shear strength of the compacted soil in the box. As the piston pushes the pusher plate into the soil, it causes the soil to shear along a failure surface. The force and displacement characteristics of this shearing action are the two most important aspects of this study and are directly related to the shear strength of the soil. The relationship between relative density and shear strength is not linear, as a small increase in density causes a substantial increase in shear strength. Figure 71 shows the results of a study by Ismael and Behbehani displaying high variation in shear strength with only slight variation in density (2014). The same relative density can be achieved by compacting soil at moisture contents both below (dry) and above (wet) the optimum moisture content. However, a soil compacted to 95% relative density on the dry side of optimum will have a different shear strength than a soil compacted to 95% relative density on the wet side of optimum. Figure 71 shows an example of soils compacted to different relative densities on the dry side of optimum (90% and 95% relative density) or at optimum (100% relative density), because the sand used in the laboratory testing program of this study were all compacted dry of optimum.

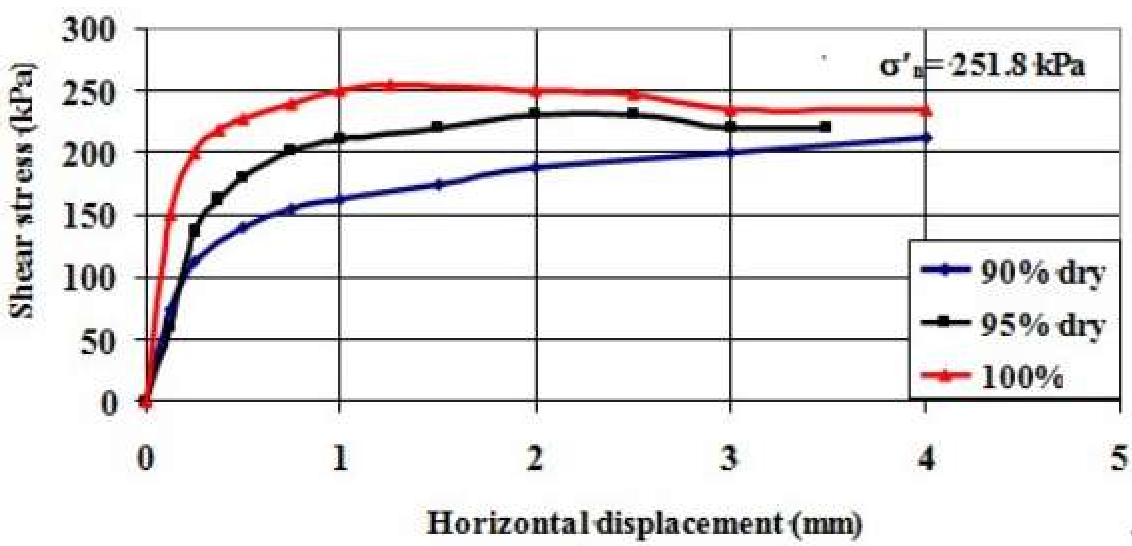

Figure 71: Shear stress versus horizontal displacement from direct shear tests on samples compacted at different relative compaction and at different normal pressures on the dry side of optimum (Ismael and Behbehani 2014)

In an effort to provide the required consistent density, a variety of compaction techniques were tested and a test was developed to determine the in-place density of the sand at any desired location within the specimen. Initial compaction techniques included hammer blows to the side of the box. While this densified the soil, densification was as inconsistent as the hammer blows applied to the specimen. A vibratory plate compactor (Figure 57) was developed. Soil was vibrated for five minutes to compact one half inch lifts of soil. This provided consistent soil density as evaluated by the technique given in Appendix F and shown in Table 1.

iii. Design Features of Benchtop Test to Provide Consistent Results

The benchtop test was designed to produce an identical soil structure for each test, with the only difference being the geometry of the reinforcement. A consistent specimen preparation scheme was devised to produce identical soil structures for each individual test. For the specimen preparation scheme to be effective, the testing apparatus was designed to provide consistent results. The three design features of the testing apparatus that help to provide consistent results are the design of the connection from the GeoJac to the pusher plate rod, the use of polypropylene fibers between the pusher plate and the box, and a single operator for all tests.

1. Connection to the GeoJac

The design of the connection between the GeoJac and the pusher plate rod is critical. The connection was designed to prevent the shaft from binding in the linear bushing while also providing torsional resistance to keep the plate from rotating. Typically, in other types of compression testing, a ball bearing is placed between two cupped shaft ends to prevent the shaft from binding. However, a ball bearing does not resist rotation about the axis of the shaft. Using a universal joint provides the benefits of the ball bearing by reducing binding of the linear bushing, but also provides torsional resistance so the plate will not rotate during the test.

2. Use of Polypropylene Fibers

As the pusher plate is advanced horizontally into the soil, a slight gap opens between the pusher plate and the box. Sand particles enter this gap to fill the void between the pusher plate and the box, creating divots on each side of the pusher plate. Loss of soil into these gaps reduces the soil support, causing a reduction in the force necessary to advance the plate. This problem is critical because the soil is lost at the edges of the plate which is the initiation point of the failure surface. Also, soil particles lodged between the plate and the box may increase the force that is necessary to advance the plate. Figure 72 shows a close up photograph of sand falling through the gap between the pusher plate and the box during a preliminary test.

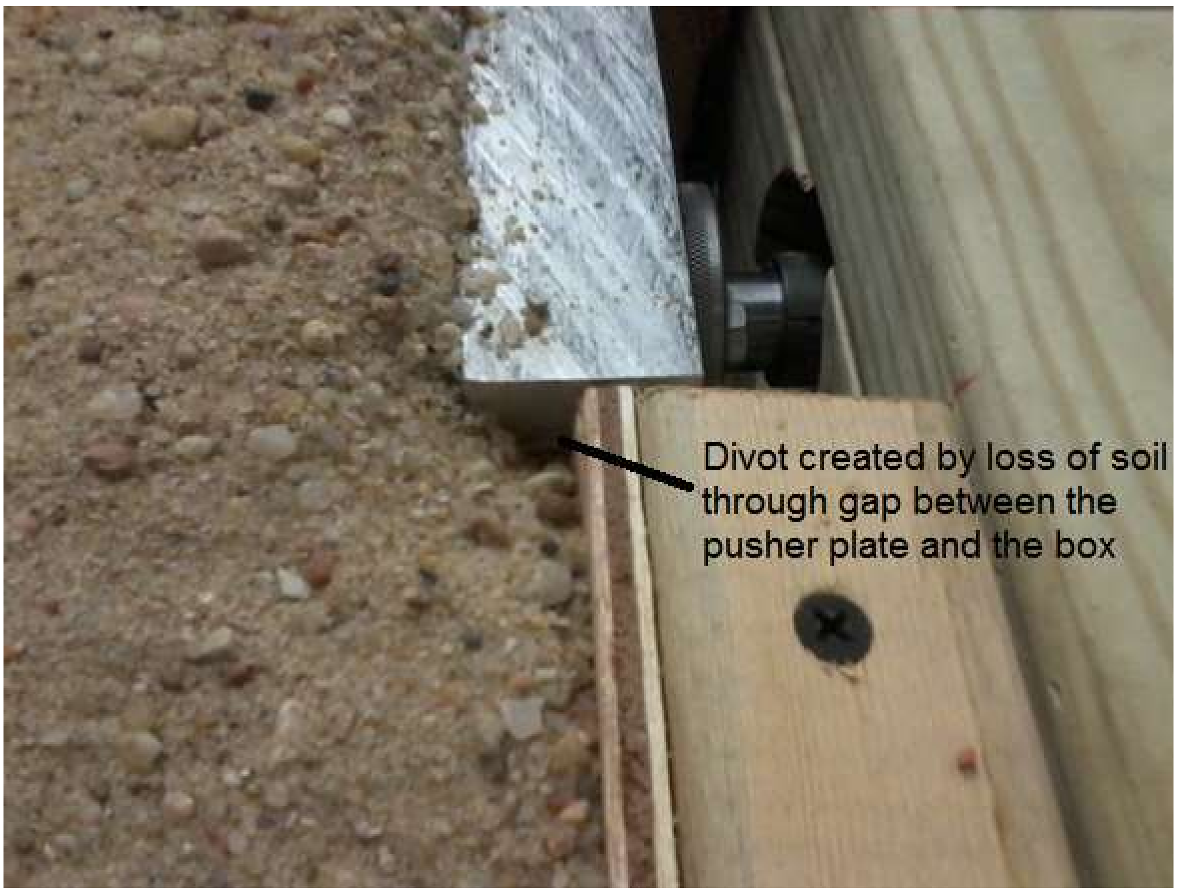

Figure 72: Sand falling through the gap between the pusher plate and the box

To mitigate the problem of sand entering the gap and causing inconsistencies from test to test, a filler material needed to be placed between the pusher plate and the box shown in Figure 73.

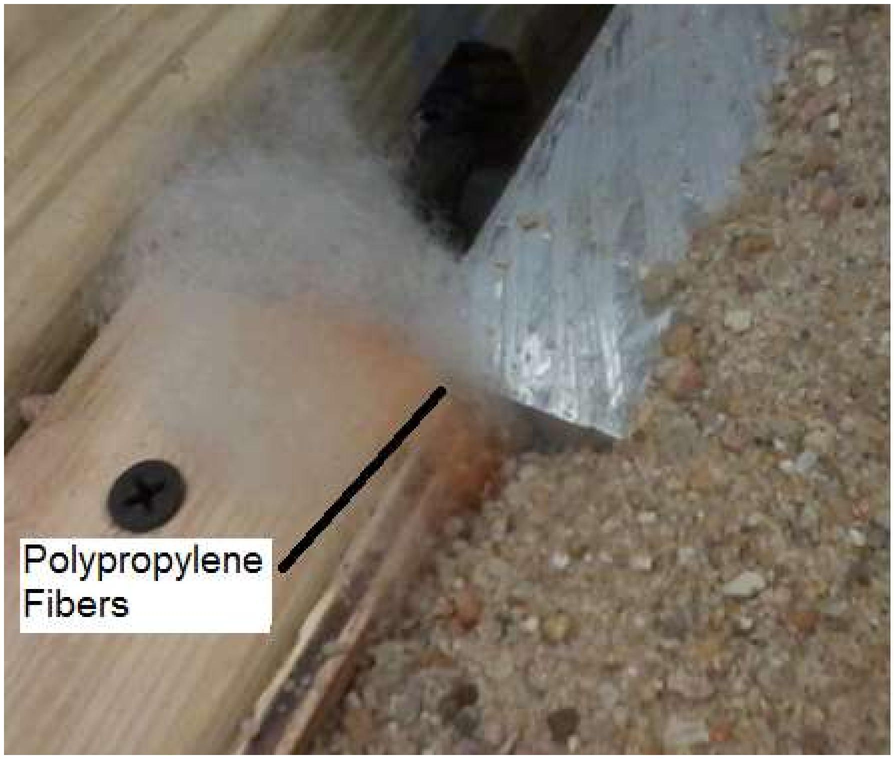

Figure 73: Polypropylene fibers mitigating soil intrusion into the pusher plate-box interface crack during testing.

The filler material should not affect the force required to advance the pusher plate, yet should be able to keep soil from filling the void. To determine the effect of the polypropylene fibers, tests were run without soil in the box. Running tests without soil provides force vs. displacement data due to the friction of the pusher plate rod travelling through the linear bushing. Ten tests were run without polypropylene fibers and six tests were run with polypropylene fibers between the plate and the box. The test results run without polypropylene fibers were compared to the test results with polypropylene fibers to determine the effect of the fibers. Figure 74 shows the results of all sixteen tests that were run without soil in the box. No significant difference was observed between the tests without polypropylene fibers and the tests containing the fibers. Thus it was concluded that polypropylene fibers are an adequate filler material because they do not significantly affect the force required to move the pusher plate.

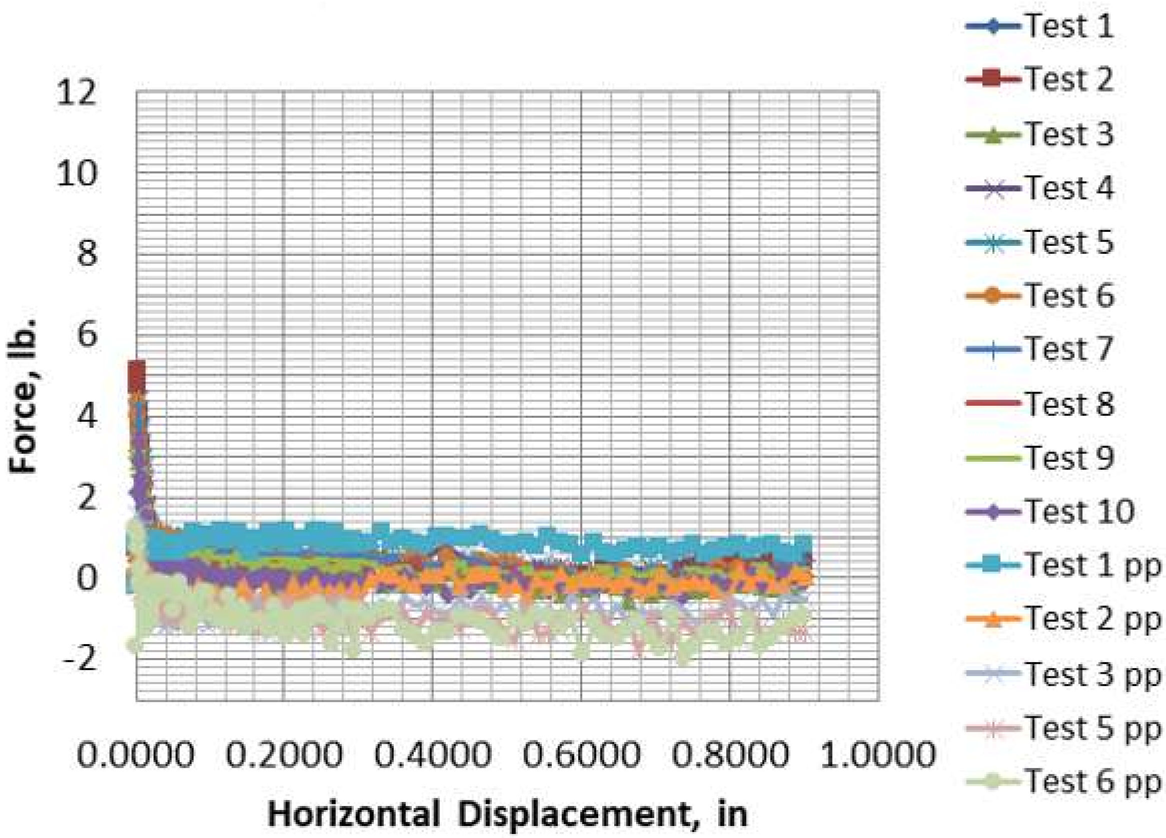

Figure 74: Force vs. Horizontal displacement of tests with no soil. "pp" denotes that polypropylene fibers were included

The filler material must also be able to keep soil from intruding in the gap. Figure 73 shows that the polypropylene fibers adequately prevent soil intrusion.

3. Single Operator

A single operator was used to construct and test each specimen. Using a single operator reduces human variability that could be present when multiple operators are used.

iv. Experimental Testing Procedure

A step by step testing procedure was used to reduce testing variability so that reinforcement configuration was the only significant variable. Elimination of other testing variables allows differences in results to be attributed only to reinforcement configuration. The majority of the testing procedure consists of constructing a soil specimen to be tested. Construction of the specimen is followed by conducting the actual test by failing the specimen with the GeoJac. It should be noted that the same soil was used for each test as stresses are low enough that crushing of soil grains was not likely to occur. Construction of the specimen is as follows:

1. Polypropylene fibers are placed between the pusher plate and the box. These fibers keep sand particles from falling in the crack between the pusher plate and the box as the pusher plate is advanced. A close up photograph of the polypropylene fibers keeping soil out of the crack during a test is shown in Figure 73.
2. 5745g of sand is weighed and placed in two rectangular pans.
3. From the lowest possible drop height, the sand from each pan is quickly dumped into the testing box along the side of the box with the pusher plate (front of box). Quickly dumping the sand and dumping from a low height reduces particle segregation.
4. The soil placement device, Figure 58, is adjusted to the proper depth and it is used to smooth out the sand, pulling from the front of the box to the back of the box (opposite the pusher plate side). As the screed is set at ½" increments and the soil is not yet compacted, excess soil will be present at the back of the box. This excess soil is smoothed evenly over the soil surface using a screed (see Figure 63).
5. The compaction device, Figure 57, is then placed atop the uncompacted lift and the vibrator activated for five minutes, compacting the specimen

6. After the compaction of each lift is complete, reinforcement is placed, if required. Reinforcement is placed with the machine direction of the paper perpendicular to the pusher plate.
7. Steps 2-6 are repeated until construction of the specimen is complete. Each specimen requires eighteen half inch sand lifts to be placed and compacted.
8. After the specimen is constructed, it is failed by pushing the pusher plate horizontally into the soil using a GeoJac at a rate of 0.02”/minute horizontally. The force on the plate and the horizontal displacement of the plate are recorded.

v. Density Variation Within Specimen

For direct comparison of test results, specimens are prepared in a consistent manner. However, it is also necessary to ensure that the specimen preparation procedure provides uniform density throughout each specimen. To evaluate density, a test was developed to directly measure soil mass and volume. The test is known as the “Water Method” density test and is described in Appendix F. This density test was performed at six different locations within a specimen prepared according to the experimental testing procedure described in the previous section. Figure 75 shows the six locations that density measurements were made. The first three density measurements were made at the soil surface, the soil was carefully excavated to a depth of 4” and the final three density measurements were made at that depth. The results of density testing are shown in Table 1 showing that there is not significant density variation within the specimen.

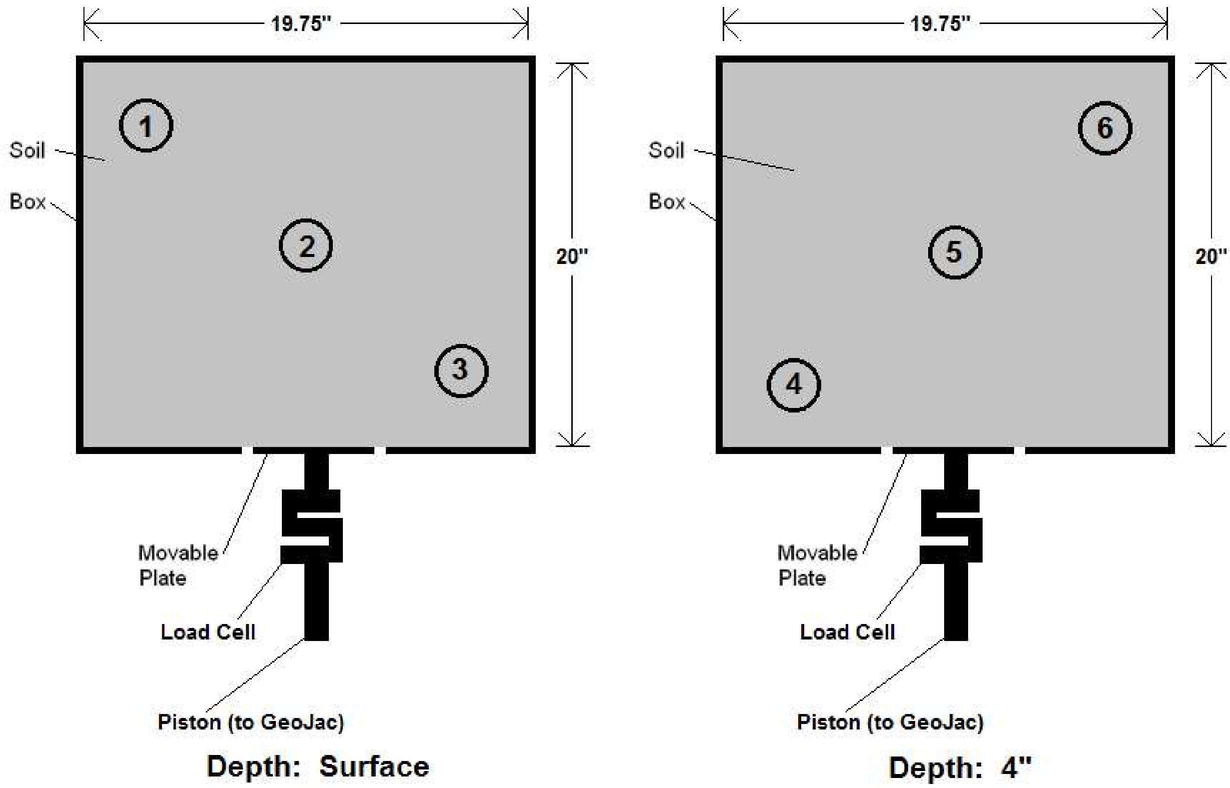

Figure 75: Plan view of test box showing the six approximate locations where density measurements were made. Note the difference in depth.

Table 1: Density test results

Location	Depth, in.	Density, pcf
1	0	111.3
2	0	110.9
3	0	112.1
4	4	110.7
5	4	110.4
6	4	111.6

vi. Soil Characterization

1. Gradation

A sieve analysis (ASTM C136) was performed on the test soil. The automatic sieve shaker used for this test is shown in Figure 76. Sieve analysis results are shown in Table 2.

Figure 76: Automatic sieve shaker

Table 2: Gradation of test soil

Sieve no.	Sieve Opening Size, mm	% Passing
4	4.750	100.0
8	2.360	90.1
16	1.180	75.6
20	0.841	63.9
50	0.300	16.3
70	0.210	8.9
100	0.149	4.4
200	0.074	0.9
Pan	0.000	0.0

The particle size distribution is presented graphically in Figure 77. As 100% of the particles passed the no. 4 sieve, it should be noted that the largest particle that could have been used in the laboratory testing is 4.75 mm (0.187 in.).

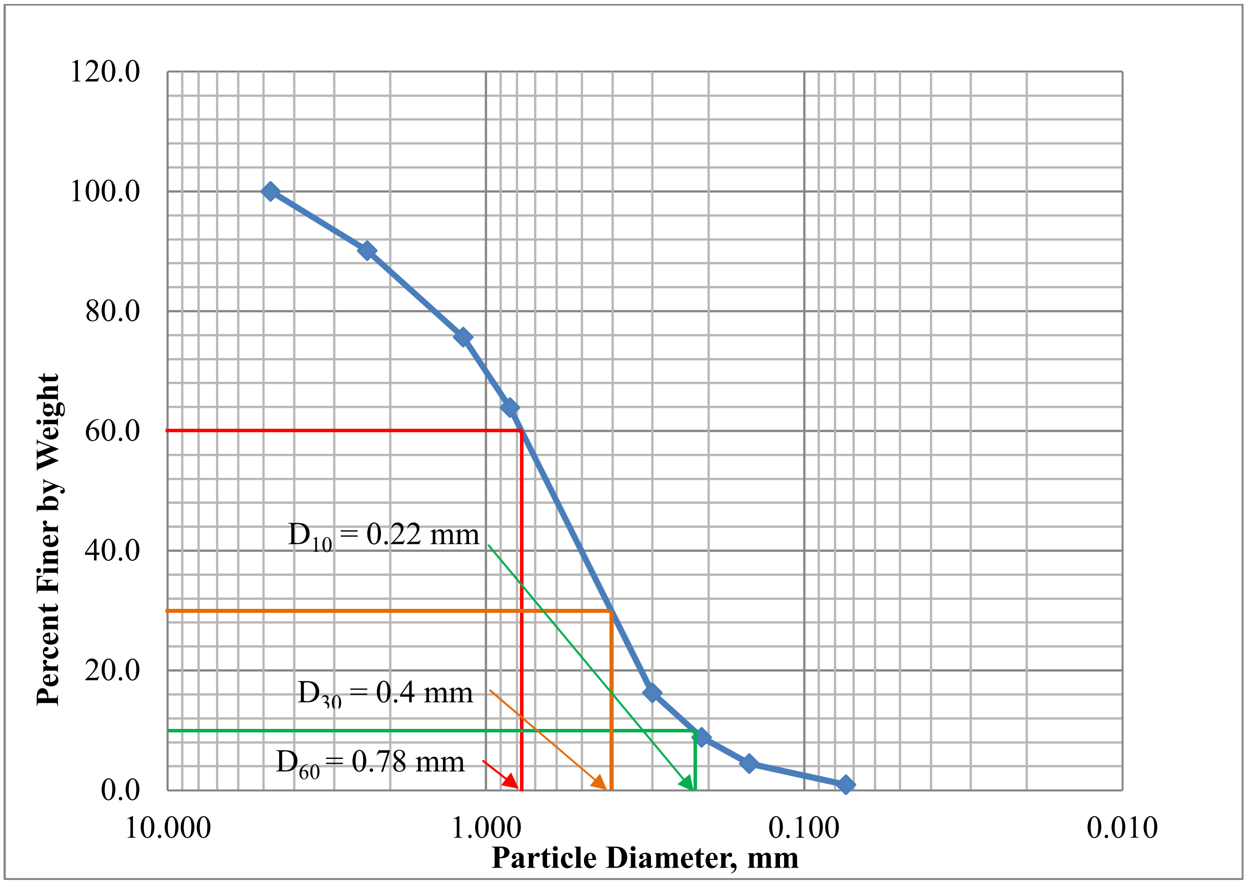

Figure 77: Particle size distribution of test soil with D_{10}, D_{30}, and D_{60} labeled

2. USCS Classification

This soil was further classified using the Unified Soil Classification System chart shown in Figure 78 (ASTM D2847). Moving from left to right on the chart: 99.1 % of the soil was retained on the no. 200 sieve, so it is coarse grained; 100% of the soil passed the no. 4 sieve, so it is a sand; The soil contains only 0.9% fines, so it is a clean sand.

Criteria for Assigning Group Symbols and Group Names Using Laboratory Tests[A]				Soil Classification	
				Group Symbol	Group Name[B]
COARSE-GRAINED SOILS More than 50 % retained on No. 200 sieve	Gravels (More than 50 % of coarse fraction retained on No. 4 sieve)	Clean Gravels (Less than 5 % fines[C])	$Cu \geq 4$ and $1 \leq Cc \leq 3$[D]	GW	Well-graded gravel[E]
			$Cu < 4$ and/or [$Cc < 1$ or $Cc > 3$][D]	GP	Poorly graded gravel[E]
		Gravels with Fines (More than 12 % fines[C])	Fines classify as ML or MH	GM	Silty gravel[E,F,G]
			Fines classify as CL or CH	GC	Clayey gravel[E,F,G]
	Sands (50 % or more of coarse fraction passes No. 4 sieve)	Clean Sands (Less than 5 % fines[H])	$Cu \geq 6$ and $1 \leq Cc \leq 3$[D]	SW	Well-graded sand[I]
			$Cu < 6$ and/or [$Cc < 1$ or $Cc > 3$][D]	SP	Poorly graded sand[I]
		Sands with Fines (More than 12 % fines[H])	Fines classify as ML or MH	SM	Silty sand[F,G,I]
			Fines classify as CL or CH	SC	Clayey sand[F,G,I]
FINE-GRAINED SOILS 50 % or more passes the No. 200 sieve	Silts and Clays Liquid limit less than 50	inorganic	PI > 7 and plots on or above "A" line[J]	CL	Lean clay[K,L,M]
			PI < 4 or plots below "A" line[J]	ML	Silt[K,L,M]
		organic	$\frac{\text{Liquid limit – oven dried}}{\text{Liquid limit – not dried}} < 0.75$	OL	Organic clay[K,L,M,N] Organic silt[K,L,M,O]
	Silts and Clays Liquid limit 50 or more	inorganic	PI plots on or above "A" line	CH	Fat clay[K,L,M]
			PI plots below "A" line	MH	Elastic silt[K,L,M]
		organic	$\frac{\text{Liquid limit – oven dried}}{\text{Liquid limit – not dried}} < 0.75$	OH	Organic clay[K,L,M,P] Organic silt[K,L,M,Q]
HIGHLY ORGANIC SOILS	Primarily organic matter, dark in color, and organic odor			PT	Peat

[A] Based on the material passing the 3-in. (75-mm) sieve.
[B] If field sample contained cobbles or boulders, or both, add "with cobbles or boulders, or both" to group name.
[C] Gravels with 5 to 12 % fines require dual symbols:
- GW-GM well-graded gravel with silt
- GW-GC well-graded gravel with clay
- GP-GM poorly graded gravel with silt
- GP-GC poorly graded gravel with clay

[D] $Cu = D_{60}/D_{10} \quad Cc = \frac{(D_{30})^2}{D_{10} \times D_{60}}$

[E] If soil contains ≥15 % sand, add "with sand" to group name.
[F] If fines classify as CL-ML, use dual symbol GC-GM, or SC-SM.
[G] If fines are organic, add "with organic fines" to group name.
[H] Sands with 5 to 12 % fines require dual symbols:
- SW-SM well-graded sand with silt
- SW-SC well-graded sand with clay
- SP-SM poorly graded sand with silt
- SP-SC poorly graded sand with clay

[I] If soil contains ≥15 % gravel, add "with gravel" to group name.
[J] If Atterberg limits plot in hatched area, soil is a CL-ML, silty clay.
[K] If soil contains 15 to <30 % plus No. 200, add "with sand" or "with gravel," whichever is predominant.
[L] If soil contains ≥30 % plus No. 200, predominantly sand, add "sand" to group name.
[M] If soil contains ≥30 % plus No. 200, predominantly gravel, add "gravelly" to group name.
[N] PI ≥ 4 and plots on or above "A" line.
[O] PI < 4 or plots below "A" line.
[P] PI plots on or above "A" line.
[Q] PI plots below "A" line.

Figure 78: Unified Soil Classification System Soil Classification Chart (ASTM D2487-11)

To determine if this sand is well graded or poorly graded, the coefficient of uniformity (C_u) and the coefficient of curvature (C_c) are calculated using Equations 21 and 22, respectively.

$$\boldsymbol{C_u = \frac{D_{60}}{D_{10}}} \qquad \text{(Eq. 21)}$$

$$\boldsymbol{C_c = \frac{(D_{30})^2}{(D_{60})(D_{10})}} \qquad \text{(Eq. 22)}$$

Where:

D_{60} is particle diameter at 60% passing
D_{10} is the particle diameter at 10% passing
D_{30} is the particle diameter at 30% passing

To be classified as well graded, the coefficient of uniformity must be greater than six and the coefficient of curvature must be between 1 and 3. The coefficient of uniformity is 3.55 and the coefficient of curvature is 0.93, classifying the soil as poorly graded. The soil lacks finer particles and is not classified as well graded by USCS. However, it still contains a wide variety of particle sizes.

3. Maximum Dry Unit Weight

The maximum dry unit weight of the compacted sand used for testing was determined with the Standard Proctor Test (ASTM D698). The test was only performed dry because the benchtop testing uses only dry soil. Figure 79 shows the soil in the proctor mold being weighed with the collar after the collar was removed and excess soil was scraped from the top of the mold.

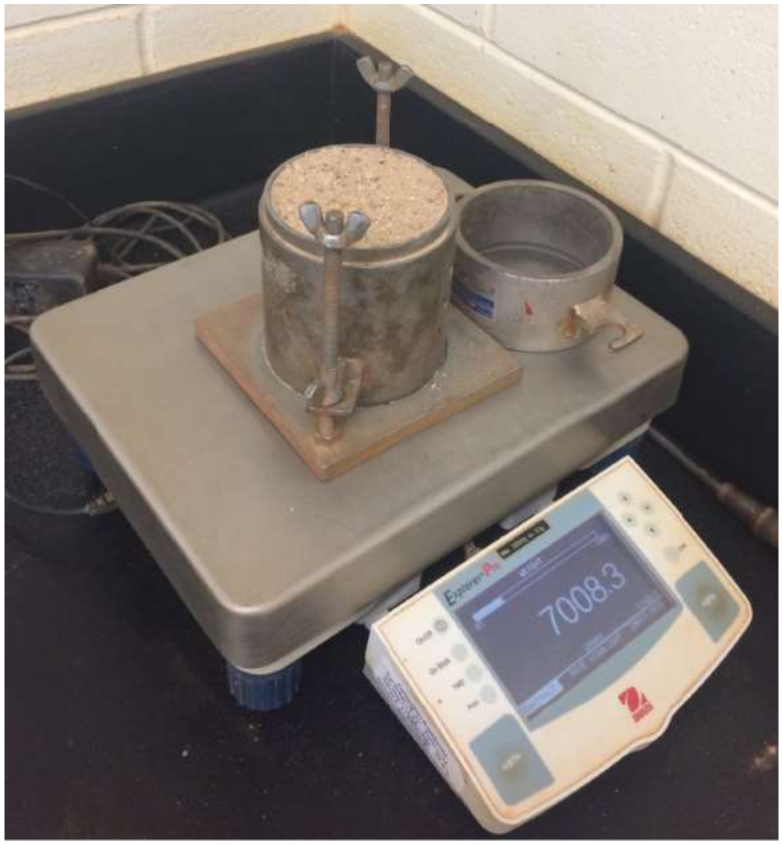

Figure 79: Proctor mold, collar, and compacted sand on balance

To determine the dry unit weight, the dry density was calculated using Equation 23 and from this dry density, the dry unit weight was calculated using Equation 24.

$$\boldsymbol{\rho_m = \frac{(M_t - M_{mol})}{V}} \qquad \text{(Eq. 23) (ASTM D698)}$$

Where: ρ_m is the moist density of the compacted specimen, equal to ρ_d in this study because water content is zero
M_t is the mass of the moist soil in mold and mold
M_{mol} is the mass of compaction mold
V is the volume of the compaction mold (944 cm^3)

$$\boldsymbol{\gamma_d = K_1 * \rho_d} \quad \text{in lbf/ft}^3 \qquad \text{(Eq. 24) (ASTM D698)}$$

Where: γ_d is the dry unit weight of compacted soil
K_1 is a conversion constant depending on density units, 62.428 for density in g/cm^3 and dry unit weight in pcf
ρ_d is the dry density of the compacted specimen

For the test soil, weight of sand and mold (+collar) was 7008.3g, weight of mold (+collar) was 5329.6g, and volume of mold was 944cm^3. Using $\boldsymbol{\rho_m} = \frac{(M_t - M_{mol})}{V}$

ρ_m = (7008.3g – 5329.6g)/944cm^3

ρ_m = 1.778 g/cm^3

Since the water content is zero, $\rho_m = \rho_d$ and $\gamma_d = K_1 * \rho_d$, Eq. 24 is used to calculate the dry unit weight.

γ_d = 62.428 * 1.778g/cm^3

γ_d = 111.0 pcf

Thus the maximum dry unit weight using standard effort is 111.0 pcf.

4. Strength Parameters

The strength parameters of the test soil were determined with triaxial testing (ASTM D4767). Tests were performed at 15 psi, 30 psi, and 45 psi confining stresses. Axial strain was plotted on the abscissa with the corresponding applied axial stress plotted on the ordinate for each deviator stress.

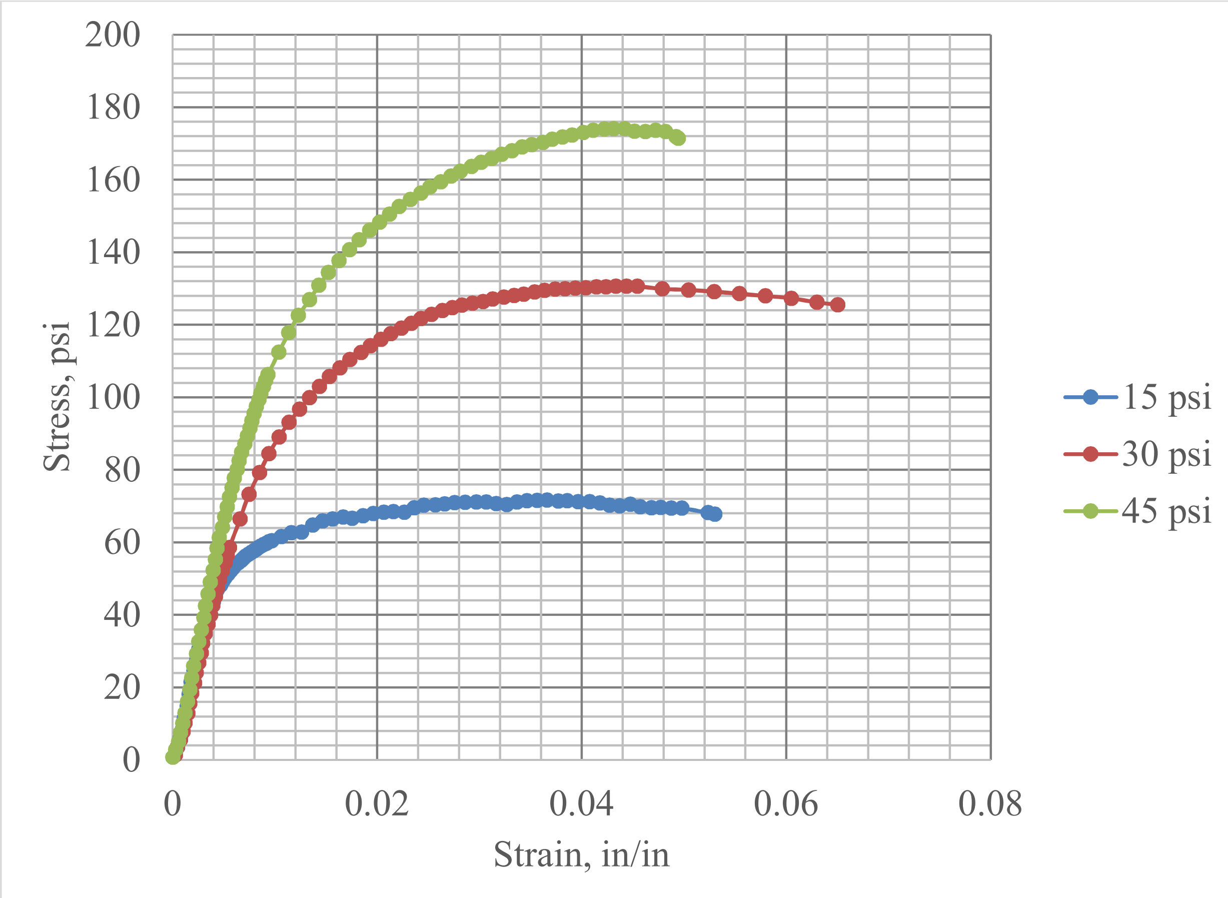

Figure 80: Stress-Strain plot for 15 psi, 30 psi, and 45 psi confining stress triaxial tests

For triaxial tests on dry sand, the deviatoric stress at failure is defined as the peak deviatoric stress observed during testing. For each of the three tests, a Mohr's circle was plotted using the major and minor effective principal stresses experienced by the specimen when the peak deviatoric stress occurred. According to Mohr-Coulomb failure criteria, a straight line failure envelope defined by these Mohr's circles will have a y-intercept representing the soil's cohesion and a slope representing the soil's angle of internal friction. Figure 81 shows Mohr's Circles and the corresponding Mohr-Coulomb failure envelope for the sand used during laboratory testing. The cohesion intercept was found to be zero and the angle of internal friction was found to be 36.6º.

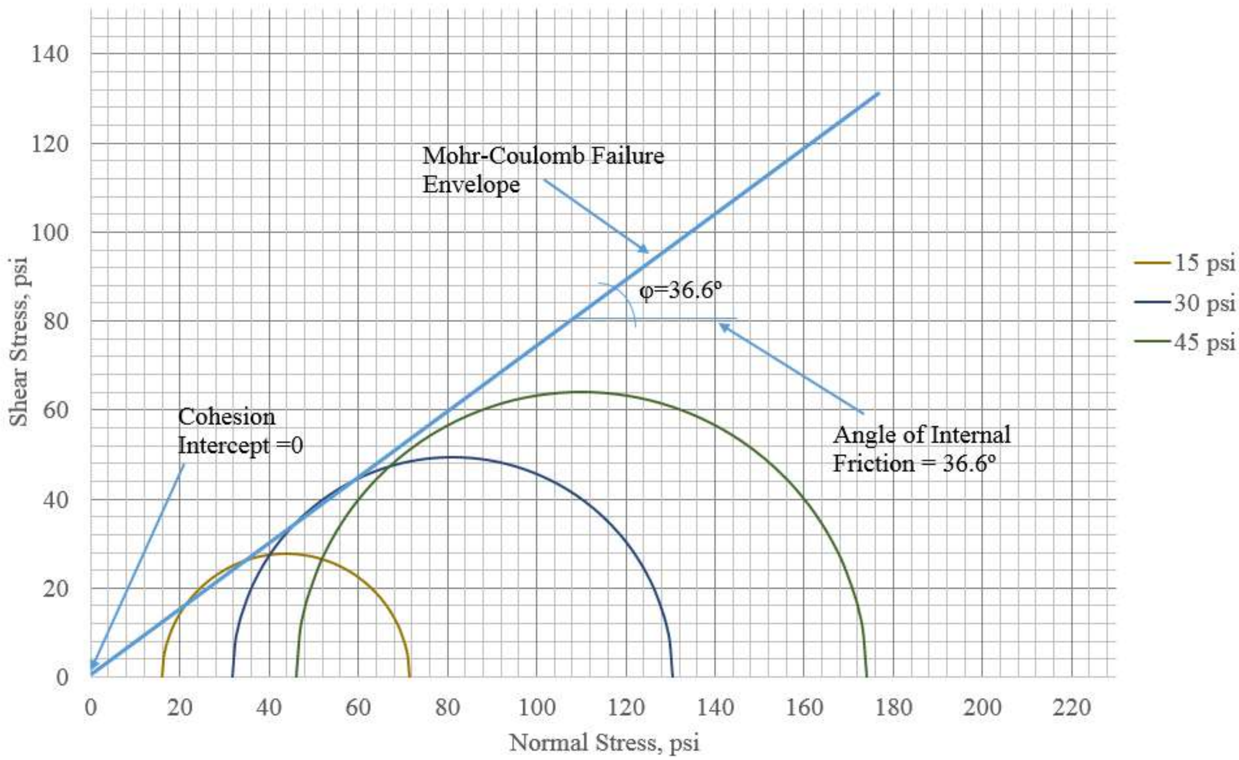

Figure 81: Mohr's circles and total stress strength parameters defined by the Mohr-Coulomb failure envelope for three confining stresses. Note that for a dry test, the total stress and effective stress strength parameters are equal.

5. Shape of soil particles

Magnified photographs of the sand particles were taken to show the variety of particle sizes and shapes. Figure 82 shows a magnified view of sand particles magnified under a 10X microscope while Figure 83 shows a single sand particle magnified under a 40X microscope.

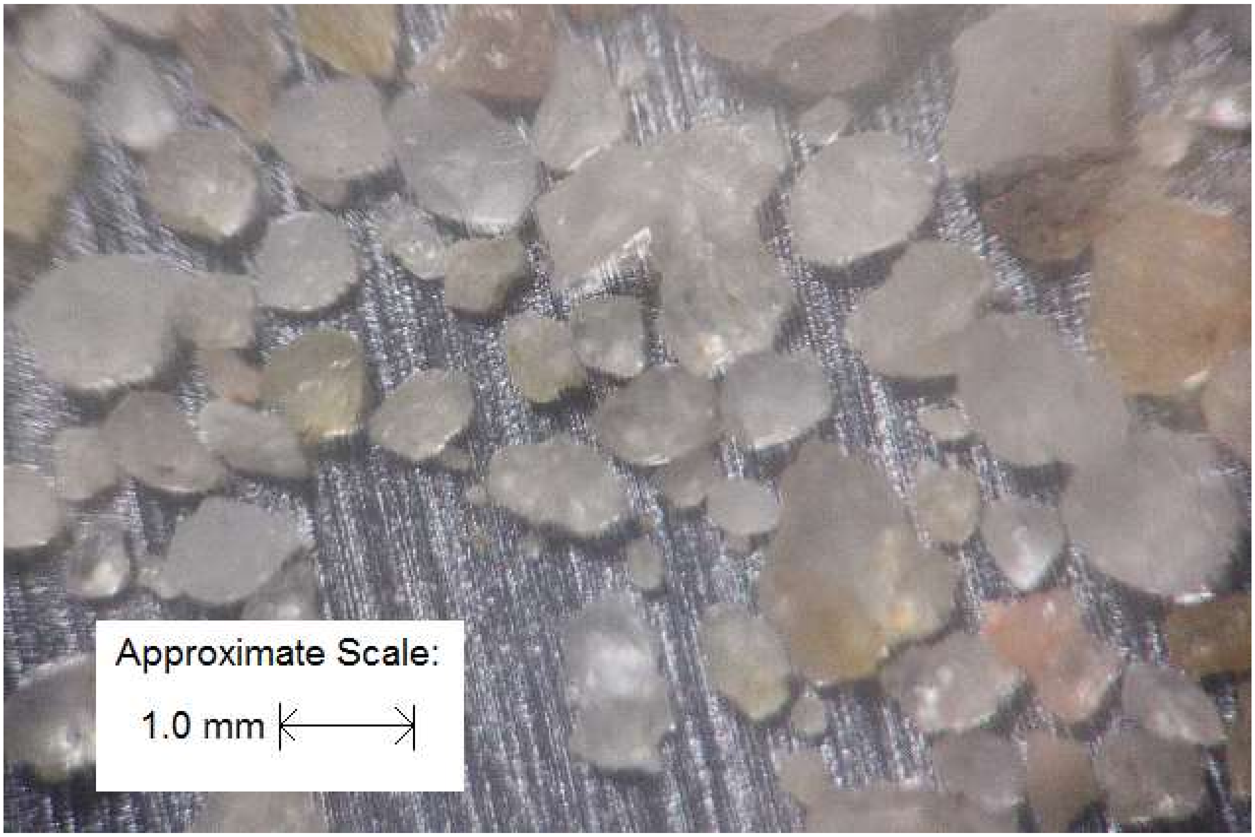

Figure 82: 10X magnified photograph showing various soil particle sizes and shapes

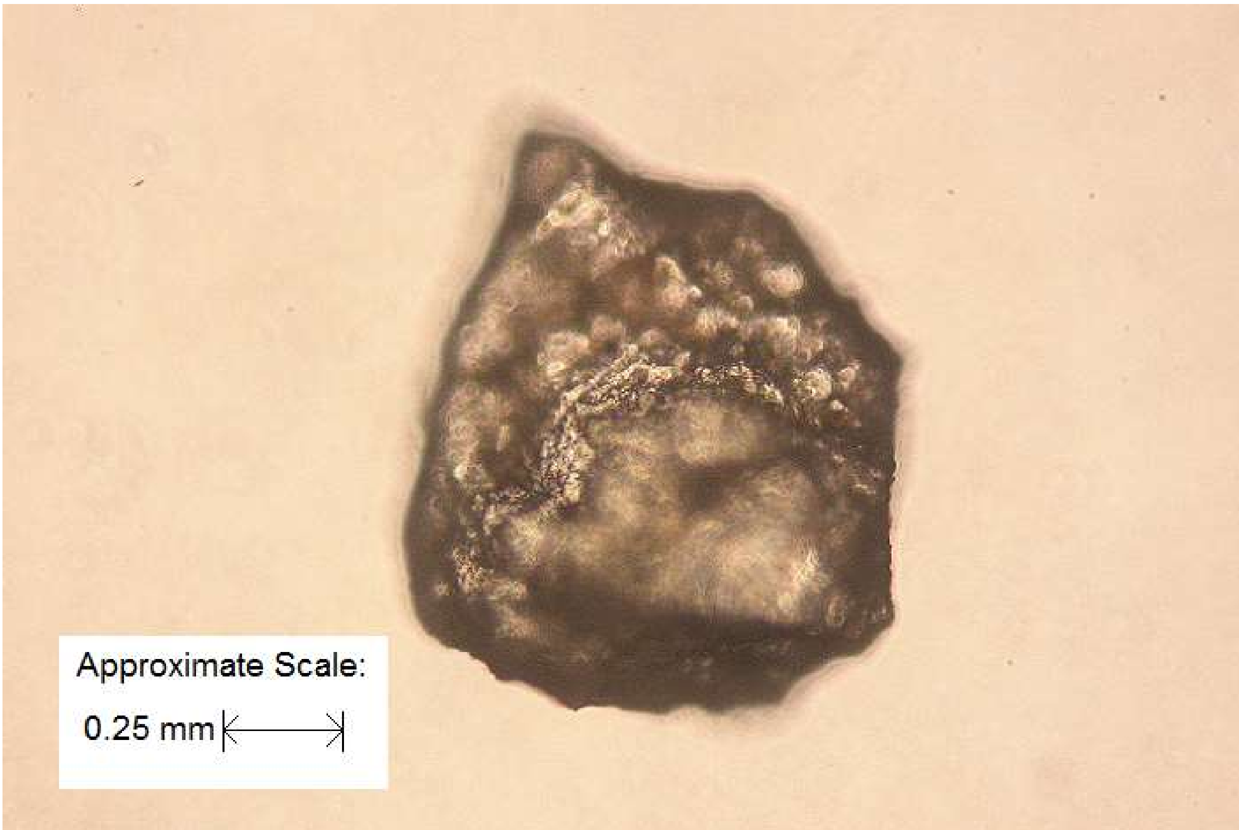

Figure 83: 40X magnified photograph of a single sand particle showing surface texture and particle shape

6. Soil Particle Mineral Type

The soil particle mineral type was determined by a professional geologist. Through visual inspection and the soil's reactivity with hydrochloric acid, the soil consists predominantly of carbonate and silicate sands (Barnwell 2018).

vii. Reinforcement Characterization

1. Flexural Rigidity

Engineering paper was used as reinforcement for laboratory testing. The flexural rigidity of the reinforcement was determined using the cantilever test described in ASTM D1388-14. The flexural rigidity of engineering paper was determined as well as that of a typical high density polyethylene geotextile and a typical polyester geotextile. The three reinforcement specimen types are shown in Figure 84.

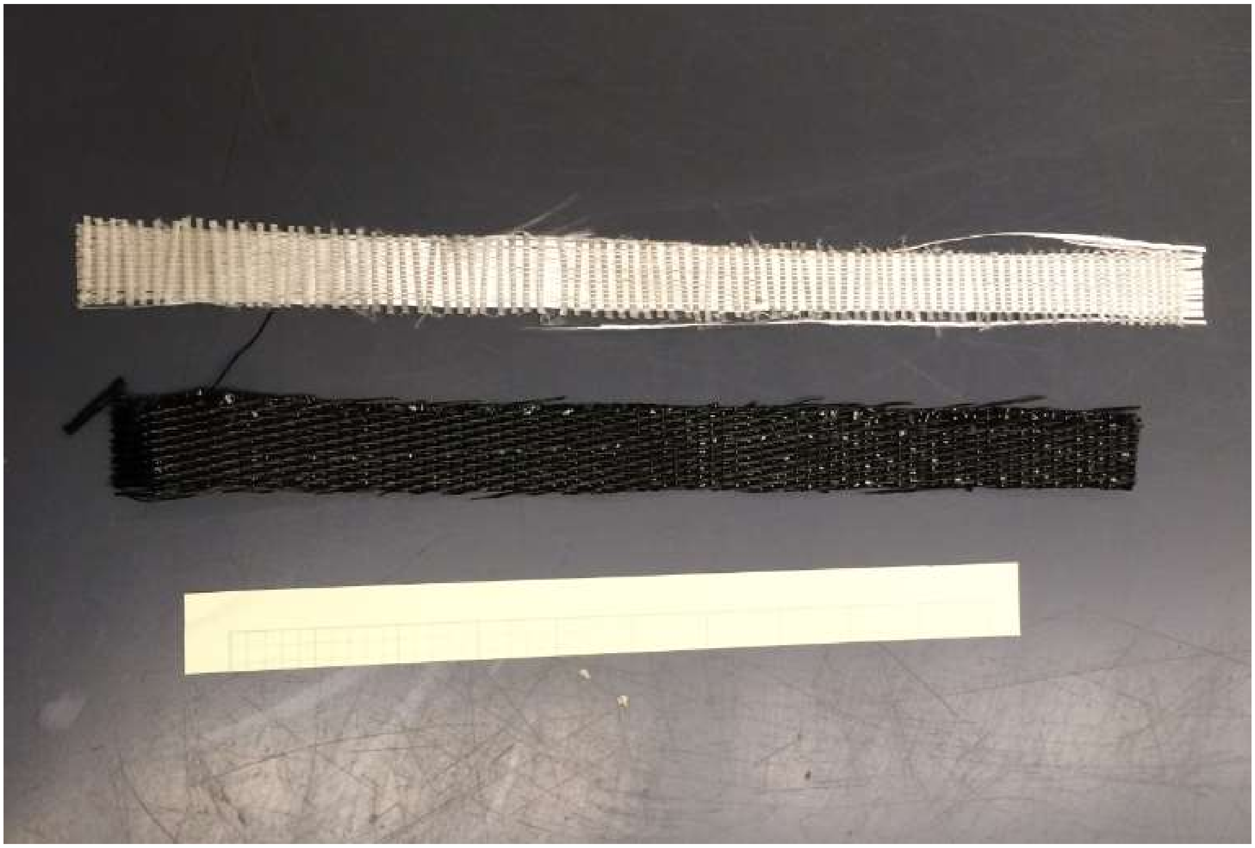

Figure 84: Reinforcement types: polyester (top), high density polyethylene (center), engineering paper (bottom)

All tests were performed using the FRL Cantilever Bending Tester shown in Figure 85. A specimen of engineering paper being tested is shown in Figure 86 with photographs of all cantilever tests shown in Appendix B.

Figure 85: FRL Cantilever Bending Tester

Figure 86: Engineering paper being tested with the FRL Cantilever Bending Tester

Four tests of each reinforcement type were performed. The test results and the average for each reinforcement type are shown in Table 3.

Table 3: Average Flexural Rigidity of Reinforcement

Reinforcement Type or Test Number	Flexural Rigidity, µjoule/m
Paper	
Test 1	3.04×10^{12}
Test 2	2.73×10^{12}
Test 3	2.73×10^{12}
Test 4	3.04×10^{12}
Average	2.88×10^{12}
Polyester woven geotextile	
Test 1	2.00×10^{13}
Test 2	2.04×10^{13}
Test 3	2.04×10^{13}
Test 4	2.36×10^{13}
Average	2.11×10^{13}
High Density Polyethylene woven geotextile	
Test 1	8.30×10^{13}
Test 2	7.20×10^{13}
Test 3	8.30×10^{13}
Test 4	6.68×10^{13}
Average	7.62×10^{13}

2. Interface Friction Angle

The interface friction angle between soil and reinforcement (paper) was determined using a tilt table test described by Narejo (2002). A sketch of the tilt table described by Narejo is shown in Figure 87. The tilt table used for testing varies from this sketch as the dimensions are 19” L x 8”W and the test specimen was attached to the bottom plate using tape instead of Velcro. The tilt table used for testing is shown in Figure 88. A protractor and plumb bob measured the tilt angle.

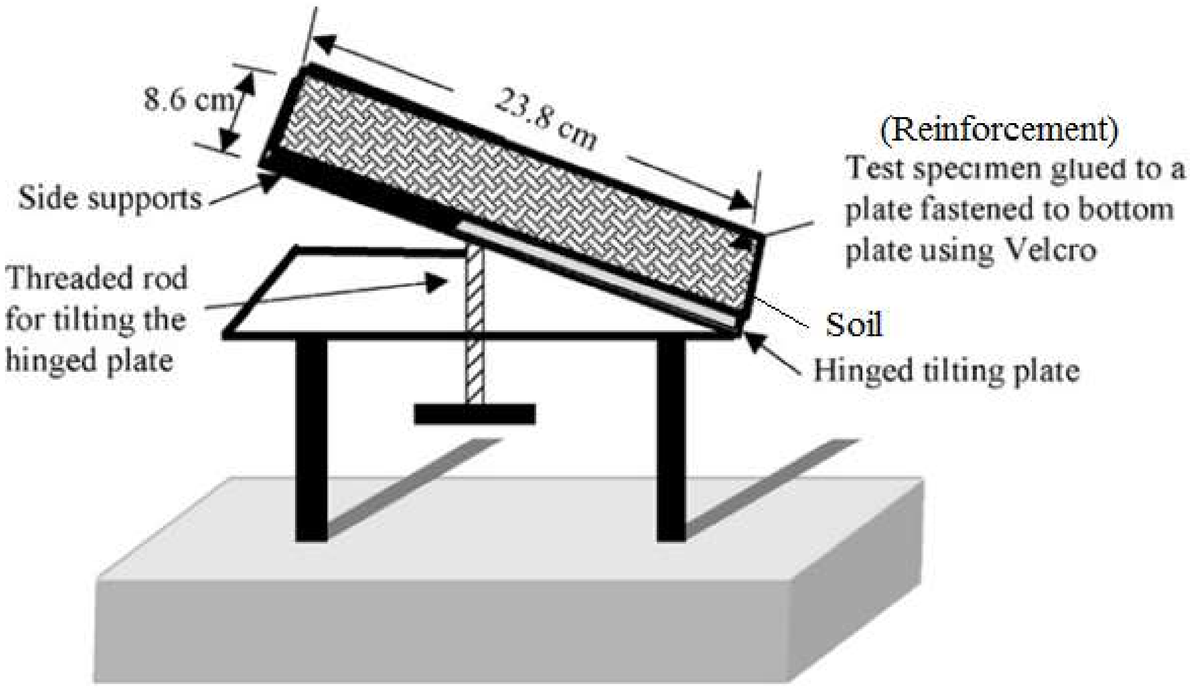

Figure 87: Sketch of tilt table device (Narejo 2002)

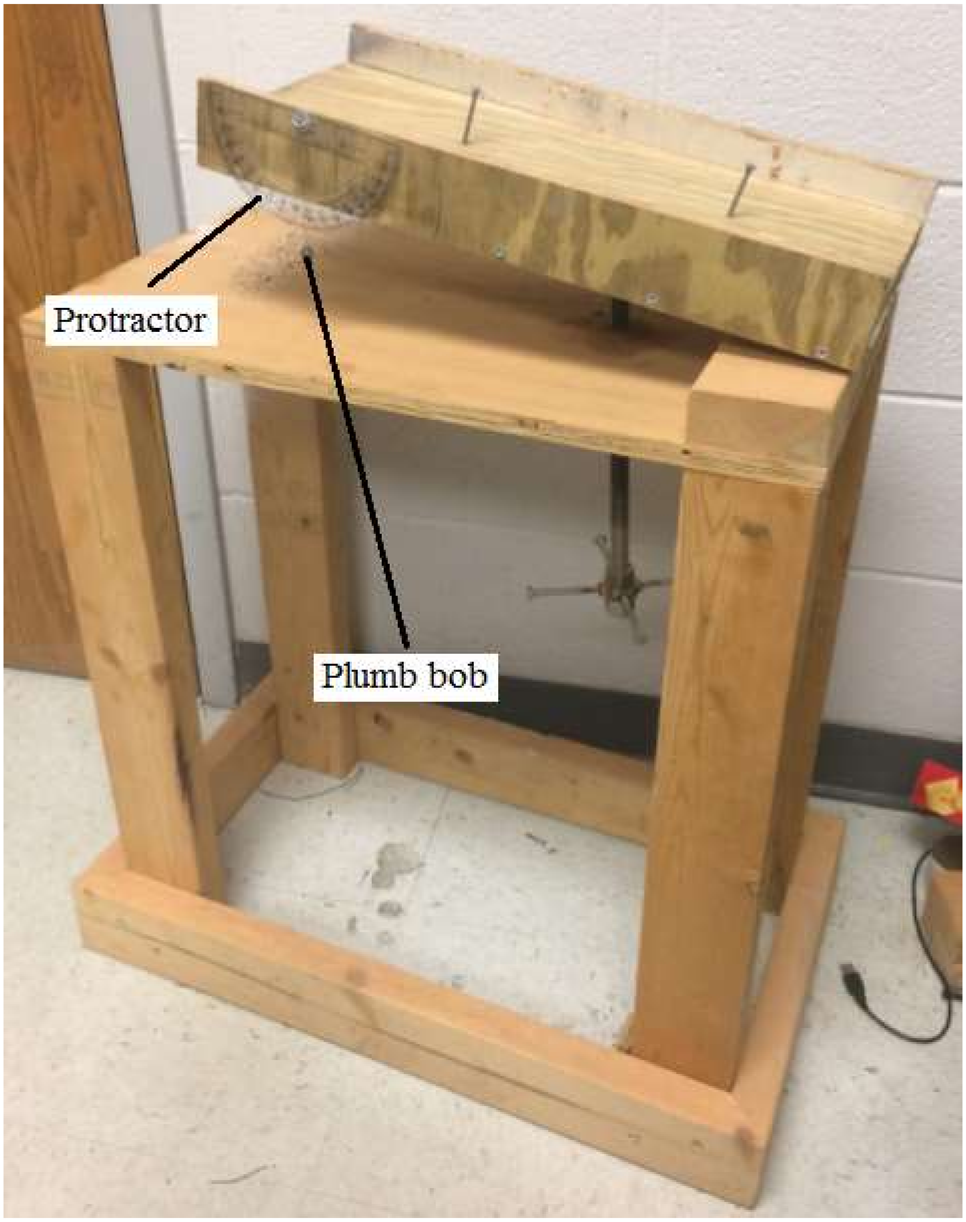

Figure 88: Tilt table used for testing with protractor and plumb bob to measure tilt angle

The specimen was prepared by taping paper reinforcement to the bottom plate, placing a layer of soil atop the reinforcement, placing the top plate on the layer of soil, and placing dead weights on the top plate to provide overburden pressure. Figure 90-93, show how the specimen was prepared. The overburden stress created by the weights in Figure 93 is 1.24 kPa. The effect of overburden pressure on friction angle was evaluated by Narejo (2002). He performed tilt tests on three different interfaces at three overburden stresses per interface. Narejo concluded that overburden stress had little effect on interface friction angle (2002). Figure 89 shows the results of Narejo's testing. Research performed by Wasti and Ozduzgun (2001) also showed that applied normal stress had little effect on interface friction results, particularly for smoother reinforcements. An overburden stress of 1.24 kPa was chosen for testing due to the little influence of overburden stress on results and because it is within the range of overburden stresses suggested by Narejo for tilt table testing.

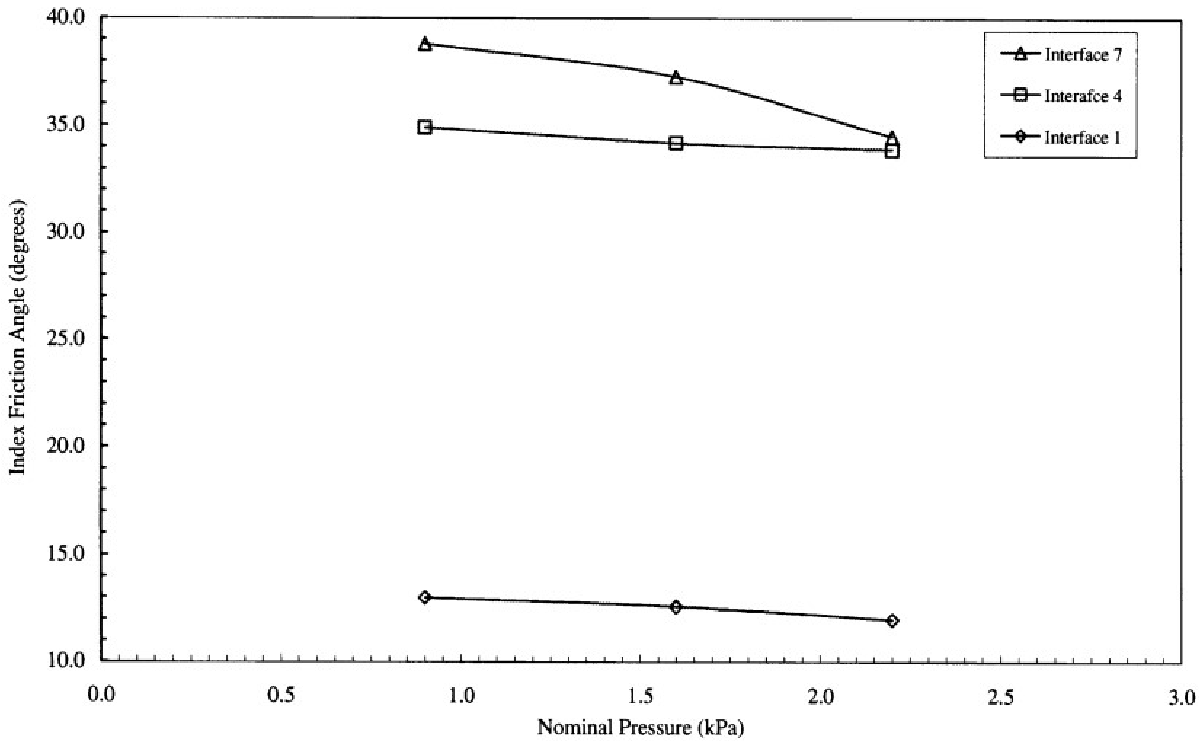

Figure 89: Influence of overburden stress on index friction angle (Narejo 2002)

Figure 90: Paper taped to bottom plate of tilt table

Figure 91: Soil placed atop paper reinforcement

Figure 92: Top plate atop soil layer

Figure 93: Dead weights placed on top plate, held in place with screws

After specimen preparation, the screw handle was turned clockwise, increasing the tilt angle until failure occurred (sliding between the sand/paper interface). The test was performed three times with the long dimension of the rectangular paper in line with the long dimension of the tilt table. Every specimen failed at a 25 degree tilt angle. The test was repeated three times with the short dimension of the rectangular paper in line with the long dimension of the tilt table. Each of these tests failed at a 25 degree tilt angle as well indicating non-directionality of the friction angle.

3. Tensile Strength and Strain

The tensile strength and strain properties of the paper reinforcement were determined using a constant rate of elongation apparatus and the testing procedure as described in TAPPI T 494 om-01 (2001). A Param XLW(EC) auto tensile tester was used to test the paper specimens and is shown in Figure 94. Figure 95 shows the testing apparatus with a paper specimen loaded into the grips before testing. Figure 96 shows the paper specimen after rupture.

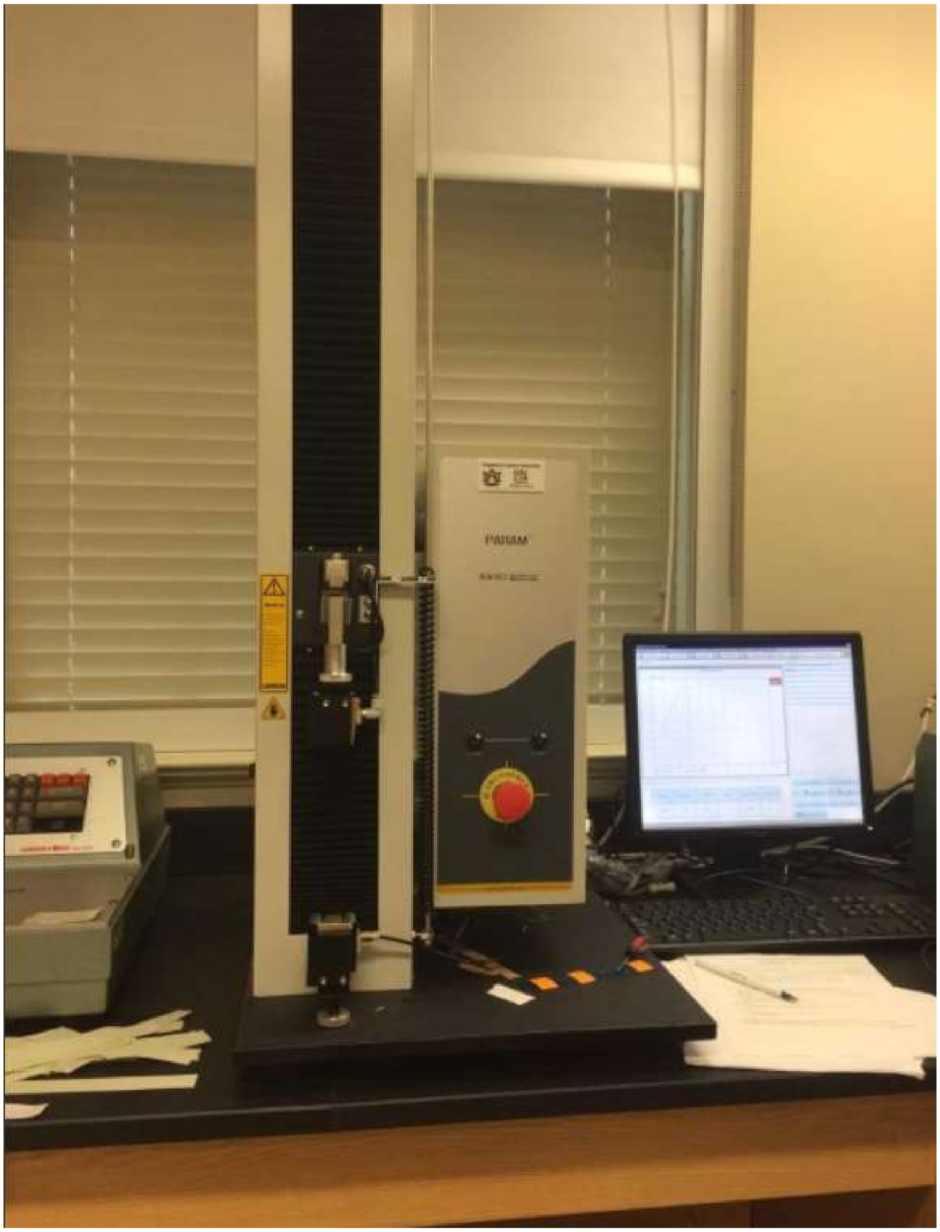

Figure 94: Param XLW(EC) auto tensile tester

Figure 95: Param XLW(EC) auto tensile tester with paper specimen ready for testing

Figure 96: Param XLW(EC) auto tensile tester with ruptured specimen

Table 4 shows the test results for the ten tests performed on specimens cut with the cross machine direction as the axis of extension. The average strength of specimens tested with the cross machine direction as the axis of extension was 20.18 MPa and the data had a standard deviation of only 0.82 MPa. Table 5 shows the test results for the ten tests performed on specimens cut with the machine direction as the axis of extension. The average strength of specimens tested with the machine direction as the axis of extension was 47.43 MPa and the data had a standard deviation of only 0.42 MPa.

Table 4: Test result summary for cross machine direction of paper reinforcement

Test Number	Maximum Force, N	Displacement, mm	Strength, MPa	Strain at specimen failure, %
1	41.179	11.1	19.609	6.2
2	43.088	11.5	20.518	6.4
3	42.627	10.3	20.299	5.8
4	40.751	9.3	19.405	5.2
5	42.298	10.2	20.142	5.7
6	39.895	9.9	18.998	5.6
7	43.450	11.0	20.691	6.2
8	43.088	9.5	20.518	5.3
9	46.018	12.4	21.913	7.0
10	41.446	9.0	19.736	5.1
Mean	**42.384**	**10.4**	**20.183**	**5.9**
Standard Deviation	**1.719**	**1.1**	**0.812**	**0.6**

Table 5: Test result summary for machine direction of paper reinforcement

Test Number	Maximum Force, N	Displacement, mm	Strength, MPa	Strain at specimen failure, %
1	103.162	3.0	49.125	1.7
2	100.726	3.0	47.965	1.7
3	102.372	3.1	48.748	1.7
4	101.088	3.0	48.137	1.7
5	100.100	3.3	47.667	1.8
6	97.072	3.0	46.225	1.7
7	101.779	3.2	48.466	1.8
8	98.013	3.0	46.673	1.7
9	94.676	3.0	45.084	1.7
10	97.039	3.1	46.209	1.8
Mean	**99.603**	**3.1**	**47.430**	**1.7**
Standard Deviation	**2.760**	**0.1**	**1.314**	**0.05**

b. FLAC3D™ Modeling Study

FLAC3D™, geotechnical finite difference modeling software, was used to model the laboratory testing.

The FLAC3D™ modeling procedure consists of five steps: Test geometry creation, calibration of FLAC3D™ model parameters to laboratory test, assignment of constitutive model and properties, application of strain to the model, and obtaining FLAC3D™ results.

i. Geometry Creation

1. Dimensions, Grid Density, and Boundary Conditions

Correct dimensions, grid density, and boundary conditions must be used to properly model the laboratory testing. The geometry of the FLAC3D™ model matches that of the laboratory testing and is a rectangular prism with dimensions of 19.75" long x 20" wide x 9" high. Increasing grid density directly increases program run time. As this particular simulation has a large number of steps, the grid density was chosen to provide the densest grid that allowed reasonable program run time (approximately 12 hours) per reinforcement geometry configuration. The bottom four inches (z=0 to z=4) were composed of one grid block per cubic inch except for the back of the box (y=19 to y=19.75) which was composed of one grid block per 0.75 cubic inches to obtain total y length of 19.75". The top five inches (z=4 to z=9) were composed of two grid blocks per cubic inch except for the back of the box (y=19 to y=19.75) which was composed of one grid block per 0.375 cubic inches. Grid blocks are shorter in the z-dimension at the top 5 inches (z=5 to z=9) to allow geogrid reinforcement elements to be easily attached to the geometry. Refer to Figure 97 for x, y, and z dimension directions. The only exception to the aforementioned grid density is that the grid density was increased to 16 grid blocks per cubic inch in the first inch of the front face of the box, where the edge of the pusher plate contacts the specimen. Figure 97 shows the grid density configuration.

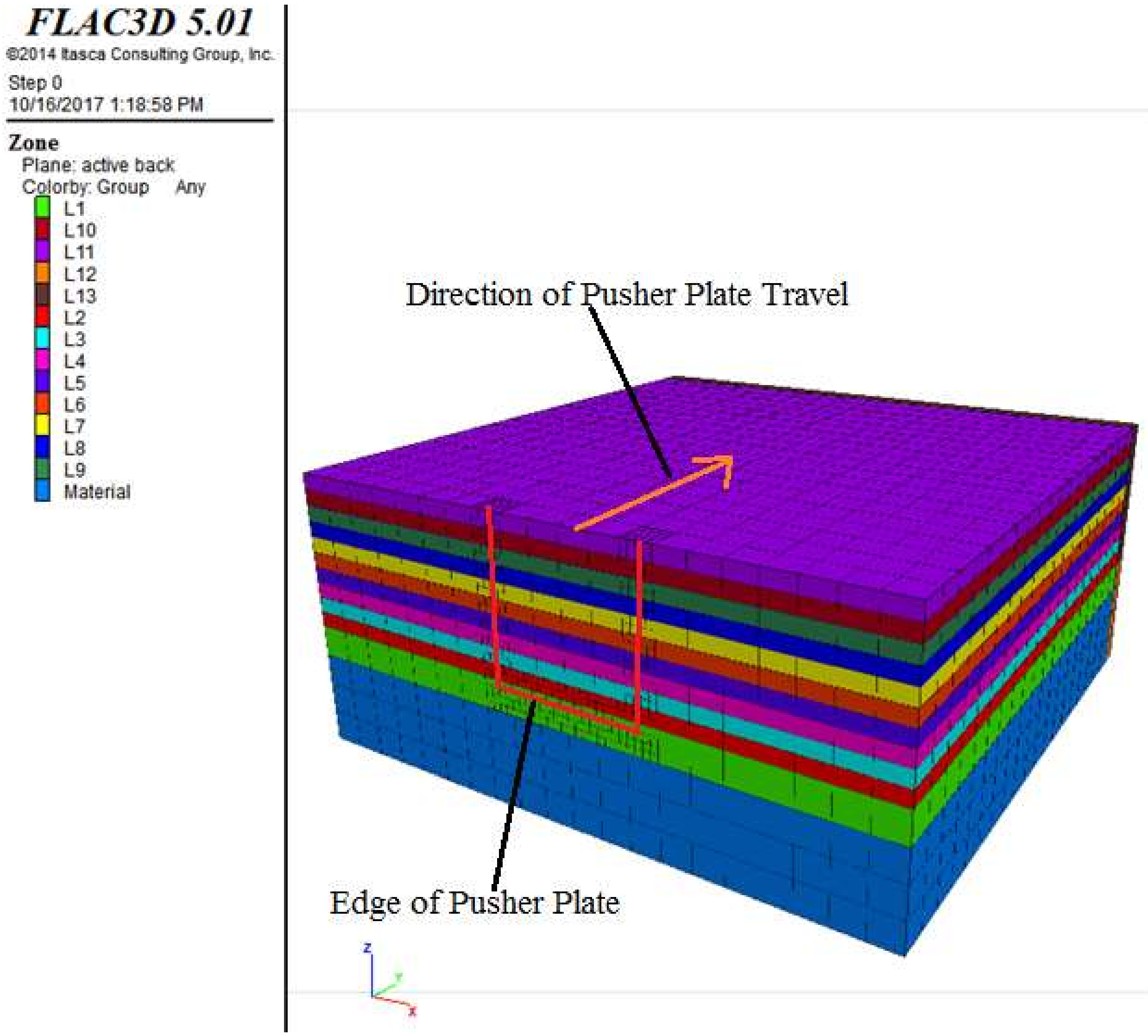

Figure 97: Geometry creation showing grid density. Different colors are used only to show different geometric elements that were joined together to create the whole geometry. The red outline indicates the edge of the pusher plate. The orange arrow indicates the direction of pusher plate travel.

The boundary conditions are designed to mimic that of the laboratory testing. The laboratory testing is performed in an open top box with four vertical sides and a bottom. Therefore, soil adjacent to any side of the box cannot move perpendicular to its respective side. FLAC3D™ allows gridpoints to be fixed and unable to move in any direction. To mimic the laboratory setup, the nodes at the bottom of the box and the four vertical sides of the box were fixed (unable to move perpendicular to their respective side). However, they are still allowed to move freely in any direction parallel to their respective sides. The fixities of the gridpoints of the vertical sides of the box and the bottom of the box are shown in Figure 98 and Figure 99, respectively. The colored lines represent the direction in which the gridpoints are not allowed to move. Each colored line represents the fixity of a gridpoint located in the center of the line.

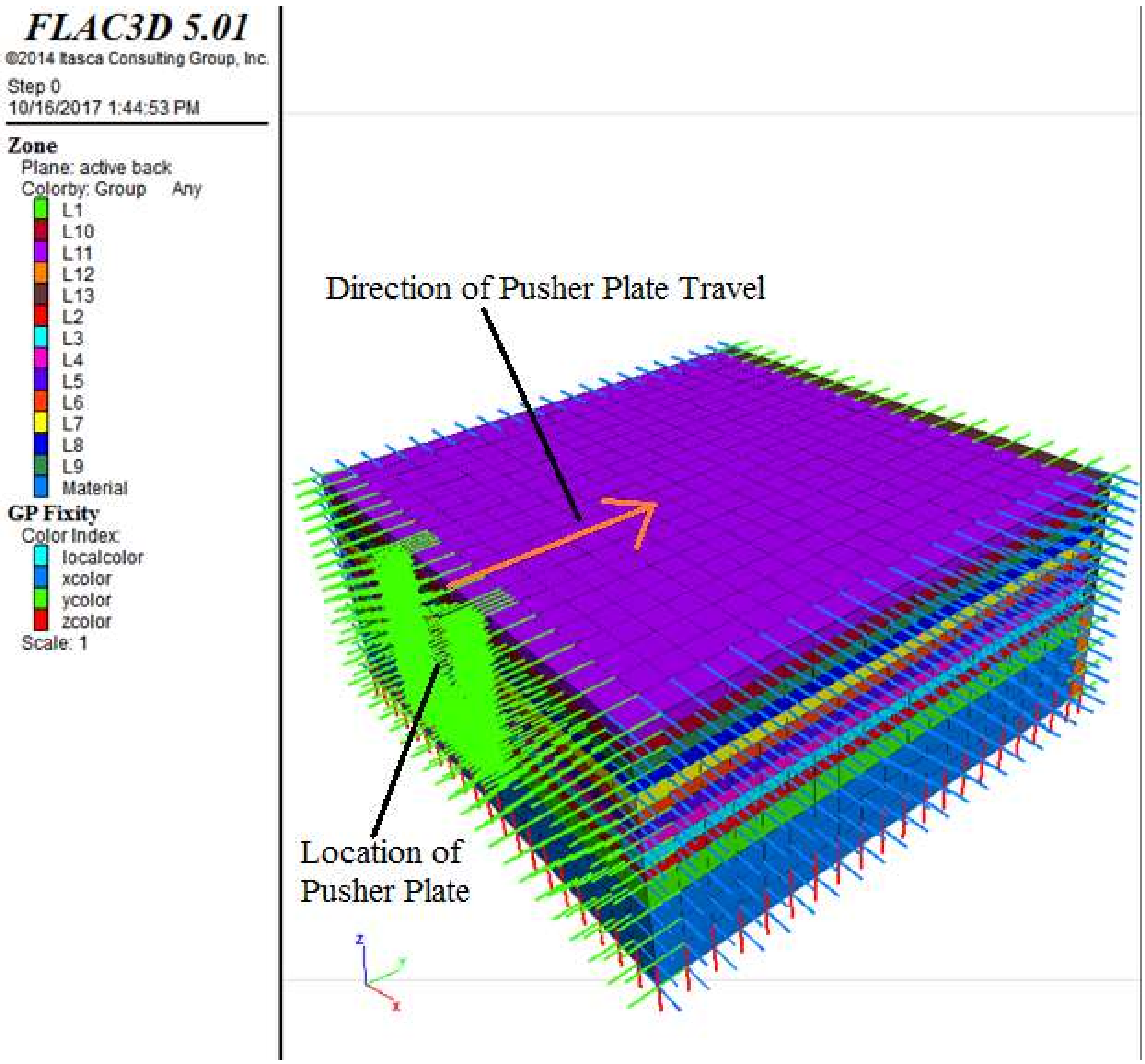

Figure 98: Gridpoint fixities of the vertical sides of the box.

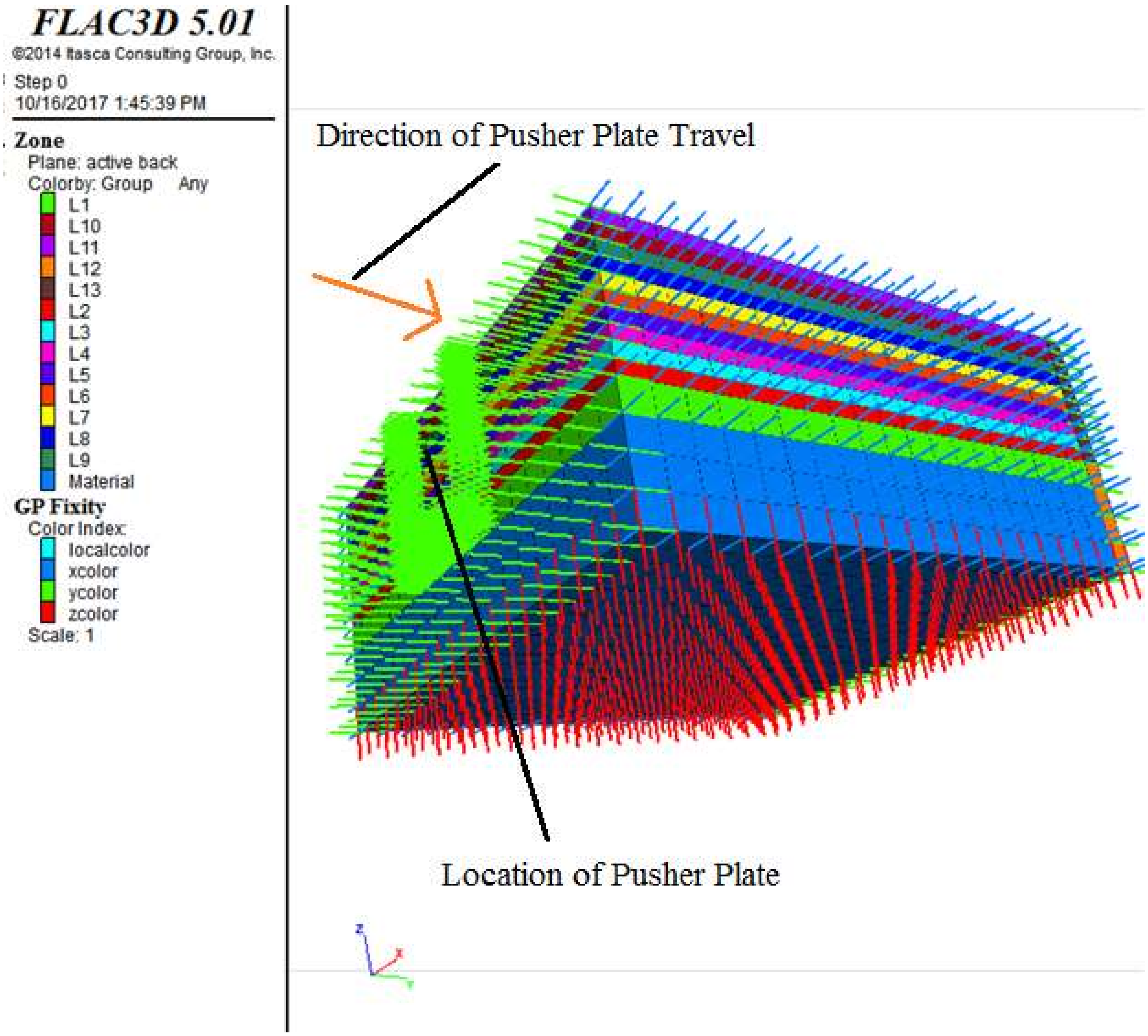

Figure 99: Gridpoint fixities of the bottom of the box

2. Reinforcement

Reinforcement was added to the model using the built in "Geogrid" structural element. Similar to the rest of the geometry, the reinforcement configurations are identical to the 12 reinforcement configurations used in the laboratory testing. Figure 100 is a cut section of a FLAC3D™ grid showing the location of reinforcement for the 8W11L10Lay geometry configuration. "8W11L10Lay" is a code used to describe the test, and will be explained in Chapter V:a.

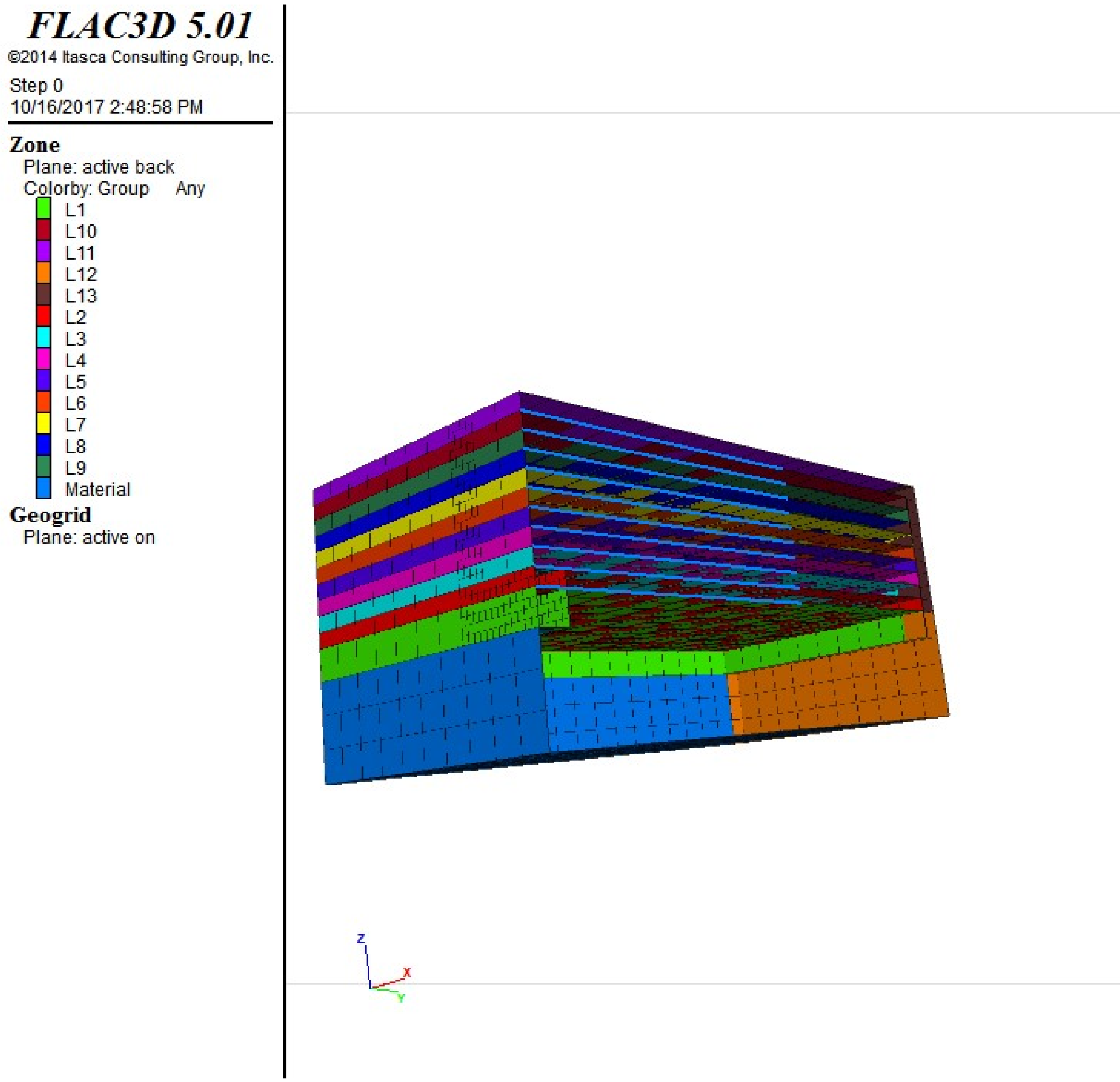

Figure 100: Cut section (x=0 to x=10) showing where reinforcement was added to the model for the 8W11L10Lay simulation. The blue horizontal lines represent the 8W8L10 Lay reinforcement.

ii. FLAC3D™ Model Parameters

The Plastic Hardening constitutive model within the FLAC3D™ software requires the user to input parameters related to the soil specimen, initial stress conditions, and any structural elements, such as reinforcement.

1. Soil

The Plastic Hardening constitutive model requires soil parameters E_{50}^{ref}, E_{ur}^{ref}, m, R_f, and ϕ. E_{50}^{ref} is the secant stiffness at 50% of the ultimate deviatoric stress when $-\sigma_3$ (from triaxial testing) is equal to p^{ref} (atmospheric pressure) and determines the stress-strain behavior before failure. E_{ur}^{ref} is the reference unloading-reloading stiffness modulus when $-\sigma_3$ (from triaxial testing) is equal to p^{ref} (atmospheric pressure). E_{ur}^{ref} influences how the model handles the stress-strain behavior associated with unloading and reloading a specimen. The elastic modulus exponent is m and is used to obtain actual E_{50} moduli from E_{50}^{ref}. R_f is the failure ratio and is used by the program as an input to the shear yield function to determine shear hardening behavior. The friction angle is ϕ and is a shear strength parameter used to determine stress-strain behavior. These can be calibrated to the model using laboratory triaxial results. Calibration was performed according to the method suggested by the Itasca™ Consulting Group (Cheng 2015), creators of FLAC3D™. The calibration procedure is in Appendix J. Table 6 shows the calibrated parameters.

Table 6: Parameters Calibrated in Appendix J

Parameter	Value
R_f	0.912
E_{50}^{ref}	5606 psi
m	0.45
ϕ	36.6º
E_{ur}^{ref}	28030 psi

To test the quality of the calibration, non-reinforced laboratory data was compared to a non-reinforced FLAC3D™ simulation. Initially, the FLAC3D™ simulated data showed a soil that was quite a bit stronger than the actual laboratory test. After a significant reduction in friction angle (ϕ), minor reduction of E_{50}^{ref} and E_{ur}^{ref}, and slight increase of m, the FLAC3D™ simulation provided output that very closely matched the laboratory test data for non-reinforced testing (see Figure 101). Table 7 lists the parameters used in the FLAC3D™ simulation to provide the output given in Figure 101.

Table 7: Parameters Used in FLAC3D™ Simulation

Parameter	Value
R_f	0.912
E_{50}^{ref}	5400 psi
m	0.49
ϕ	18.3º
E_{ur}^{ref}	27000 psi

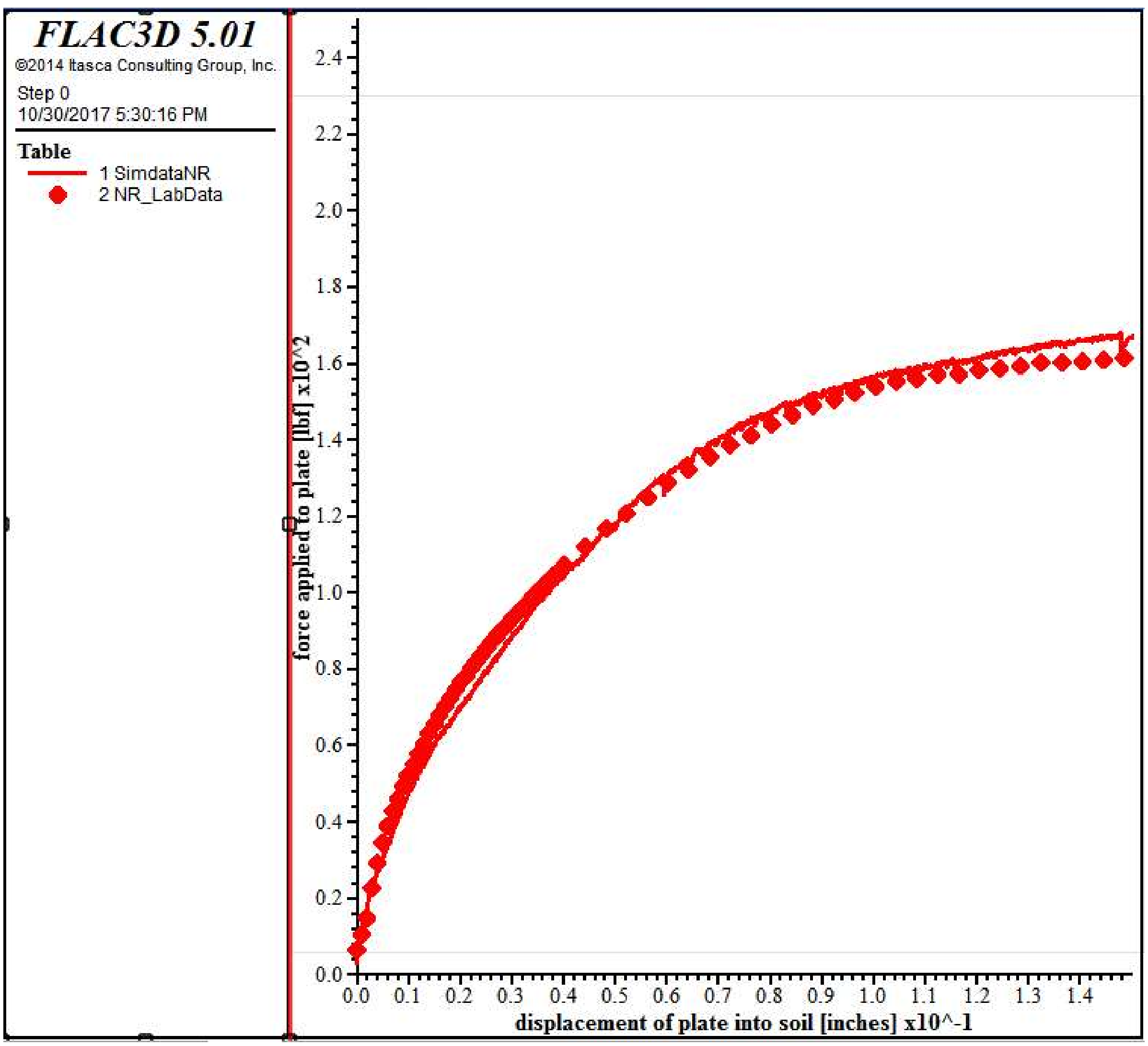

Figure 101: Force vs. Displacement plot for FLAC3D™ simulated data (solid line) and laboratory data (diamond points) for non-reinforced soil

2. Stress Initialization

FLAC3D™ allows the user to input initial stress conditions on the yz, xz, and xy-planes and in the x, y, and z-directions, respectively. The xy-plane represents the bottom of the soil. The initial stresses here were calculated by multiplying the unit weight of soil times the depth of soil. Estimation of the initial horizontal forces (sxx and syy) must consider that vibratory compaction had just occurred on the soil specimen. Research by Chen and Fang (2008) concludes a fairly uniform horizontal stress distribution exists on granular soils compacted with vibration. NAVFAC (1986) also estimates a uniform horizontal stress distribution when vibratory compaction is used. Both of these stress distributions have zero horizontal earth pressure at the soil surface but quickly reach the uniform stress value at a very shallow depth. Due to this, a uniform stress distribution was used for the initial horizontal stresses. However, NAVFAC provides a slight overestimation of the horizontal stresses when compared with the data collected by Chen and Fang. To estimate the magnitude of the uniform horizontal stress distribution, McCarthy (2007) suggests an at-rest earth pressure coefficient value ranging from 0.3 to 0.5. An initial at-rest earth pressure coefficient value of 0.3 was used, but reduced to 0.25, as it provided a better data fit between laboratory and FLAC3D™ results, shown in Figure 101. The initial stress acting on the z-plane in the z-direction was 0.60 psi, while the initial stress acting on both the y-plane in the y-direction and the x plane in the x direction were estimated to be 0.15 psi.

3. Reinforcement

The built-in FLAC3D™ Geogrid structural element was used to model the reinforcement. The Geogrid structural element behaves as an isotropic or orthotropic linear elastic material. Geogrid structural elements exhibit shear-directed frictional interaction with the FLAC3D™ grid in the plane tangent to the geogrid surface. The Geogrid structural element was selected because it is typically used in applications where a flexible membrane that has important shear interaction with the adjacent soil. In this application, geogrid input properties were thickness, Poisson's Ratio, coupling spring friction angle, Young's modulus, and coupling spring stiffness per unit area. To determine reinforcement thickness, a two hundred sheet pad of engineering paper was measured at approximately 19/32" thick, this number was divided by the two hundred sheets to obtain a thickness of 0.0029" thick. A value of 0.33 was used for Poisson's ratio as suggested by Schulgasser (1983). From laboratory testing, the paper-soil interface friction angle was 25° and the soil friction angle was 36.6°. The ratio between the interface friction angle and the soil friction angle was 0.68. To keep this same ratio, the friction angle of the FLAC3D™ soil was multiplied by the ratio of 0.68 to obtain 12.5º. A value of 13º was used for coupling spring friction angle. As Young's modulus and coupling spring stiffness per unit area were not measured, typical values presented in Itasca™ FLAC3D™ examples were used and then modified until the laboratory data and FLAC3D™ simulated data were fairly similar, Figure 102. Young's modulus was 130,000 psi and coupling spring stiffness per unit area was 2.3×10^9 lb/in^3.

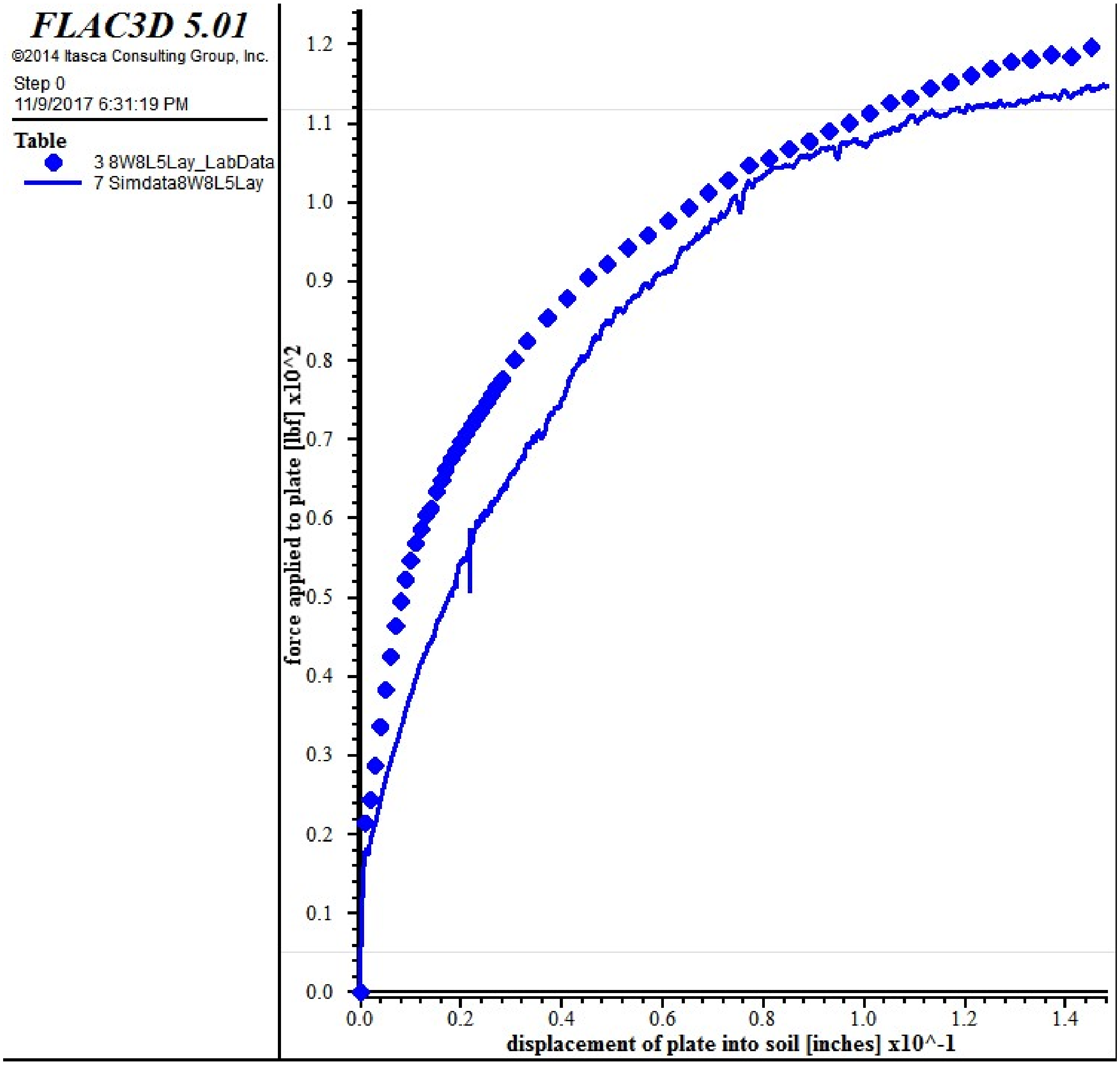

Figure 102: Laboratory data and FLAC3D™ simulated data for 8W8L5Lay reinforcement geometry. The blue diamonds represent laboratory data. The blue solid line represents FLAC3D™ simulated data

After a close match was obtained for the 8W8L5Lay configuration, the properties of soil and reinforcement were held constant. The rest of the reinforcement geometries were simulated with reinforcement geometry configuration as the only variable.

iii. Choice of Constitutive Model

Sixteen constitutive models are available in FLAC3D™ and are categorized into null, elastic, and plastic model groups. This section summarizes each of the sixteen constitutive models, discusses the features of the Plastic Hardening constitutive model, and discusses why the Plastic Hardening constitutive model was chosen for this simulation.

1. Null Model Group

The null model is the only constitutive model in the null model group. Null constitutive models are assigned to represent material that is removed or excavated. Stresses in zones that are assigned the null constitutive model are set to zero.

2. Elastic Model Group

Elastic models are characterized by reversible deformations upon unloading. The models in this group have linear and path-independent stress-strain response. The elastic model group contains the following three constitutive models: elastic, isotropic model, elastic, orthotropic model, and elastic, transversely isotropic model.

a. Elastic, isotropic model

The elastic, isotropic model is the simplest representation of material behavior offered in FLAC3D™. This model is only valid for homogeneous, isotropic, continuous materials that exhibit linear stress-strain behavior and no hysteresis upon unloading.

b. Elastic, orthotropic model

The elastic, orthotropic model allows different elastic material properties to be assigned to three mutually perpendicular planes.

c. Elastic, transversely isotropic model

The elastic, transversely isotropic model allows simulation of layered elastic materials in which there are distinctly different elastic moduli in directions normal and parallel to the layers.

3. Plastic Model Group

The plastic model group allows permanent, path-dependent deformations due to nonlinear stress-strain behavior. The plastic model group contains the following twelve constitutive models: Drucker-Prager, Mohr-Coulomb, ubiquitous-joint, strain-hardening/softening, bilinear strain-hardening/softening ubiquitous-joint, double-yield, modified Cam-clay, Hoek-Brown, modified Hoek-Brown, Cysoil, simplified Cysoil, and Plastic Hardening.

a. Drucker-Prager model

The Drucker-Prager model used in FLAC3D™ uses Drucker-Prager failure criterion with a tension cutoff. This model may be useful to model soft clay materials with low friction angles. However, this model is not generally recommended by FLAC3D™ to model geologic materials and is included to permit comparison of results with other numerical programs.

b. Mohr-Coulomb model

The Mohr-Coulomb model used in FLAC3D™ uses Mohr-Coulomb failure criterion with a tension cutoff. This constitutive model is often used to model sand and concrete with FLAC3D™.

c. Ubiquitous-joint model

The ubiquitous-joint model is an anisotropic plasticity model that allows for the modeling of weak planes within a solid. This model uses Mohr-Coulomb failure criterion with a tension cutoff.

d. Strain-hardening/softening model

The strain-hardening/softening model allows modeling of materials that change strength as they are strained. This model allows nonlinear softening and hardening behavior to be modeled by using prescribed variations of Mohr-Coulomb model properties as functions of deviatoric plastic strain.

e. Bilinear strain-hardening/softening ubiquitous joint model

The bilinear strain-hardening/softening ubiquitous joint model allows for the modeling of weak planes within materials that change strength as they are strained. This constitutive model allows nonlinear softening and hardening behavior to be modeled by using prescribed variations of ubiquitous-joint model properties as functions of deviatoric and tensile plastic strain. The bilinear option allows modeling of material strength properties as they vary with mean stress.

f. Double-yield model

The double-yield model represents materials in which there may be significant, irreversible compaction in addition to shear yielding. Additionally, this model allows for modeling of strain softening/hardening behavior.

g. Modified Cam-clay model

The modified Cam-clay model is an incremental hardening/softening elastoplastic model. This model is used to represent materials where the influence of volume change on bulk property and resistance to shear needs to be considered and is commonly used to model soft clay.

h. Hoek-Brown model

The Hoek-Brown model is used to model intact rock and rock masses. It utilizes a failure criterion with a nonlinear failure surface and is based on the relationship between major and minor principal stresses. The model incorporates a plasticity flow rule that varies as a function of confining stress level.

i. Modified Hoek-Brown model

This model is provided as an alternative to the Hoek-Brown model. The modified Hoek-Brown model characterizes post-failure plastic flow by simple flow rule choices given in terms of a user-specified dilation angle. The model also contains a tensile strength limit similar to the Mohr-Coulomb model. This model allows a factor of safety to be calculated based on the strength reduction method.

j. Cysoil model

The Cysoil model is intended to provide a comprehensive representation of the nonlinear behavior of soils. This model includes frictional strain-hardening and softening shear behavior, an elliptic volumetric cap with strain-hardening behavior, and an elastic modulus function of plastic volumetric strain. The model provides a more accurate representation of the loading/unloading response of soils.

k. Simplified Cysoil model

The simplified Cysoil model utilizes built-in features including a friction-hardening law that uses hyperbolic model parameters as a direct input as well as a Mohr-Coulomb failure envelope with two built-in dilations laws.

l. Plastic Hardening model

The plastic hardening model is an elasto-plastic model intended to provide a more realistic representation of pre-failure stress-strain relation. The model allows different stiffnesses to be used for primary loading and unloading/reloading. The plastic hardening model yield surface is not fixed in the principal stress space, allowing it to expand due to an increase in plastic strain. The model accounts for shear hardening and volumetric hardening.

4. Features of the Plastic Hardening model

The Plastic Hardening model is a shear and volumetric hardening constitutive model that can be easily calibrated using lab tests or in-situ tests. The Plastic Hardening model is suitable for both cohesionless and cohesive soils. It is well established and widely used for a variety of applications including soil-structure interaction. The Plastic Hardening model's ability to accurately model soil-structure interaction makes it particularly attractive for this research that includes geogrid structural elements in addition to soil. The seven main features of the Plastic Hardening model follow:

a. Hyperbolic stress-strain relationship in axial drained compression

b. Plastic strain in mobilizing friction

c. Plastic strain in primary compression

d. Stress-dependent stiffness according to a power law

e. Elastic unloading/reloading compared to virgin loading

f. Memory of pre-consolidation stress

g. Mohr-Coulomb failure criterion

Aside from the elastic unloading/reloading compared to virgin loading and the memory of pre-consolidation stress, the other five main features of the plastic hardening model were expected to provide stress-strain behavior that closely mimicked that of the laboratory testing. After considering the constitutive models available in FLAC3D™ and discussion with Mr. Augusto Lucarelli of the Itasca™ Consulting Group, Inc., the Plastic Hardening model was chosen due to its features that should provide similar stress-strain behavior to that of the laboratory testing in addition to its ability to accurately model soil-structure interaction.

iv. Application of Pusher Plate Strain to the Model

In the laboratory testing, the pusher plate applied consistent strain perpendicular to the face of the soil specimen. To model this in FLAC3D™, the gridpoints corresponding to the location of the pusher plate were given a small velocity in the y-direction (into the soil specimen). This y-velocity represents the distance that the gridpoints corresponding to the pusher plate will move into the soil specimen per step. A y-velocity of 0.125×10^{-6} was assigned to the gridpoints corresponding to the pusher plate for 1,200,000 steps totaling 0.15” of deformation into the soil specimen. To determine the y-velocity, a very small velocity was first used and the velocity was increased slowly until inertial effects were seen. The highest velocity where inertial effects were not observed was used to reduce steps and reduce overall program run time.

v. Obtaining FLAC3D™ Results

To obtain the FLAC3D™ results, histories were recorded of: a gridpoint within the pusher plate range to represent displacement; the summation of the forces in the y-direction of all of the gridpoints within the pusher plate range to represent force on the plate. After histories are recorded, force vs. displacement data were plotted in FLAC3D™ and also written to a text file used in Excel for further analysis.

Chapter IV: Presentation of Results

This chapter presents the results of laboratory testing and FLAC3D™ modeling.

a. Laboratory Testing

Thirty nine laboratory tests were performed with varying reinforcement geometry configurations to determine the effect of reinforcement on load-deformation characteristics as well as failure surface location. A description of the laboratory test is provided in Chapter III:a.iv. Testing Procedure.

Nomenclature of each of the thirty nine laboratory tests is as follows:

- NR stands for Non-Reinforced, A number 2 or 3 following the NR string indicates the second or third run.
- Reinforced specimens are in the form _W_L_Lay. W stands for Wide, L stands for Long and Lay is the number of Layers in the specimen. The blanks are filled with geometric information or layer numbering information. For example 8W8L5Lay would be read as, "8 inches wide, 8 inches long, 5 layers of reinforcement." A number 2 or 3 following the _W_L_Lay string indicates the second or third run of the same geometry.
- Three widths were tested: Plate (P) which is the 5.5" width of the pusher plate, 8" (8), and 11" (11). Two lengths were tested: 8" (8) and 11" (11). Two layering schemes were tested: 10 layers (10) and 5 layers (5). 10 layer specimens are spaced at 0.5" vertical spacing and 5 layer specimens are spaced at 1" vertical spacing.

i. Load-Deformation Characteristics

During laboratory testing, load-deformation data were recorded with GeoJac software and plotted using an Excel spreadsheet. Figure 103 is a typical load-deformation plot showing how key information is obtained. Key information from a load-deformation plot is: Peak Force, displacement where Peak Force occurred, Residual Force, and stiffness at 50% of the Peak Force value. Peak Force is defined as the largest force applied to the specimen during a test. Displacement where Peak Force occurred is the horizontal plate displacement into the specimen corresponding to the Peak Force. As the test was terminated at 0.6 inches, Residual Force is defined as the force applied to the specimen at 0.6 inches of displacement. Stiffness at 50% of the Peak Force value, K_{50}, is the slope of the line defined by the point of origin and the point on the load-deformation plot where 50% of the Peak Force value occurs.

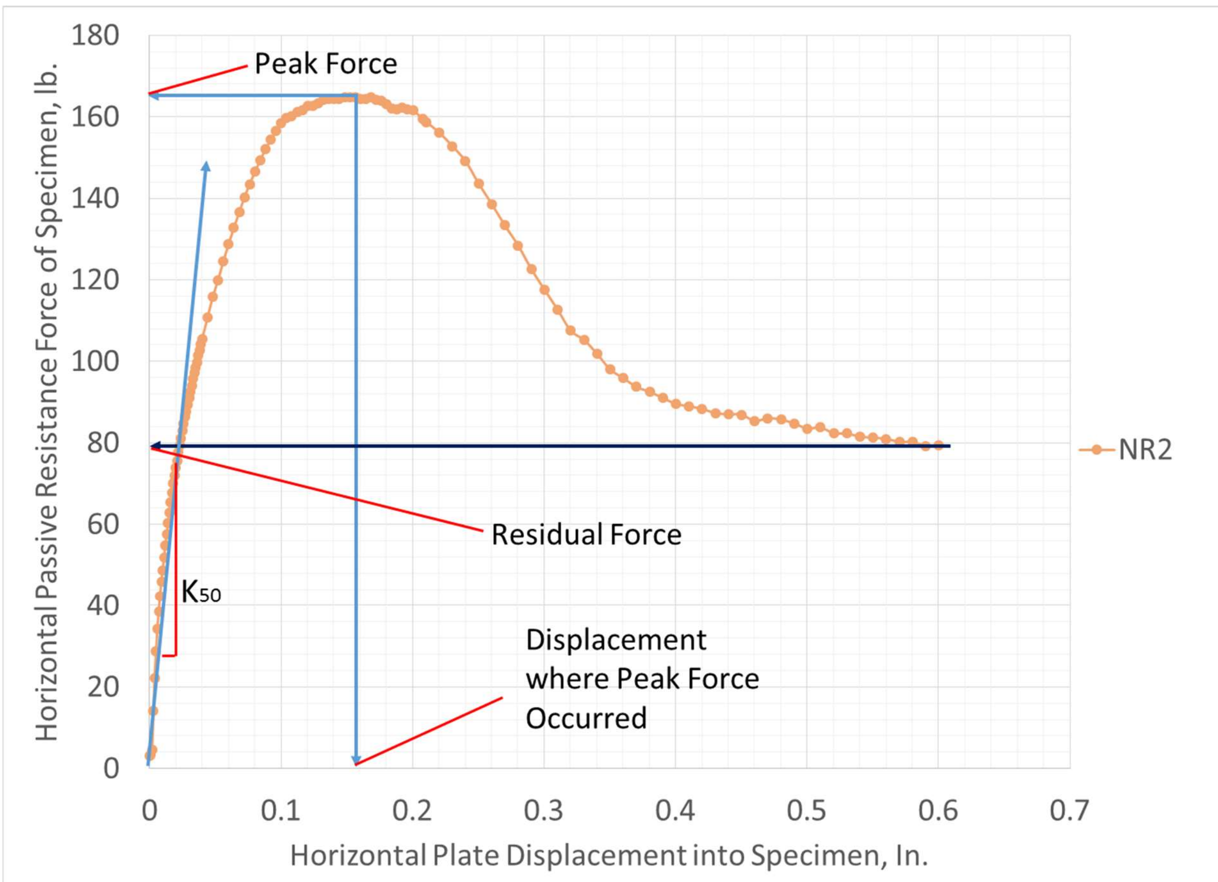

Figure 103: Typical Load-Deformation Plot with Peak Force, Residual Force, Displacement where Peak Force occurred, and Stiffness at 50% of Peak Force (K_{50}) labeled

Table 8 gives the Peak Force, Residual Force, displacement where Peak Force occurred, and stiffness at 50% of Peak Force data for the thirty nine laboratory tests.

Table 8: Summary of Peak Force, Peak Force Displacement, Residual Force, and K_{50} Data for Laboratory Tests

Test Name	Peak Force, lb.	Residual Force, lb.	Peak Force Displacement, in.	K_{50}, lb./in.
8W8L5Lay	133.65	82.77	0.188	3969
8W8L5Lay2	114.79	61.25	0.186	4988
8W8L10Lay	131.89	76.27	0.176	5072
8W8L10Lay2	123.37	61.25	0.157	5140
8W11L5Lay	124.10	87.09	0.168	4773
8W11L5Lay2	123.02	80.24	0.159	5169
8W11L10Lay	145.03	80.04	0.100	7259
8W11L10Lay2	151.90	85.94	0.141	7165
11W8L5Lay	143.69	105.44	0.184	5322
11W8L5Lay2	127.47	89.92	0.183	5058
11W8L10Lay	148.53	96.20	0.124	5847
11W8L10Lay2	141.40	82.16	0.124	5050
11W11L5Lay	125.88	92.10	0.098	7676
11W11L5Lay2	126.16	97.50	0.081	7008
11W11L10Lay	157.40	83.69	0.096	7870
11W11L10Lay2	154.62	102.98	0.072	7092
PW8L5Lay	122.15	81.24	0.184	2395
PW8L5Lay2	120.72	63.97	0.165	3773
PW8L10Lay	118.83	61.06	0.180	4951
PW8L10Lay2	126.13	59.83	0.158	4204
PW11L5Lay	113.36	75.74	0.135	4360
PW11L5Lay2	124.52	68.08	0.184	4016
PW11L10Lay	117.30	70.81	0.113	5586
PW11L10Lay2	122.60	65.98	0.080	6811
NR1	157.68	74.36	0.149	3937
NR2	164.89	79.34	0.156	3383
8W8L5Lay3	113.14	75.60	0.160	4526
8W8L10Lay3	131.42	64.87	0.128	6917
8W11L5Lay3	111.69	64.08	0.142	5585
8W11L10Lay3	120.91	59.43	0.071	6232
11W8L5Lay3	114.45	83.50	0.173	4769
11W8L10Lay3	120.98	106.27	0.078	5260
11W11L5Lay3	107.84	81.54	0.141	5392
11W11L10Lay3	124.30	95.65	0.056	5947
PW8L5Lay3	79.37	63.22	0.192	4008
PW8L10Lay3	80.34	72.93	0.110	4671
PW11L5Lay3	100.00	73.79	0.184	4808
PW11L10Lay3	90.73	71.79	0.072	4775
NR3	162.88	71.57	0.152	3381.2

ii. Failure Surface Definition

The failure surface for one test of each reinforcement geometry was defined using painted horizontal layers according to the procedure outlined in Chapter III:a.i.7. Additionally, creases in the reinforcement indicate areas of shear strain in the confined soil. These creases allow a failure surface to be defined in a fashion similar to the surface defined by painting soil layers. However, this surface can only be defined within the boundaries of the reinforcement geometry. Failure surface location interpretation should take this into account. Failure surface contours with respect to depth from the test soil surface are presented in Appendix G for the creased reinforcement as well as the painted horizontal layer instrumentation scheme. Appendix H shows the mid plate failure surface on a vertical plane which is derived from the data presented in Appendix G.

b. FLAC3D™ Modeling

i. Introduction

Thirteen FLAC3D™ simulations were performed with varying reinforcement geometries to determine the effect of reinforcement on load-deformation characteristics. The FLAC3D™ simulations modeled the same geometry configurations tested in the laboratory.

Each test was given a code name. The code key for the thirteen FLAC3D™ simulations is: NR stands for Non-Reinforced. Reinforced specimens are in the form _W_L_Lay. W stands for Wide (the y direction), L stands for Long (the x direction) and Lay is the number of reinforcement Layers in the specimen. The blanks are filled with geometric information or layer numbering information. For example, 8W8L5Lay would be read as, "8 inches wide, 8 inches long, 5 layers of reinforcement." Three widths were simulated: Plate (P) which is the 5.5" width of the pusher plate, 8" (8), and 11" (11). Two lengths were tested: 8" (8) and 11" (11). Two layering schemes were tested: 10 layers (10) and 5 layers (5). 10 layer specimens have 0.5" vertical spacing and 5 layer specimens have 1" vertical spacing.

ii. Load-Deformation Characteristics

During FLAC3D™ simulations, load-deformation data were recorded with FLAC3D™ software, exported to a text file, and plotted using a Microsoft Excel spreadsheet. A typical load-deformation plot showing how key information is obtained is shown in Figure 104. The key data from load-deformation plots are: Peak Force, and stiffness at 50% of the Peak Force value. Peak Force is defined as the largest force applied to the specimen during a test. Stiffness at 50% of the Peak Force value, K_{50}, is the slope of the line defined by the point of origin and the point on the load-deformation plot where 50% of the Peak Force value occurs, a secant stiffness.

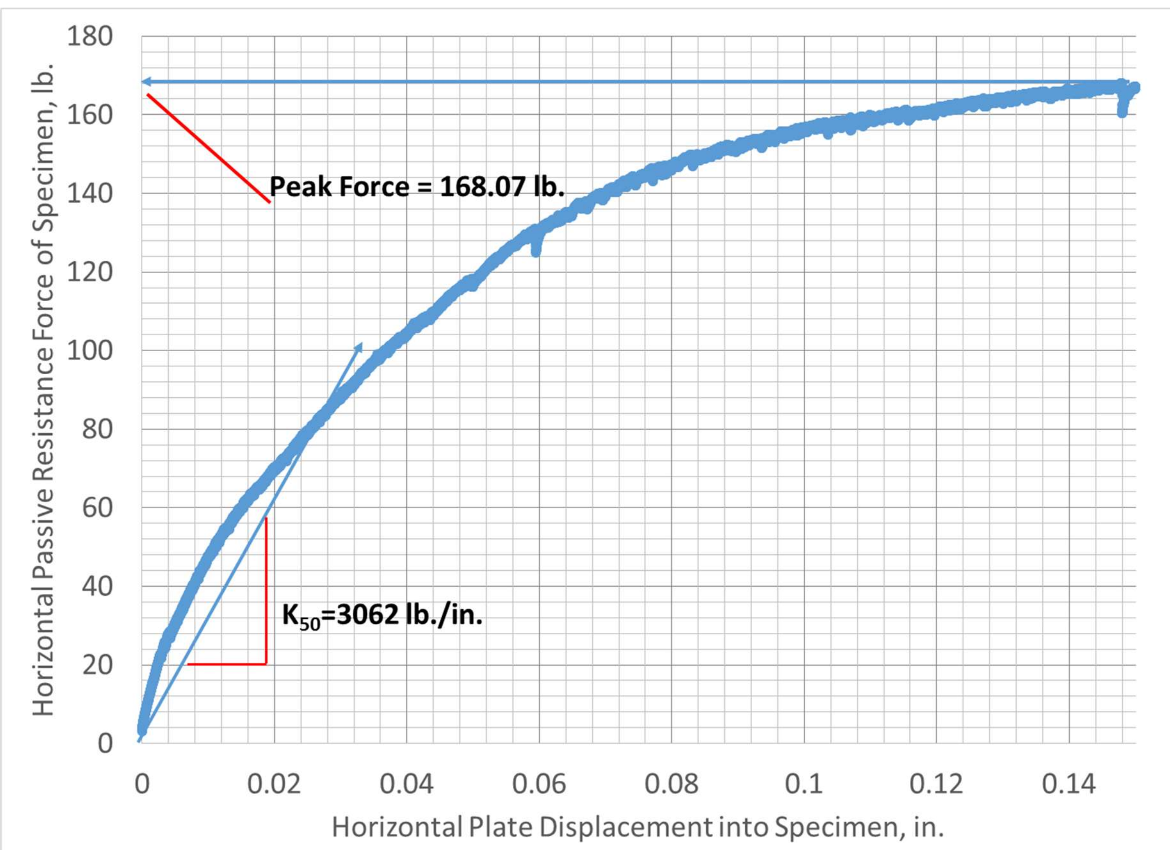

Figure 104: Typical FLAC3D™ Load-Deformation Plot with Peak Force and Stiffness at 50% of Peak Force (K_{50}) labeled

Peak Force and stiffness at 50% of Peak Force data are summarized for each of the thirty nine FLAC3D™ simulations in Table 9.

Table 9: Summary of Peak Force and K_{50} Data for FLAC3D™ simulations. PW is the width of the pusher plate (5.5")

Test Name	Peak Force, lb.	K_{50}, lb./in.
8W8L5Lay	114.92	2612
8W8L10Lay	119.94	3415
8W11L5Lay	121.60	2911
8W11L10Lay	123.55	3831
11W8L5Lay	116.37	2629
11W8L10Lay	121.12	3953
11W11L5Lay	114.93	2953
11W11L10Lay	123.09	3679
PW8L5Lay	114.90	2786
PW8L10Lay	117.97	3646
PW11L5Lay	115.73	2853
PW11L10Lay	134.40	3117
NR (not reinforced)	168.07	3062

Chapter V: Analysis and Discussion of Results

Thirty nine laboratory tests were performed with varying reinforcement geometry configurations to determine the effect of reinforcement spacing, width, length, and surface area on load-deformation characteristics and failure surface location.

a. Laboratory Testing

The suite of tests performed during laboratory testing was designed to isolate the geometric variables vertical spacing, reinforcement width, and reinforcement length. Peak Force, Residual Force, the displacement where Peak Force occurred, and the stiffness at 50% of the Peak Force (K_{50}) were identified as key points of interest because each of these are important descriptors of the response of mechanically stabilized soil when loaded passively. The effect of each geometric variable on each key point of interest is examined in this section. The effect of each geometric variable on the location of the failure surface is also examined.

i. Effect of Reinforcement Vertical Spacing

1. Load Deformation Characteristics

a. Peak Force

To determine the effect of reinforcement vertical spacing on Peak Force, Peak Force vs. vertical spacing was plotted for each reinforcement width and length combination. After plotting, an initial observation was made, linear regression analysis was performed for data with vertical spacing as the only measurable variable, analysis of variance (ANOVA) was performed for data with vertical spacing as the only measurable variable, and linear regression analysis was performed for all of the data points with length and width as known variables.

i. Initial Observation

Initial observation was made after plotting Peak Force vs. vertical spacing, Figure 105.

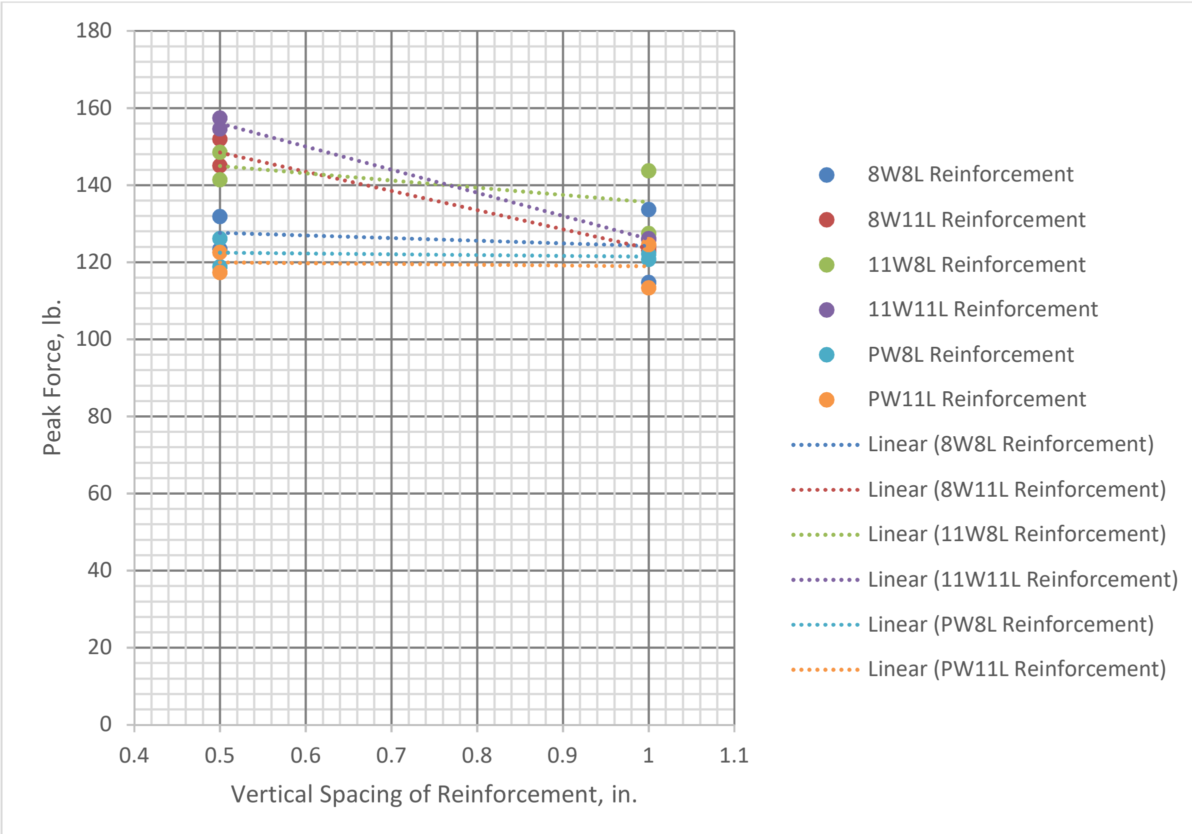

Figure 105: Peak Force vs. vertical spacing for various reinforcement widths and lengths with linear trend lines (results of 24 tests)

After plotting, linear trend lines were added for each width and length combination to determine if any data trends were apparent. Table 10 shows the observed trends.

Table 10: Observed trends for Peak Force values as vertical spacing increases from 0.5” to 1”

Width and Length Combination	Peak Force Trend as Vertical Spacing Increases
PW8L	None
PW11L	None
8W8L	None
8W11L	Decrease
11W8L	Slight Decrease
11W11L	Decrease

While two tests showed a decrease in Peak Force as vertical spacing increased, most tests showed either no discernable trend or only a slight trend. Due to this, the initial observation is made that reinforcement vertical spacing has negligible effect on Peak Force.

ii. Single Variable Linear Regression Analysis

A linear regression analysis was performed to determine the significance of change in Peak Force when the single variable, reinforcement vertical spacing, is modified. Six sets of reinforcement widths and lengths were tested. For each reinforcement width and length set, two tests of two different reinforcement vertical spacings were evaluated resulting in four data points. A t-test was performed at a 90% confidence interval. For each data set, a t* value was calculated and compared to a t value corresponding to a 90% confidence interval and 4 data points. Two alternatives exist for the two sided test: acceptance of the null hypothesis, or acceptance of the alternate hypothesis. The null hypothesis concludes that there is no relationship between Peak Force and reinforcement vertical spacing. The alternate hypothesis concludes that there is a relationship between Peak Force and reinforcement vertical spacing. If the t* value is greater than the t value, the alternate hypothesis is chosen. If the t* value is less than or equal to the t value, the null hypothesis is chosen. P-values were also computed as p-values less than the level of significance support the alternate hypothesis. Each data set was plotted with reinforcement vertical spacing on the abscissa and Peak Force on the ordinate. A linear best fit line was added and the slope of this line was computed. Table 11 summarizes the linear regression analysis.

Table 11: Linear regression analysis results for effect of reinforcement vertical spacing on Peak Force. "Null Hypothesis" indicates that there is not a statistically significant relationship between the two variables, while "Alternate Hypothesis" indicates that there is a statistically significant relationship.

Reinforcement Width and Length	|t*|	t(0.95;2)	Decision	P-Value	Best Fit Line Slope
PW8L	0.28	2.92	Null Hypothesis	0.805	-2.09
PW11L	0.16	2.92	Null Hypothesis	0.89	-2.02
8W8L	0.33	2.92	Null Hypothesis	0.77	-6.82
8W11L	7.16	2.92	Alternate Hypothesis	0.019	-49.81
11W8L	1.06	2.92	Null Hypothesis	0.4	-18.77
11W11L	21.47	2.92	Alternate Hypothesis	0.002	-59.98

From the linear regression analysis, four of six data sets show that a relationship does not exist between reinforcement vertical spacing and Peak Force. All of the decisions are supported by corresponding p-values. Best fit lines have only negative slopes, showing that a negative relationship between reinforcement vertical spacing and Peak Force may be a possibility but is still unlikely. Due to four tests failing the t-test, a relationship between vertical spacing and Peak Force is unlikely.

iii. Analysis of Variance

A single factor ANOVA was performed to determine if the mean value of the Peak Force data populations are equal when the single variable, reinforcement vertical spacing, is modified. Six sets of reinforcement widths and lengths were tested. For each reinforcement width and length set, two tests of two different reinforcement vertical spacings were evaluated resulting in four data points. A 90% confidence interval was used for the ANOVA. For each data set, an F value was computed as well as a critical F value. The alternate hypothesis states that at least one of the means of each data population is different. The null hypothesis states that the means of each data population are equal. If F exceeds $F_{critical}$, the null hypothesis is rejected and at least one of the means of the populations is different. Table 12 shows the results of the ANOVA.

Table 12: Results of ANOVA for Peak Force data as vertical spacing increases from 0.5" to 1"

Reinforcement Width and Length	F	$F_{critical}$	Decision
PW8L	0.079	8.526	Null Hypothesis
PW11L	0.027	8.526	Null Hypothesis
8W8L	0.109	8.526	Null Hypothesis
8W11L	51.300	8.526	Alternate Hypothesis
11W8L	1.122	8.526	Null Hypothesis
11W11L	460.829	8.526	Alternate Hypothesis

All six ANOVA results support the linear regression analysis results.

b. Residual Force

To determine the effect of reinforcement vertical spacing on Residual Force, Residual Force vs. vertical spacing was plotted for each reinforcement width and length combination. After plotting, an initial observation was made, linear regression analysis was performed for data with vertical spacing as the only measurable variable, analysis of variance (ANOVA) was performed for data with vertical spacing as the only measurable variable, and linear regression analysis was performed for all of the data points with length and width as known variables.

i. Initial Observation

Initial observation was made after plotting Residual Force vs. vertical spacing, Figure 106.

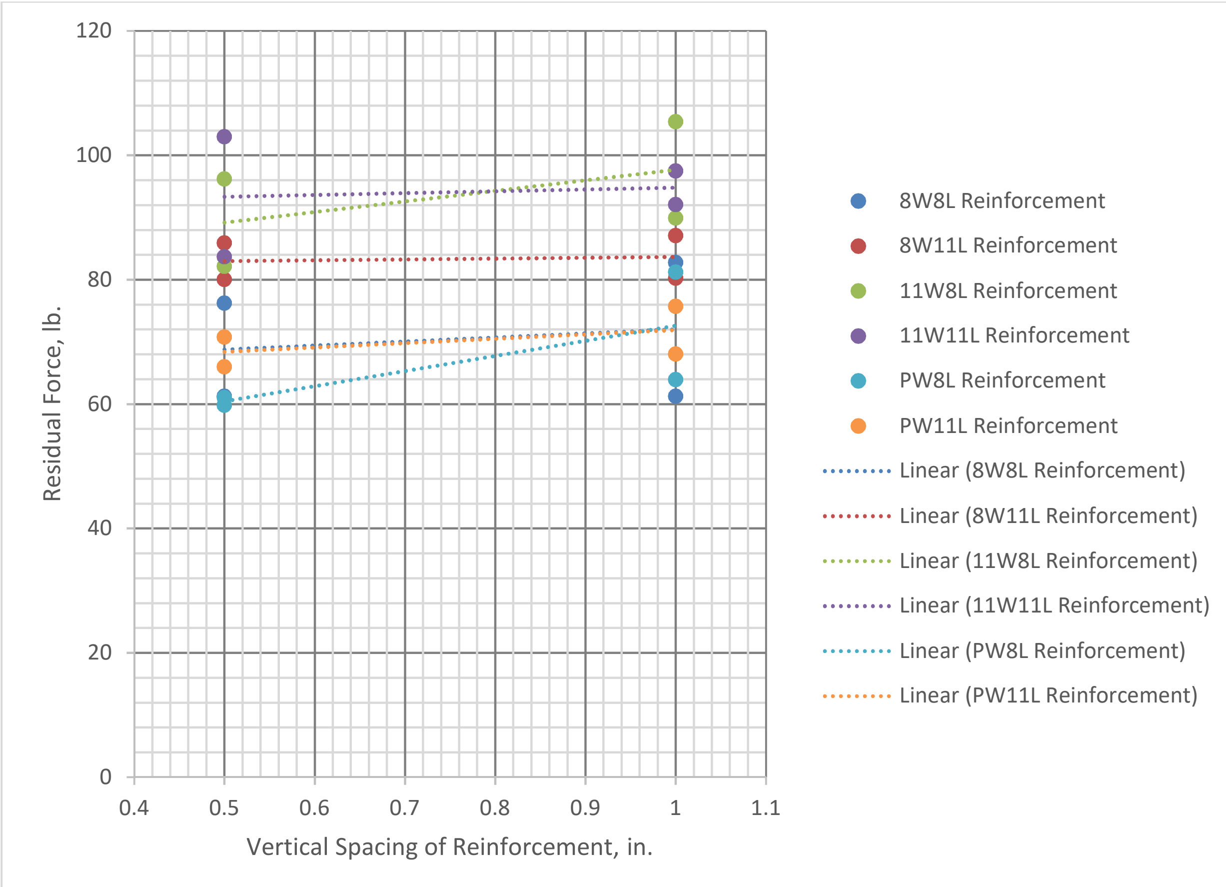

Figure 106: Residual Force vs. vertical spacing for various reinforcement width and lengths with linear trend lines (results of 24 tests)

After plotting, linear trend lines were added for each width and length combination to determine if any data trends were apparent. Table 13 shows the observed trends.

Table 13: Observed trends for Residual Force values as vertical spacing increases from 0.5" to 1"

Width and Length Combination	Residual Force Trend as Vertical Spacing Increases
PW8L	Slight Increase
PW11L	None
8W8L	None
8W11L	None
11W8L	Slight Increase
11W11L	None

While two tests showed a slight increase as vertical spacing increased, most tests showed no discernable trend. Due to this, the initial observation is made that reinforcement vertical spacing has negligible effect on Residual Force.

ii. Single Variable Linear Regression Analysis

A linear regression analysis was performed to determine the significance of change in Residual Force when the single variable, reinforcement vertical spacing, is modified. Six sets of reinforcement widths and lengths were tested. For each reinforcement width and length set, two tests of two different reinforcement vertical spacings were evaluated resulting in four data points. A t-test was performed at a 90% confidence interval. For each data set, a t* value was calculated and compared to a t value corresponding to a 90% confidence interval and 4 data points. Two alternatives exist for the two sided test: acceptance of the null hypothesis, or acceptance of the alternate hypothesis. The null hypothesis concludes that there is no relationship between Residual Force and reinforcement vertical spacing. The alternate hypothesis concludes that there is a relationship between Residual Force and reinforcement vertical spacing. If the t* value is greater than the t value, the alternate hypothesis is chosen. If the t* value is less than or equal to the t value, the null hypothesis is chosen. P-values were also computed as p-values less than the level of significance support the alternate hypothesis. Each data set was plotted with reinforcement vertical spacing on the abscissa and Residual Force on the ordinate. A linear best fit line was added and the slope of this line was computed. Table 14 summarizes the linear regression analysis.

Table 14: Linear regression analysis results for effect of reinforcement vertical spacing on Residual Force. "Null Hypothesis" indicates that there is not a statistically significant relationship between the two variables, while "Alternate Hypothesis" indicates that there is a statistically significant relationship.

Reinforcement Width and Length	|t*|	t(0.95;2)	Decision	P-Value	Best Fit Line Slope
PW8L	1.4	2.92	Null Hypothesis	0.3	23.52
PW11L	0.78	2.92	Null Hypothesis	0.52	7.03
8W8L	0.25	2.92	Null Hypothesis	0.83	6.5
8W11L	0.149	2.92	Null Hypothesis	0.89	1.35
11W8L	0.812	2.92	Null Hypothesis	0.5	17
11W11L	0.146	2.92	Null Hypothesis	0.9	2.93

From the linear regression analysis, all of the six data sets show that a relationship does not exist between reinforcement vertical spacing and Residual Force. All of the decisions are supported by corresponding p-values. Best fit lines have only positive slopes, showing that a positive relationship between reinforcement vertical spacing and Residual Force may be a possibility but is still unlikely. Due to all tests failing the t-test, a relationship between vertical spacing and Residual Force is unlikely.

iii. Analysis of Variance

A single factor ANOVA was performed to determine if the mean value of the Residual Force data populations are equal when the single variable, reinforcement vertical spacing, is modified. Six sets of reinforcement widths and lengths were tested. For each reinforcement width and length set, two tests of two different reinforcement vertical spacings were evaluated resulting in four data points. A 90% confidence interval was used for the ANOVA. For each data set, an F value was computed as well as a critical F value. The alternate hypothesis states that at least one of the means of each data population is different. The null hypothesis states that the means of each data population are equal. If F exceeds $F_{critical}$, the null hypothesis is rejected and at least one of the means of the populations is different. Table 15 shows the results of the ANOVA.

Table 15: Results of ANOVA for Residual Force data as vertical spacing increases from 0.5" to 1"

Reinforcement Width and Length	F	$F_{critical}$	Decision
PW8L	1.973	8.526	Null Hypothesis
PW11L	0.602	8.526	Null Hypothesis
8W8L	0.061	8.526	Null Hypothesis
8W11L	0.022	8.526	Null Hypothesis
11W8L	0.660	8.526	Null Hypothesis
11W11L	0.021	8.526	Null Hypothesis

All six ANOVA results support the linear regression analysis results.

c. Peak Force Displacement

To determine the effect of reinforcement vertical spacing on Peak Force Displacement, Peak Force Displacement vs. vertical spacing was plotted for each reinforcement width and length combination. After plotting, an initial observation was made, linear regression analysis was performed for data with vertical spacing as the only measurable variable, analysis of variance (ANOVA) was performed for data with vertical spacing as the only measurable variable, and linear regression analysis was performed for all of the data points with length and width as known variables.

i. Initial Observation

Initial observation was made after plotting Peak Force Displacement vs. vertical spacing, Figure 107.

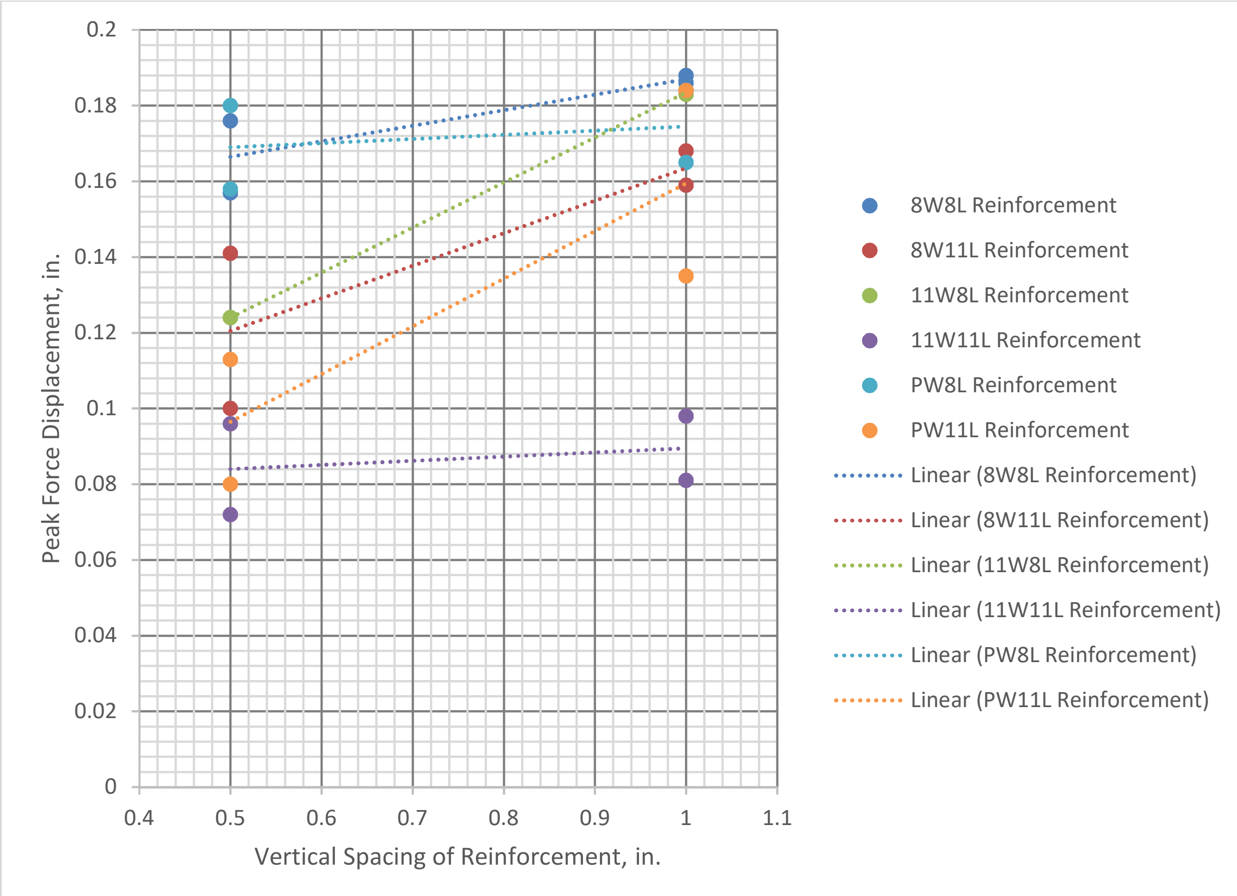

Figure 107: Peak Force Displacement vs. vertical spacing for various reinforcement width and lengths with linear trend lines (results of 24 tests)

After plotting, linear trend lines were added for each width and length combination to determine if any data trends were apparent. Table 16 shows the observed trends.

Table 16: Observed trends for Peak Force Displacement values as vertical spacing increases from 0.5” to 1”

Width and Length Combination	Peak Force Displacement Trend as Vertical Spacing Increases
PW8L	Slight Increase
PW11L	Increase
8W8L	Increase
8W11L	Increase
11W8L	Increase
11W11L	Slight Increase

Four tests showed a definite increase in Peak Force Displacement while two test showed at least a slight increase in Peak Force Displacement with increasing vertical spacing. Due to this, the initial observation is made that increasing reinforcement vertical spacing results in an increased Peak Force Displacement.

ii. Single Variable Linear Regression Analysis

A linear regression analysis was performed to determine the significance of change in Peak Force Displacement when the single variable, reinforcement vertical spacing, is modified. Six sets of reinforcement widths and lengths were tested. For each reinforcement width and length set, two tests of two different reinforcement vertical spacings were evaluated resulting in four data points. A t-test was performed at a 90% confidence interval. For each data set, a t* value was calculated and compared to a t value corresponding to a 90% confidence interval and 4 data points. Two alternatives exist for the two sided test: acceptance of the null hypothesis or acceptance of the alternate hypothesis. The null hypothesis concludes that there is no relationship between Peak Force Displacement and reinforcement vertical spacing. The alternate hypothesis concludes that there is a relationship between Peak Force Displacement and reinforcement vertical spacing. If the t* value is greater than the t value, the alternate hypothesis is chosen. If the t* value is less than or equal to the t value, the null hypothesis is chosen. P-values were also computed as p-values less than the level of significance support the alternate hypothesis. Each data set was plotted with reinforcement vertical spacing on the abscissa and Peak Force Displacement on the ordinate. A linear best fit line was added and the slope of this line was computed. Table 17 summarizes the linear regression analysis.

Table 17: Linear regression analysis results for effect of reinforcement vertical spacing on Peak Force Displacement. "Null Hypothesis" indicates that there is not a statistically significant relationship between the two variables, while "Alternate Hypothesis" indicates that there is a statistically significant relationship.

Reinforcement Width and Length	|t*|	t(0.95;2)	Decision	P-Value	Best Fit Line Slope
PW8L	0.378	2.92	Null Hypothesis	0.74	0.011
PW11L	2.13	2.92	Null Hypothesis	0.167	0.011
8W8L	2.14	2.92	Null Hypothesis	0.17	0.041
8W11L	2.05	2.92	Null Hypothesis	0.18	0.086
11W8L	119	2.92	Alternate Hypothesis	7E-06	0.119
11W11L	0.374	2.92	Null Hypothesis	0.74	0.011

From the linear regression analysis, five of the six data sets show that a relationship does not exist between reinforcement vertical spacing and Peak Force Displacement. All of the decisions are supported by corresponding p-values. Best fit lines have only positive slopes, showing that a positive relationship between reinforcement vertical spacing and Peak Force Displacement may be a possibility but is still unlikely. Due to all but one test failing the t-test, a relationship between vertical spacing and Peak Force Displacement is unlikely.

iii. Analysis of Variance

A single factor ANOVA was performed to determine if the mean value of the Peak Force Displacement data populations are equal when the single variable, reinforcement vertical spacing, is modified. Six sets of reinforcement widths and lengths were tested. For each reinforcement width and length set, two tests of two different reinforcement vertical spacings were evaluated resulting in four data points. A 90% confidence interval was used for the ANOVA. For each data set, an F value was computed as well as a critical F value. The alternate hypothesis states that at least one of the means of each data population is different. The null hypothesis states that the means of each data population are equal. If F exceeds $F_{critical}$, the null hypothesis is rejected and at least one of the means of the populations is different. Table 18 shows the results of the ANOVA.

Table 18: Results of ANOVA for Peak Force Displacement data as vertical spacing increases from 0.5" to 1"

Reinforcement Width and Length	F	$F_{critical}$	Decision
PW8L	0.143	8.526	Null Hypothesis
PW11L	4.549	8.526	Null Hypothesis
8W8L	4.605	8.526	Null Hypothesis
8W11L	4.198	8.526	Null Hypothesis
11W8L	14161	8.526	Alternate Hypothesis
11W11L	0.021	8.526	Null Hypothesis

All six ANOVA results support the linear regression analysis results.

d. K_{50}

To determine the effect of reinforcement vertical spacing on K_{50}, K_{50} vs. vertical spacing was plotted for each reinforcement width and length combination. After plotting, an initial observation was made, linear regression analysis was performed for data with vertical spacing as the only measurable variable, analysis of variance (ANOVA) was performed for data with vertical spacing as the only measurable variable, and linear regression analysis was performed for all of the data points with length and width as known variables.

i. Initial Observation

Initial observation was made after plotting K_{50} vs. vertical spacing, Figure 108.

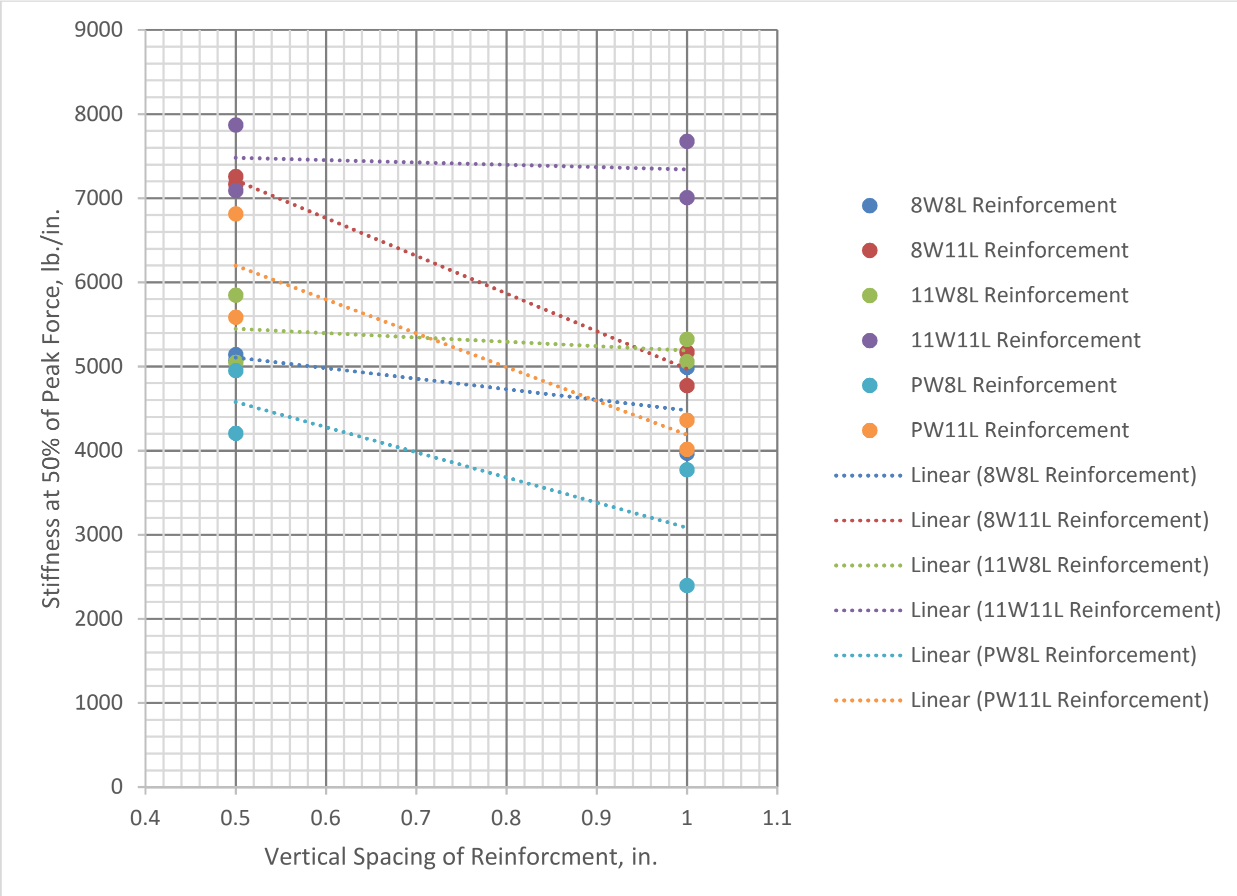

Figure 108: K_{50} vs. vertical spacing for various reinforcement width and lengths with linear trend lines (results of 24 tests)

After plotting, linear trend lines were added for each width and length combination to determine if any data trends were apparent. Table 19 shows the observed trends.

Table 19: Observed trends for K_{50} values as vertical spacing increases from 0.5” to 1”

Width and Length Combination	**K_{50} Trend as Vertical Spacing Increases**
PW8L	Decrease
PW11L	Decrease
8W8L	None
8W11L	Decrease
11W8L	None
11W11L	None

Half of the tests showed a noticeable decrease in K_{50} with increasing vertical spacing while the other half showed no trend. However, the tests showing no real trend had a very slight decrease in K_{50} with increasing vertical spacing. Due to this, the initial observation is made that increasing reinforcement vertical spacing results in a decreased K_{50} value.

ii. Single Variable Linear Regression Analysis

A linear regression analysis was performed to determine the significance of change in K_{50} when the single variable, reinforcement vertical spacing, is modified. Six sets of reinforcement widths and lengths were tested. For each reinforcement width and length set, two tests of two different reinforcement vertical spacings were evaluated resulting in four data points. A t-test was performed at a 90% confidence interval. For each data set, a t* value was calculated and compared to a t value corresponding to a 90% confidence interval and 4 data points. Two alternatives exist for the two sided test: acceptance of the null hypothesis, or acceptance of the alternate hypothesis. The null hypothesis concludes that there is no relationship between K_{50} and reinforcement vertical spacing. The alternate hypothesis concludes that there is a relationship between K_{50} and reinforcement vertical spacing. If the t* value is greater than the t value, the alternate hypothesis is chosen. If the t* value is less than or equal to the t value, the null hypothesis is chosen. P-values were also computed as p-values less than the level of significance support the alternate hypothesis. Each data set was plotted with reinforcement vertical spacing on the abscissa and K_{50} on the ordinate. A linear best fit line was added and the slope of this line was computed. Table 20 summarizes the linear regression analysis.

Table 20: Linear regression analysis results for effect of reinforcement vertical spacing on K_{50}. "Null Hypothesis" indicates that there is not a statistically significant relationship between the two variables, while "Alternate Hypothesis" indicates that there is a statistically significant relationship.

Reinforcement Width and Length	|t*|	t(0.95;2)	Decision	P-Value	Best Fit Line Slope
PW8L	1.9	2.92	Null Hypothesis	0.2	-2987
PW11L	3.16	2.92	Alternate Hypothesis	0.087	-4021
8W8L	1.23	2.92	Null Hypothesis	0.34	-1255
8W11L	11.01	2.92	Alternate Hypothesis	0.008	-4482
11W8L	0.615	2.92	Null Hypothesis	0.6	-517
11W11L	0.271	2.92	Null Hypothesis	0.81	-278

From the linear regression analysis, four of the six data sets show that a relationship does not exist between reinforcement vertical spacing and K_{50}. All of the decisions are supported by corresponding p-values. Best fit lines have only negative slopes, showing that a negative relationship between reinforcement vertical spacing and K_{50} may be a possibility but is still unlikely. Due to four of six data sets failing the t-test, a relationship between vertical spacing and K_{50} is unlikely.

iii. Analysis of Variance

A single factor ANOVA was performed to determine if the mean value of the Peak Force data populations are equal when the single variable, reinforcement vertical spacing, is modified. Six sets of reinforcement widths and lengths were tested. For each reinforcement width and length set, two tests of two different reinforcement vertical spacings were evaluated resulting in four data points. A 90% confidence interval was used for the ANOVA. For each data set, an F value was computed as well as a critical F value. The alternate hypothesis states that at least one of the means of each data population is different. The null hypothesis states that the means of each data population are equal. If F exceeds $F_{critical}$, the null hypothesis is rejected and at least one of the means of the populations is different. Table 21 shows the results of the ANOVA.

Table 21: Results of ANOVA for Peak Force data as vertical spacing increases from 0.5" to 1"

Reinforcement Width and Length	F	$F_{critical}$	Decision
PW8L	3.631	8.526	Null Hypothesis
PW11L	9.987	8.526	Alternate Hypothesis
8W8L	1.51	8.526	Null Hypothesis
8W11L	121.268	8.526	Alternate Hypothesis
11W8L	0.379	8.526	Null Hypothesis
11W11L	0.073	8.526	Null Hypothesis

All six ANOVA results support the linear regression analysis results.

2. Failure Surface Location

To evaluate the effect of reinforcement vertical spacing on the failure surface location, the mid-plate failure surface location was plotted for each width and length combination, allowing reinforcement vertical spacing to be the only variable in the reinforcement geometry for each plot. The data presented in Figures 109-114 are from the failure surfaces determined using painted layers.

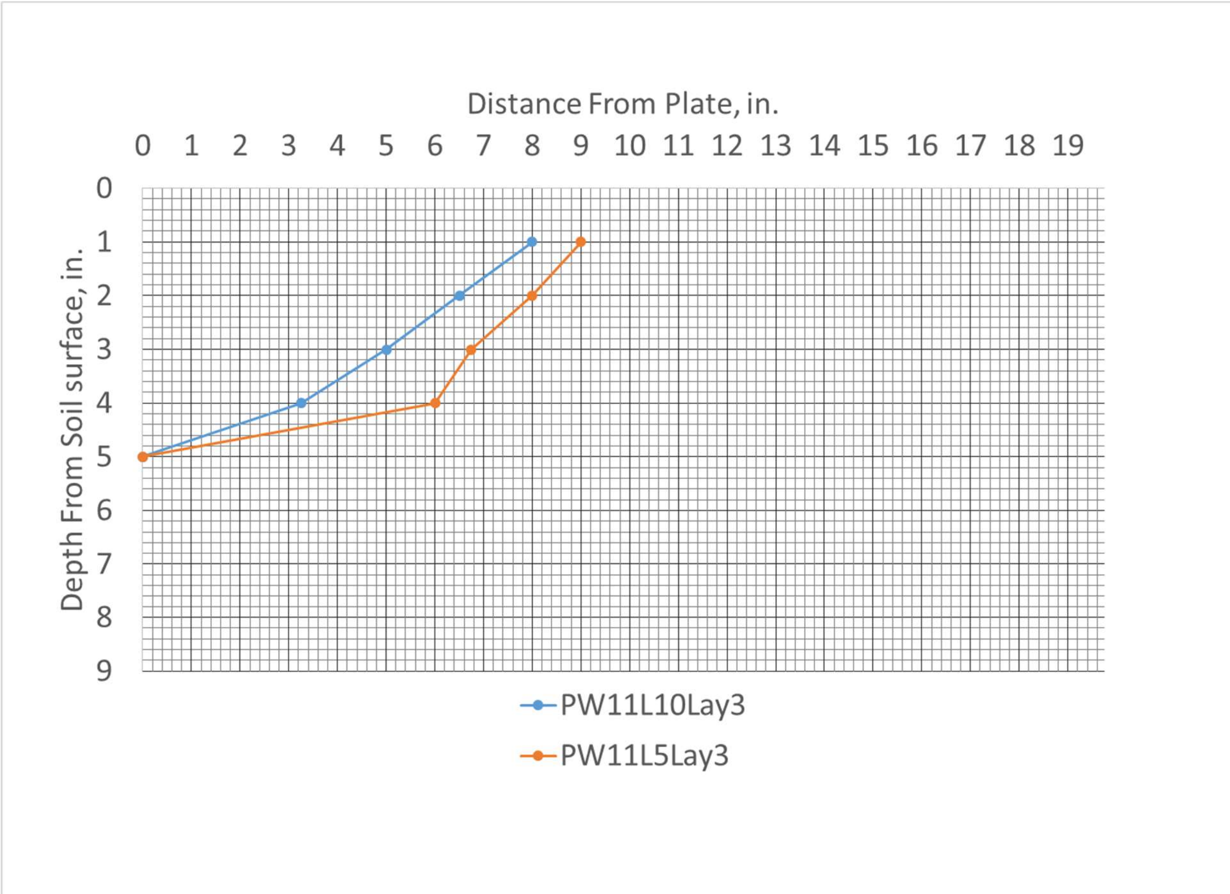

Figure 109: Mid-Plate failure surface location of tests PW11L10Lay3 and PW11L5Lay3

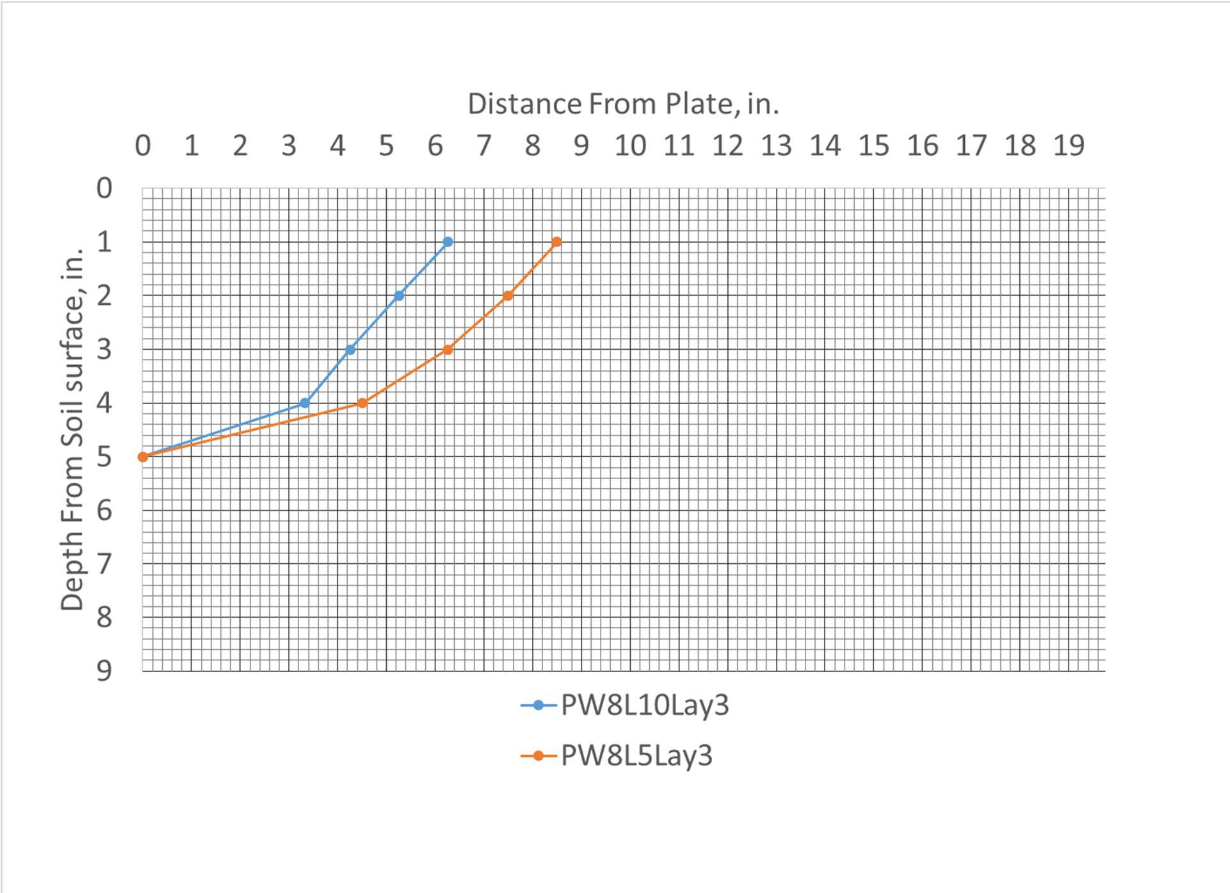

Figure 110: Mid-Plate failure surface location of tests PW8L10Lay3 and PW8L5Lay3

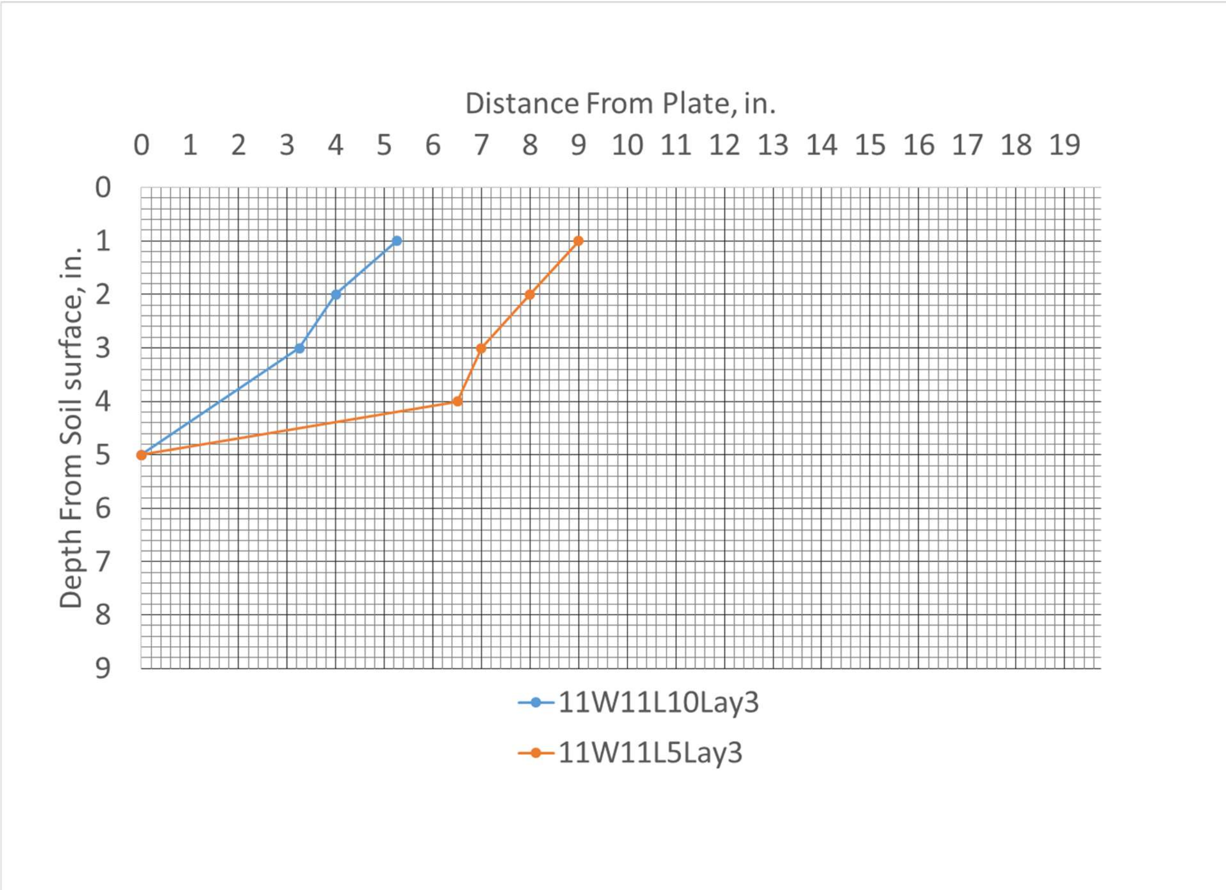

Figure 111: Mid-Plate failure surface location of tests 11W11L10Lay3 and 11W11L5Lay3

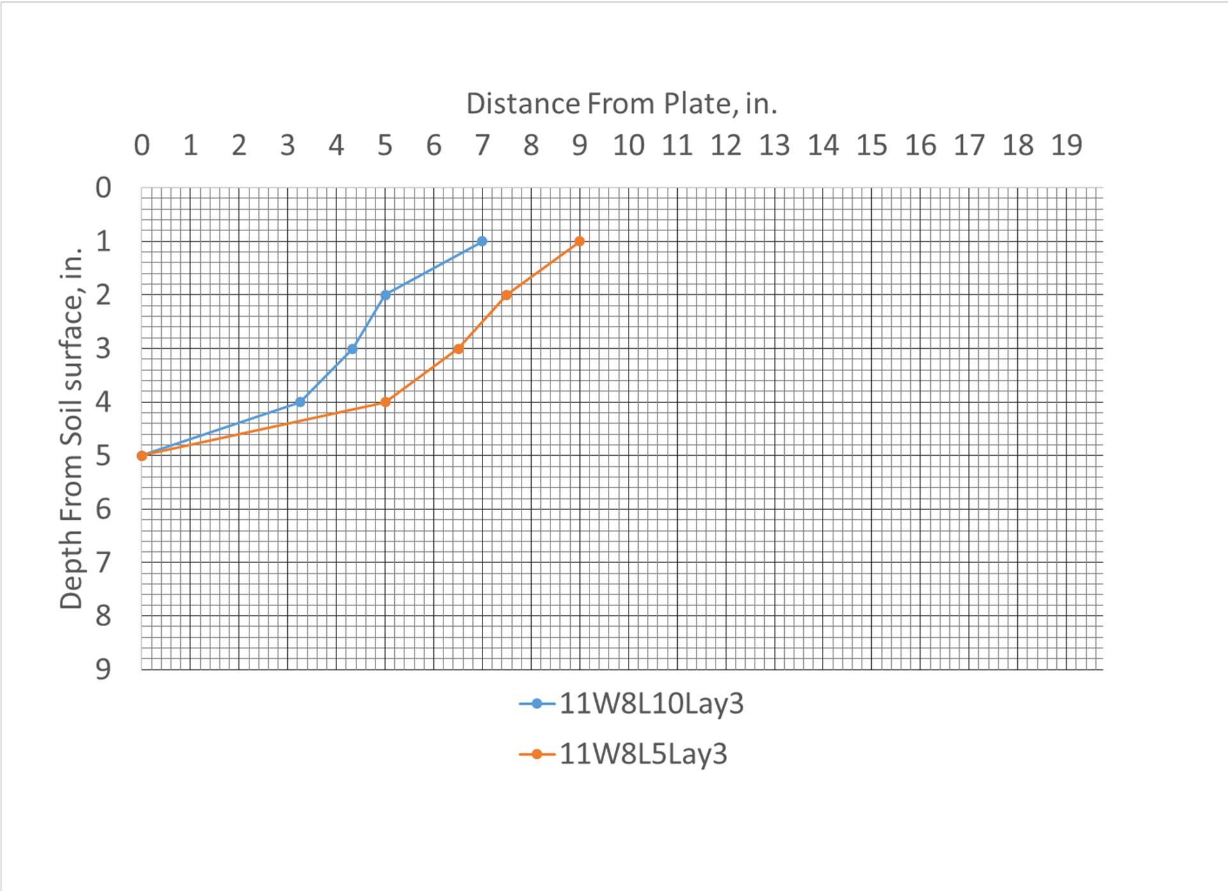

Figure 112: Mid-Plate failure surface location of tests 11W8L10Lay3 and 11W8L5Lay3

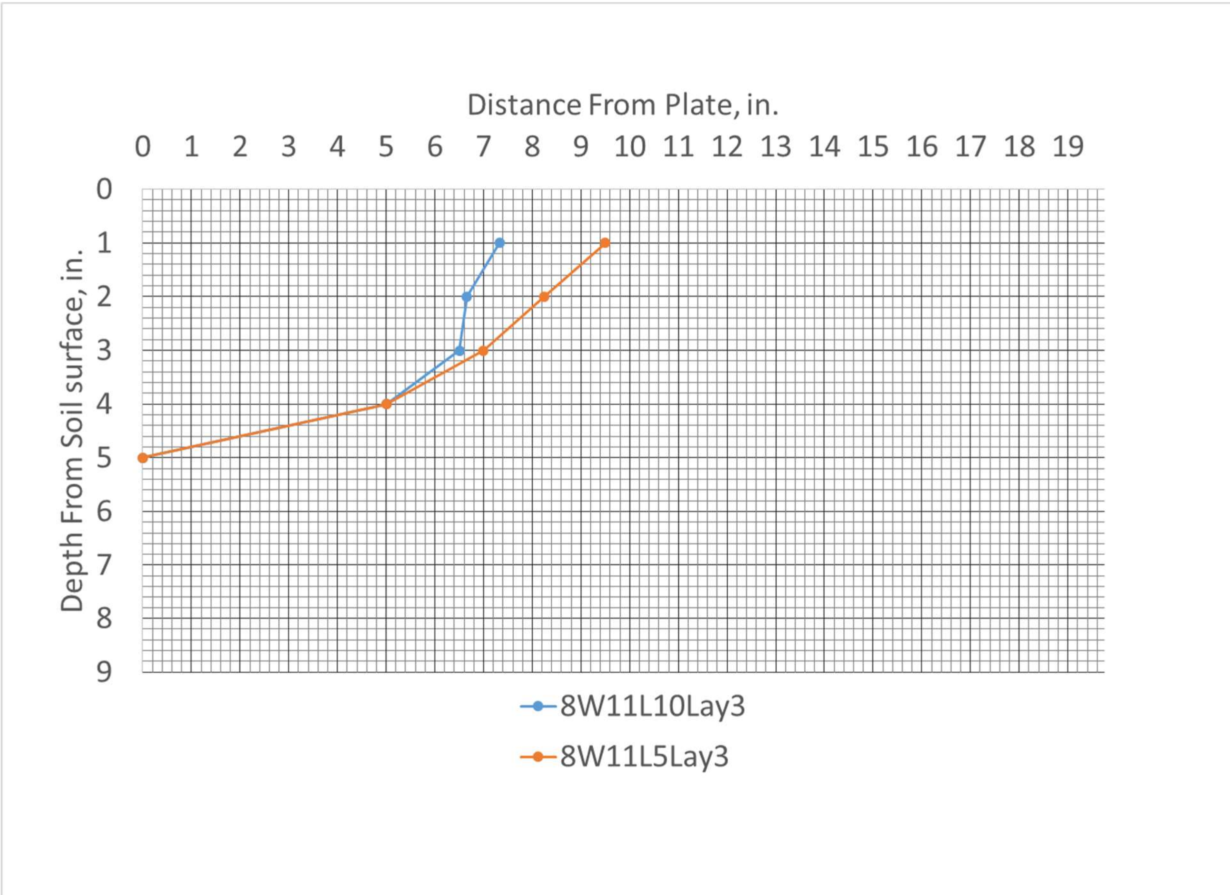

Figure 113: Mid-Plate failure surface location of tests 8W11L10Lay3 and 8W11L5Lay3

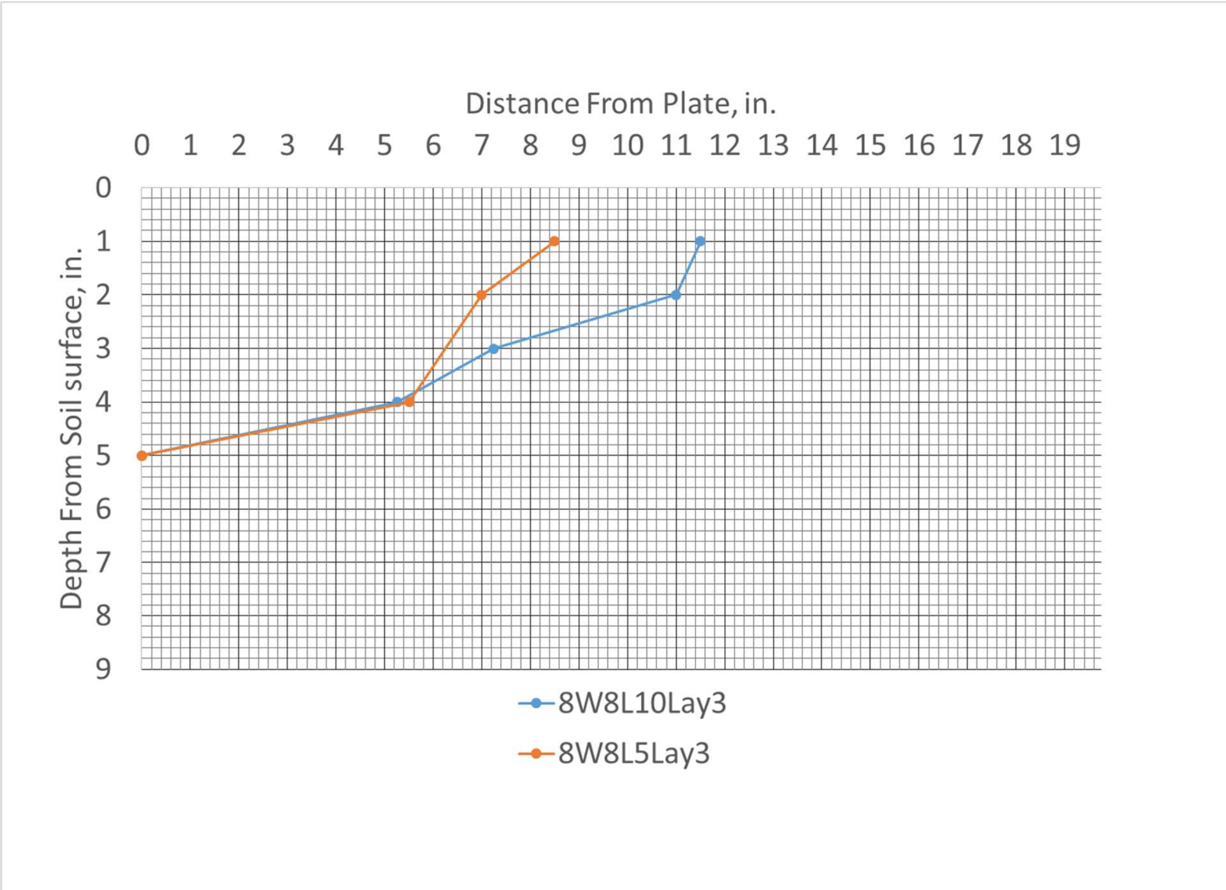

Figure 114: Mid-Plate failure surface location of tests 8W8L10Lay3 and 8W8L5Lay3

With width and length held constant, five of six pairs of tests showed a longer failure surface when the reinforcement vertical spacing is increased from 0.5” to 1.” Typically a longer failure surface indicates a stronger soil structure. This is expected as the addition of more weak planes (the reinforcement) into the soil structure is likely to reduce the passive resistance of the structure.

ii. Effect of Reinforcement Width

1. Load Deformation Characteristics

a. Peak Force

To determine the effect of reinforcement width on Peak Force, Peak Force vs. reinforcement width was plotted for each reinforcement length and vertical spacing combination.

After plotting, an initial observation was made, linear regression analysis was performed for data with reinforcement width as the only measurable variable, analysis of variance (ANOVA) was performed for data with reinforcement width as the only measurable variable, and linear regression analysis was performed for all of the data points with length and vertical spacing as known variables.

i. Initial Observation

Initial observation was made after plotting Peak Force vs. reinforcement width, Figure 115.

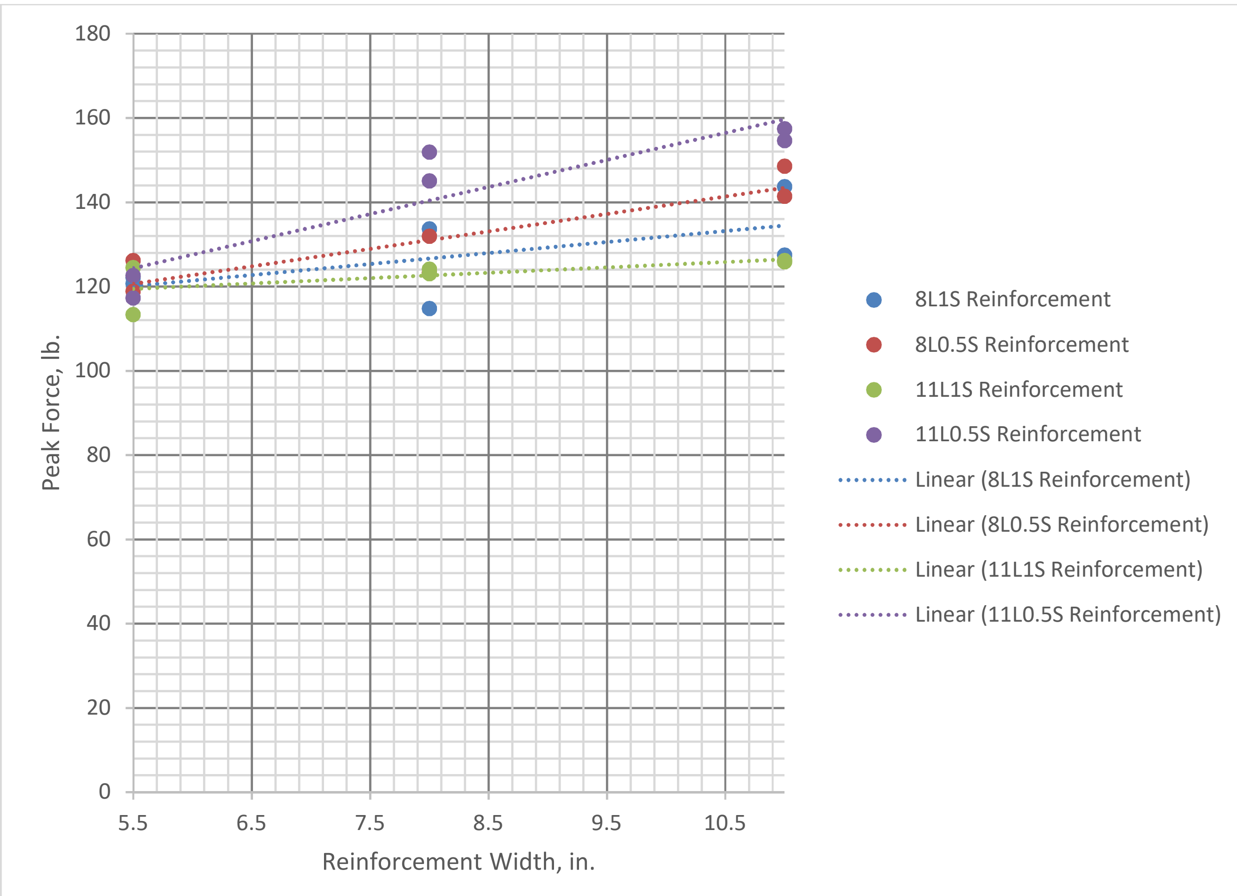

Figure 115: Peak Force vs. reinforcement width for various reinforcement lengths and spacings with linear trend lines (results of 24 tests)

After plotting, linear trend lines were added for each length and spacing combination to determine if any data trends were apparent. Table 22 shows the observed trends.

Table 22: Observed trends for Peak Force values as reinforcement width increases from 5.5" to 8" to 11"

Length and Spacing Combination	Peak Force Trend as Reinforcement Width Increases
8L5Lay	Increase
8L10Lay	Increase
11L5Lay	Increase
11L10Lay	Increase

All of the tests showed a noticeable increase in Peak Force as reinforcement width increased. Due to this, the initial observation is made that increasing reinforcement width results in increasing Peak Force values.

ii. Single Variable Linear Regression Analysis

A linear regression analysis was performed to determine the significance of change in Peak Force when the single variable, reinforcement width, is modified. Four sets of reinforcement lengths and spacings were tested. For each reinforcement length and spacing set, two tests of three different reinforcement widths were evaluated resulting in six data points. A t-test was performed at a 90% confidence interval. For each data set, a t* value was calculated and compared to a t value corresponding to a 90% confidence interval and 6 data points. Two alternatives exist for the two sided test: acceptance of the null hypothesis or acceptance of the alternate hypothesis. The null hypothesis concludes that there is no relationship between Peak Force and reinforcement width. The alternate hypothesis concludes that there is a relationship between Peak Force and reinforcement width. If the t* value is greater than the t value, the alternate hypothesis is chosen. If the t* value is less than or equal to the t value, the null hypothesis is chosen. P-values were also computed as p-values less than the level of significance support the alternate hypothesis. Each data set was plotted with reinforcement width on the abscissa and Peak Force on the ordinate. A linear best fit line was added and the slope of this line was computed. Table 23 summarizes the linear regression analysis.

Table 23: Linear regression analysis results for effect of reinforcement width on Peak Force. "Null Hypothesis" indicates that there is not a statistically significant relationship between the two variables, while "Alternate Hypothesis" indicates that there is a statistically significant relationship.

Reinforcement Length and Spacing	|t*|	t(0.95;4)	Decision	P-Value	Best Fit Line Slope
8L5Lay	1.59	2.13	Null Hypothesis	0.187	2.61
8L10Lay	4.12	2.13	Alternate Hypothesis	0.015	4.14
11L5Lay	1.73	2.13	Null Hypothesis	0.158	1.27
11L10Lay	4.60	2.13	Alternate Hypothesis	0.010	6.42

From the linear regression analysis, only half of the data sets show a relationship between reinforcement width and Peak Force. All of the decisions are supported by corresponding p-values. However, all best fit lines have a positive slope indicating the possibility that Peak Force increases with increasing reinforcement width. However, due to only half of the data sets showing a statistical relationship between reinforcement width and Peak Force, it is concluded that a positive relationship may exist between reinforcement width and Peak Force, but not for each individual test.

iii. Analysis of Variance

A single factor ANOVA was performed to determine if the mean values of the Peak Force data populations are equal when the single variable, reinforcement width, is modified. Four sets of reinforcement lengths and spacings were tested. For each reinforcement length and spacing set, two tests of three different reinforcement widths were evaluated resulting in six data points. A 90% confidence interval was used for the ANOVA. For each data set, an F value was computed as well as a critical F value. The alternate hypothesis states that at least one of the means of each data population is different. The null hypothesis states that the means of each data population are equal. If F exceeds $F_{critical}$, the null hypothesis is rejected and at least one of the means of the populations is different. Table 24 shows the results of the ANOVA.

Table 24: Results of ANOVA for Peak Force data as reinforcement width increases from 5.5" to 8" to 11"

Reinforcement Length and Spacing	F	$F_{critical}$	Decision
8L5Lay	1.085	5.462	Null Hypothesis
8L10Lay	9.423	5.462	Alternate Hypothesis
11L5Lay	1.233	5.462	Null Hypothesis
11L10Lay	52.288	5.462	Alternate Hypothesis

All four ANOVA results support the linear regression analysis results.

b. Residual Force

To determine the effect of reinforcement width on Residual Force, Residual Force vs. reinforcement width was plotted for each reinforcement length and vertical spacing combination. After plotting, an initial observation was made, linear regression analysis was performed for data with reinforcement width as the only measurable variable, analysis of variance (ANOVA) was performed for data with reinforcement width as the only measurable variable, and linear regression analysis was performed for all of the data points with length and vertical spacing as known variables.

i. Initial Observation

Initial observation was made after Residual Force vs. reinforcement width, Figure 116.

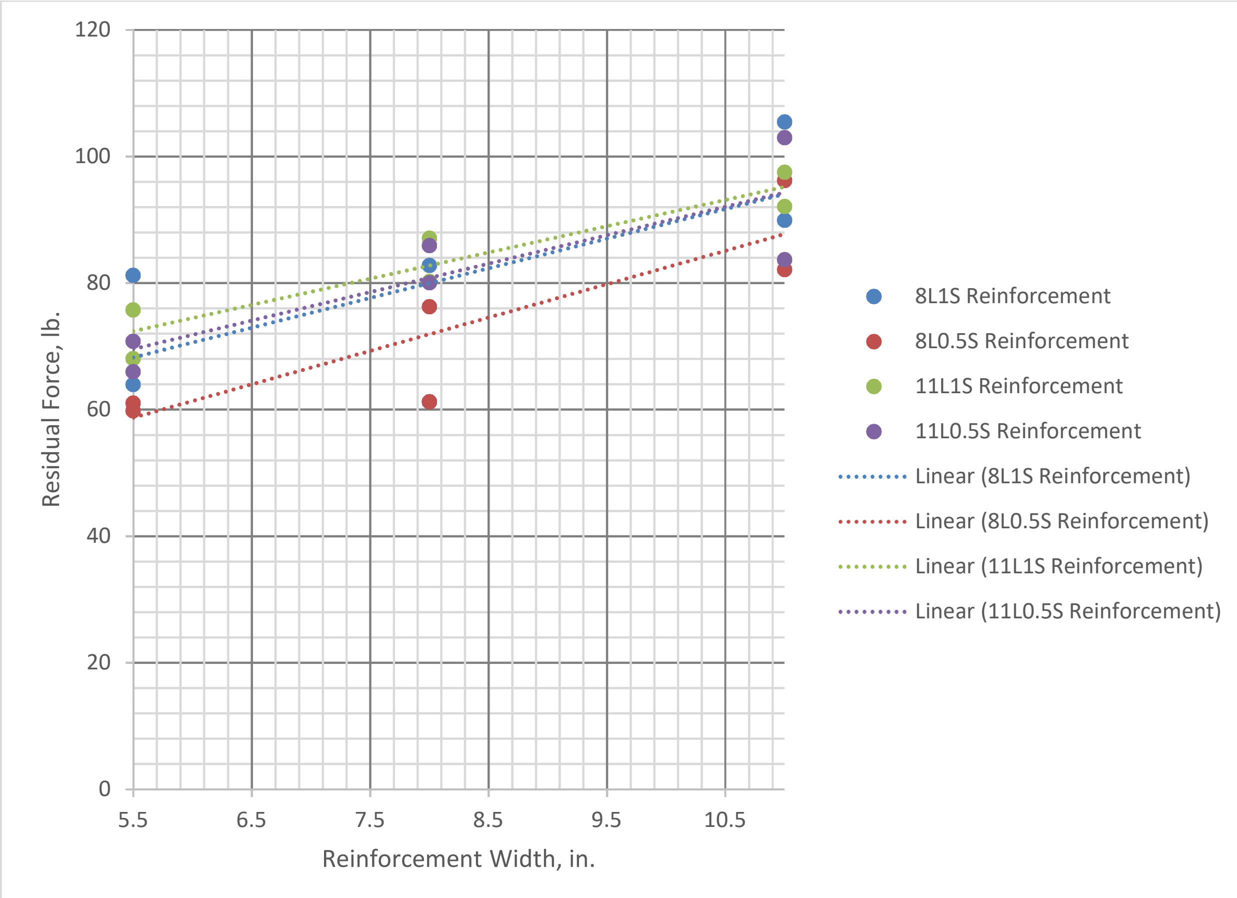

Figure 116: Residual Force vs. reinforcement width for various reinforcement lengths and spacings with linear trend lines (results of 24 tests)

After plotting, linear trend lines were added for each length and spacing combination to determine if any data trends were apparent. Table 25 shows the observed trends.

Table 25: Observed trends for Peak Force values as reinforcement width increases from 5.5” to 8” to 11”

Length and Spacing Combination	Residual Force Trend as Reinforcement Width Increases
8L5Lay	Increase
8L10Lay	Increase
11L5Lay	Increase
11L10Lay	Increase

All of the tests showed a noticeable increase in Residual Force as reinforcement width increased. Due to this, the initial observation is made that increasing reinforcement width results in increasing Residual Force values.

ii. Single Variable Linear Regression Analysis

A linear regression analysis was performed to determine the significance of change in Residual Force when the single variable, reinforcement width, is modified. Four sets of reinforcement lengths and spacings were tested. For each reinforcement length and spacing set, two tests of three different reinforcement widths were evaluated resulting in six data points. A t-test was performed at a 90% confidence interval. For each data set, a t* value was calculated and compared to a t value corresponding to a 90% confidence interval and 6 data points. Two alternatives exist for the two sided test: acceptance of the null hypothesis or acceptance of the alternate hypothesis. The null hypothesis concludes that there is no relationship between Residual Force and reinforcement width. The alternate hypothesis concludes that there is a relationship between Residual Force and reinforcement width. If the t* value is greater than the t value, the alternate hypothesis is chosen. If the t* value is less than or equal to the t value, the null hypothesis is chosen. P-values were also computed as p-values less than the level of significance support the alternate hypothesis. Each data set was plotted with reinforcement width on the abscissa and Residual Force on the ordinate. A linear best fit line was added and the slope of this line was computed. Table 26 summarizes the linear regression analysis.

Table 26: Linear regression analysis results for effect of reinforcement width on Residual Force. "Null Hypothesis" indicates that there is not a statistically significant relationship between the two variables, while "Alternate Hypothesis" indicates that there is a statistically significant relationship.

Reinforcement Length and Spacing	|t*|	t(0.95;4)	Decision	P-Value	Best Fit Line Slope
8L5Lay	1.96	2.13	Null Hypothesis	0.121	4.69
8L10Lay	3.74	2.13	Alternate Hypothesis	0.020	5.28
11L5Lay	5.47	2.13	Alternate Hypothesis	0.005	4.15
11L10Lay	3.27	2.13	Alternate Hypothesis	0.031	4.50

From the linear regression analysis, three out of four data sets show a relationship between reinforcement width and Residual Force. All of the decisions are supported by corresponding p-values. All best fit lines have a positive slope indicating that Residual Force likely increases with increasing reinforcement width. The one test that concluded that a relationship did not exist barely failed the test. The other three tests easily passed the test concluding that a positive relationship exists. Due to only one test barely failing the t-test, it is very likely that a positive relationship exists between Residual Force and reinforcement width.

iii. Analysis of Variance

A single factor ANOVA was performed to determine if the mean values of the Residual Force data populations are equal when the single variable, reinforcement width, is modified. Four sets of reinforcement lengths and spacings were tested. For each reinforcement length and spacing set, two tests of three different reinforcement widths were evaluated resulting in six data points. A 90% confidence interval was used for the ANOVA. For each data set, an F value was computed as well as a critical F value. The alternate hypothesis states that at least one of the means of each data population is different. The null hypothesis states that the means of each data population are equal. If F exceeds $F_{critical}$, the null hypothesis is rejected and at least one of the means of the populations is different. Table 27 shows the results of the ANOVA.

Table 27: Results of ANOVA for Residual Force data as reinforcement width increases from 5.5" to 8" to 11"

Reinforcement Length and Spacing	F	$F_{critical}$	Decision
8L5Lay	2.570	5.462	Null Hypothesis
8L10Lay	6.184	5.462	Alternate Hypothesis
11L5Lay	11.667	5.462	Alternate Hypothesis
11L10Lay	4.379	5.462	Null Hypothesis

Three of the four ANOVA results support the linear regression analysis results.

c. Peak Force Displacement

To determine the effect of reinforcement width on Peak Force Displacement, Peak Force Displacement vs. reinforcement width was plotted for each reinforcement length and vertical spacing combination. After plotting, an initial observation was made, linear regression analysis was performed for data with reinforcement width as the only measurable variable, analysis of variance (ANOVA) was performed for data with reinforcement width as the only measurable variable, and linear regression analysis was performed for all of the data points with length and vertical spacing as known variables.

i. Initial Observation

Initial observation was made after plotting Peak Force Displacement vs. reinforcement width, Figure 117.

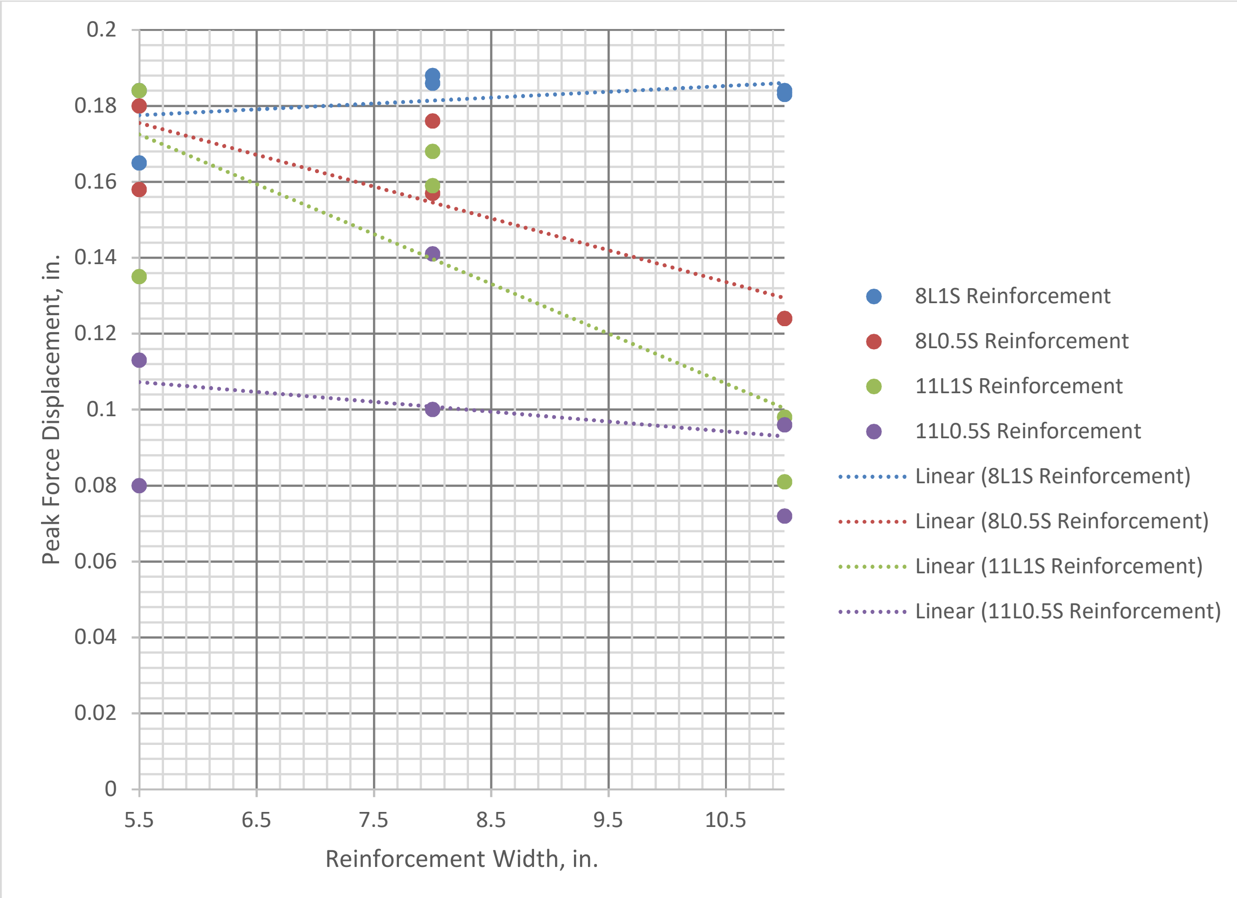

Figure 117: Peak Force Displacement vs. reinforcement width for various reinforcement lengths and spacings with linear trend lines (results of 24 tests)

After plotting, linear trend lines were added for each length and spacing combination to determine if any data trends were apparent. Table 28 shows the observed trends.

Table 28: Observed trends for Peak Force Displacement values as reinforcement width increases from 5.5" to 8" to 11"

Length and Spacing Combination	Peak Force Displacement Trend as Reinforcement Width Increases
8L5Lay	None
8L10Lay	None
11L5Lay	None
11L10Lay	None

No tests showed a noticeable trend in Peak Force Displacement with increasing reinforcement width. Due to this, the initial observation is made that increasing reinforcement width has no effect on Peak Force Displacement.

ii. Single Variable Linear Regression Analysis

A linear regression analysis was performed to determine the significance of change in Peak Force Displacement when the single variable, reinforcement width, is modified. Four sets of reinforcement lengths and spacings were tested. For each reinforcement length and spacing set, two tests of three different reinforcement widths were evaluated resulting in six data points. A t-test was performed at a 90% confidence interval. For each data set, a t* value was calculated and compared to a t value corresponding to a 90% confidence interval and 6 data points. Two alternatives exist for the two sided test: acceptance of the null hypothesis or acceptance of the alternate hypothesis. The null hypothesis concludes that there is no relationship between Peak Force Displacement and reinforcement width. The alternate hypothesis concludes that there is a relationship between Peak Force Displacement and reinforcement width. If the t* value is greater than the t value, the alternate hypothesis is chosen. If the t* value is less than or equal to the t value, the null hypothesis is chosen. P-values were also computed as p-values less than the level of significance support the alternate hypothesis. Each data set was plotted with reinforcement width on the abscissa and Peak Force Displacement on the ordinate. A linear best fit line was added and the slope of this line was computed. Table 29 summarizes the linear regression analysis.

Table 29: Linear regression analysis results for effect of reinforcement width on Peak Force Displacement. "Null Hypothesis" indicates that there is not a statistically significant relationship between the two variables, while "Alternate Hypothesis" indicates that there is a statistically significant relationship.

Reinforcement Length and Spacing	|t*|	t(0.95;4)	Decision	P-Value	Best Fit Line Slope
8L5Lay	1.02	2.13	Null Hypothesis	0.364	0.0015
8L10Lay	3.16	2.13	Alternate Hypothesis	0.034	-0.0084
11L5Lay	2.60	2.13	Alternate Hypothesis	0.060	-0.0130
11L10Lay	0.54	2.13	Null Hypothesis	0.620	-0.0026

From the linear regression analysis, two out of four data sets show a relationship between reinforcement width and Peak Force Displacement. All of the decisions are supported by corresponding p-values. Some best fit lines have a positive slope, while others have a negative slope indicating that a relationship between Peak Force Displacement and reinforcement width is unlikely. Due to half of the tests failing the t-test and positive and negative best fit line slopes, it is unlikely that a relationship exists between Peak Force Displacement and reinforcement width.

iii. Analysis of Variance

A single factor ANOVA was performed to determine if the mean values of the Peak Force Displacement data populations are equal when the single variable, reinforcement width, is modified. Four sets of reinforcement lengths and spacings were tested. For each reinforcement length and spacing set, two tests of three different reinforcement widths were evaluated resulting in six data points. A 90% confidence interval was used for the ANOVA. For each data set, an F value was computed as well as a critical F value. The alternate hypothesis states that at least one of the means of each data population is different. The null hypothesis states that the means of each data population are equal. If F exceeds $F_{critical}$, the null hypothesis is rejected and at least one of the means of the populations is different. Table 30 shows the results of the ANOVA.

Table 30: Results of ANOVA for Peak Force Displacement data as reinforcement width increases from 5.5" to 8" to 11"

Reinforcement Length and Spacing	F	$F_{critical}$	Decision
8L5Lay	1.363	5.462	Null Hypothesis
8L10Lay	9.083	5.462	Alternate Hypothesis
11L5Lay	7.501	5.462	Alternate Hypothesis
11L10Lay	1.234	5.462	Null Hypothesis

All four ANOVA results support the linear regression analysis results..

d. K_{50}

To determine the effect of reinforcement width on K_{50}, K_{50} vs. reinforcement width was plotted for each reinforcement length and vertical spacing combination. After plotting, an initial observation was made, linear regression analysis was performed for data with reinforcement width as the only measurable variable, analysis of variance (ANOVA) was performed for data with reinforcement width as the only measurable variable, and linear regression analysis was performed for all of the data points with length and vertical spacing as known variables.

i. Initial Observation

Initial observation was made after plotting K_{50} vs. reinforcement width, Figure 118.

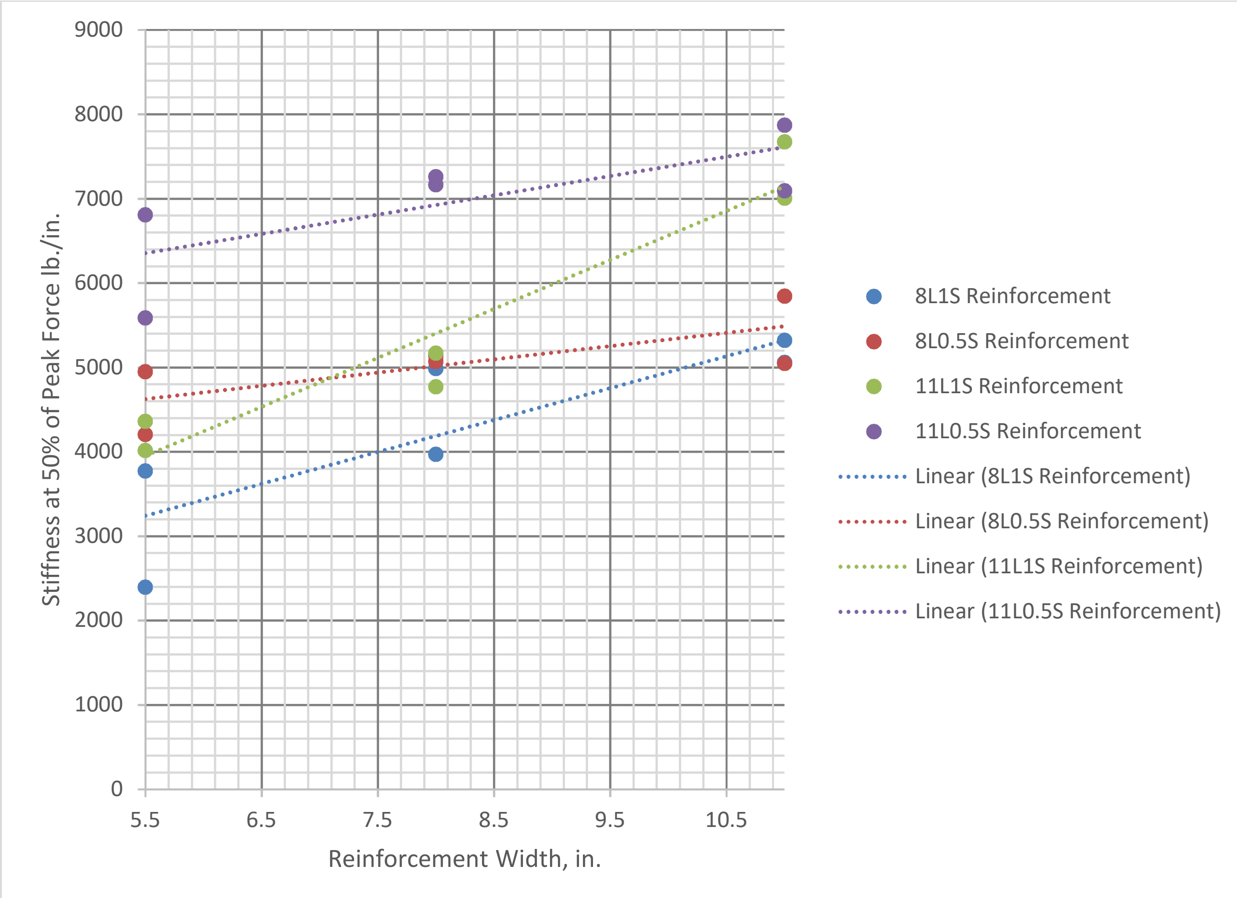

Figure 118: K_{50} vs. reinforcement width for various reinforcement lengths and spacings with linear trend lines (results of 24 tests)

After plotting, linear trend lines were added for each length and spacing combination to determine if any data trends were apparent. Table 31 shows the observed trends.

Table 31: Observed trends for Peak Force values as reinforcement width increases from 5.5” to 8” to 11”

Width and Length Combination	K_{50} Trend as Reinforcement Width Increases
8L5Lay	Increase
8L10Lay	Increase
11L5Lay	Increase
11L10Lay	Increase

All of the tests showed a noticeable increase in K_{50} as reinforcement width is increased. Due to this, the initial observation is made that increasing reinforcement width results in an increased K_{50} value.

ii. Single Variable Linear Regression Analysis

A linear regression analysis was performed to determine the significance of change in K_{50} when the single variable, reinforcement width, is modified. Four sets of reinforcement lengths and spacings were tested. For each reinforcement length and spacing set, two tests of three different reinforcement widths were evaluated resulting in six data points. A t-test was performed at a 90% confidence interval. For each data set, a t* value was calculated and compared to a t value corresponding to a 90% confidence interval and 6 data points. Two alternatives exist for the two sided test: acceptance of the null hypothesis or acceptance of the alternate hypothesis. The null hypothesis concludes that there is no relationship between K_{50} and reinforcement width. The alternate hypothesis concludes that there is a relationship between K_{50} and reinforcement width. If the t* value is greater than the t value, the alternate hypothesis is chosen. If the t* value is less than or equal to the t value, the null hypothesis is chosen. P-values were also computed as p-values less than the level of significance support the alternate hypothesis. Each data set was plotted with reinforcement width on the abscissa and K_{50} on the ordinate. A linear best fit line was added and the slope of this line was computed. Table 32 summarizes the linear regression analysis.

Table 32: Linear regression analysis results for effect of reinforcement width on K_{50}. "Null Hypothesis" indicates that there is not a statistically significant relationship between the two variables, while "Alternate Hypothesis" indicates that there is a statistically significant relationship.

Reinforcement Length and Spacing	|t*|	t(0.95;4)	Decision	P-Value	Best Fit Line Slope
8L5Lay	3.14	2.13	Alternate Hypothesis	0.035	378.10
8L10Lay	2.19	2.13	Alternate Hypothesis	0.094	156.91
11L5Lay	6.65	2.13	Alternate Hypothesis	0.003	580.60
11L10Lay	2.20	2.13	Alternate Hypothesis	0.090	228.45

From the linear regression analysis, all four data sets show a relationship between reinforcement width and K_{50}. All of the decisions are supported by corresponding p-values. All best fit lines have a positive slope indicating a positive relationship between reinforcement width and K_{50}. Due to all of the tests passing the t-test and all having positive best fit line slopes, it is very likely that a positive relationship exists between reinforcement width and K_{50}.

iii. Analysis of Variance

A single factor ANOVA was performed to determine if the mean values of the K_{50} data populations are equal when the single variable, reinforcement width, is modified. Four sets of reinforcement lengths and spacings were tested. For each reinforcement length and spacing set, two tests of three different reinforcement widths were evaluated resulting in six data points. A 90% confidence interval was used for the ANOVA. For each data set, an F value was computed as well as a critical F value. The alternate hypothesis states that at least one of the means of each data population is different. The null hypothesis states that the means of each data population are equal. If F exceeds $F_{critical}$, the null hypothesis is rejected and at least one of the means of the populations is different. Table 33 shows the results of the ANOVA.

Table 33: Results of ANOVA for K_{50} data as reinforcement width increases from 5.5" to 8" to 11"

Reinforcement Length and Spacing	F	$F_{critical}$	Decision
8L5Lay	4.580	5.462	Null Hypothesis
8L10Lay	1.929	5.462	Null Hypothesis
11L5Lay	44.866	5.462	Alternate Hypothesis
11L10Lay	2.595	5.462	Null Hypothesis

Only one ANOVA result supports the linear regression analysis results.

2. Failure Surface Location

To evaluate the effect of reinforcement width on the failure surface location, the location of the failure surface breaking mid-plate plane was plotted for each vertical spacing and length combination, allowing reinforcement width to be the only variable in the reinforcement geometry for each plot. The data presented in Figures 119-122 are from the failure surfaces determined with painted layers.

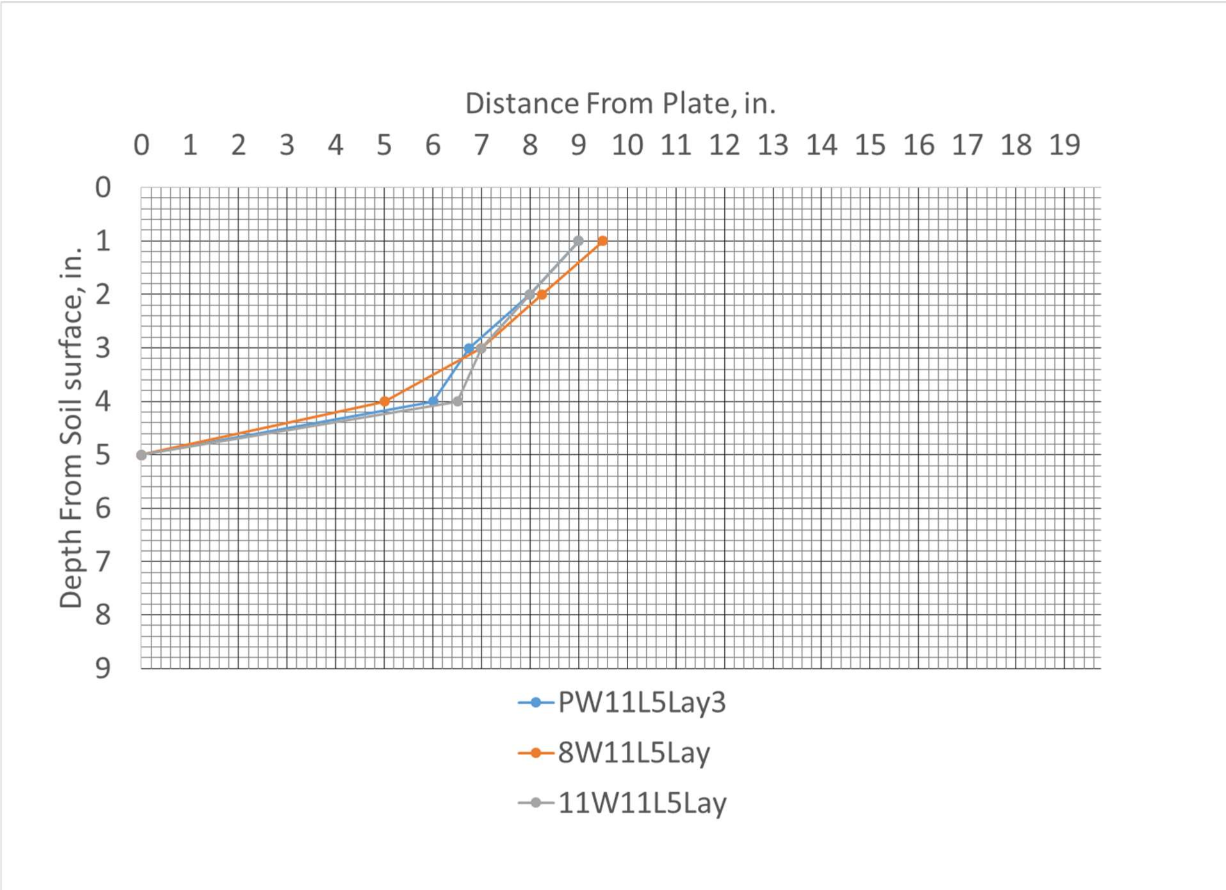

Figure 119: Mid-Plate failure surface location of tests PW11L5Lay3, 8W11L5Lay3, and 11W11L5Lay

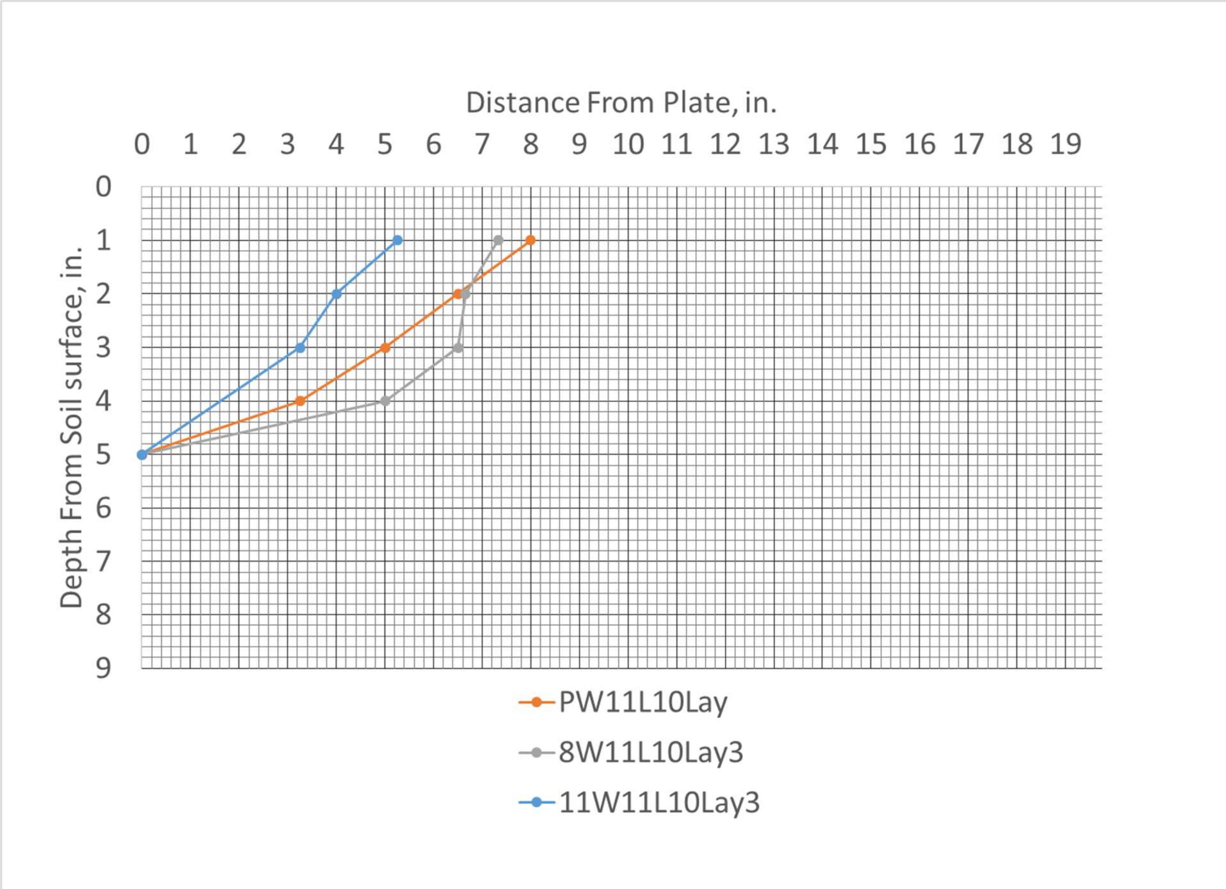

Figure 120: Mid-Plate failure surface location of tests PW11L10Lay3, 8W11L10Lay3, and 11W11L10Lay3

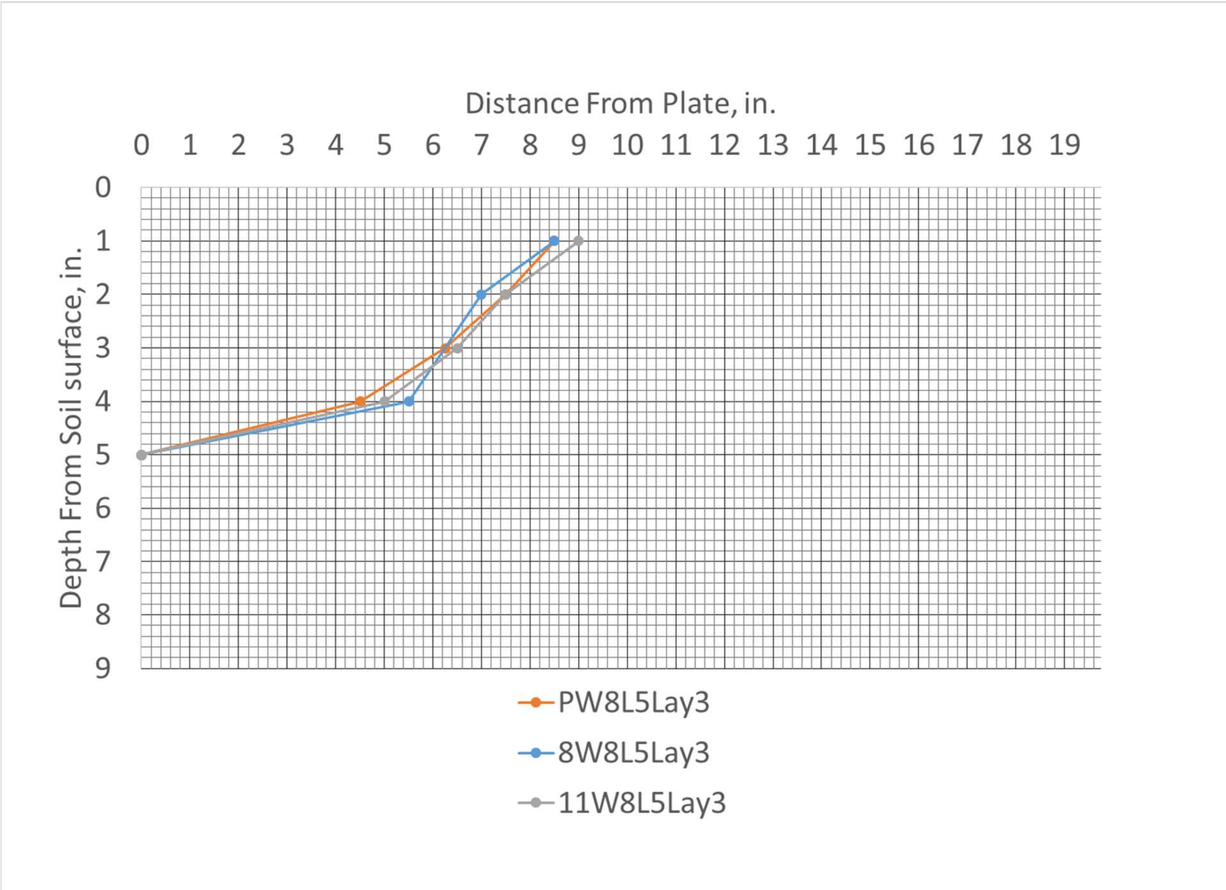

Figure 121: Mid-Plate failure surface location of tests PW8L5Lay3, 8W8L5Lay3, and 11W8L5Lay3

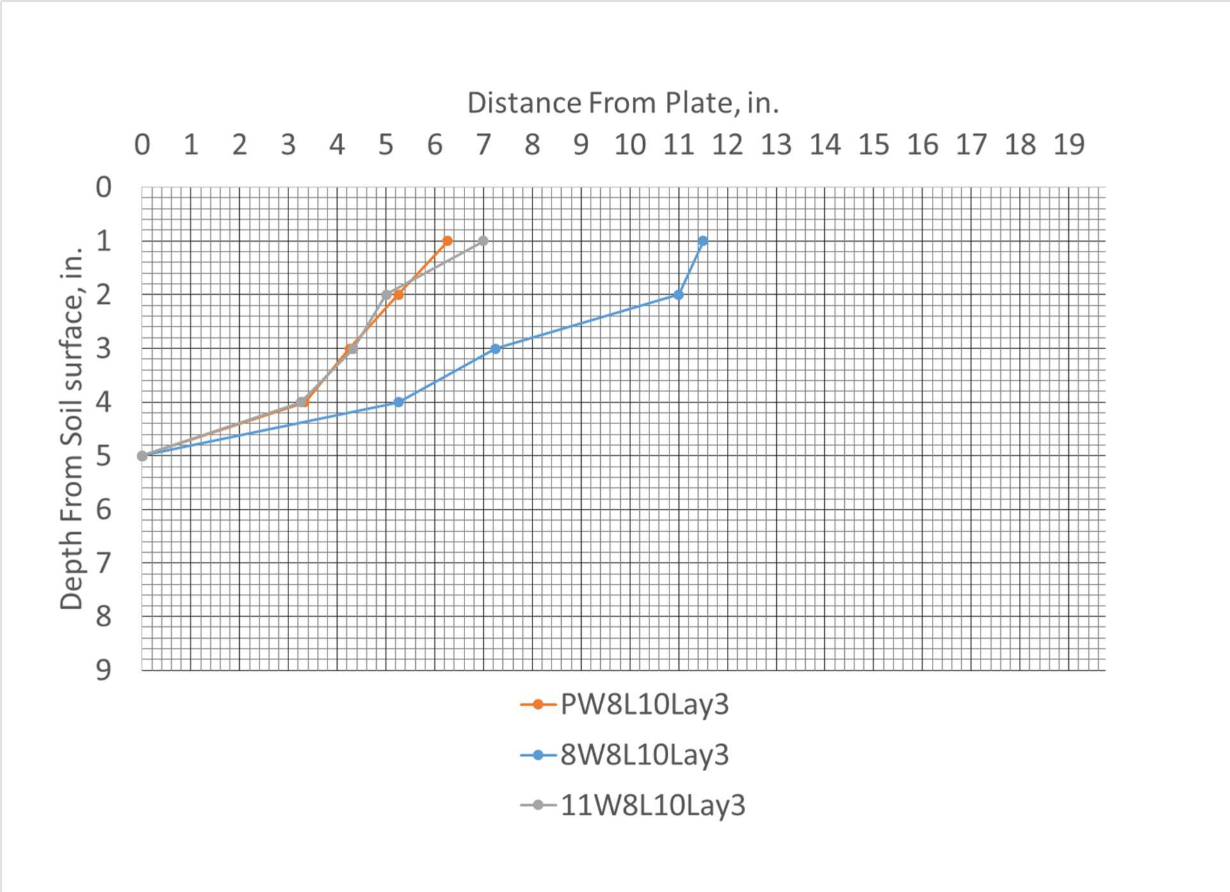

Figure 122: Mid-Plate failure surface location of tests PW8L10Lay3, 8W8L10Lay3, and 11W8L10Lay3

For each trio of tests plotted, no trends were observed between failure surface location and reinforcement width.

iii. Effect of Reinforcement Length

1. Load Deformation Characteristics

a. Peak Force

To determine the effect of reinforcement length on Peak Force, Peak Force vs. reinforcement length was plotted for each reinforcement width and spacing combination. After plotting, an initial observation was made, linear regression analysis was performed for data with reinforcement length as the only measurable variable, analysis of variance (ANOVA) was performed for data with reinforcement length as the only measurable variable, and linear regression analysis was performed for all of the data points with vertical spacing and width as known variables.

i. Initial Observation

Initial observation was made after plotting Peak Force vs. vertical spacing, Figure 123.

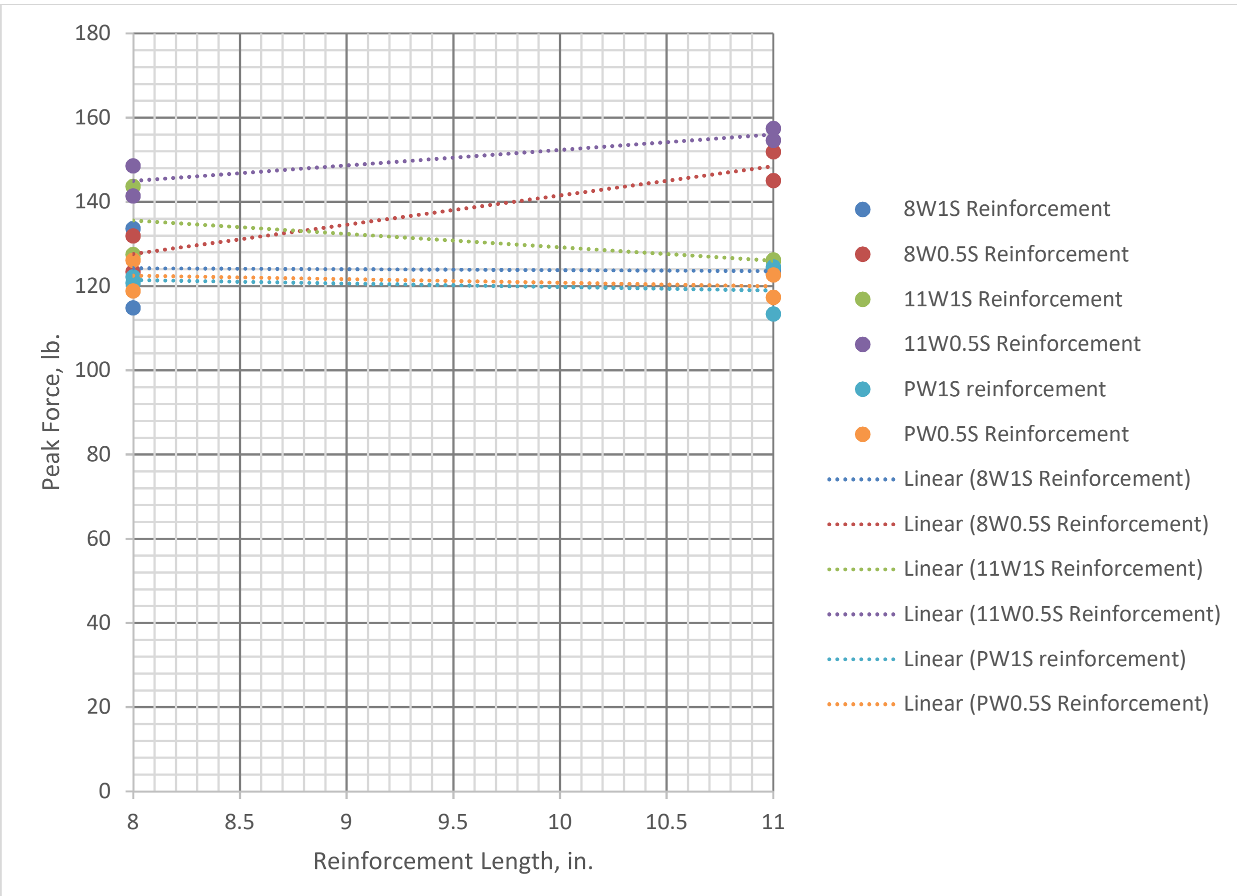

Figure 123: Peak Force vs. reinforcement length for various reinforcement width and spacings with linear trend lines (results of 24 tests)

After plotting, linear trend lines were added for each width and spacing combination to determine if any data trends were apparent. Table 34 shows the observed trends.

Table 34: Observed trends for Peak Force values as reinforcement length increases from 8" to 11"

Width and Spacing Combination	Peak Force Trend as Reinforcement Length Increases
PW5Lay	None
PW10Lay	None
8W5Lay	None
8W10Lay	Increase
11W5Lay	None
11W10Lay	Slight Increase

Most tests showed no relationship between reinforcement length and Peak Force. Due to this, the initial observation is made that increasing reinforcement length has no effect on Peak Force values.

ii. Single Variable Linear Regression Analysis

A linear regression analysis was performed to determine the significance of change in Peak Force when the single variable, reinforcement length, is modified. Six sets of reinforcement widths and spacings were tested. For each reinforcement width and spacing set, two tests of two different reinforcement lengths were evaluated resulting in four data points. A t-test was performed at a 90% confidence interval. For each data set, a t* value was calculated and compared to a t value corresponding to a 90% confidence interval and 4 data points. Two alternatives exist for the two sided test: acceptance of the null hypothesis or acceptance of the alternate hypothesis. The null hypothesis concludes that there is no relationship between Peak Force and reinforcement width. The alternate hypothesis concludes that there is a relationship between Peak Force and reinforcement width. If the t* value is greater than the t value, the alternate hypothesis is chosen. If the t* value is less than or equal to the t value, the null hypothesis is chosen. P-values were also computed as p-values less than the level of significance support the alternate hypothesis. Each data set was plotted with reinforcement length on the abscissa and Peak Force on the ordinate. A linear best fit line was added and the slope of this line was computed. Table 35 summarizes the linear regression analysis.

Table 35: Linear regression analysis results for effect of reinforcement length on Peak Force. "Null Hypothesis" indicates that there is not a statistically significant relationship between the two variables, while "Alternate Hypothesis" indicates that there is a statistically significant relationship.

Reinforcement Width and Spacing	|t*|	t(0.95;2)	Decision	P-Value	Best Fit Line Slope
PW5Lay	0.44	2.92	Null Hypothesis	0.7	-0.832
PW10Lay	0.56	2.92	Null Hypothesis	0.63	-0.843
8W5Lay	0.07	2.92	Null Hypothesis	0.95	-0.22
8W10Lay	3.81	2.92	Alternate Hypothesis	0.063	6.945
11W5Lay	1.18	2.92	Null Hypothesis	0.36	-3.19
11W10Lay	2.89	2.92	Null Hypothesis	0.102	3.68

From the linear regression analysis, a relationship between reinforcement length and Peak Force does not exist in five of the six data sets. All of the decisions are supported by corresponding p-values. Best fit lines have positive and negative slopes, furthering the evidence that a relationship does not exist. Only one of the tests passed the t-test so it is very unlikely that a relationship exists between reinforcement length and Peak Force.

iii. Analysis of Variance

A single factor ANOVA was performed to determine if the mean value of the Peak Force data populations are equal when the single variable, reinforcement length, is modified. Six sets of reinforcement widths and spacings were tested. For each reinforcement width and spacing set, two tests of two different reinforcement lengths were evaluated resulting in four data points. A 90% confidence interval was used for the ANOVA. For each data set, an F value was computed as well as a critical F value. The alternate hypothesis states that at least one of the means of each data population is different. The null hypothesis states that the means of each data population are equal. If F exceeds $F_{critical}$, the null hypothesis is rejected and at least one of the means of the populations is different. Table 36 shows the results of the ANOVA.

Table 36: Results of ANOVA for Peak Force data as reinforcement length increases from 8" to 11"

Reinforcement Width and Spacing	F	$F_{critical}$	Decision
PW5Lay	0.197	8.562	Null Hypothesis
PW10Lay	0.315	8.562	Null Hypothesis
8W5Lay	0.005	8.562	Null Hypothesis
8W10Lay	14.496	8.562	Alternate Hypothesis
11W5Lay	1.389	8.562	Null Hypothesis
11W10Lay	8.332	8.562	Null Hypothesis

All six ANOVA results support the linear regression analysis results..

b. Residual Force

To determine the effect of reinforcement length on Residual Force, Residual Force vs. reinforcement length was plotted for each reinforcement vertical spacing and width combination. After plotting, an initial observation was made, linear regression analysis was performed for data with reinforcement length as the only measurable variable, analysis of variance (ANOVA) was performed for data with reinforcement length as the only measurable variable, and linear regression analysis was performed for all of the data points with vertical spacing and width as known variables.

i. Initial Observation

Initial observation was made after plotting Residual Force vs. vertical spacing, Figure 124.

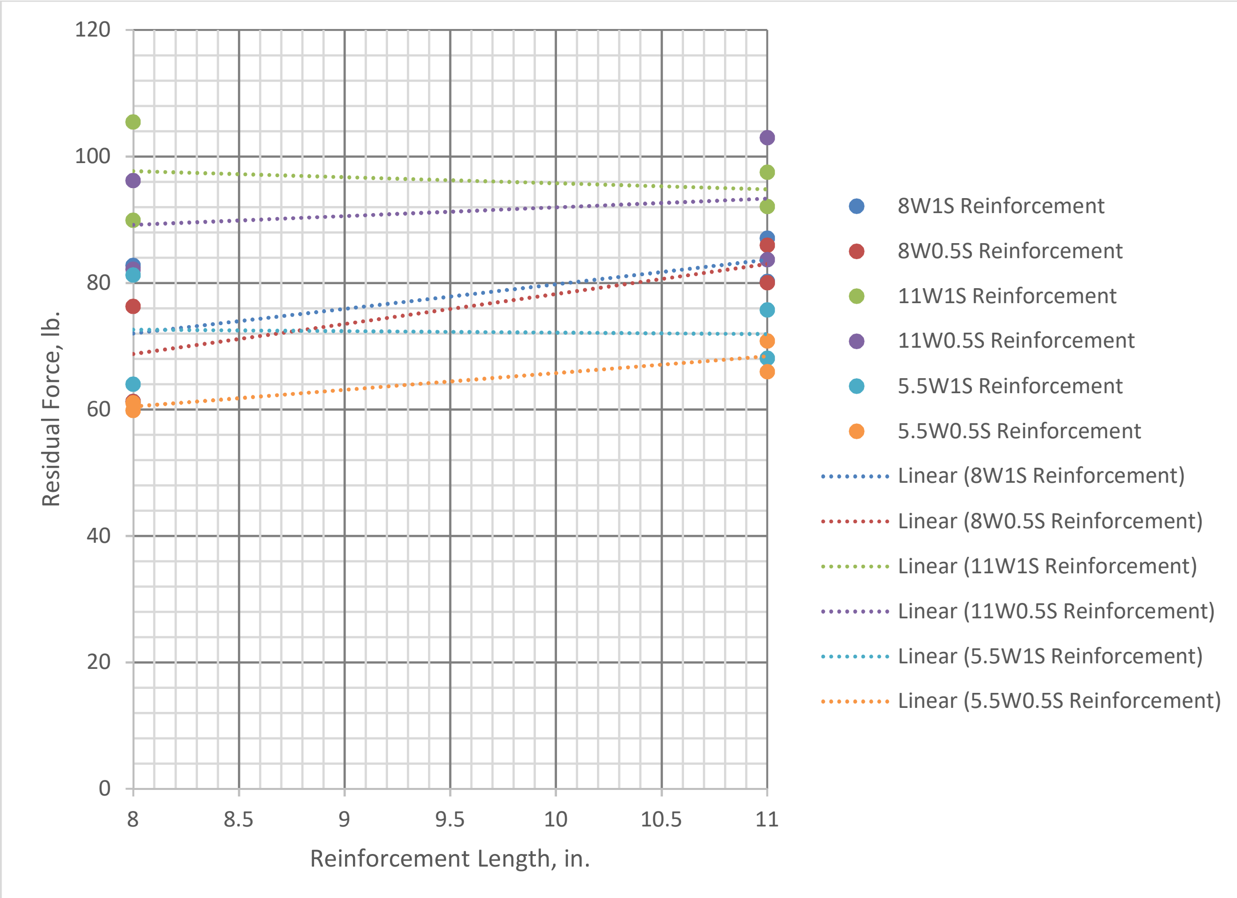

Figure 124: Residual Force vs. reinforcement length for various reinforcement width and spacings with linear trend lines (results of 24 tests)

After plotting, linear trend lines were added for each width and spacing combination to determine if any data trends were apparent. Table 37 shows the observed trends.

Table 37: Observed trends for Residual Force values as reinforcement length increases from 8" to 11"

Width and Spacing Combination	Residual Force Trend as Reinforcement Length Increases
PW5Lay	None
PW10Lay	Increase
8W5Lay	Increase
8W10Lay	Increase
11W5Lay	None
11W10Lay	None

Half of the tests showed no relationship between reinforcement length and Residual Force. The other half showed a slight increase in Residual Force as reinforcement length increased. Due to this, the initial observation is made that increasing reinforcement length has no effect on Residual Force values.

ii. Single Variable Linear Regression Analysis

A linear regression analysis was performed to determine the significance of change in Residual Force when the single variable, reinforcement length, is modified. Six sets of reinforcement widths and spacings were tested. For each reinforcement width and spacing set, two tests of two different reinforcement lengths were evaluated resulting in four data points. A t-test was performed at a 90% confidence interval. For each data set, a t* value was calculated and compared to a t value corresponding to a 90% confidence interval and 4 data points. Two alternatives exist for the two sided test: acceptance of the null hypothesis or acceptance of the alternate hypothesis. The null hypothesis concludes that there is no relationship between Residual Force and reinforcement width. The alternate hypothesis concludes that there is a relationship between Residual Force and reinforcement width. If the t* value is greater than the t value, the alternate hypothesis is chosen. If the t* value is less than or equal to the t value, the null hypothesis is chosen. P-values were also computed as p-values less than the level of significance support the alternate hypothesis. Each data set was plotted with reinforcement length on the abscissa and Residual Force on the ordinate. A linear best fit line was added and the slope of this line was computed. Table 38 summarizes the linear regression analysis.

Table 38: Linear regression analysis results for effect of reinforcement length on Residual Force. "Null Hypothesis" indicates that there is not a statistically significant relationship between the two variables, while "Alternate Hypothesis" indicates that there is a statistically significant relationship.

Reinforcement Width and Spacing	|t*|	t(0.95;2)	Decision	P-Value	Best Fit Line Slope
PW5Lay	0.073	2.92	Null Hypothesis	0.95	-0.23
PW10Lay	3.19	2.92	Alternate Hypothesis	0.085	2.65
8W5Lay	1.03	2.92	Null Hypothesis	0.41	3.885
8W10Lay	1.76	2.92	Null Hypothesis	0.22	4.743
11W5Lay	0.35	2.92	Null Hypothesis	0.76	-0.96
11W10Lay	0.348	2.92	Null Hypothesis	0.76	1.385

From the linear regression analysis, five of six data sets show that no relationship exists between reinforcement length and Residual Force. All of the decisions are supported by corresponding p-values. Best fit lines have positive and negative slopes, furthering the evidence that a relationship is nonexistent. Only one of the tests passed the t-test so it is very unlikely that a relationship exists between reinforcement length and Residual Force.

iii. Analysis of Variance

A single factor ANOVA was performed to determine if the mean value of the Residual Force data populations are equal when the single variable, reinforcement length, is modified. Six sets of reinforcement widths and spacings were tested. For each reinforcement width and spacing set, two tests of two different reinforcement lengths were evaluated resulting in four data points. A 90% confidence interval was used for the ANOVA. For each data set, an F value was computed as well as a critical F value. The alternate hypothesis states that at least one of the means of each data population is different. The null hypothesis states that the means of each data population are equal. If F exceeds $F_{critical}$, the null hypothesis is rejected and at least one of the means of the populations is different. Table 39 shows the results of the ANOVA.

Table 39: Results of ANOVA for Residual Force data as reinforcement length increases from 8" to 11"

Reinforcement Width and Spacing	F	$F_{critical}$	Decision
PW5Lay	0.005	8.562	Null Hypothesis
PW10Lay	10.177	8.562	Alternate Hypothesis
8W5Lay	1.065	8.562	Null Hypothesis
8W10Lay	3.110	8.562	Null Hypothesis
11W5Lay	0.123	8.562	Null Hypothesis
11W10Lay	0.121	8.562	Null Hypothesis

All six ANOVA results support the linear regression analysis results.

c. Peak Force Displacement

To determine the effect of reinforcement length on Peak Force Displacement, Peak Force Displacement vs. reinforcement length was plotted for each reinforcement width and spacing combination. After plotting, an initial observation was made, linear regression analysis was performed for data with reinforcement length as the only measurable variable, analysis of variance (ANOVA) was performed for data with reinforcement length as the only measurable variable, and linear regression analysis was performed for all of the data points with vertical spacing and width as known variables.

i. Initial Observation

Initial observation was made after plotting Peak Force Displacement vs. vertical spacing, Figure 125.

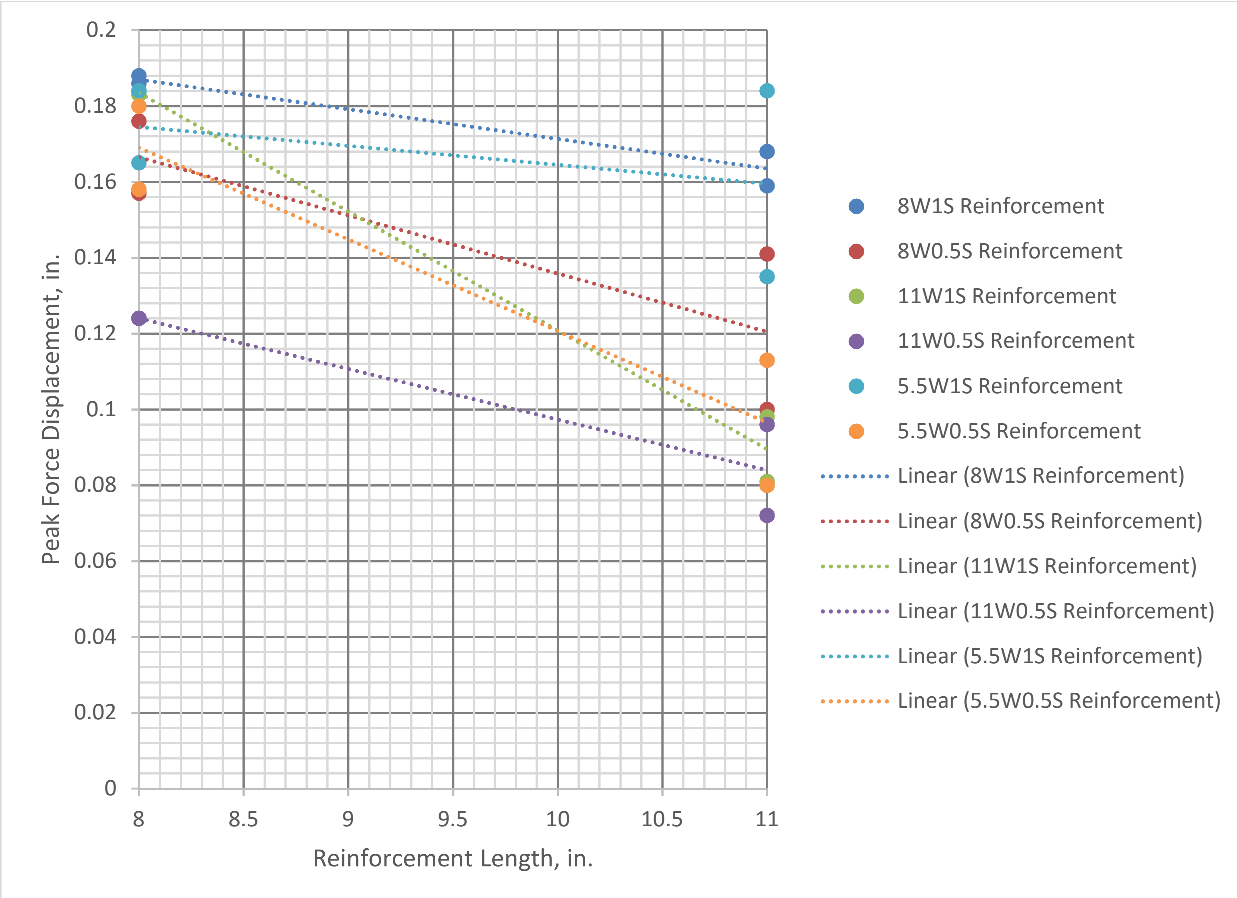

Figure 125: Peak Force Displacement vs. reinforcement length for various reinforcement width and spacings with linear trend lines (results of 24 tests)

After plotting, linear trend lines were added for each width and spacing combination to determine if any data trends were apparent. Table 40 shows the observed trends.

Table 40: Observed trends for Peak Force Displacement values as reinforcement length increases from 8" to 11"

Width and Spacing Combination	Peak Force Displacement Trend as Reinforcement Length Increases
PW5Lay	None
PW10Lay	Decrease
8W5Lay	Decrease
8W10Lay	Decrease
11W5Lay	Decrease
11W10Lay	Decrease

Most of the test showed a noticeable decrease in Peak Force Displacement as reinforcement length increased. Due to this, the initial observation is made that increasing reinforcement length results in a decrease in Peak Force Displacement values.

ii. Single Variable Linear Regression Analysis

A linear regression analysis was performed to determine the significance of change in Peak Force Displacement when the single variable, reinforcement length, is modified. Six sets of reinforcement widths and spacings were tested. For each reinforcement width and spacing set, two tests of two different reinforcement lengths were evaluated resulting in four data points. A t-test was performed at a 90% confidence interval. For each data set, a t* value was calculated and compared to a t value corresponding to a 90% confidence interval and 4 data points. Two alternatives exist for the two sided test,: acceptance of the null hypothesis or acceptance of the alternate hypothesis. The null hypothesis concludes that there is no relationship between Peak Force Displacement and reinforcement width. The alternate hypothesis concludes that there is a relationship between Peak Force Displacement and reinforcement width. If the t* value is greater than the t value, the alternate hypothesis is chosen. If the t* value is less than or equal to the t value, the null hypothesis is chosen. P-values were also computed as p-values less than the level of significance support the alternate hypothesis. Each data set was plotted with reinforcement length on the abscissa and Peak Force Displacement on the ordinate. A linear best fit line was added and the slope of this line was computed. Table 41 summarizes the linear regression analysis.

Table 41: Linear regression analysis results for effect of reinforcement length on Peak Force Displacement. "Null Hypothesis" indicates that there is not a statistically significant relationship between the two variables, while "Alternate Hypothesis" indicates that there is a statistically significant relationship.

Reinforcement Width and Spacing	|t*|	t(0.95;2)	Decision	P-Value	Best Fit Line Slope
PW5Lay	.057	2.92	Null Hypothesis	0.63	-0.005
PW10Lay	3.66	2.92	Alternate Hypothesis	0.067	-0.0242
8W5Lay	5.1	2.92	Alternate Hypothesis	0.036	-0.0078
8W10Lay	2.04	2.92	Null Hypothesis	0.18	-0.0153
11W5Lay	11.03	2.92	Alternate Hypothesis	0.008	-0.03
11W10Lay	3.33	2.92	Alternate Hypothesis	0.08	-0.0133

From the linear regression analysis, four of six data sets show that a relationship exists between reinforcement length and Peak Force Displacement. All of the decisions are supported by corresponding p-values. Best fit lines have only negative slopes, indicating that a negative relationship between reinforcement length and Peak Force Displacement is a possibility.

iii. Analysis of Variance

A single factor ANOVA was performed to determine if the mean value of the Peak Force Displacement data populations are equal when the single variable, reinforcement length, is modified. Six sets of reinforcement widths and spacings were tested. For each reinforcement width and spacing set, two tests of two different reinforcement lengths were evaluated resulting in four data points. A 90% confidence interval was used for the ANOVA. For each data set, an F value was computed as well as a critical F value. The alternate hypothesis states that at least one of the means of each data population is different. The null hypothesis states that the means of each data population are equal. If F exceeds $F_{critical}$, the null hypothesis is rejected and at least one of the means of the populations is different. Table 42 shows the results of the ANOVA.

Table 42: Results of ANOVA for Peak Force Displacement data as reinforcement length increases from 8” to 11”

Reinforcement Width and Spacing	F	$F_{critical}$	Decision
PW5Lay	0.326	8.562	Null Hypothesis
PW10Lay	13.366	8.562	Alternate Hypothesis
8W5Lay	25.988	8.562	Alternate Hypothesis
8W10Lay	4.145	8.562	Null Hypothesis
11W5Lay	121.876	8.562	Alternate Hypothesis
11W10Lay	11.111	8.562	Alternate Hypothesis

All six ANOVA results support the linear regression analysis results.

d. K_{50}

To determine the effect of reinforcement length on K_{50}, K_{50} vs. reinforcement length was plotted for each reinforcement width and spacing combination. After plotting, an initial observation was made, linear regression analysis was performed for data with reinforcement length as the only measurable variable, analysis of variance (ANOVA) was performed for data with reinforcement length as the only measurable variable, and linear regression analysis was performed for all of the data points with vertical spacing and width as known variables.

i. Initial Observation

Initial observation was made after plotting K_{50} vs. vertical spacing, Figure 126.

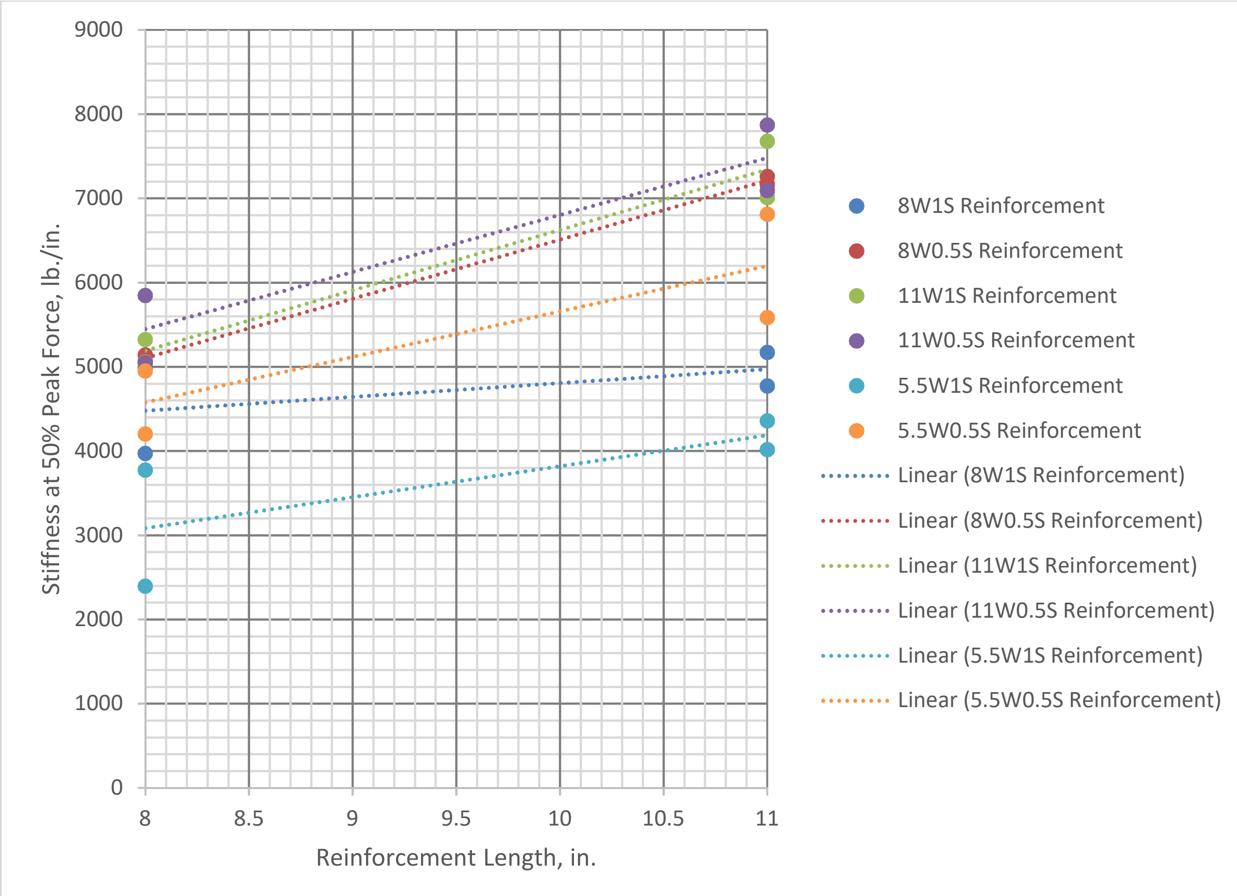

Figure 126: K_{50} vs. reinforcement length for various reinforcement width and spacings with linear trend lines (results of 24 tests)

After plotting, linear trend lines were added for each width and spacing combination to determine if any data trends were apparent. Table 43 shows the observed trends.

Table 43: Observed trends for K_{50} values as reinforcement length increases from 8" to 11"

Width and Spacing Combination	K_{50} Trend as Reinforcement Length Increases
PW5Lay	None
PW10Lay	Increase
8W5Lay	None
8W10Lay	Increase
11W5Lay	Increase
11W10Lay	Increase

Most tests showed a noticeable increase in K_{50} values as reinforcement length is increased. Due to this, the initial observation is made that increasing reinforcement length results in increased K_{50} values.

ii. Single Variable Linear Regression Analysis

A linear regression analysis was performed to determine the significance of change in K_{50} when the single variable, reinforcement length, is modified. Six sets of reinforcement widths and spacings were tested. For each reinforcement width and spacing set, two tests of two different reinforcement lengths were evaluated resulting in four data points. A t-test was performed at a 90% confidence interval. For each data set, a t* value was calculated and compared to a t value corresponding to a 90% confidence interval and 4 data points. Two alternatives exist for the two sided test: acceptance of the null hypothesis or acceptance of the alternate hypothesis. The null hypothesis concludes that there is no relationship between K_{50} and reinforcement width. The alternate hypothesis concludes that there is a relationship between K_{50} and reinforcement width. If the t* value is greater than the t value, the alternate hypothesis is chosen. If the t* value is less than or equal to the t value, the null hypothesis is chosen. P-values were also computed as p-values less than the level of significance support the alternate hypothesis. Each data set was plotted with reinforcement length on the abscissa and K_{50} on the ordinate. A linear best fit line was added and the slope of this line was computed. Table 44 summarizes the linear regression analysis.

Table 44: Linear regression analysis results for effect of reinforcement length on K_{50}. "Null Hypothesis" indicates that there is not a statistically significant relationship between the two variables, while "Alternate Hypothesis" indicates that there is a statistically significant relationship.

Reinforcement Width and Spacing	|t*|	t(0.95;2)	Decision	P-Value	Best Fit Line Slope
PW5Lay	1.55	2.92	Null Hypothesis	0.26	368
PW10Lay	2.26	2.92	Null Hypothesis	0.15	540.3
8W5Lay	0.9	2.92	Null Hypothesis	0.46	164.17
8W10Lay	36.3	2.92	Alternate Hypothesis	0.00076	702
11W5Lay	5.99	2.92	Alternate Hypothesis	0.027	717
11W10Lay	3.65	2.92	Alternate Hypothesis	0.068	677.5

From the linear regression analysis, three of six data sets show that a relationship exists between reinforcement length and K_{50}. All of the decisions are supported by corresponding p-values. Best fit lines have only positive slopes, showing that a positive relationship between reinforcement length and K_{50} is a possibility.

iii. Analysis of Variance

A single factor ANOVA was performed to determine if the mean value of the K_{50} data populations are equal when the single variable, reinforcement length, is modified. Six sets of reinforcement widths and spacings were tested. For each reinforcement width and spacing set, two tests of two different reinforcement lengths were evaluated resulting in four data points. A 90% confidence interval was used for the ANOVA. For each data set, an F value was computed as well as a critical F value. The alternate hypothesis states that at least one of the means of each data population is different. The null hypothesis states that the means of each data population are equal. If F exceeds $F_{critical}$, the null hypothesis is rejected and at least one of the means of the populations is different. Table 45 shows the results of the ANOVA.

Table 45: Results of ANOVA for K_{50} data as reinforcement length increases from 8" to 11"

Reinforcement Width and Spacing	F	$F_{critical}$	Decision
PW5Lay	2.417	8.562	Null Hypothesis
PW10Lay	5.106	8.562	Null Hypothesis
8W5Lay	0.811	8.562	Null Hypothesis
8W10Lay	1318.049	8.562	Alternate Hypothesis
11W5Lay	35.906	8.562	Alternate Hypothesis
11W10Lay	13.321	8.562	Alternate Hypothesis

All six ANOVA results support the linear regression analysis results.

2. Failure Surface Location

To evaluate the effect of reinforcement length on the failure surface location, the mid-plate failure surface location was plotted for each vertical spacing and width combination, allowing reinforcement length to be the only variable in the reinforcement geometry for each plot. The data presented in Figures 127-132 are from the failure surfaces determined with painted layers.

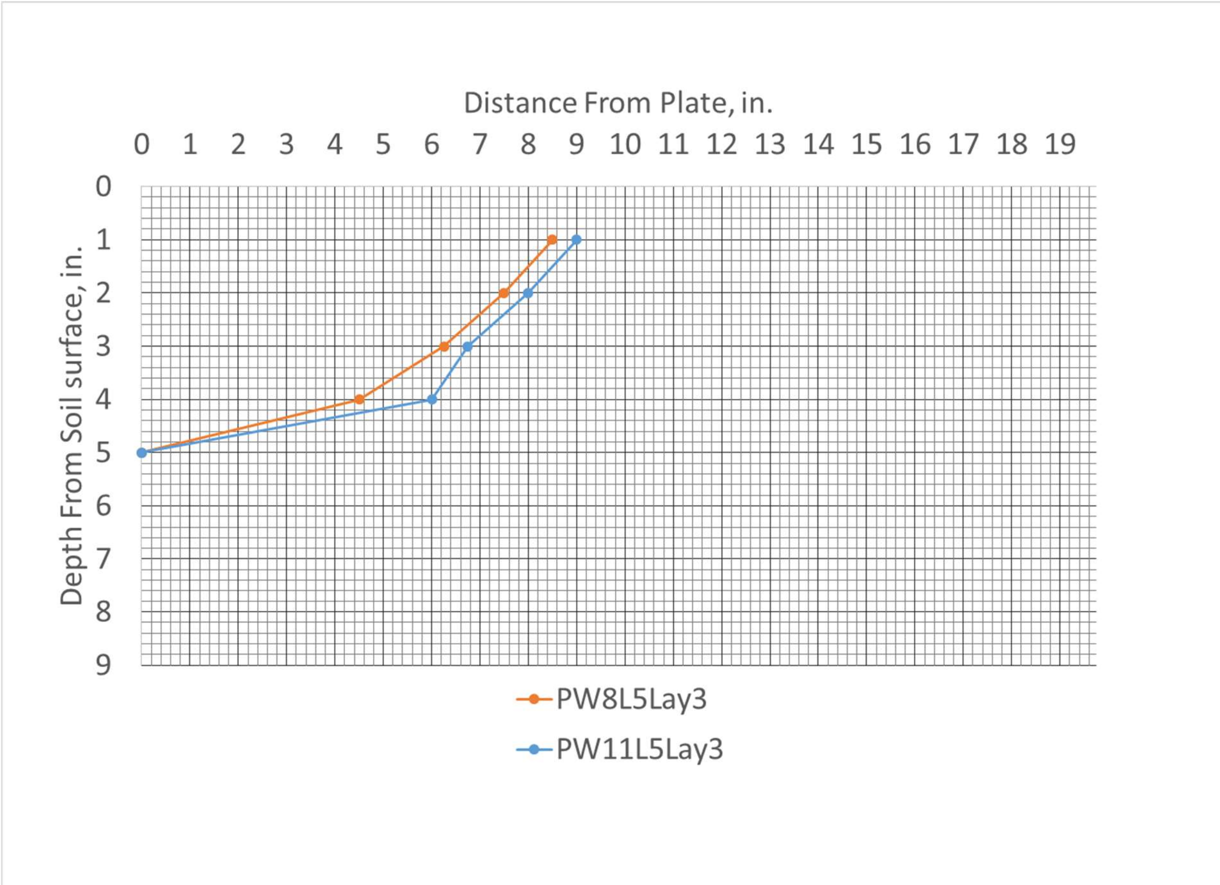

Figure 127: Mid-Plate failure surface location of tests PW8L5Lay3 and PW11L5Lay3

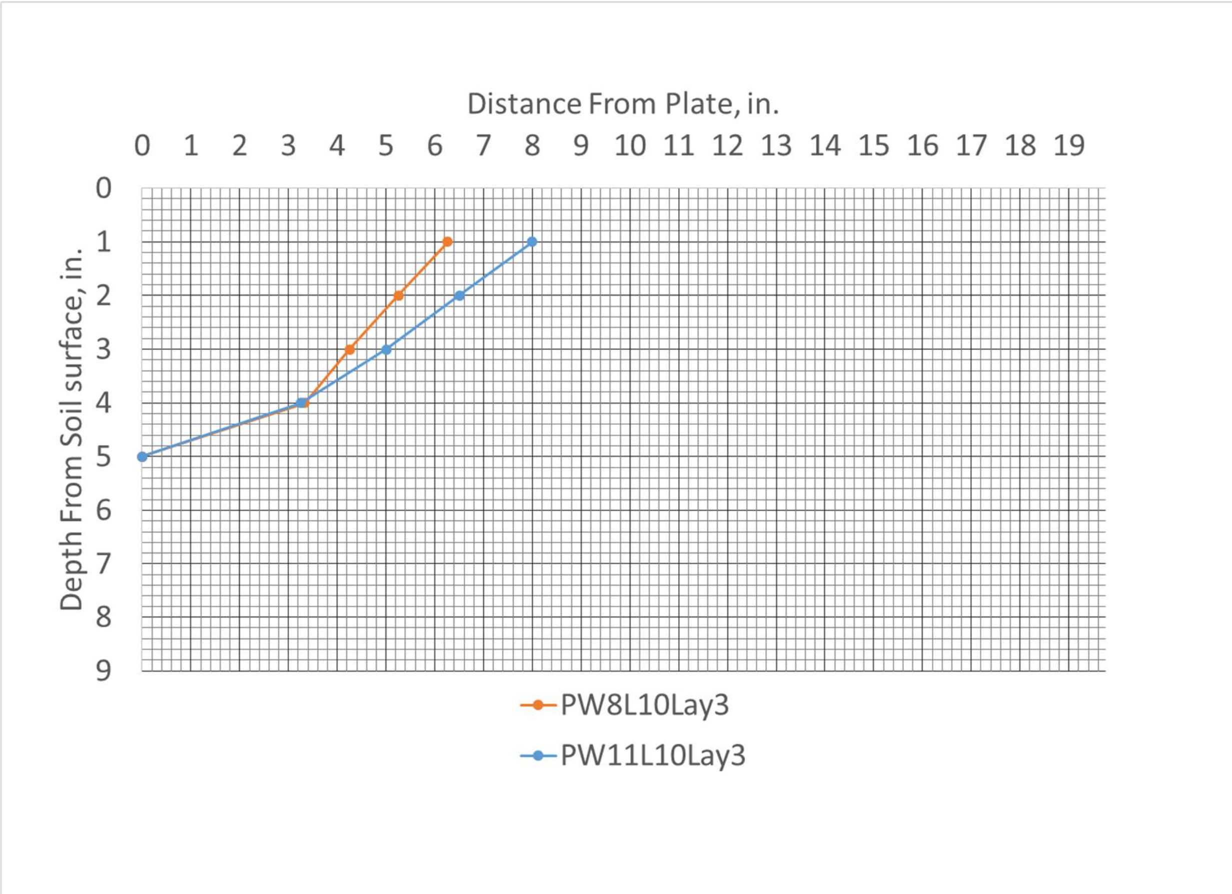

Figure 128: Mid-Plate failure surface location of tests PW8L10Lay3 and PW11L10Lay3

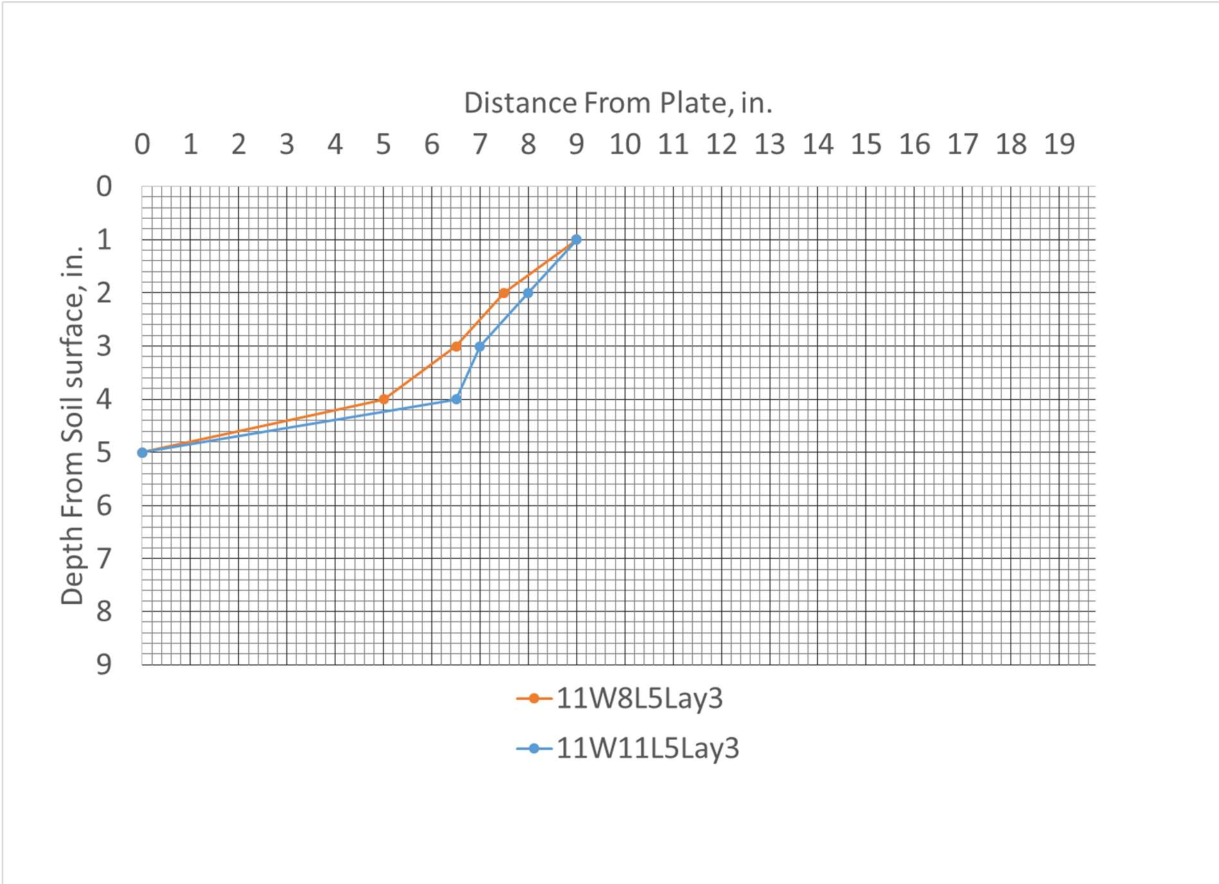

Figure 129: Mid-Plate failure surface location of tests 11W8L5Lay3 and 11W11L5Lay3

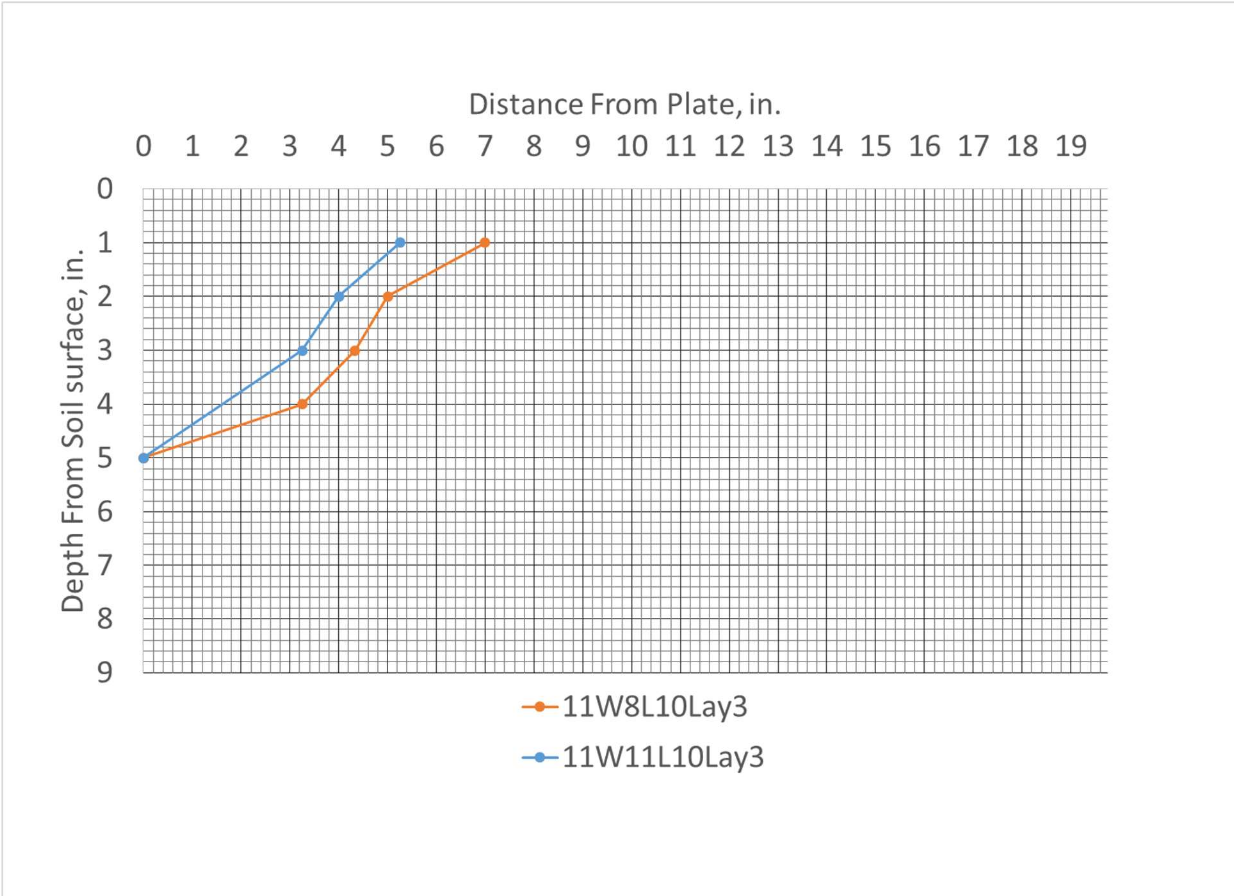

Figure 130: Mid-Plate failure surface location of tests 11W8L10Lay3 and 11W11L10Lay3

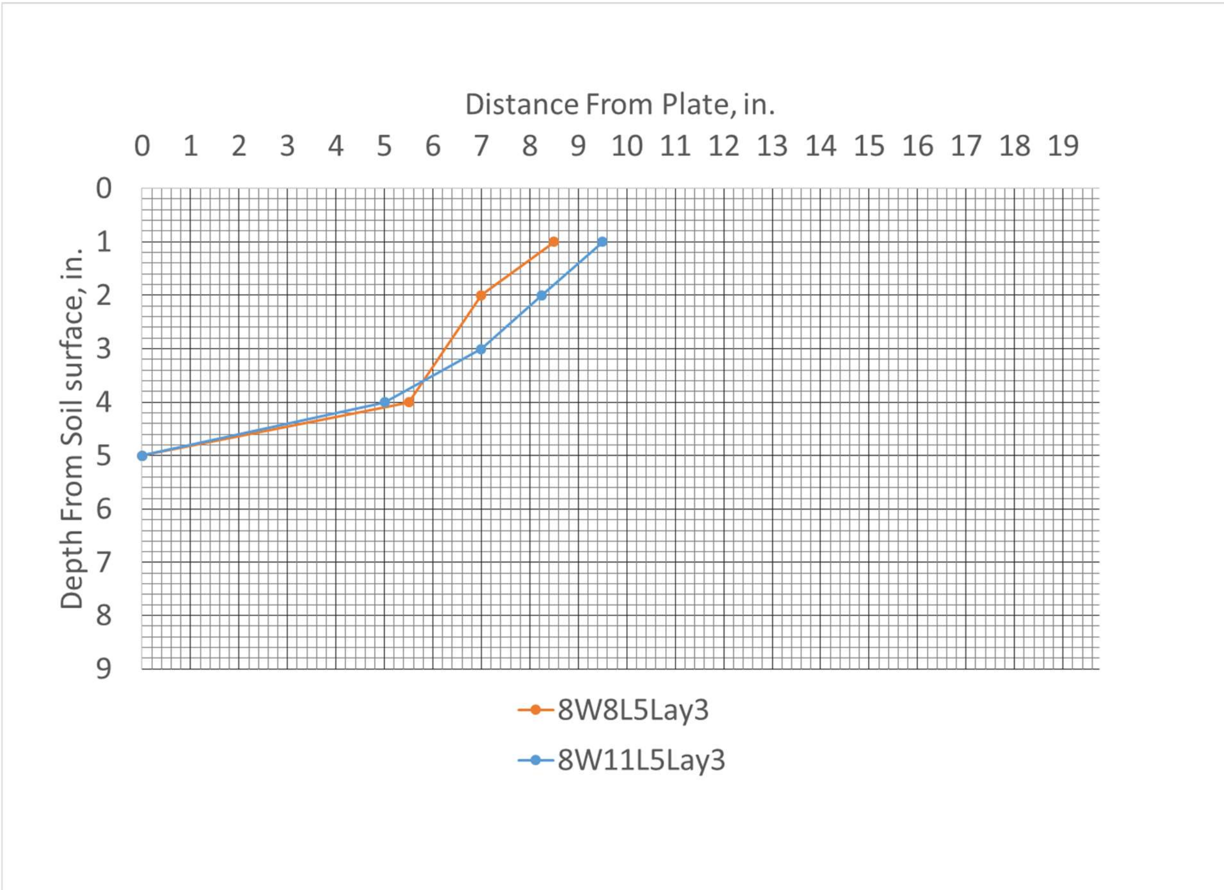

Figure 131: Mid-Plate failure surface location of tests 8W8L5Lay3 and 8W11L5Lay3

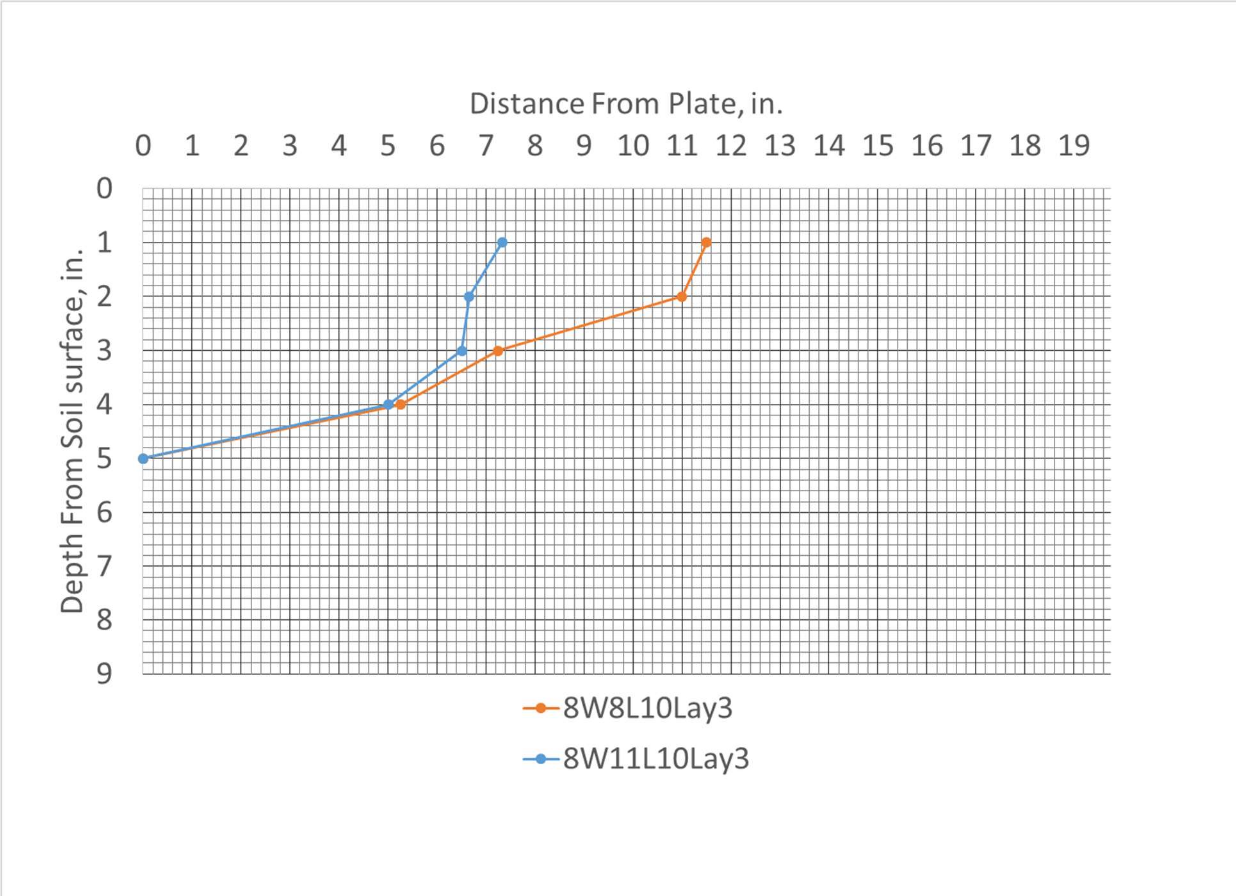

Figure 132: Mid-Plate failure surface location of tests 8W8L10Lay3 and 8W11L10Lay3

As length increased, four of the six pairs of test showed increasing failure surface length while two of the six showed decreasing failure surface length. It was expected that as length increased, the longer weak layer would lead to a shorter failure surface length. There is no discernable pattern present with regard to failure surface location and reinforcement length.

iv. Effect of Reinforcement Surface Area

1. Load Deformation Characteristics

a. Peak Force

To determine the effect of reinforcement surface area on Peak Force, Peak Force vs. surface area was plotted. After plotting, an initial observation was made, linear regression analysis was performed for data with surface area as the only measurable variable, and analysis of variance (ANOVA) was performed for data with surface area as the only measurable variable.

i. Initial Observation

Initial observation was made after plotting Peak Force vs. reinforcement surface area, Figure 133.

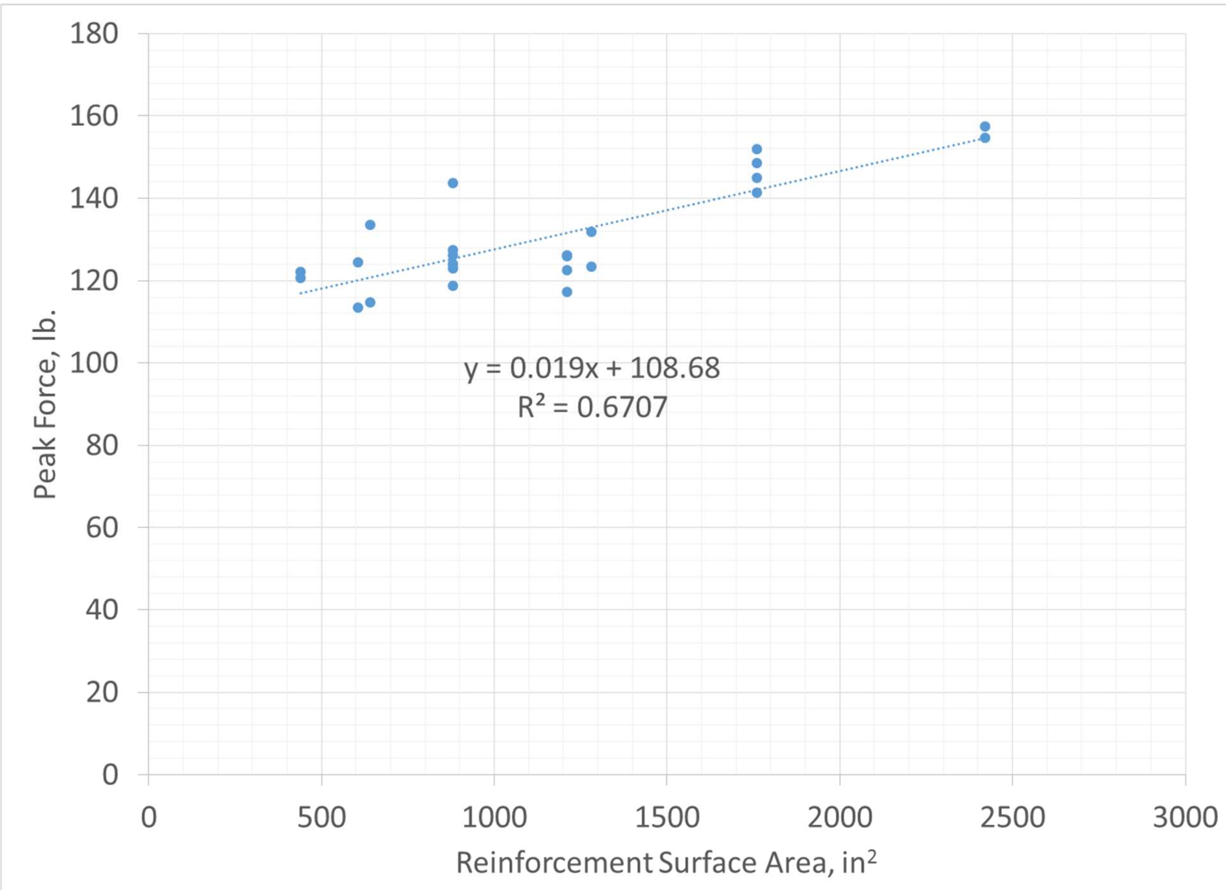

Figure 133: Peak Force vs. reinforcement surface area (results of 24 tests)

With the addition of a trend line, it is likely that there is a positive relationship between reinforcement surface area and Peak Force.

ii. Single Variable Linear Regression Analysis

A linear regression analysis was performed to determine the significance of change in Peak Force when the single variable, reinforcement surface area, is modified. Twenty four data points are present for this linear regression. A t-test was performed at a 90% confidence interval. A t* value was calculated and compared to a t value corresponding to a 90% confidence interval and 24 data points. Two alternatives exist for the two sided test,: acceptance of the null hypothesis or acceptance of the alternate hypothesis. The null hypothesis concludes that there is no relationship between Peak Force and reinforcement surface area. The alternate hypothesis concludes that there is a relationship between Peak Force and reinforcement surface area. If the t* value is greater than the t value, the alternate hypothesis is chosen. If the t* value is less than or equal to the t value, the null hypothesis is chosen. P-values were also computed as p-values less than the level of significance support the alternate hypothesis. Each data set was plotted with reinforcement surface area on the abscissa and Peak Force on the ordinate. A linear best fit line was added and the slope of this line was computed. Table 46 summarizes the linear regression analysis.

Table 46: Linear regression analysis results for Peak Force vs. reinforcement surface area. "Null Hypothesis" indicates that there is not a statistically significant relationship between the two variables, while "Alternate Hypothesis" indicates that there is a statistically significant relationship.

|t*|	t(0.95;22)	Decision	P-Value	Best Fit Line Slope
6.693	1.717	Alternate Hypothesis	9.96E-07	0.019

The linear regression analysis shows that a positive relationship exists between Peak Force and reinforcement surface area. The decision is supported by a corresponding p-value.

iii. Analysis of Variance

A single factor ANOVA was performed to determine if the mean values of the Peak Force data population are equal when the single variable, reinforcement surface area, is modified. Eight surface areas were tested. A 90% confidence interval was used for the

ANOVA. For the data set, an F value was computed as well as a critical F value. The alternate hypothesis states that at least one of the means of each data population is different. The null hypothesis states that the means of each data population are equal. If F exceeds $F_{critical}$, the null hypothesis is rejected and at least one of the means of the populations is different. Table 47 shows the results of the ANOVA.

Table 47: Results of ANOVA for Peak Force data vs. reinforcement surface area. "Null Hypothesis" indicates that there is not a statistically significant relationship between the two variables, while "Alternate Hypothesis" indicates that there is a statistically significant relationship.

F	$F_{critical}$	Decision
9.485	2.128	Alternate Hypothesis

The ANOVA result supports the linear regression analysis result.

b. Residual Force

To determine the effect of reinforcement surface area on Residual Force, Residual Force vs. surface area was plotted. After plotting, an initial observation was made, linear regression analysis was performed for data with surface area as the only measurable variable, and analysis of variance (ANOVA) was performed for data with surface area as the only measurable variable.

i. Initial Observation

Initial observation was made after plotting Residual Force vs. reinforcement surface area, Figure 134.

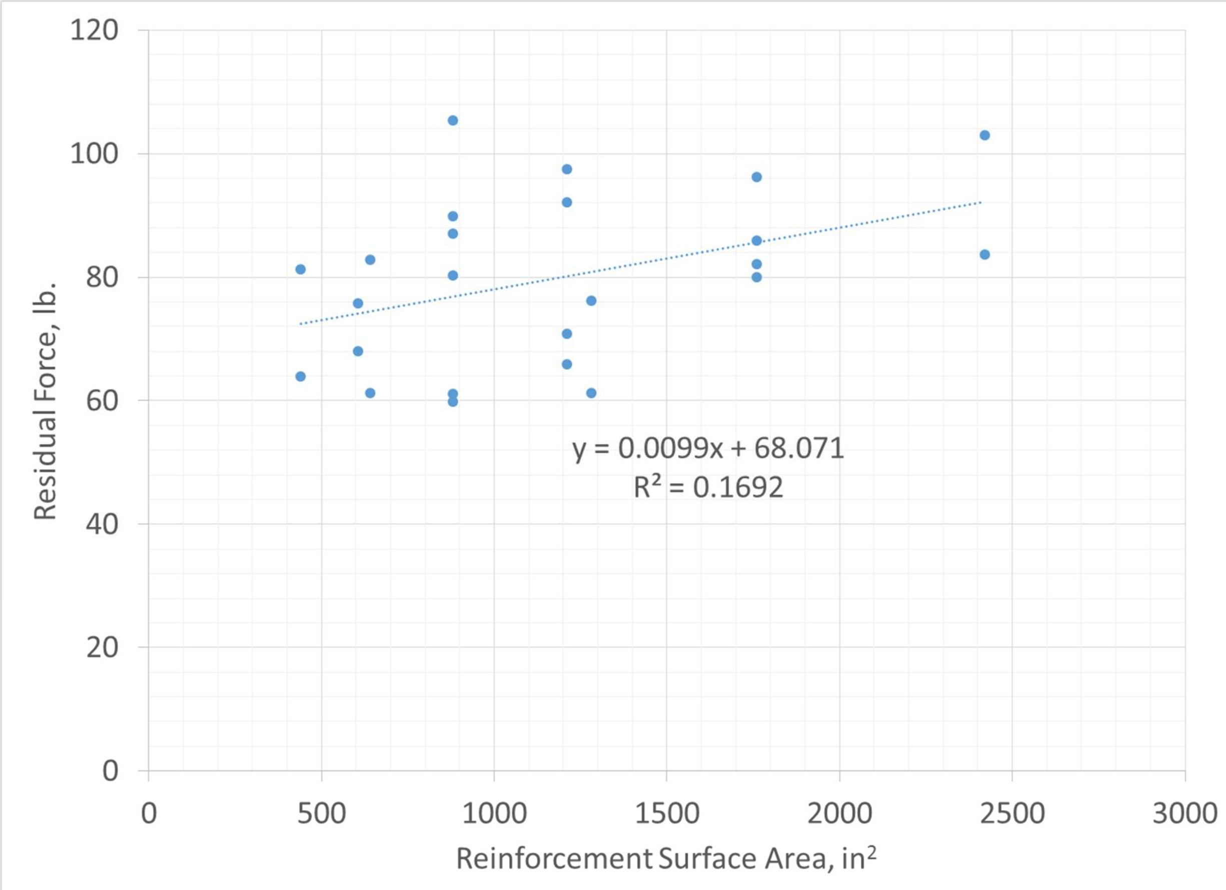

Figure 134: Residual Force vs. reinforcement surface area (results of 24 tests)

With the addition of a trend line, it is possible that there is a positive relationship between reinforcement surface area and Residual Force. However, quite a bit of scatter exists in the plot so the apparent positive relationship may not be statistically significant.

ii. Single Variable Linear Regression Analysis

A linear regression analysis was performed to determine the significance of change in Residual Force when the single variable, reinforcement surface area, is modified. Twenty four data points are present for this linear regression. A t-test was performed at a 90% confidence interval. A t* value was calculated and compared to a t value corresponding to a 90% confidence interval and 24 data points. Two alternatives exist for the two sided test: acceptance of the null hypothesis or acceptance of the alternate hypothesis. The null hypothesis concludes that there is no relationship between Residual Force and reinforcement surface area. The alternate hypothesis concludes that there is a relationship between Residual Force and reinforcement surface area. If the t* value is greater than the t value, the alternate hypothesis is chosen. If the t* value is less than or equal to the t value, the null hypothesis is chosen. P-values were also computed as p-values less than the level of significance support the alternate hypothesis. Each data set was plotted with reinforcement surface area on the abscissa and Residual Force on the ordinate. A linear best fit line was added and the slope of this line was computed. Table 48 summarizes the linear regression analysis.

Table 48: Linear regression analysis results for Residual Force vs. reinforcement surface area. "Null Hypothesis" indicates that there is not a statistically significant relationship between the two variables, while "Alternate Hypothesis" indicates that there is a statistically significant relationship.

|t*|	t(0.95;22)	Decision	P-Value	Best Fit Line Slope
2.116	1.717	Alternate Hypothesis	4.50E-02	0.01

The linear regression analysis shows that a positive relationship exists between Residual Force and reinforcement surface area. The decision is supported by a corresponding p-value.

iii. Analysis of Variance

A single factor ANOVA was performed to determine if the mean values of the Residual Force data population are equal when the single variable, reinforcement surface area, is modified. A 90% confidence interval was used for the ANOVA. For the data set, an F value was computed as well as a critical F value. The alternate hypothesis states that at least one of the means of each data population is different. The null hypothesis states that the means of each data population are equal. If F exceeds $F_{critical}$, the null hypothesis is rejected and at least one of the means of the populations is different. Table 49 shows the results of the ANOVA.

Table 49: Results of ANOVA for Residual Force data vs. reinforcement surface area. "Null Hypothesis" indicates that there is not a statistically significant relationship between the two variables, while "Alternate Hypothesis" indicates that there is a statistically significant relationship.

F	$F_{critical}$	Decision
0.824	2.128	Null Hypothesis

The ANOVA result did not support the linear regression analysis result.

c. Peak Force Displacement

To determine the effect of reinforcement surface area on Peak Force Displacement, Peak Force Displacement vs. surface area was plotted. After plotting, an initial observation was made, linear regression analysis was performed for data with surface area as the only measurable variable, and analysis of variance (ANOVA) was performed for data with surface area as the only measurable variable.

i. Initial Observation

Initial observation was made after plotting Peak Force Displacement vs. reinforcement surface area, Figure 135.

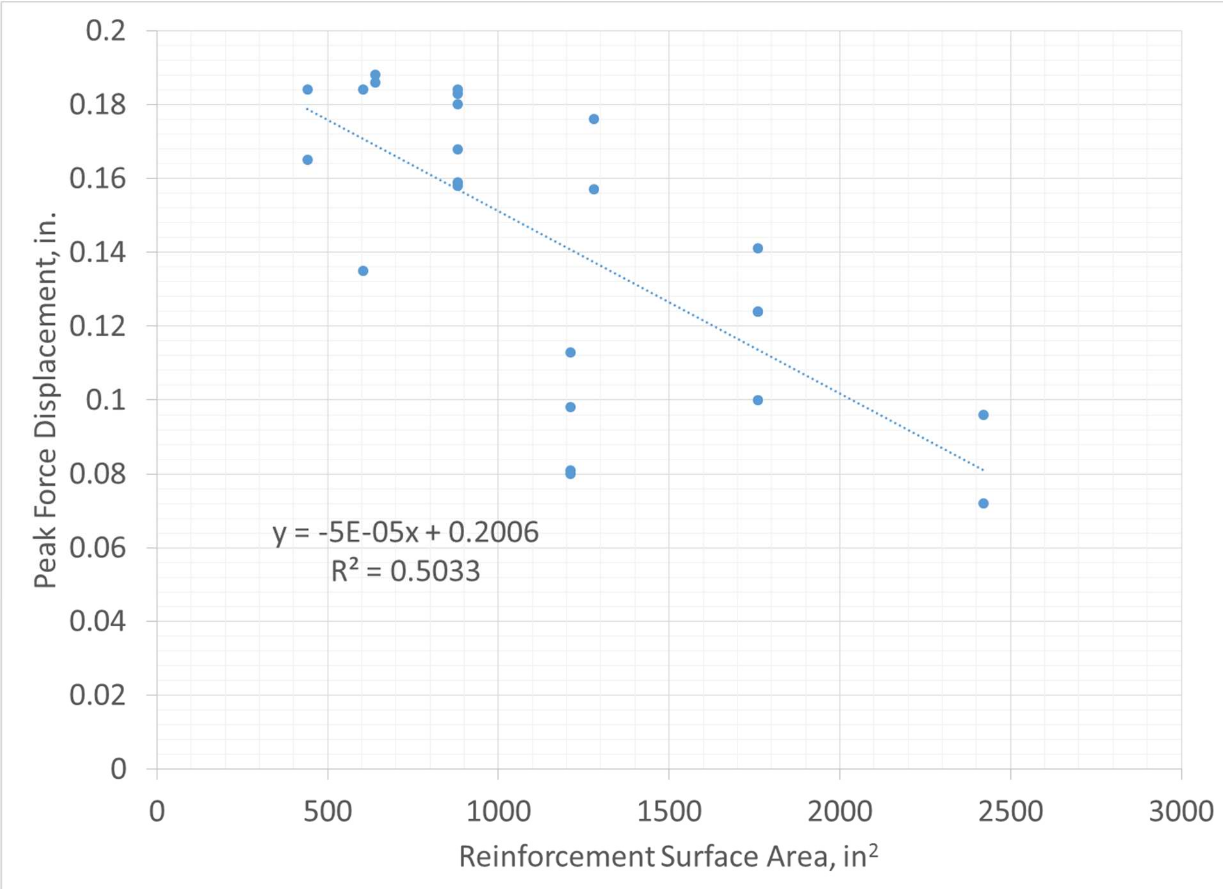

Figure 135: Peak Force Displacement vs. reinforcement surface area (results of 24 tests)

With the addition of a trend line, it is likely that there is a negative relationship between reinforcement surface area and Peak Force Displacement.

ii. Single Variable Linear Regression Analysis

A linear regression analysis was performed to determine the significance of change in Peak Force Displacement when the single variable, reinforcement surface area, is modified. Twenty four data points are present for this linear regression. A t-test was performed at a 90% confidence interval. A t* value was calculated and compared to a t value corresponding to a 90% confidence interval and 24 data points. Two alternatives exist for the two sided test: acceptance of the null hypothesis or acceptance of the alternate hypothesis. The null hypothesis concludes that there is no relationship between Peak Force Displacement and reinforcement surface area. The alternate hypothesis concludes that there is a relationship between Peak Force Displacement and reinforcement surface area. If the t* value is greater than the t value, the alternate hypothesis is chosen. If the t* value is less than or equal to the t value, the null hypothesis is chosen. P-values were also computed as p-values less than the level of significance support the alternate hypothesis. Each data set was plotted with reinforcement surface area on the abscissa and Peak Force Displacement on the ordinate. A linear best fit line was added and the slope of this line was computed. Table 50 summarizes the linear regression analysis.

Table 50: Linear regression analysis results for Peak Force Displacement vs. reinforcement surface area. "Null Hypothesis" indicates that there is not a statistically significant relationship between the two variables, while "Alternate Hypothesis" indicates that there is a statistically significant relationship.

|t*|	t(0.95;22)	Decision	P-Value	Best Fit Line Slope
4.72	1.717	Alternate Hypothesis	1.00E-04	-5.00E-05

The linear regression analysis shows that a negative relationship exists between Peak Force Displacement and reinforcement surface area. The decision is supported by a corresponding p-value.

iii. Analysis of Variance

A single factor ANOVA was performed to determine if the mean values of the Peak Force Displacement data population are equal when the single variable, reinforcement surface area, is modified. A 90% confidence interval was used for the ANOVA. For the data set, an F value was computed as well as a critical F value. The alternate hypothesis states that at least one of the means of each data population is different. The null hypothesis states that the means of each data population are equal. If F exceeds $F_{critical}$, the null hypothesis is rejected and at least one of the means of the populations is different. Table 51 shows the results of the ANOVA.

Table 51: Results of ANOVA for Peak Force Displacement data vs. reinforcement surface area. "Null Hypothesis" indicates that there is not a statistically significant relationship between the two variables, while "Alternate Hypothesis" indicates that there is a statistically significant relationship.

F	$F_{critical}$	Decision
17.194	2.128	Alternate Hypothesis

The ANOVA result supports the linear regression analysis result.

d. K_{50}

To determine the effect of reinforcement surface area on K_{50}, K_{50} vs. surface area was plotted. After plotting, an initial observation was made, linear regression analysis was performed for data with surface area as the only measurable variable, and analysis of variance (ANOVA) was performed for data with surface area as the only measurable variable.

i. Initial Observation

Initial observation was made after plotting K_{50} vs. reinforcement surface area, Figure 136.

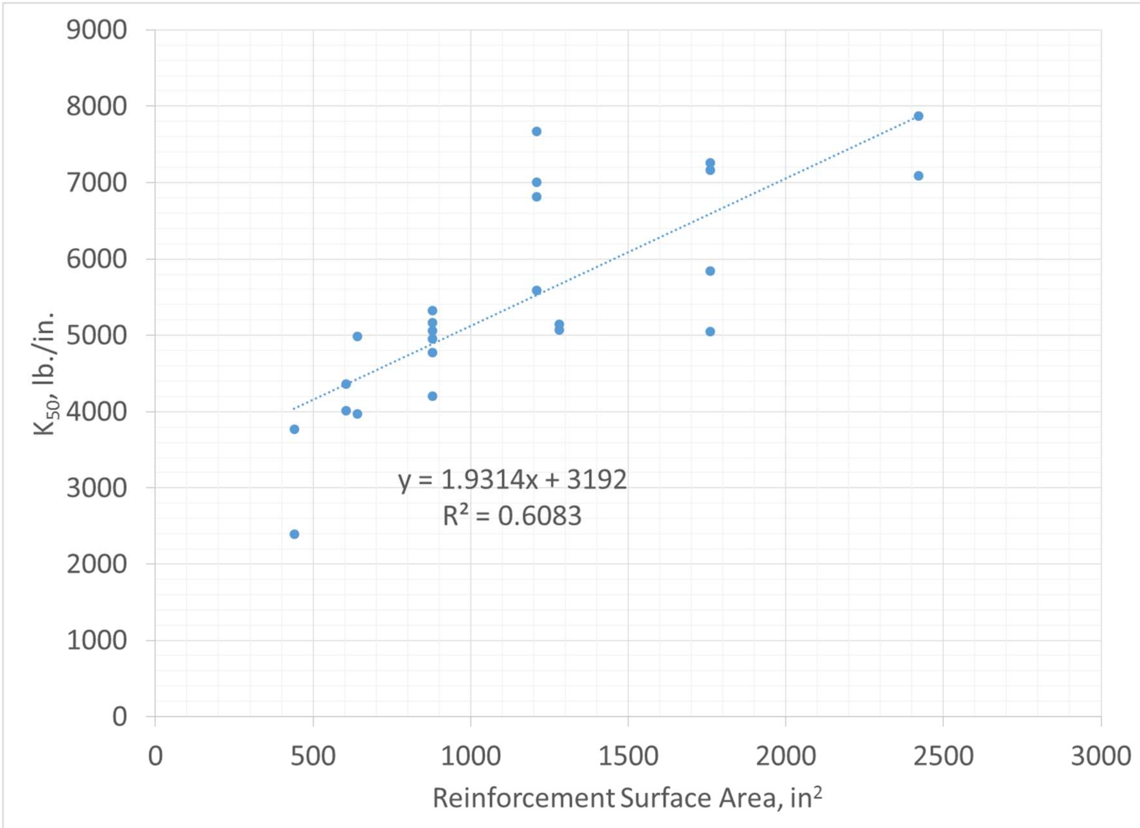

Figure 136: K_{50} vs. reinforcement surface area (results of 24 tests)

With the addition of a trend line, it is likely that there is a positive relationship between reinforcement surface area and K_{50}.

ii. Single Variable Linear Regression Analysis

A linear regression analysis was performed to determine the significance of change in K_{50} when the single variable, reinforcement surface area, is modified. Twenty four data points are present for this linear regression. A t-test was performed at a 90% confidence interval. A t* value was calculated and compared to a t value corresponding to a 90% confidence interval and 24 data points. Two alternatives exist for the two sided test: acceptance of the null hypothesis or acceptance of the alternate hypothesis. The null hypothesis concludes that there is no relationship between K_{50} and reinforcement surface area. The alternate hypothesis concludes that there is a relationship between K_{50} and reinforcement surface area. If the t* value is greater than the t value, the alternate hypothesis is chosen. If the t* value is less than or equal to the t value, the null hypothesis is chosen. P-values were also computed as p-values less than the level of significance support the alternate hypothesis. Each data set was plotted with reinforcement surface area on the abscissa and K_{50} force on the ordinate. A linear best fit line was added and the slope of this line was computed. Table 52 summarizes the linear regression analysis.

Table 52: Linear regression analysis results for K_{50} vs. reinforcement surface area. "Null Hypothesis" indicates that there is not a statistically significant relationship between the two variables, while "Alternate Hypothesis" indicates that there is a statistically significant relationship.

|t*|	t(0.95;22)	Decision	P-Value	Best Fit Line Slope
5.84	1.717	Alternate Hypothesis	7.01E-06	1.93

The linear regression analysis shows that a positive relationship exists between K_{50} and reinforcement surface area. The decision is supported by a corresponding p-value.

iii. Analysis of Variance

A single factor ANOVA was performed to determine if the mean value of the Peak Force data populations are equal when the single variable, reinforcement vertical spacing, is modified. A 90% confidence interval was used for the ANOVA. For each data set, an F value was computed as well as a critical F value. The alternate hypothesis states that at least one of the means of each data population is different. The null hypothesis states that the means of each data population are equal. If F exceeds $F_{critical}$, the null hypothesis is rejected and at least one of the means of the populations is different. Table 53 shows the results of the ANOVA.

Table 53: Results of ANOVA for K_{50} data vs. reinforcement surface area. "Null Hypothesis" indicates that there is not a statistically significant relationship between the two variables, while "Alternate Hypothesis" indicates that there is a statistically significant relationship.

F	$F_{critical}$	Decision
10.039	2.128	Alternate Hypothesis

The ANOVA result supports the linear regression analysis result.

2. Failure Surface Location

To evaluate the effect of reinforcement surface area on the failure surface location, the mid-plate failure surface location was plotted for each test with the test name and surface area in square inches (in parentheses) and is shown in Figure 137. The data presented in the plots are from the failure surfaces determined with painted layers.

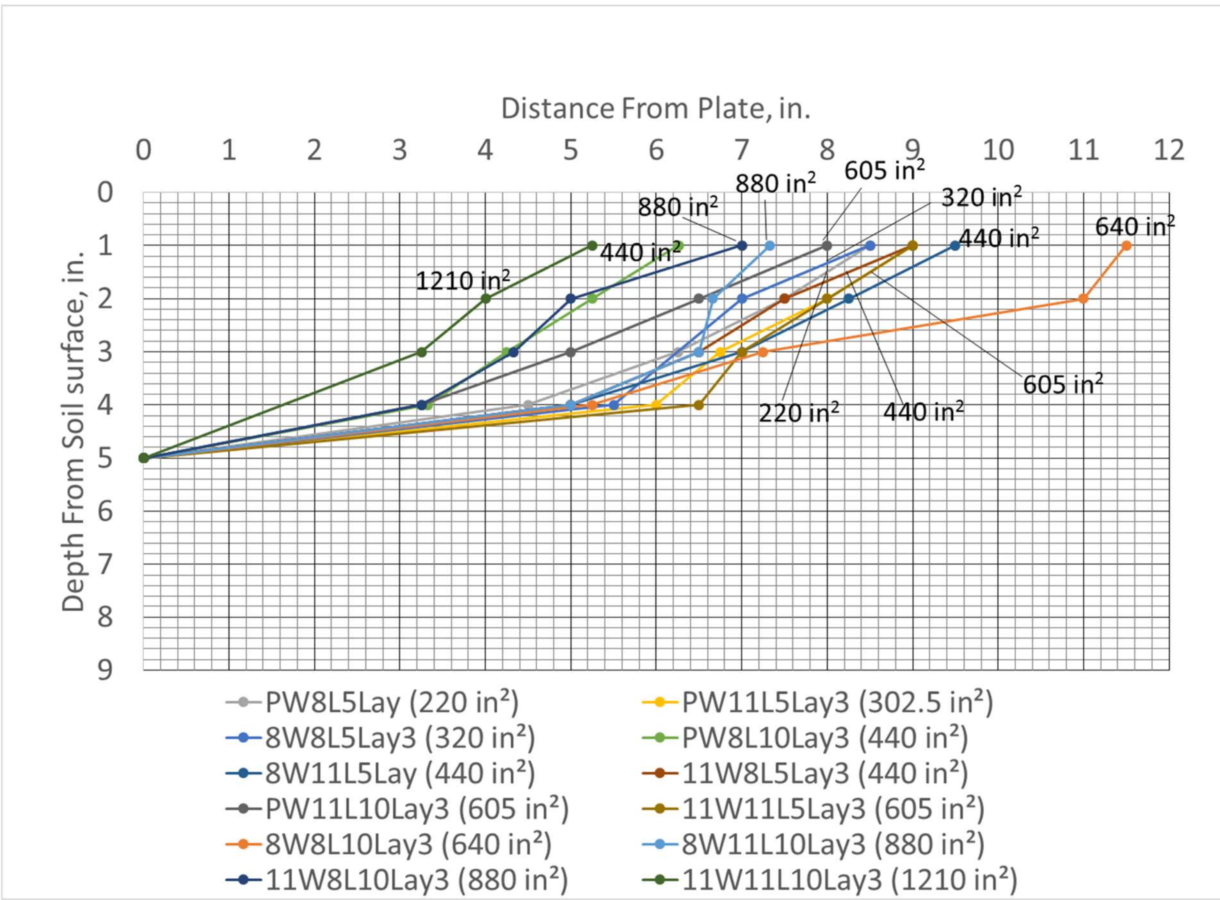

Figure 137: Mid-Plate failure surface for all length, width, and vertical spacing combinations with reinforcement surface area in square inches in parentheses. Numbers on the plot indicate reinforcement surface area for each configuration in square inches.

From the plot, no discernable relationship is shown between failure surface location and reinforcement surface area.

v. Complete Data Set Linear Regression Analyses

1. Peak Force

A linear regression analysis was performed to determine the overall effect of reinforcement vertical spacing, length, and width on Peak Force. The regression was performed with pairs of spacing and Peak Force, length and Peak Force, and width and Peak Force. For each geometric parameter that is varied, the other two geometric parameters are also varied. The regression represents the relationship between the three geometric parameters and Peak Force with a variety of variables present. Table 54 summarizes the results of the linear regression.

Table 54: Results of linear regression analysis for overall effect of geometric parameters on Peak Force. "Null Hypothesis" indicates that there is not a statistically significant relationship between the two variables, while "Alternate Hypothesis" indicates that there is a statistically significant relationship.

Geometric Parameter	|t*|	t(0.95;22)	Decision	P-Value	Best Fit Line Slope
Vertical Spacing	2.39	1.72	Alternate Hypothesis	0.026	-23.248
Length	0.51	1.72	Null Hypothesis	0.61	0.9242
Width	3.85	1.72	Alternate Hypothesis	0.0009	3.612

From the linear regression results, a negative relationship exists between vertical spacing and Peak Force, a positive relationship exists between width and Peak Force, and no relationship exists between length and Peak Force. P-values support all results.

2. Residual Force

A linear regression analysis was performed to determine the overall effect of reinforcement vertical spacing, length, and width on Residual Force. The regression was performed with pairs of spacing and Residual Force, length and Residual Force, and width and Residual Force. For each geometric parameter that is varied, the other two geometric parameters are also varied. The regression represents the relationship between the three geometric reinforcement parameters and Residual Force with a variety of variables present. Table 55 summarizes the results of the linear regression.

Table 55: Results of linear regression analysis for overall effect of geometric parameters on Residual Force. "Null Hypothesis" indicates that there is not a statistically significant relationship between the two variables, while "Alternate Hypothesis" indicates that there is a statistically significant relationship.

Geometric Parameter	|t*|	t(0.95;22)	Decision	P-Value	Best Fit Line Slope
Vertical Spacing	0.88	1.72	Null Hypothesis	0.39	9.855
Length	1.03	1.72	Null Hypothesis	0.31	1.9119
Width	5.91	1.72	Alternate Hypothesis	0.000006	4.65

From the linear regression results, a positive relationship exists between width and Residual Force, no relationship exists between vertical spacing and Residual Force, and no relationship exists between length and Residual Force. P-values support all results.

3. Peak Force Displacement

A linear regression analysis was performed to determine the overall effect of reinforcement vertical spacing, length, and width on Peak Force Displacement. The regression was performed with pairs of spacing and Peak Force Displacement, length and Peak Force Displacement, and width and Peak Force Displacement. For each geometric parameter that is varied, the other two geometric parameters are also varied. The regression represents the relationship between the three geometric parameters and Peak Force Displacement with a variety of variables present. Table 56 summarizes the results of the linear regression.

Table 56: Results of linear regression analysis for overall effect of geometric parameters on Peak Force Displacement. "Null Hypothesis" indicates that there is not a statistically significant relationship between the two variables, while "Alternate Hypothesis" indicates that there is a statistically significant relationship.

Geometric Parameter	|t*|	t(0.95;22)	Decision	P-Value	Best Fit Line Slope
Vertical Spacing	2.22	1.72	Alternate Hypothesis	0.037	0.0657
Length	3.82	1.72	Alternate Hypothesis	0.0009	-0.0162
Width	1.64	1.72	Null Hypothesis	0.115	-0.0056

From the linear regression results, a negative relationship exists between length and Peak Force Displacement, a positive relationship exists between vertical spacing and Peak Force Displacement, and no relationship exists between width and Peak Force Displacement. P-values support all results.

4. K_{50}

A linear regression analysis was performed to determine the overall effect of reinforcement vertical spacing, length, and width on K_{50}. The regression was performed with pairs of spacing and Peak Force Displacement, length and Peak Force Displacement, and width and Peak Force Displacement. For each geometric parameter that is varied, the other two geometric parameters are also varied. The regression represents the relationship between the three geometric parameters and Peak Force Displacement with a variety of variables present. Table 57 summarizes the results of the linear regression.

Table 57: Results of linear regression analysis for overall effect of geometric parameters on K_{50}. "Null Hypothesis" indicates that there is not a statistically significant relationship between the two variables, while "Alternate Hypothesis" indicates that there is a statistically significant relationship.

Geometric Parameter	|t*|	t(0.95;22)	Decision	P-Value	Best Fit Line Slope
Vertical Spacing	2.12	1.72	Alternate Hypothesis	0.045	-2256.7
Length	3.33	1.72	Alternate Hypothesis	0.003	528.22
Width	3.109	1.72	Alternate Hypothesis	0.005	336.02

From the linear regression results, a negative relationship exists between vertical spacing and K_{50}, a positive relationship exists between length and K_{50}, and a positive relationship exists between width and K_{50}. P-values support all results.

vi. Complete Data Set Analysis of Variance

1. Peak Force

A single factor ANOVA was performed to determine if the mean value of the Peak Force data populations are equal when each of the single variables reinforcement vertical spacing, reinforcement width, and reinforcement length are modified. A 90% confidence interval was used for the ANOVA. For each data set, an F value was computed as well as a critical F value. The alternate hypothesis states that at least one of the means of each data population is different. The null hypothesis states that the means of each data population are equal. If F exceeds $F_{critical}$, the null hypothesis is rejected and at least one of the means of the populations is different. Table 58 shows the results of the ANOVA.

Table 58: Results of ANOVA for Peak Force data as reinforcement geometric parameters are modified

Geometric Parameter	F	$F_{critical}$	Decision
Vertical Spacing	5.712	2.949	Alternate Hypothesis
Length	0.261	2.949	Null Hypothesis
Width	7.135	2.949	Alternate Hypothesis

All three ANOVA results support the linear regression analysis results.

2. Residual Force

A single factor ANOVA was performed to determine if the mean value of the Residual Force data populations are equal when each of the single variables reinforcement vertical spacing, reinforcement width, and reinforcement length are modified. A 90% confidence interval was used for the ANOVA. For each data set, an F value was computed as well as a critical F value. The alternate hypothesis states that at least one of the means of each data population is different. The null hypothesis states that the means of each data population are equal. If F exceeds $F_{critical}$, the null hypothesis is rejected and at least one of the means of the populations is different. Table 59 shows the results of the ANOVA.

Table 59: Results of ANOVA for Residual Force data as reinforcement geometric parameters are modified

Geometric Parameter	F	$F_{critical}$	Decision
Vertical Spacing	0.775	2.949	Null Hypothesis
Length	1.064	2.949	Null Hypothesis
Width	17.524	2.949	Alternate Hypothesis

All three ANOVA results support the linear regression analysis results.

3. Peak Force Displacement

A single factor ANOVA was performed to determine if the mean value of the Peak Force Displacement data populations are equal when each of the single variables reinforcement vertical spacing, reinforcement width, and reinforcement length are modified. A 90% confidence interval was used for the ANOVA. For each data set, an F value was computed as well as a critical F value. The alternate hypothesis states that at least one of the means of each data population is different. The null hypothesis states that the means of each data population are equal. If F exceeds $F_{critical}$, the null hypothesis is rejected and at least one of the means of the populations is different. Table 60 shows the results of the ANOVA.

Table 60: Results of ANOVA for Peak Force Displacement data as reinforcement geometric parameters are modified

Geometric Parameter	F	$F_{critical}$	Decision
Vertical Spacing	4.921	2.949	Alternate Hypothesis
Length	14.595	2.949	Alternate Hypothesis
Width	2.436	2.949	Null Hypothesis

All three ANOVA results support the linear regression analysis results.

4. K_{50}

A single factor ANOVA was performed to determine if the mean value of the K_{50} data populations are equal when each of the single variables reinforcement vertical spacing, reinforcement width, and reinforcement length are modified. A 90% confidence interval was used for the ANOVA. For each data set, an F value was computed as well as a critical F value. The alternate hypothesis states that at least one of the means of each data population is different. The null hypothesis states that the means of each data population are equal. If F exceeds $F_{critical}$, the null hypothesis is rejected and at least one of the means of the populations is different. Table 61 shows the results of the ANOVA.

Table 61: Results of ANOVA for K_{50} data as reinforcement geometric parameters are modified

Geometric Parameter	F	$F_{critical}$	Decision
Vertical Spacing	4.513	2.949	Alternate Hypothesis
Length	11.119	2.949	Alternate Hypothesis
Width	4.633	2.949	Alternate Hypothesis

All three ANOVA results support the linear regression analysis results.

vii. Summary of Laboratory Results

Table 62 summarizes the laboratory testing data analysis for initial observation, single variable linear regression analysis, overall linear regression analysis, and mid-plate failure surface location. From this table, it is shown that generally, initial observation, single variable linear regression analysis, and overall linear regression analysis agree on the effect of reinforcement geometry on the measured parameters. However, more trends were apparent with the overall linear regression analysis than the other two methods. In particular, the overall linear regression analysis showed three apparent trends relating to vertical spacing that were not observed with the single linear regression analysis.

A total of 74 of 79 ANOVA analyses supported the linear regression analyses. While all 79 ANOVA analyses did not support the linear regression analyses, this was expected as two different analysis methods were used. Using different analytical methods on the same set of data often results in differing analysis results (Silberzahn et al. 2018). All of the situations where ANOVA analyses did not support linear regression analyses occurred in situations where both ANOVA and linear regression results were near the significance threshold value and are a result of differing analysis methods. This reasoning was also confirmed by Dr. Rob Bubb.

Table 62: Summary of Relationships Between Measured Parameters and Independent Variables from Laboratory Testing Data Analysis

Initial Observation				
Measured Parameter	**Vertical Spacing**	**Width**	**Length**	**Surface Area**
Peak Force	None	Positive	None	Positive
Residual Force	None	Positive	None	Positive
Peak Force Displacement	Positive	None	Negative	Negative
K_{50}	Negative	Positive	Positive	Positive

Single Variable Linear Regression Analysis				
Measured Parameter	**Vertical Spacing**	**Width**	**Length**	**Surface Area**
Peak Force	None	None	None	Positive
Residual Force	None	Positive	None	Positive
Peak Force Displacement	None	None	Negative	Negative
K_{50}	None	Positive	Positive	Positive

Complete Data Set Linear Regression Analysis				
Measured Parameter	**Vertical Spacing**	**Width**	**Length**	
Peak Force	Negative	Positive	None	
Residual Force	None	Positive	None	
Peak Force Displacement	Positive	None	Negative	
K_{50}	Negative	Positive	Positive	

Mid-Plate Surface Location				
	Vertical Spacing	**Width**	**Length**	**Surface Area**
Observed Pattern	Longer surface with increased spacing	None	None	None

b. FLAC3D™ Modeling

All of the geometries deployed in the experimental phase of this research were modeled with FLAC3D™, with the intent of confirming that the FLAC3D™ model produced the same results as the physical modeling. The results and analysis, and comparison of laboratory and FLAC3D™ results and analysis, follow.

i. Effect of Reinforcement Vertical Spacing on Load Deformation Characteristics

1. Peak Force

To determine the effect of reinforcement vertical spacing on Peak Force, Peak Force vs. vertical spacing was plotted for each reinforcement width and length combination. An observation was made after plotting Peak Force vs. vertical spacing, Figure 138.

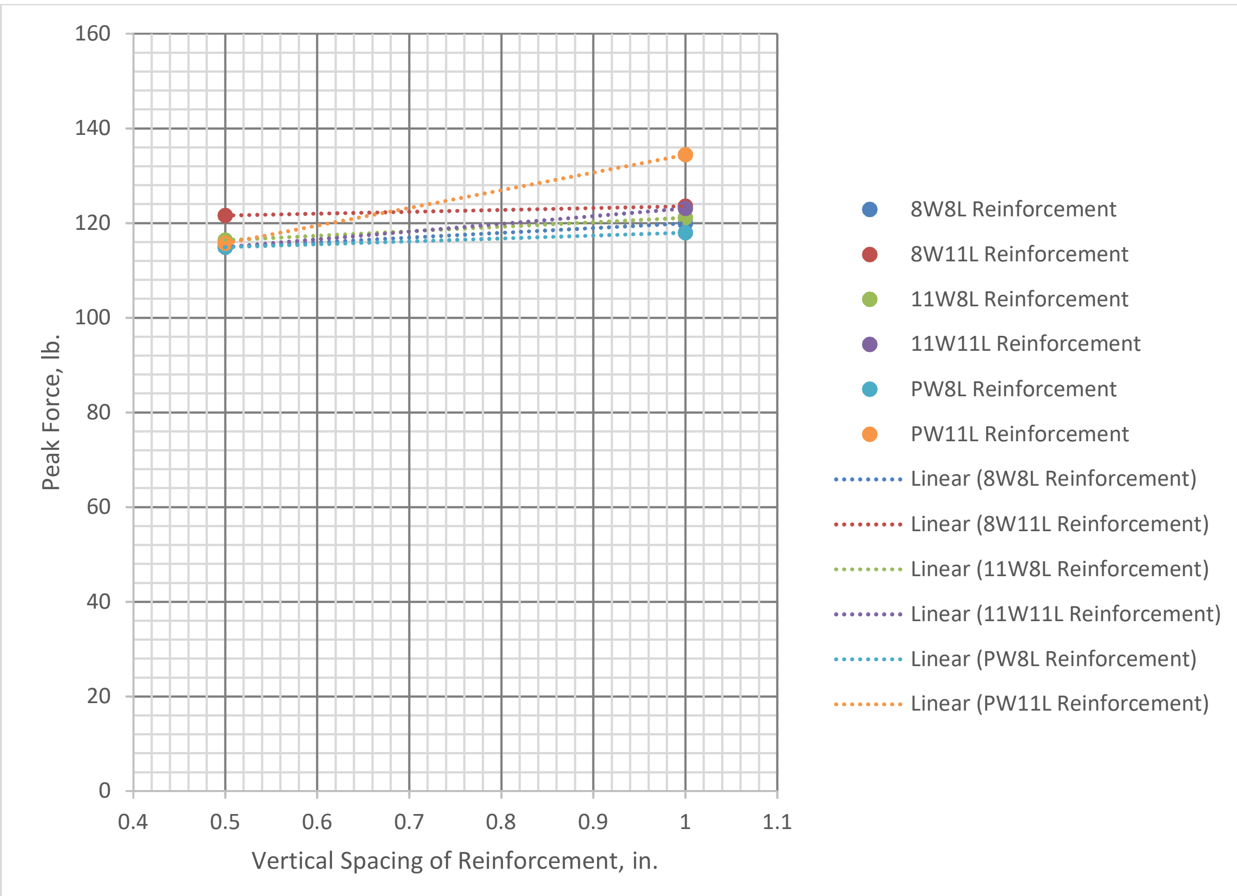

Figure 138: Peak Force vs. vertical spacing for various reinforcement widths and lengths with linear trend lines (results of 12 tests)

After plotting, linear trend lines were added for each width and length combination to determine if any data trends were apparent. Table 63 shows the observed trends.

Table 63: Observed trends for Peak Force values as vertical spacing increases from 0.5" to 1"

Width and Length Combination	Peak Force Trend as Vertical Spacing Increases
PW8L	Increase
PW11L	Increase
8W8L	Increase
8W11L	Increase
11W8L	Increase
11W11L	Increase

All simulations showed an increase in Peak Force as vertical spacing increased. Due to this, the observation is made that increasing reinforcement vertical spacing increases Peak Force.

2. K_{50}

To determine the effect of reinforcement vertical spacing on K_{50}, K_{50} vs. vertical spacing was plotted for each reinforcement width and length combination. An observation was made after plotting K_{50} vs. vertical spacing, Figure 139.

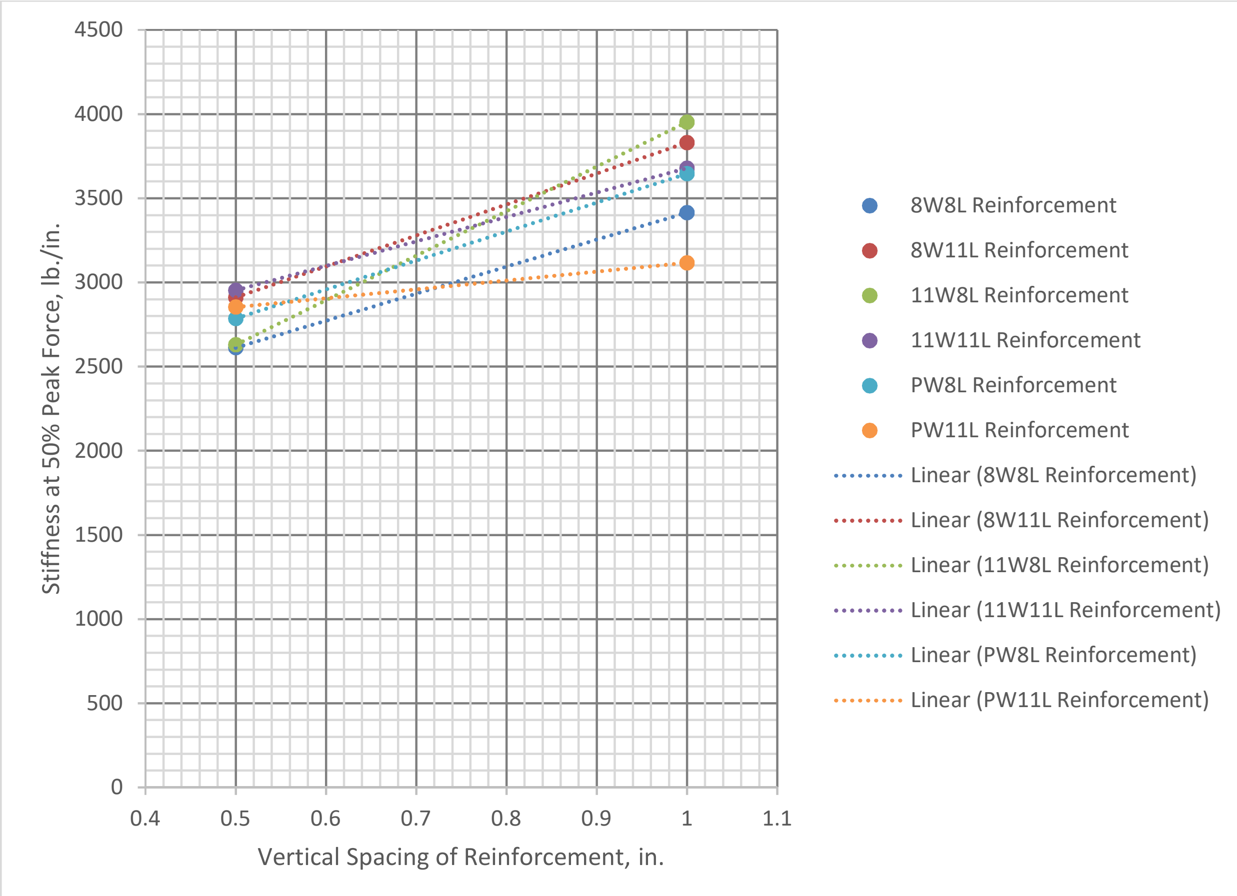

Figure 139: K_{50} vs. vertical spacing for various reinforcement widths and lengths with linear trend lines (results of 12 tests)

After plotting, linear trend lines were added for each width and spacing combination to determine if any data trends were apparent. Table 64 shows the observed trends.

Table 64: Observed trends for K_{50} values as vertical spacing increases from 0.5” to 1”

Width and Spacing Combination	K_{50} Trend as Vertical Spacing Increases
PW5Lay	Increase
PW10Lay	Increase
8W5Lay	Increase
8W10Lay	Increase
11W5Lay	Increase
11W10Lay	Increase

All simulations showed a noticeable increase in K_{50} values as vertical spacing of reinforcement is increased. Due to this, the observation is made that vertical spacing of reinforcement results in increased K_{50} values.

ii. Effect of Reinforcement Width on Load Deformation Characteristics

1. Peak Force (Load)

To determine the effect of reinforcement width on Peak Force, Peak Force vs. reinforcement width was plotted for each reinforcement vertical spacing and length combination. An observation was made after plotting Peak Force vs. reinforcement width, Figure 140.

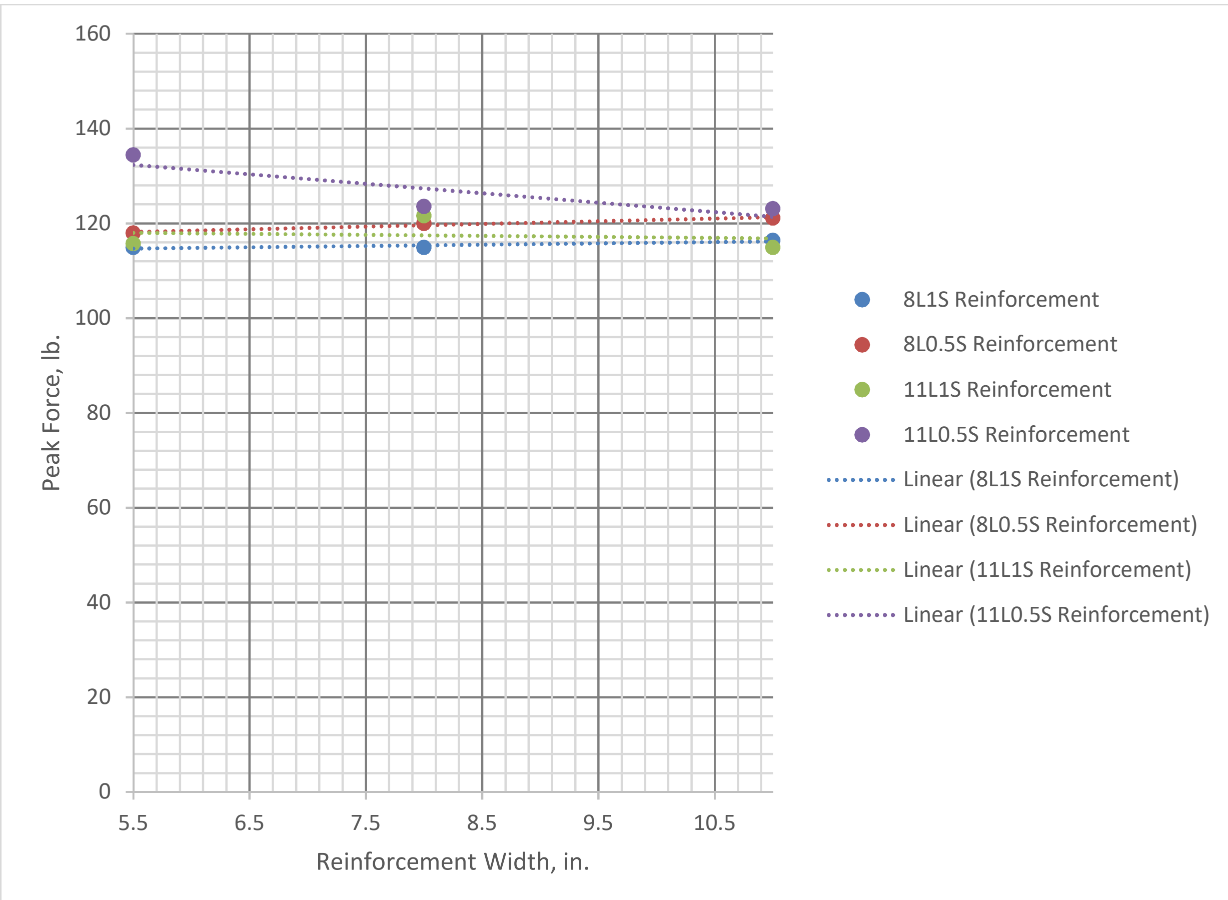

Figure 140: Peak Force vs. reinforcement width for various reinforcement vertical spacings and lengths with linear trend lines (results of 12 tests)

After plotting, linear trend lines were added for each length and spacing combination to determine if any data trends were apparent. Table 65 shows the observed trends.

Table 65: Observed trends for Peak Force values as reinforcement width increases from 5.5" to 8" to 11"

Length and Spacing Combination	Peak Force Trend as Reinforcement Width Increases
8L5Lay	Increase
8L10Lay	Increase
11L5Lay	None
11L10Lay	Decrease

The simulations showed varying trends as reinforcement width was increased. Two had a very slight increase while one had no trend and one even had a decreasing trend. Due to the inconsistency of trends, the observation is made that increasing reinforcement width has no effect on Peak Force values.

2. K_{50}

To determine the effect of reinforcement width on K_{50}, K_{50} vs. reinforcement width was plotted for each reinforcement width and vertical spacing combination. An observation was made after plotting K_{50} vs. reinforcement width, Figure 141.

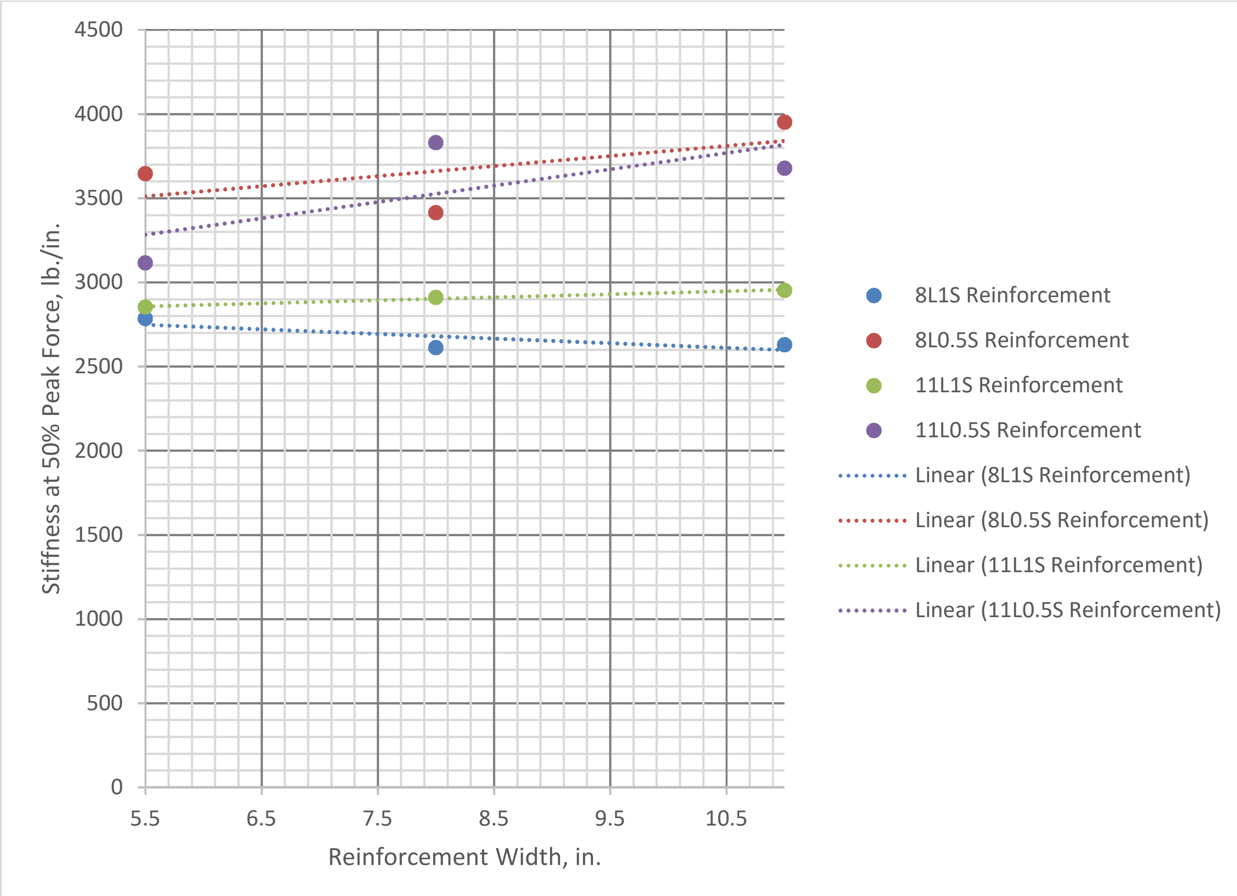

Figure 141: K_{50} vs. reinforcement width for various reinforcement vertical spacings and lengths with linear trend lines (results of 12 tests)

After plotting, linear trend lines were added for each length and spacing combination to determine if any data trends were apparent. Table 66 shows the observed trends.

Table 66: Observed trends for Peak Force values as reinforcement width increases from 5.5” to 8” to 11”

Width and Length Combination	K_{50} Trend as Reinforcement Width Increases
8L5Lay	None
8L10Lay	None
11L5Lay	Increase
11L10Lay	None

The simulations showed varying changes in K_{50} as reinforcement width is increased. Due to this, the observation is made that increasing reinforcement width does not change the K_{50} value.

iii. Effect of Reinforcement Length on Load Deformation Characteristics

1. Peak Force (Load)

To determine the effect of reinforcement length on Peak Force, Peak Force vs. reinforcement length was plotted for each reinforcement width and vertical spacing combination. An observation was made after plotting K_{50} vs. reinforcement length, Figure 142.

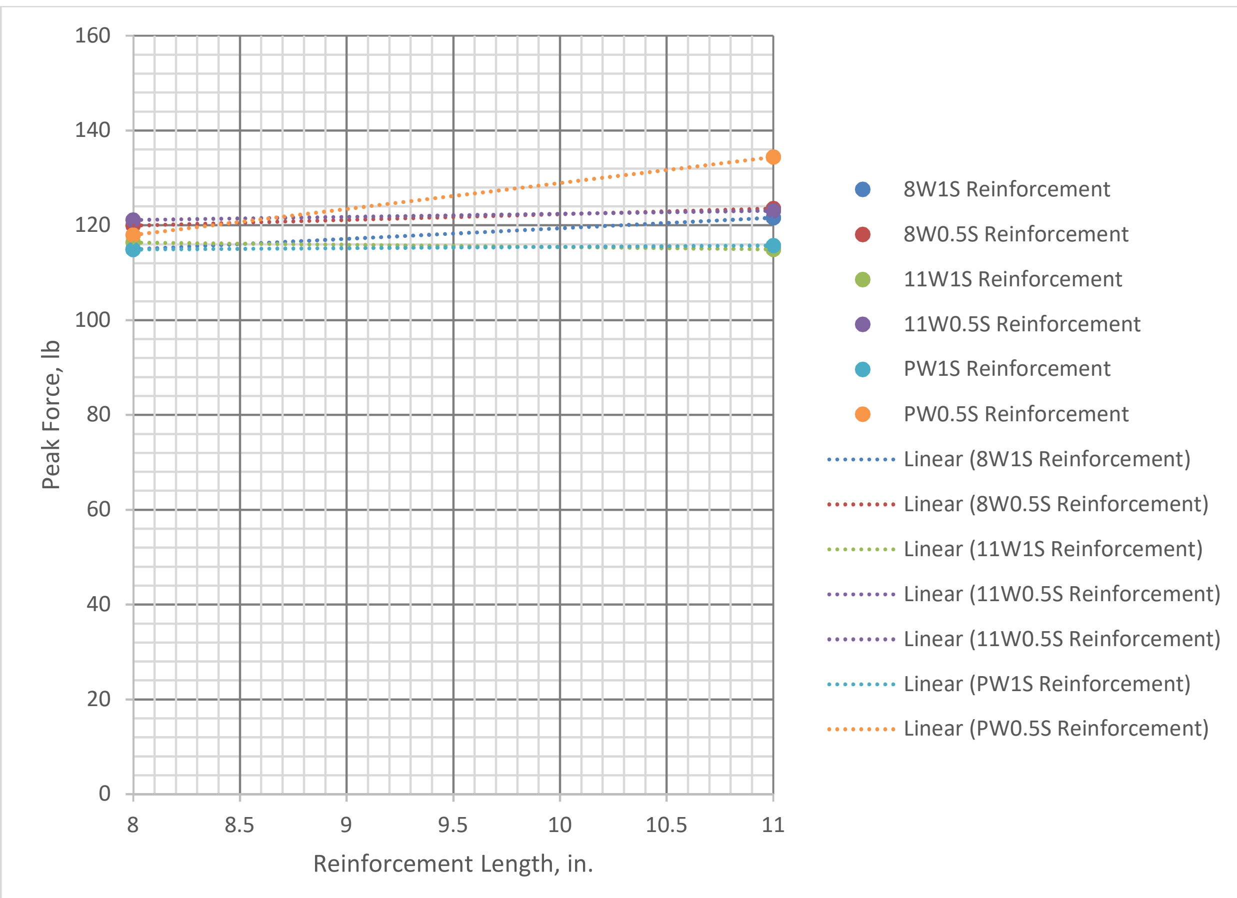

Figure 142: Peak Force vs. reinforcement length for various reinforcement vertical spacings and widths with linear trend lines (results of 12 tests)

After plotting, linear trend lines were added for each width and spacing combination to determine if any data trends were apparent. Table 67 shows the observed trends.

Table 67: Observed trends for Peak Force values as reinforcement length increases from 8" to 11"

Width and Spacing Combination	Peak Force Trend as Reinforcement Length Increases
PW5Lay	Increase
PW10Lay	Increase
8W5Lay	Increase
8W10Lay	Increase
11W5Lay	Decrease
11W10Lay	Increase

All but one simulation showed an increase in Peak Force as reinforcement length increased. Due to this, the observation is made that increasing reinforcement length increases Peak Force values.

2. K_{50}

To determine the effect of reinforcement length on K_{50}, K_{50} vs. reinforcement length was plotted for each reinforcement width and vertical spacing combination. An observation was made after plotting K_{50} vs. reinforcement length, Figure 143.

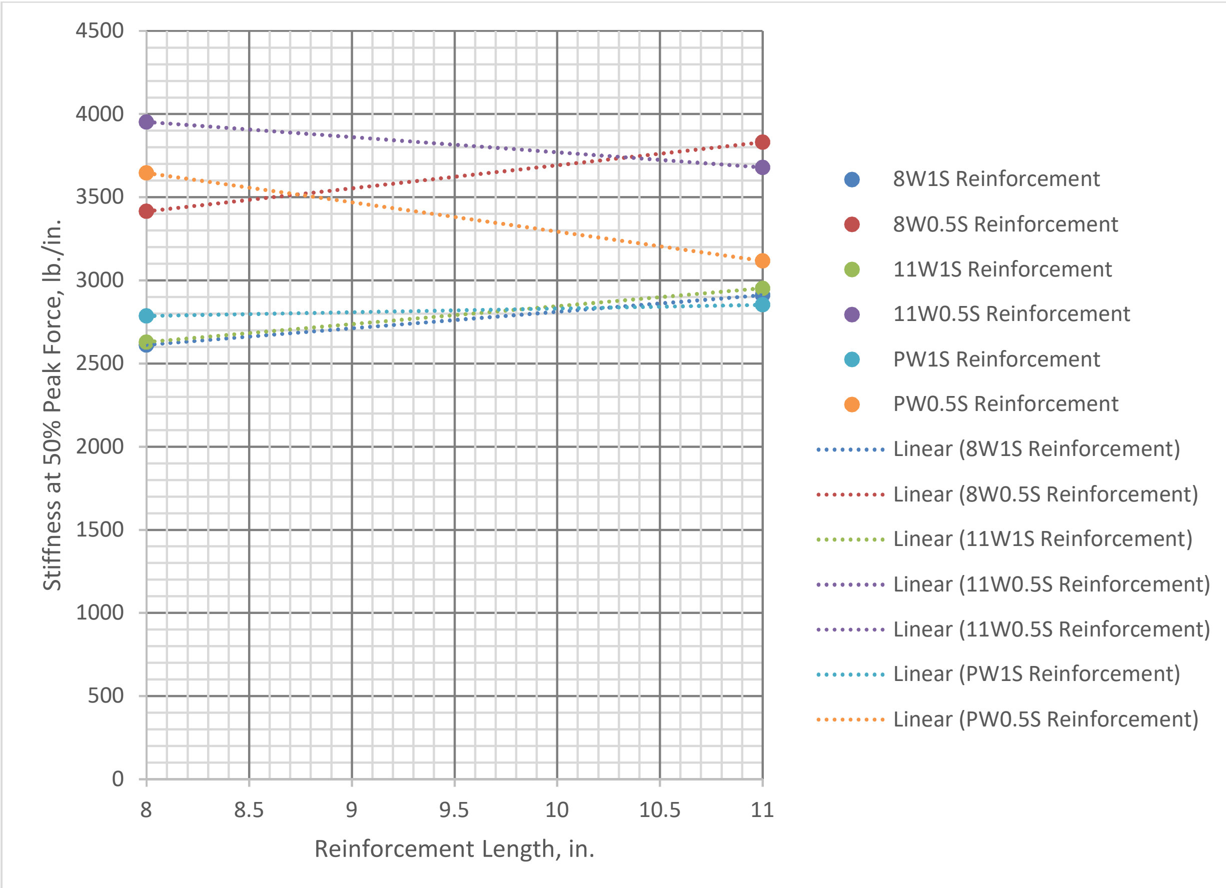

Figure 143: K_{50} vs. reinforcement length for various reinforcement vertical spacings and widths with linear trend lines (results of 12 tests)

After plotting, linear trend lines were added for each width and spacing combination to determine if any data trends were apparent. Table 68 shows the observed trends.

Table 68: Observed trends for K_{50} values as reinforcement length increases from 8" to 11"

Width and Spacing Combination	K_{50} Trend as Reinforcement Length Increases
PW5Lay	Increase
PW10Lay	Decrease
8W5Lay	Increase
8W10Lay	Increase
11W5Lay	Increase
11W10Lay	Decrease

The trends show an increase for four simulations and a decrease for two simulations in K_{50} values as reinforcement length is increased. Due to this, the observation is made that there is no trend between reinforcement length and K_{50} values.

iv. Effect of Reinforcement Surface Area

1. Peak Force

a. Initial Observation

Initial observation was made after plotting Peak Force vs. reinforcement surface area for all tests, Figure 144.

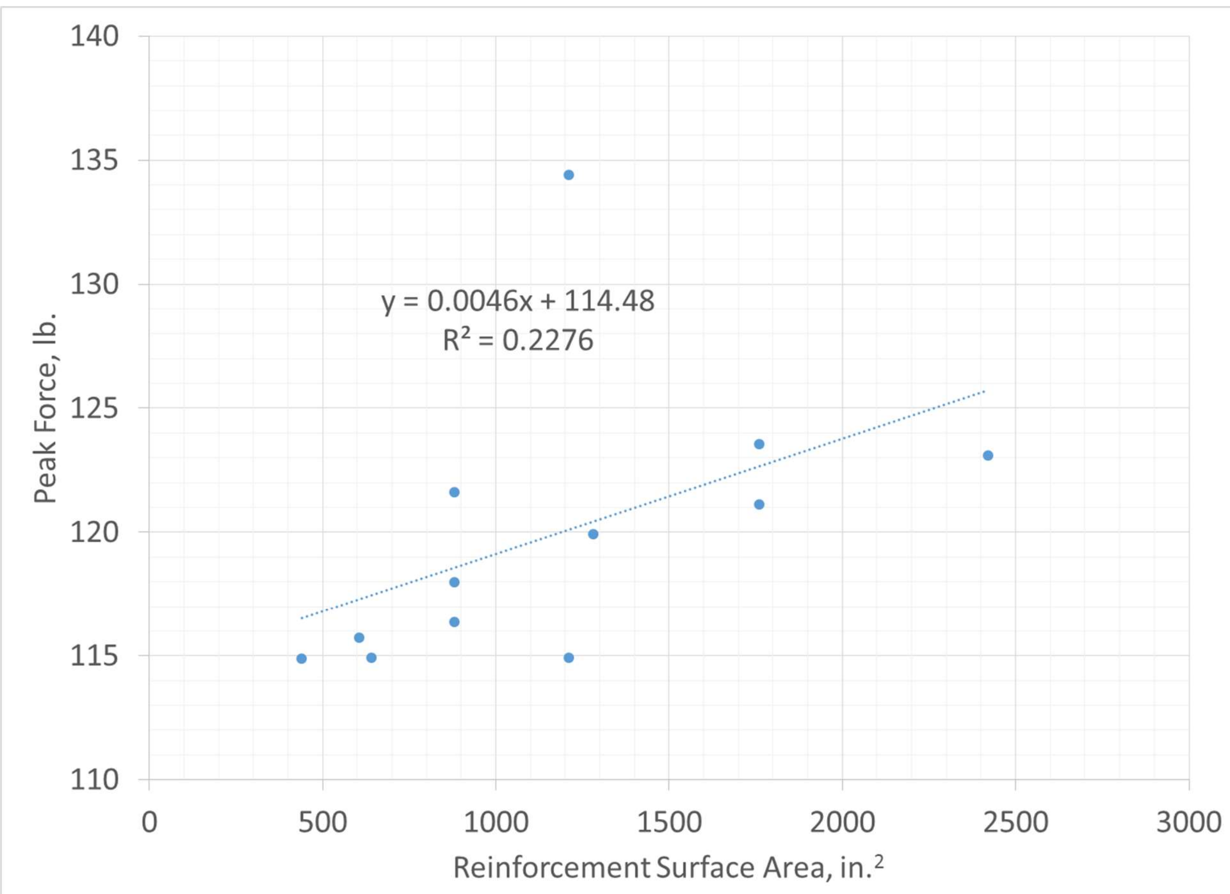

Figure 144: Peak Force vs. reinforcement surface area (results of 12 tests)

After the addition of a trend line, a positive correlation appears to exist between Peak Force and reinforcement surface area.

b. Single Variable Linear Regression Analysis

A linear regression analysis was performed to determine the significance of change in Peak Force when the single variable, reinforcement surface area, is modified. Twelve data points are present for this linear regression. A t-test was performed at a 90% confidence interval. A t* value was calculated and compared to a t value corresponding to a 90% confidence interval and 12 data points. Two alternatives exist for the two sided test: acceptance of the null hypothesis or acceptance of the alternate hypothesis. The null hypothesis concludes that there is no relationship between Peak Force and reinforcement surface area. The alternate hypothesis concludes that there is a relationship between Peak Force and reinforcement surface area. If the t* value is greater than the t value, the alternate hypothesis is chosen. If the t* value is less than or equal to the t value, the null hypothesis is chosen. P-values were also computed as p-values less than the level of significance support the alternate hypothesis. Each data set was plotted with reinforcement surface area on the abscissa and Peak Force on the ordinate. A linear best fit line was added and the slope of this line was computed. Table 69 summarizes the linear regression analysis.

Table 69: Linear regression analysis results for Peak Force vs. reinforcement surface area. "Null Hypothesis" indicates that there is not a statistically significant relationship between the two variables, while "Alternate Hypothesis" indicates that there is a statistically significant relationship.

|t*|	t(0.95;10)	Decision	P-Value	Best Fit Line Slope
1.717	1.812	Null Hypothesis	1.17E-01	0.0046

The linear regression results indicate that there is not a statistically significant relationship between Peak Force and reinforcement surface area. However, there is a strong outlier (PW11L10Lay). Elimination of this outlier provides the linear regression results shown in Table 70.

Table 70: Linear regression analysis results for Peak Force vs. reinforcement surface area after elimination of outlier. "Null Hypothesis" indicates that there is not a statistically significant relationship between the two variables, while "Alternate Hypothesis" indicates that there is a statistically significant relationship.

$\lvert t^* \rvert$	t(0.95;9)	Decision	P-Value	Best Fit Line Slope
3.847	1.833	Alternate Hypothesis	3.90E-03	0.0044

After elimination of the outlier, the linear regression results indicate that there is a statistically significant positive relationship between Peak Force and reinforcement surface area.

2. K_{50}

a. Initial Observation

Initial observation was made after plotting K_{50} vs. reinforcement surface area for all tests, Figure 145.

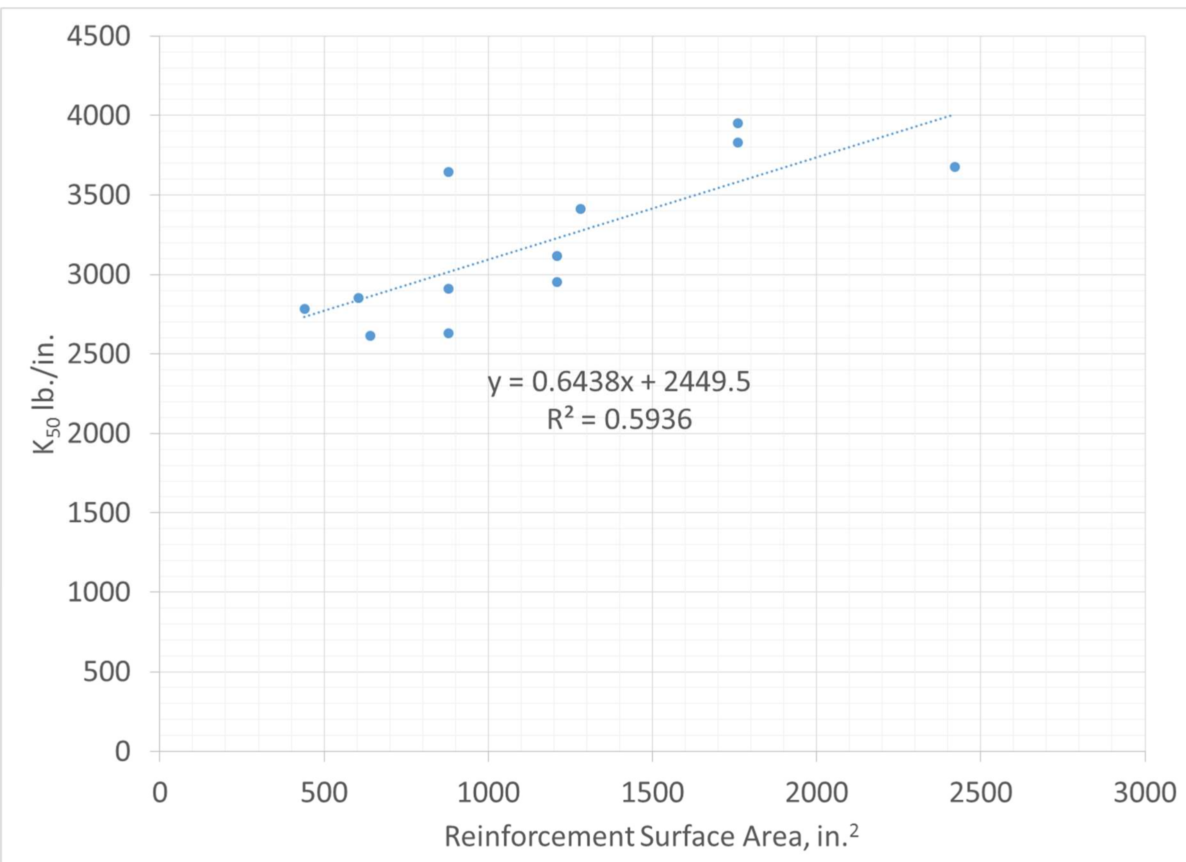

Figure 145: K_{50} vs. reinforcement surface area (results of 12 tests)

After the addition of a trend line, a positive correlation appears to exist between K_{50} and reinforcement surface area.

b. Single Variable Linear Regression Analysis

A linear regression analysis was performed to determine the significance of change in K_{50} when the single variable, reinforcement surface area, is modified. Twelve data points are present for this linear regression. A t-test was performed at a 90% confidence interval. A t* value was calculated and compared to a t value corresponding to a 90% confidence interval and 12 data points. Two alternatives exist for the two sided test,: acceptance of the null hypothesis or acceptance of the alternate hypothesis. The null hypothesis concludes that there is no relationship between K_{50} and reinforcement surface area. The alternate hypothesis concludes that there is a relationship between K_{50} and reinforcement surface area. If the t* value is greater than the t value, the alternate hypothesis is chosen. If the t* value is less than or equal to the t value, the null hypothesis is chosen. P-values were also computed as p-values less than the level of significance support the alternate hypothesis. Each data set was plotted with reinforcement surface area on the abscissa and K_{50} on the ordinate. A linear best fit line was added and the slope of this line was computed. Table 71 summarizes the linear regression analysis.

Table 71: Linear regression analysis results for K_{50} vs. reinforcement surface area. "Null Hypothesis" indicates that there is not a statistically significant relationship between the two variables, while "Alternate Hypothesis" indicates that there is a statistically significant relationship.

|t*|	t(0.95;10)	Decision	P-Value	Best Fit Line Slope
3.822	1.812	Alternate Hypothesis	3.30E-03	0.643

The results of the linear regression analysis indicate that a positive correlation exists between K_{50} and reinforcement surface area.

v. Summary of FLAC3D™ Results

Table 72 summarizes the FLAC3D™ data analysis. FLAC3D™ results do not vary from test to test, so the trends observed in the initial observation are statistically significant. Because there were variances in Peak Force and K_{50} values for the same surface area, a linear regression analysis was performed on that data. The trends observed for the linear regression analysis agreed with the initial observation and are shown in Table 72.

Table 72: Summary of FLAC3D™ Data Analysis

Initial Observation				
Measured Parameter	**Vertical Spacing**	**Width**	**Length**	**Surface Area**
Peak Force	None	None	None	Positive
K_{50}	Positive	None	None	Positive

Single Variable Linear Regression Analysis	
Measured Parameter	**Surface Area**
Peak Force	Positive
K_{50}	Positive

c. Comparison of Laboratory Data Analysis with FLAC3D™ Data Analysis

Comparison of laboratory data and FLAC3D™ data shows how well FLAC3D™ modeled the laboratory data in terms of trends resulting from reinforcement geometry variances. While the FLAC3D™ data plots and the laboratory data plots were quite similar, it is important to see how different parameters from data analysis compare between laboratory and FLAC3D™ results. Since the "initial observation" is statistically significant for the vertical spacing, width, and length FLAC3D™ data, it will be compared to the single variable linear regression analysis of the vertical spacing, width, and length laboratory data. Also, the single variable linear analysis for "surface area" of FLAC3D™ will be compared to the single variable linear regression analysis for surface area of the laboratory results.

Table 73 compares the laboratory data analysis with the FLAC3D™ data analysis. Overall, the FLAC3D™ data analysis compares favorably with the laboratory data analysis. There are divergences.

- The FLAC3D™ data shows a positive relationship between vertical spacing and K_{50} while the laboratory data showed no trend.
- The FLAC3D™ data shows a positive relationship between vertical spacing and Peak Force while the laboratory data showed no trend.
- The laboratory data showed positive trends between both width and length and K_{50} where the FLAC3D™ data showed no trend.

Both FLAC3D™ and the laboratory data showed positive relationships between Peak Force and surface area, and K_{50} and surface area. Both FLAC3D™ and the laboratory data showed no relationship between Peak Force and vertical spacing, Peak Force and width, and Peak Force and length.

Table 73: Comparison of Laboratory Data Analysis with FLAC3D™ Data Analysis. Reported FLAC3D™ values for vertical spacing, width, and length are initial observations. Reported FLAC3D™ values for surface area are from single variable linear regression analysis. All reported values for laboratory (Lab) data are single variable linear regression analysis.

Measured Parameter	Vertical Spacing (Lab/FLAC3D™)	Width (Lab/FLAC3D™)	Length (Lab/FLAC3D™)	Surface Area (Lab/FLAC3D™)
Peak Force	None/None	None/None	None/None	Positive/ Positive
K_{50}	None/ Positive	Positive/ None	Positive/ None	Positive/ Positive

The slope of a trend line indicates how much a geometric parameter affects a measured parameter. The following comparisons are made to observe the difference between how measured parameters in FLAC3D™ respond to changing surface area and how measured parameters in the laboratory testing respond to changing surface area. These comparisons indicate how sensitive the measured parameters are to a change in a surface area for FLAC3D™ and laboratory testing, respectively.

First, the slopes of the FLAC3D™ data trend lines are compared with the slopes of the laboratory data trend lines to see if the FLAC3D™ sensitivity compares favorably with the laboratory data sensitivity. Table 74 shows how the FLAC3D™ data and laboratory data compare in terms of their slopes of the best fit line used for single variable linear regression analysis for K_{50} vs. surface area and Peak Force vs. surface area. The laboratory slopes for both K_{50} vs. surface area and Peak Force vs. surface area were approximately three times higher than the FLAC3D™ data indicating that the FLAC3D™ program was not as sensitive to changes in reinforcement geometry as what was observed in laboratory testing.

Second, the ratio of slopes for K_{50} vs. surface area and Peak Force vs. surface area for the FLAC3D™ data are compared with those of the laboratory data to determine if the ratio of sensitivity of K_{50} to changes in surface area and the sensitivity of Peak Force to changes in surface area are similar for both FLAC3D™ and laboratory data. For FLAC3D™, the ratio of slopes for K_{50} vs. surface area and Peak Force vs. surface area is 146 while the ratio of these same slopes for the laboratory data is 102. This means that in FLAC3D™ (data from Tables 70 and 71), a change in surface area affects K_{50} than 146 times more than it affects Peak Force, and a change in surface area affects K_{50} 102 times more than it affects Peak Force in the laboratory data (data from Tables 46 and 52). This indicates that the FLAC3D™ model compares favorably with the laboratory data in terms of how sensitive each measured parameter is to a change in surface area.

Table 74: Comparison of FLAC3D™ and laboratory data best fit line slopes for single variable linear regression analysis of K_{50} vs. surface area and Peak Force vs. Surface Area

	Slope	
	FLAC3D™	**Laboratory**
K_{50} vs. Surface Area	0.643	1.93
Peak Force vs. Surface Area	0.0044	0.019

Chapter VI: Conclusions

The research objectives presented in Chapter I, c. were met by performing laboratory work and finite difference modeling to evaluate the performance of mechanically stabilized earth structures subjected to passive forces. The conclusions presented in this section were drawn from the results.

a. Summary of Work

The primary research objective was to determine the load-deformation response of mechanically stabilized soil subjected to passive forces. To determine this load-deformation response, a laboratory test was developed to provide passive forces to scale soil specimens with varying reinforcement configurations. After development, this laboratory test was performed on thirty-nine soil specimens: three test repetitions of thirteen different reinforcement configurations. Load-deformation data were collected, plotted, and analyzed for each of the thirty-nine tests. In addition to load-deformation data, the location of the failure surface was obtained for thirteen of the thirty-nine tests.

Additionally, finite difference modeling of the laboratory test was performed using FLAC3D™ software to determine the load-deformation response. The finite difference model mimics the geometry of the laboratory test as well as the soil and reinforcement parameters. The soil parameters were characterized through sieve analysis, USCS classification, Proctor density testing, and triaxial testing. The reinforcement parameters were characterized through flexural rigidity testing, interface friction testing, and tensile strength and strain testing. The FLAC3D™ model was applied to the thirteen laboratory test configurations.

b. Conclusions

From the research, the following conclusions can be made about the effect of horizontal sheet reinforcement on the engineering performance of model, mechanically stabilized soil subjected to passive loading:

1. Every reinforced laboratory test exhibited lower Peak Force values than the average of the three non-reinforced laboratory tests. The average non-reinforced laboratory test exhibited Peak Force values from 2.8% to 103.8% greater than the reinforced laboratory tests. The conclusion is made that the addition of reinforcement to a soil structure causes a decrease in Peak Force values. (Table 8) This conclusion is logical because adding reinforcement introduces a weak plane at the bottom of the pusher plate that is parallel to the direction of pusher plate travel. A weak plane in this location likely has a high contact area with the failure surface. A reduction of shear strength at the failure surface results in less force required to advance the pusher plate into the specimen.
2. Every reinforced laboratory test exhibited higher K_{50} values than the average of the three non-reinforced laboratory tests. The average non-reinforced laboratory test exhibited K_{50} values between 5.5% and 54.7% less than the reinforced laboratory tests. The conclusion is made that the addition of reinforcement to a soil structure causes an increase in K_{50} values. (Table 8) This conclusion is logical because at low displacements (where K_{50} is measured) a passive failure surface has not fully mobilized and caused shear strength reduction. At low displacements, the portion of the reinforcement that is in contact with the pusher plate is likely in tension and provides additional specimen resistance and higher K_{50} values. Additionally, the highest increase in K_{50} values occurred with wider specimens that would experience the highest tensile forces.

3. Peak Force Displacement and Residual Force values showed increases and decreases when comparing non-reinforced laboratory tests with reinforced laboratory tests. Therefore the conclusion is made that the addition of reinforcement to a soil structure has a non-determinate effect on Peak Force Displacement and on Residual Force. (Table 8) This conclusion is logical because there are a variety of reinforcement geometry variables at play. Some reinforcement geometry variables may have a greater effect than others resulting in a different effects on Peak Force Displacement and Residual Force and a non-determinate effect when considering the general addition of reinforcement.
4. FLAC3D™ models laboratory testing well and may be used to predict performance of additional laboratory tests. (Chapter 5, Section c.)
5. Mechanically stabilized soils loaded passively react consistently and predictably and can be modeled effectively.
6. Although all reinforced specimens were weaker than the non-reinforced specimens (lower Peak Force), additional reinforcement (increasing reinforcement surface area) provided a strength increase amongst the reinforced specimens as evidenced by positive trends between Peak Force and surface area, Residual Force and surface area, and K_{50} and surface area in the laboratory testing as well as a positive trend between Peak Force and surface area and between K_{50} and surface area for the FLAC3D™ modeling. No other relationships were discovered with respect to surface area. (Chapter V, Section a, part iv. for laboratory data and Chapter V, Section b, part iv. for FLAC3D™ data) This conclusion is logical because a large strength reduction occurs due to the layer of reinforcement placed at the base of the

pusher plate (explained in Conclusion no. 1), but additional reinforcement surface area increases the amount of reinforcement intersecting and extending beyond the failure surface. It is likely that this reinforcement is in tension at locations of failure surface intersection resulting in additional force required to advance the pusher plate into the specimen, particularly at larger displacements with a fully mobilized failure surface, resulting in increasing Peak Force and Residual Force values. Increased K_{50} values is explained in Conclusion no. 2.

7. Among reinforced laboratory tests, increasing vertical spacing of reinforcement results in decreasing Peak Force values (Table 54), negligible effect on Residual Force values (Table 55), increasing Peak Force Displacement values (Table 56), and decreasing K_{50} values (Table 57). This conclusion is logical because greater vertical spacing reduces the amount of reinforcement intersecting and extending beyond the failure surface resulting in lower Peak Force (See Conclusion no. 6). Decreased K_{50} values would logically require greater displacement to occur to reach the Peak Force (increased Peak Force Displacement). The negligible effect on Residual Force may be explained by the variety of other geometric factors that may affect Residual Force.

8. Among reinforced laboratory tests, increasing reinforcement length results in a negligible effect on Peak Force values (Table 54), a negligible effect on Residual Force values (Table 55), decreasing Peak Force Displacement values (Table 56), and Increasing K_{50} values (Table 57). The negligible effects on Residual Force and Peak Force may be explained by the variety of other geometric factors that may affect them. It is logical that increasing K_{50} values would cause decreasing

Peak Force Displacement values as decreased K_{50} values would require less displacement to occur to reach the Peak Force.

9. Among reinforced laboratory tests, increasing reinforcement width results in increasing Peak Force values (Table 54), increasing Residual Force values (Table 55), negligible effect on Peak Force Displacement values (Table 56), and increasing K_{50} values (Table 57). This conclusion is logical because as reinforcement width increases, the amount of reinforcement intersecting and extending beyond the failure surface increases resulting in greater Peak Force and Residual Force values (see Conclusion no. 6). The increase in K_{50} values is explained in Conclusion no. 2. As K_{50} and Peak Force increase, the negligible effect on Peak Force Displacement is supported as no change would necessarily be required in the required displacement to obtain the Peak Force.

10. Among FLAC3D™ tests, increasing vertical spacing of reinforcement results in increasing Peak Force values (Table 63) and increasing K_{50} values (Table 64). This conclusion is logical because increasing vertical spacing reduces the amount of weak planes present in the specimen resulting in higher Peak Force and K_{50} values.

11. Among FLAC3D™ tests, increasing reinforcement width results in negligible effects to both Peak Force values and K_{50} values (Tables 65 and 66, respectively). This conclusion is logical because the negligible effect may be explained by the variety of other geometric factors that may affect Peak Force and K_{50}.

12. Among FLAC3D™ tests, increasing reinforcement length results in increasing Peak Force values (Table 67) and has a negligible effect on K_{50} values (Table 68).

This conclusion is logical because increasing reinforcement length increases the amount of reinforcement intersecting and extending beyond the failure surface (see Conclusion no. 6). The negligible effect on K_{50} may be explained by the variety of other geometric factors that affect it.

13. There does not appear to be a discernable pattern between failure surface location and reinforcement length, width, or surface area. Due to this, the conclusion is made that reinforcement length, width, and surface area do not have a predictable effect on the failure surface location. (Chapter V, Section a, part ii, 2 for reinforcement width, Chapter V, Section a part iii, 2 for reinforcement length, and Chapter V, Section a, part iv, 2 for reinforcement surface area)

14. Increasing vertical spacing of reinforcement results in longer failure surfaces. (Chapter V, Section a, part i, 2) This conclusion is logical because as vertical spacing is increased, the amount of weak planes in the specimen is decreased. Typically, stronger soils are associated with longer failure surfaces. The decreased number of weak planes increases soil strength and causes a longer failure surface.

Chapter VII: Inferences from Research

The research consists solely of scale MSE structures and FLAC3D^{TM} simulations of these structures. Although the MSE structures were scale size, shearing these structures using passive force provided load-displacement data that are expected with dense, dry granular material. As shear displacement increases, the shearing resistance of the soil climbs, reaches a peak value, and falls to a residual value. This indicates that the parameters measured in this study, Peak Force, Residual Force, Peak Force Displacement, and K_{50}, are likely to exist and be significant performance indicators of full-scale MSE structures subjected to passive forces. FLAC3D^{TM} software is commonly used to simulate full-scale geotechnical situations and should be capable of modeling full-scale MSE structures loaded passively. The performance indicators from this study are predictable as reinforcement geometry changes. It is expected that these performance indicators will also be predictable as geometry varies in full-scale MSE structures. Thus, a design procedure may be developed to control performance of MSE structures loaded passively by varying reinforcement geometry. However, scale effects likely exist between this study and full-scale MSE structures and should be considered as a design procedure is developed.

Chapter VIII: Suggestions for Further Research

a. Laboratory testing and modeling should be performed for reinforcement lengths and widths with aspect ratios that are not approximately one.

b. Research should be performed with geogrid reinforcement where strike-through occurs and a friction angle reduction may not be a significant factor because of the increased particle-to-particle interaction when compared to the reinforcement used in this research, which did not allow particle interaction to occur through the reinforcement.

c. Research should be performed to determine if adding additional reinforcement or increasing length and width can eventually make the composite structure stronger in terms of Peak Force than non-reinforced soil.

d. Research should be performed to increase the capability of the FLAC3D™ model to predict mechanically stabilized soil behavior when loaded passively well beyond the strain required to achieve Peak Force.

e. Large scale tests loading reinforced specimens passively should be investigated.

f. FLAC3D™ should be used to determine the optimal reinforcement configuration for a given outcome, beyond those configurations used in this study.

Chapter IX: References

Abu-Hejleh, N. (2006). "Flowfill and MSE Bridge Approaches: Performance, Cost, and Recommendations for Improvements." Report no. CDOT-DTD-R-2006-2. Colorado Dept. of Trans. Research Branch, Denver, CO.

Adams, M., Nicks, J., Stabile, T., Wu, J., Schlatter, W., Hartmann, J. (2011) "Geosynthetic Reinforced Soil Integrated Bridge System, Interim Implementation Guide." Federal Highway Administration, Office of Infrastructure Research and Development, Washington, D.C.

ASTM (2007). "D4719-07 Standard Test Methods for Prebored Pressuremeter Testing in Soils." Annual Book of ASTM Standards, ASTM International, West Conshohocken, Pennsylvania.

ASTM (2011). "D1586-11 Standard Test Method for Standard Penetration Test (SPT) and Split-Barrel Sampling of Soils." Annual Book of ASTM Standards, ASTM International, West Conshohocken, Pennsylvania.

ASTM (2011). "D2487-11 Standard Practice for Classification of Soils for Engineering Purposes (Unified Soil Classification System)." Annual Book of ASTM Standards, ASTM International, West Conshohocken, Pennsylvania.

ASTM (2011). "D3080/D3080M-11 Standard Test Method for Direct Shear Test of Soils Under Consolidated Drained Conditons." Annual Book of ASTM Standards, ASTM International, West Conshohocken, Pennsylvania.

ASTM (2011). "D4767-11 Standard Test Method for Consolidated Undrained Triaxial Compression Test for Cohesive Soils." Annual Book of ASTM Standards, ASTM International, West Conshohocken, Pennsylvania.

ASTM (2012). "D698-12 Standard Test Methods for Laboratory Compaction Characteristics of Soil Using Standard Effort (12,400 ft-lbf/ft^3 (600 kN-m/m^3))" Annual Book of ASTM Standards, ASTM International, West Conshohocken, Pennsylvania.

ASTM (2012). "D5778-12 Standard Test Method for Electronic Friction Cone and Piezocone Penetration Testing of Soils." Annual Book of ASTM Standards, ASTM International, West Conshohocken, Pennsylvania.

ASTM (2014). "C136/C136M-14 Standard Test Method for Sieve Analysis of Fine and Coarse Aggregates." Annual Book of ASTM Standards, ASTM International, West Conshohocken, Pennsylvania.

ASTM (2014). "D1388-14 Standard Test Method for Stiffness of Fabrics." Annual Book of ASTM Standards, ASTM International, West Conshohocken, Pennsylvania.

ASTM (2015). "D1556/1556M-15 Standard Test Method for Density and Unit Weight of Soil in Place by Sand-Cone Method." Annual Book of ASTM Standards, ASTM International, West Conshohocken, Pennsylvania.

ASTM (2015). "D2573/D2573M-15 Standard Test Method for Field Vane Shear Test in Saturated Fine-Grained Soils." Annual Book of ASTM Standards, ASTM International, West Conshohocken, Pennsylvania.

ASTM (2016). "D3441-16 Standard Test Method for Mechanical Cone Penetration Testing of Soils." Annual Book of ASTM Standards, ASTM International, West Conshohocken, Pennsylvania.

ASTM (2016). "D4633-16 Standard Test Method for Energy Measurement for Dynamic Penetrometers." Annual Book of ASTM Standards, ASTM International, West Conshohocken, Pennsylvania.

Barnwell, B. (2018). Personal Communication. bbarnwell@adem.alabama.gov. 1400 Coliseum Blvd. Montgomery, AL 36110.

Bell, F. (2002). Engineering Treatment of Soils. CRC Press, Boca Raton, FL.

Bowles, J. E. (1996). *Foundation Analysis and Design 5th ed.* McGraw Hill, New York.

BS 1377 (1990). BS1377: Part 7: 1990 Method 4.4 – Determination of the in-situ vane shear strength of weak cohesive soils

Bubb, R. (2019). Personal Communication, Lecturer of Statistics and Research Methods, Auburn University.

Cassard, A., Kern, F., and Mathieu, G. (1979). Use of Reinforcement Techniques in Earth Dams. *C.R. Coll. Int. Renforcement des Sols*, Paris.

Chabal, J.P., Tardiu, B., Cureber, P., and Batsand, J. (1983). A Novel Reinforced Fill Dam. VIII ESCMFE, Helsinki.

Chen, T. and Fang, Y. (2008). Earth Pressure due to Vibratory Compaction. Journal of Geotechnical and Geoenvironmental Engineering. ASCE.

Cheng, J. (2015). Technical Memorandum. Plastic Hardening Model: Theory and Exmples. Itasca™ Consulting Group, Inc. Minneapolis, Minnesota.

Chinese Report (1979). *Testing and Research of Tank Foundation in Zheijiang Refinery Factory*. Zheijiang University, Hangzhow, China.

Clayton, C. R. I., Matthews, M.C., and Simons, N. E. (1995). Site Investigation 2nd ed. Department of Civil Engineering, University of Surrey. Wiley-Blackwell, England.

Coulomb, C. A. (1776). "Essi sur une application des regles de Maximums et Minimums à quelques Problèmes de Statique, relatifs à l'Architecture," *Memoires de Mathematique et de Physique,* Présentés à l'Academie Royale des Sciences, Paris, Vol. 3, 38.

Das, B. M. (2002). *Soil Mechanics Laboratory Manual 6th ed.* Oxford University Press, New York.

Das, B. M. (2004). *Principles of Foundation Engineering 5th ed*. Thomson, United States.

Das, B. M. (2005). *Fundamentals of Geotechnical Engineering 2nd ed.* Thomson, United States.

Das, B. M. (2006). *Principles of Geotechnical Engineering 6th ed*. Thomson, United States.

Day, R. W. (2001). *Soil Testing Manual.* McGraw Hill, New York.

Degroot, D. J., Poirier, S. E., and Landon, M. M. (2005). Sample Disturbance-Soft Clays. Studia Geotechnica et Mechanica, Vol. XXVII, No. 3-4, 2005.

Engineering News Record (1983). Old Fill Dam Gets Fast Safety Lift. January.

Holtz, R. D. and Kovacs, W. D. (1981). An Introduction to Geotechnical Engineering. Prentice Hall, Upper Saddle River, NJ.

Horvath, J.S. (2000). "Integral Abutment Bridges: Problems and Innovative Solutions Using EPS Geofoam and Other Geosynthetics. Report no. CE/GE-00-2. Manhattan College School of Engineering, Bronx, NY.

Ismael, N.F. and Behbehani M. (2014). "Influence of Relative Compaction on the Shear Strength of Compacted surface Sands." International Journal of Environmental Science and Development, Vol. 5, No. 1, February 2014.

Jones, C.J.F.P. (1996). Earth Reinforcement and Soil Structures. Thomas Telford. ASCE Press.

Koerner, R.M. (2005). *Designing With Geosynthetics. 5th ed.* Pearson Prentice Hall, Upper Saddle River, NJ.

Kulhawy, F.H. and Mayne, P.W. (1990). *Manual on Estimating Soil Properties for Foundation Design,* Final Report (EL-6800) submitted to Electric Power Research Institute (ERPI), Palo Alto, California.

Lee, K.L. (1965). "Triaxial Compressive Strength of Saturated Sands Under Seismic Loading Conditions." PhD Dissertation, University of California at Berkeley, 521 pp.

Lutenegger, A. J. (1987). "Suggested Method for Performing the Bore hole Shear Test." *Geotechnical Testing Journal*, GTJODJ, Vol. 10, No. 1

McCarthy, D. (2007). Essentials of Soil Mechanics and Foundations, Basic Geotechnics. 7th ed. Pearson Prentice Hall, Upper Saddle River, NJ.

Mohr, O. (1900). Welche Umstände bedingen die Elastizitätsgrenze und den Bruch eines Materials*? Zeitschrift des Vereins Deutscher Ingenieure.*

Narejo, D. (2003). "A Simple Tilt Table Device to Measure Index Friction Angle of Geosynthetics." Geotextiles and Geomembranes, Vol. 21. Pages 49-57. Elsevier.

NAVFAC (1986). Soils And Foundations Design Manuals. Naval Facilities Engineering Command, Alexandria, Virginia. < http://web.mst.edu/~rogersda/u mrcourses/ge441/dm7_01.pdf>.

Reinforced Earth Company (2008). Reinforced Earth ®. < http://www.recocanada.com /reinforced_earth.php>. (July 20, 2016).

Samtani, N. and Nowatzki, E. (2006). "Soils and Foundations Manual, Vol 2." Federal Highway Administration, Washington, DC.

Schulgasser, K. (1983). "The In-Plane Poisson Ratio of Paper." Fibre Science and Technology. Applied Science Publishers Ltd, England.

Shukla, S.K., Lopes, M.L., Das B.M., Palmeira, E.M., Bordeau, P.L., Ashmawy, A.K., Perkins, S.W., Berg R.R., Christopher, B.R., Tan, S.A., Ingold, T.S., Zanzinger, H., Gartung, E., Singh, D.N., Duquennoi, C., Bathurst, R.J., Hatami, K., and Alfaro, M.C. (2002). Geosynthetics and Their Applications. Thomas Telford Press, London, England.

TAPPI (2001). "T 494 om-01 Tensile Properties of Paper and Paperboard (Using Constant Rate of Elongation Apparatus)." TAPPI Standards and Suggested Methods, Technical Association of the Pulp and Paper Industry, Peachtree Corners, Georgia.

Terzaghi, Karl (1925). *Erdbaumechanik auf Bodenphysikalischer Grundlage*. F. Deuticke.

Wasti, Y. and Ozduzgun, B. (2001). Geomembrane-Geotextile Interface Shear Properties as Determined by Inclined Board and Direct Shear Box Tests. Geotextiles and Geomembranes, Vol. 19. Pages 45-57. Elsevier.

Winterkorn, H. F. and Fang, H. (1975). *Foundation Engineering Handbook*. Van Nostrand Reinhold Ltd. New York, New York.

Silberzahn, R., Uhlmann, E. L., Martin, D. P., Anselmi, P., Aust, F., Awtrey, E., … Nosek, B. A. (2018). Many Analysts, One Data Set: Making Transparent How Variations in Analytic Choices Affect Results. *Advances in Methods and Practices in Psychological Science*, *1*(3), 337–356. <https://doi.org/10.1177/2515245917747646>.

APPENDICES

List of Tables in Appendices

List of Figures in Appendices

APPENDIX A: BENCHTOP TESTING REINFORCEMENT PHOTOGRAPHS

A.1 Introduction

Photographs were taken of the reinforcement that was recovered from each benchtop test. Each piece of reinforcement was marked with a pen where the failure plane(s) appeared to occur in the specimen due to a fold in the reinforcement. The grid is a Plexiglass sheet placed over the excavated reinforcement.

A.2 Photographs of Test 8W8L5Lay

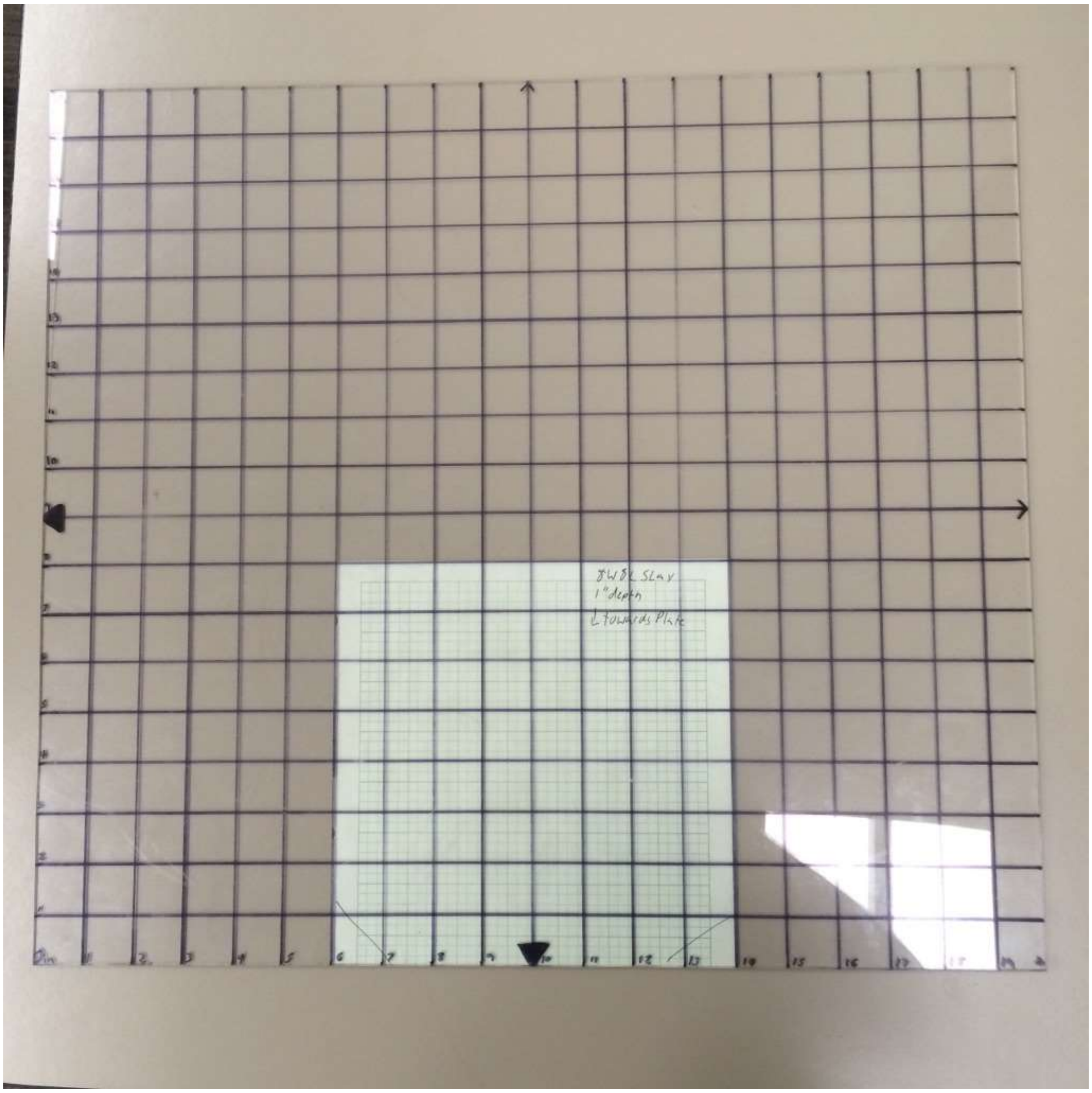

Figure 146: Test 8W8L5Lay 1" Depth

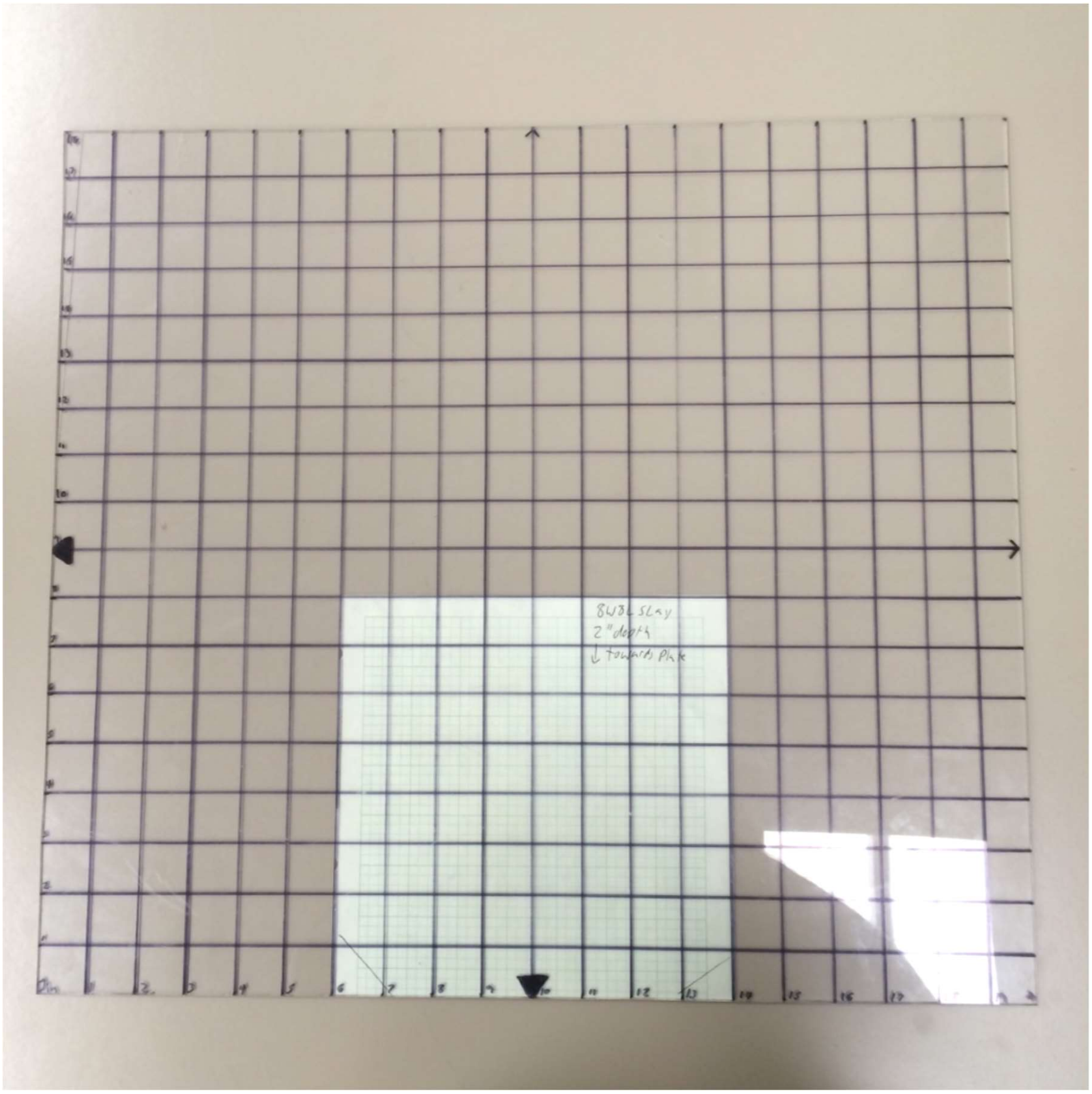

Figure 147: Test 8W8L5Lay 2" Depth

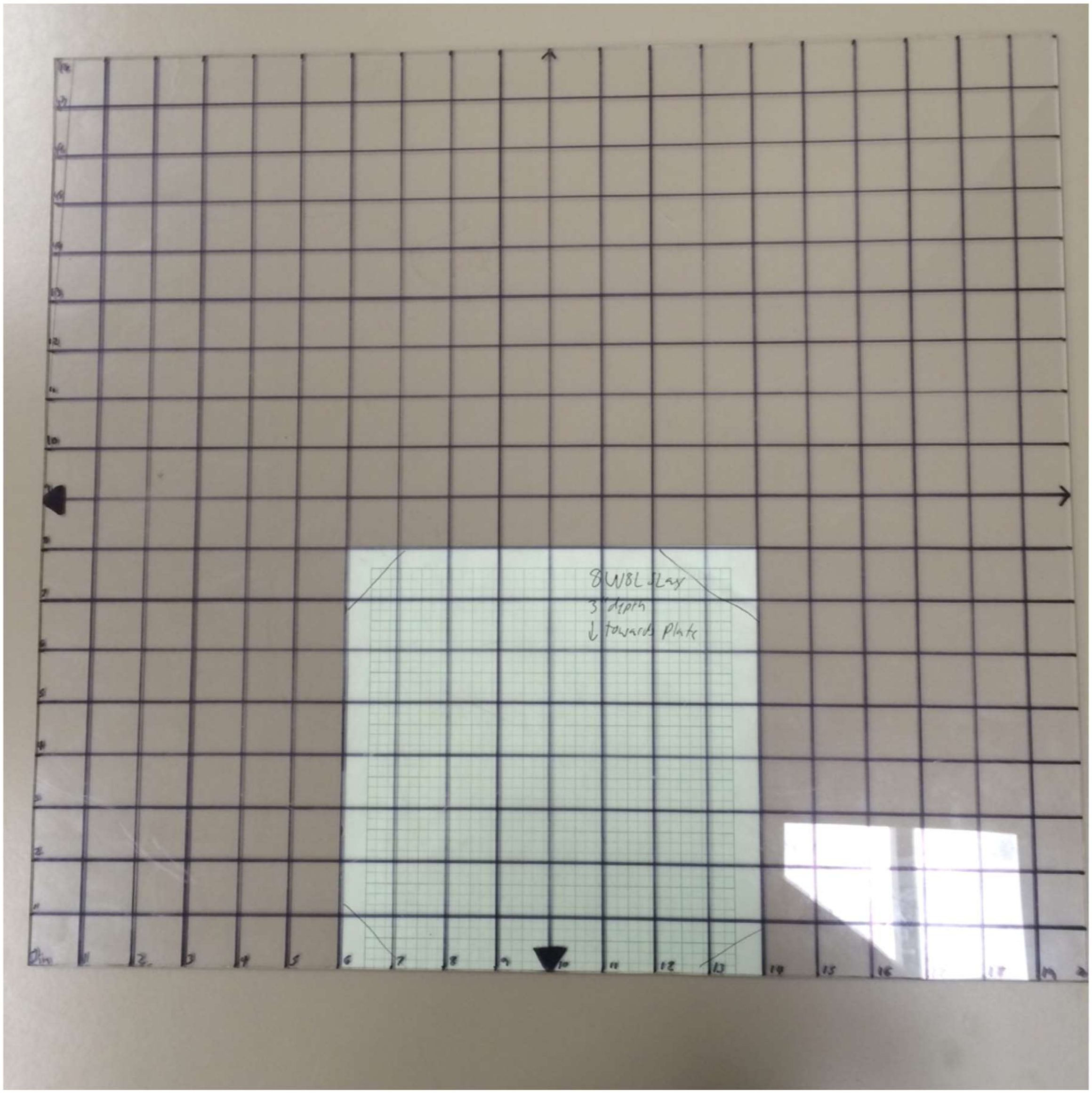

Figure 148: Test 8W8L5Lay 3" Depth

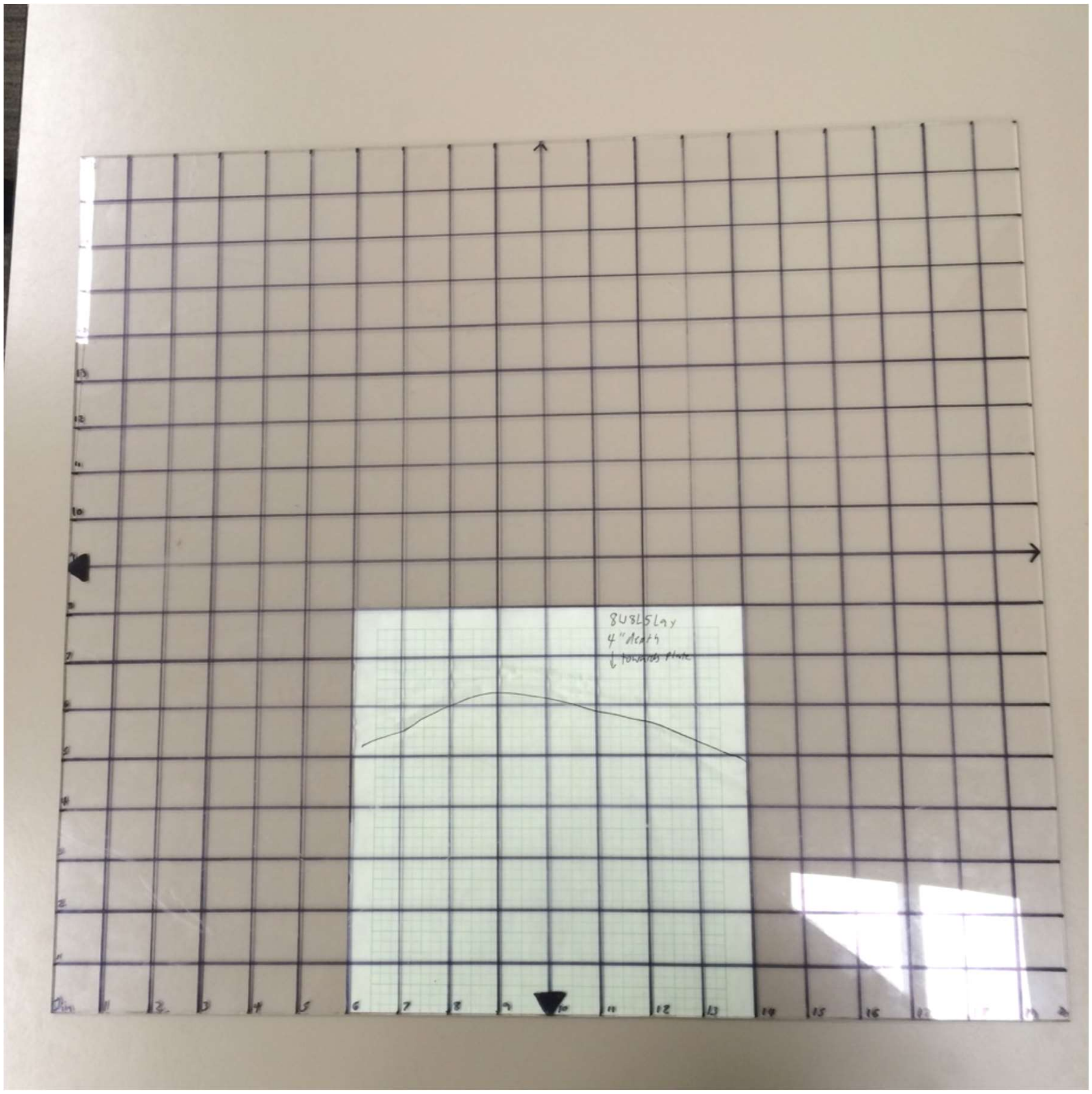

Figure 149: Test 8W8L5Lay 4" Depth

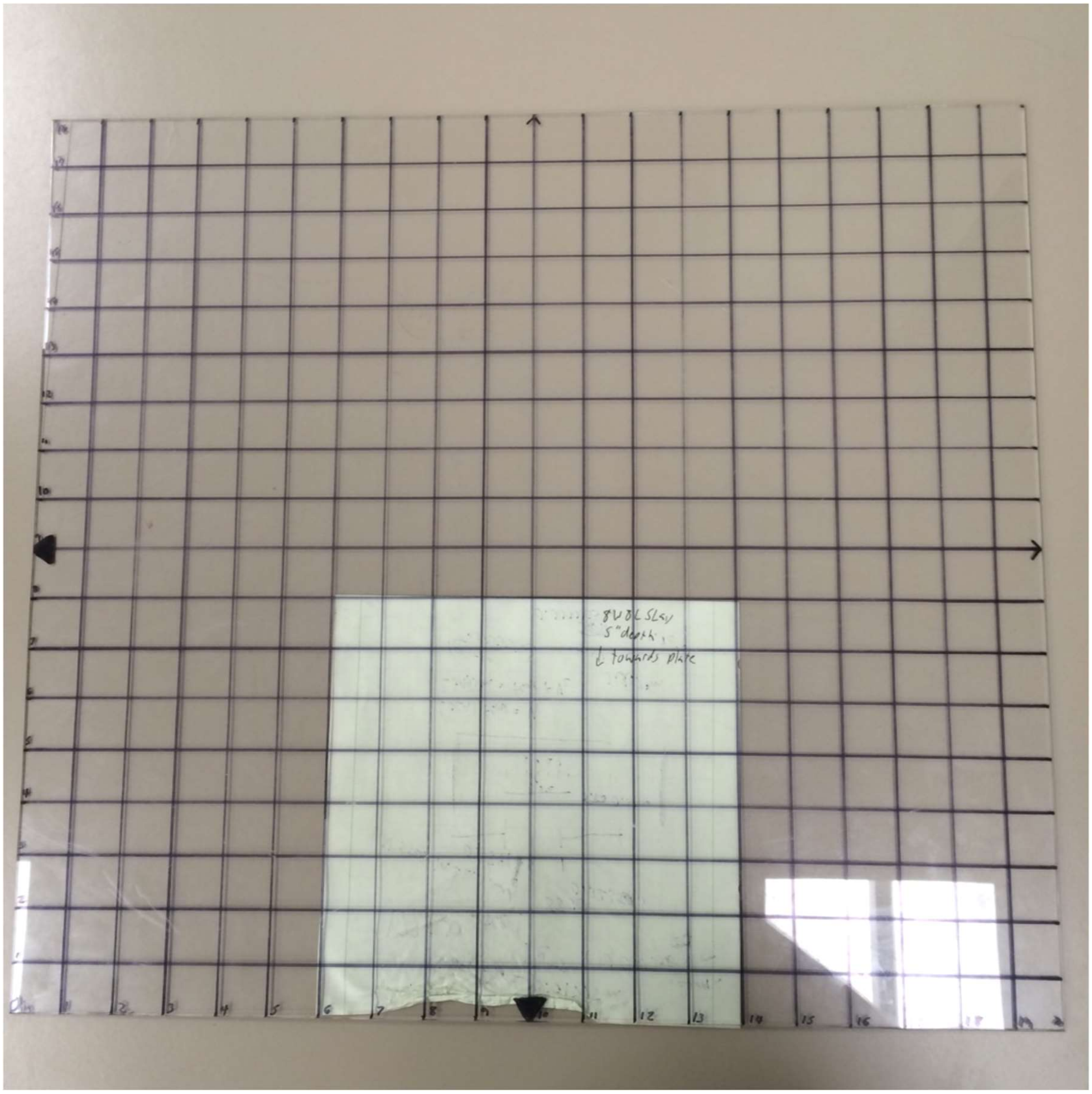

Figure 150: Test 8W8L5Lay 5” Depth

A.3 Photographs of Test 8W8L5Lay2

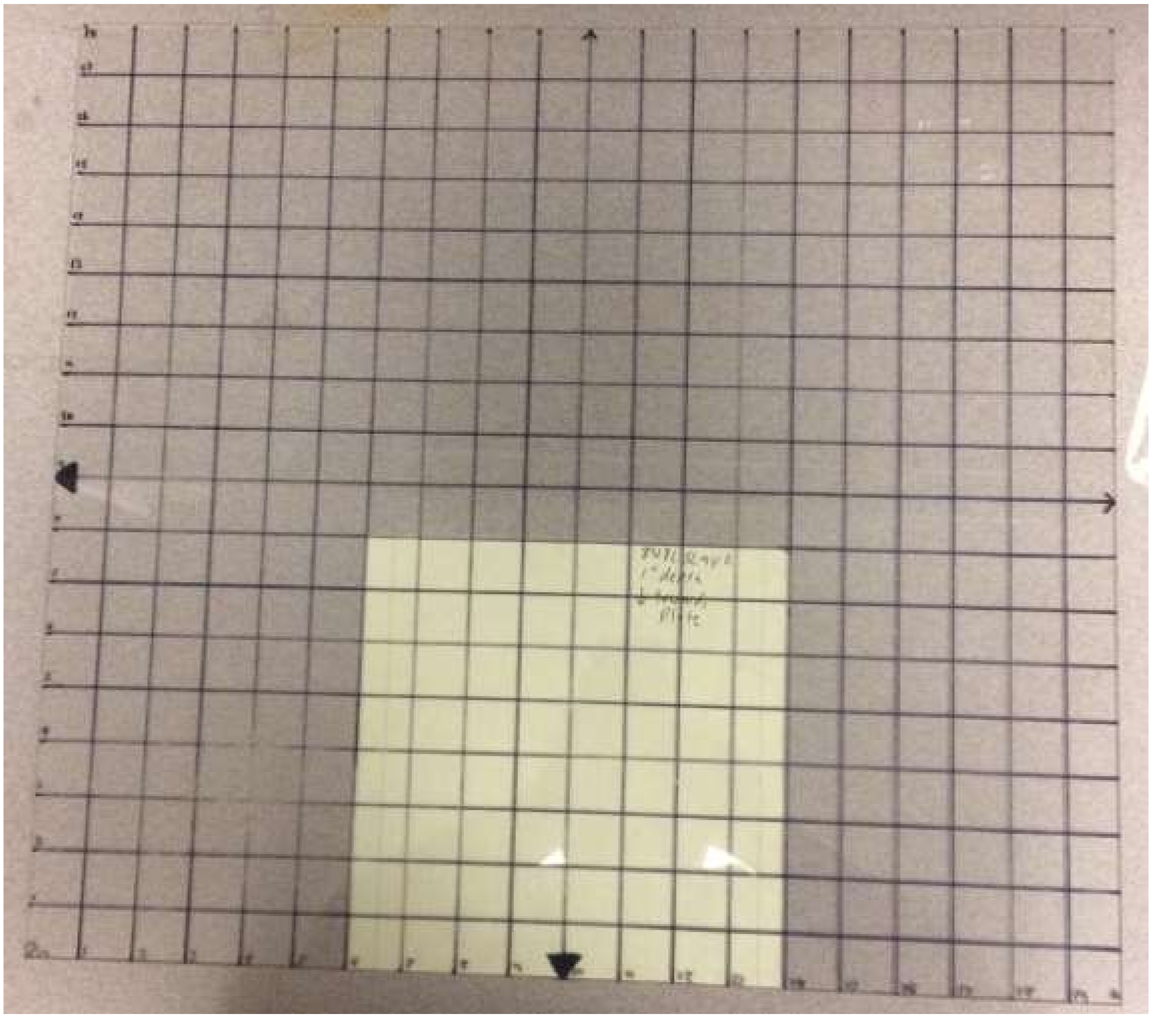

Figure 151: Test 8W8L5Lay2 1" Depth

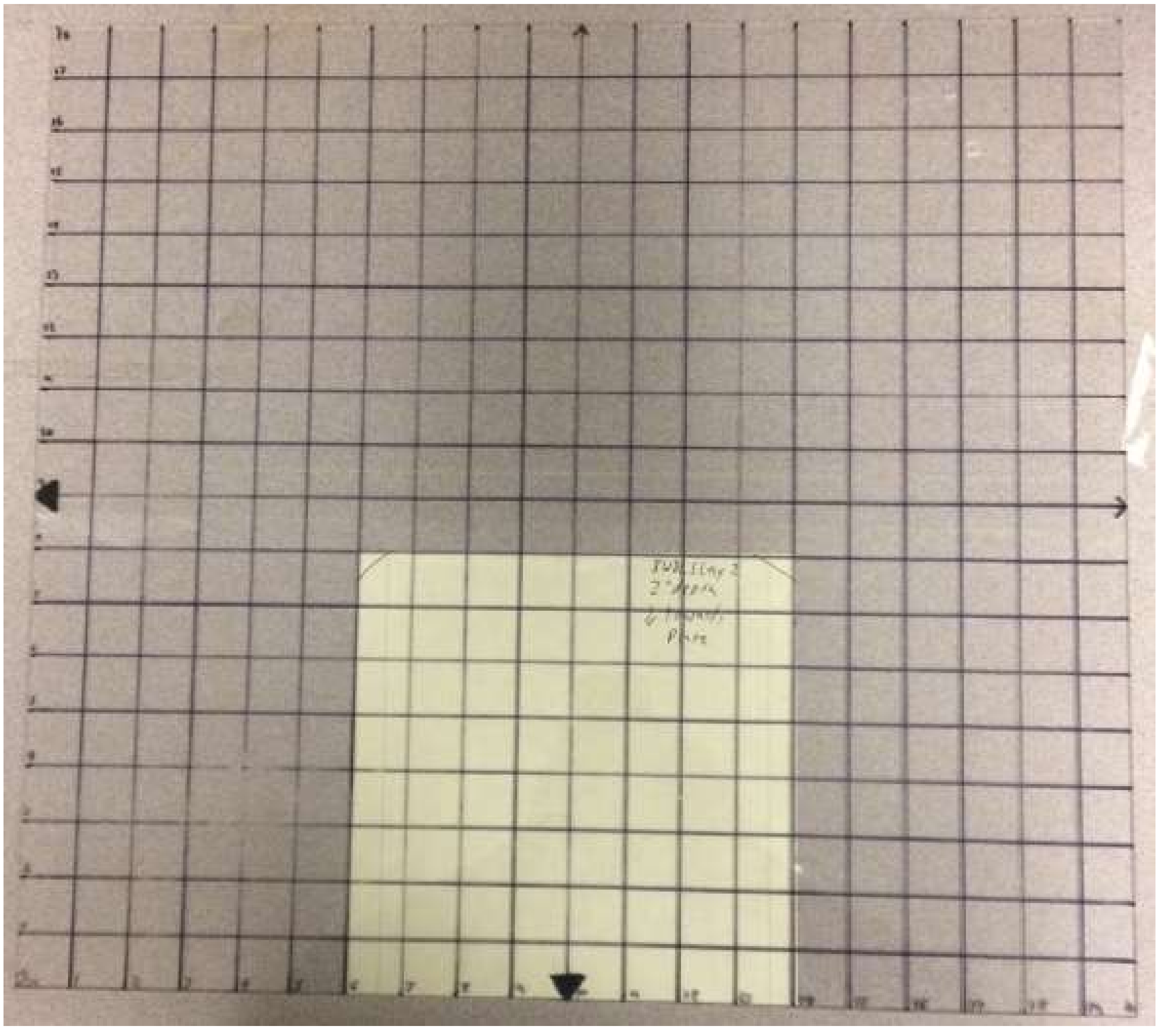

Figure 152: Test 8W8L5Lay2 2" Depth

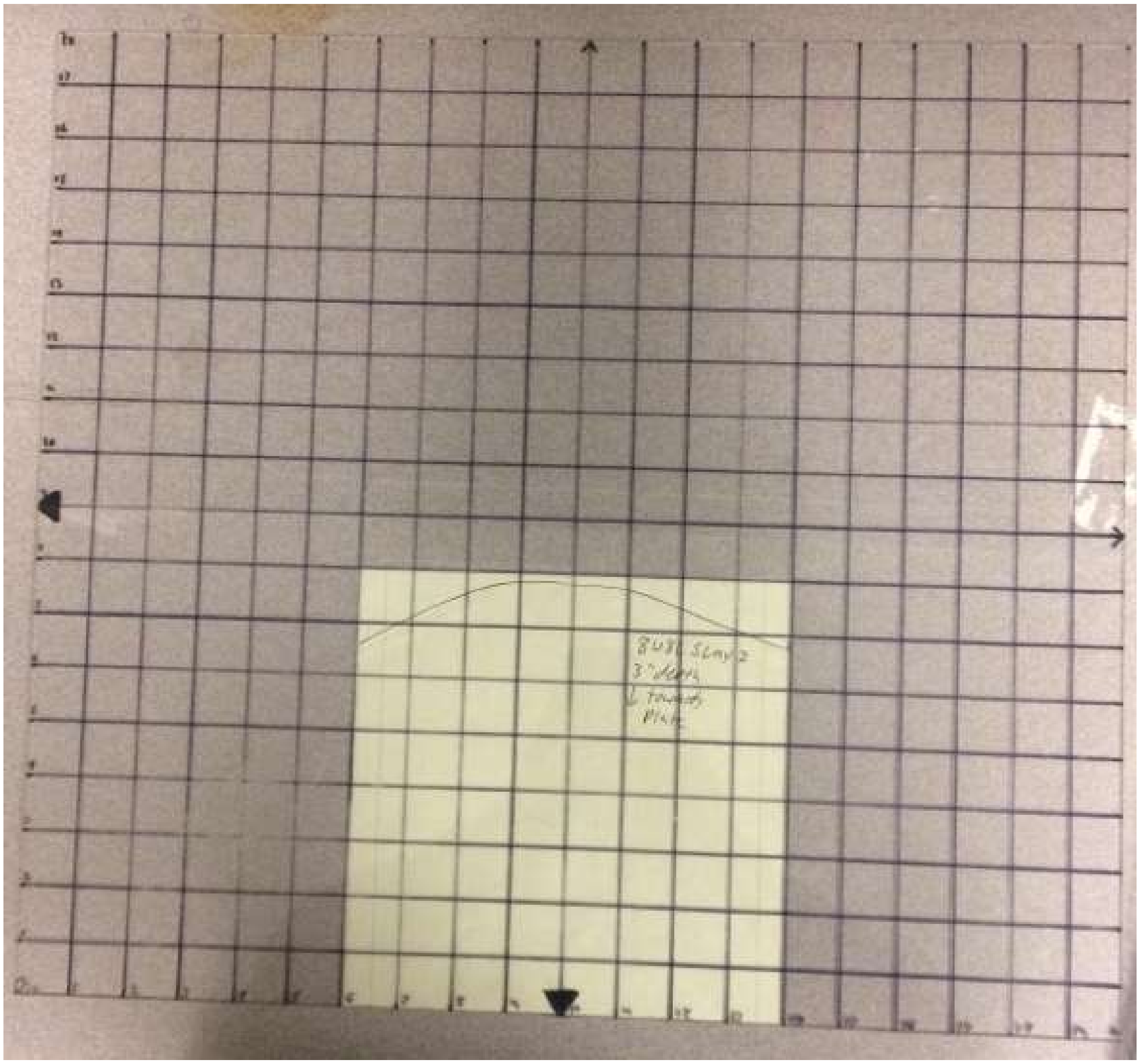

Figure 153: Test 8W8L5Lay2 3" Depth

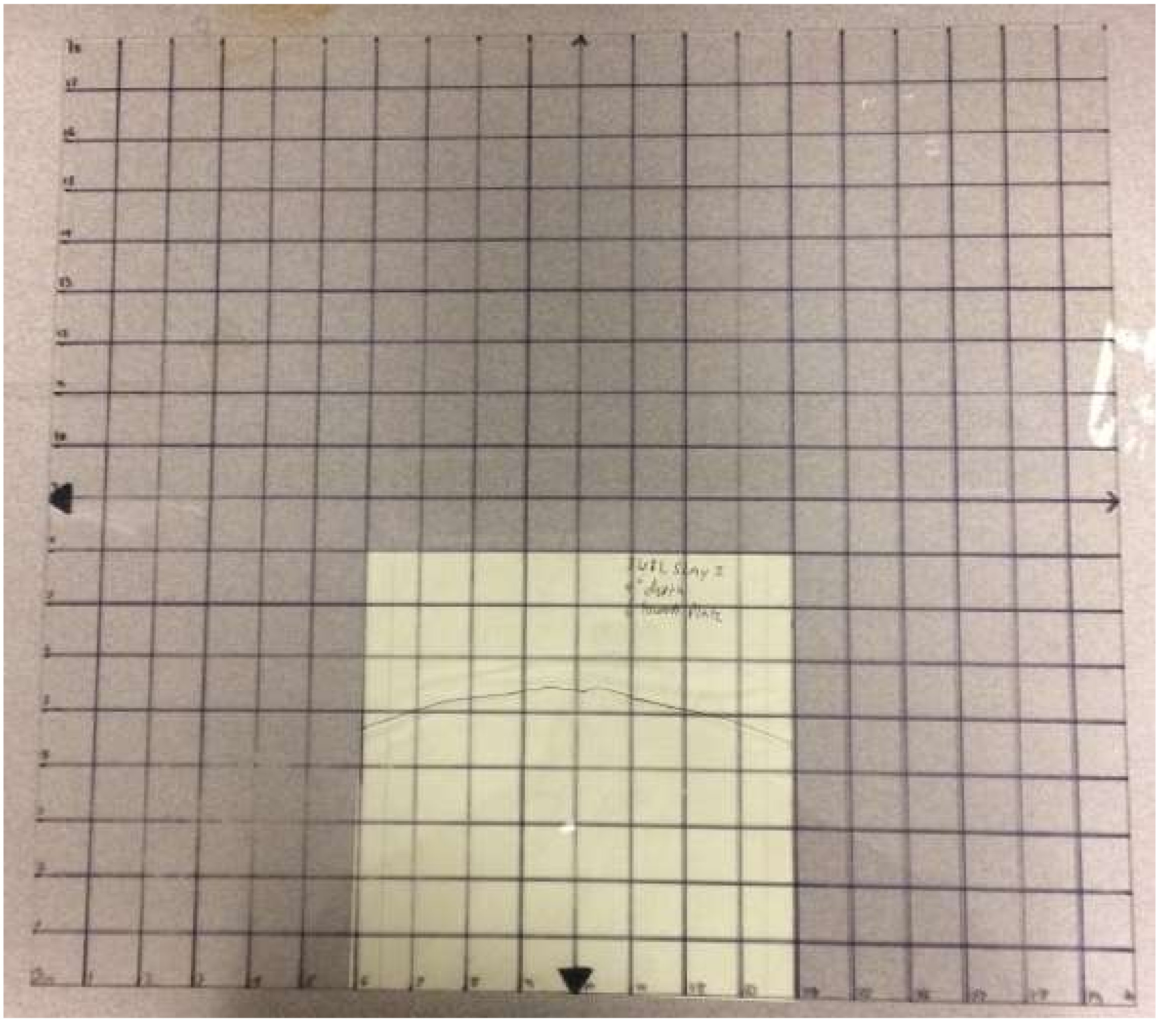

Figure 154: Test 8W8L5Lay 4” Depth

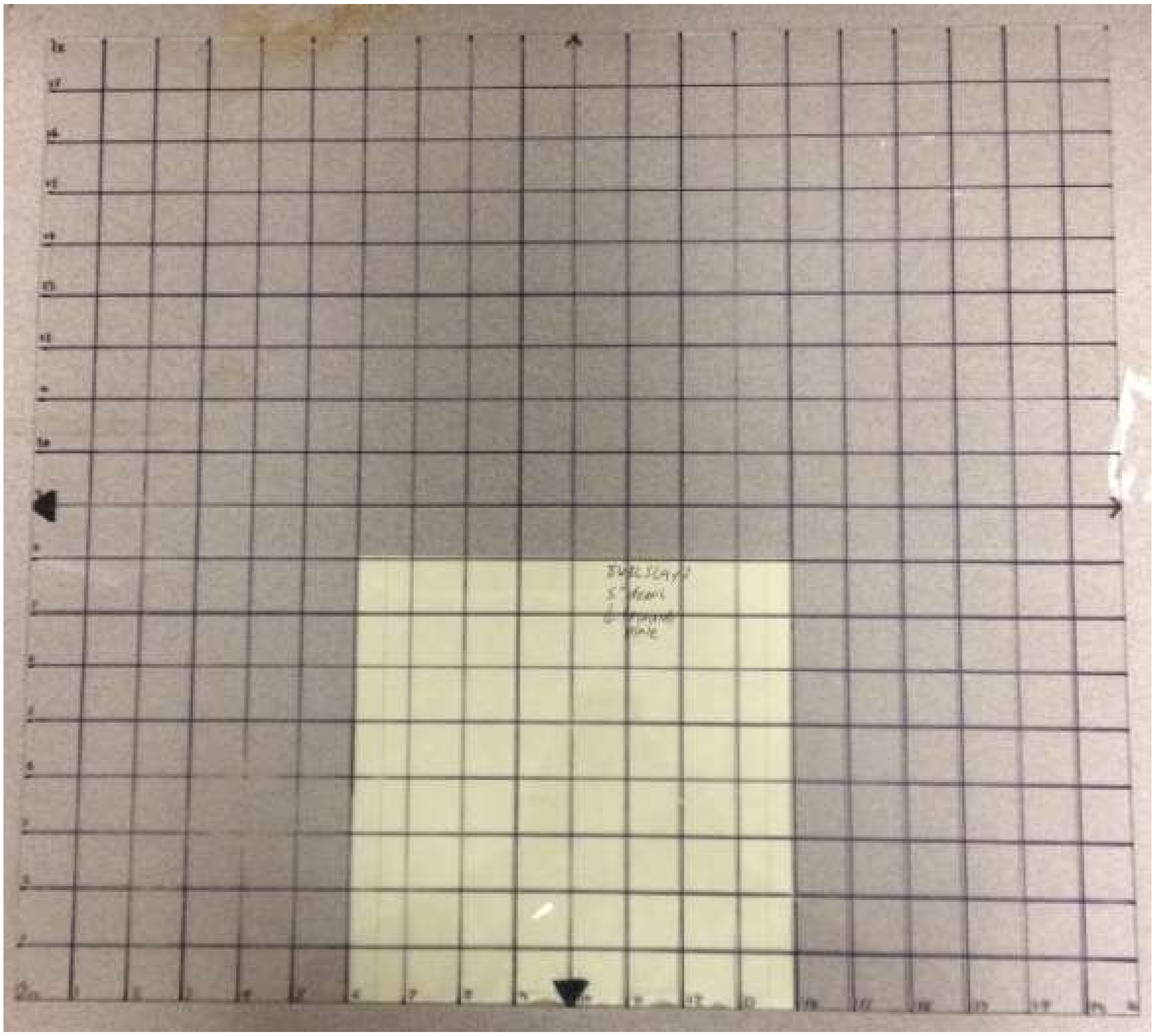

Figure 155: Test 8W8L5Lay 5” Depth

A.3 Photographs of Test 11W8L5Lay

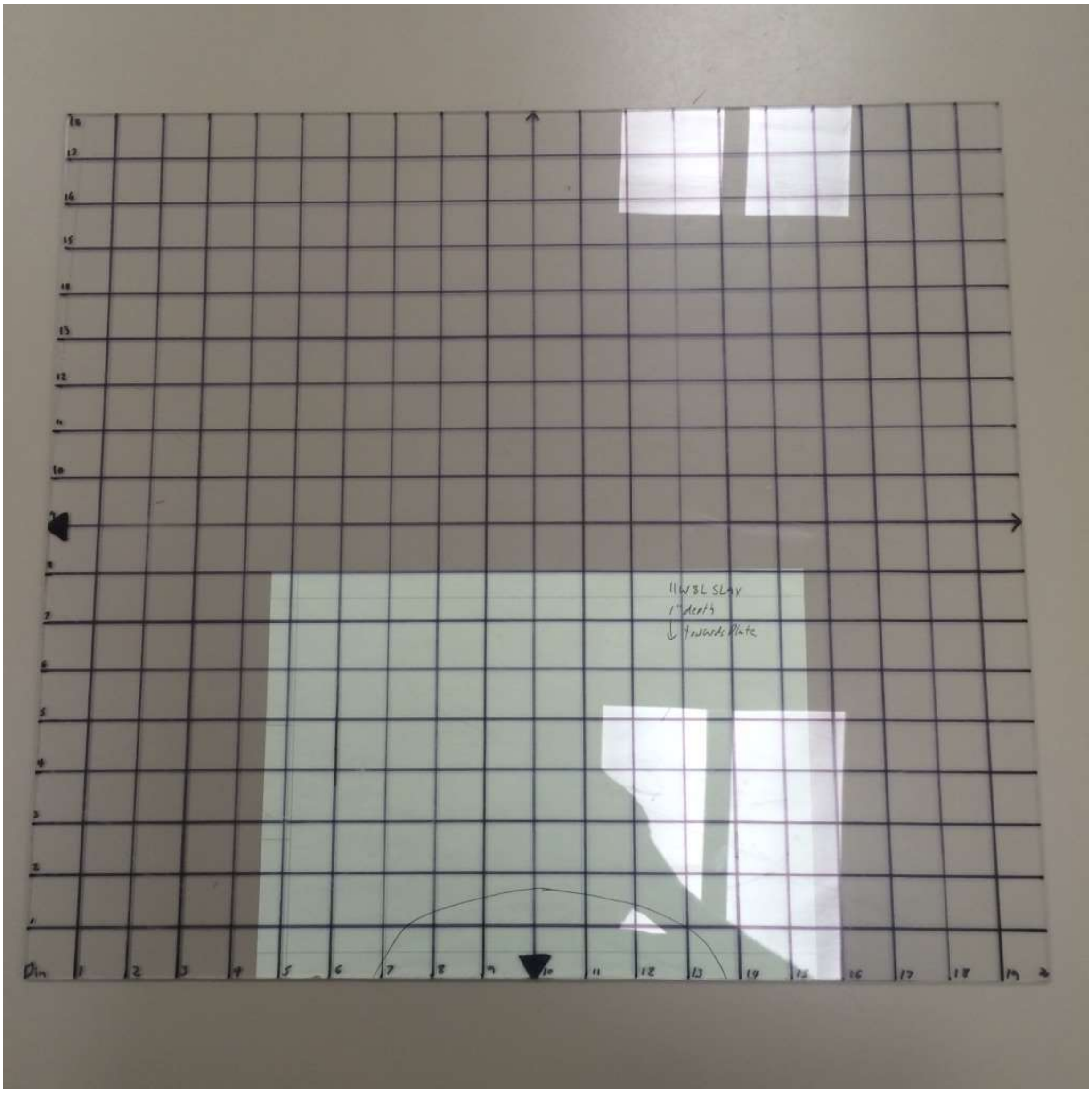

Figure 156: Test 11W8L5Lay 1" Depth

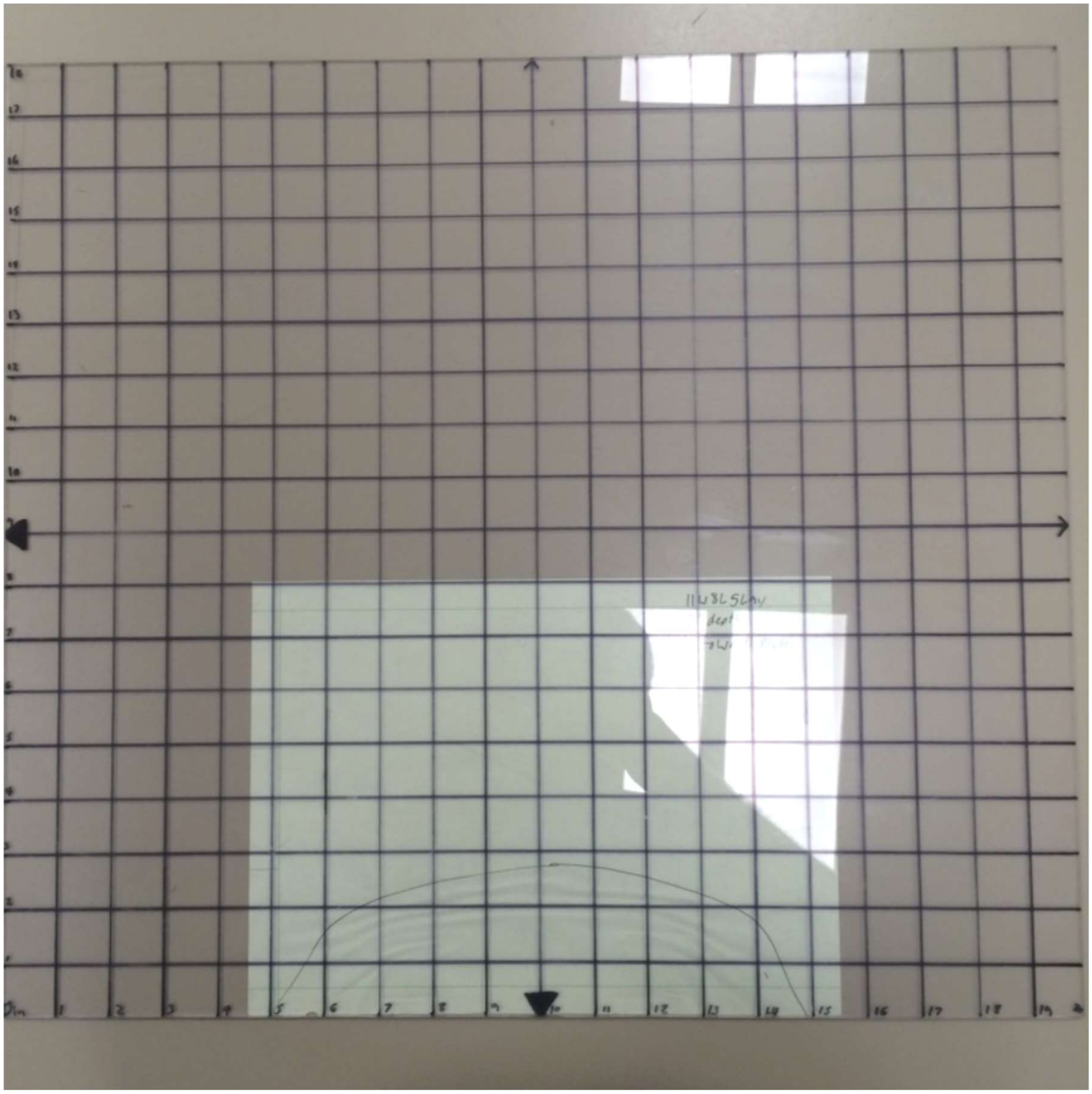

Figure 157: Test 11W8L5Lay 2" Depth

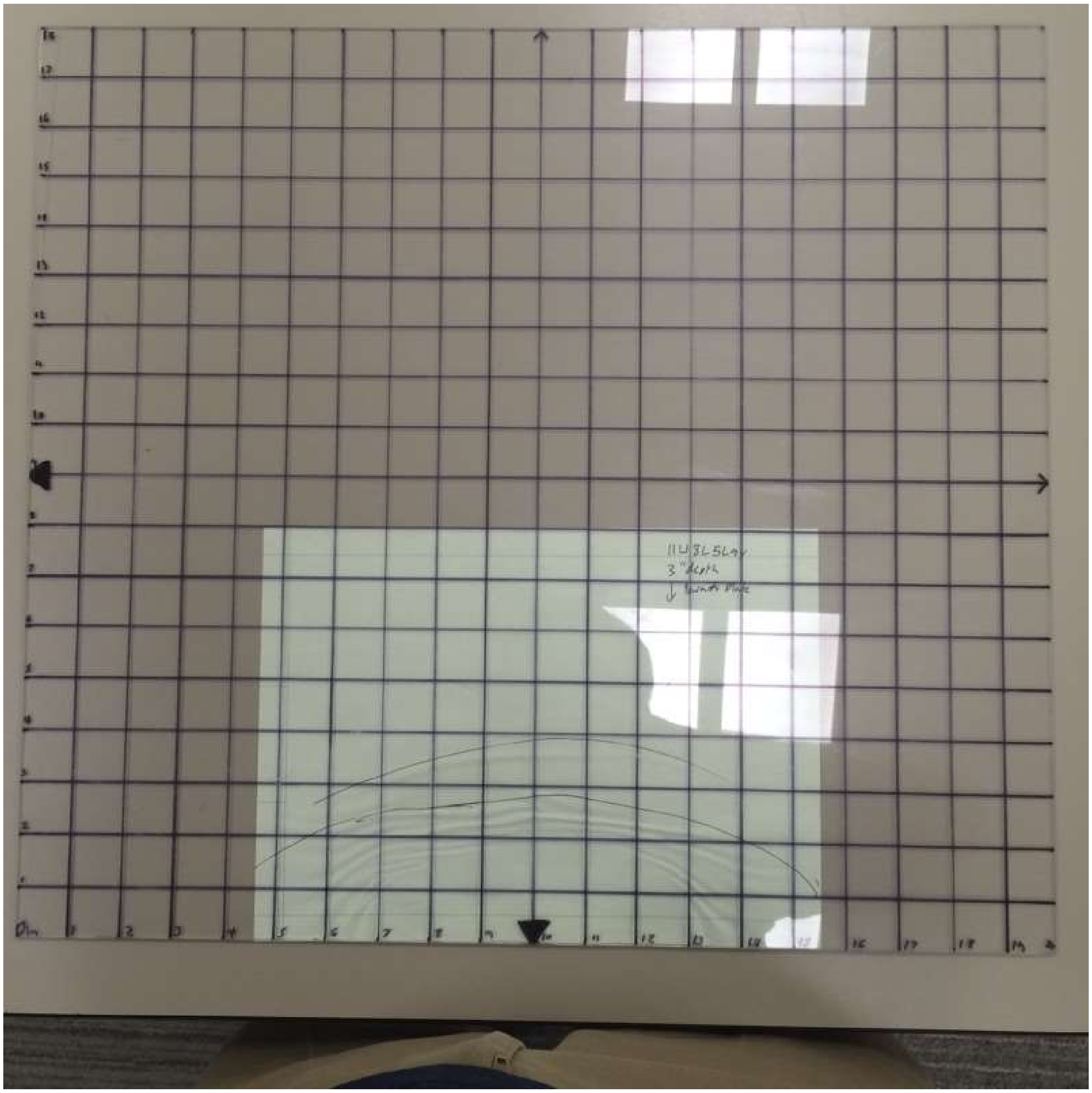

Figure 158: Test 11W8L5Lay 3” Depth

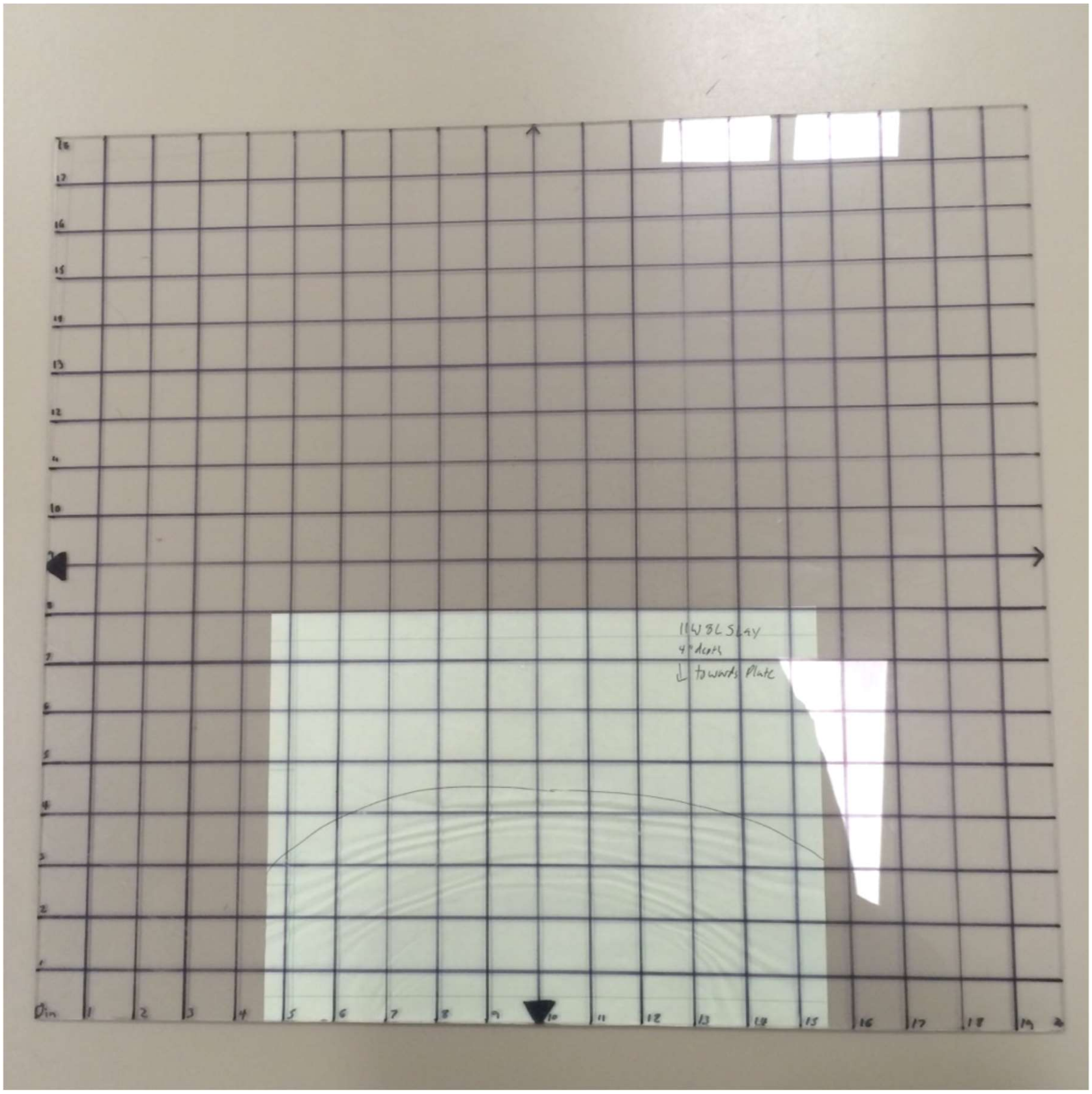

Figure 159: Test 11W8L5Lay 4" Depth

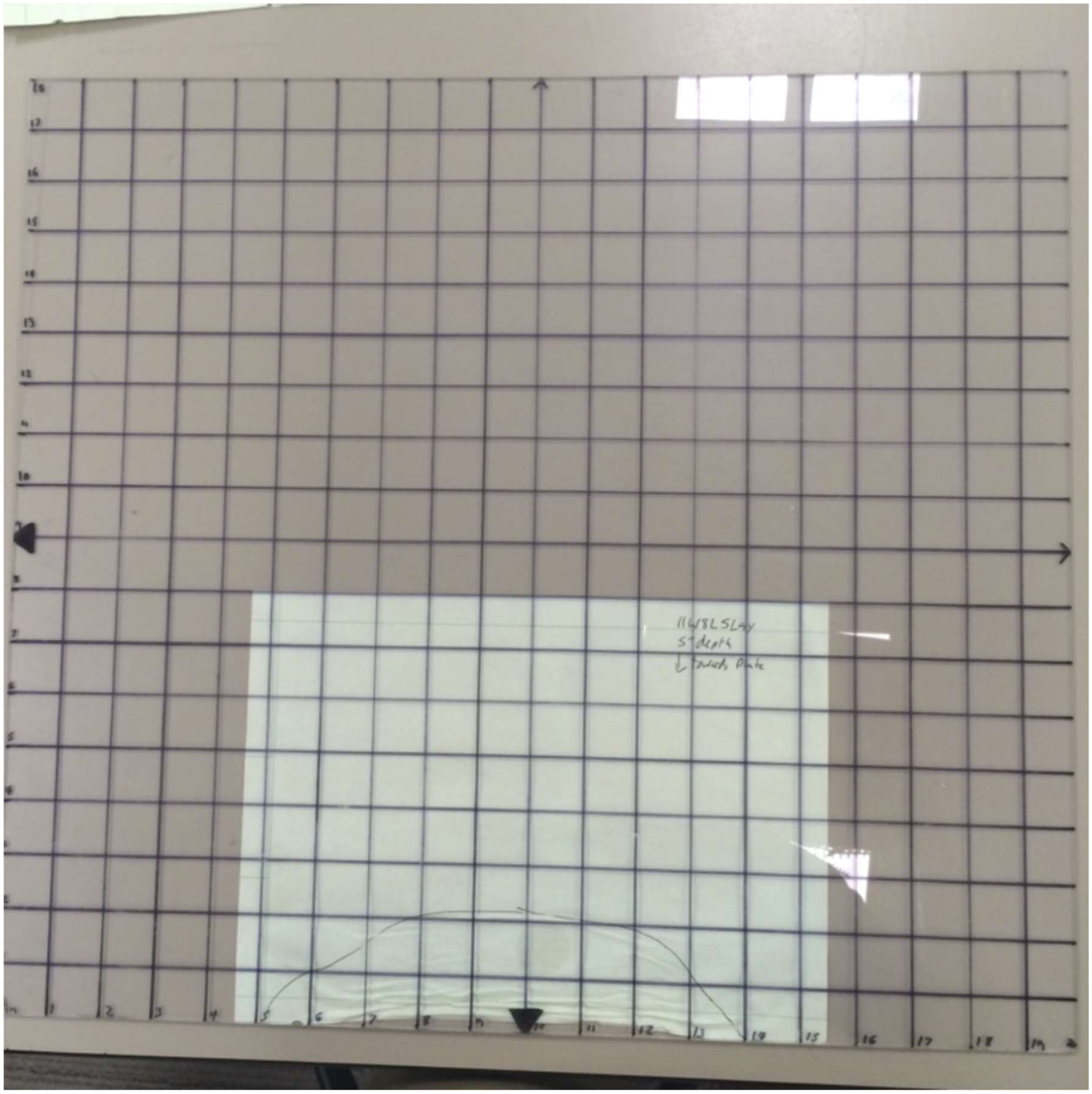

Figure 160: Test 11W8L5Lay 5” Depth

A.4 Photographs of Test 11W8L10Lay

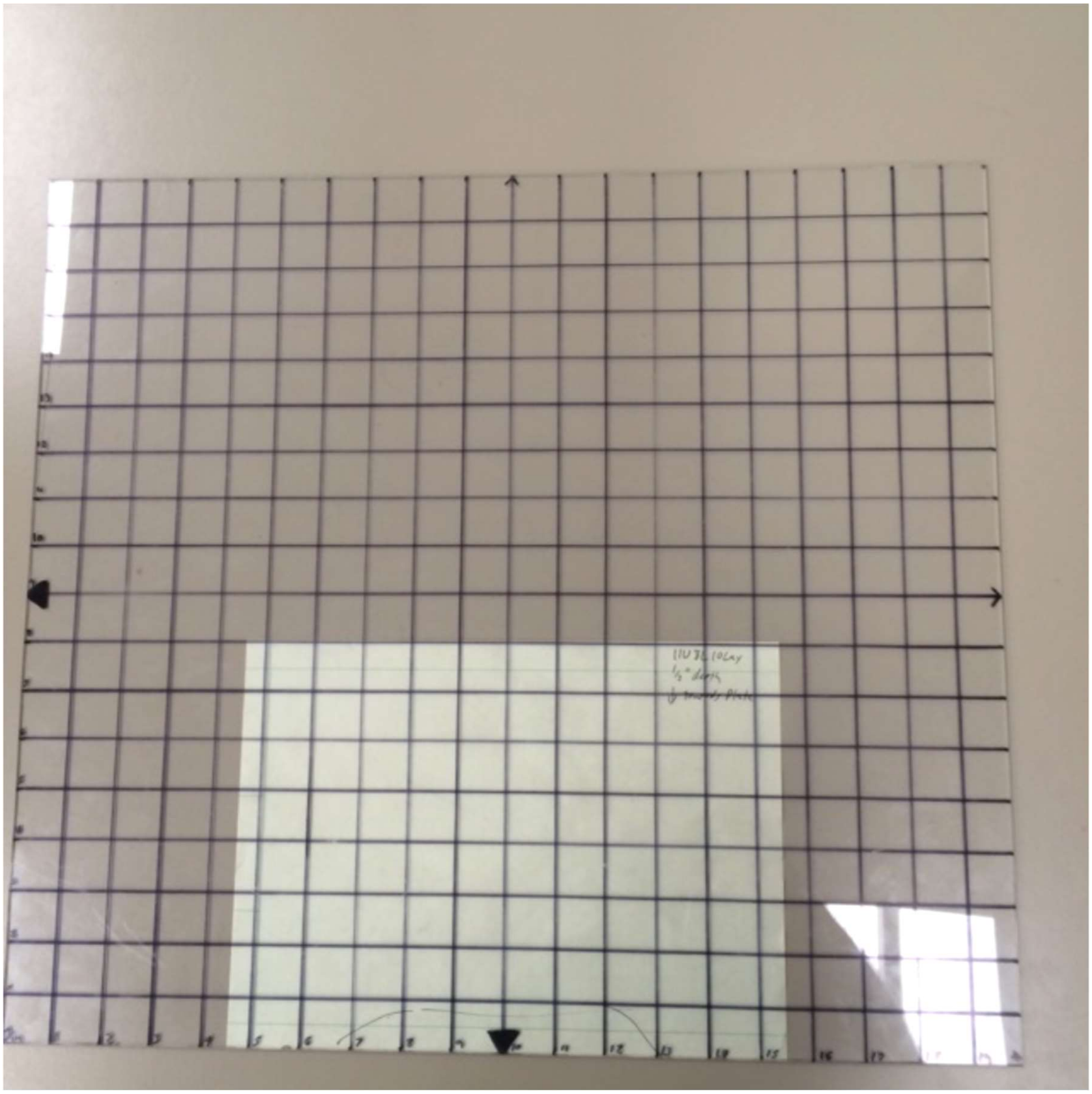

Figure 161: Test 11W8L10Lay 0.5” Depth

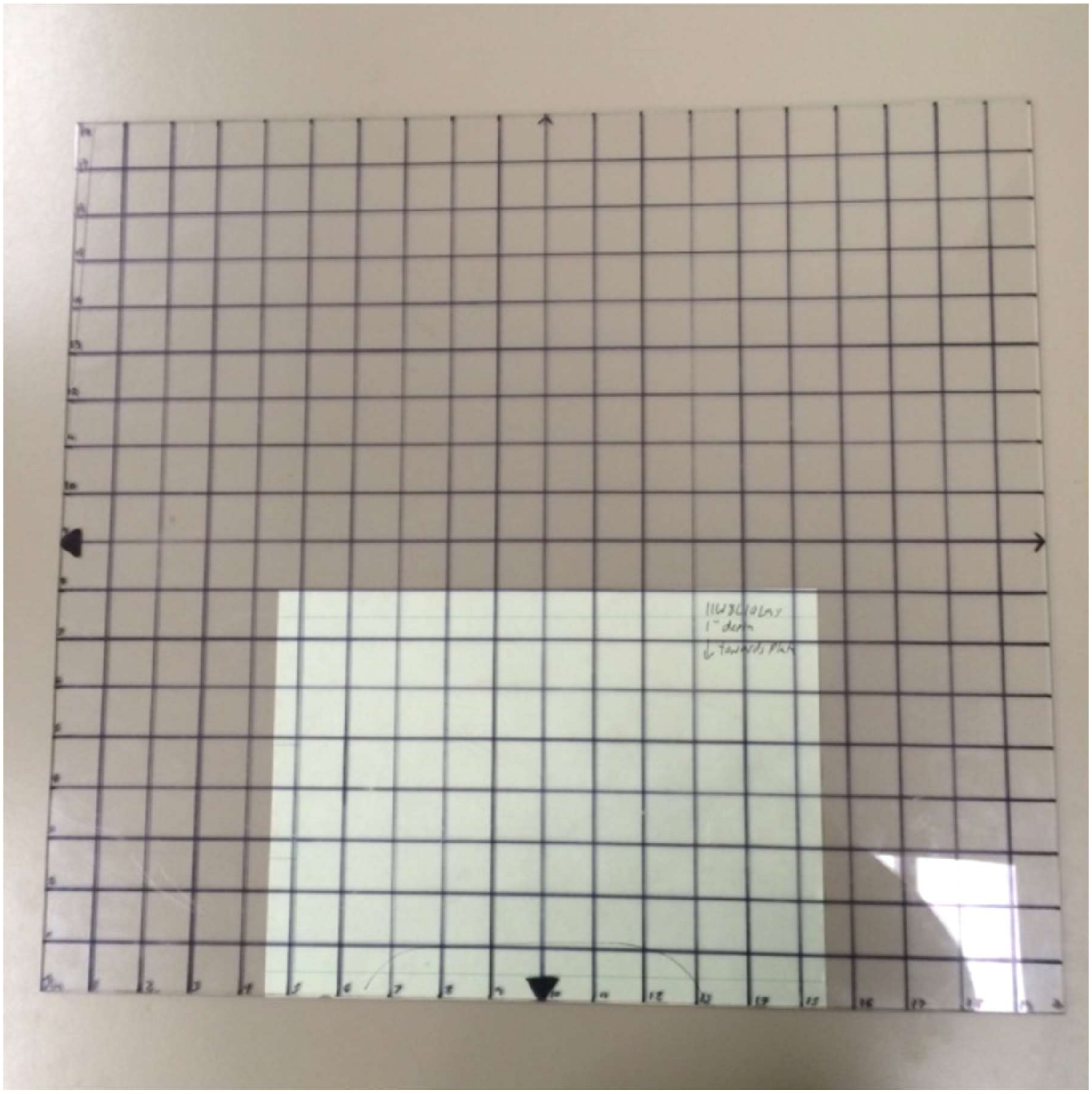

Figure 162: Test 11W8L10Lay 1" Depth

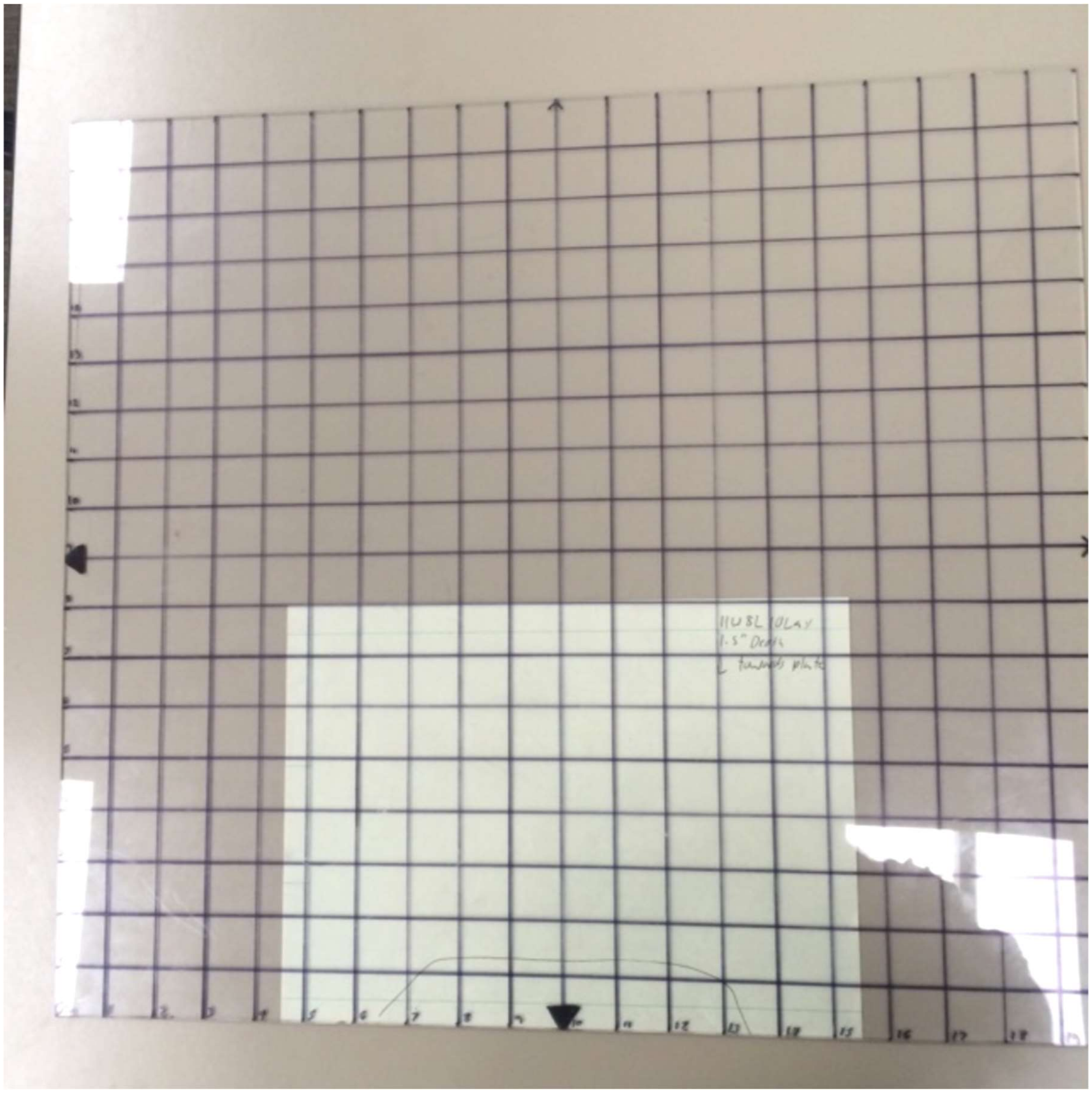

Figure 163: Test 11W8L10Lay 1.5" Depth

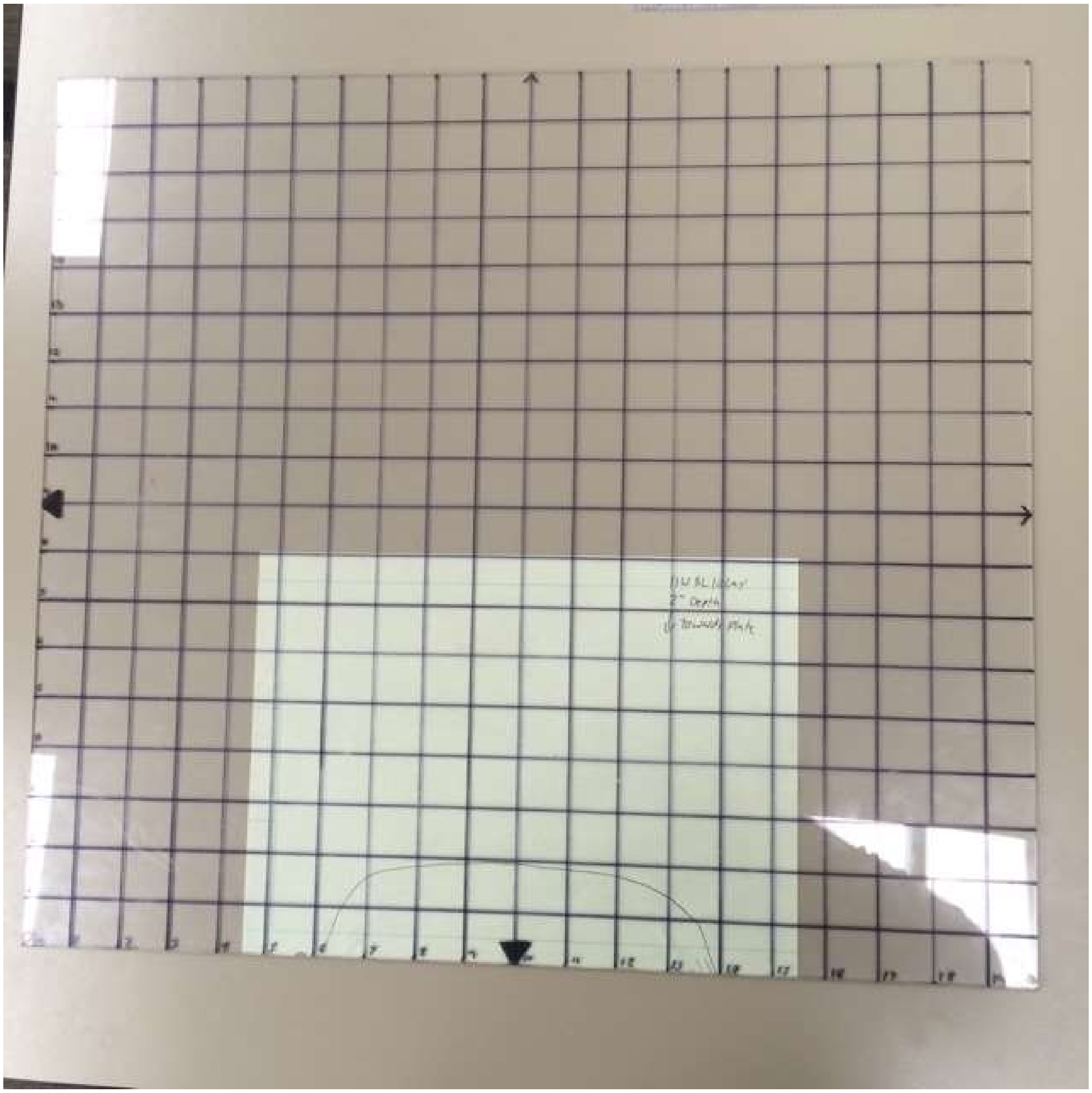

Figure 164: Test 11W8L10Lay 2" Depth

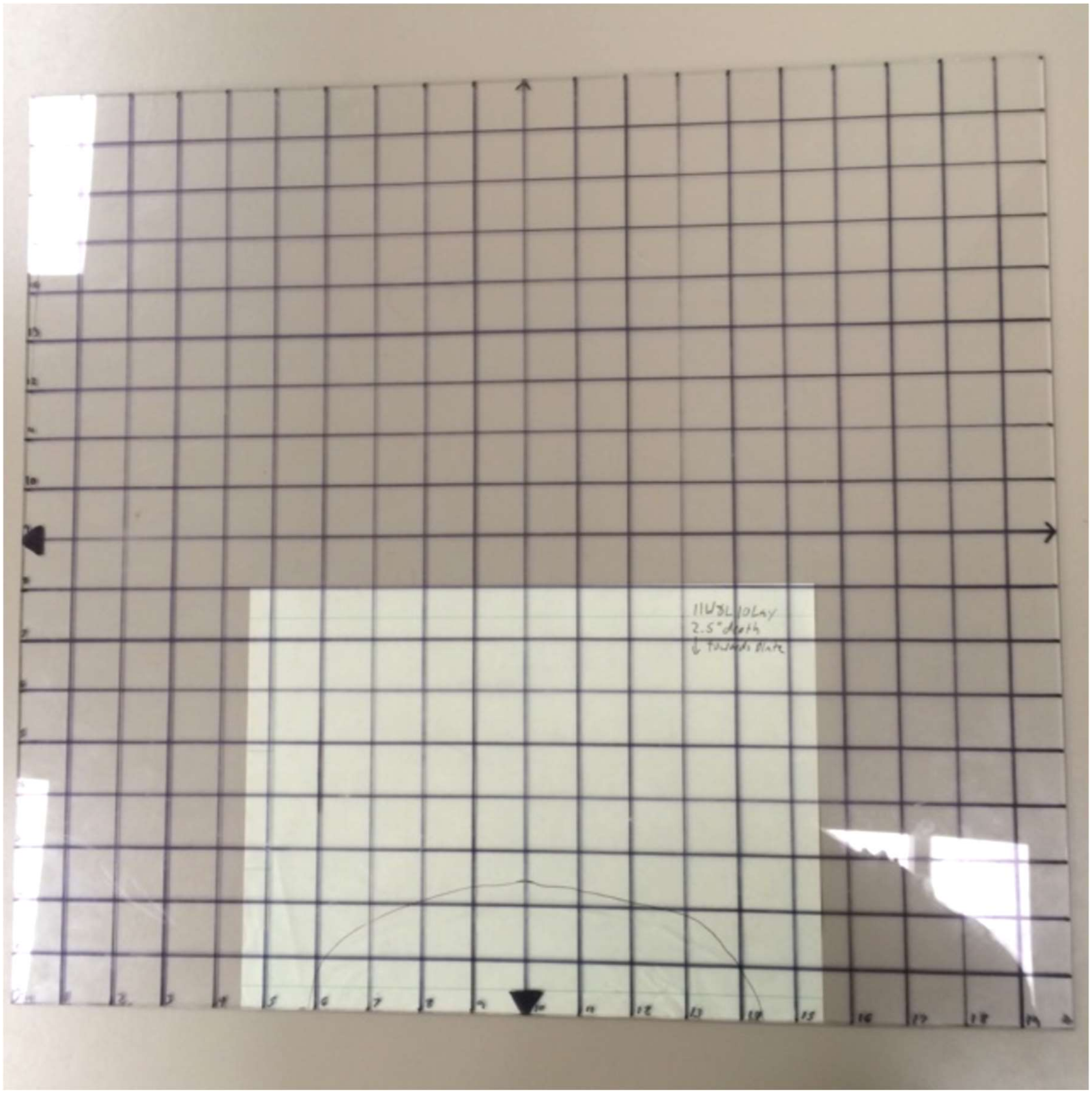

Figure 165: Test 11W8L10Lay 2.5" Depth

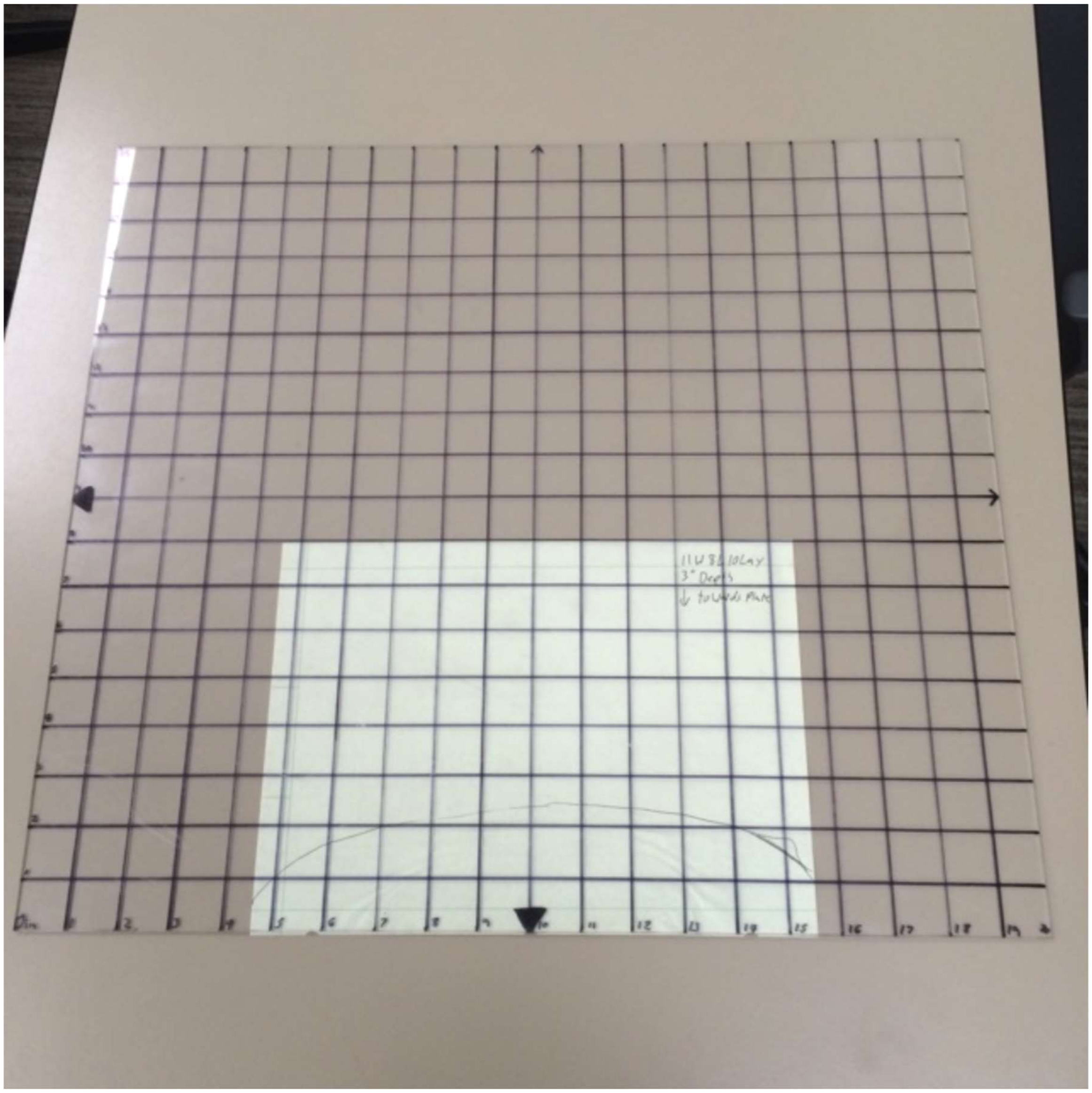

Figure 166: Test 11W8L10Lay 3" Depth

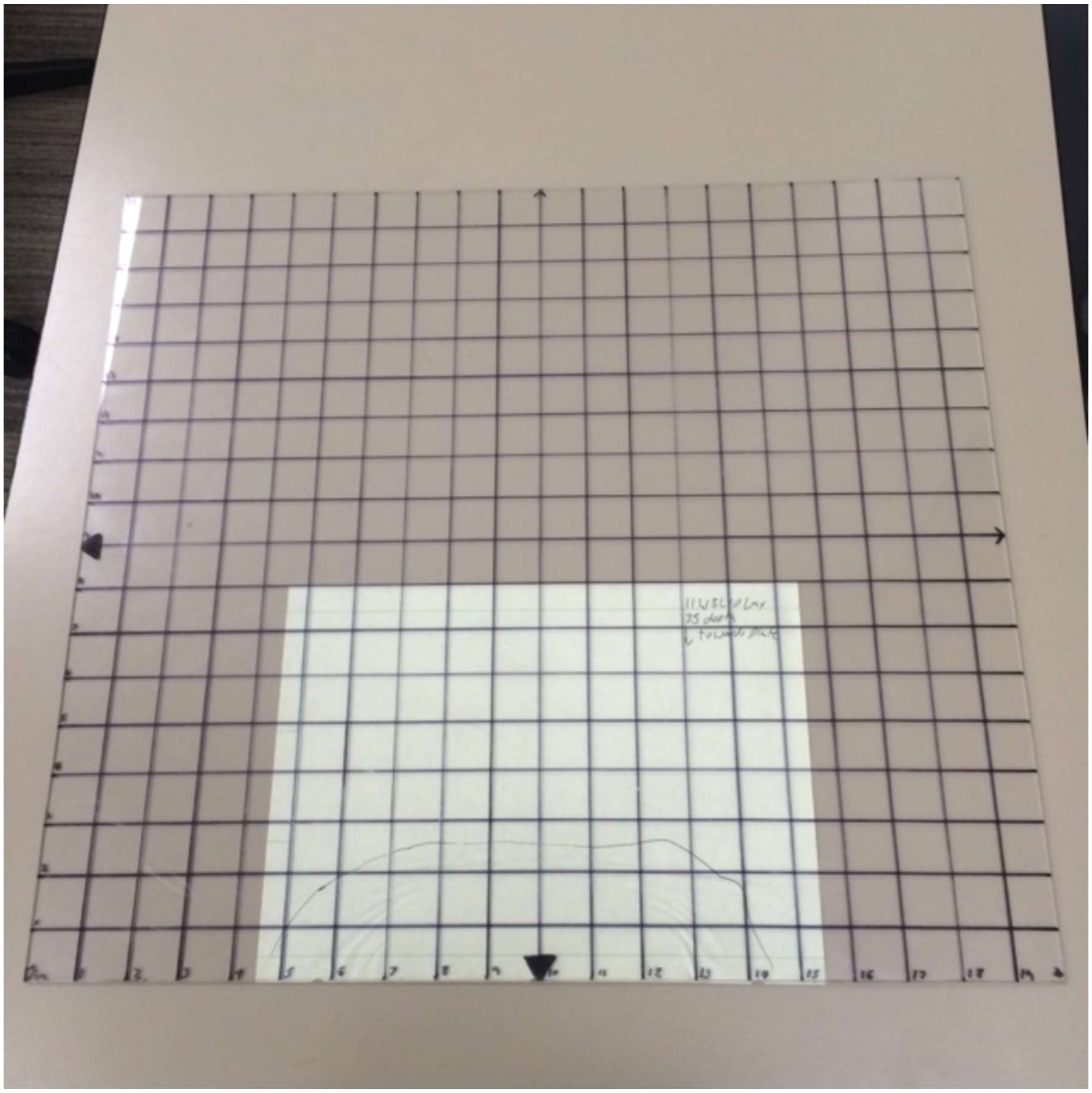

Figure 167: Test 11W8L10Lay 3.5” Depth

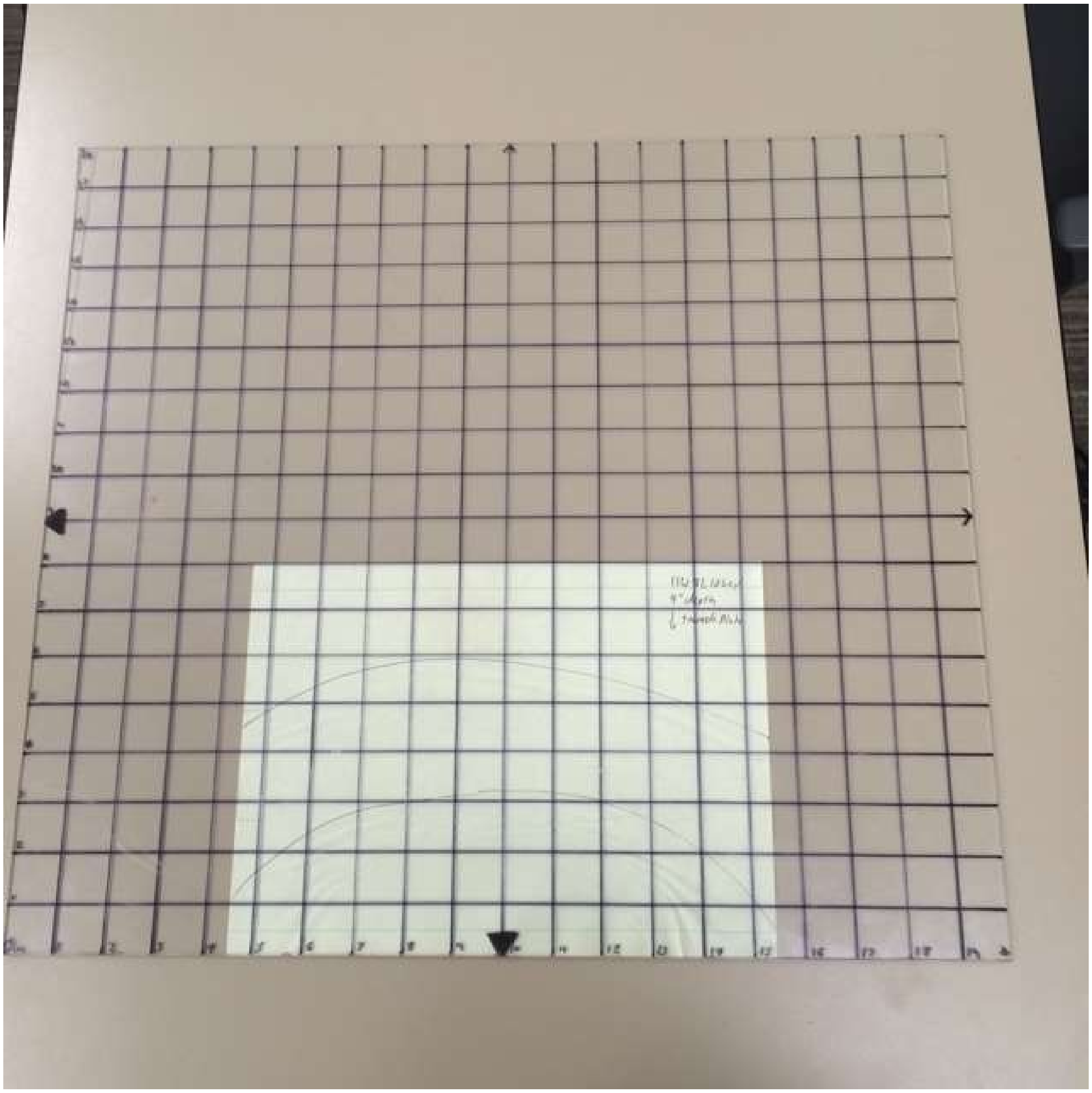

Figure 168: Test 11W8L10Lay 4” Depth

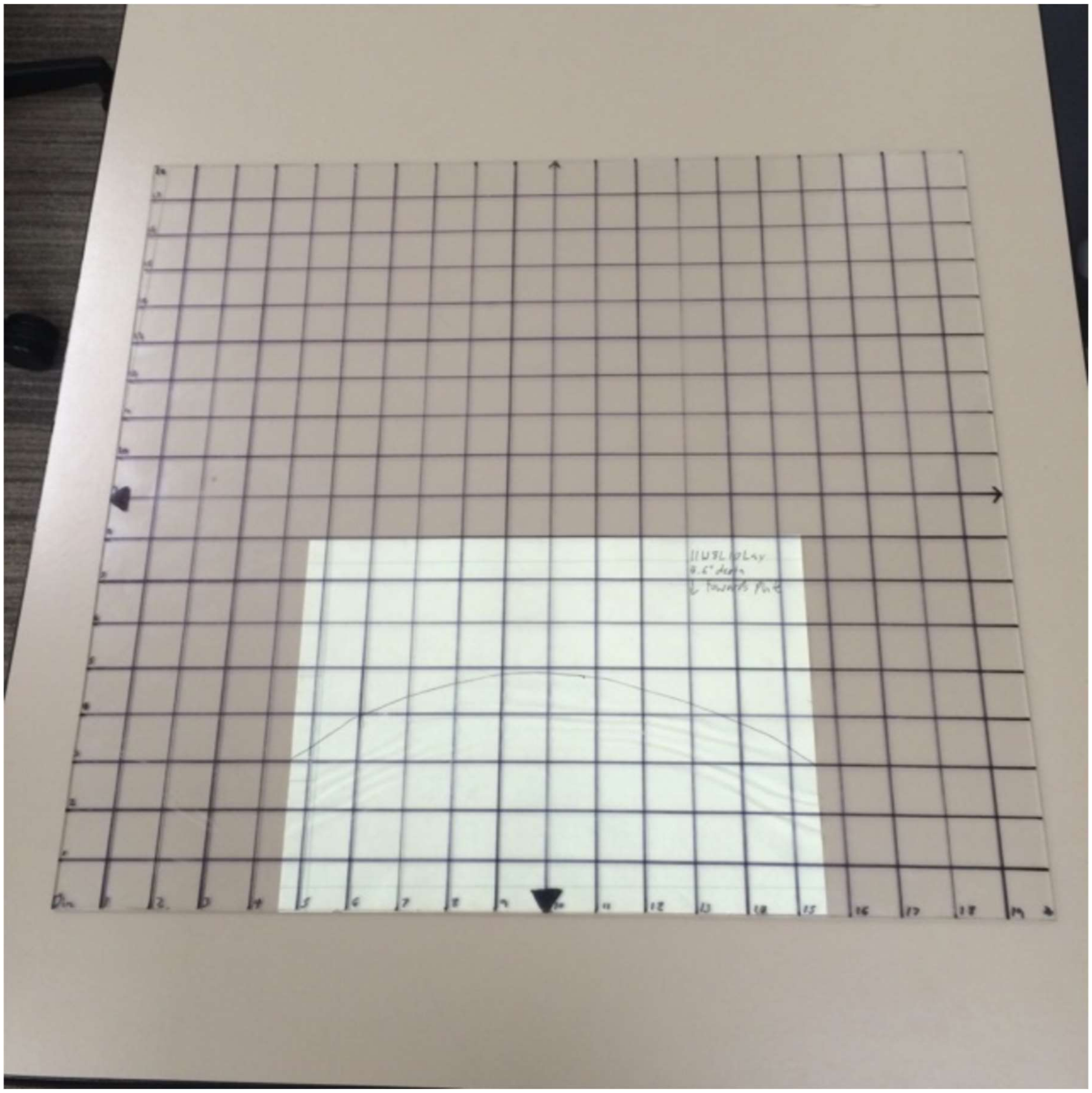

Figure 169: Test 11W8L10Lay 4.5" Depth

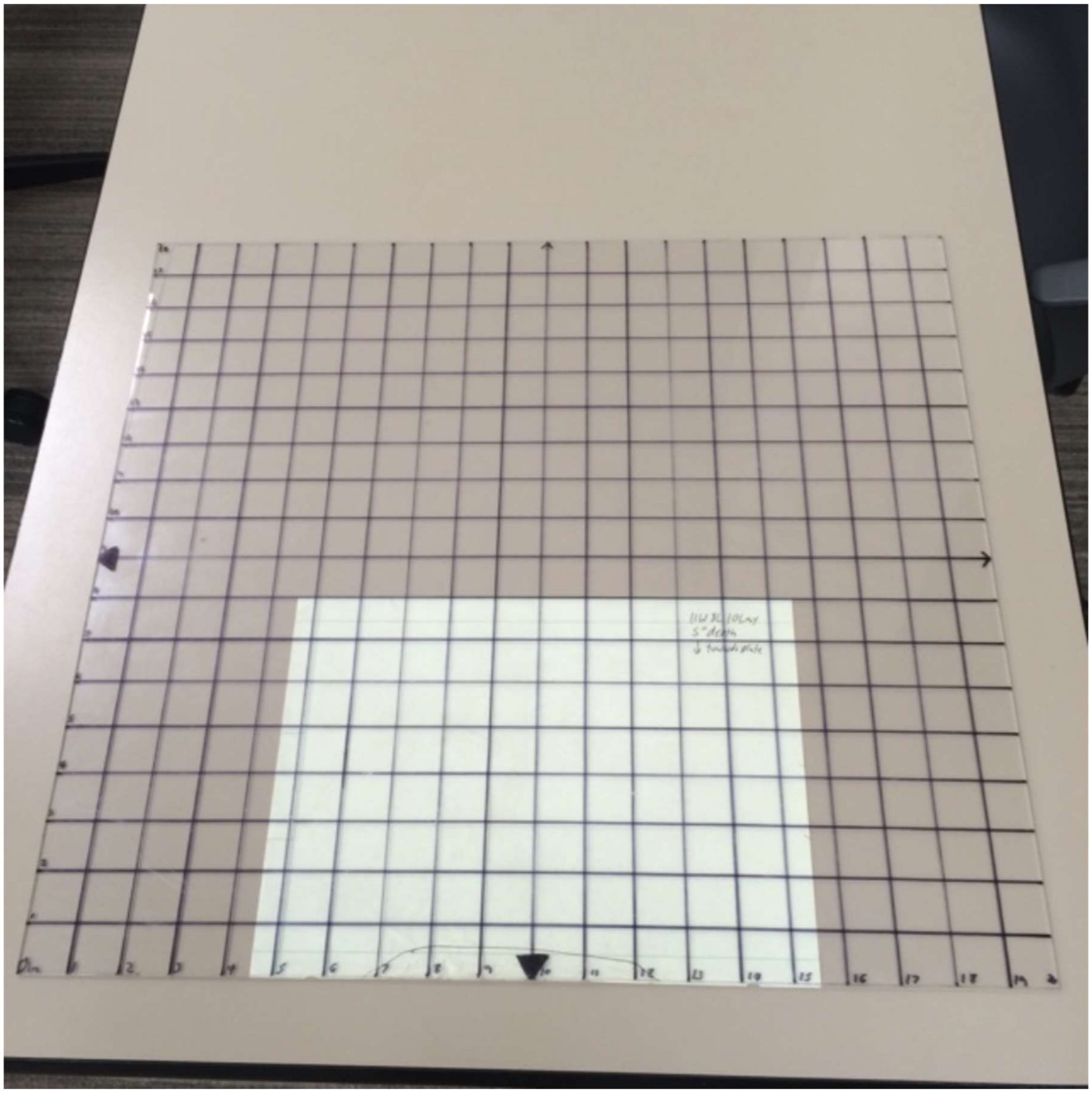

Figure 170: Test 11W8L10Lay 5" Depth

A.5 Photographs of Test 11W8L10Lay2

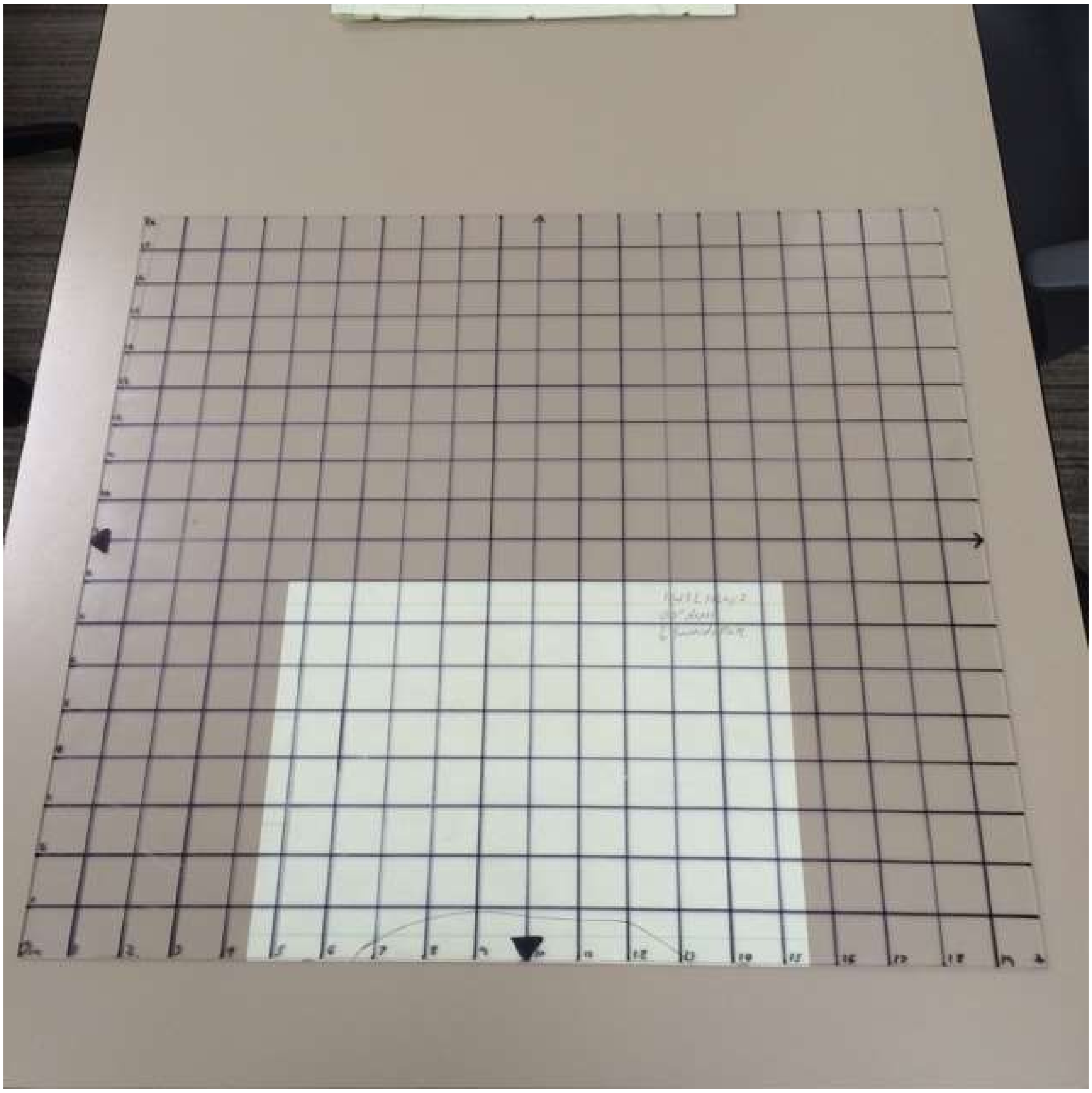

Figure 171: Test 11W8L10Lay2 0.5" Depth

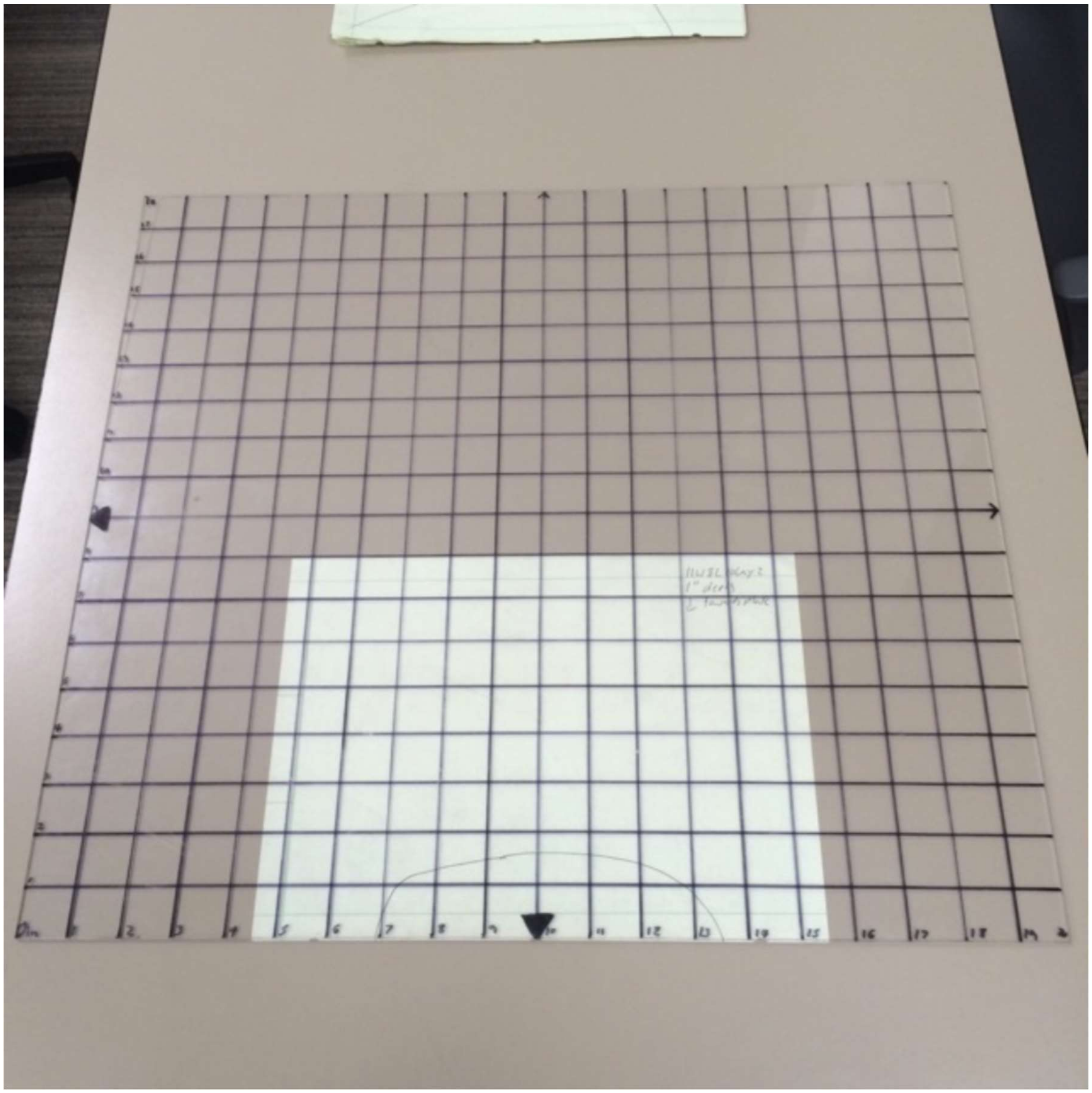

Figure 172: Test 11W8L10Lay2 1" Depth

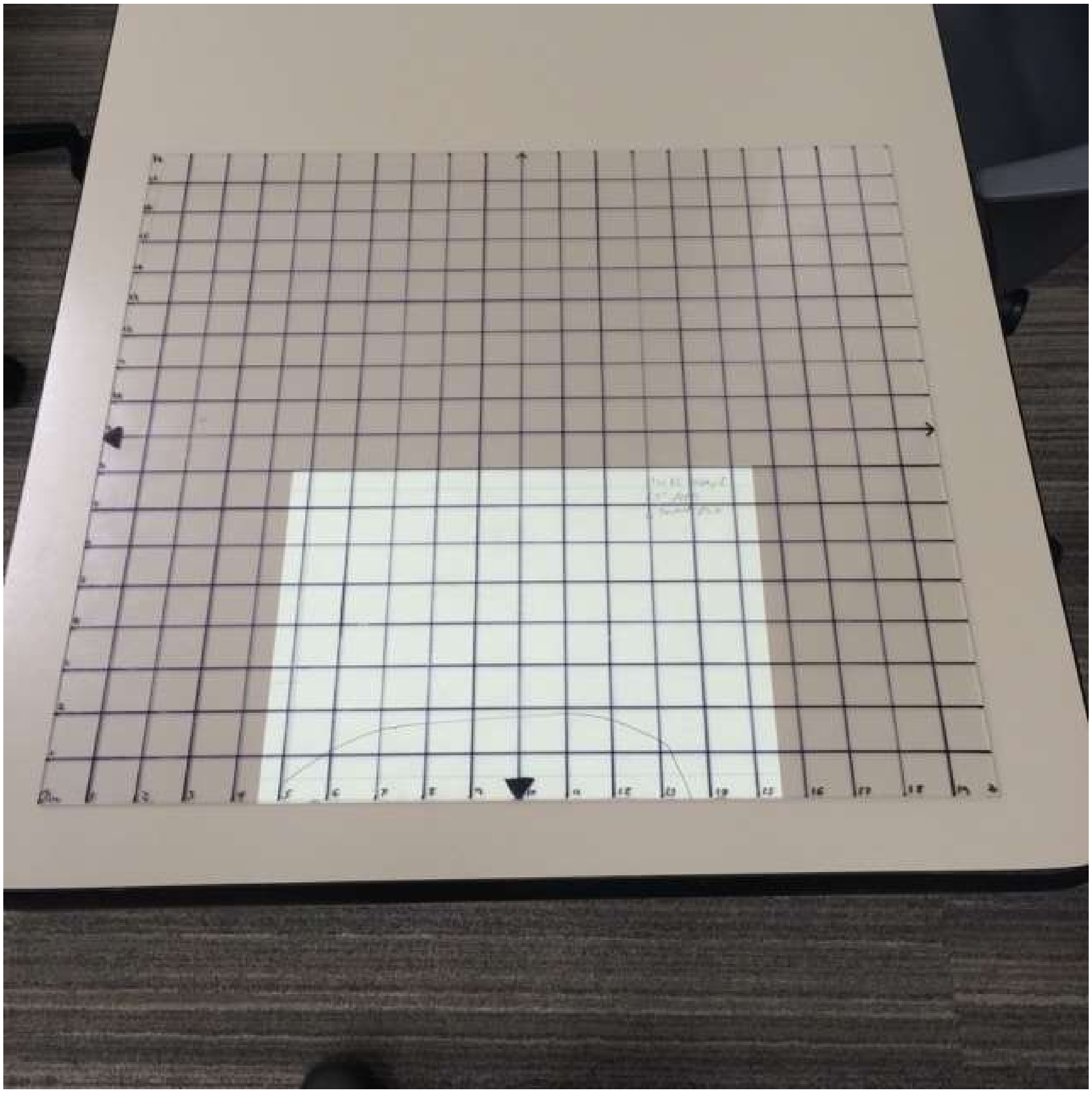

Figure 173: Test 11W8L10Lay2 1.5" Depth

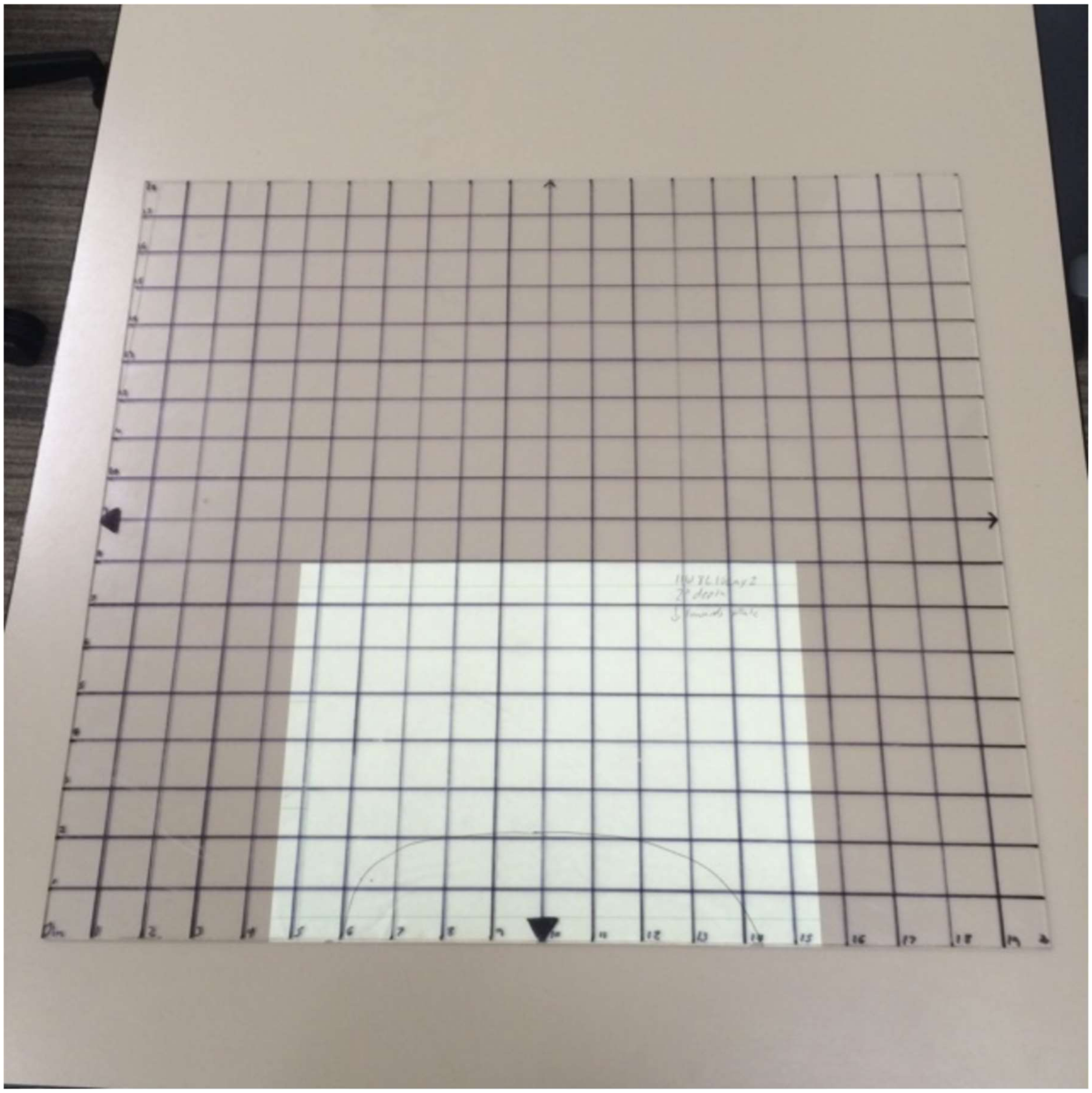

Figure 174: Test 11W8L10Lay2 2" Depth

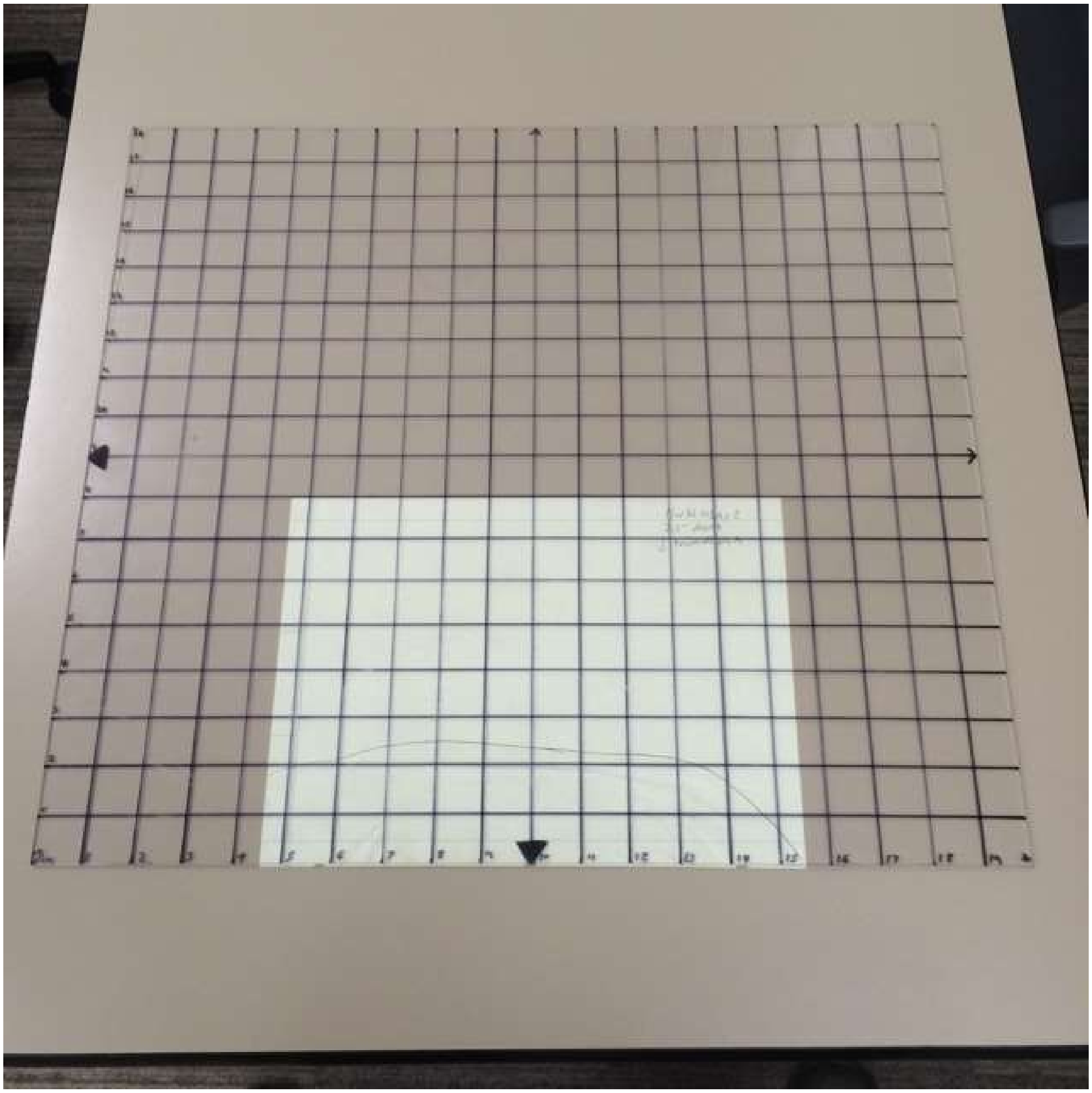

Figure 175: Test 11W8L10Lay2 2.5" Depth

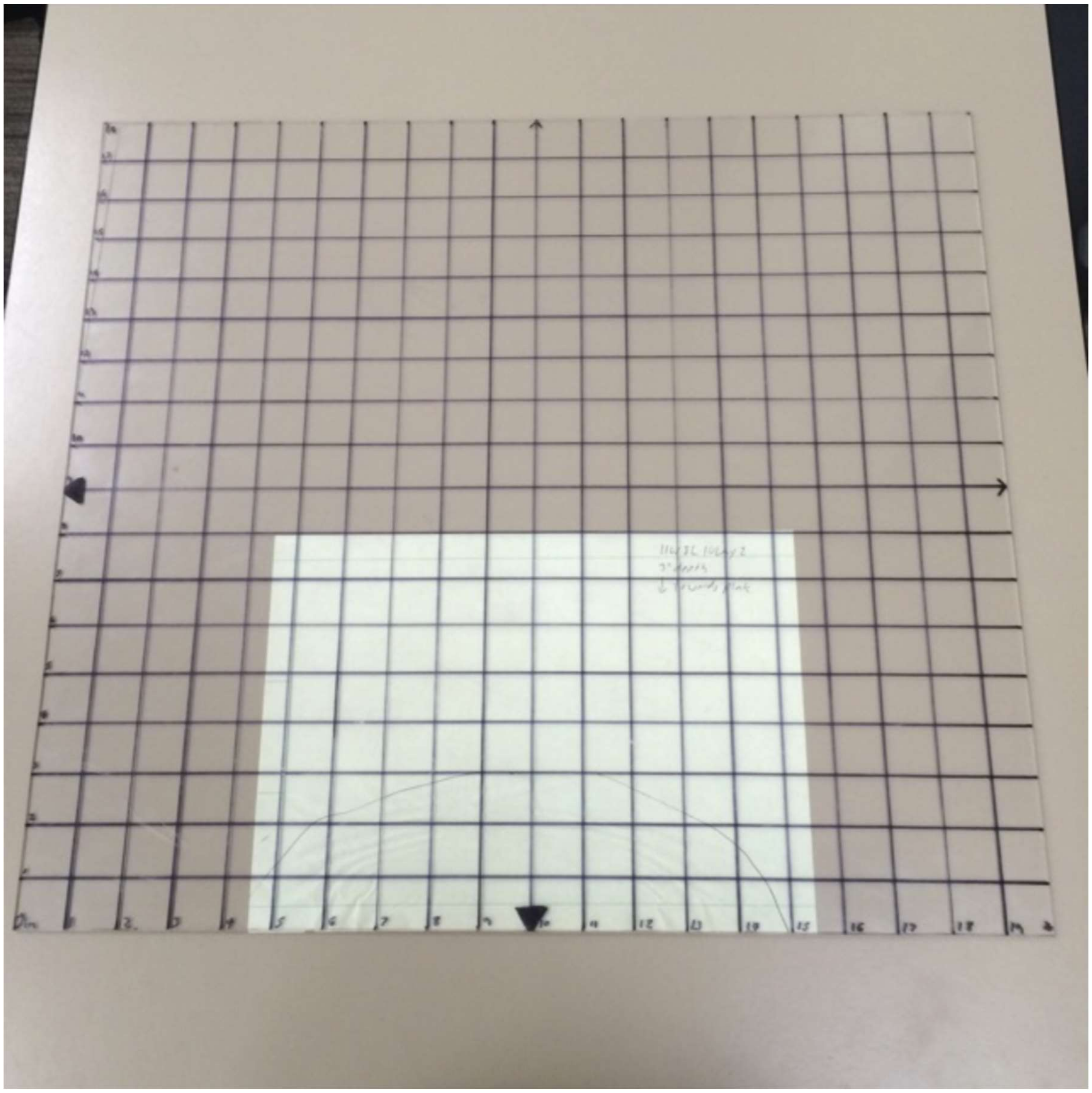

Figure 176: Test 11W8L10Lay2 3” Depth

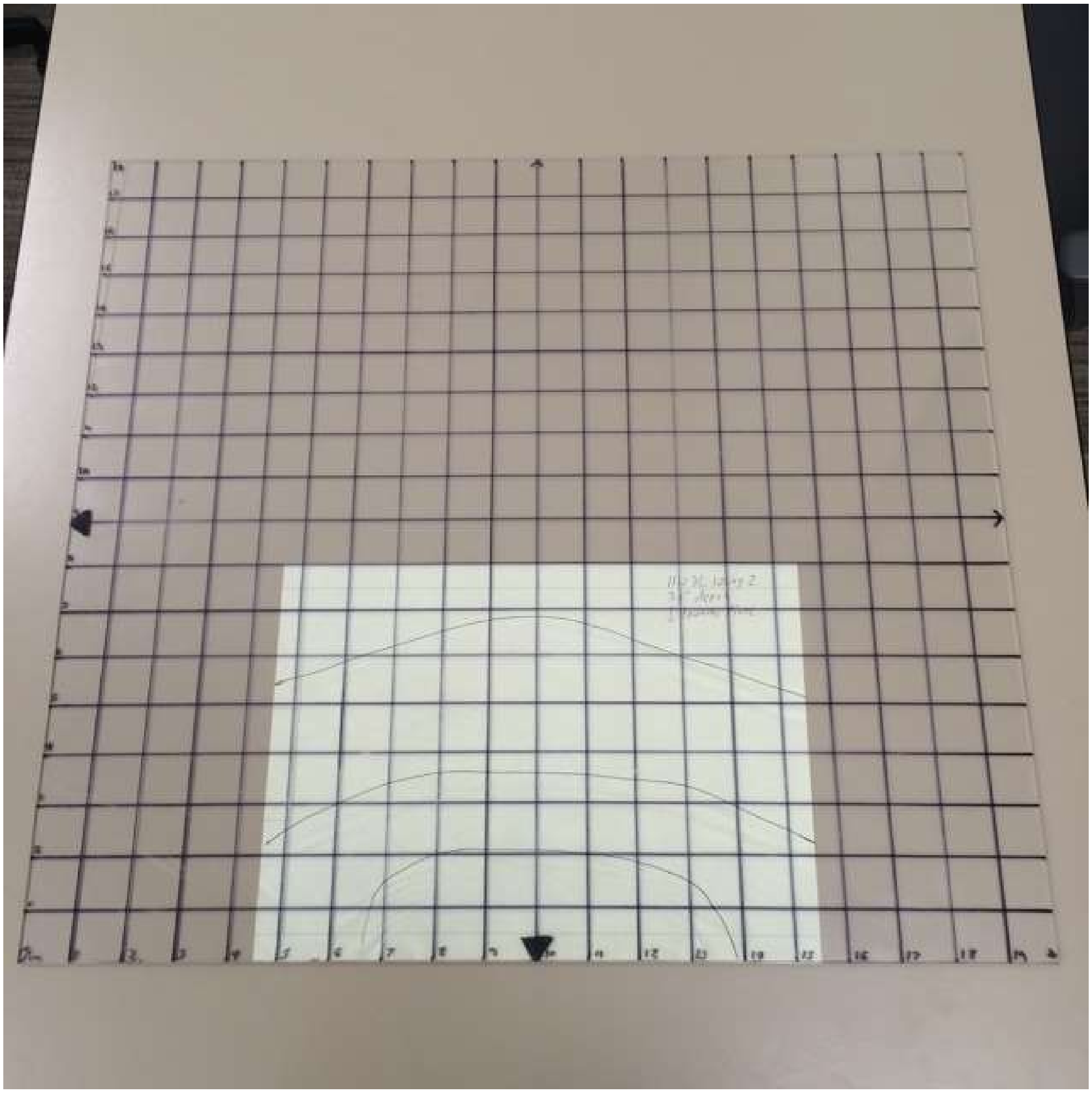

Figure 177: Test 11W8L10Lay2 3.5” Depth

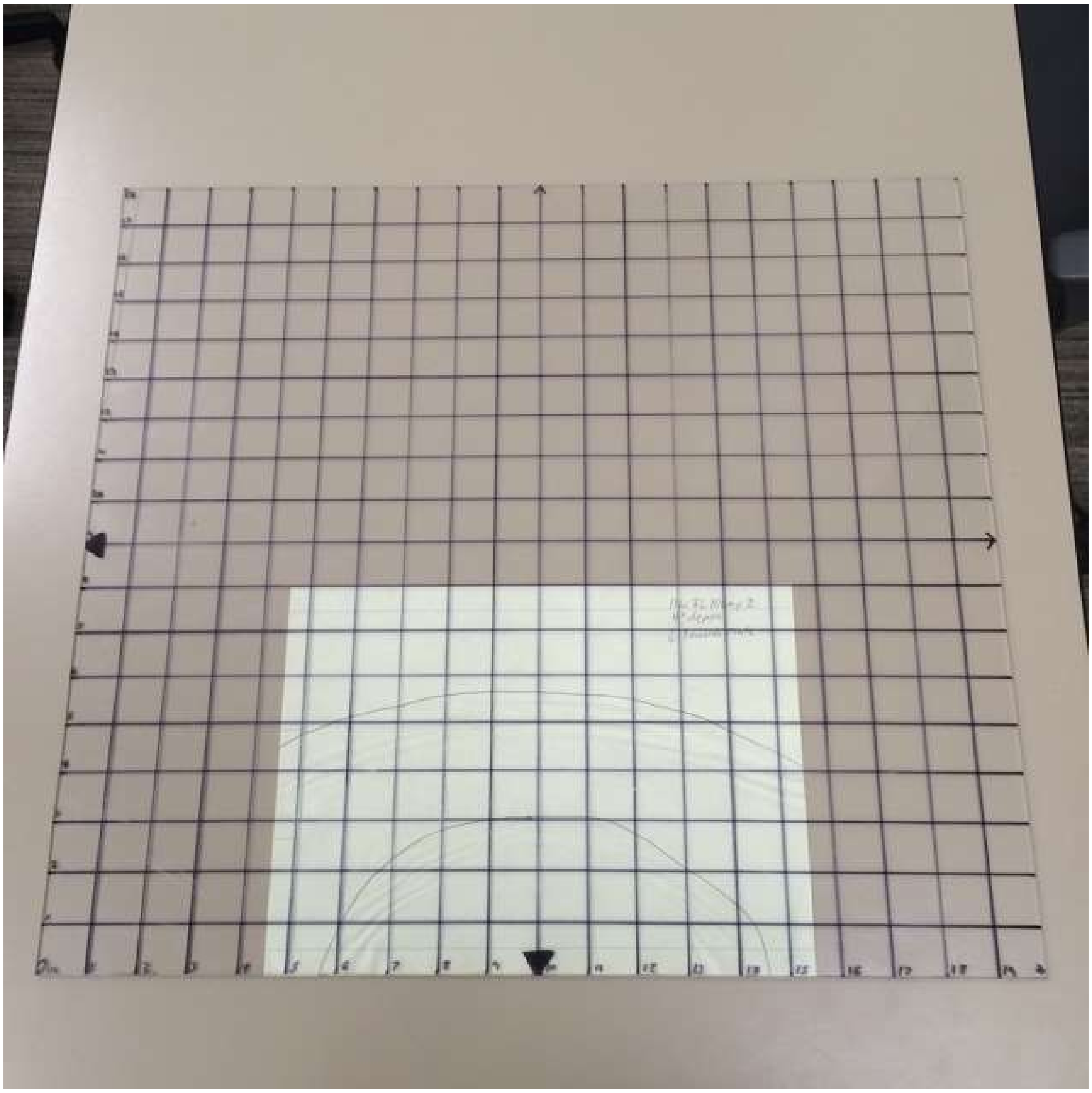

Figure 178: Test 11W8L10Lay2 4” Depth

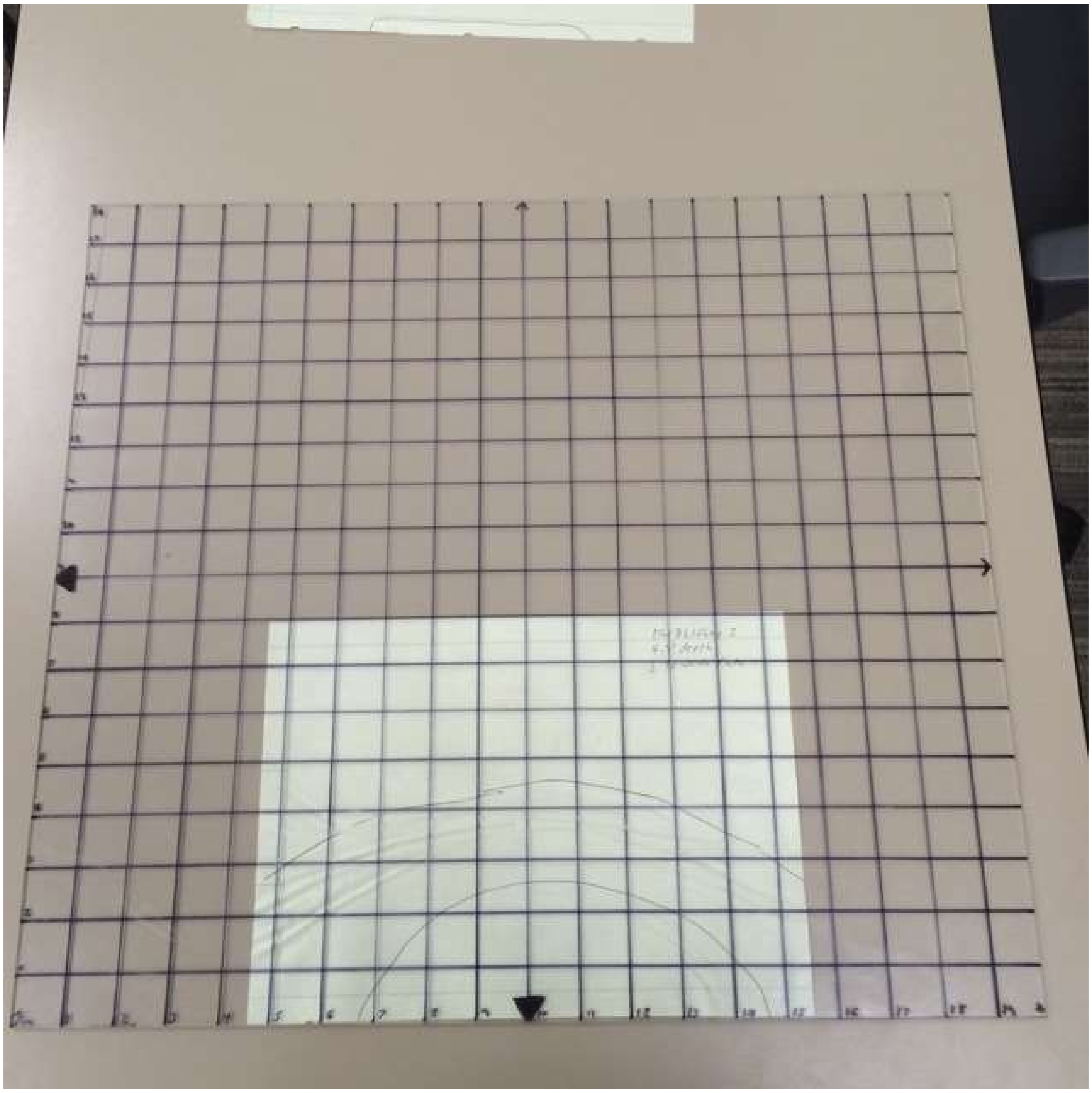

Figure 179: Test 11W8L10Lay2 4.5" Depth

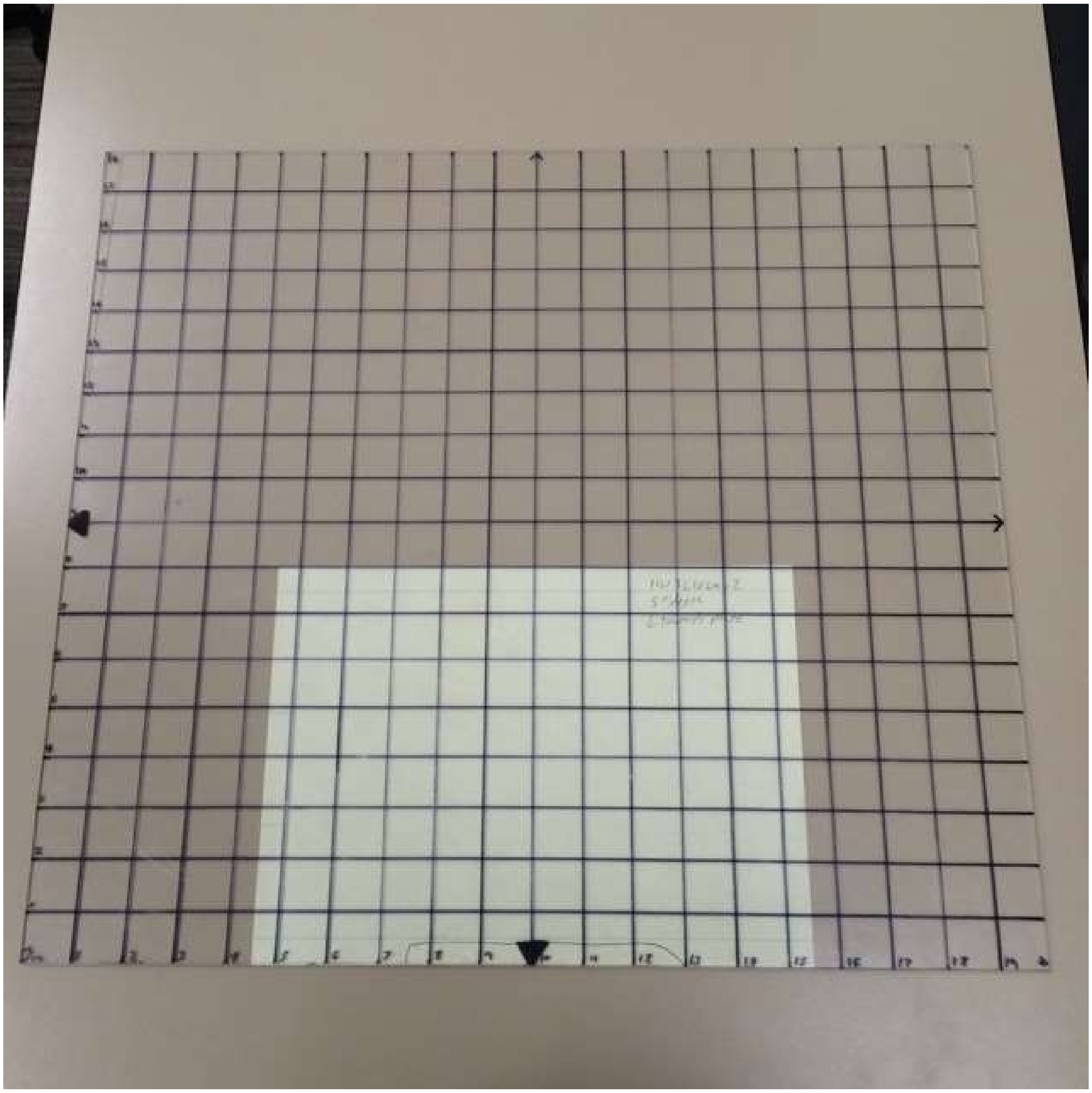

Figure 180: Test 11W8L10Lay2 5" Depth

A.7 Photographs of Test PW8L5Lay

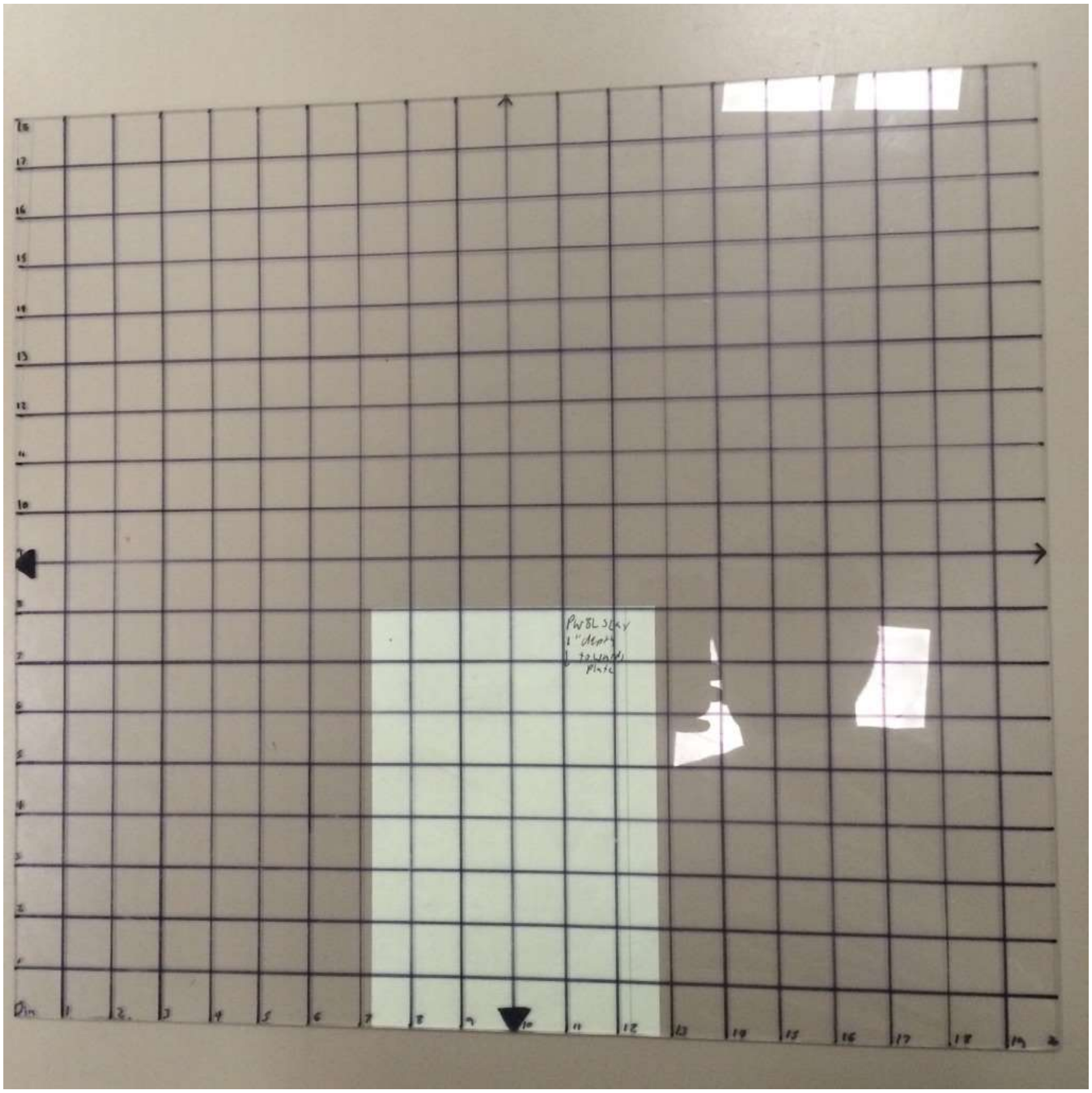

Figure 181: Test PW8L5Lay 1" Depth

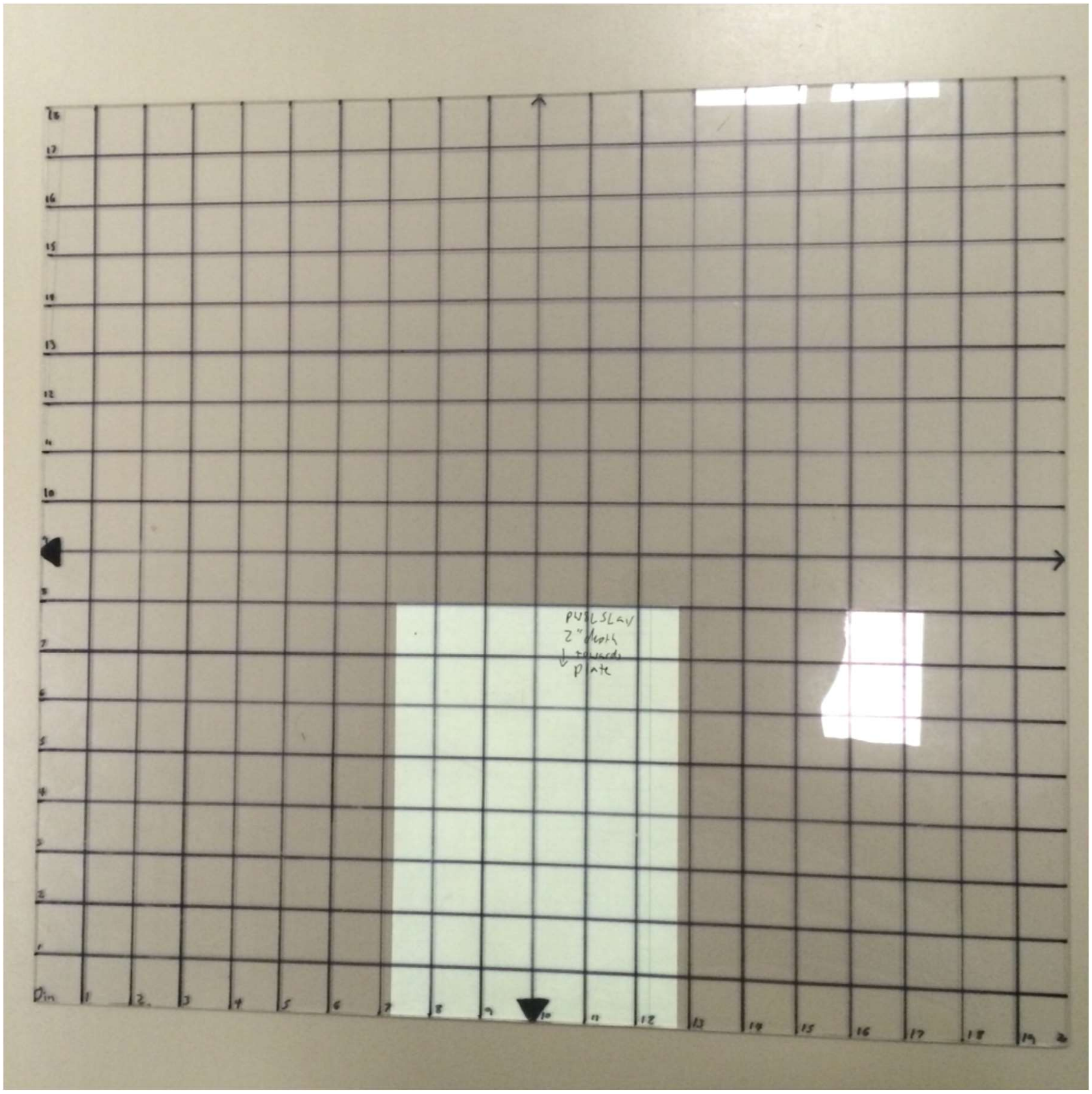

Figure 182: Test PW8L5Lay 2” Depth

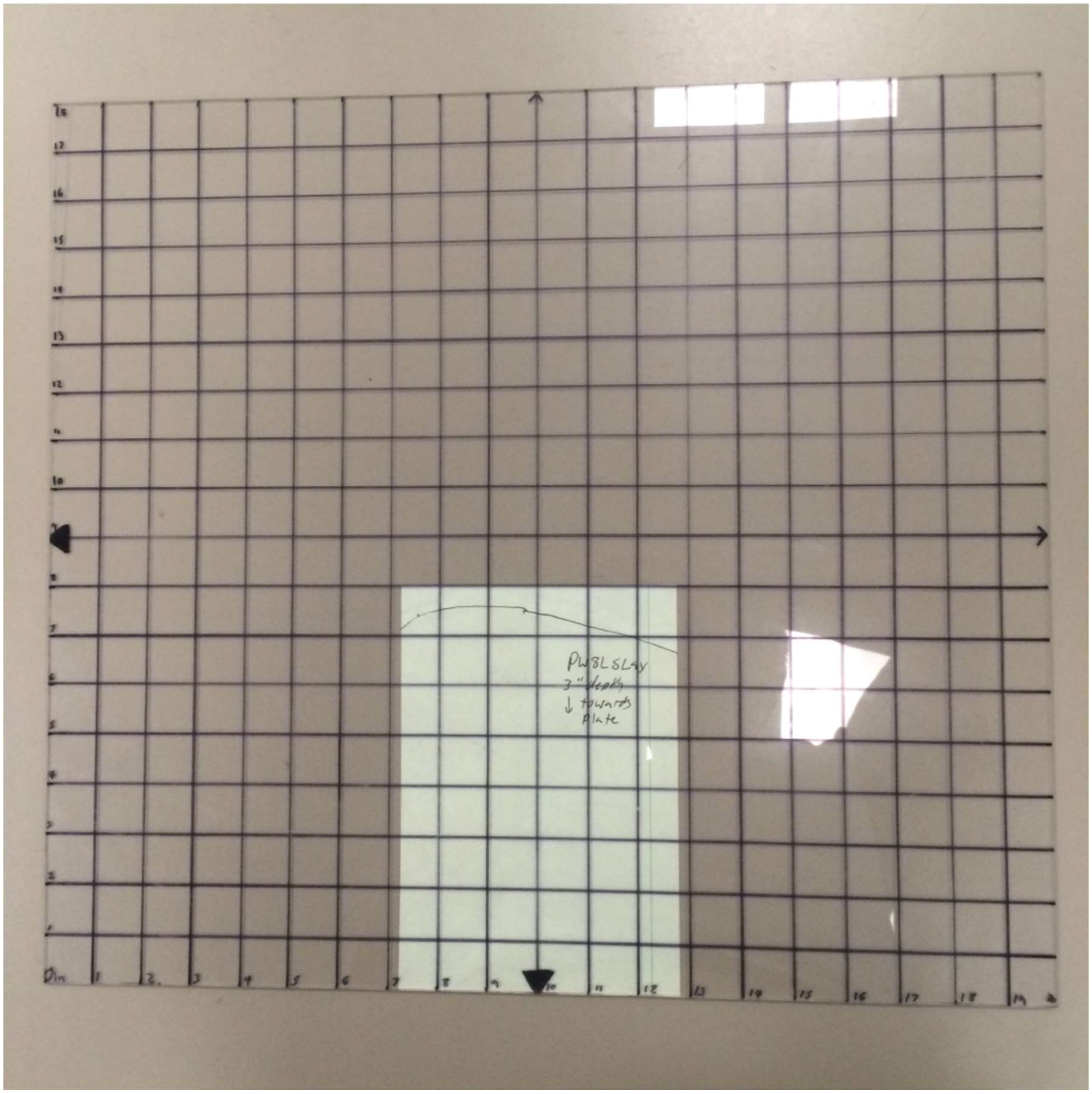

Figure 183: Test PW8L5Lay 3" Depth

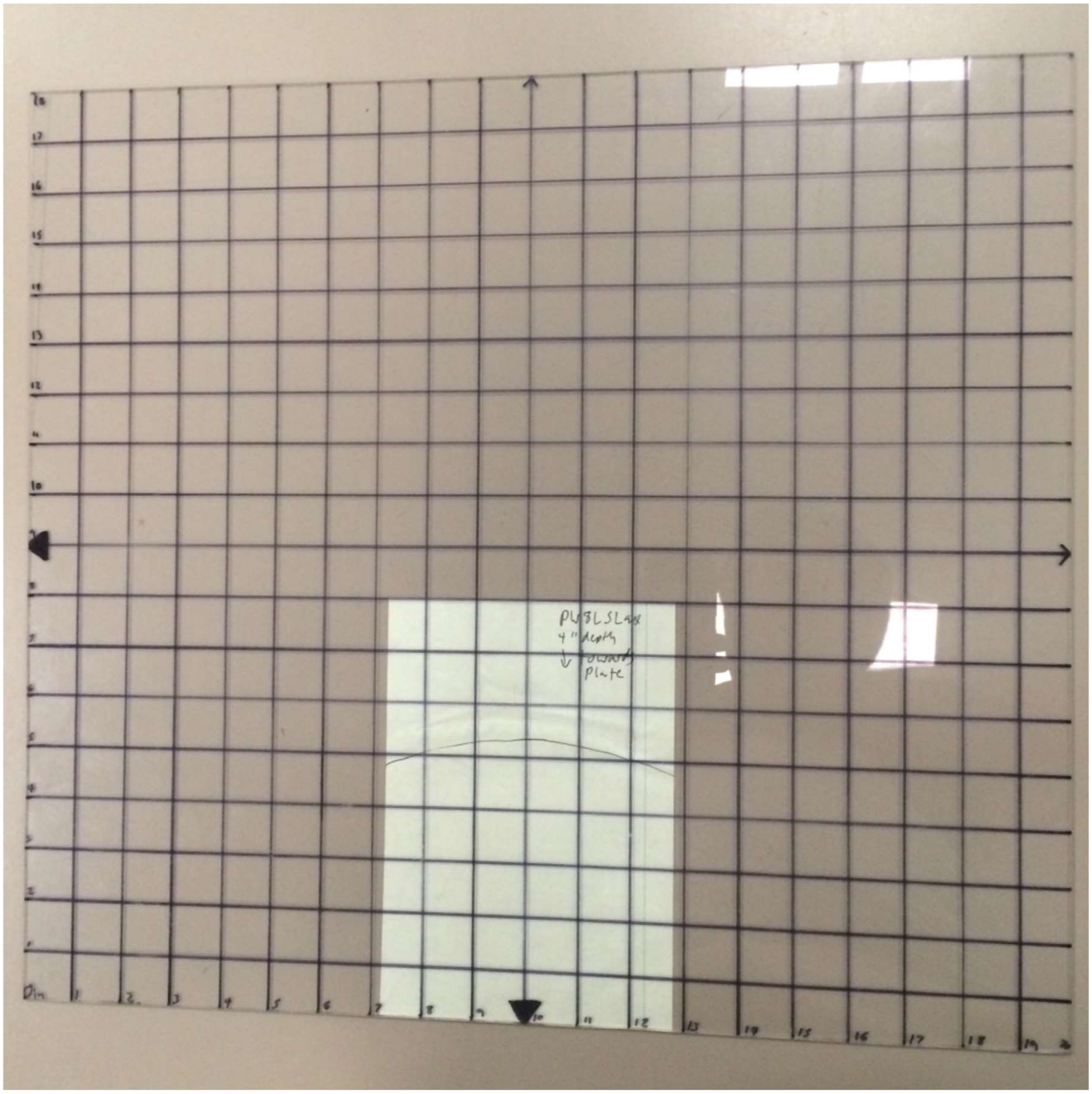

Figure 184: Test PW8L5Lay 4" Depth

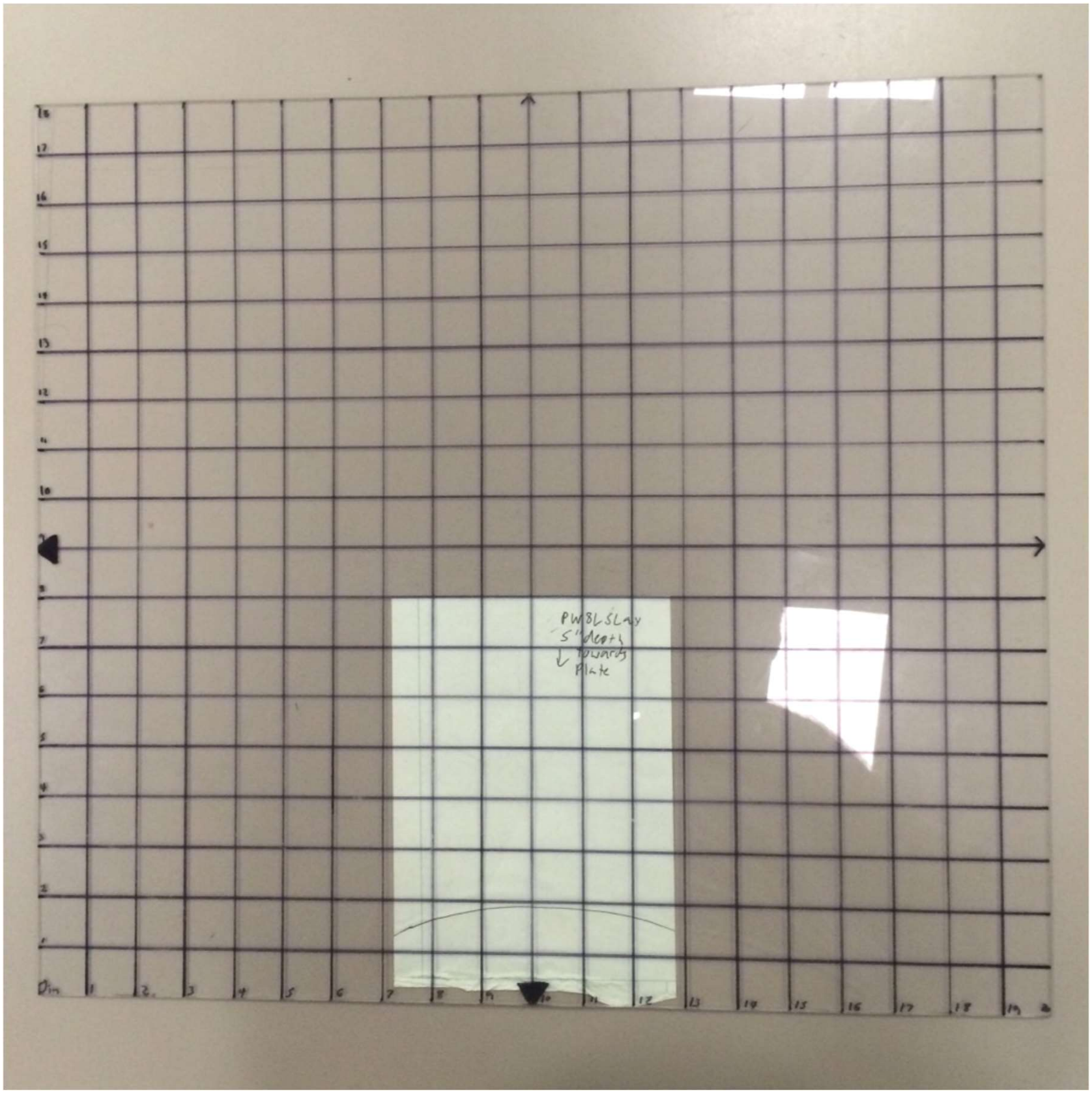

Figure 185: Test PW8L5Lay 5” Depth

A.8 Photographs of Test PW8L5Lay2

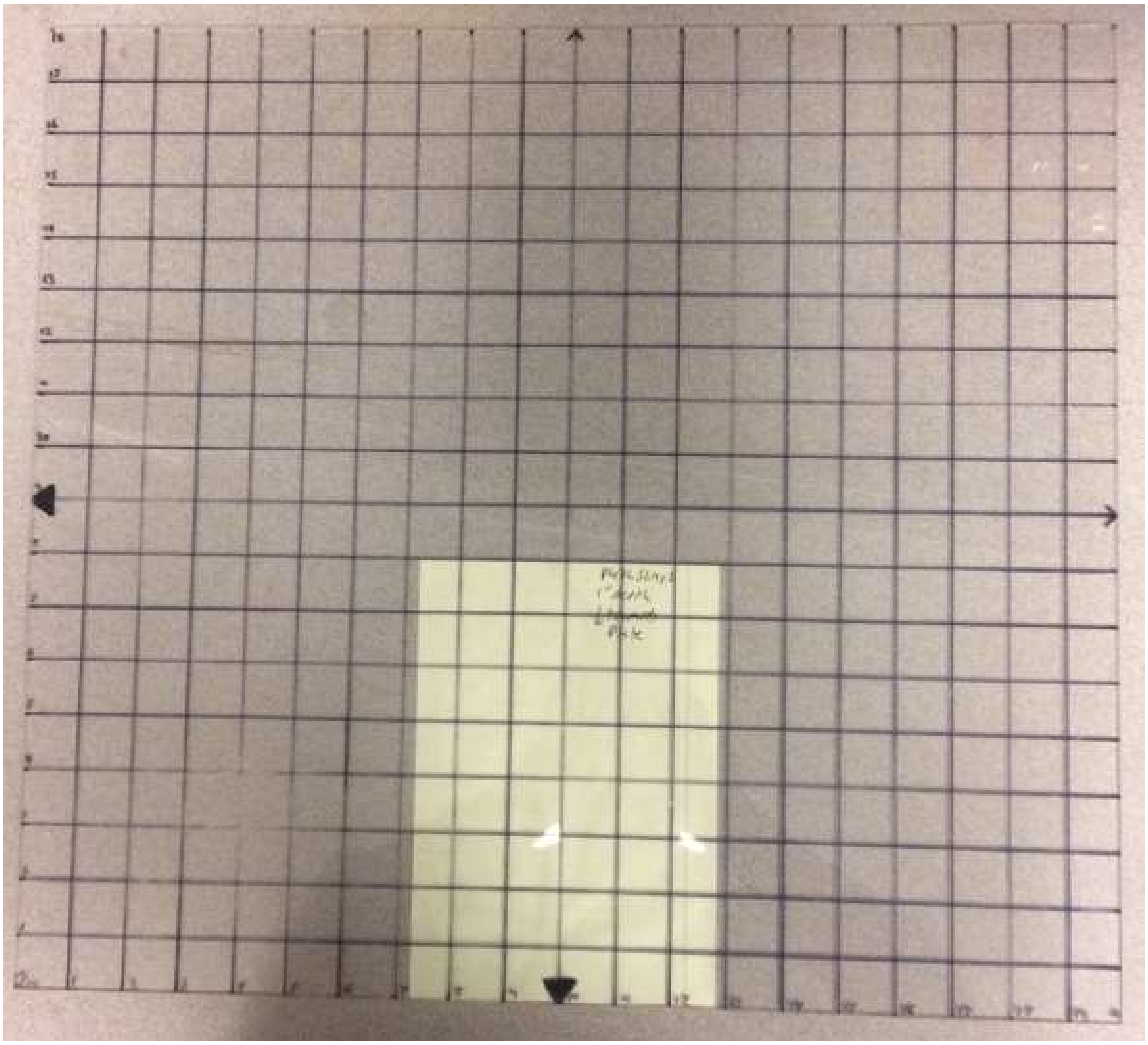

Figure 186: Test PW8L5Lay2 1" Depth

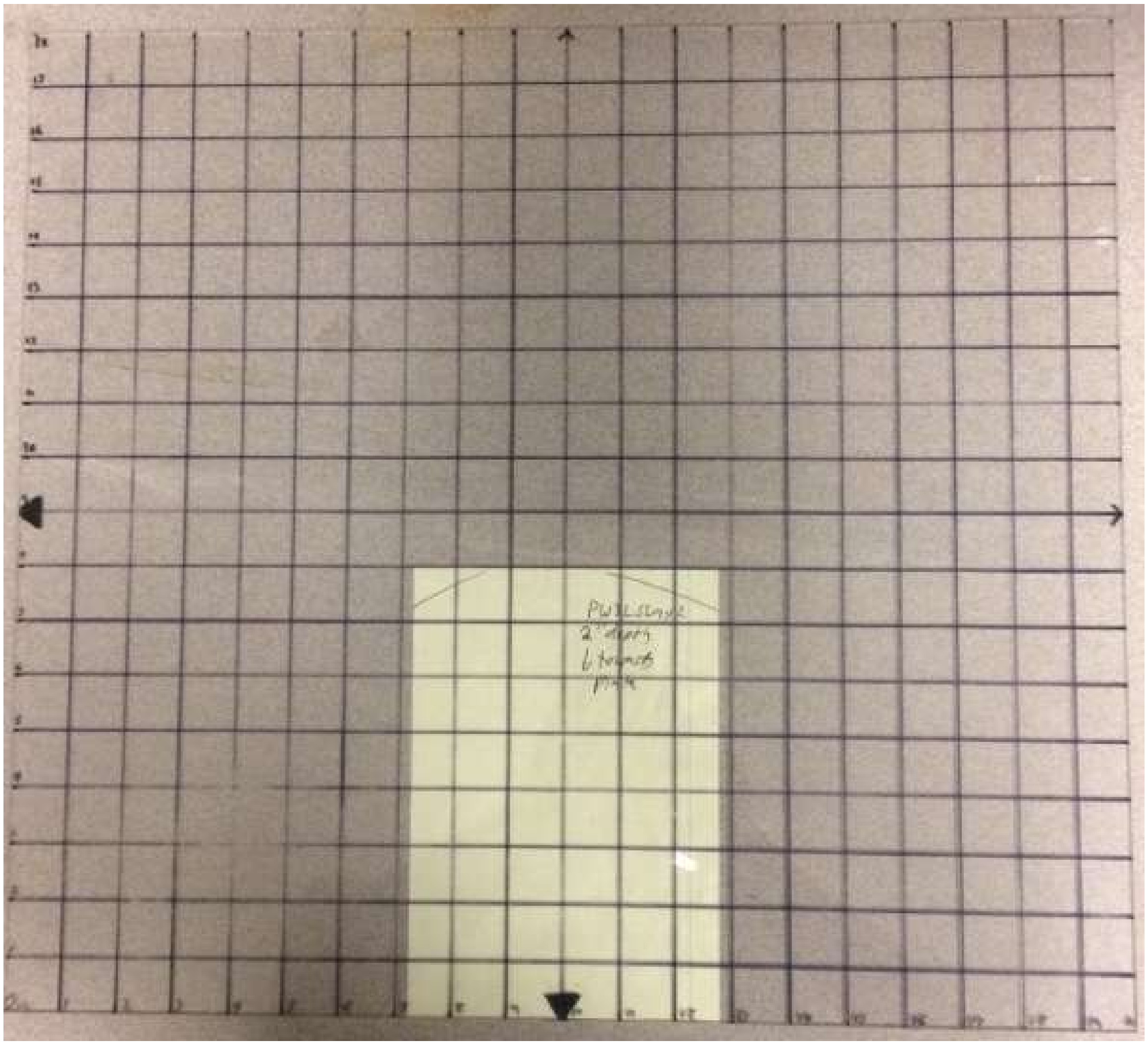

Figure 187: Test PW8L5Lay2 2” Depth

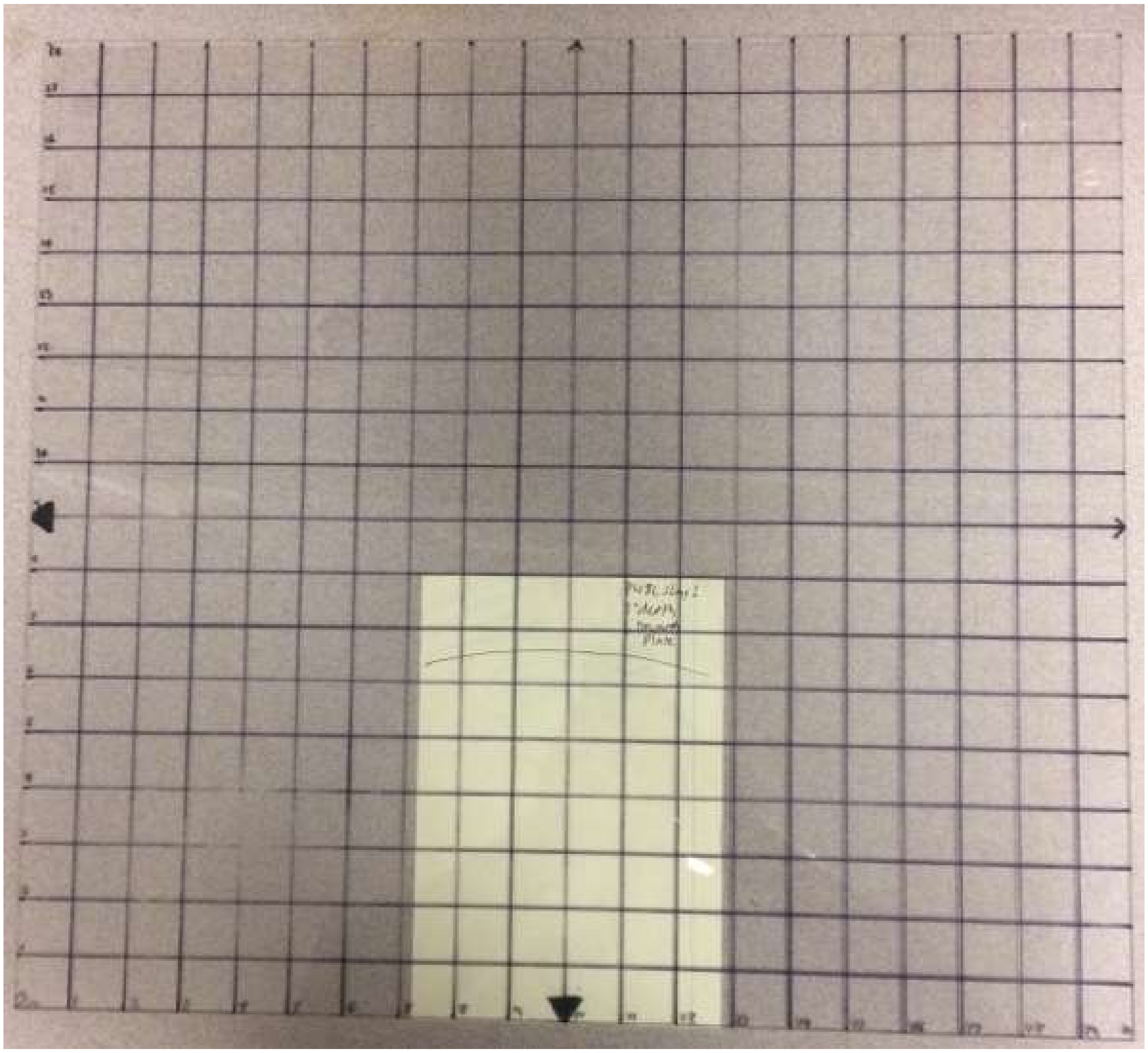

Figure 188: Test PW8L5Lay2 3" Depth

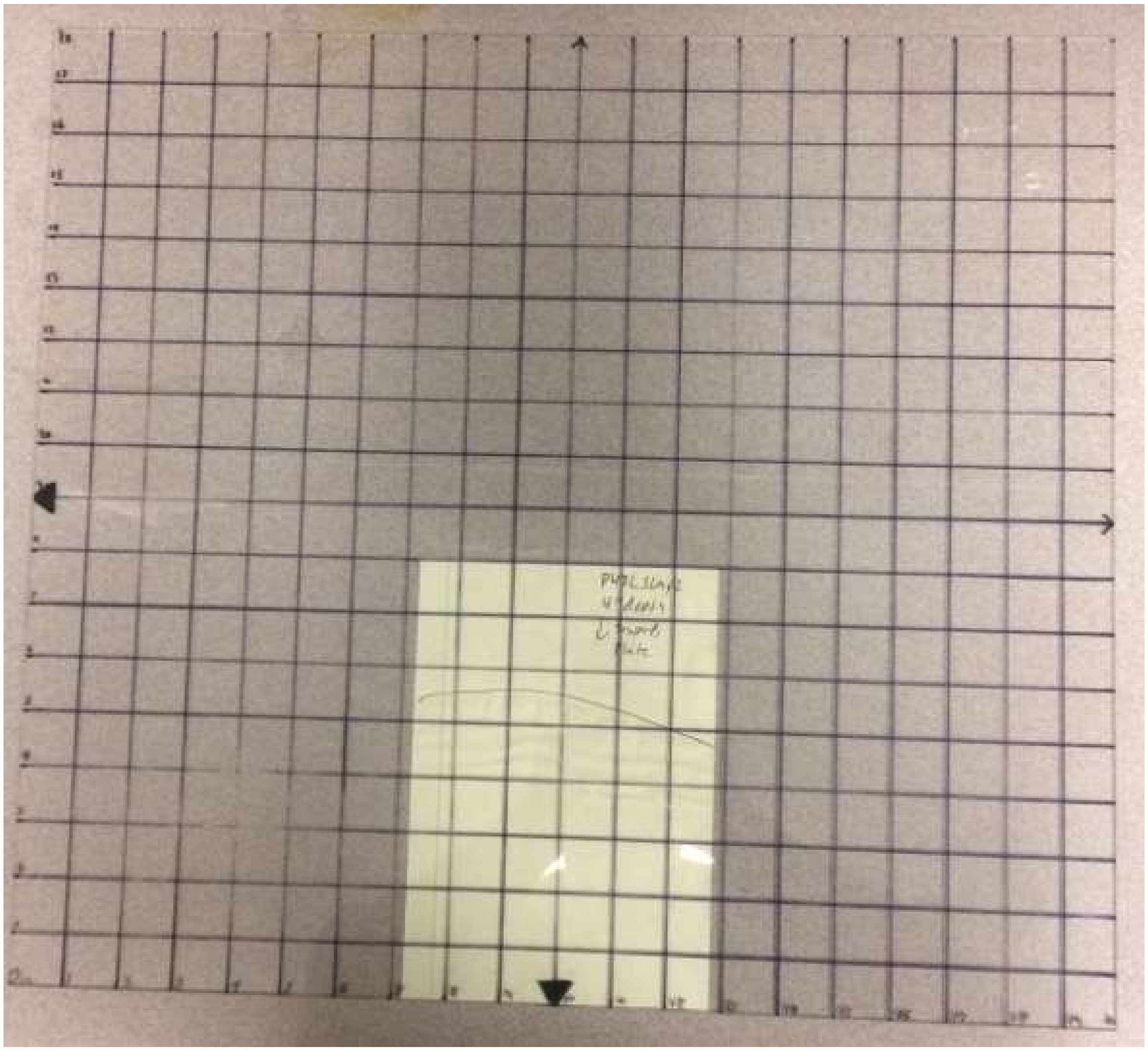

Figure 189: Test PW8L5Lay2 4” Depth

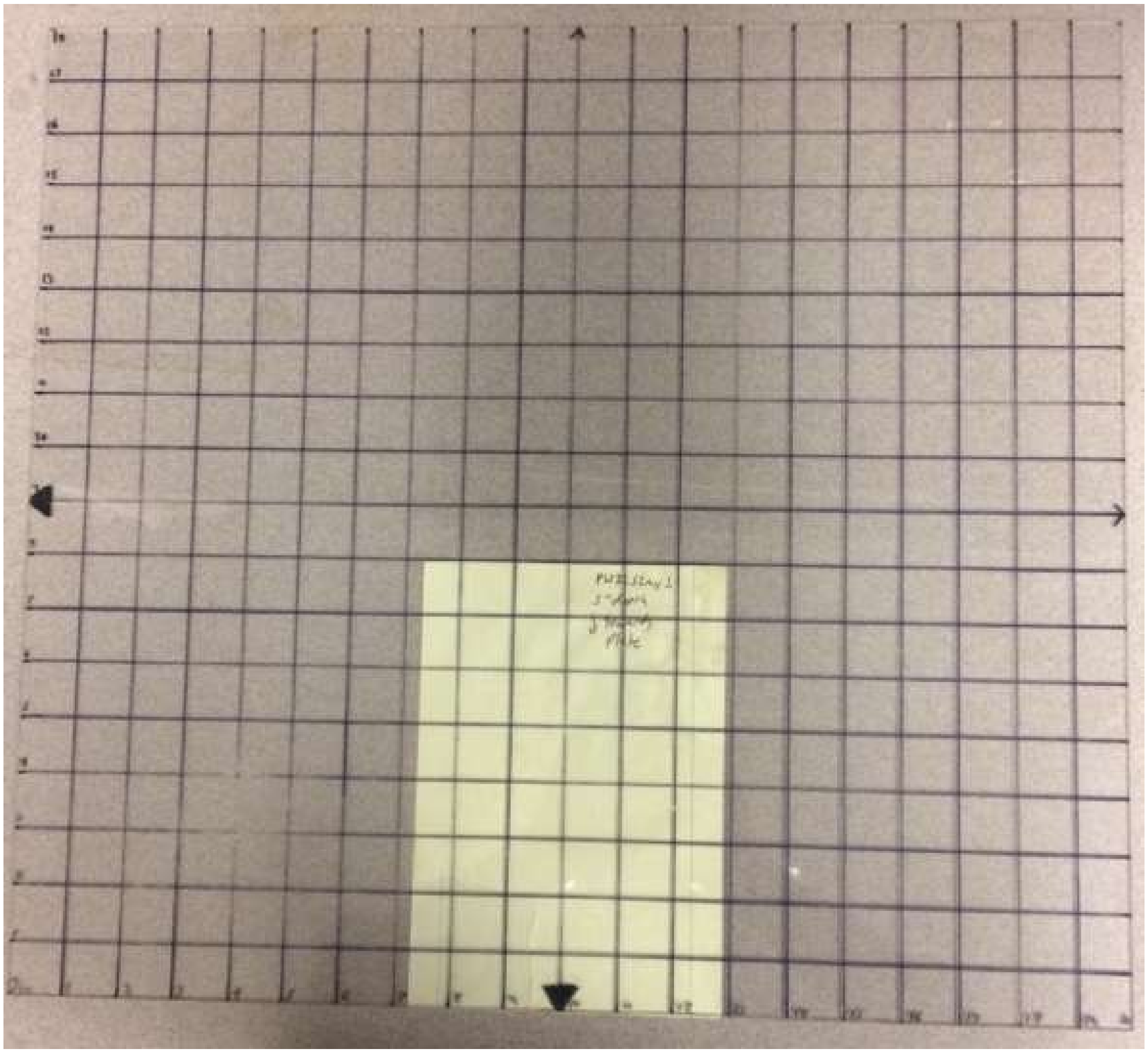

Figure 190: Test PW8L5Lay2 5" Depth

A.8 Photographs of Test PW8L10Lay

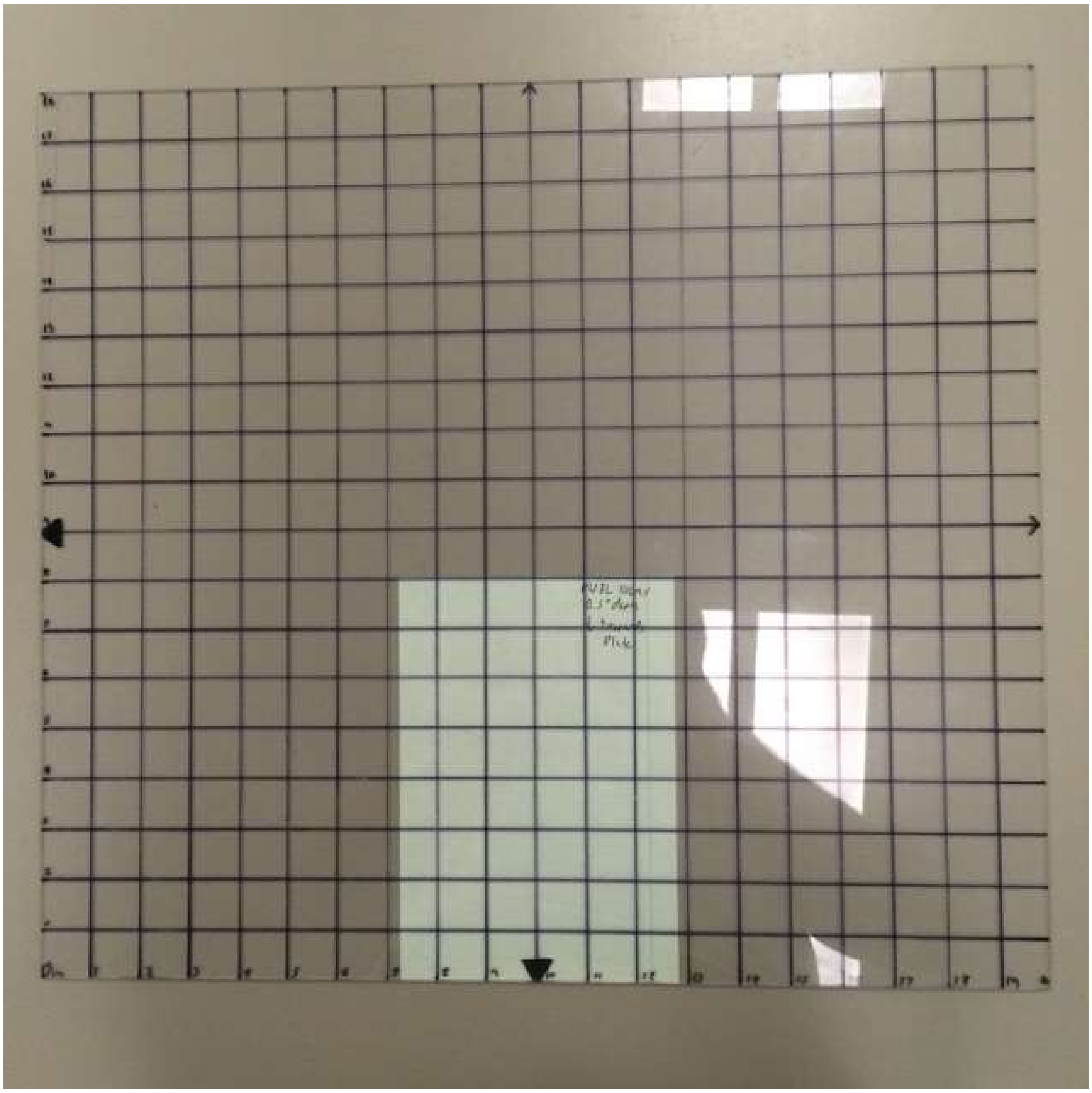

Figure 191: Test PW8L10Lay 0.5" Depth

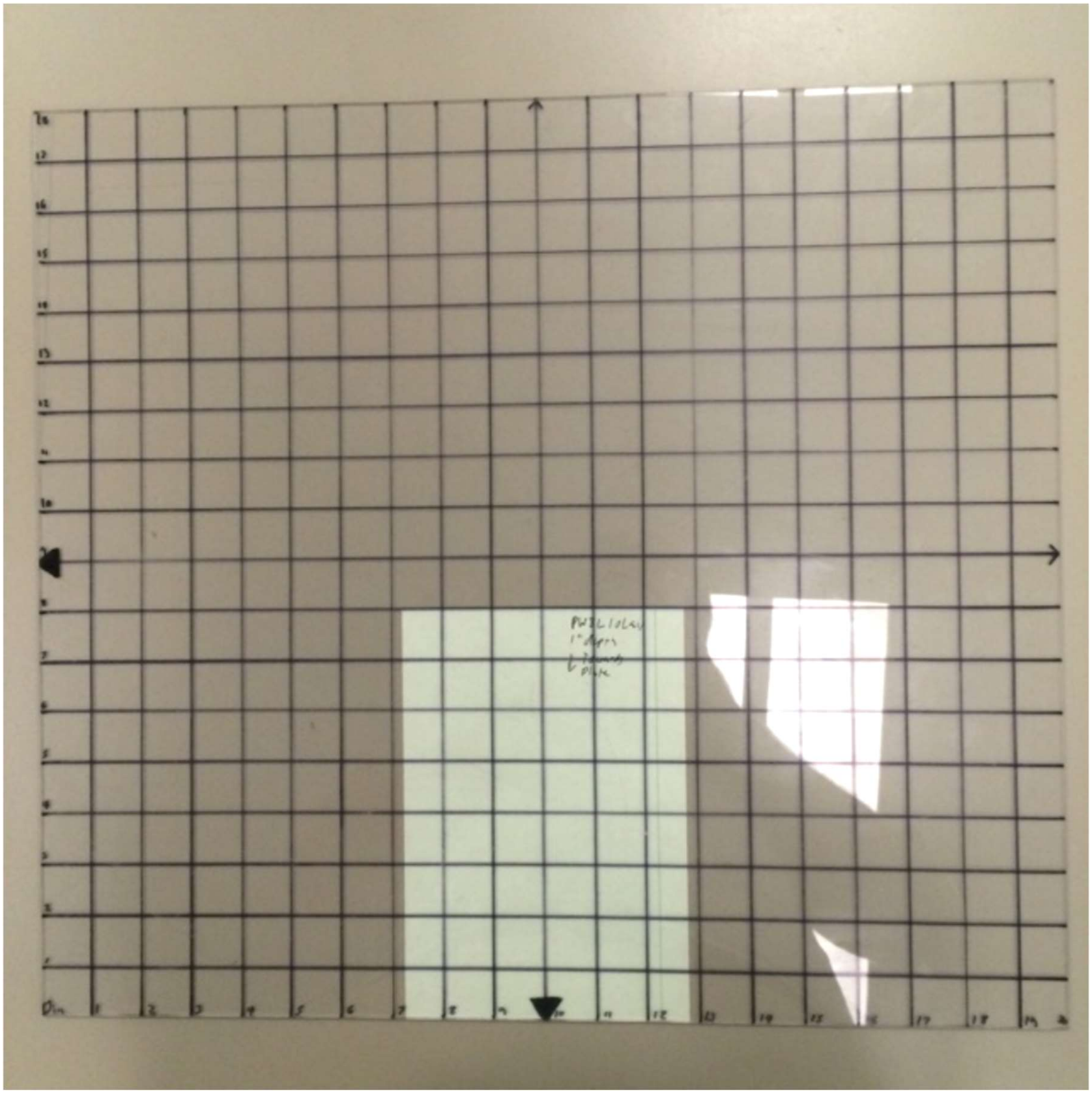

Figure 192: Test PW8L10Lay 1” Depth

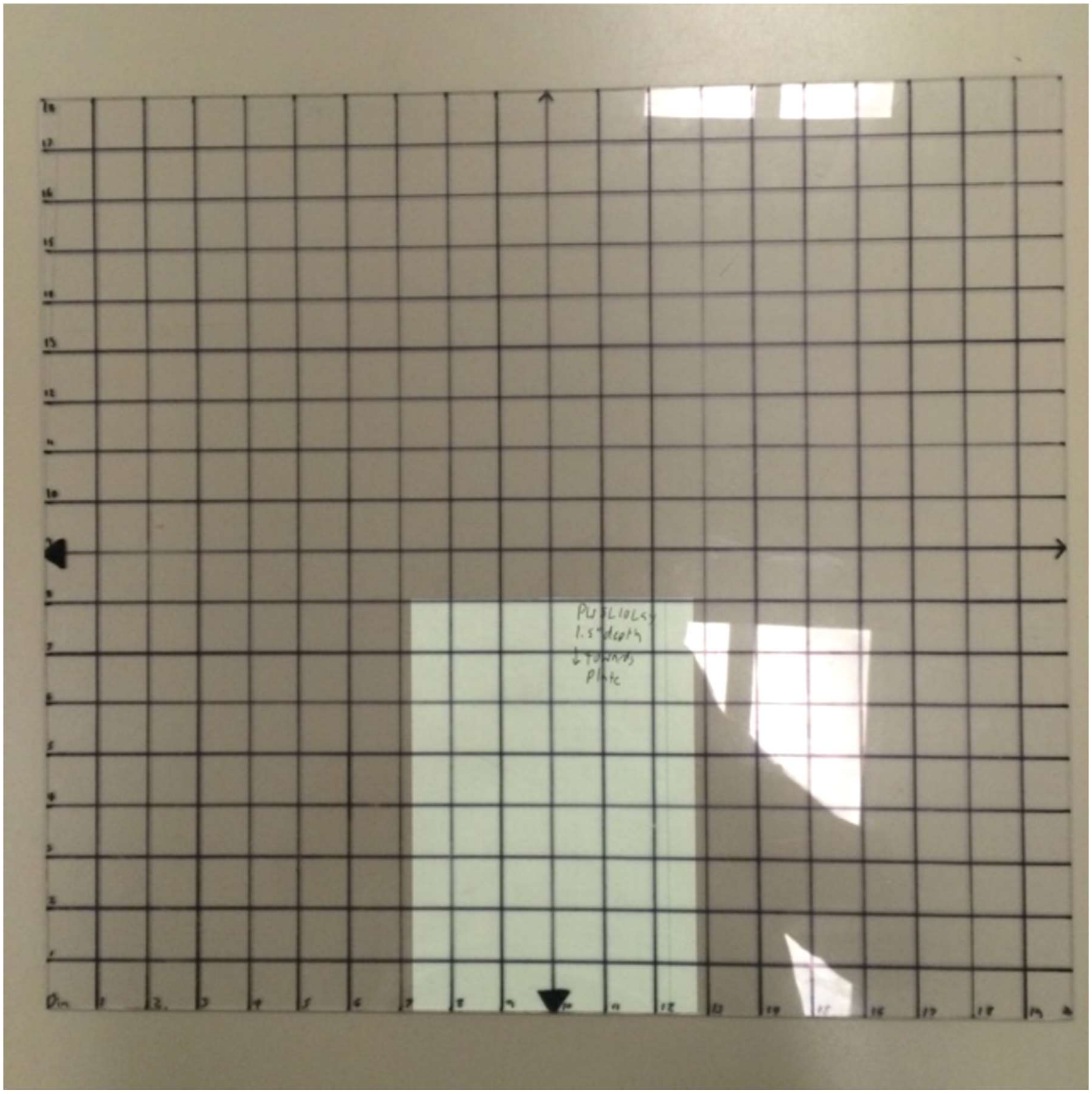

Figure 193: Test PW8L10Lay 1.5" Depth

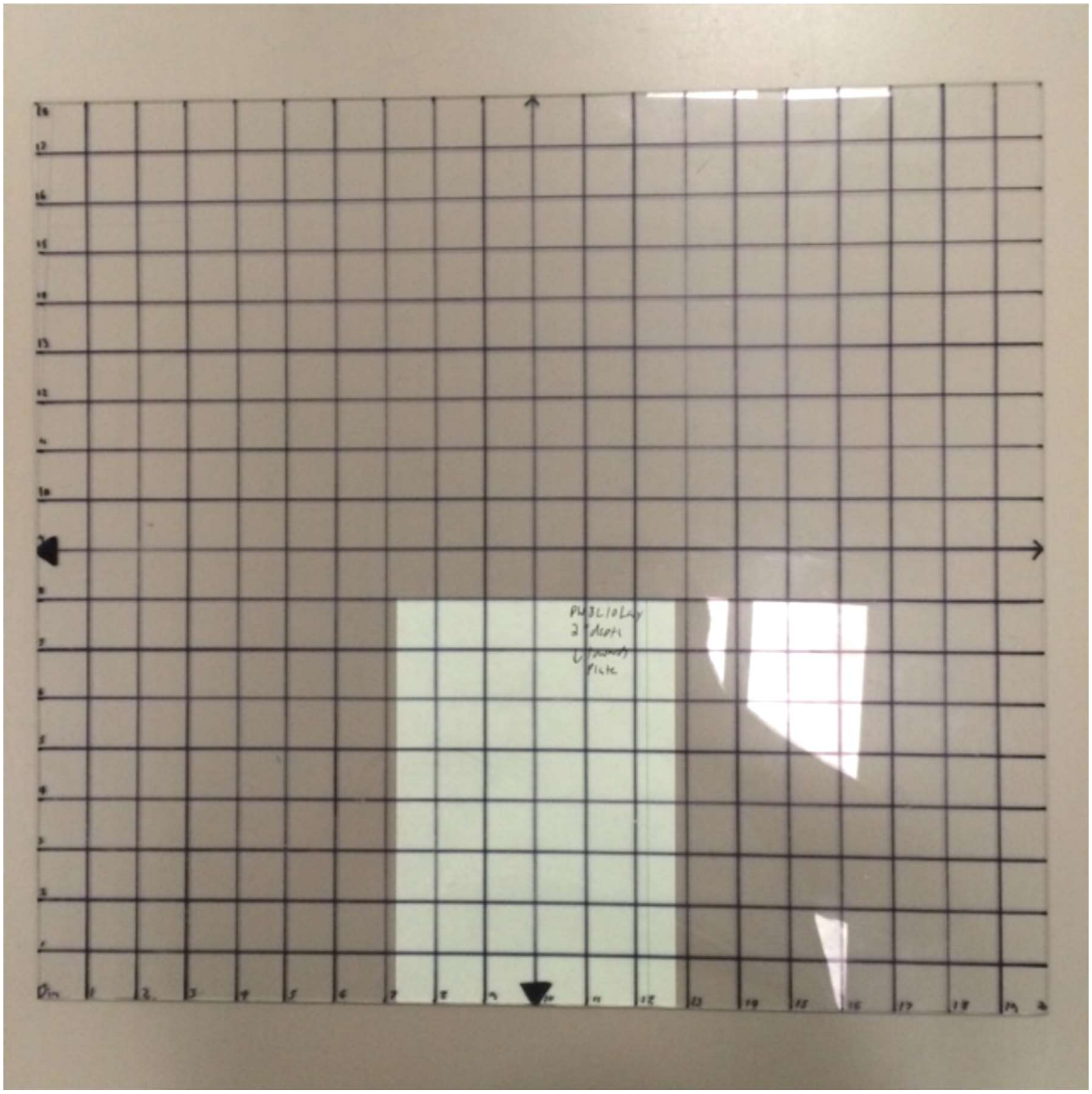

Figure 194: Test PW8L10Lay 2” Depth

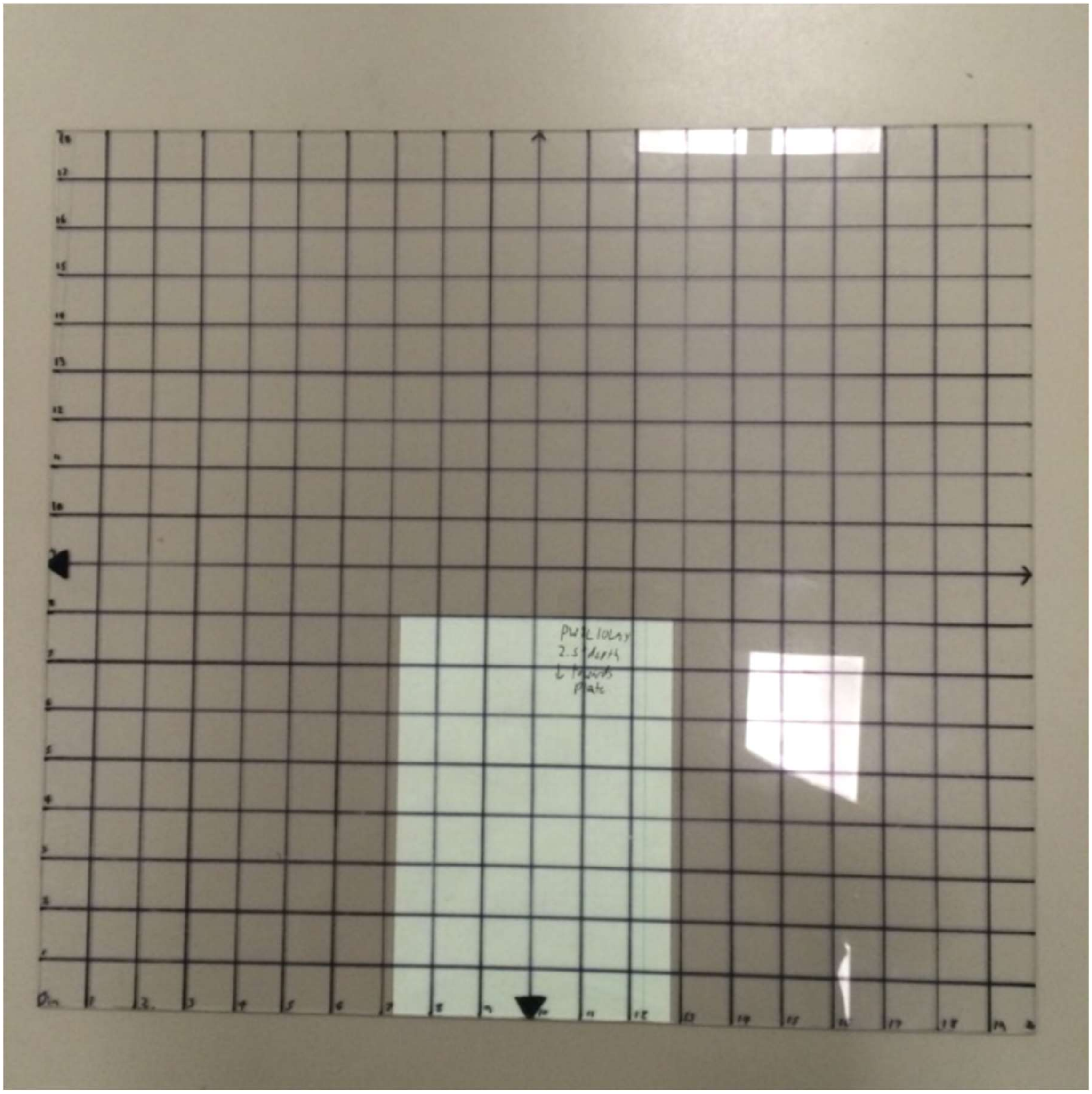

Figure 195: Test PW8L10Lay 2.5" Depth

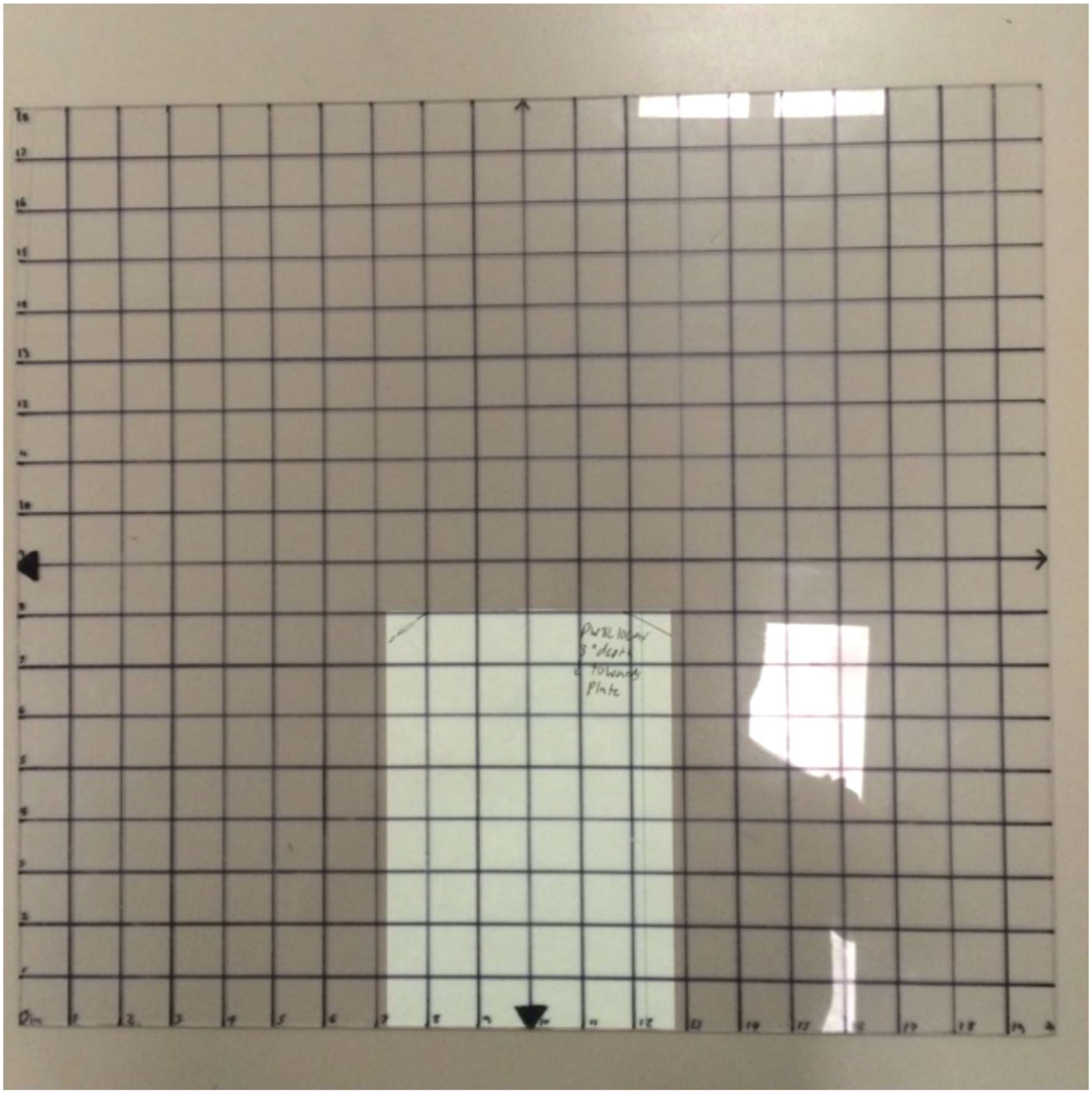

Figure 196: Test PW8L10Lay 3" Depth

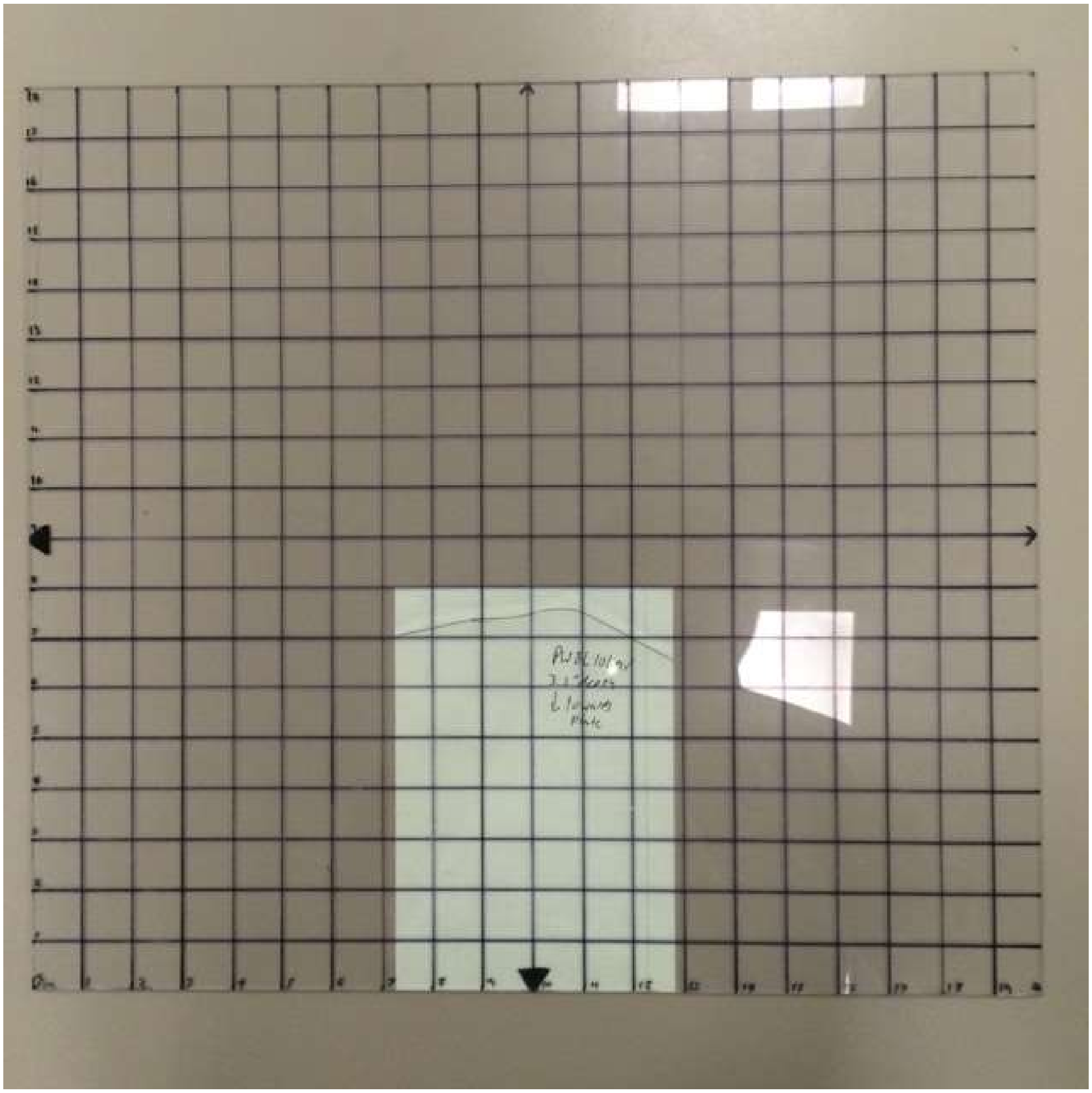

Figure 197: Test PW8L10Lay 3.5" Depth

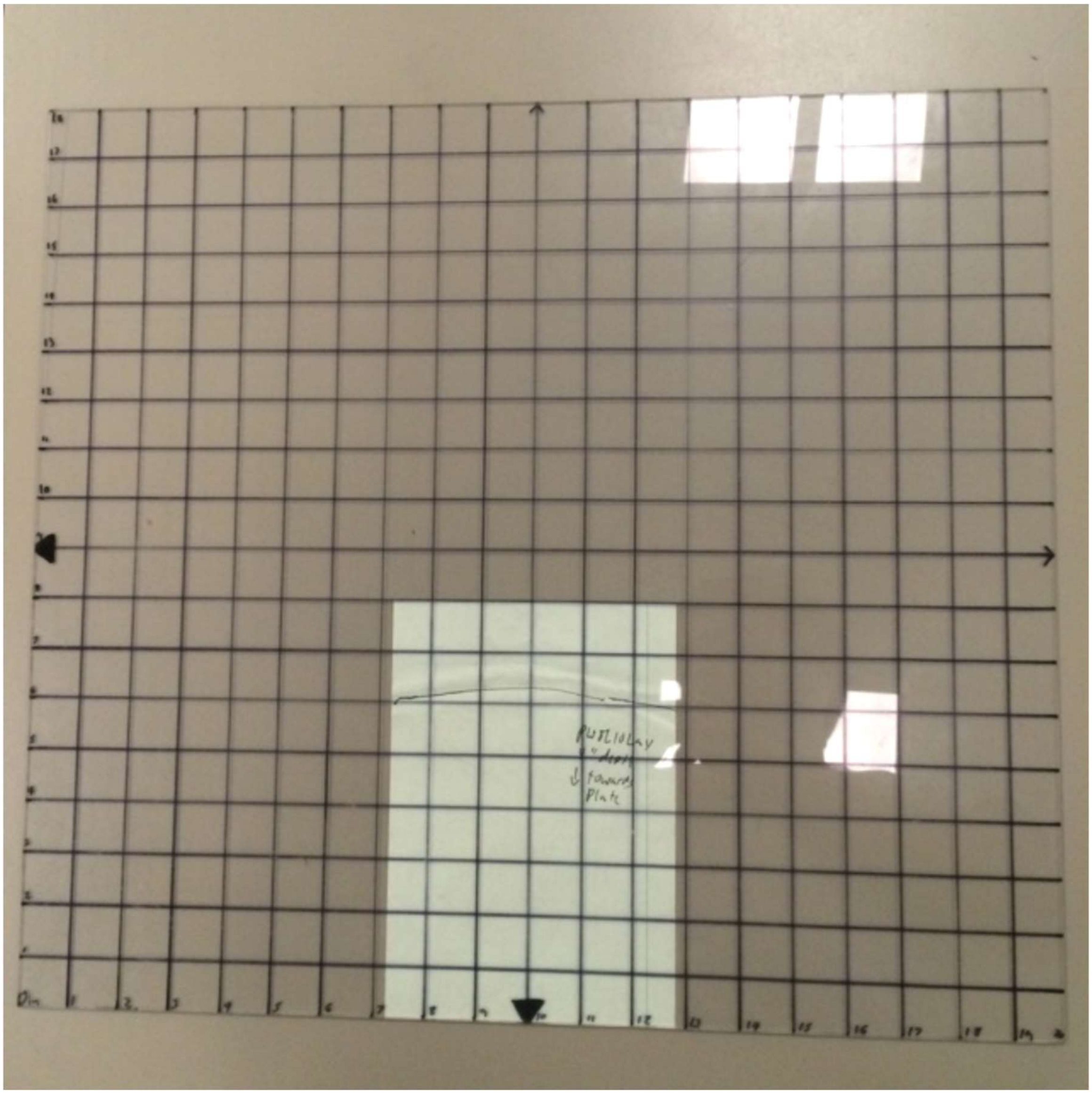

Figure 198: Test PW8L10Lay 4” Depth

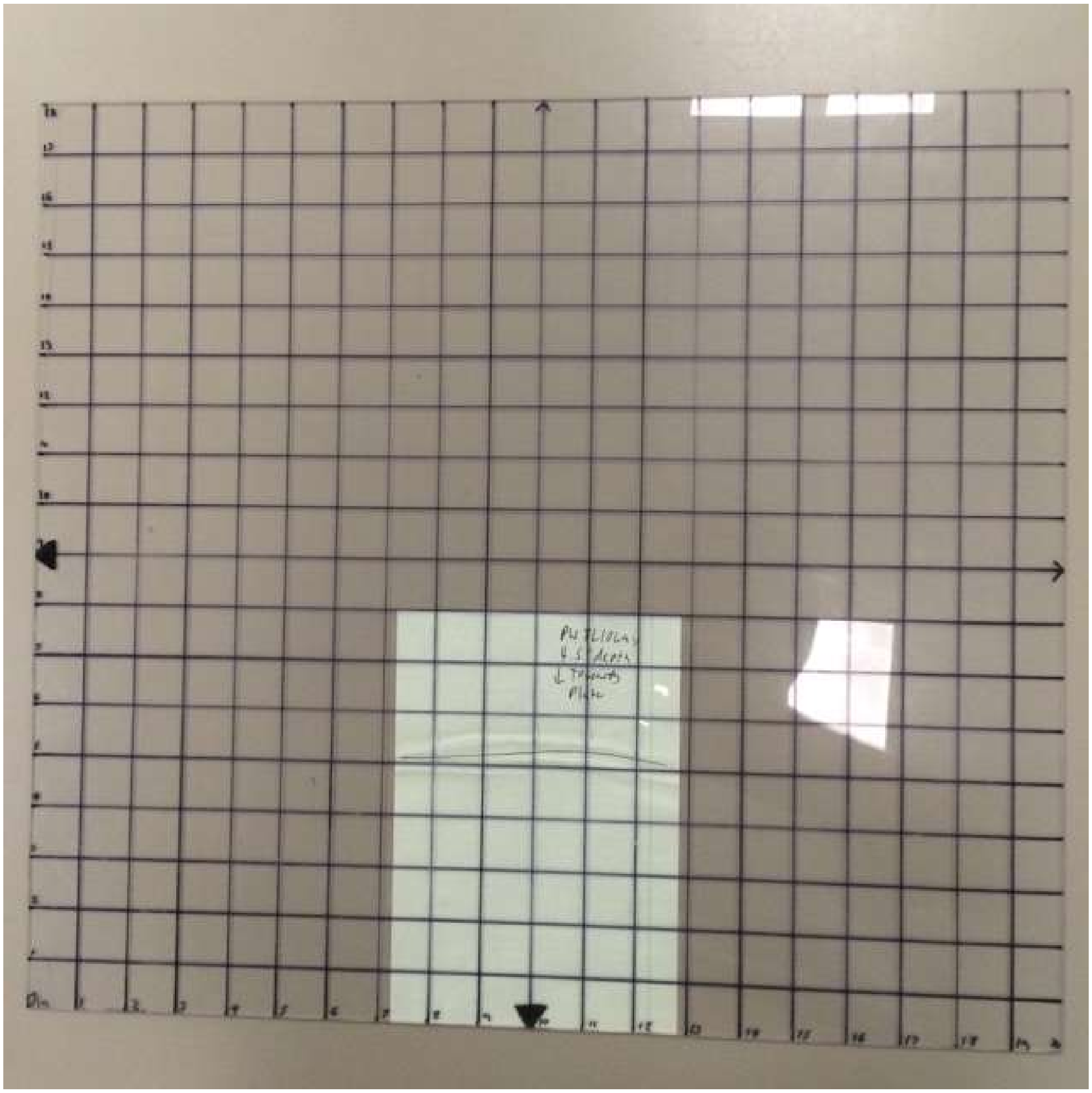

Figure 199: Test PW8L10Lay 4.5” Depth

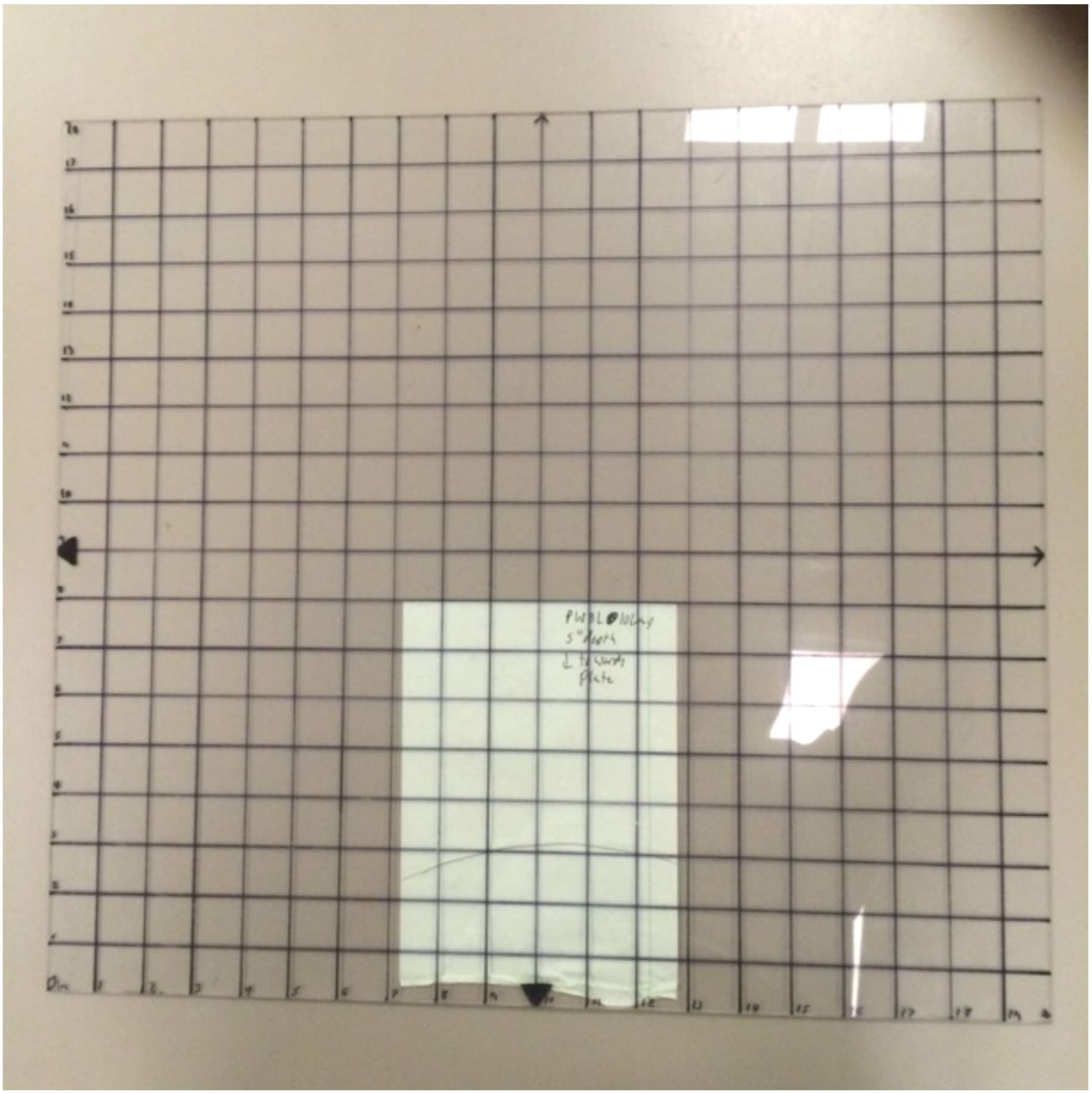

Figure 200: Test PW8L10Lay 5" Depth

A.9 Photographs of Test PW8L10Lay2

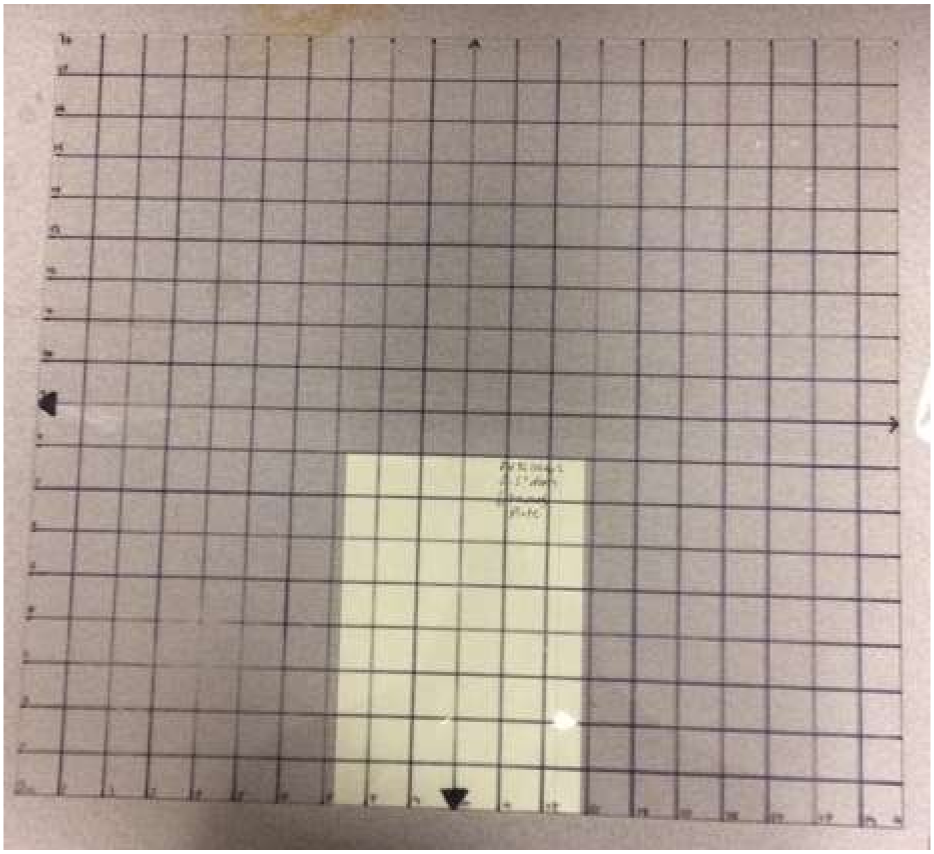

Figure 201: Test PW8L10Lay2 0.5" Depth

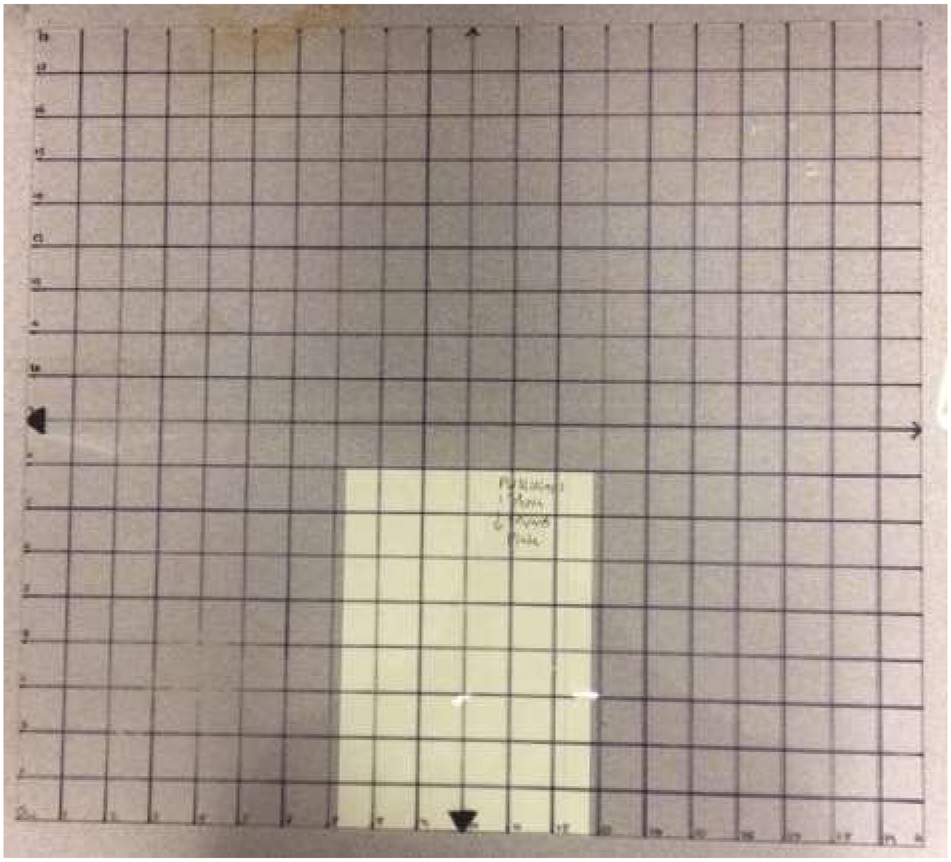

Figure 202: Test PW8L10Lay2 1" Depth

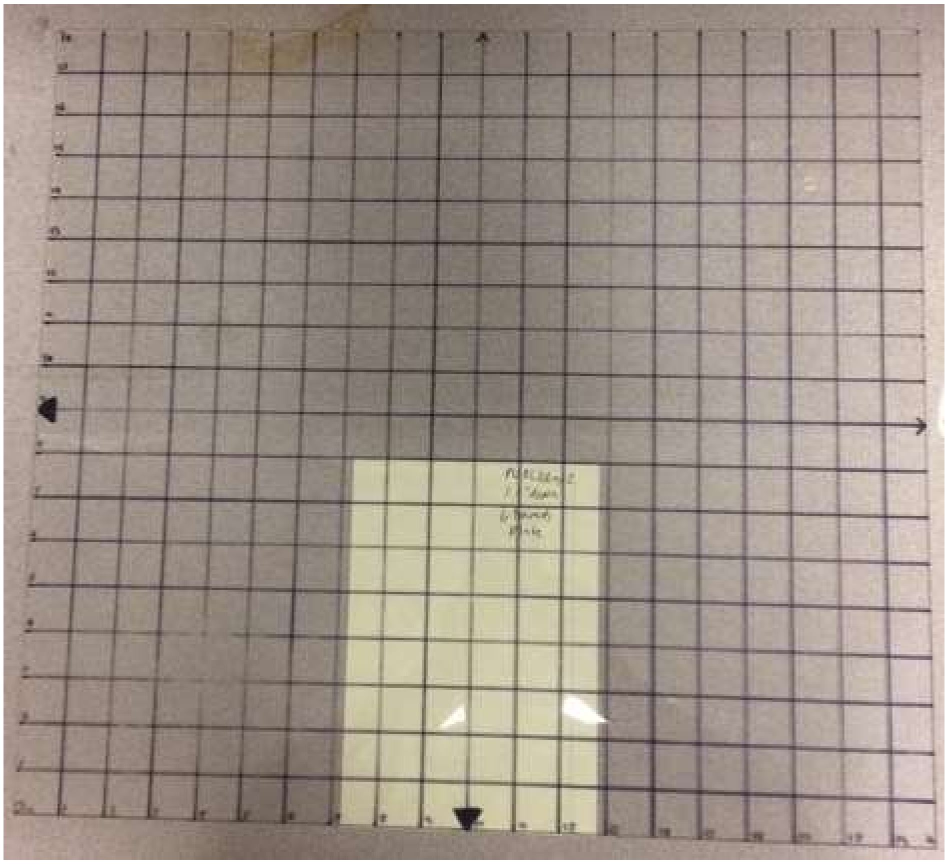
Figure 203: Test PW8L10Lay2 1.5" Depth

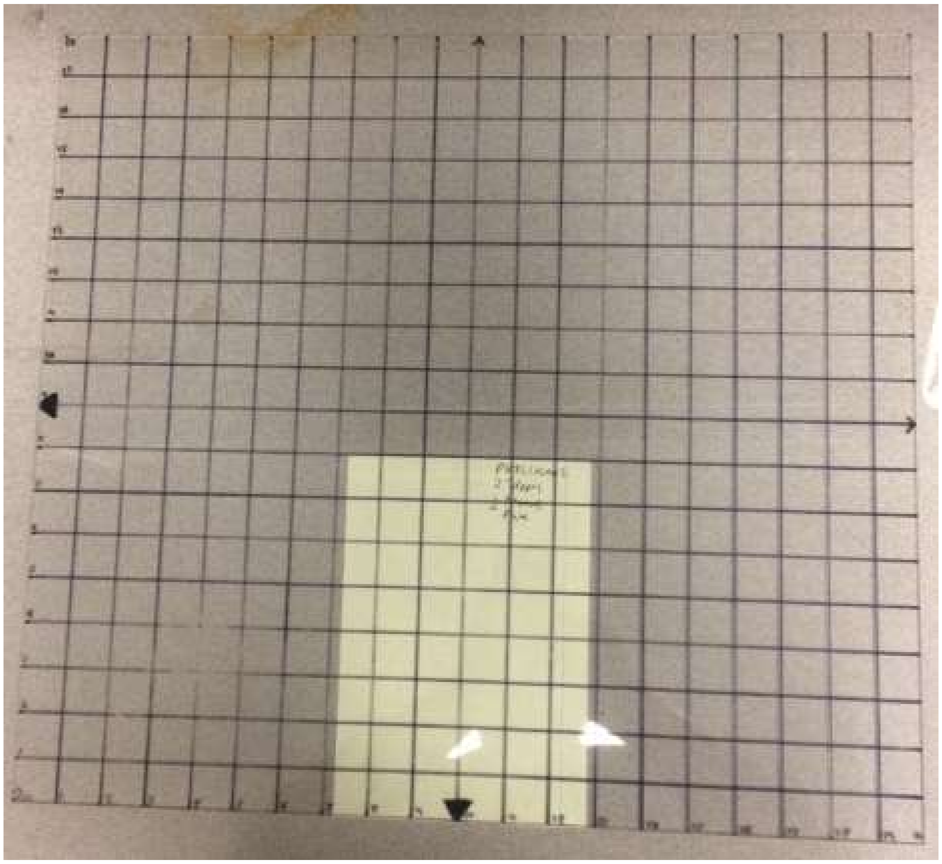

Figure 204: Test PW8L10Lay2 2” Depth

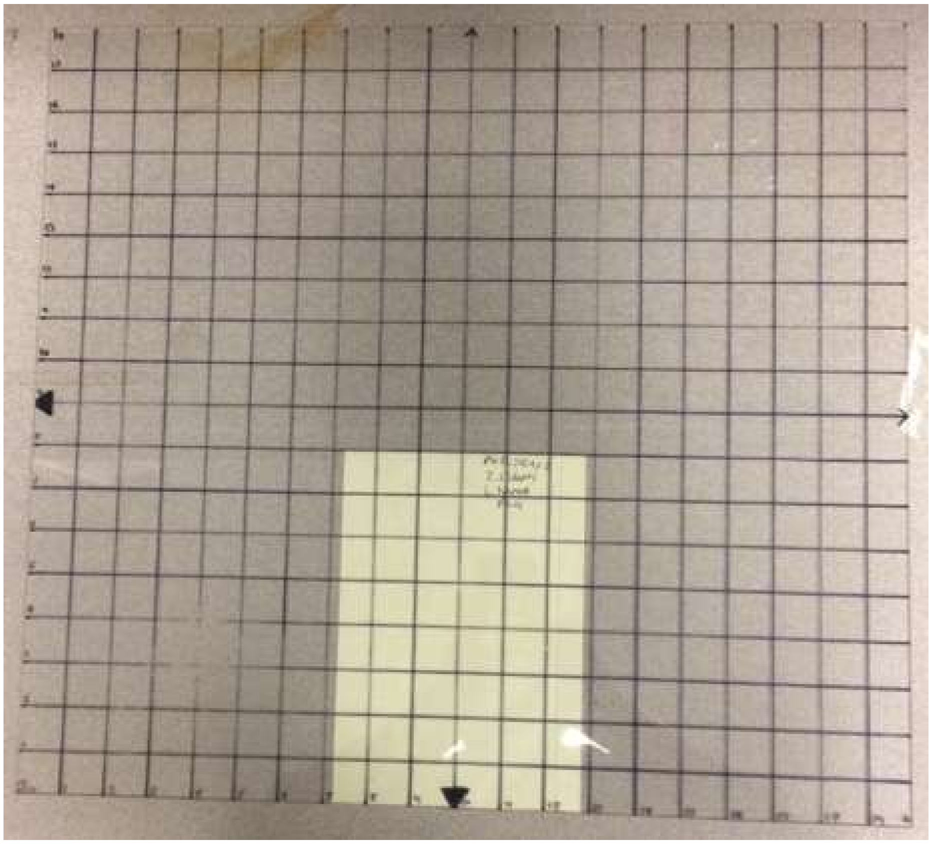

Figure 205: Test PW8L10Lay2 2.5" Depth

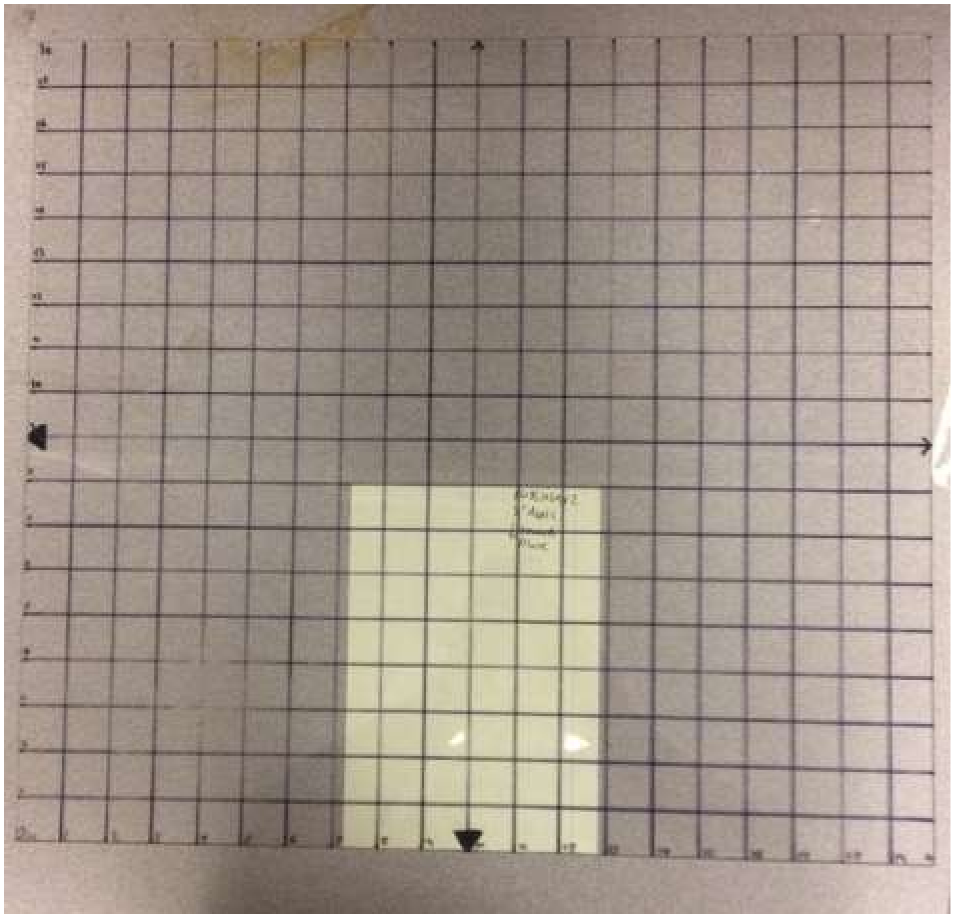

Figure 206: Test PW8L10Lay2 3” Depth

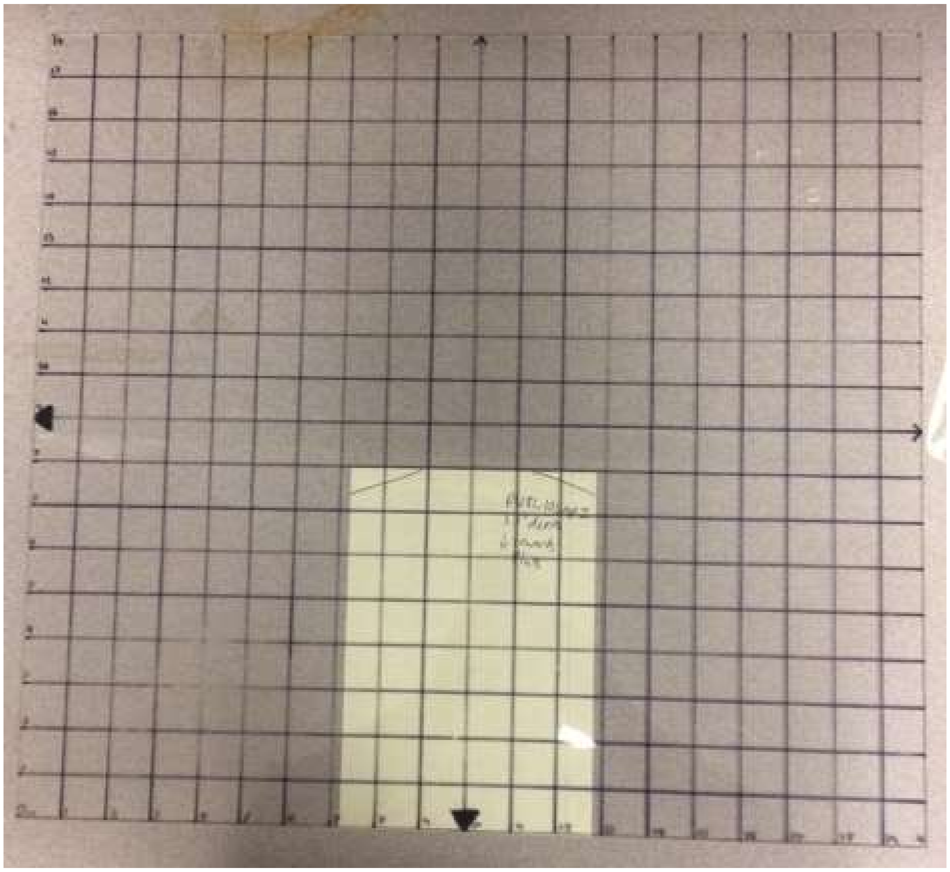

Figure 207: Test PW8L10Lay2 3.5" Depth

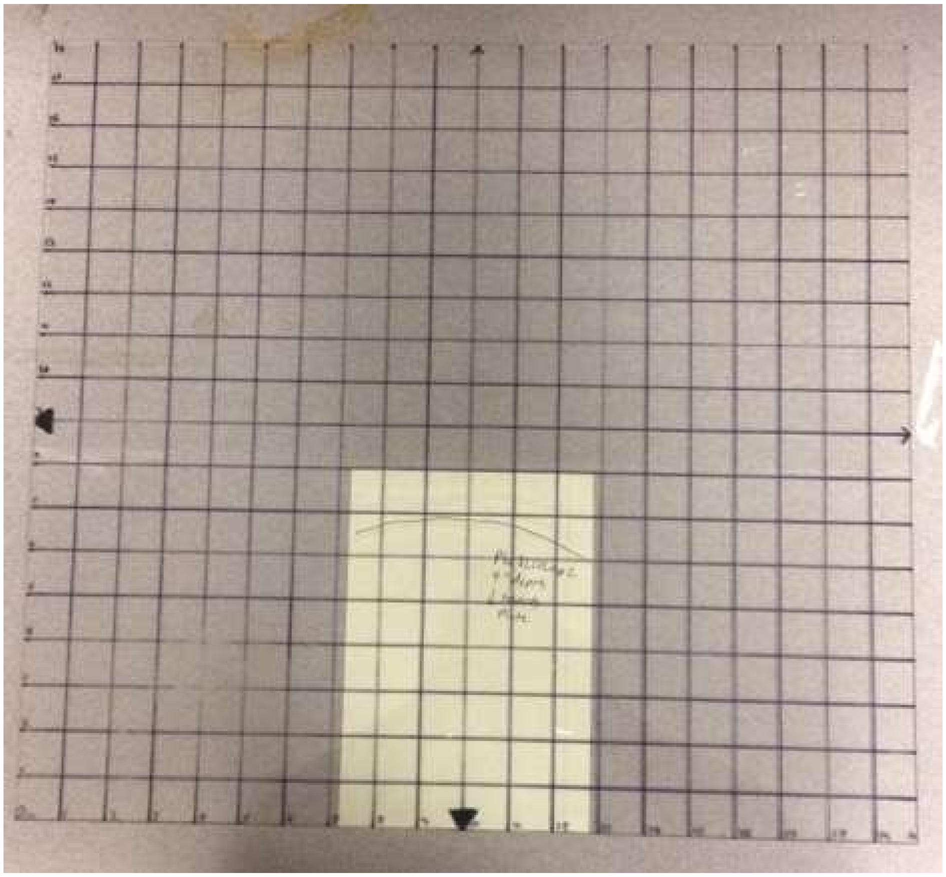

Figure 208: Test PW8L10Lay2 4" Depth

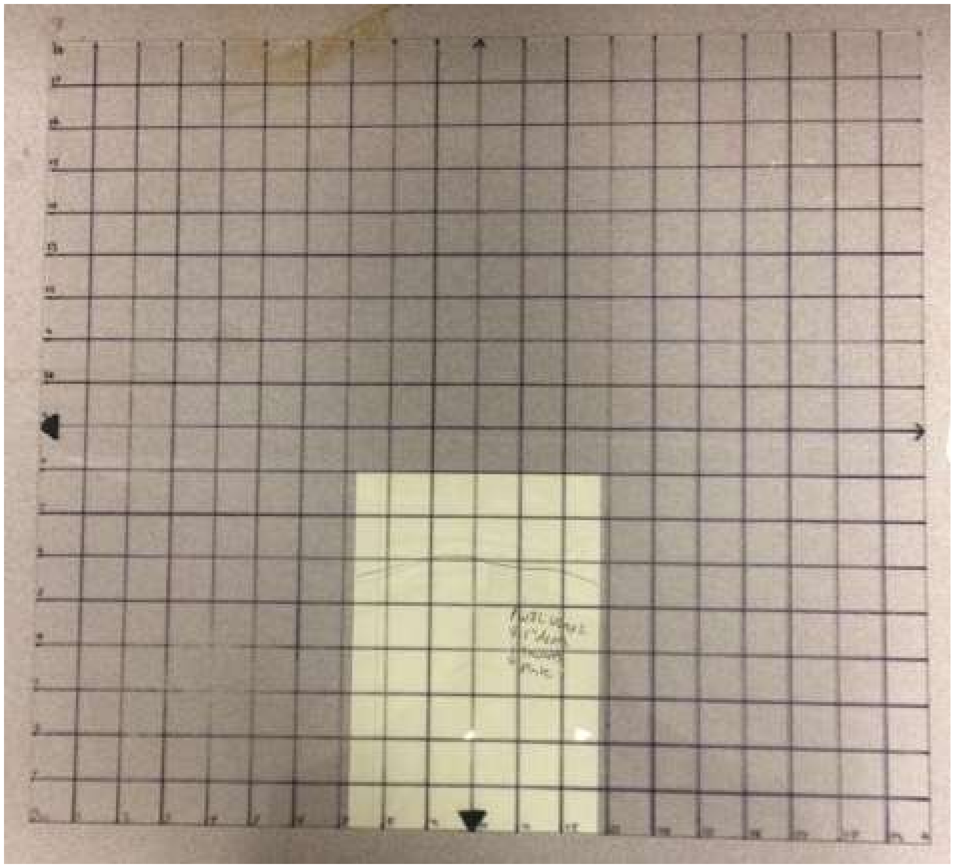

Figure 209: Test PW8L10Lay2 4.5" Depth

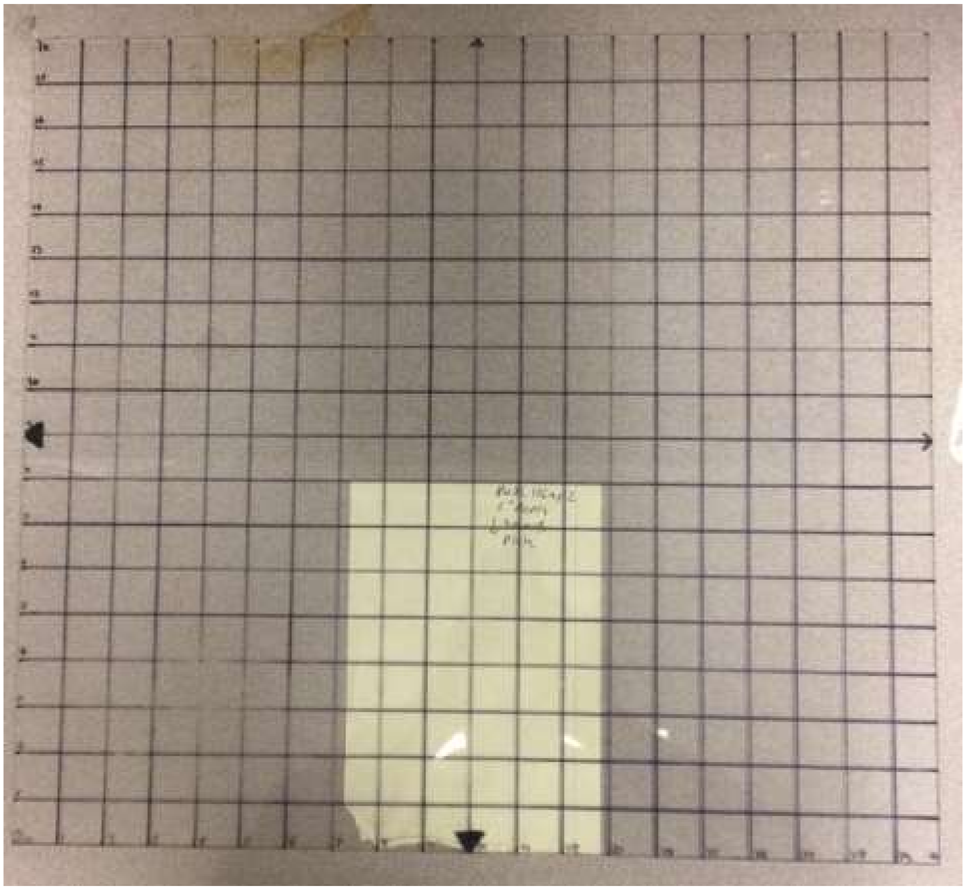

Figure 210: Test PW8L10Lay2 5” Depth

A.9 Photographs of Test PW11L5Lay

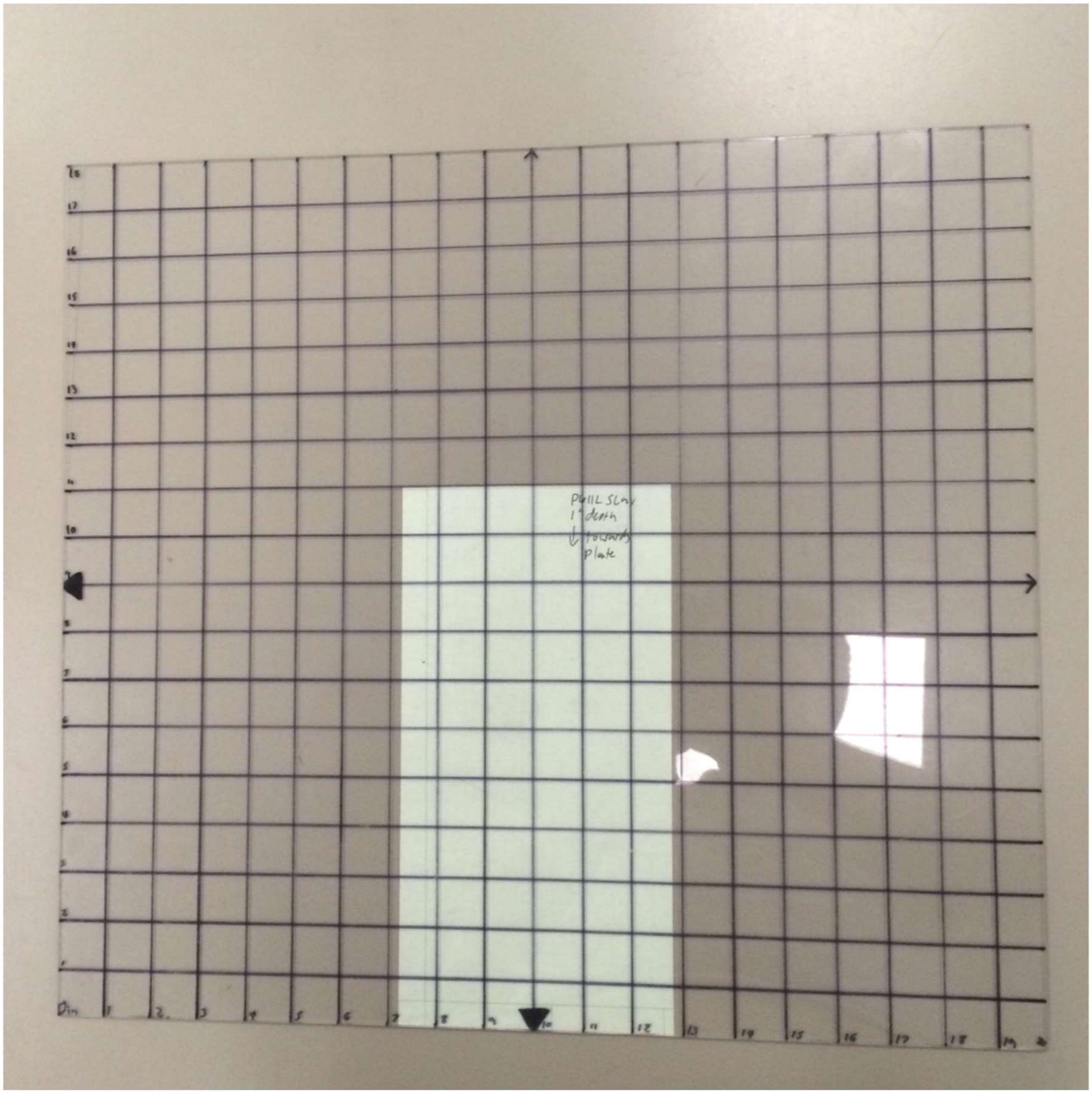

Figure 211: Test PW11L5Lay 1" Depth

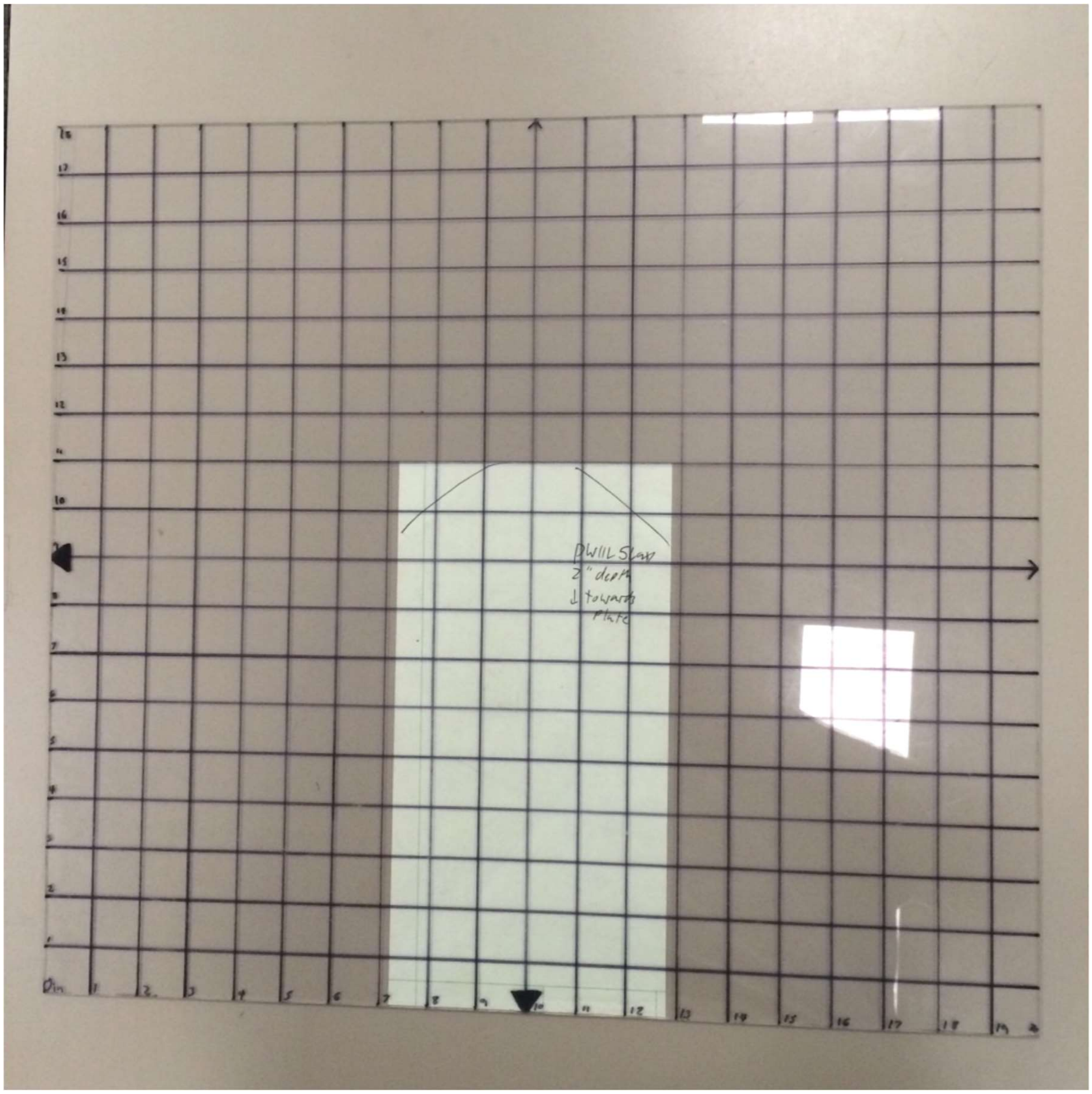

Figure 212: Test PW11L5Lay 2” Depth

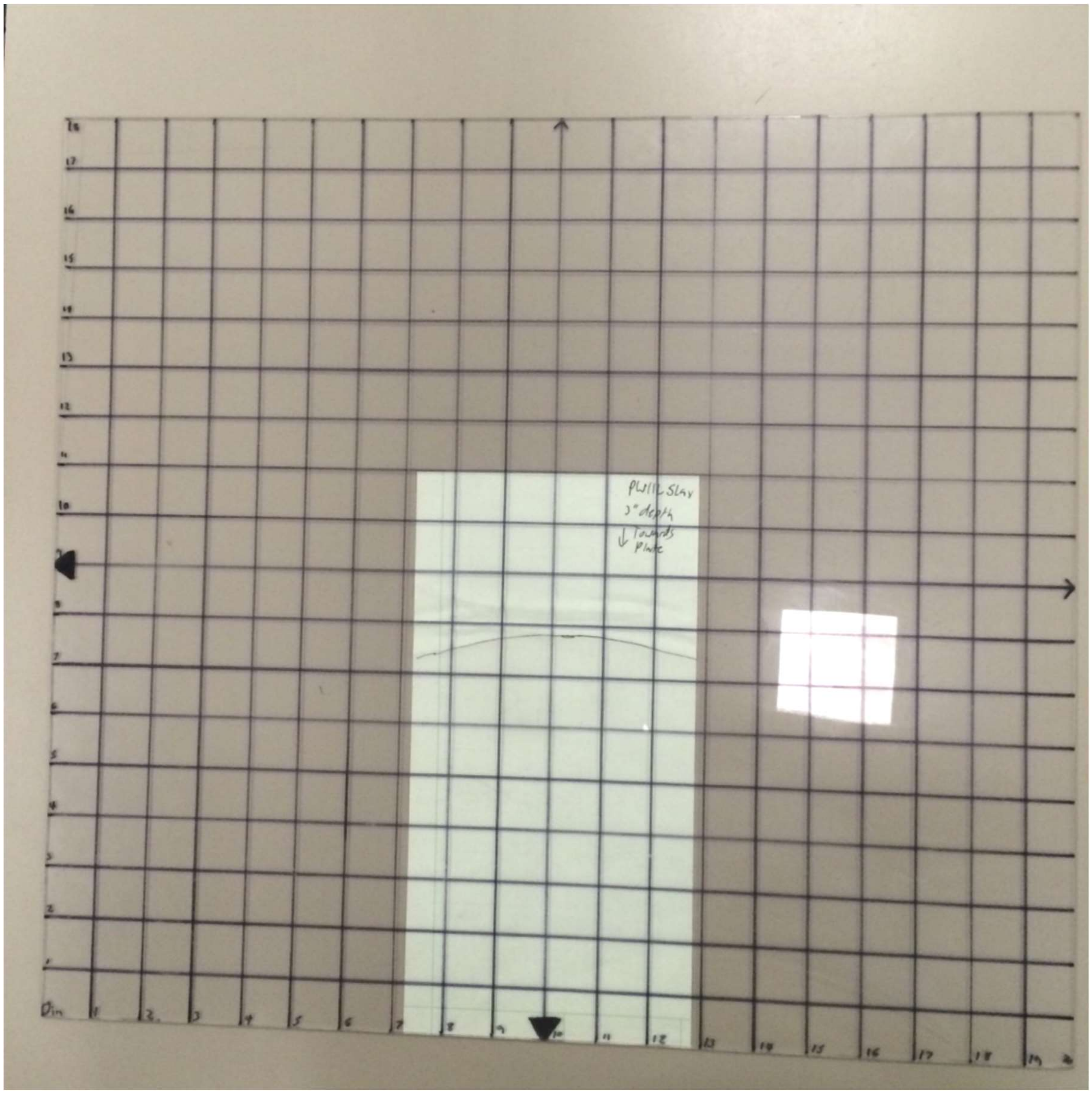

Figure 213 Test PW11L5Lay 3” Depth

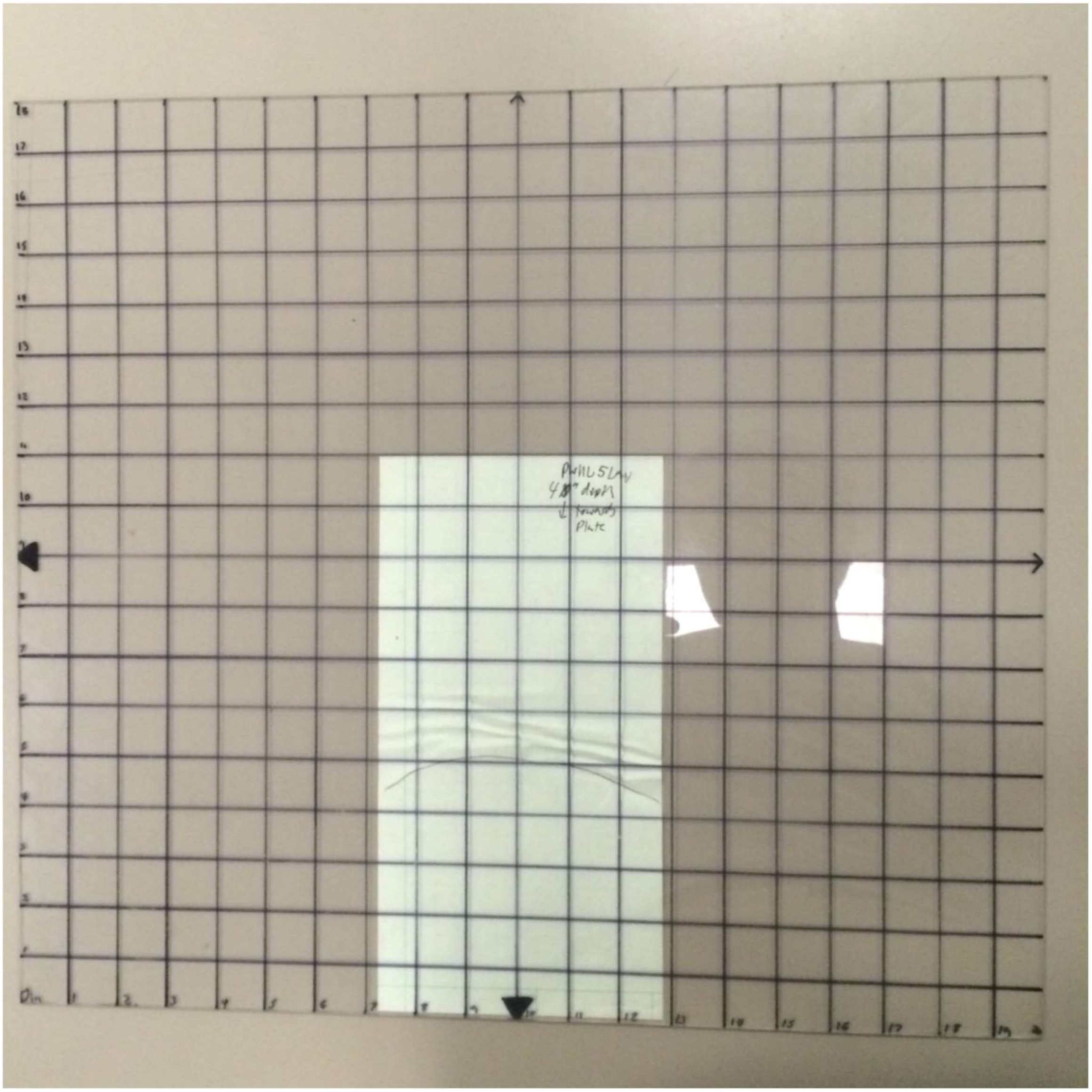

Figure 214: Test PW11L5Lay 4" Depth

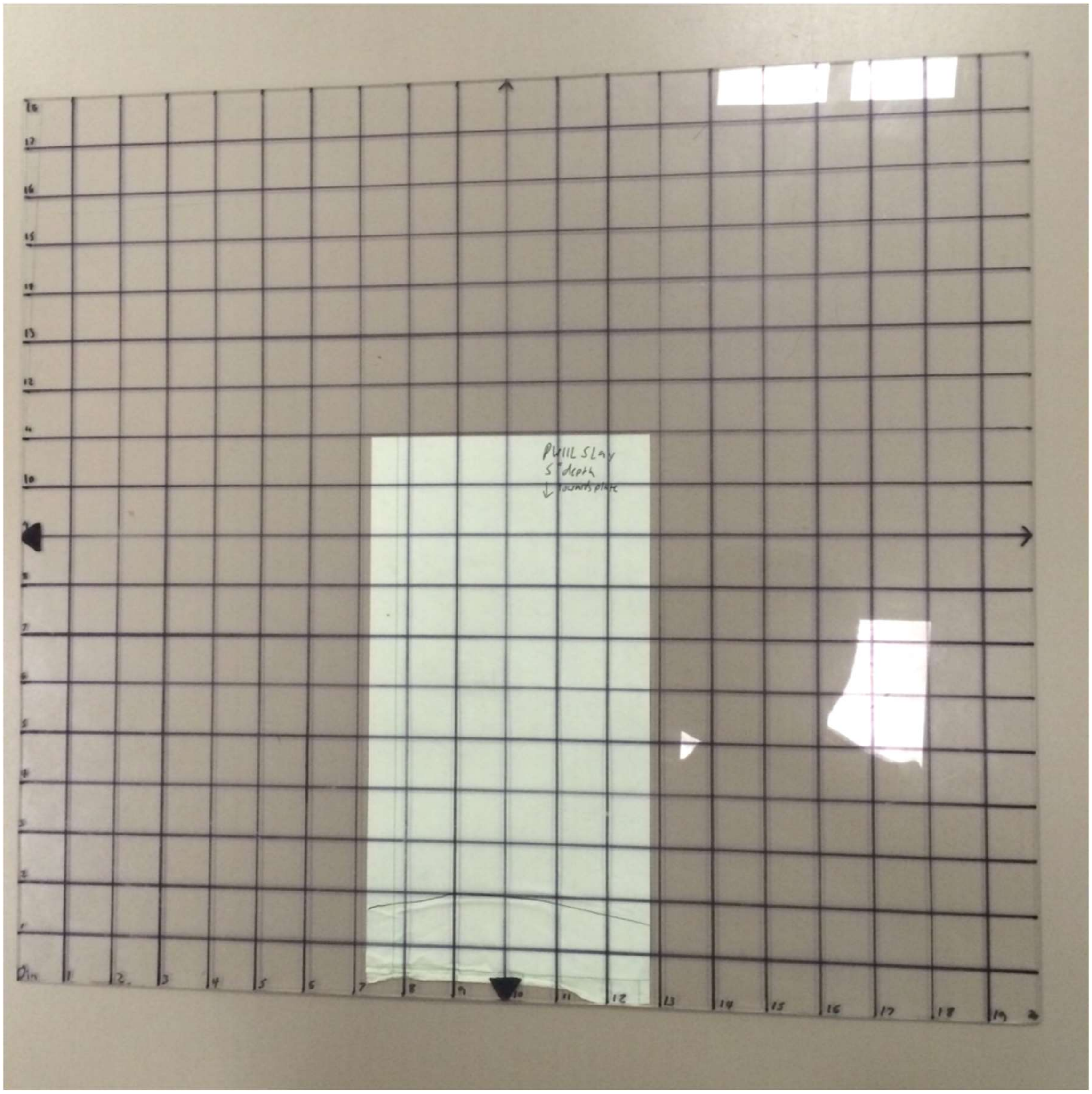

Figure 215: Test PW11L5Lay 5" Depth

A.10 Photographs of Test PW11L5Lay2

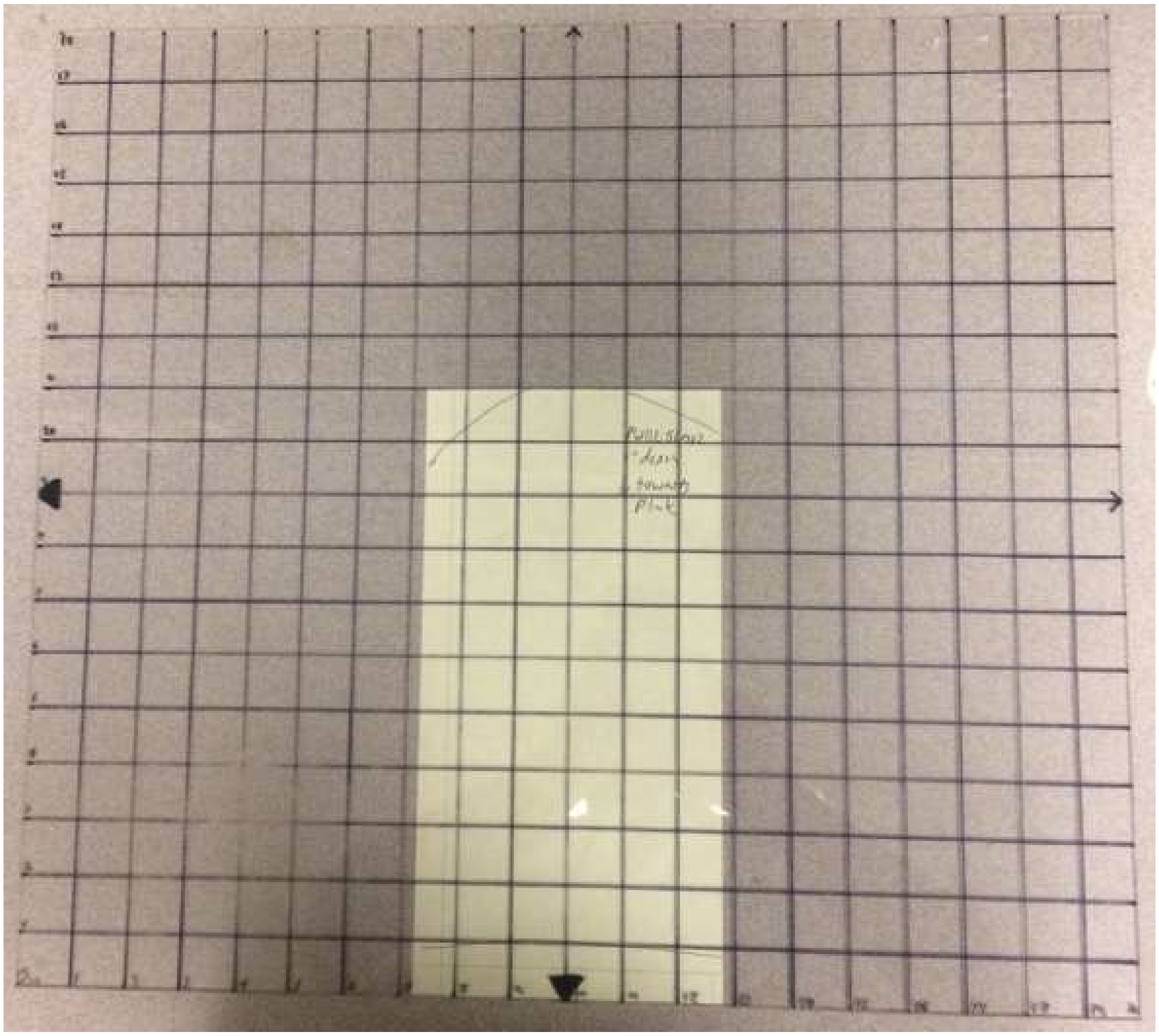

Figure 216: Test PW11L5Lay2 1" Depth

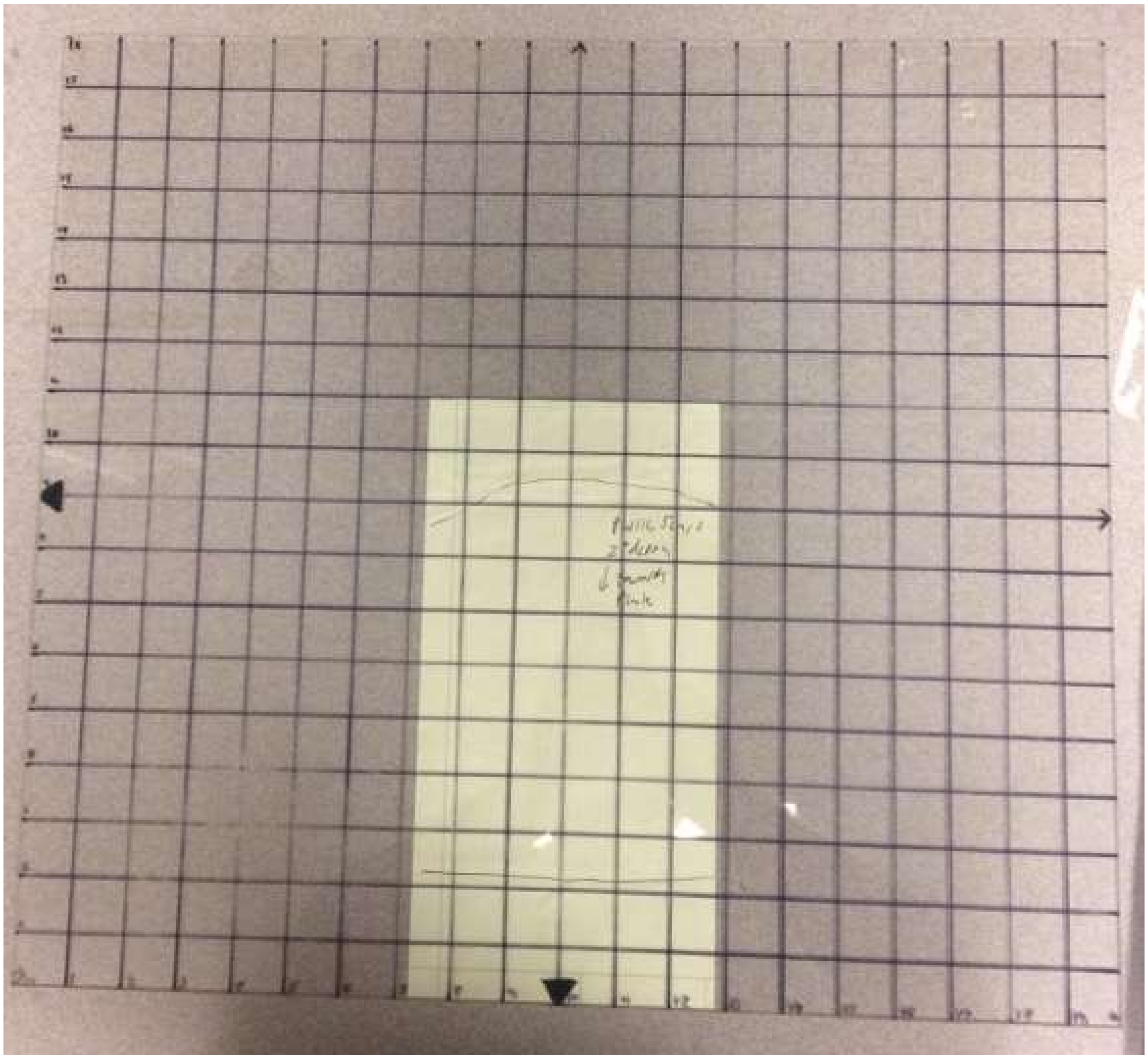

Figure 217: Test PW11L5Lay2 2" Depth

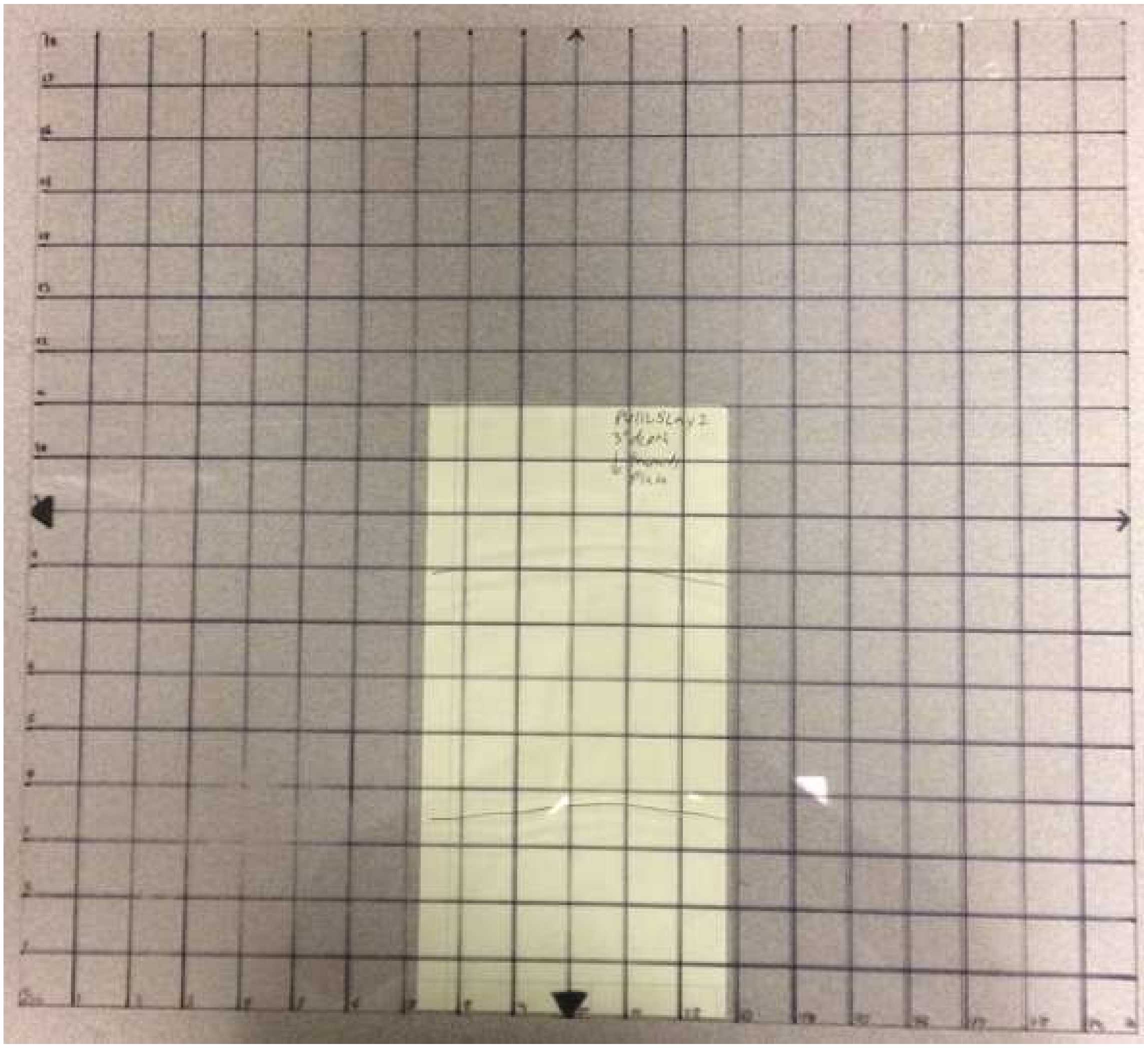

Figure 218: Test PW11L5Lay2 3” Depth

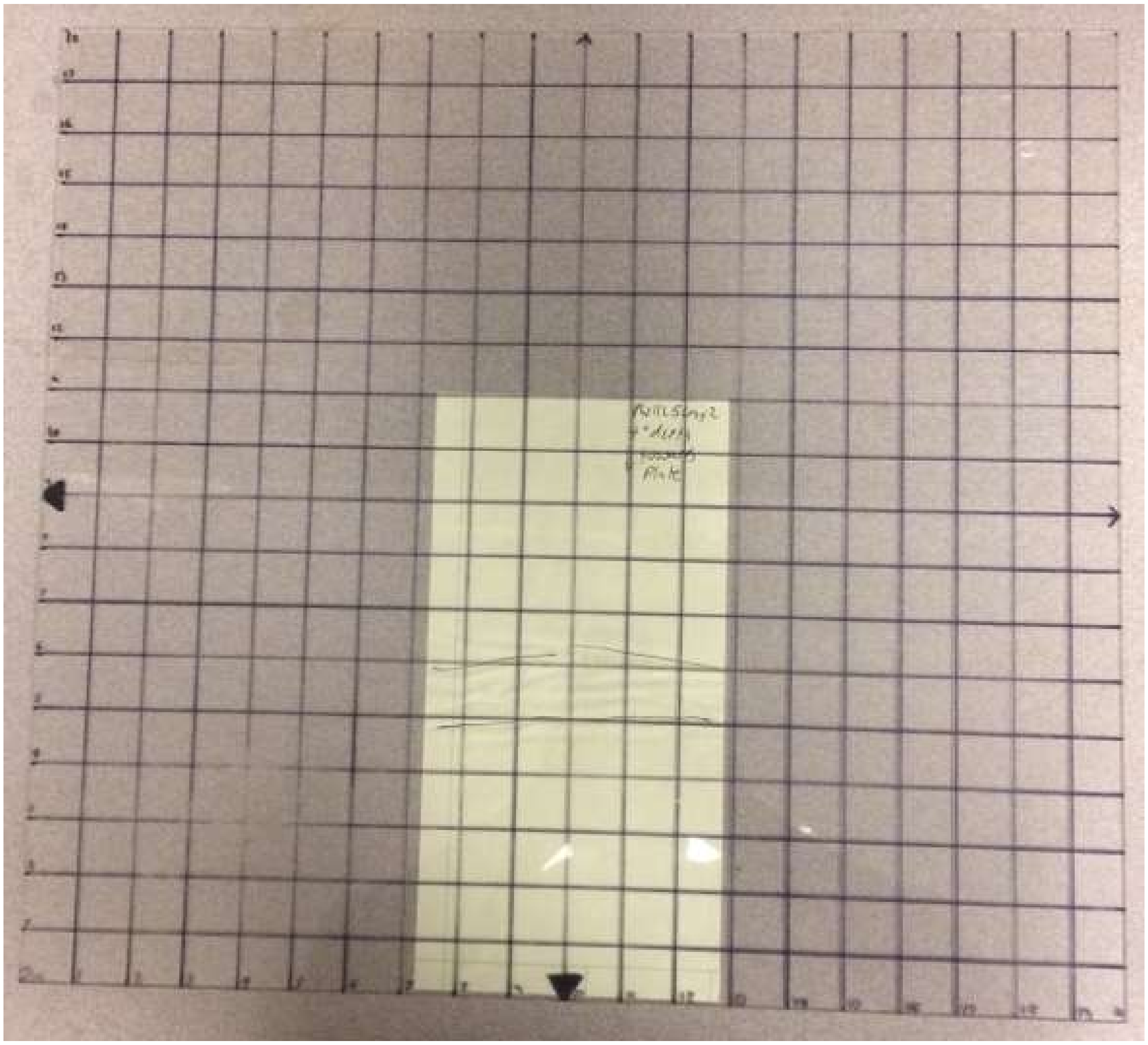

Figure 219: Test PW11L5Lay2 4” Depth

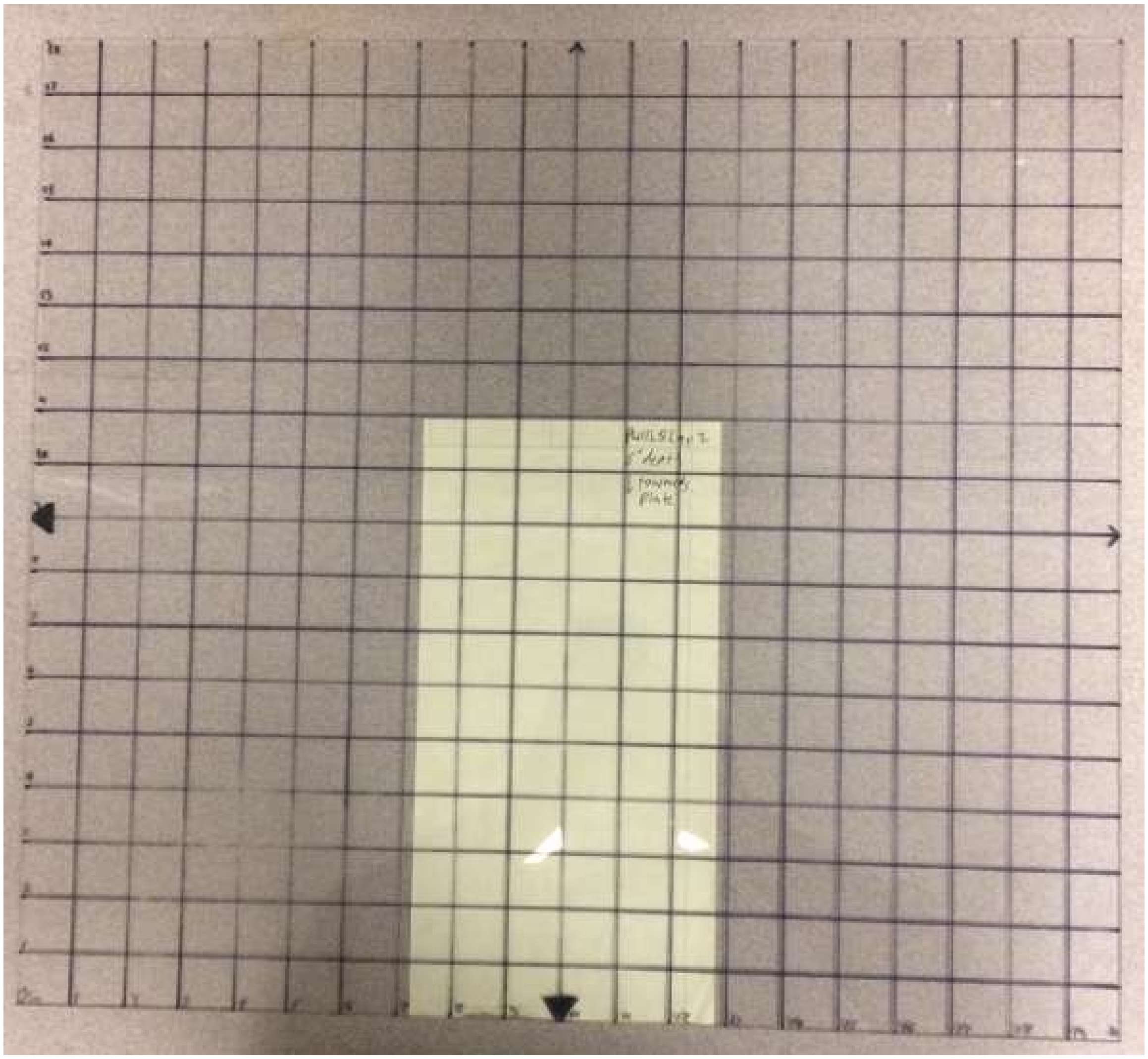
Figure 220: Test PW11L5Lay2 5” Depth

A.10 Photographs of Test PW11L10Lay

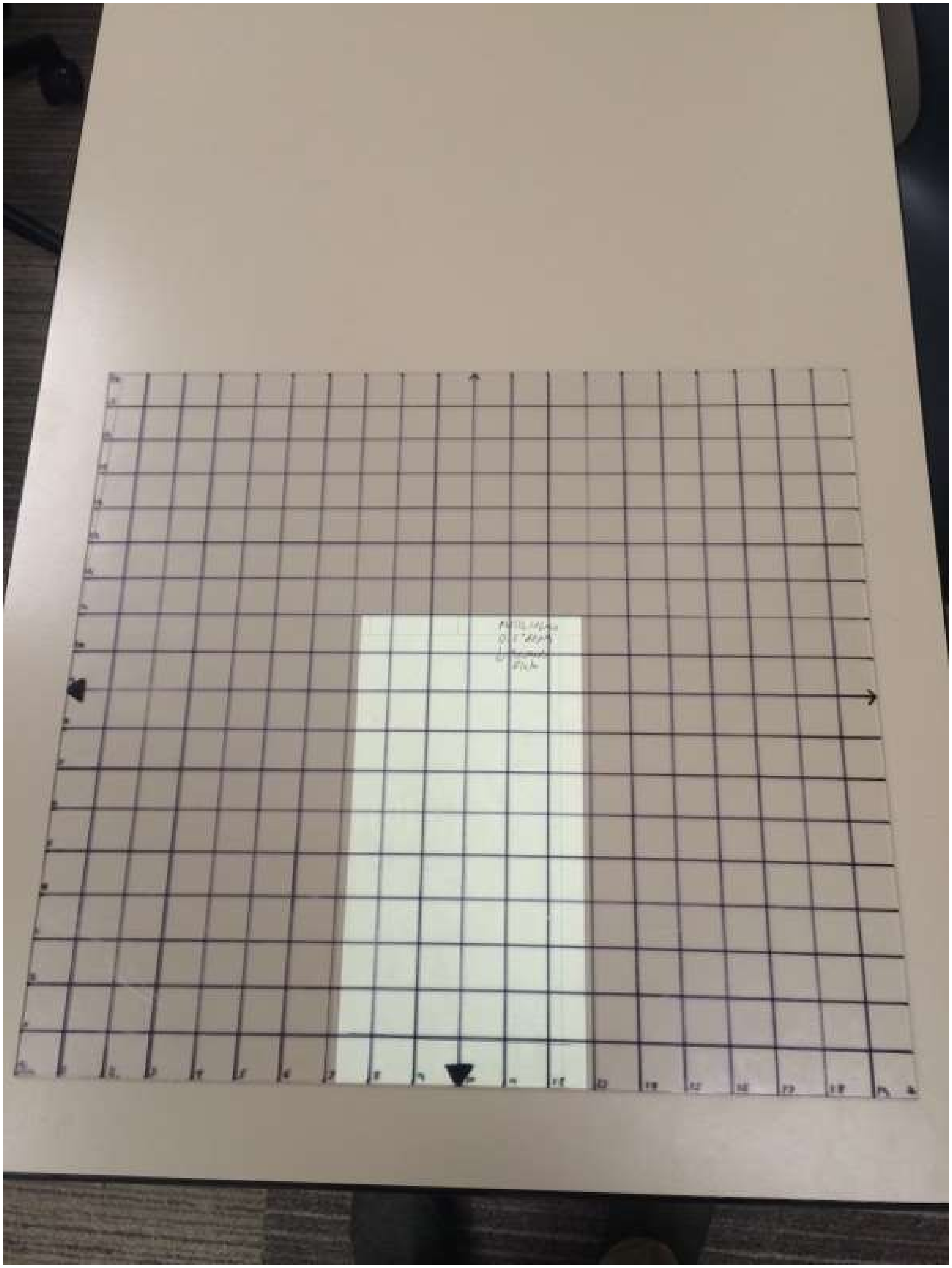

Figure 221: Test PW11L10Lay 0.5" Depth

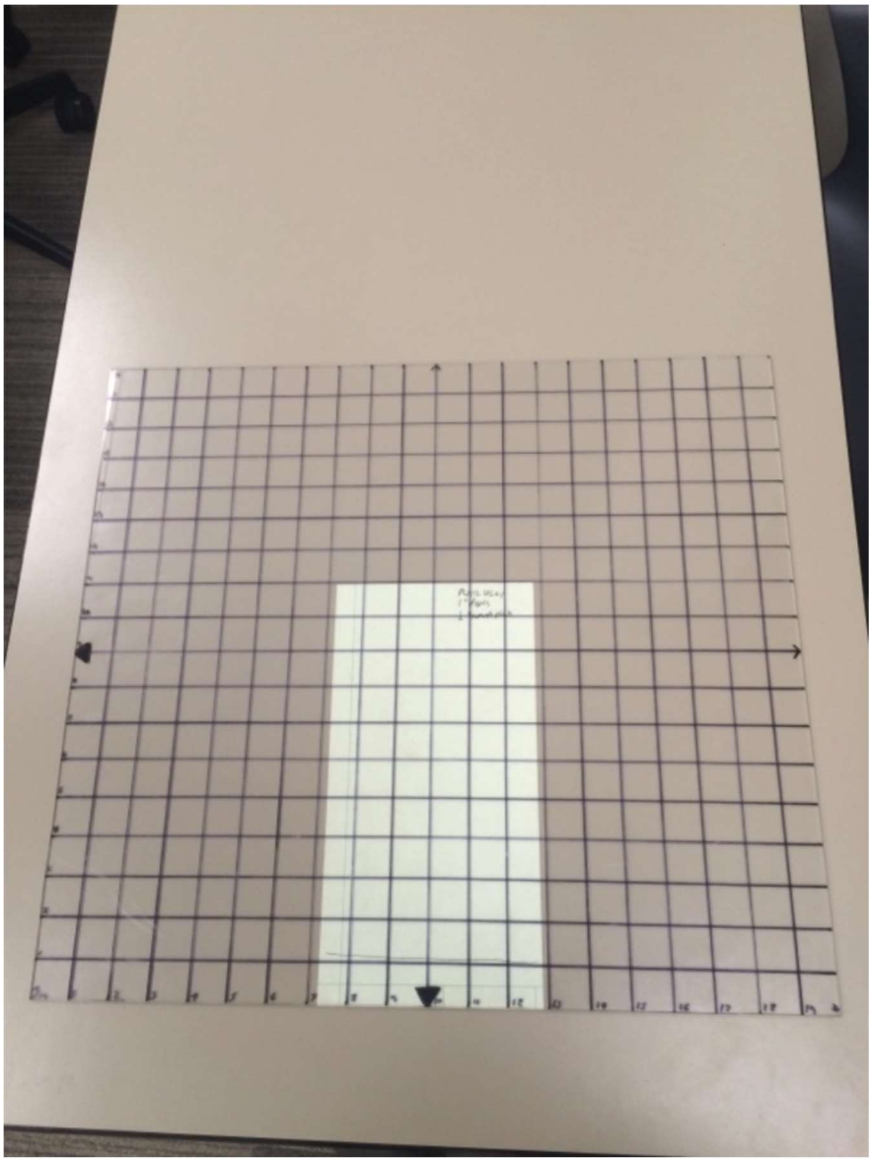

Figure 222: Test PW11L10Lay 1" Depth

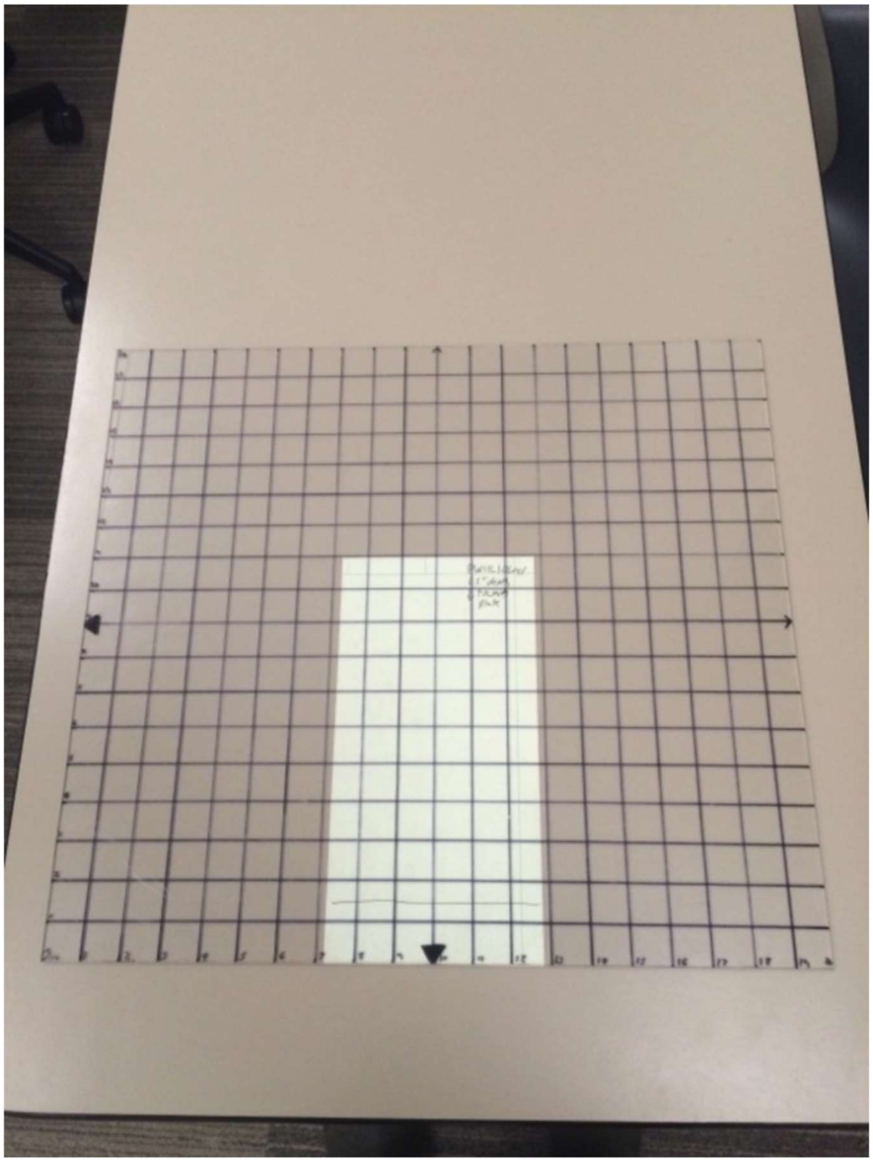

Figure 223: Test PW11L10Lay 1.5” Depth

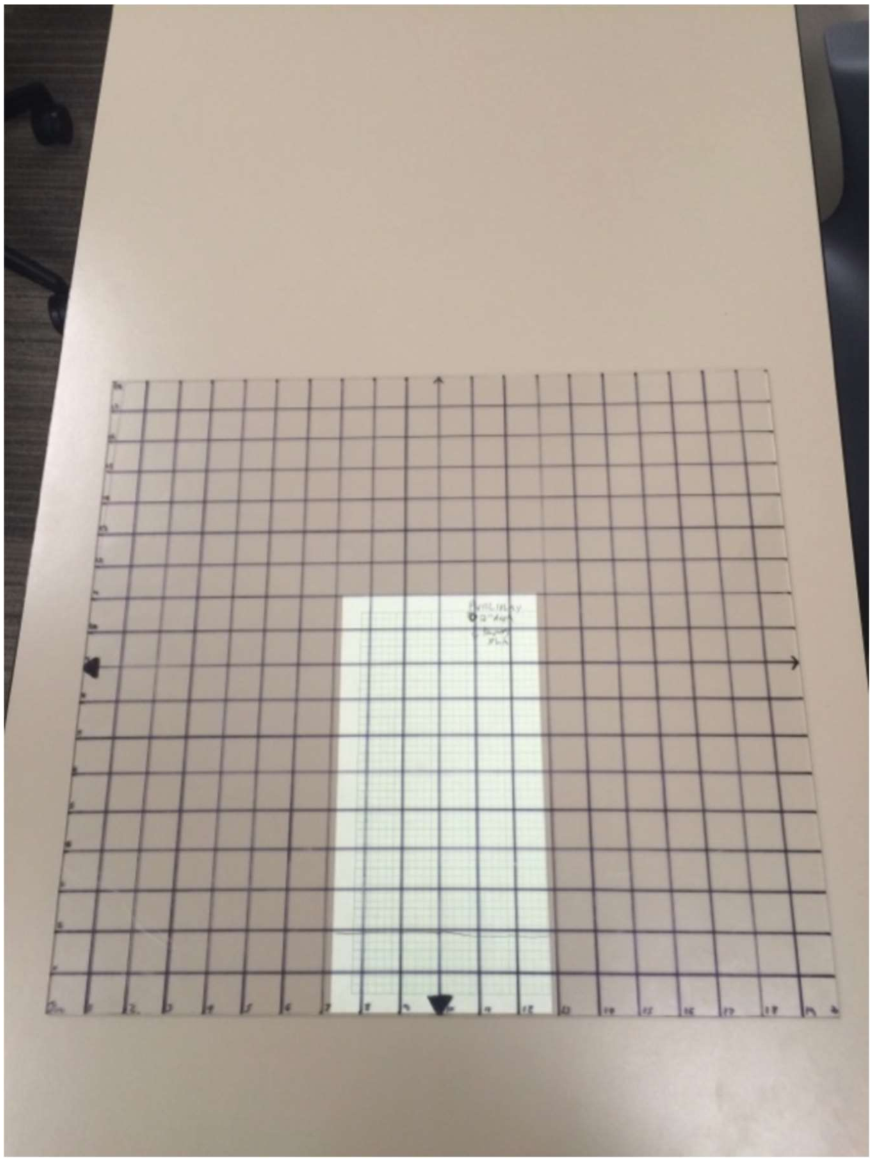

Figure 224: Test PW11L10Lay 2" Depth

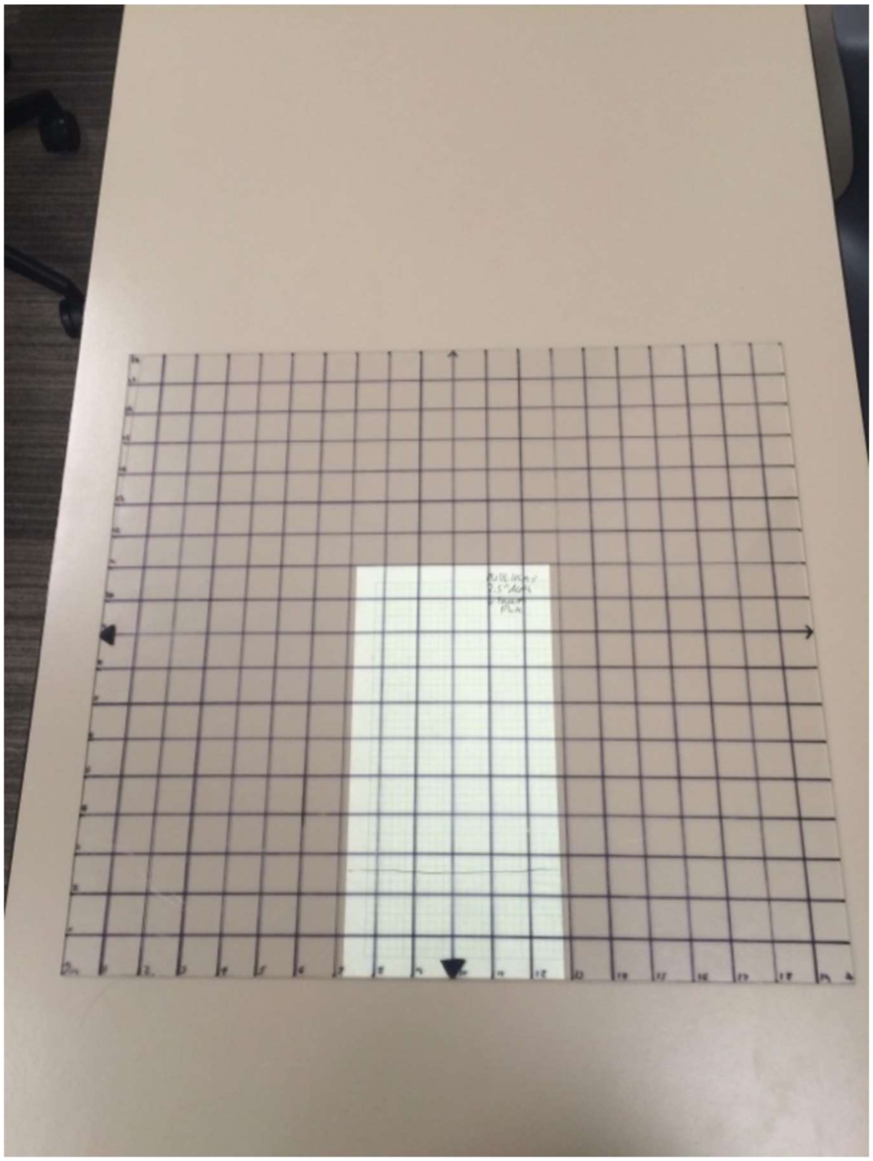

Figure 225 Test PW11L10Lay 2.5" Depth

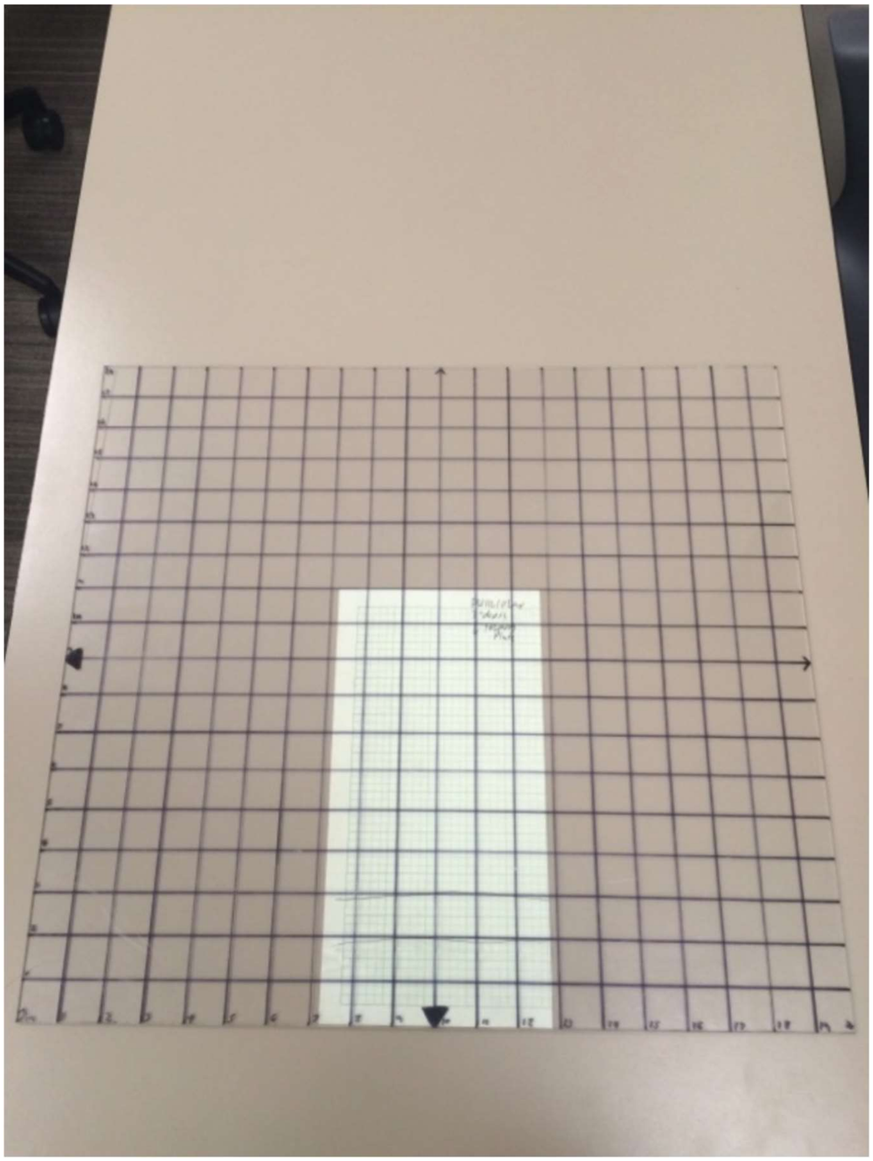

Figure 226: Test PW11L10Lay 3" Depth

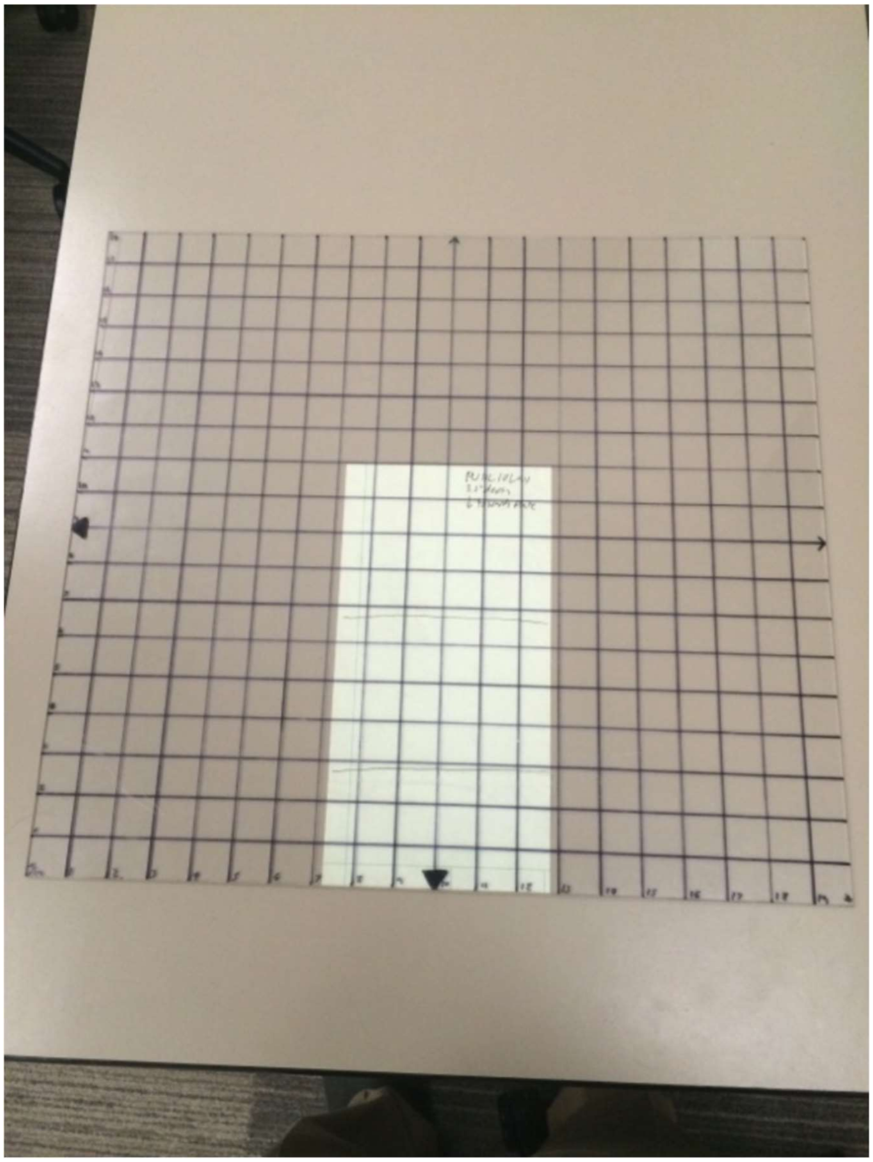

Figure 227 Test PW11L10Lay 3.5” Depth

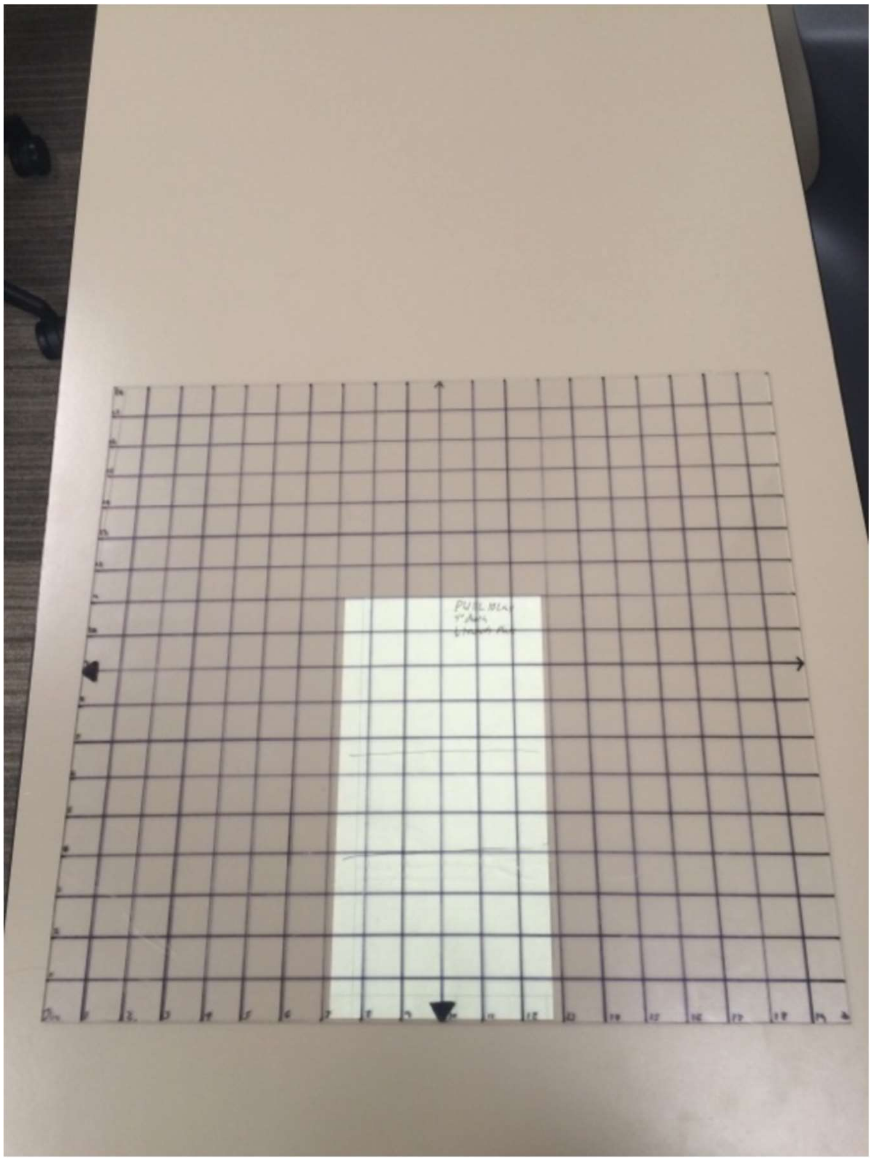

Figure 228: Test PW11L10Lay 4" Depth

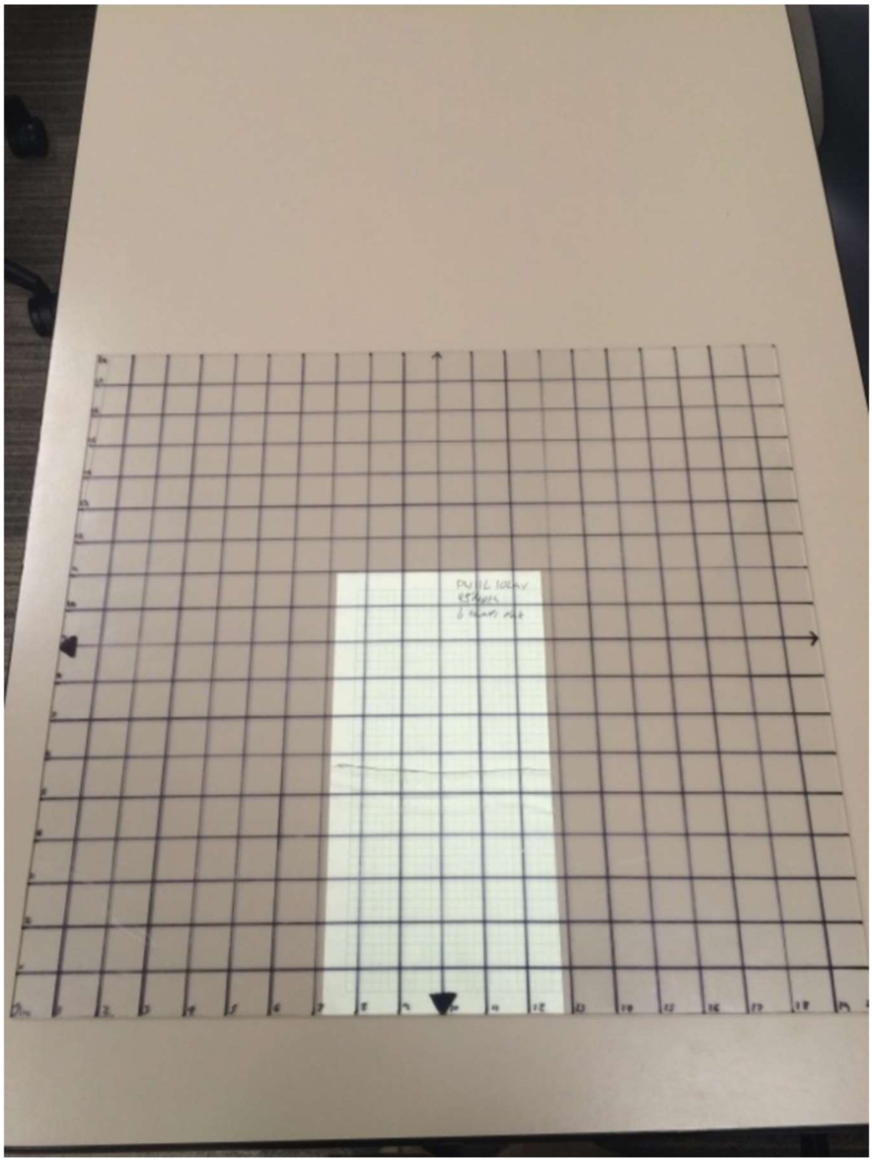

Figure 229: Test PW11L10Lay 4.5” Depth

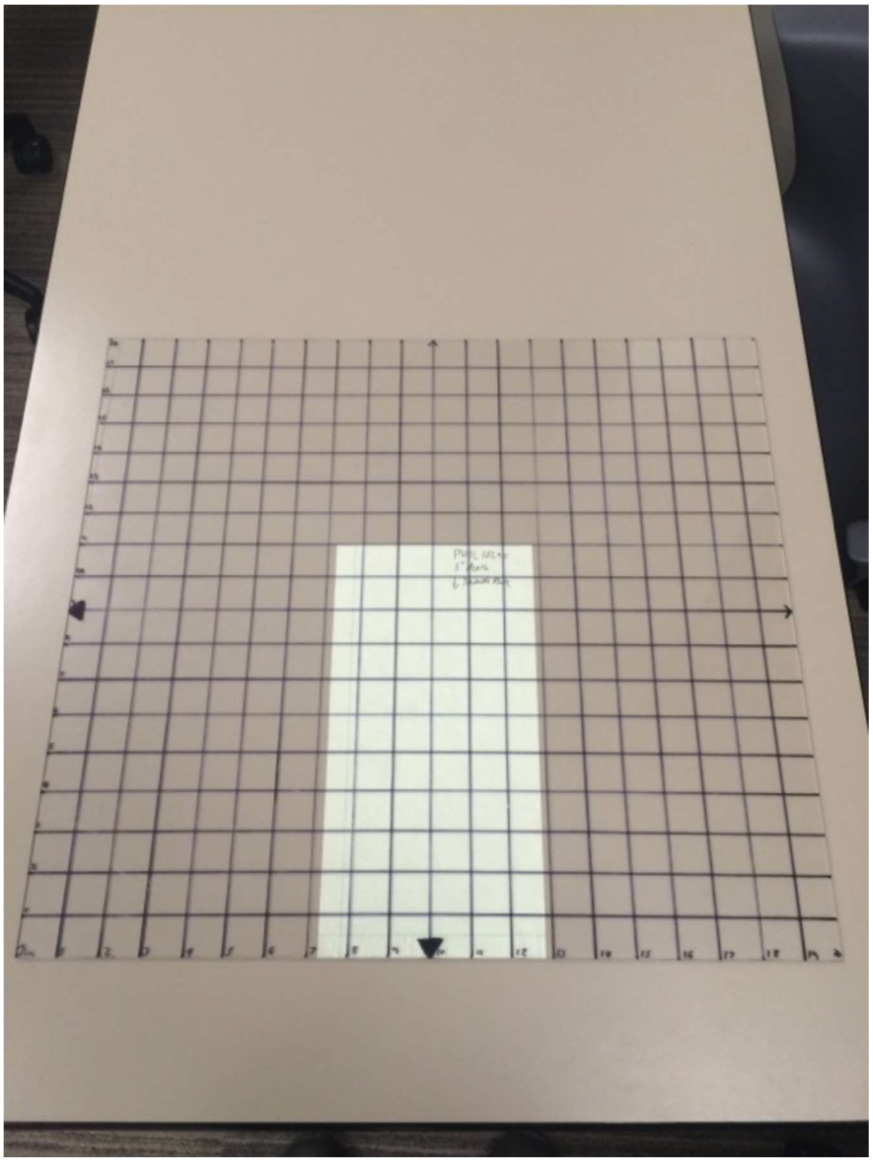

Figure 230: Test PW11L10Lay 5” Depth

A.11 Photographs of Test PW11L10Lay2

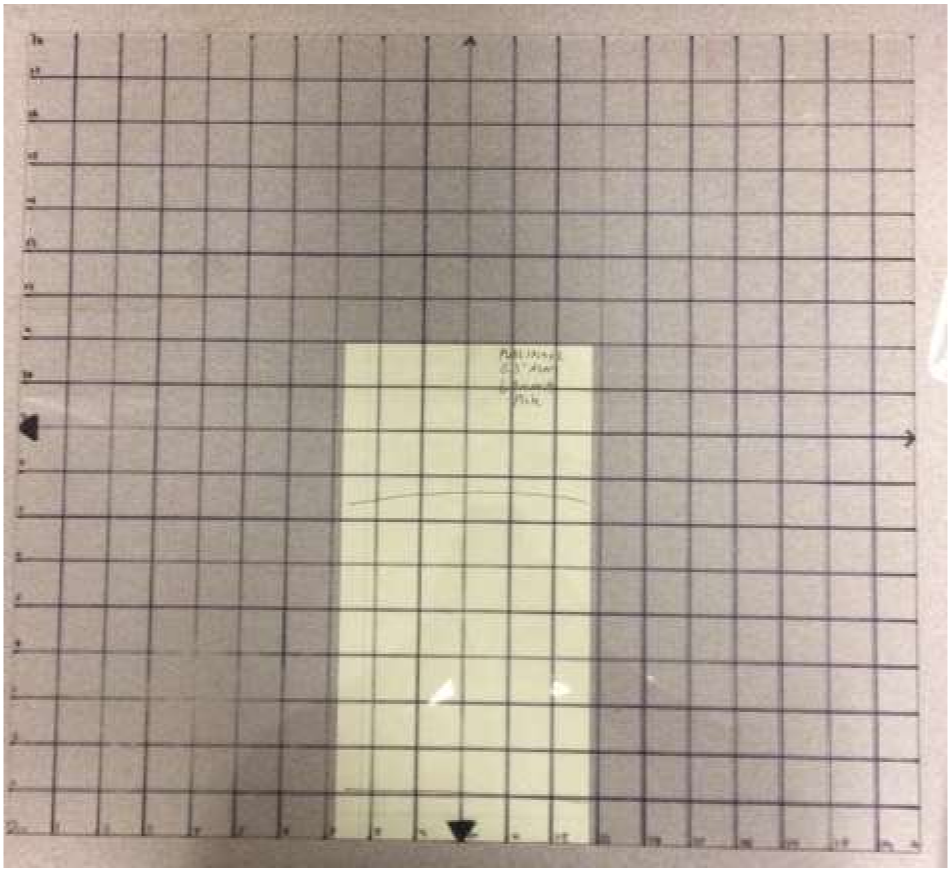

Figure 231: Test PW11L10Lay2 0.5" Depth

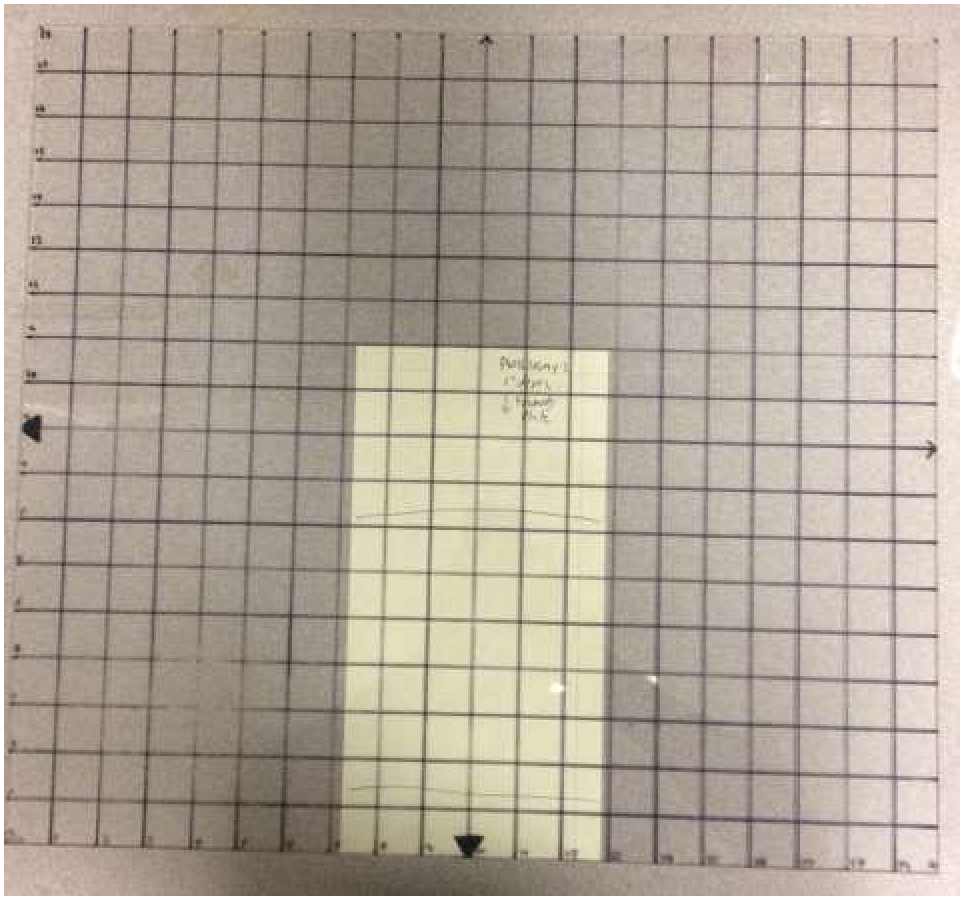

Figure 232: Test PW11L10Lay2 1” Depth

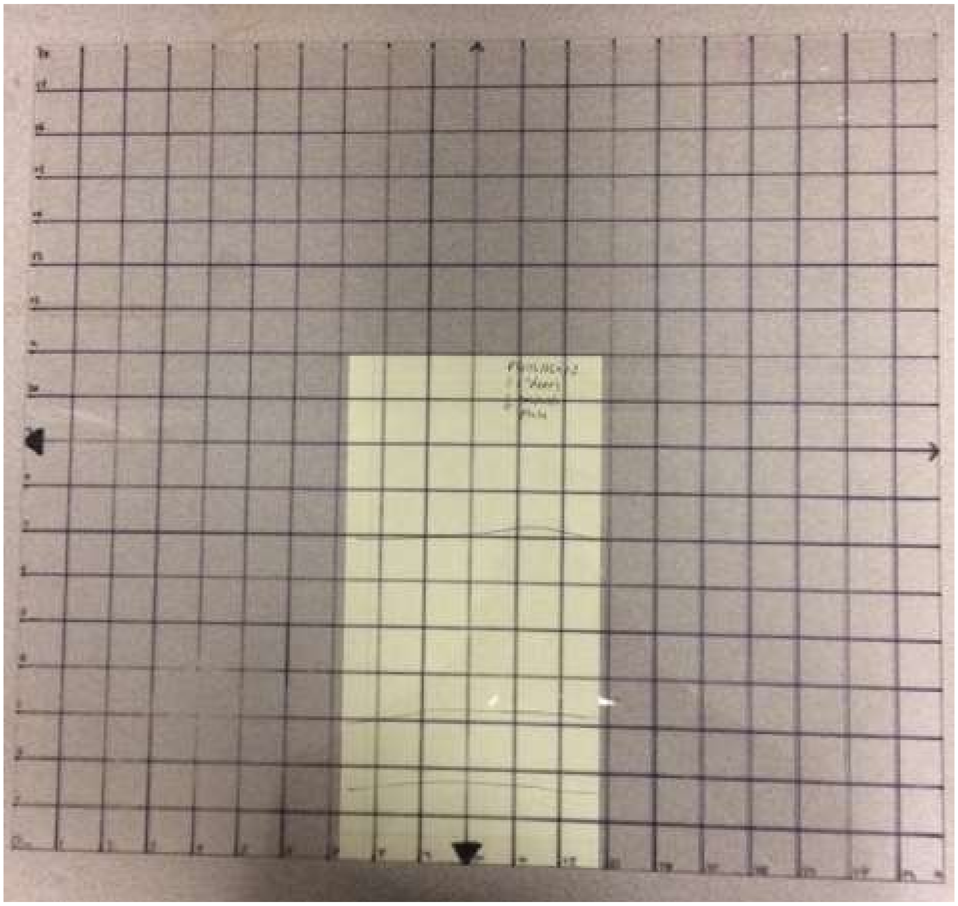

Figure 233: Test PW11L10Lay2 1.5” Depth

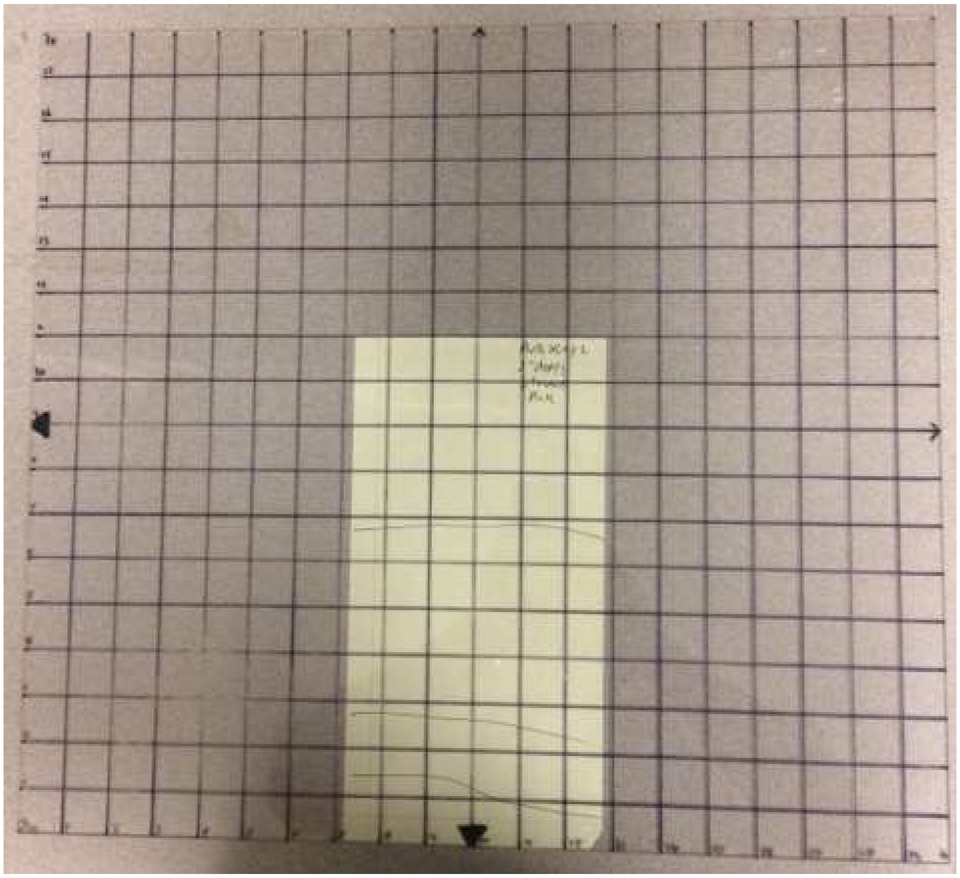

Figure 234: Test PW11L10Lay2 2" Depth

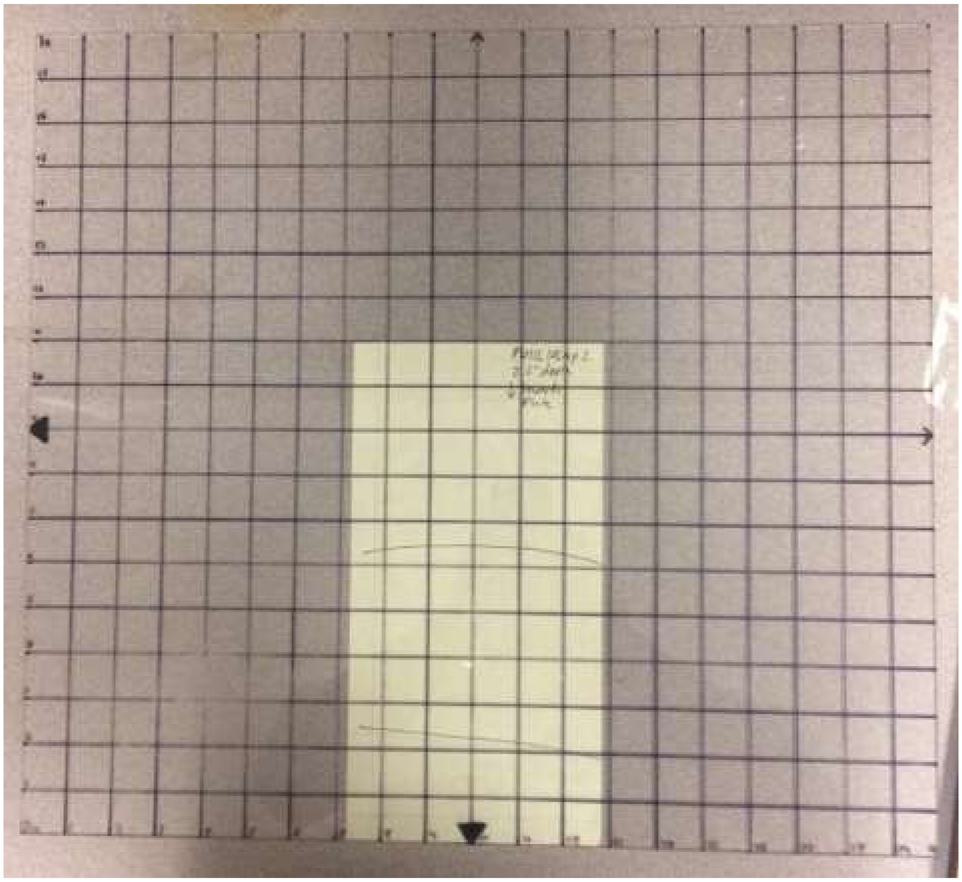

Figure 235: Test PW11L10Lay2 2.5" Depth

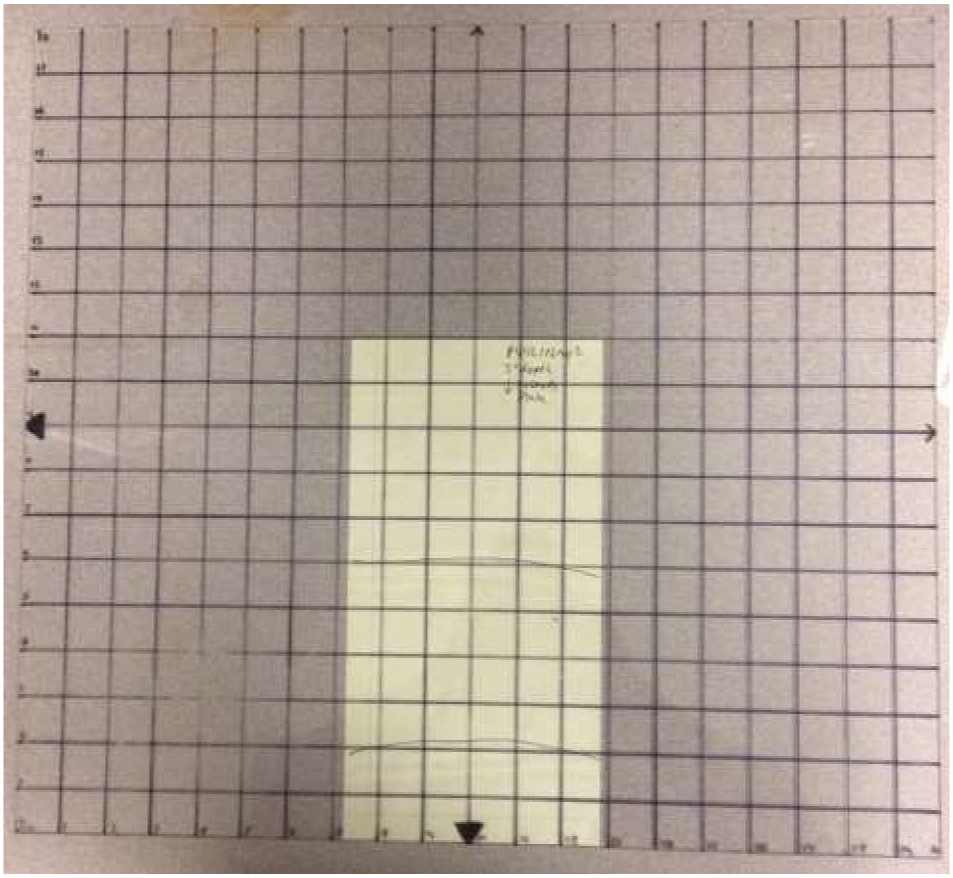

Figure 236: Test PW11L10Lay2 3" Depth

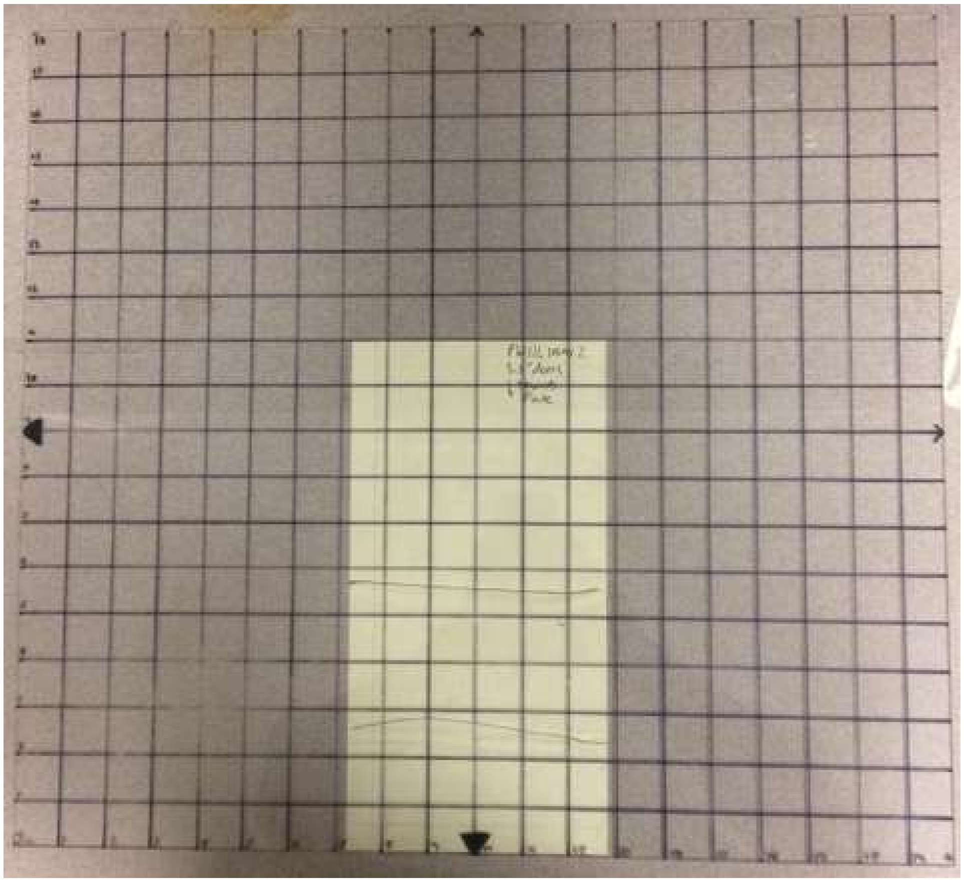

Figure 237: Test PW11L10Lay2 3.5" Depth

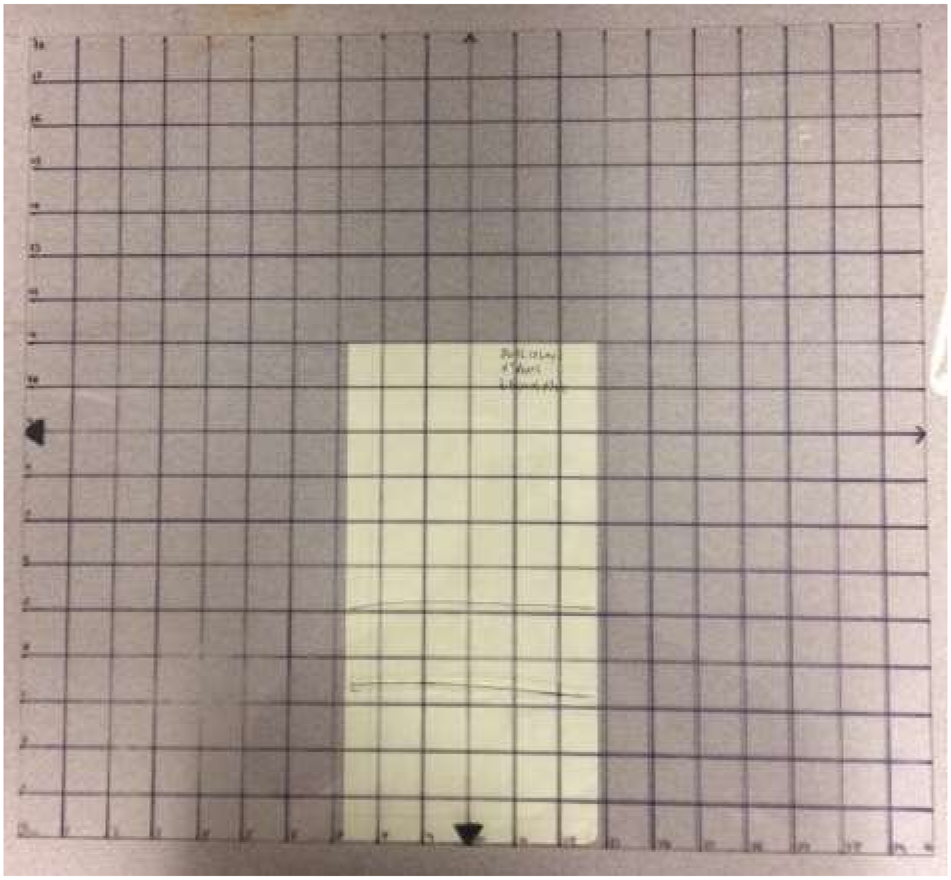

Figure 238: Test PW11L10Lay2 4” Depth

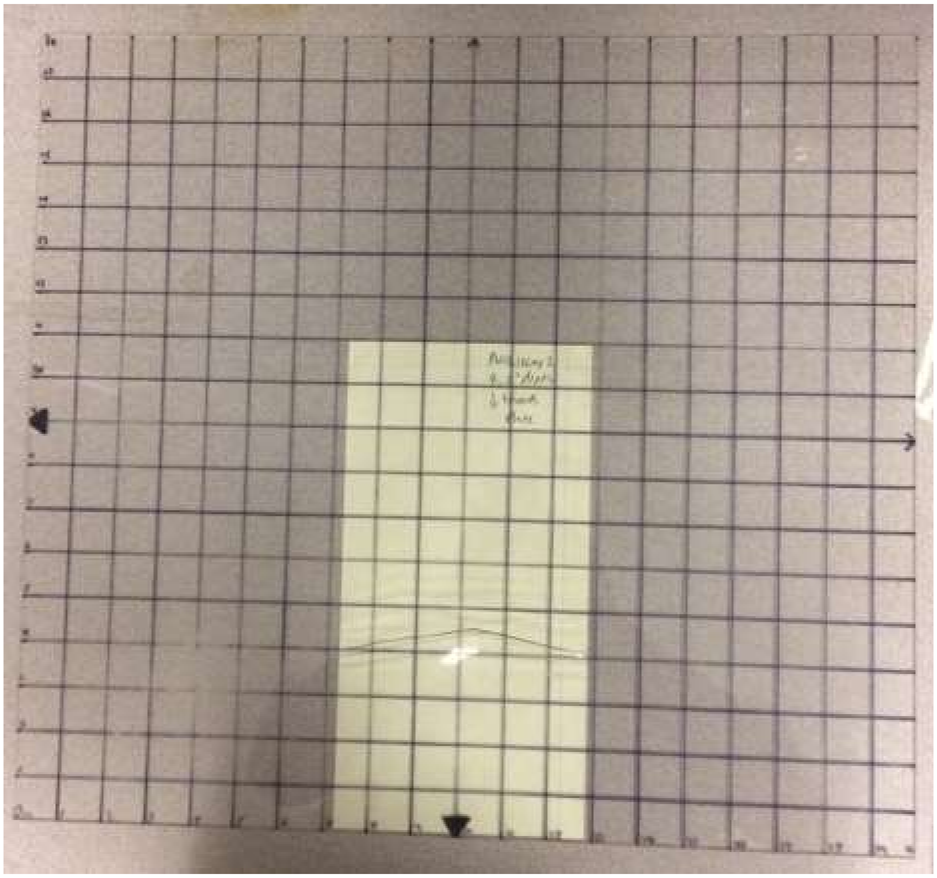

Figure 239: Test PW11L10Lay2 4.5" Depth

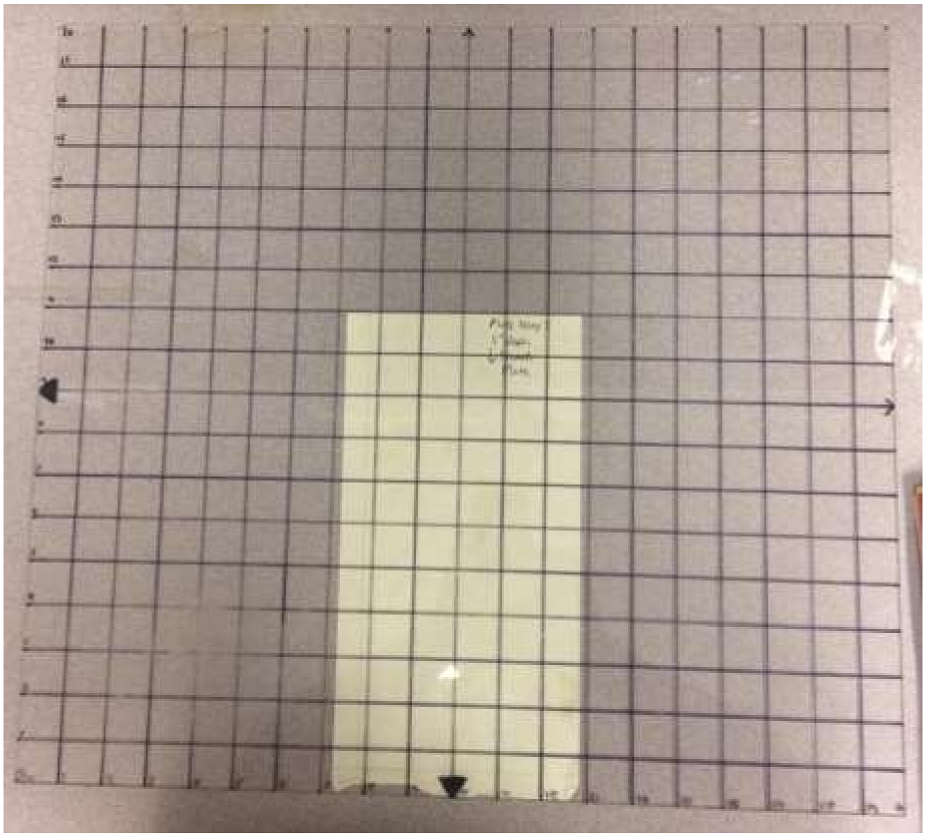

Figure 240: Test PW11L10Lay2 5” Depth

A.11 Photographs of Test 8W8L10Lay

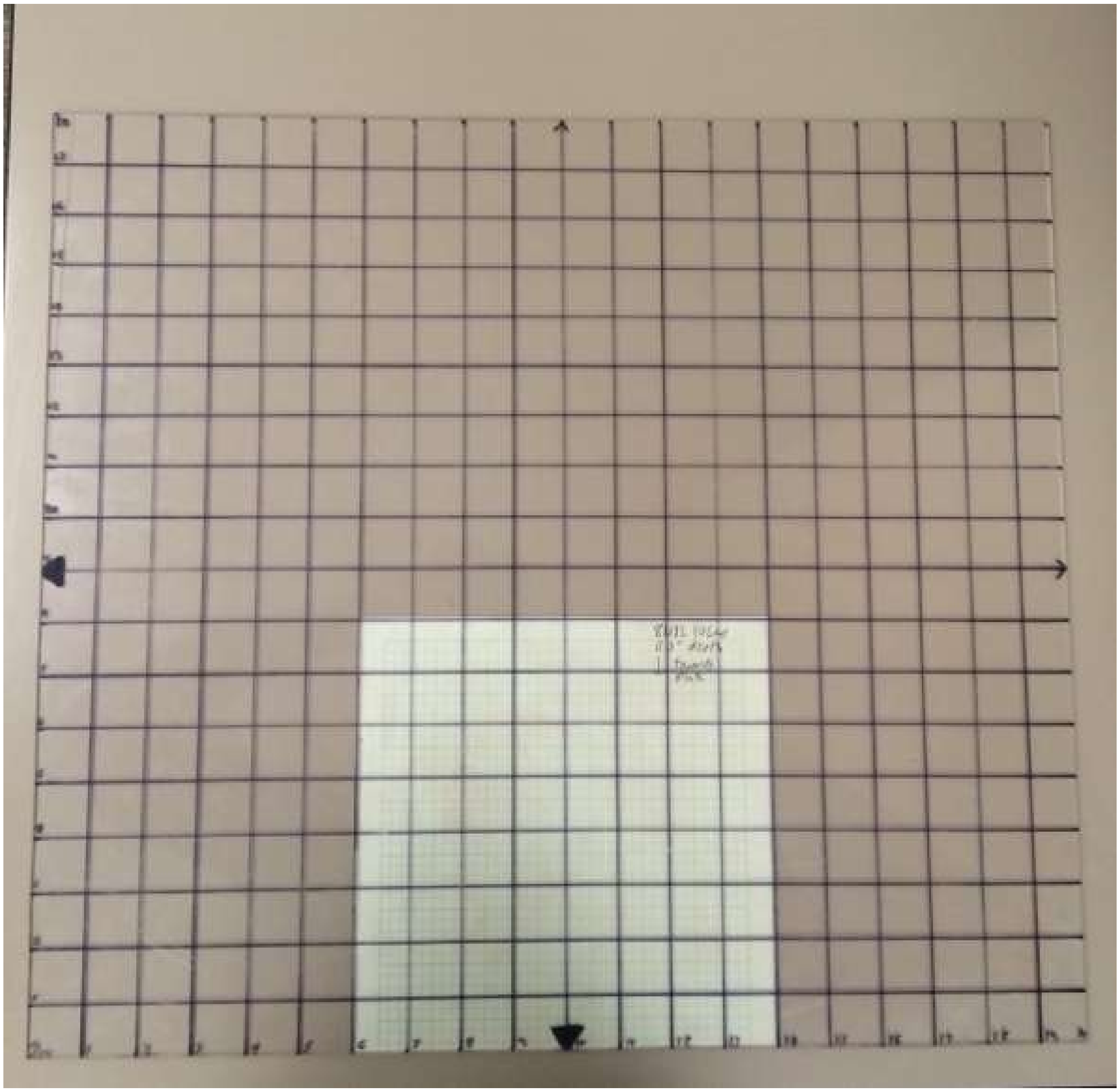

Figure 241: Test 8W8L10Lay 0.5” Depth

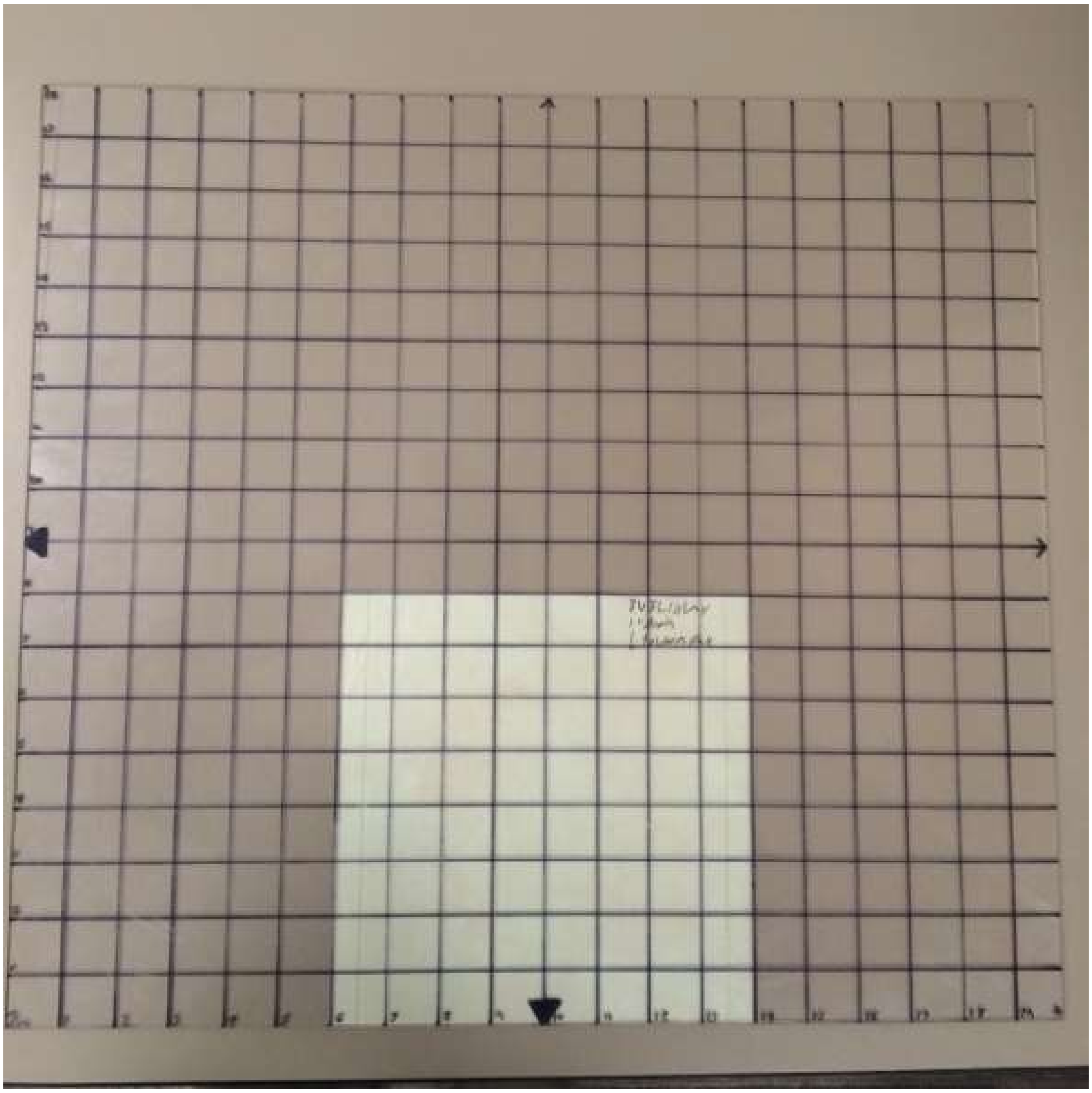

Figure 242: Test 8W8L10Lay 1" Depth

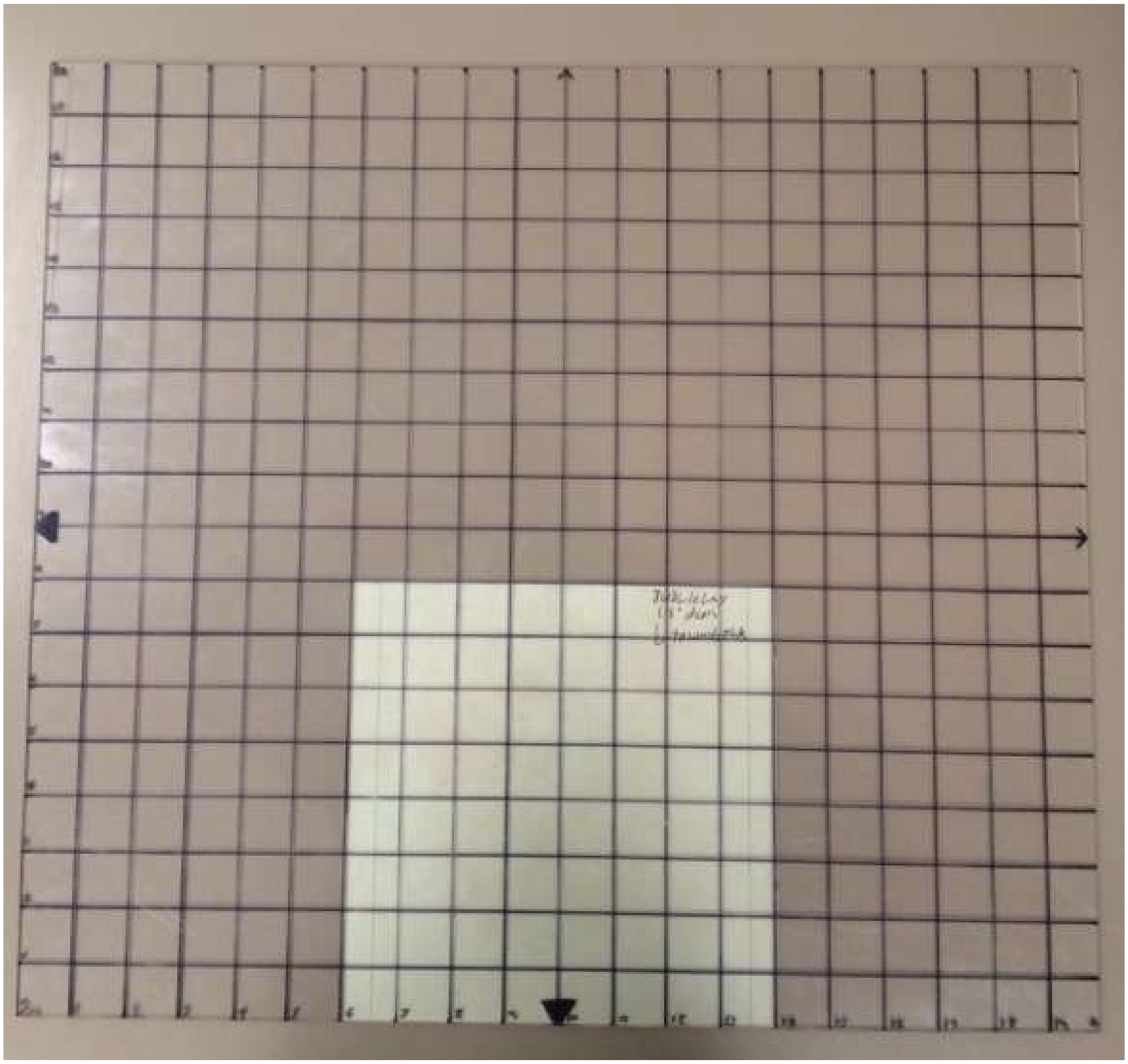

Figure 243: Test 8W8L10Lay 1.5” Depth

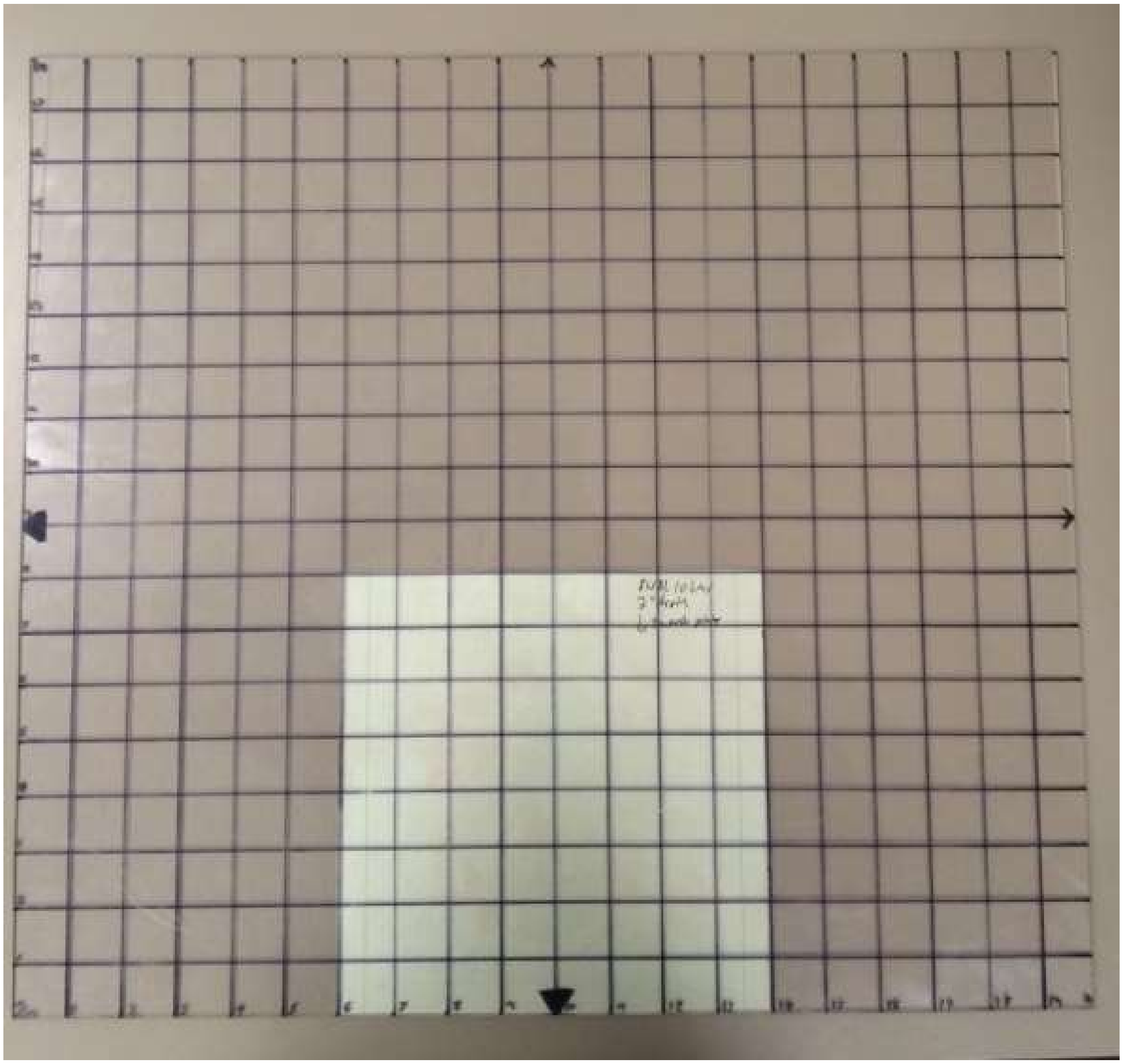

Figure 244: Test 8W8L10Lay 2” Depth

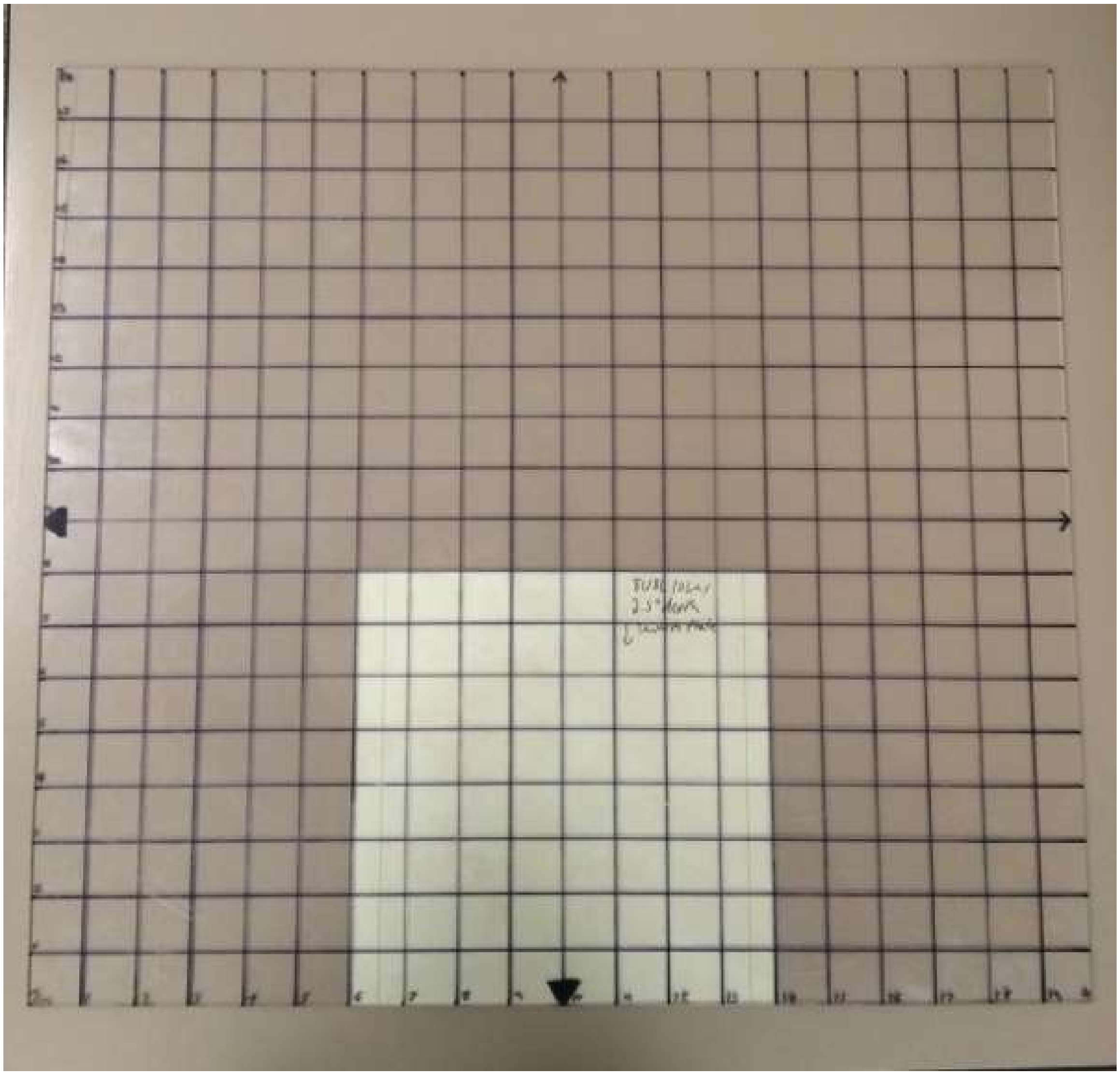

Figure 245: Test 8W8L10Lay 2.5" Depth

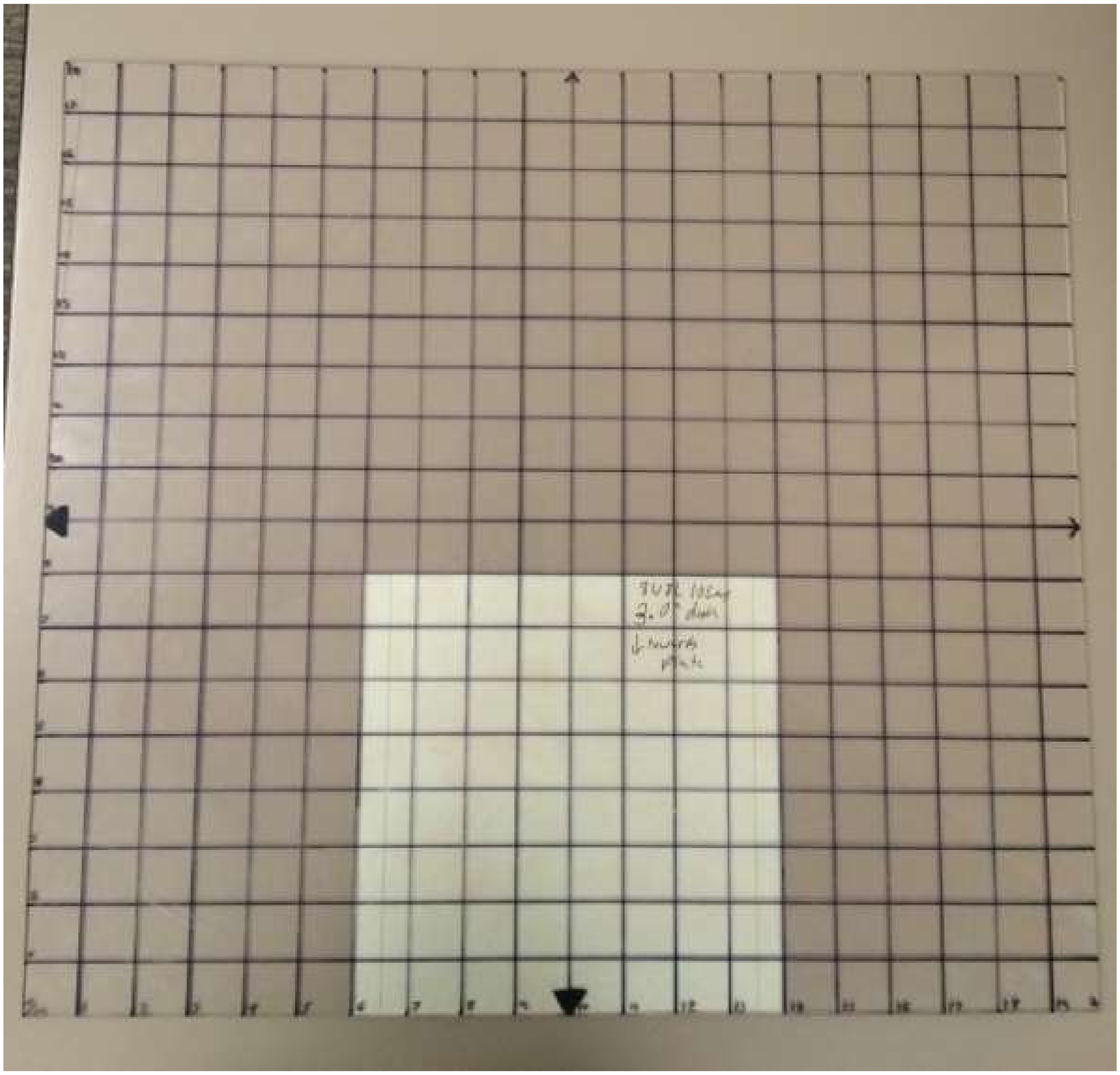

Figure 246: Test 8W8L10Lay 3" Depth

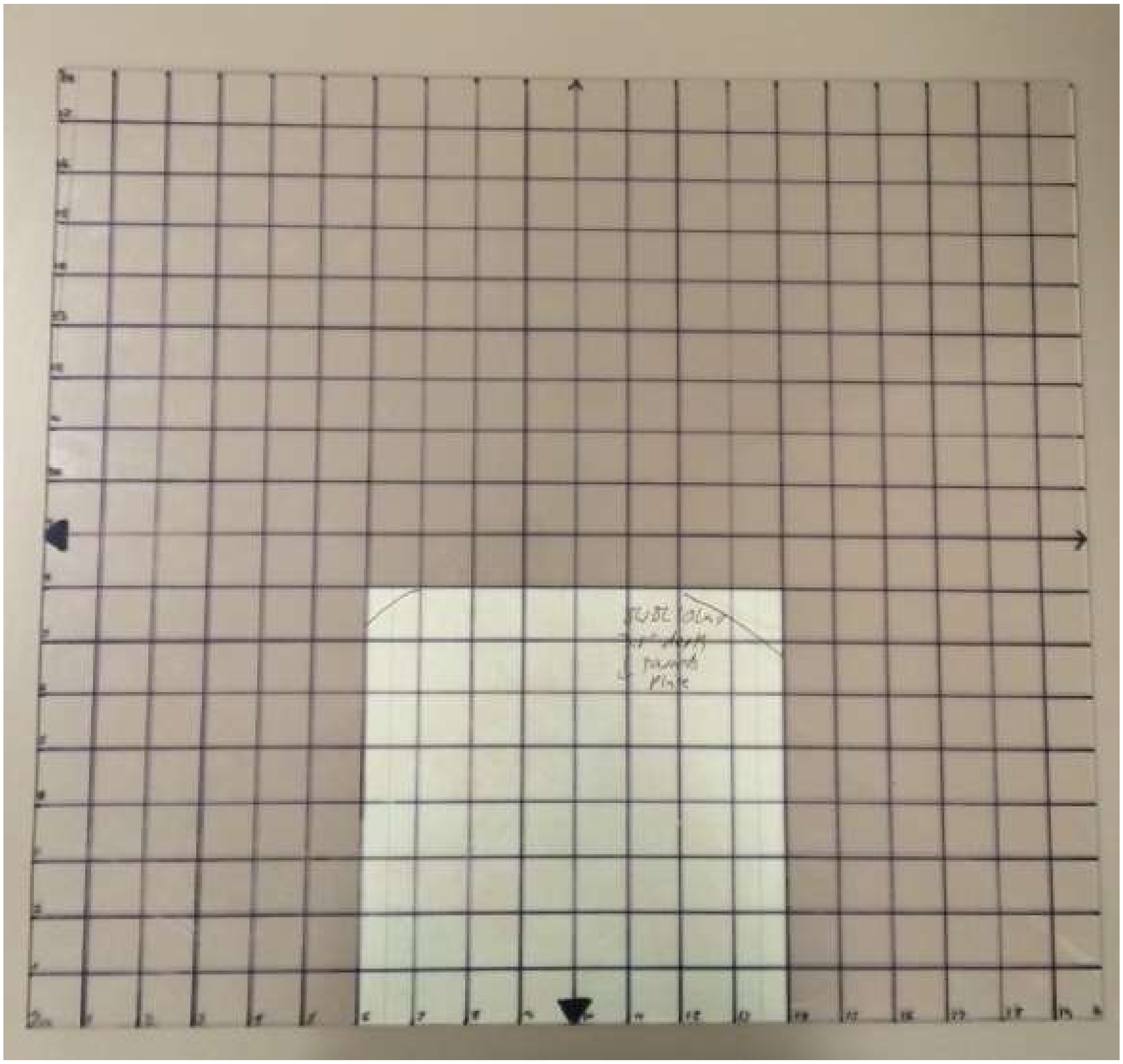

Figure 247: Test 8W8L10Lay 3.5" Depth

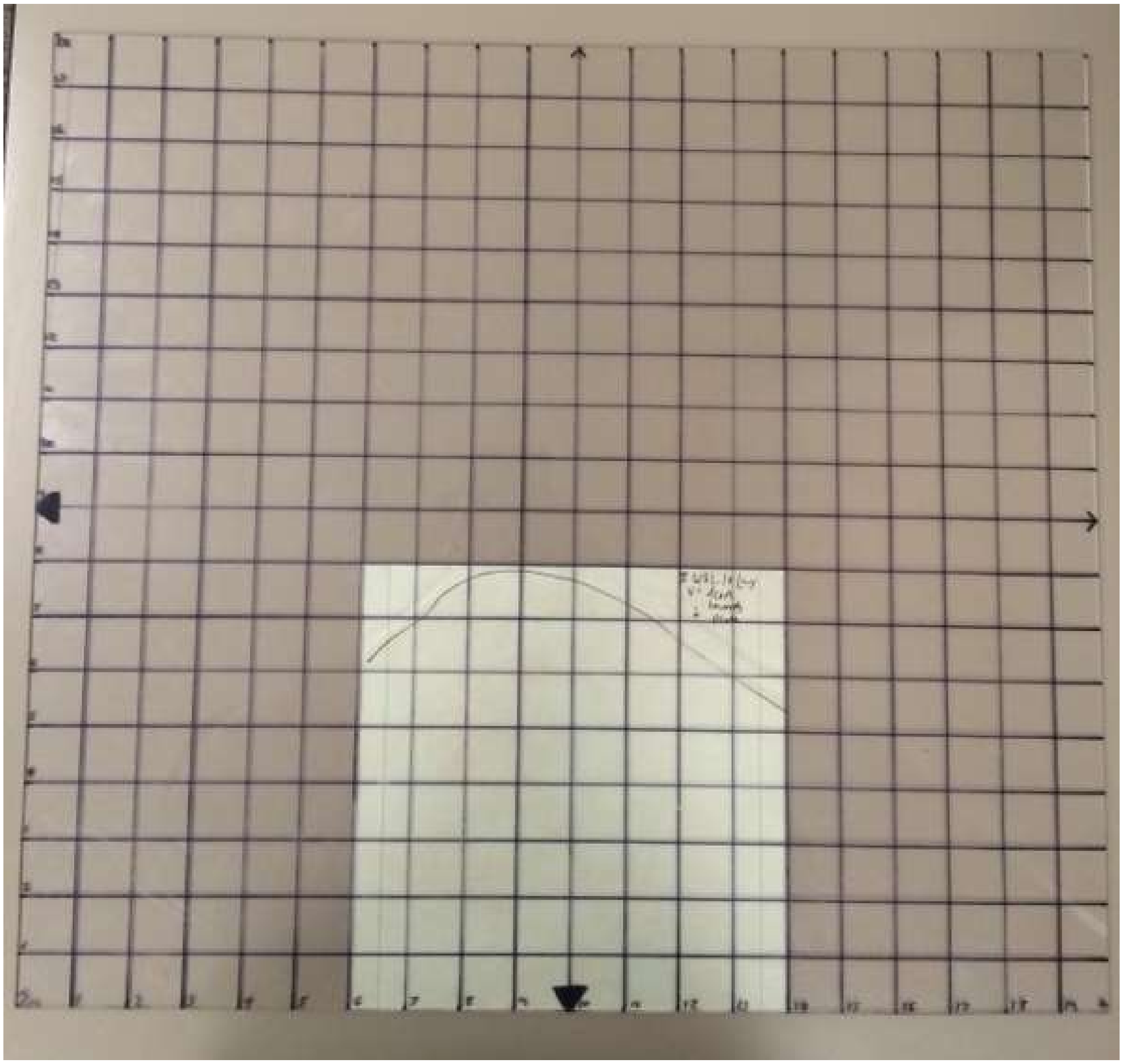

Figure 248: Test 8W8L10Lay 4” Depth

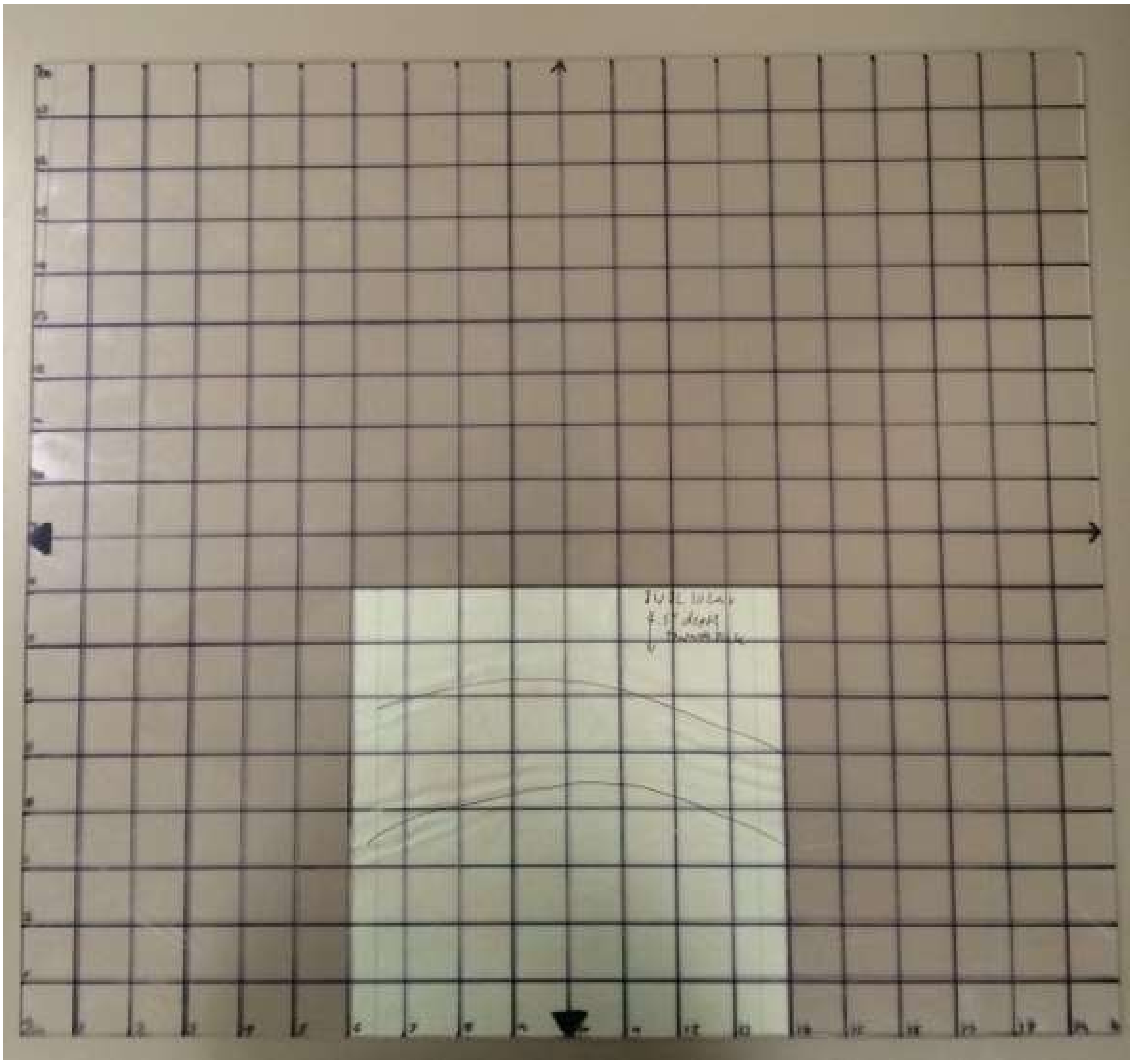

Figure 249: 8W8L10Lay 4.5” Depth

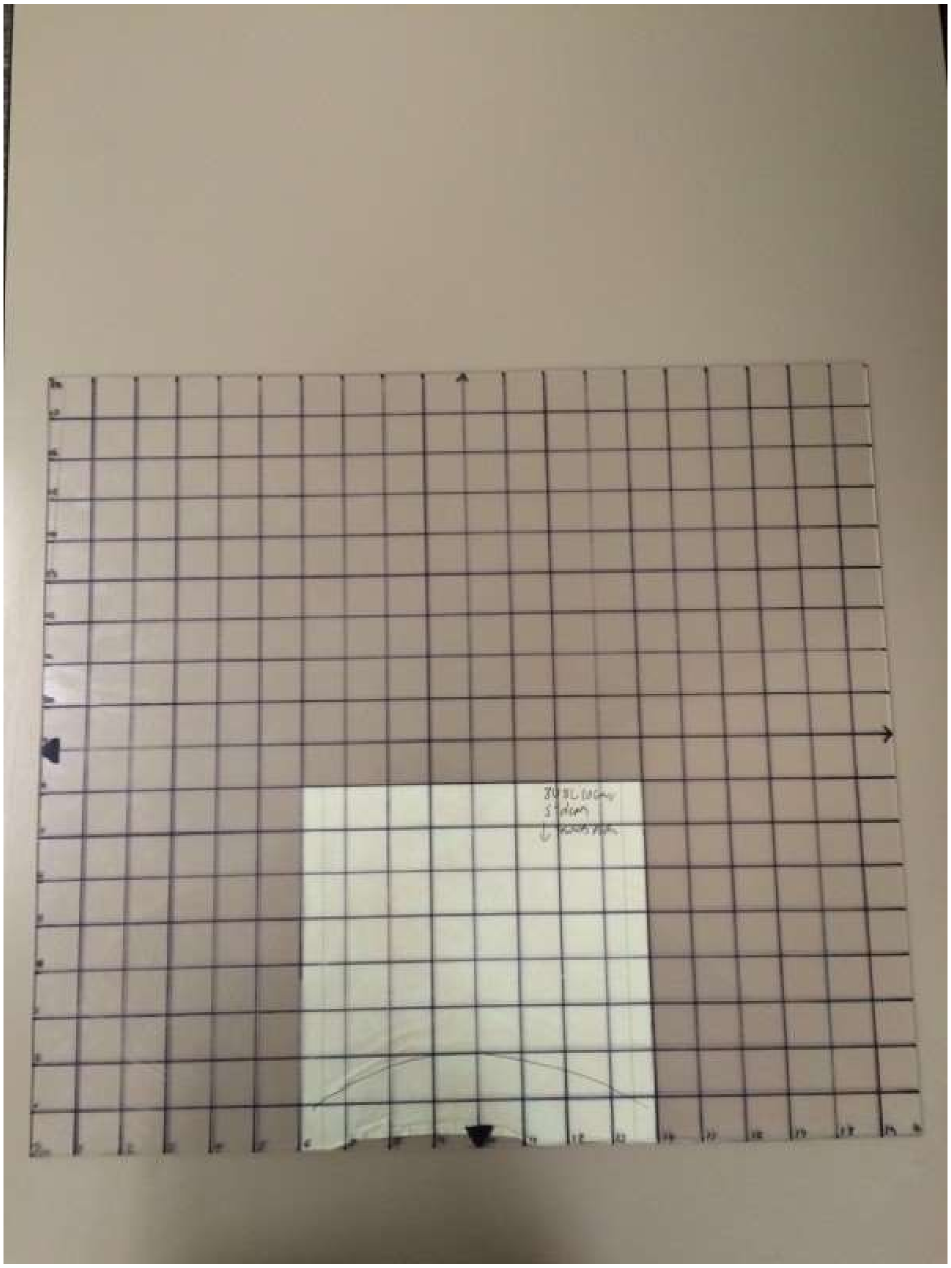

Figure 250: Test 8W8L10Lay 5” Depth

A.12 Photographs of Test 8W8L10Lay2

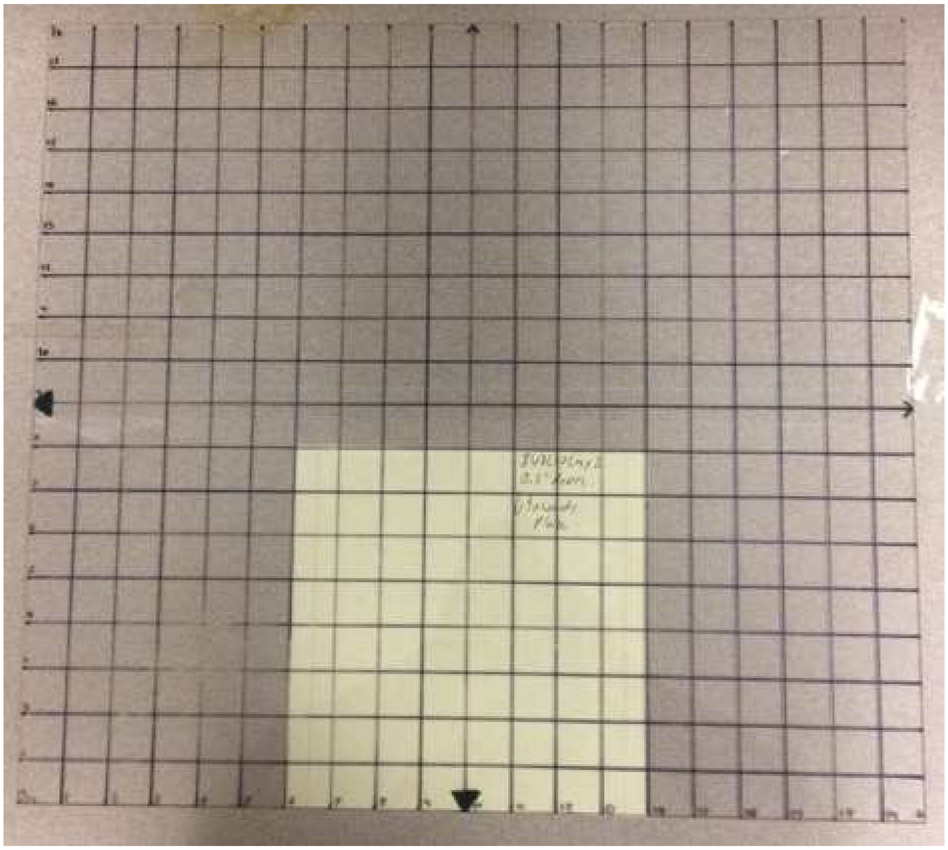

Figure 251: Test 8W8L10Lay2 0.5” Depth

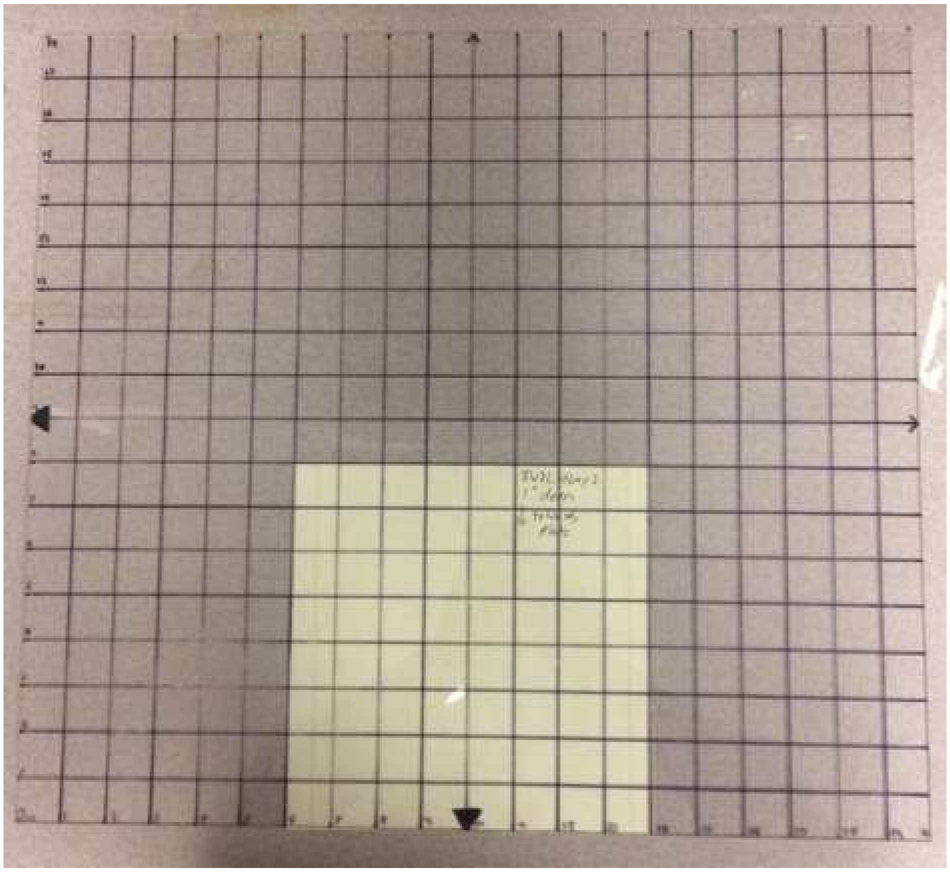

Figure 252: Test 8W8L10Lay2 1" Depth

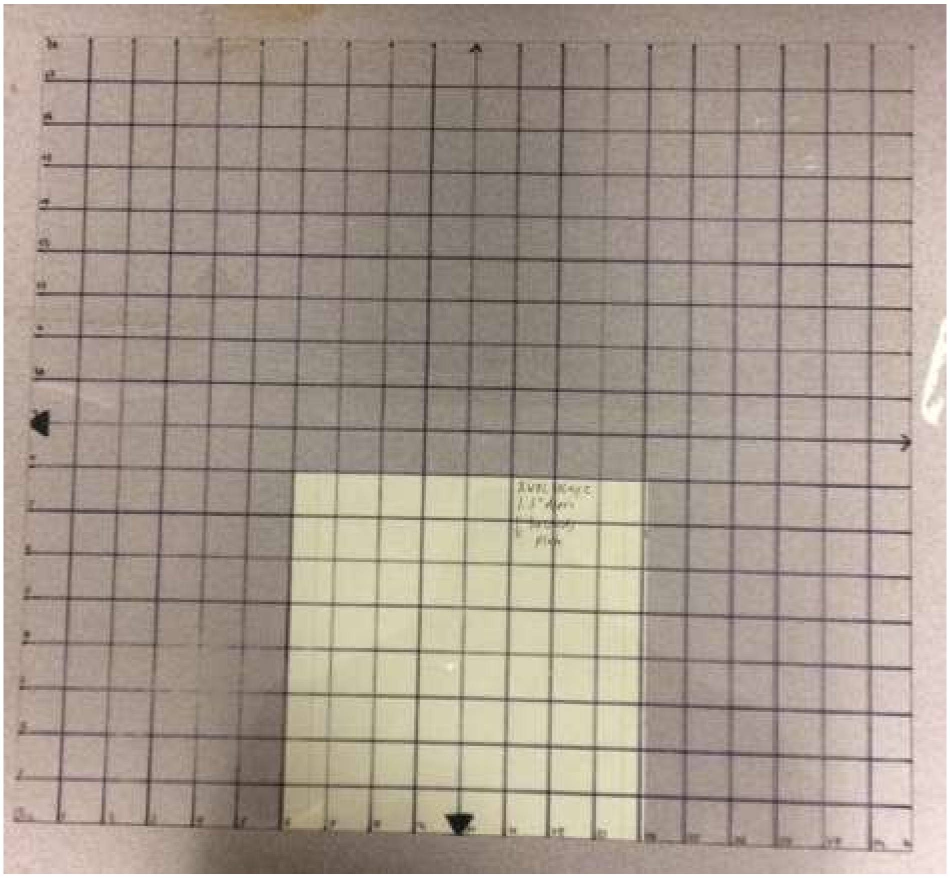

Figure 253: Test 8W8L10Lay2 1.5" Depth

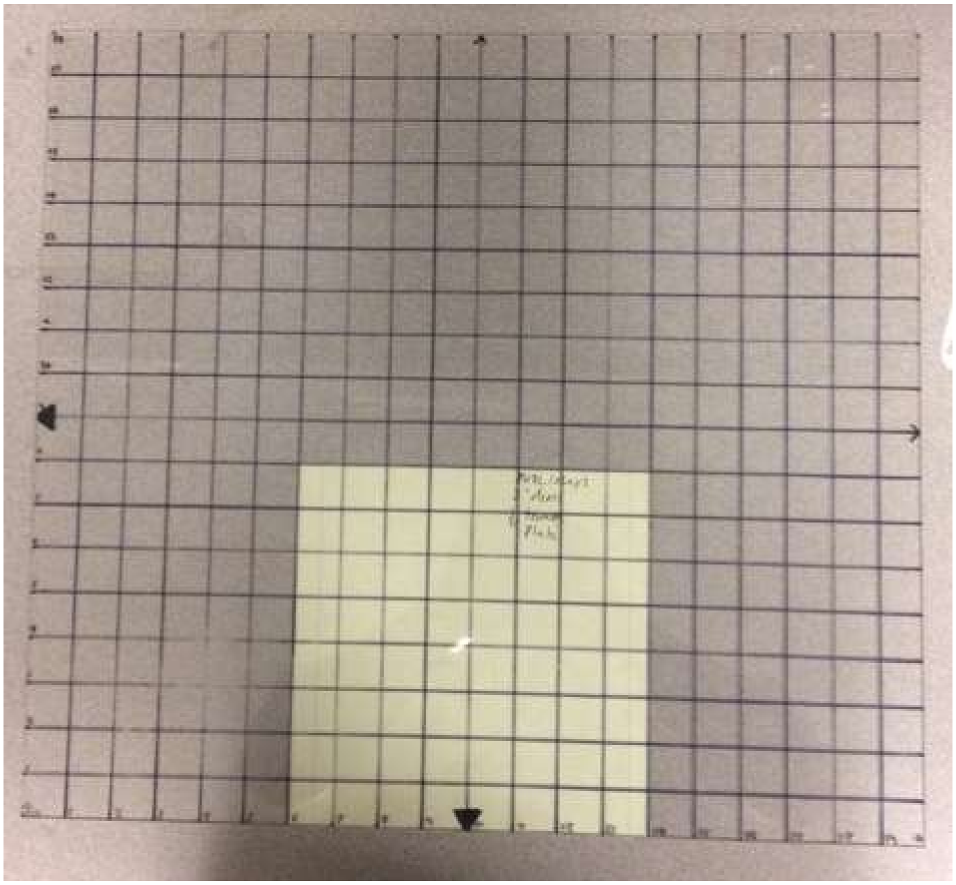

Figure 254: Test 8W8L10Lay2 2” Depth

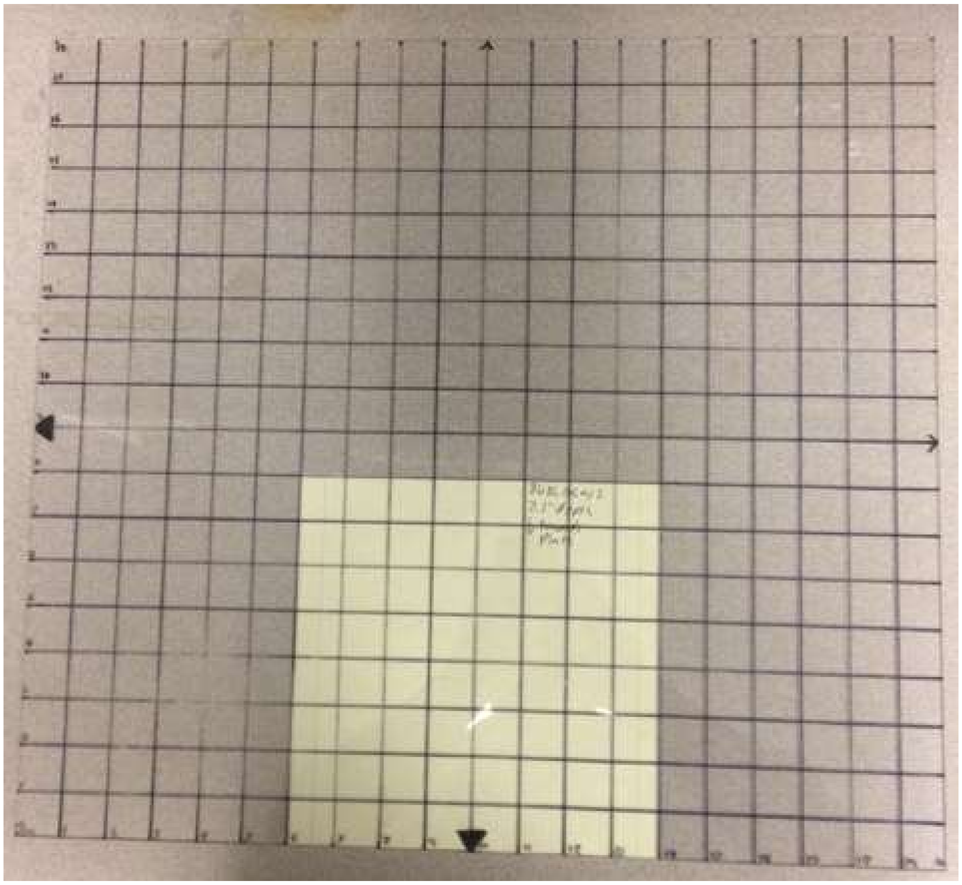

Figure 255: Test 8W8L10Lay2 2.5" Depth

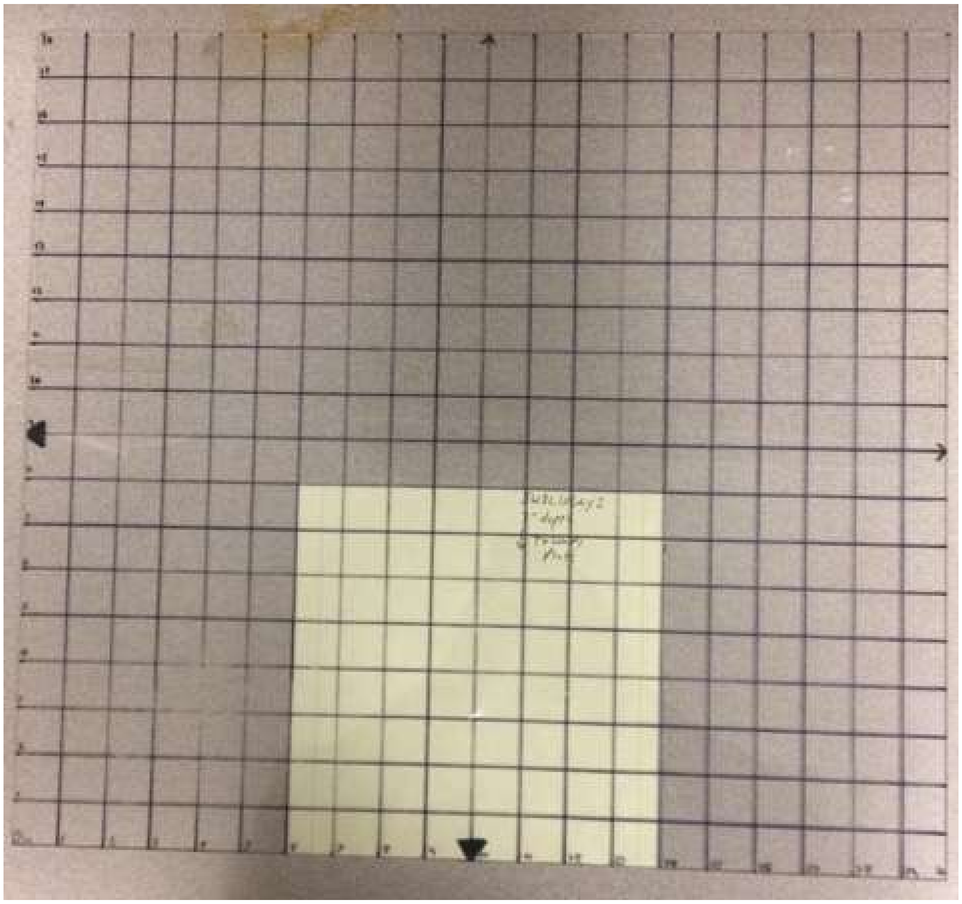

Figure 256: Test 8W8L10Lay2 3” Depth

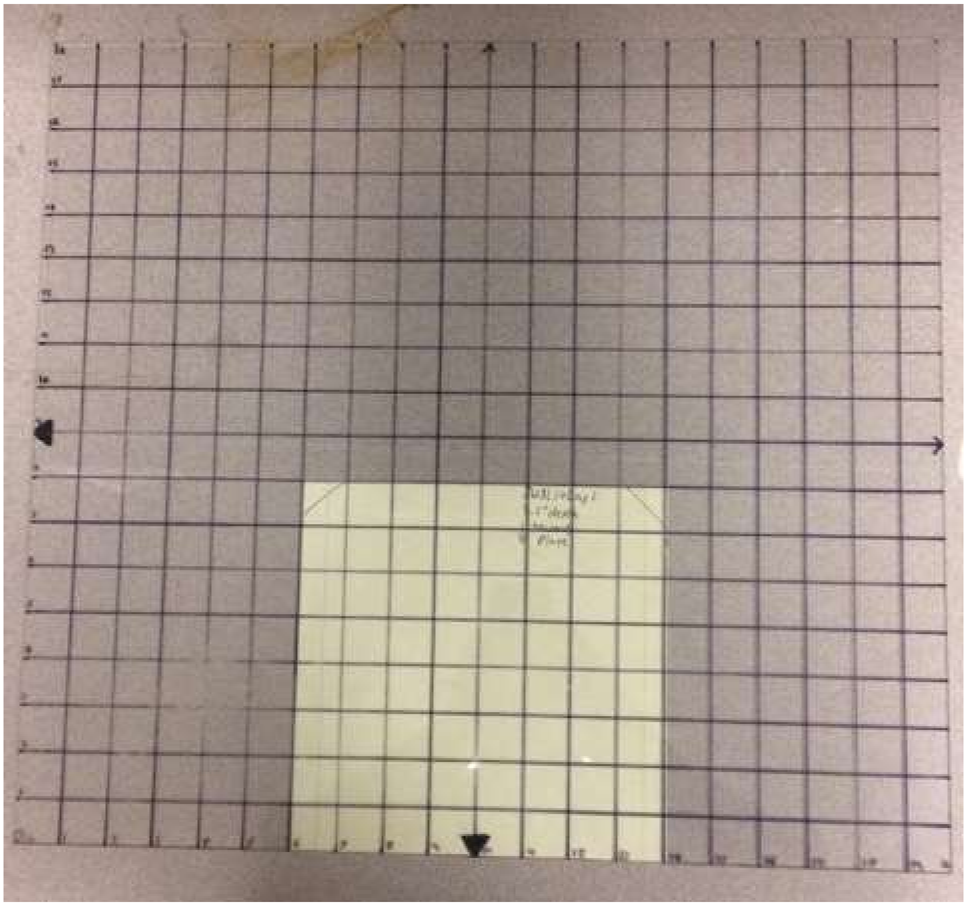

Figure 257: Test 8W8L10Lay2 3.5" Depth

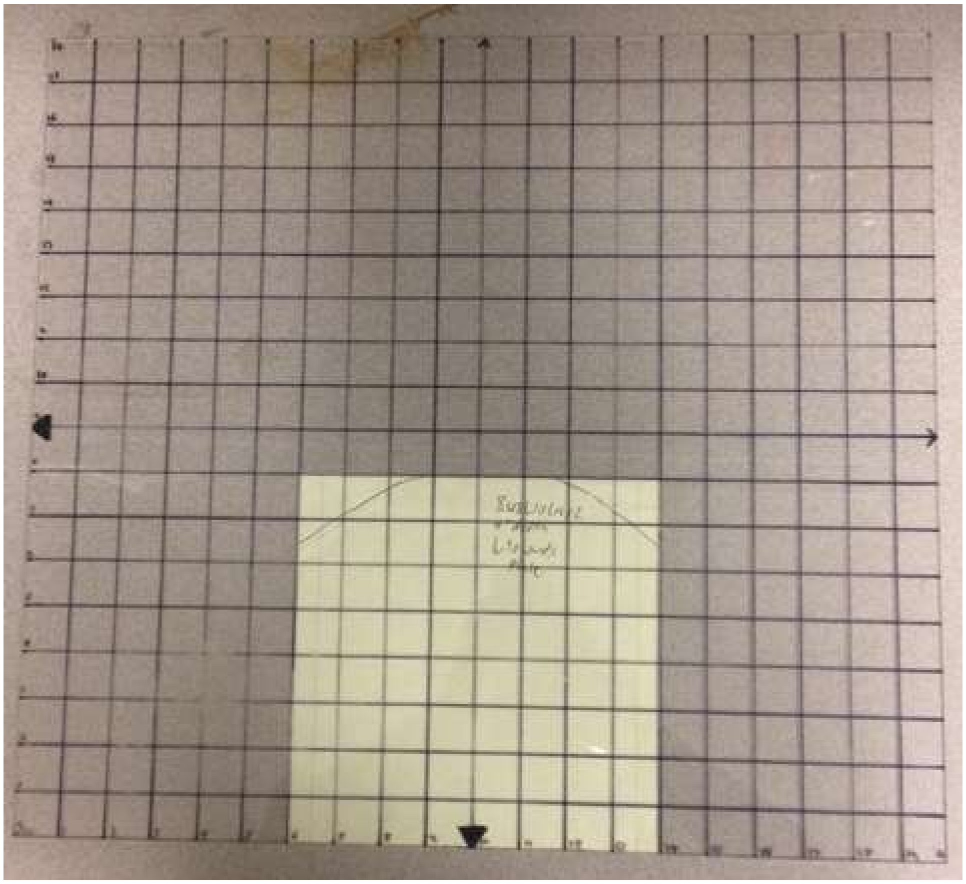

Figure 258: Test 8W8L10Lay2 4" Depth

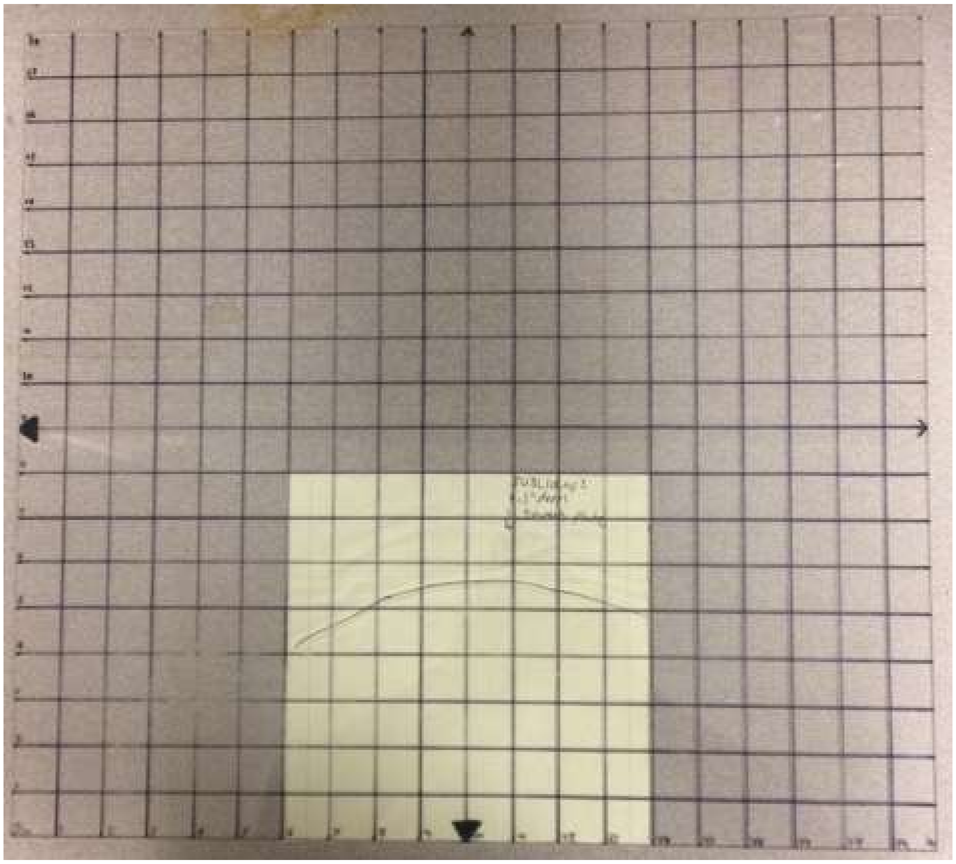

Figure 259: Test 8W8L10Lay2 4.5” Depth

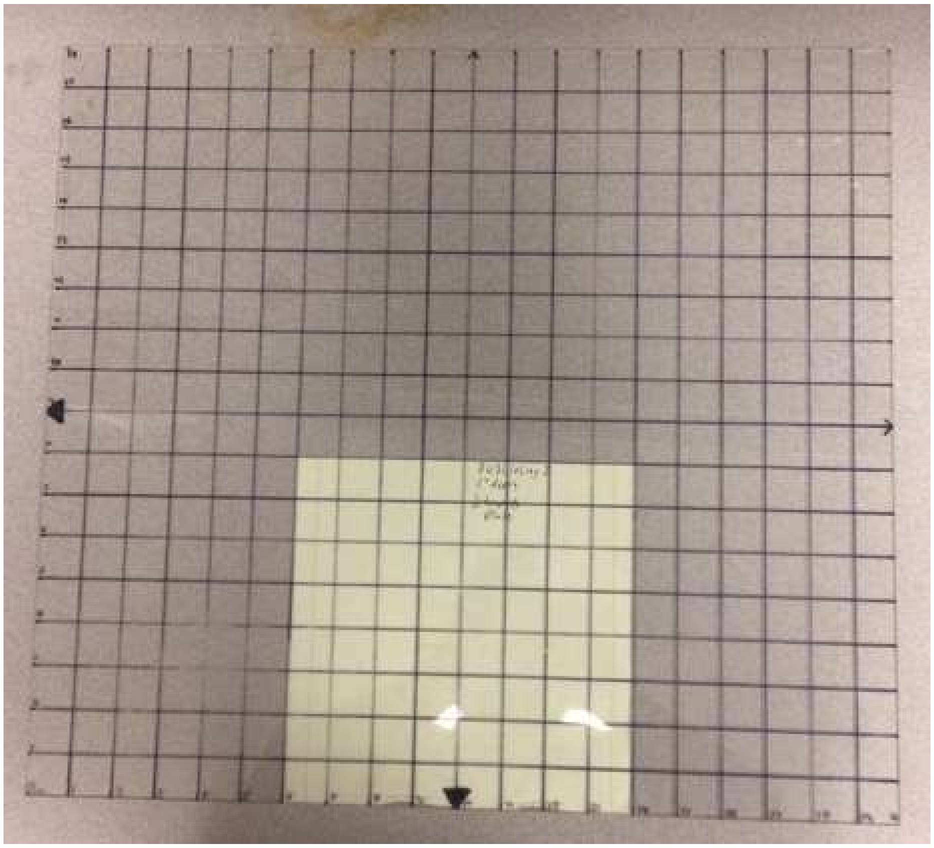

Figure 260: Test 8W8L10Lay2 5” Depth

A.12 Photographs of Test 11W8L5Lay3

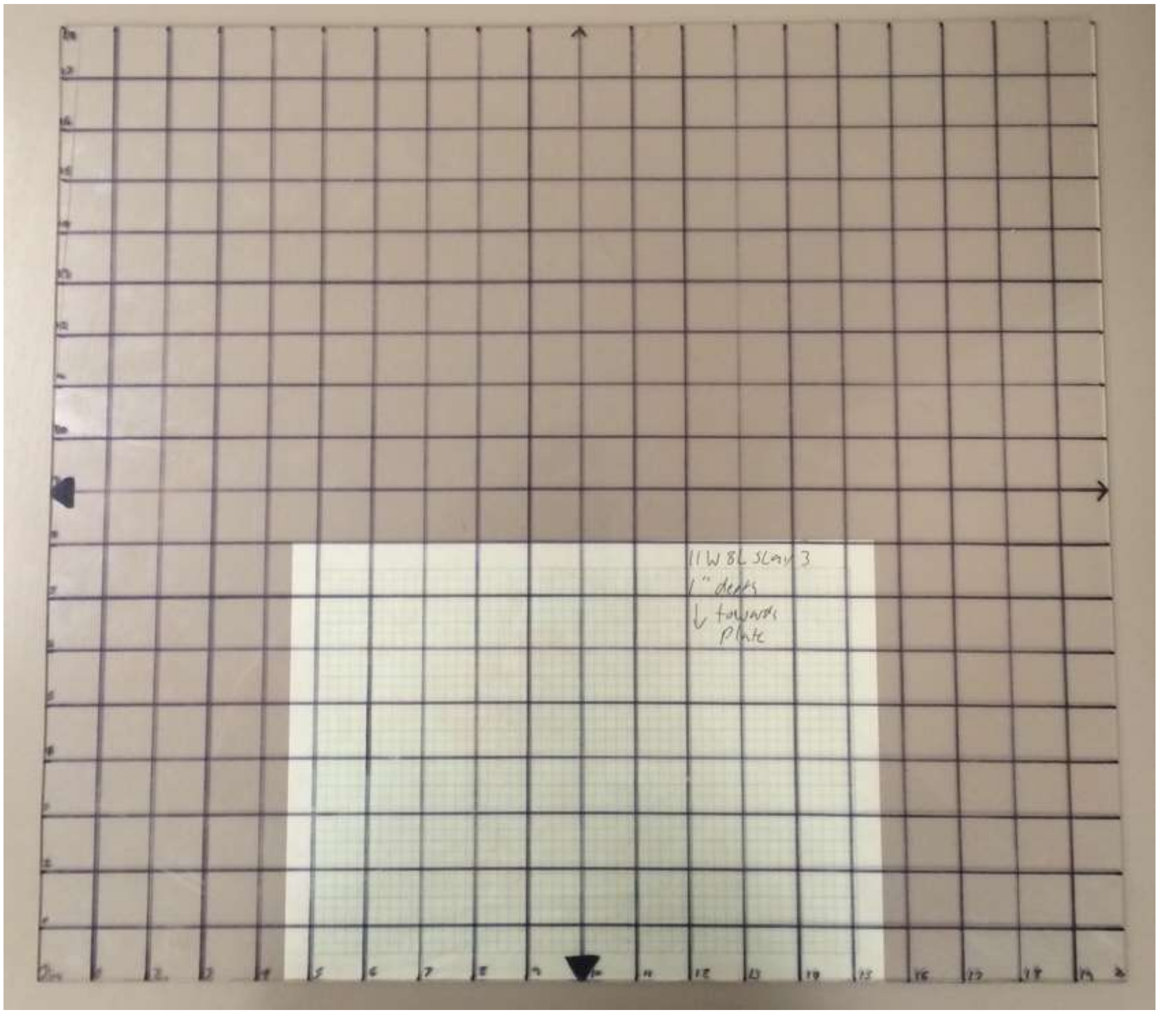

Figure 261: Test 11W8L5Lay3 1” Depth

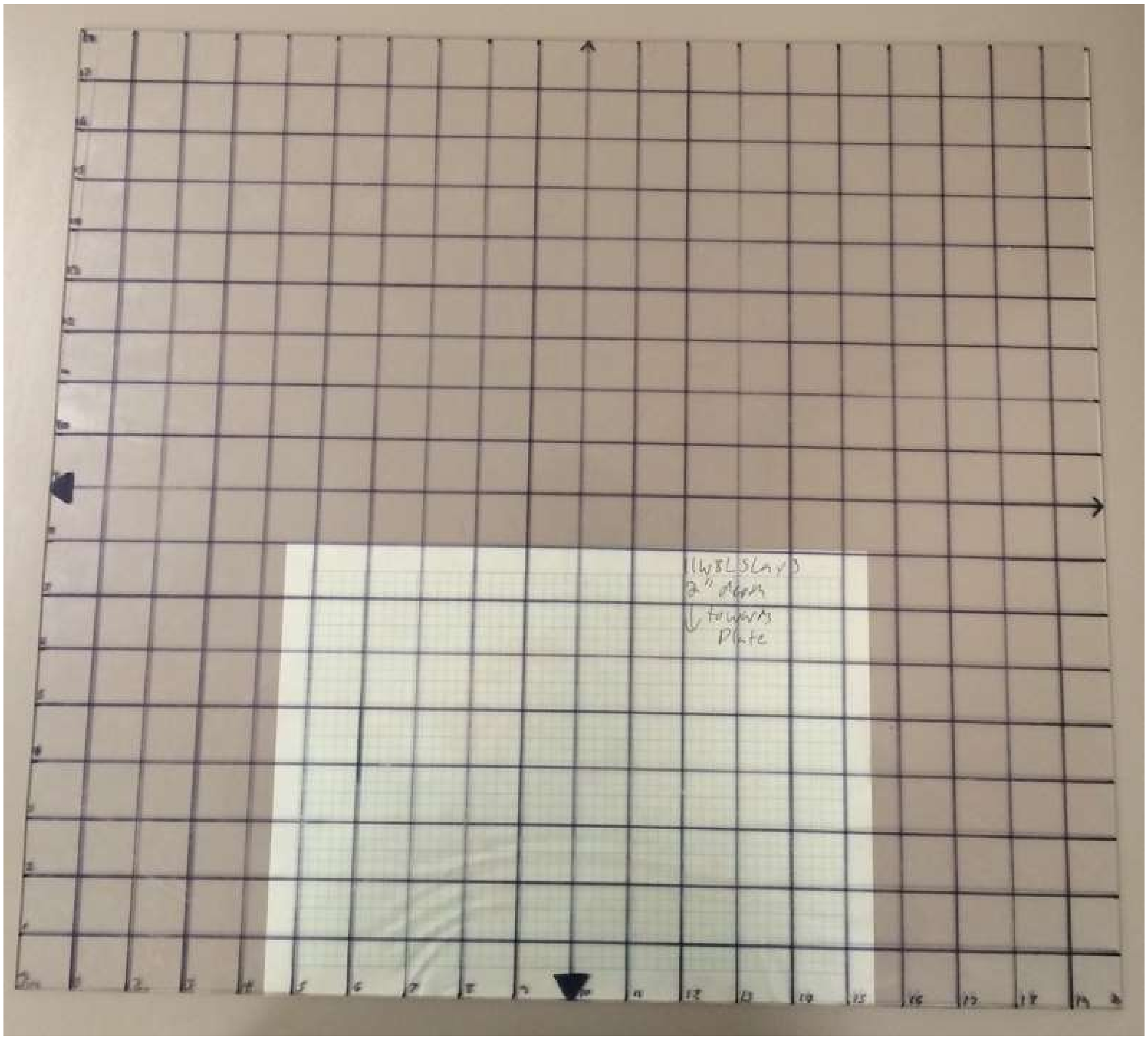

Figure 262: Test 11W8L5Lay3 2" Depth

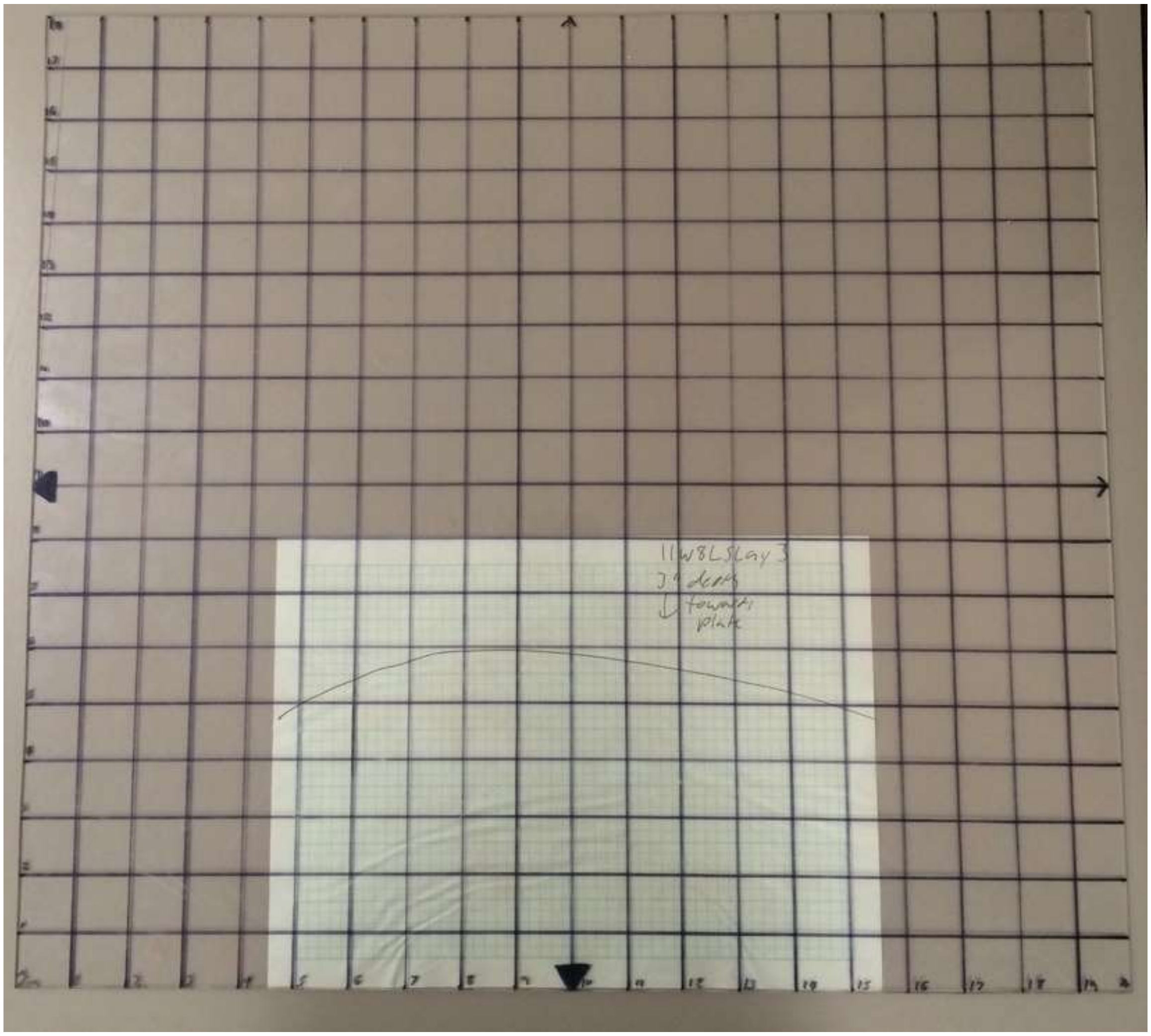

Figure 263: Test 11W8L5Lay3 3" Depth

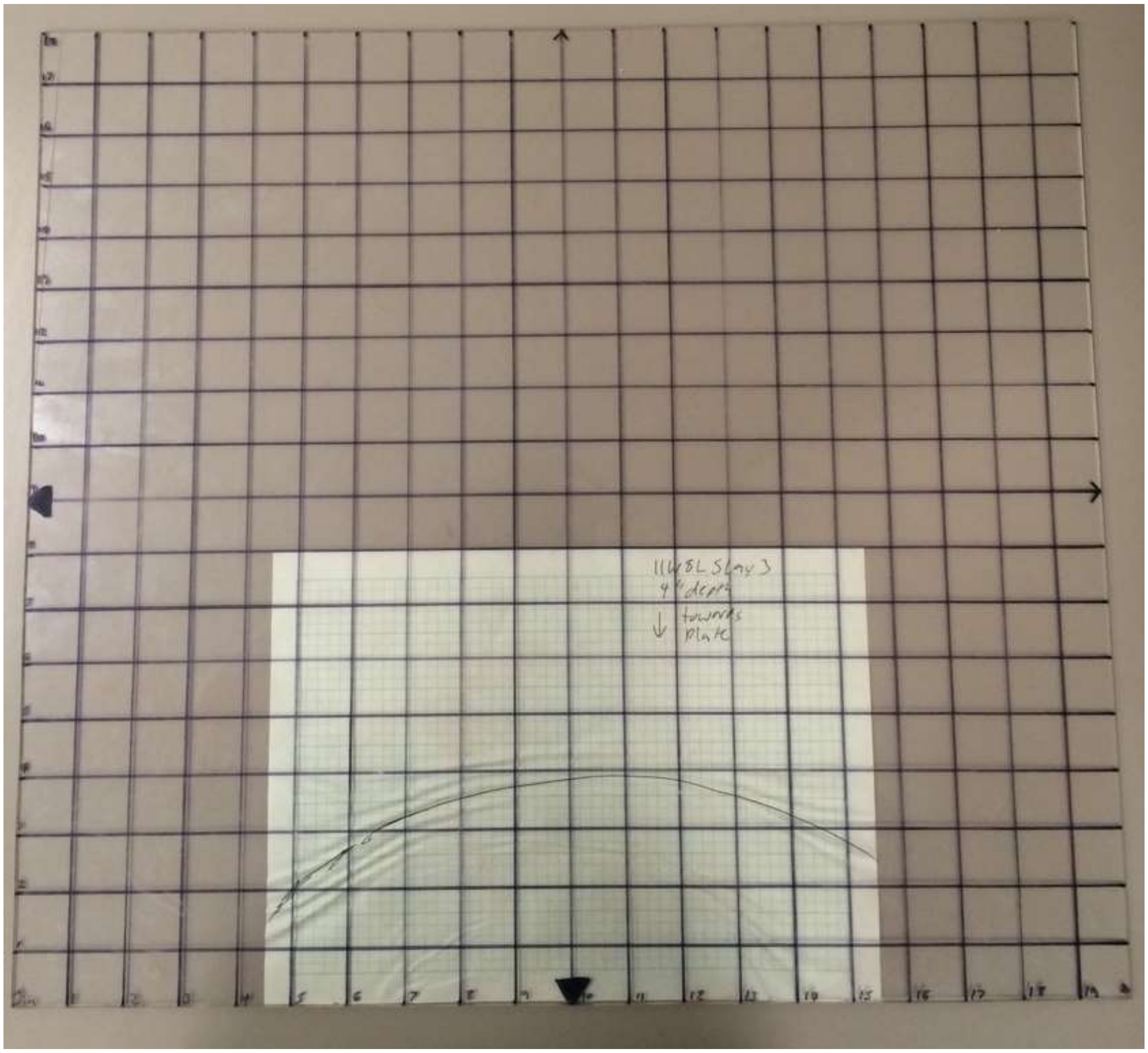

Figure 264: Test 11W8L5Lay3 4" Depth

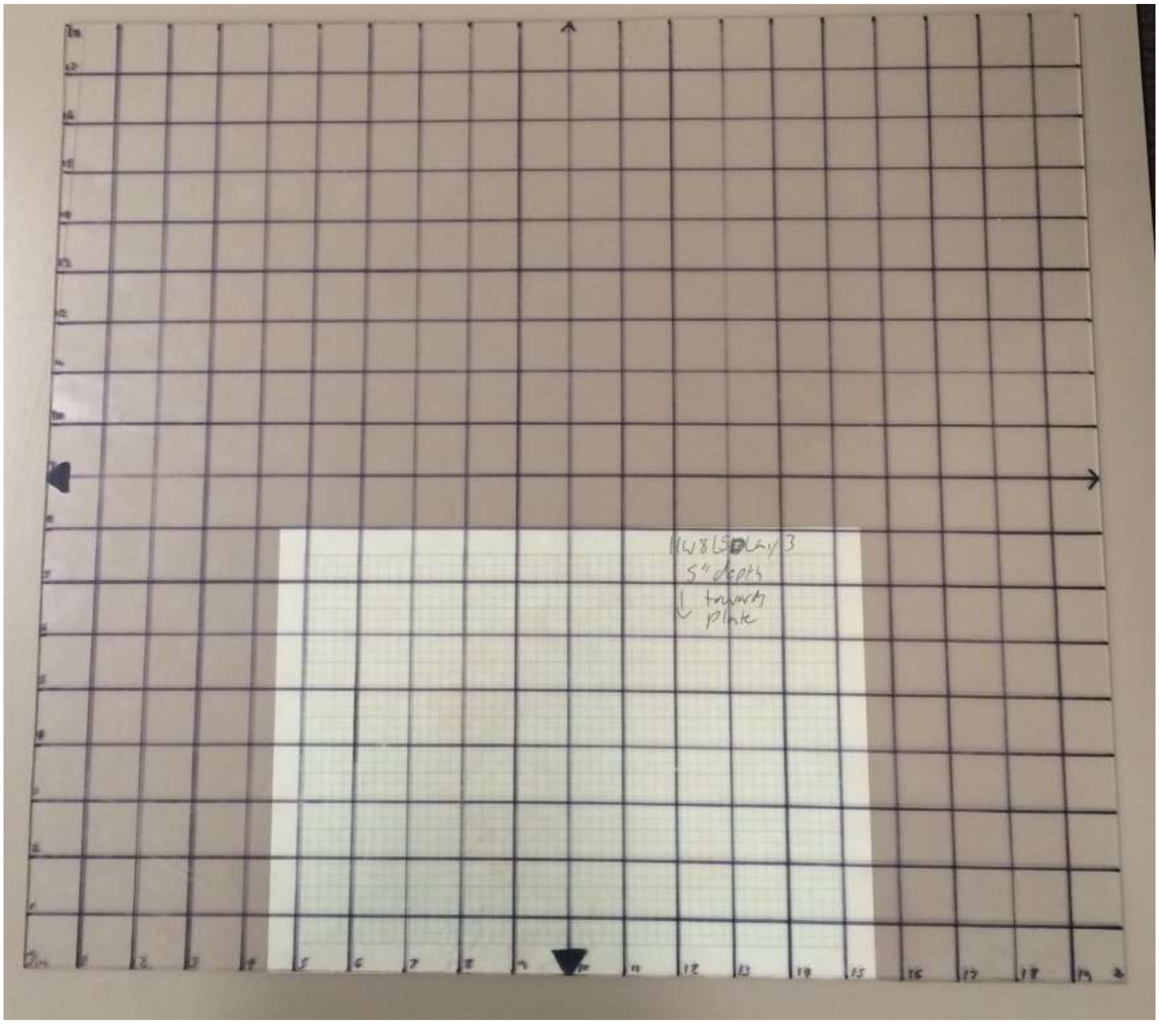

Figure 265: Test 11W8L5Lay3 5” Depth

A.13 Photographs of Test 11W8L5Lay2

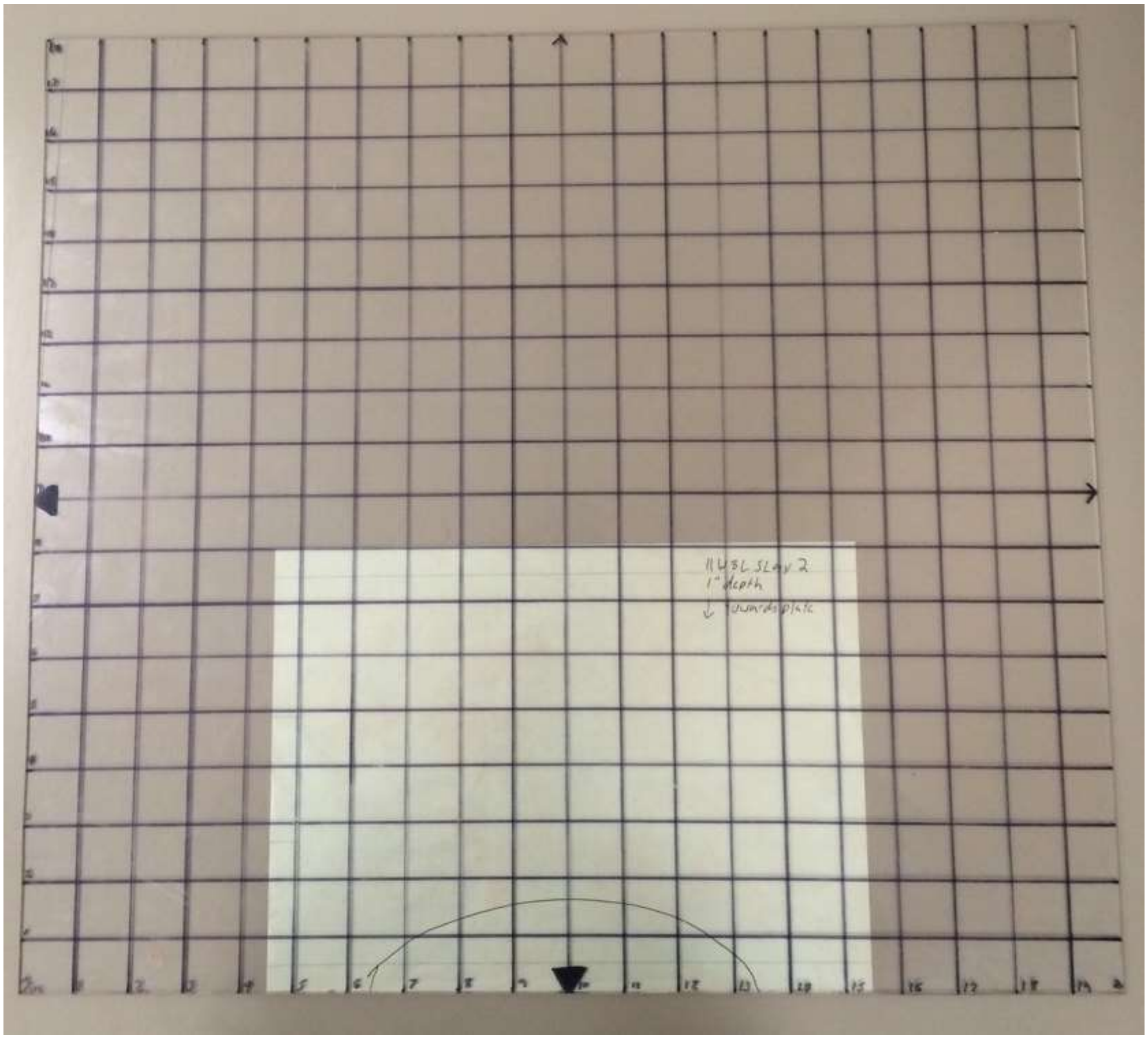

Figure 266: Test 11W8L5Lay2 1" Depth

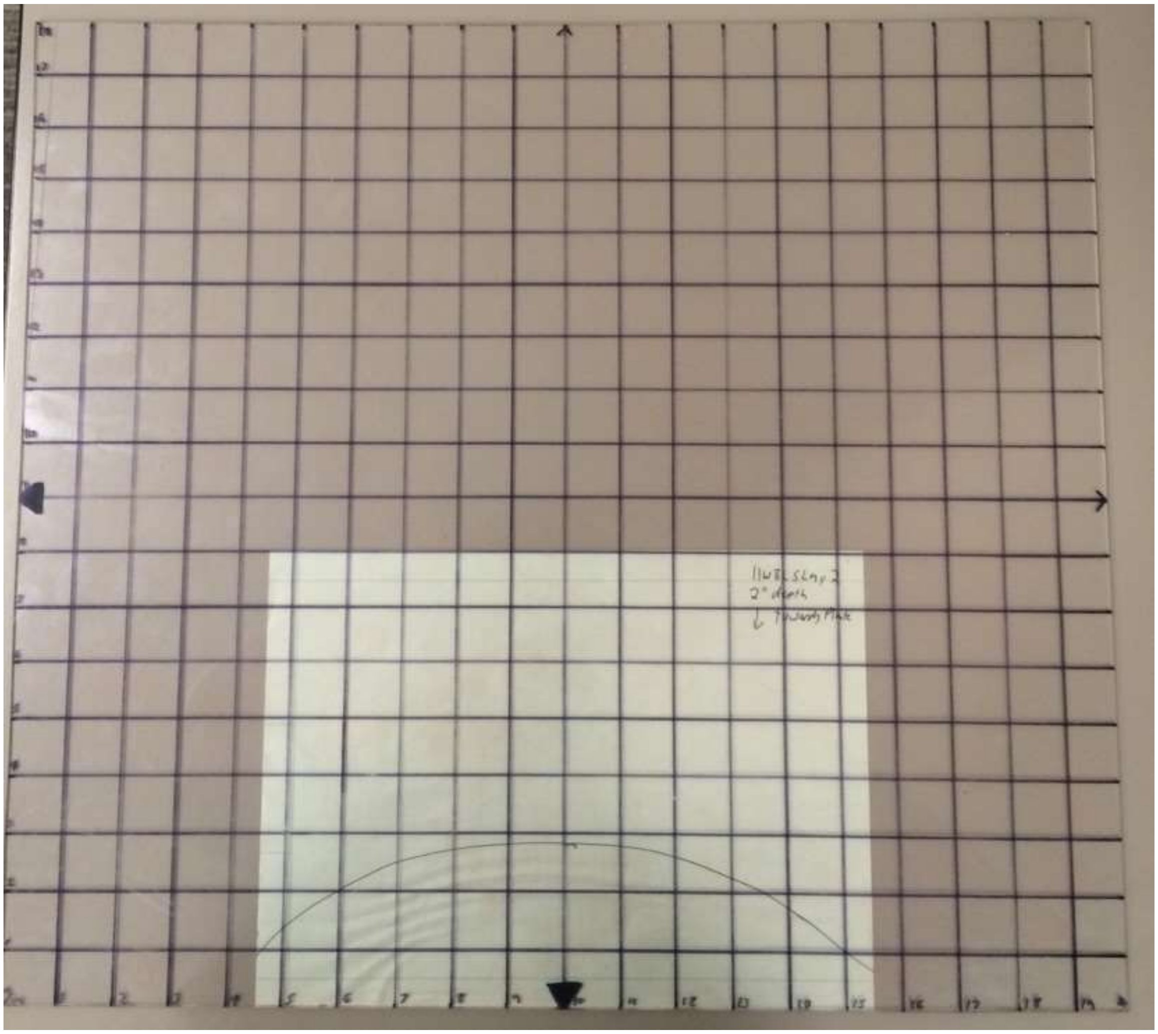

Figure 267: Test 11W8L5Lay2 2” Depth

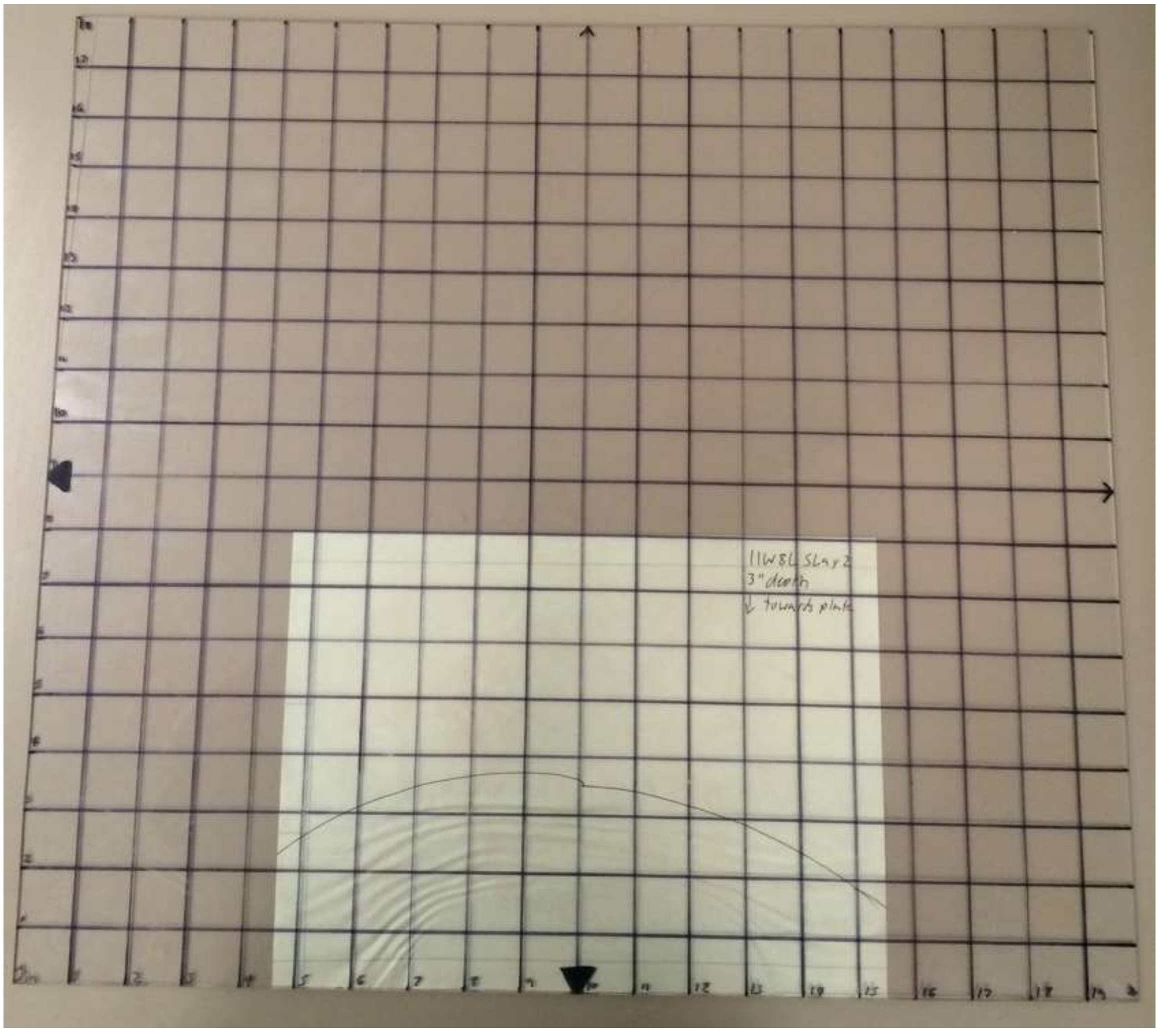

Figure 268: Test 11W8L5Lay2 3" Depth

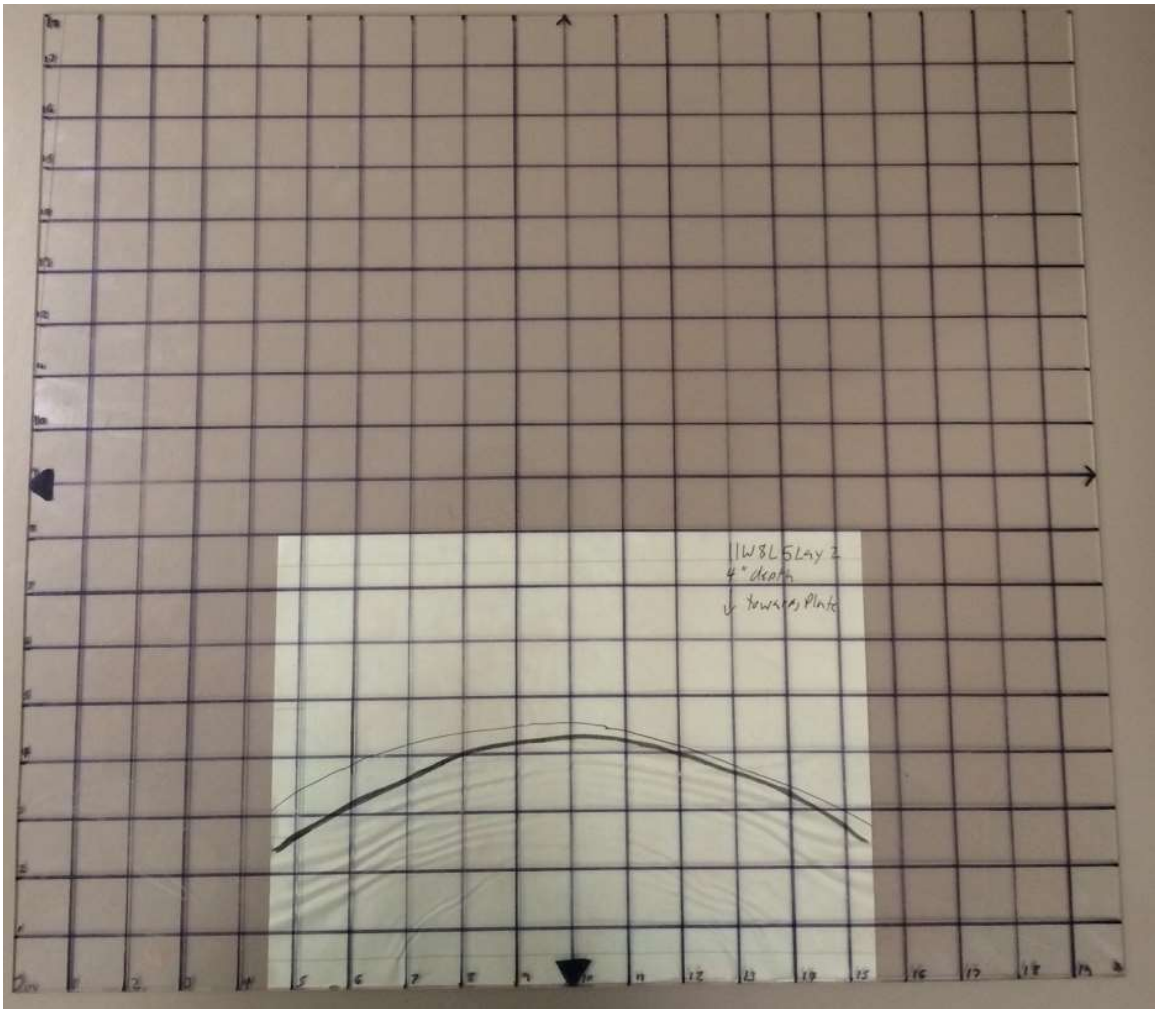

Figure 269: Test 11W8L5Lay2 4" Depth

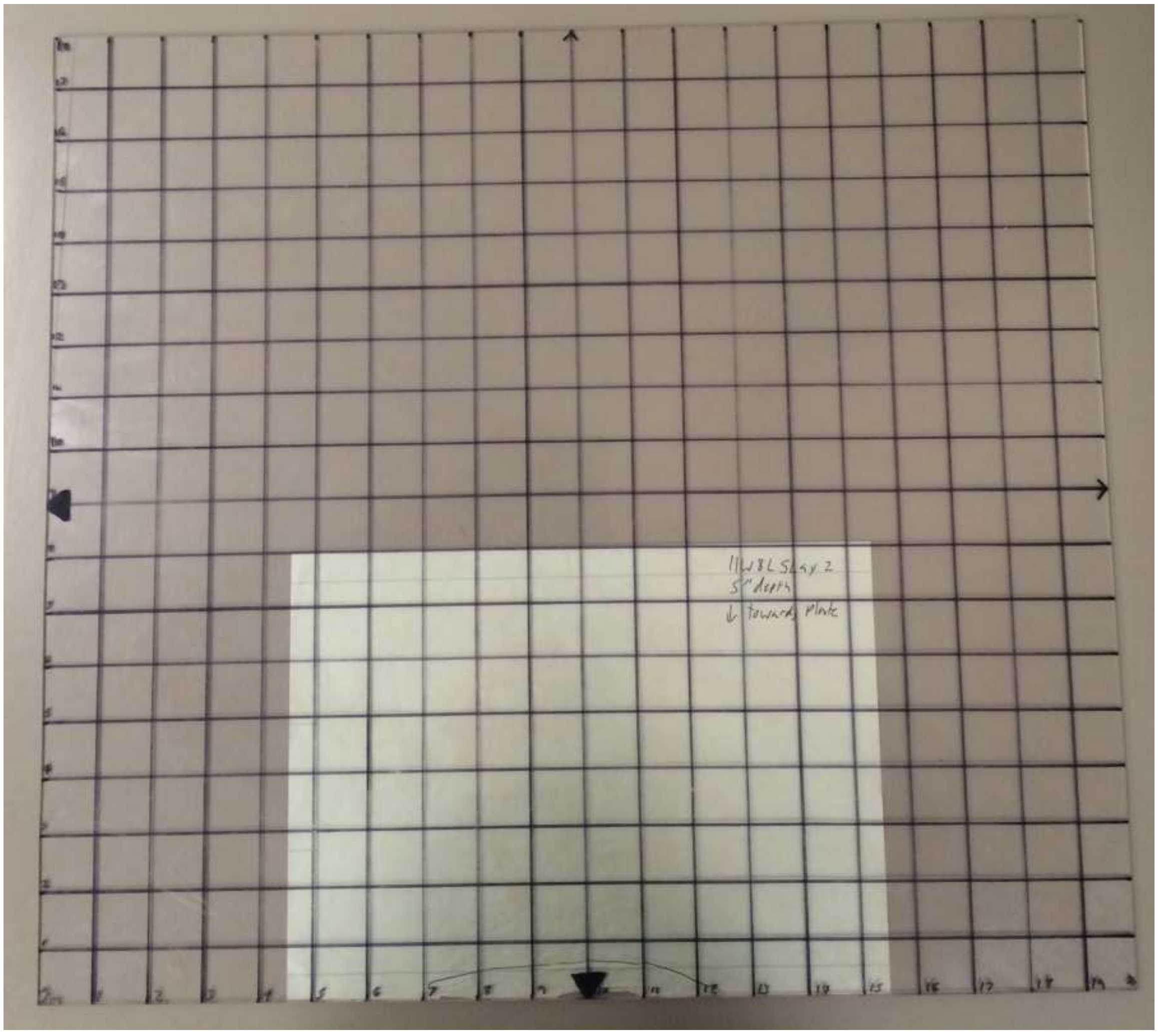

Figure 270: Test 11W8L5Lay2 5" Depth

A.14 Photographs of Test PW8L5Lay3

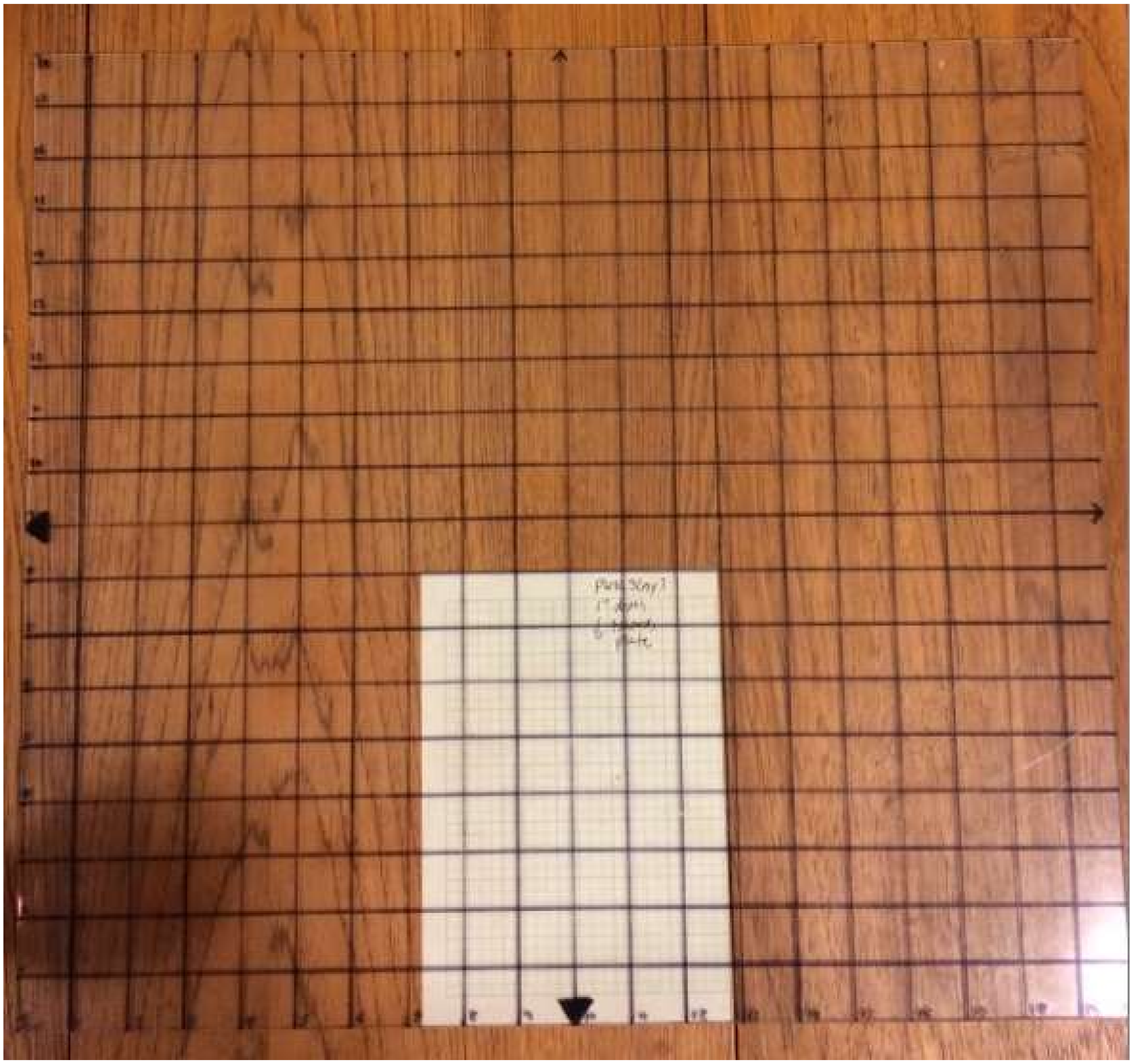

Figure 271: Test PW8L5Lay3 1" Depth

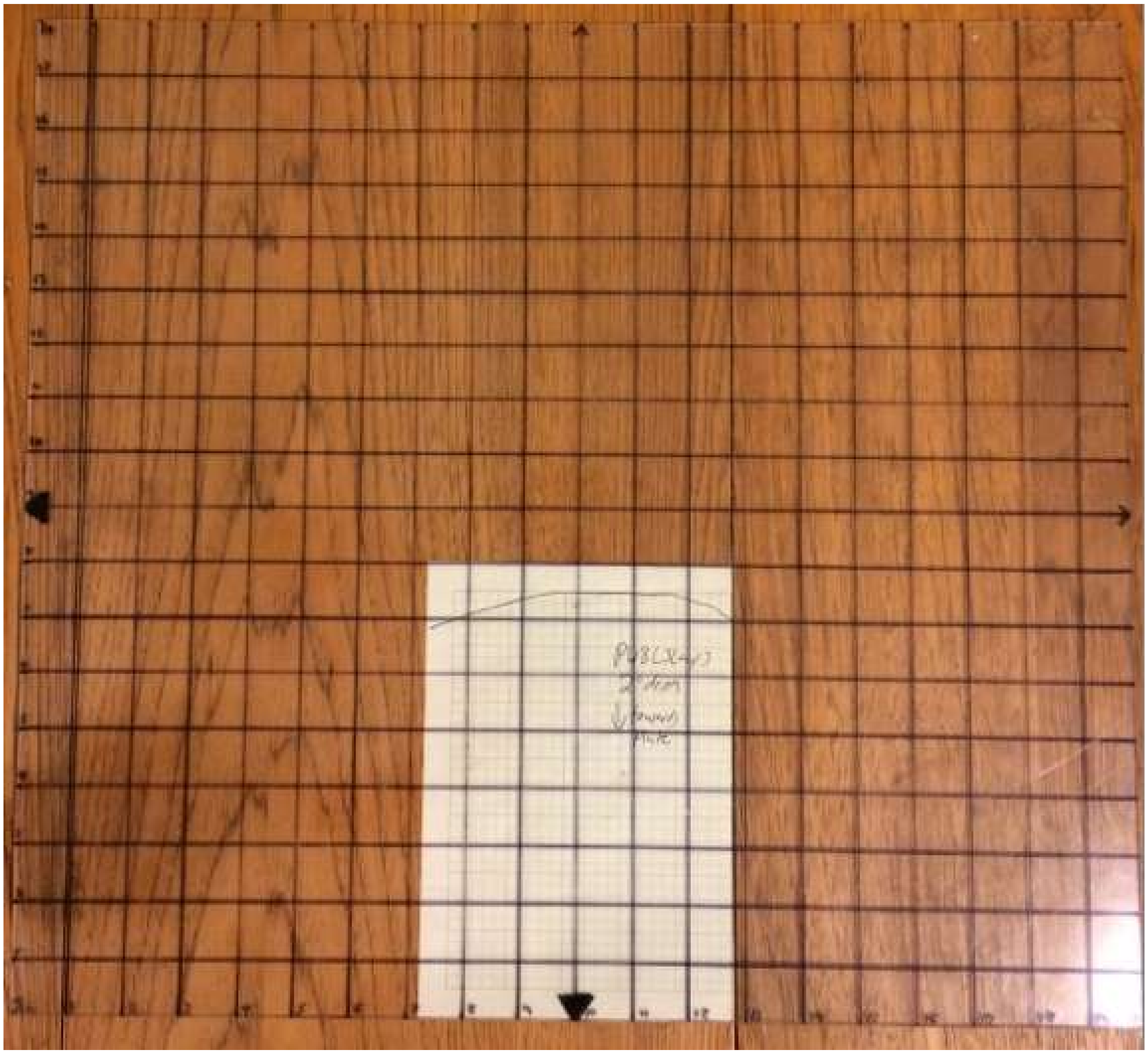

Figure 272: Test PW8L5Lay3 2" Depth

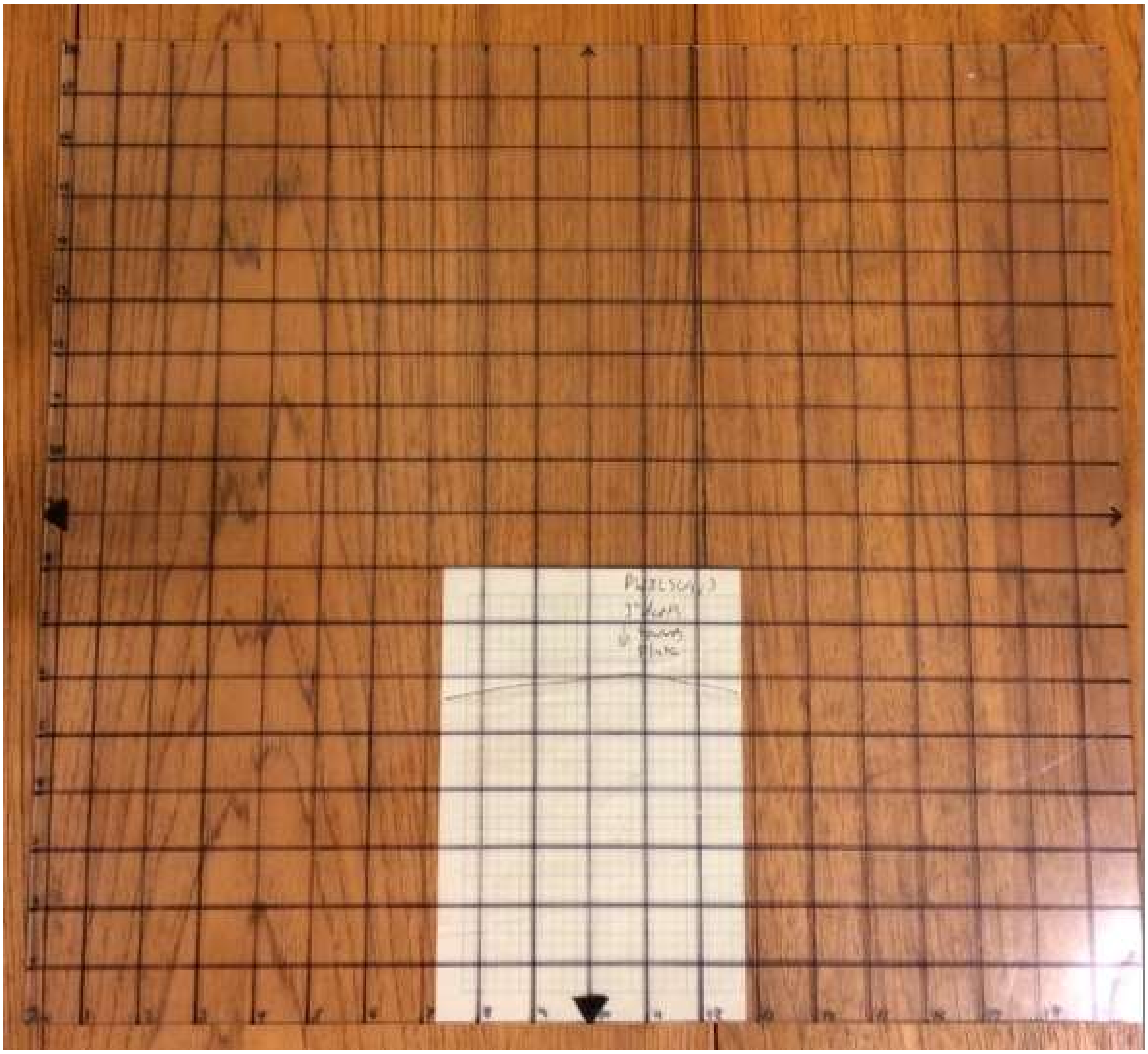

Figure 273: Test PW8L5Lay3 3” Depth

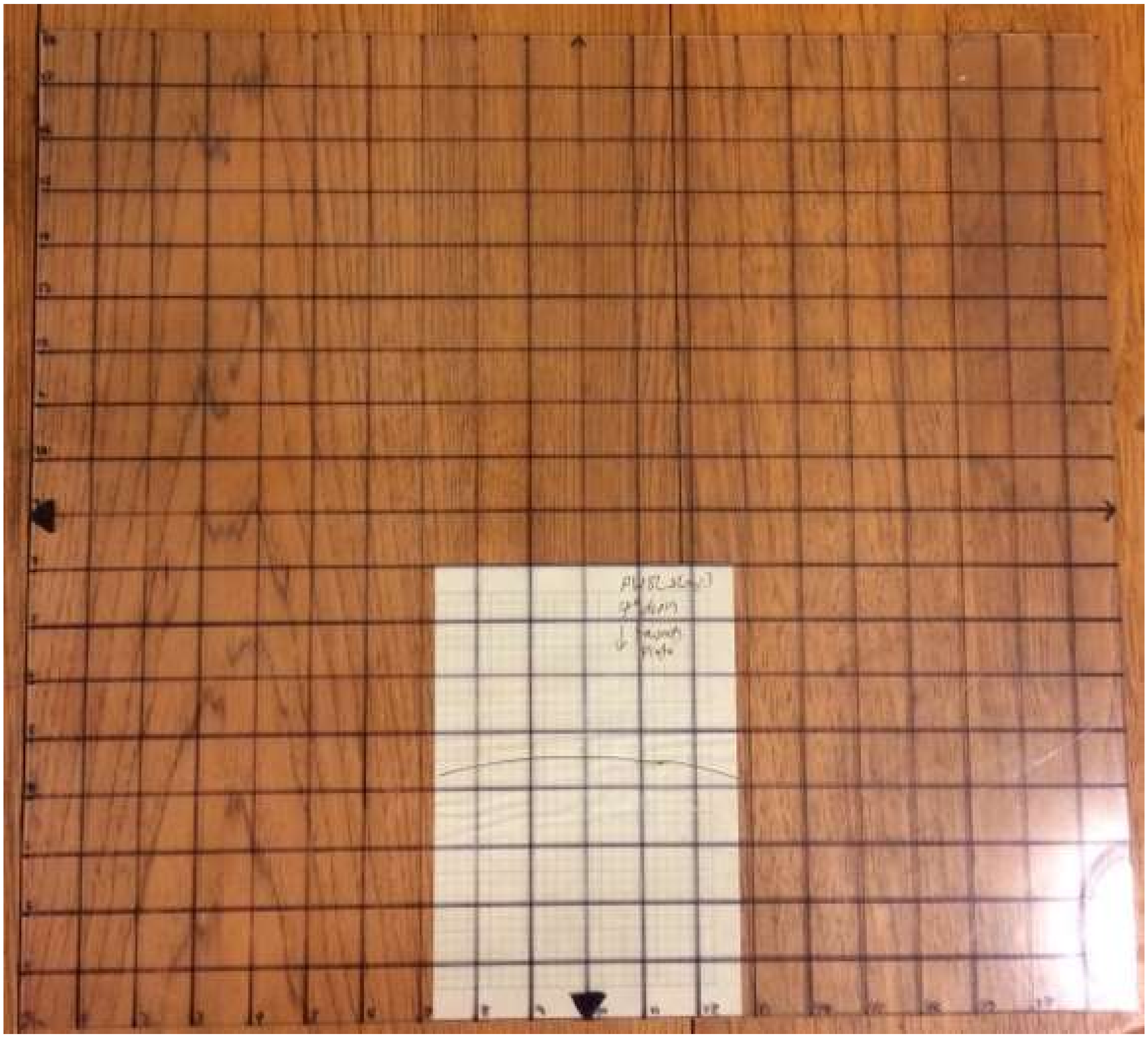

Figure 274: Test PW8L5Lay3 4" Depth

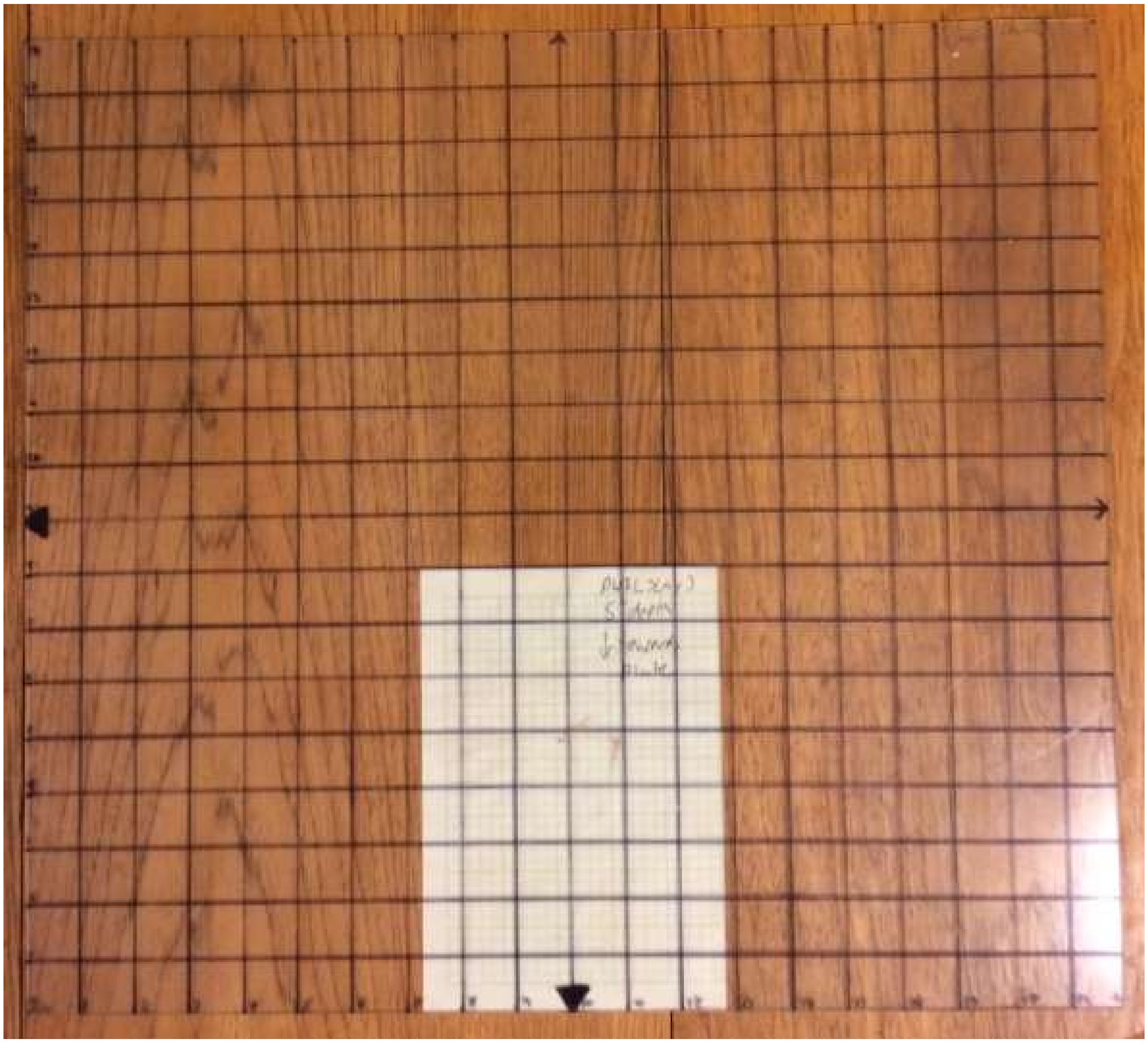

Figure 275: Test PW8L5Lay3 5” Depth

A.15 Photographs of Test PW8L10Lay3

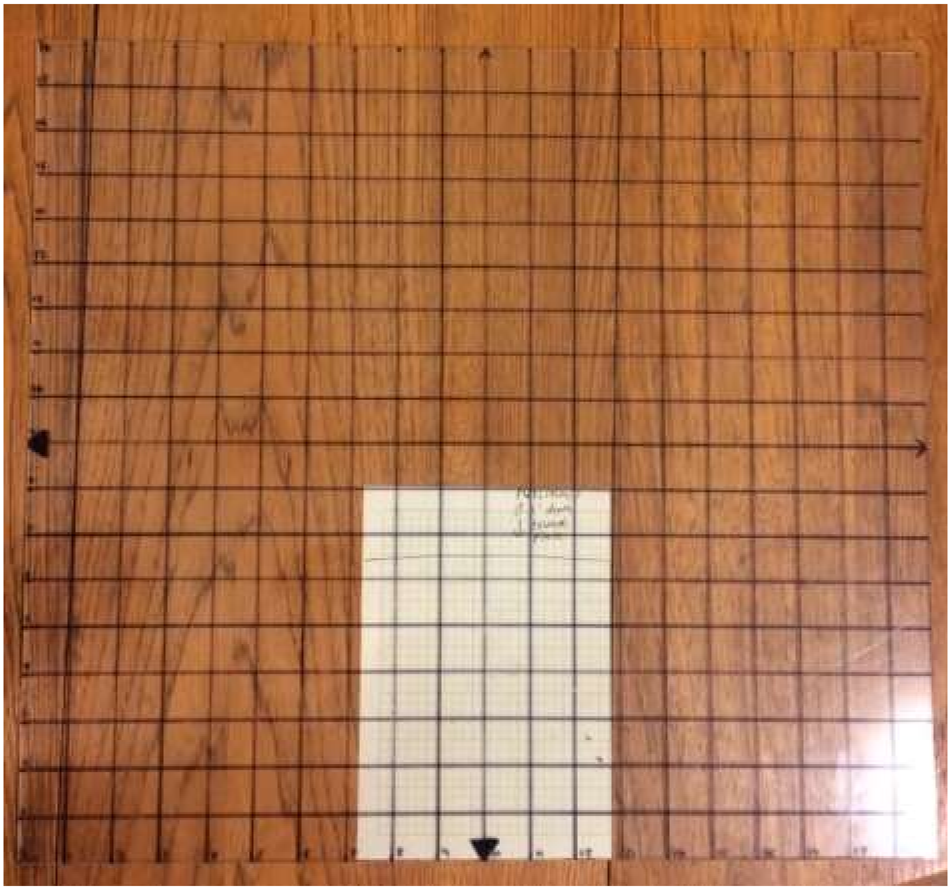

Figure 276: Test PW8L10Lay3 0.5” Depth

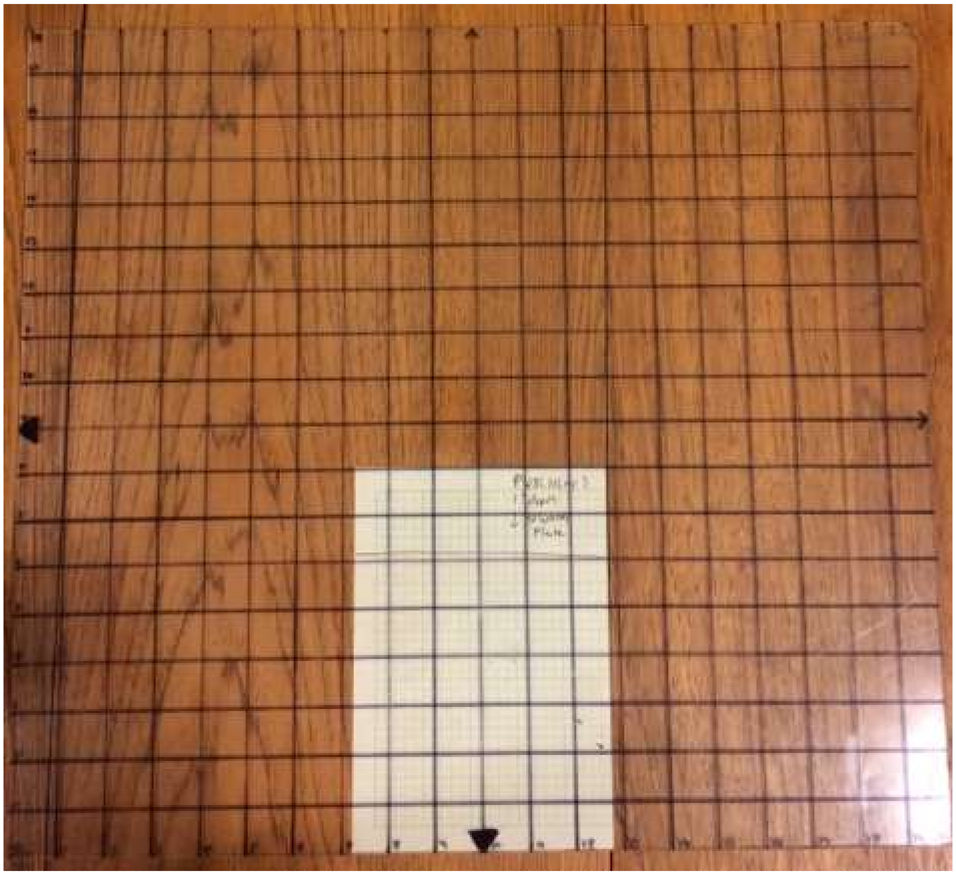

Figure 277: Test PW8L10Lay3 1" Depth

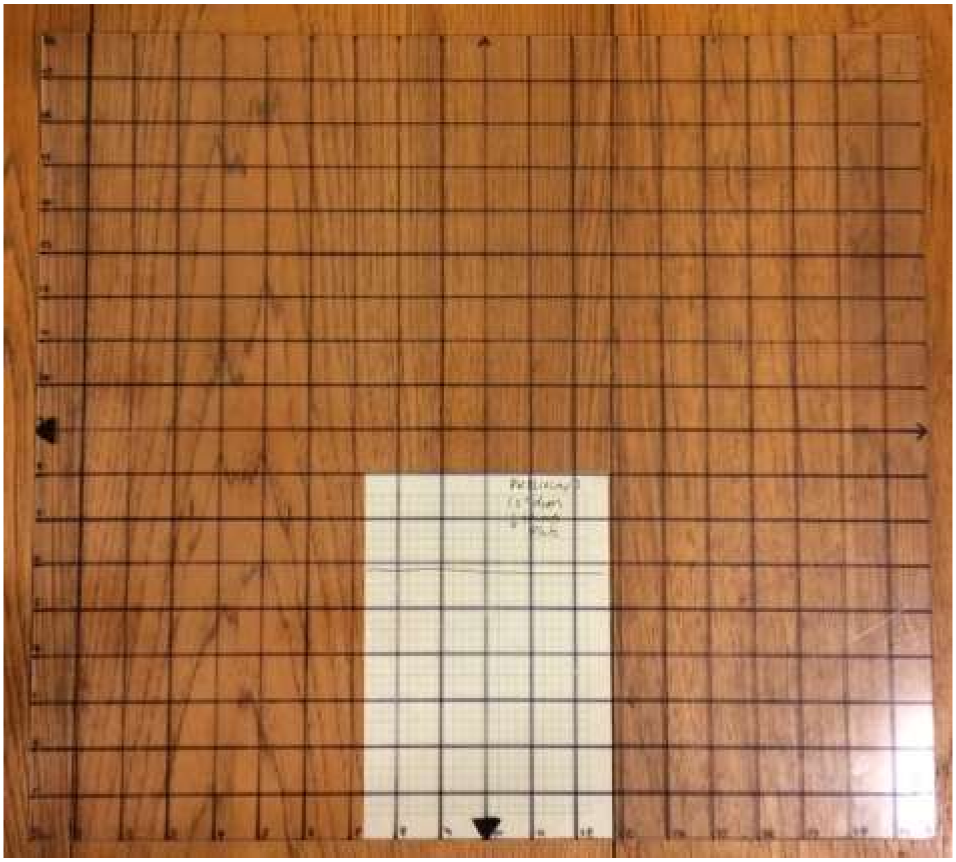

Figure 278: Test PW8L10Lay3 1.5” Depth

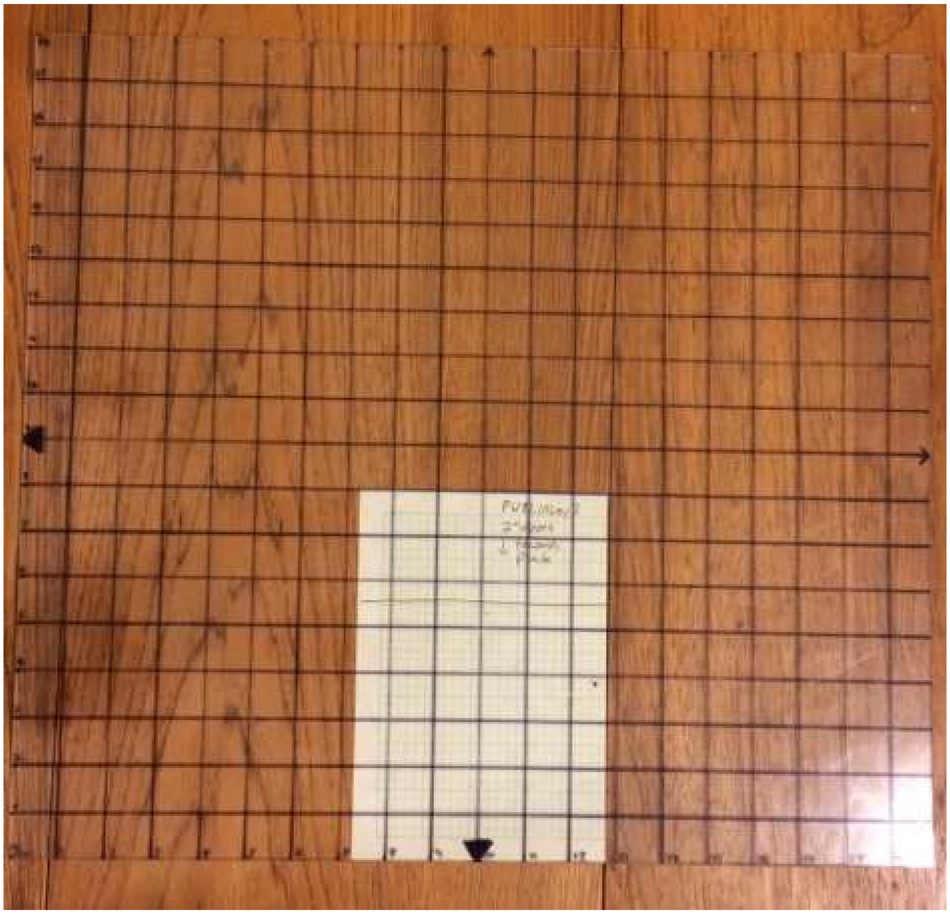

Figure 279: Test PW8L10Lay3 2” Depth

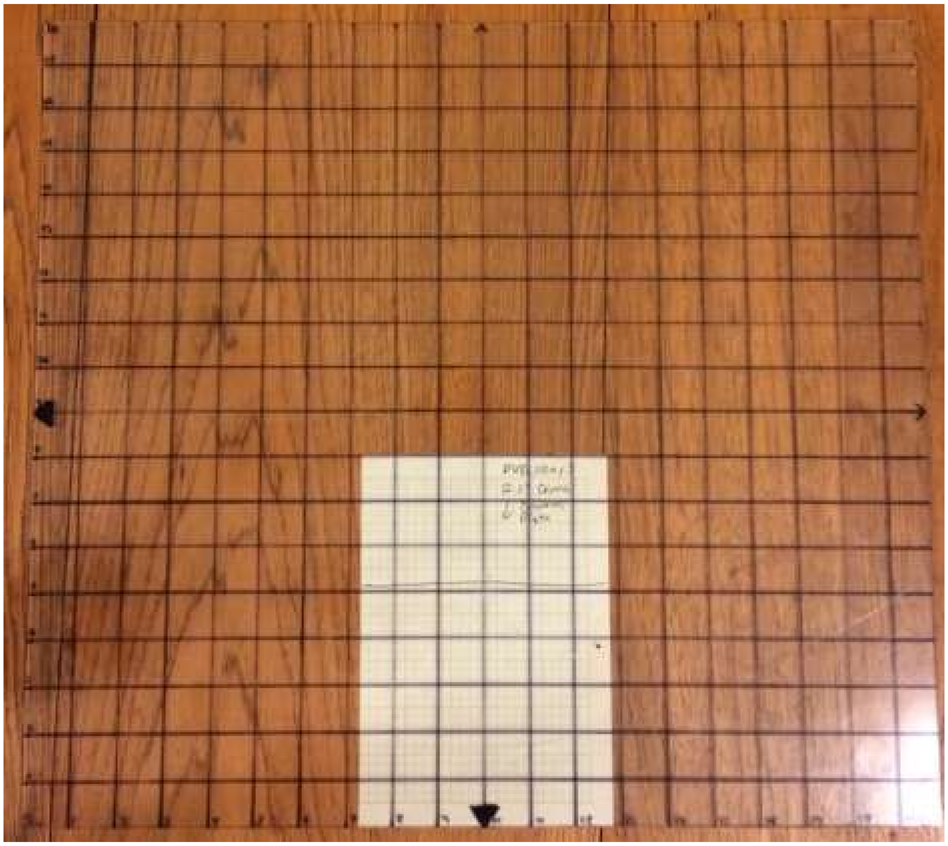

Figure 280: Test PW8L10Lay3 2.5" Depth

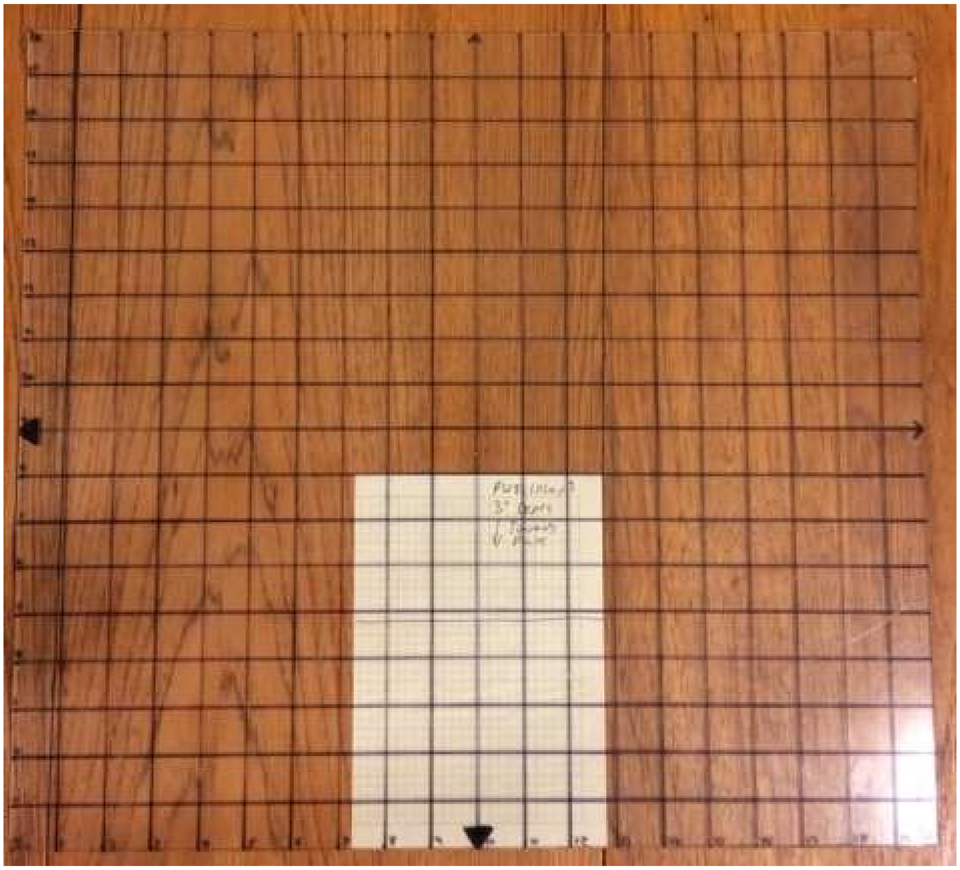

Figure 281: Test PW8L10Lay3 3" Depth

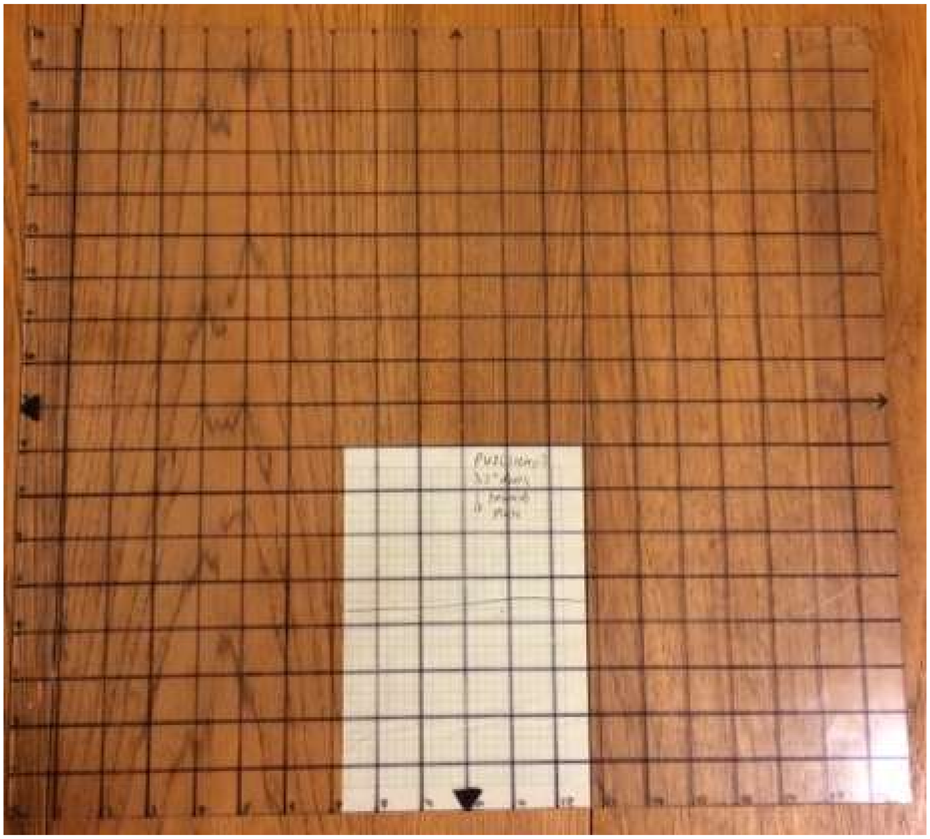

Figure 282: Test PW8L10Lay3 3.5" Depth

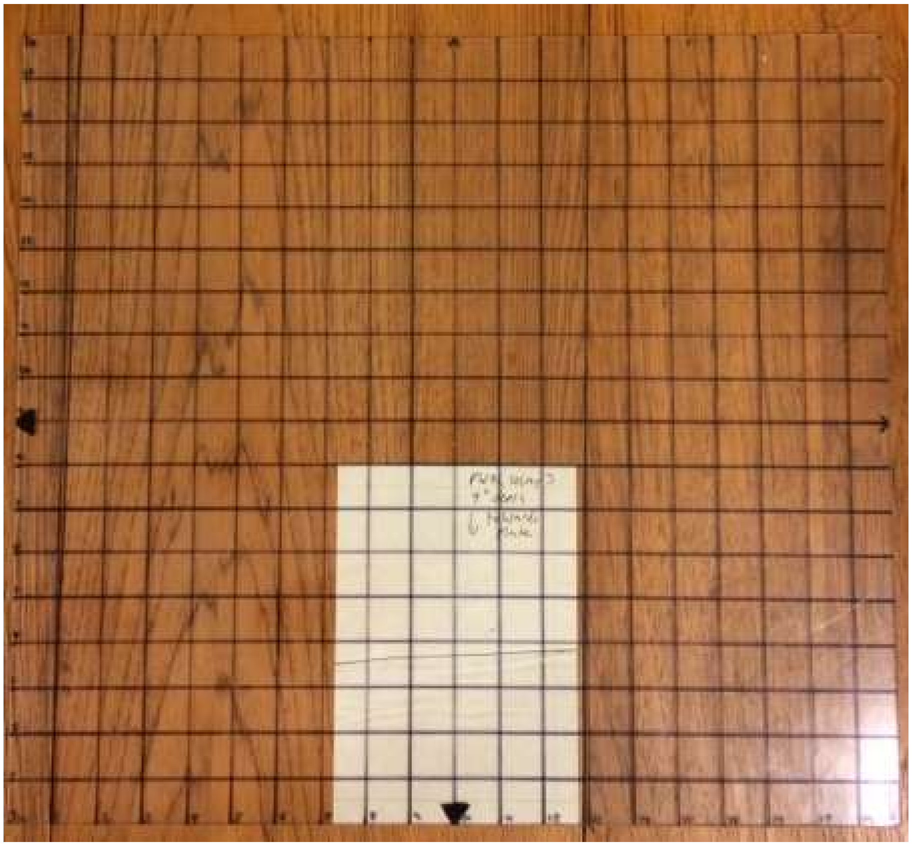

Figure 283: Test PW8L10Lay3 4” Depth

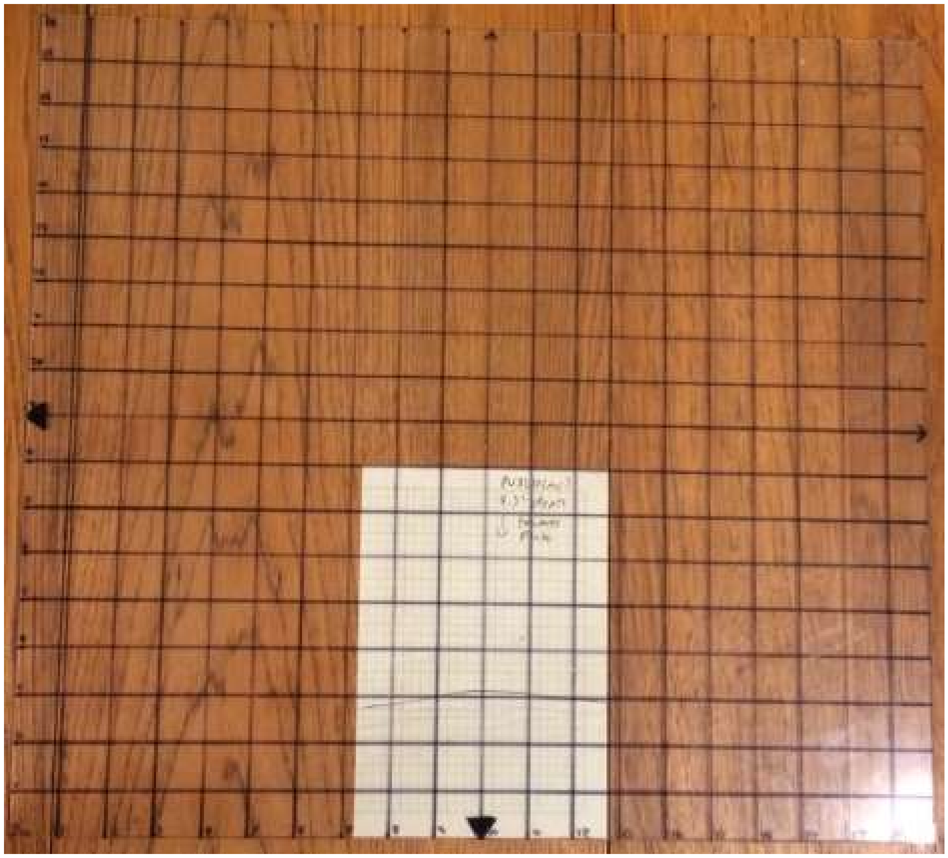

Figure 284: Test PW8L10Lay3 4.5” Depth

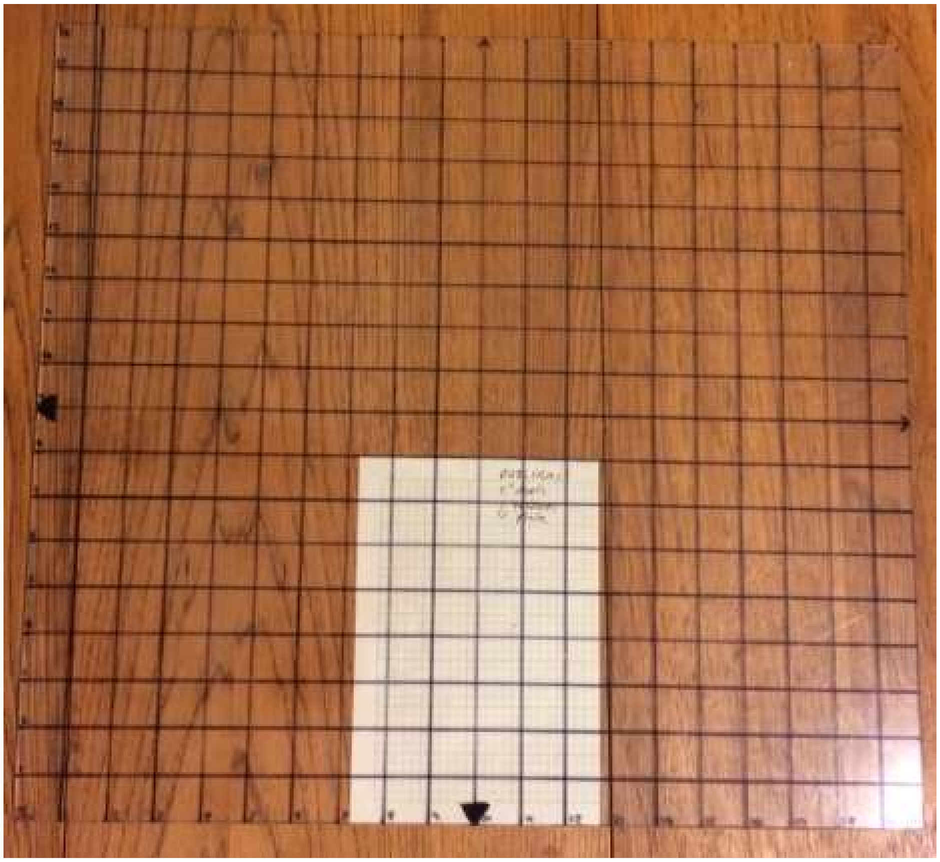

Figure 285: Test PW8L10Lay3 5” Depth

A.16 Photographs of Test PW11L5Lay3

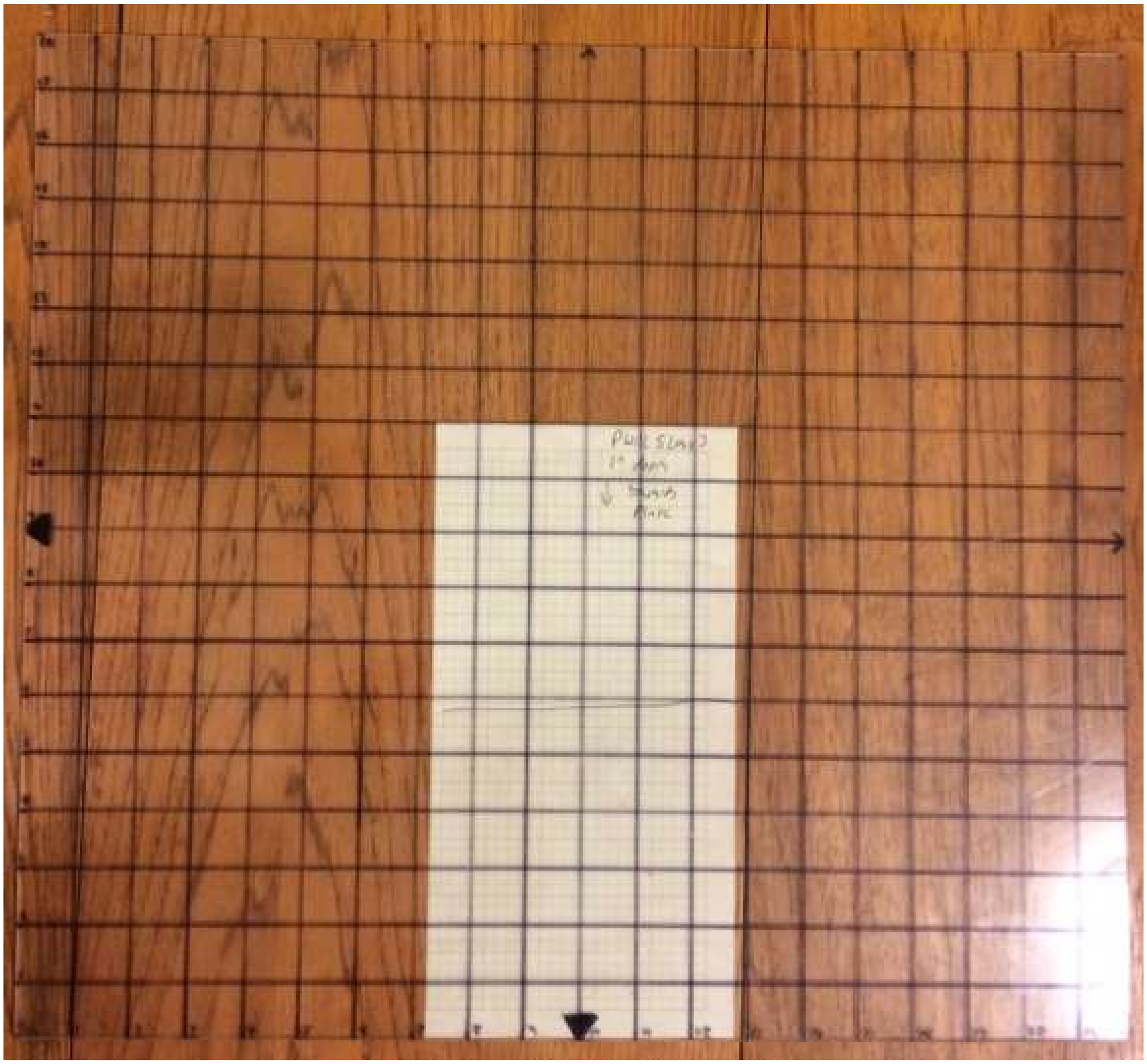

Figure 286: Test PW11L5Lay3 1" Depth

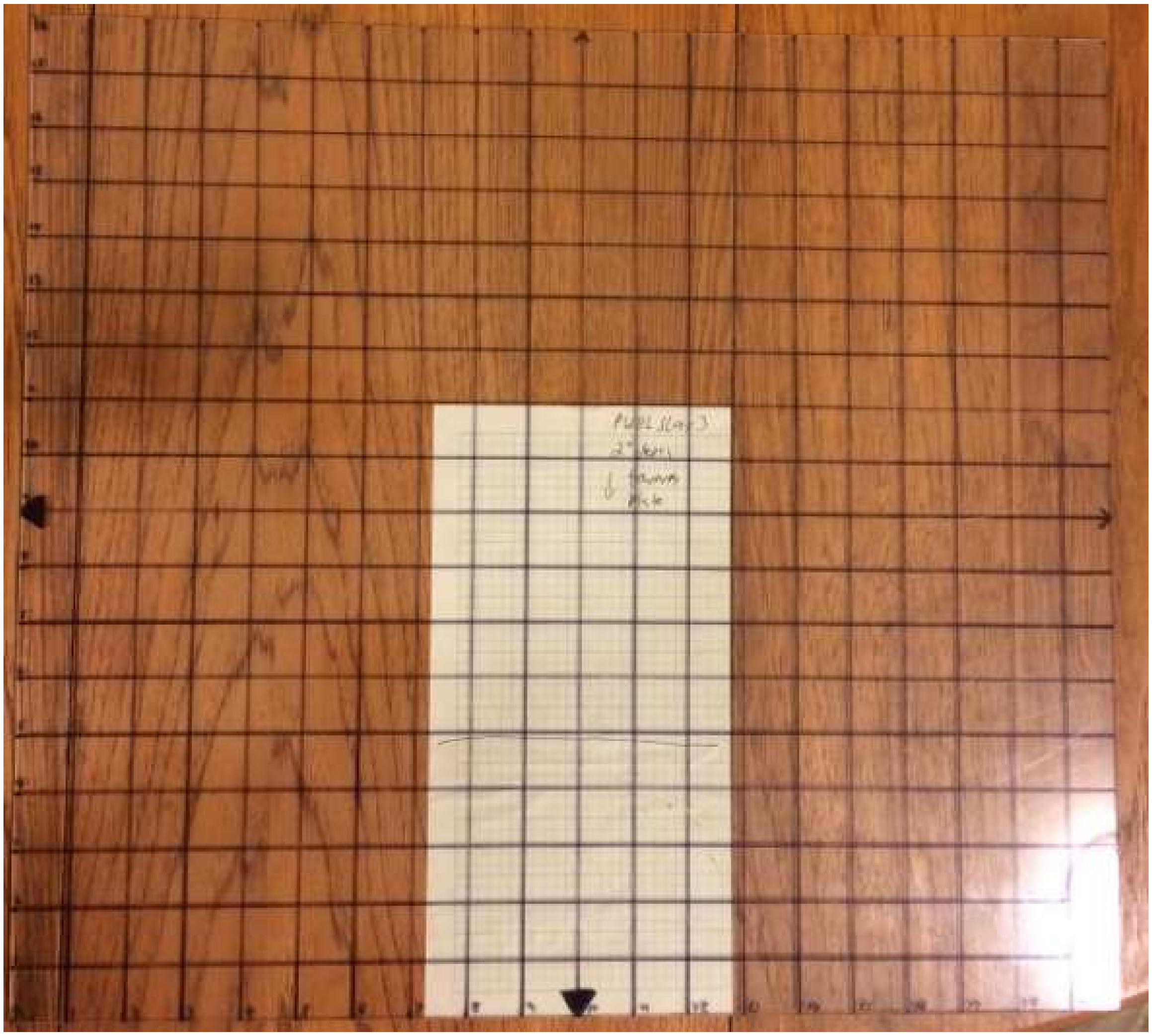

Figure 287: Test PW11L5Lay3 2" Depth

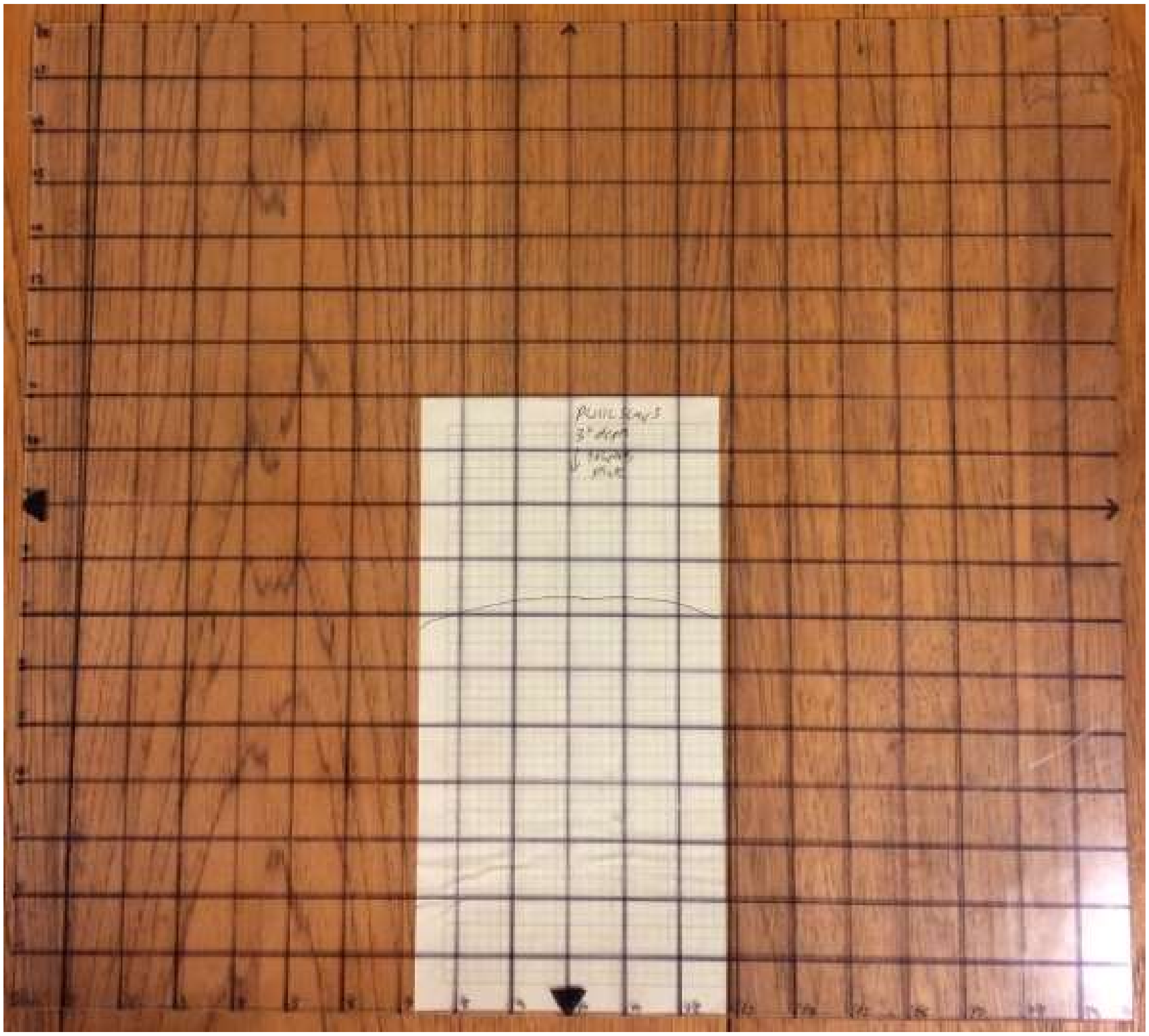

Figure 288: Test PW11L5Lay3 3" Depth

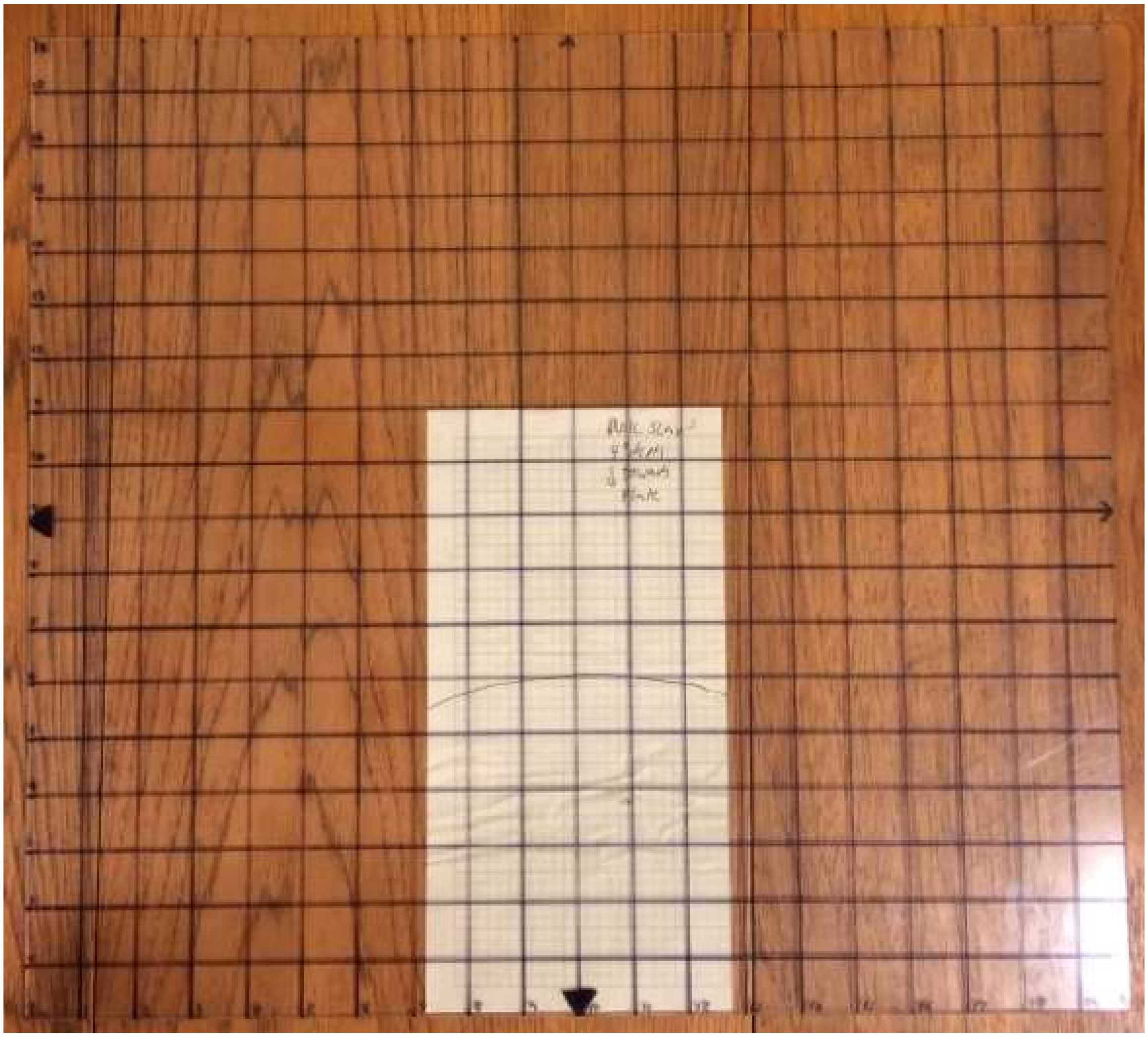

Figure 289: Test PW11L5Lay3 4” Depth

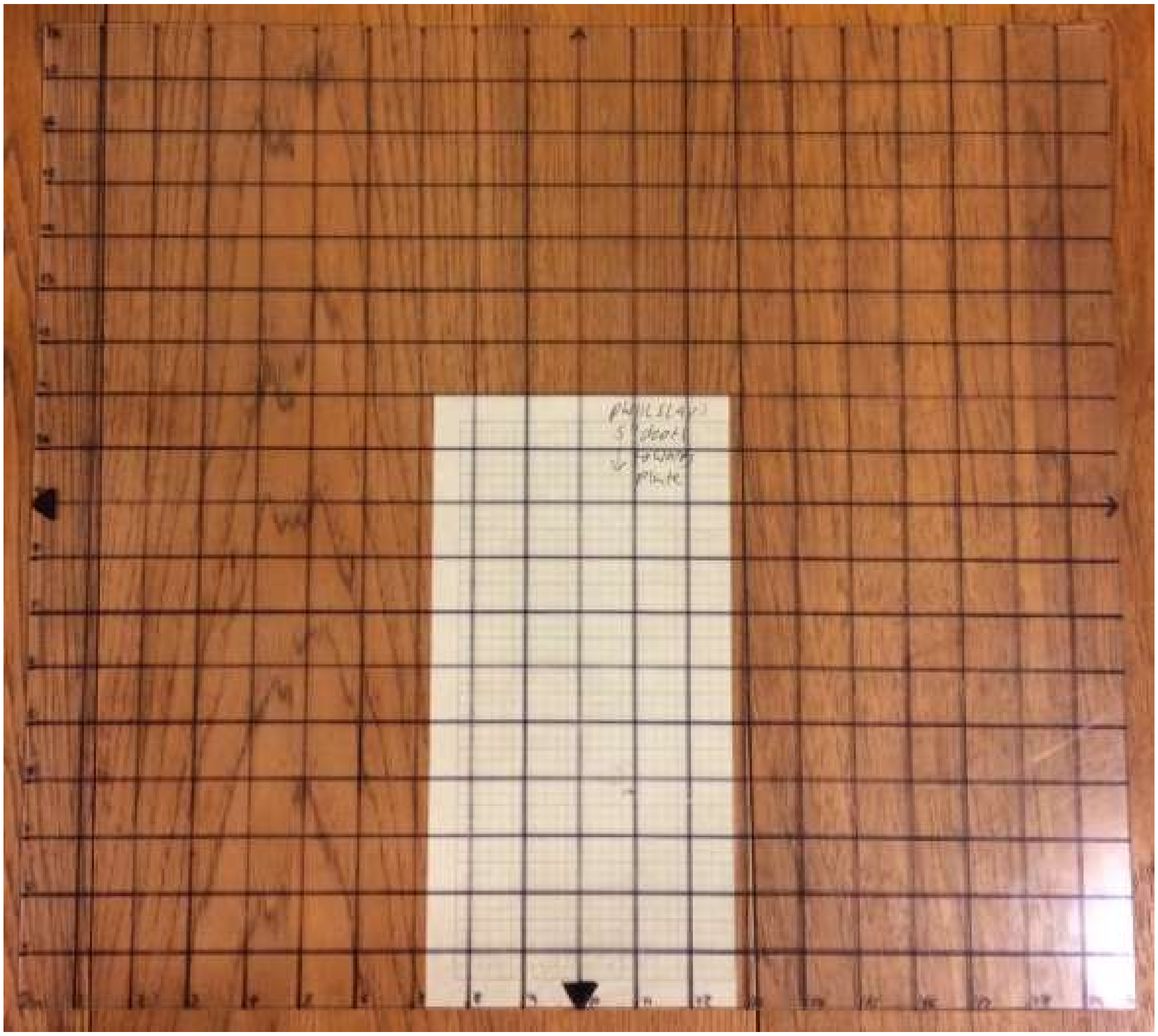

Figure 290: Test PW11L5Lay3 5” Depth

A.17 Photographs of Test PW11L10Lay3

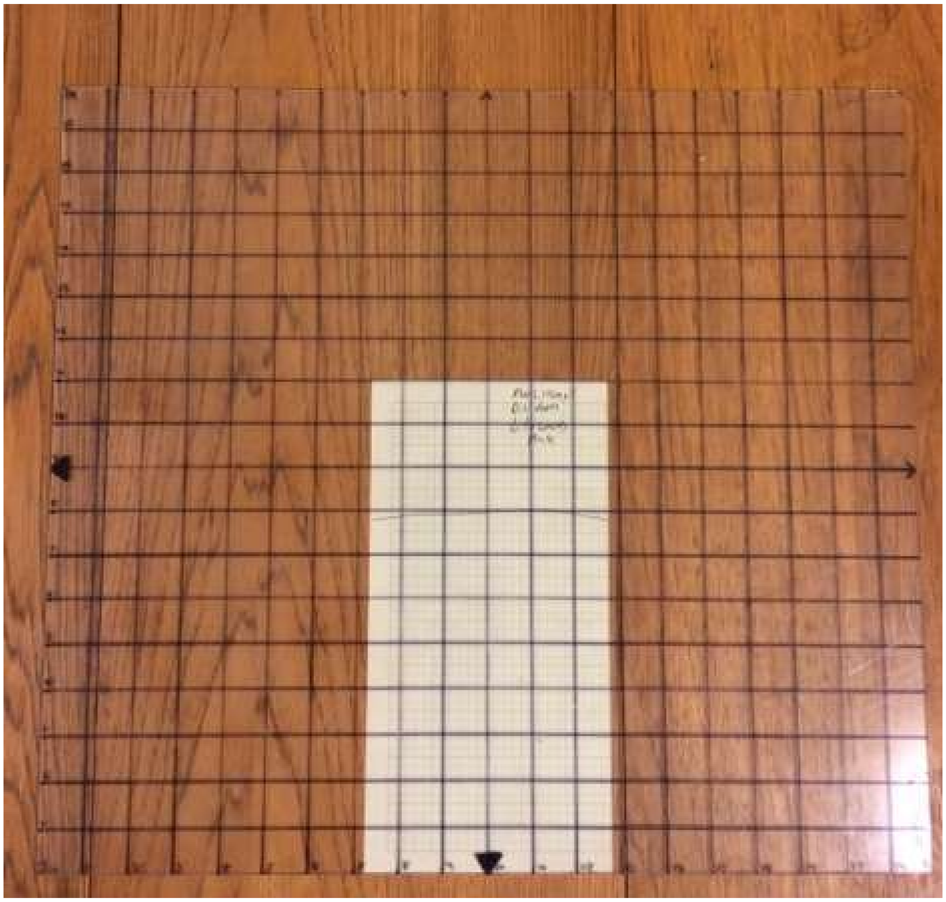

Figure 291: Test PW11L10Lay3 0.5" Depth

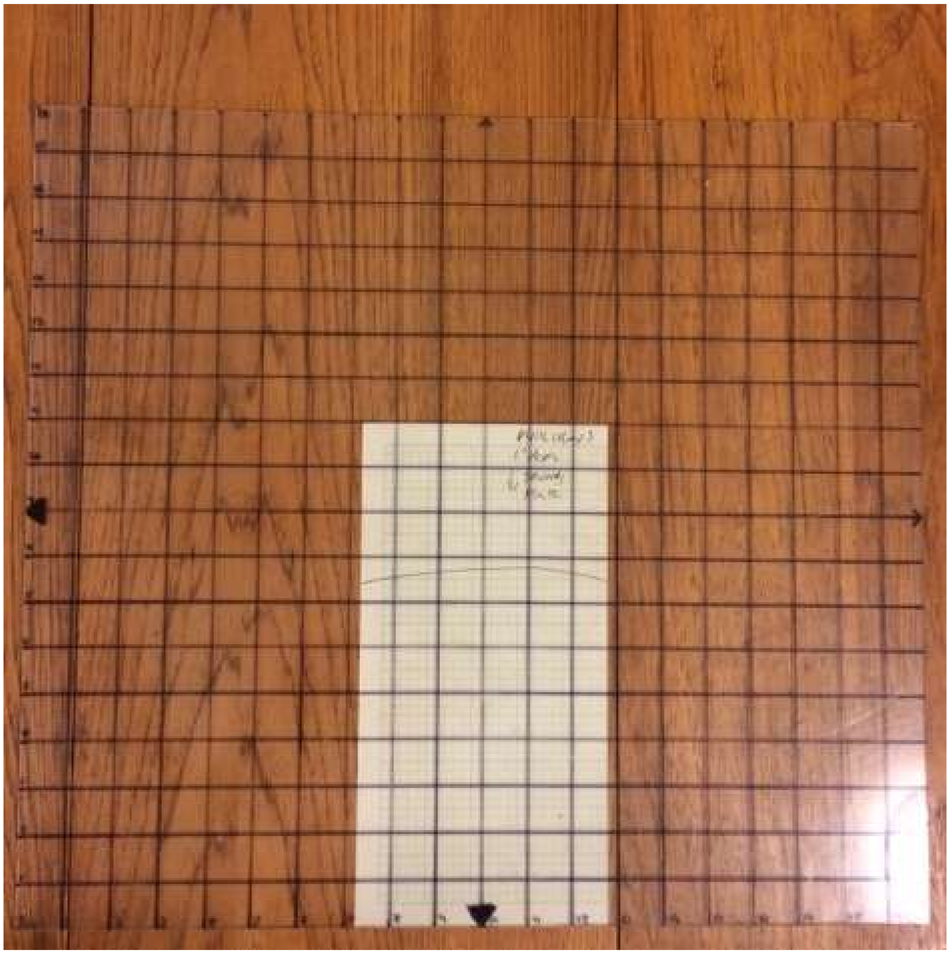

Figure 292: Test PW11L10Lay3 1” Depth

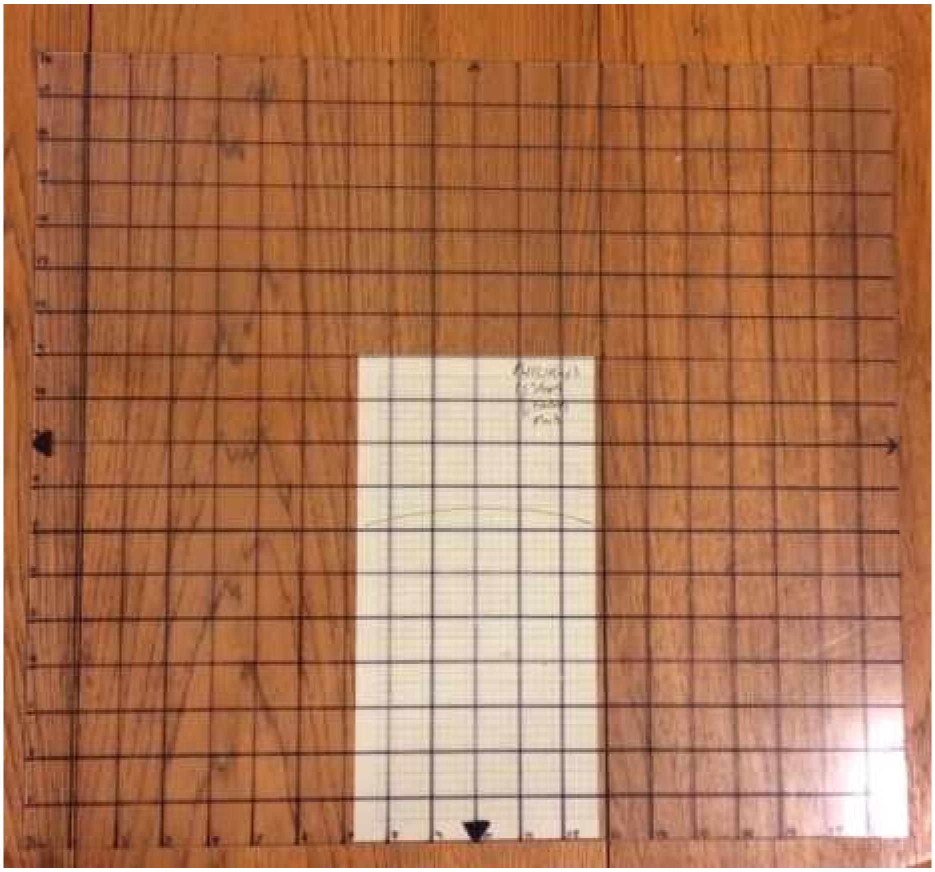

Figure 293: Test PW11L10Lay3 1.5" Depth

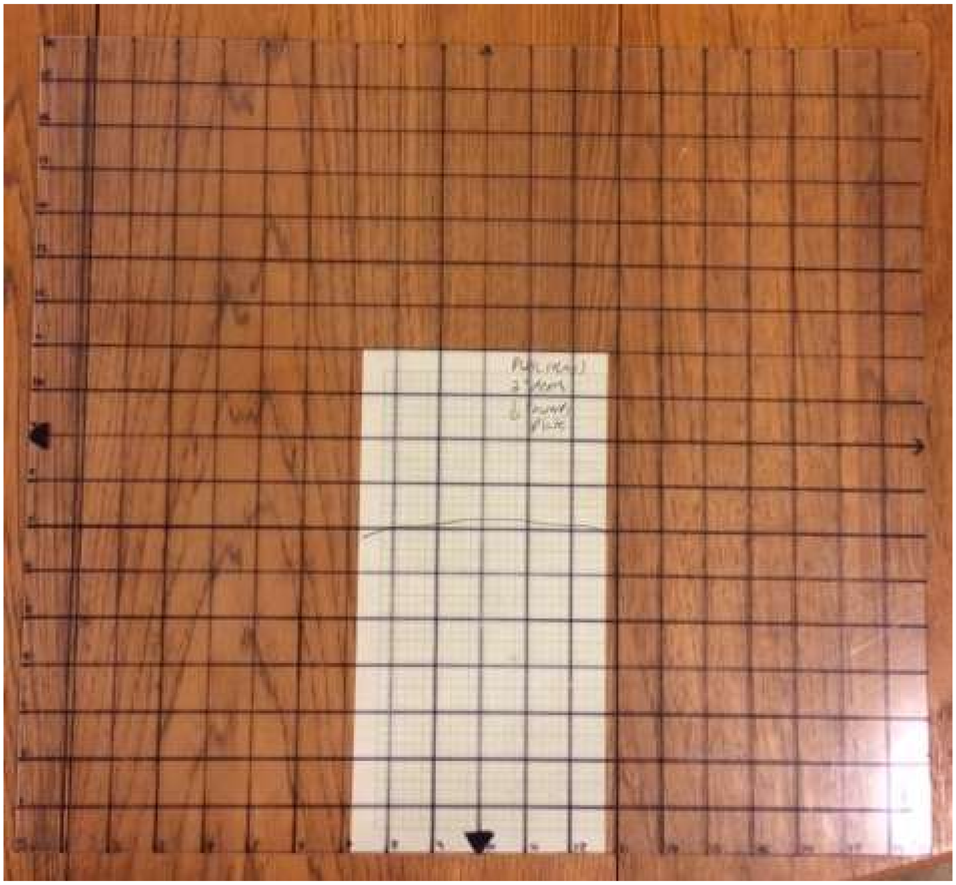

Figure 294: Test PW11L10Lay3 2" Depth

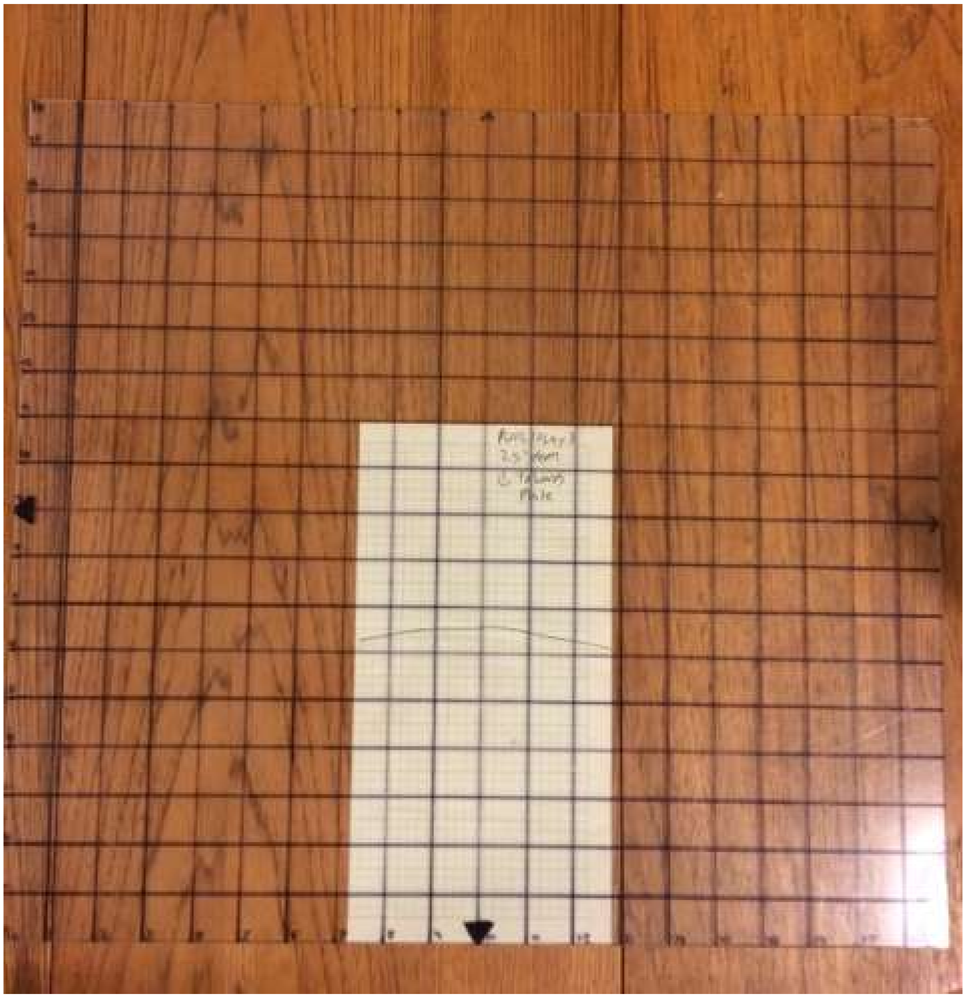

Figure 295: Test PW11L10Lay3 2.5" Depth

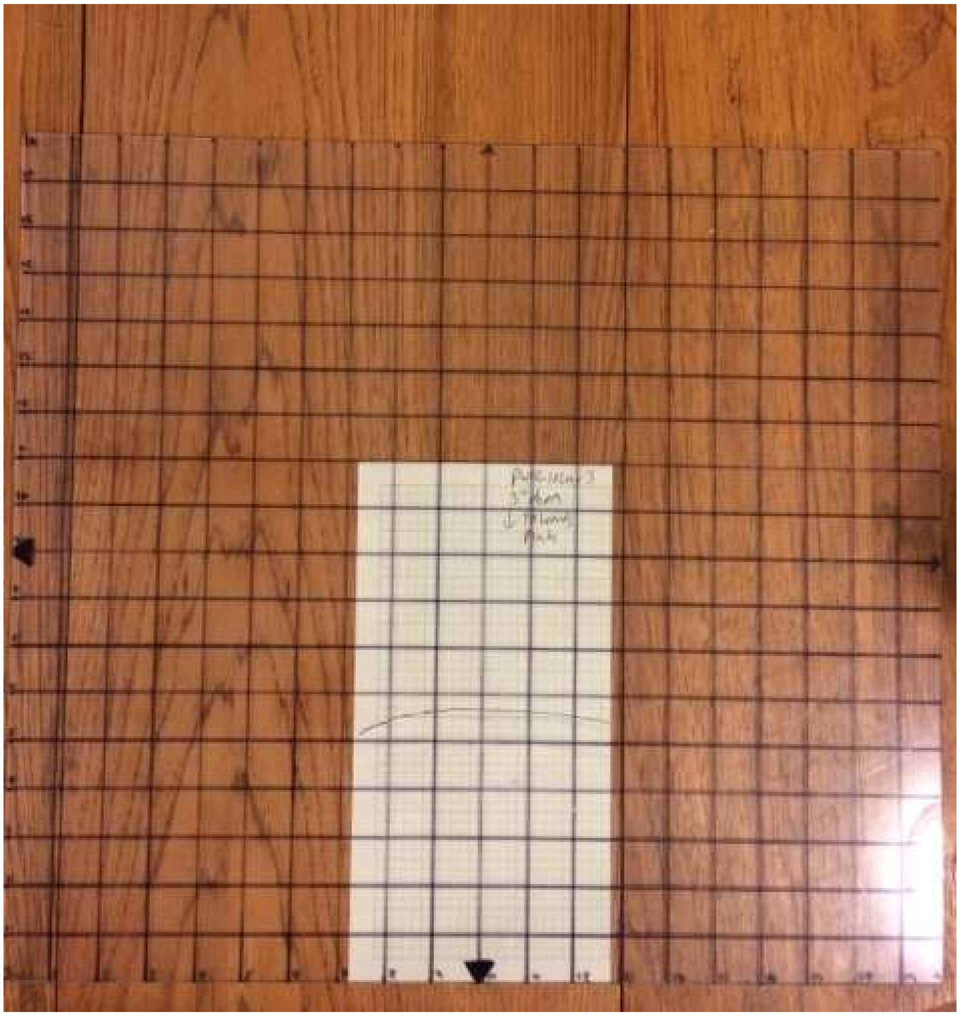

Figure 296: Test PW11L10Lay3 3” Depth

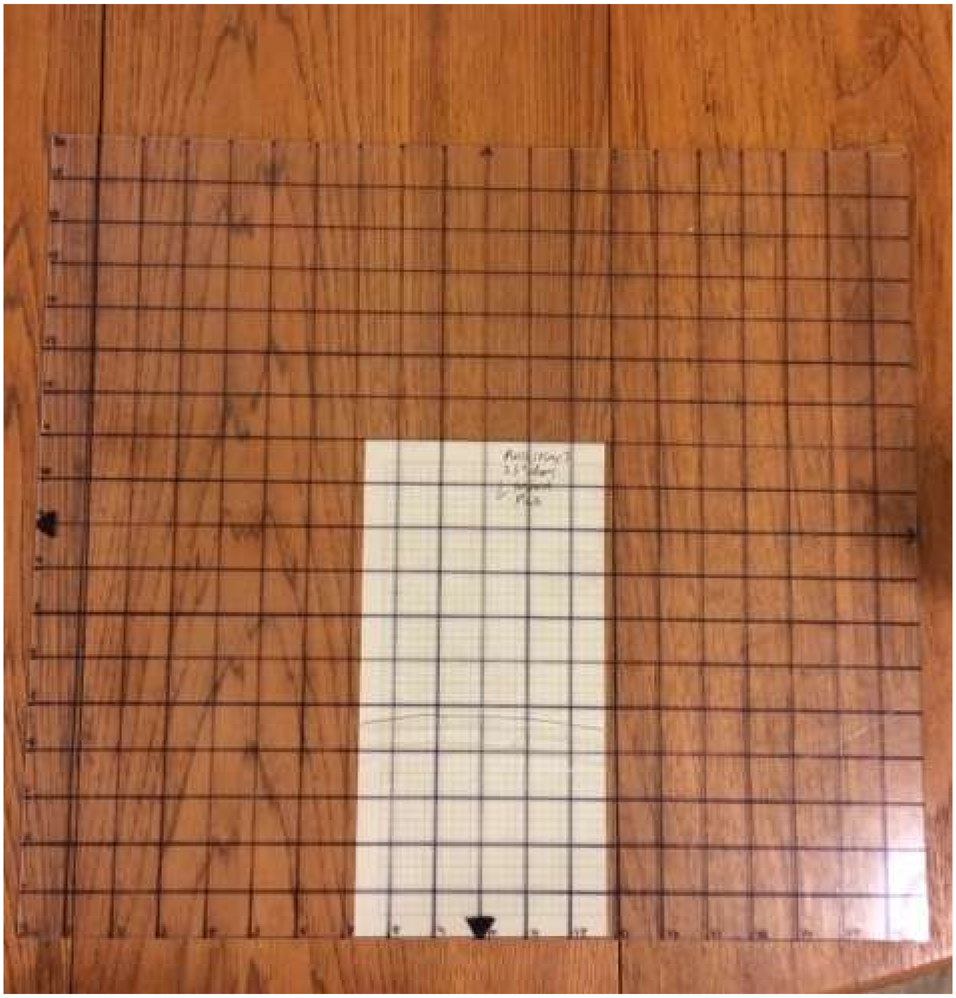

Figure 297: Test PW11L10Lay3 3.5" Depth

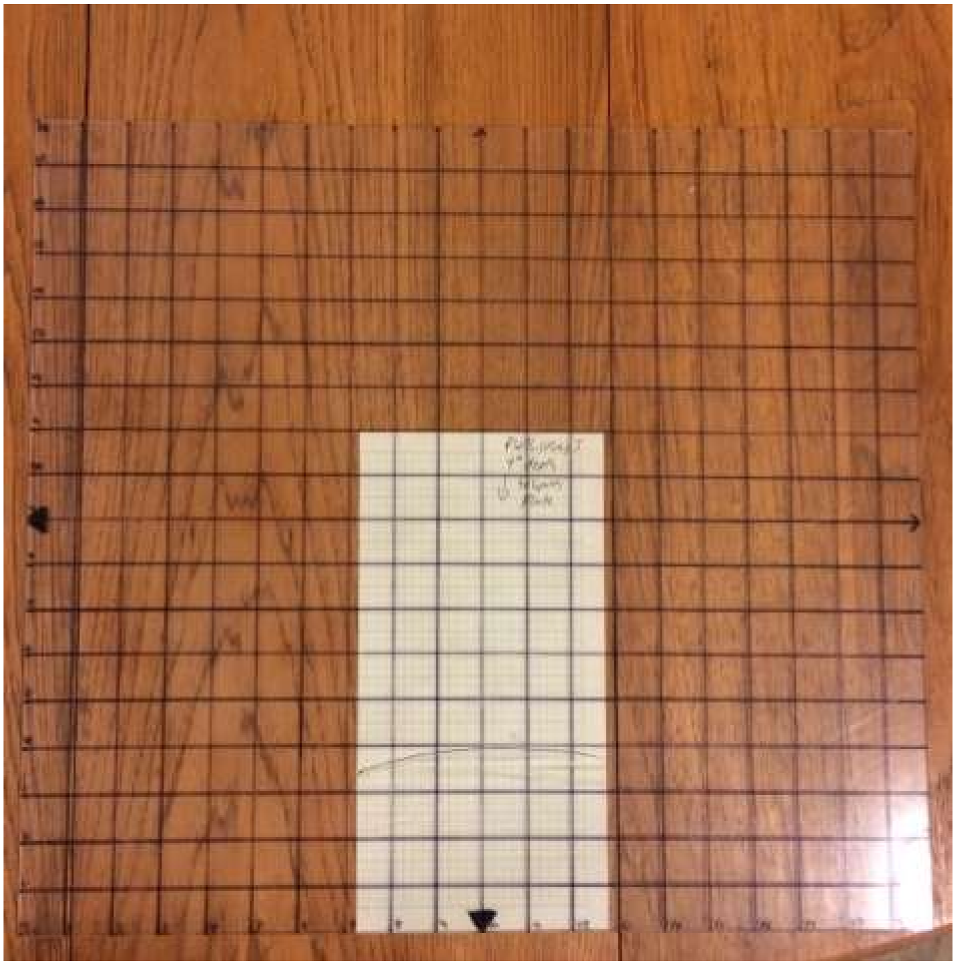

Figure 298: Test PW11L10Lay3 4” Depth

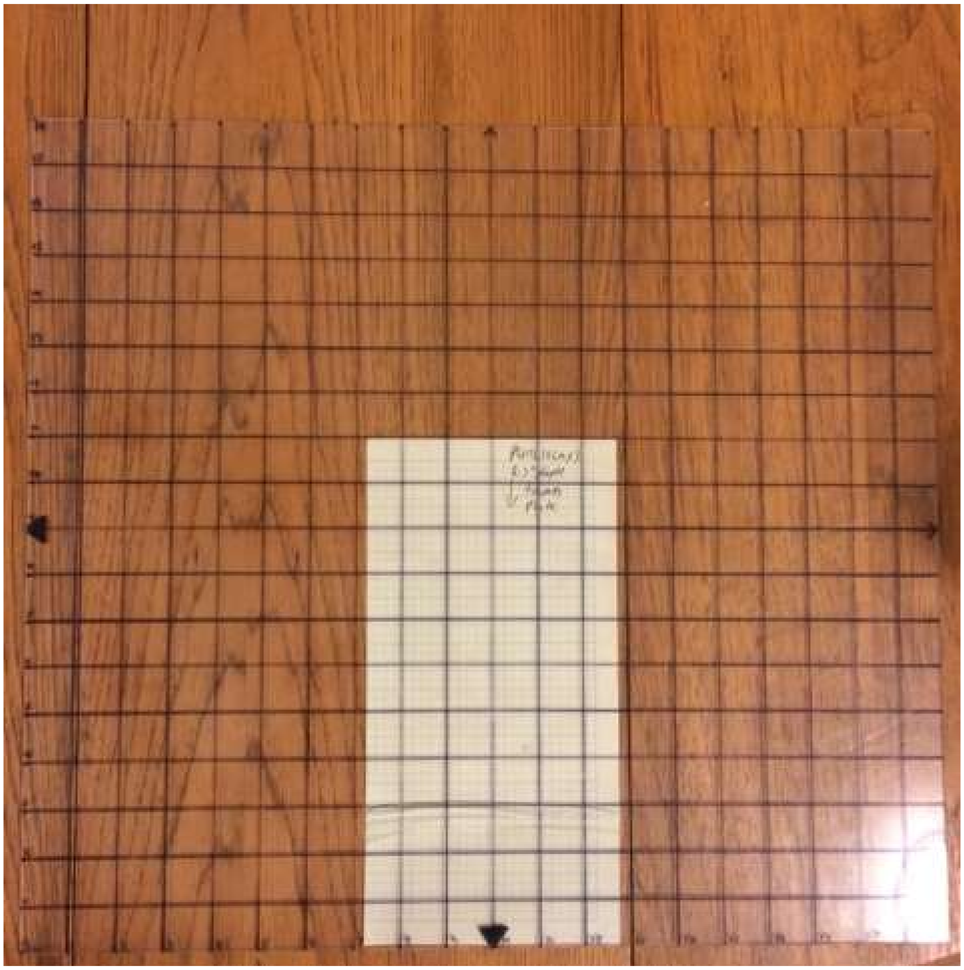

Figure 299: Test PW11L10Lay3 4.5” Depth

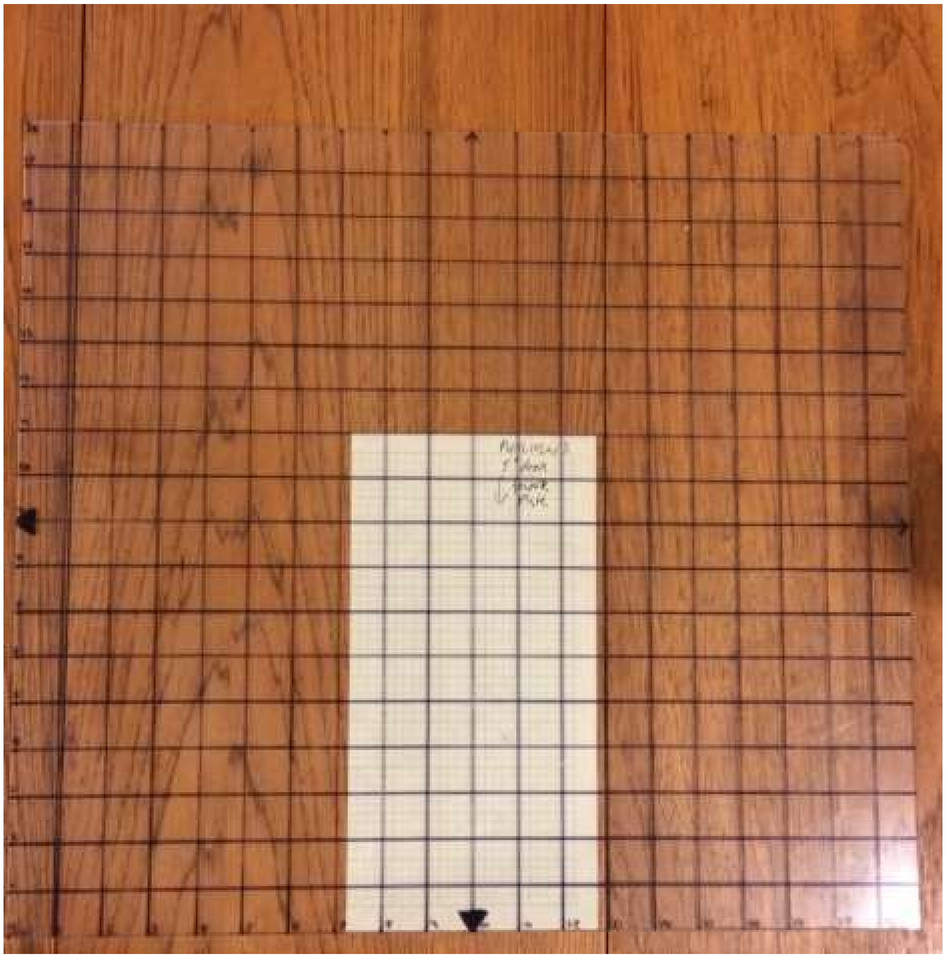

Figure 300: Test PW11L10Lay3 5" Depth

A.18 Photographs of Test 8W11L5Lay

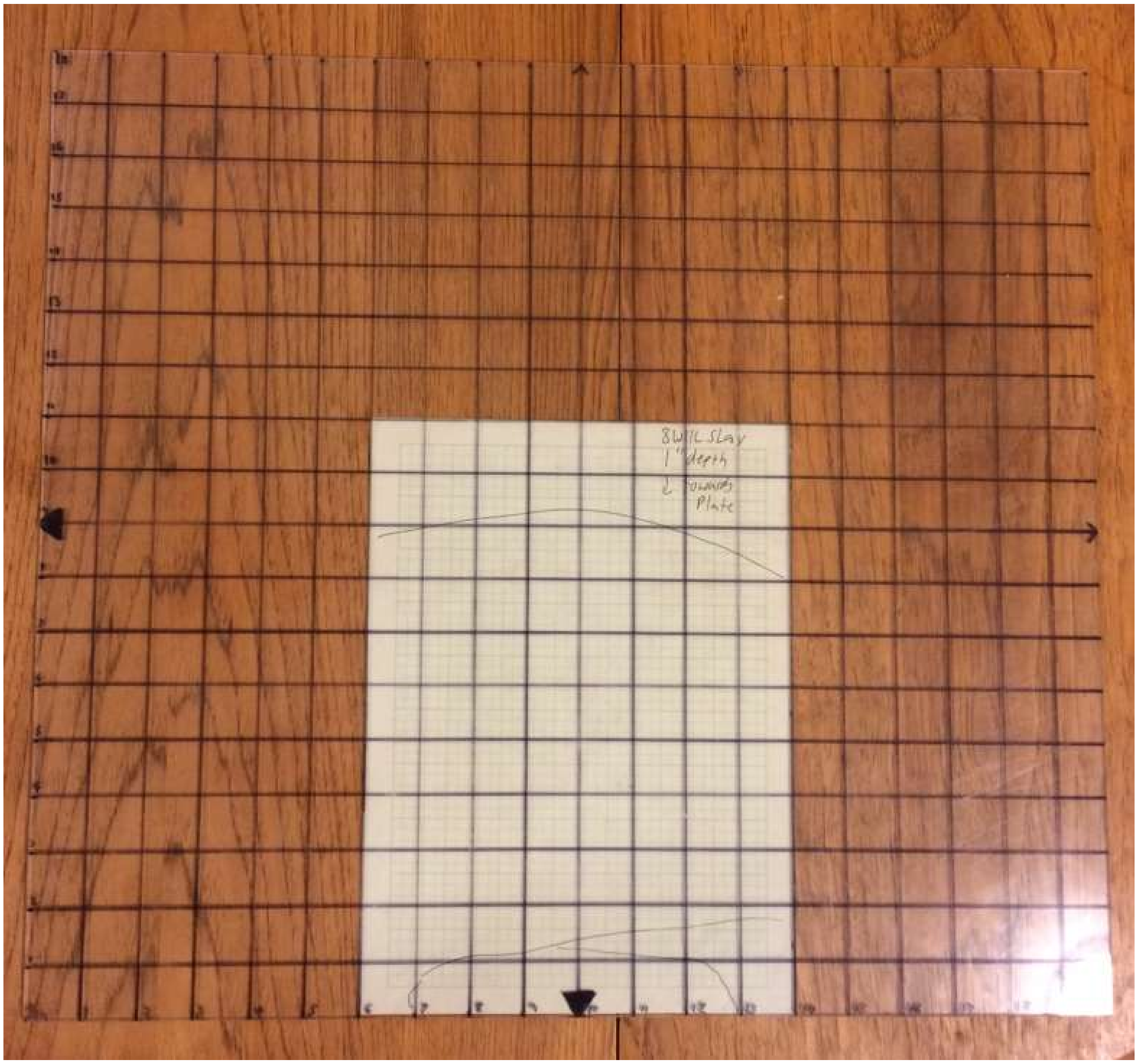

Figure 301: Test 8W11L5Lay 1" Depth

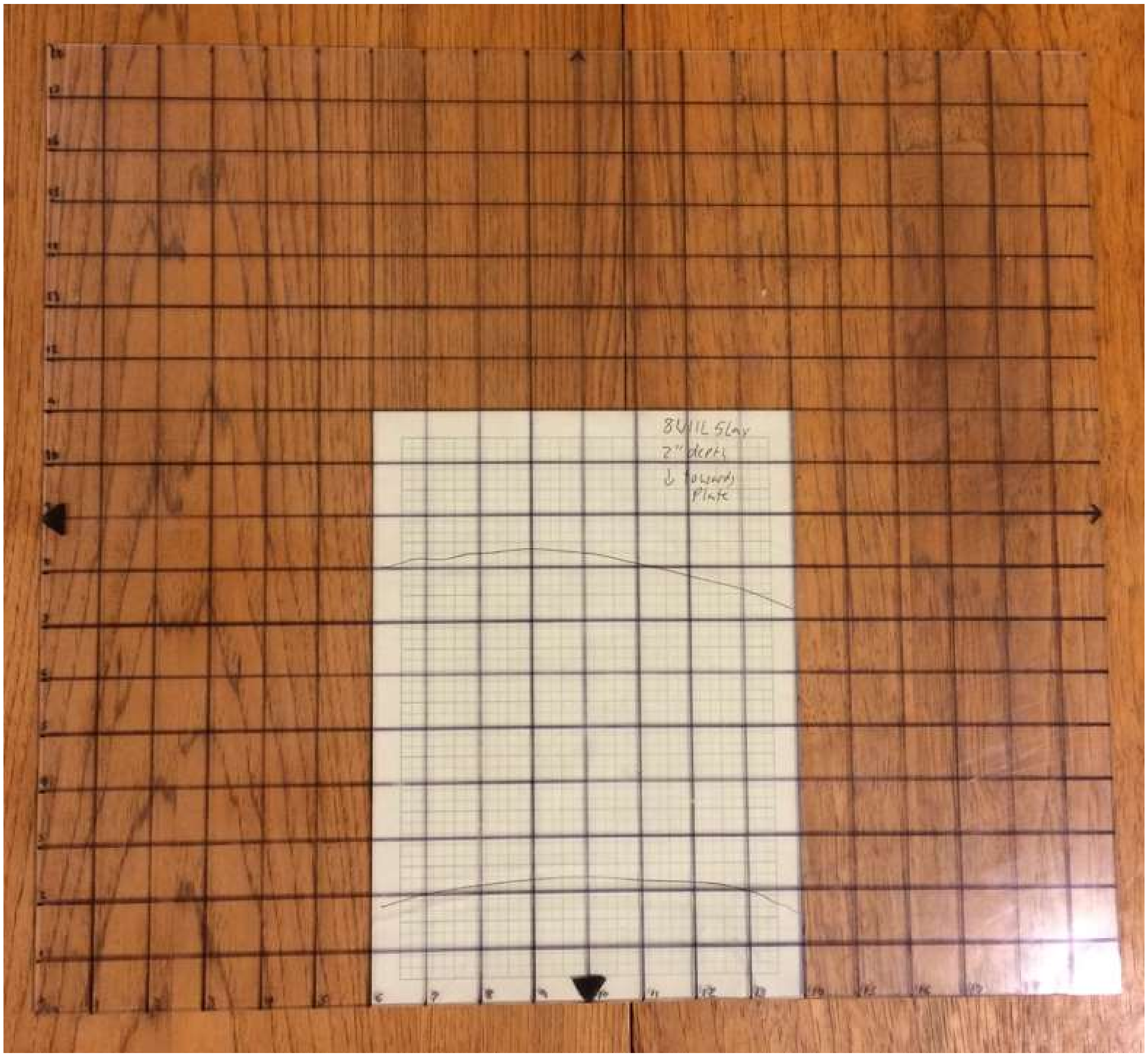

Figure 302: Test 8W11L5Lay 2" Depth

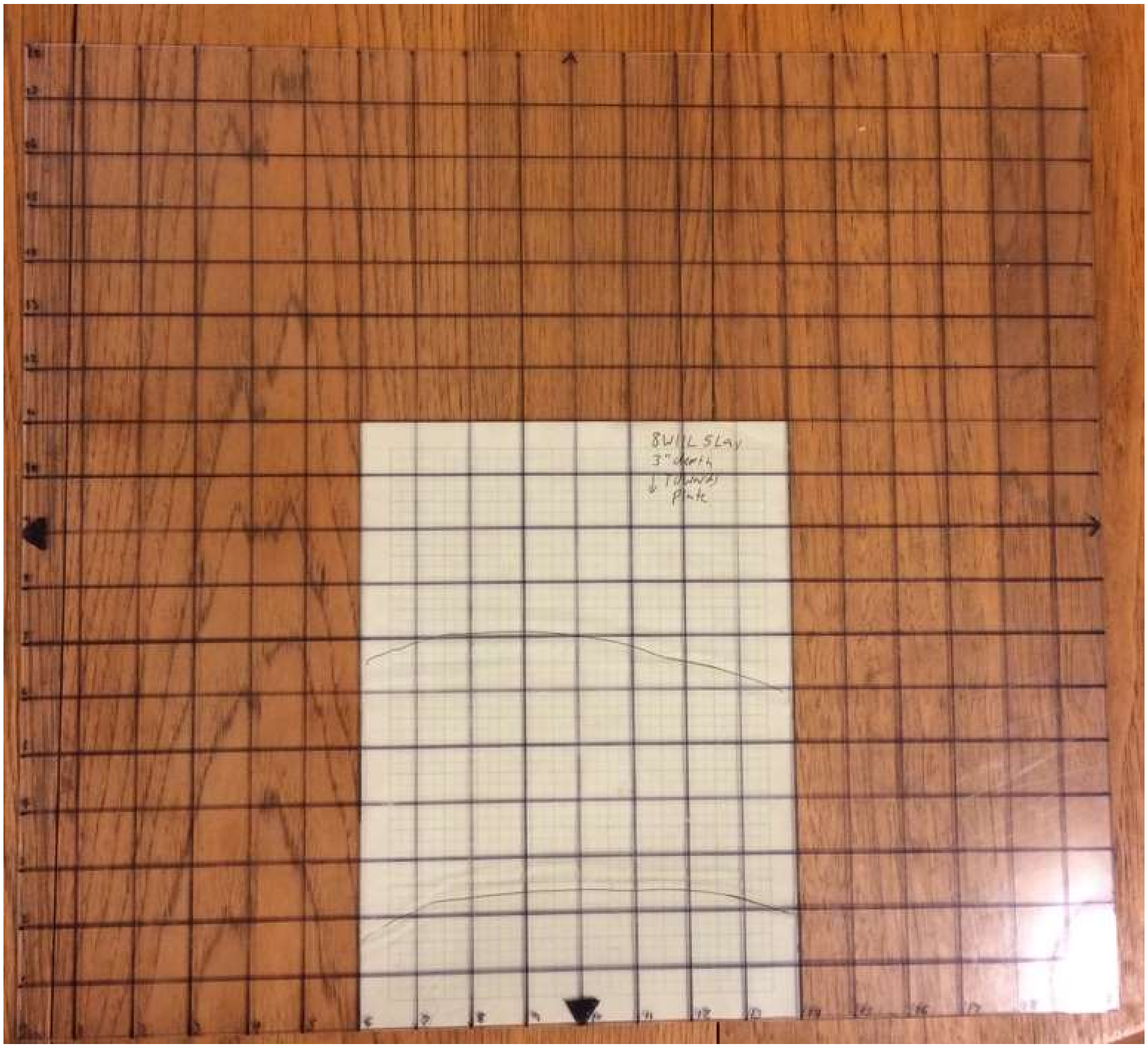

Figure 303: Test 8W11L5Lay 3" Depth

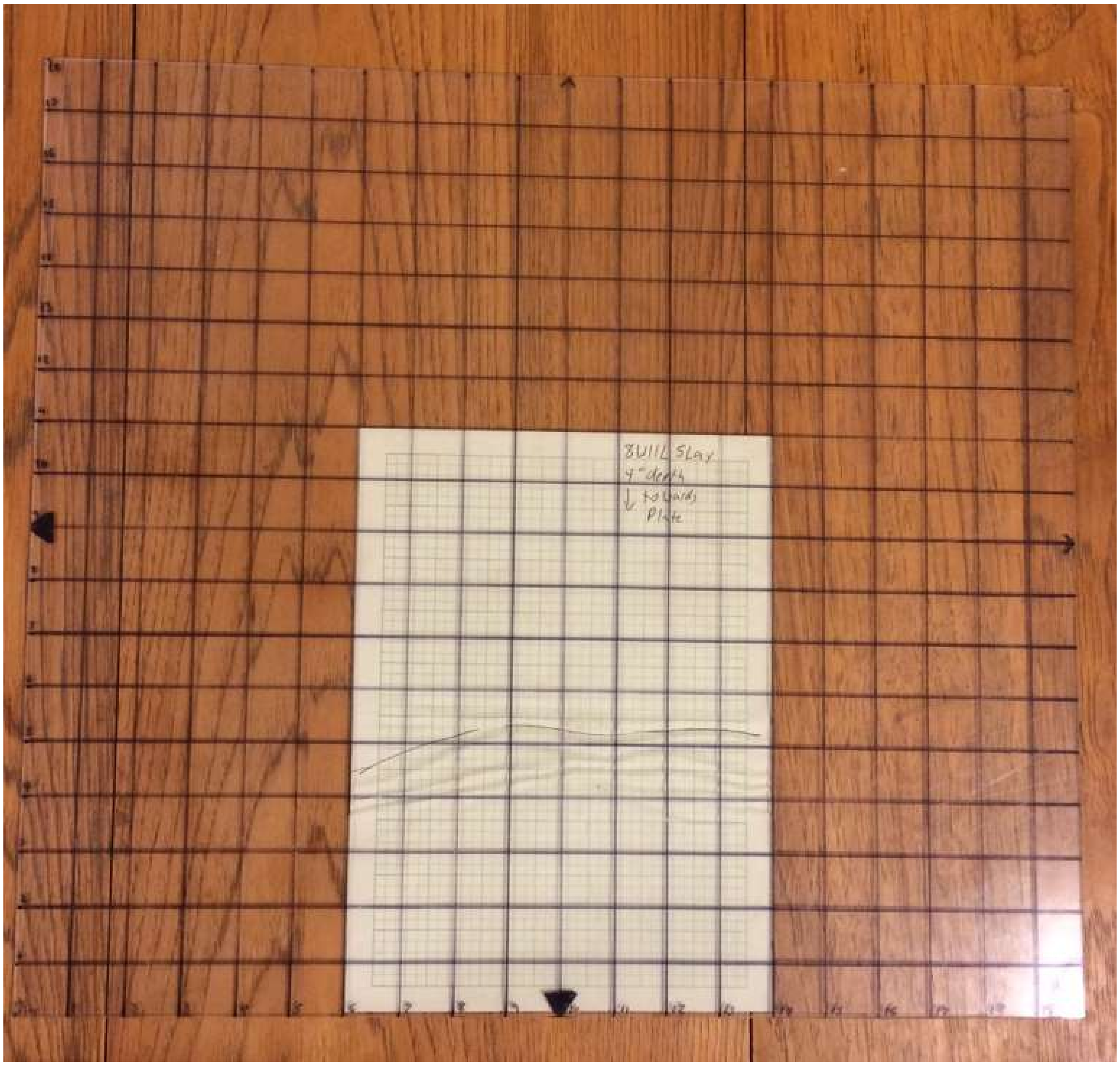

Figure 304: Test 8W11L5Lay 4" Depth

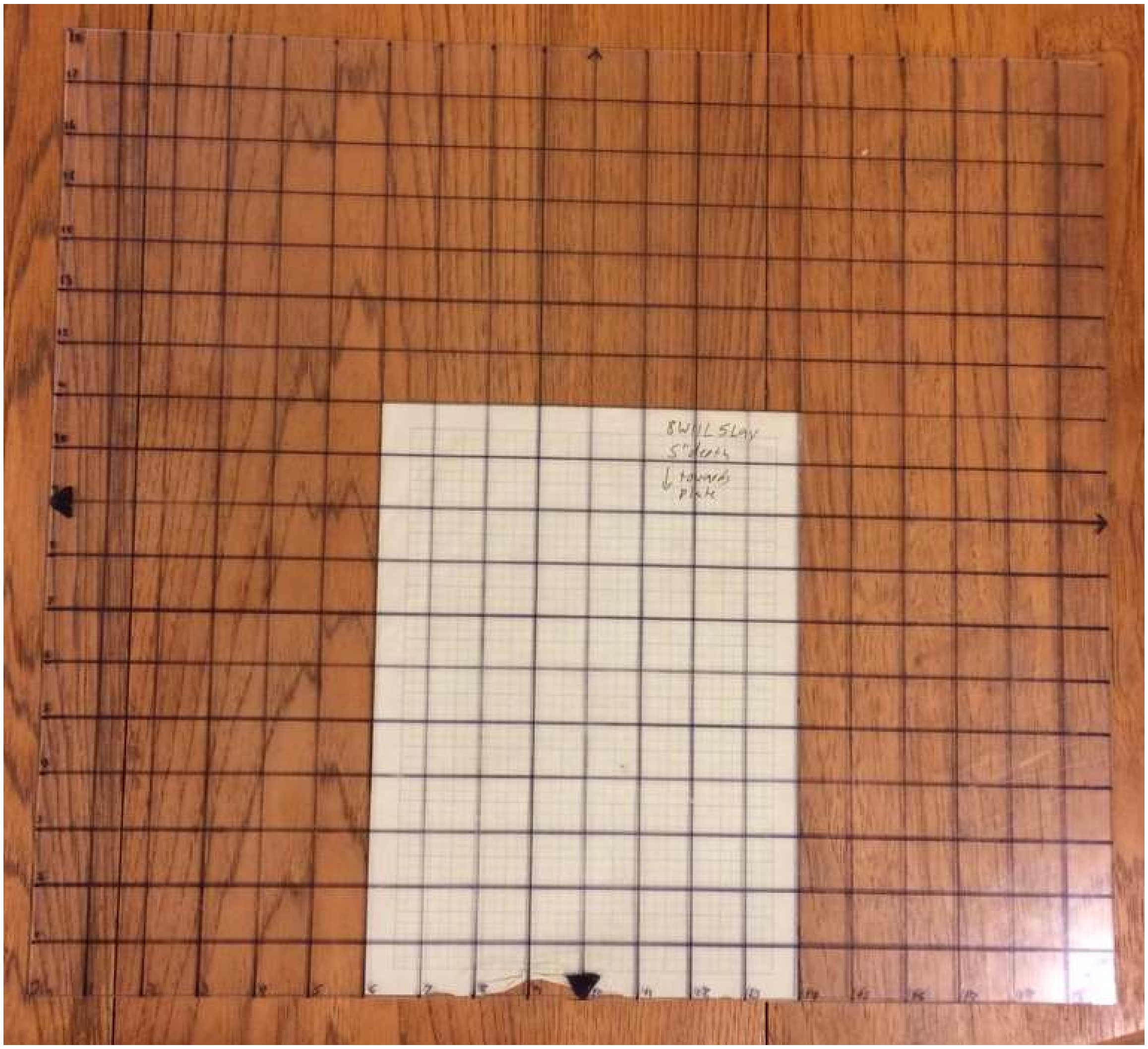

Figure 305: Test 8W11L5Lay 5" Depth

A.19 Photographs of Test 8W11L10Lay

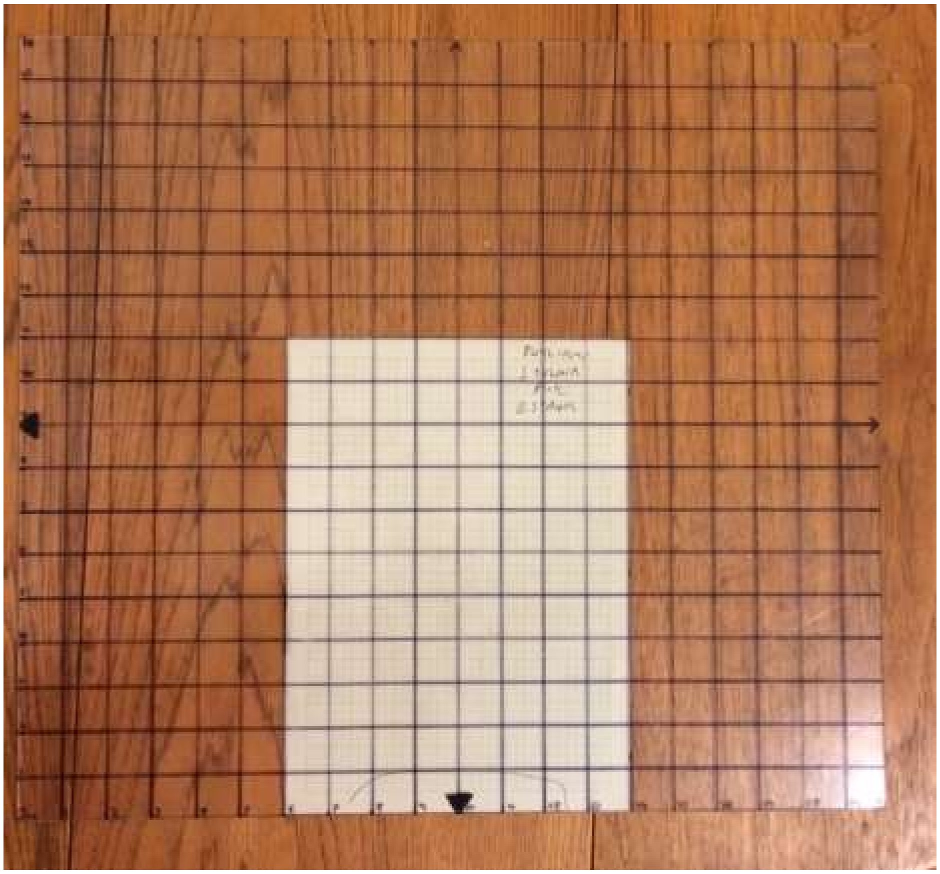

Figure 306: Test 8W11L10Lay 0.5" Depth

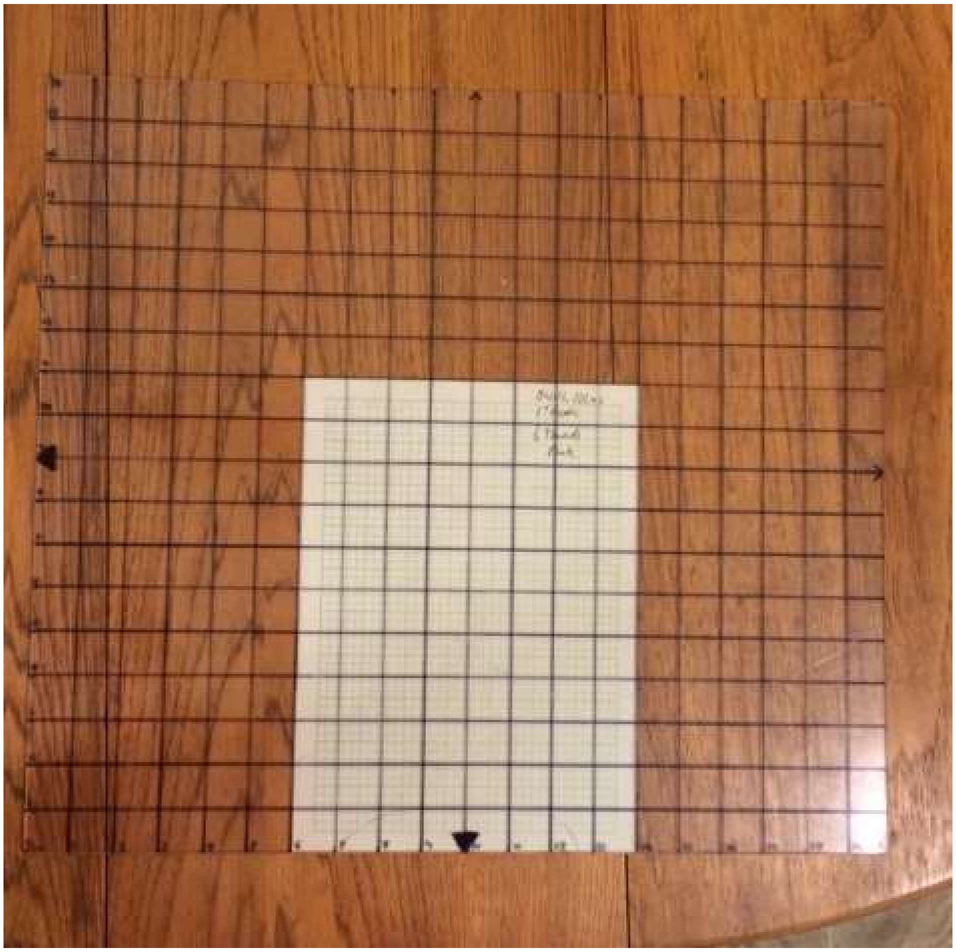

Figure 307: Test 8W11L10Lay 1" Depth

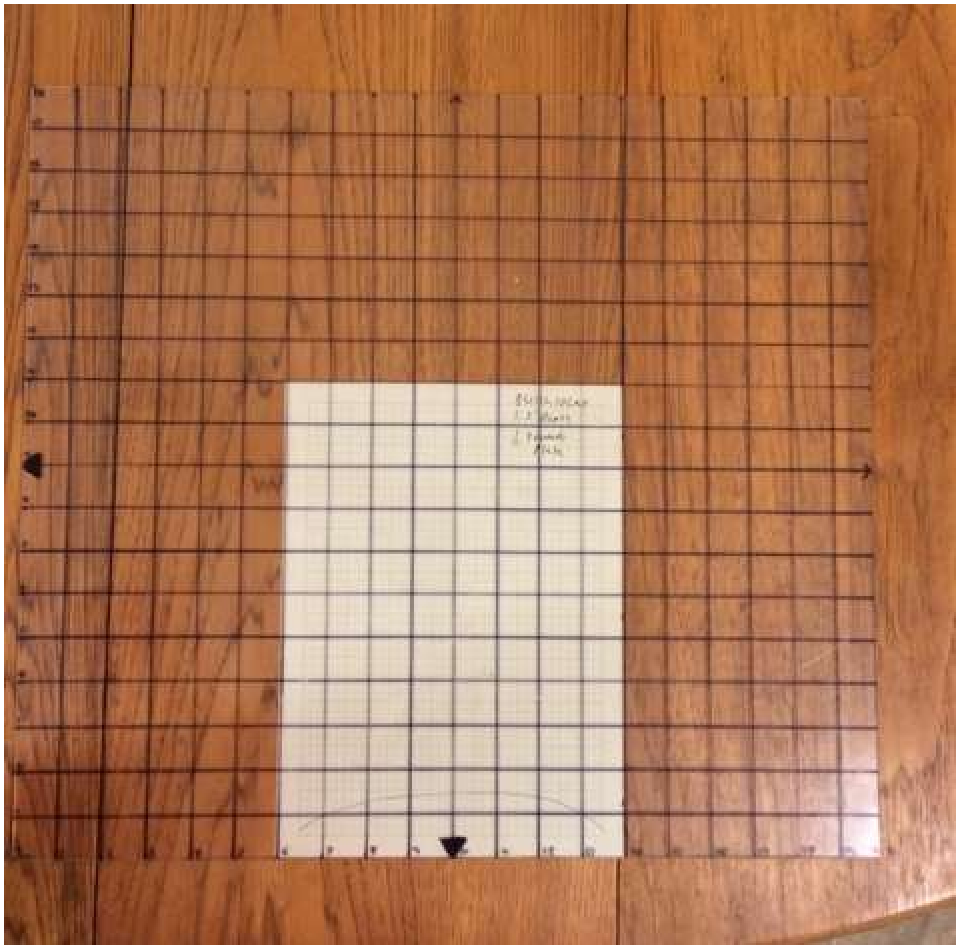

Figure 308: Test 8W11L10Lay 1.5" Depth

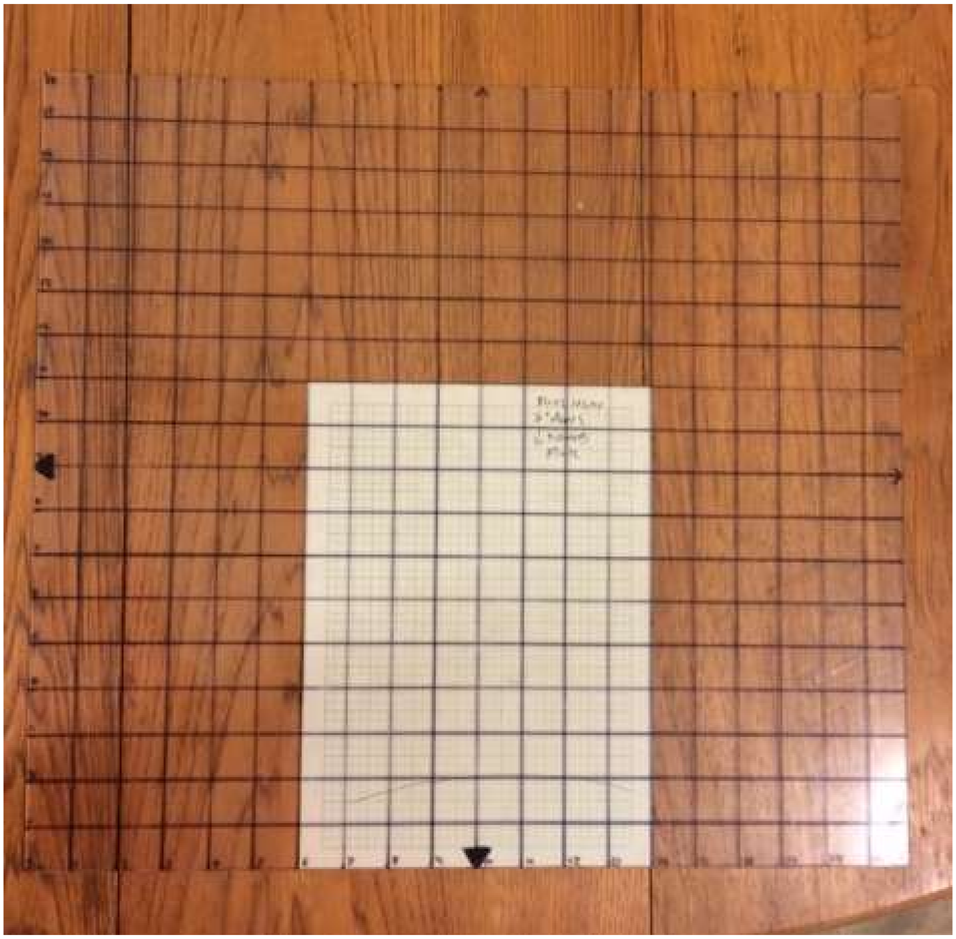

Figure 309: Test 8W11L10Lay 2" Depth

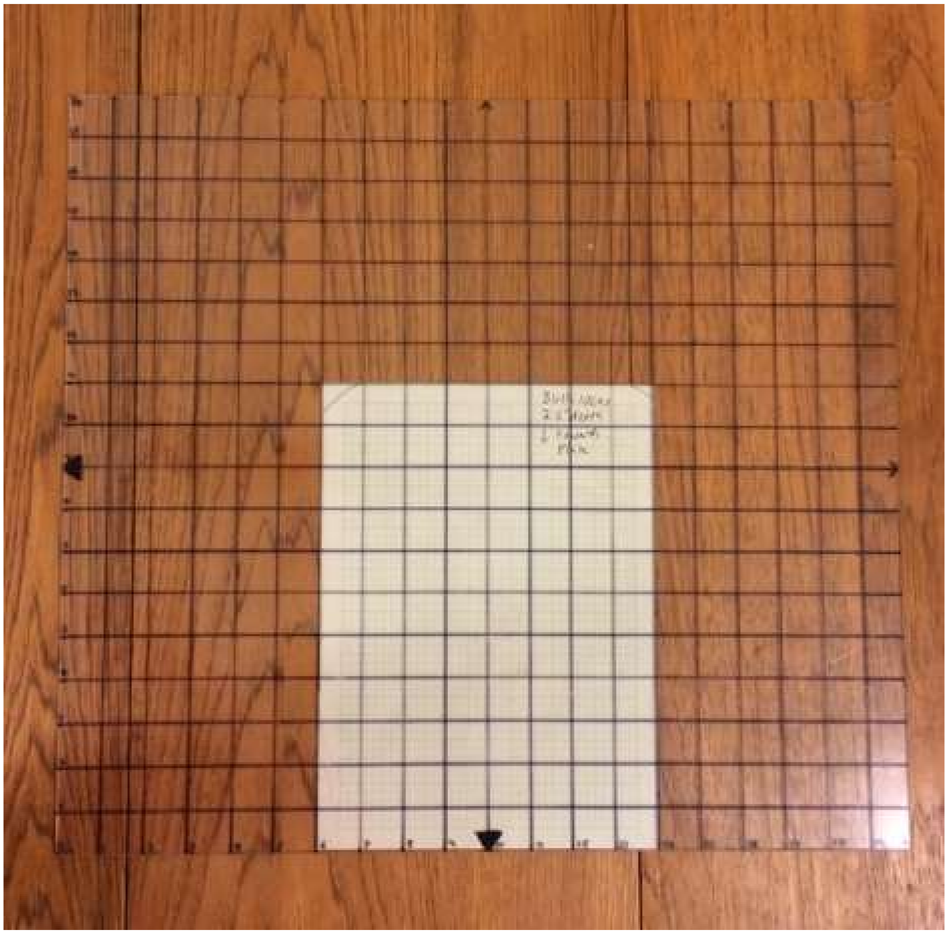

Figure 310: Test 8W11L10Lay 2.5” Depth

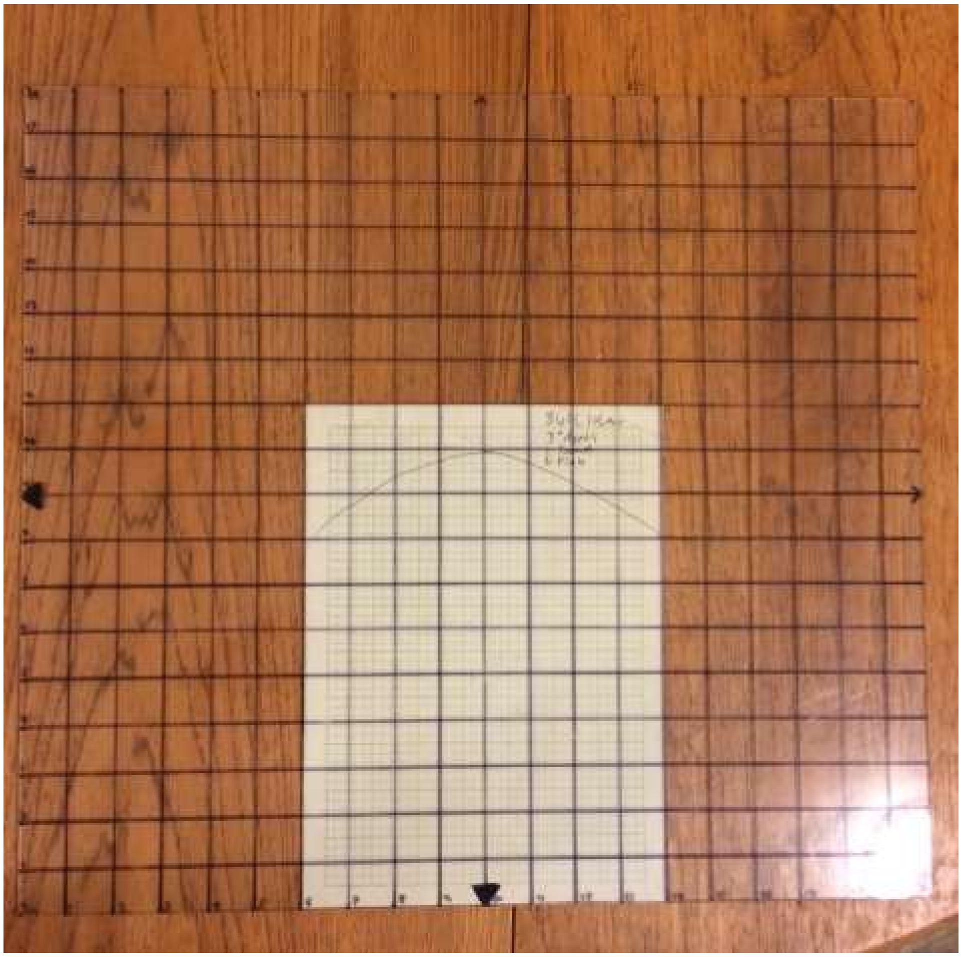

Figure 311: Test 8W11L10Lay 3” Depth

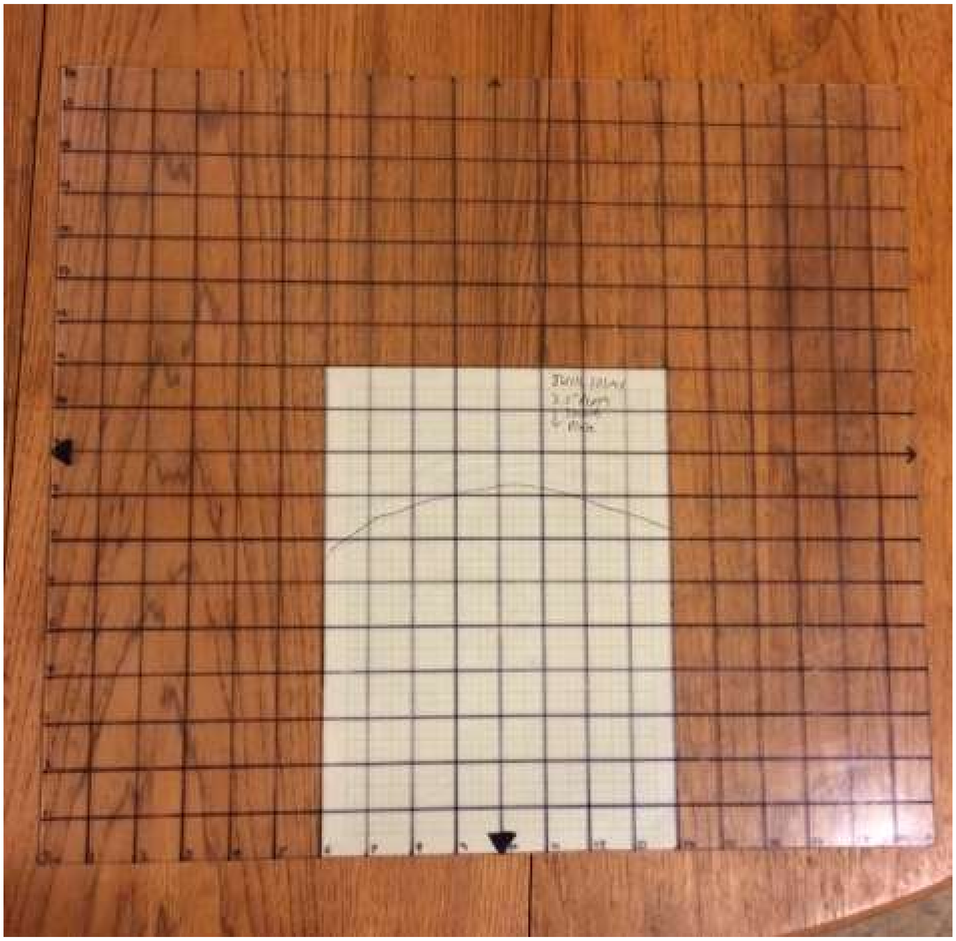

Figure 312: Test 8W11L10Lay 3.5" Depth

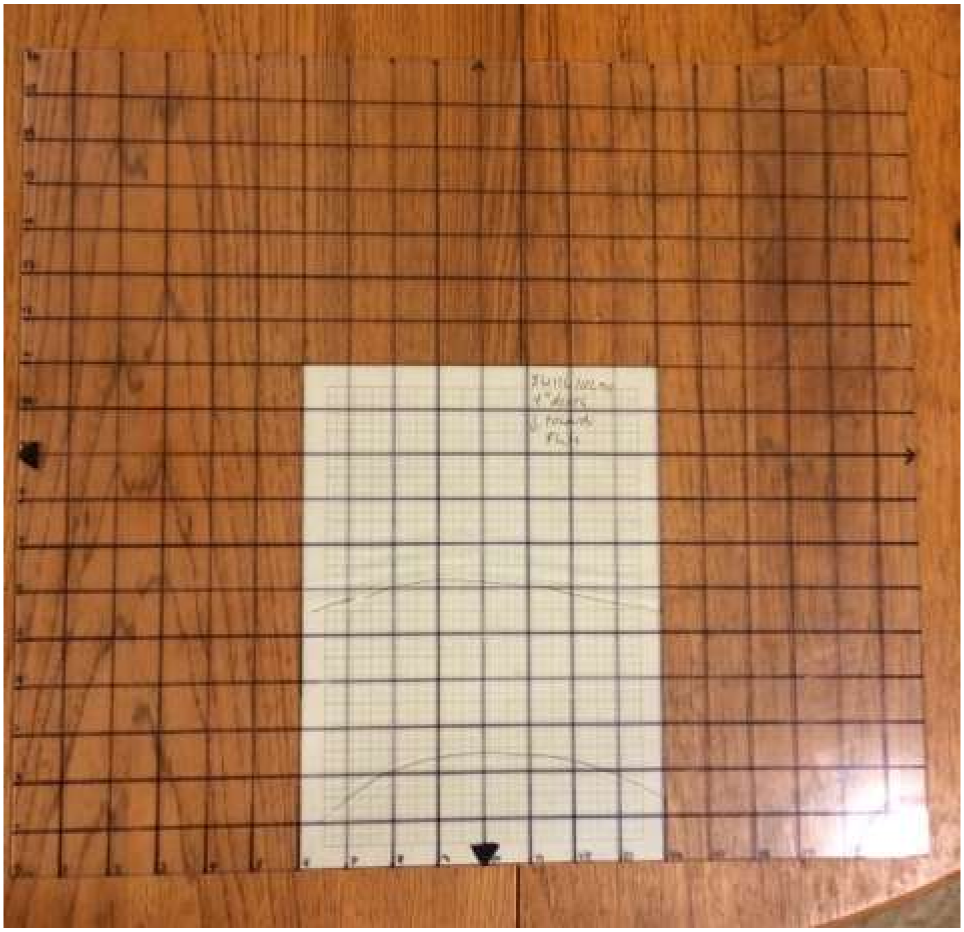

Figure 313: Test 8W11L10Lay 4" Depth

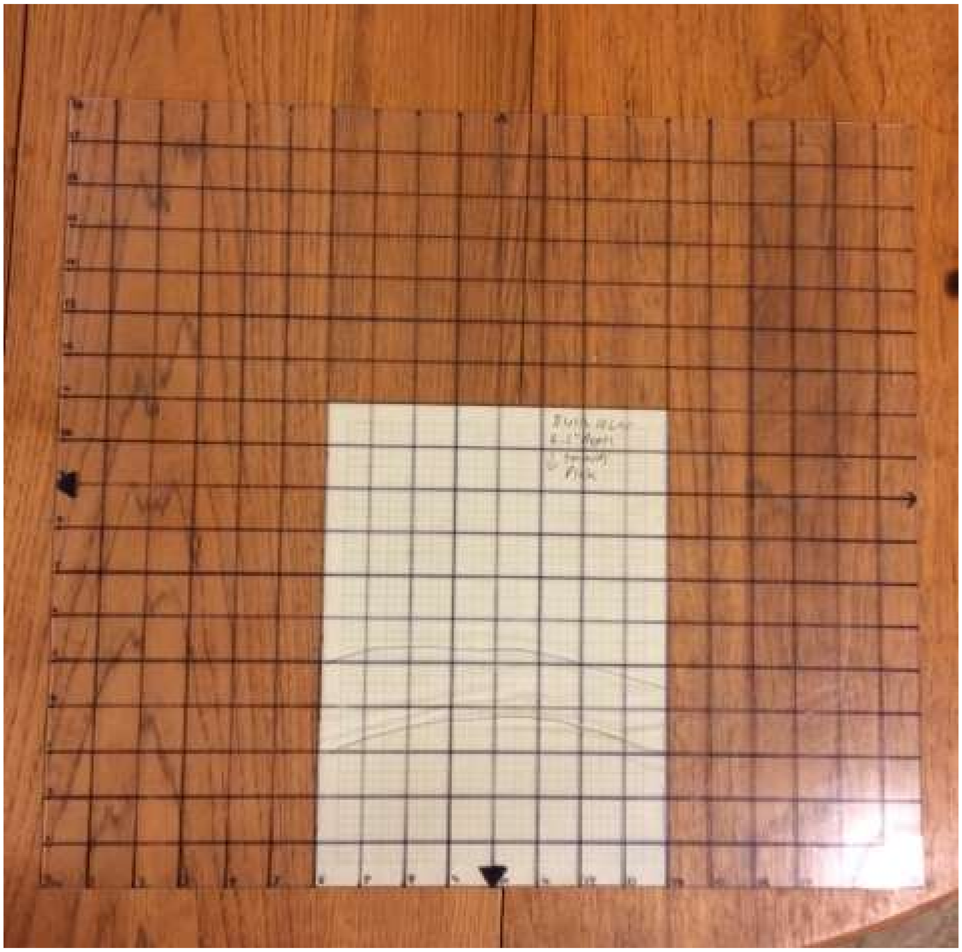

Figure 314: Test 8W11L10Lay 4.5” Depth

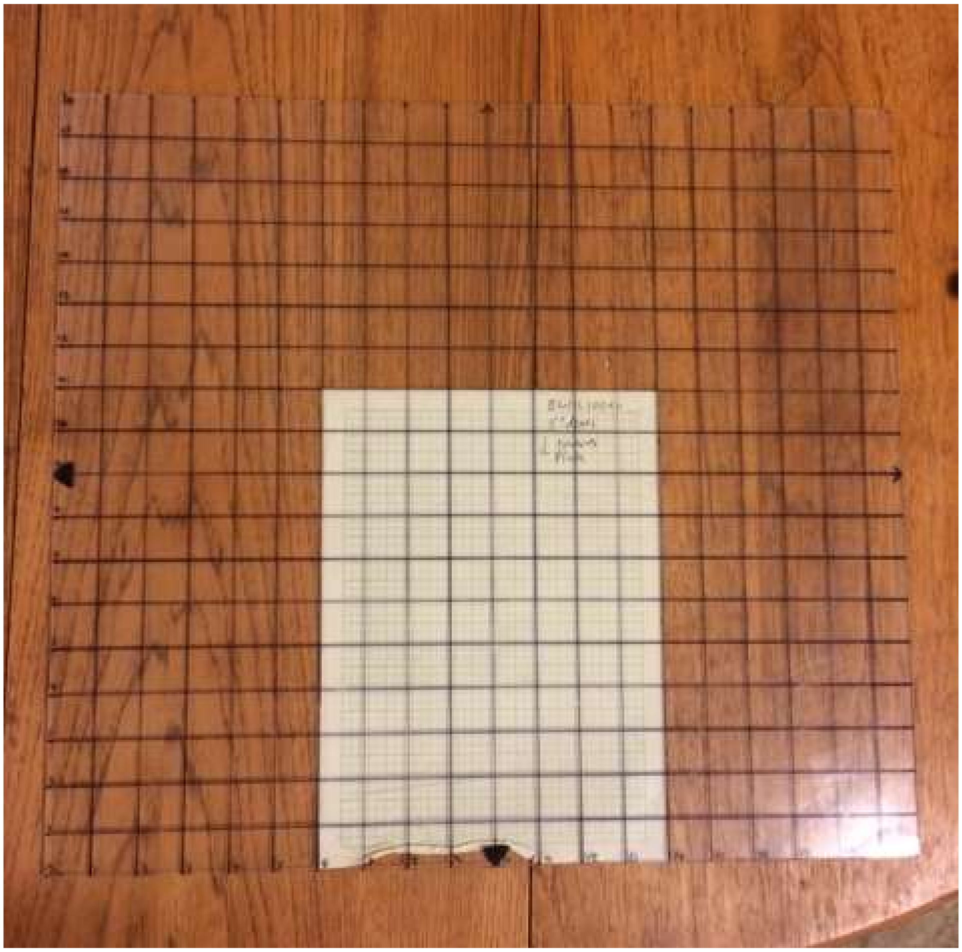

Figure 315: Test 8W11L10Lay 5" Depth

A.20 Photographs of Test 8W11L10Lay2

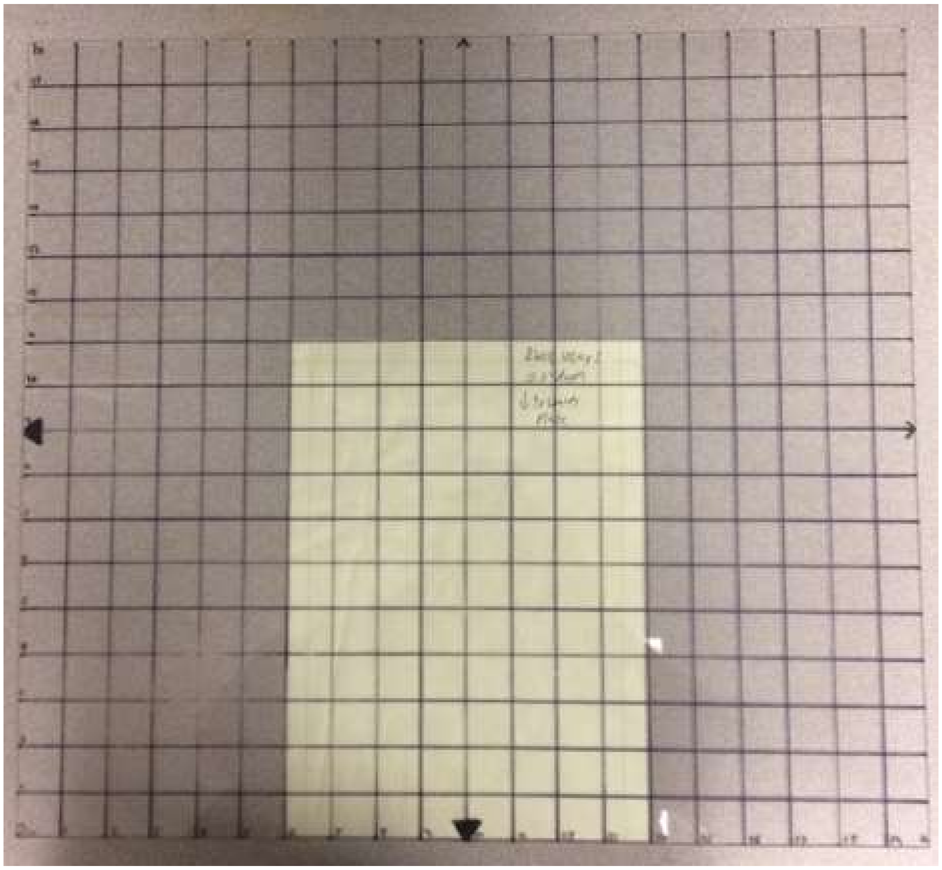

Figure 316: Test 8W11L10Lay2 0.5" Depth

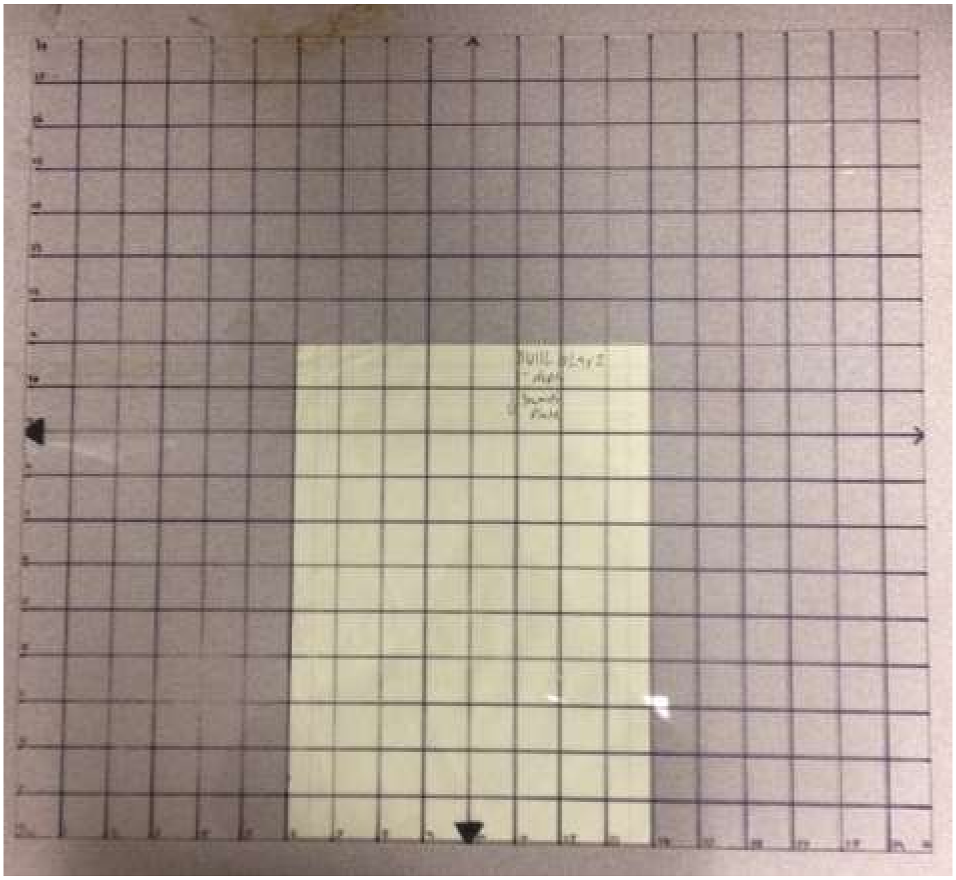

Figure 317: Test 8W11L10Lay2 1" Depth

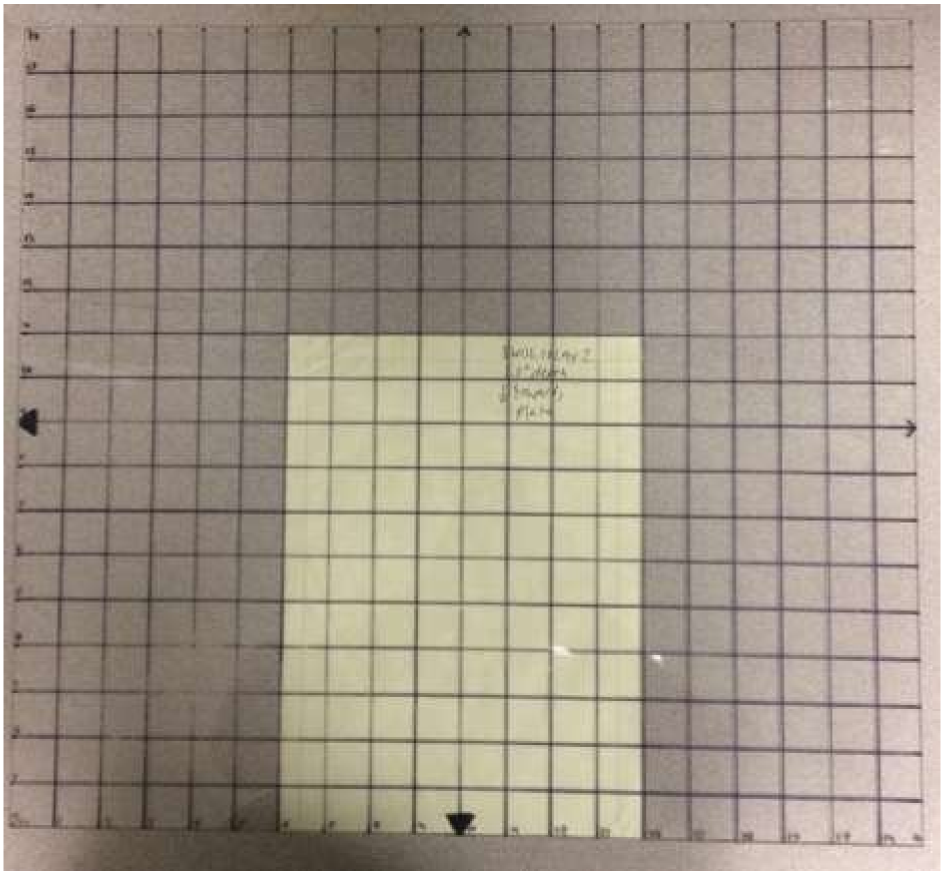

Figure 318: Test 8W11L10Lay2 1.5” Depth

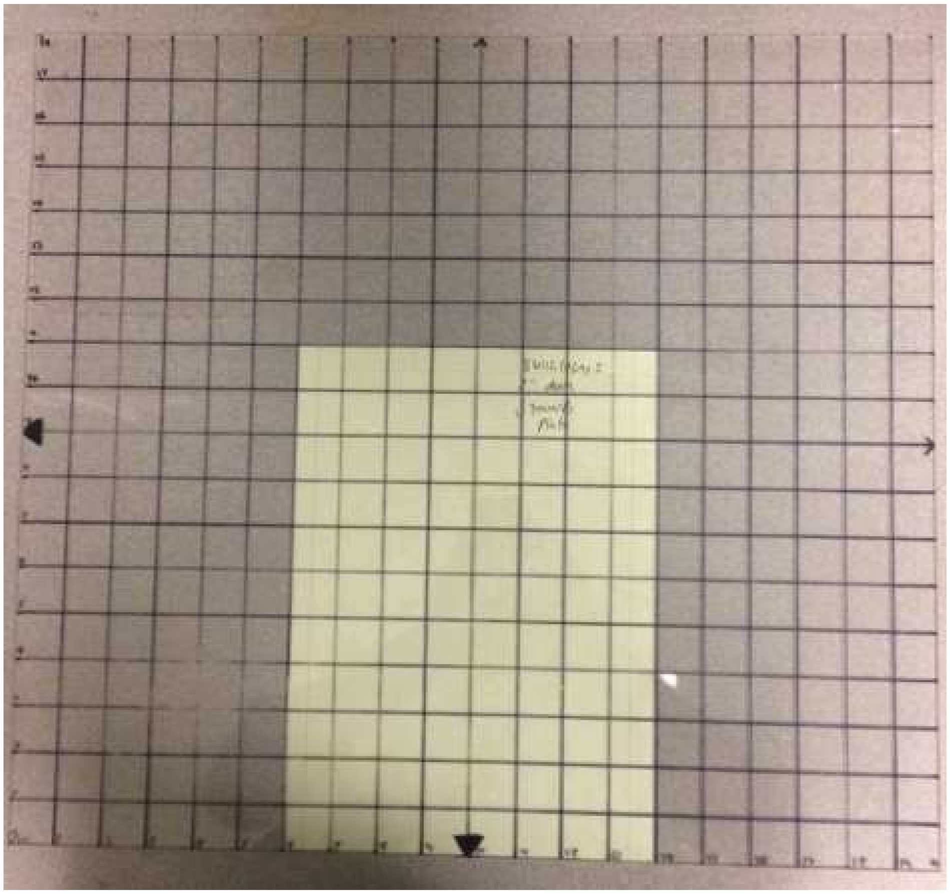

Figure 319: Test 8W11L10Lay2 2" Depth

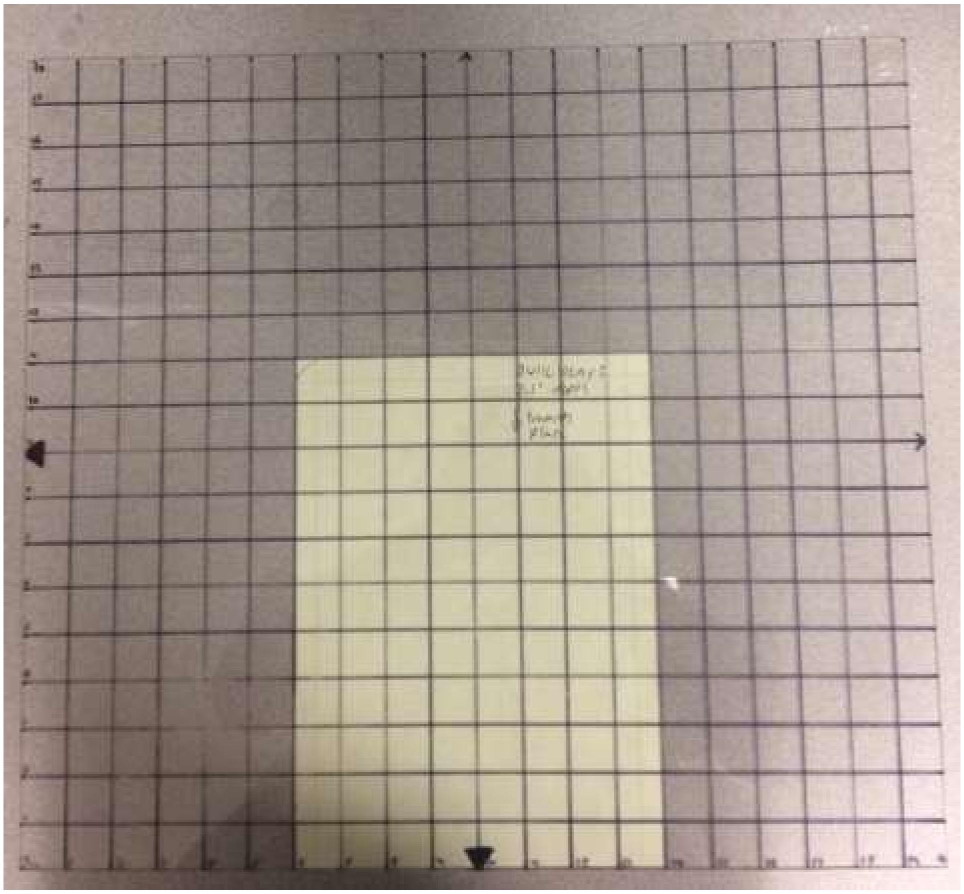

Figure 320: Test 8W11L10Lay2 2.5” Depth

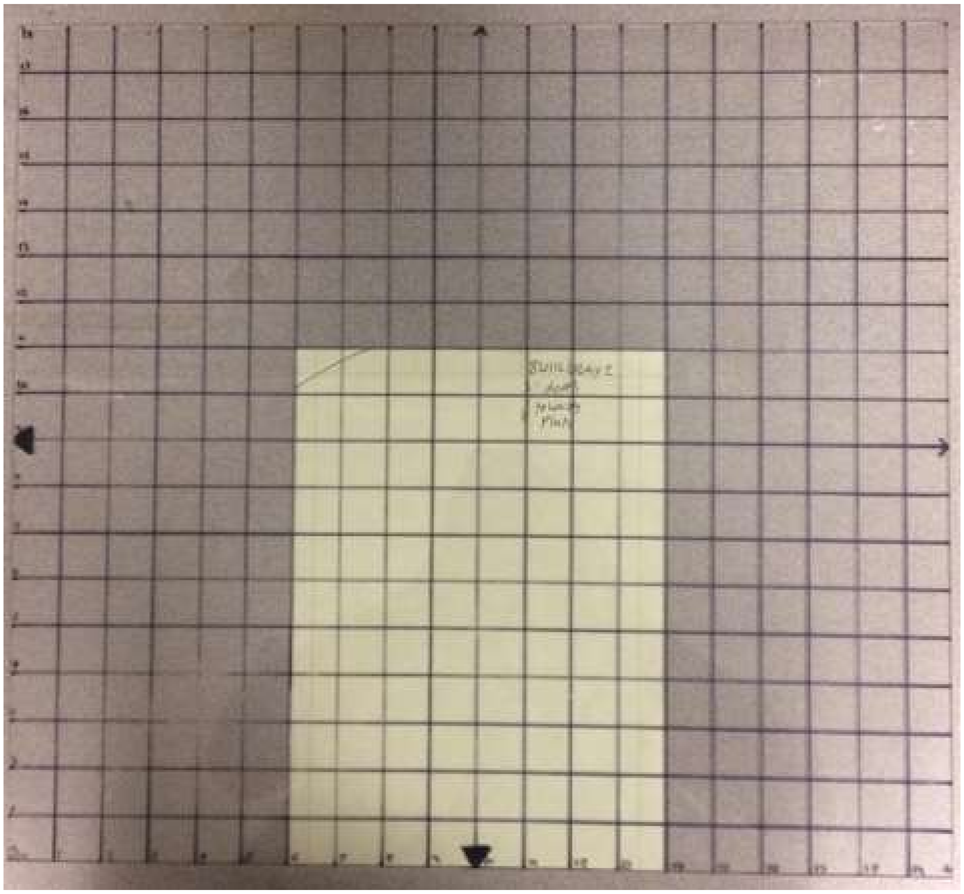

Figure 321: Test 8W11L10Lay2 3" Depth

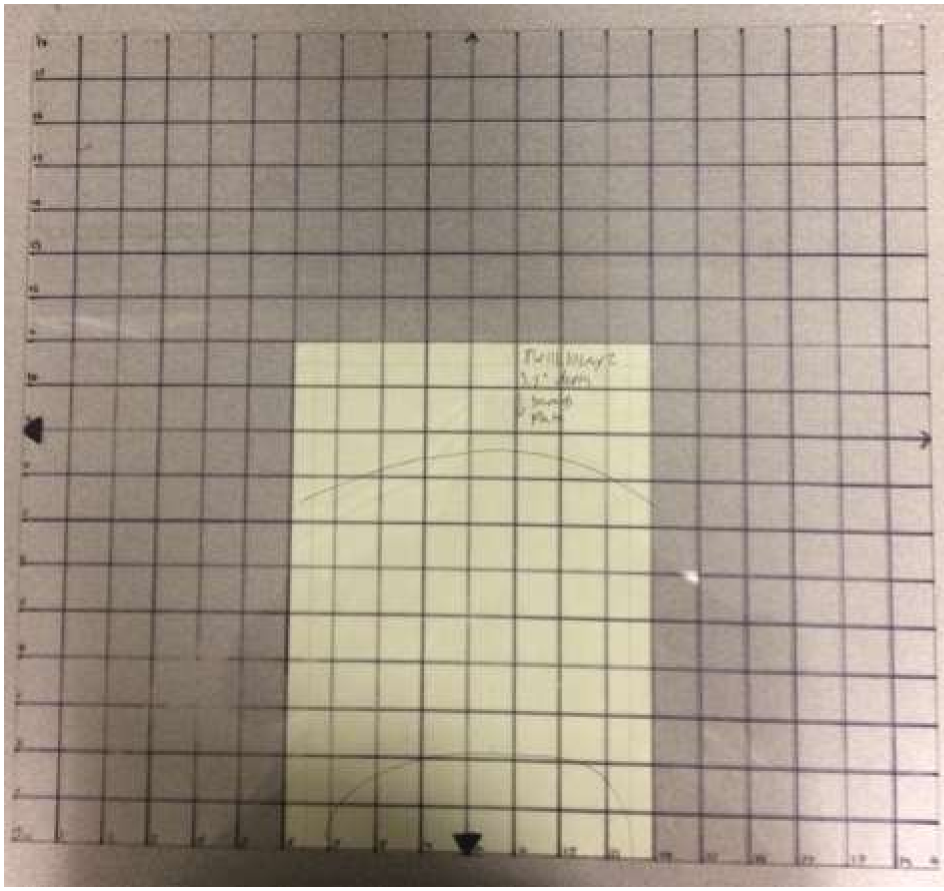

Figure 322: Test 8W11L10Lay2 3.5” Depth

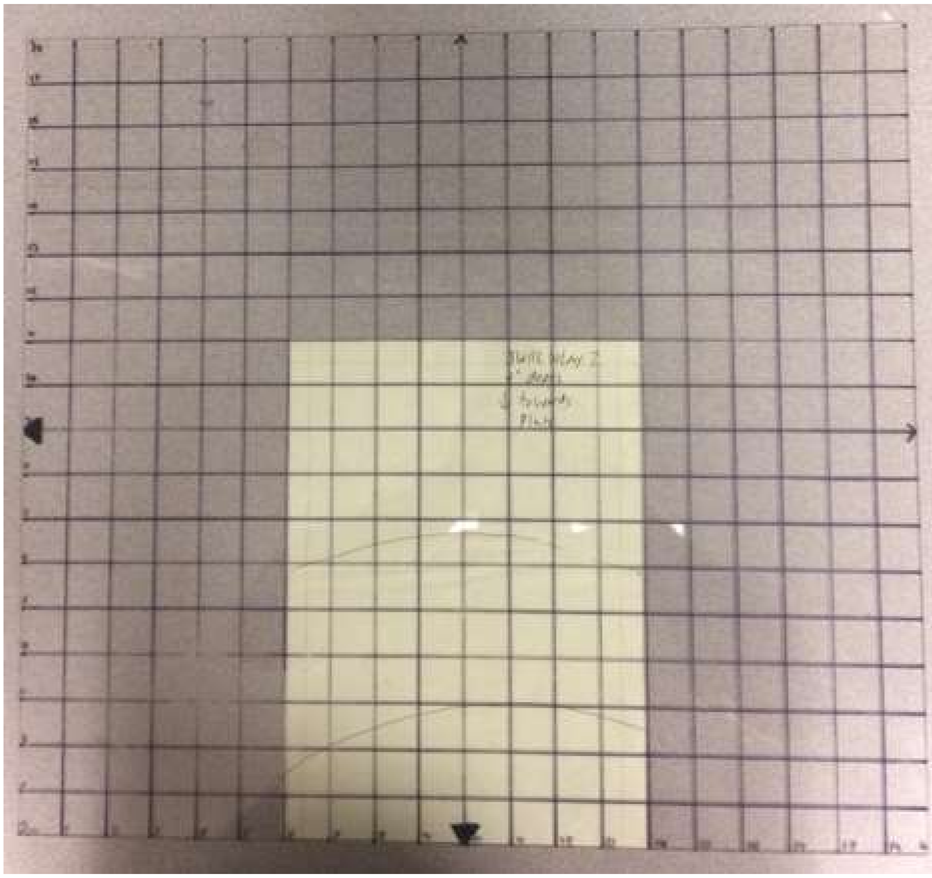

Figure 323: Test 8W11L10Lay2 4” Depth

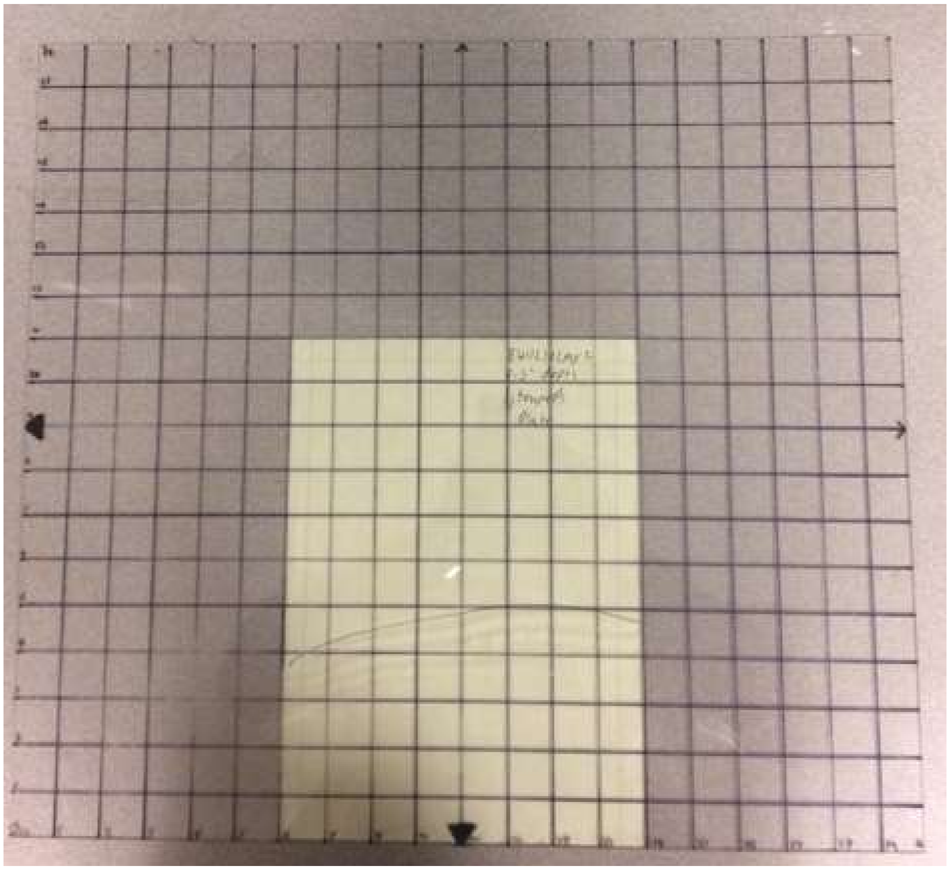

Figure 324: Test 8W11L10Lay2 4.5" Depth

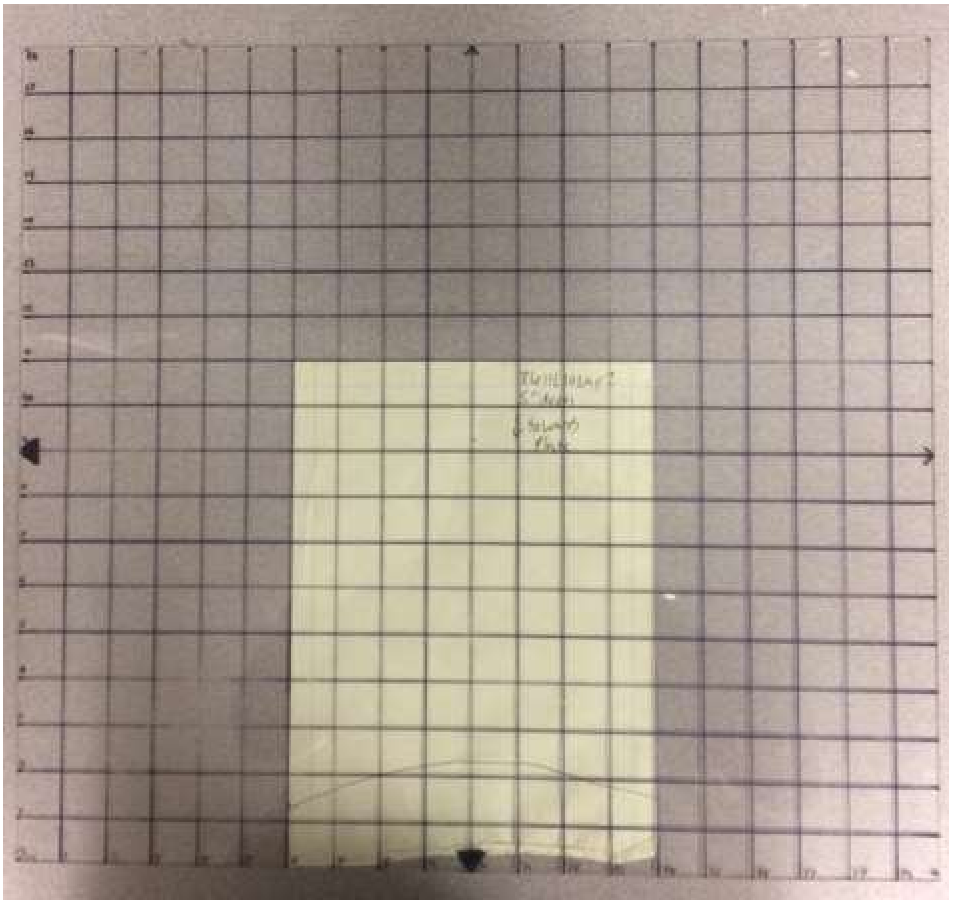

Figure 325: Test 8W11L10Lay2 5" Depth

A.20 Photographs of Test 8W11L5Lay2

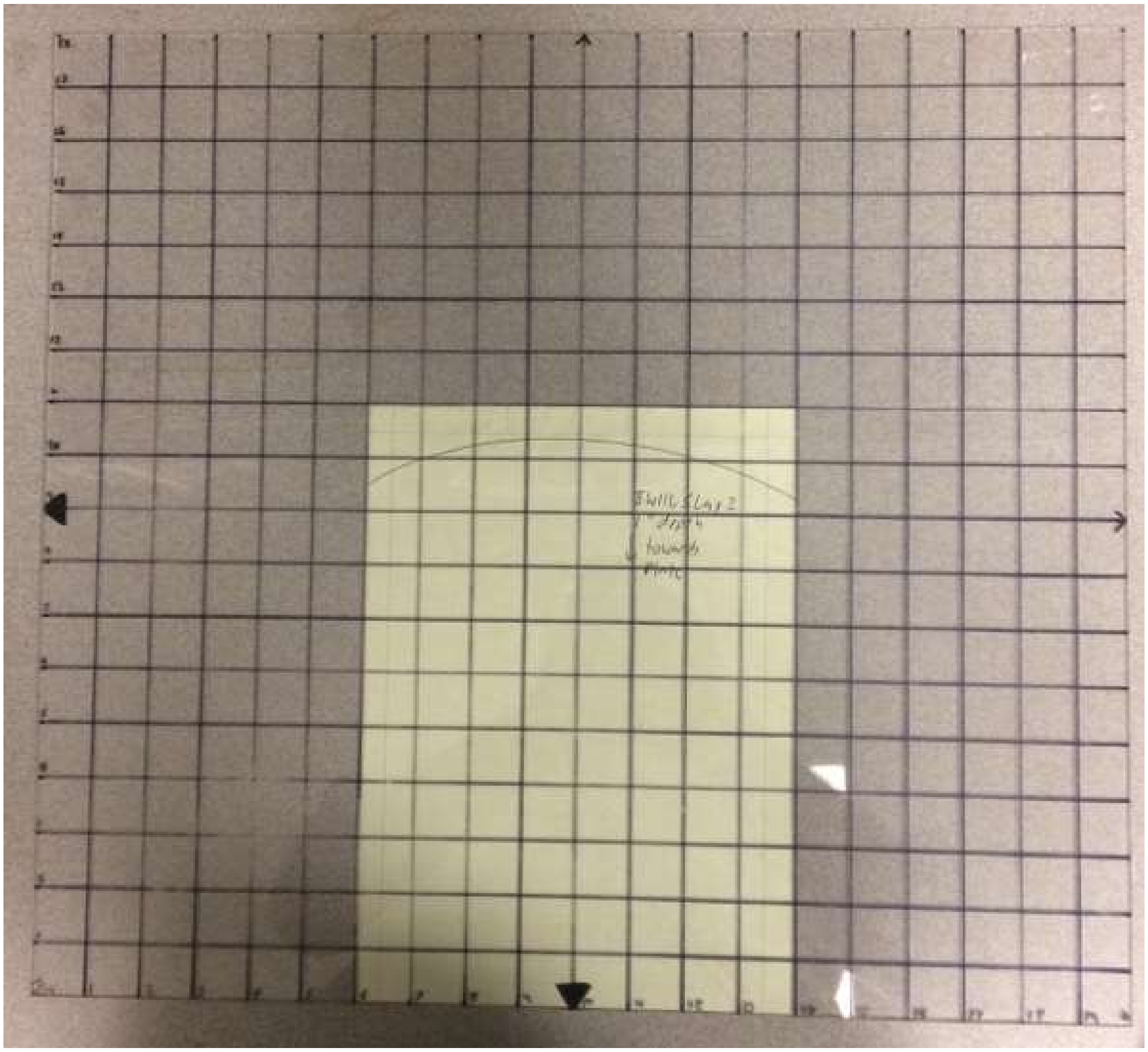

Figure 326: Test 8W11L5Lay2 1” Depth

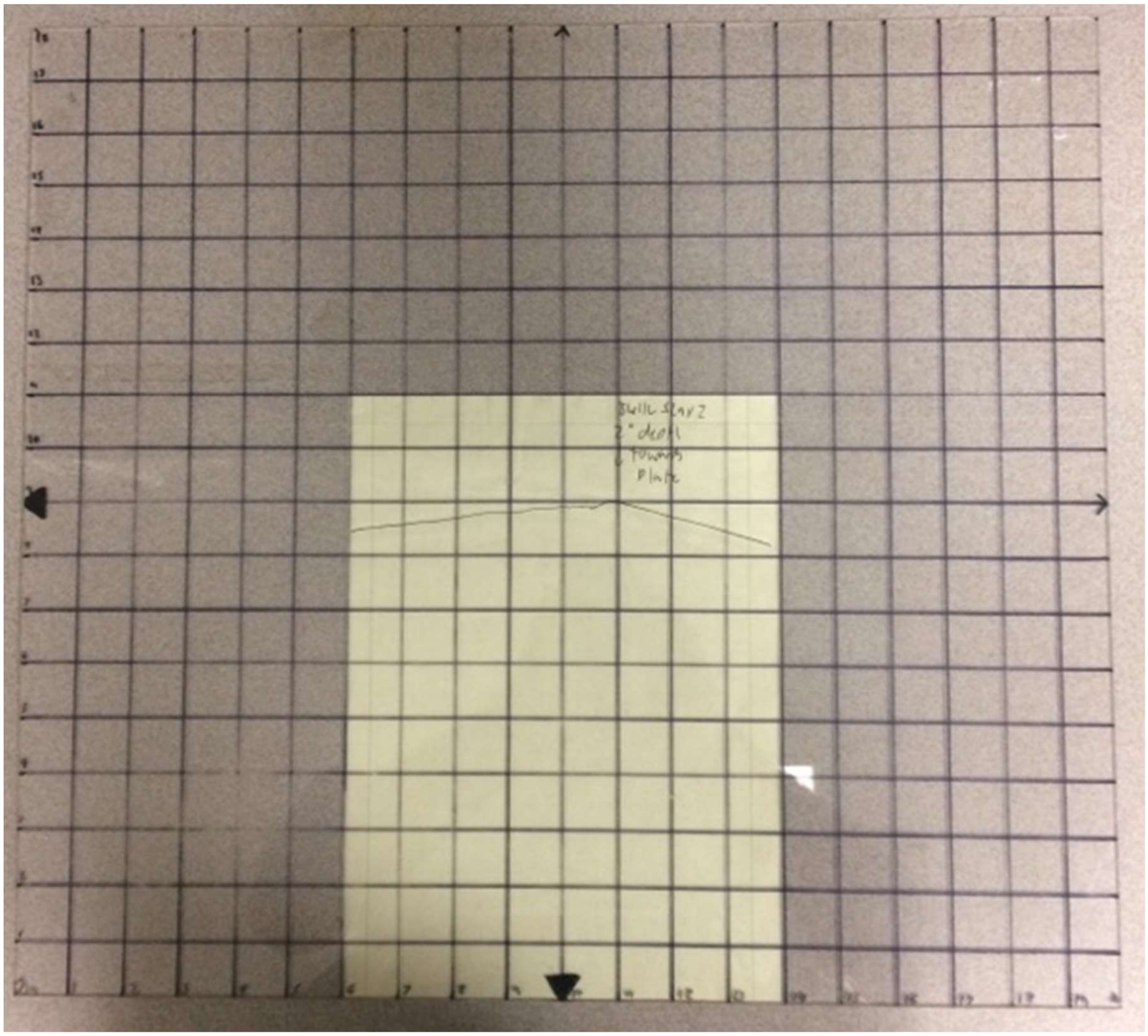

Figure 327: Test 8W11L5Lay2 2” Depth

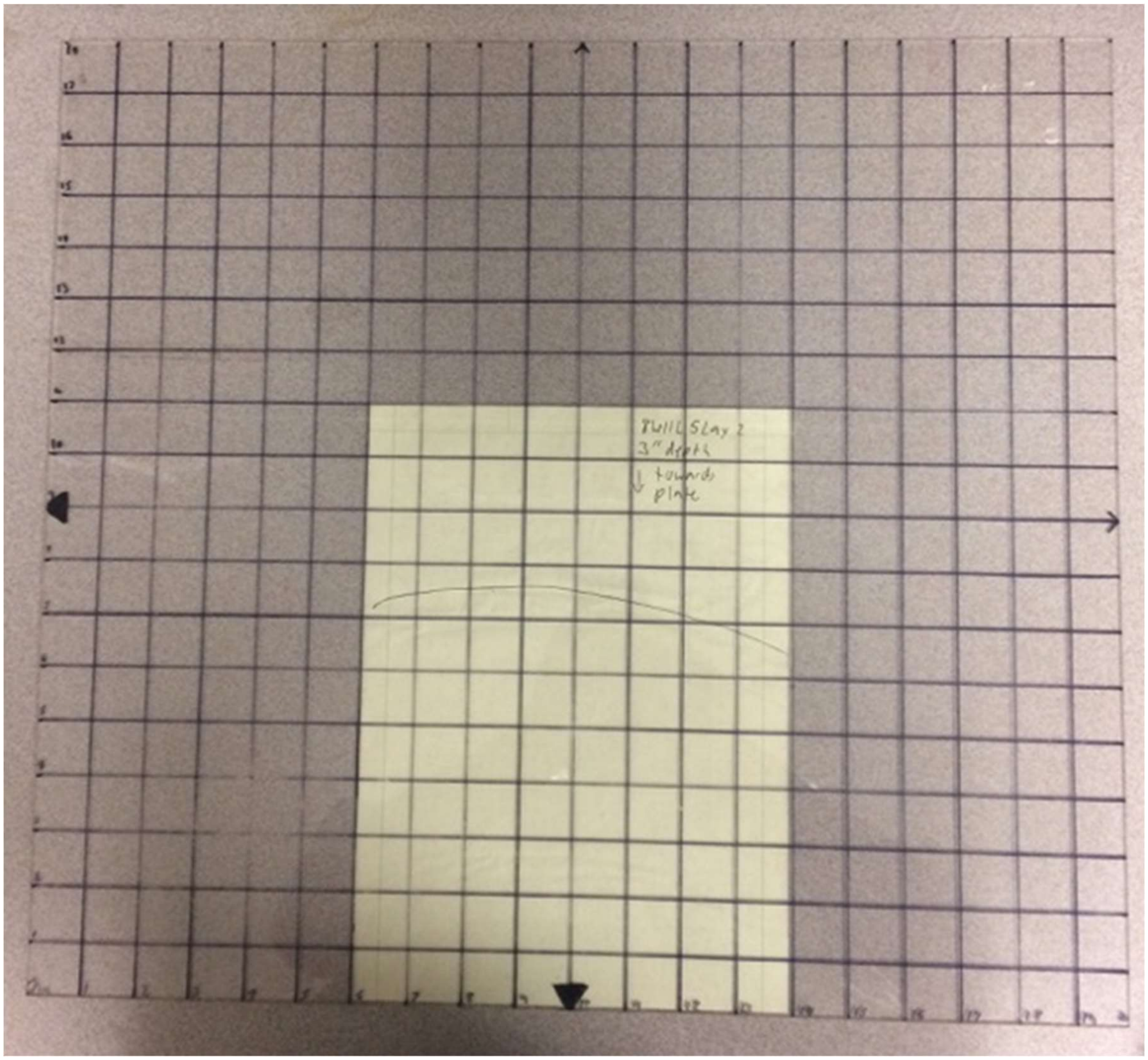

Figure 328: Test 8W11L5Lay2 3” Depth

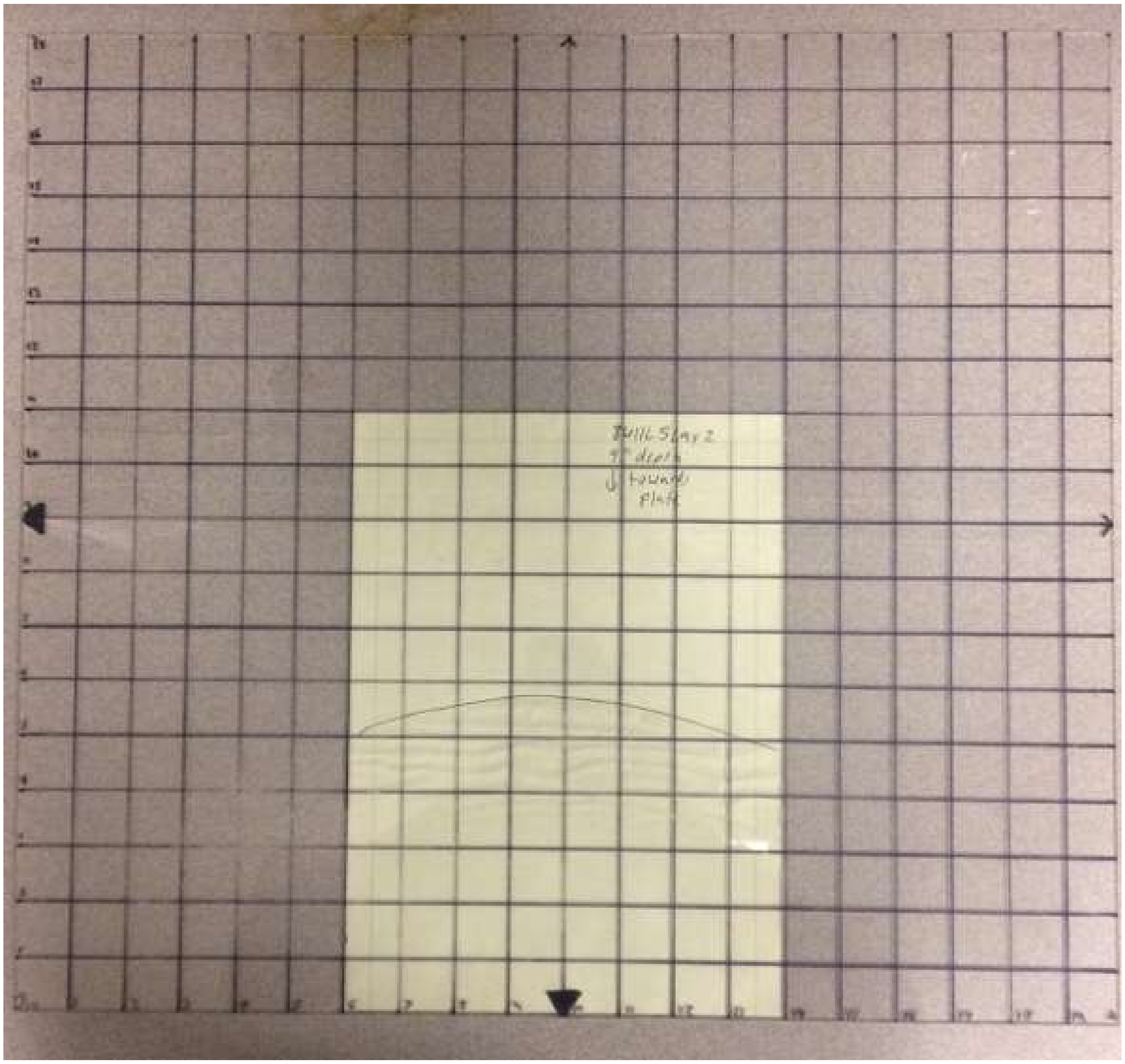

Figure 329: Test 8W11L5Lay2 4” Depth

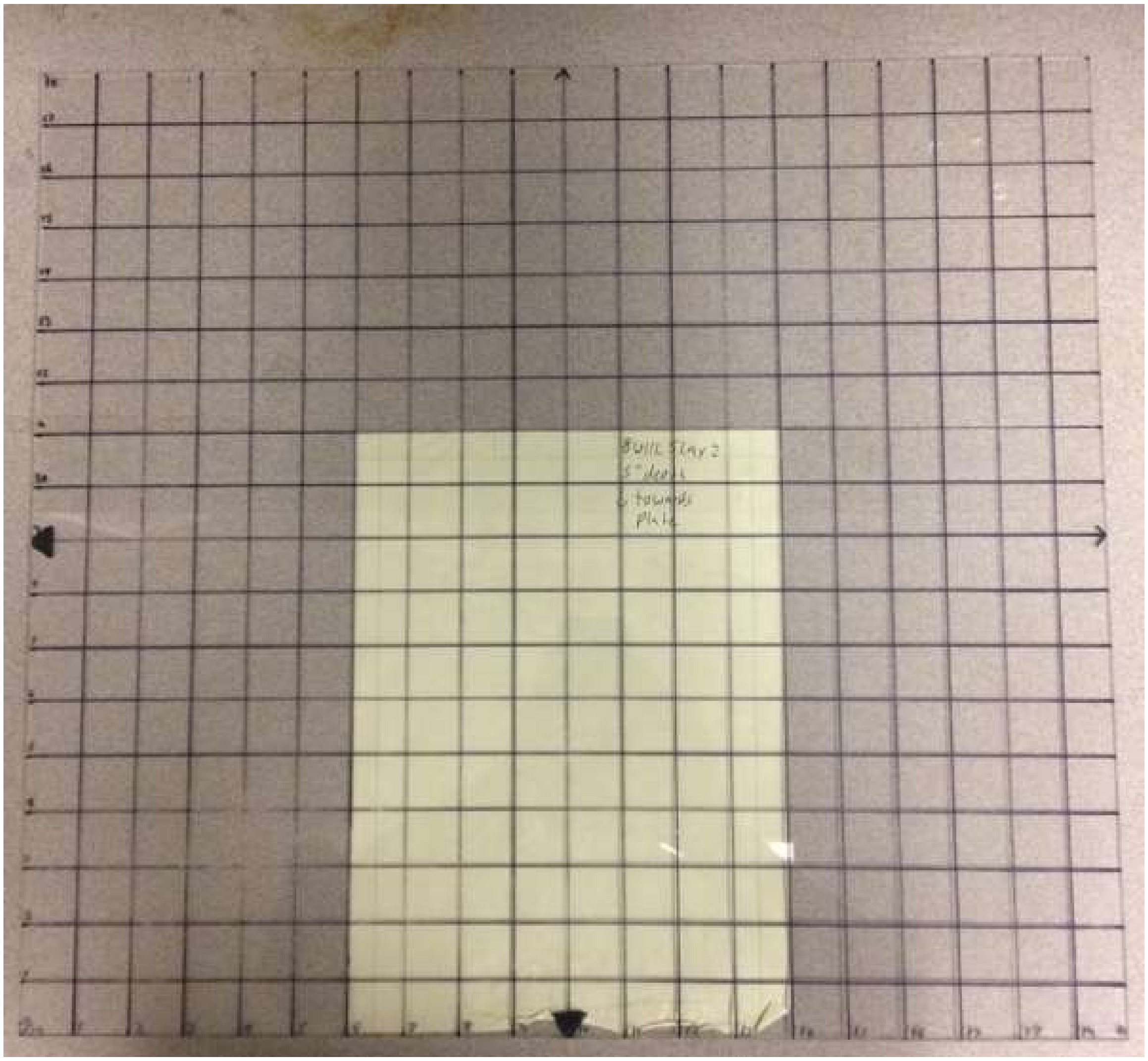

Figure 330: Test 8W11L5Lay2 5” Depth

A.20 Photographs of Test 11W11L10Lay

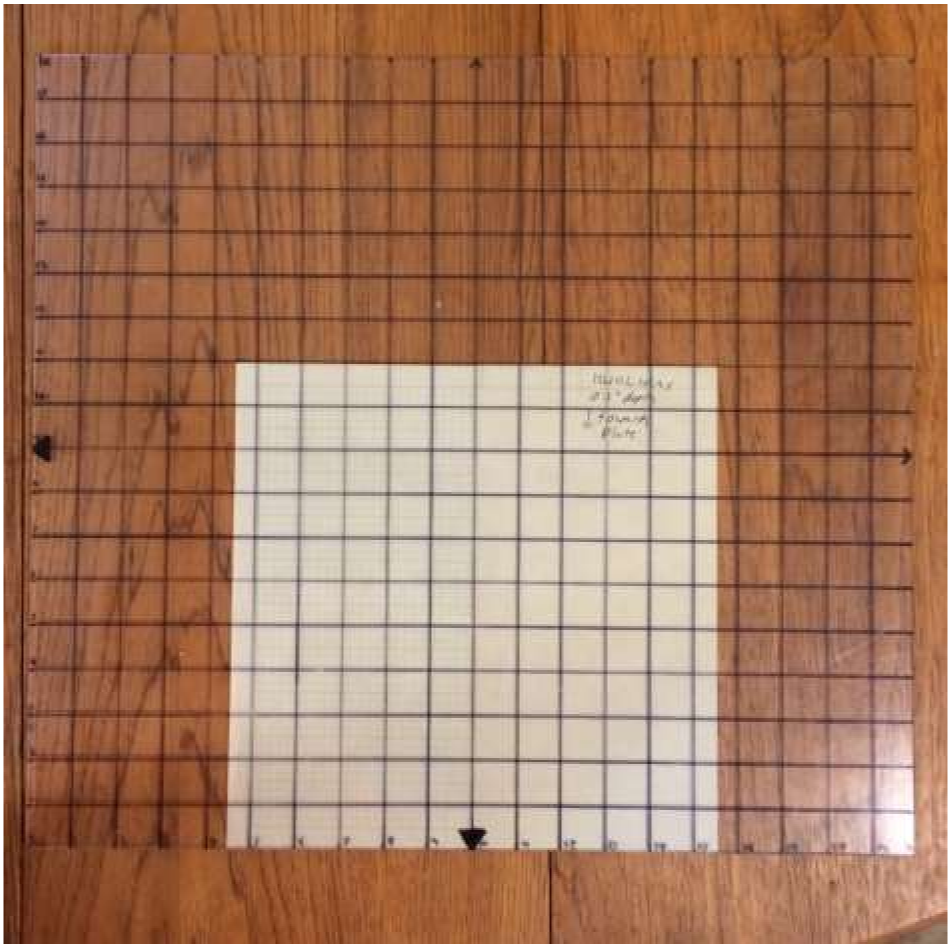

Figure 331: Test 11W11L10Lay 0.5" Depth

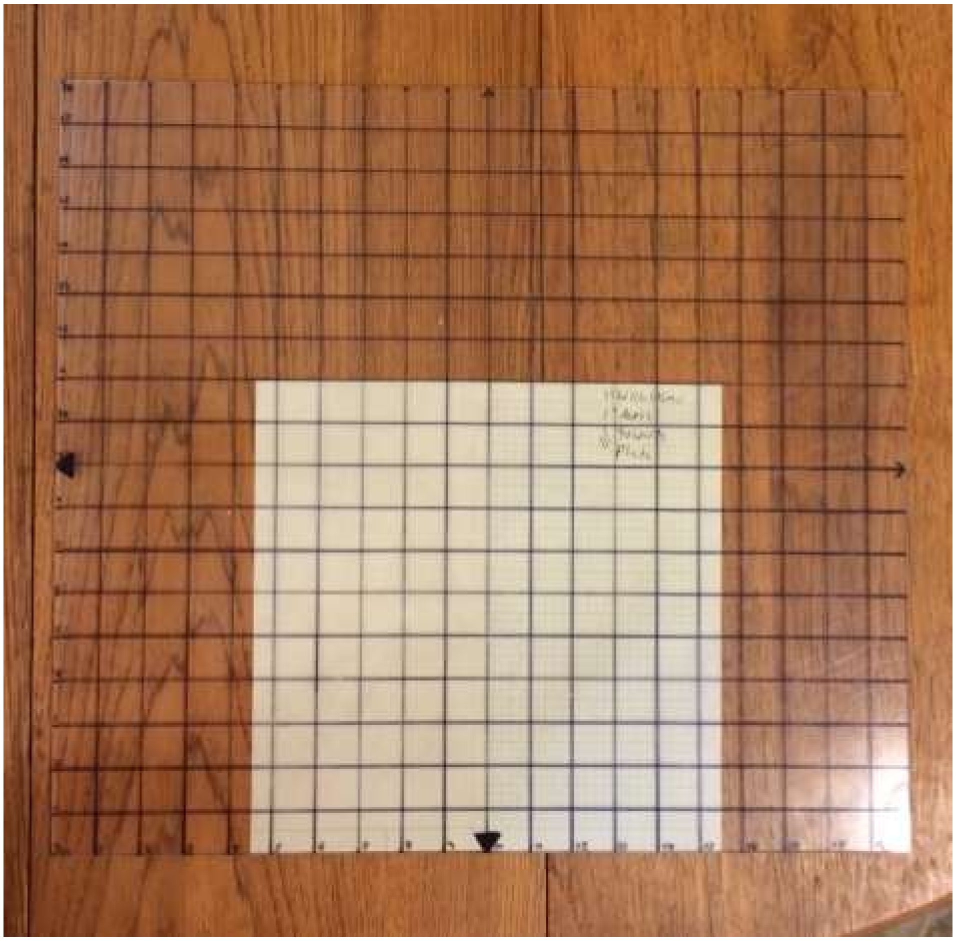

Figure 332: Test 11W11L10Lay 1" Depth

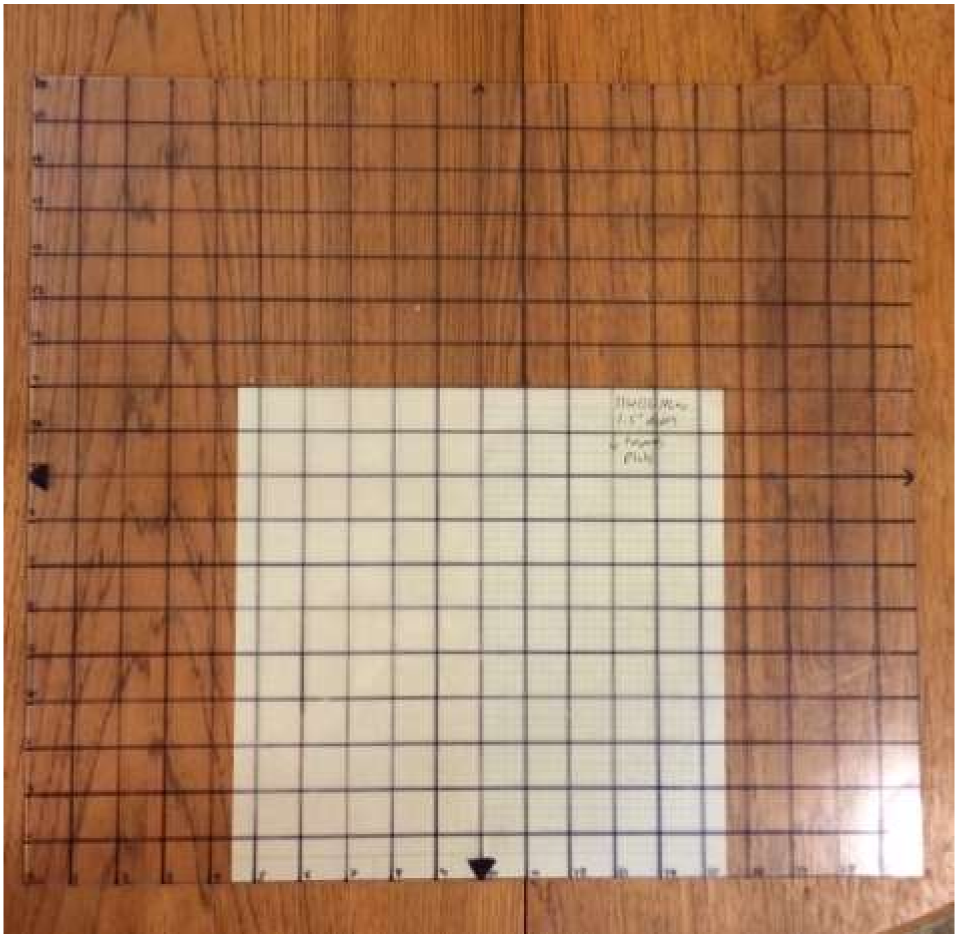

Figure 333: Test 11W11L10Lay 1.5" Depth

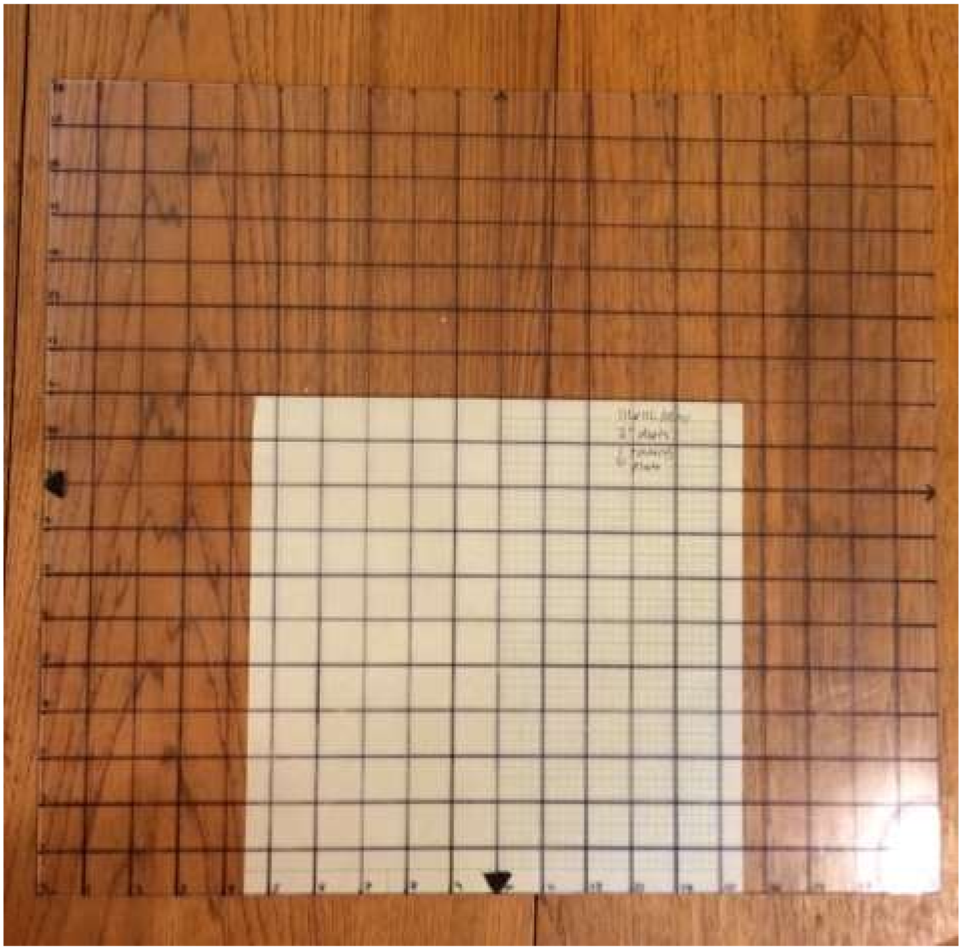

Figure 334: Test 11W11L10Lay 2" Depth

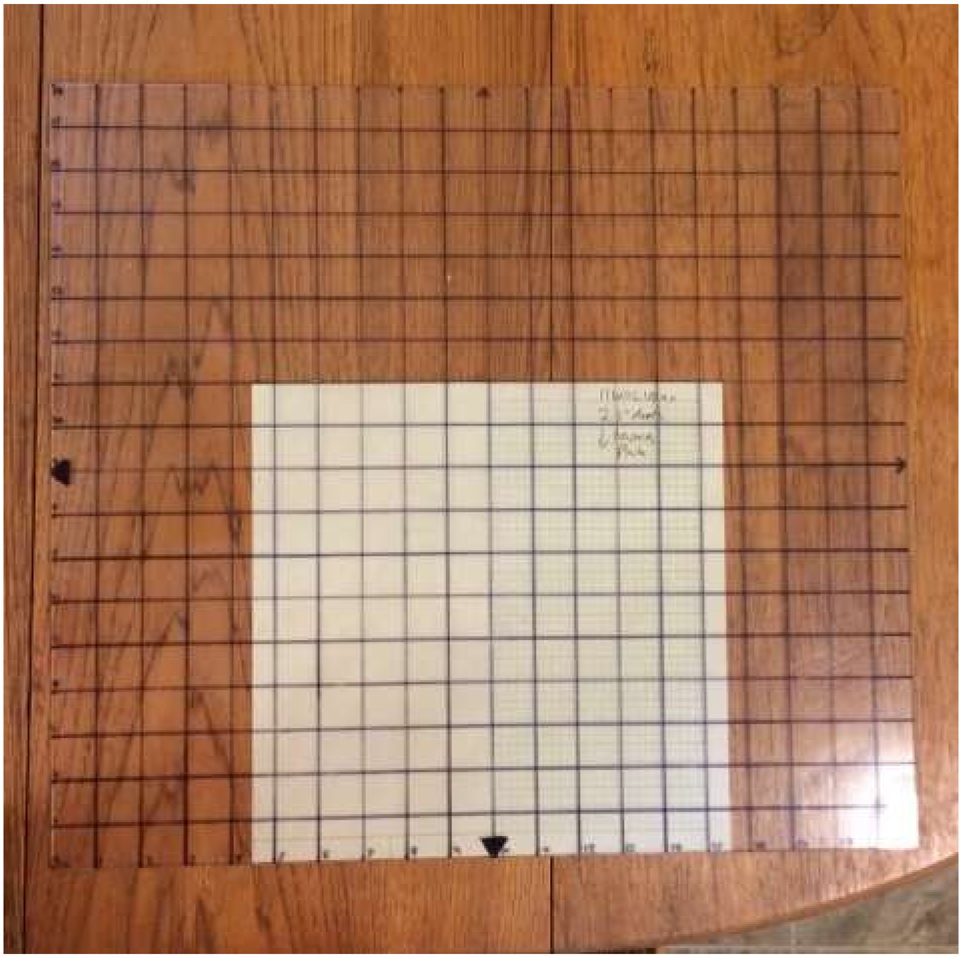

Figure 335: Test 11W11L10Lay 2.5" Depth

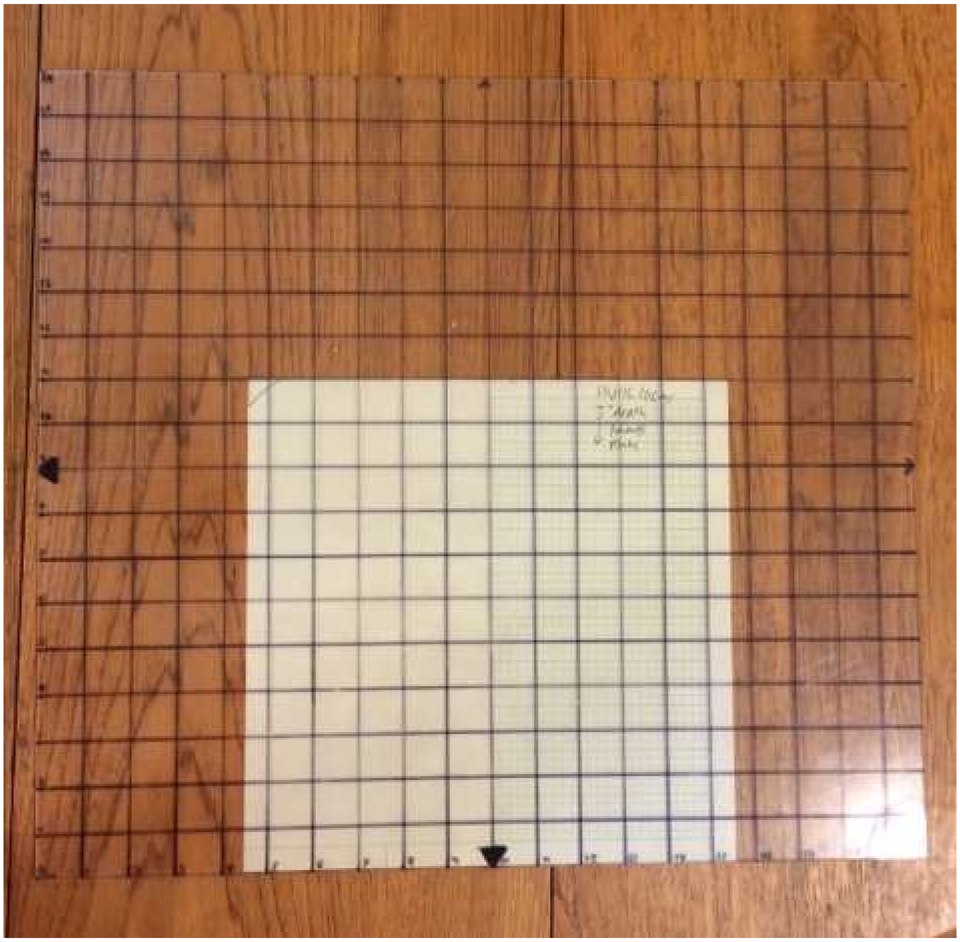

Figure 336: Test 11W11L10Lay 3” Depth

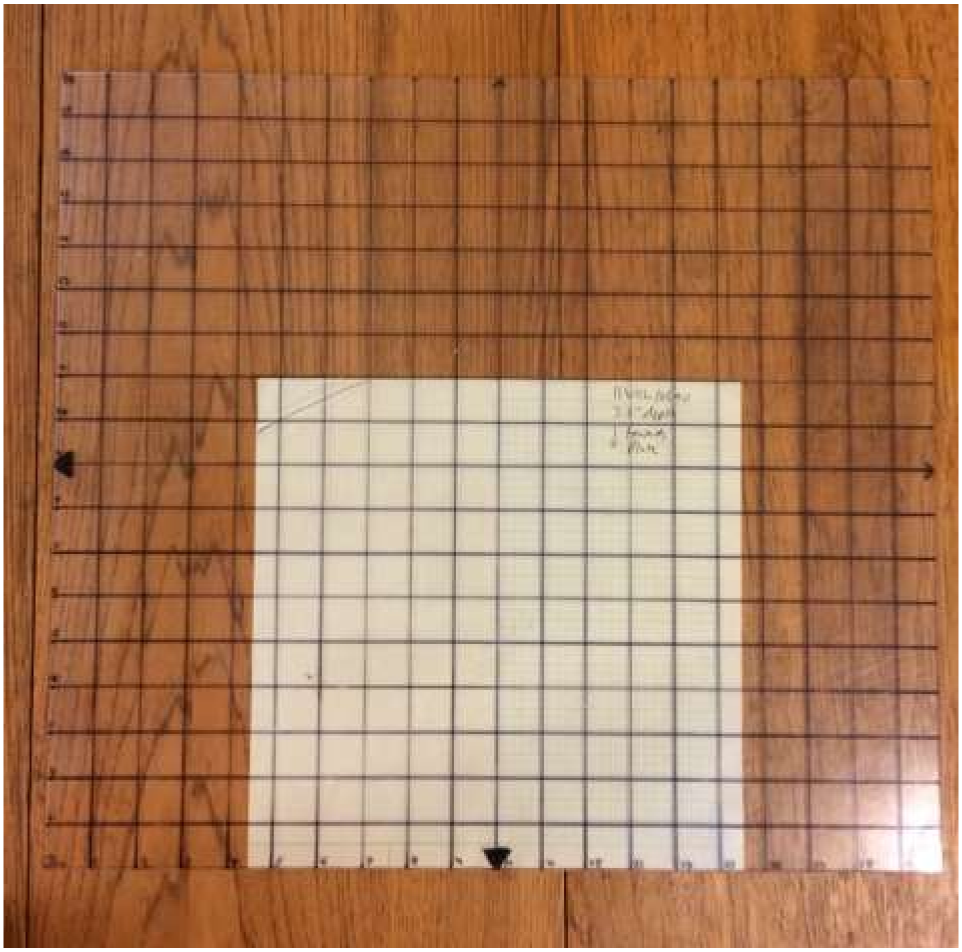

Figure 337: Test 11W11L10Lay 3.5" Depth

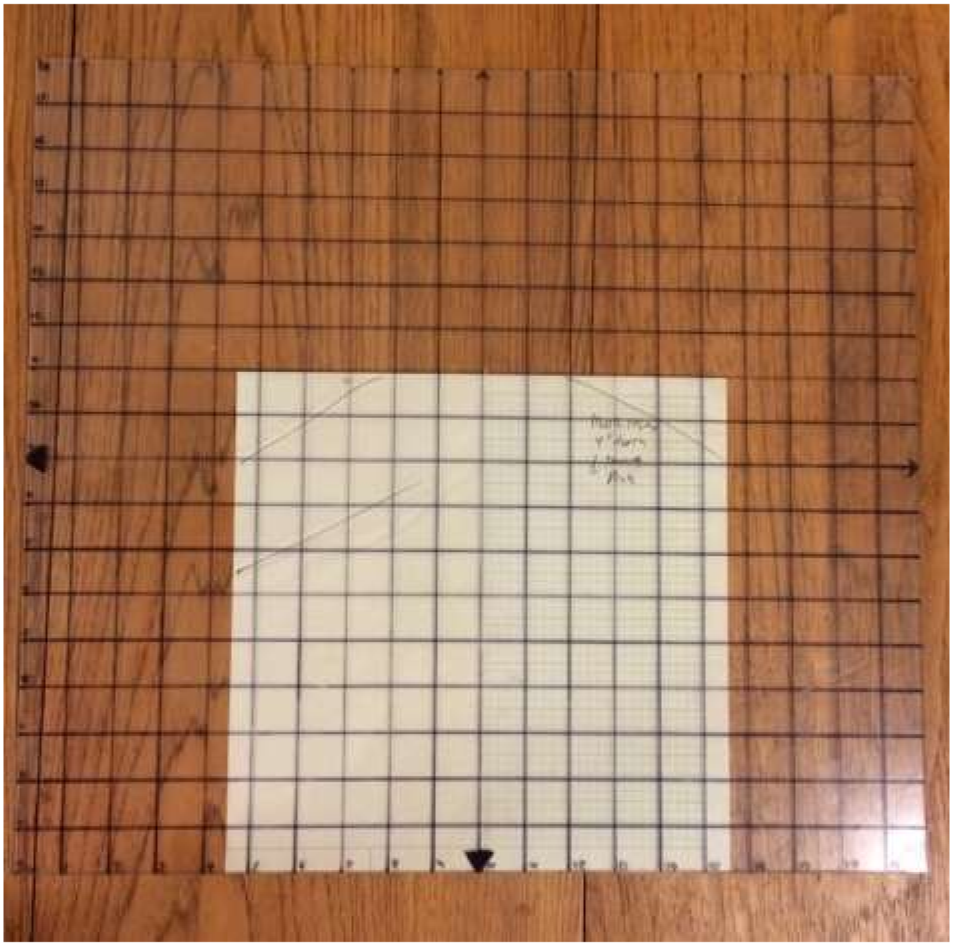

Figure 338: Test 11W11L10Lay 4” Depth

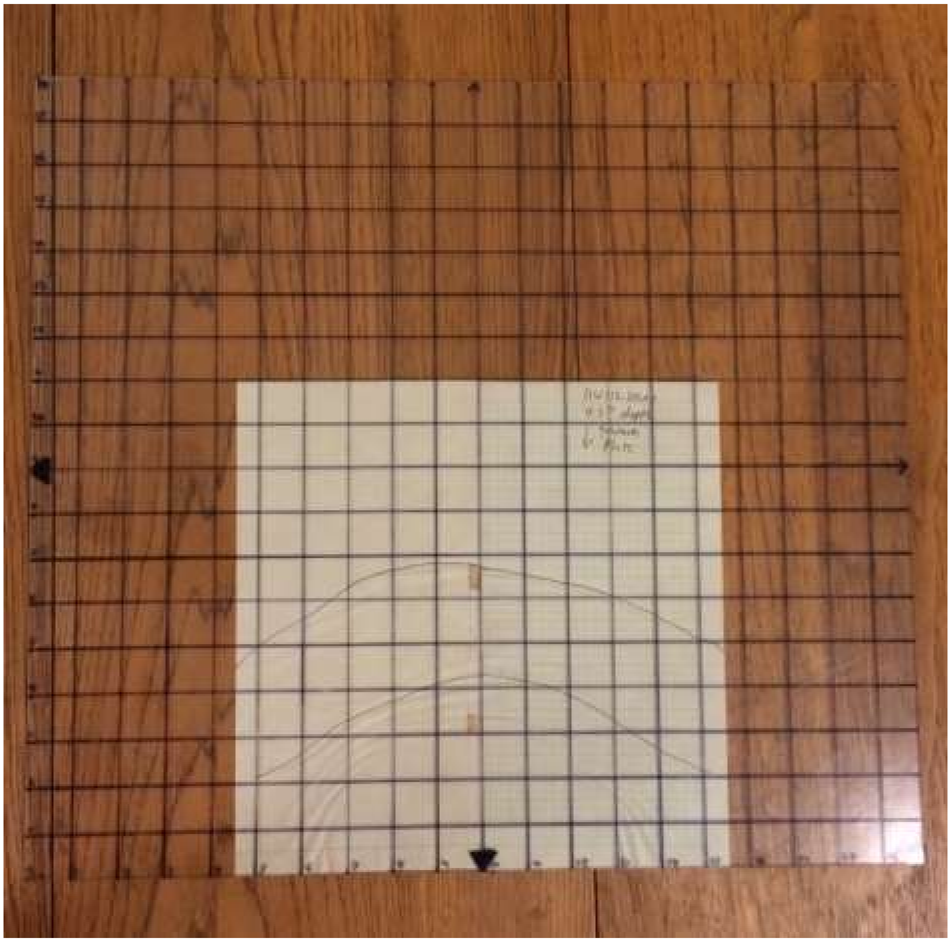

Figure 339: Test 11W11L10Lay 4.5" Depth

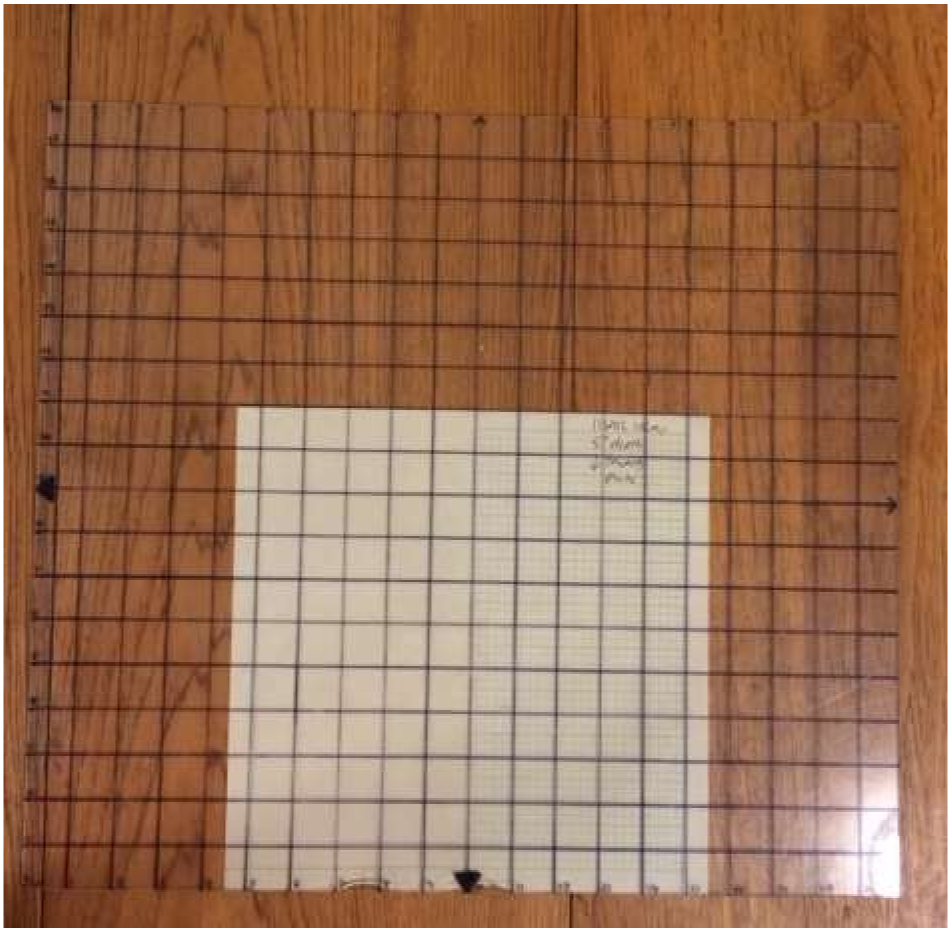

Figure 340: Test 11W11L10Lay 5" Depth

A.21 Photographs of Test 11W11L10Lay2

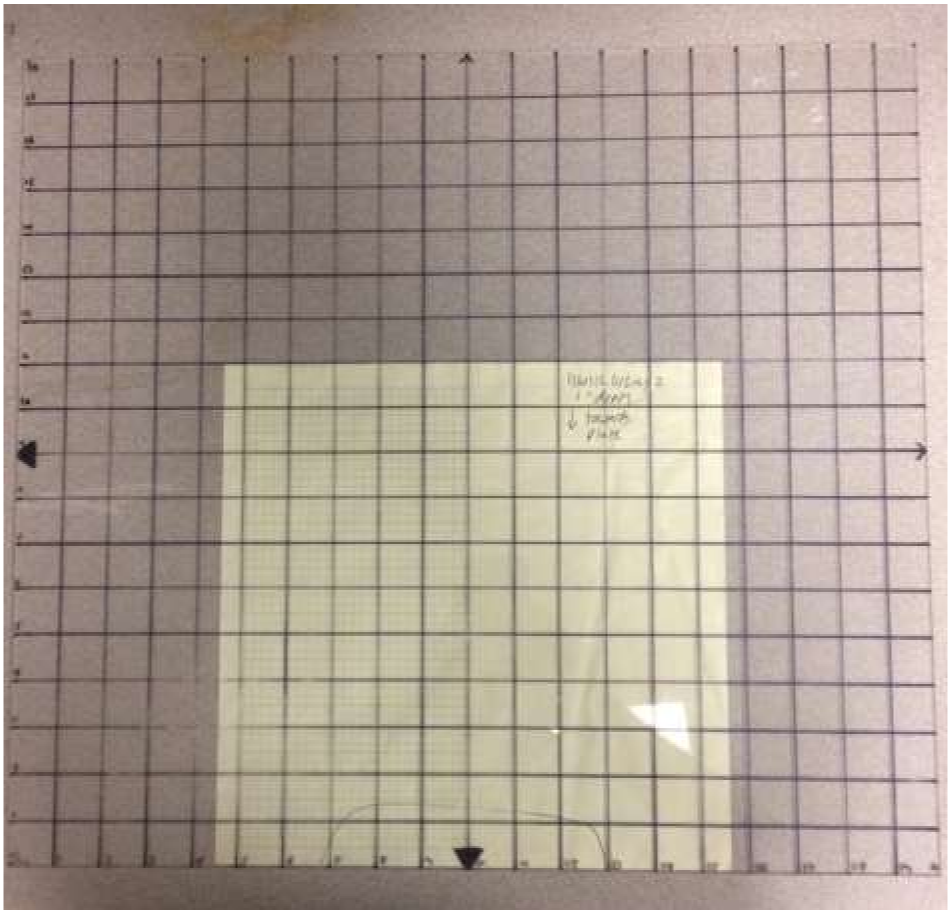

Figure 341: Test 11W11L10Lay2 1" Depth

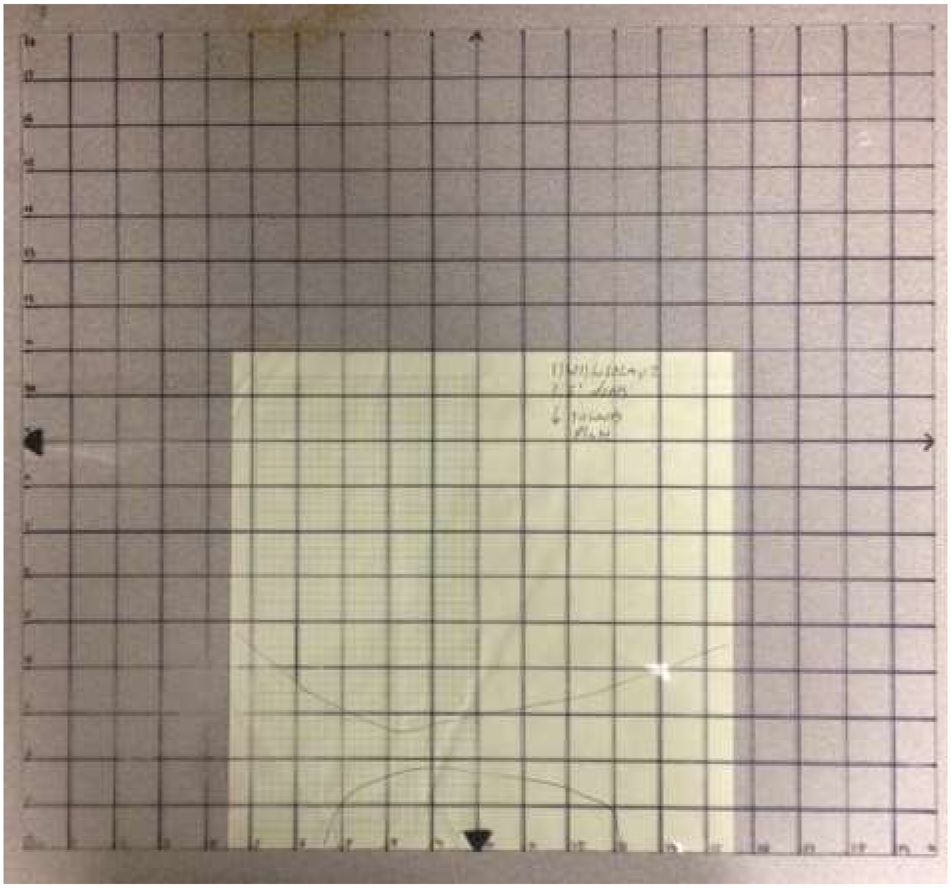

Figure 342: Test 11W11L10Lay2 1.5" Depth

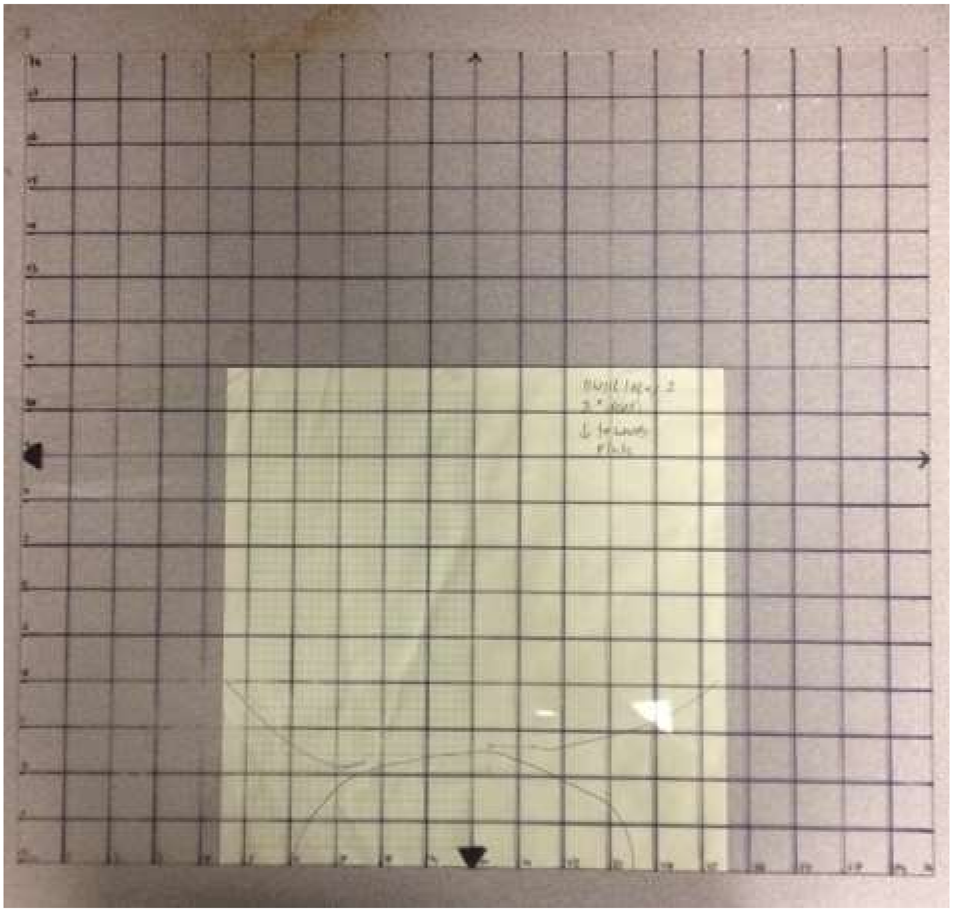

Figure 343: Test 11W11L10Lay2 2" Depth

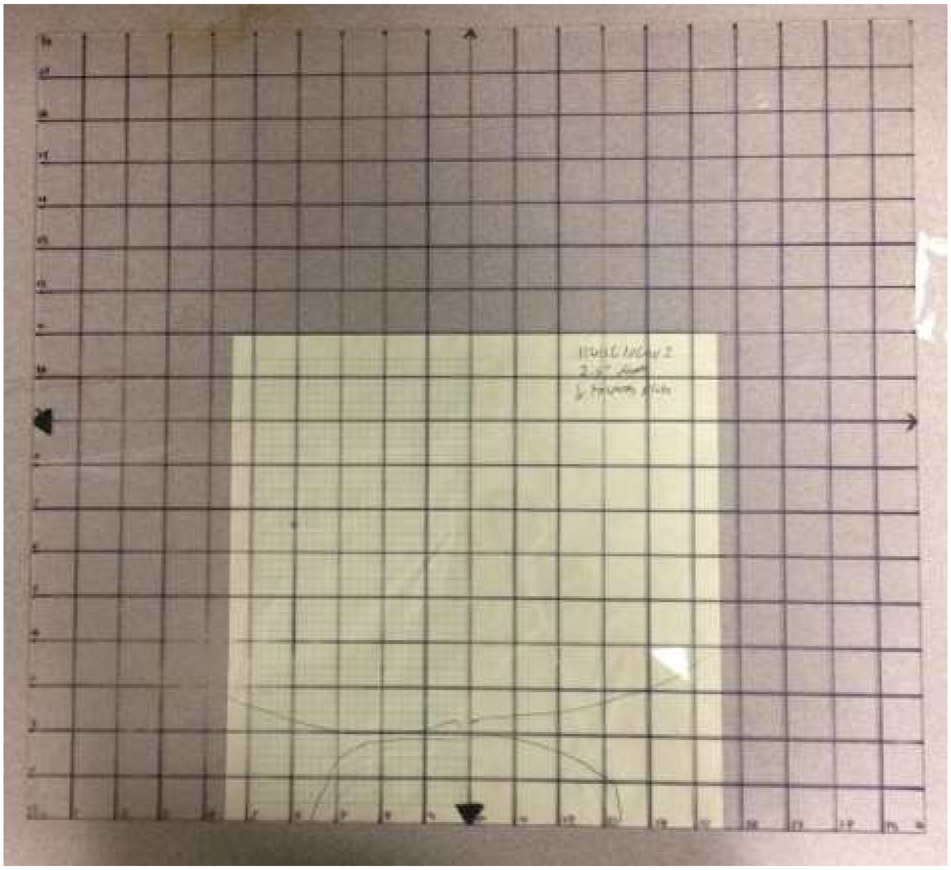

Figure 344: Test 11W11L10Lay2 2.5” Depth

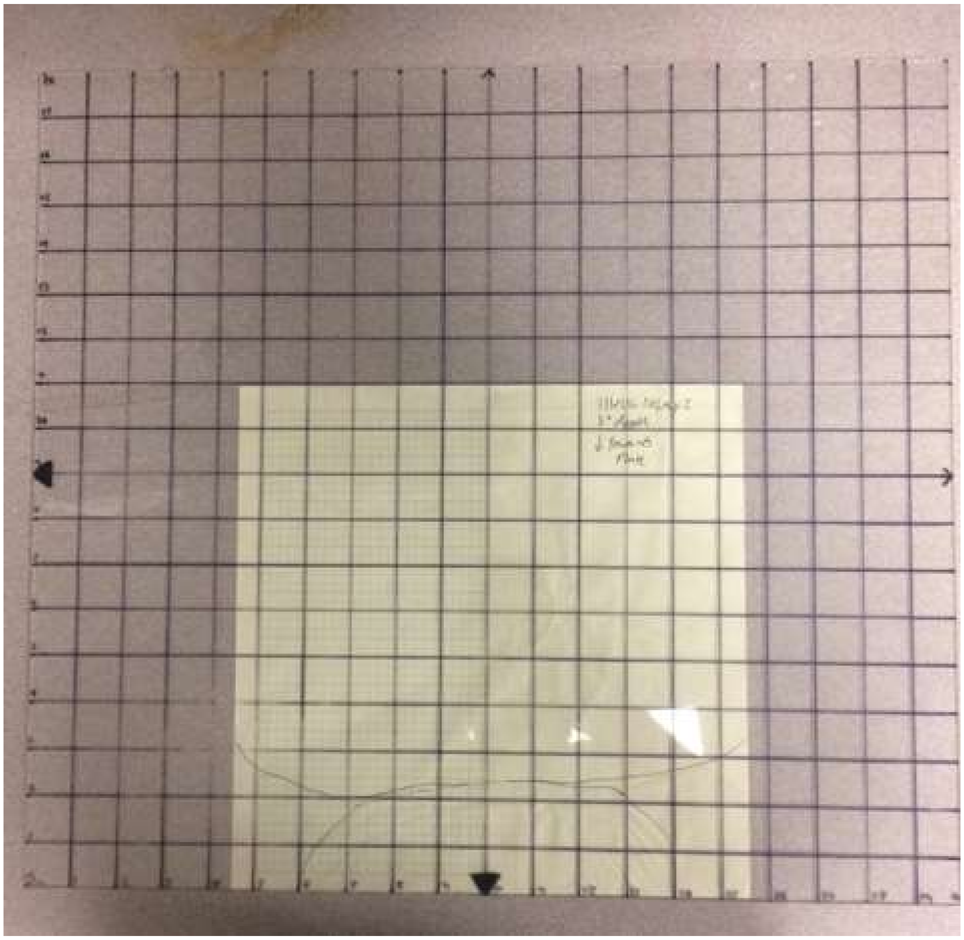

Figure 345: Test 11W11L10Lay2 3" Depth

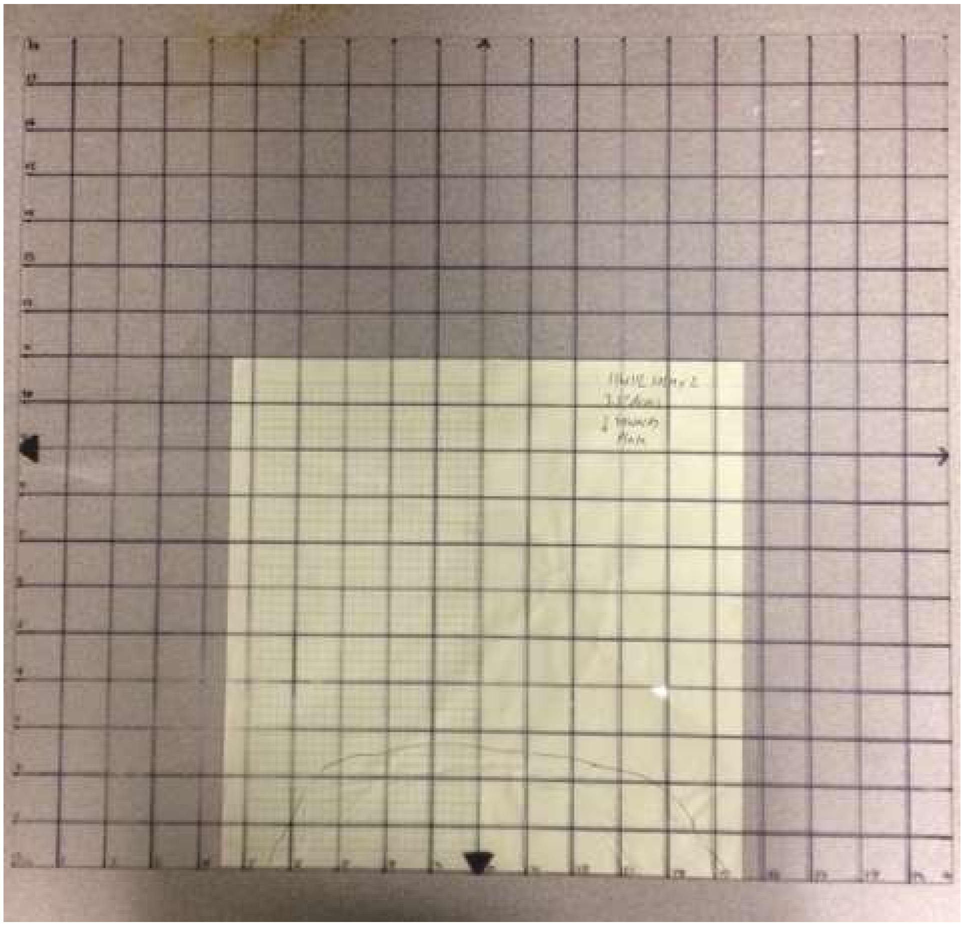

Figure 346: Test 11W11L10Lay2 3.5” Depth

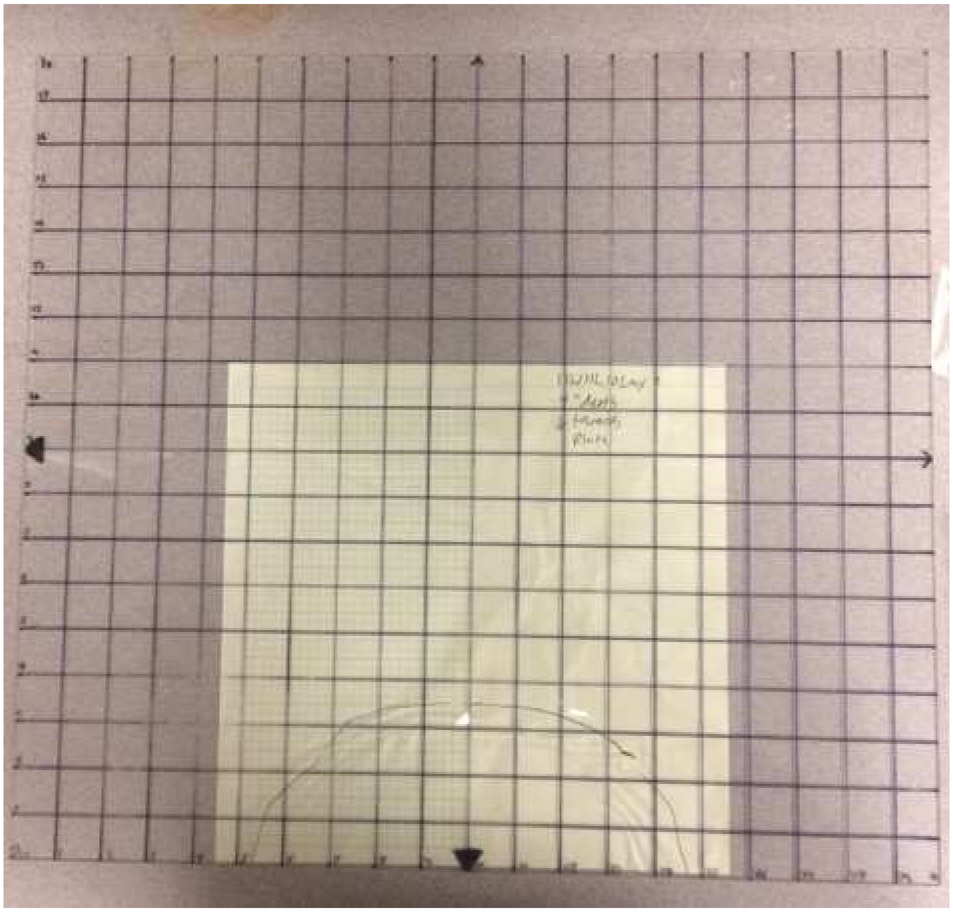

Figure 347: Test 11W11L10Lay2 4” Depth

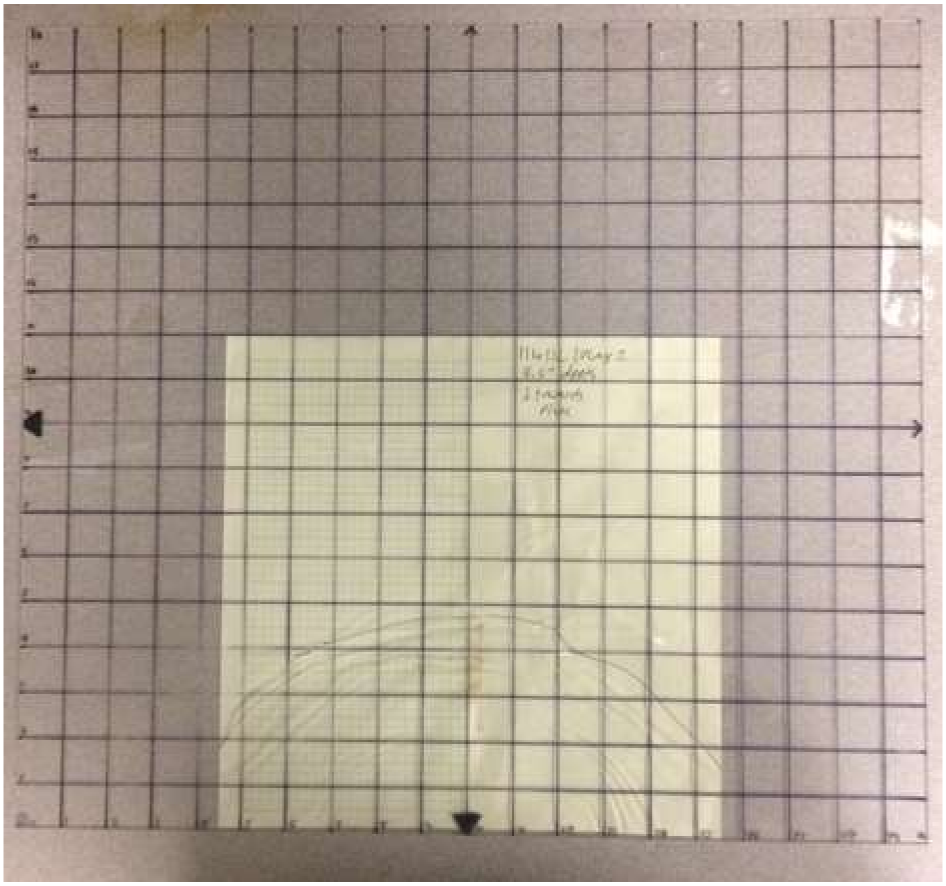

Figure 348: Test 11W11L10Lay2 4.5" Depth

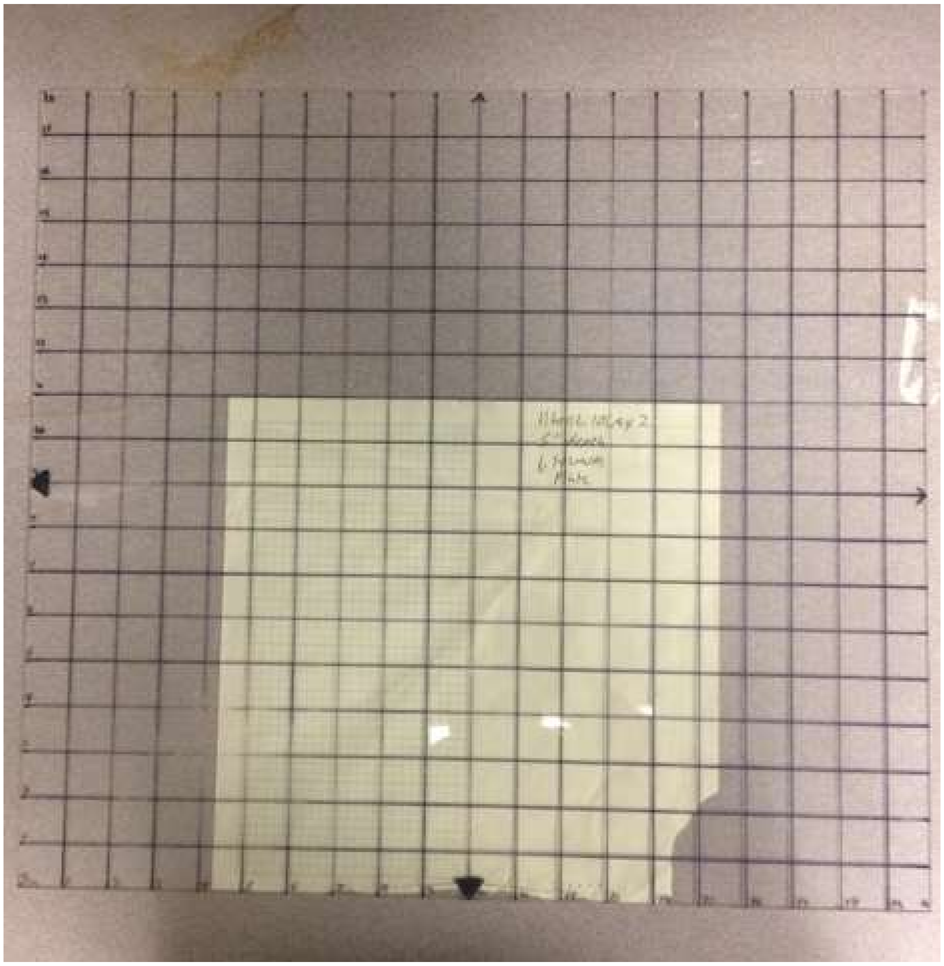

Figure 349: Test 11W11L10Lay2 5" Depth

A.21 Photographs of Test 11W11L5Lay

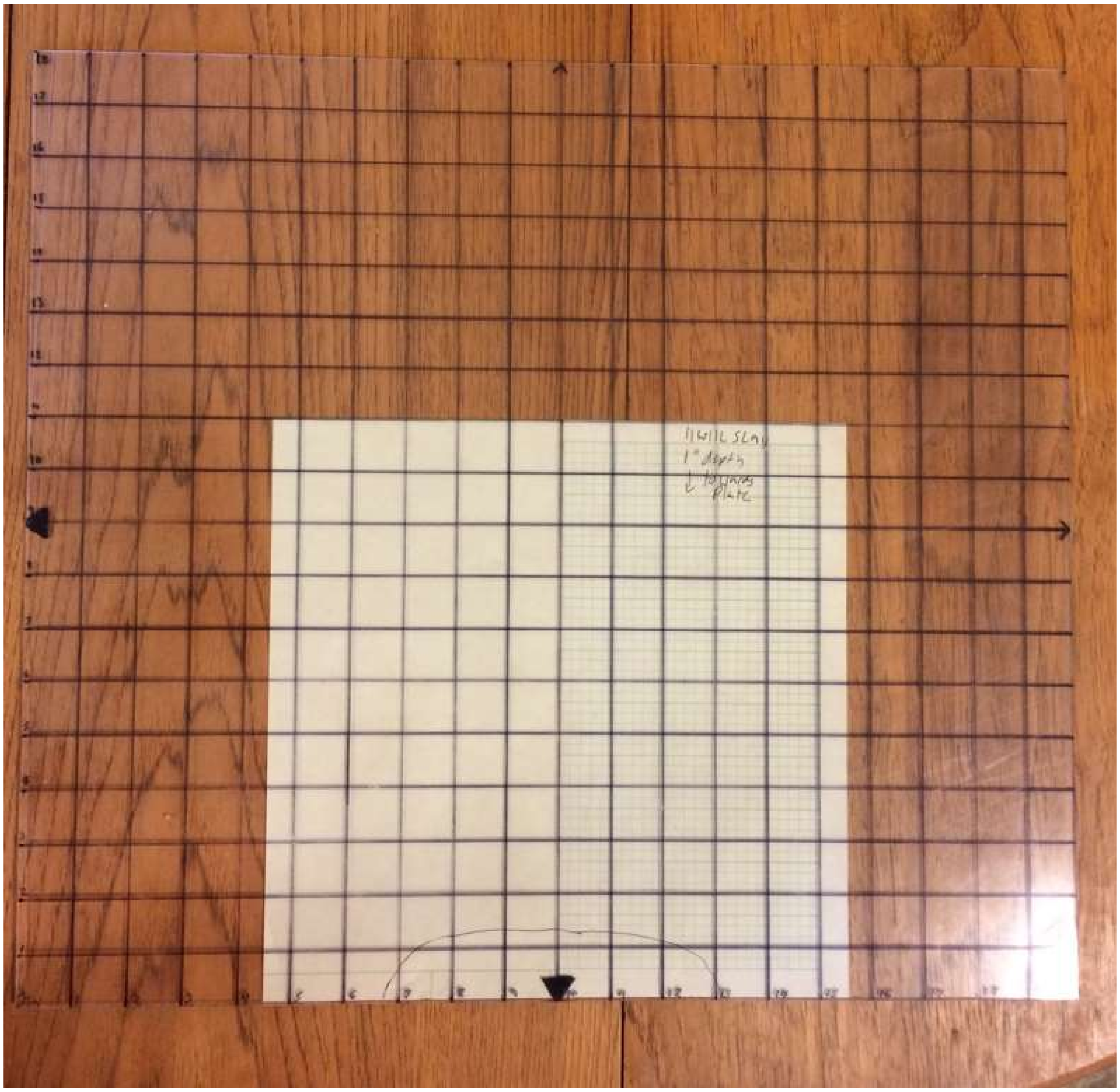

Figure 350: Test 11W11L5Lay 1" Depth

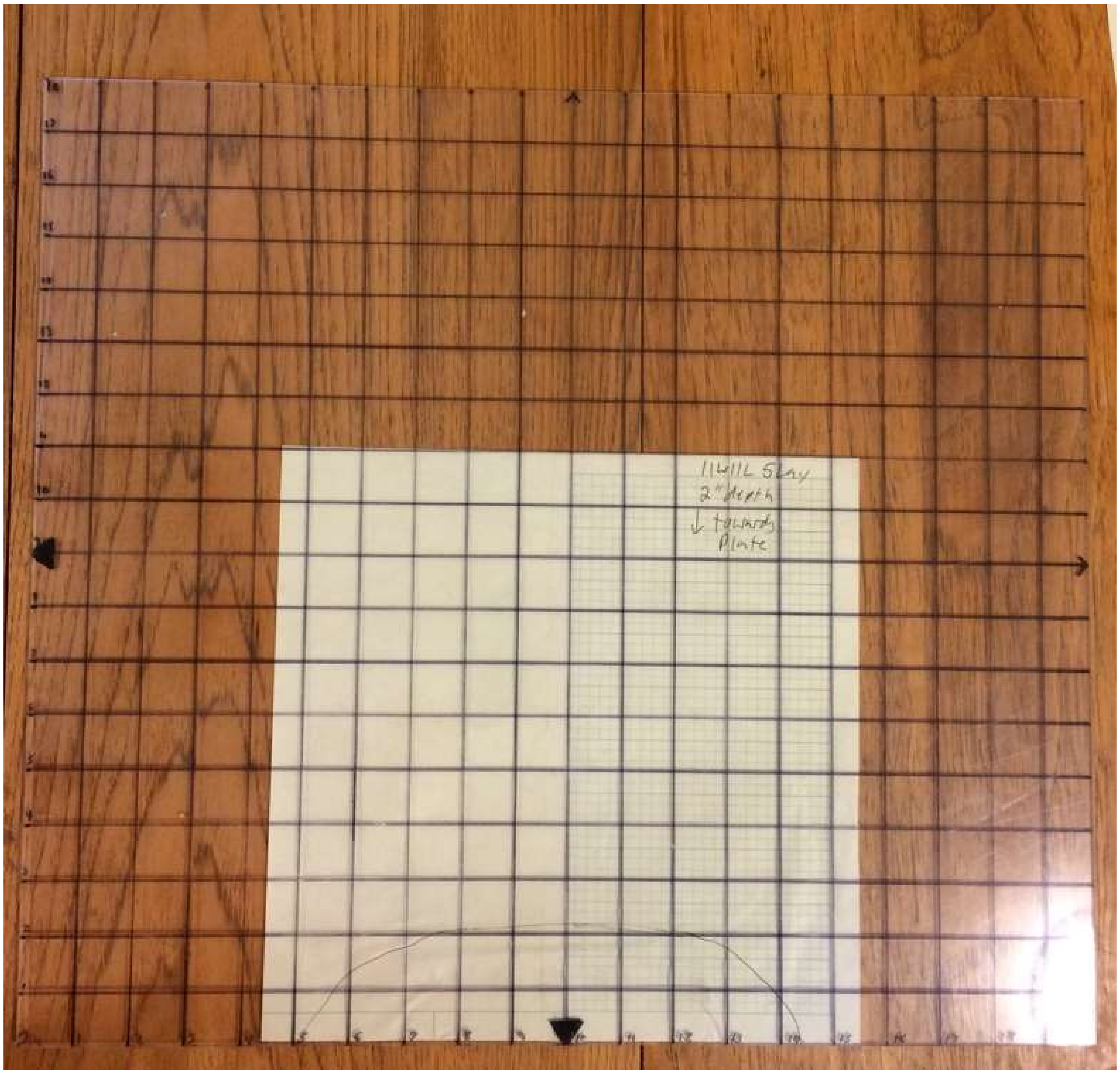

Figure 351: Test 11W11L5Lay 2" Depth

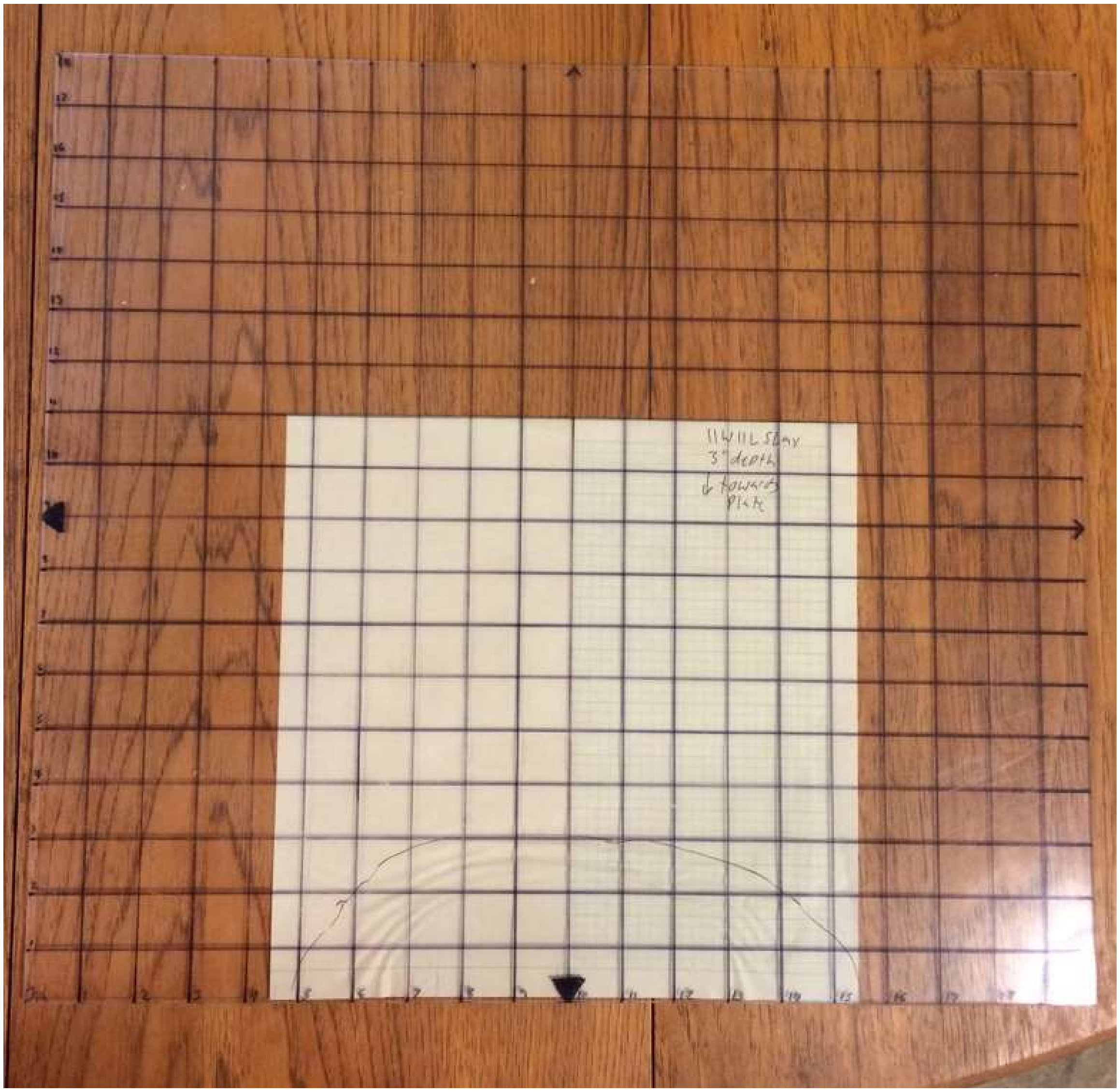

Figure 352: Test 11W11L5Lay 3" Depth

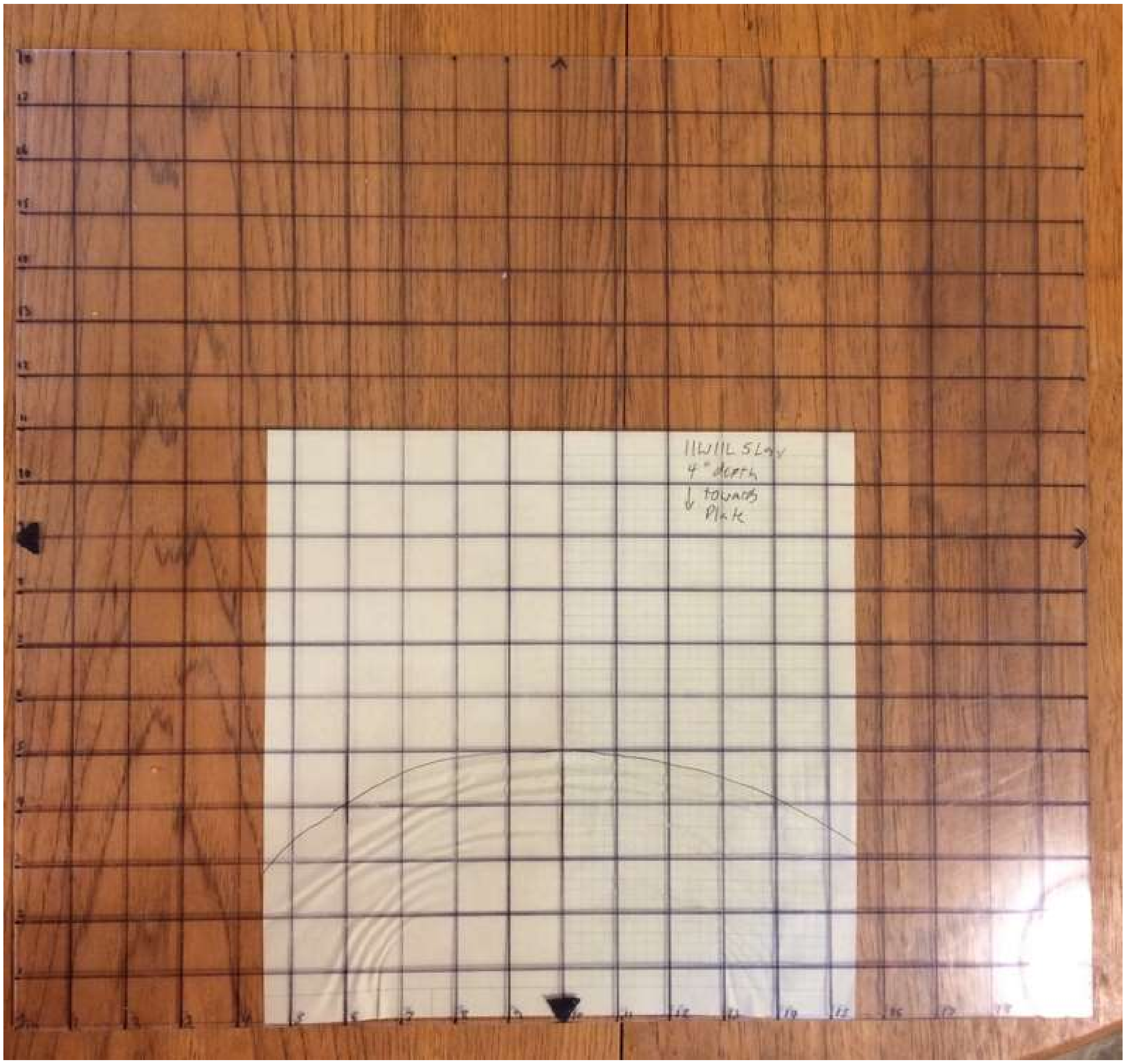

Figure 353: Test 11W11L5Lay 4" Depth

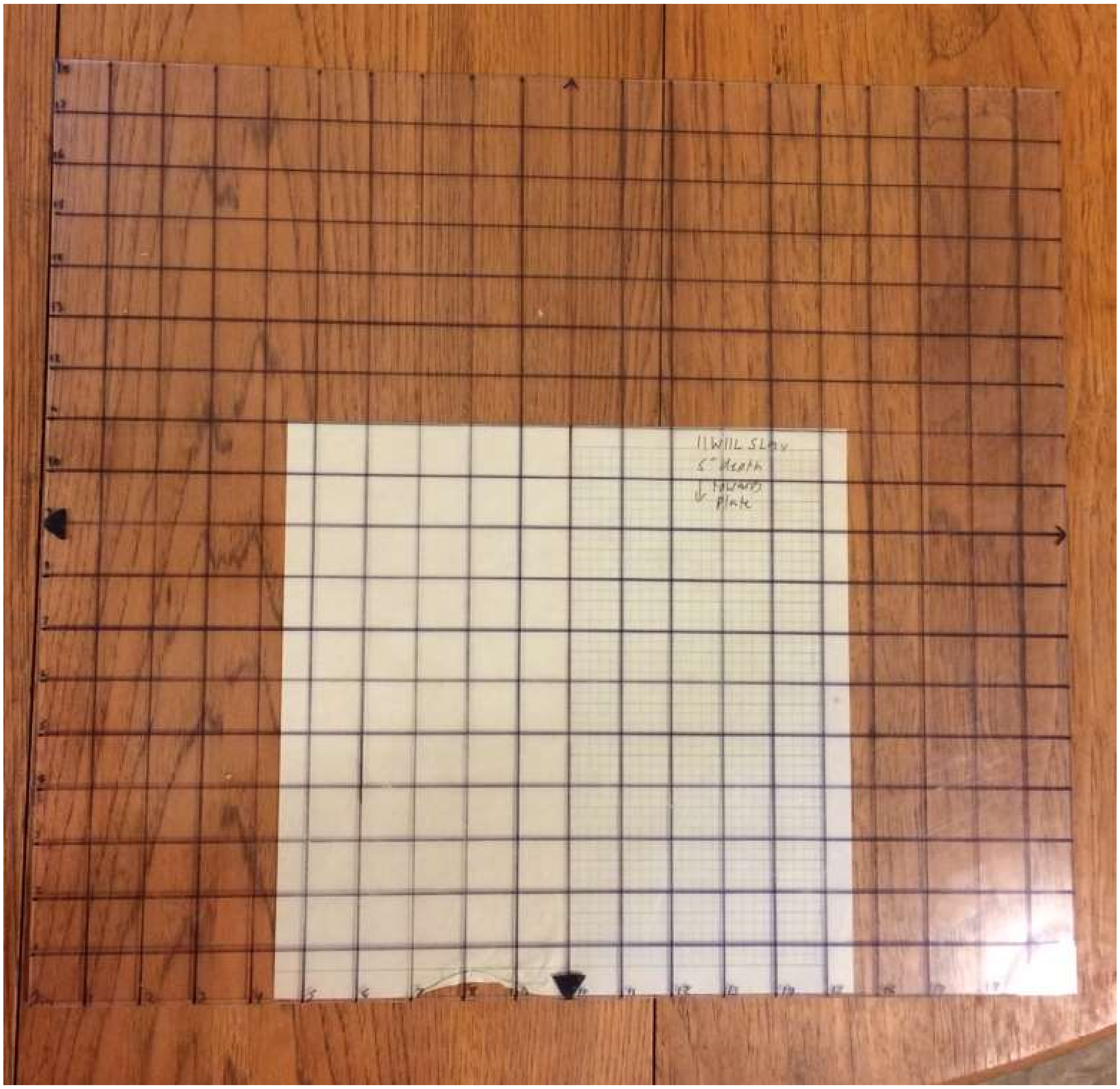

Figure 354: Test 11W11L5Lay 5” Depth

A.21 Photographs of Test 11W11L5Lay2

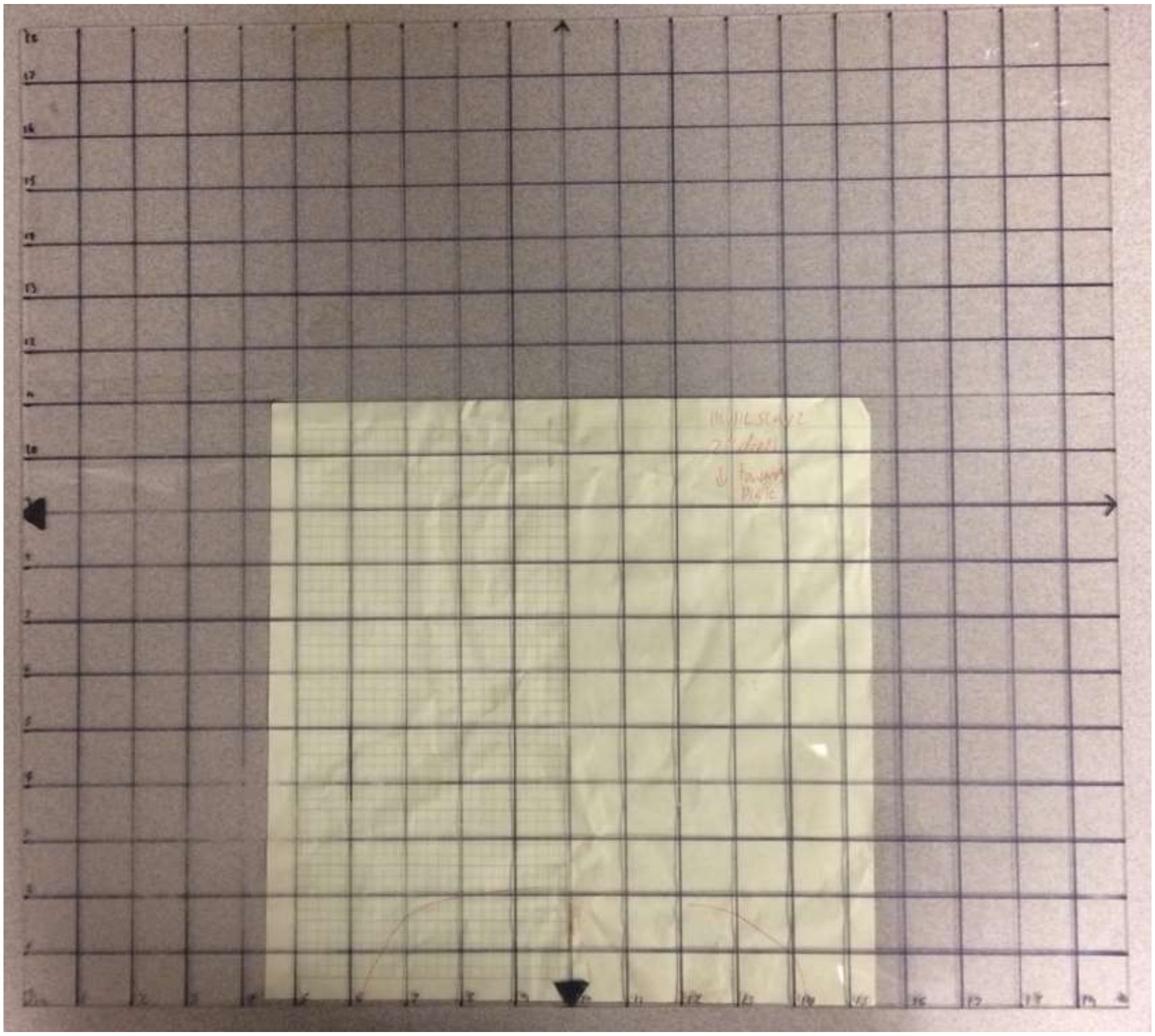

Figure 355: Test 11W11L5Lay2 2" Depth

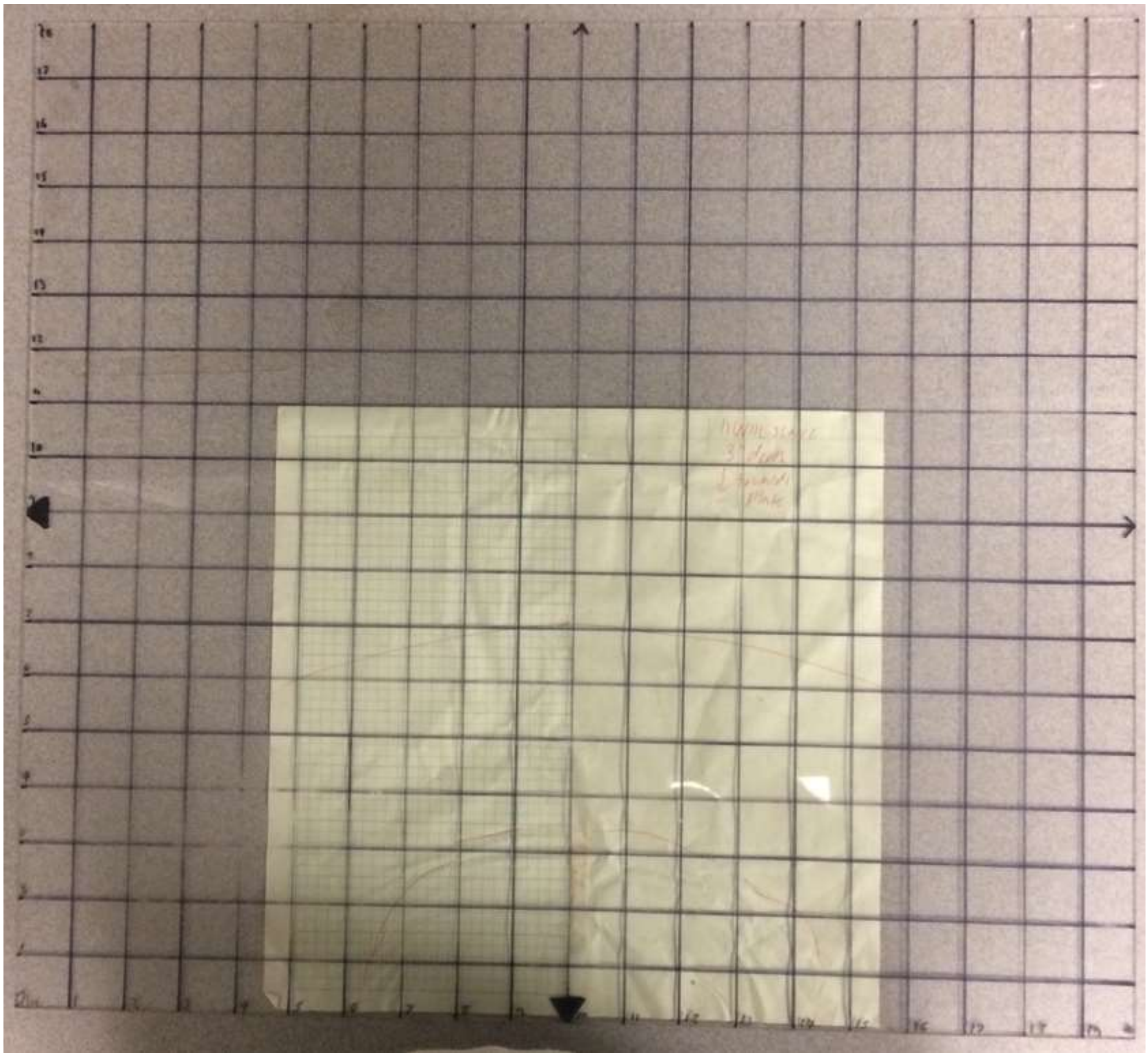

Figure 356: Test 11W11L5Lay2 3” Depth

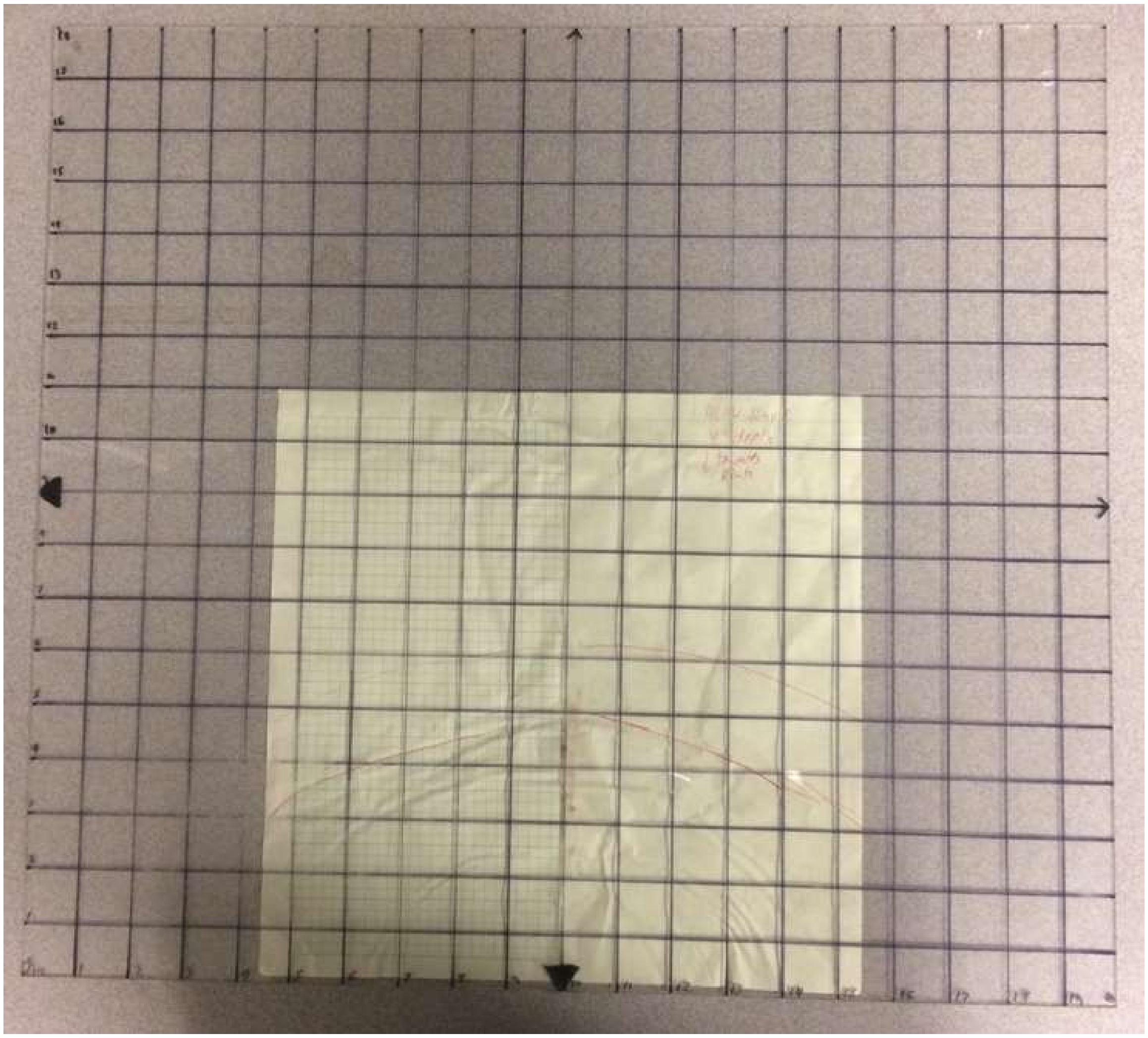

Figure 357: Test 11W11L5Lay2 4” Depth

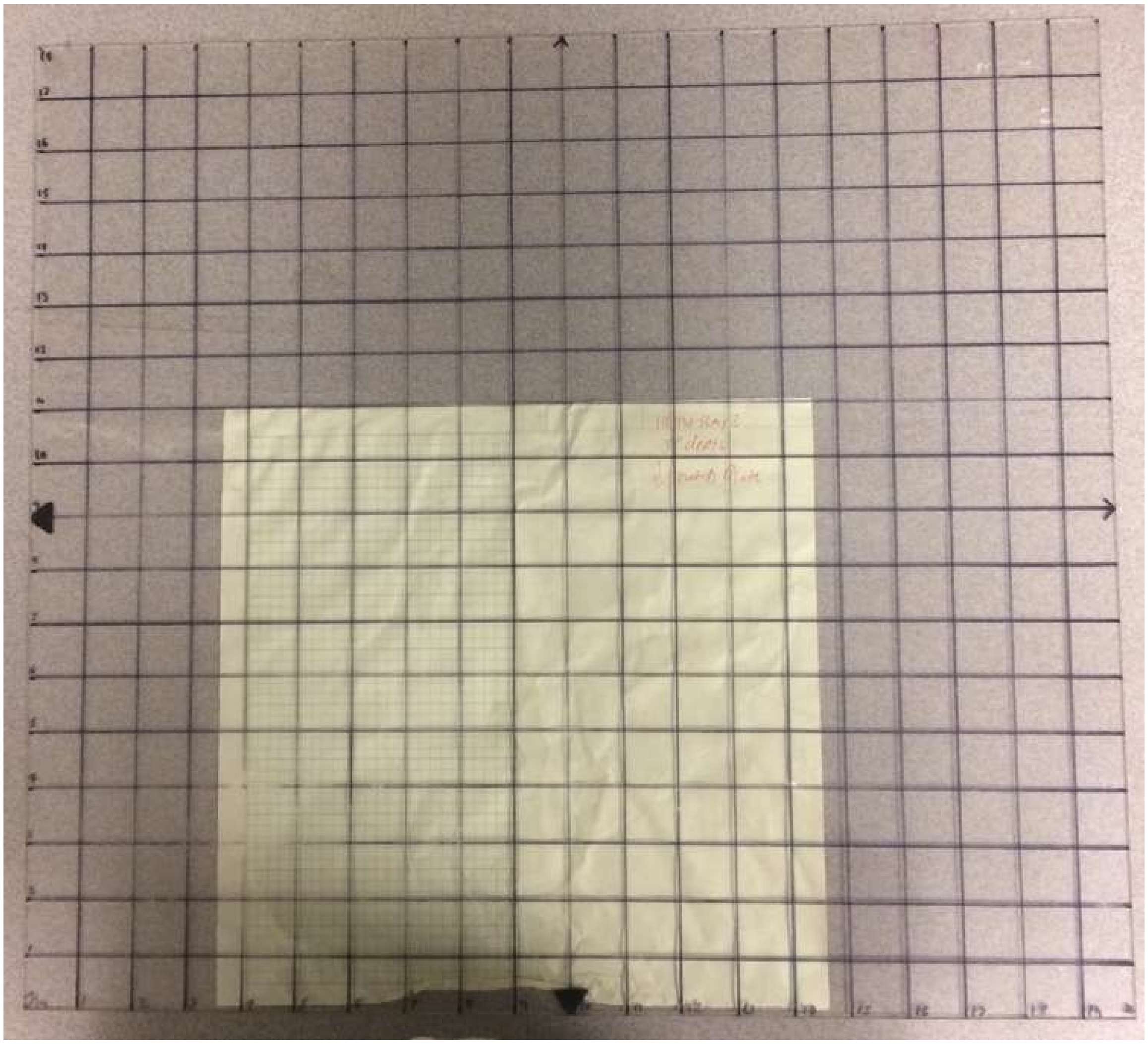

Figure 358: Test 11W11L5Lay2 5" Depth

A.21 Photographs of Test 8W8L5Lay3

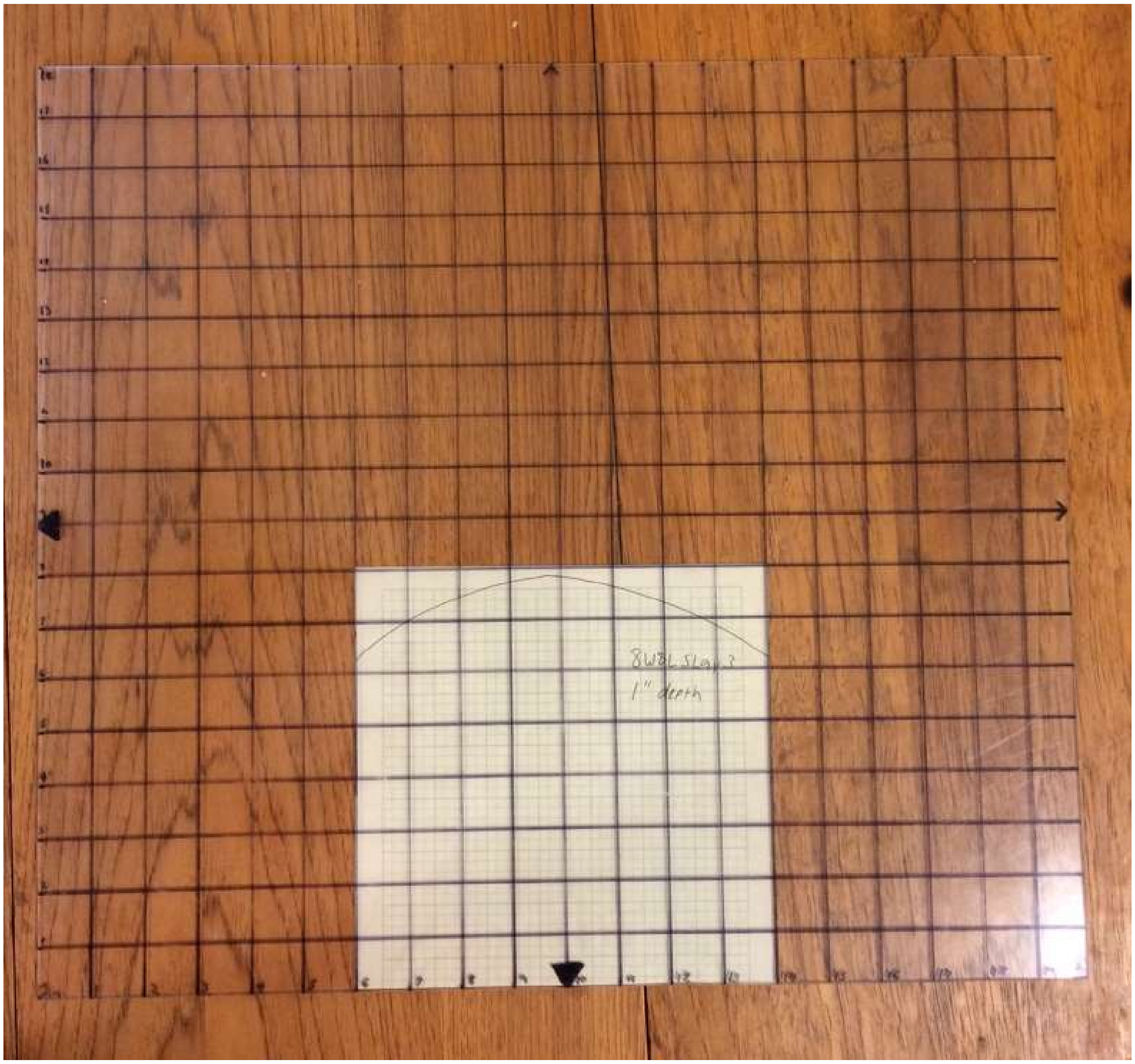

Figure 359: Test 8W8L5Lay3 1" Depth

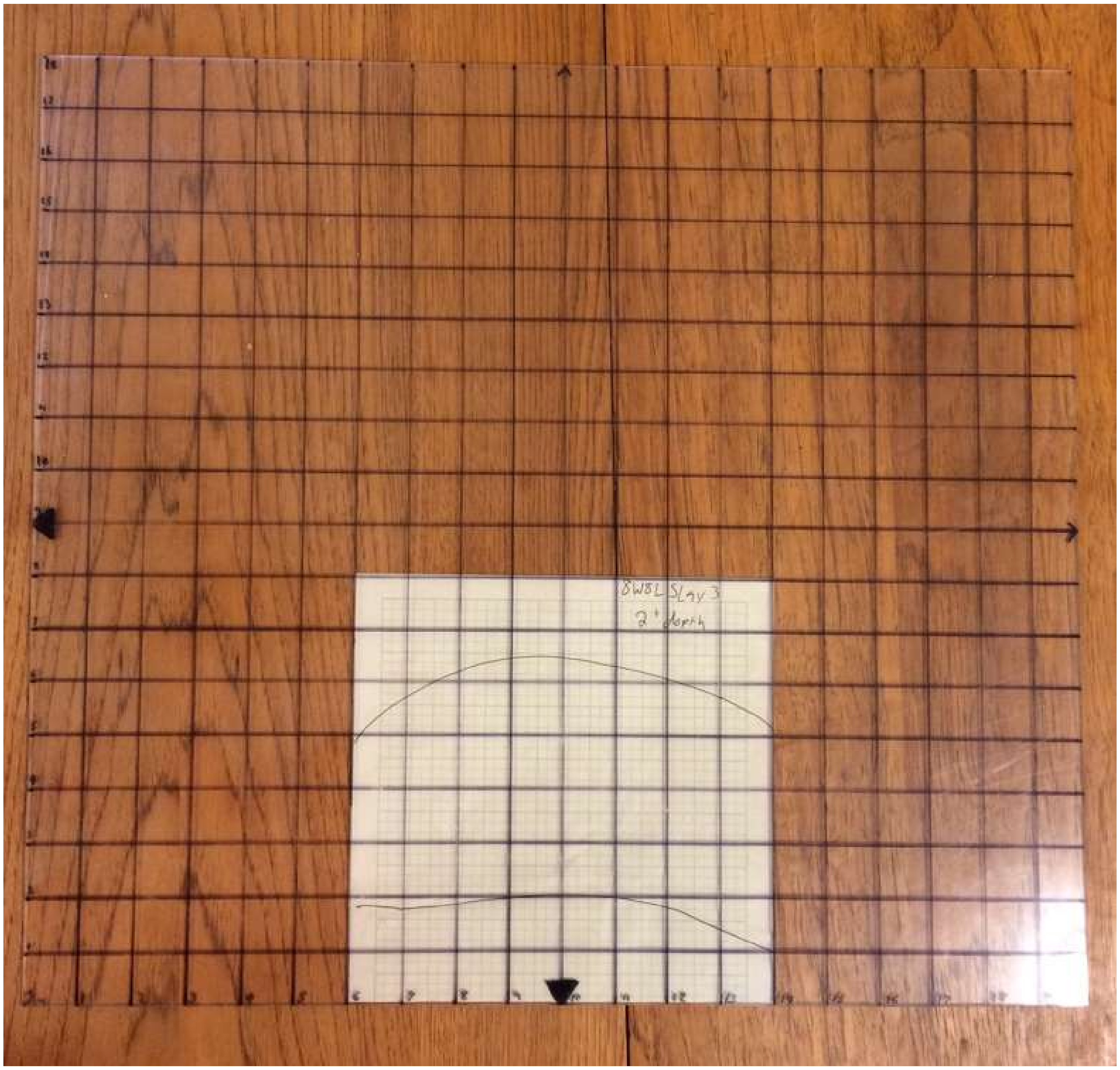

Figure 360: Test 8W8L5Lay3 2" Depth

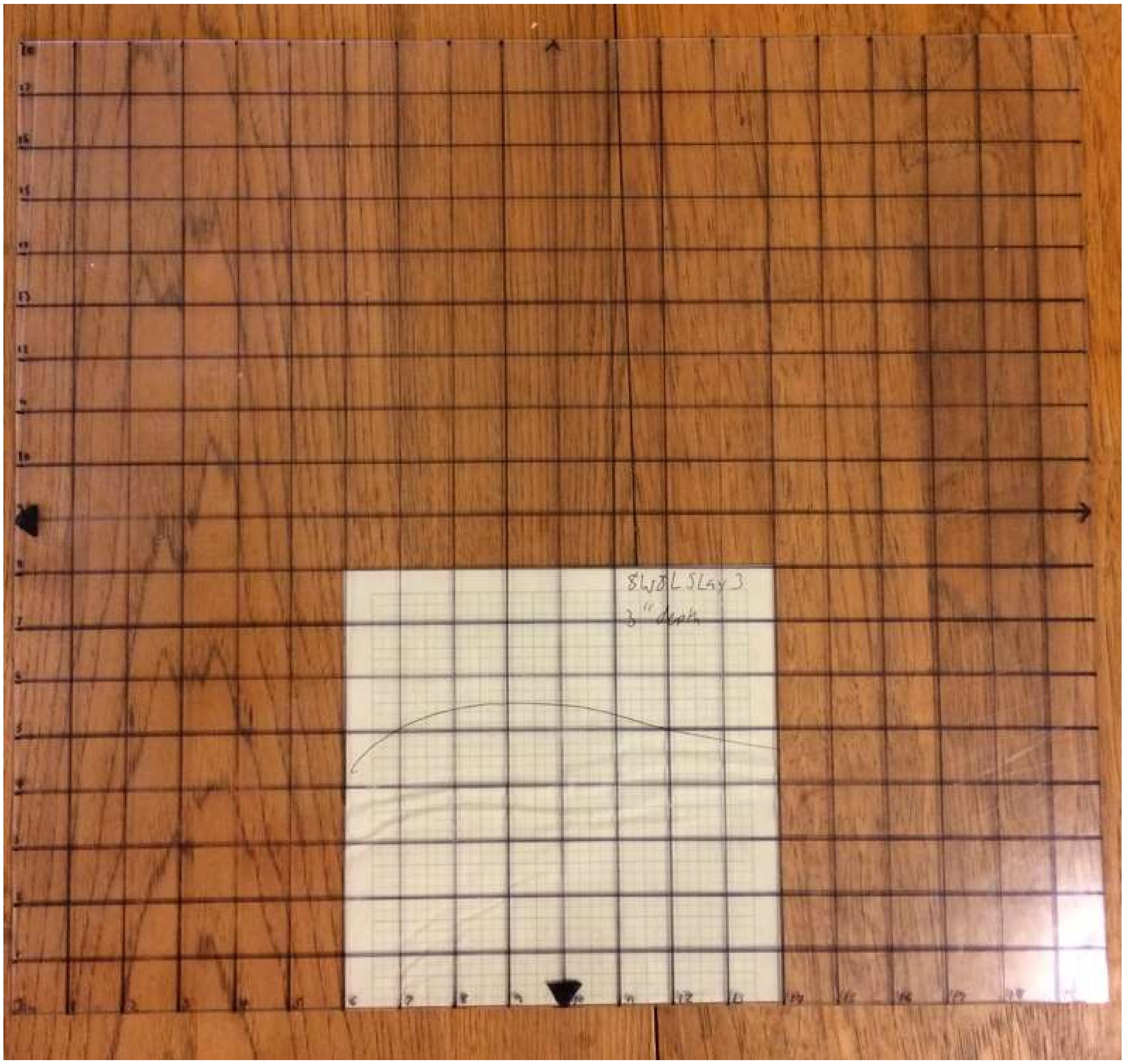

Figure 361: Test 8W8L5Lay3 3" Depth

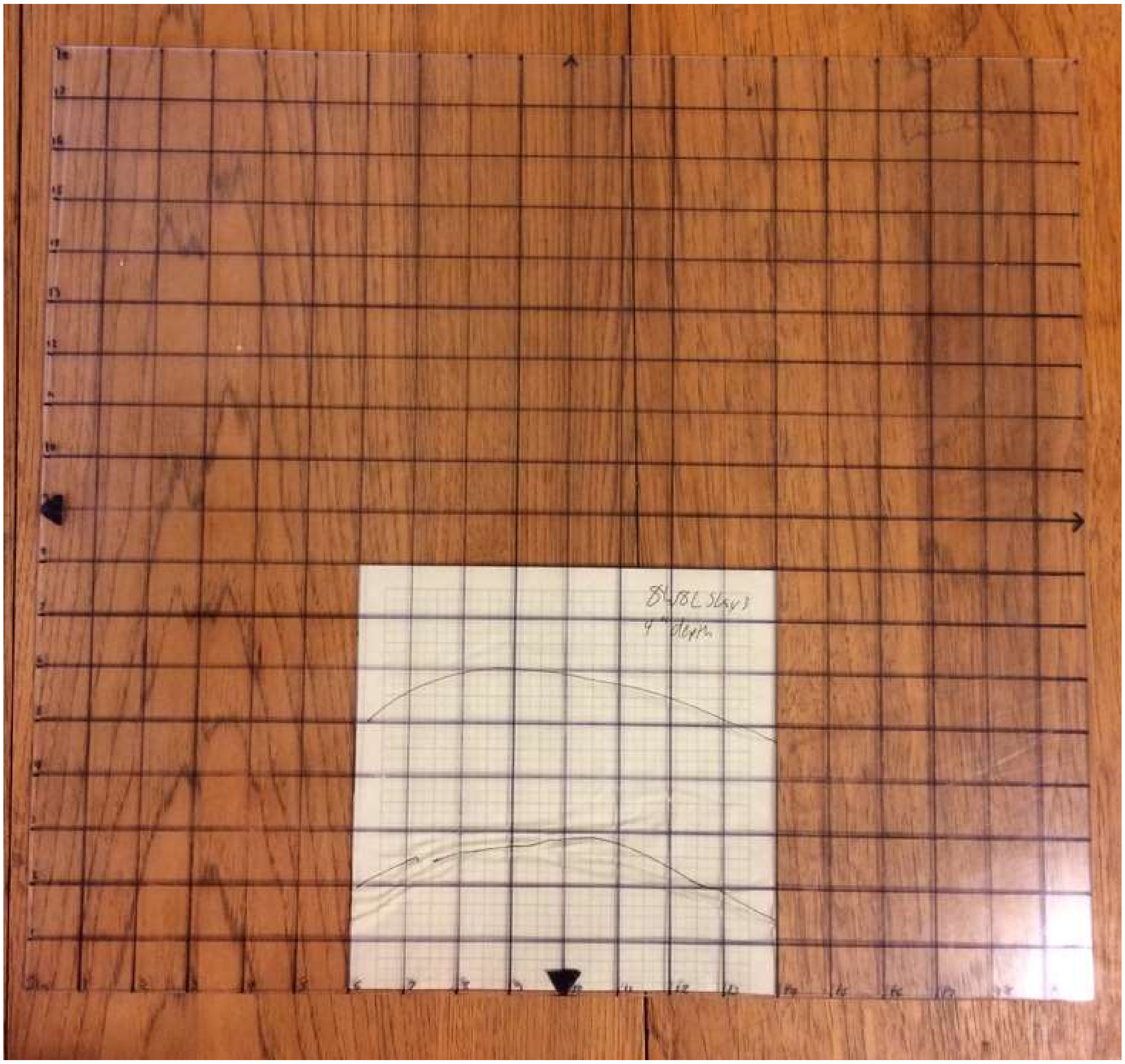

Figure 362: Test 8W8L5Lay3 4" Depth

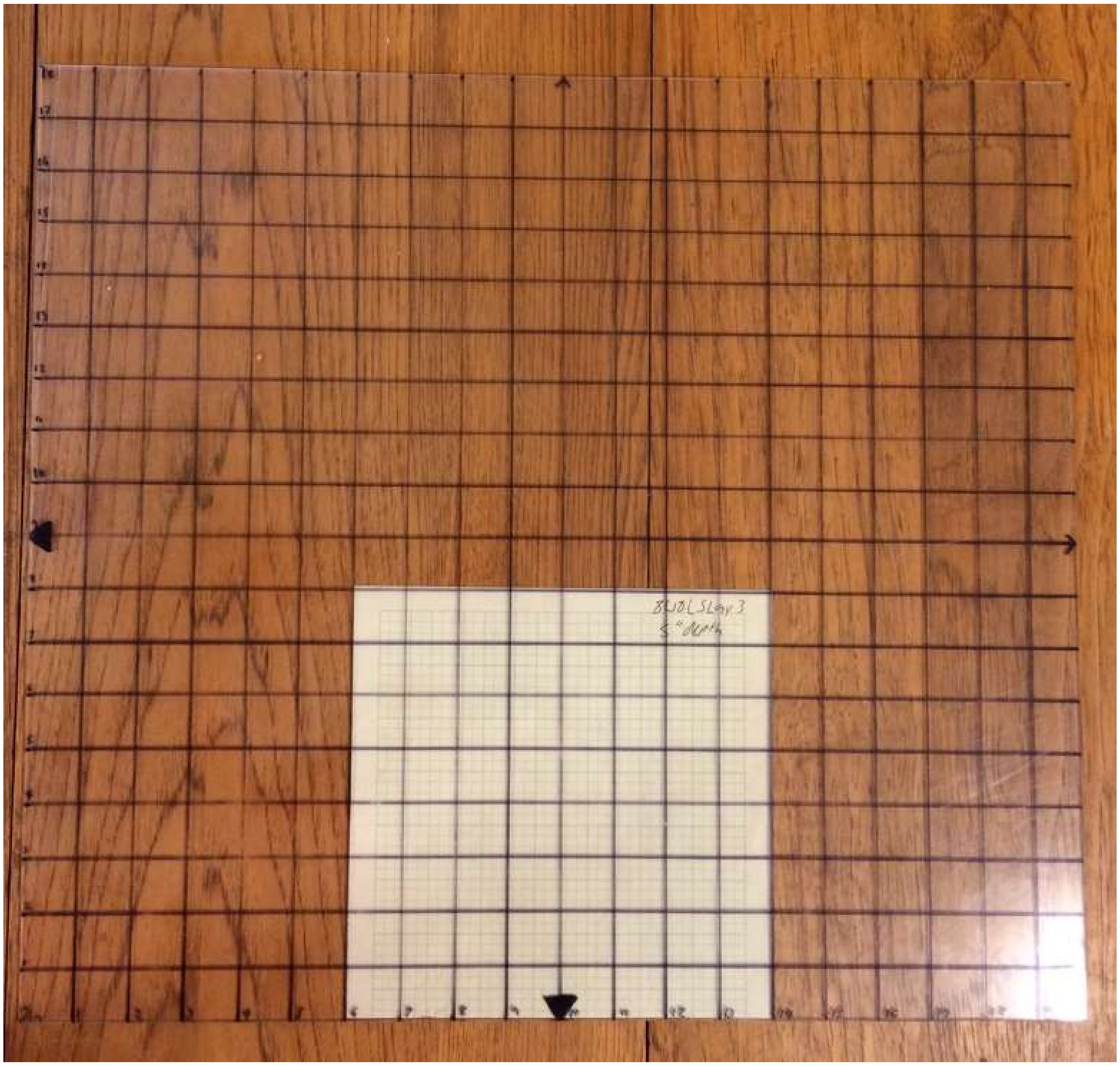

Figure 363: Test 8W8L5Lay3 5” Depth

A.22 Photographs of Test 8W8L10Lay3

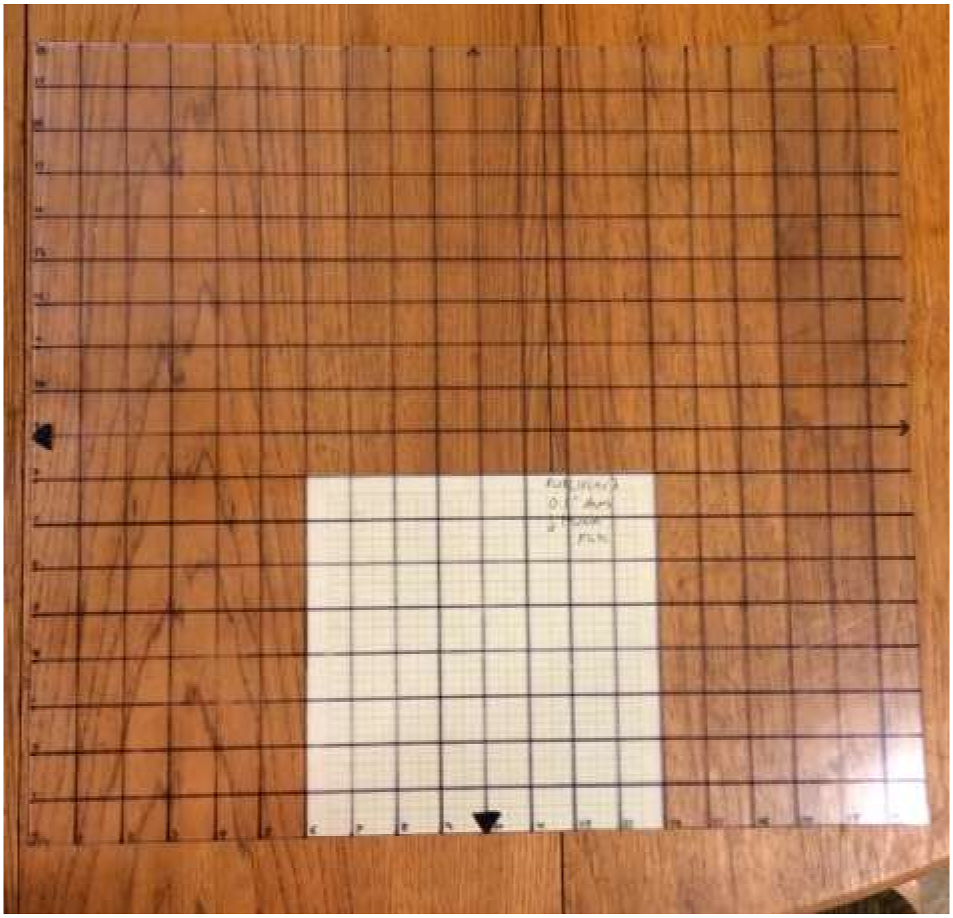

Figure 364: Test 8W8L10Lay3 0.5” Depth

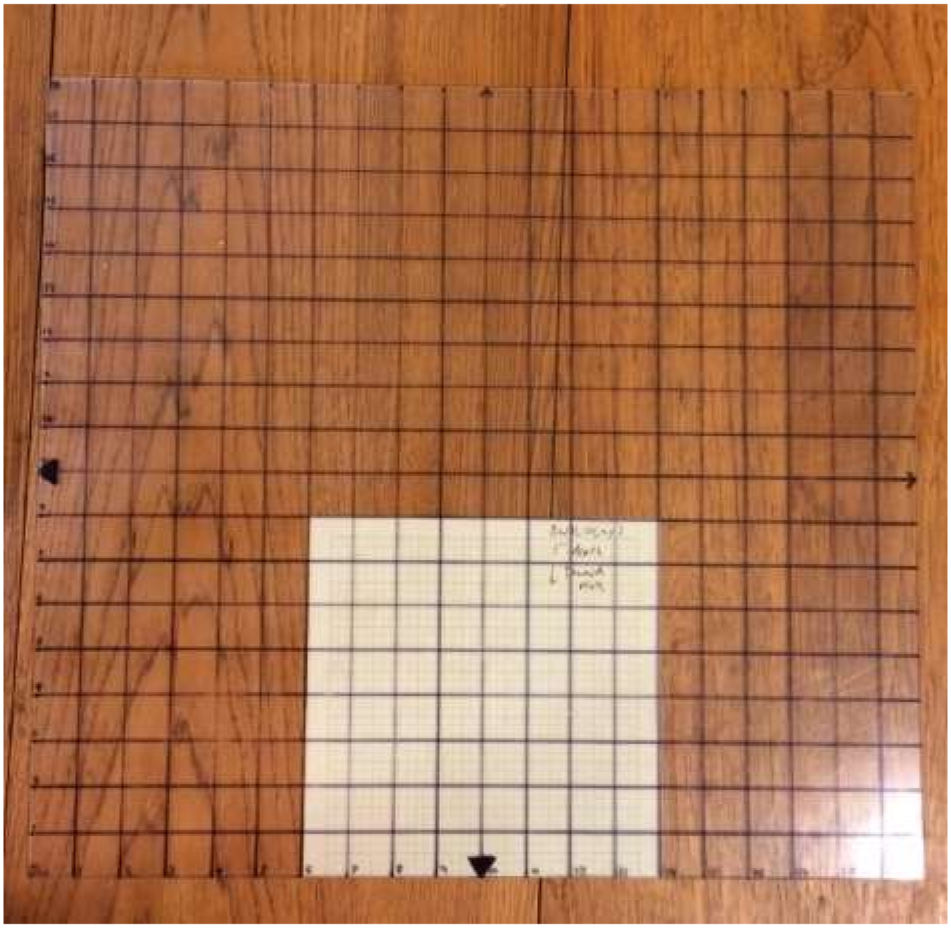

Figure 365: Test 8W8L10Lay3 1" Depth

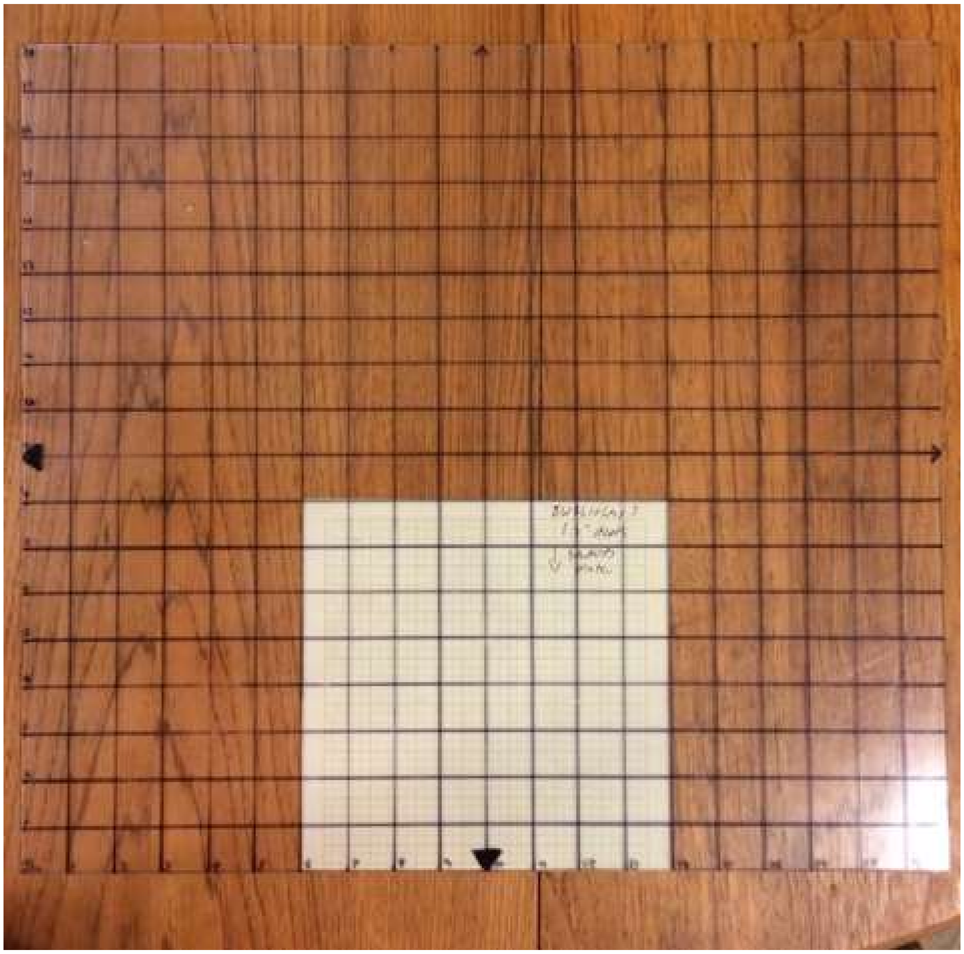

Figure 366: Test 8W8L10Lay3 1.5” Depth

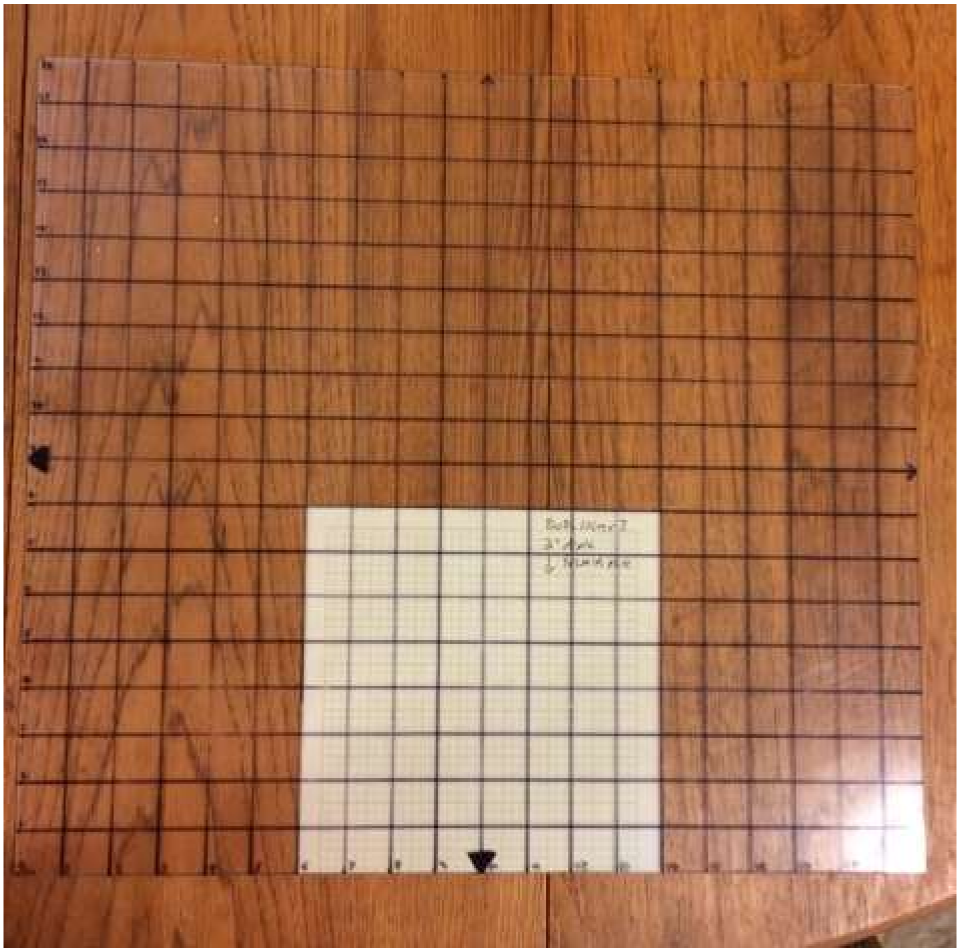

Figure 367: Test 8W8L10Lay3 2” Depth

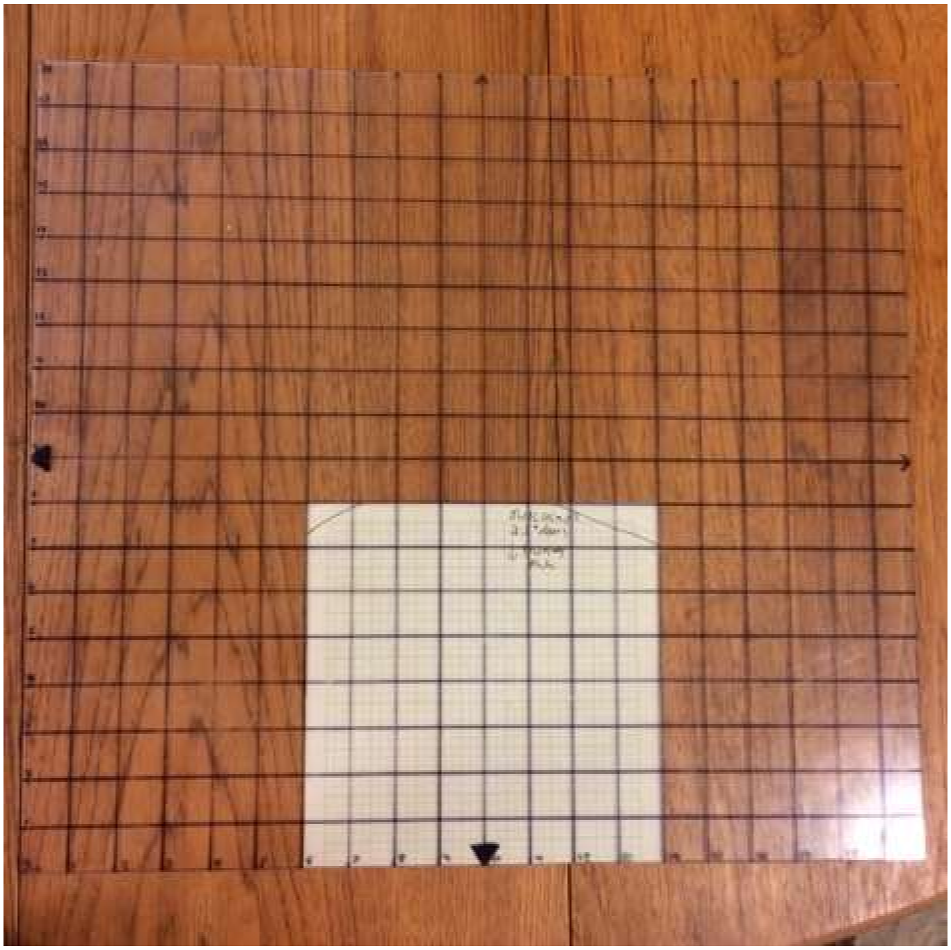

Figure 368: Test 8W8L10Lay3 2.5" Depth

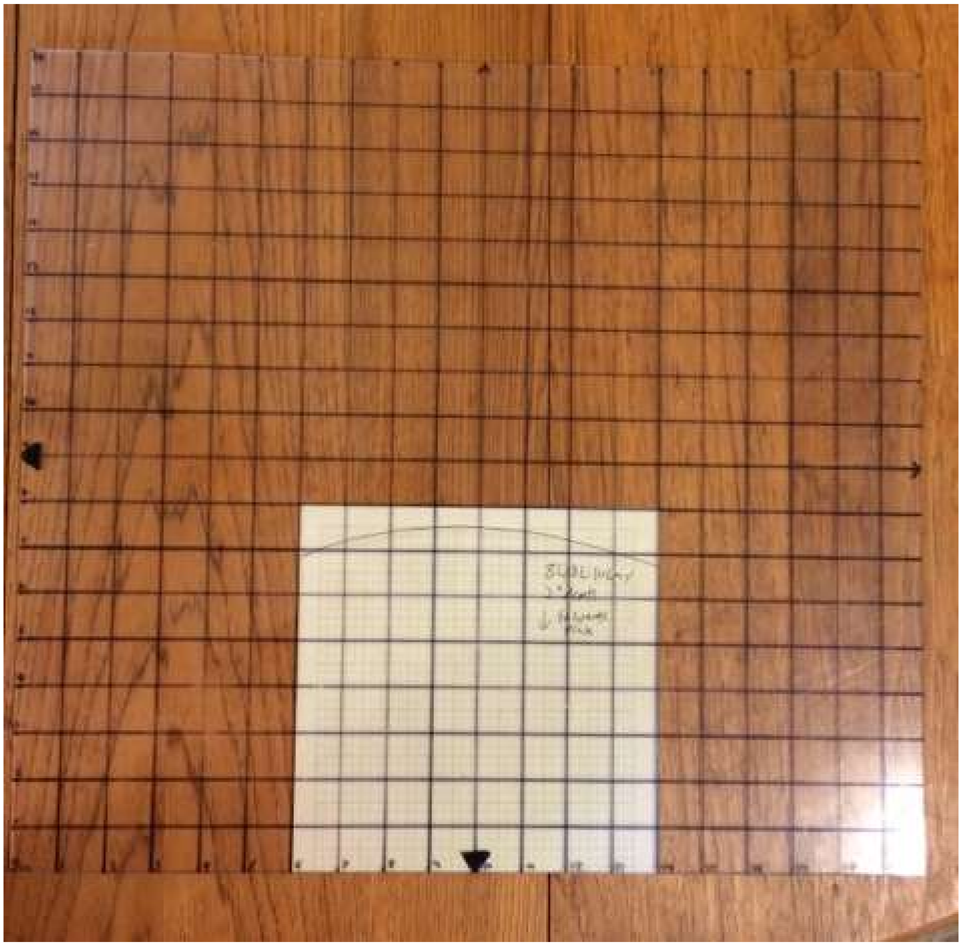

Figure 369: Test 8W8L10Lay3 3" Depth

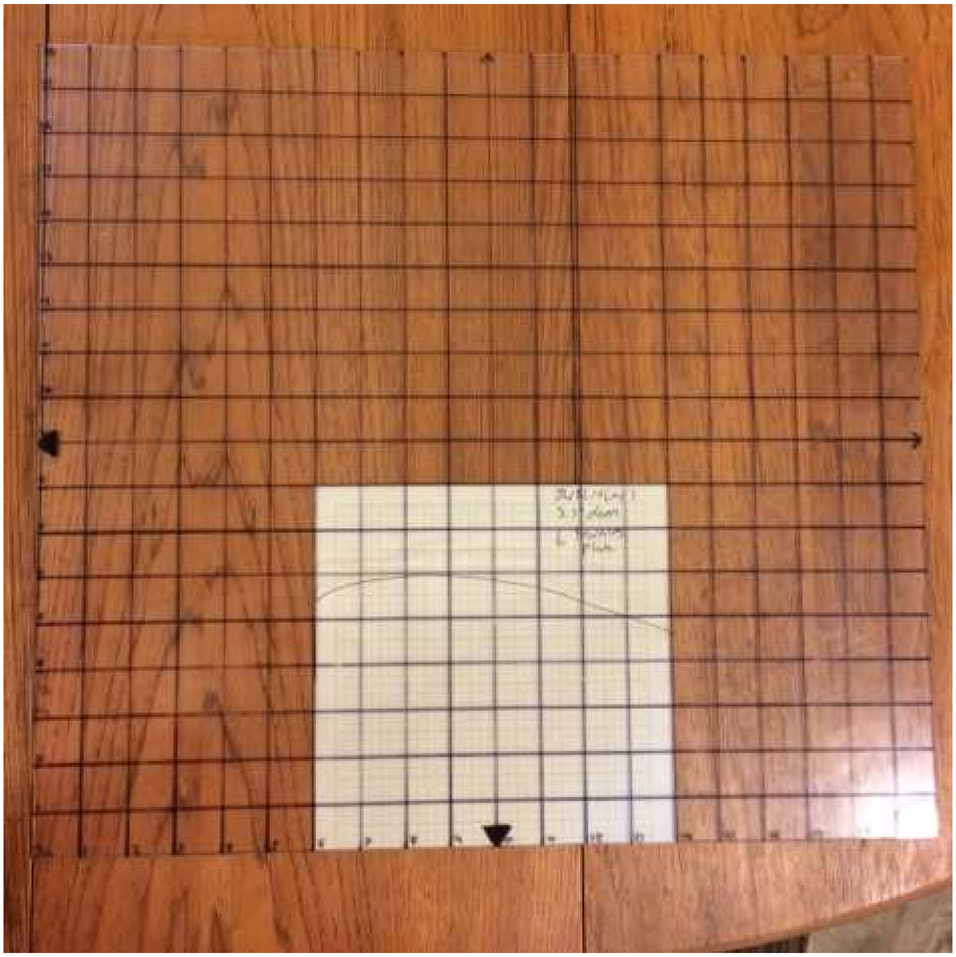

Figure 370: Test 8W8L10Lay3 3.5" Depth

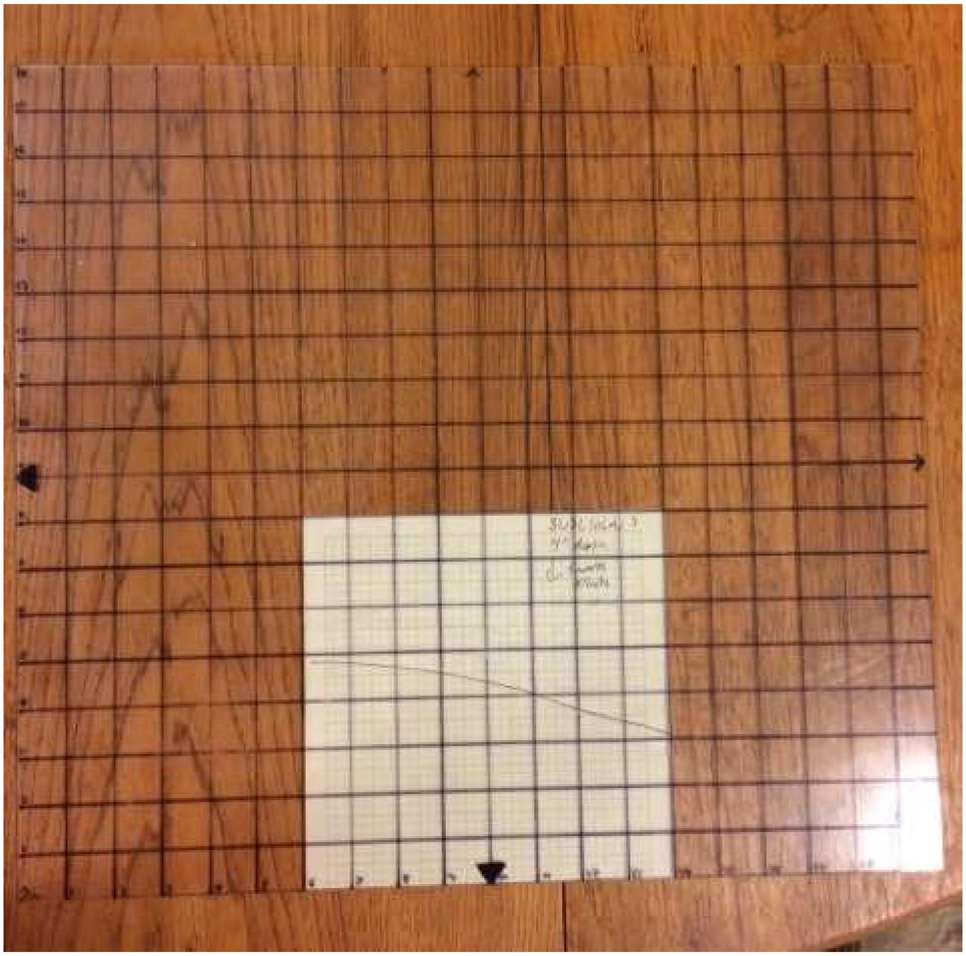

Figure 371: Test 8W8L10Lay3 4" Depth

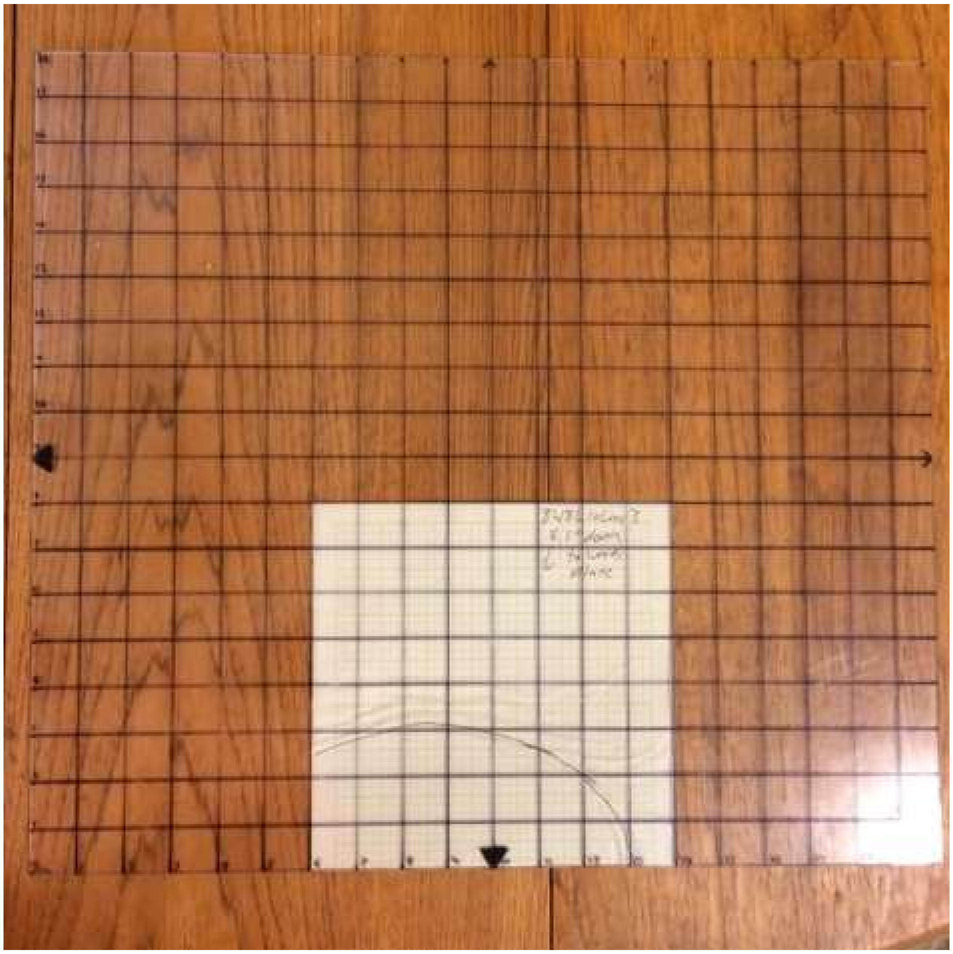

Figure 372: Test 8W8L10Lay3 4.5" Depth

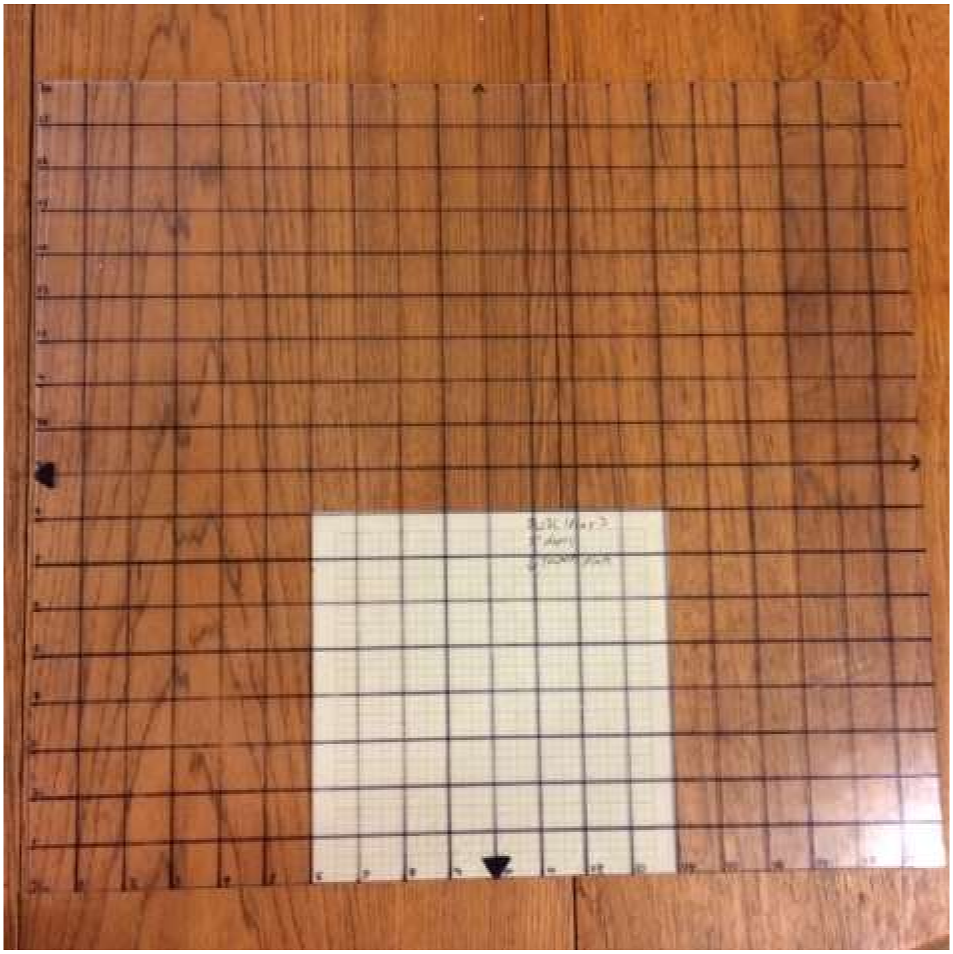

Figure 373: Test 8W8L10Lay3 5" Depth

A.23 Photographs of Test 8W11L5Lay3

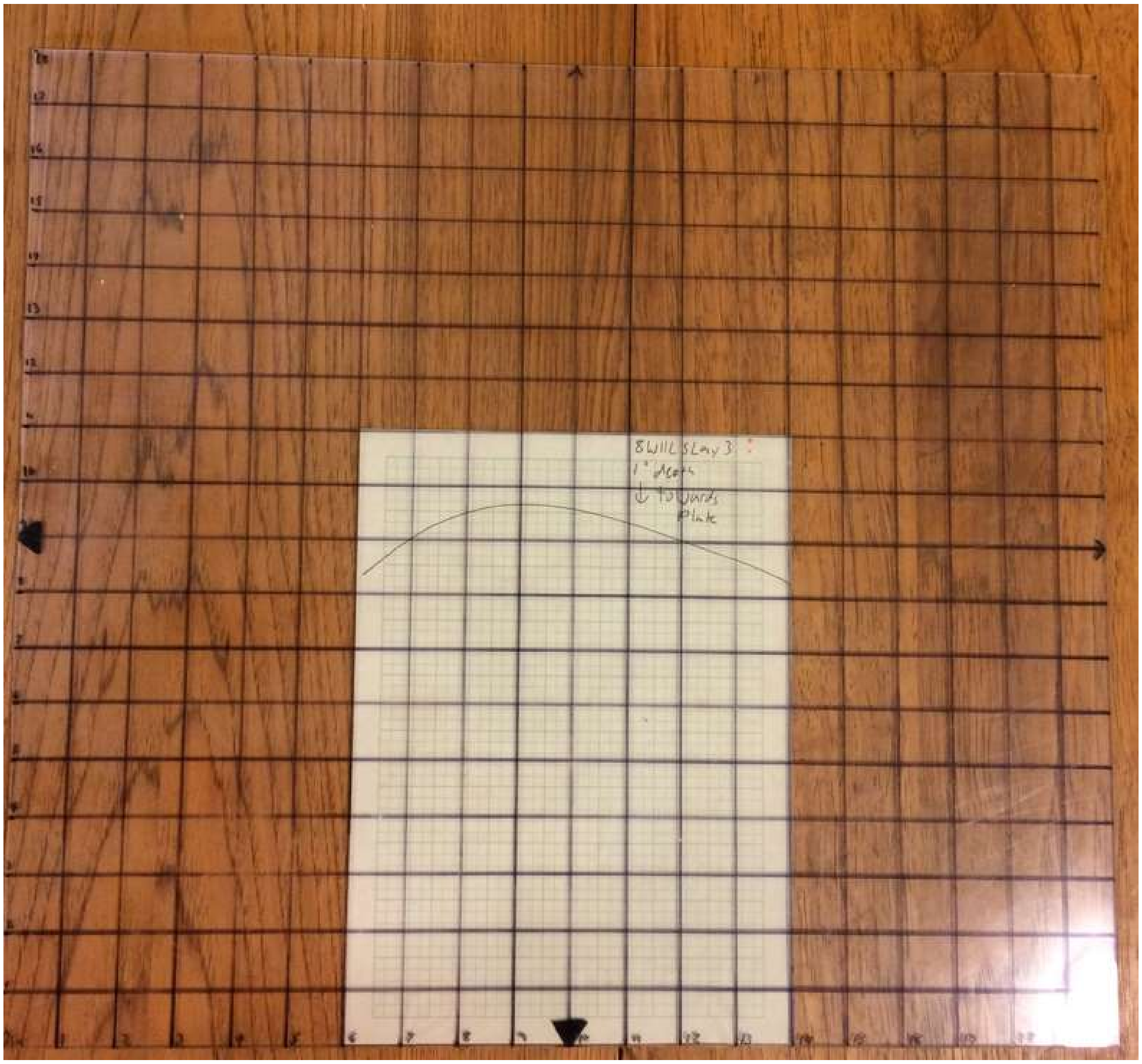

Figure 374: Test 8W11L5Lay3 1” Depth

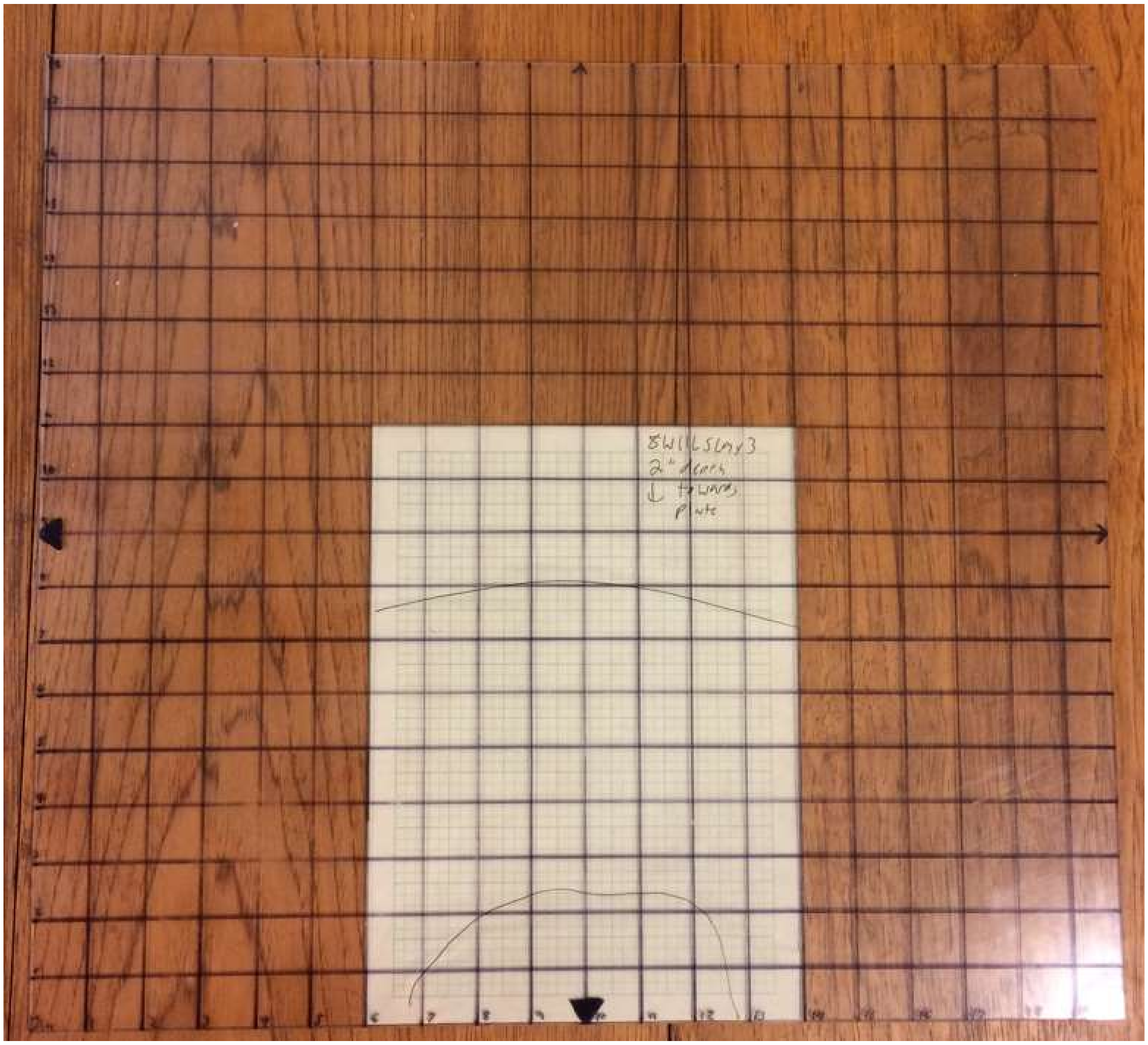

Figure 375: Test 8W11L5Lay3 2" Depth

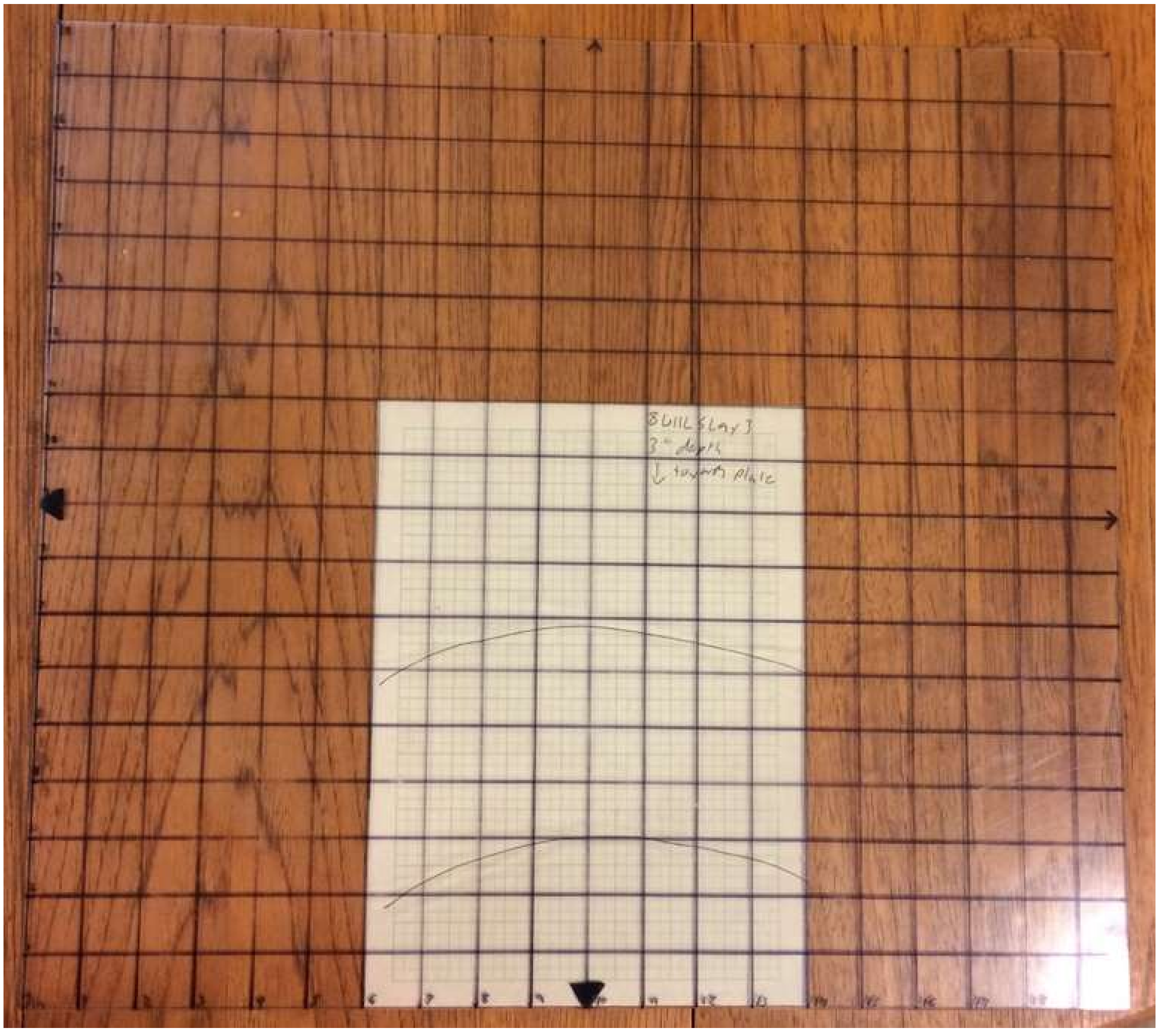

Figure 376: Test 8W11L5Lay3 3” Depth

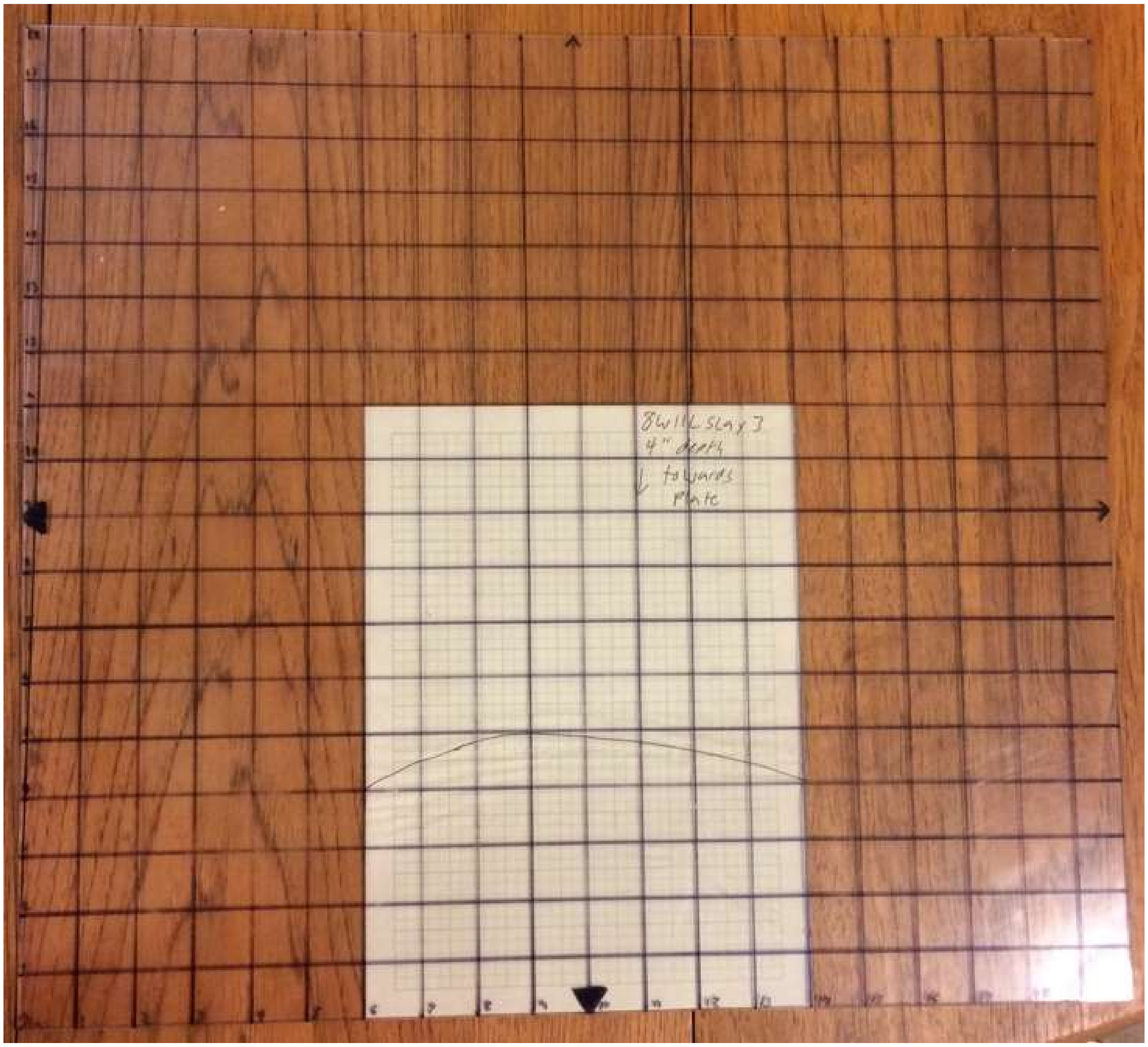

Figure 377: Test 8W11L5Lay3 4" Depth

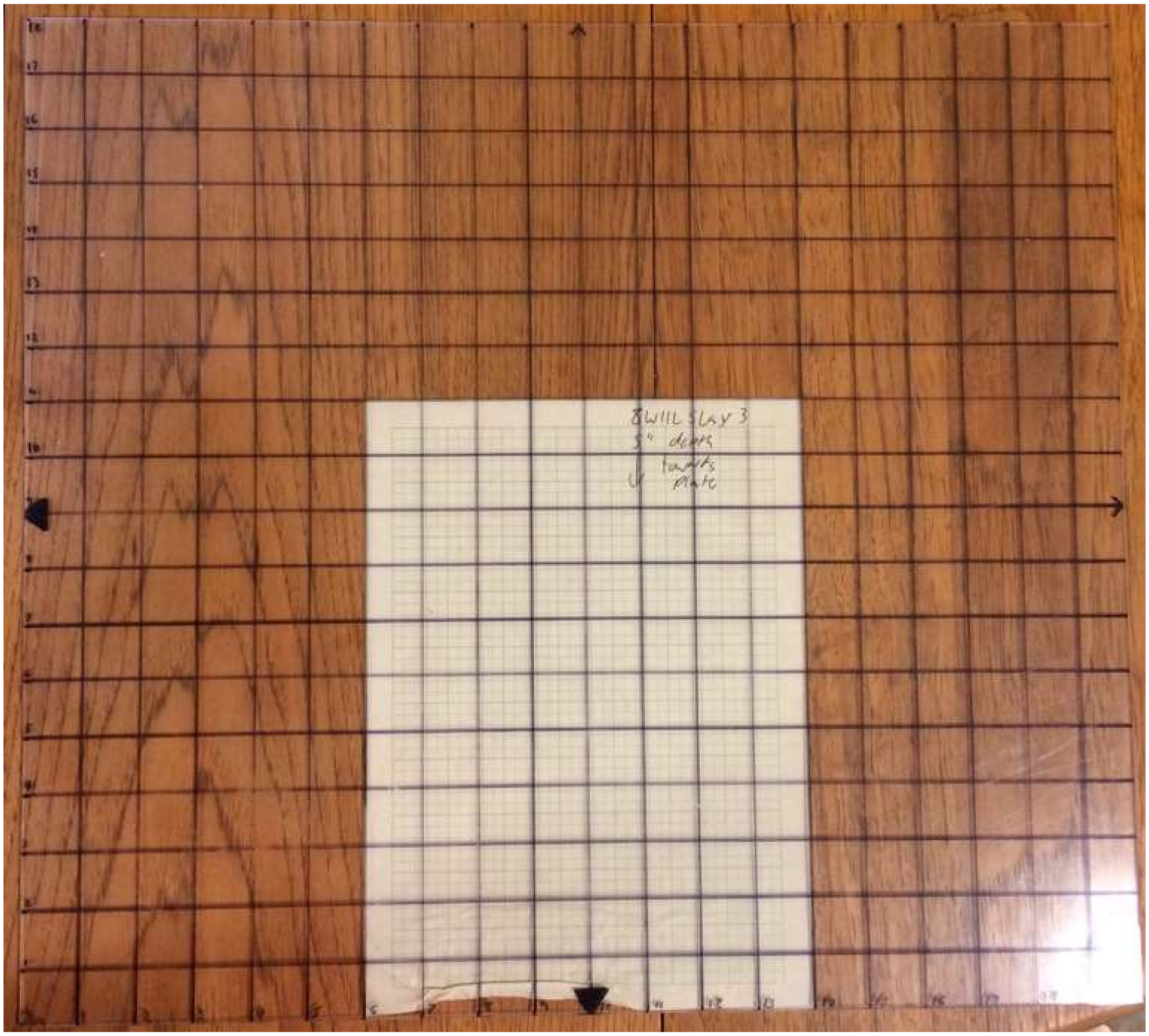

Figure 378: Test 8W11L5Lay3 5" Depth

A.24 Photographs of Test 8W11L10Lay3

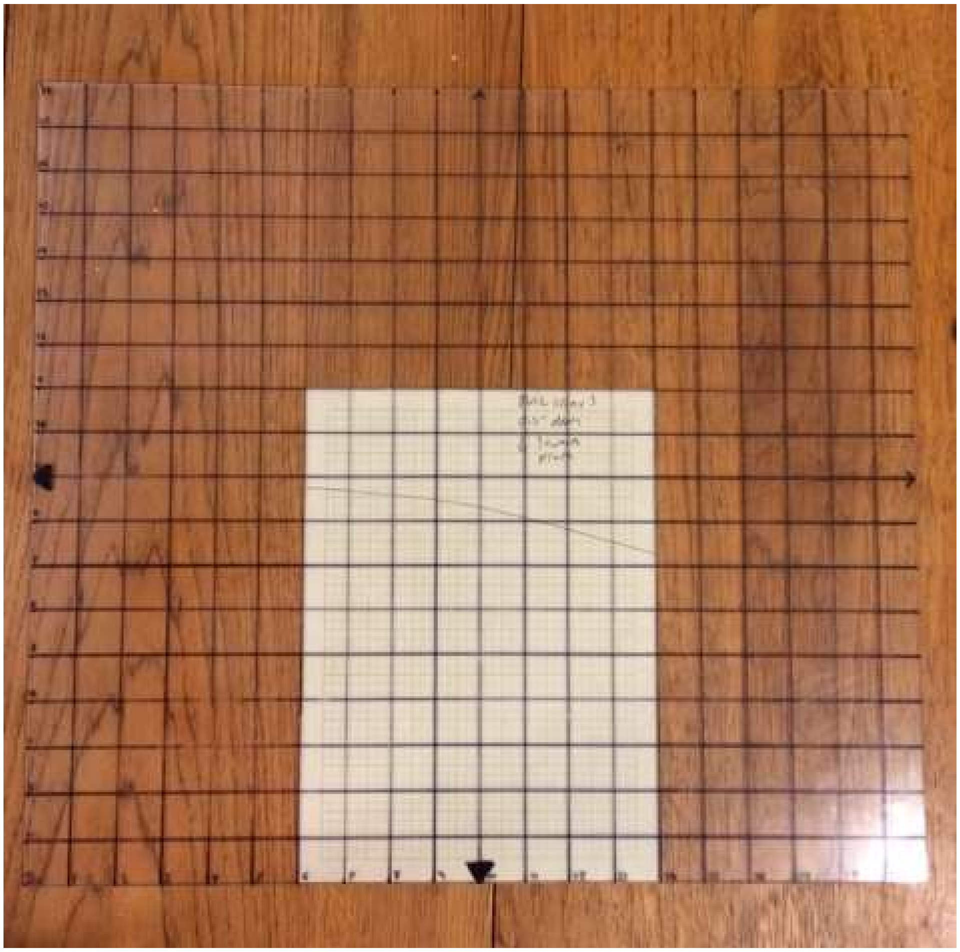

Figure 379: Test 8W11L10Lay3 0.5" Depth

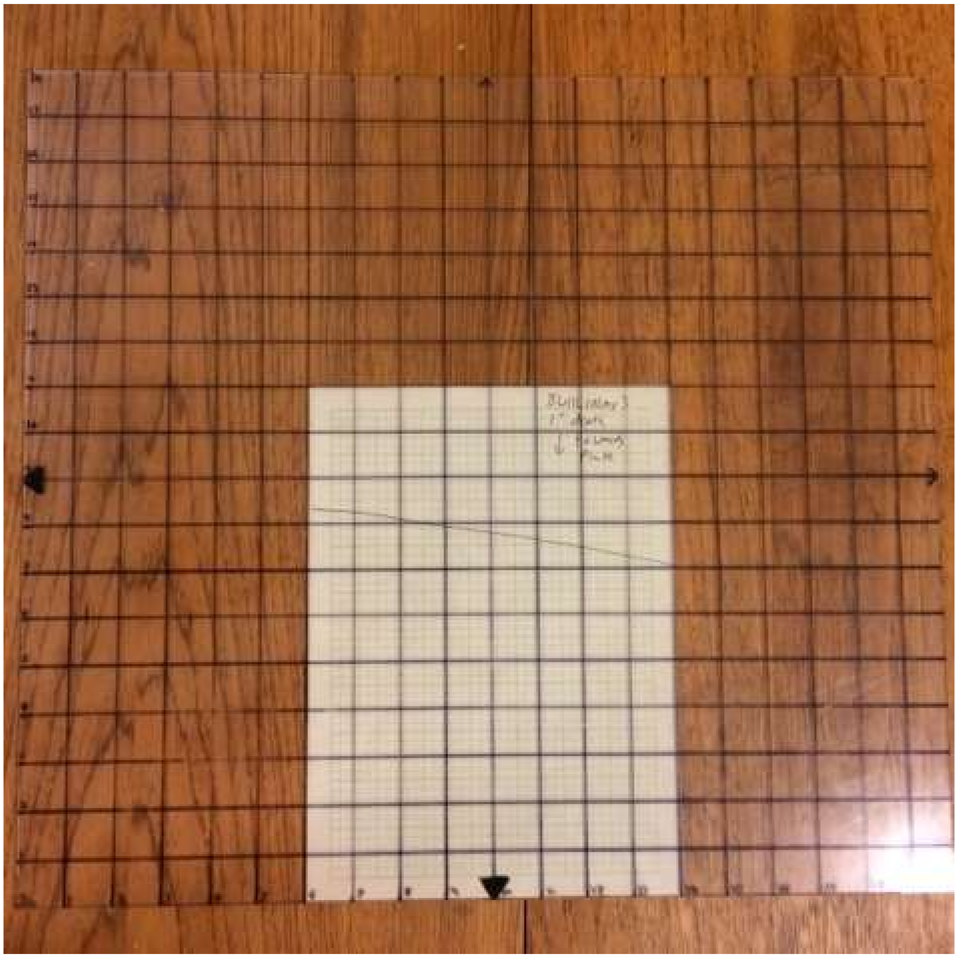

Figure 380: Test 8W11L10Lay3 1" Depth

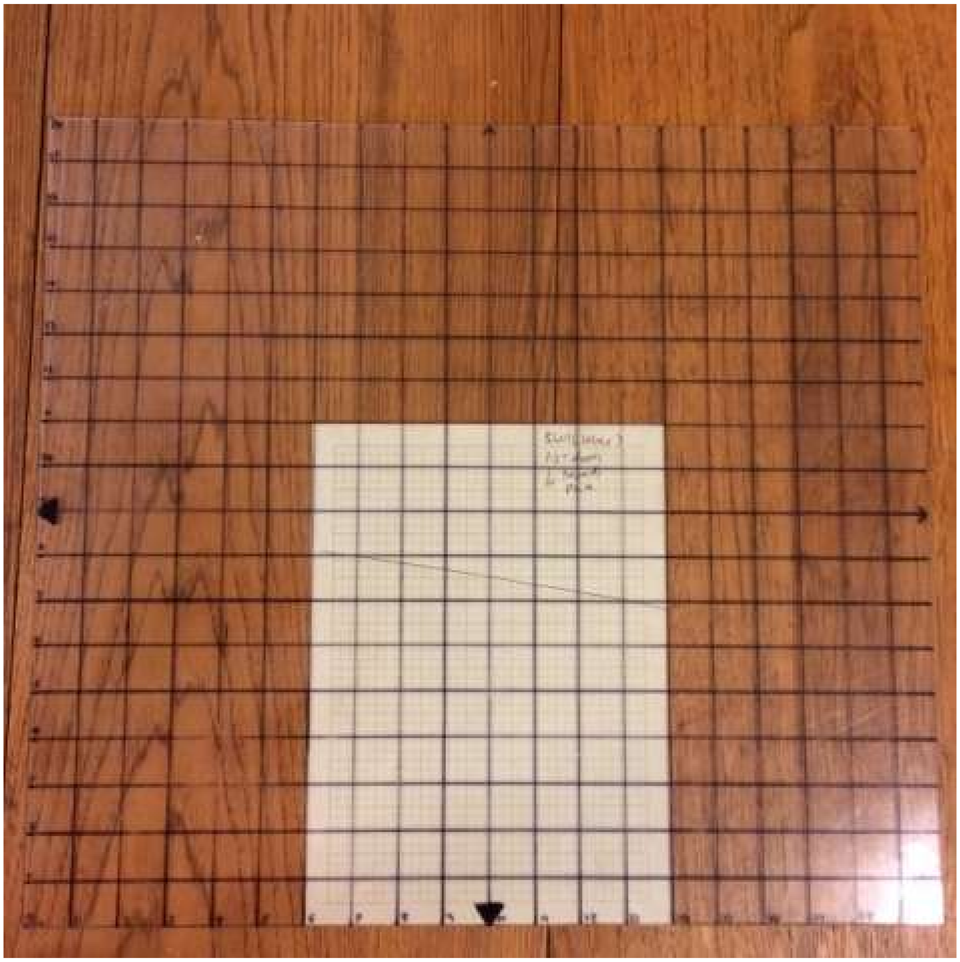

Figure 381: Test 8W11L10Lay3 1.5" Depth

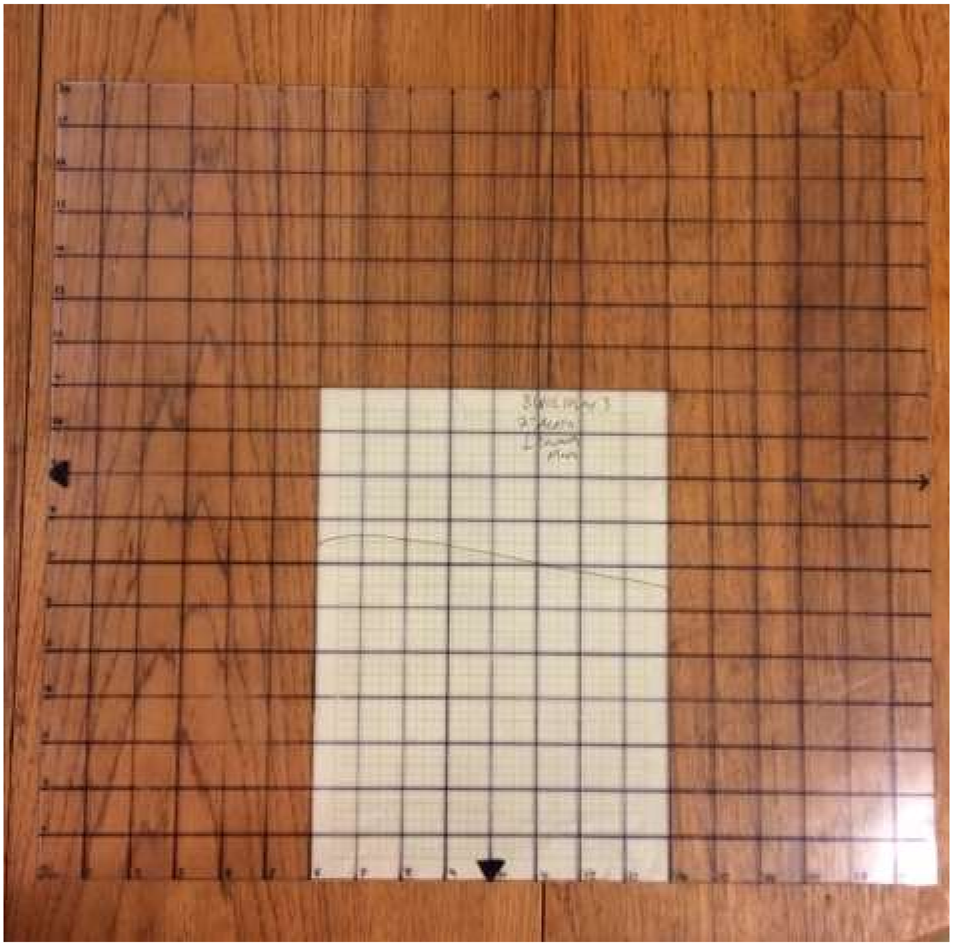

Figure 382: Test 8W11L10Lay3 2" Depth

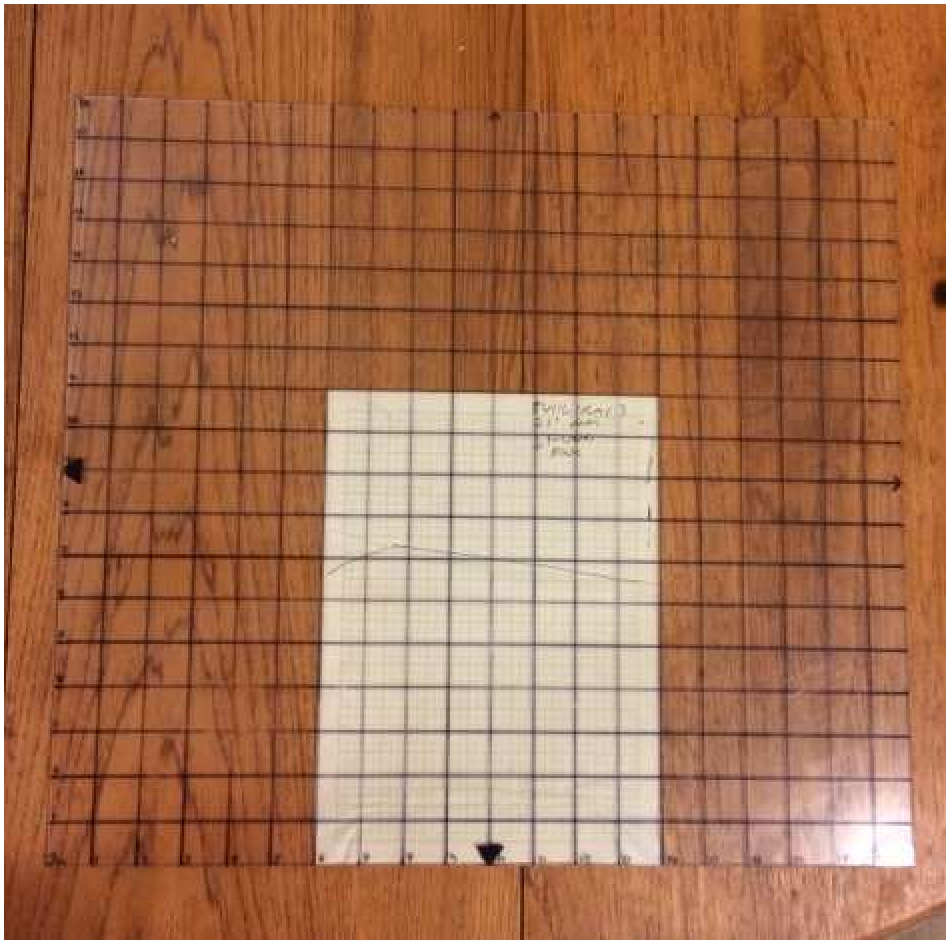

Figure 383: Test 8W11L10Lay3 2.5" Depth

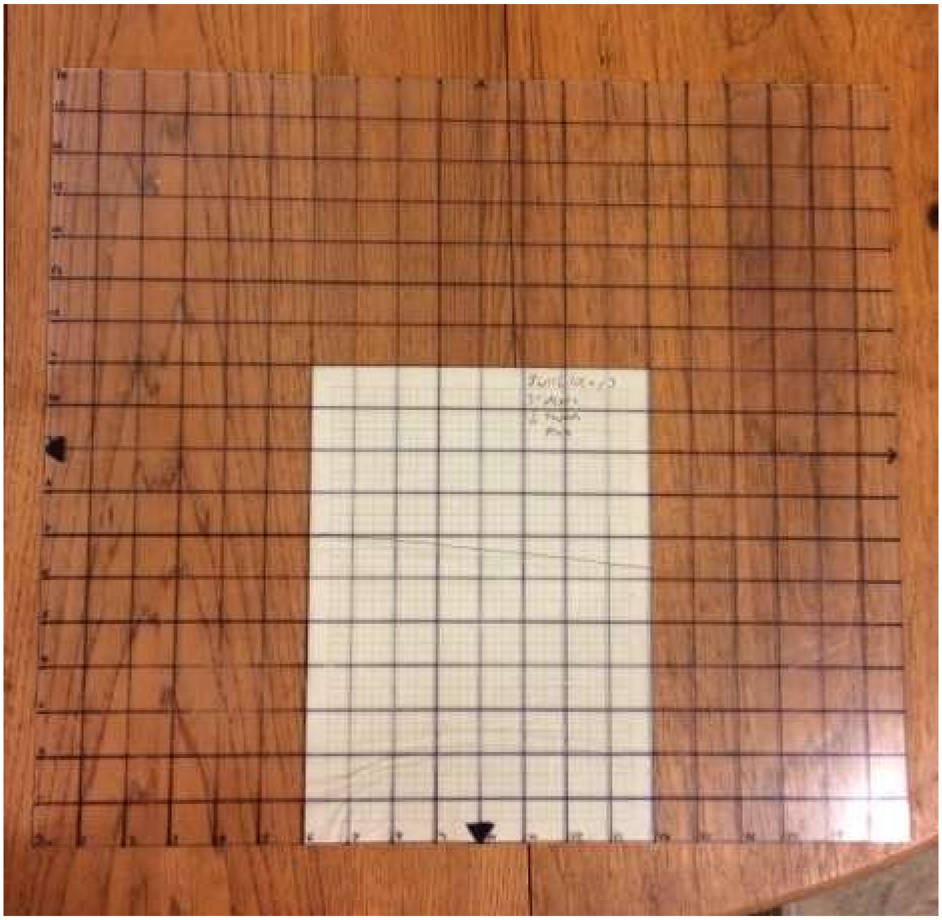

Figure 384: Test 8W11L10Lay3 3” Depth

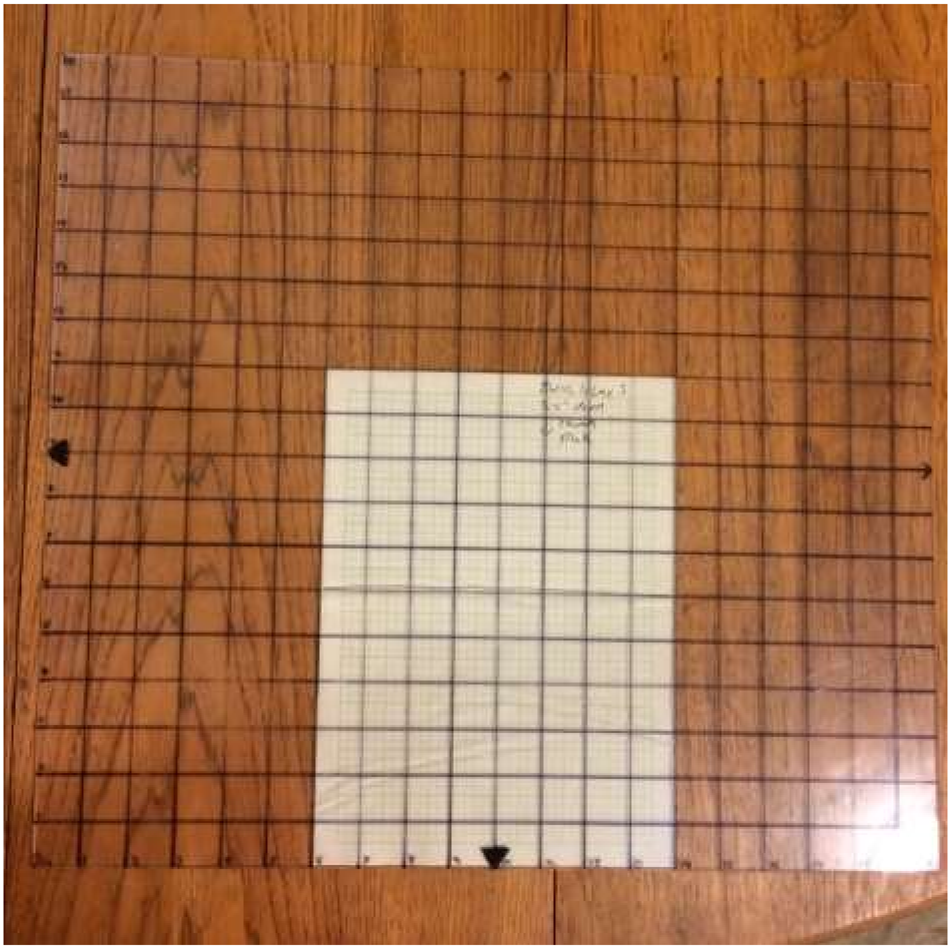

Figure 385: Test 8W11L10Lay3 3.5" Depth

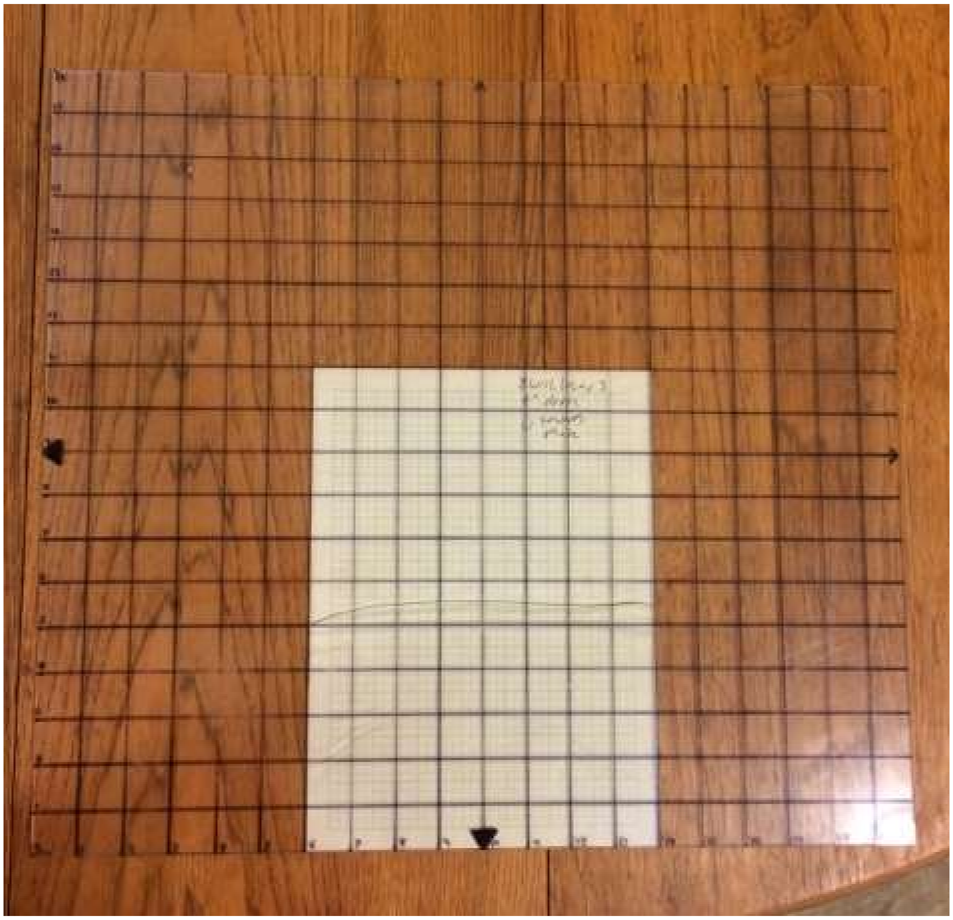

Figure 386: Test 8W11L10Lay3 4” Depth

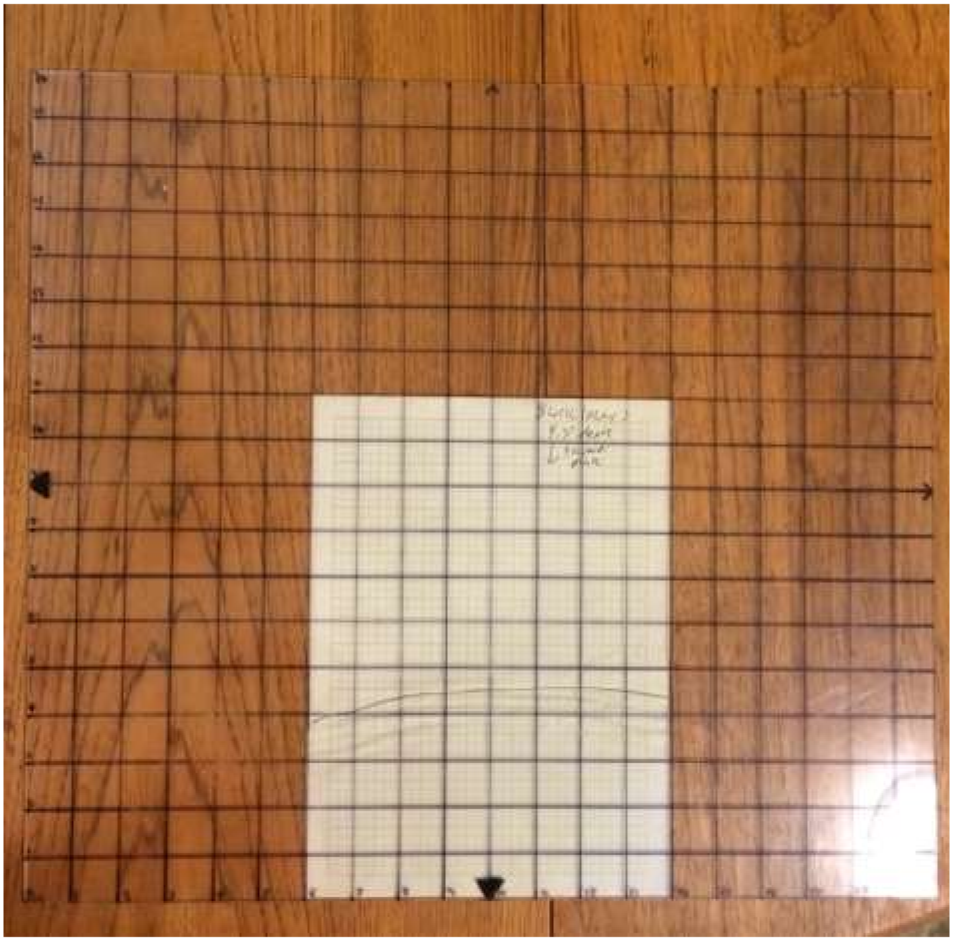

Figure 387: Test 8W11L10Lay3 4.5" Depth

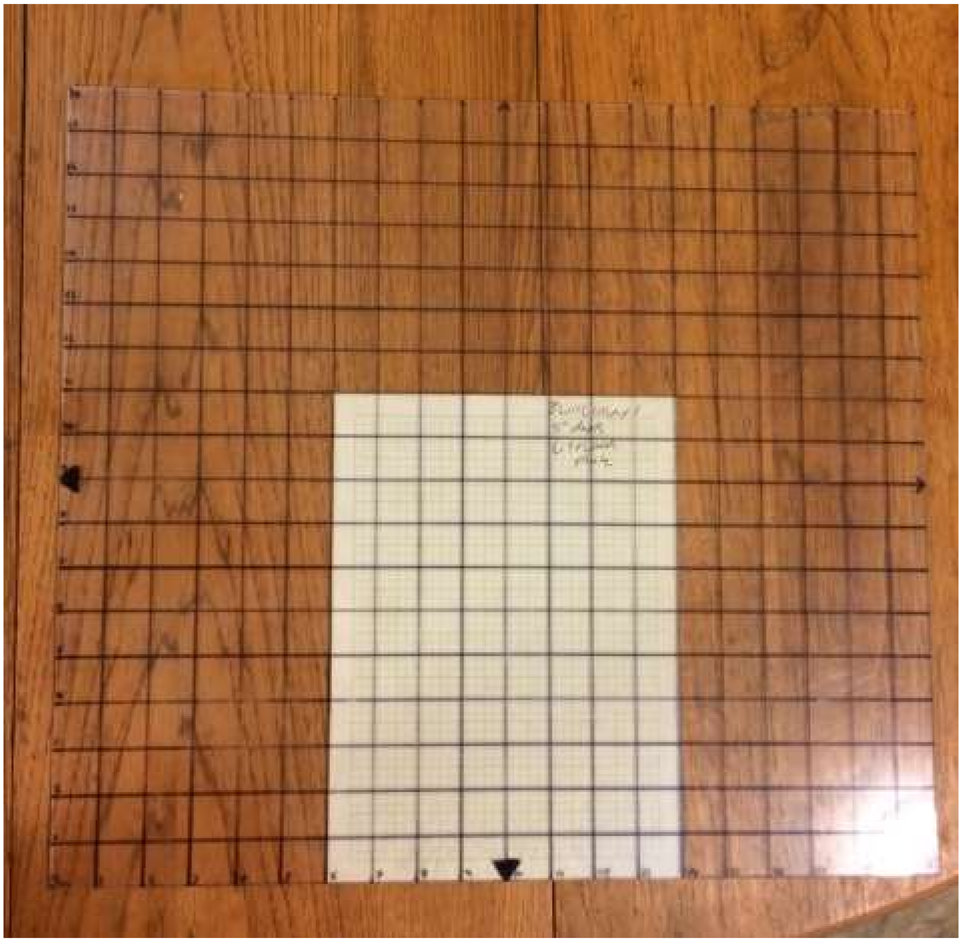

Figure 388: Test 8W11L10Lay3 5" Depth

A.24 Photographs of Test 11W8L10Lay3

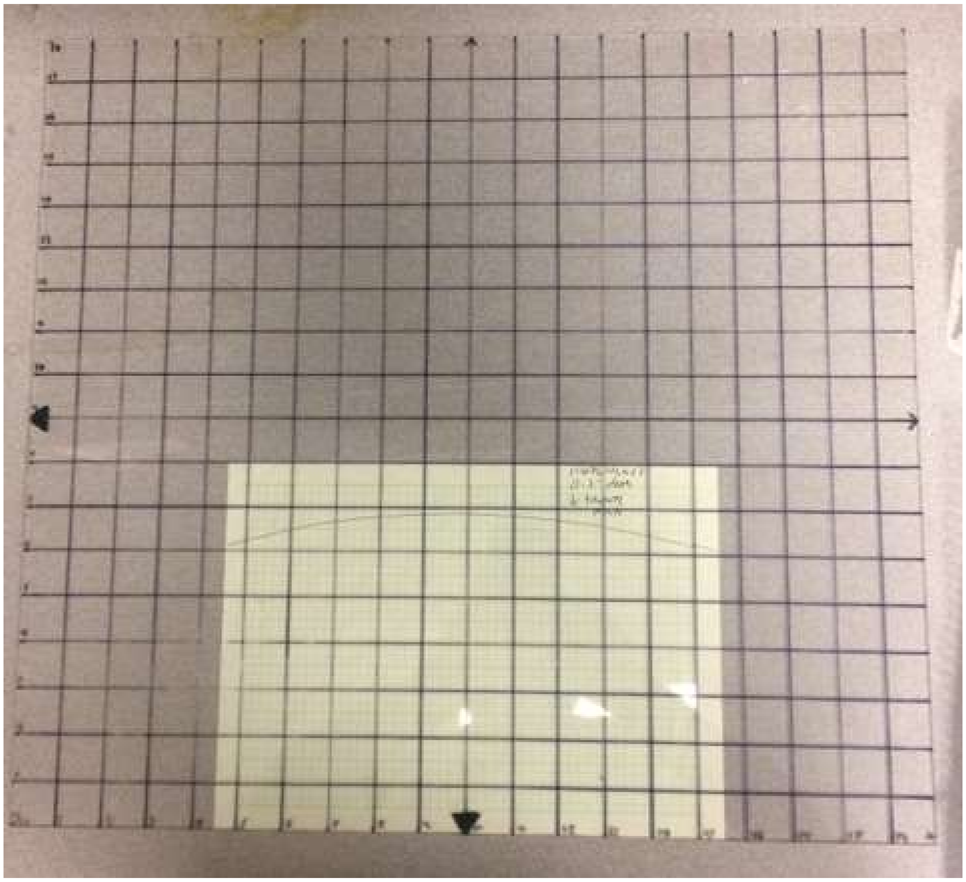

Figure 389: Test 11W8L10Lay3 0.5" Depth

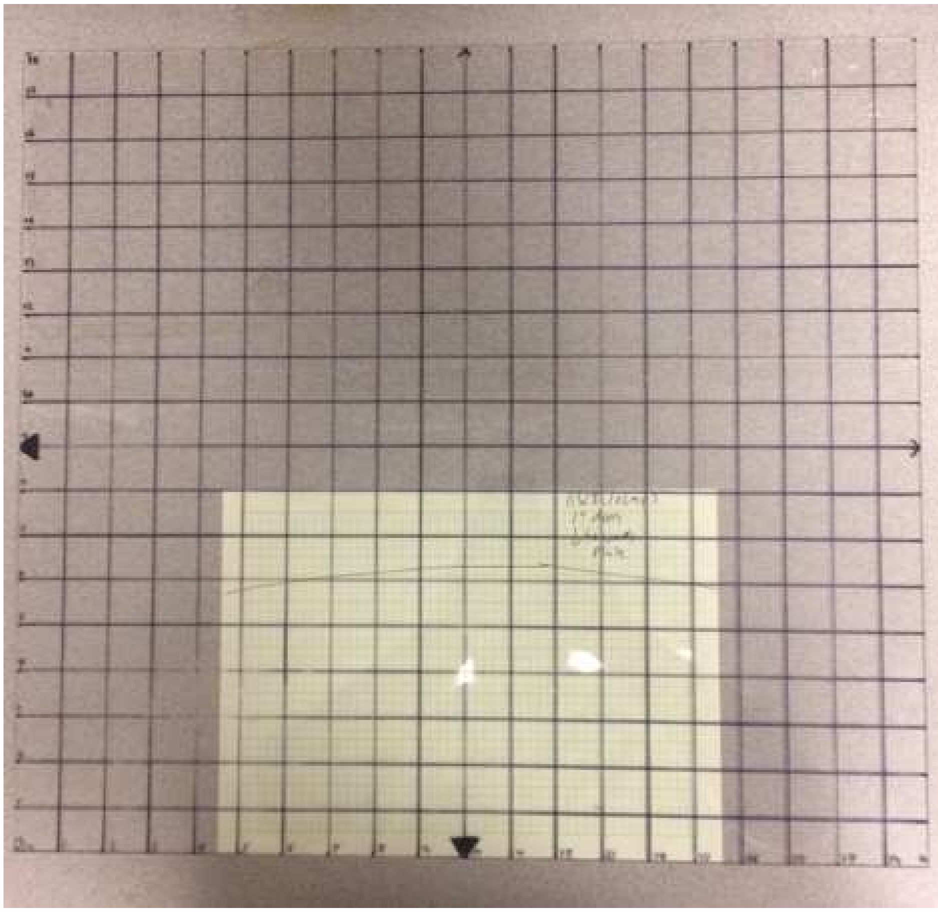

Figure 390: Test 11W8L10Lay3 1” Depth

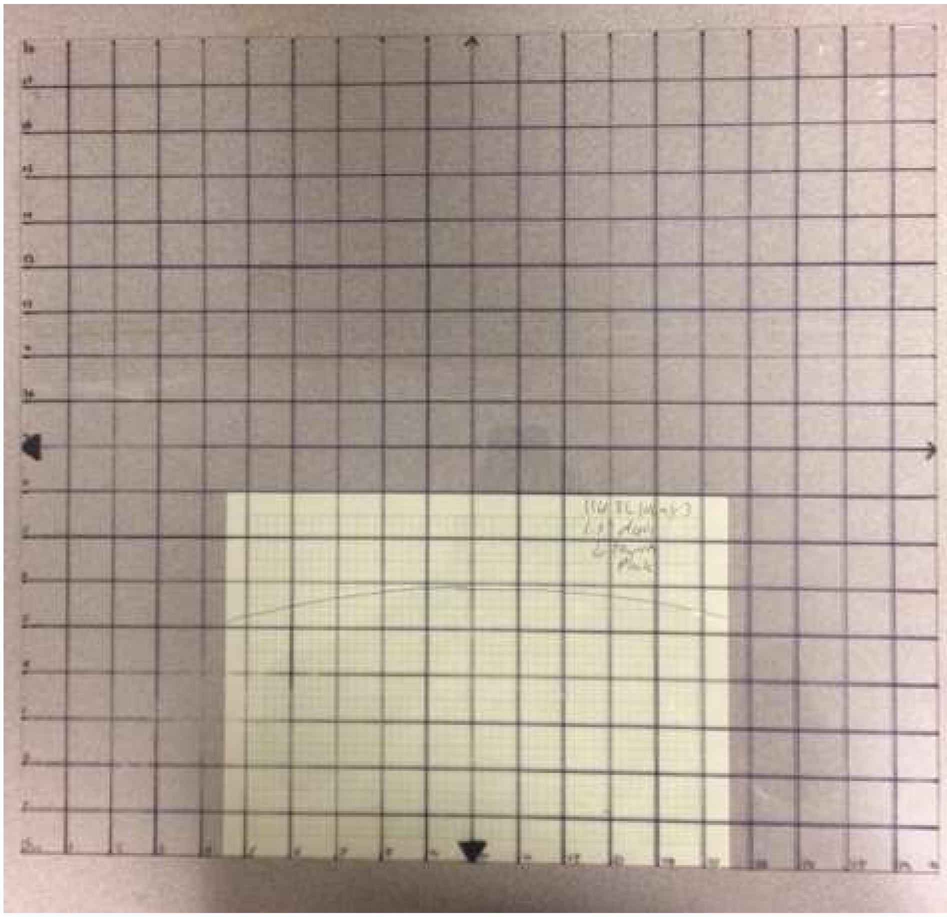

Figure 391: Test 11W8L10Lay3 1.5” Depth

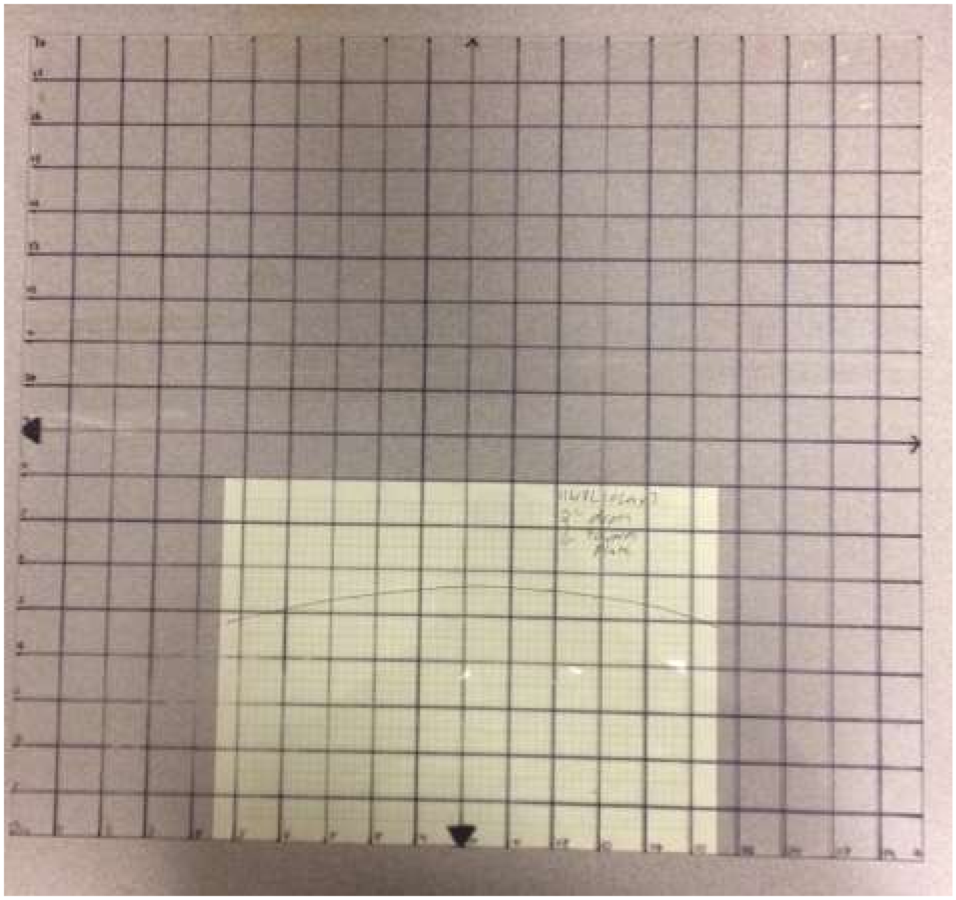

Figure 392: Test 11W8L10Lay3 2” Depth

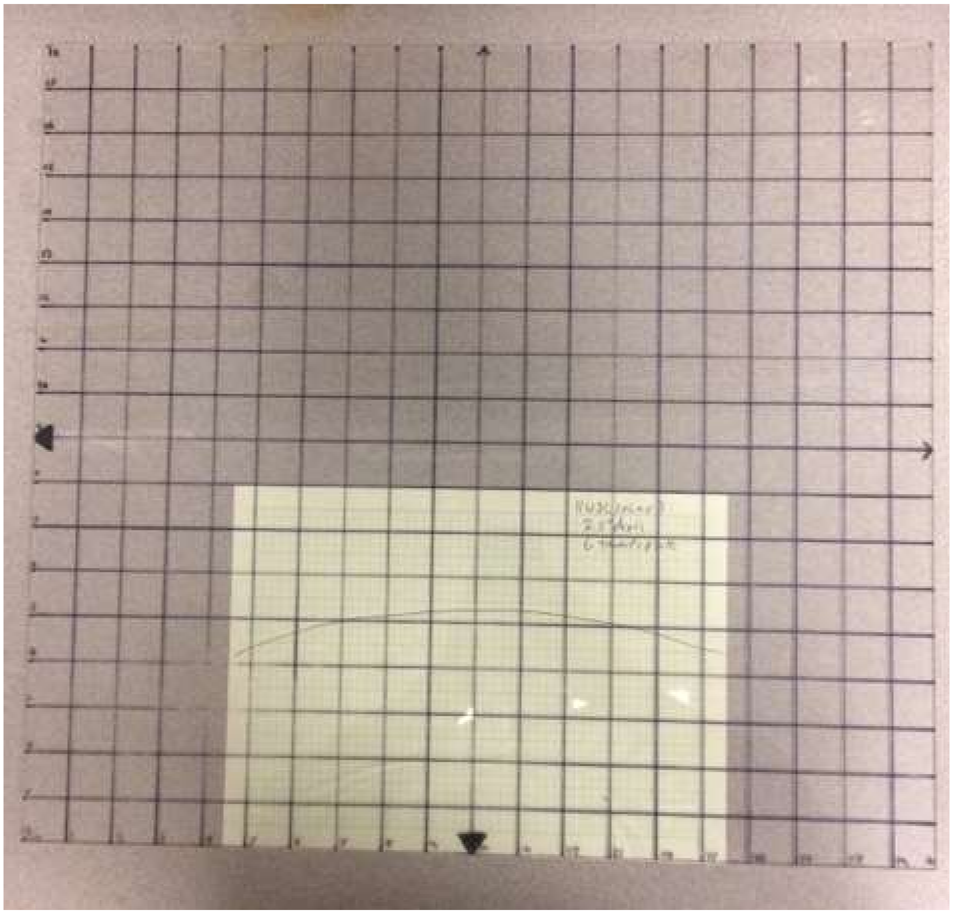

Figure 393: Test 11W8L10Lay3 2.5" Depth

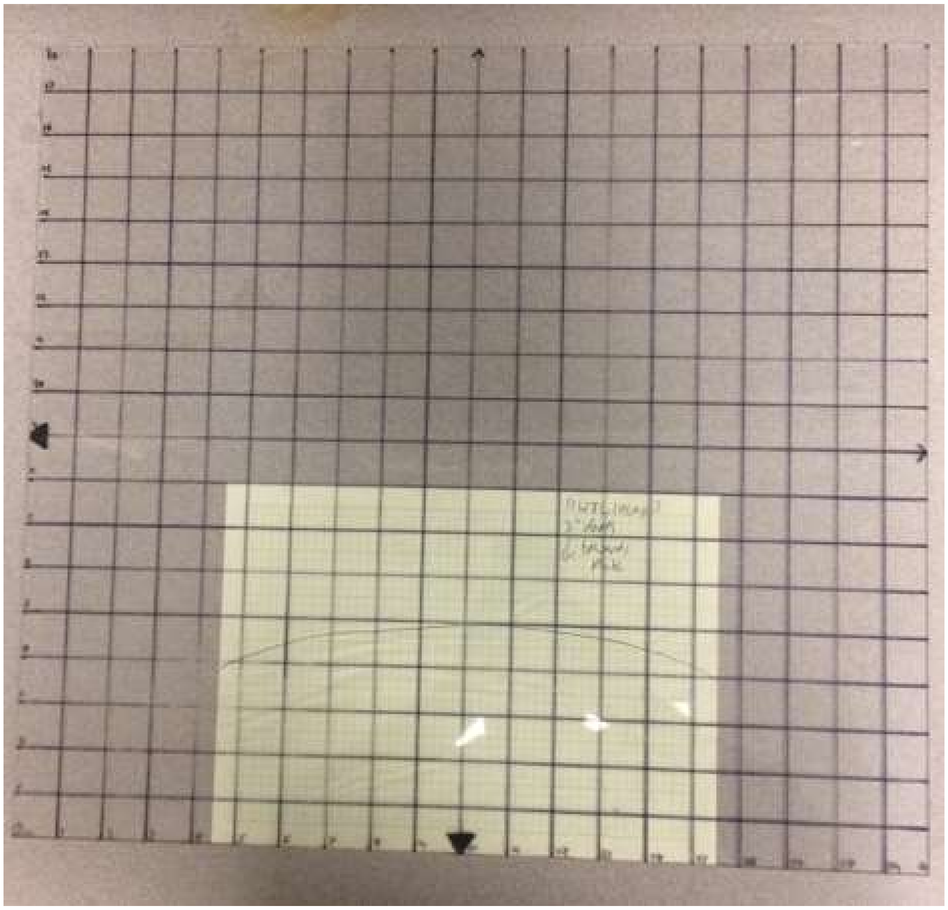

Figure 394: Test 11W8L10Lay3 3” Depth

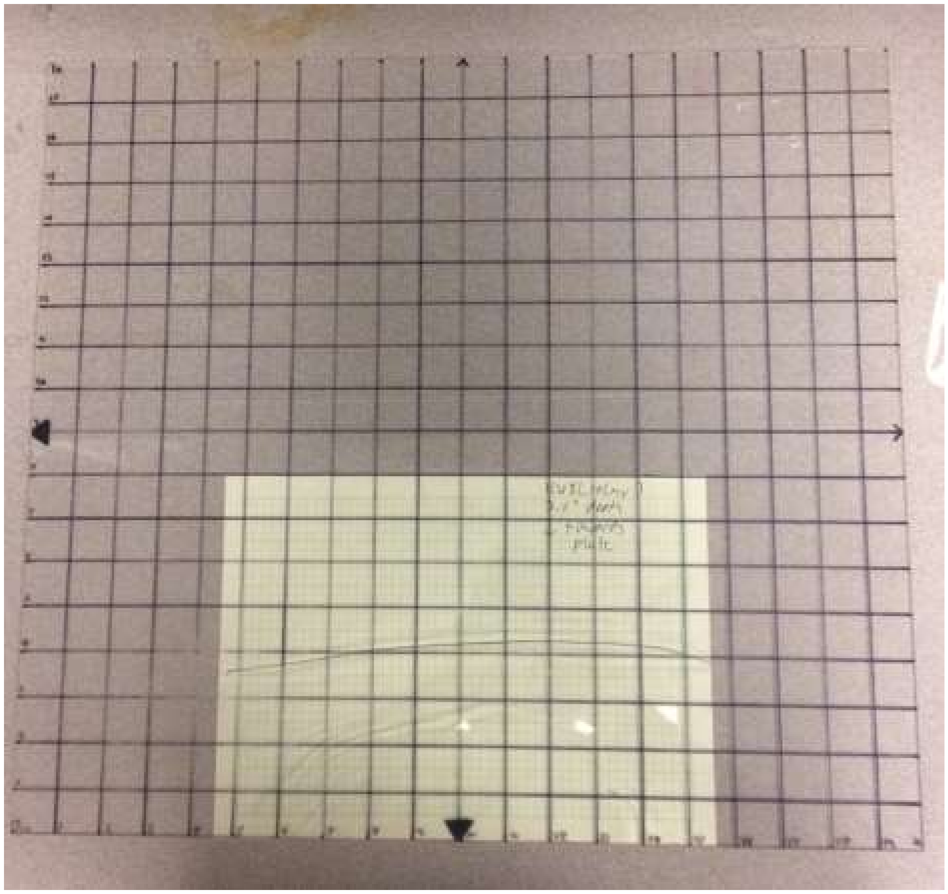

Figure 395: Test 11W8L10Lay3 3.5" Depth

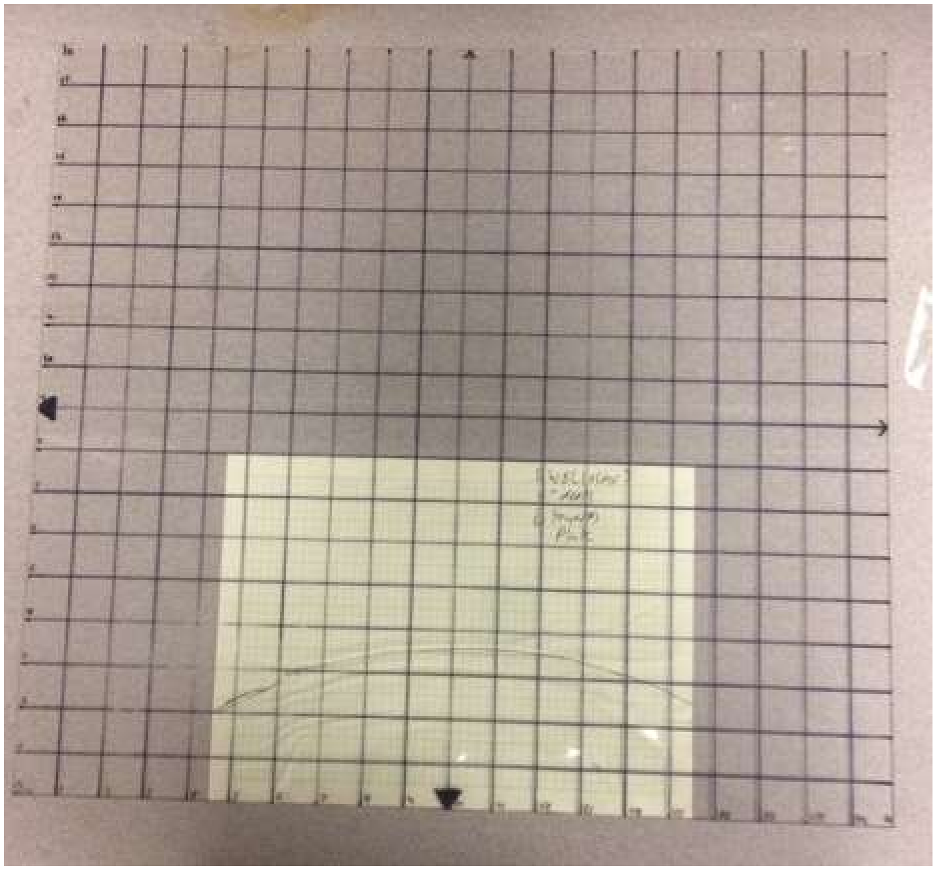

Figure 396: Test 11W8L10Lay3 4” Depth

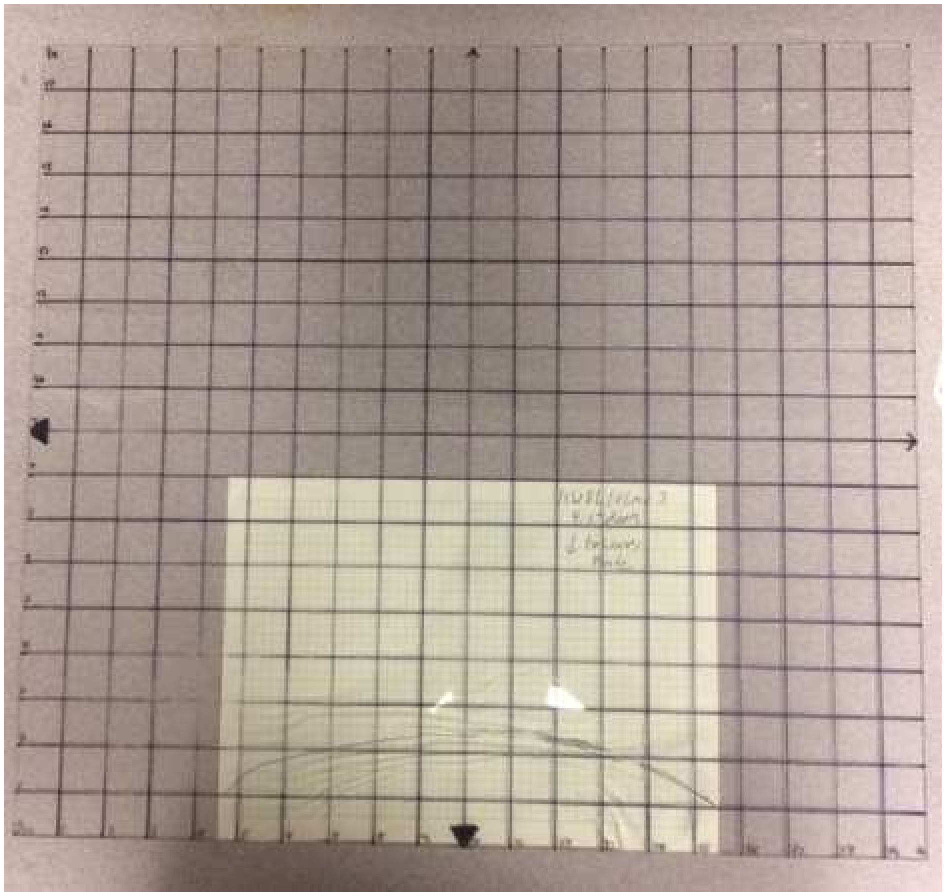

Figure 397: Test 11W8L10Lay3 4.5" Depth

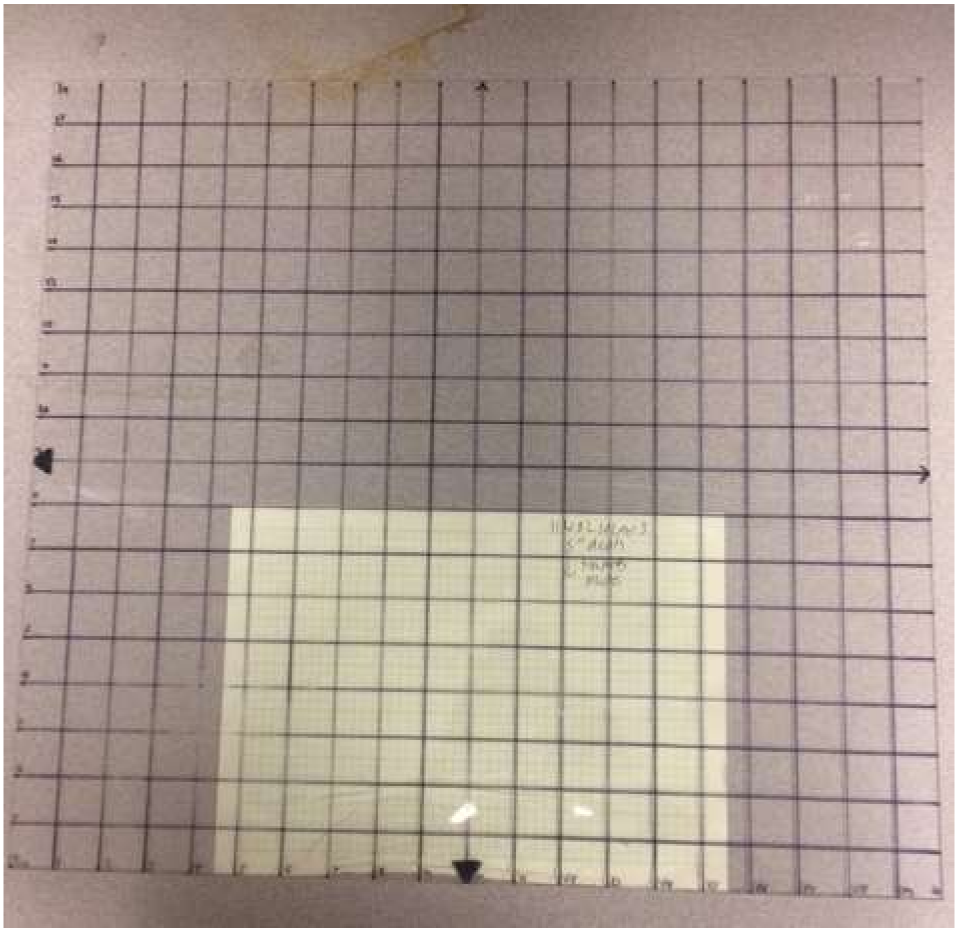

Figure 398: Test 11W8L10Lay3 5" Depth

A.24 Photographs of Test 11W11L5Lay3

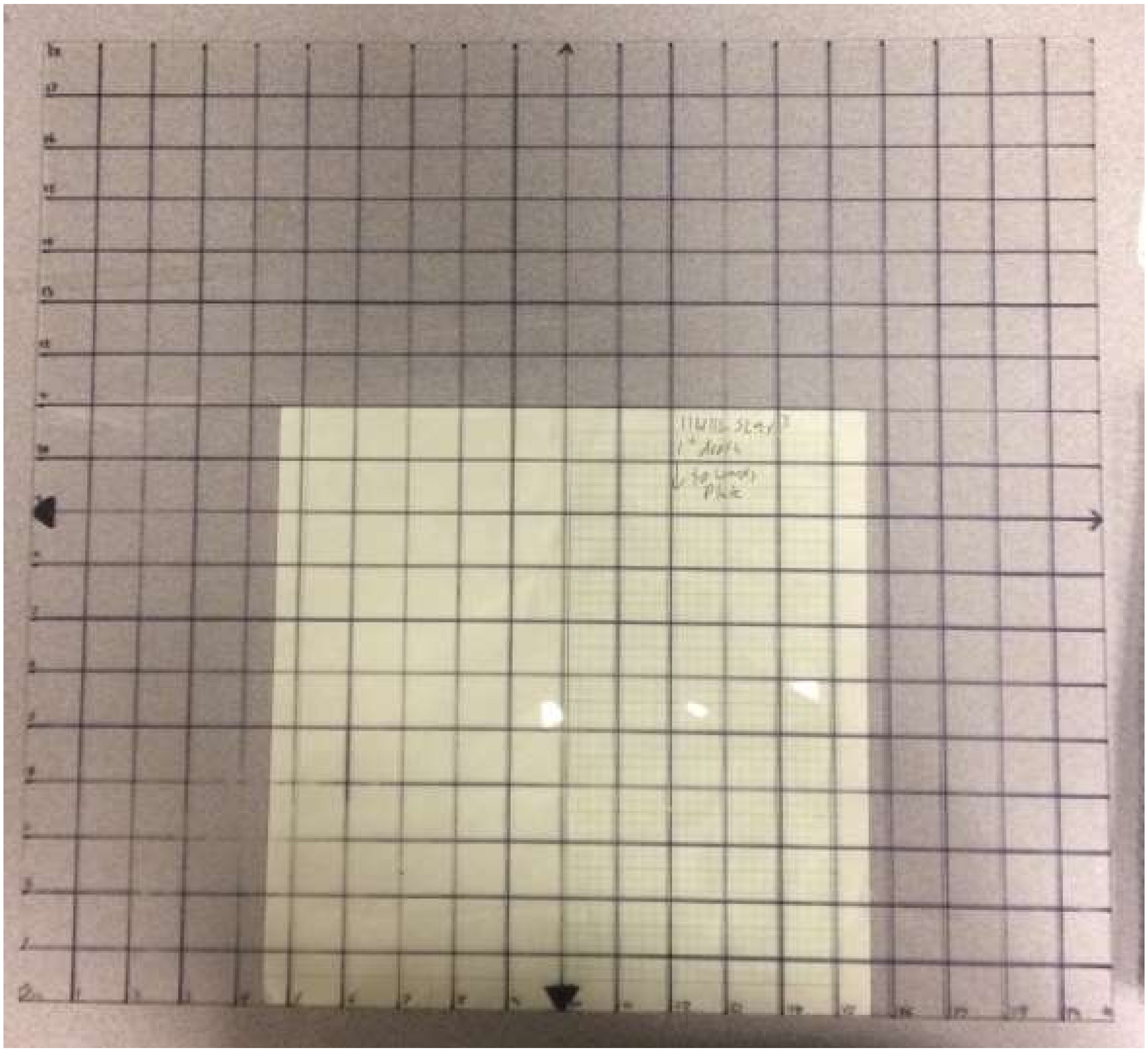

Figure 399: Test 11W11L5Lay3 1" Depth

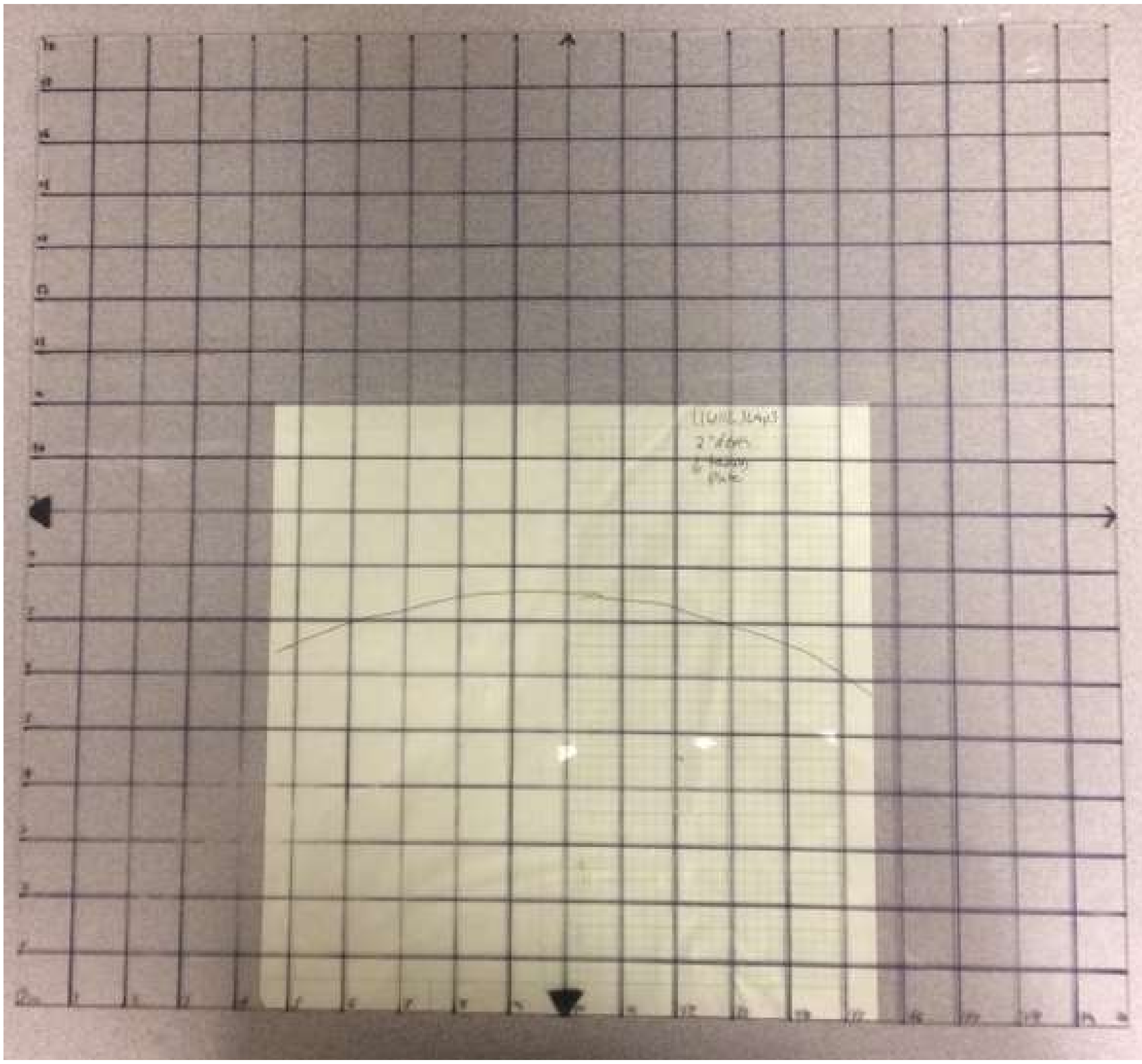

Figure 400: Test 11W11L5Lay3 2” Depth

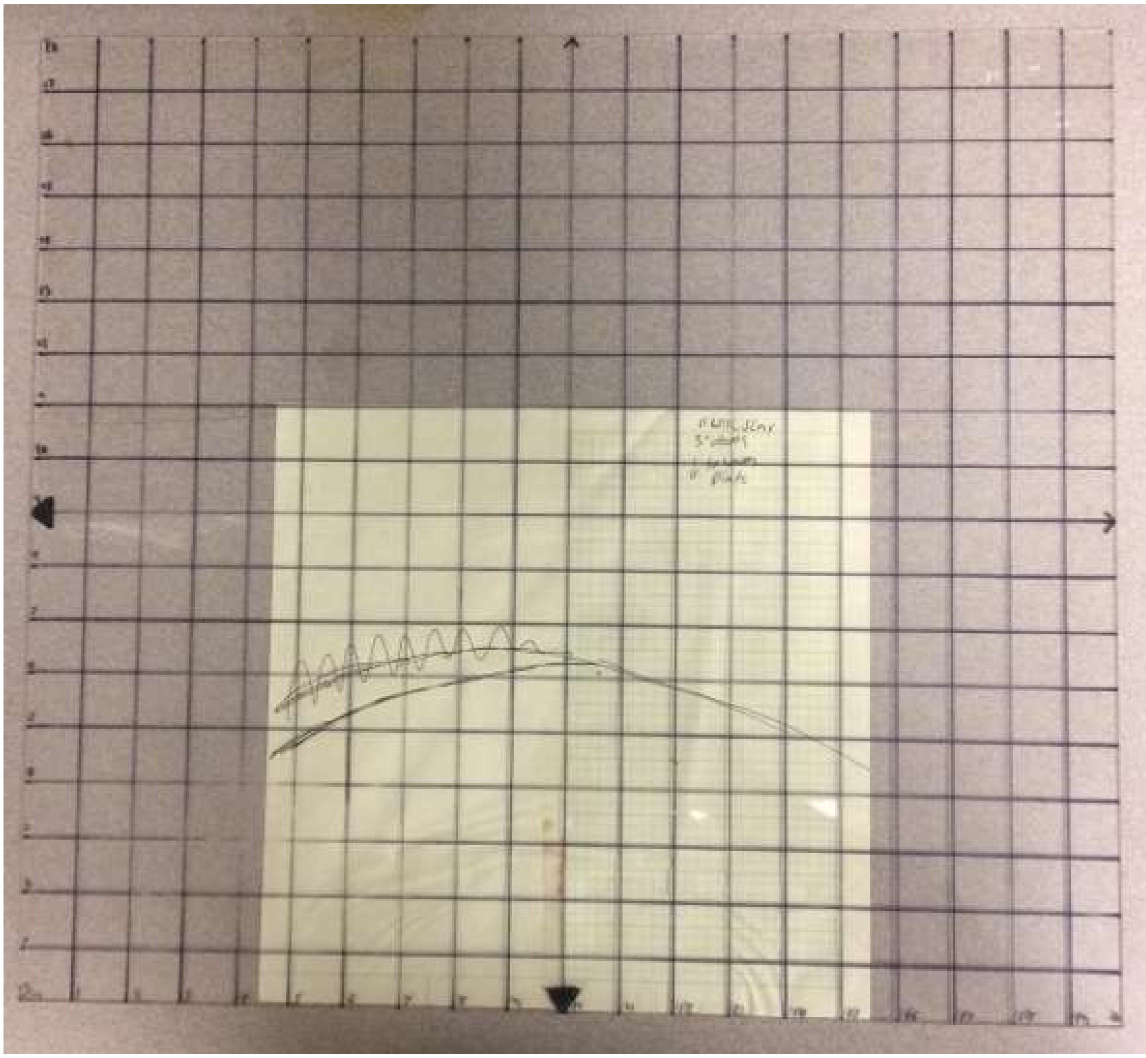

Figure 401: Test 11W11L5Lay3 3” Depth

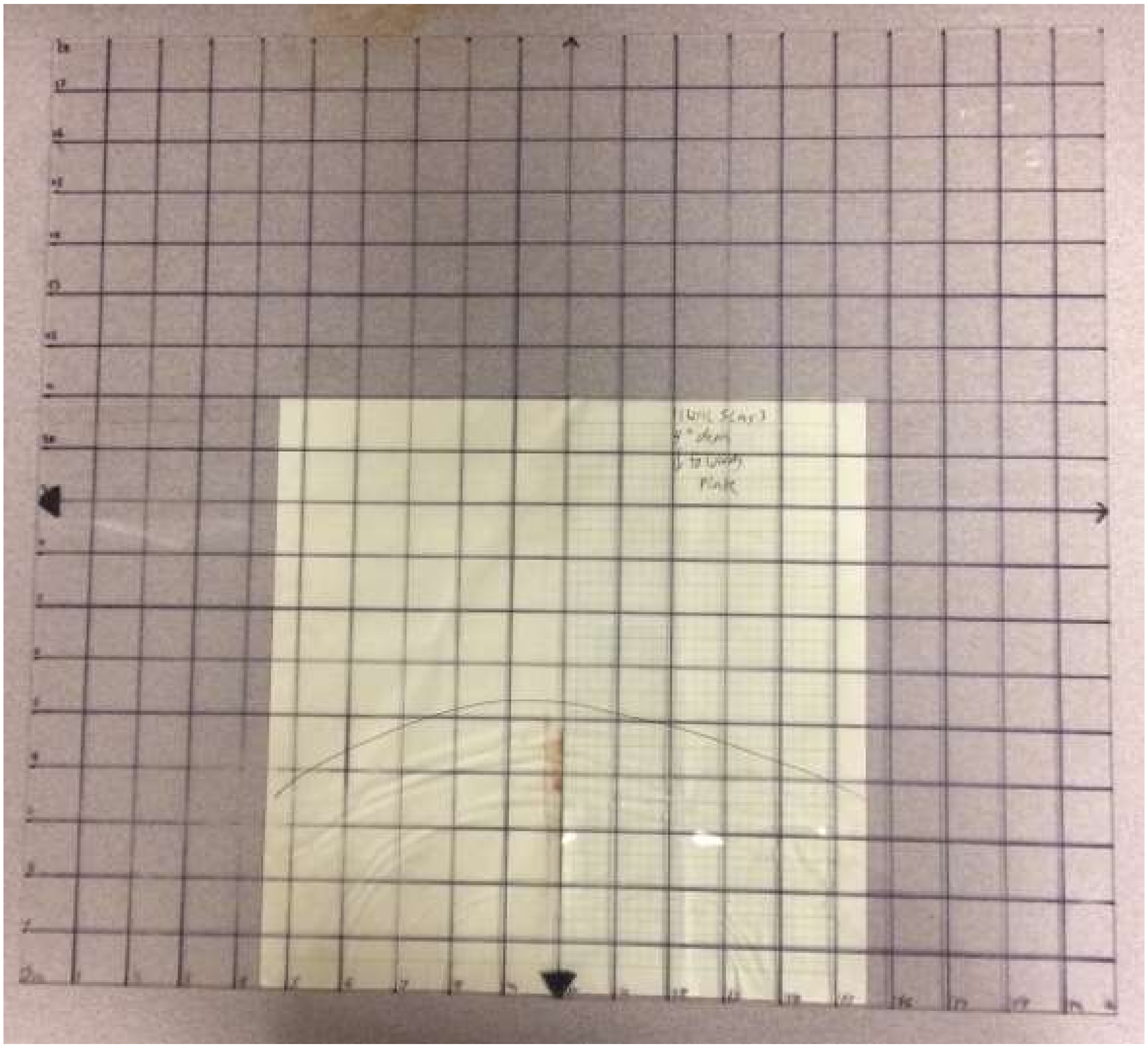

Figure 402: Test 11W11L5Lay3 4" Depth

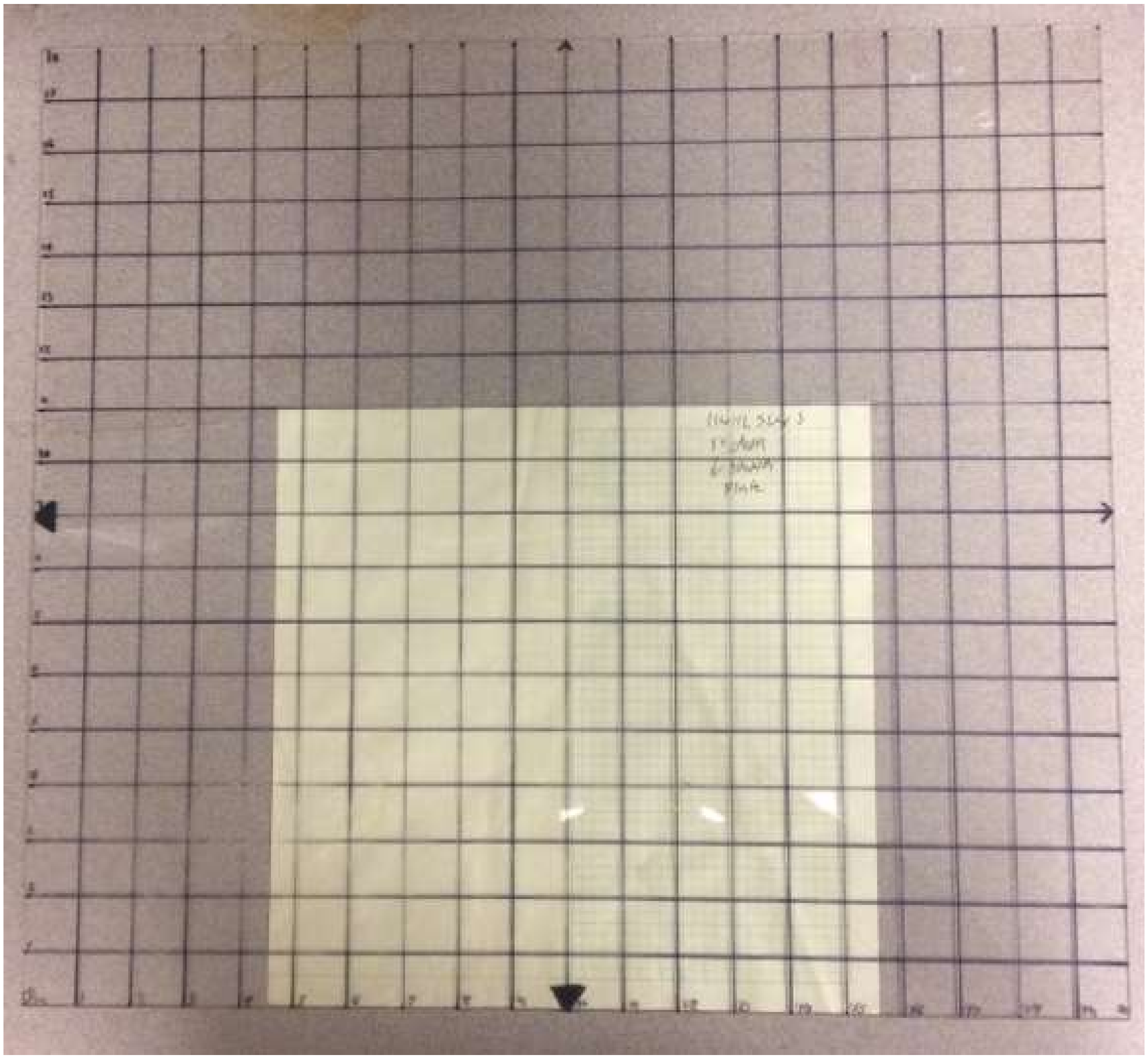

Figure 403: Test 11W11L5Lay3 5” Depth

A.24 Photographs of Test 11W11L10Lay3

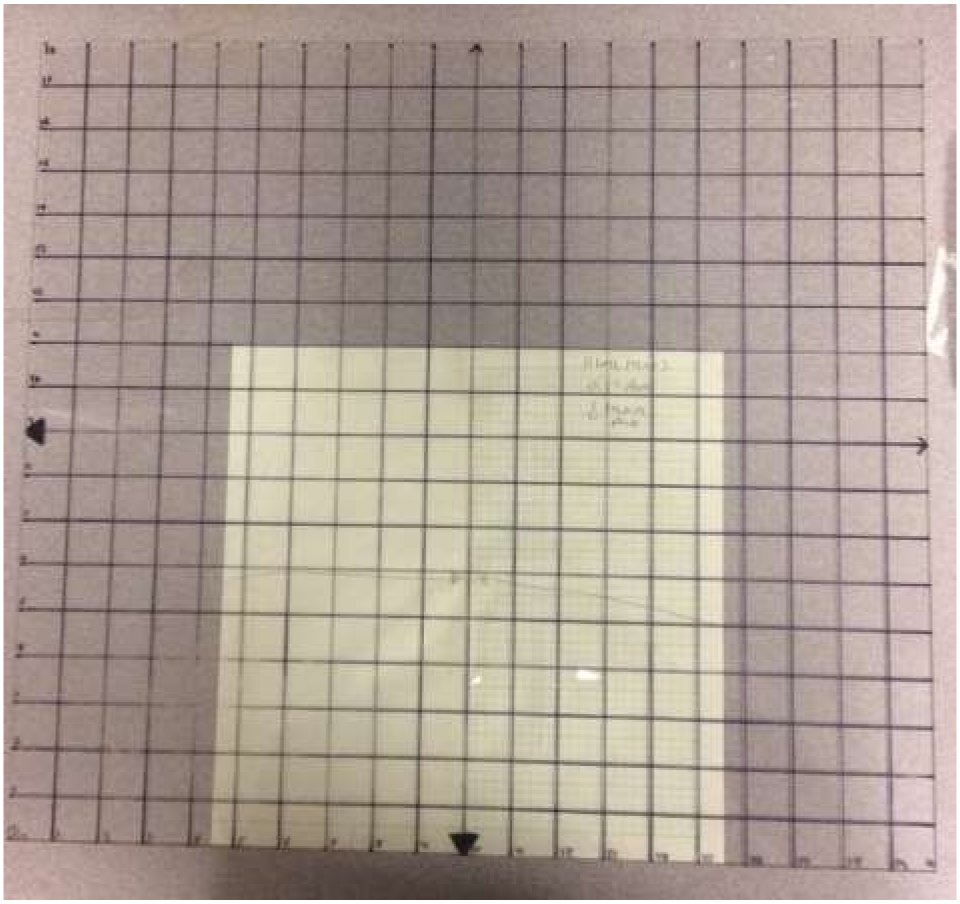

Figure 404: Test 11W11L10Lay3 0.5" Depth

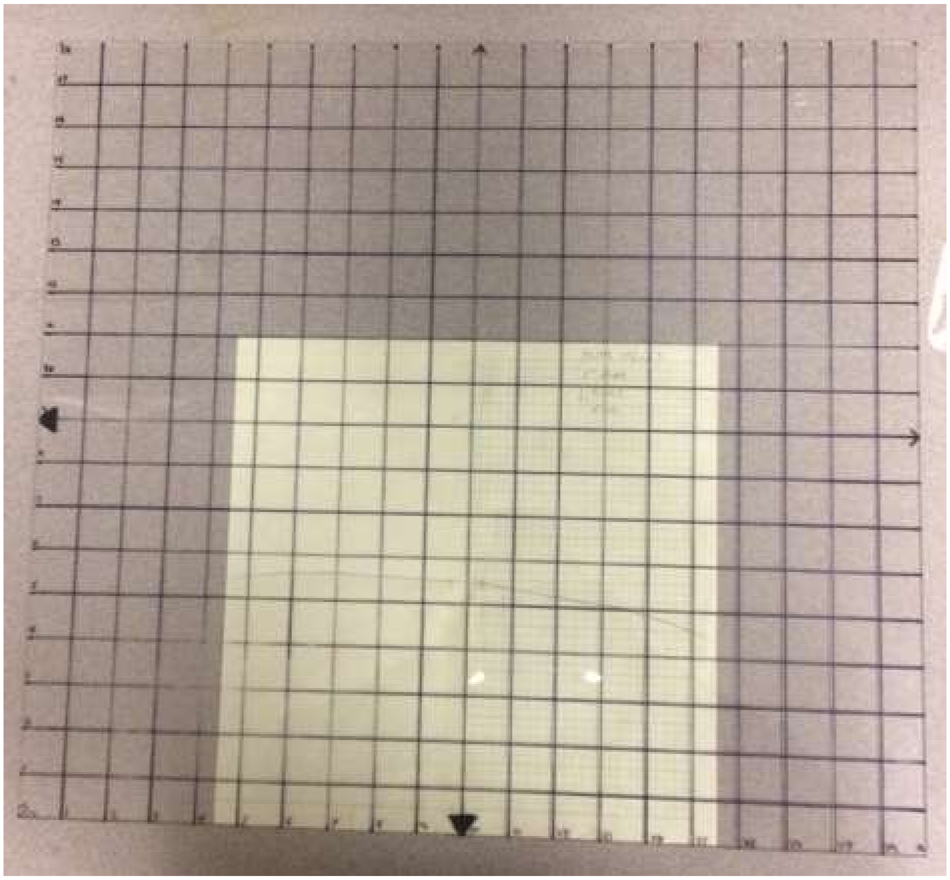

Figure 405: Test 11W11L10Lay3 1” Depth

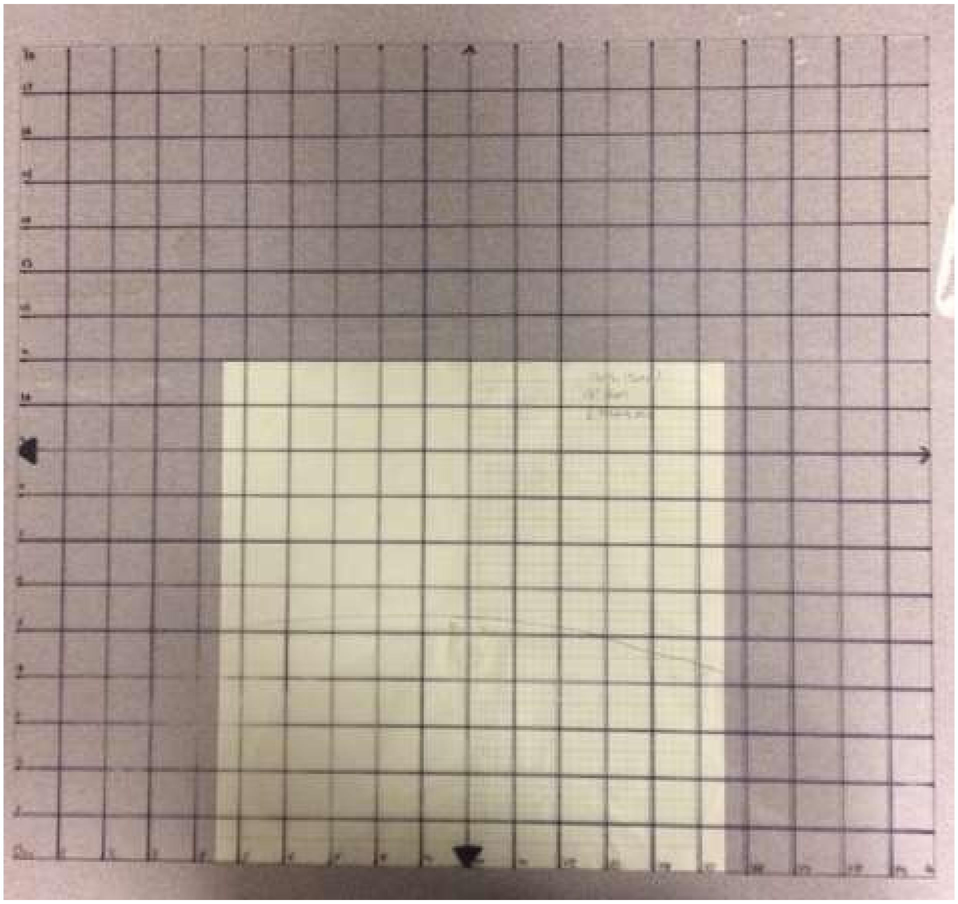

Figure 406: Test 11W11L10Lay3 1.5” Depth

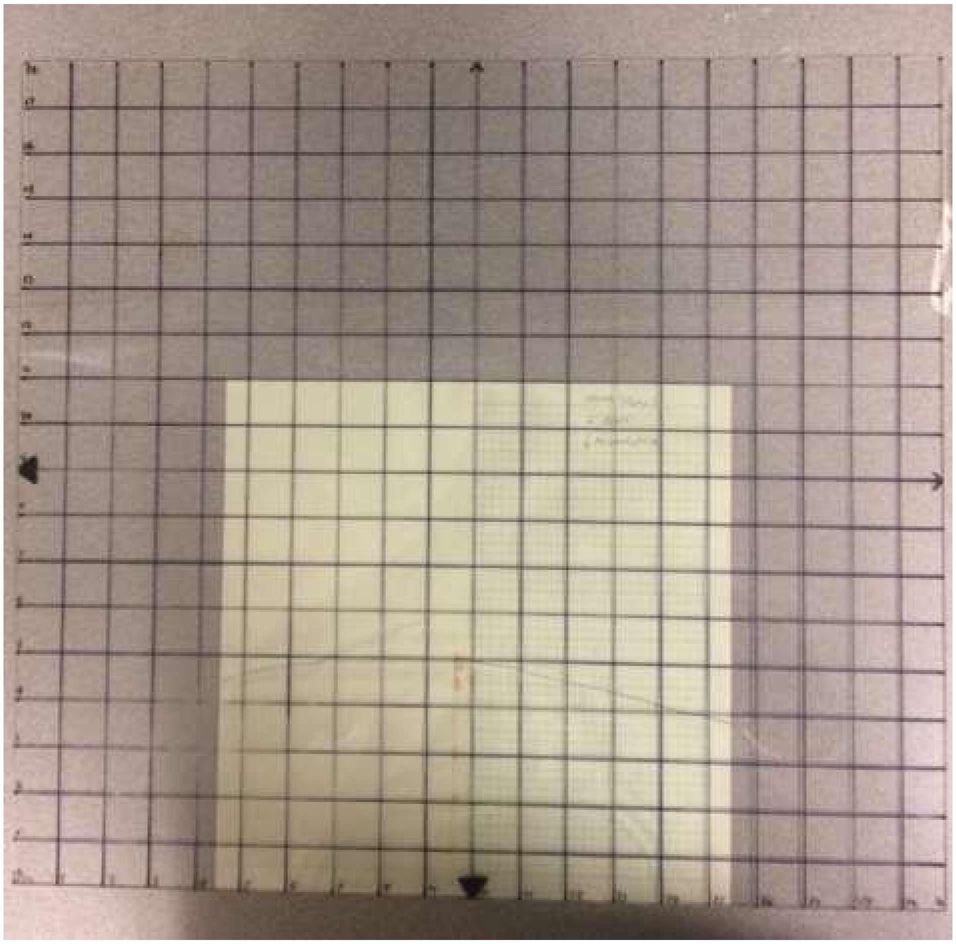

Figure 407: Test 11W11L10Lay3 2" Depth

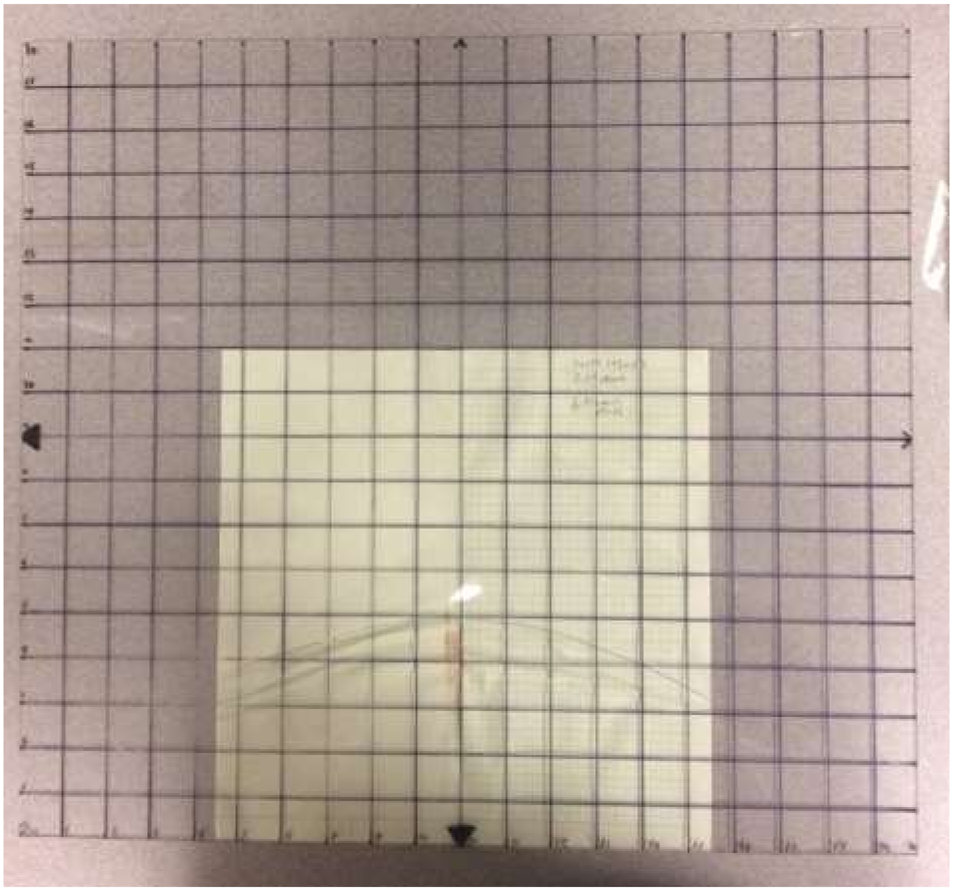

Figure 408: Test 11W11L10Lay3 2.5” Depth

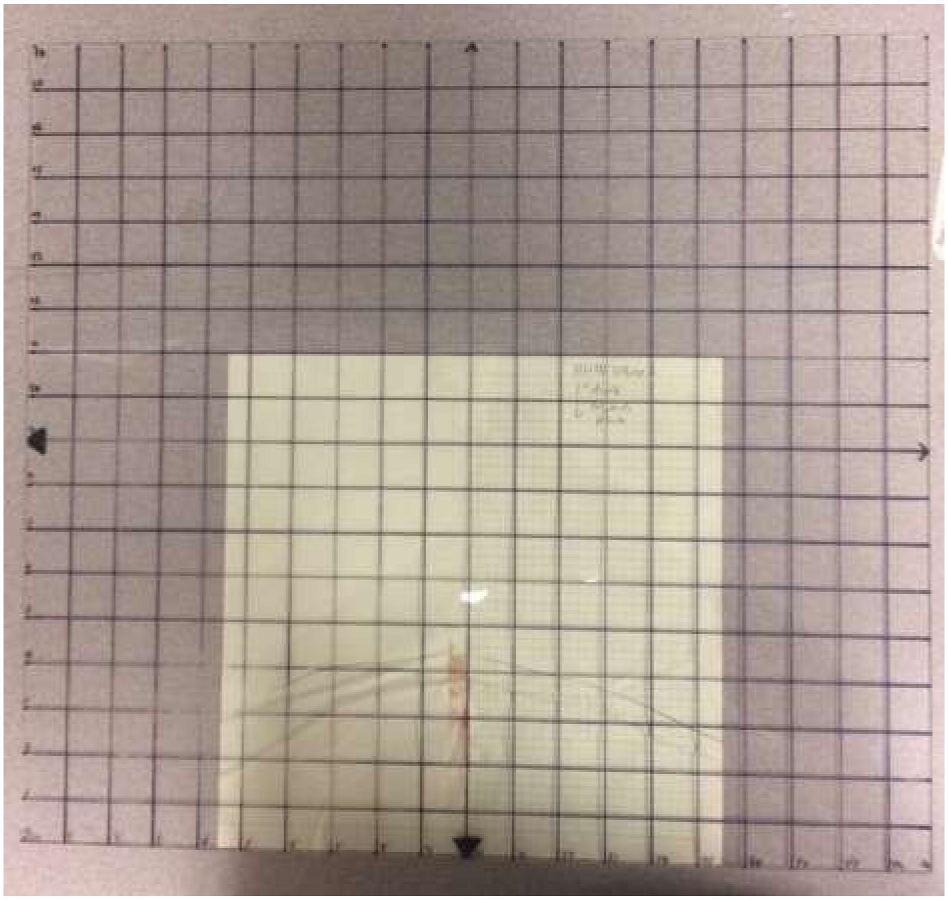

Figure 409: Test 11W11L10Lay3 3” Depth

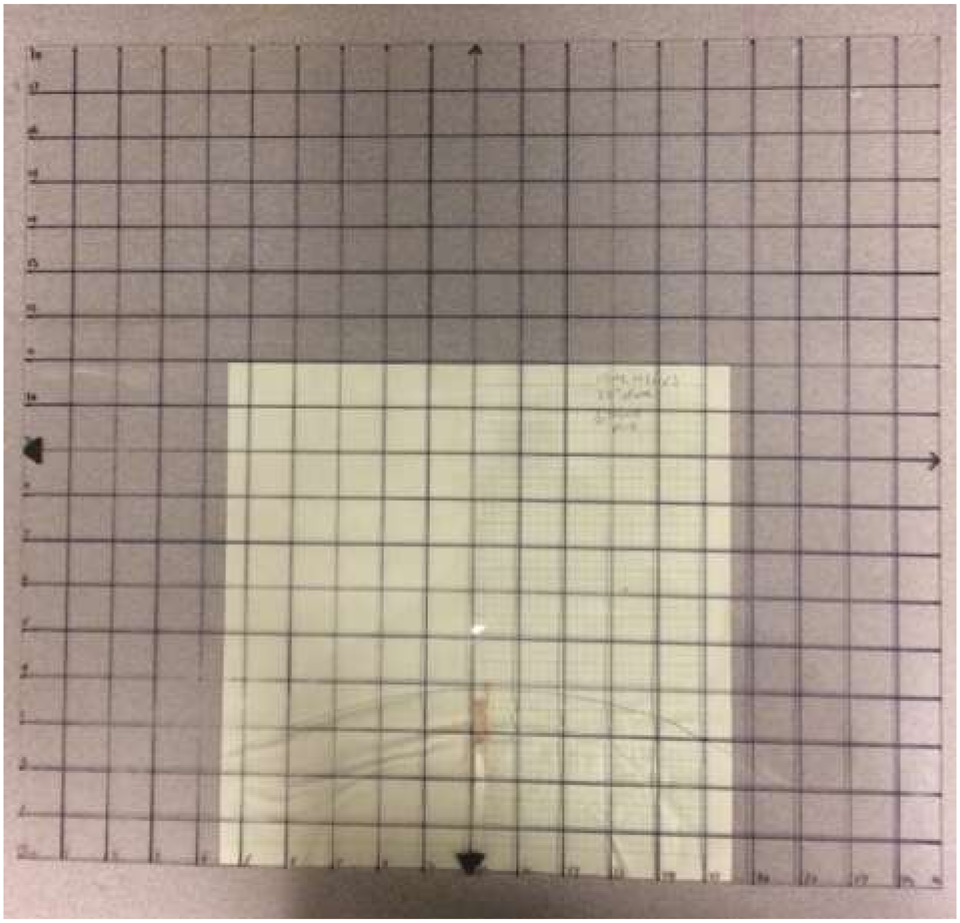

Figure 410: Test 11W11L10Lay3 3.5" Depth

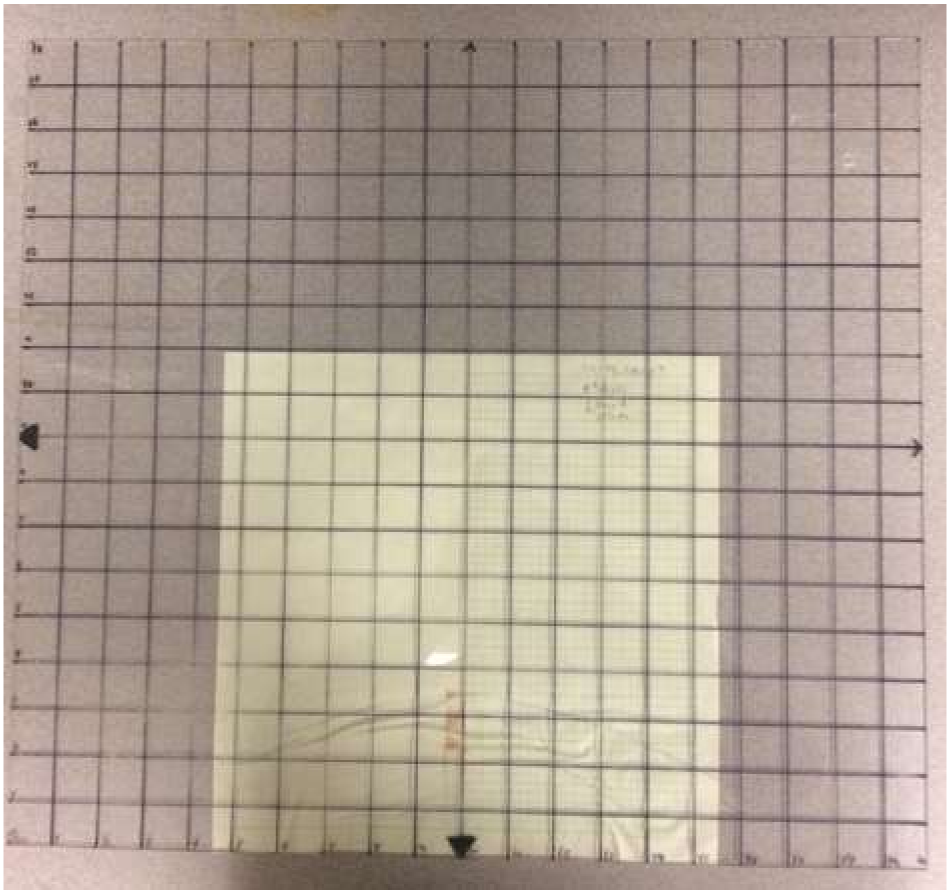

Figure 411: Test 11W11L10Lay3 4" Depth

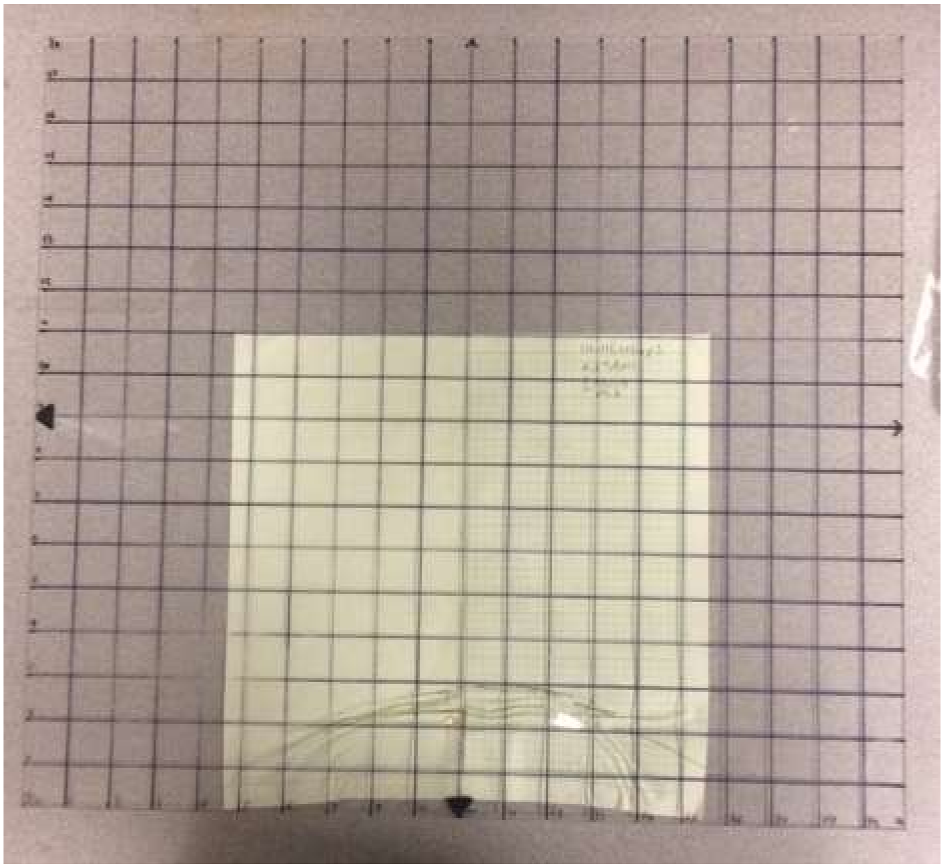

Figure 412: Test 11W11L10Lay3 4.5” Depth

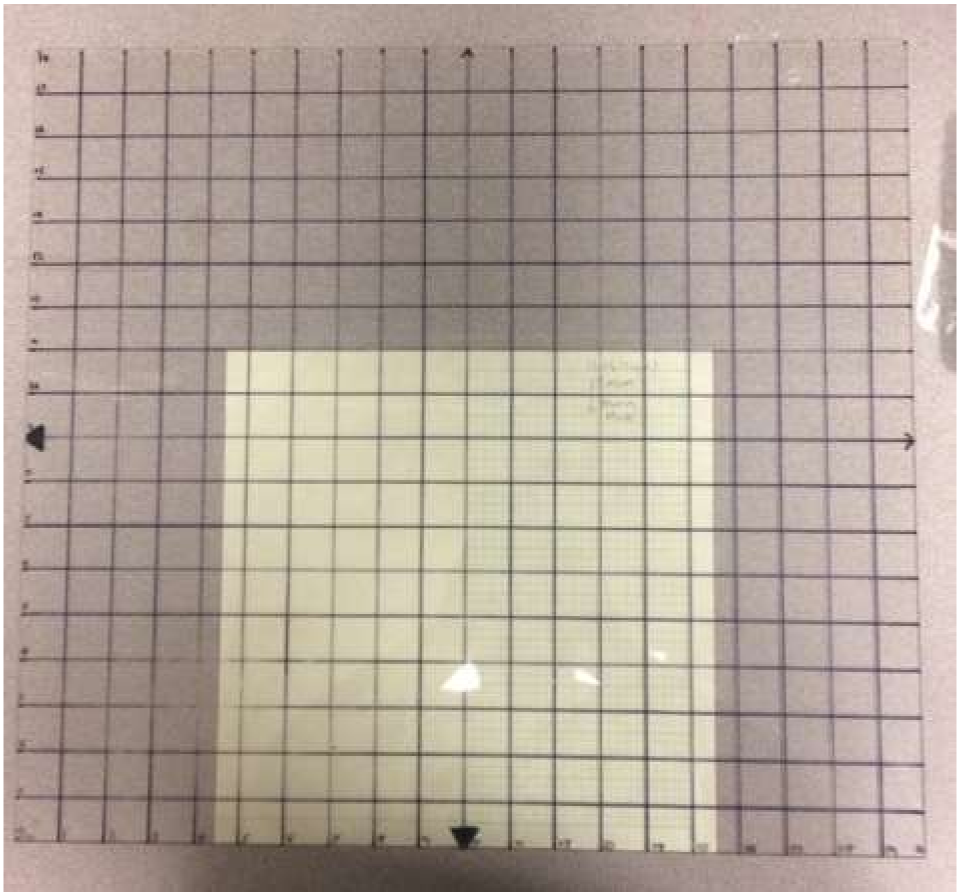

Figure 413: Test 11W11L10Lay3 5” Depth

APPENDIX B: FLEXURAL RIGIDITY TESTING PHOTOGRAPHS

B.1 Introduction

Photographs were taken of the each type of reinforcement that was tested in flexural rigidity.

B.2 Photograph of Engineering Paper Test 1

Figure 414: Engineering paper cantilever Test 1

B.3 Photograph of Engineering Paper Test 2

Figure 415: Engineering paper cantilever Test 2

B.4 Photograph of Engineering Paper Test 3

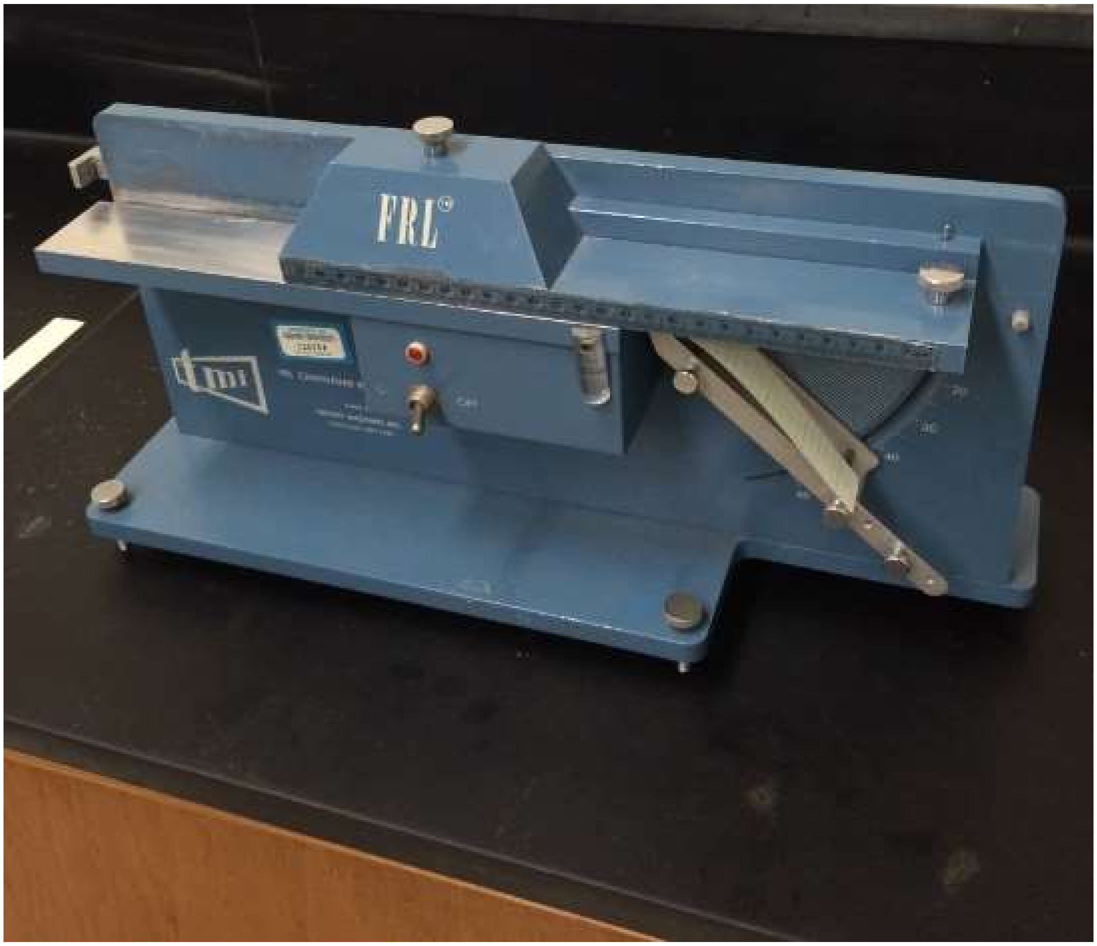

Figure 416: Engineering paper cantilever Test 3

B.5 Photograph of Engineering Paper Test 4

Figure 417: Engineering paper cantilever Test 4

B.6 Photograph of Polyester Test 1

Figure 418: Polyester Cantilever Test 1

B.7 Photograph of Polyester Test 2

Figure 419: Polyester Cantilever Test 2

B.8 Photograph of Polyester Test 3

Figure 420: Polyester Cantilever Test 3

B.9 Photograph of Polyester Test 4

Figure 421: Polyester Cantilever Test 4

B.10 Photograph of High Density Polyethylene Test 1

Figure 422: High density polyethylene Cantilever Test 1

B.11 Photograph of High Density Polyethylene Test 2

Figure 423: High density polyethylene Cantilever Test 2

B.12 Photograph of High Density Polyethylene Test 3

Figure 424: High density polyethylene Cantilever Test 3

B.13 Photograph of High Density Polyethylene Test 4

Figure 425: High density polyethylene Cantilever Test 4

APPENDIX C: PHOTOGRAPHS OF PAINTED SURFACES SHOWING FAILURE SURFACE DEFINITION

C.1 Introduction

To determine the location of the failure surface within the specimen, photographs were taken of each scraped painted layer overlain with a piece of plexiglass with a one inch square grid to show where the failure surface contacted each painted horizontal layer. When the test is performed, the pusher plate is forced into the soil specimen. Some of the soil in the box does not move, while other soil moves in the direction of the plate and also upwards. The upward deformation of failed soil also carried the previously planar horizontal paint layer upwards. After the test is performed, soil layers are gently scraped off using the soil placement device shown in Figure 63. The soil and paint that moved vertically is scraped off, leaving the soil and paint that did not move behind, as shown in Figure 64. A piece of clear plexiglass with a grid of 1” squares is placed atop the scraped soil and paint allowing three dimensional coordinates of the failure surface to be obtained; see Figure 65.

C.2 Photographs of Test 8W8L5Lay3

Figure 426: Test 8W8L5Lay3, 1" depth

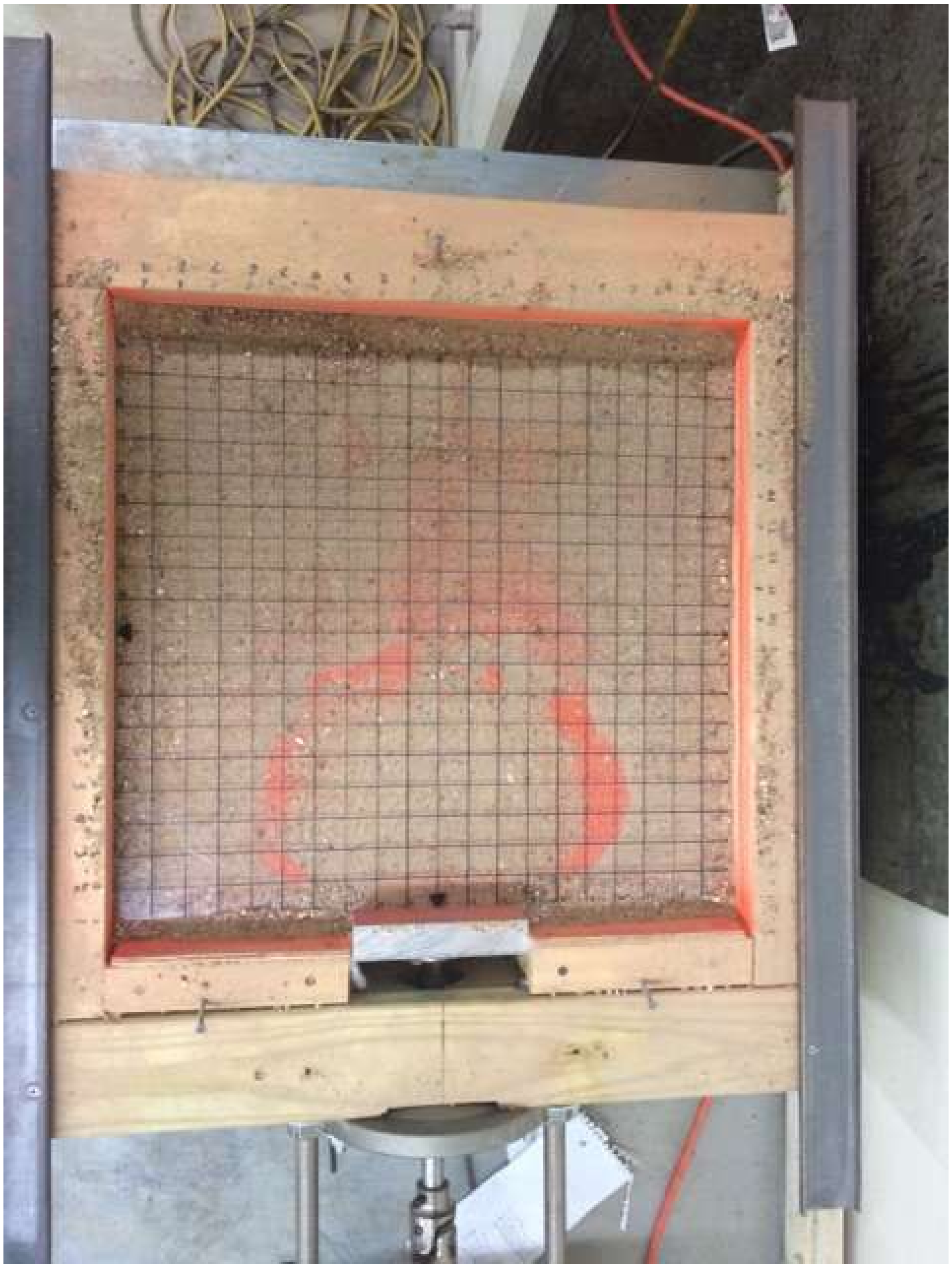

Figure 427: Test 8W8L5Lay3, 2” depth

Figure 428: Test 8W8L5Lay3, 4” depth

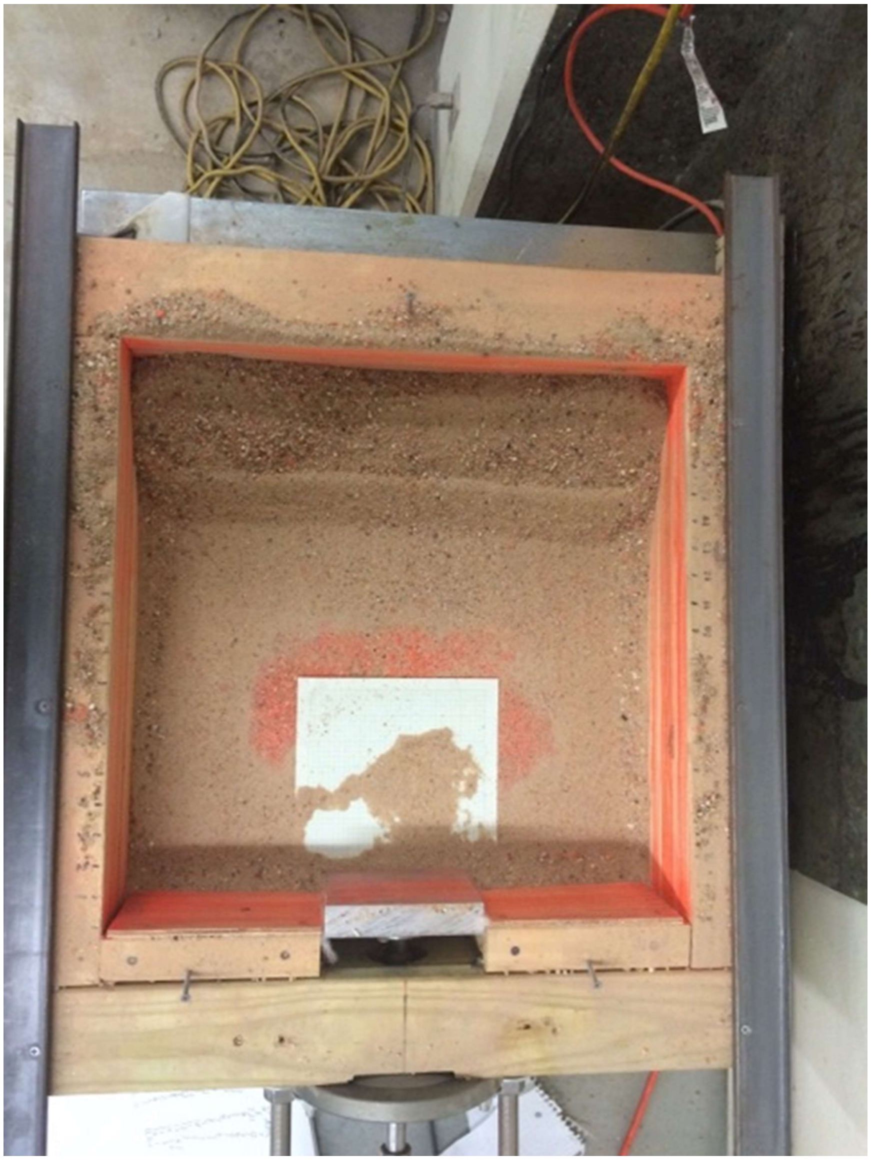

Figure 429: Test 8W8L5Lay3, 5” depth

C.3 Photographs of Test 8W8L10Lay3

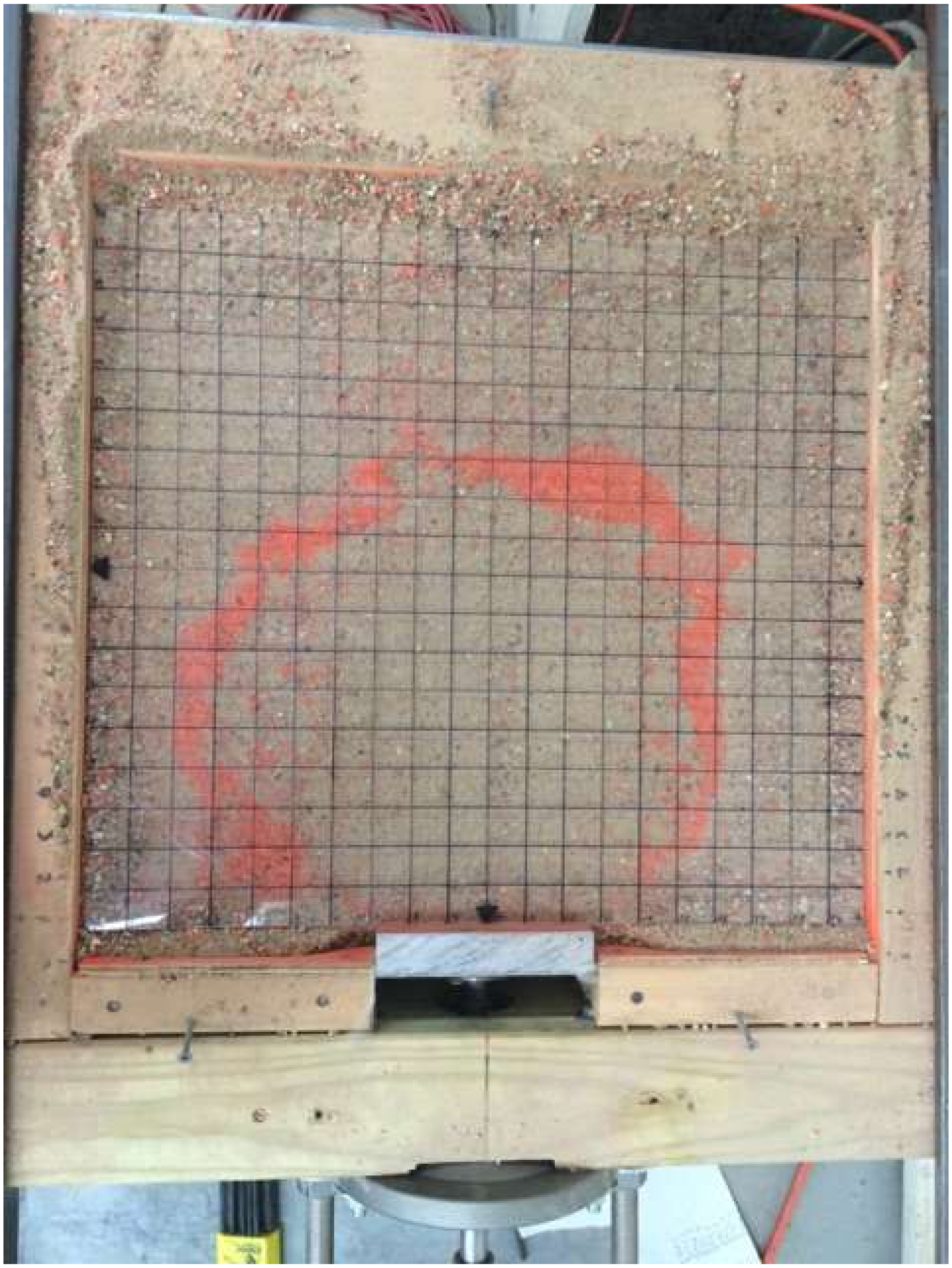

Figure 430: Test 8W8L10Lay3, 1" Depth

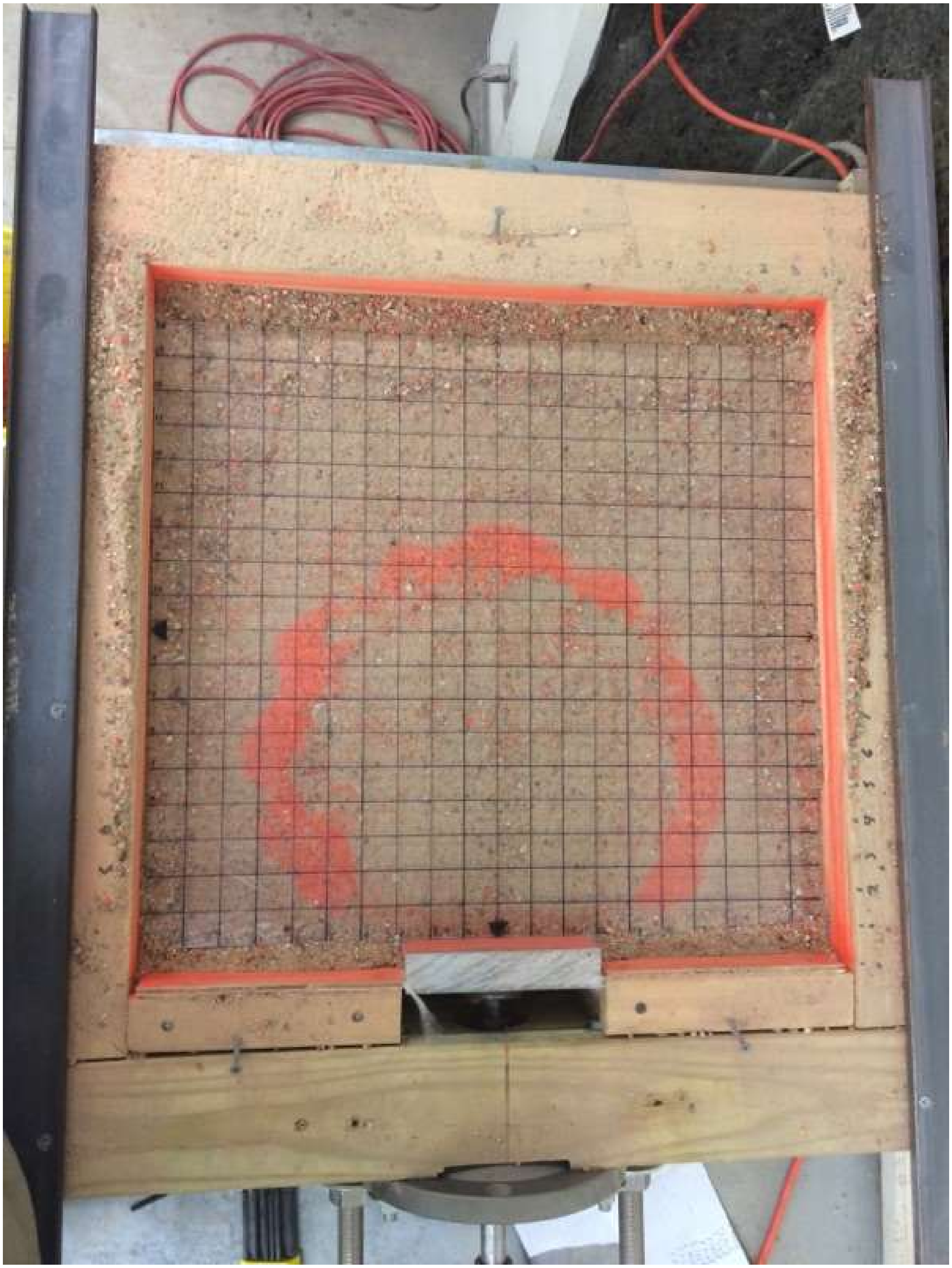

Figure 431: Test 8W8L10Lay3, 2" Depth

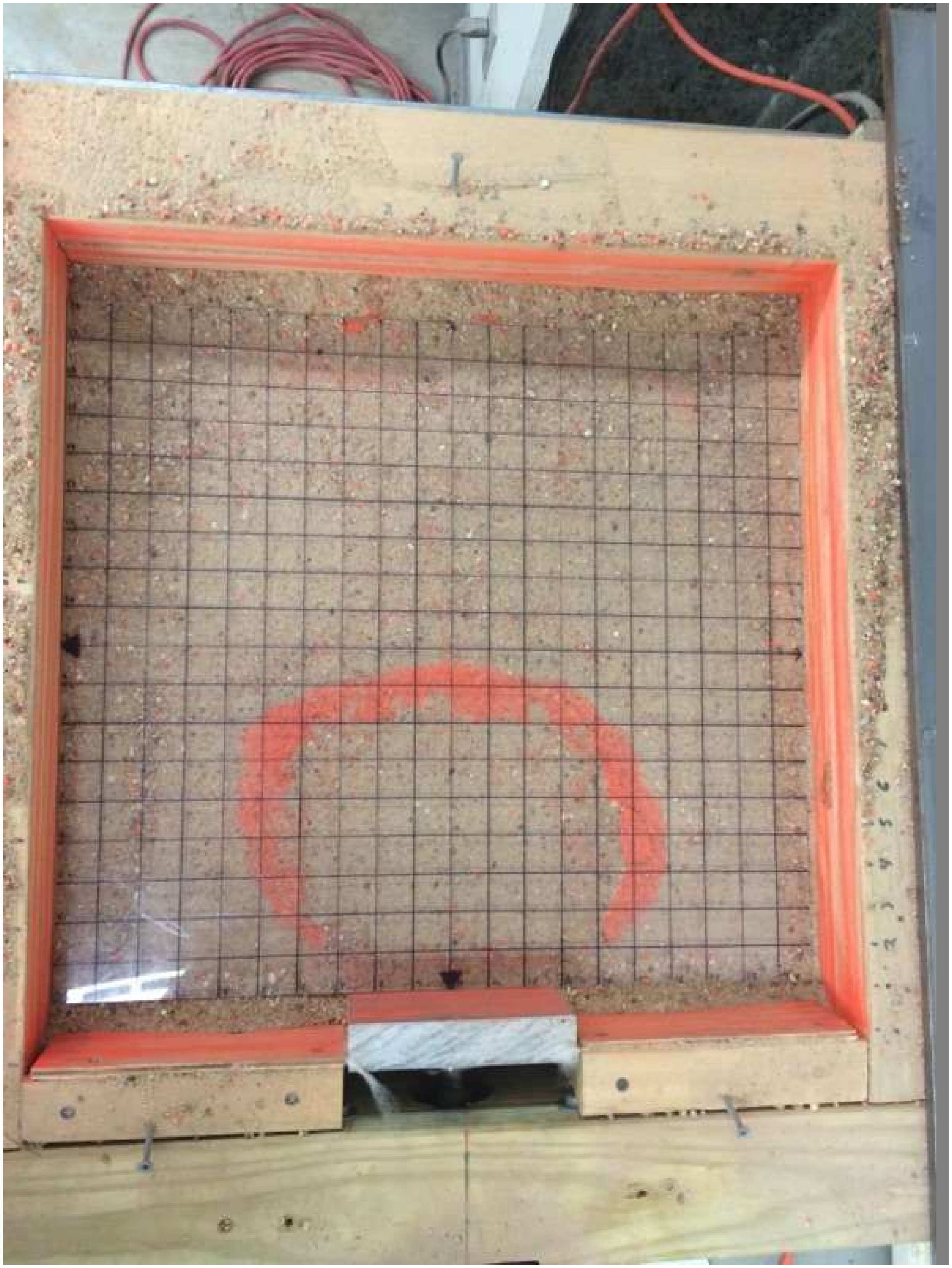

Figure 432: Test 8W8L10Lay3, 3” Depth

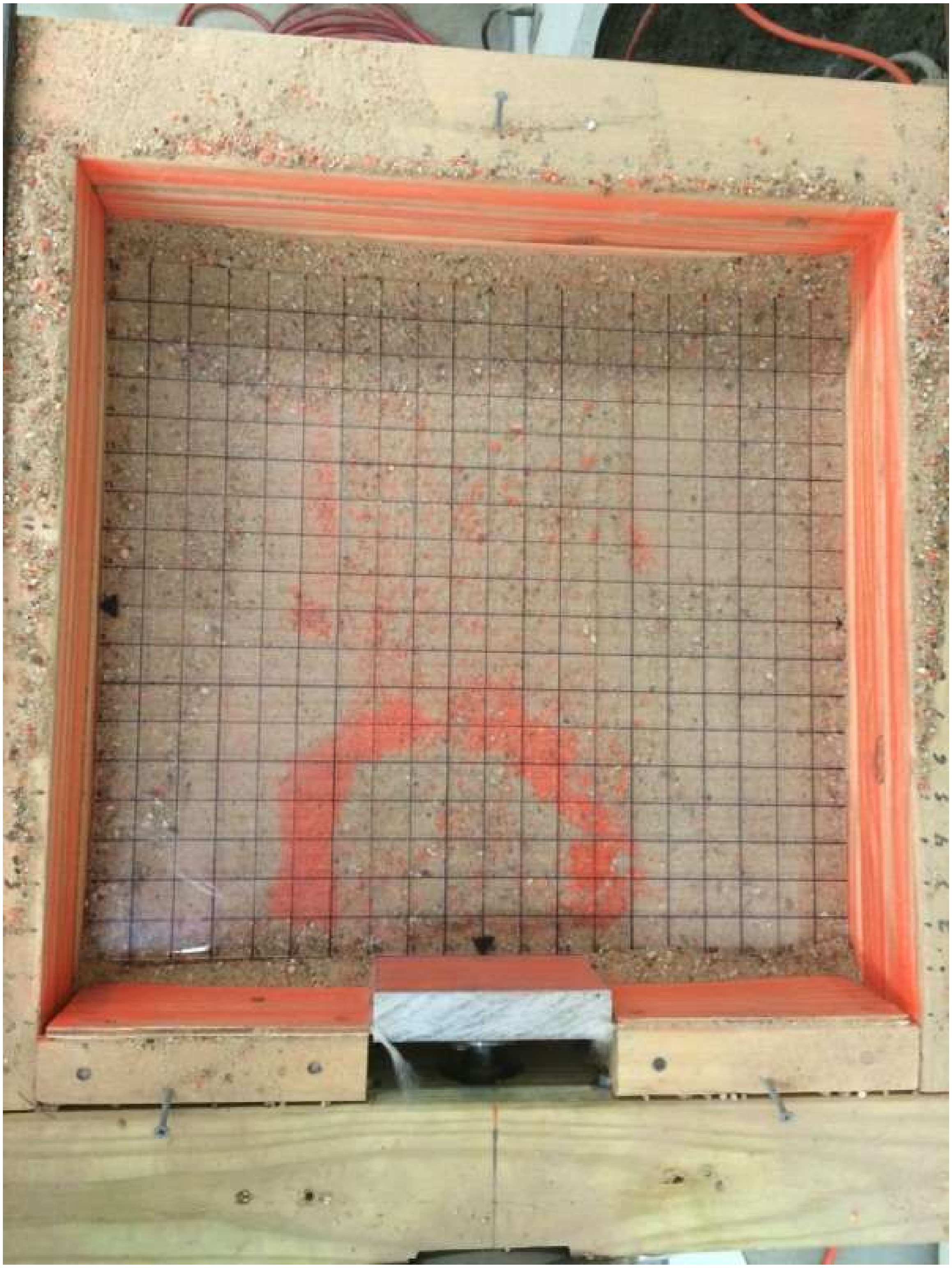

Figure 433: Test 8W8L10Lay3, 4” Depth

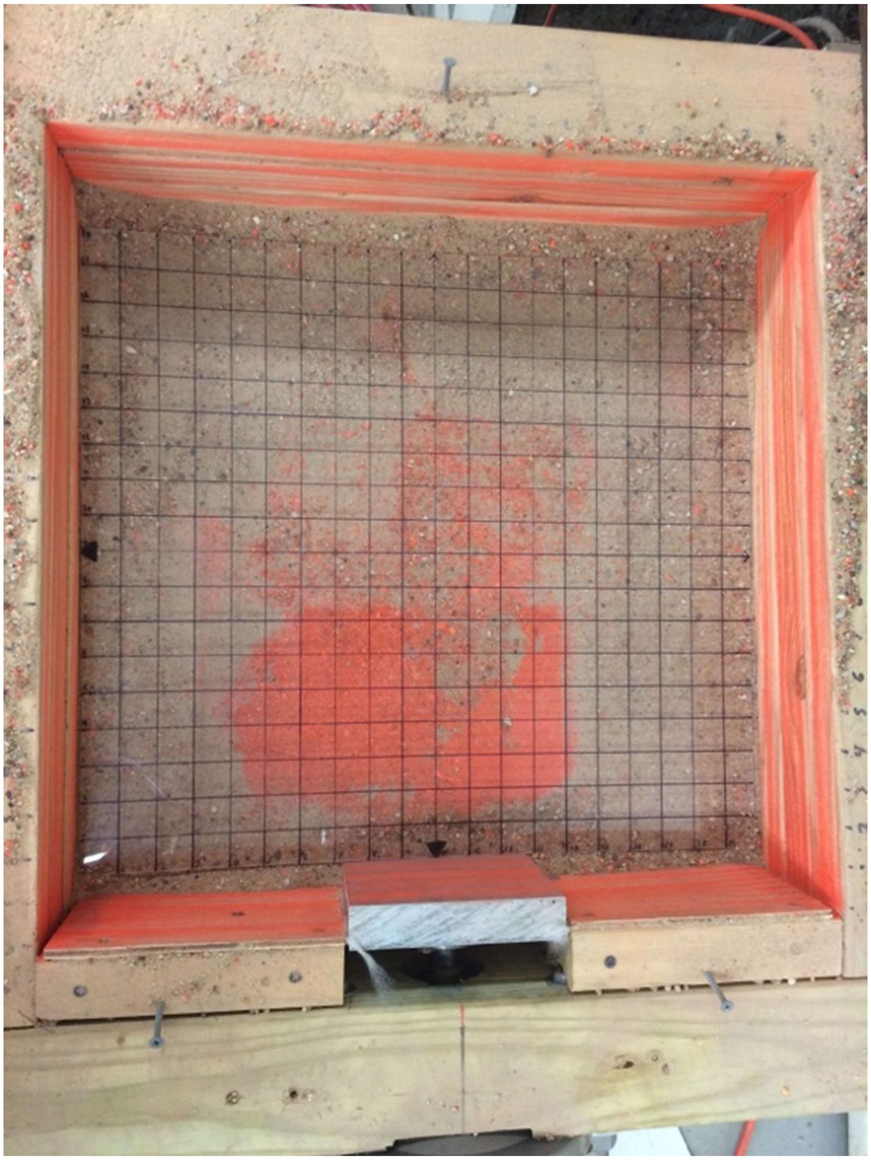

Figure 434: Test 8W8L10Lay3, 5” Depth

C.4 Photographs of Test 8W11L5Lay3

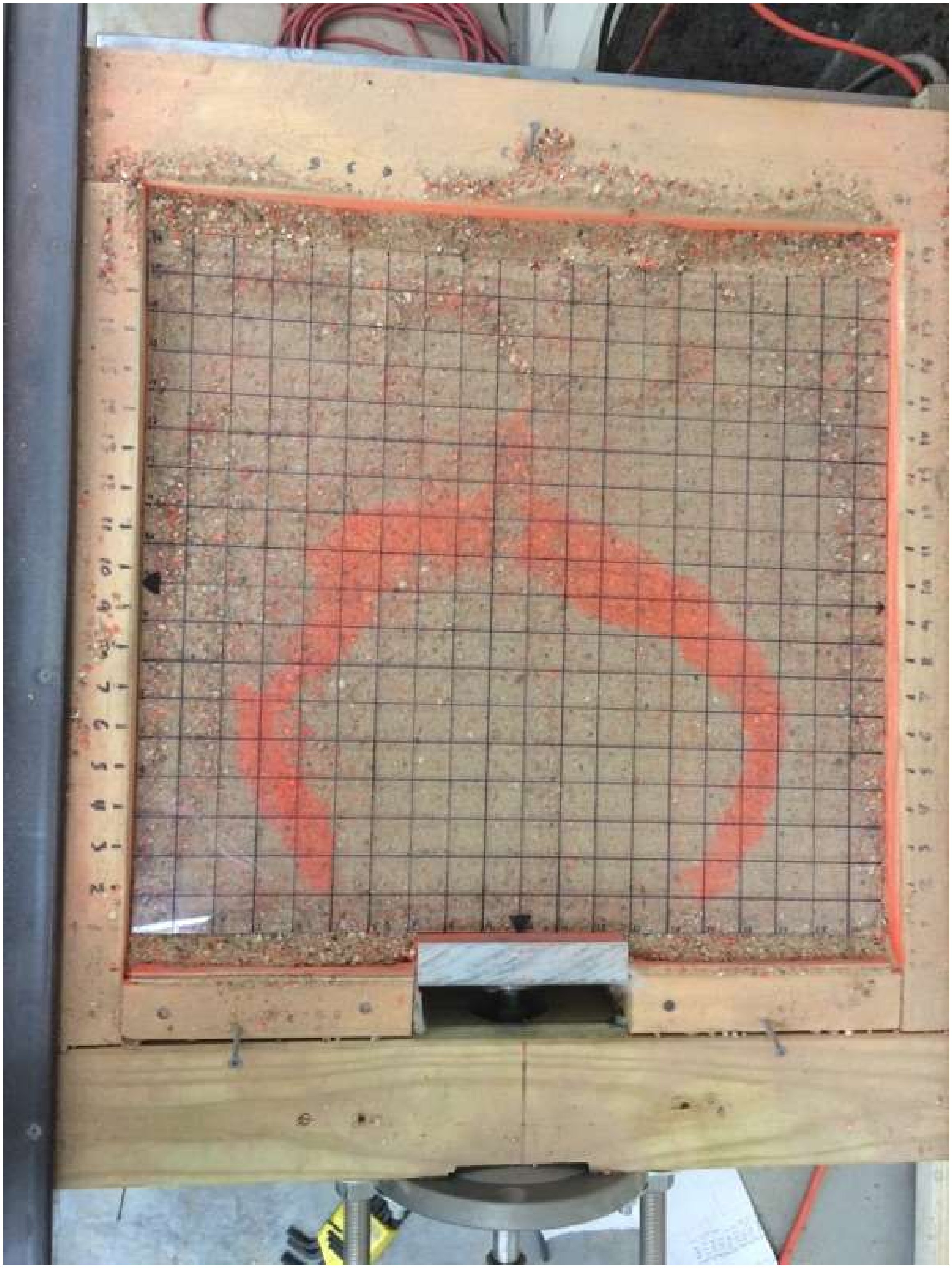

Figure 435: Test 8W11L5Lay3, 1" depth

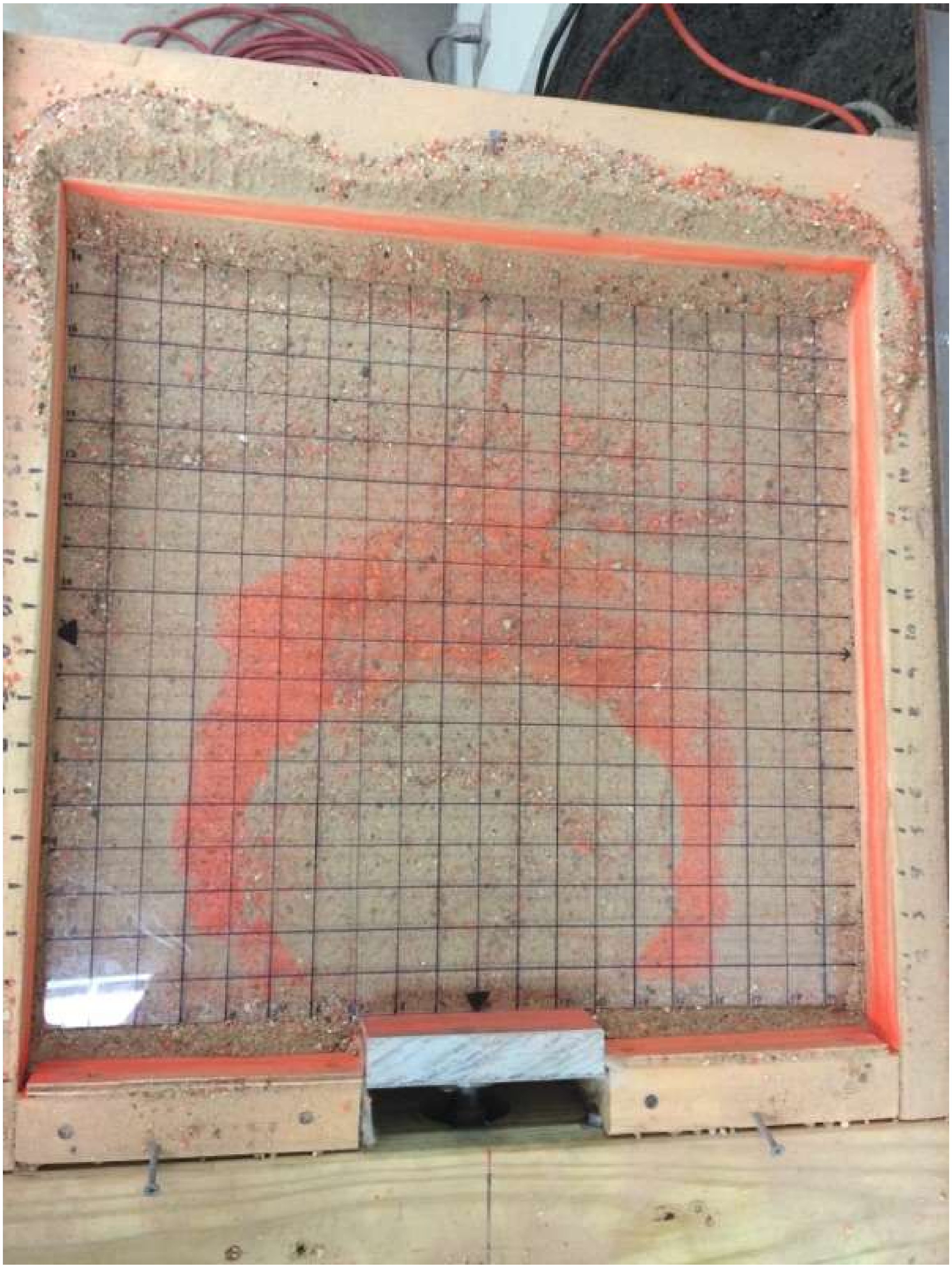

Figure 436: Test 8W11L5Lay3, 2” depth

Figure 437: Test 8W11L5Lay3, 3” depth

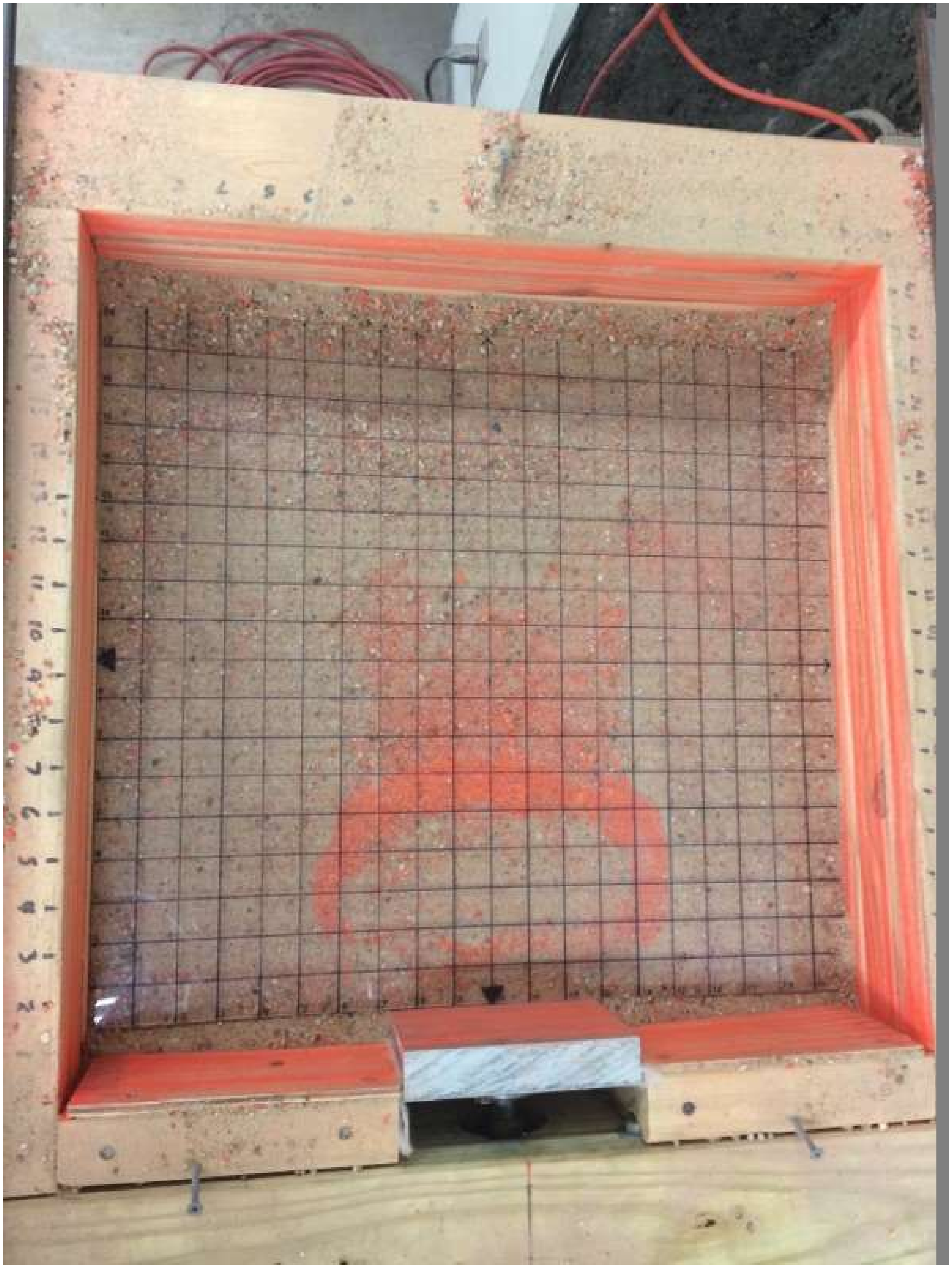

Figure 438: Test 8W11L5Lay3, 4” depth

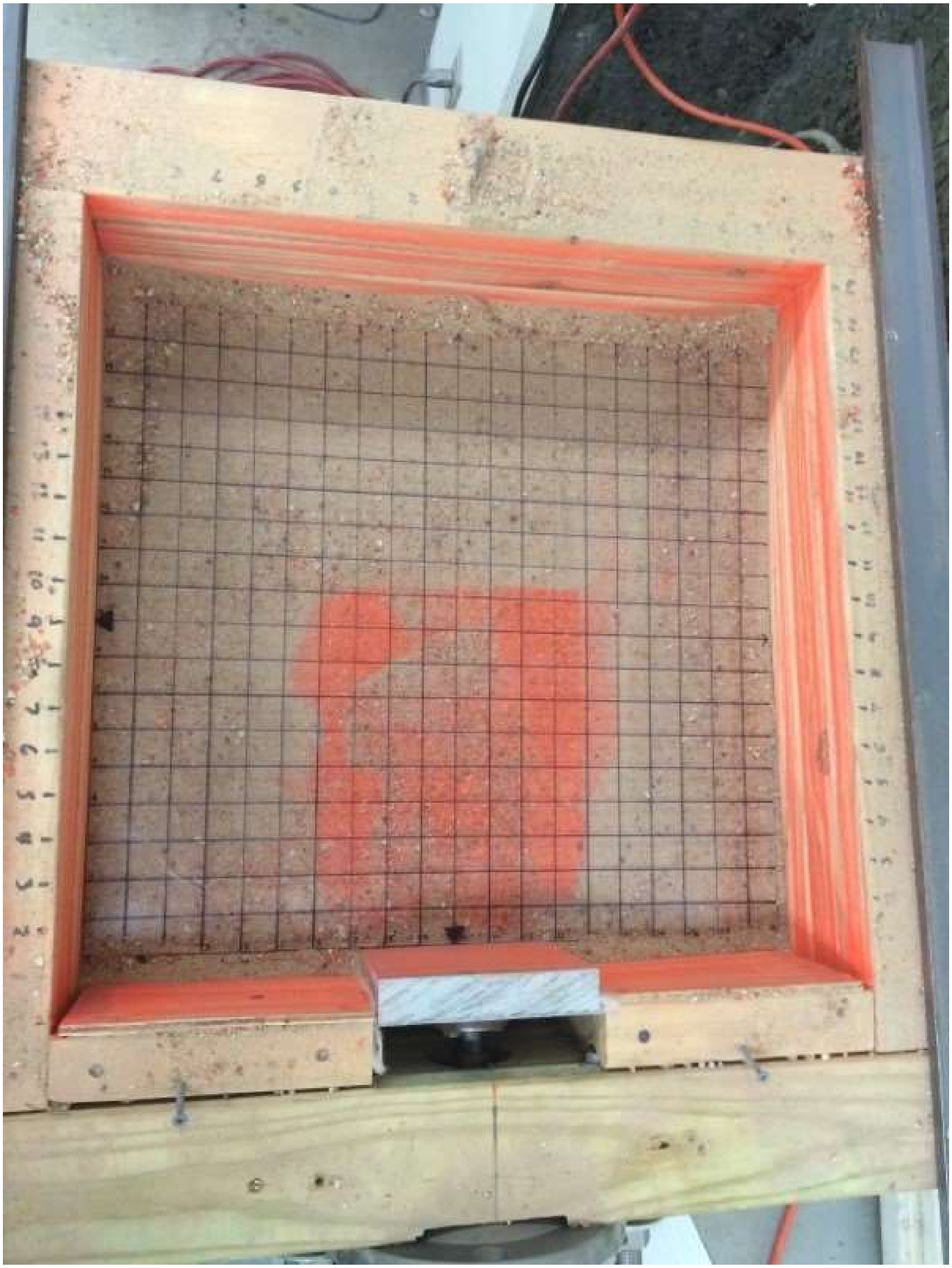

Figure 439: Test 8W11L5Lay3, 5" depth

C.5 Photographs of Test 8W11L10Lay3

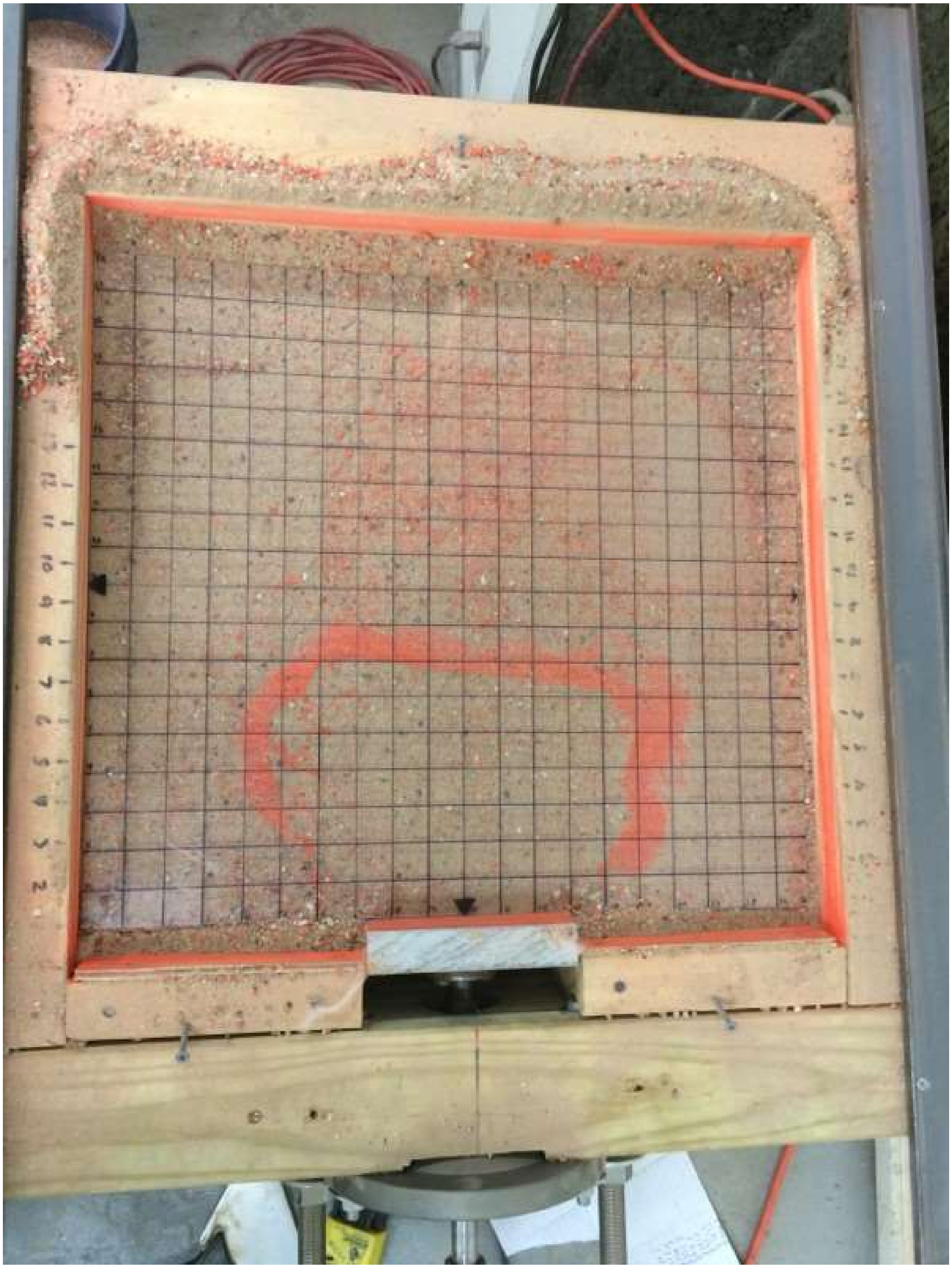

Figure 440: Test 8W11L10Lay3, 1" depth

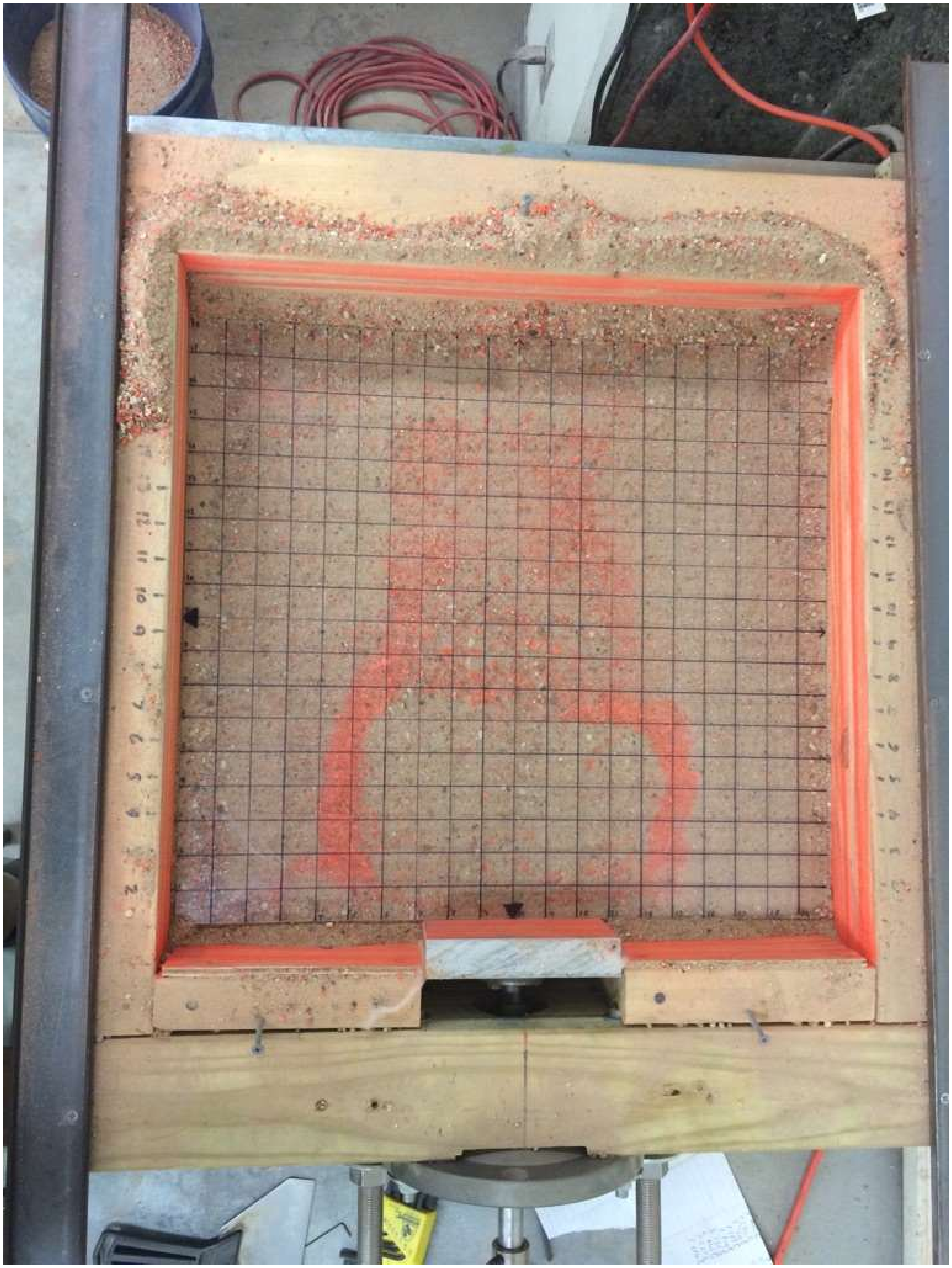

Figure 441: Test 8W11L10Lay3, 2" depth

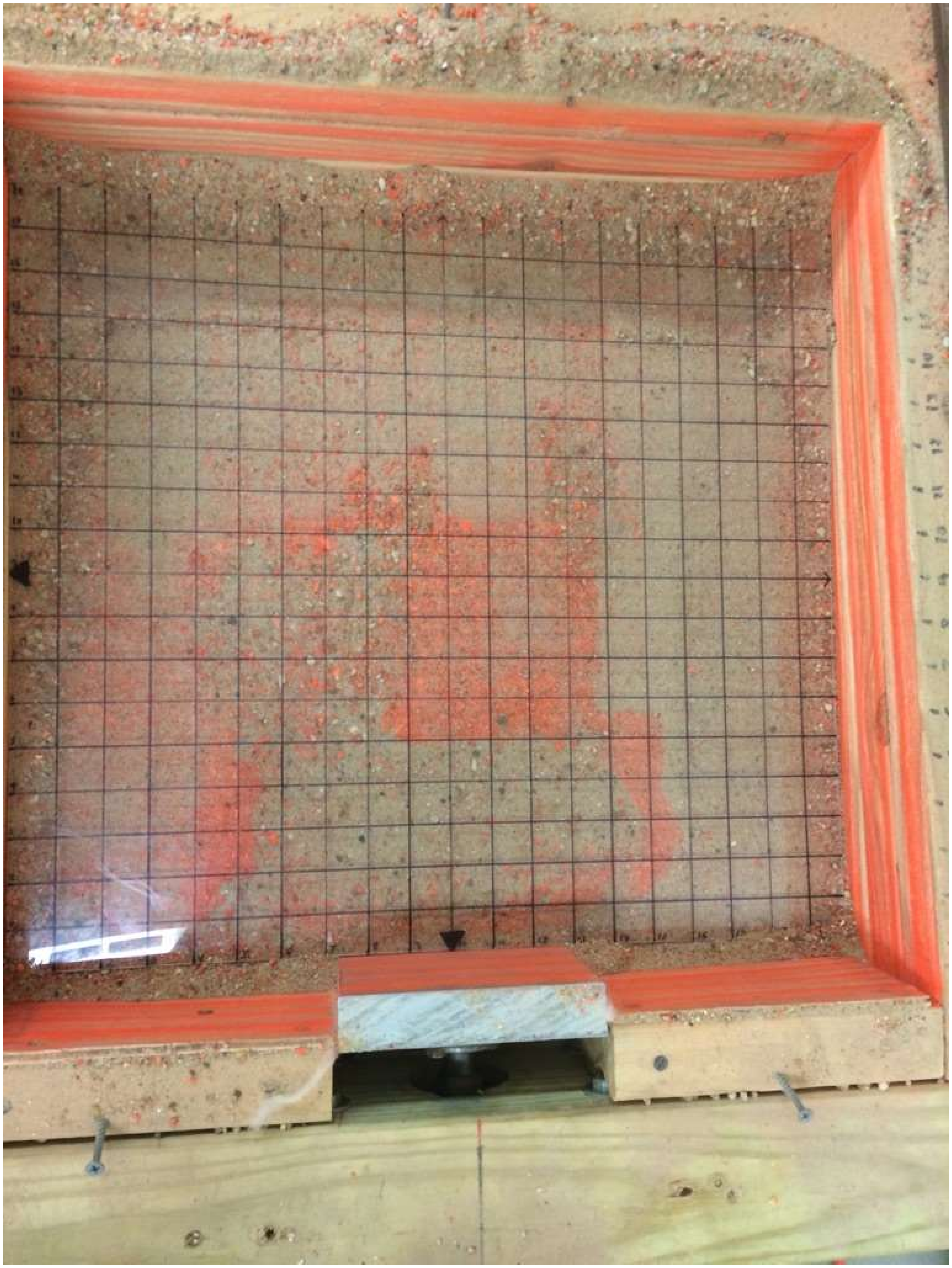

Figure 442: Test 8W11L10Lay3, 4" depth

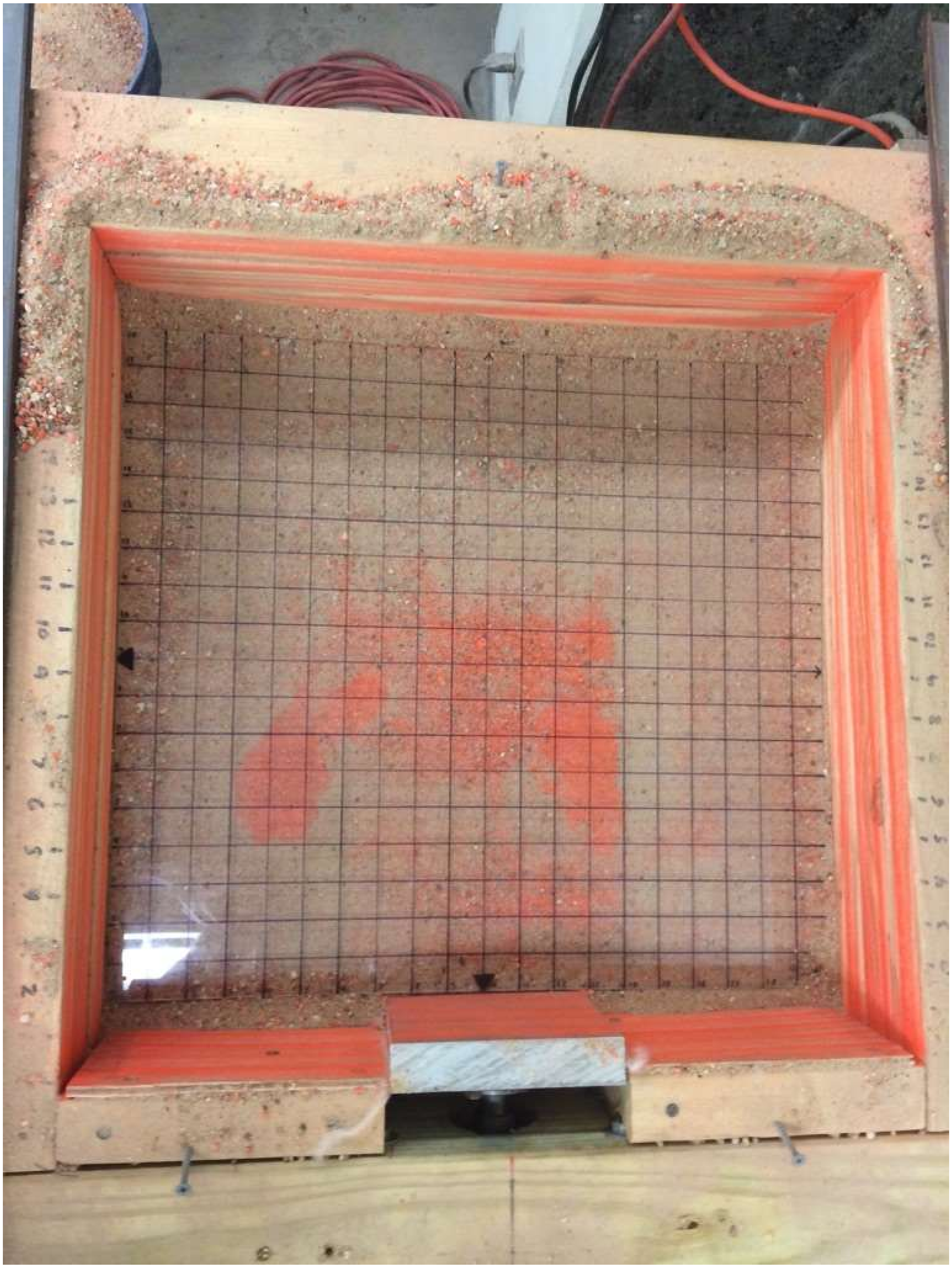

Figure 443: Test 8W11L10Lay3, 5” depth

C.6 Photographs of Test 11W8L5Lay3

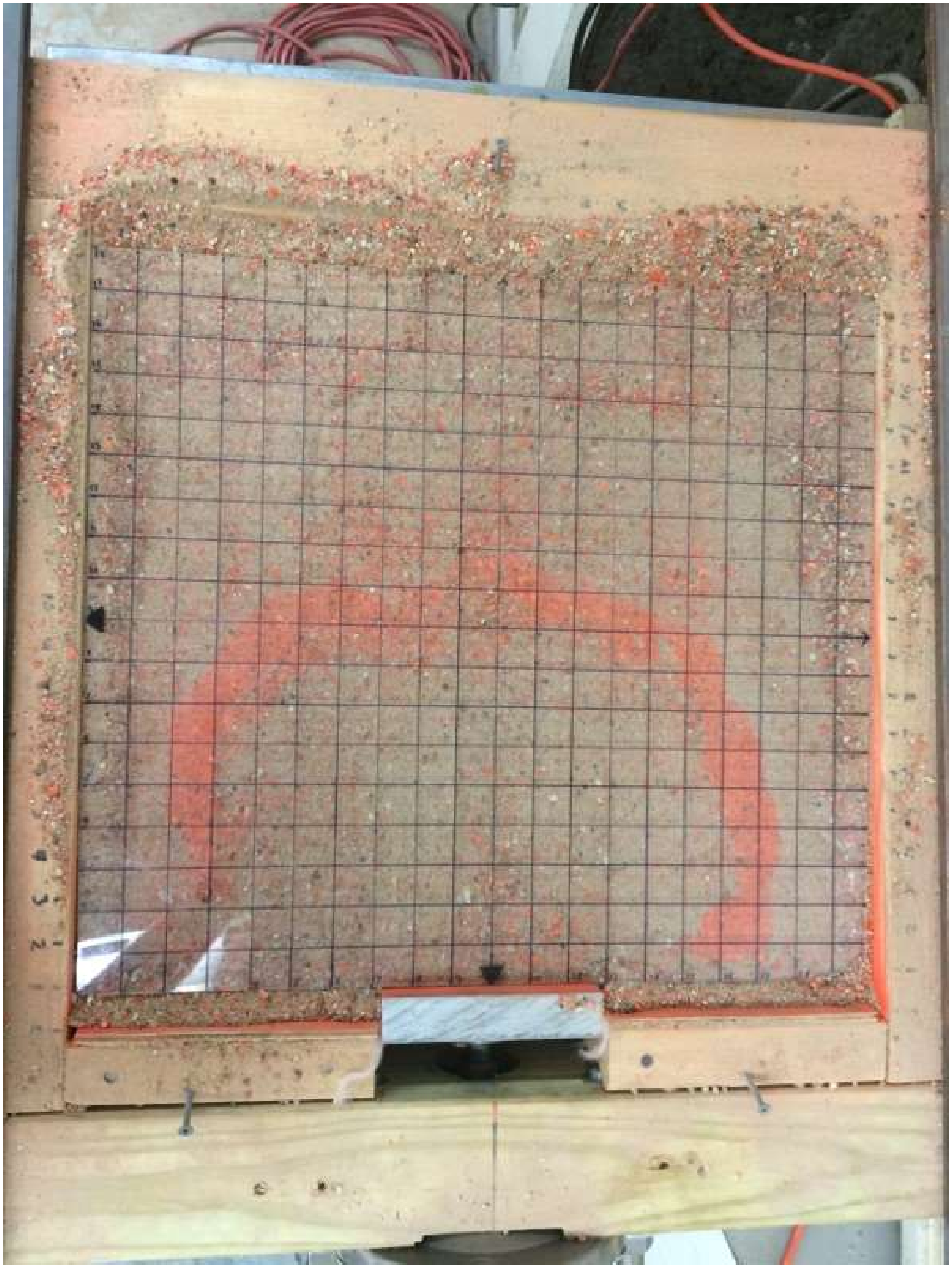

Figure 444: Test 11W8L5Lay3, 1" depth

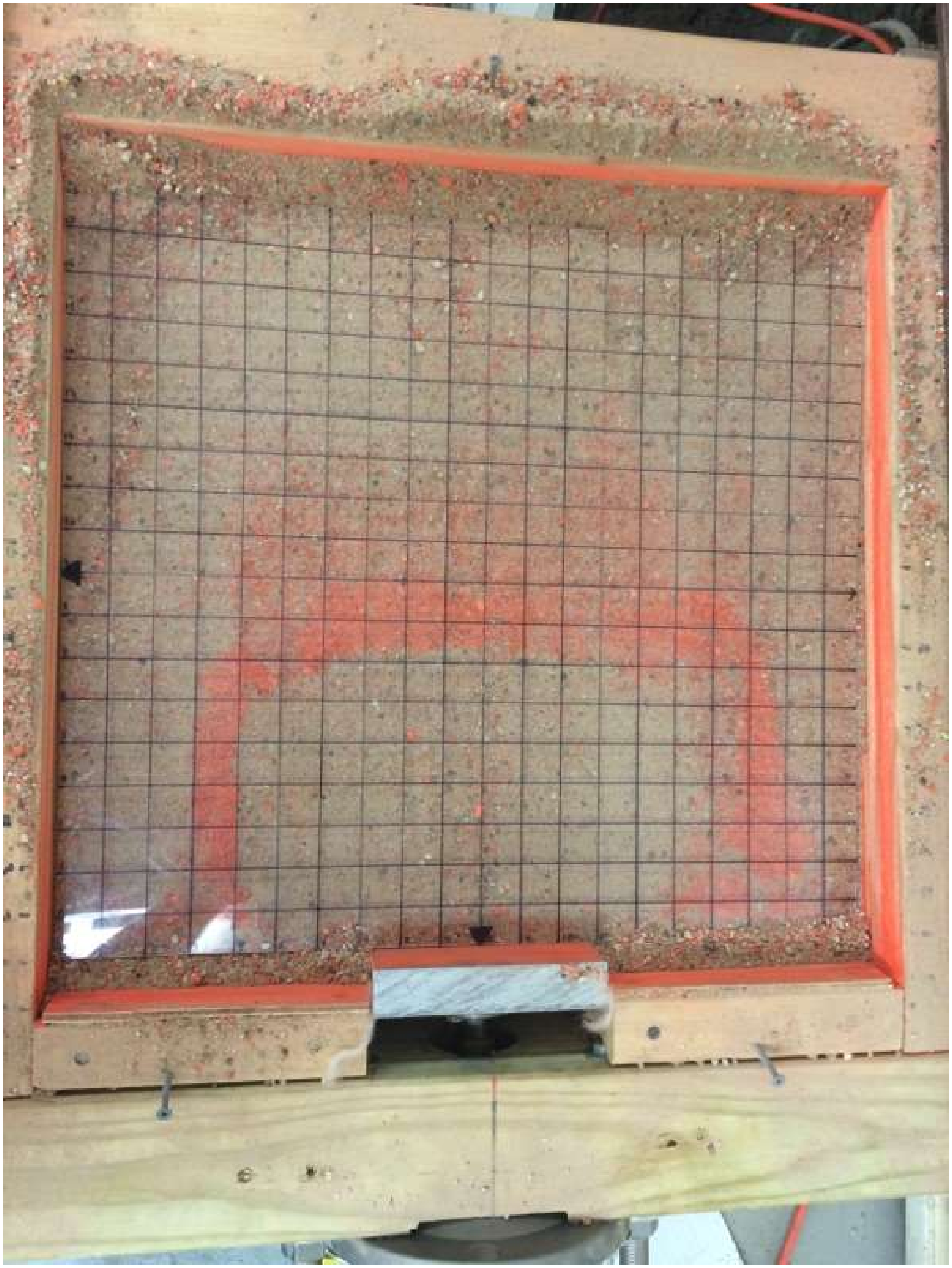

Figure 445: Test 11W8L5Lay3, 2” depth

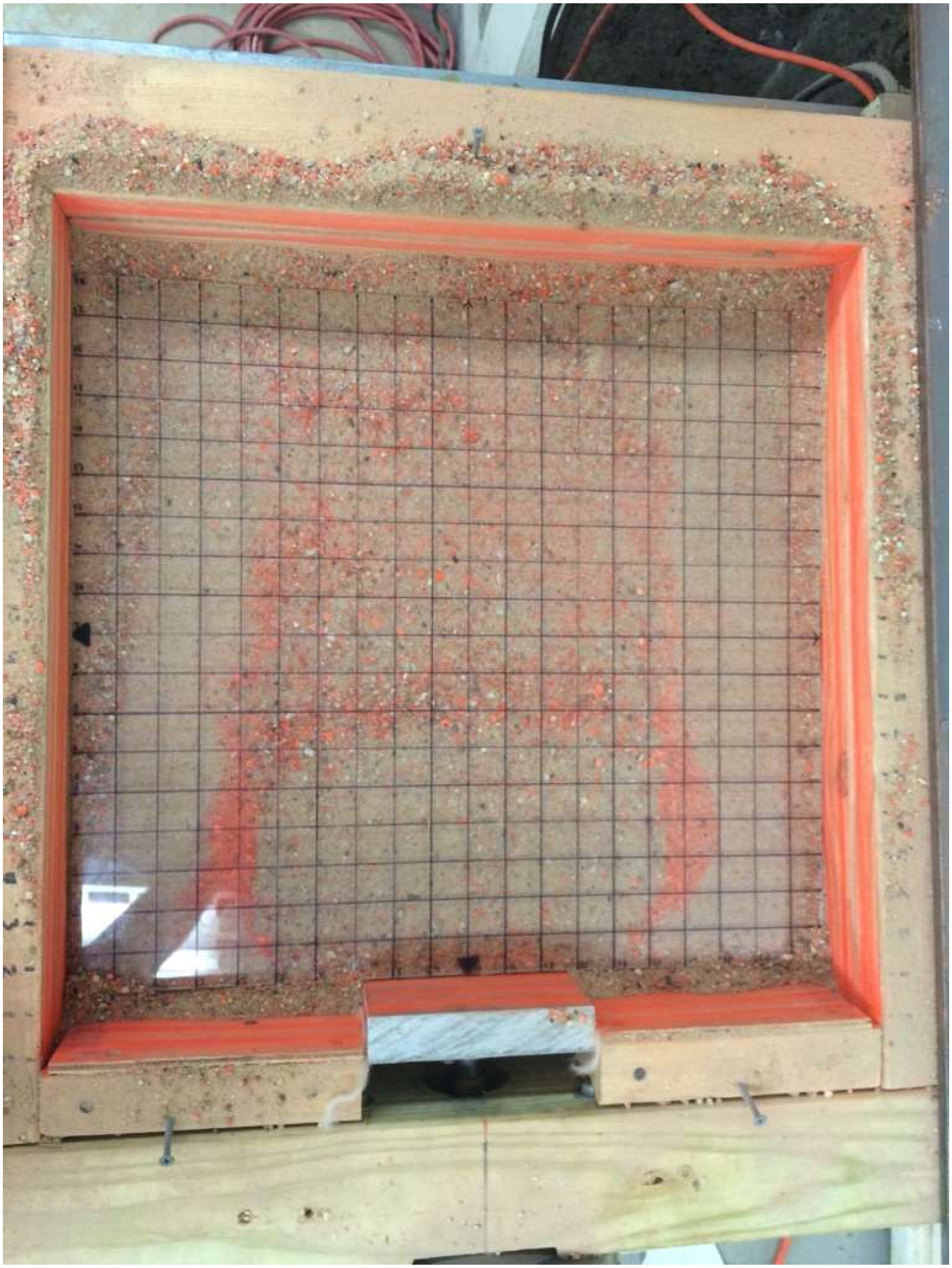

Figure 446: Test 11W8L5Lay3, 3" depth

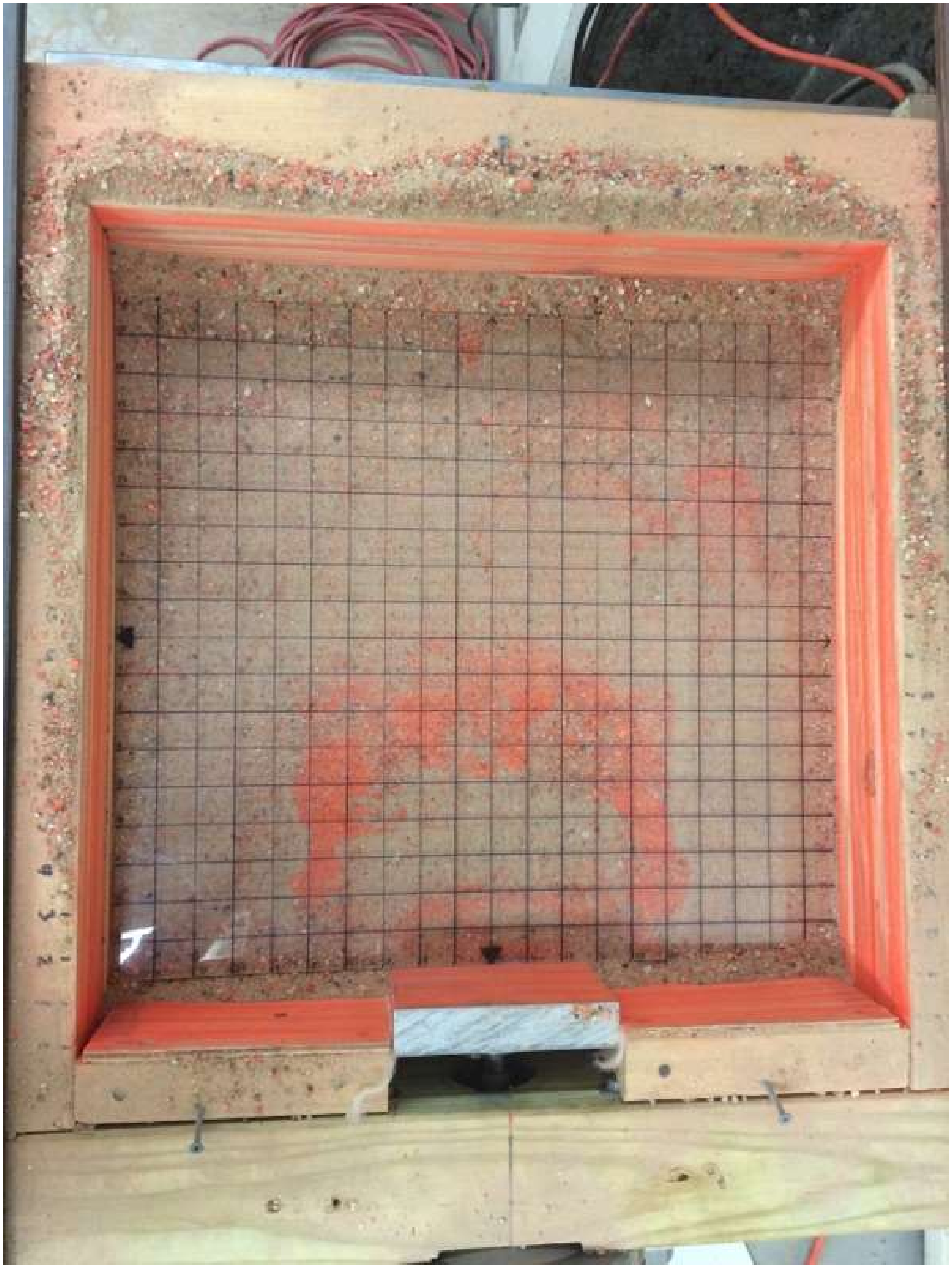

Figure 447: Test 11W8L5Lay3, 4” depth

C.7 Photographs of Test 11W8L10Lay3

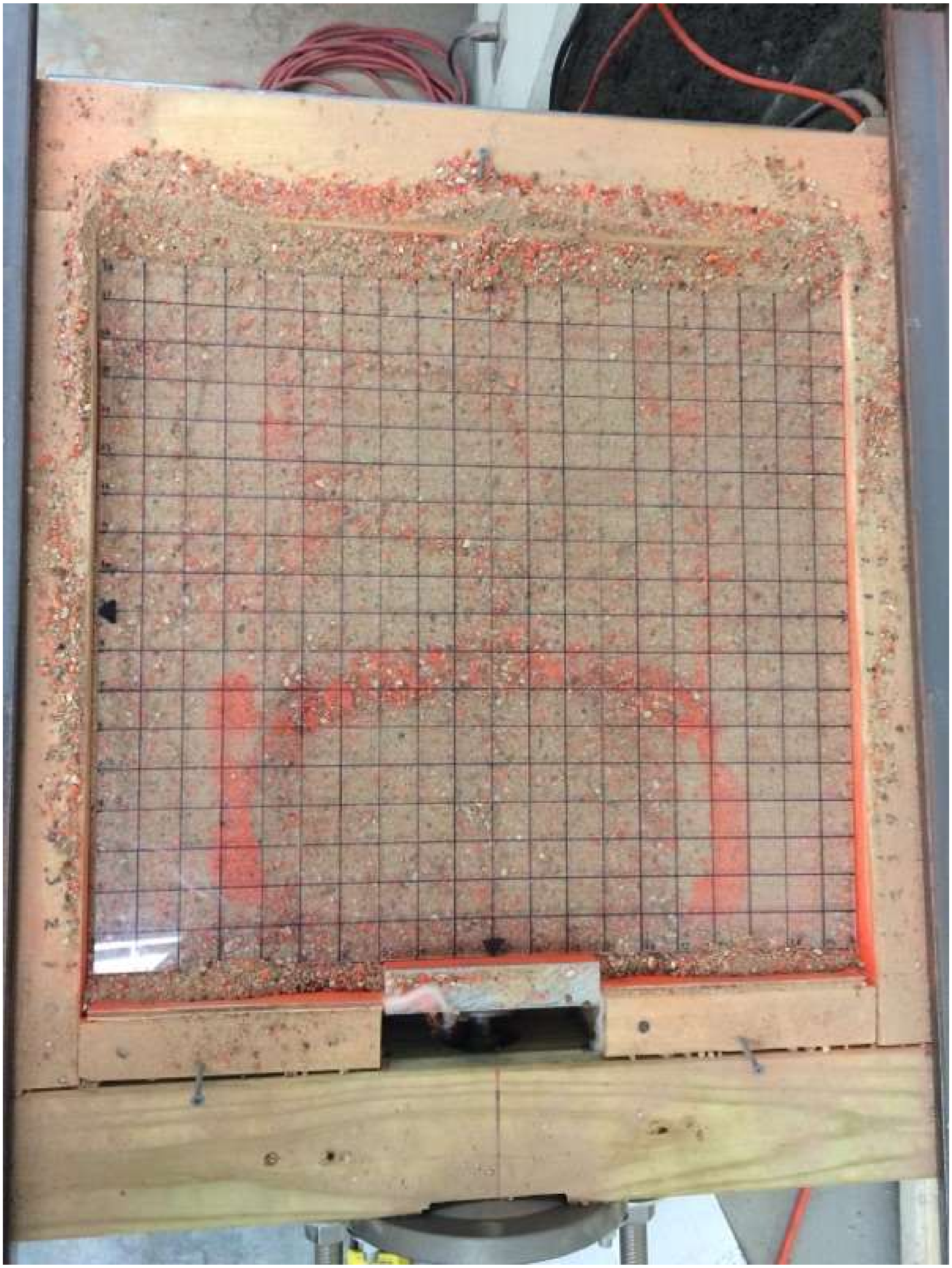

Figure 448: Test 11W8L10Lay3, 1" depth

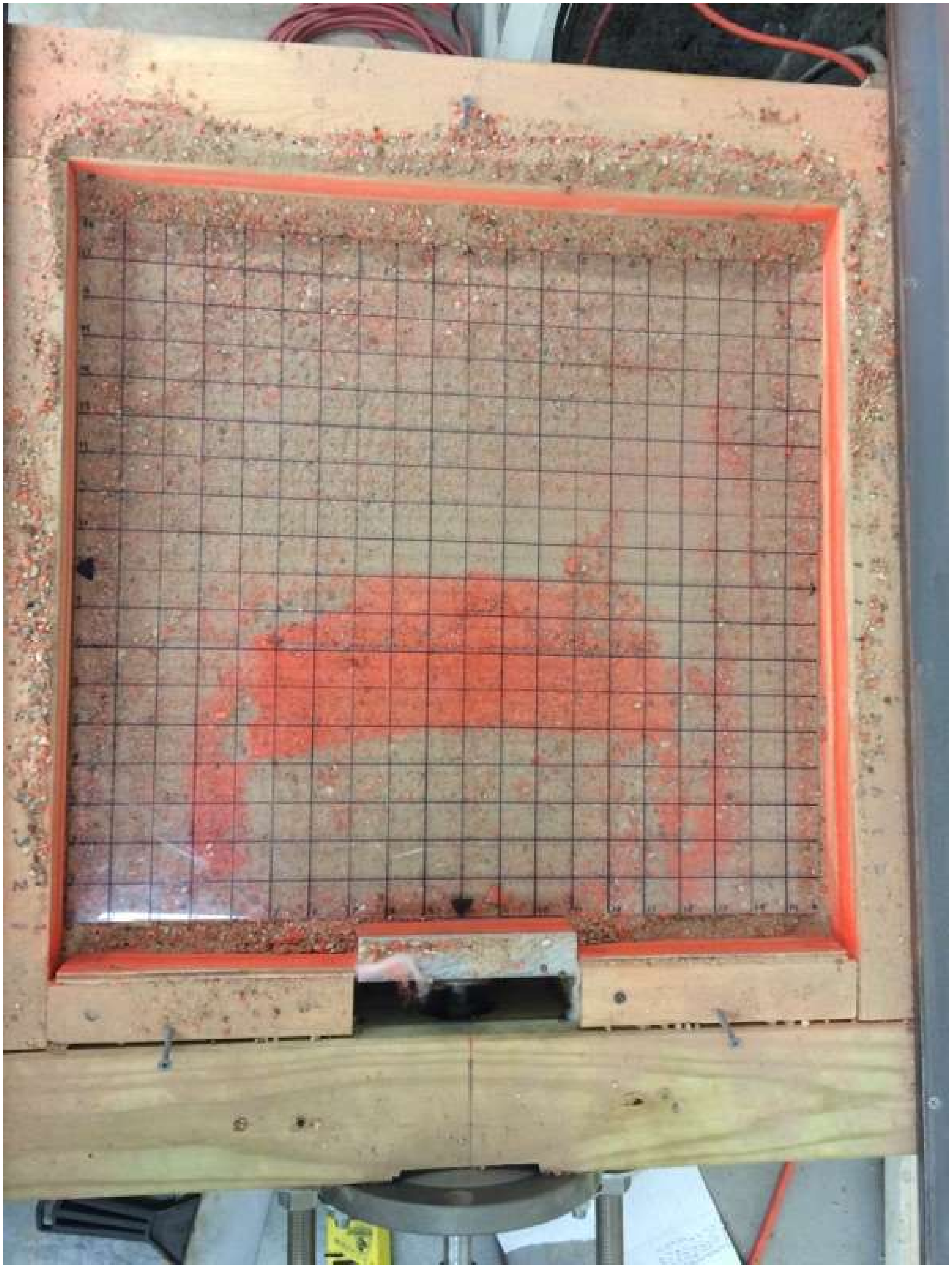

Figure 449: Test 11W8L10Lay3, 2” depth

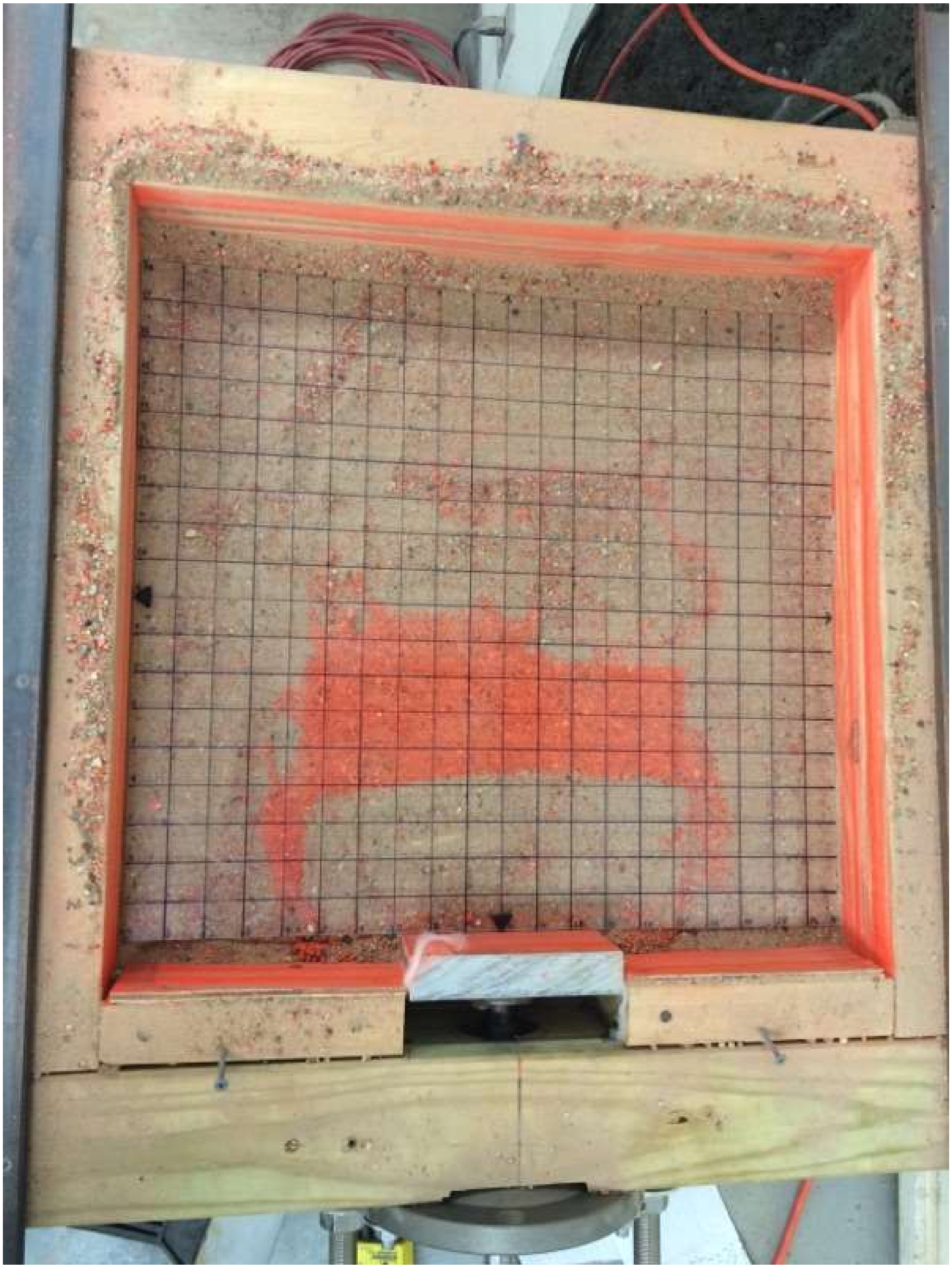

Figure 450: Test 11W8L10Lay3, 3” depth

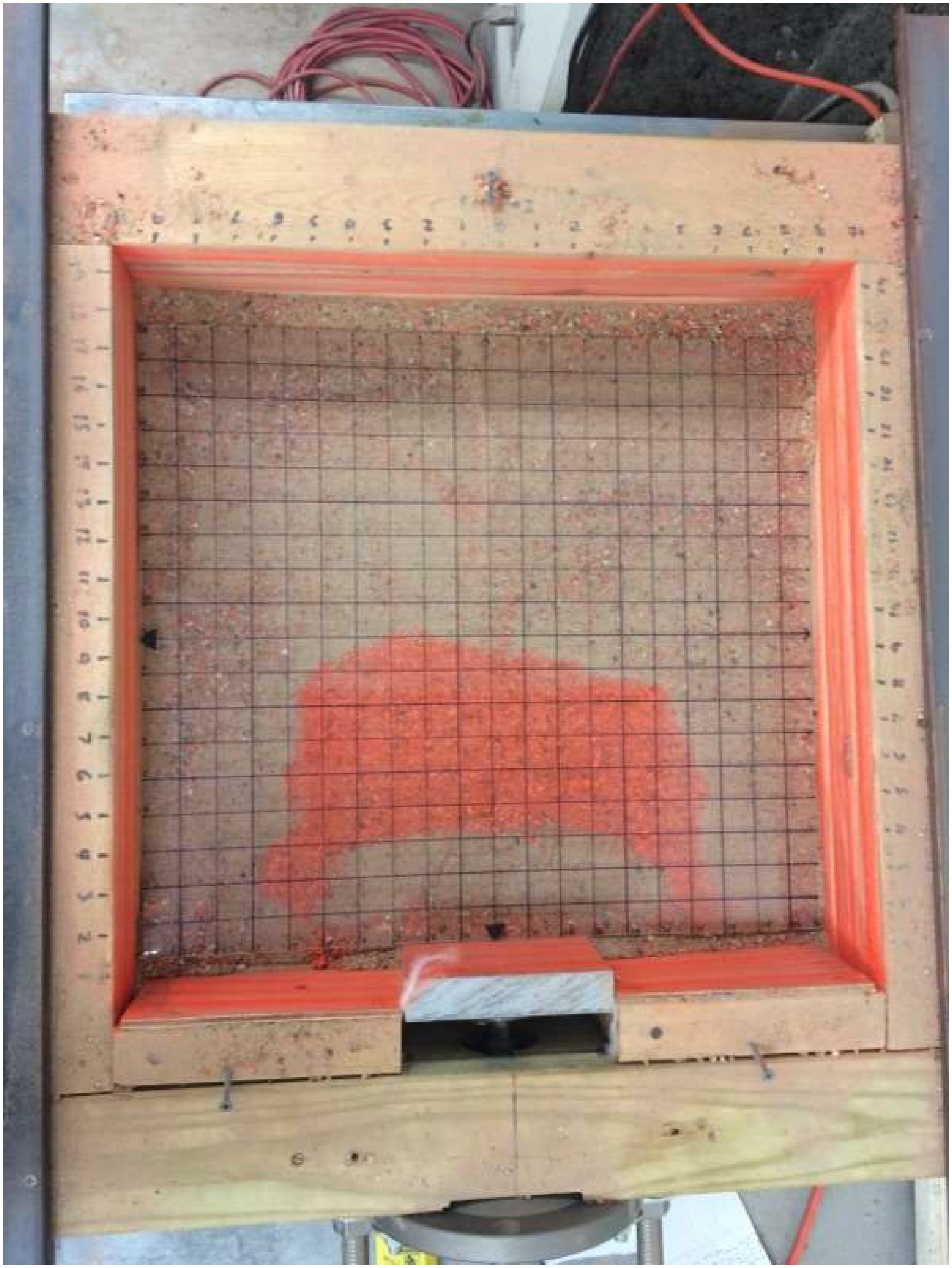

Figure 451: Test 11W8L10Lay3, 4” depth

Figure 452: Test 11W8L10Lay3, 5" depth

C.8 Photographs of Test 11W11L5Lay3

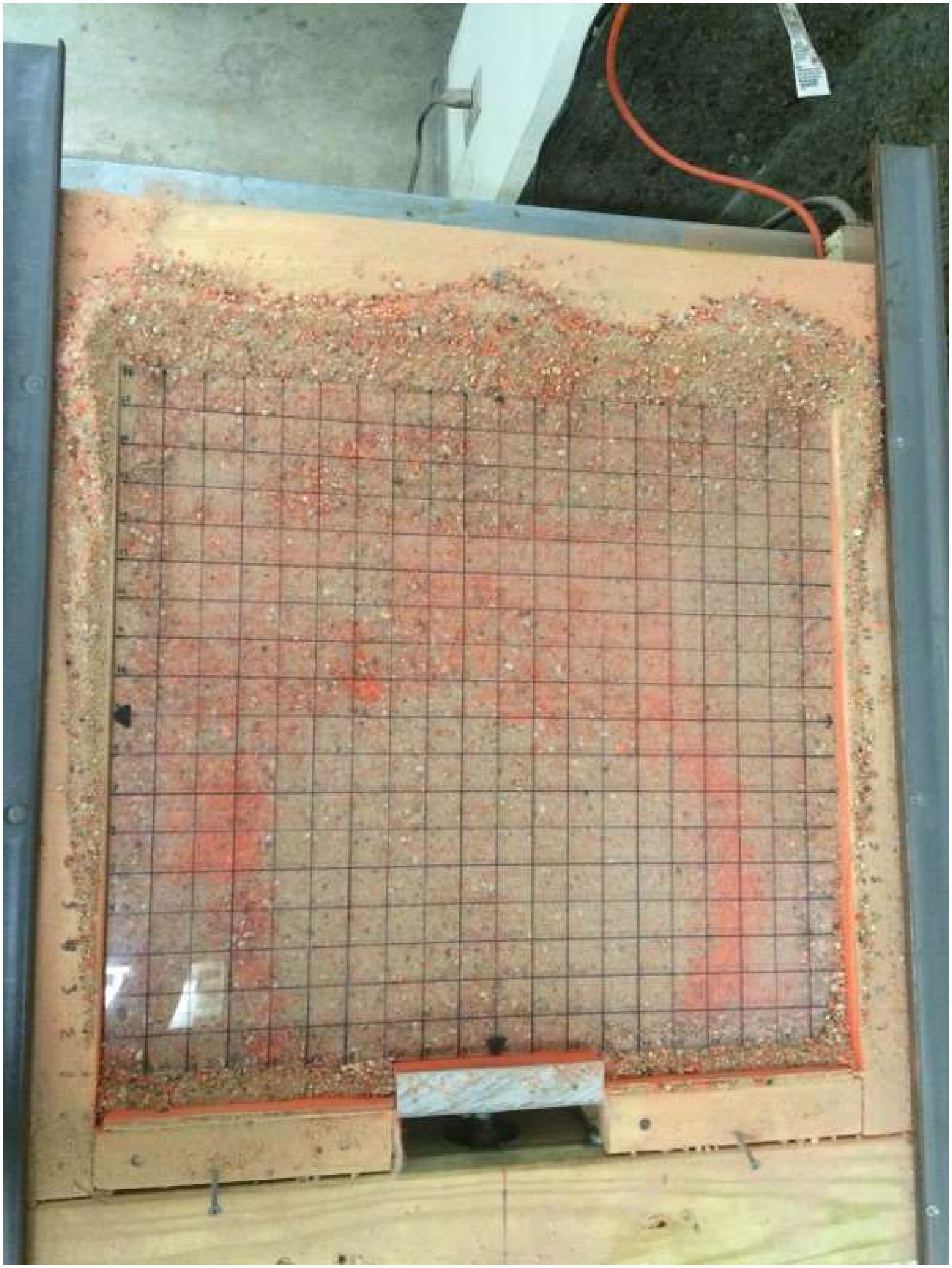

Figure 453: Test 11W11L5Lay3, 1” depth

Figure 454: Test 11W11L5Lay3, 2” depth

Figure 455: Test 11W11L5Lay3, 3” depth

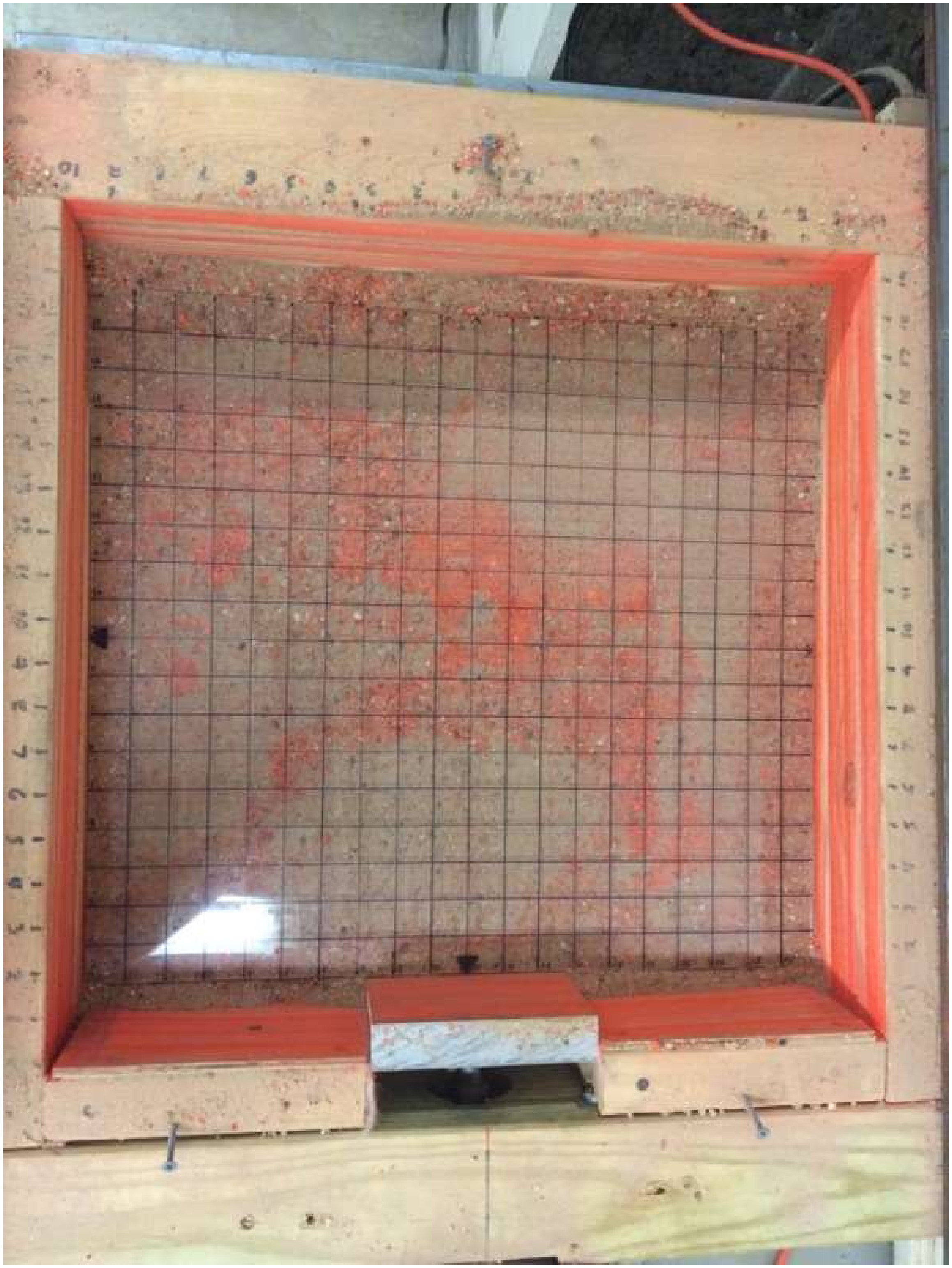

Figure 456: Test 11W11L5Lay3, 4” depth

Figure 457: Test 11W11L5Lay3, 5" depth

C.9 Photographs of Test 11W11L10Lay3

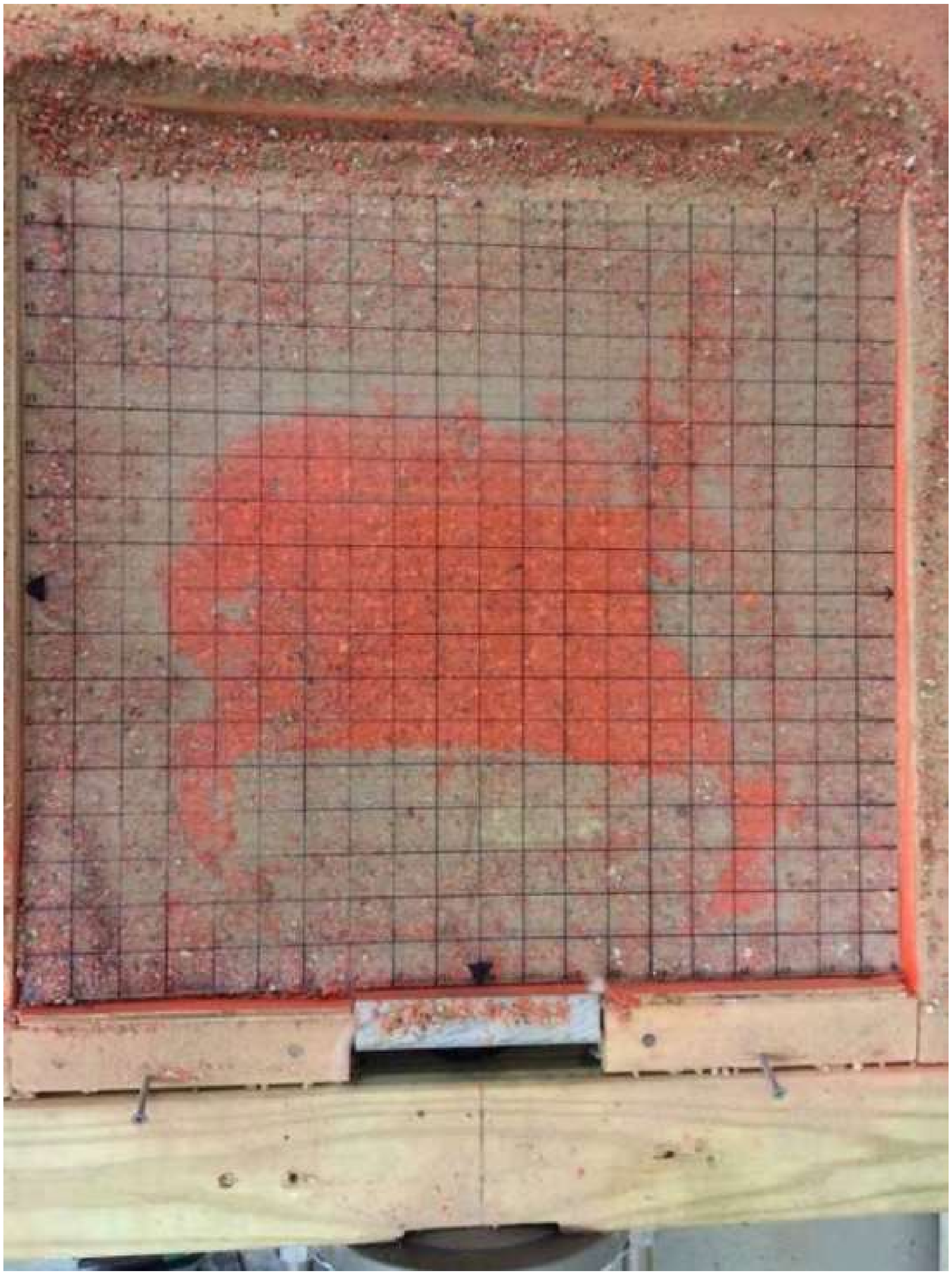

Figure 458: Test 11W11L10Lay3, 2” depth

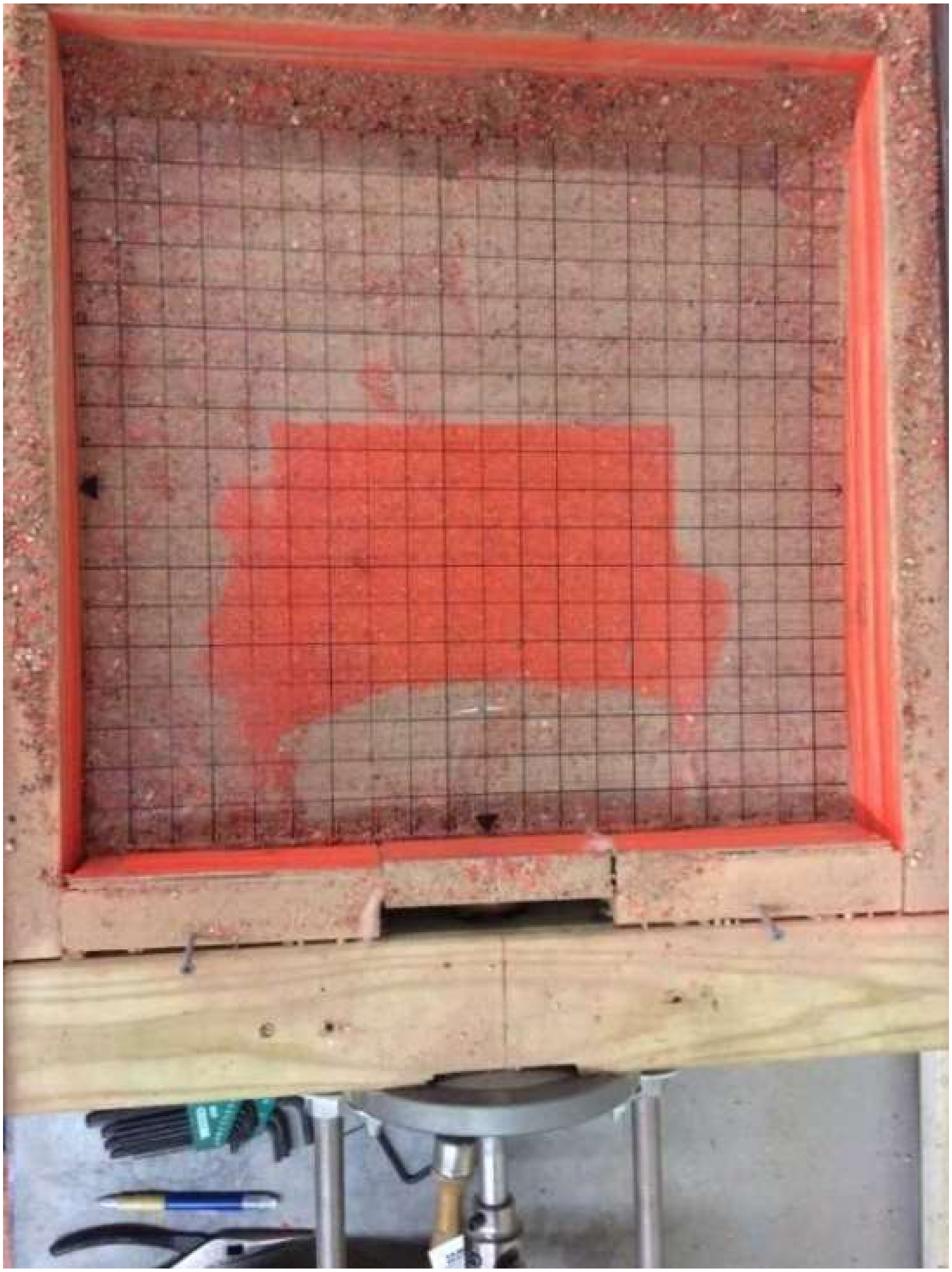

Figure 459: Test 11W11L10Lay3, 3" depth

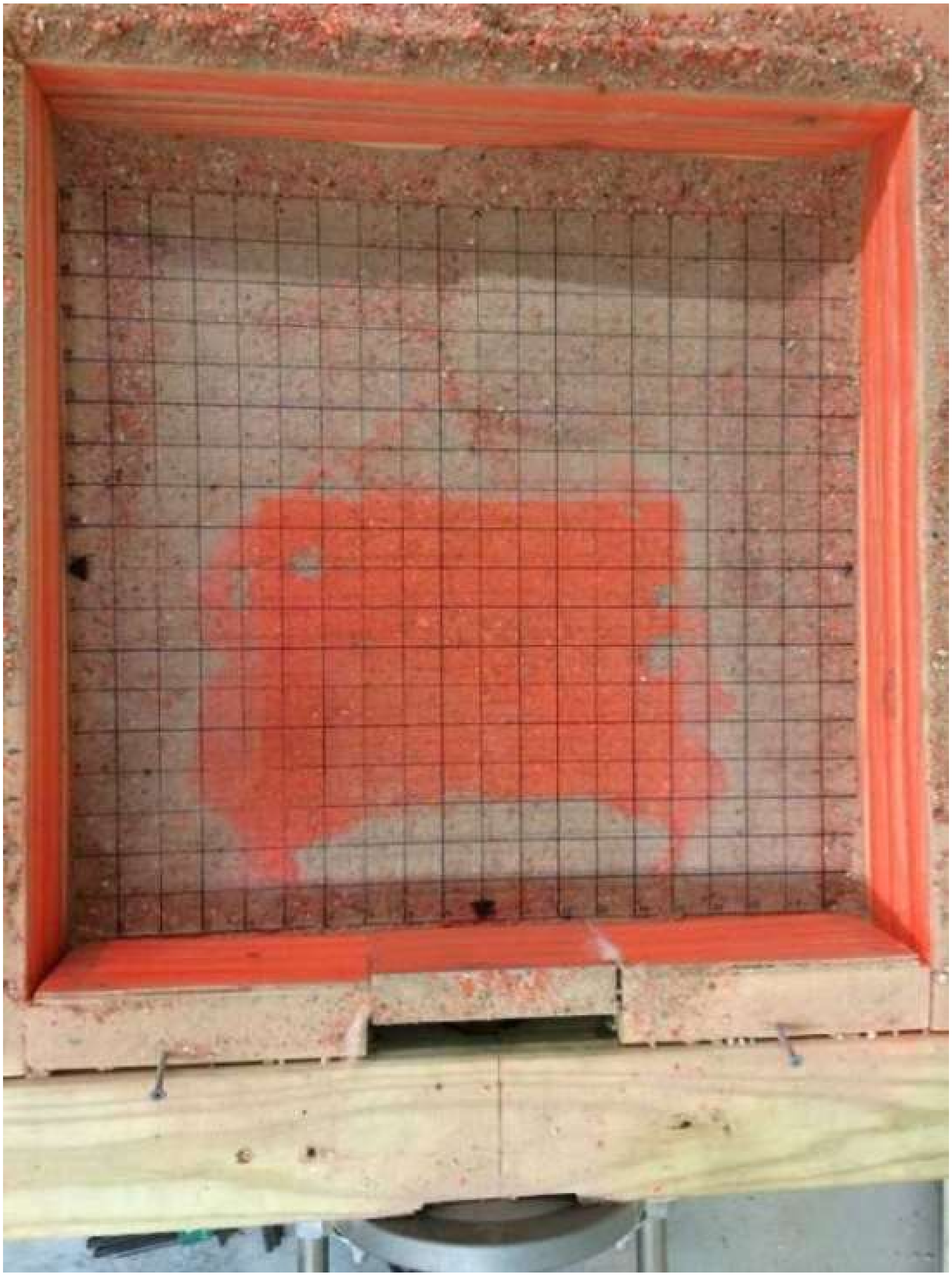

Figure 460: Test 11W11L10Lay3, 4" depth

C.10 Photographs of Test PW8L5Lay3

Figure 461: Test PW8L5Lay3, 1" depth

Figure 462: Test PW8L5Lay3, 2" depth

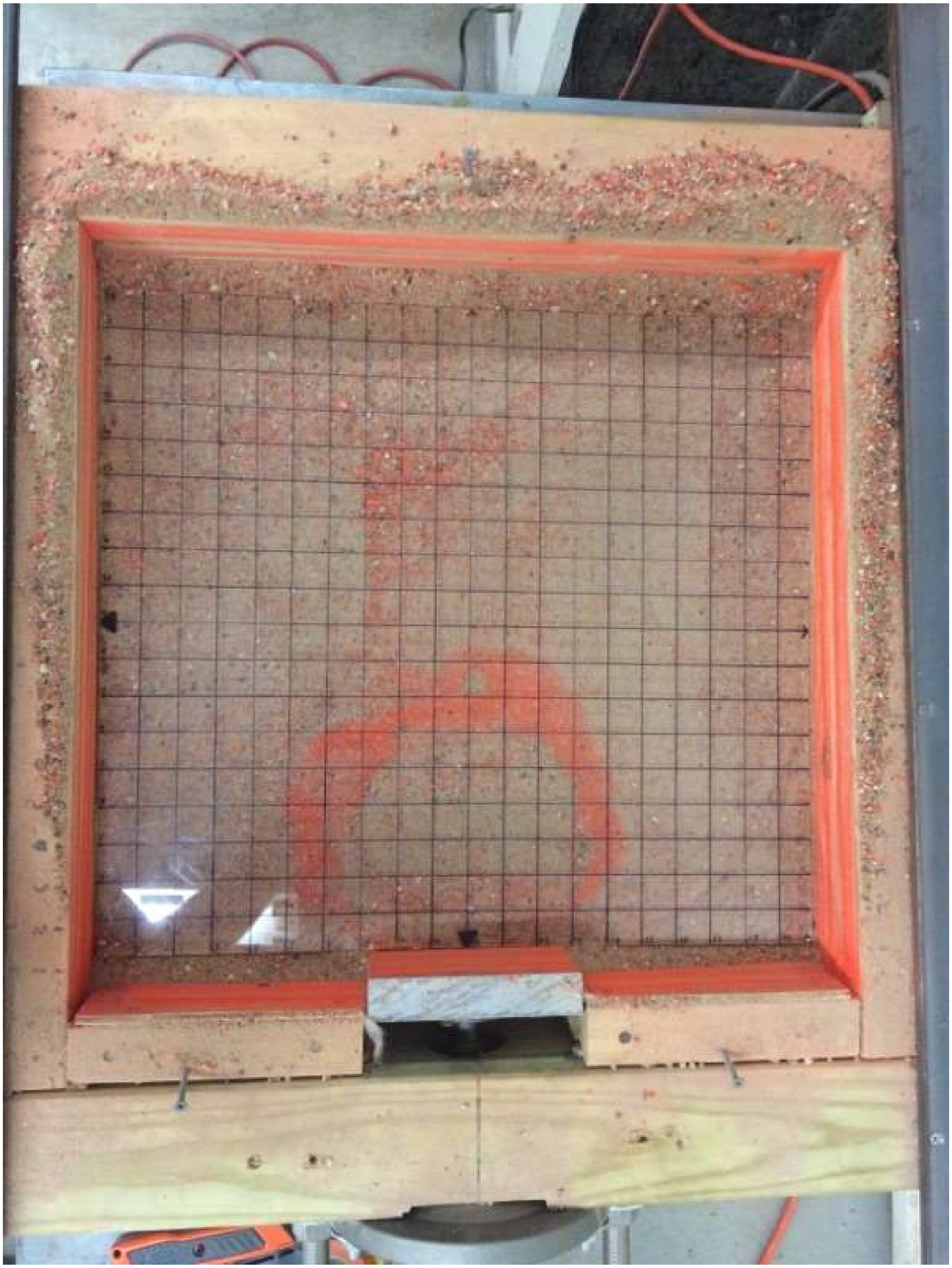

Figure 463: Test PW8L5Lay3, 3” depth

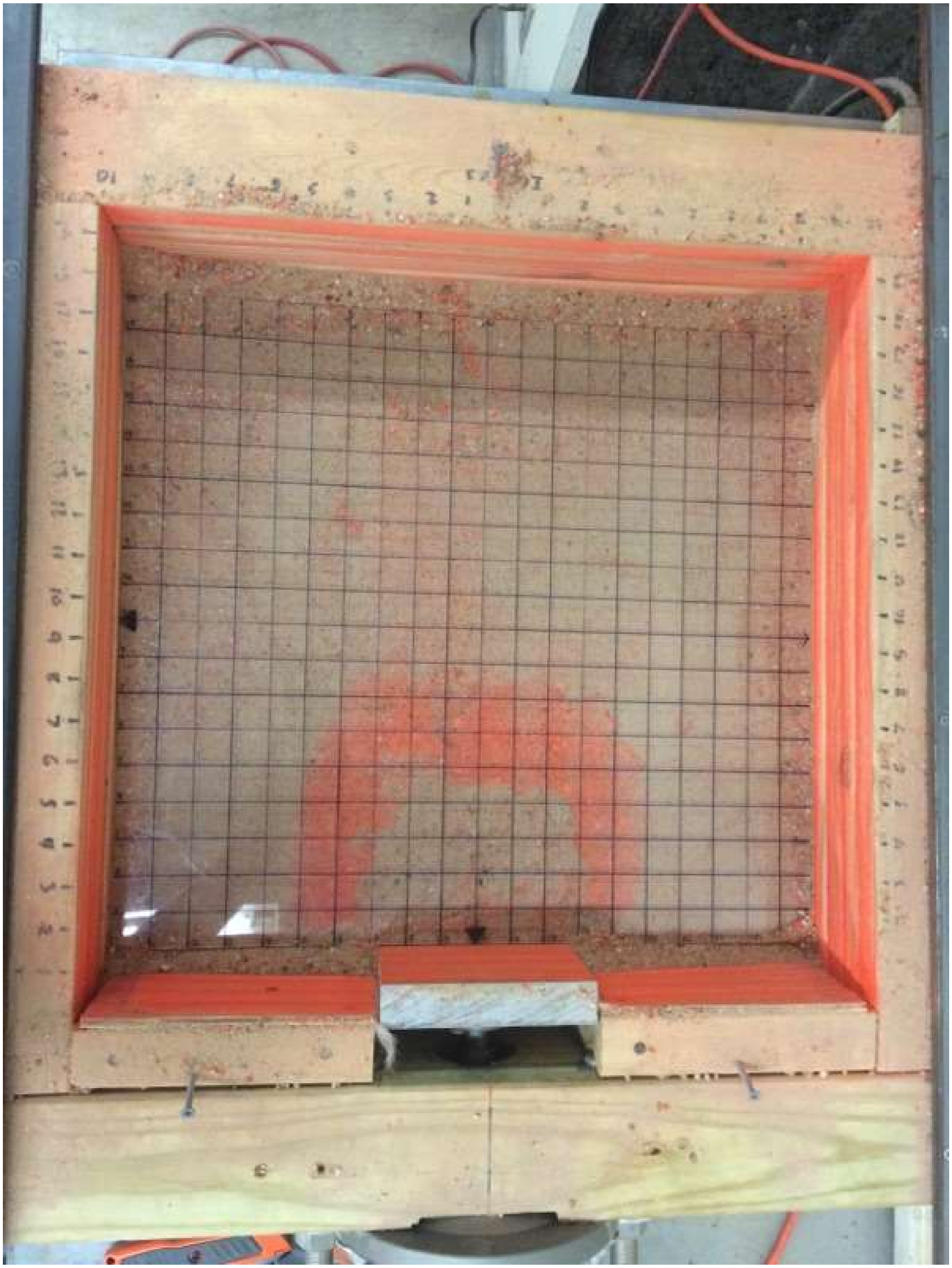

Figure 464: Test PW8L5Lay3, 4” depth

Figure 465: Test PW8L5Lay3, 5" depth

C.11 Photographs of Test PW8L10Lay3

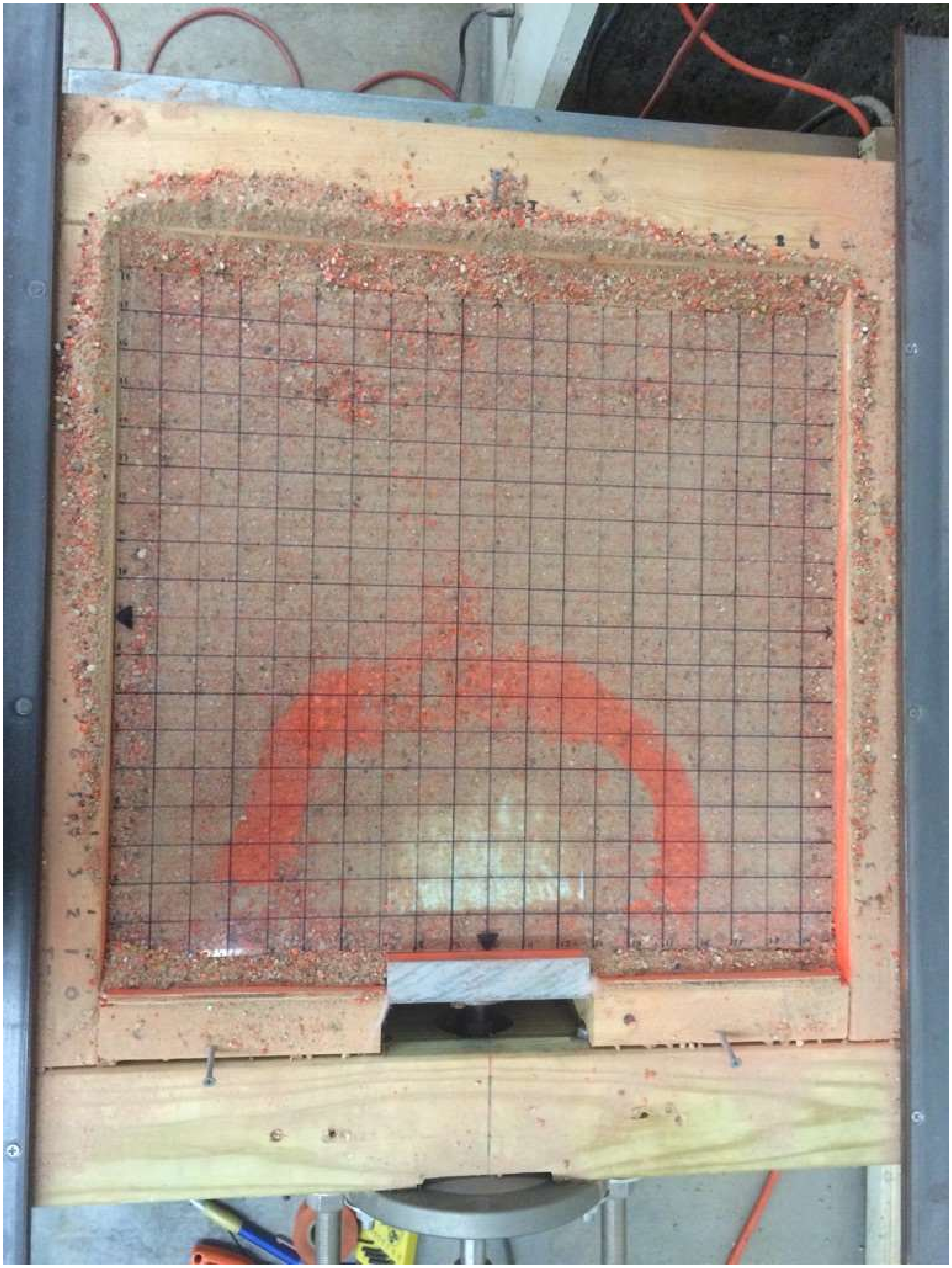

Figure 466: Test PW8L10Lay3, 1" depth

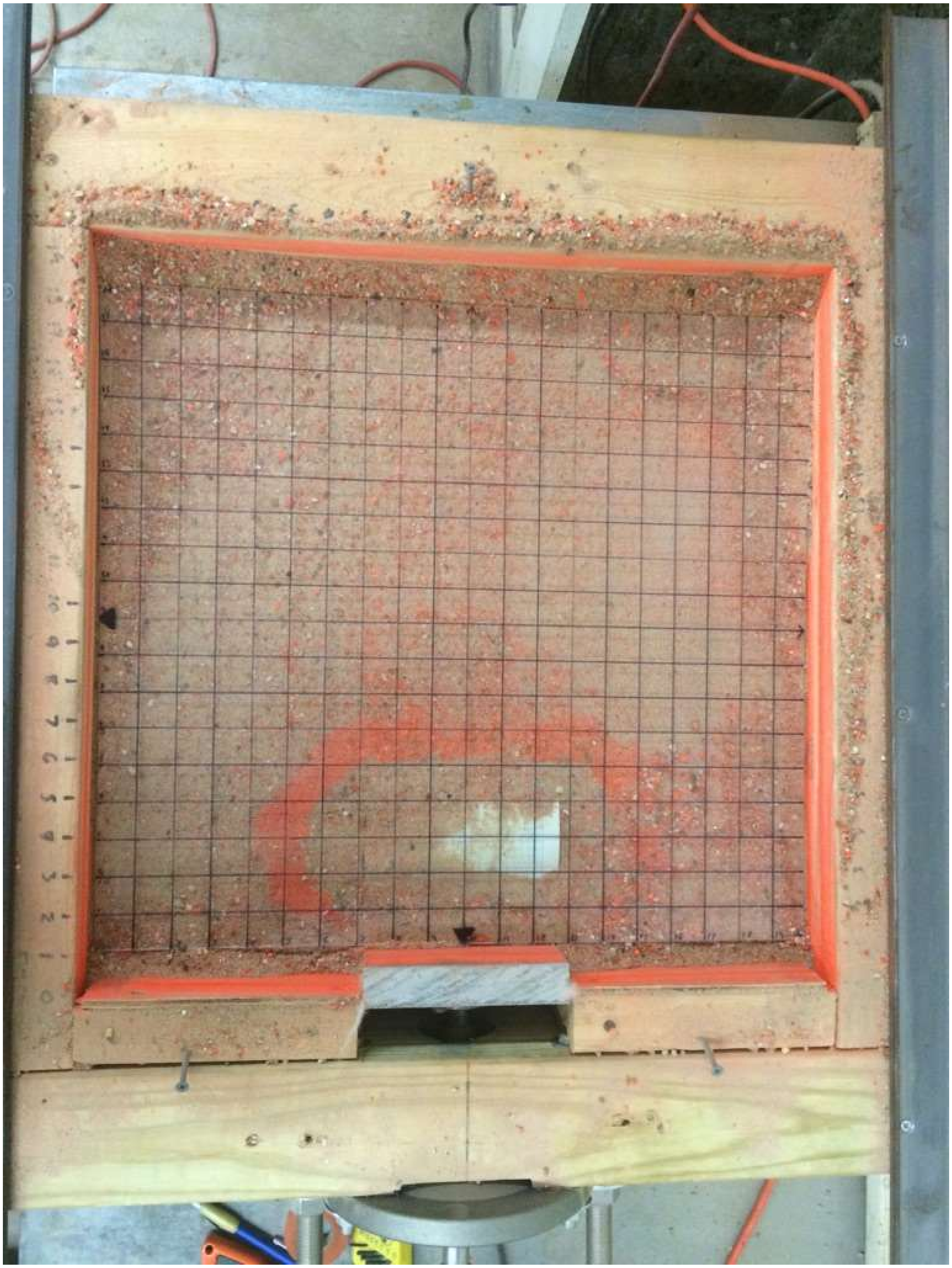

Figure 467: Test PW8L10Lay3, 2” depth

Figure 468: Test PW8L10Lay3, 4” depth

Figure 469: Test PW8L10Lay3, 5" depth

C.12 Photographs of Test PW11L5Lay3

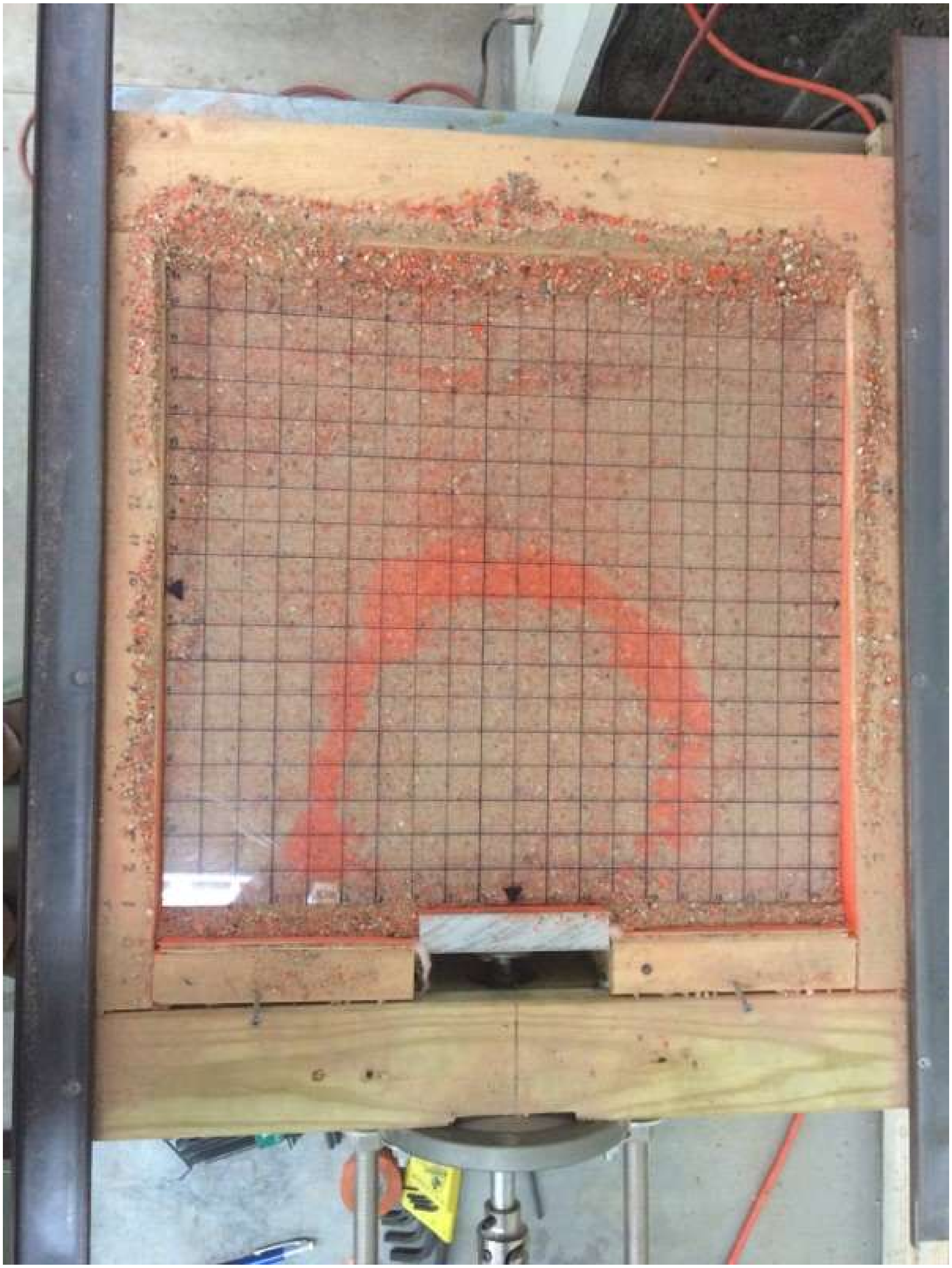

Figure 470: Test PW11L5Lay3, 1" depth

Figure 471: Test PW11L5Lay3, 2” depth

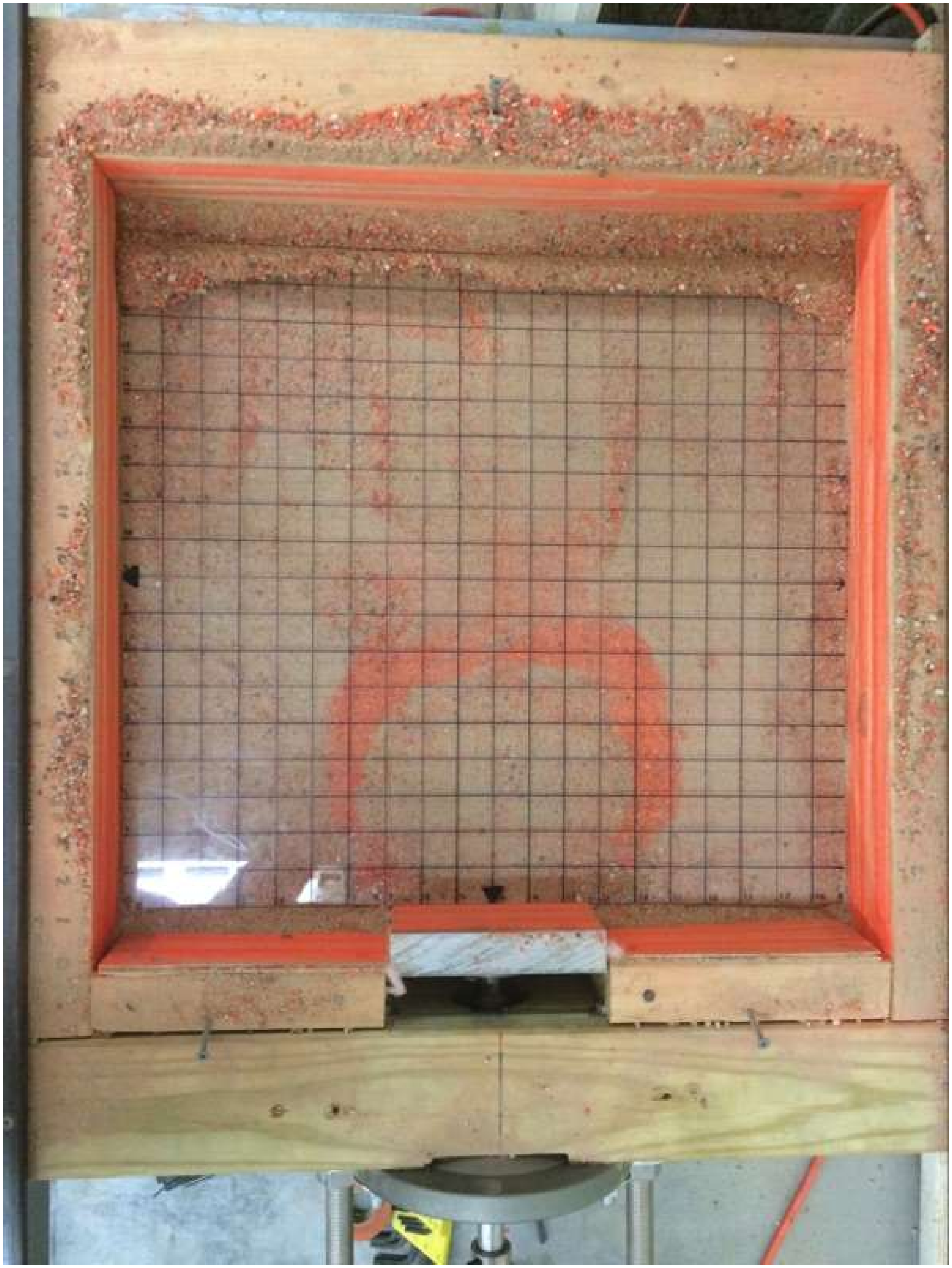

Figure 472: Test PW11L5Lay3, 3" depth

Figure 473: Test PW11L5Lay3, 4” depth

Figure 474: Test PW11L5Lay3, 5” depth

C.13 Photographs of Test PW11L10Lay3

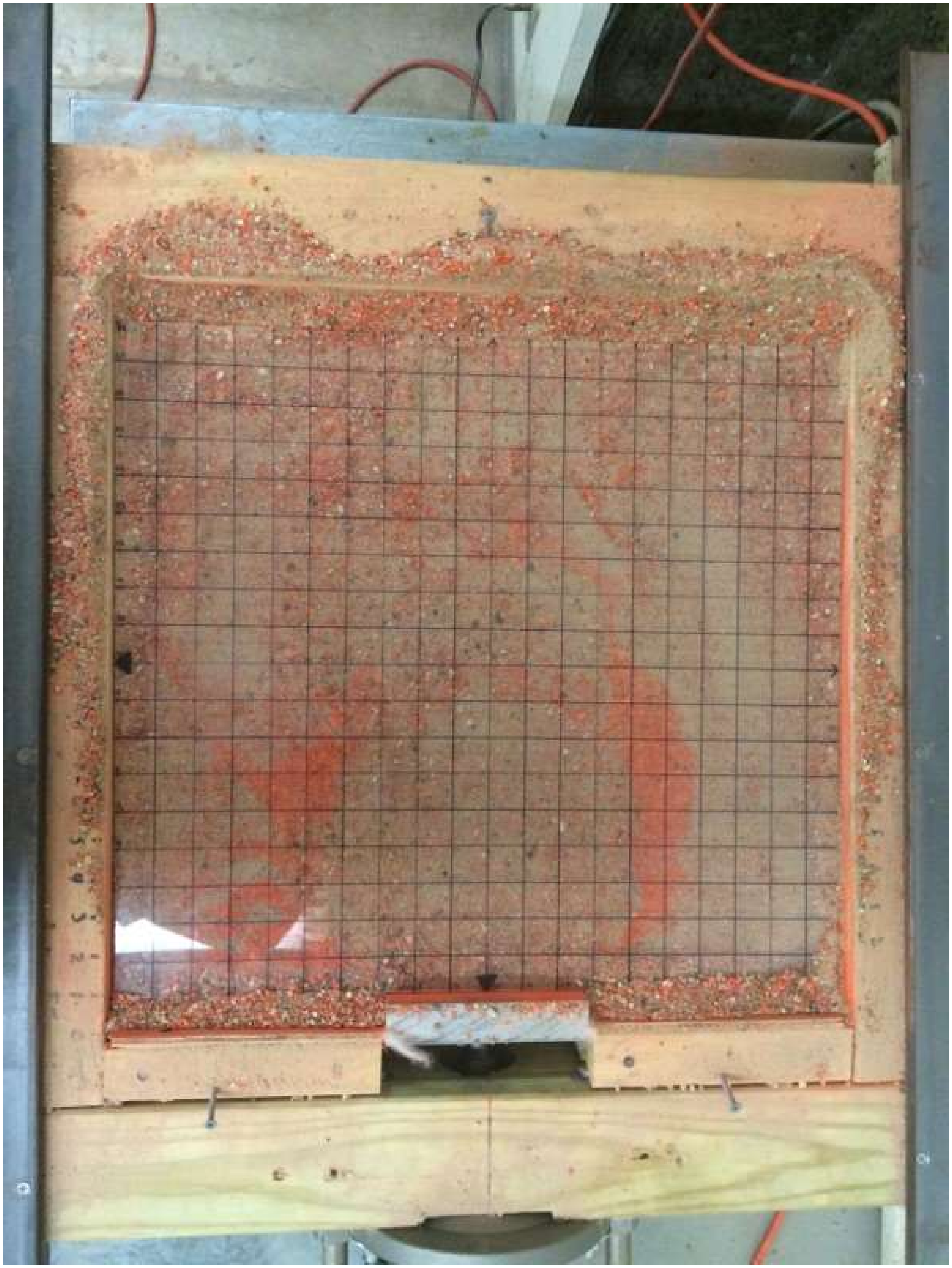

Figure 475: Test PW11L10Lay3, 1” depth

Figure 476: Test PW11L10Lay3, 3” depth

Figure 477: Test PW11L10Lay3, 4” depth

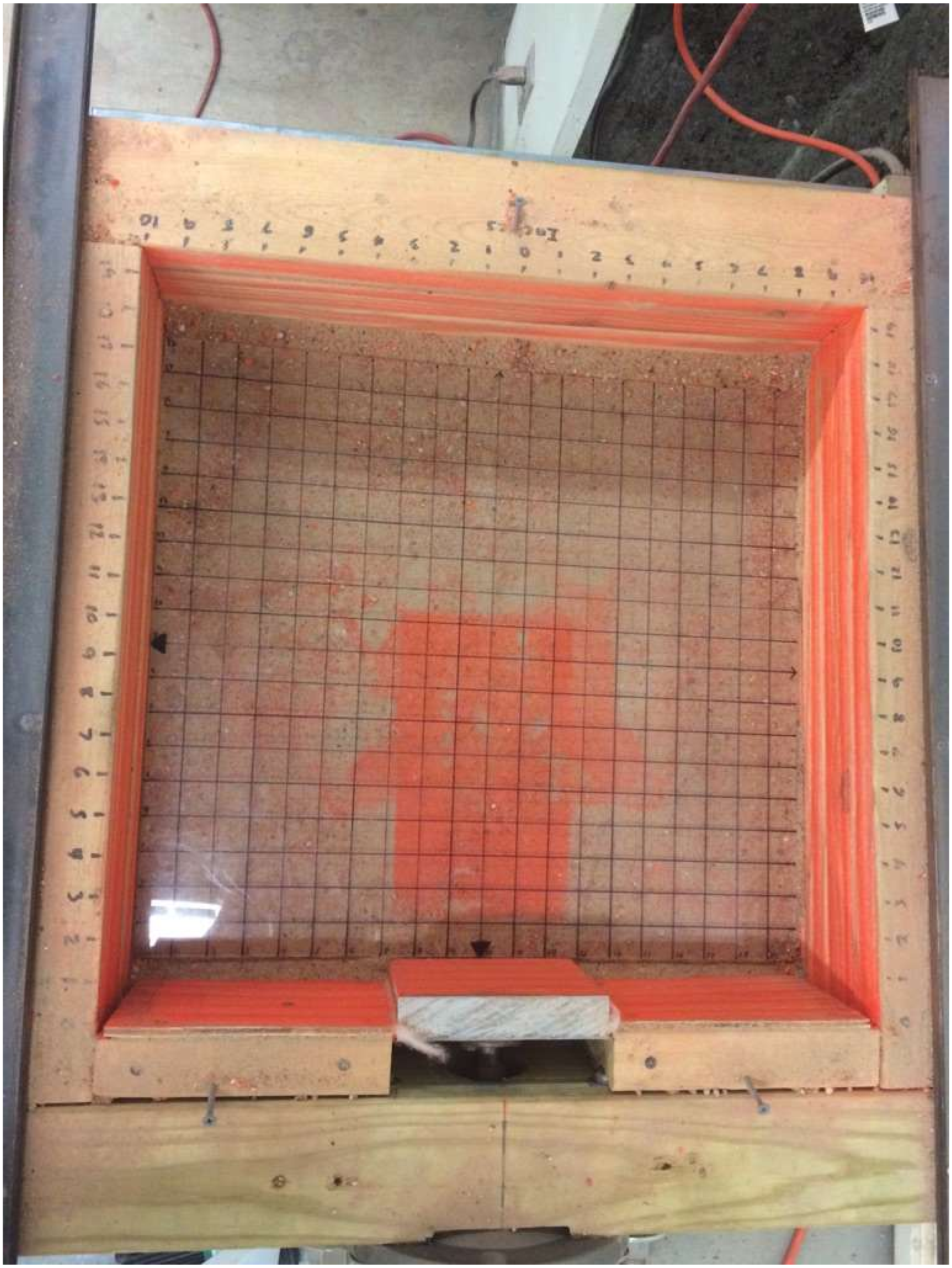

Figure 478: Test PW11L10Lay3, 5" depth

C.14 Photographs of Test NR3

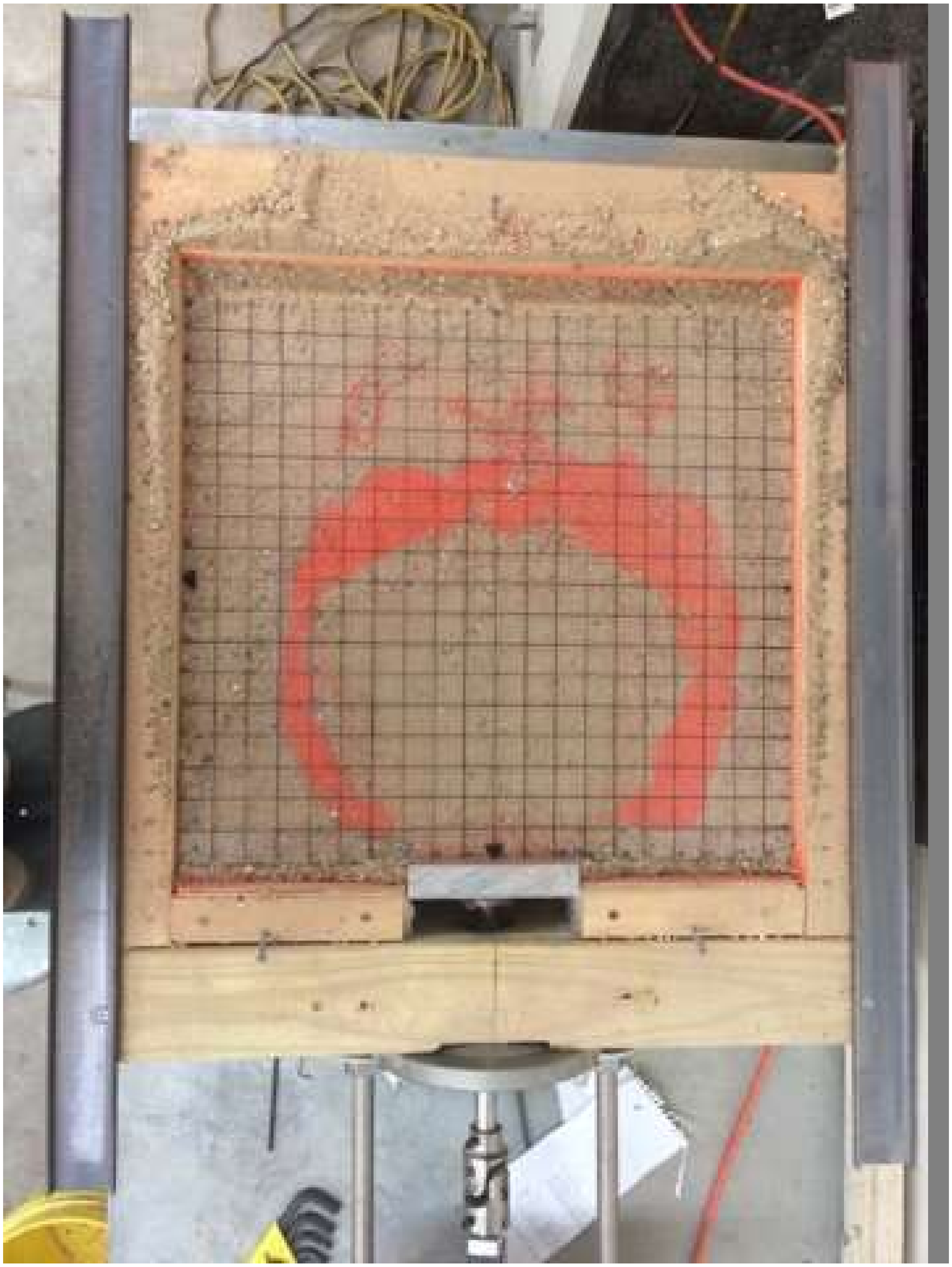

Figure 479: Test NR3, 1" depth

Figure 480: Test NR3, 2” depth

Figure 481: Test NR3, 3” depth

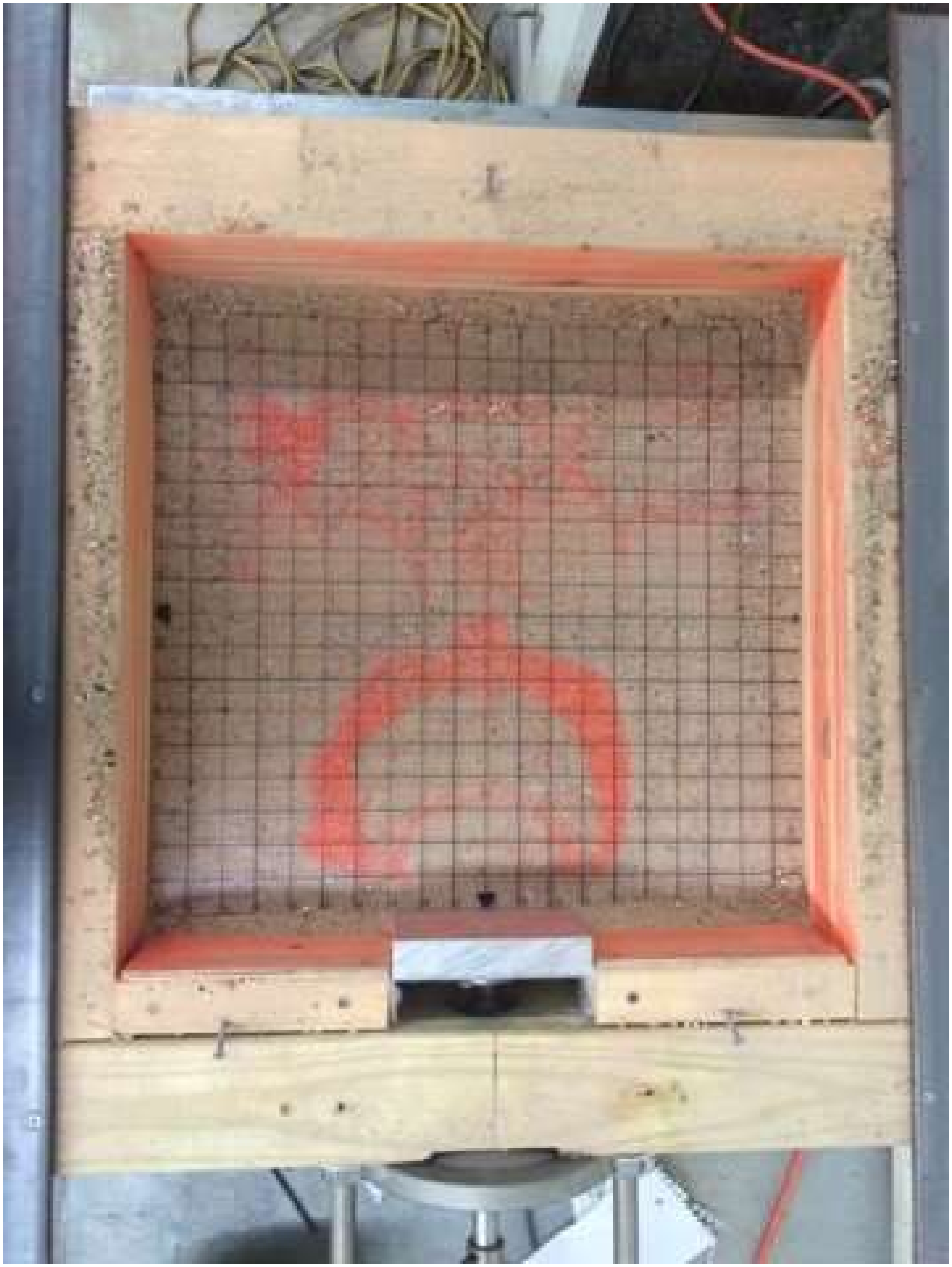

Figure 482: Test NR3, 4" depth

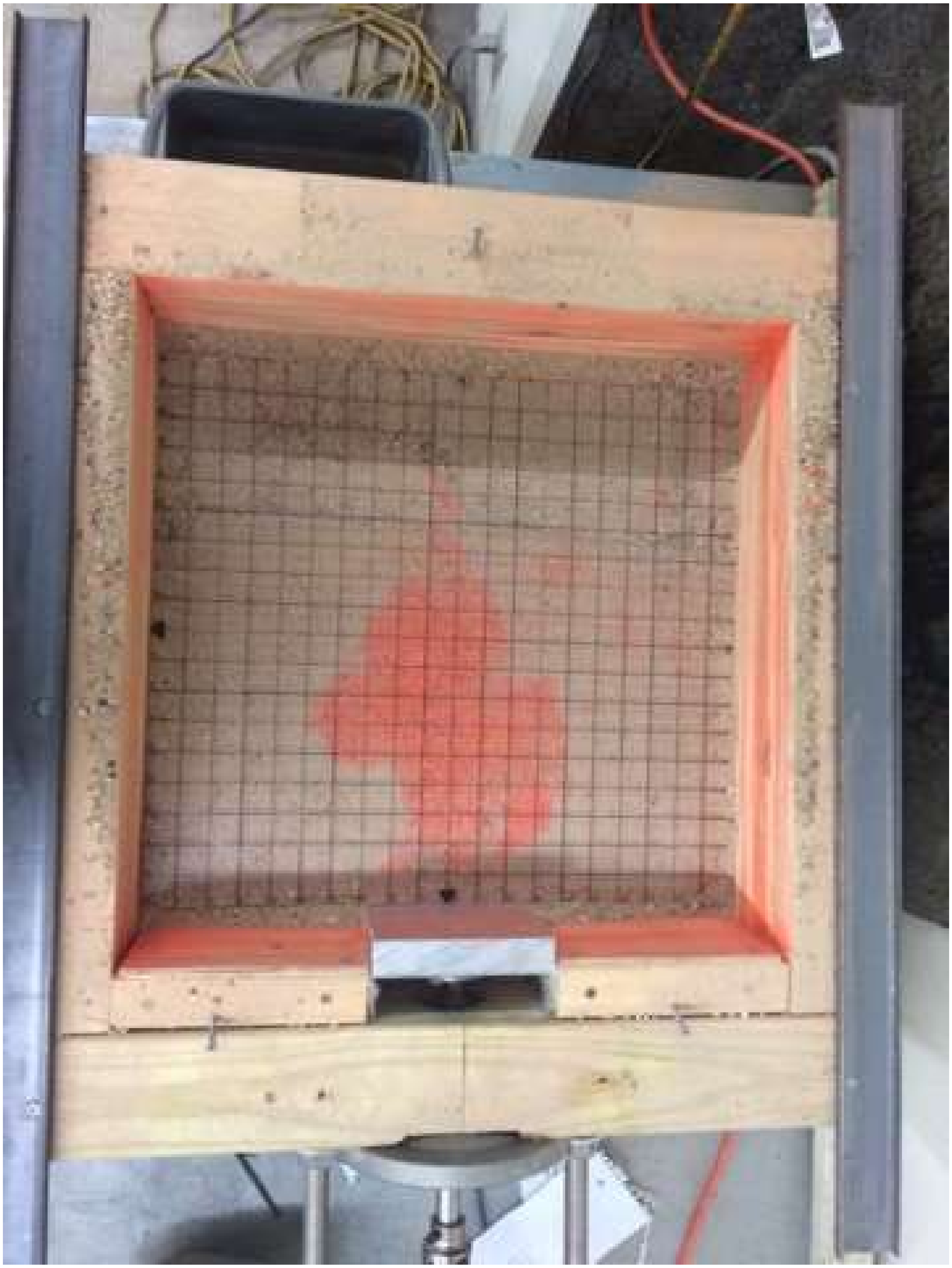

Figure 483: Test NR3, 5” depth

APPENDIX D: LOAD DISPLACEMENT PLOTS FROM RAW DATA

D.1 Introduction

Load-displacement data were taken during laboratory testing using GeoJac software and were plotted using Microsoft Excel. Peak Force, Residual Force, displacement where the Peak Force occurred, and the stiffness at 50% of the Peak Force were determined using each plot and are shown on the plot.

D.2 Load-Displacement Plot of Test 8W8L5Lay

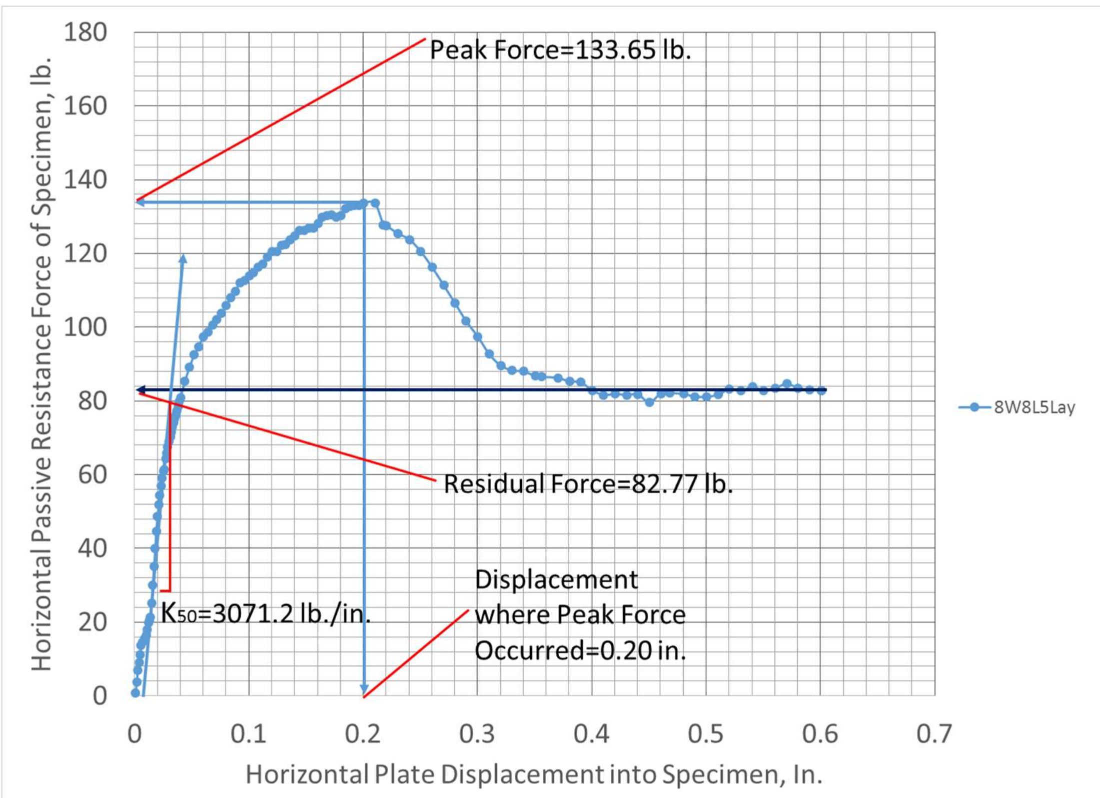

Figure 484: Load-Displacement Plot of Test 8W8L5Lay

D.3 Load-Displacement Plot of Test 8W8L5Lay2

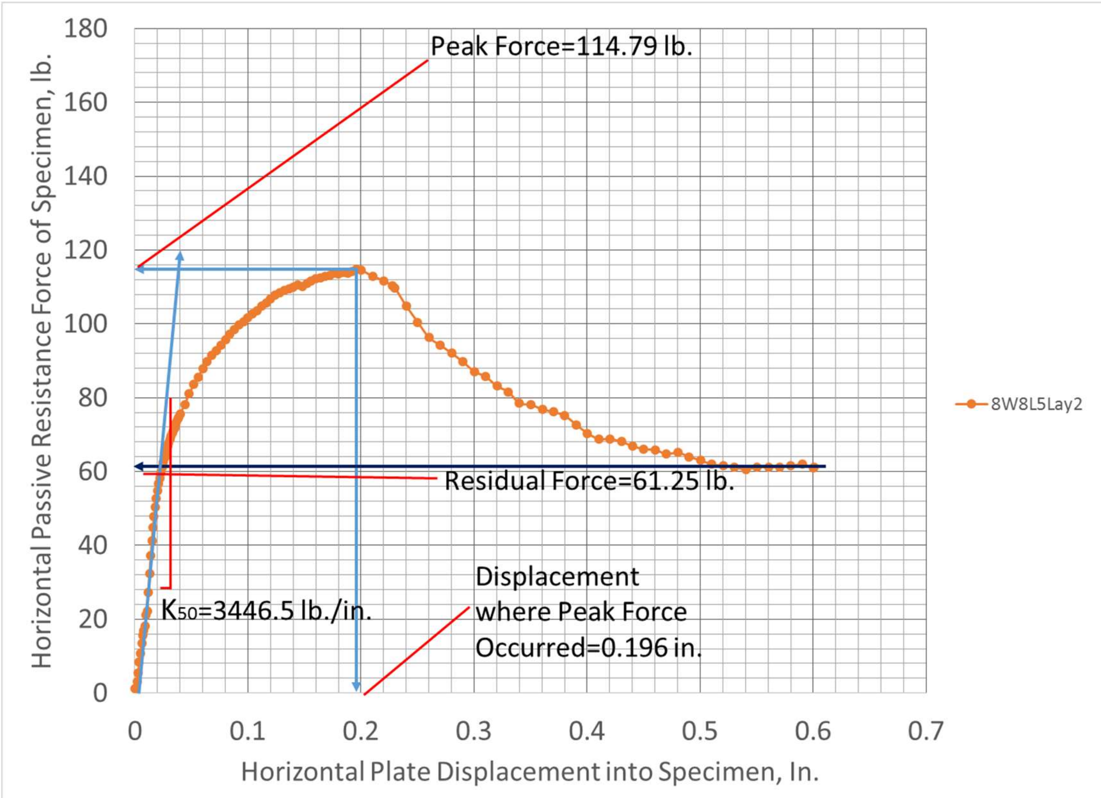

Figure 485: Load-Displacement Plot of Test 8W8L5Lay2

D.4 Load-Displacement Plot of Test 8W8L10Lay

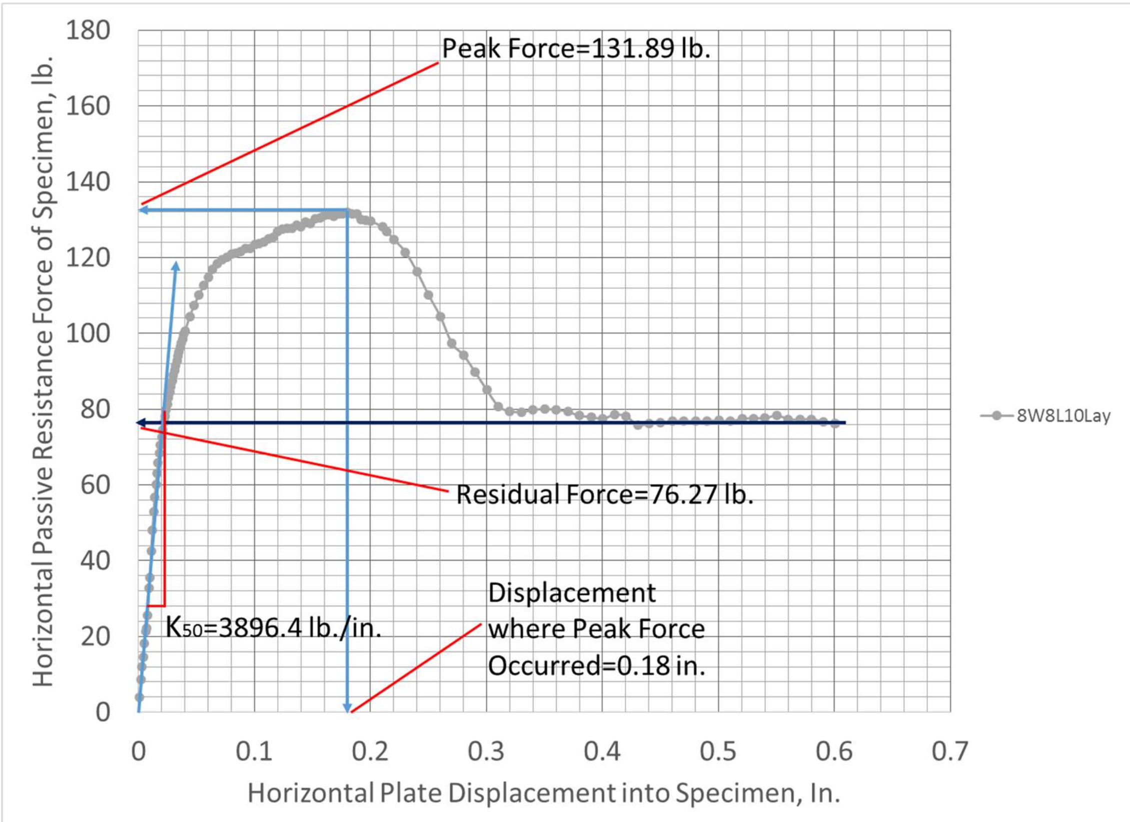

Figure 486: Load-Displacement Plot of Test 8W8L10Lay

D.5 Load-Displacement Plot of Test 8W8L10Lay2

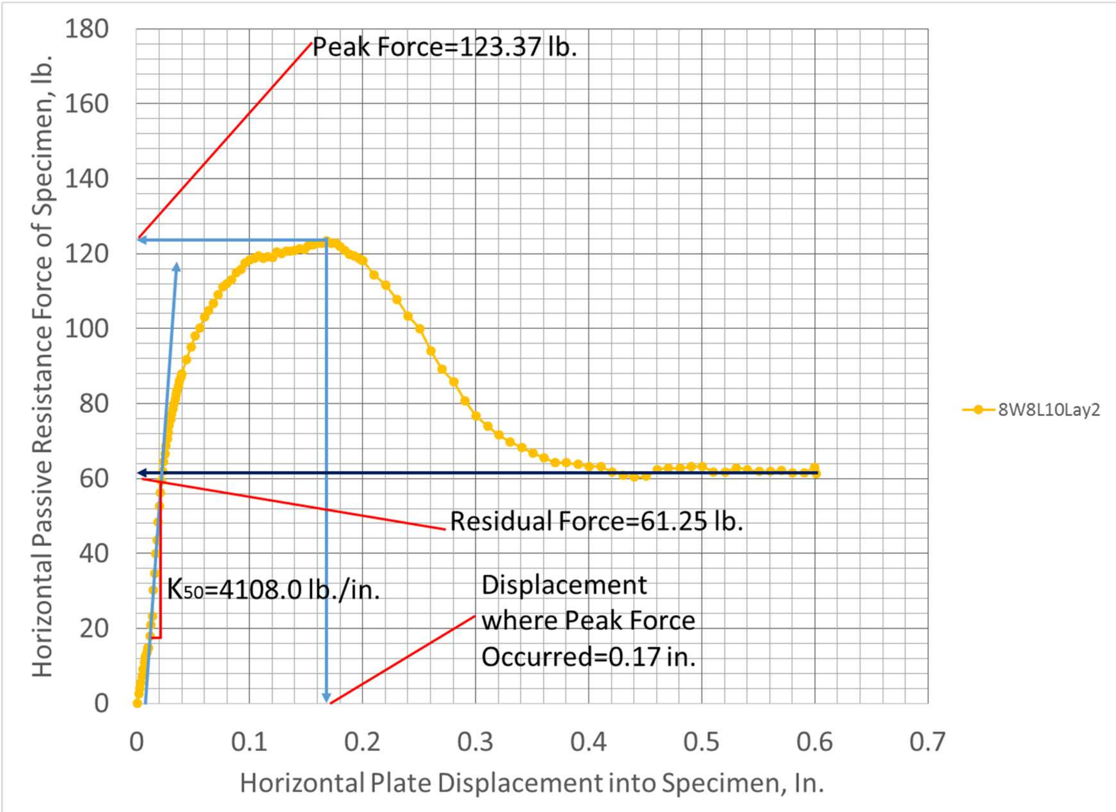

Figure 487: Load-Displacement Plot of Test 8W11L10Lay2

D.6 Load-Displacement Plot of Test 8W11L5Lay

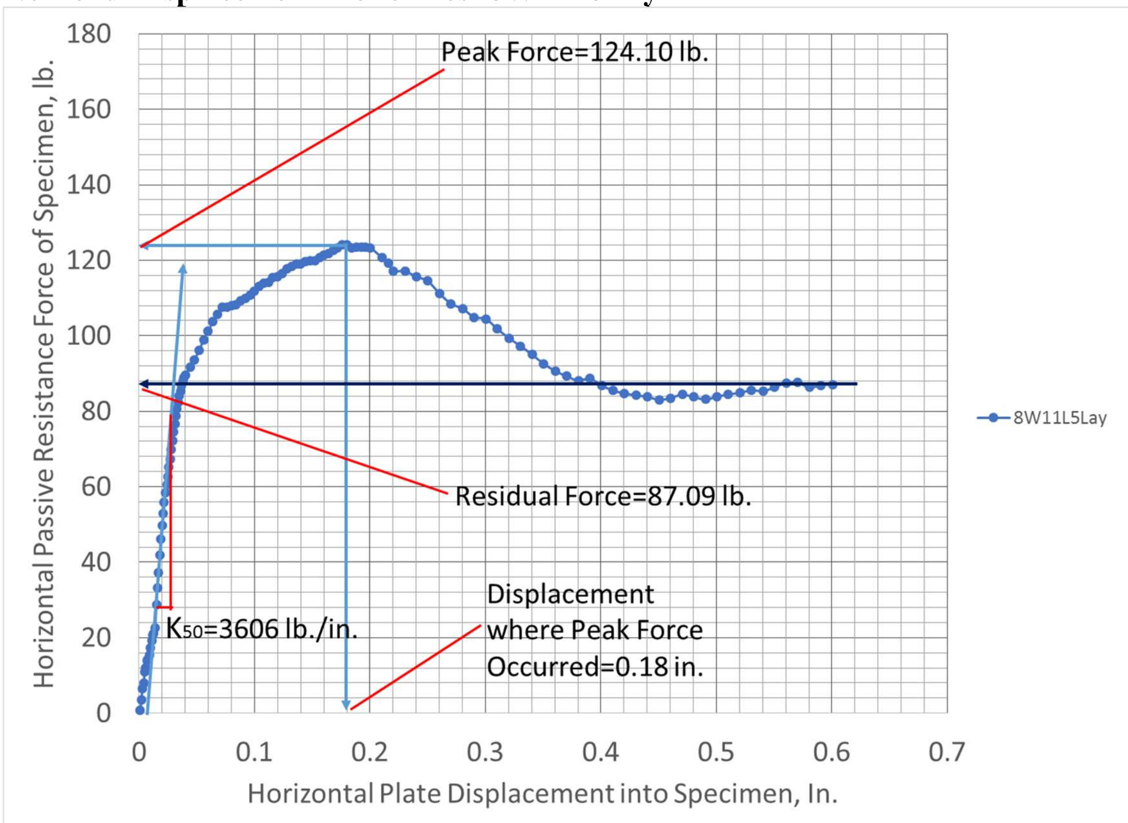

Figure 488: Load-Displacement Plot of Test 8W11L5Lay

D.7 Load-Displacement Plot of Test 8W11L5Lay2

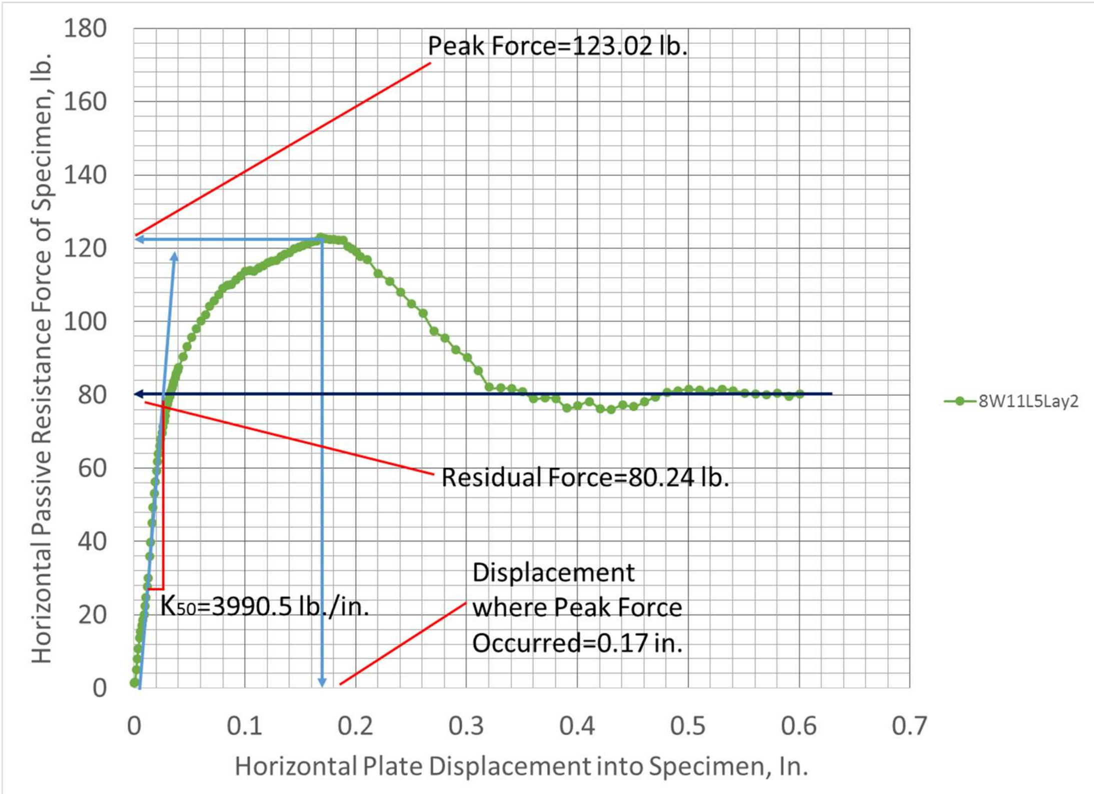

Figure 489: Load-Displacement Plot of Test 8W11L5Lay2

D.8 Load-Displacement Plot of Test 8W11L10Lay

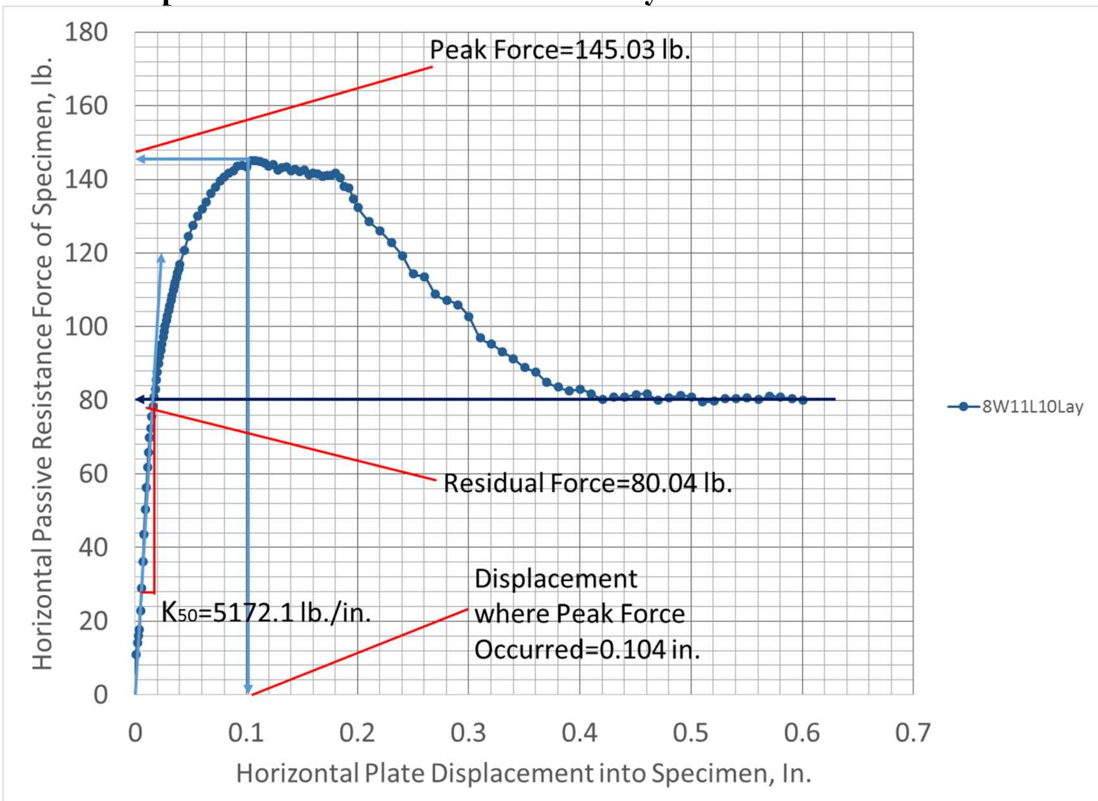

Figure 490: Load-Displacement Plot of Test 8W11L10Lay

D.9 Load-Displacement Plot of Test 8W11L10Lay2

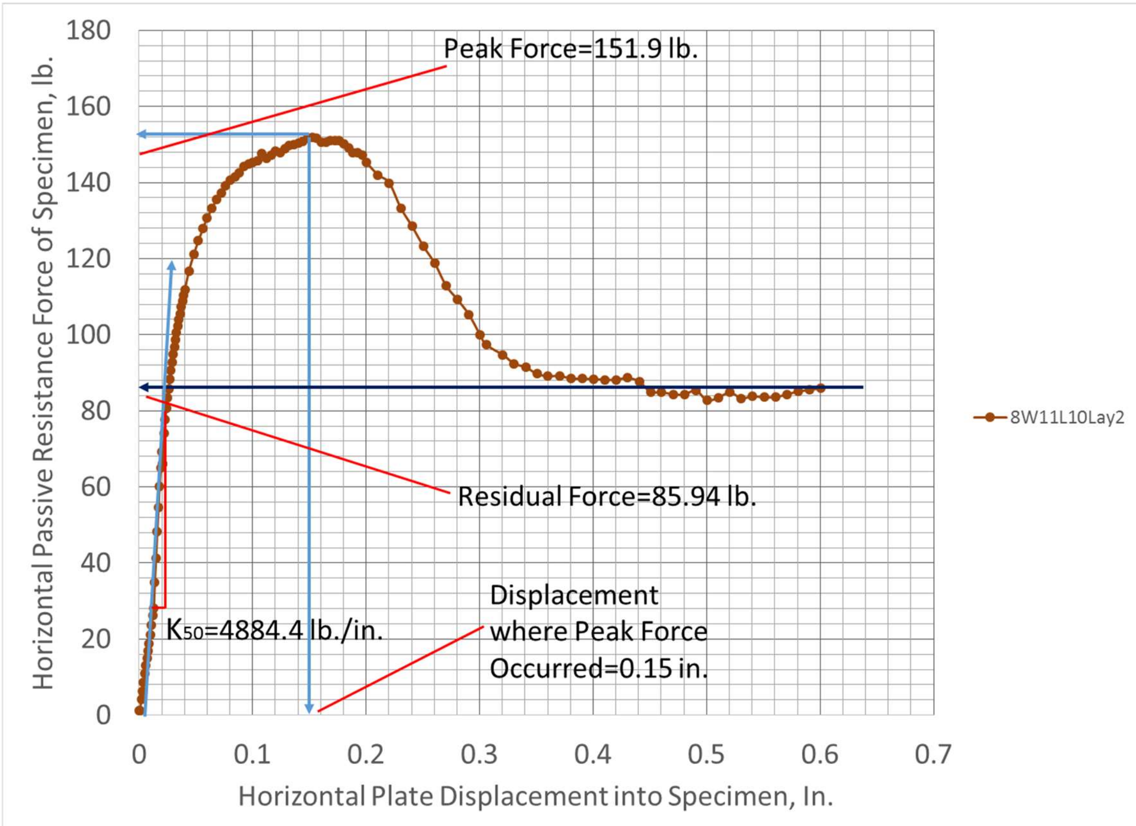

Figure 491: Load-Displacement Plot of Test 8W11L10Lay2

D.10 Load-Displacement Plot of Test 11W8L5Lay

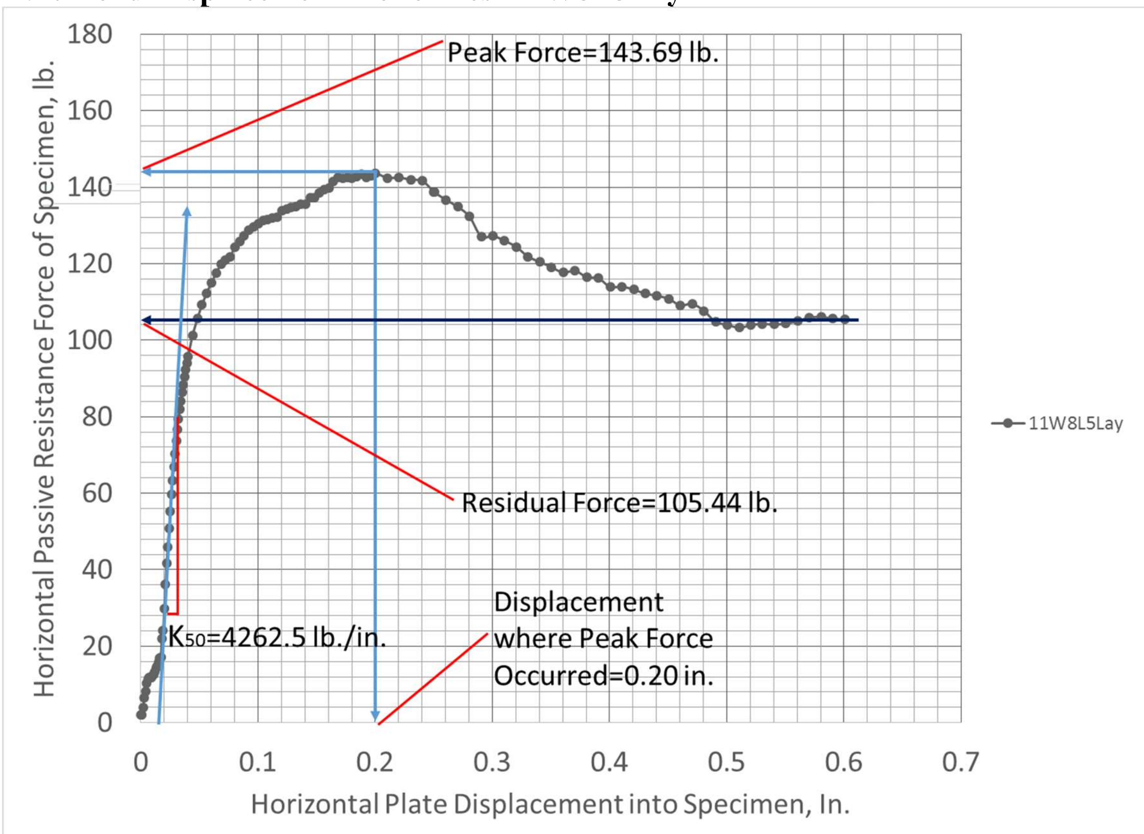

Figure 492: Load-Displacement Plot of Test 11W8L5Lay

D.11 Load-Displacement Plot of Test 11W8L5Lay2

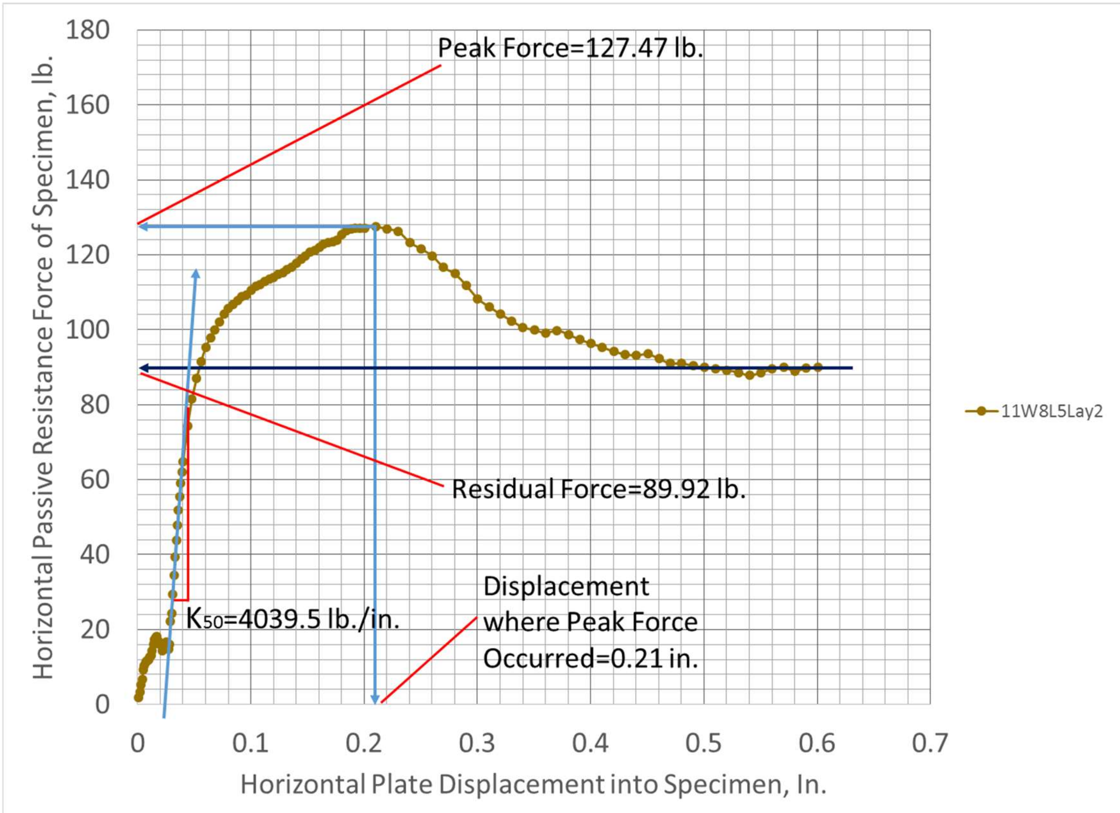

Figure 493: Load-Displacement Plot of Test 11W8L5Lay2

D.12 Load-Displacement Plot of Test 11W8L10Lay

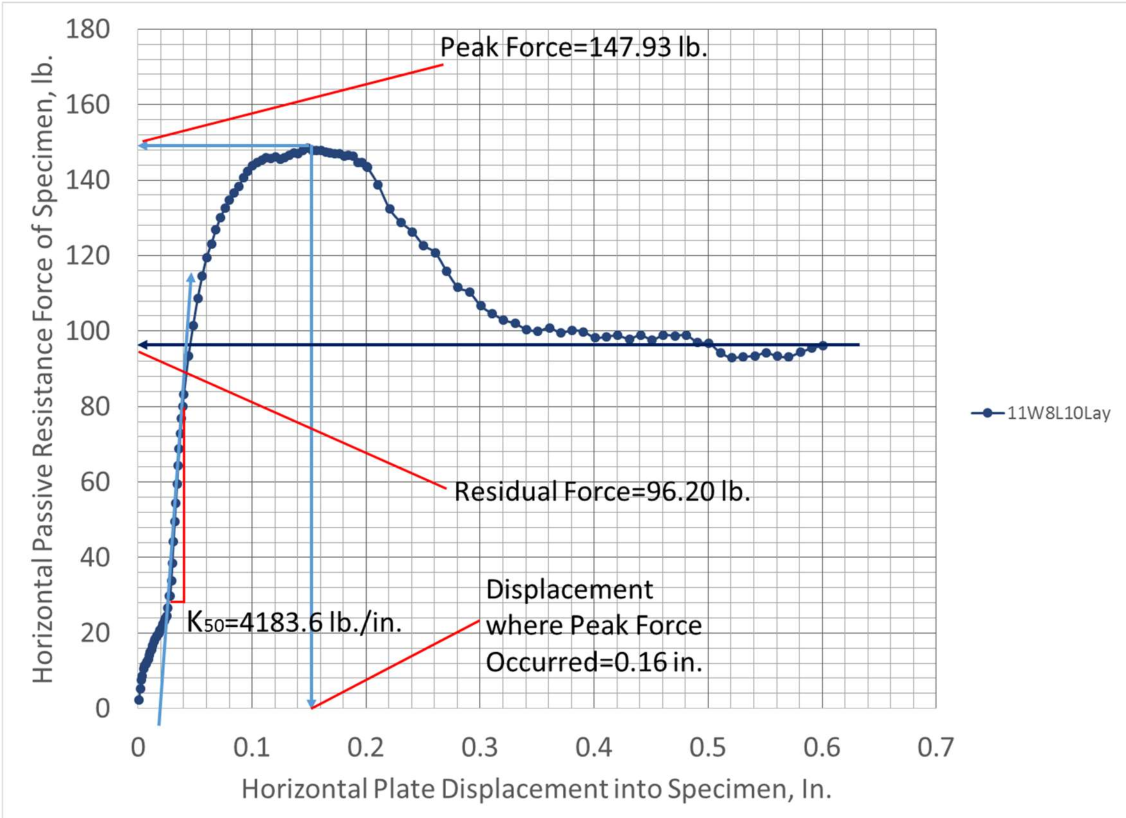

Figure 494: Load-Displacement Plot of Test 11W8L10Lay

D.13 Load-Displacement Plot of Test 11W8L10Lay2

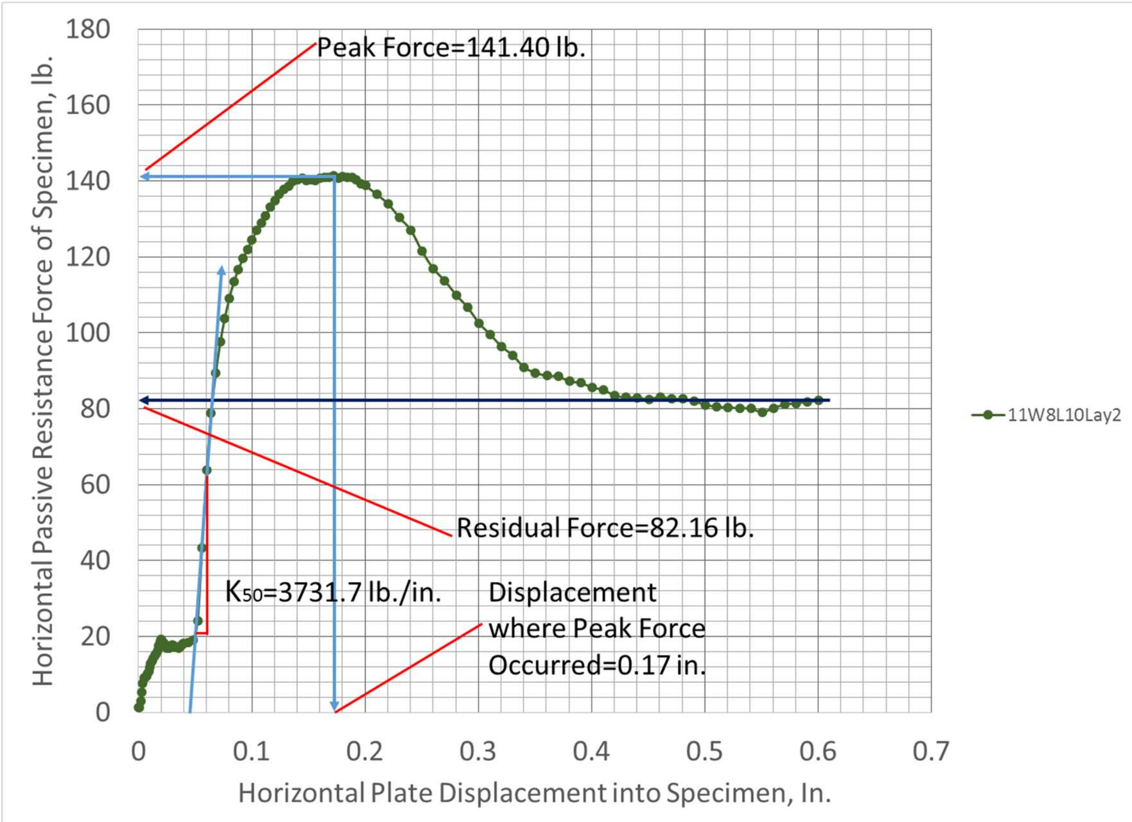

Figure 495: Load-Displacement Plot of Test 11W8L10Lay2

D.14 Load-Displacement Plot of Test 11W11L5Lay

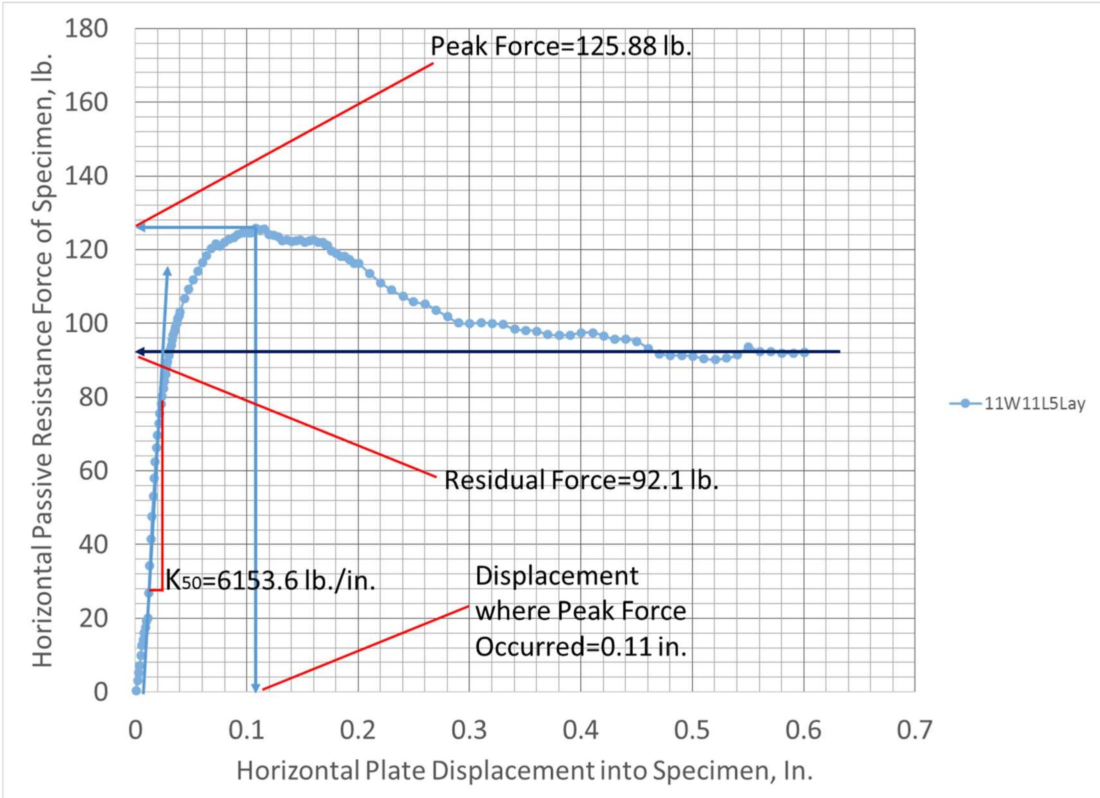

Figure 496: Load-Displacement Plot of Test 11W11L5Lay

D.15 Load-Displacement Plot of Test 11W11L5Lay2

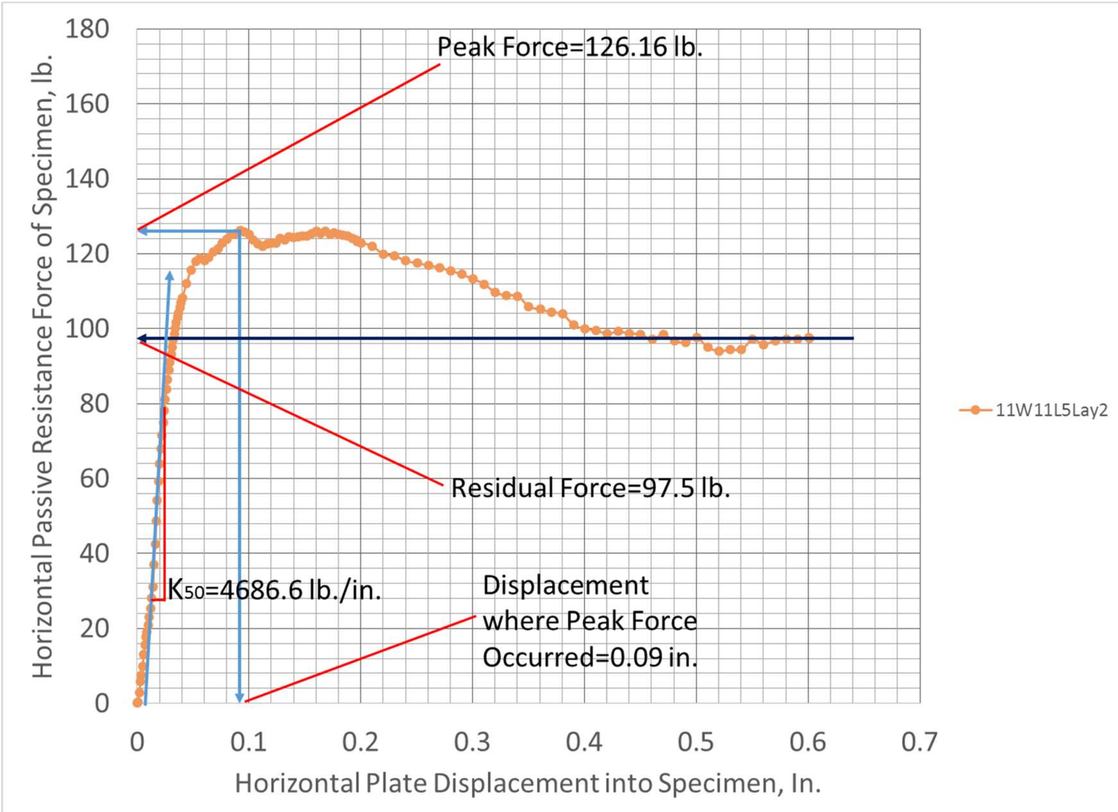

Figure 497: Load-Displacement Plot of Test 11W11L5Lay2

D.16 Load-Displacement Plot of Test 11W11L10Lay

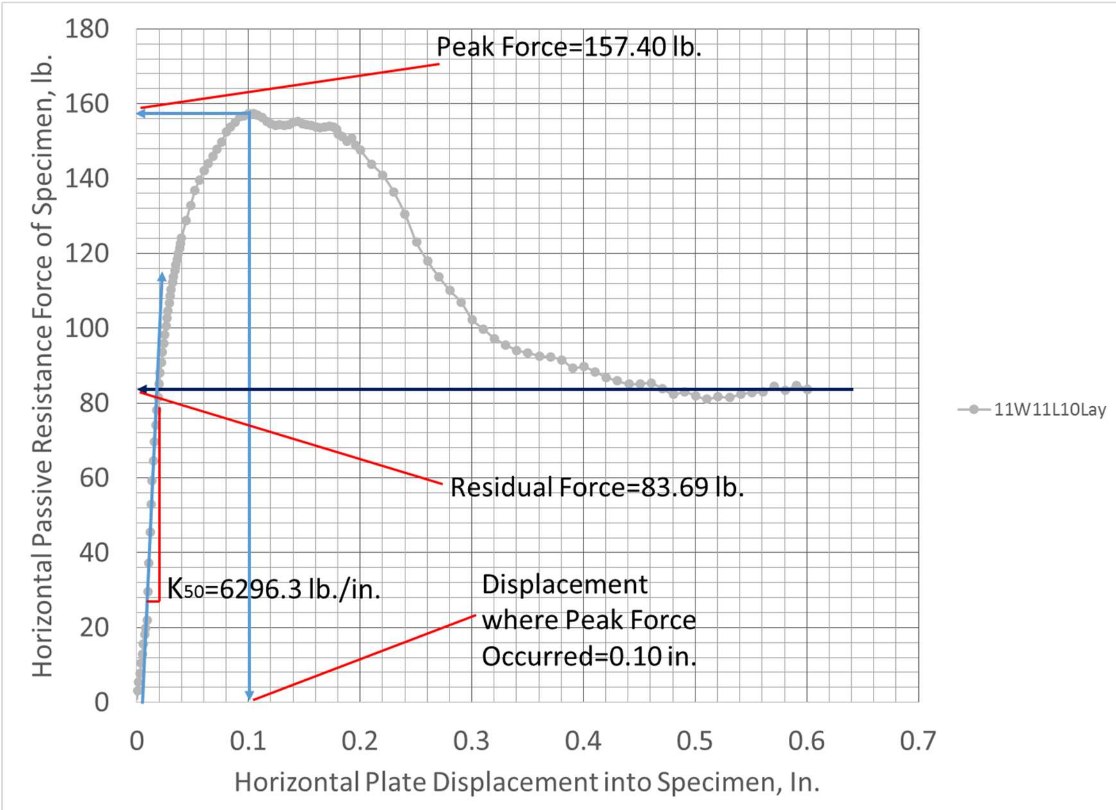

Figure 498: Load-Displacement Plot of Test 11W11L10Lay

D.17 Load-Displacement Plot of Test 11W11L10Lay2

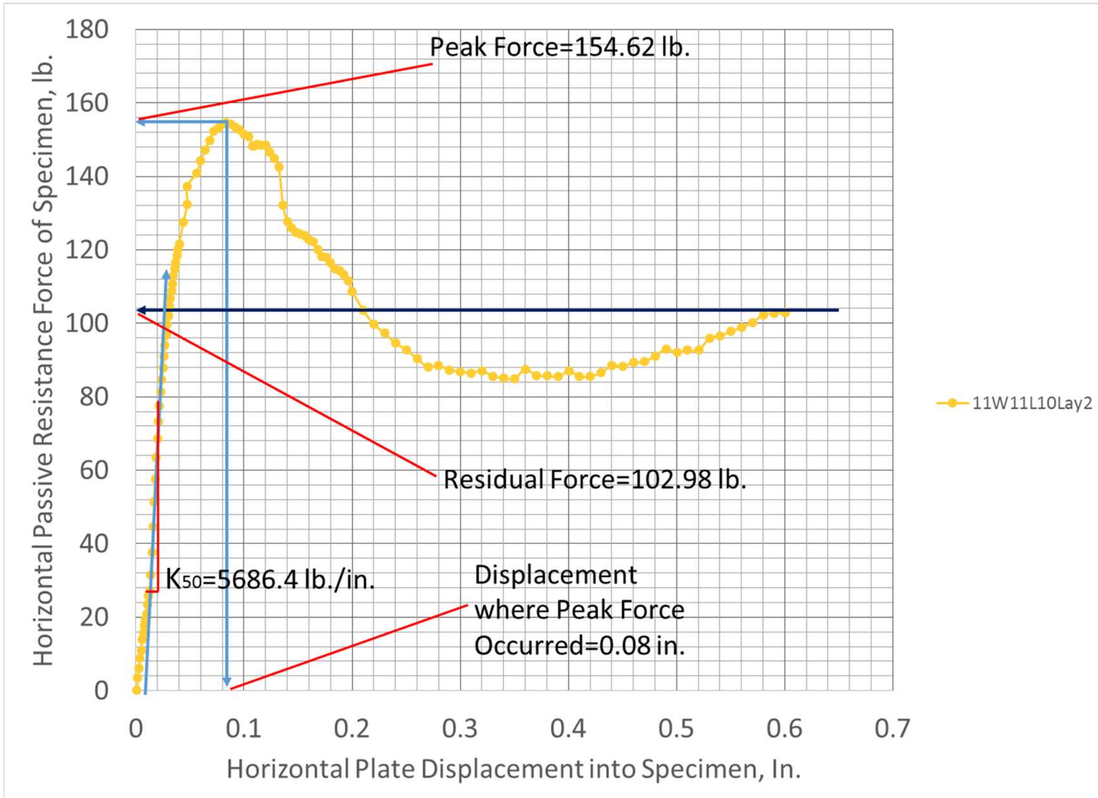

Figure 499: Load-Displacement Plot of Test 11W11L10Lay2

D.18 Load-Displacement Plot of Test PW8L5Lay

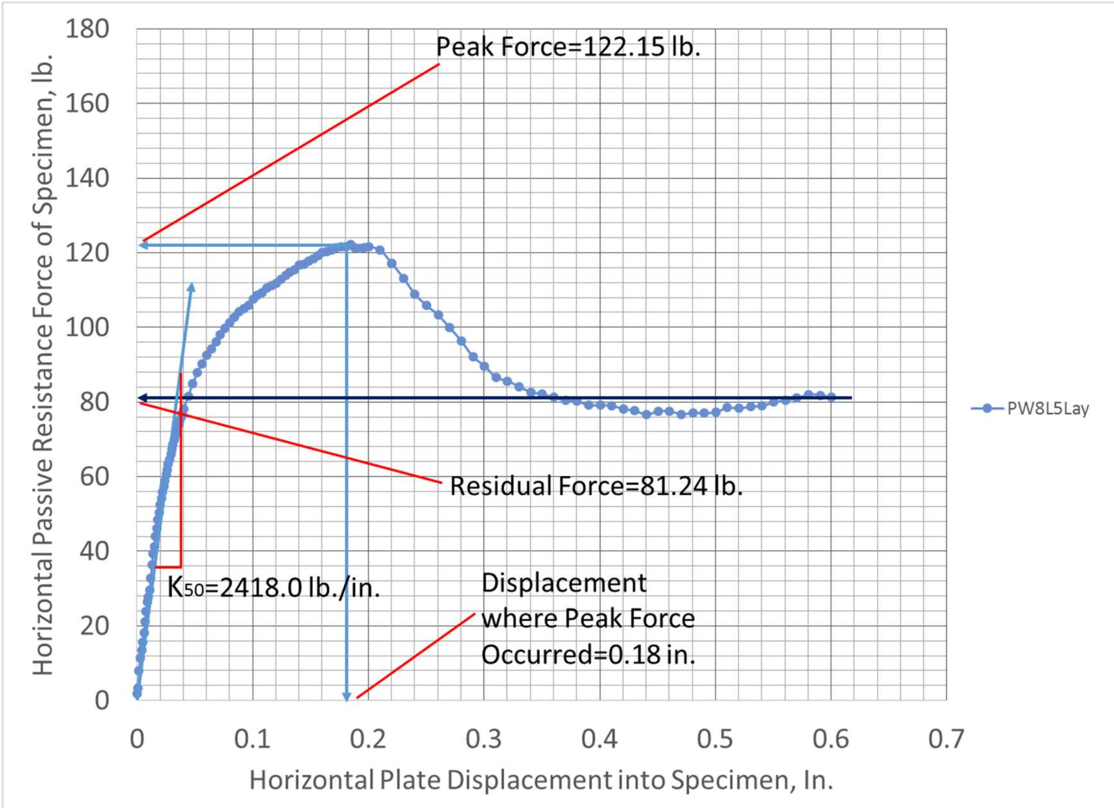

Figure 500: Load-Displacement Plot of Test PW8L5Lay

D.19 Load-Displacement Plot of Test PW8L5Lay2

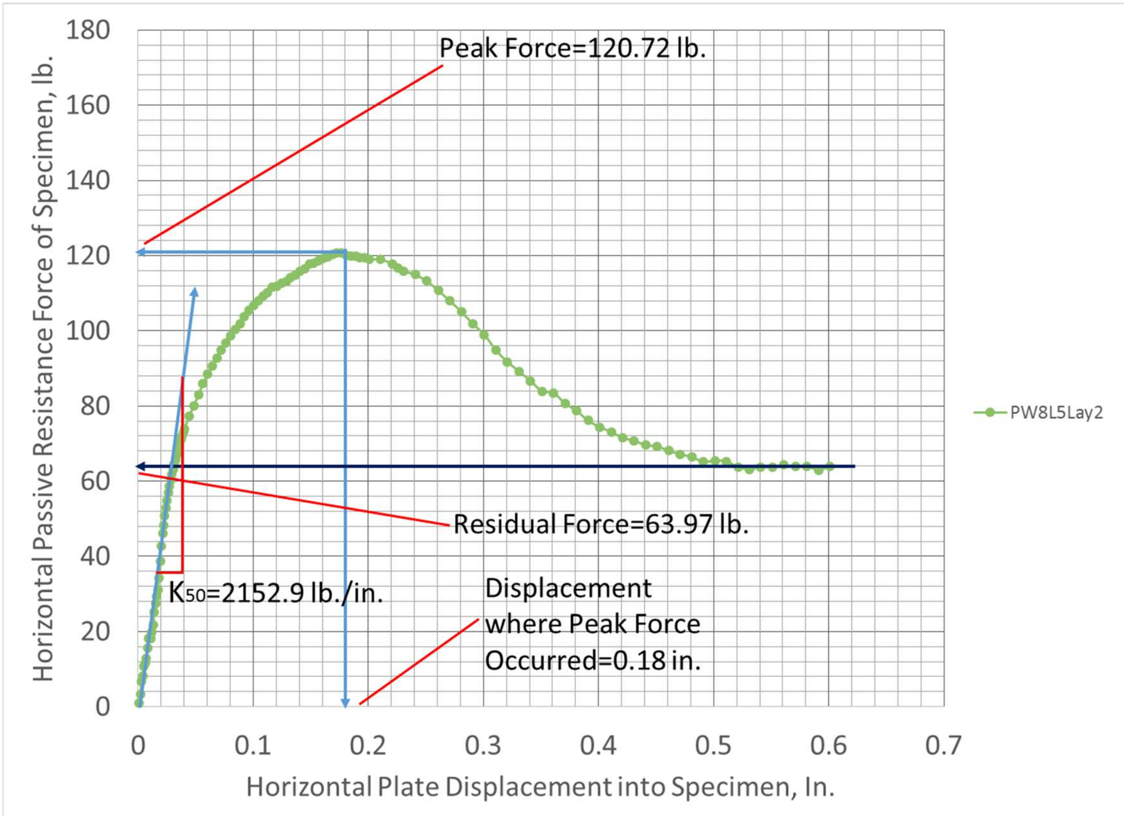

Figure 501: Load-Displacement Plot of Test PW8L5Lay2

D.20 Load-Displacement Plot of Test PW8L10Lay

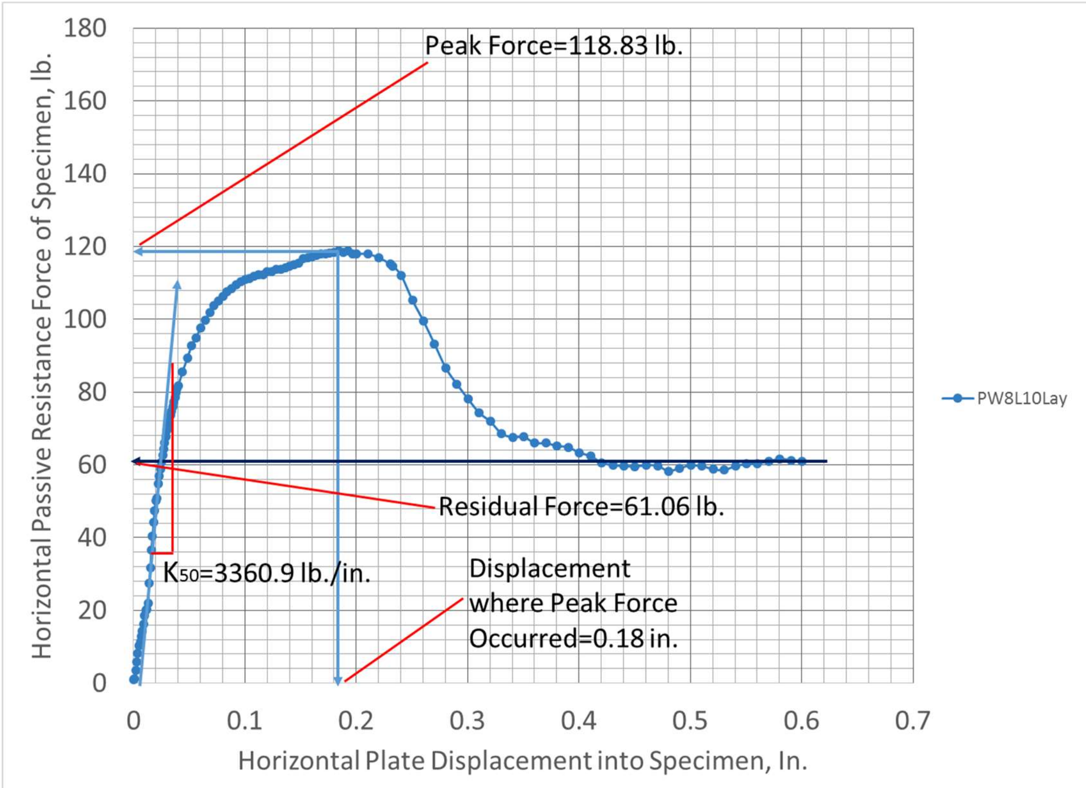

Figure 502: Load-Displacement Plot of Test PW8L10Lay

D.21 Load-Displacement Plot of Test PW8L10Lay2

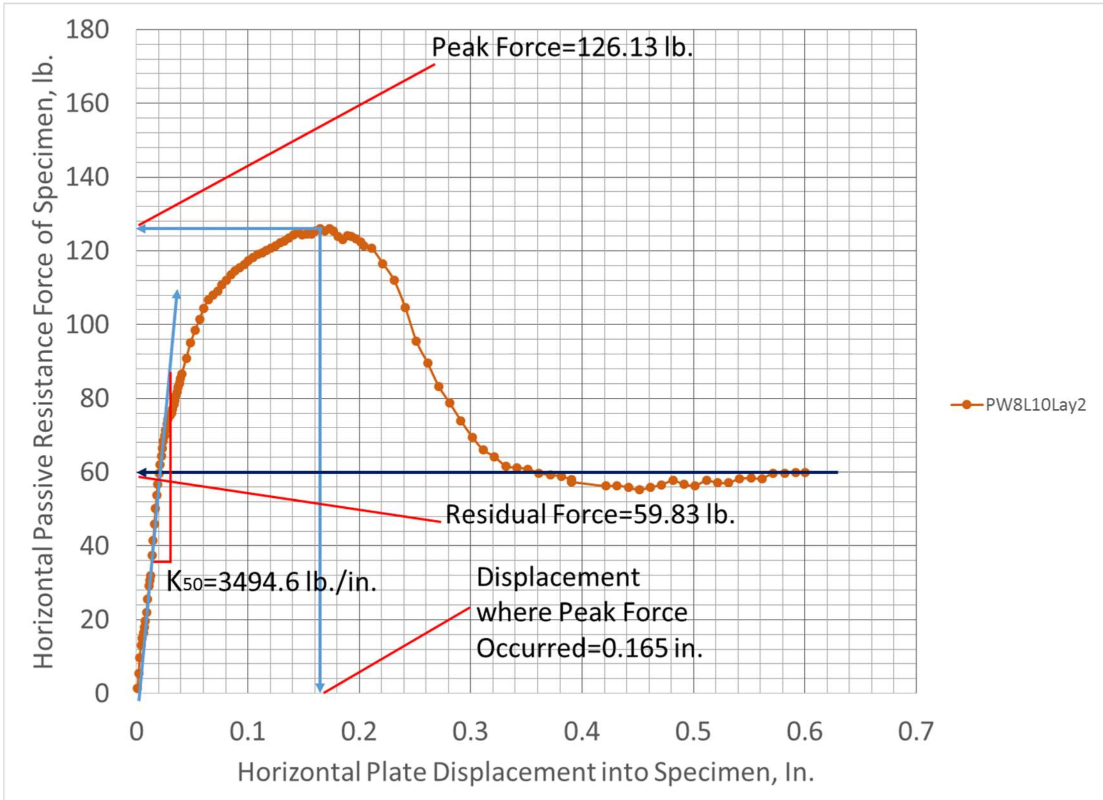

Figure 503: Load-Displacement Plot of Test PW8L10Lay2

D.22 Load-Displacement Plot of Test PW11L5Lay

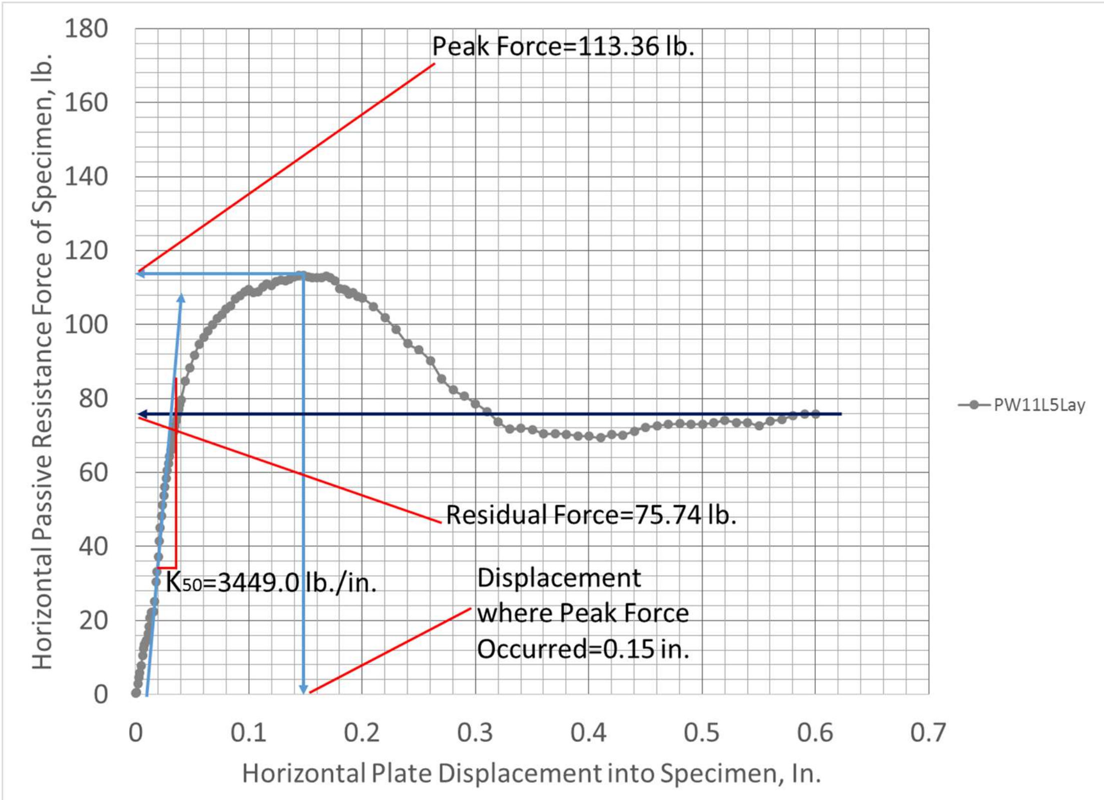

Figure 504: Load-Displacement Plot of Test PW11L5Lay

D.23 Load-Displacement Plot of Test PW11L5Lay2

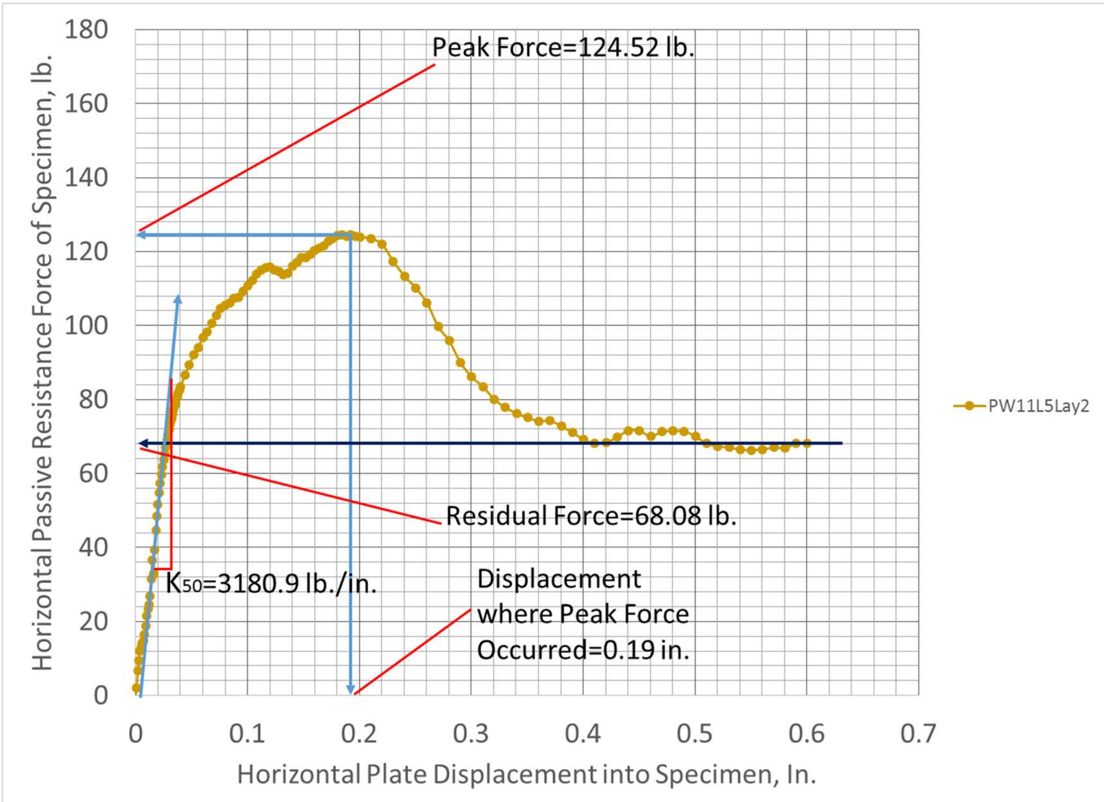

Figure 505: Load-Displacement Plot of Test PW11L5Lay2

D.24 Load-Displacement Plot of Test PW11L10Lay

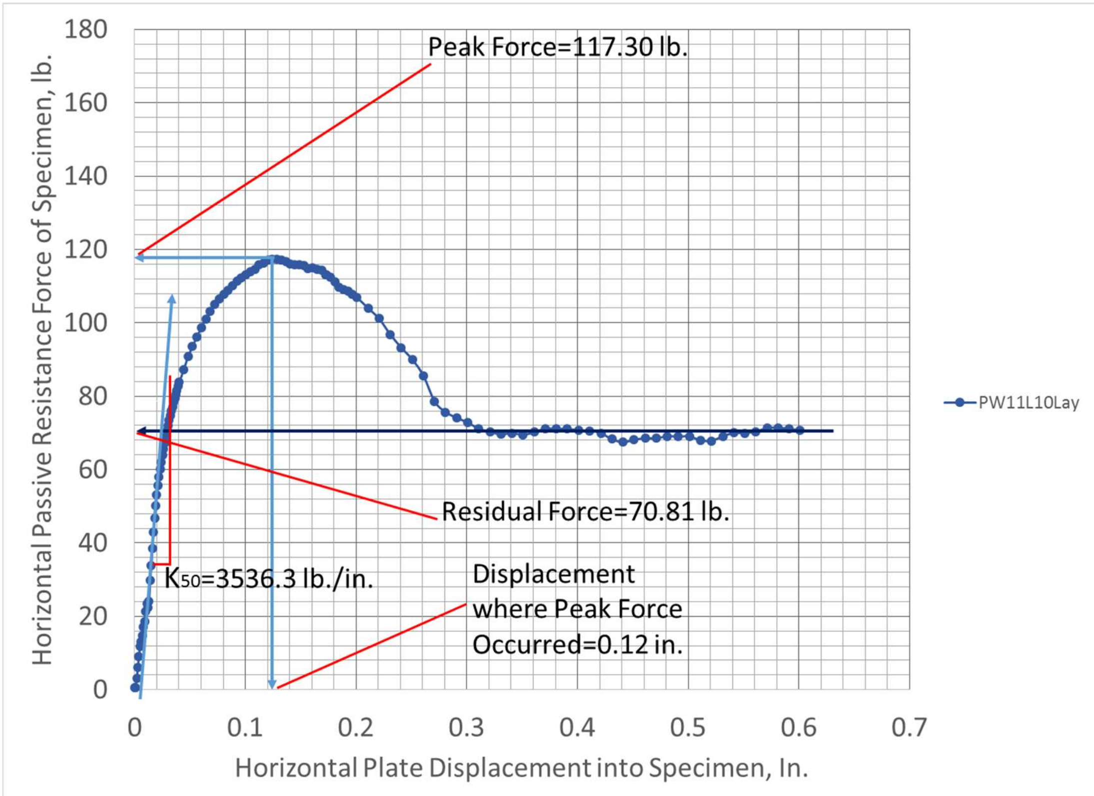

Figure 506: Load-Displacement Plot of Test PW11L10Lay

D.25 Load-Displacement Plot of Test PW11L10Lay2

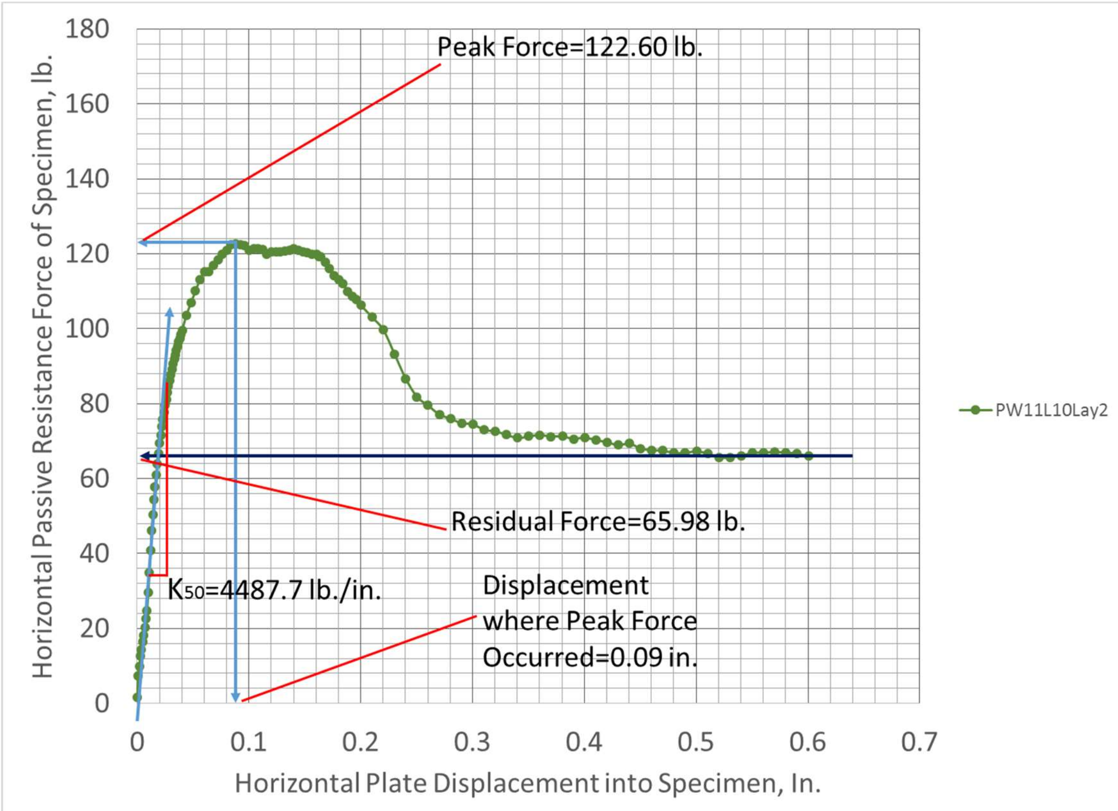

Figure 507: Load-Displacement Plot of Test PW11L10Lay2

D.26 Load-Displacement Plot of Test NR1

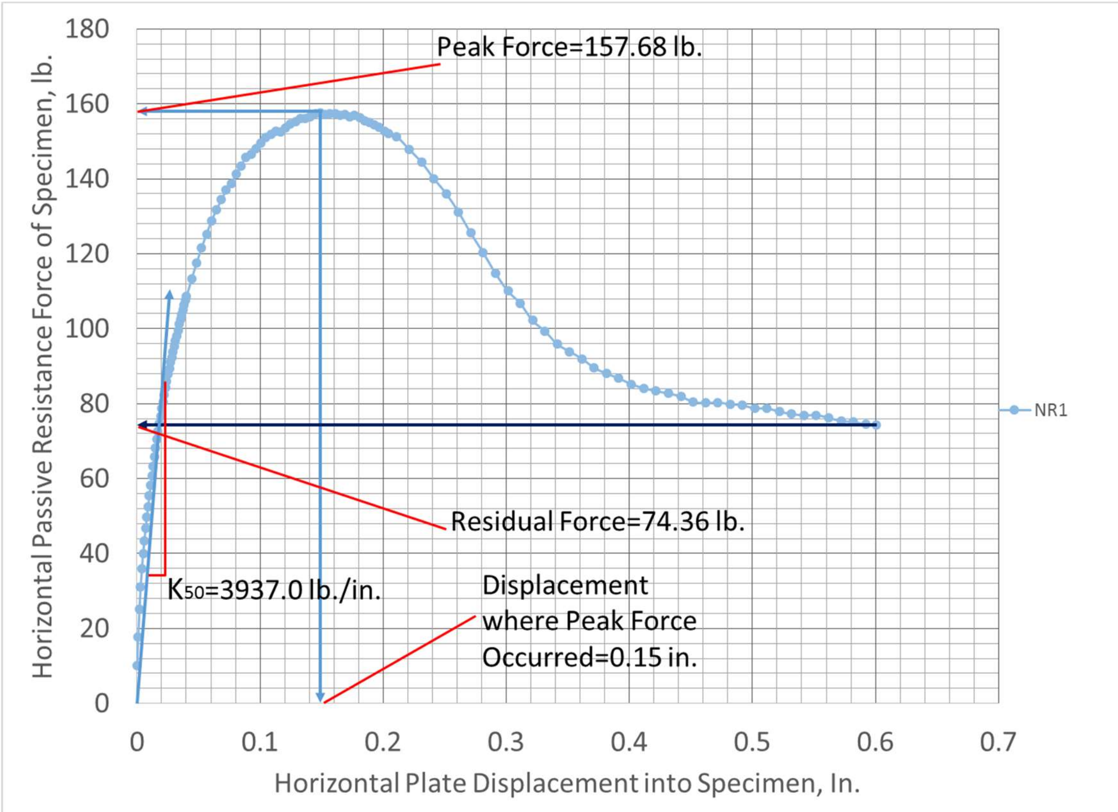

Figure 508: Load-Displacement Plot of Test NR1

D.27 Load-Displacement Plot of Test NR2

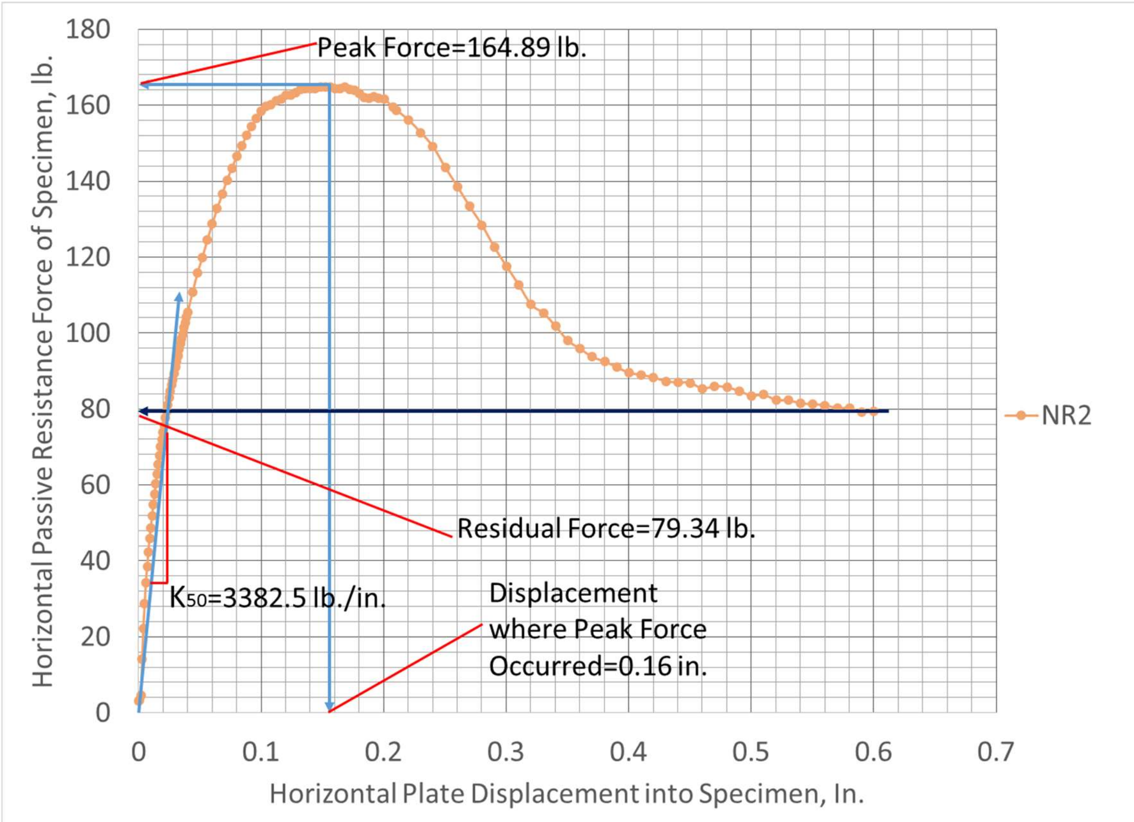

Figure 509: Load-Displacement Plot of Test NR2

D.28 Load-Displacement Plot of Test 8W8L5Lay3 (Painted)

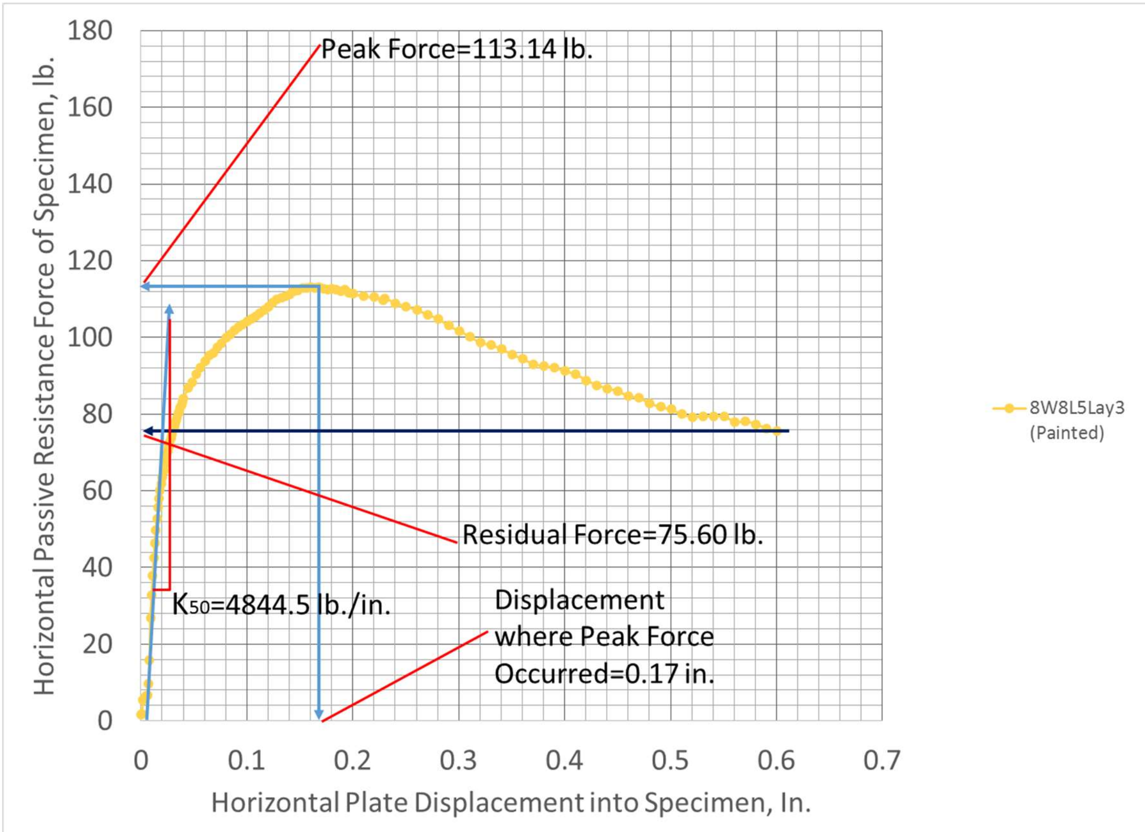

Figure 510: Load-Displacement Plot of Test 8W8L5Lay3 (Painted)

D.29 Load-Displacement Plot of Test 8W8L10Lay3 (Painted)

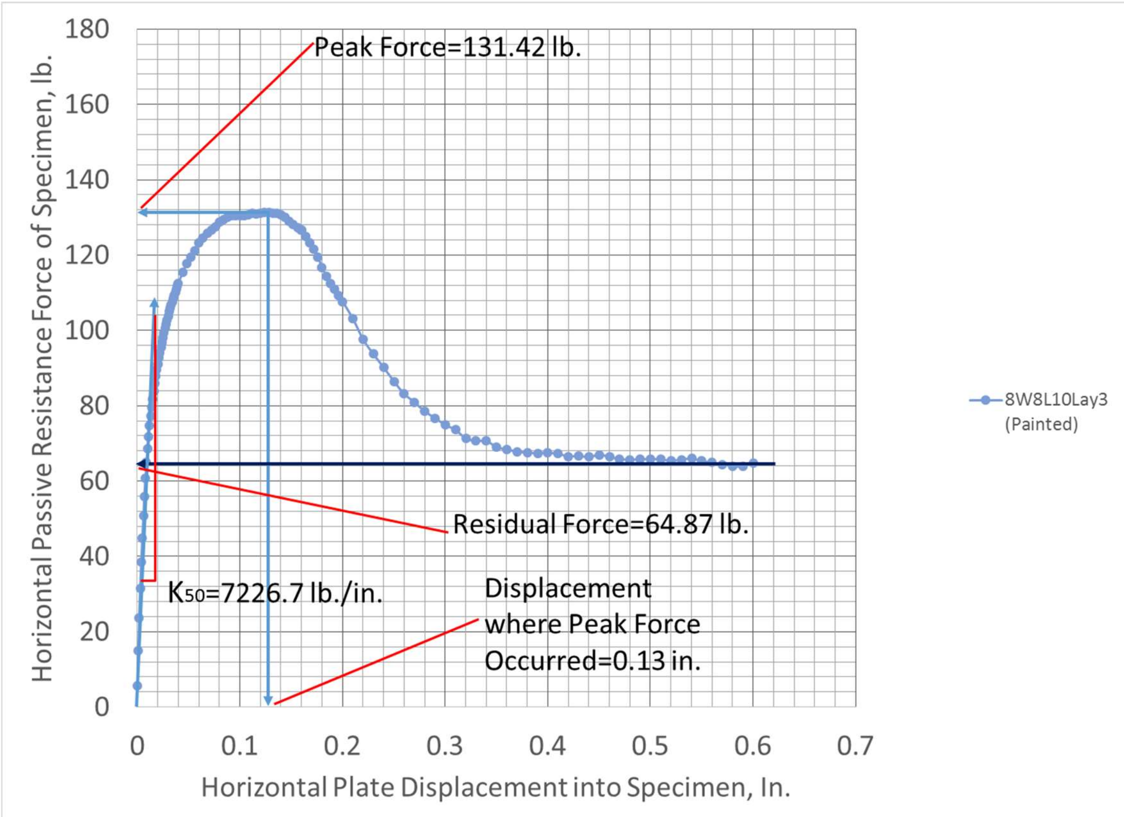

Figure 511: Load-Displacement Plot of Test 8W8L10Lay3 (Painted)

D.30 Load-Displacement Plot of Test 8W11L5Lay3 (Painted)

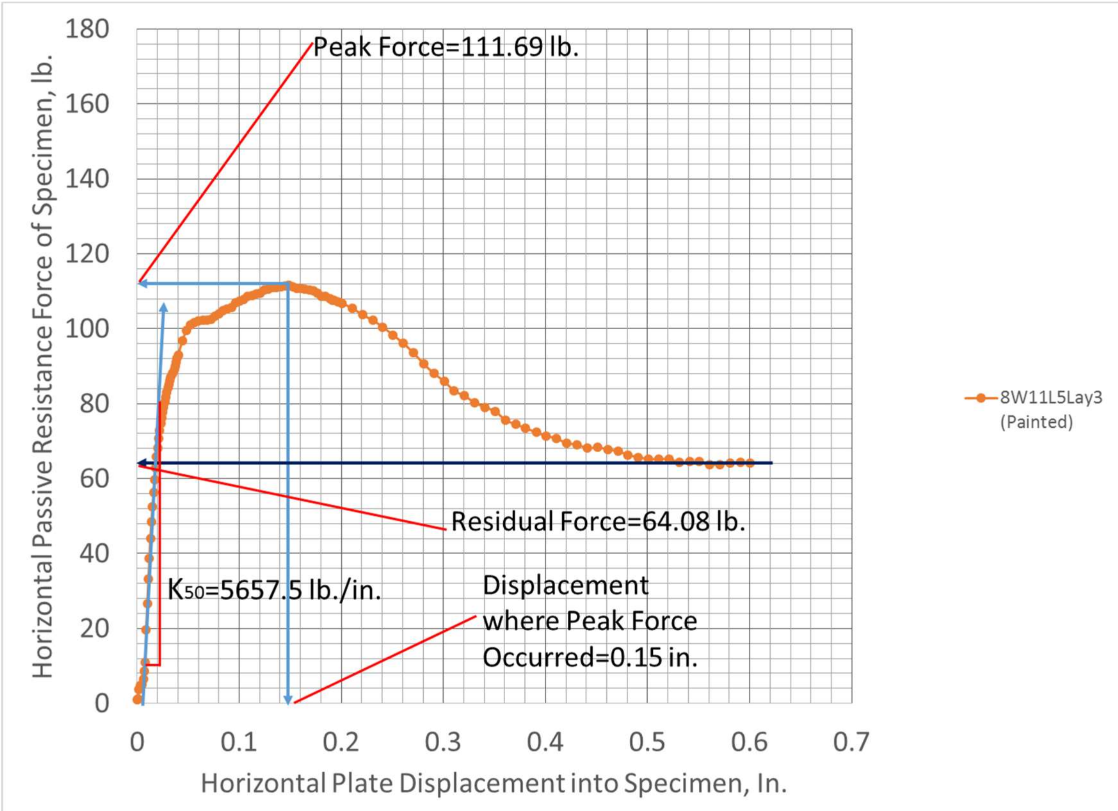

Figure 512: Load-Displacement Plot of Test 8W11L5Lay3 (Painted)

D.31 Load-Displacement Plot of Test 8W11L10Lay3 (Painted)

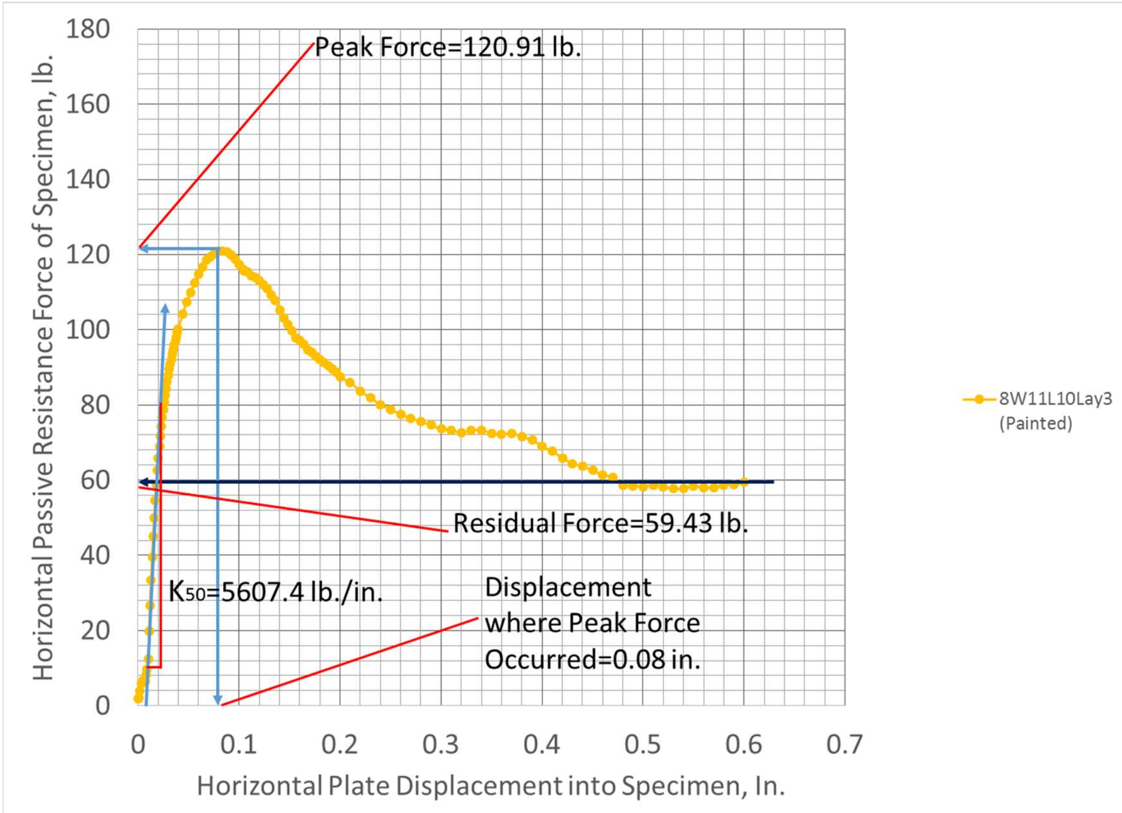

Figure 513: Load-Displacement Plot of Test 8W11L10Lay3 (Painted)

D.32 Load-Displacement Plot of Test 11W8L5Lay3 (Painted)

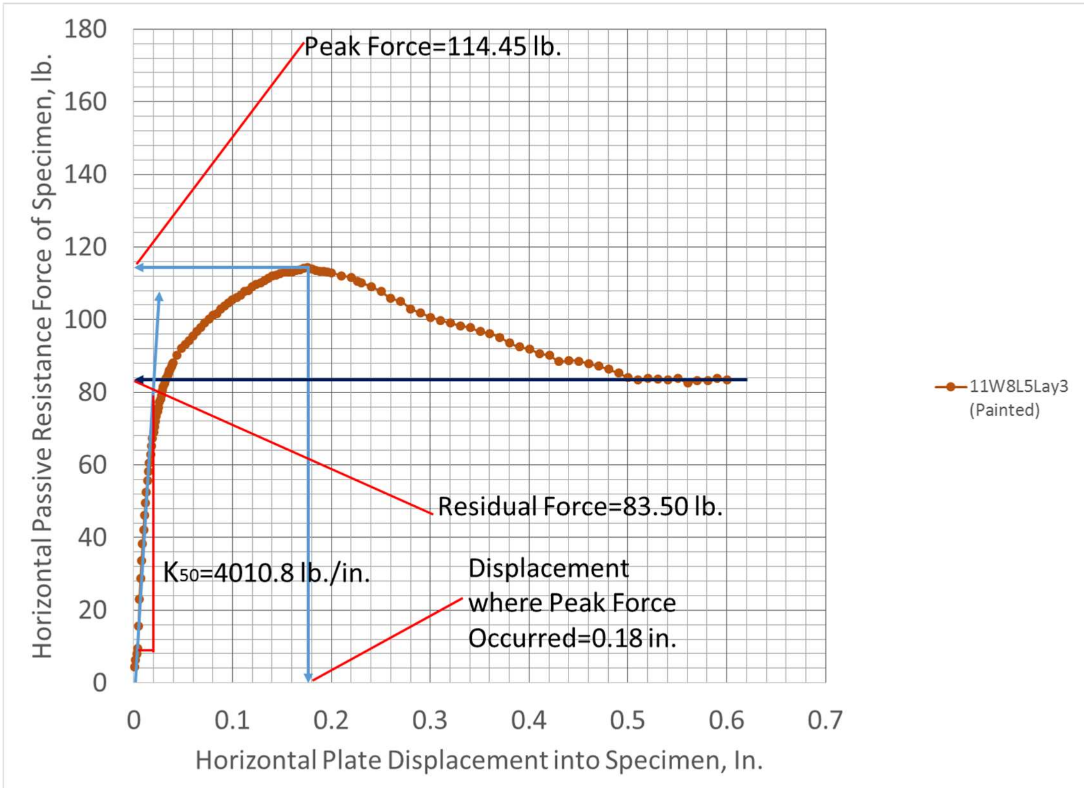

Figure 514: Load-Displacement Plot of Test 11W8L5Lay3 (Painted)

D.33 Load-Displacement Plot of Test 11W8L10Lay3 (Painted)

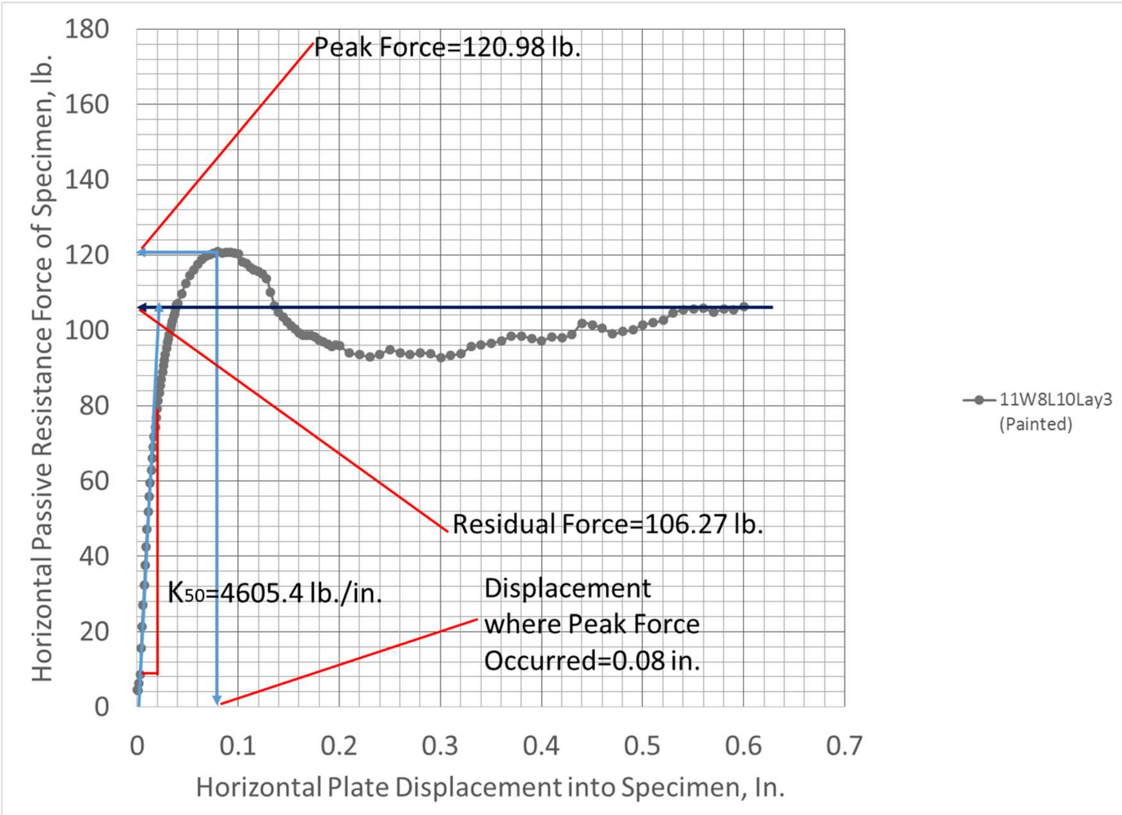

Figure 515: Load-Displacement Plot of Test 11W8L10Lay3 (Painted)

D.34 Load-Displacement Plot of Test 11W11L5Lay3 (Painted)

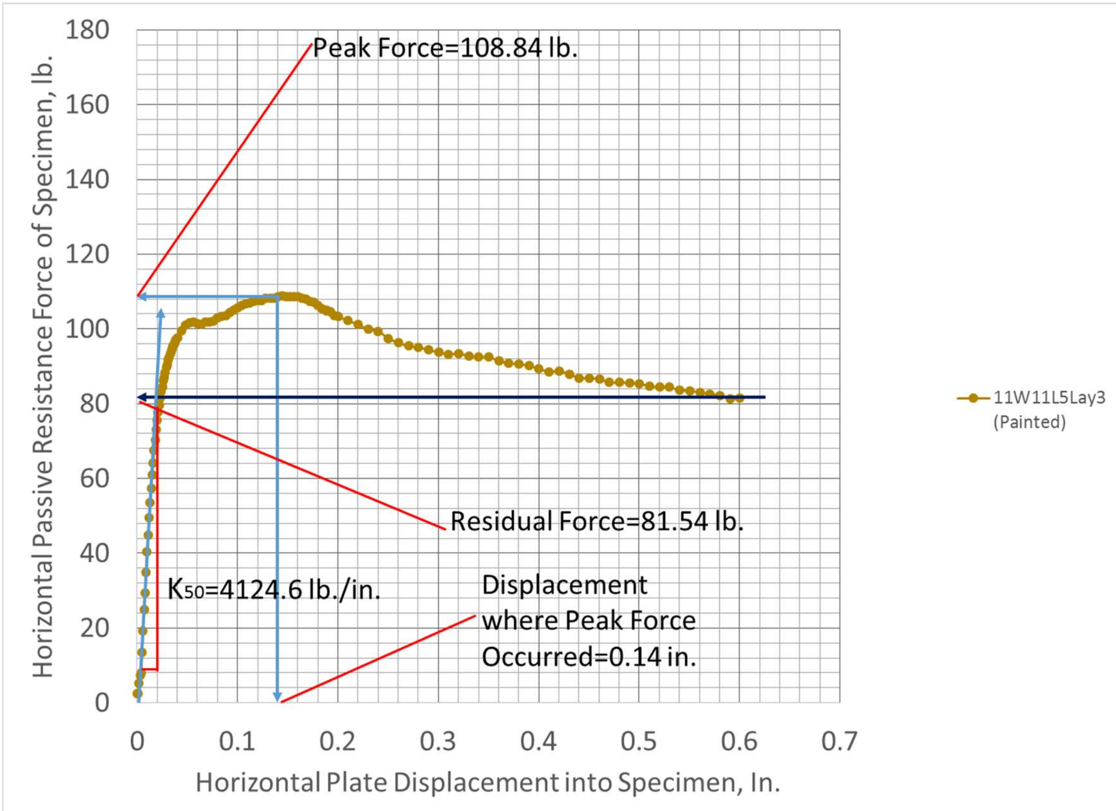

Figure 516: Load-Displacement Plot of Test 11W11L5Lay3 (Painted)

D.35 Load-Displacement Plot of Test 11W11L10Lay3 (Painted)

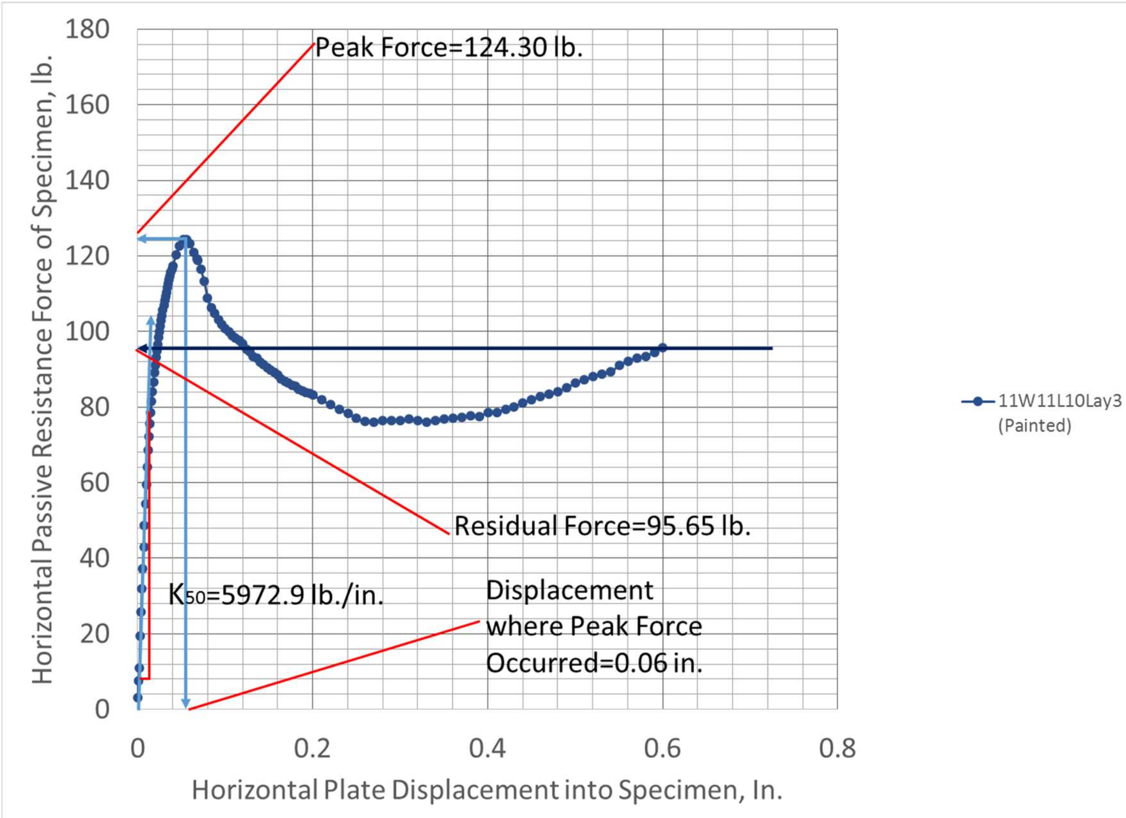

Figure 517: Load-Displacement Plot of Test 11W11L10Lay3 (Painted)

D.36 Load-Displacement Plot of Test PW8L5Lay3 (Painted)

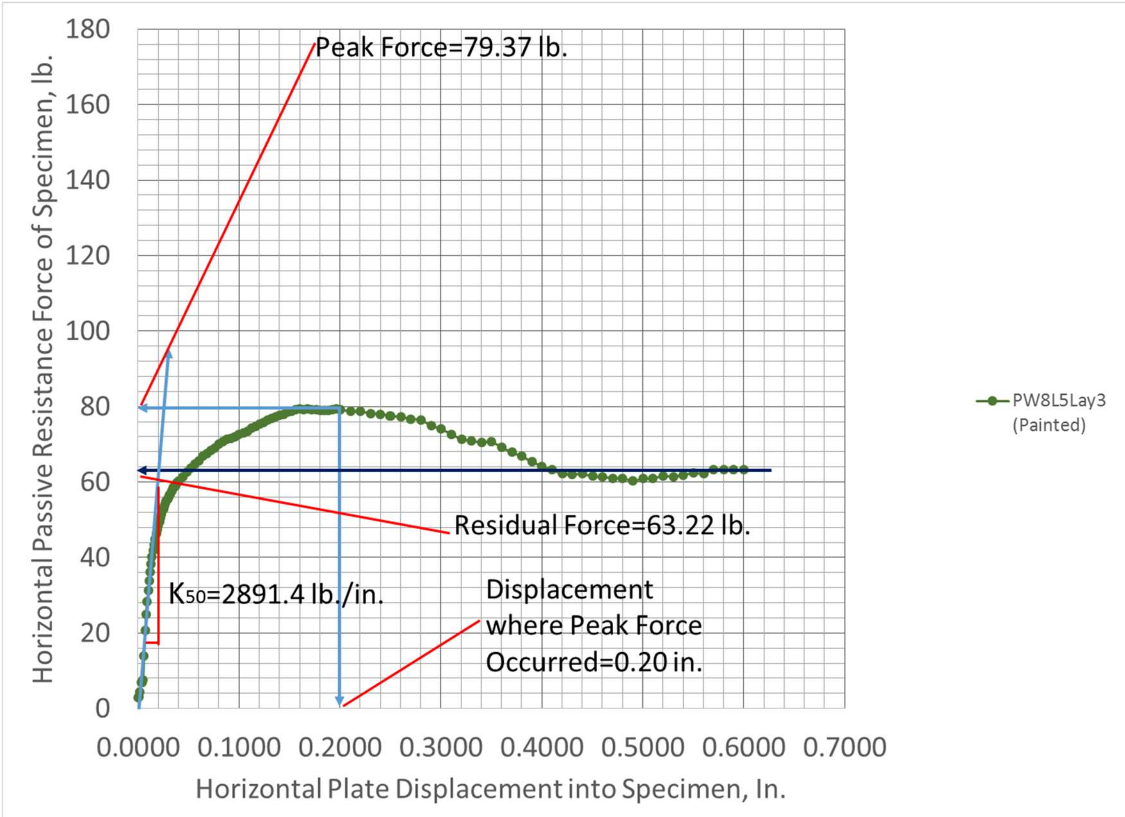

Figure 518: Load-Displacement Plot of Test PW8L5Lay3 (Painted)

D.37 Load-Displacement Plot of Test PW8L10Lay3 (Painted)

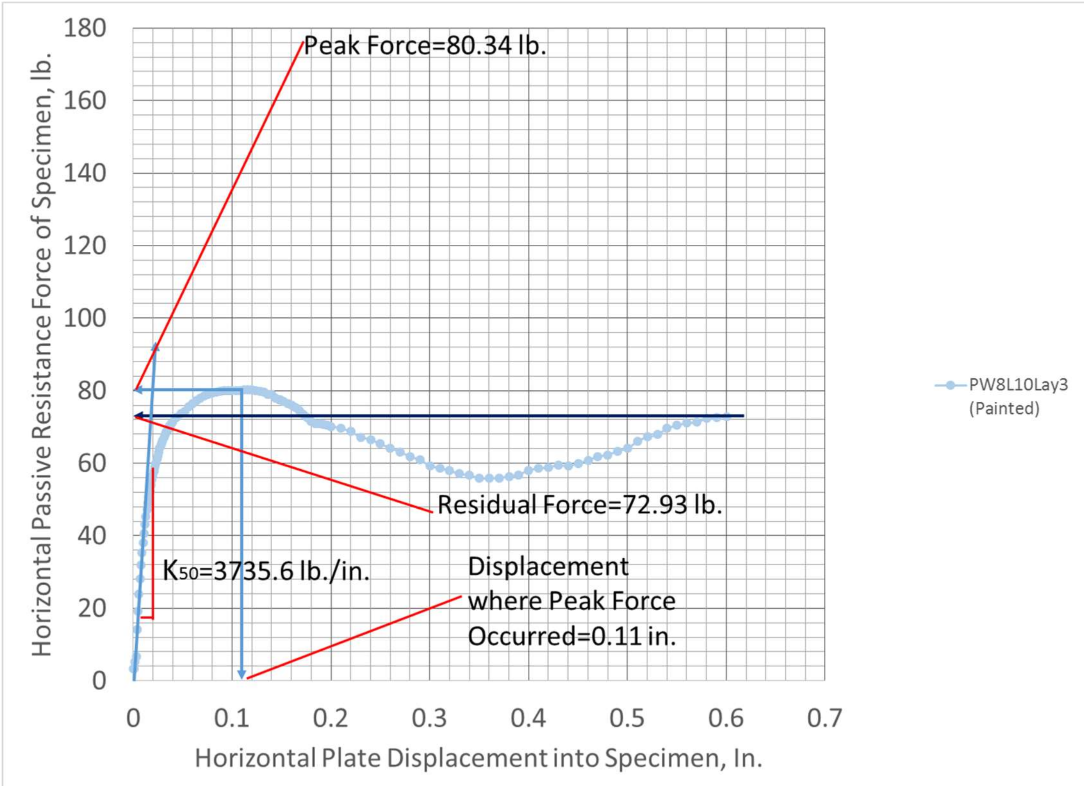

Figure 519: Load-Displacement Plot of Test PW8L10Lay3 (Painted)

D.38 Load-Displacement Plot of Test PW11L5Lay3 (Painted)

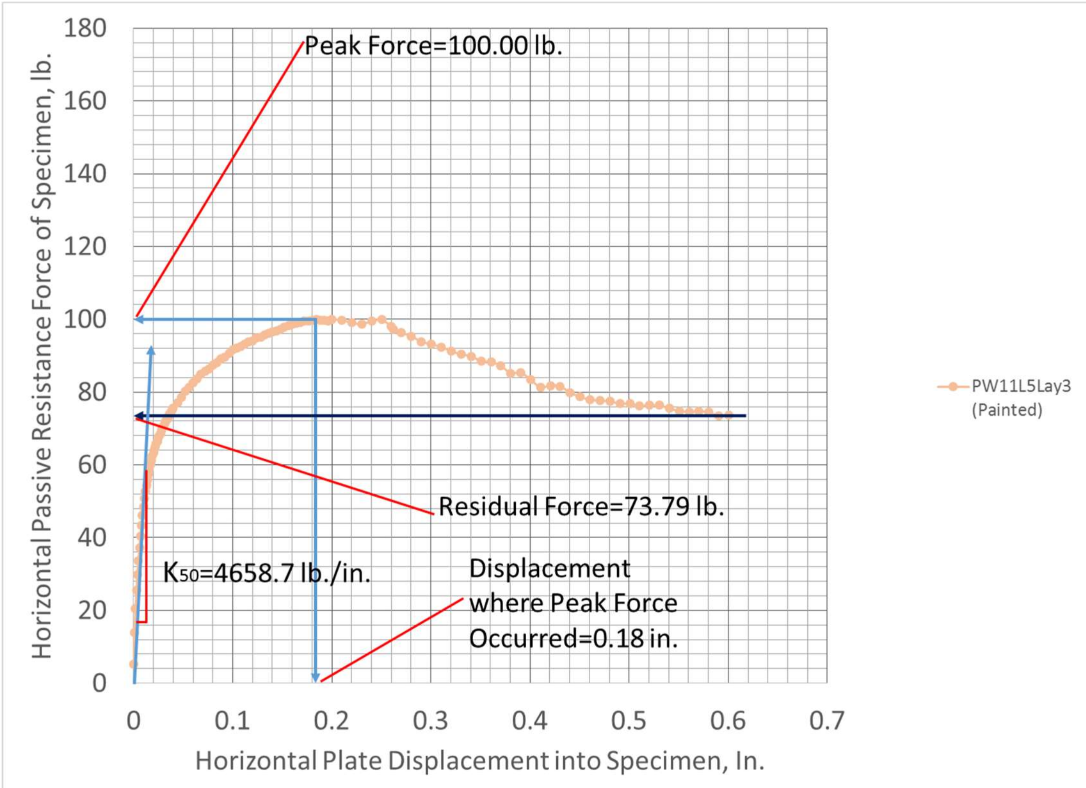

Figure 520: Load-Displacement Plot of Test PW11L5Lay3 (Painted)

D.39 Load-Displacement Plot of Test PW11L10Lay3 (Painted)

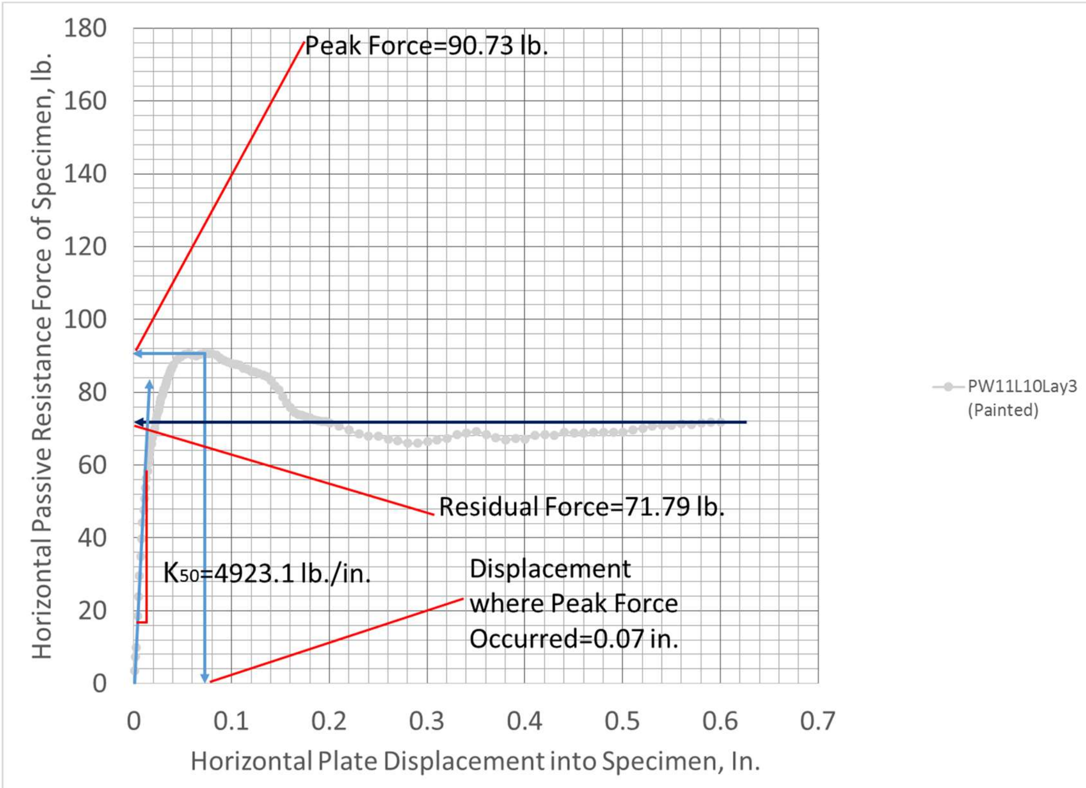

Figure 521: Load-Displacement Plot of Test PW11L10Lay3 (Painted)

D.40 Load-Displacement Plot of Test NR3 (Painted)

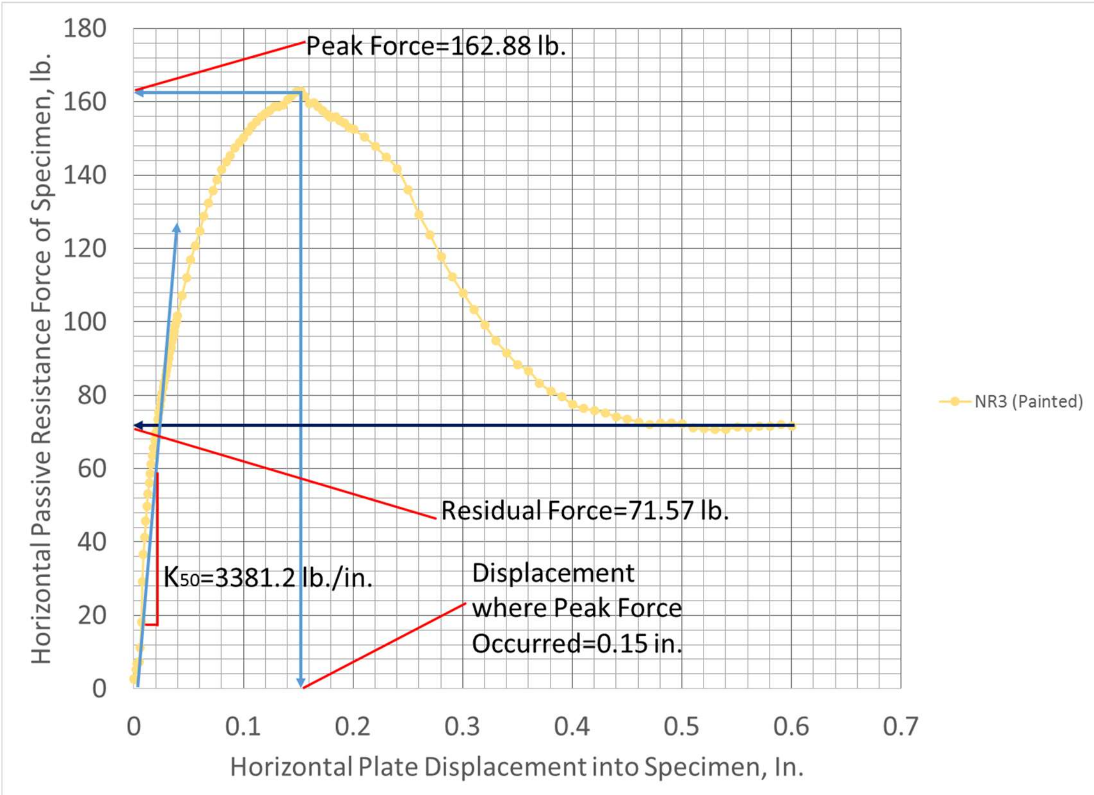

Figure 522: Load-Displacement Plot of Test NR3 (Painted)

APPENDIX E: ADJUSTED LOAD DISPLACEMENT PLOTS

E.1 Introduction

Load-displacement data were taken during laboratory testing using GeoJac software and were plotted using Microsoft Excel. Some tests required some small displacement before the plate was seated properly. This small displacement was subtracted from the following plots so that all tests begin to resist passive loading at zero displacement. Peak Force, Residual Force, displacement where the Peak Force occurred, and the stiffness at 50% of the Peak Force were determined using each plot and are shown on the plot.

E.2 Load-Displacement Plot of Test 8W8L5Lay

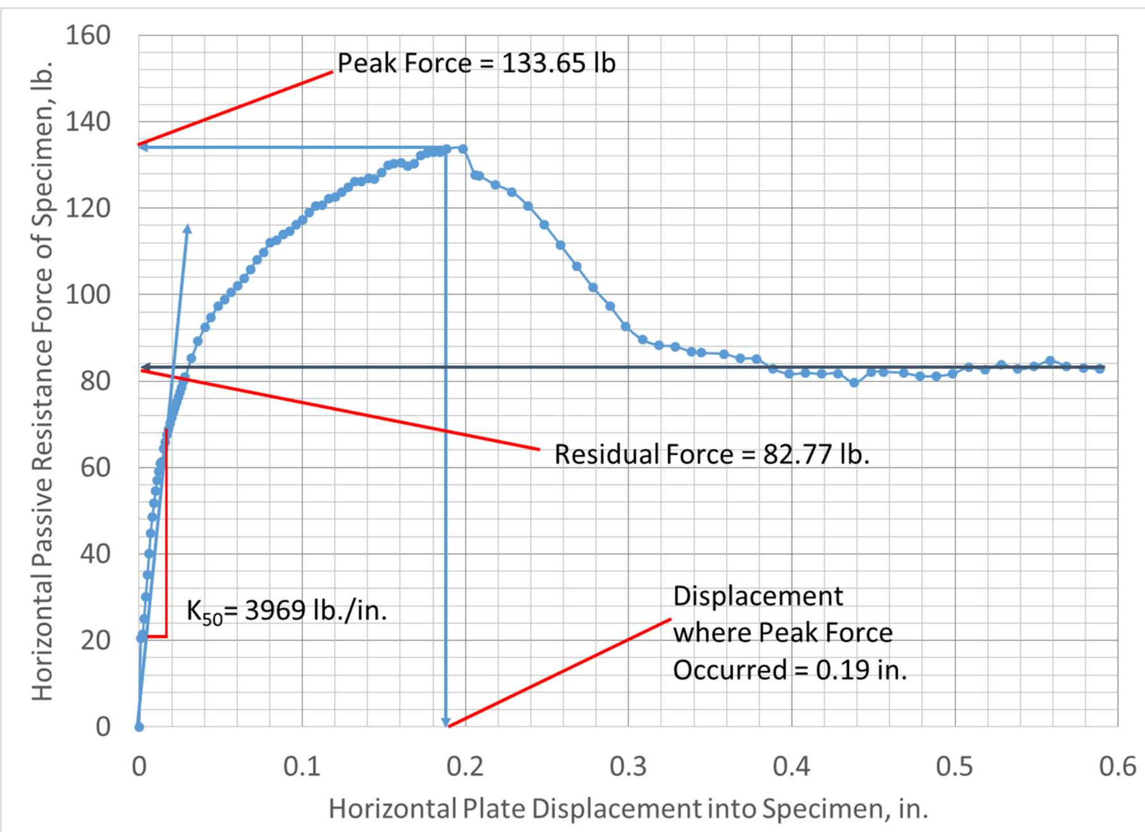

Figure 523: Load-Displacement Plot of Test 8W8L5Lay

E.3 Load-Displacement Plot of Test 8W8L5Lay2

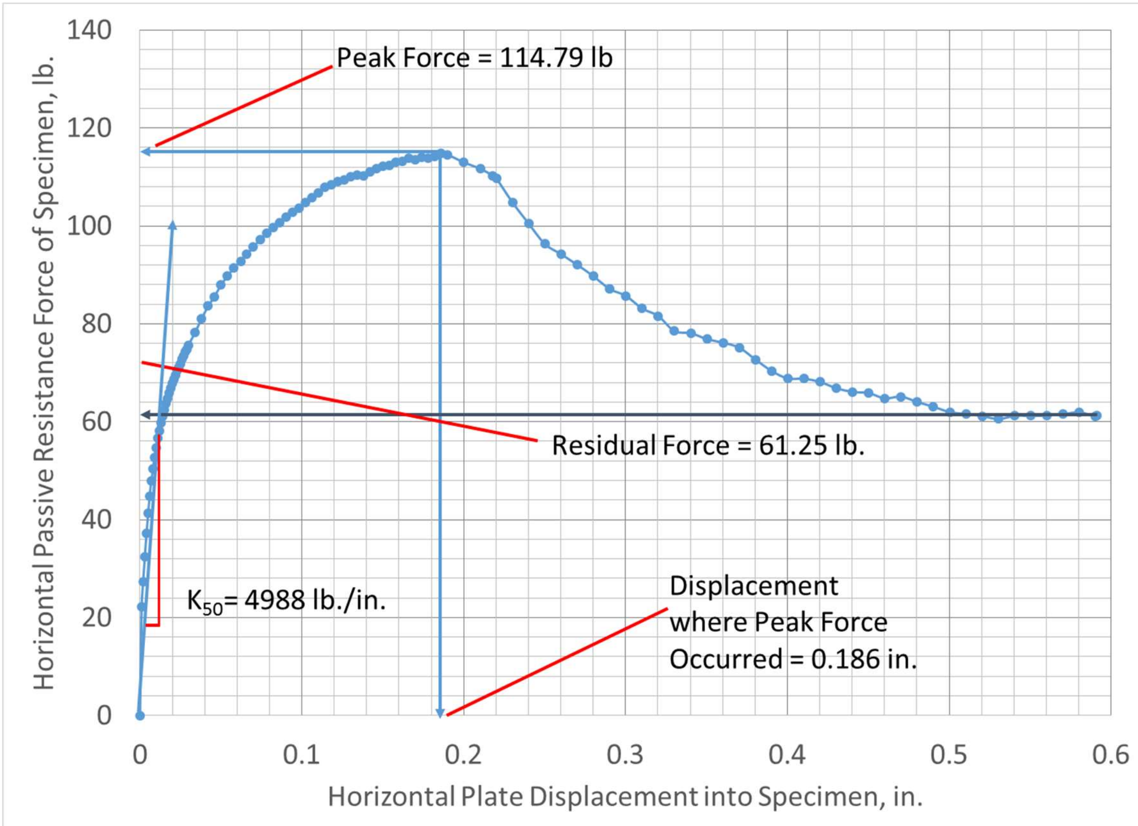

Figure 524: Load-Displacement Plot of Test 8W8L5Lay2

E.4 Load-Displacement Plot of Test 8W8L10Lay

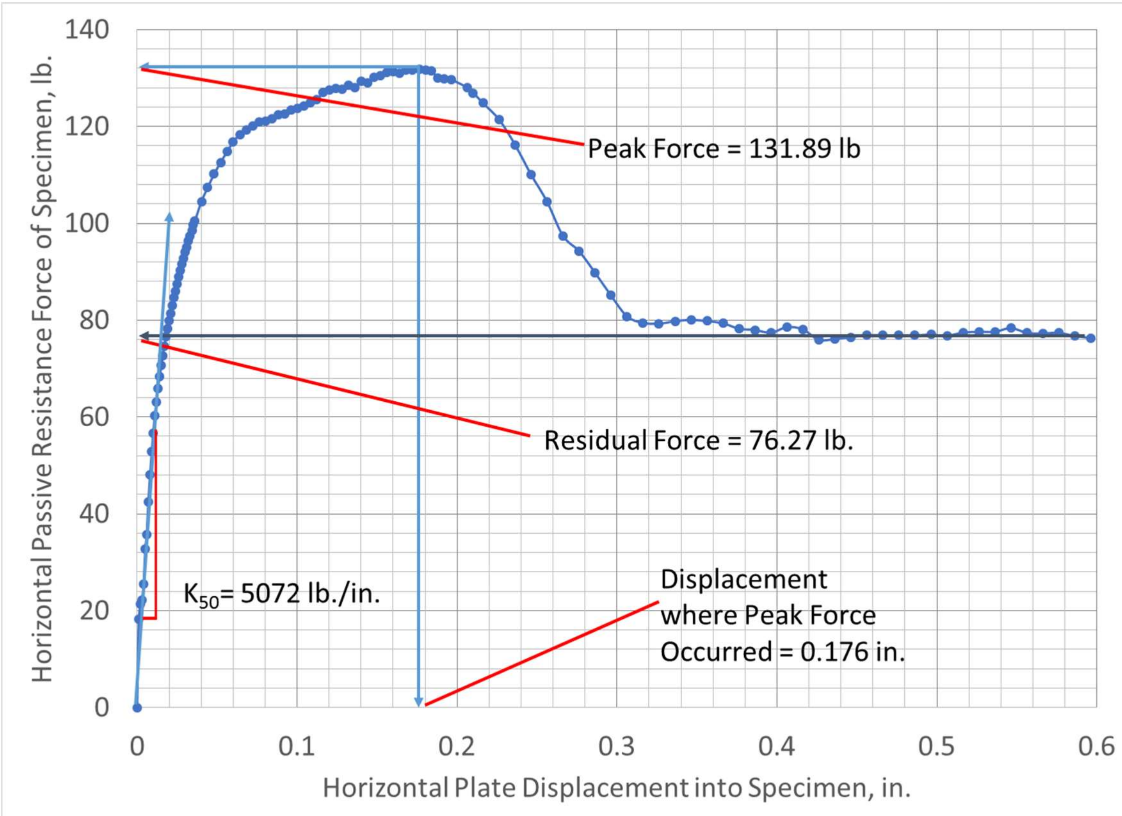

Figure 525: Load-Displacement Plot of Test 8W8L10Lay

E.5 Load-Displacement Plot of Test 8W8L10Lay2

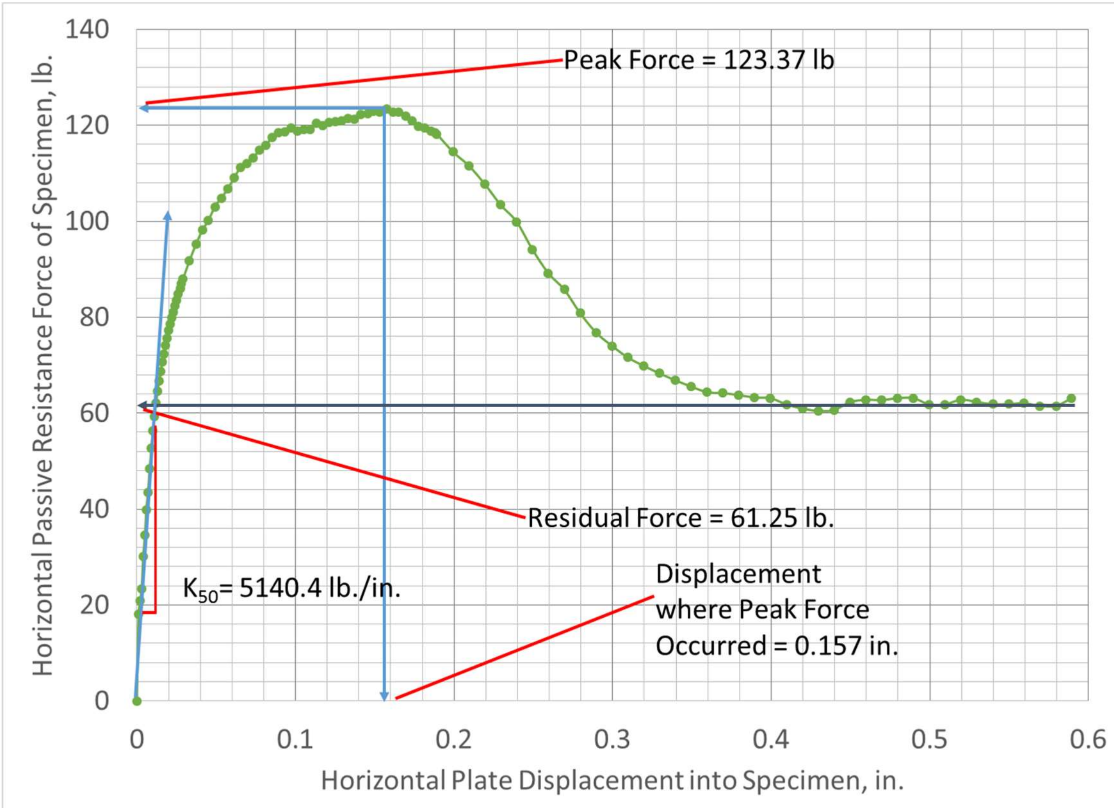

Figure 526: Load-Displacement Plot of Test 8W11L10Lay2

E.6 Load-Displacement Plot of Test 8W11L5Lay

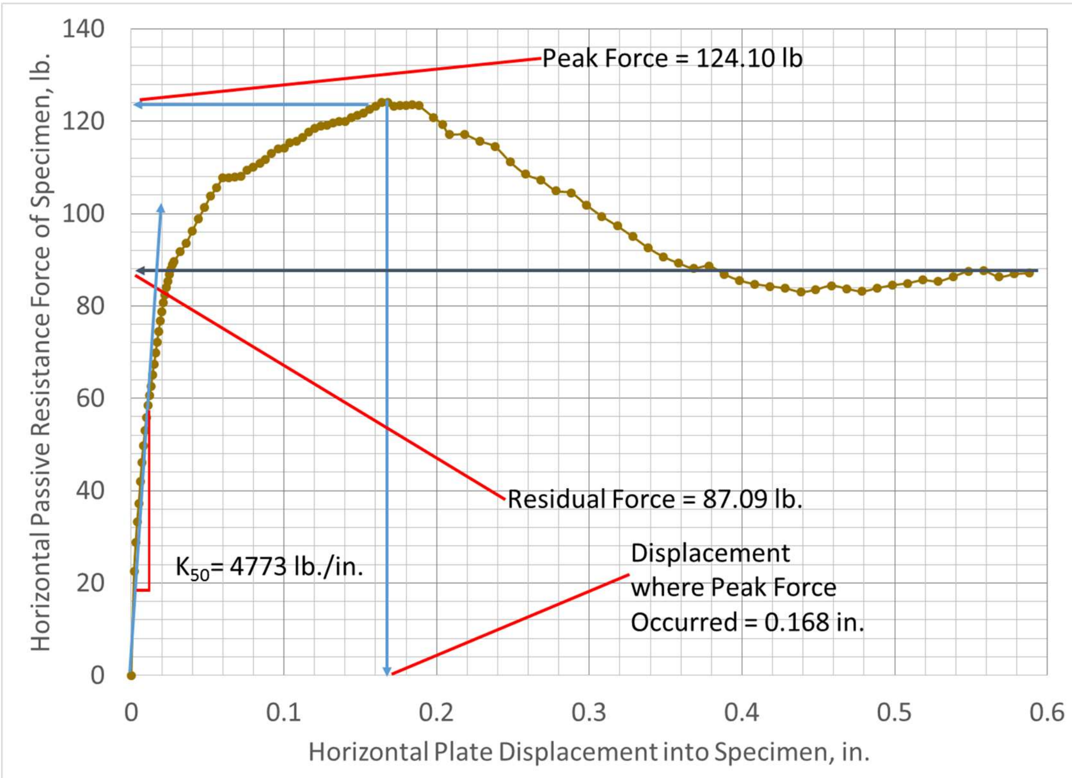

Figure 527: Load-Displacement Plot of Test 8W11L5Lay

E.7 Load-Displacement Plot of Test 8W11L5Lay2

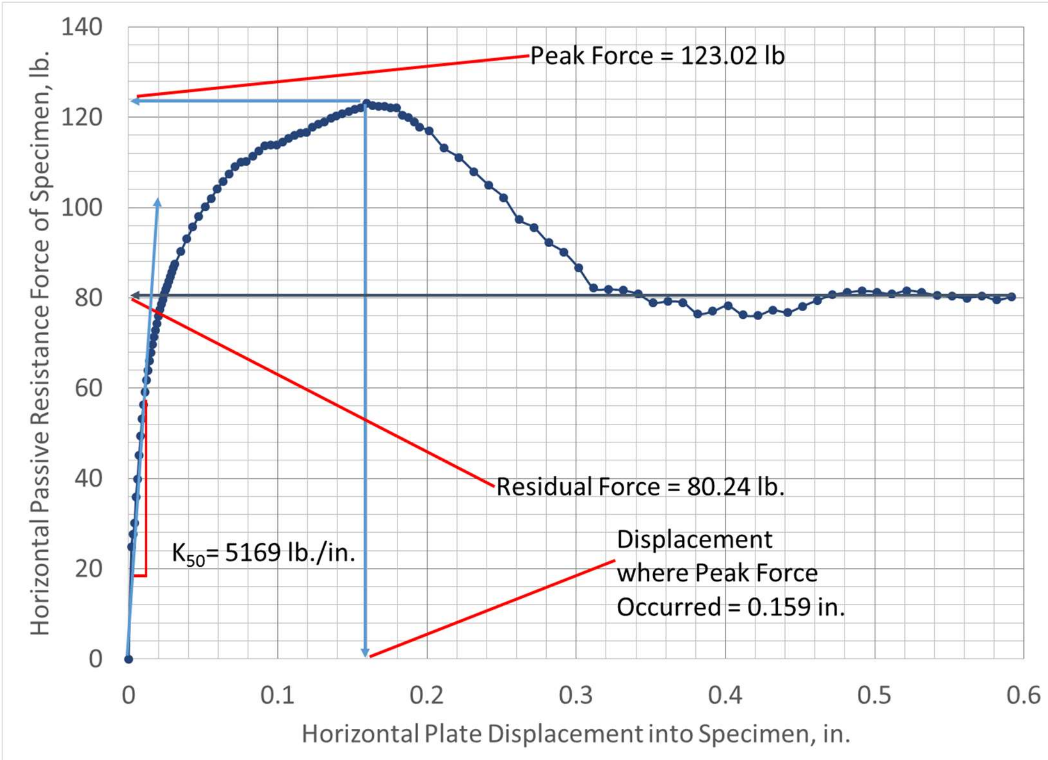

Figure 528: Load-Displacement Plot of Test 8W11L5Lay2

E.8 Load-Displacement Plot of Test 8W11L10Lay

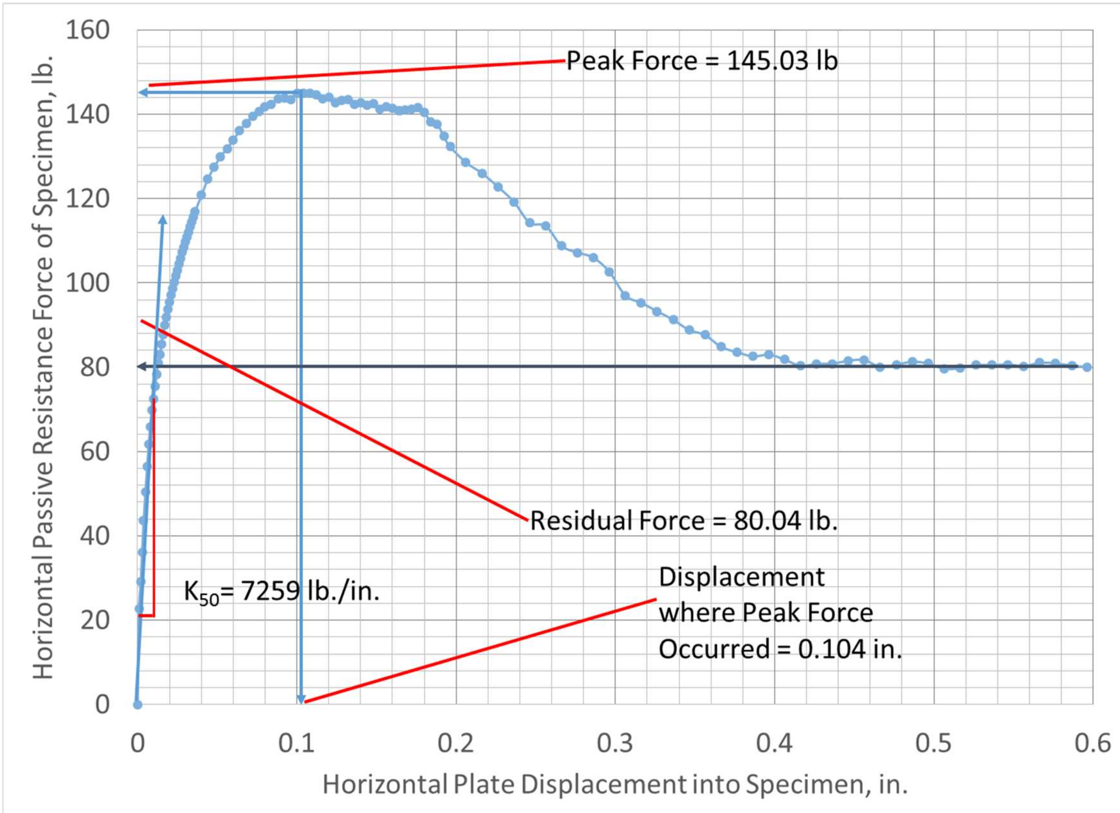

Figure 529: Load-Displacement Plot of Test 8W11L10Lay

E.9 Load-Displacement Plot of Test 8W11L10Lay2

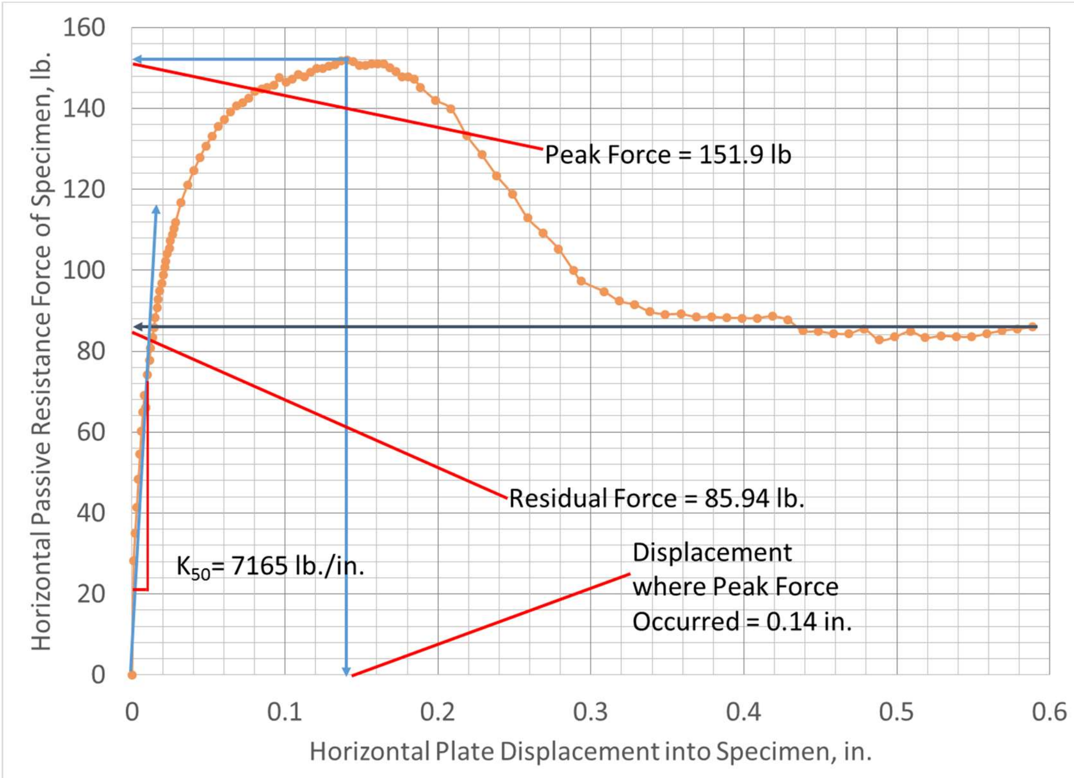

Figure 530: Load-Displacement Plot of Test 8W11L10Lay2

E.10 Load-Displacement Plot of Test 11W8L5Lay

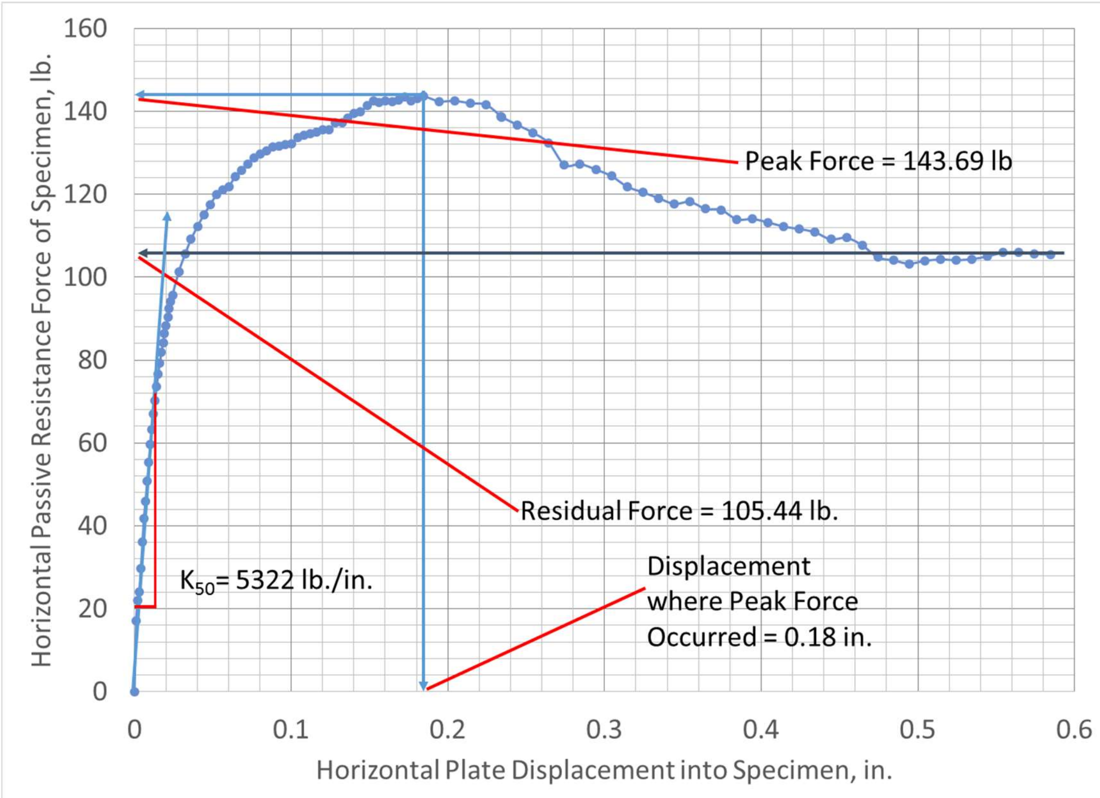

Figure 531: Load-Displacement Plot of Test 11W8L5Lay

E.11 Load-Displacement Plot of Test 11W8L5Lay2

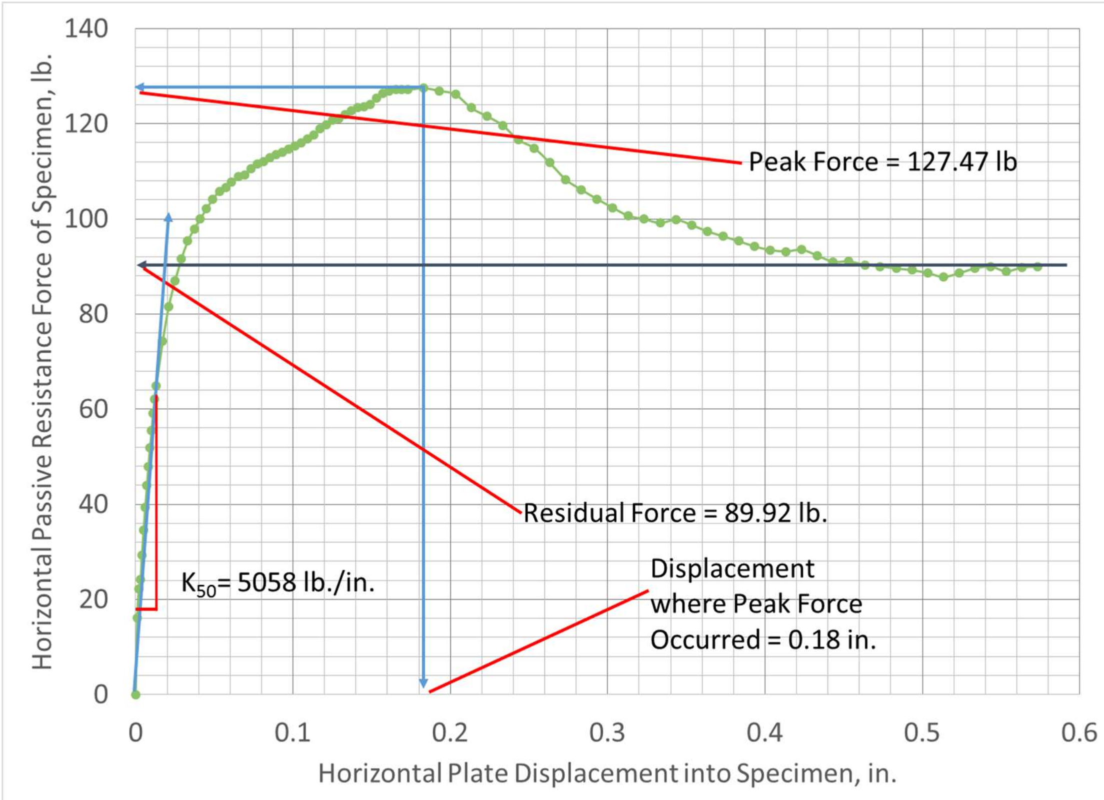

Figure 532: Load-Displacement Plot of Test 11W8L5Lay2

E.12 Load-Displacement Plot of Test 11W8L10Lay

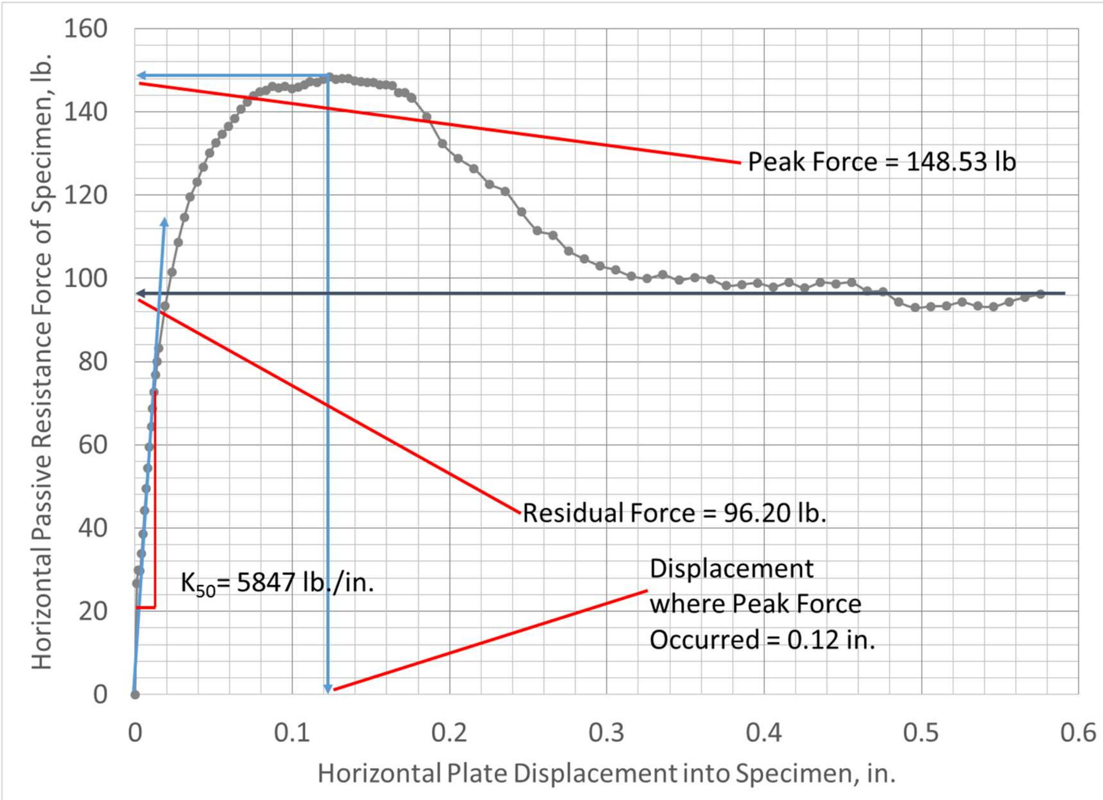

Figure 533: Load-Displacement Plot of Test 11W8L10Lay

E.13 Load-Displacement Plot of Test 11W8L10Lay2

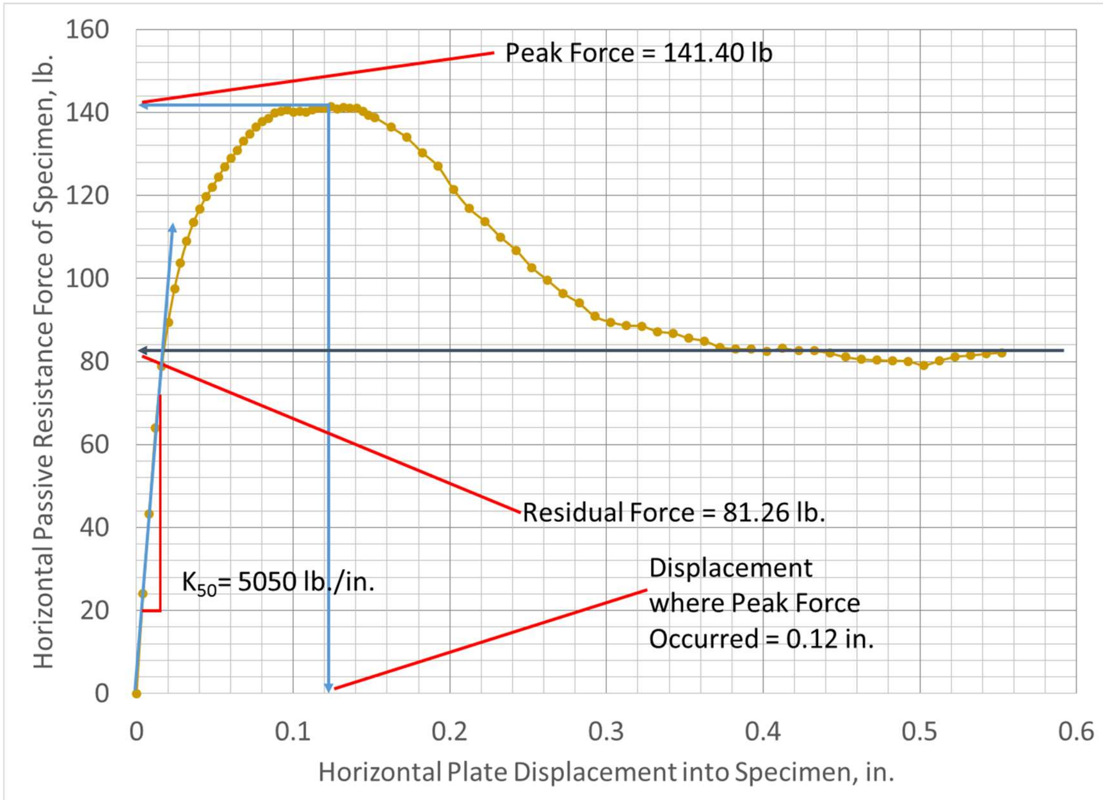

Figure 534: Load-Displacement Plot of Test 11W8L10Lay2

E.14 Load-Displacement Plot of Test 11W11L5Lay

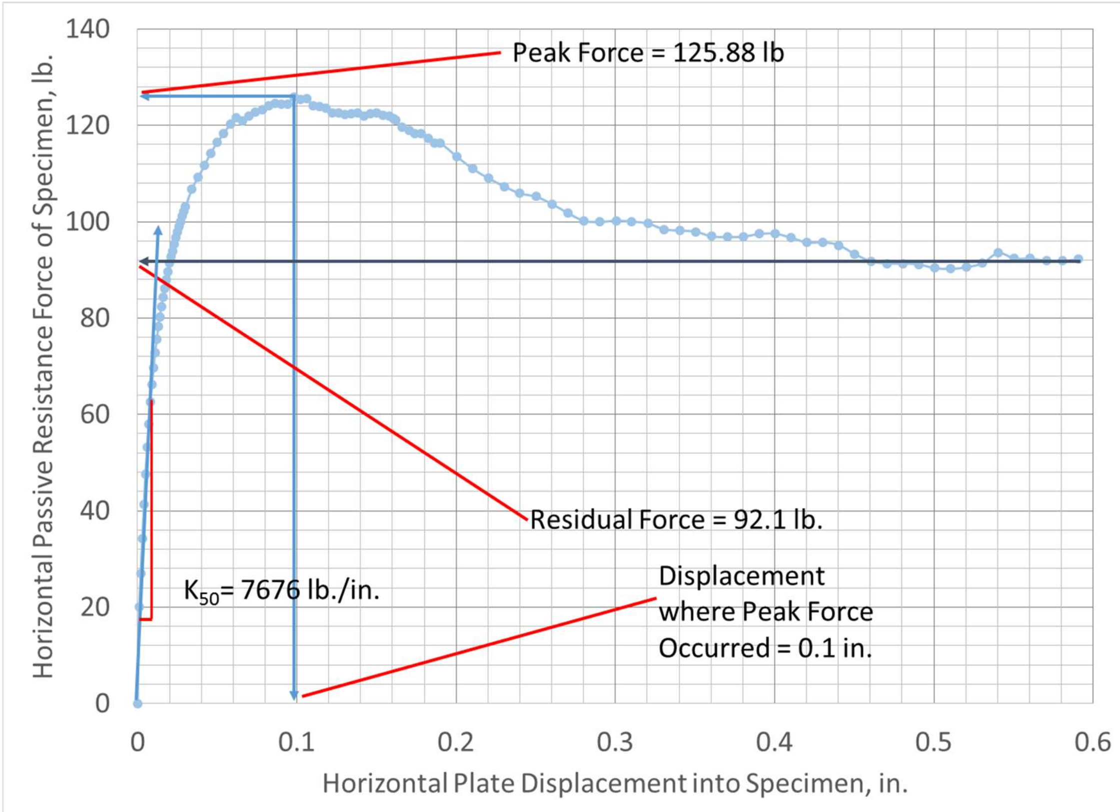

Figure 535: Load-Displacement Plot of Test 11W11L5Lay

E.15 Load-Displacement Plot of Test 11W11L5Lay2

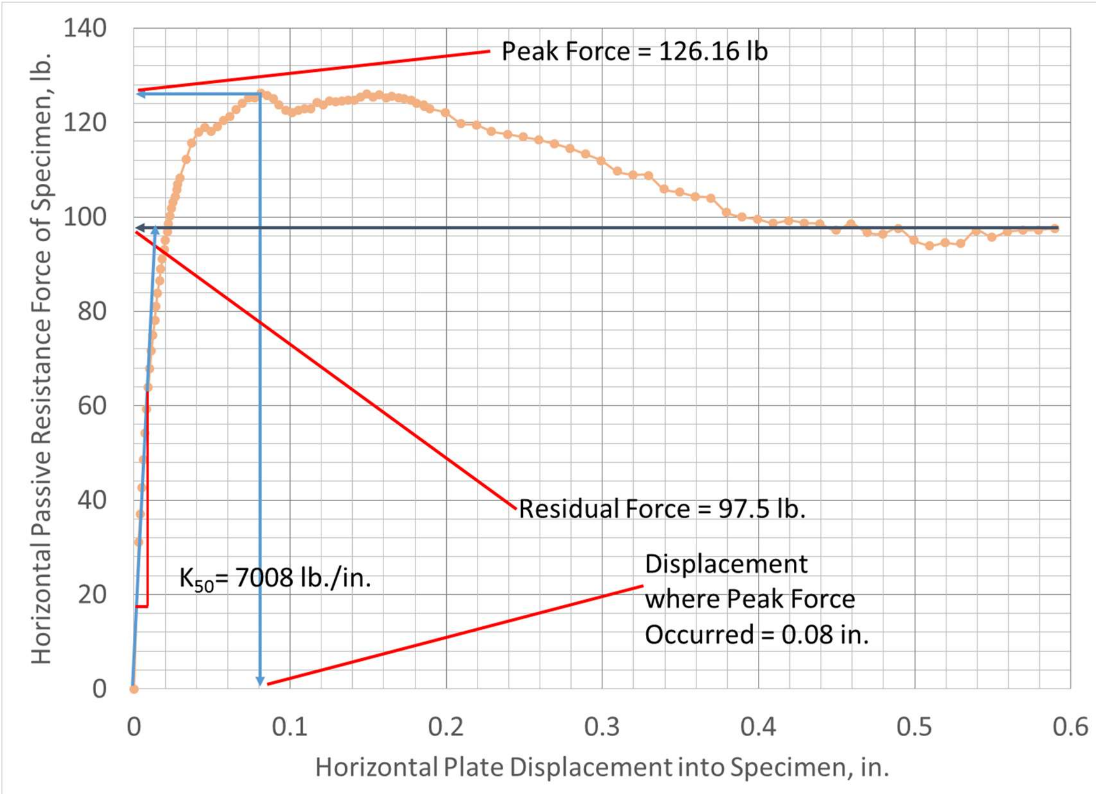

Figure 536: Load-Displacement Plot of Test 11W11L5Lay2

E.16 Load-Displacement Plot of Test 11W11L10Lay

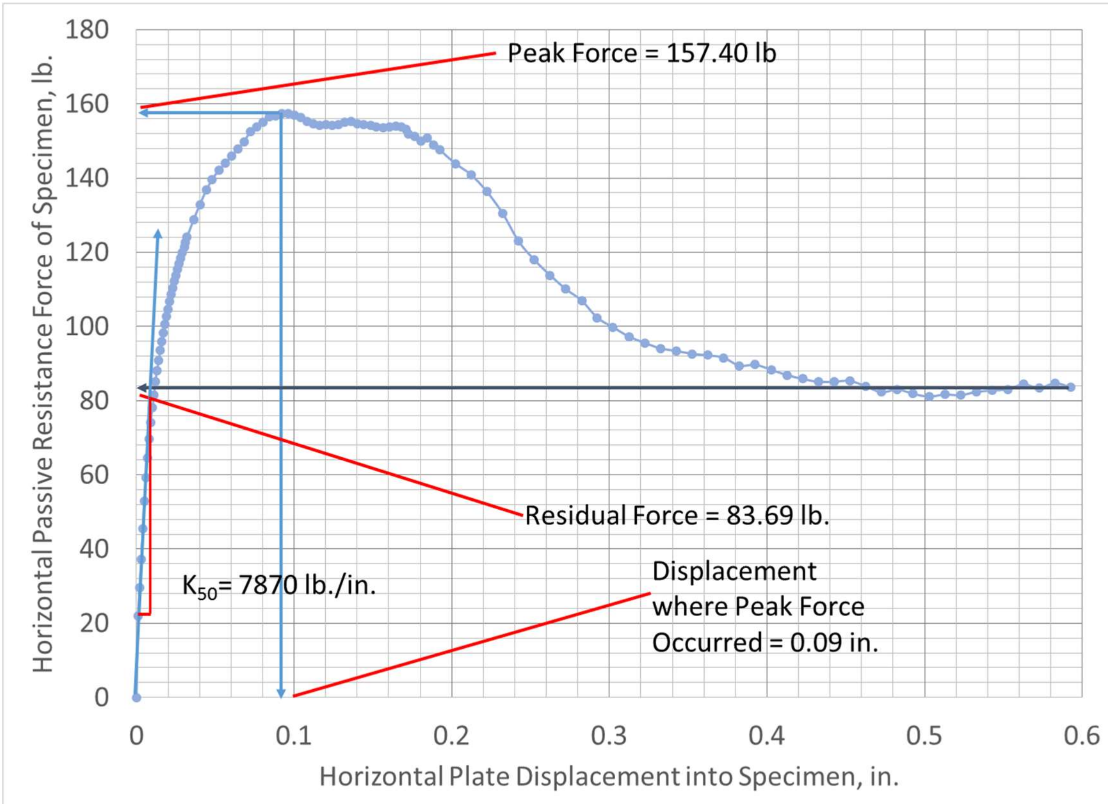

Figure 537: Load-Displacement Plot of Test 11W11L10Lay

E.17 Load-Displacement Plot of Test 11W11L10Lay2

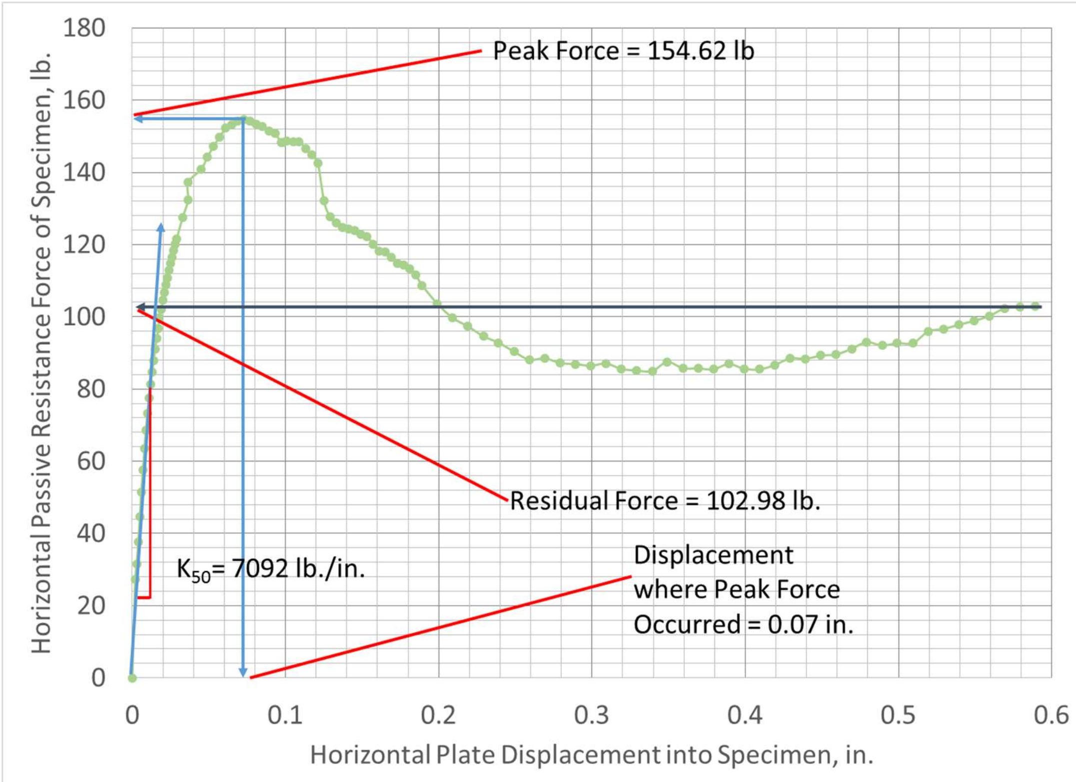

Figure 538: Load-Displacement Plot of Test 11W11L10Lay2

E.18 Load-Displacement Plot of Test PW8L5Lay

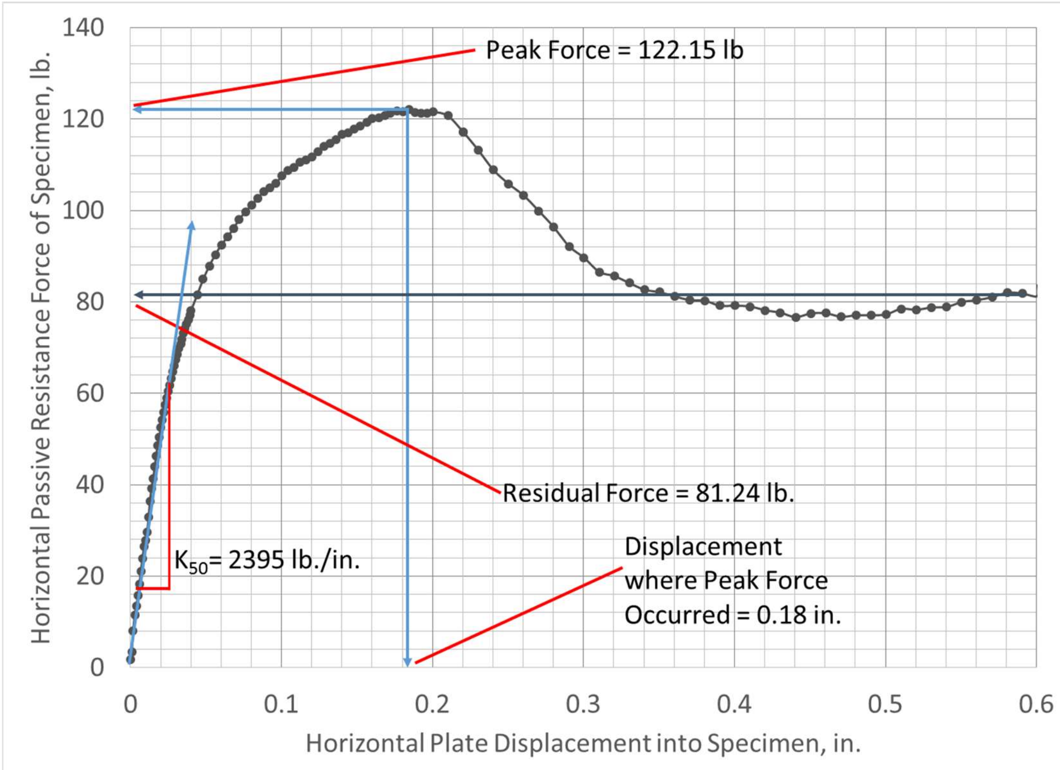

Figure 539: Load-Displacement Plot of Test PW8L5Lay

E.19 Load-Displacement Plot of Test PW8L5Lay2

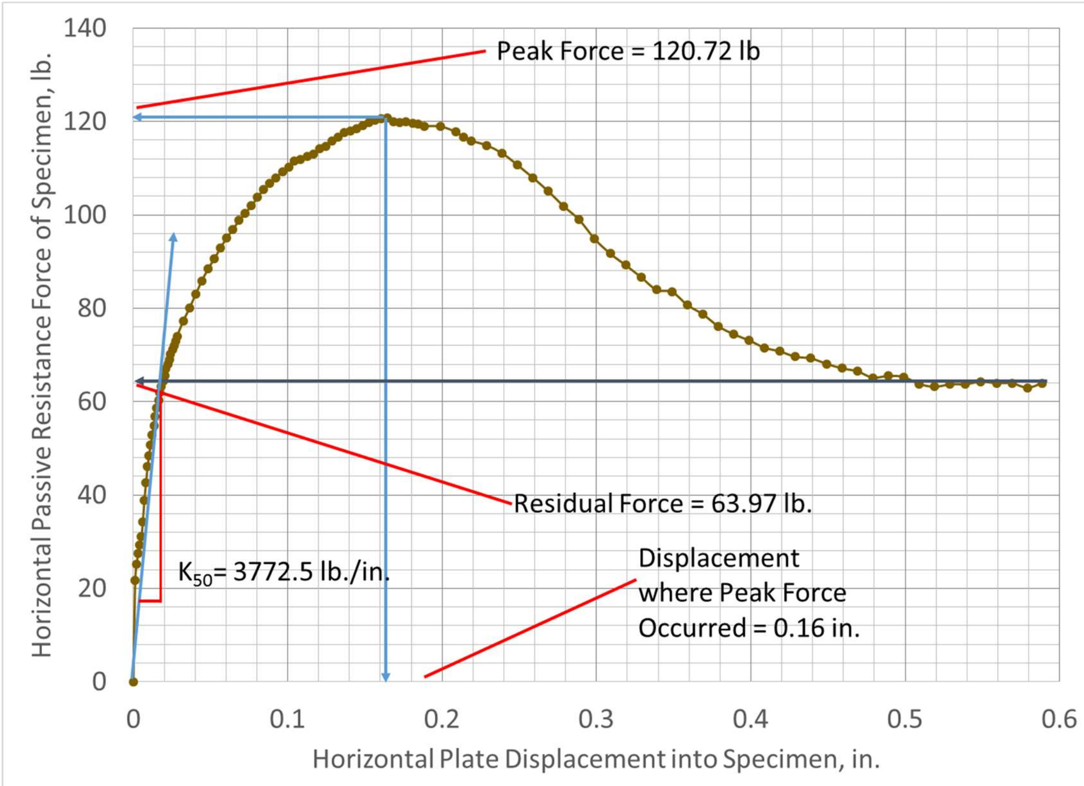

Figure 540: Load-Displacement Plot of Test PW8L5Lay2

E.20 Load-Displacement Plot of Test PW8L10Lay

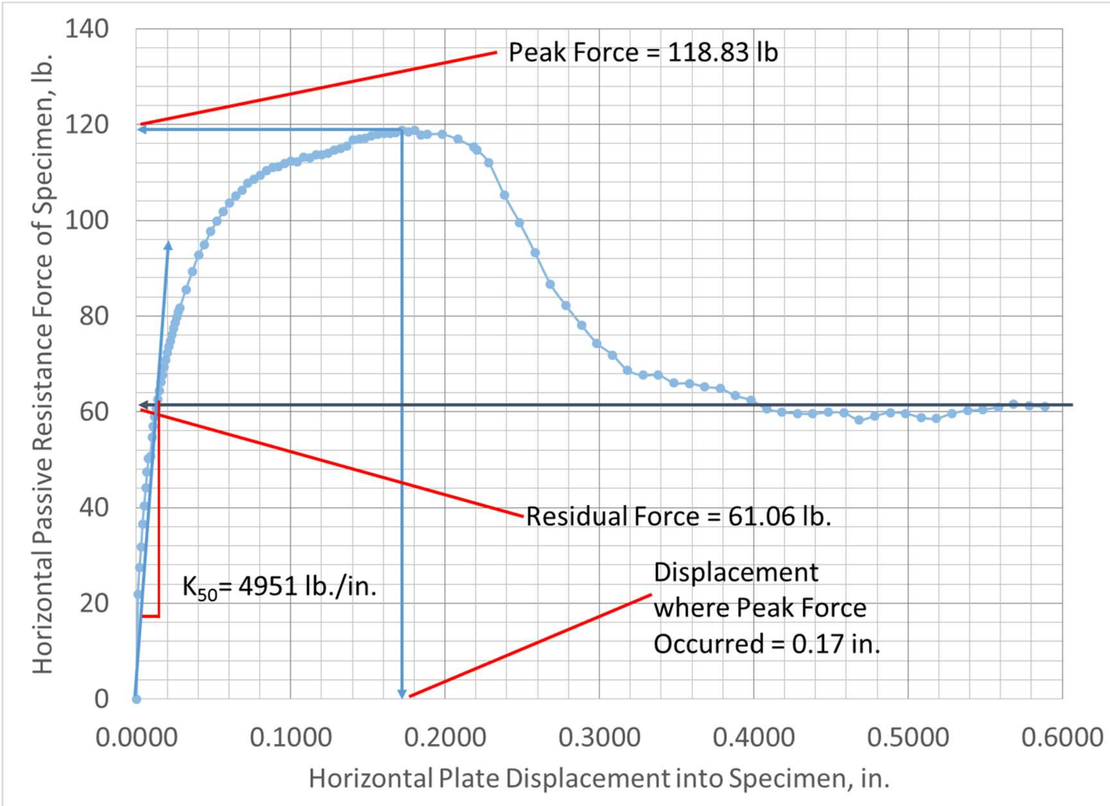

Figure 541: Load-Displacement Plot of Test PW8L10Lay

E.21 Load-Displacement Plot of Test PW8L10Lay2

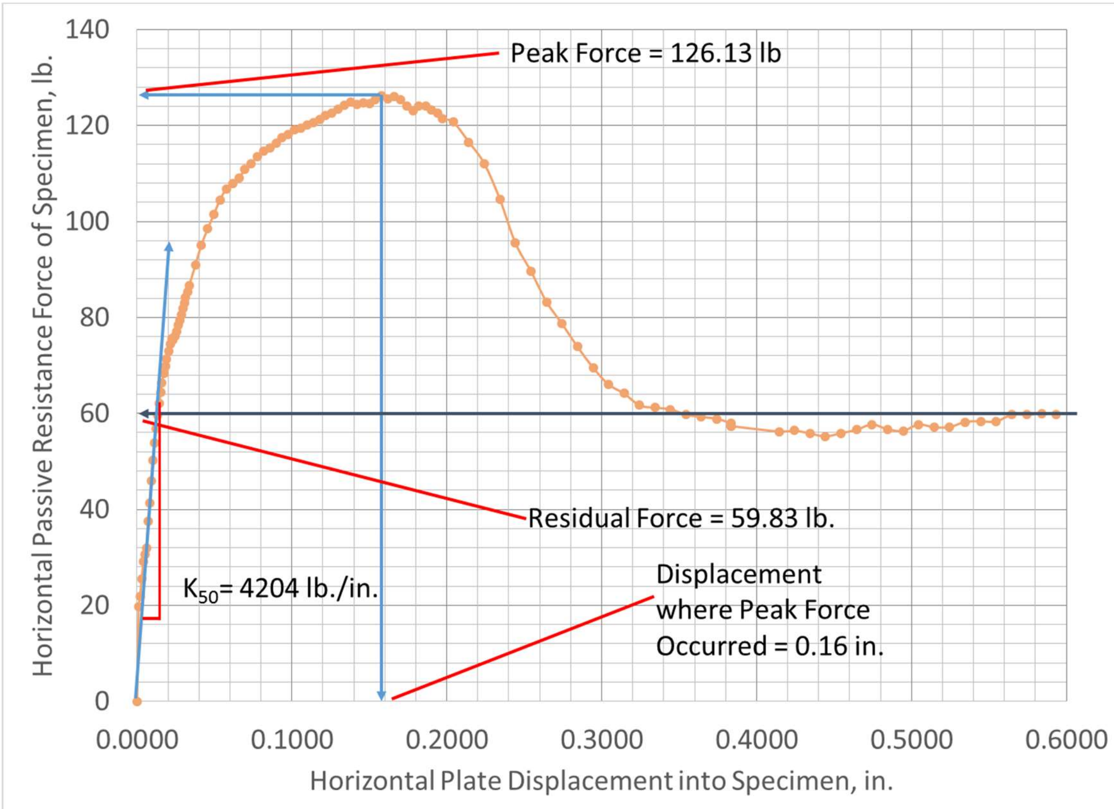

Figure 542: Load-Displacement Plot of Test PW8L10Lay2

E.22 Load-Displacement Plot of Test PW11L5Lay

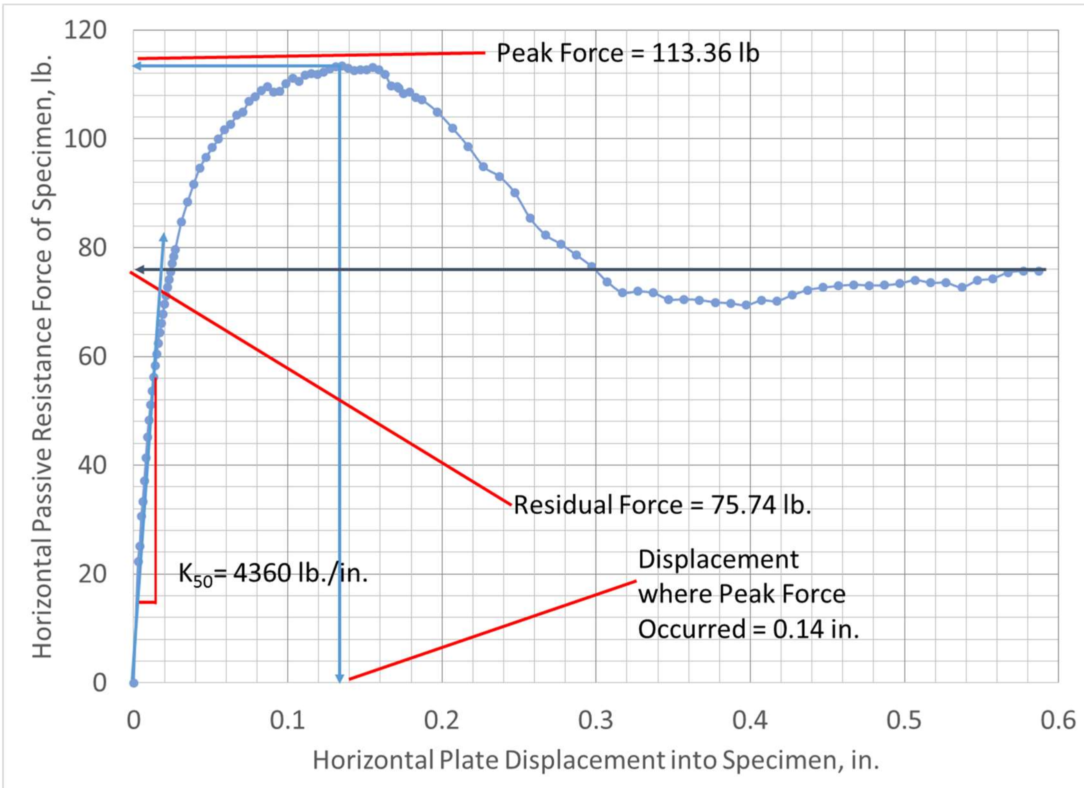

Figure 543: Load-Displacement Plot of Test PW11L5Lay

E.23 Load-Displacement Plot of Test PW11L5Lay2

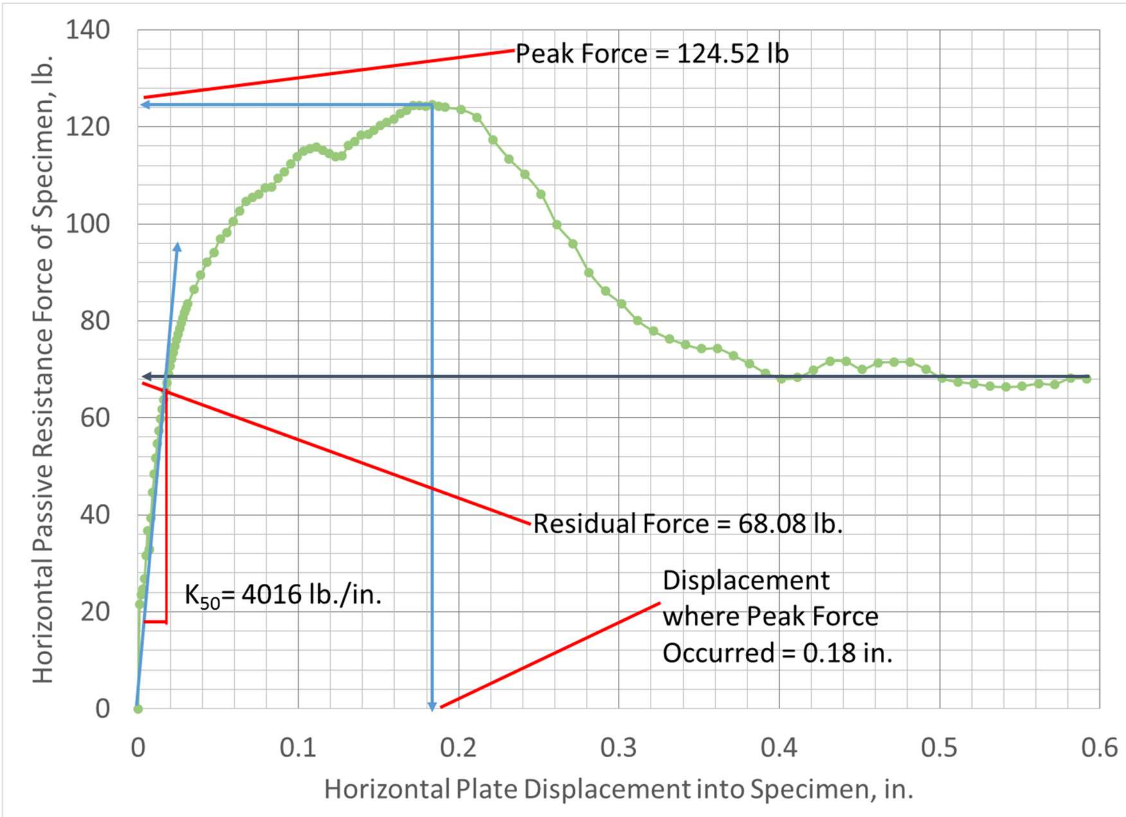

Figure 544: Load-Displacement Plot of Test PW11L5Lay2

E.24 Load-Displacement Plot of Test PW11L10Lay

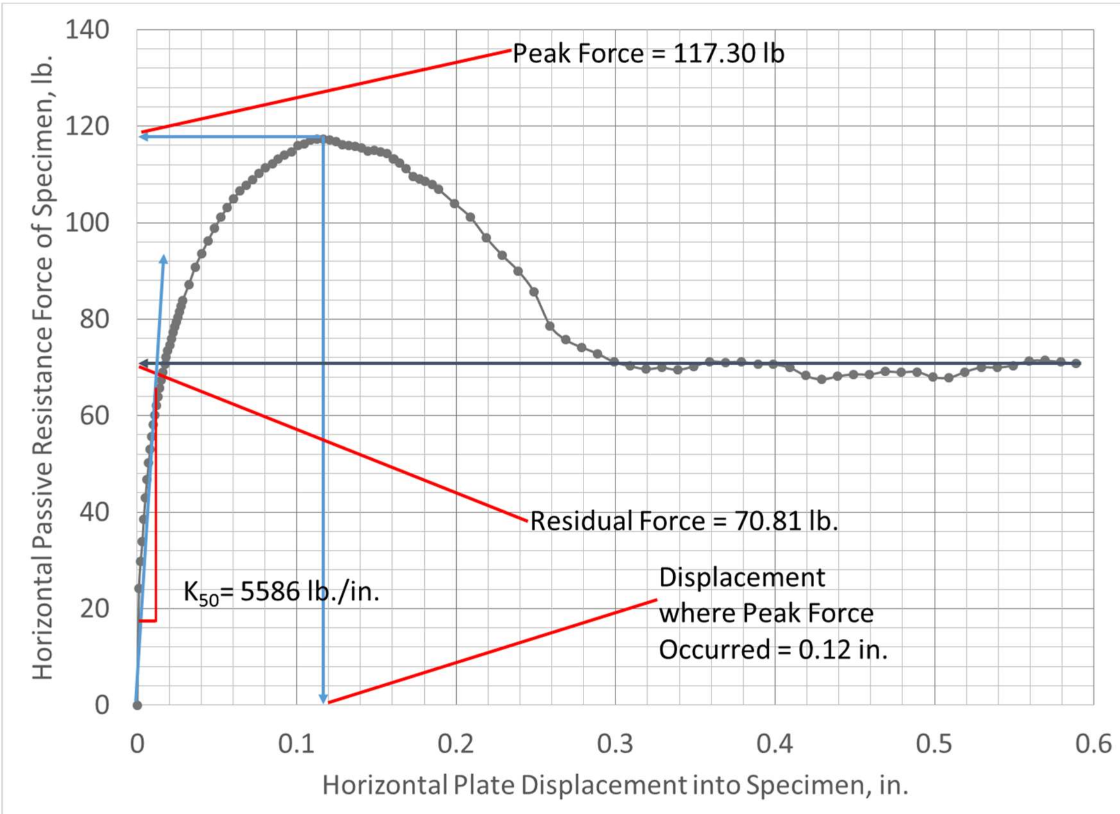

Figure 545: Load-Displacement Plot of Test PW11L10Lay

E.25 Load-Displacement Plot of Test PW11L10Lay2

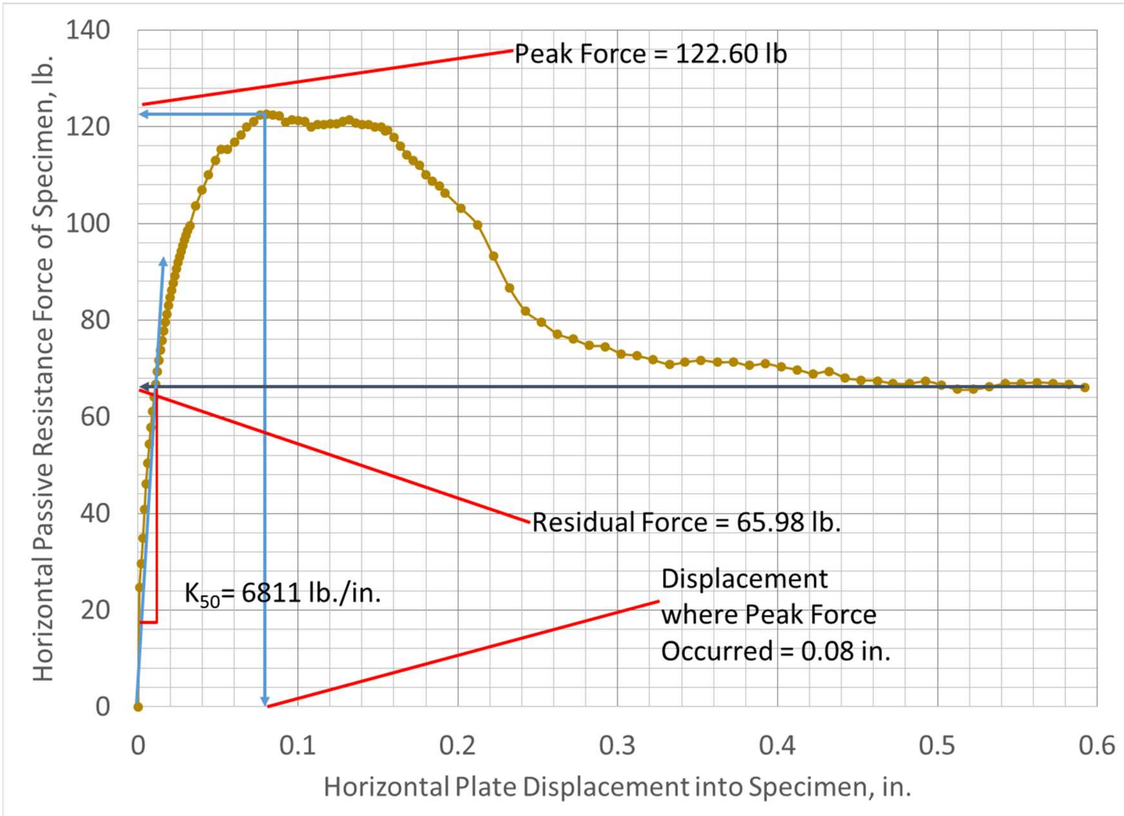

Figure 546: Load-Displacement Plot of Test PW11L10Lay2

E.26 Load-Displacement Plot of Test NR1

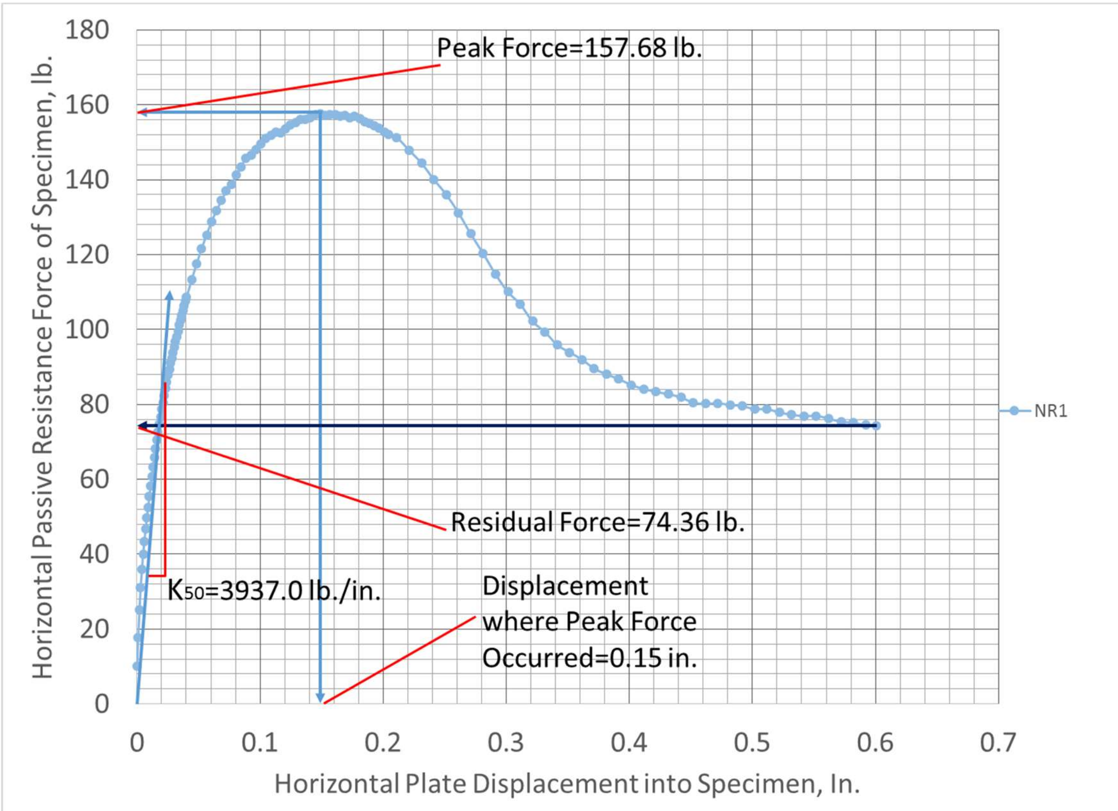

Figure 547: Load-Displacement Plot of Test NR1

E.27 Load-Displacement Plot of Test NR2

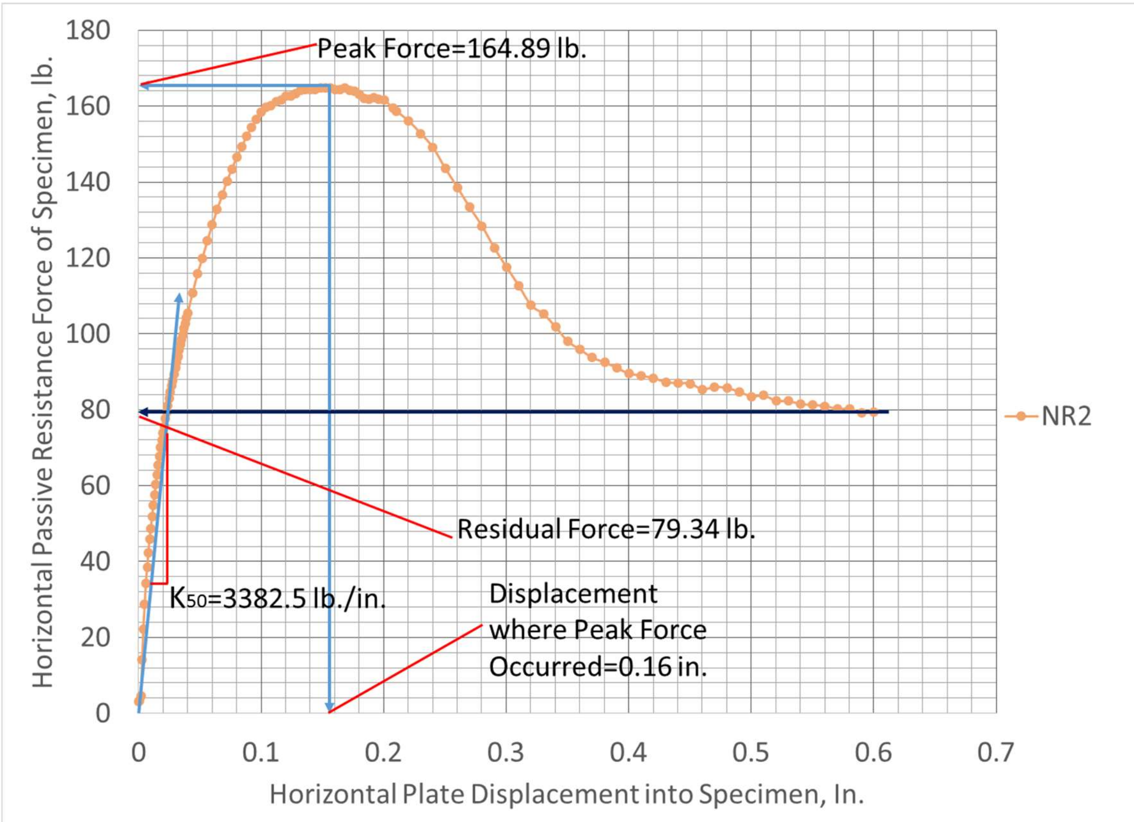

Figure 548: Load-Displacement Plot of Test NR2

E.28 Load-Displacement Plot of Test 8W8L5Lay3 (Painted)

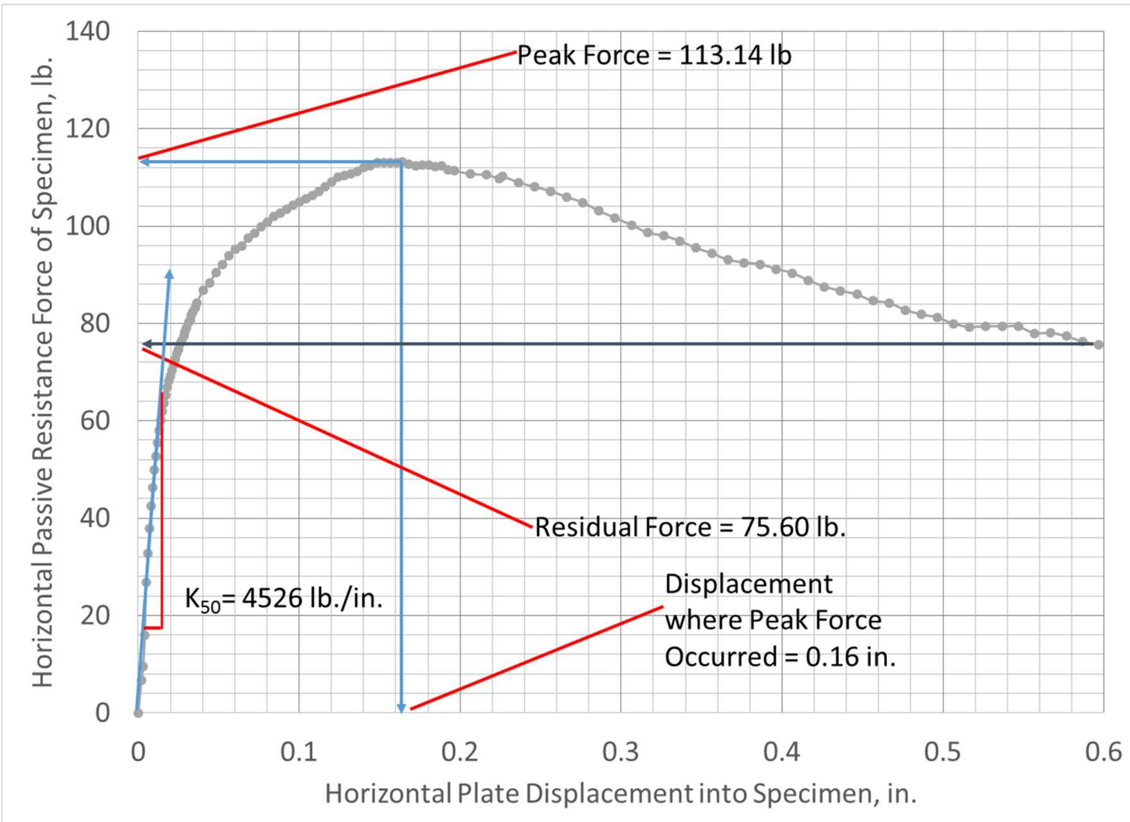

Figure 549: Load-Displacement Plot of Test 8W8L5Lay3 (Painted)

E.29 Load-Displacement Plot of Test 8W8L10Lay3 (Painted)

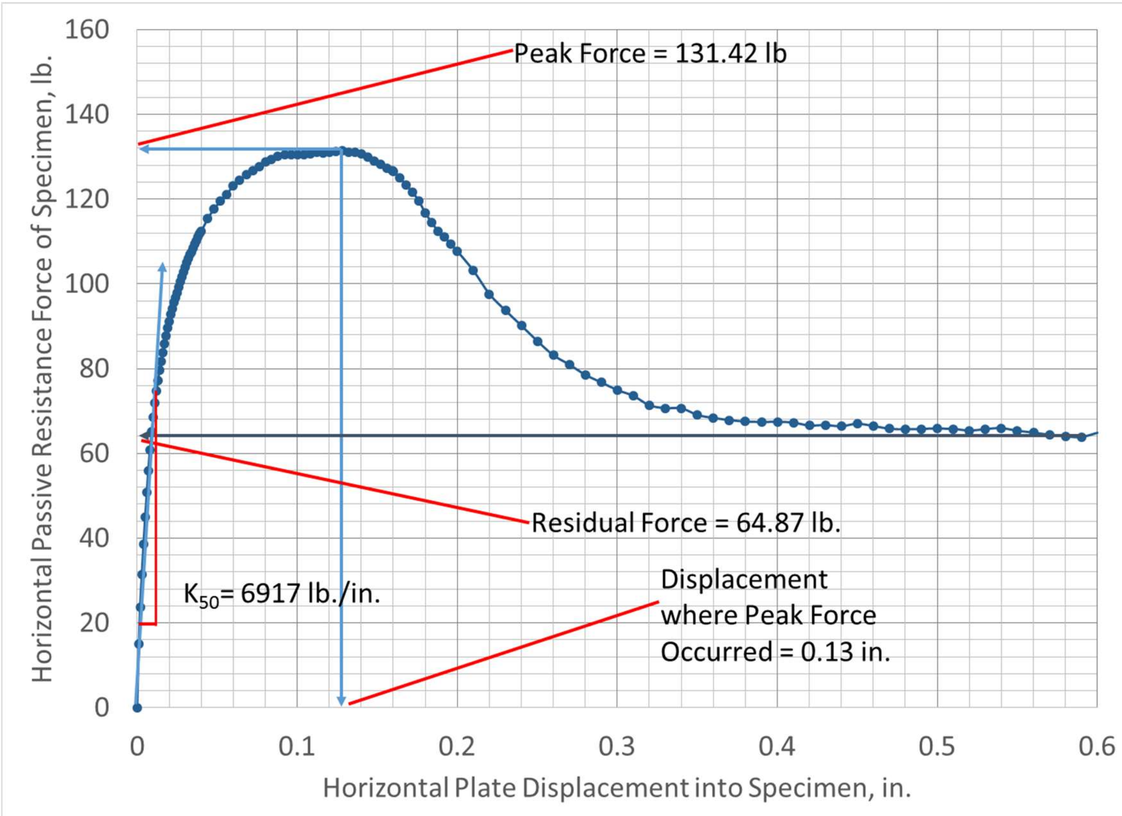

Figure 550: Load-Displacement Plot of Test 8W8L10Lay3 (Painted)

E.30 Load-Displacement Plot of Test 8W11L5Lay3 (Painted)

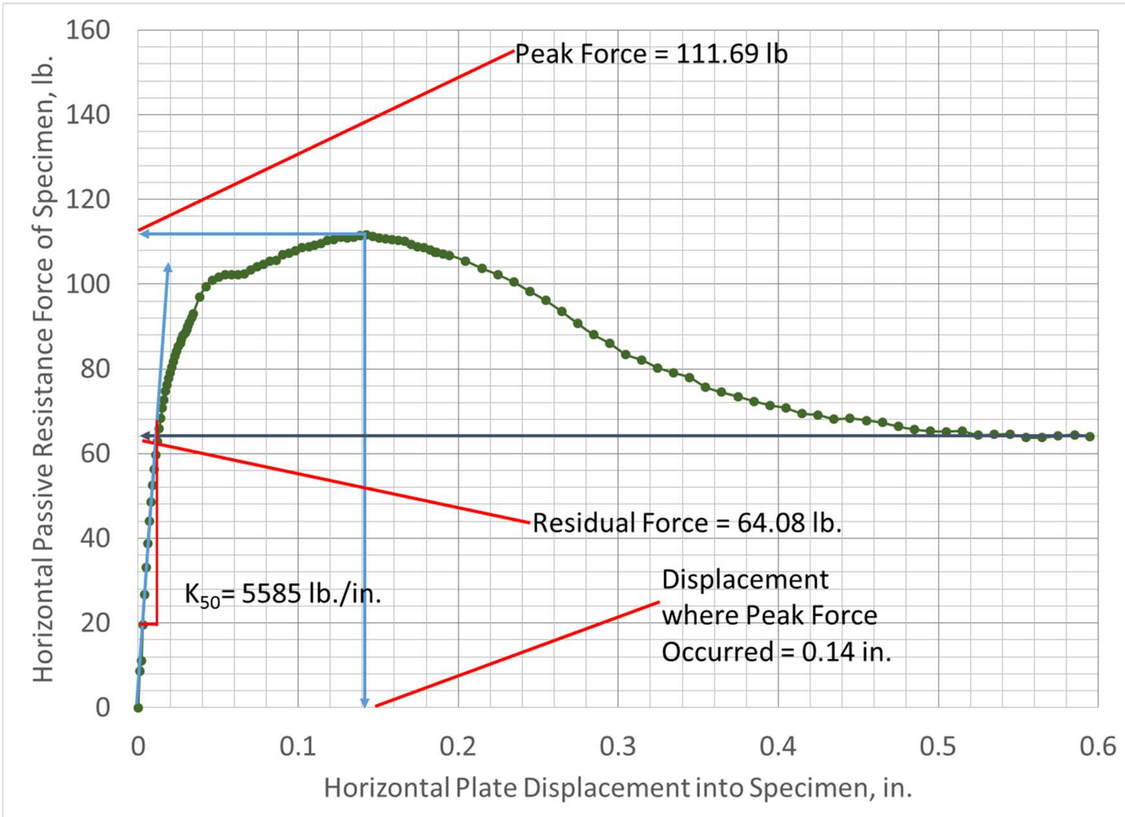

Figure 551: Load-Displacement Plot of Test 8W11L5Lay3 (Painted)

E.31 Load-Displacement Plot of Test 8W11L10Lay3 (Painted)

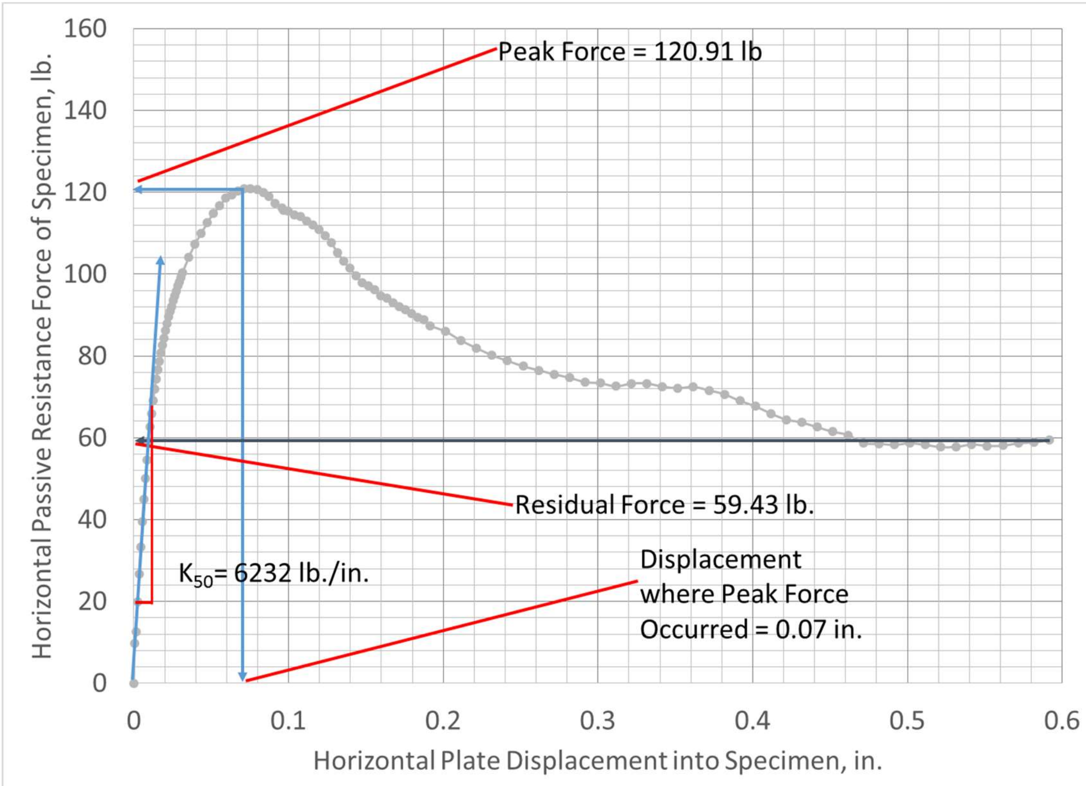

Figure 552: Load-Displacement Plot of Test 8W11L10Lay3 (Painted)

E.32 Load-Displacement Plot of Test 11W8L5Lay3 (Painted)

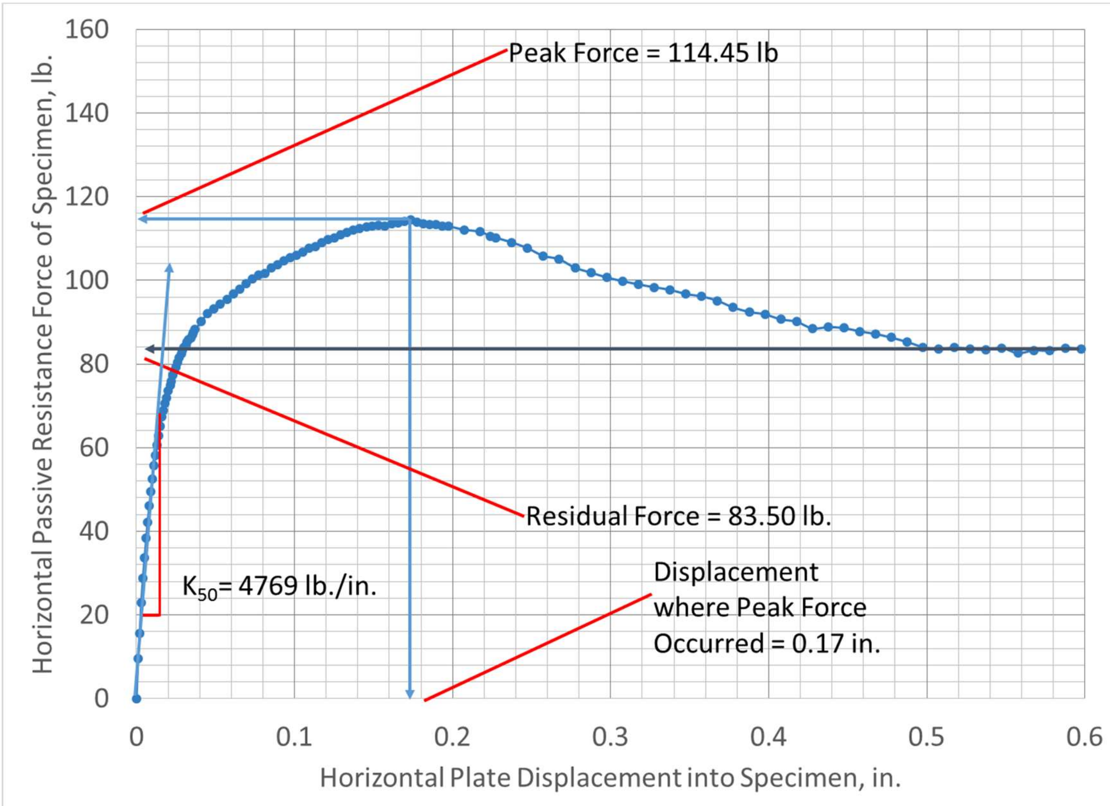

Figure 553: Load-Displacement Plot of Test 11W8L5Lay3 (Painted)

E.33 Load-Displacement Plot of Test 11W8L10Lay3 (Painted)

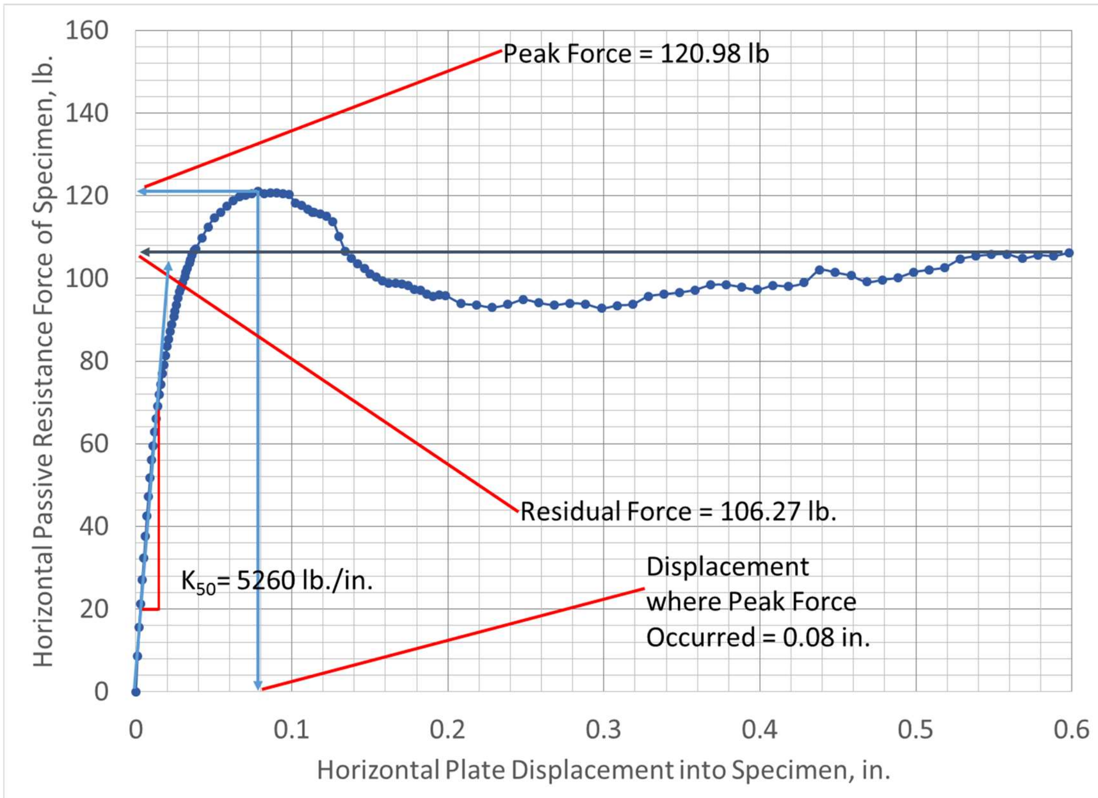

Figure 554: Load-Displacement Plot of Test 11W8L10Lay3 (Painted)

E.34 Load-Displacement Plot of Test 11W11L5Lay3 (Painted)

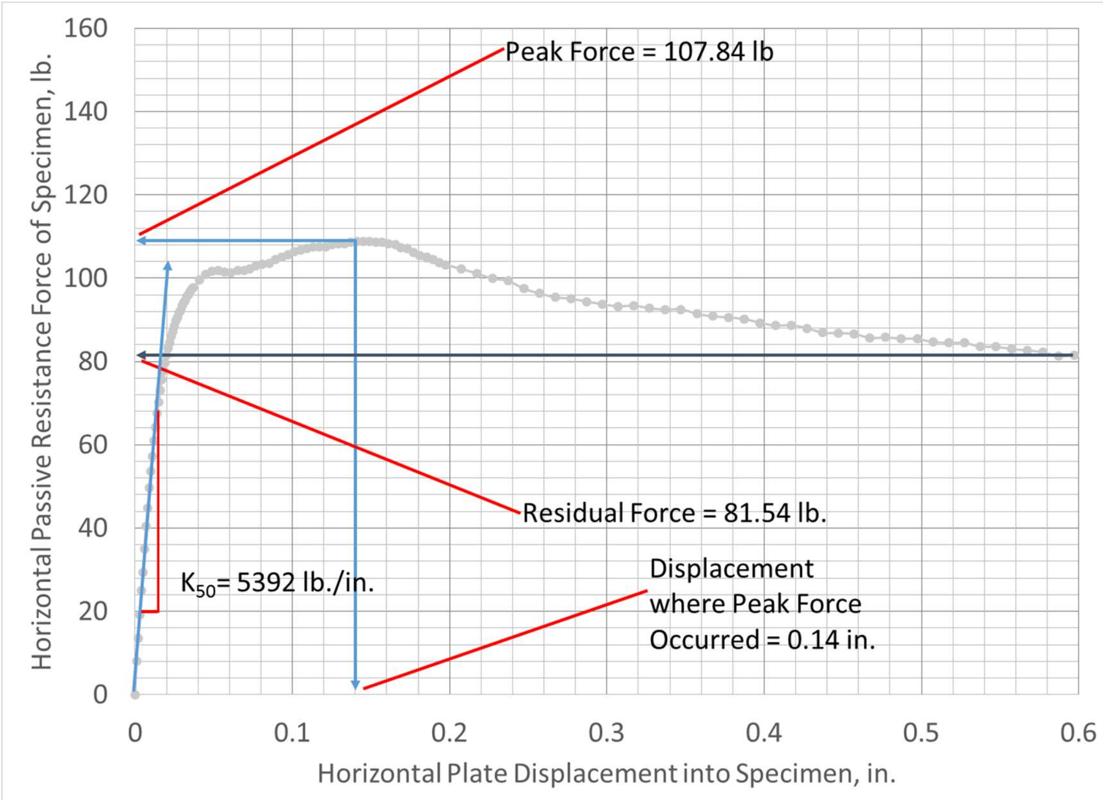

Figure 555: Load-Displacement Plot of Test 11W11L5Lay3 (Painted)

E.35 Load-Displacement Plot of Test 11W11L10Lay3 (Painted)

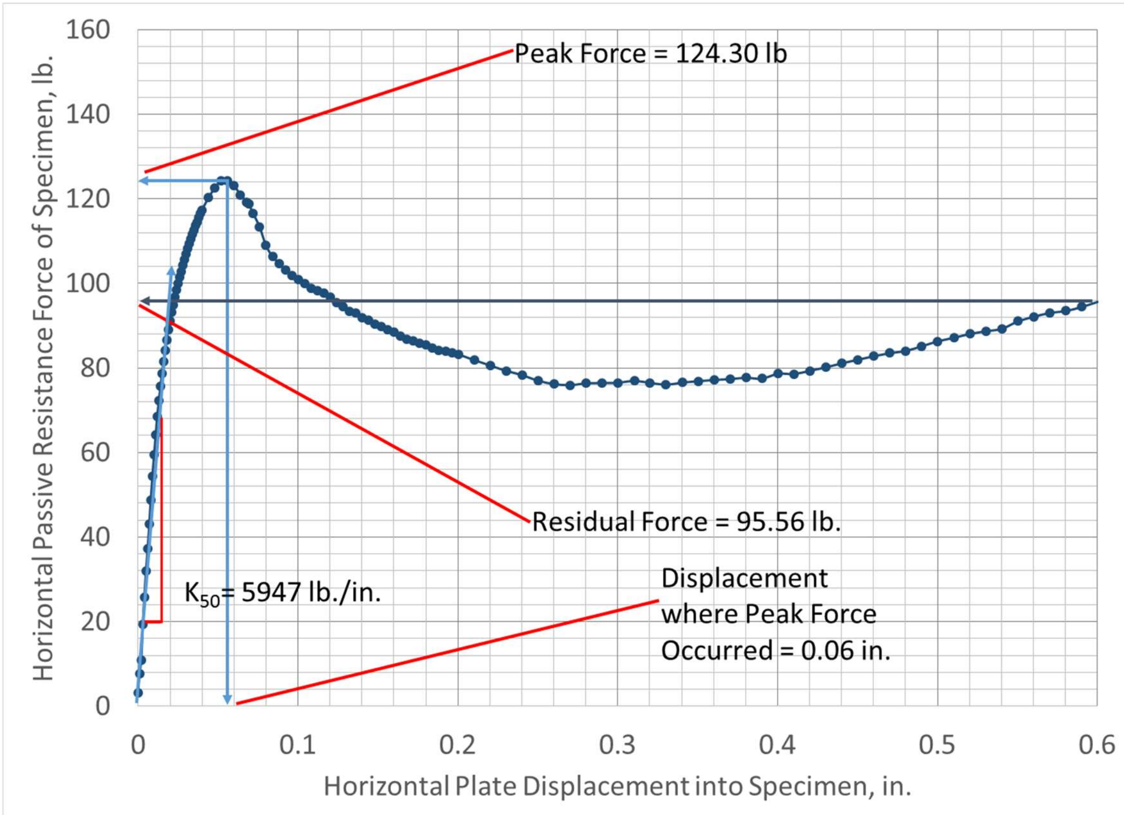

Figure 556: Load-Displacement Plot of Test 11W11L10Lay3 (Painted)

E.36 Load-Displacement Plot of Test PW8L5Lay3 (Painted)

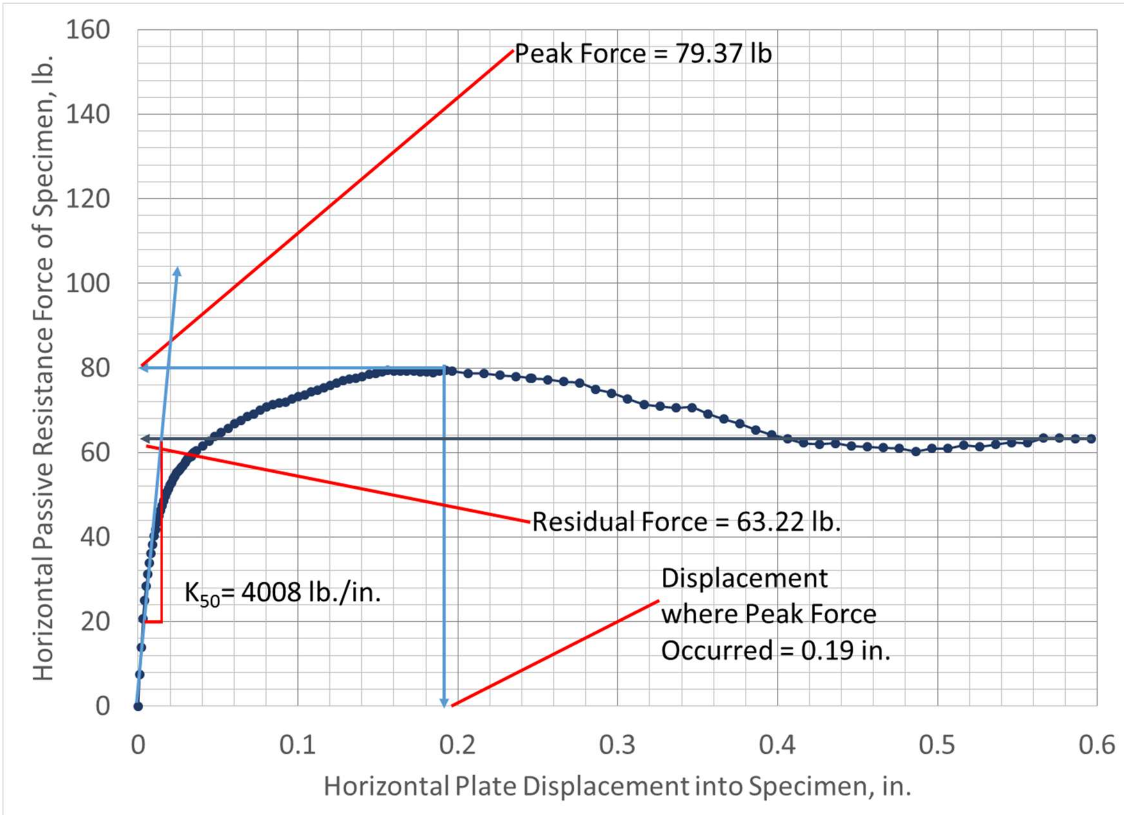

Figure 557: Load-Displacement Plot of Test PW8L5Lay3 (Painted)

E.37 Load-Displacement Plot of Test PW8L10Lay3 (Painted)

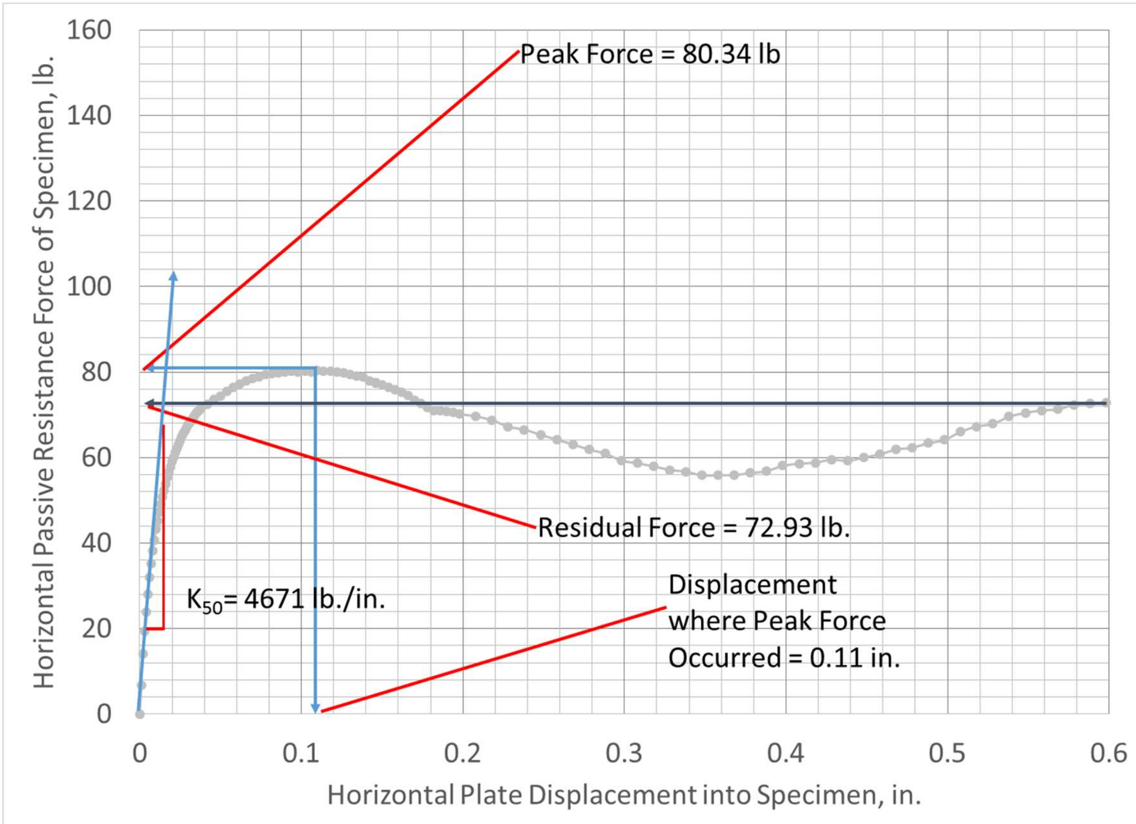

Figure 558: Load-Displacement Plot of Test PW8L10Lay3 (Painted)

E.38 Load-Displacement Plot of Test PW11L5Lay3 (Painted)

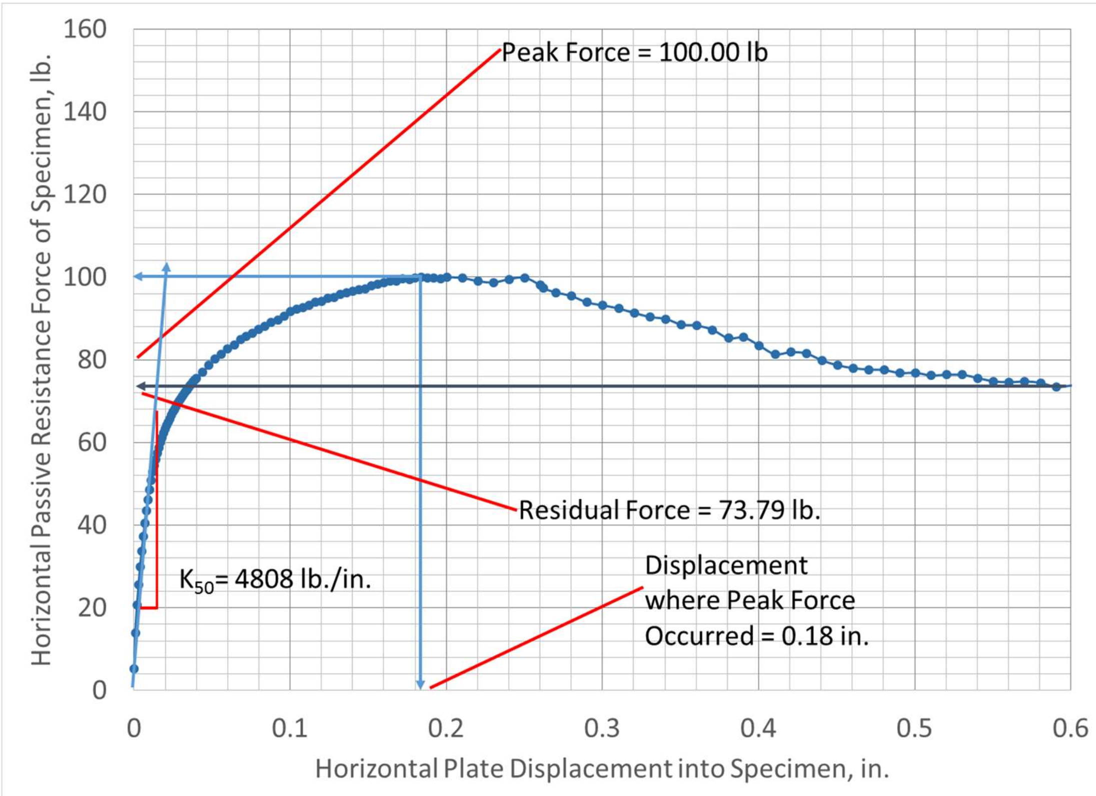

Figure 559: Load-Displacement Plot of Test PW11L5Lay3 (Painted)

E.39 Load-Displacement Plot of Test PW11L10Lay3 (Painted)

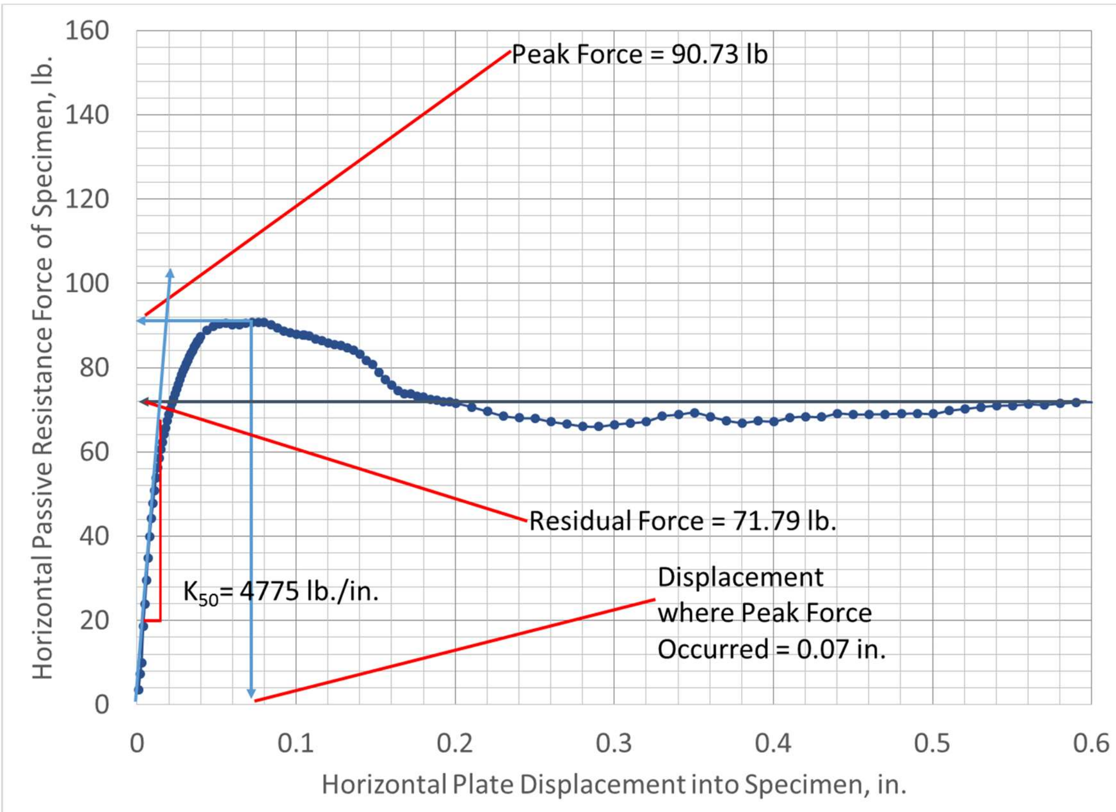

Figure 560: Load-Displacement Plot of Test PW11L10Lay3 (Painted)

E.40 Load-Displacement Plot of Test NR3 (Painted)

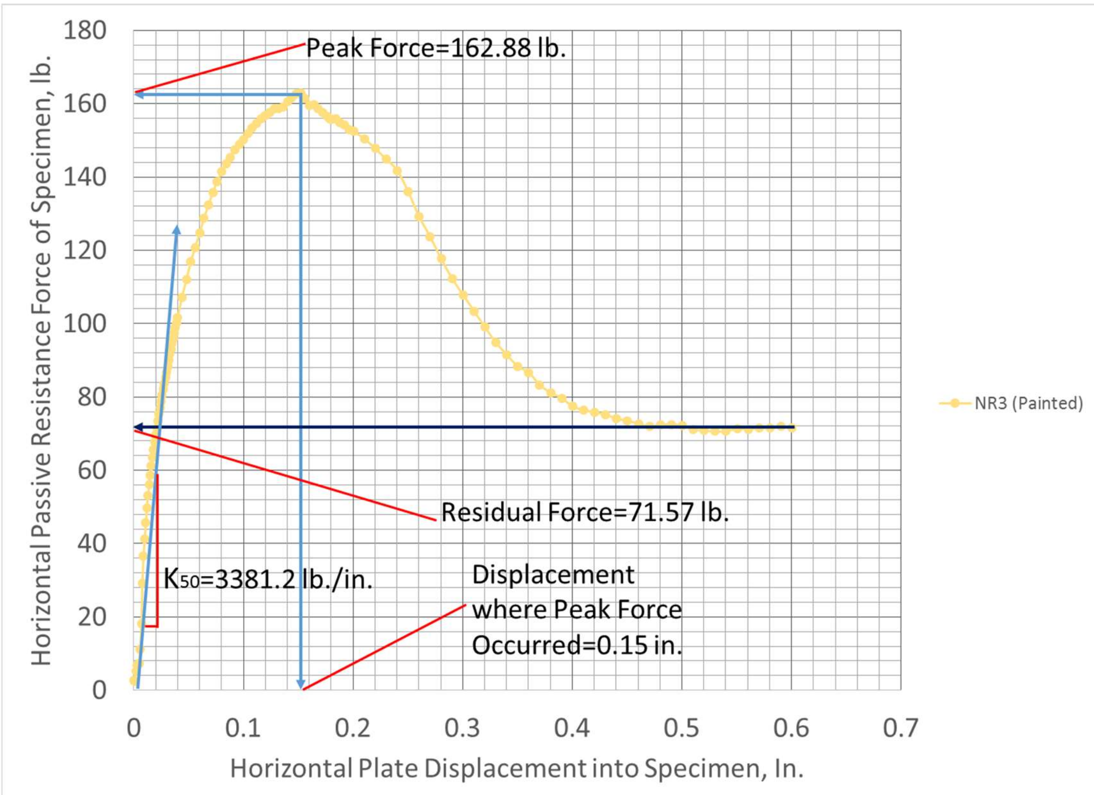

Figure 561: Load-Displacement Plot of Test NR3 (Painted)

APPENDIX F: “WATER METHOD” DENSITY TEST

F.1 Introduction

To verify that soil density is consistent within each specimen, a test was developed to directly measure in place density. The principle of the test is similar to a sand cone, where an excavation is made, a substance of known density fills the excavation, and density can be determined by dividing the mass of the excavated material (wet or dry) by the volume of the substance of known density required to fill the excavation (obtained by dividing the mass of the substance by the known density of the substance). Additional information on sand cone testing can be found in ASTM D1556/D1556M-15. The sane cone test is not a viable option because the same soil is used for each benchtop test, and it would be impossible to remove all of the alien sand that would be introduced by using a sand cone. To avoid this problem, water was used in place of sand and the test was slightly modified. The test procedure is as follows:

1. Using a spray bottle, carefully moisten the soil in the area to be excavated (Figure 562). Moistening soil provides apparent cohesion between the sand particles so that the excavation remains open.

Figure 562: Moistening soil prior to excavation

2. Using a spoon, carefully excavate an approximate hemisphere with a diameter of about three inches. Place excavated soil in a pre-weighed moisture tin and oven dry soil. Record tin weight and weight of oven dried soil and tin.
3. Place plastic wrap in excavation. Plastic wrap acts as a barrier between soil and water to be added so that the water cannot seep into the soil.
4. Fill a wash bottle with water, weigh the full wash bottle and record. Using the wash bottle, fill the excavation with water until the top of the water is just slightly above the soil surface. Filling to slightly above the soil surface takes into account the convex meniscus formed due to the water-plastic wrap interface. Weigh the wash bottle after filling the excavation and record.
5. The density of the soil can be calculated using the following equation:

$$\rho_d = \frac{M_{tin+soil} - M_{tin}}{M_{w+bottle,before} - M_{w+bottle,after}} \qquad \text{(Eq. 25)}$$

Where: ρ_d is the dry density of the soil, g/cm^3
$M_{tin+soil}$ is the mass of the moisture tin and dry soil, g
M_{tin} is the mass of the moisture tin, g

$M_{w+bottle,before}$ is the mass of the water and wash bottle before filling the excavation, g

$M_{w+bottle,after}$ is the mas of the water and wash bottle after filling the excavation, g

The equation assumes the density of water is $1 g/cm^3$. Knowing this, $M_{w+bottle,before} - M_{w+bottle,after}$ is the mass of water, in grams, that was required to fill the excavation which is equal to the volume of the water, in cm^3, required to fill the excavation. Thus, mass of excavated soil and volume of excavated soil are both directly measured and their ratio yields the true density.

APPENDIX G: FAILURE SURFACE CONTOURS FROM REINFORCEMENT AND PAINTED LAYER INSTRUMENTATION

G.1 Introduction

In many tests, the passive failure surface occurred through reinforcement layers. As shearing occurred at the failure surface interface, the reinforcement was deformed at the intersection of the reinforcement and the failure surface. Deformation was indicated by folds and kinks in the reinforcement.

Reinforcement layers were carefully excavated, the deformation marked, and the reinforcement placed under a plexiglass grid, allowing x and y coordinates of the deformation to be obtained. Photographs of every reinforcement layer under the plexiglass grid are in Appendix A. After obtaining x and y coordinates for each reinforcement layer, contours were drawn to show the plan view of the failure surface location at each reinforcement depth. The red square on each plot outlines the edges of the reinforcement. The initial pusher plate location is at y=0 and between x=7.25 and x=12.75.

In the third test for each reinforcement configuration, painted horizontal layers were used to delineate the failure surface. Contours were drawn using the x and y coordinates determined by placing a plexiglass grid over paint layers exposed by excavation. The initial pusher plate location is at y=0 and between x=7.25 and x=12.75. All plots are plan view looking straight down from above the test. Photographs of every painted layer under the plexiglass grid are shown in Appendix C.

G.2 Failure Surface Contours of test 8W8L5Lay

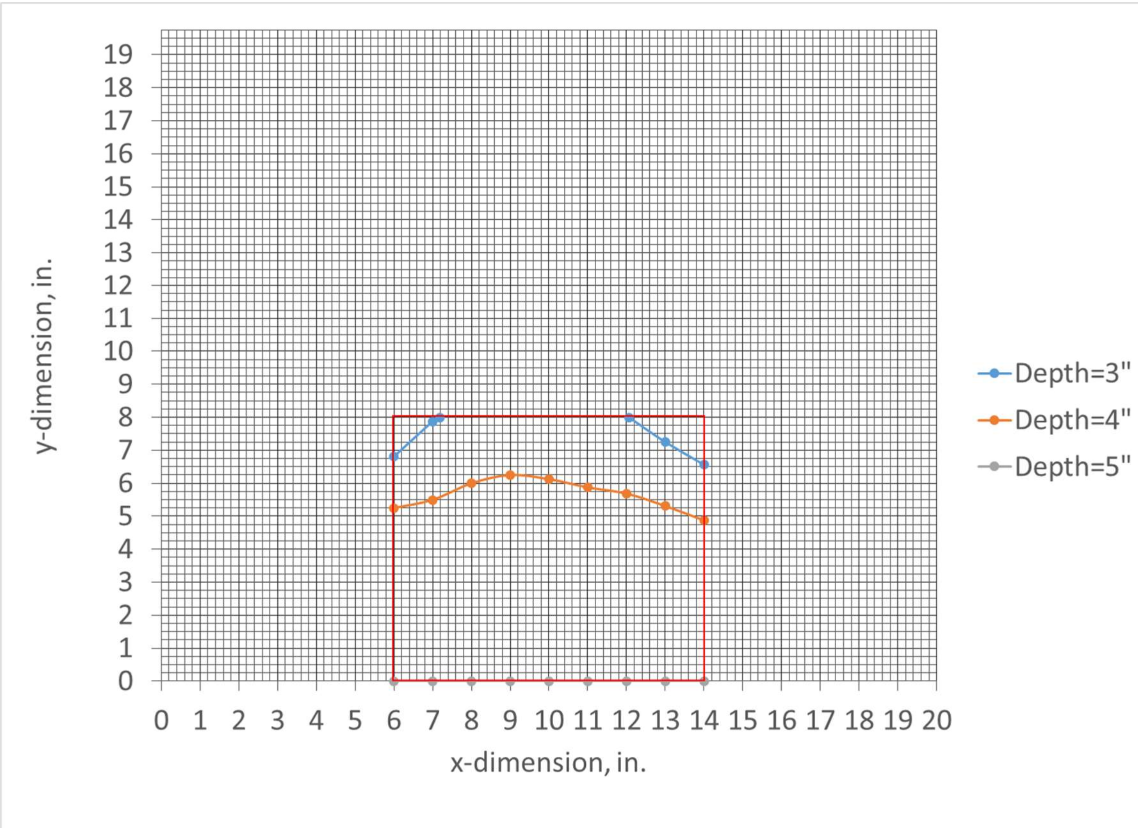

Figure 563: Failure Surface Contours of test 8W8L5Lay

G.3 Failure Surface Contours of test 8W8L5Lay2

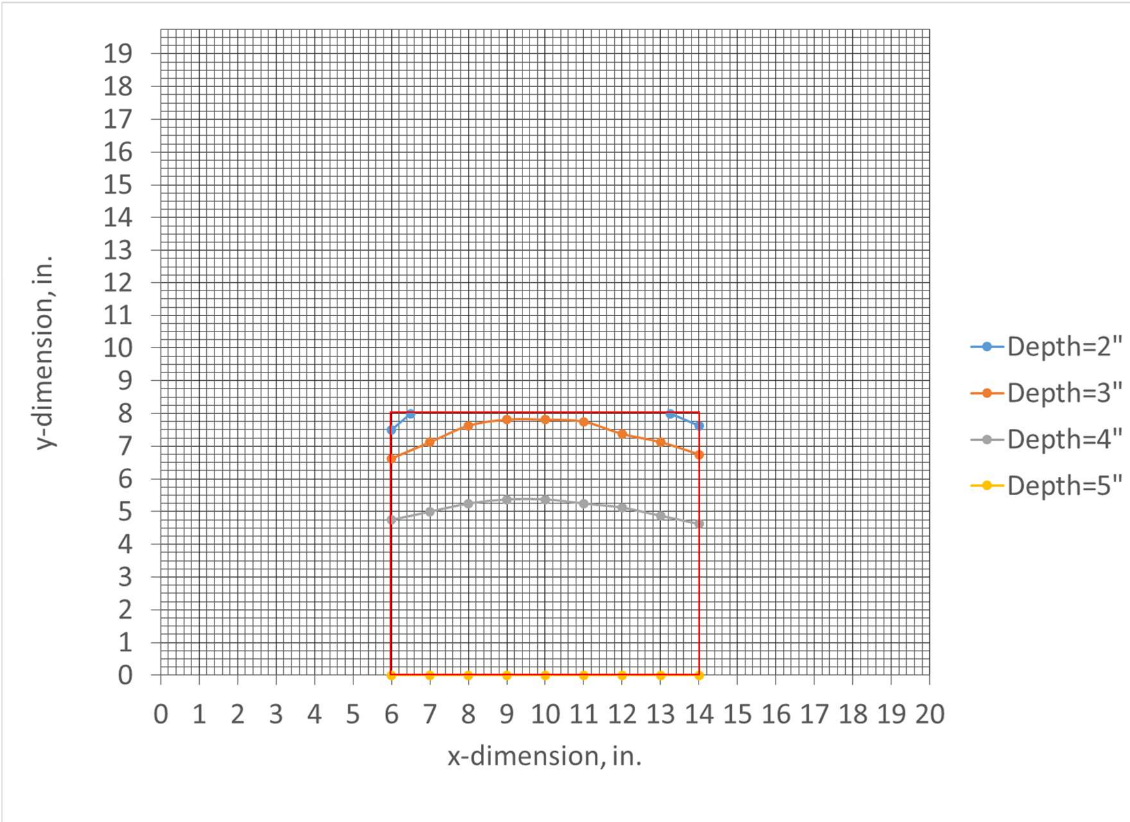

Figure 564: Failure Surface Contours of test 8W8L5Lay2

G.4 Failure Surface Contours of test 8W8L5Lay3

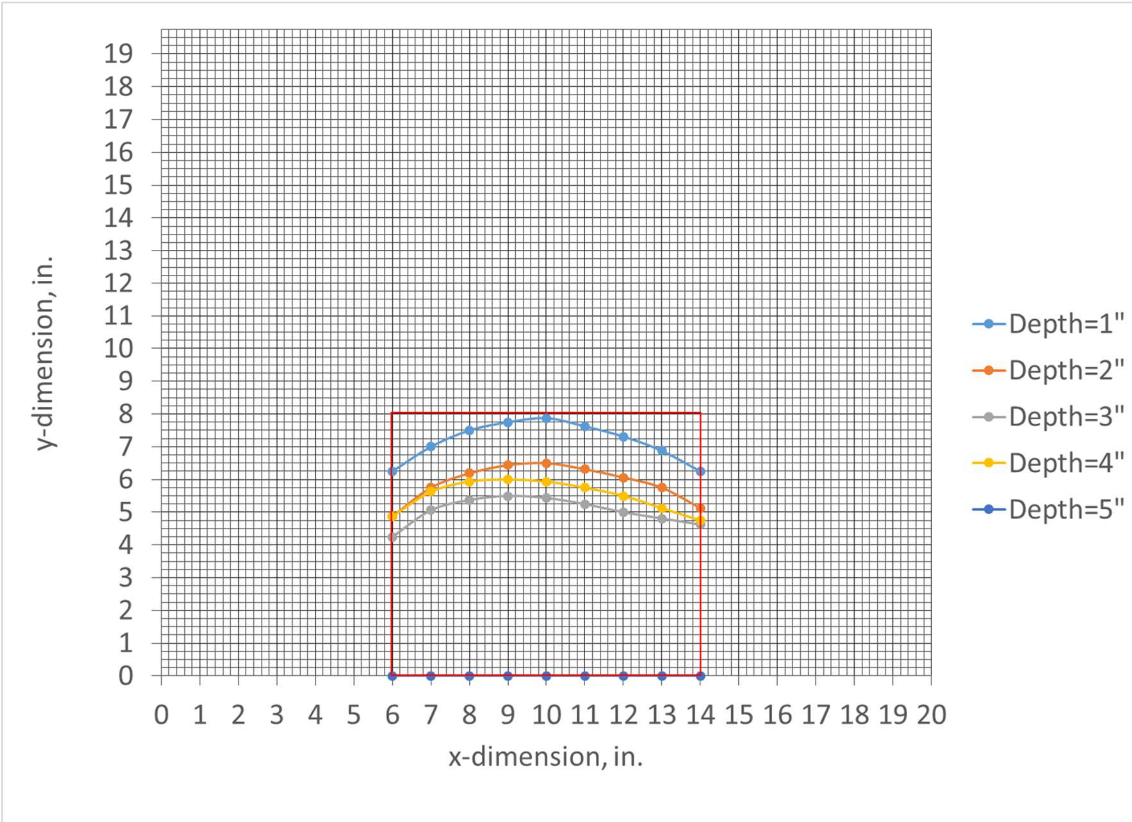

Figure 565: Failure Surface Contours of test 8W8L5Lay3

G.5 Failure Surface Contours of test 8W8L10Lay

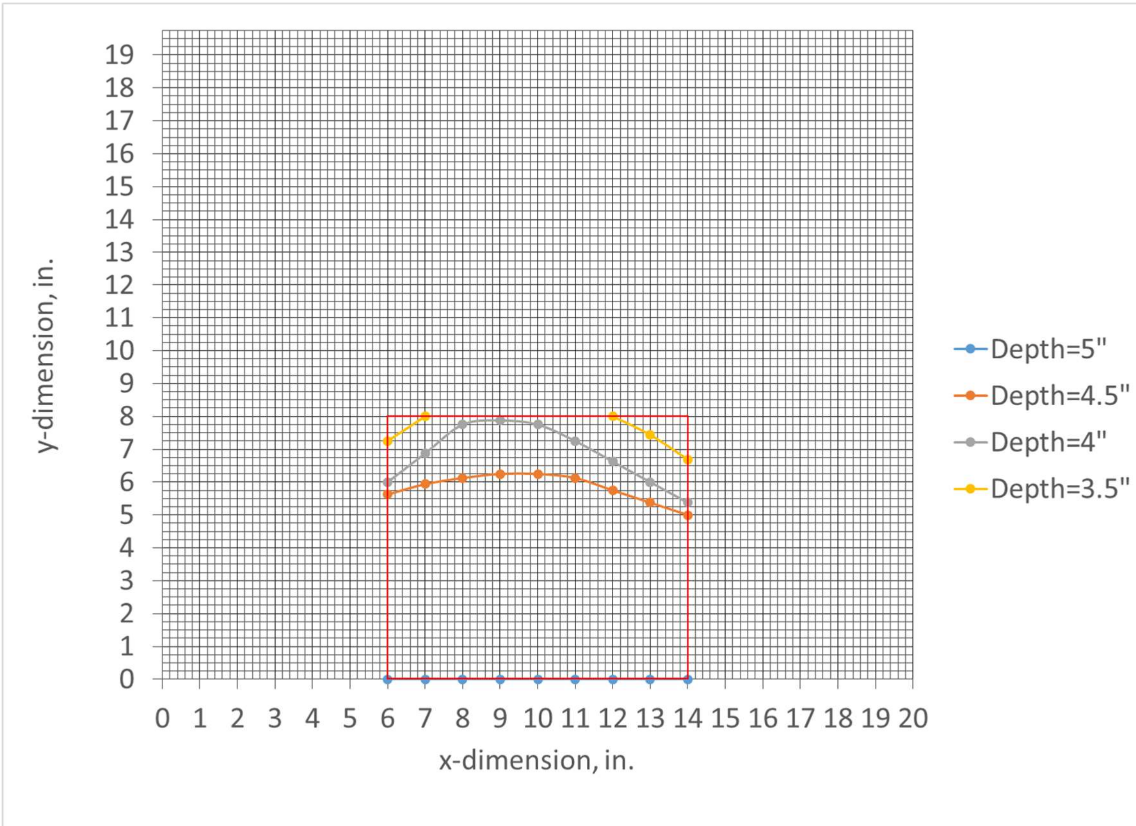

Figure 566: Failure Surface Contours of test 8W8L10Lay

G.6 Failure Surface Contours of test 8W8L10Lay2

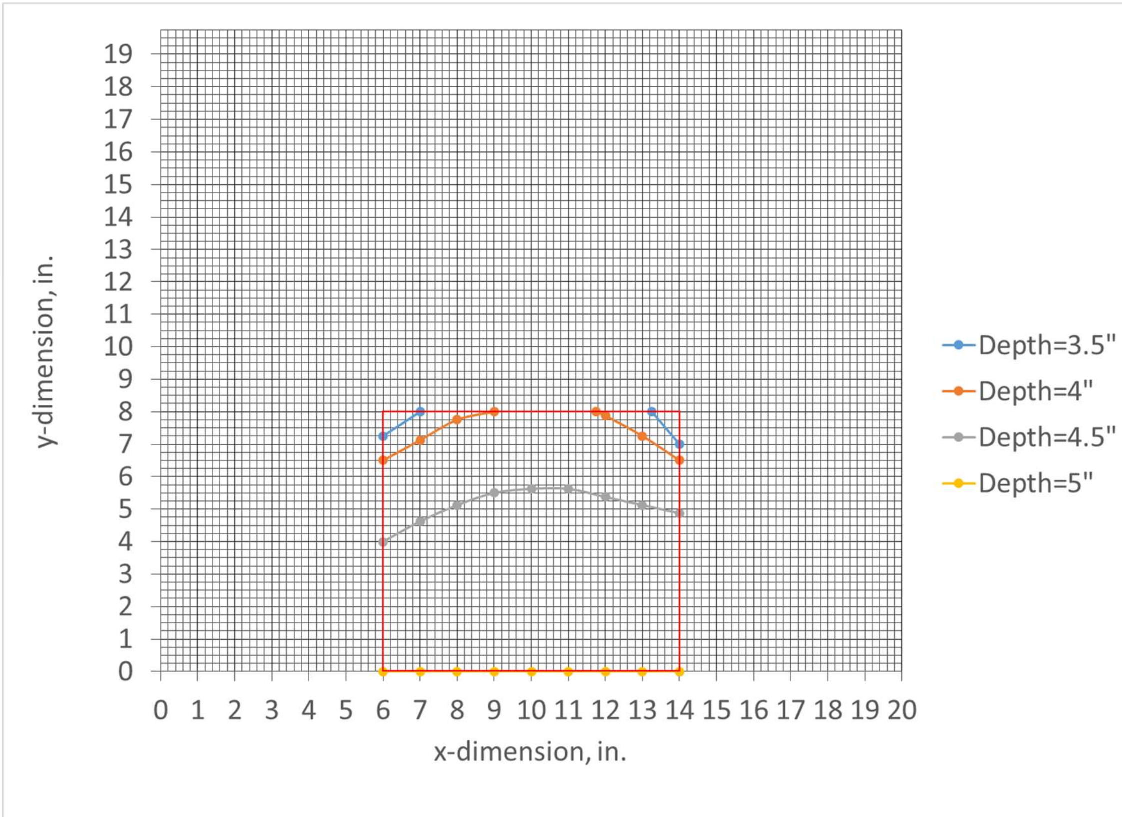

Figure 567: Failure Surface Contours of test 8W8L10Lay2

G.7 Failure Surface Contours of test 8W8L10Lay3

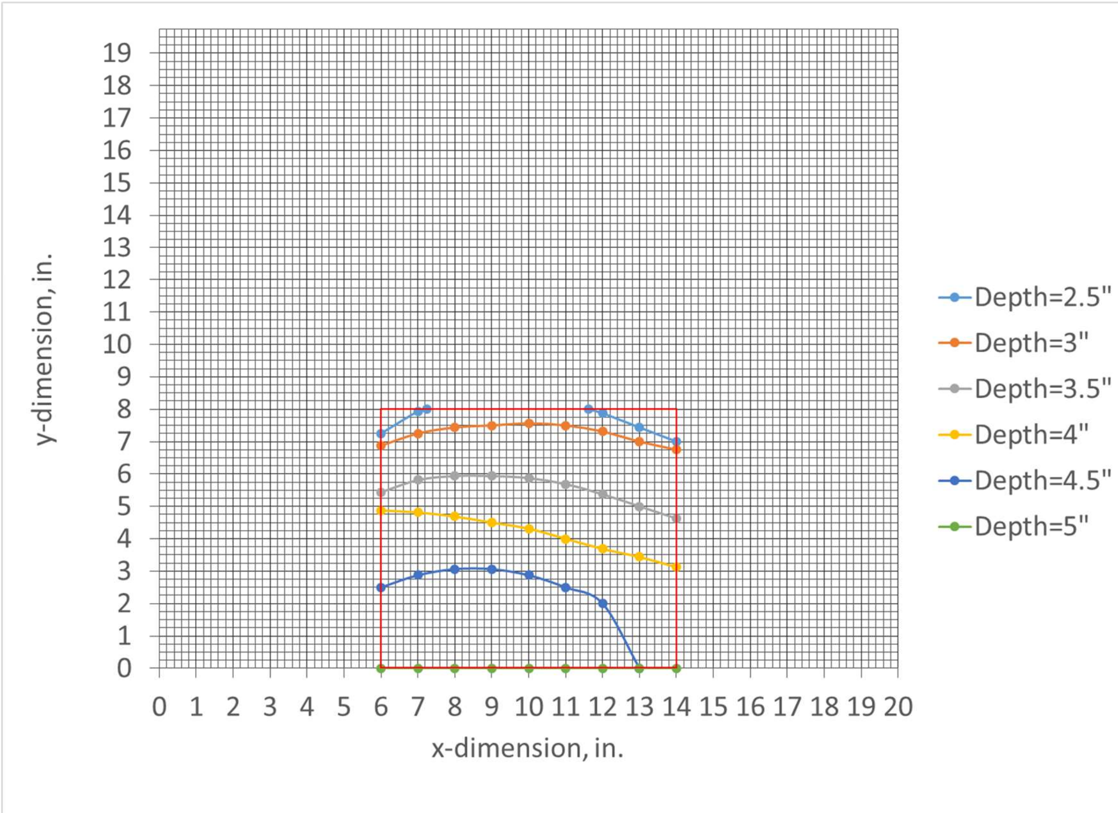

Figure 568: Failure Surface Contours of test 8W8L10Lay3

G.8 Failure Surface Contours of test 8W11L5Lay

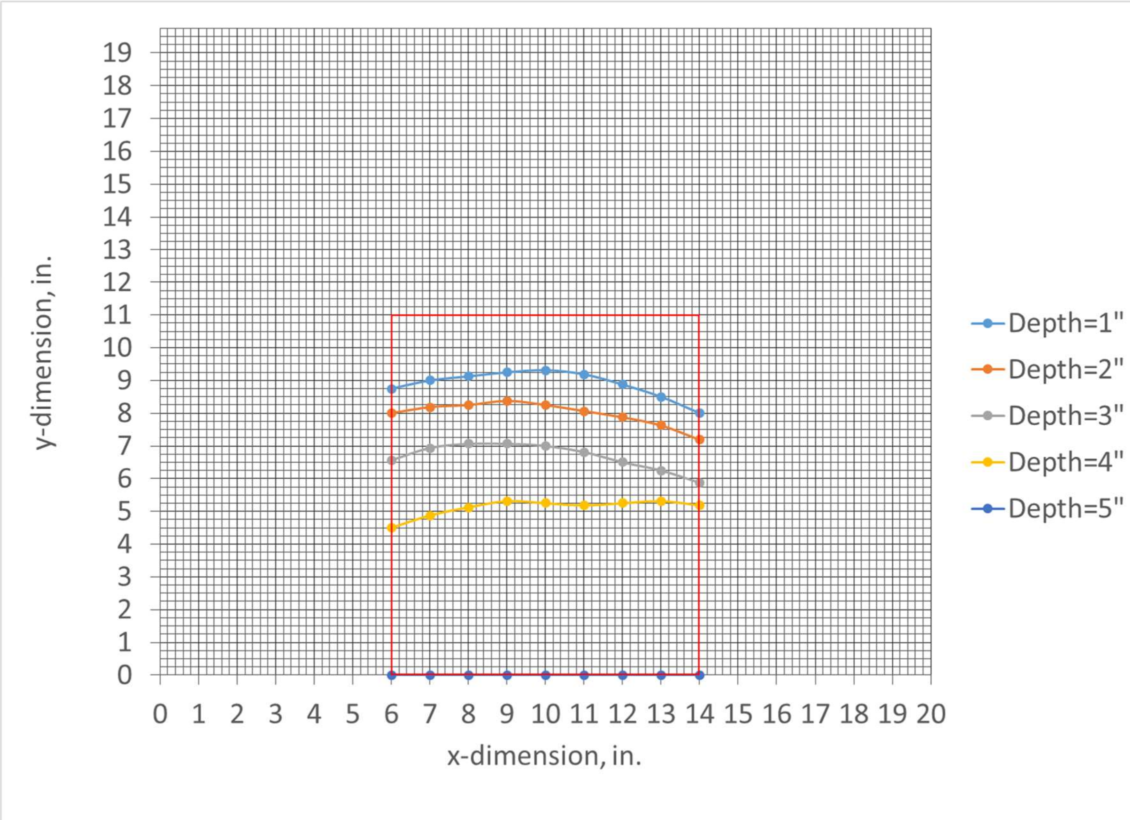

Figure 569: Failure Surface Contours of test 8W11L5Lay

G.9 Failure Surface Contours of test 8W11L5Lay2

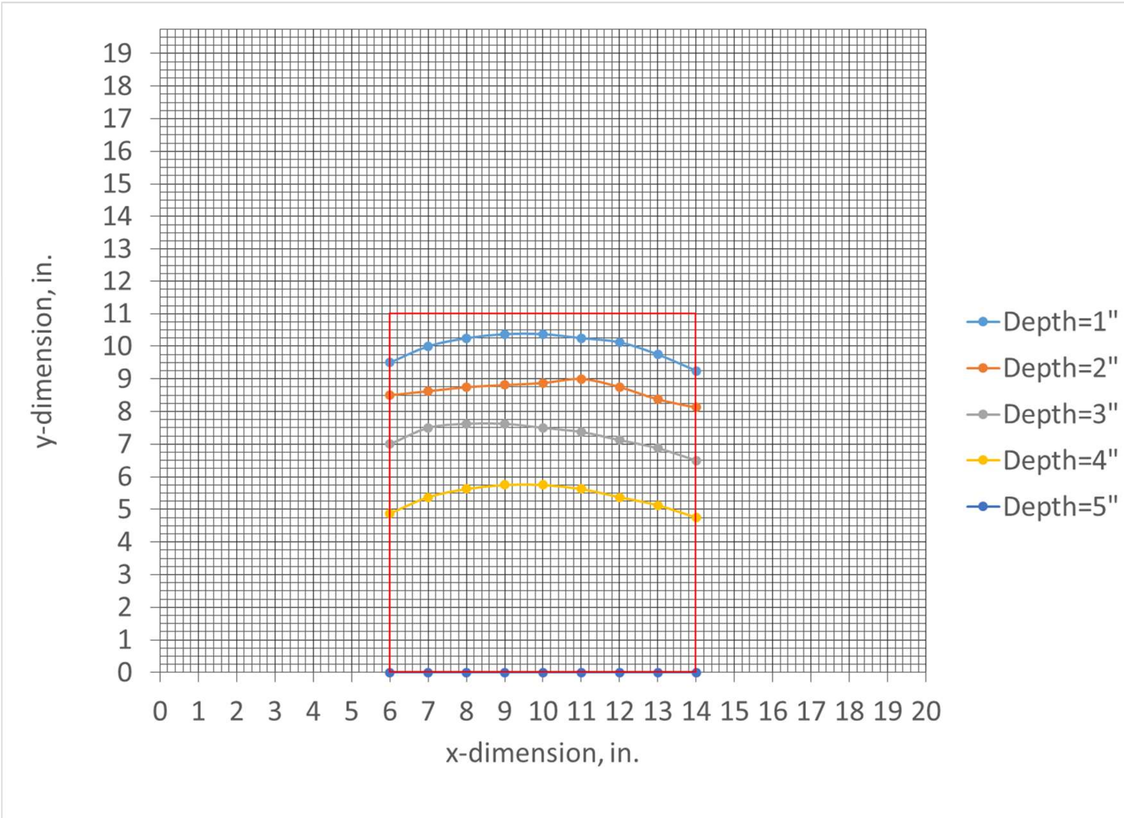

Figure 570: Failure Surface Contours of test 8W11L5Lay2

G.10 Failure Surface Contours of test 8W11L5Lay3

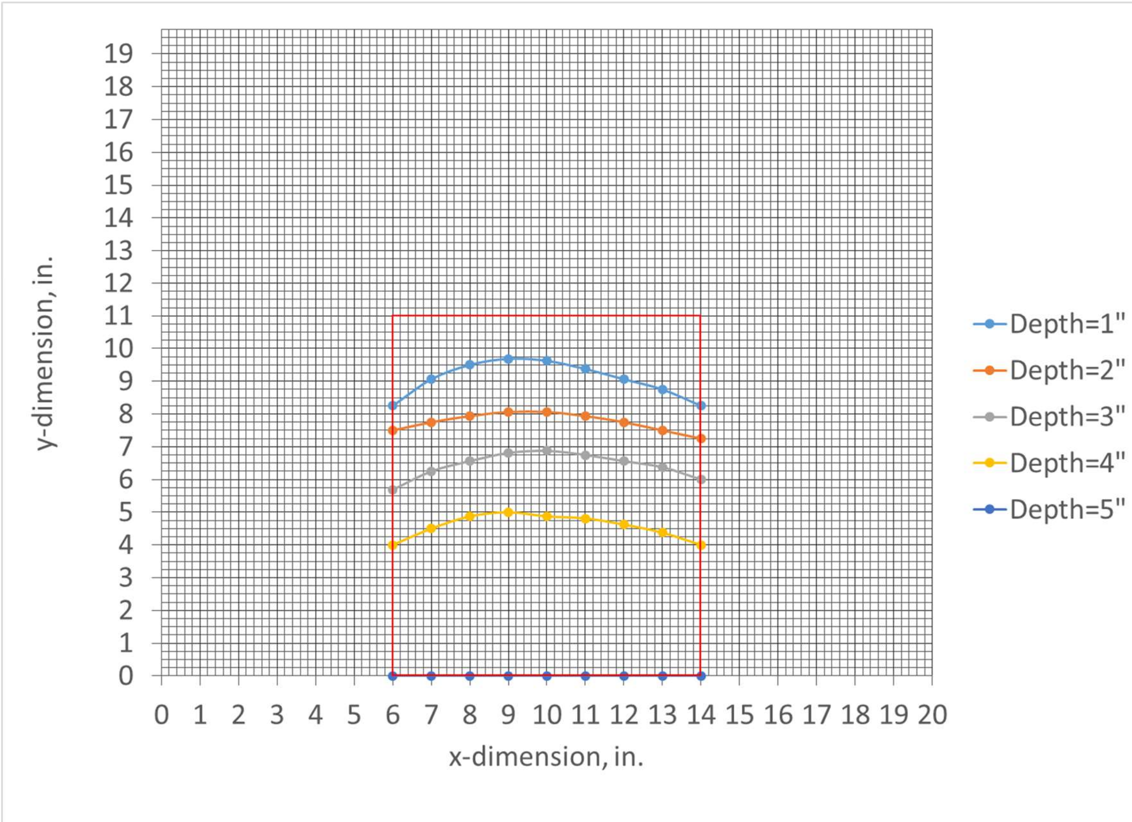

Figure 571: Failure Surface Contours of test 8W11L5Lay3

G.11 Failure Surface Contours of test 8W11L10Lay

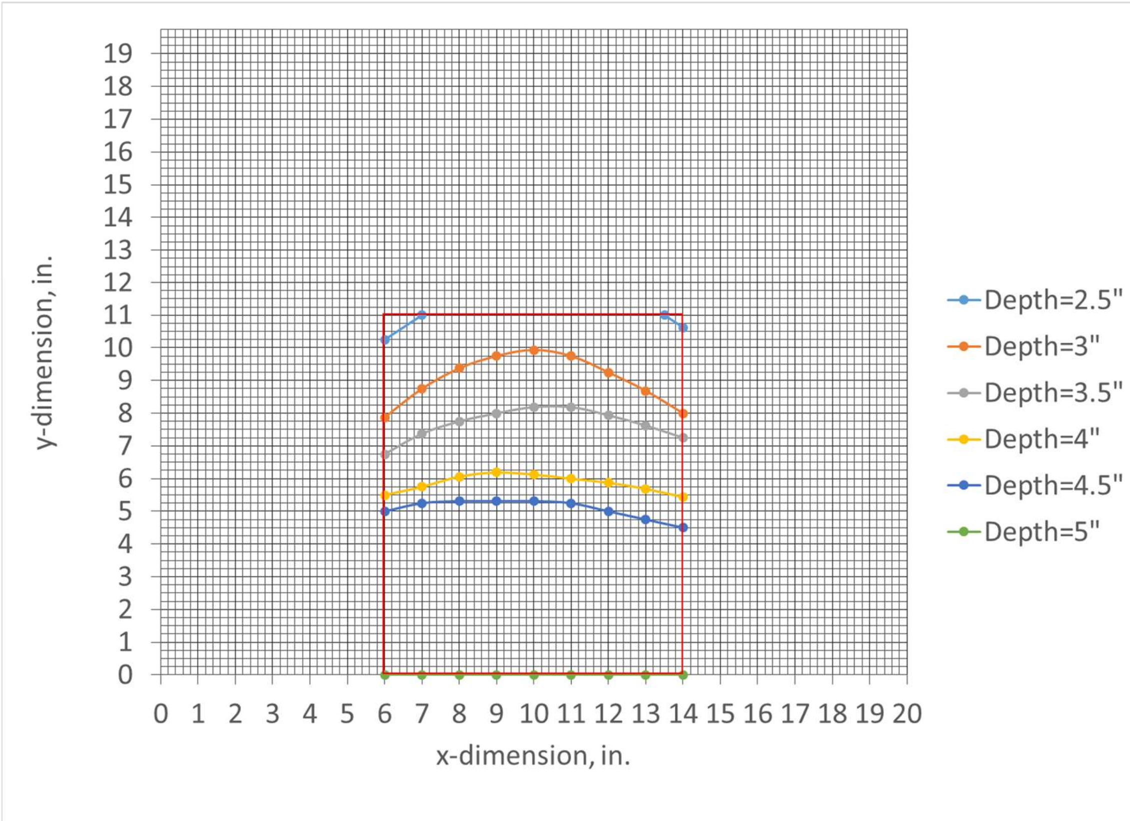

Figure 572: Failure Surface Contours of test 8W11L10Lay

G.12 Failure Surface Contours of test 8W11L10Lay2

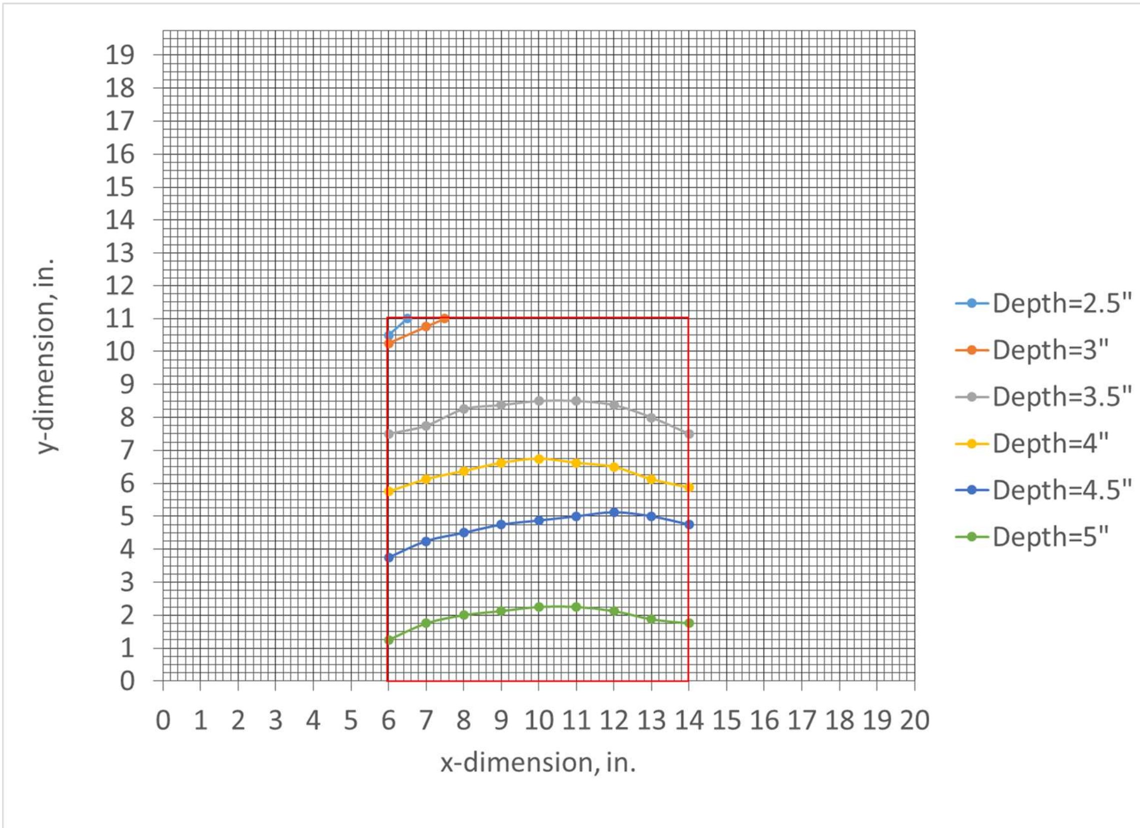

Figure 573: Failure Surface Contours of test 8W11L10Lay2

G.13 Failure Surface Contours of test 8W11L10Lay3

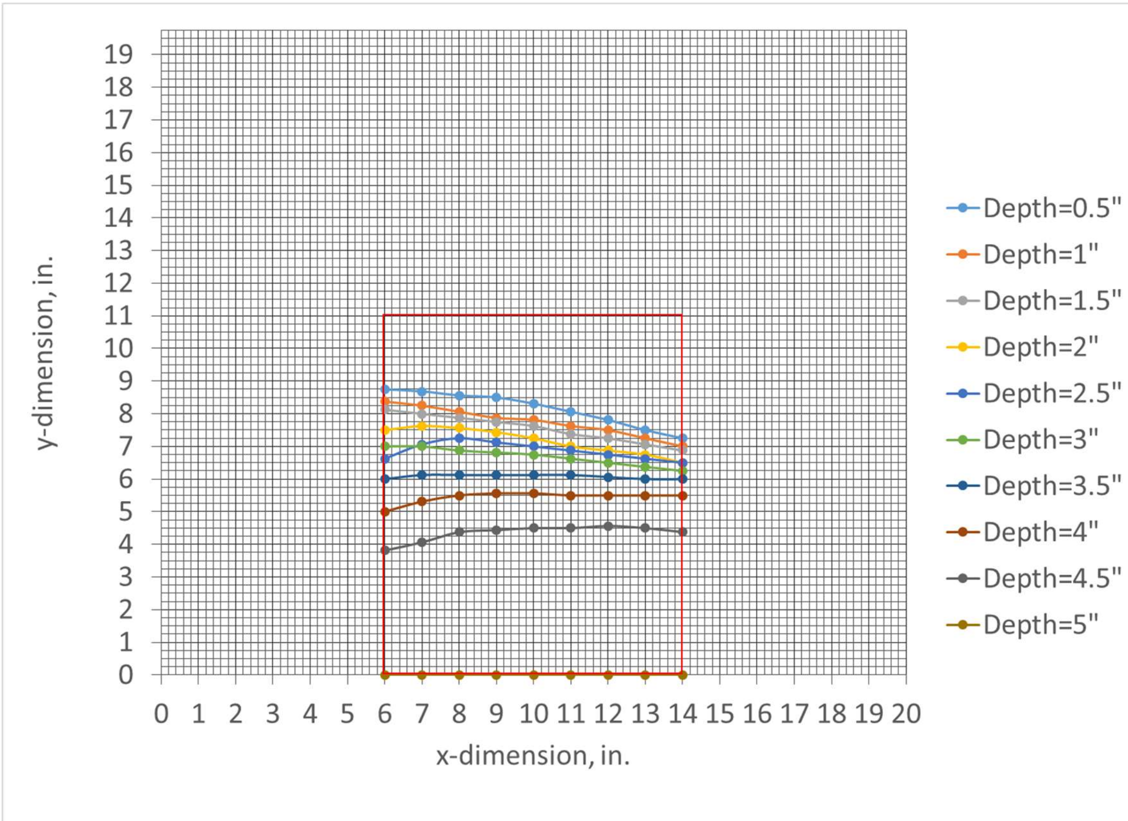

Figure 574: Failure Surface Contours of test 8W11L10Lay3

G.14 Failure Surface Contours of test 11W8L5Lay

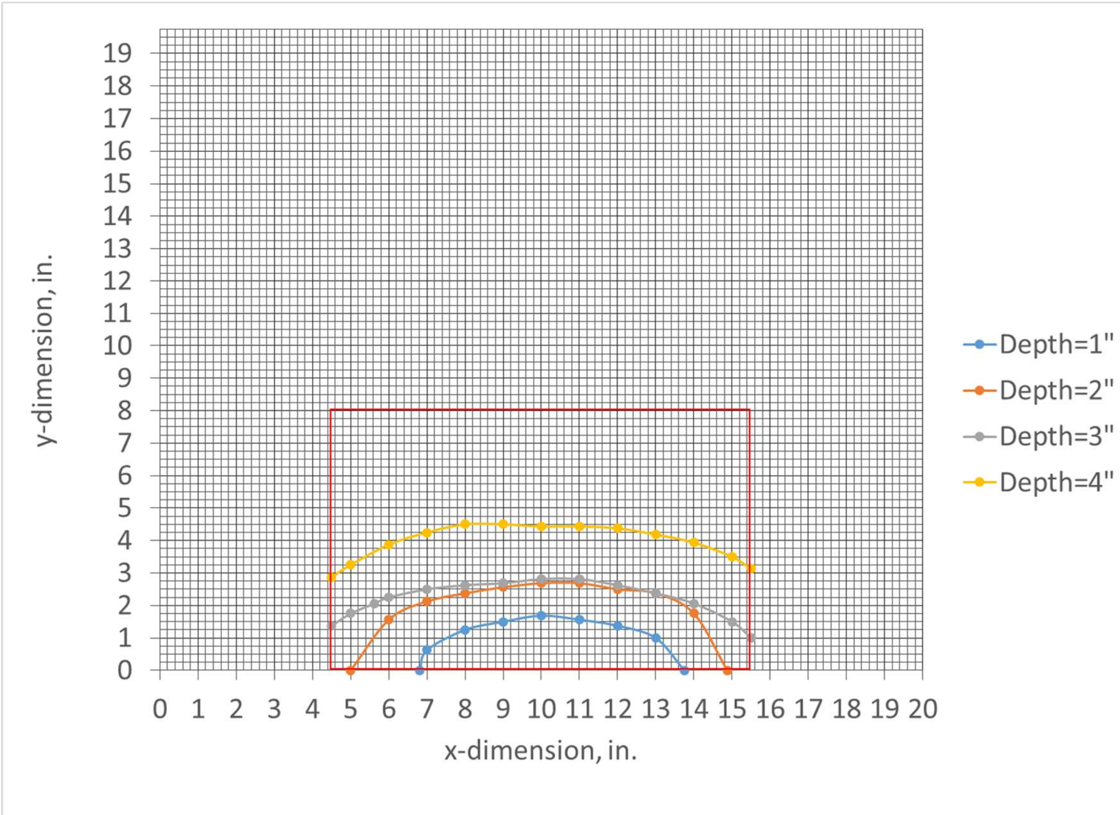

Figure 575: Failure Surface Contours of test 11W8L5Lay

G.15 Failure Surface Contours of test 11W8L5Lay2

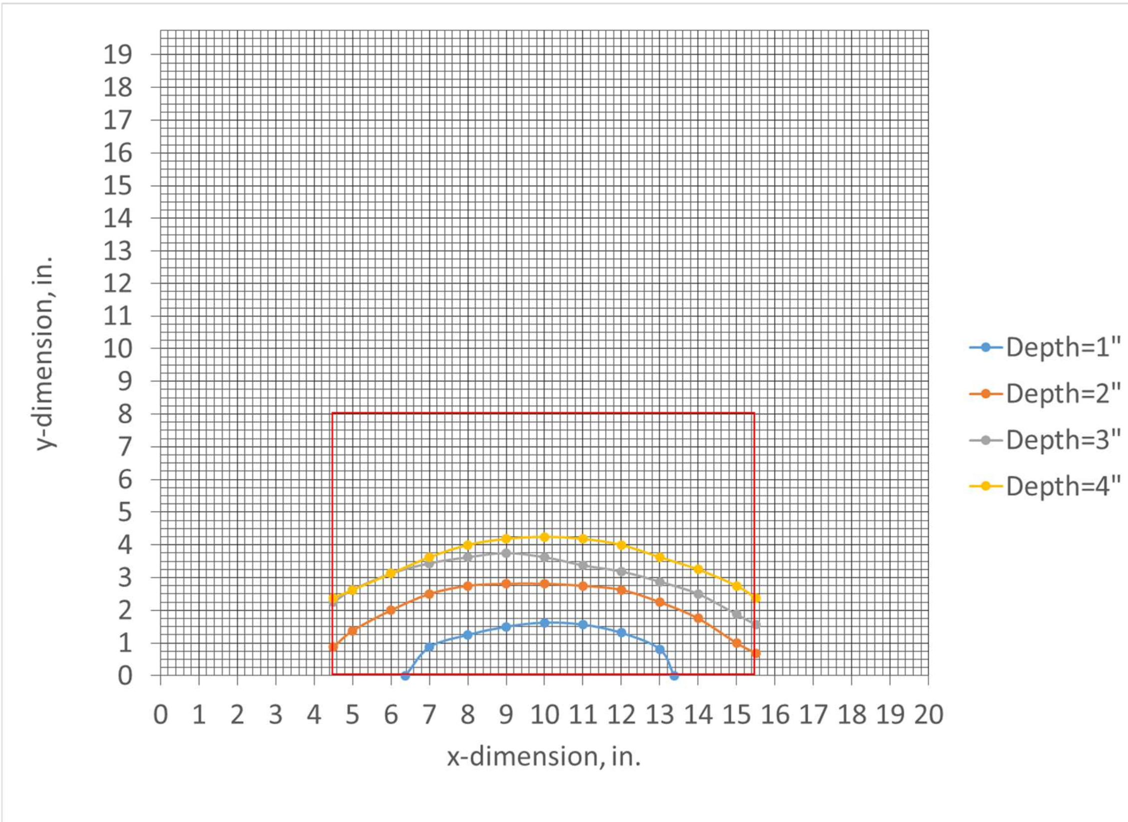

Figure 576: Failure Surface Contours of test 11W8L5Lay2

G.16 Failure Surface Contours of test 11W8L5Lay3

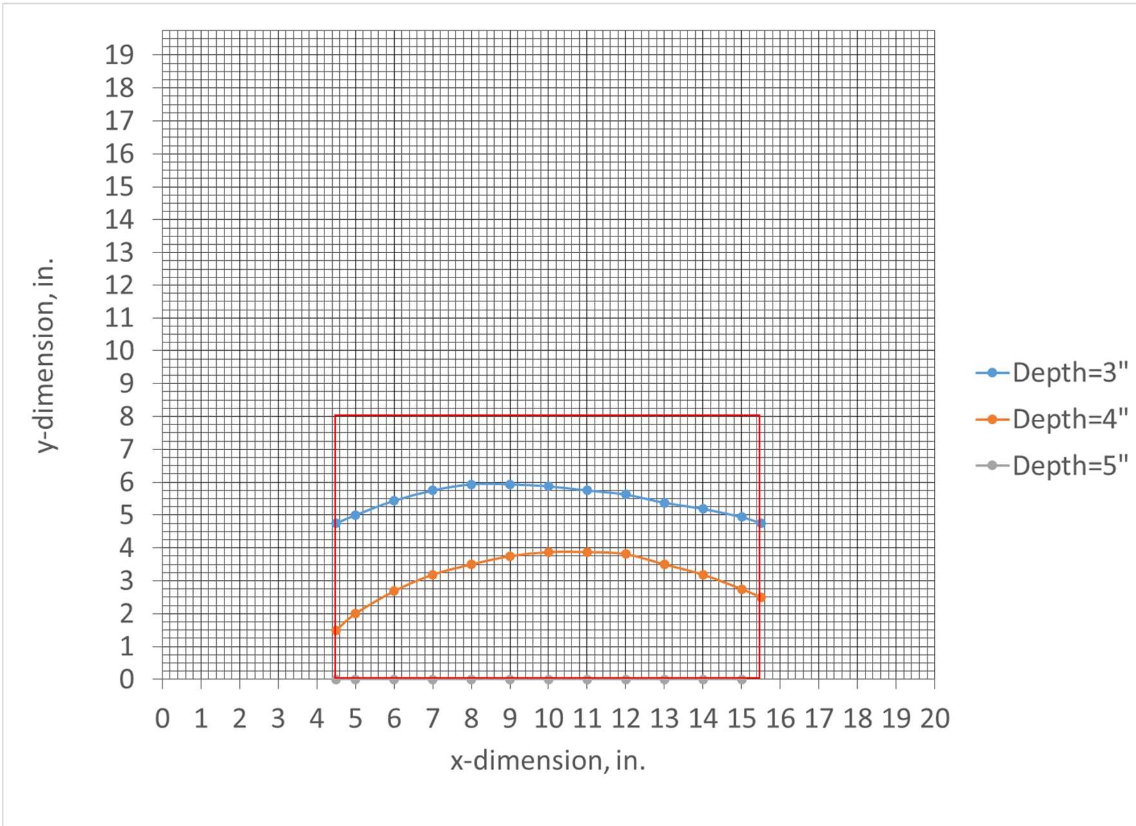

Figure 577: Failure Surface Contours of test 11W8L5Lay3

G.17 Failure Surface Contours of test 11W8L10Lay

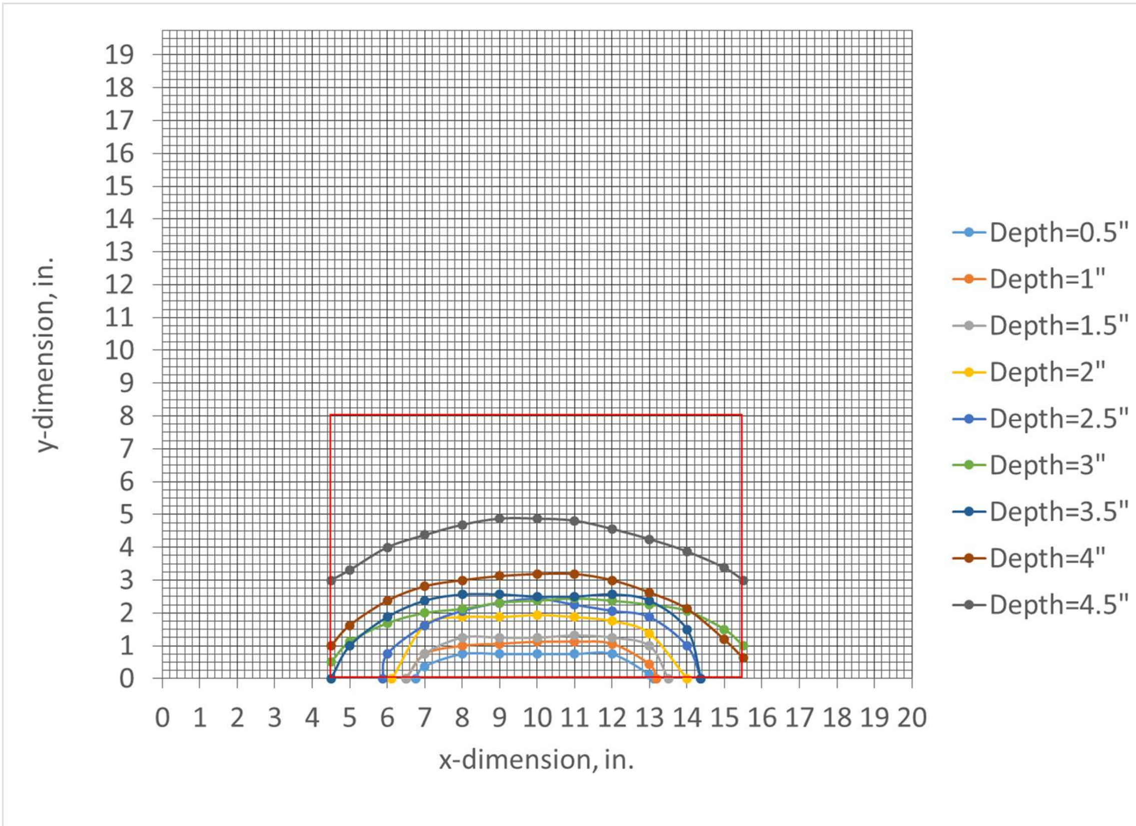

Figure 578: Failure Surface Contours of test 11W8L10Lay

G.18 Failure Surface Contours of test 11W8L10Lay2

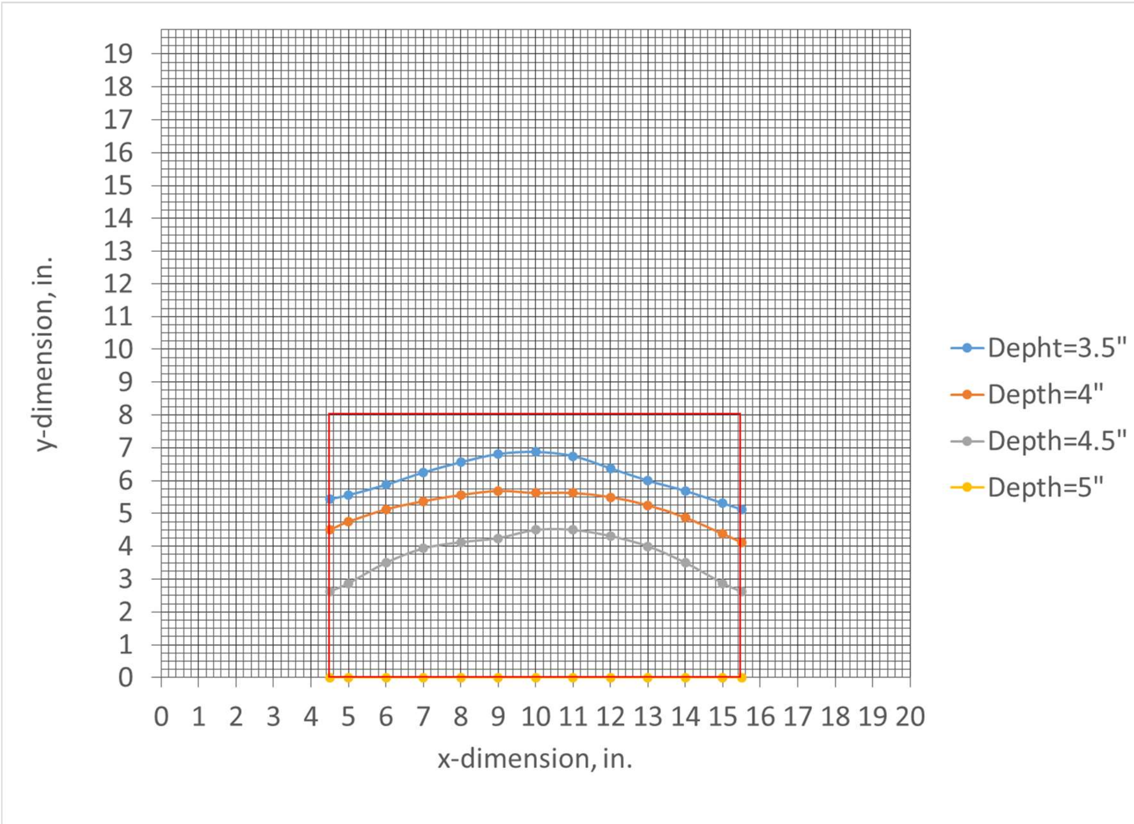

Figure 579: Failure Surface Contours of test 11W8L10Lay2

G.19 Failure Surface Contours of test 11W8L10Lay3

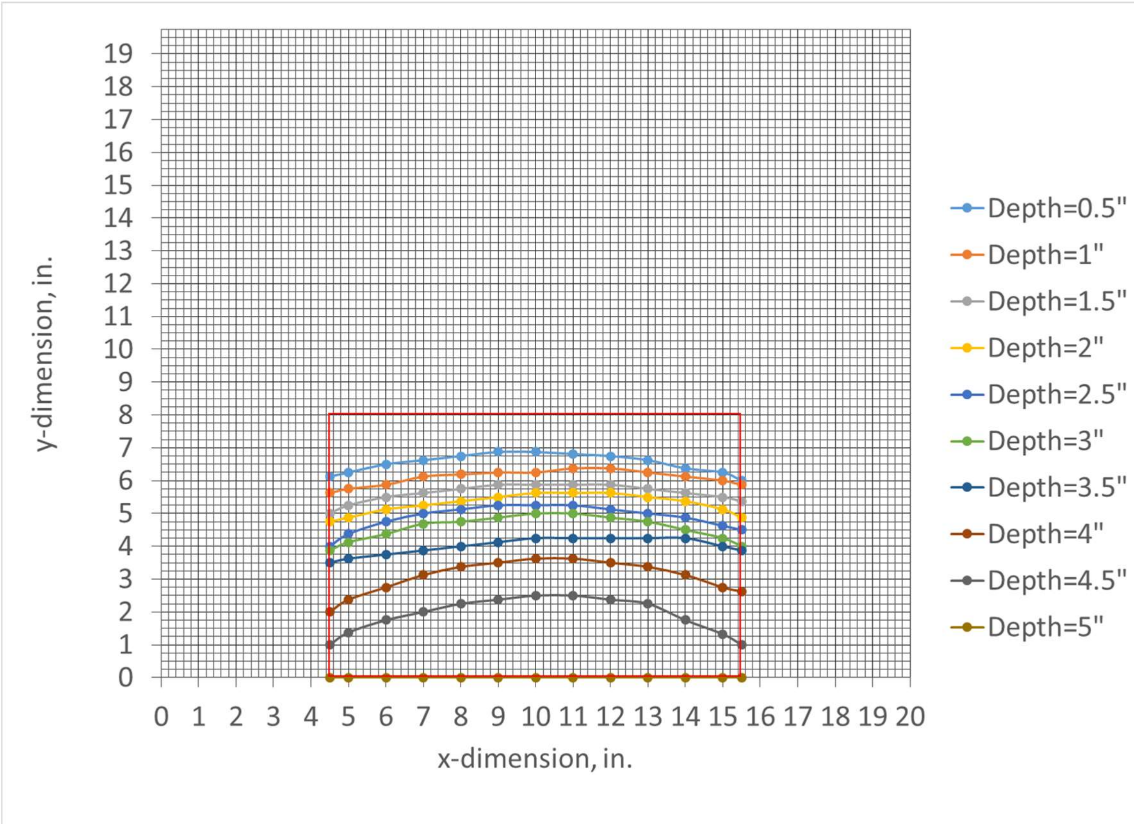

Figure 580: Failure Surface Contours of test 11W8L10Lay3

G.20 Failure Surface Contours of test 11W11L5Lay

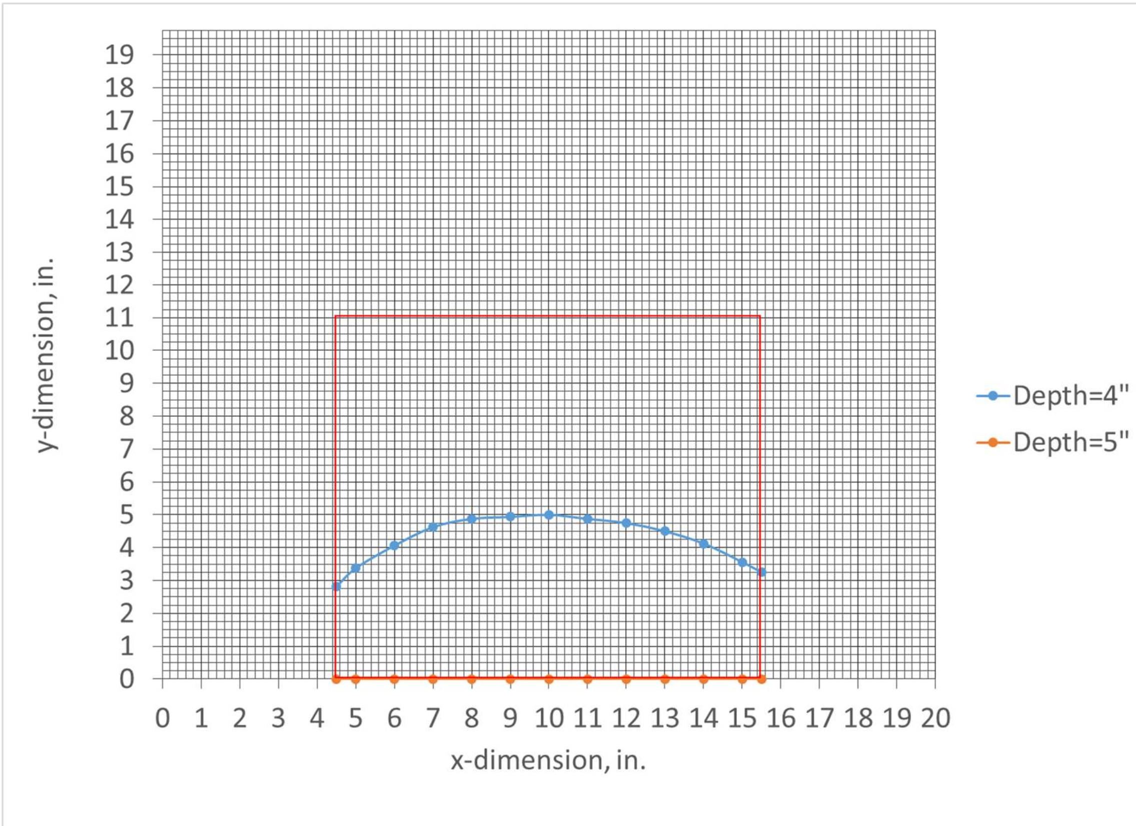

Figure 581: Failure Surface Contours of test 11W11L5Lay

G.21 Failure Surface Contours of test 11W11L5Lay2

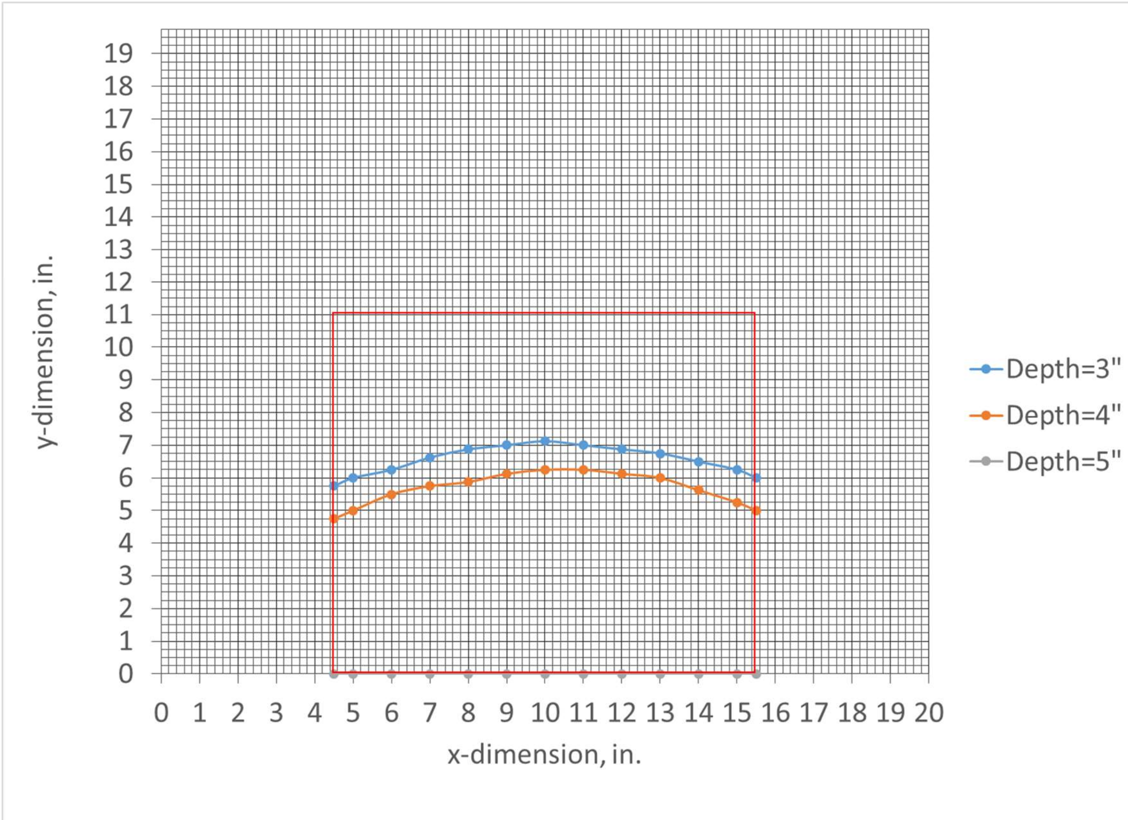

Figure 582: Failure Surface Contours of test 11W11L5Lay2

G.22 Failure Surface Contours of test 11W11L5Lay3

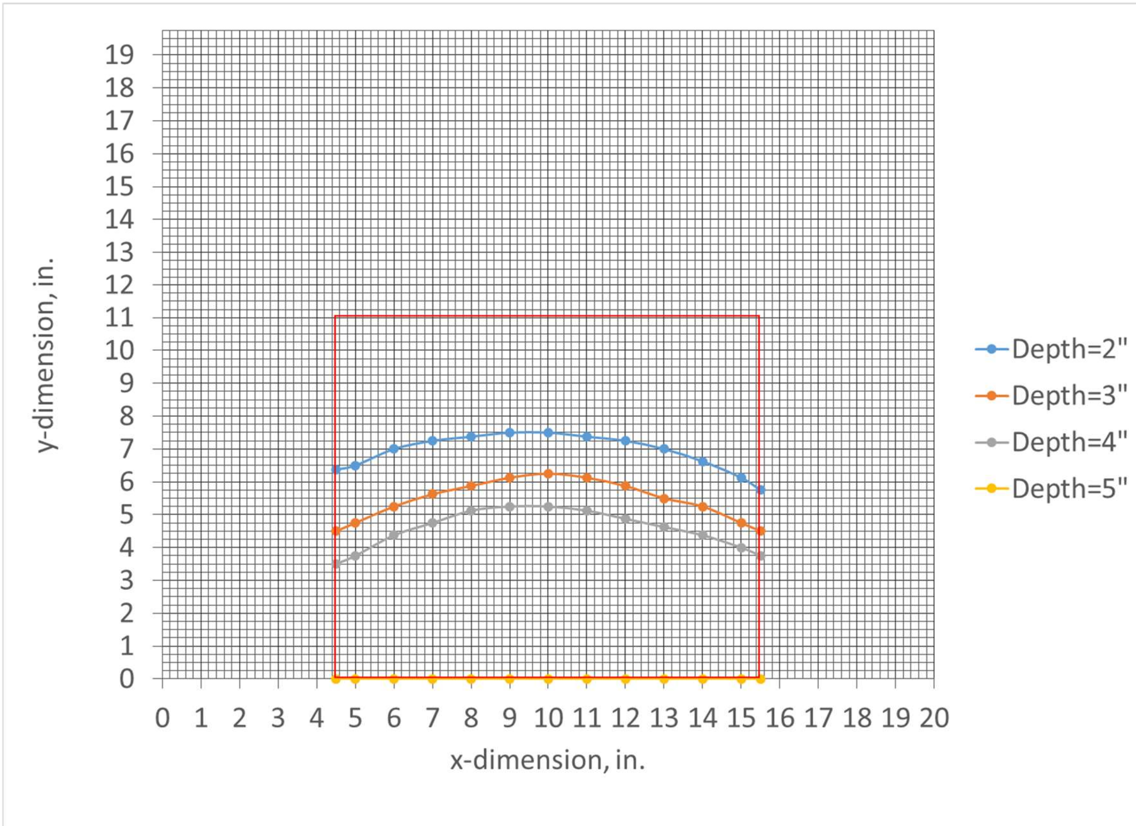

Figure 583: Failure Surface Contours of test 11W11L5Lay3

G.23 Failure Surface Contours of test 11W11L10Lay

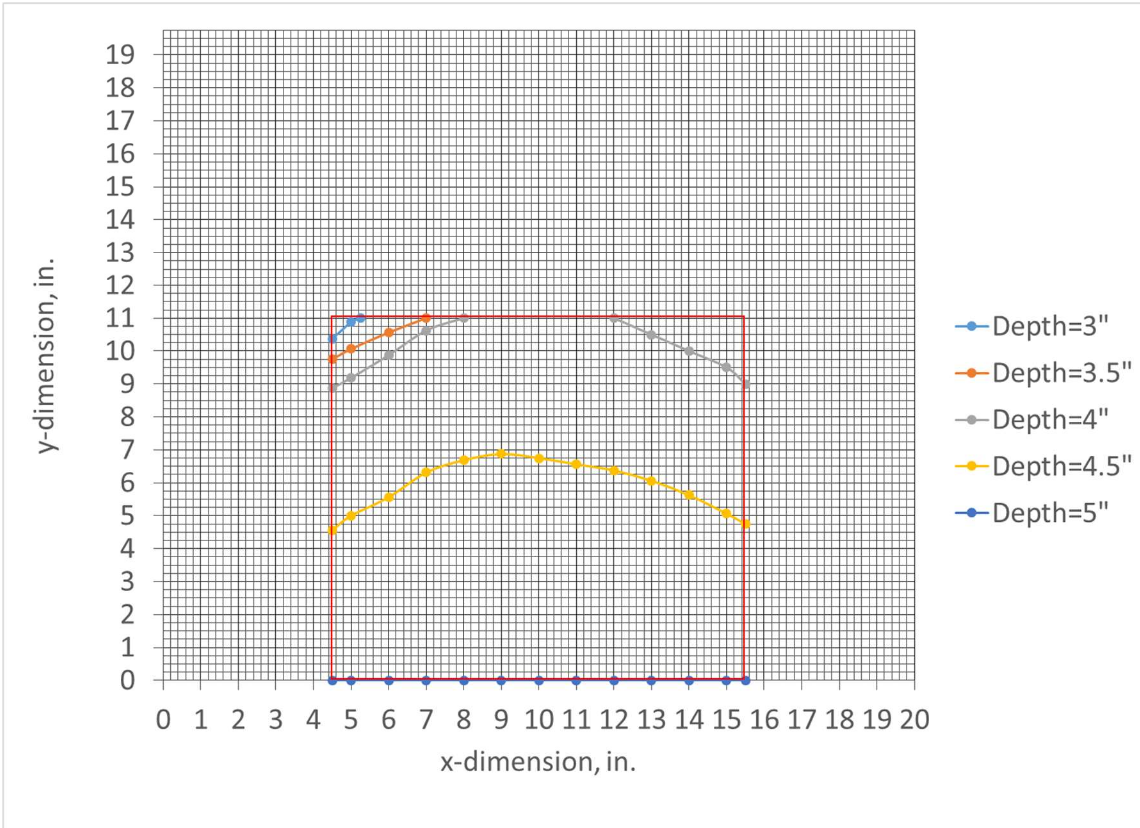

Figure 584: Failure Surface Contours of test 11W11L10Lay

G.24 Failure Surface Contours of test 11W11L10Lay2

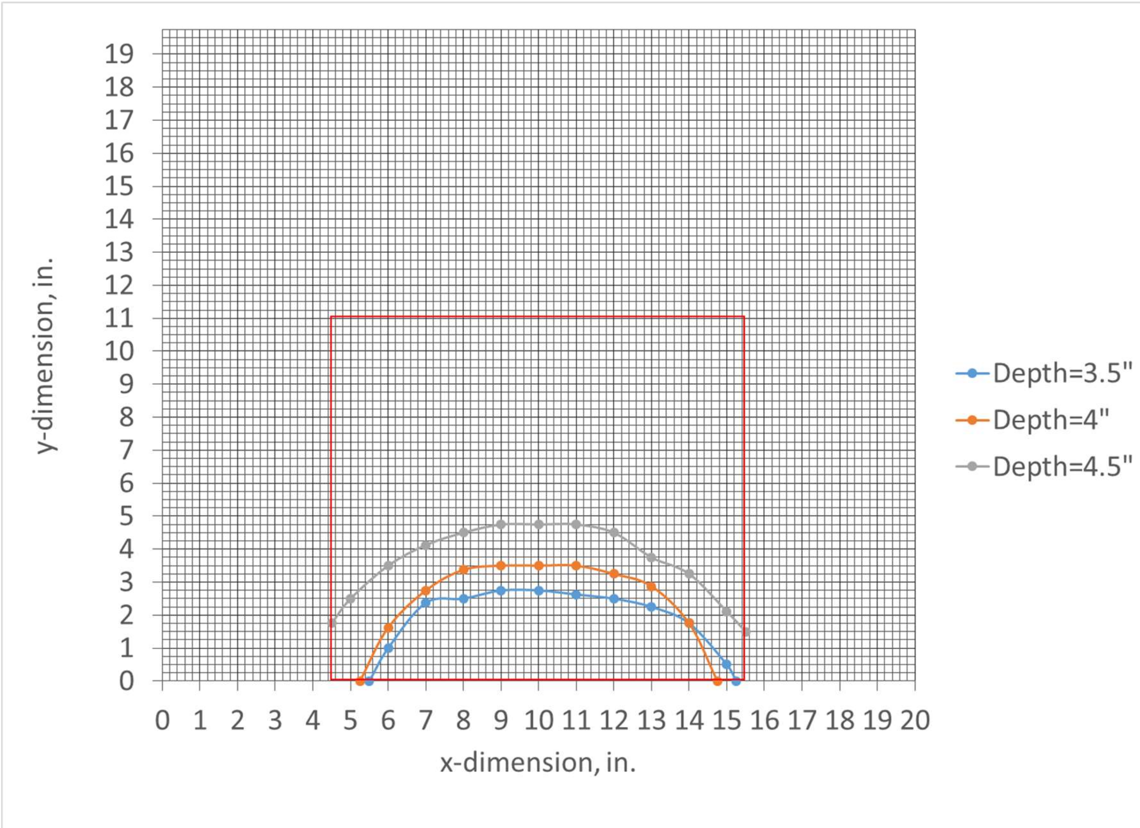

Figure 585: Failure Surface Contours of test 11W11L10Lay2

G.25 Failure Surface Contours of test 11W11L10Lay3

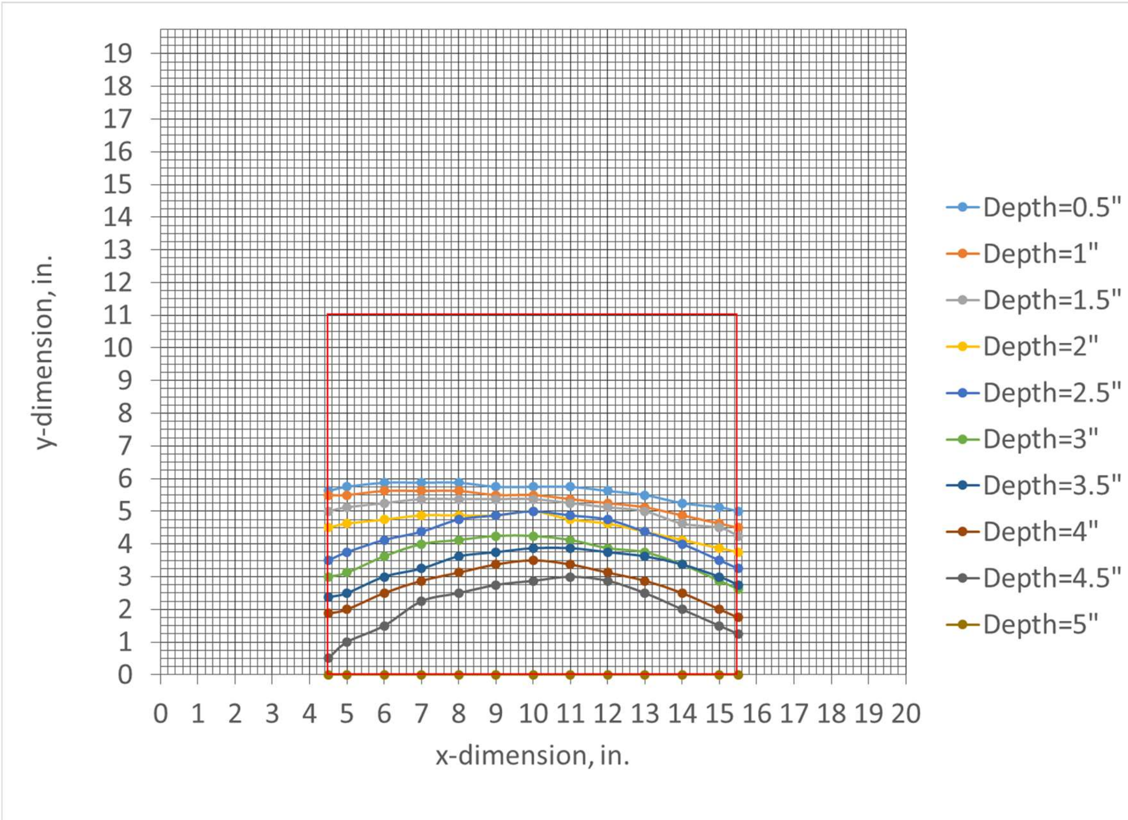

Figure 586: Failure Surface Contours of test 11W11L10Lay3

G.26 Failure Surface Contours of test PW8L5Lay

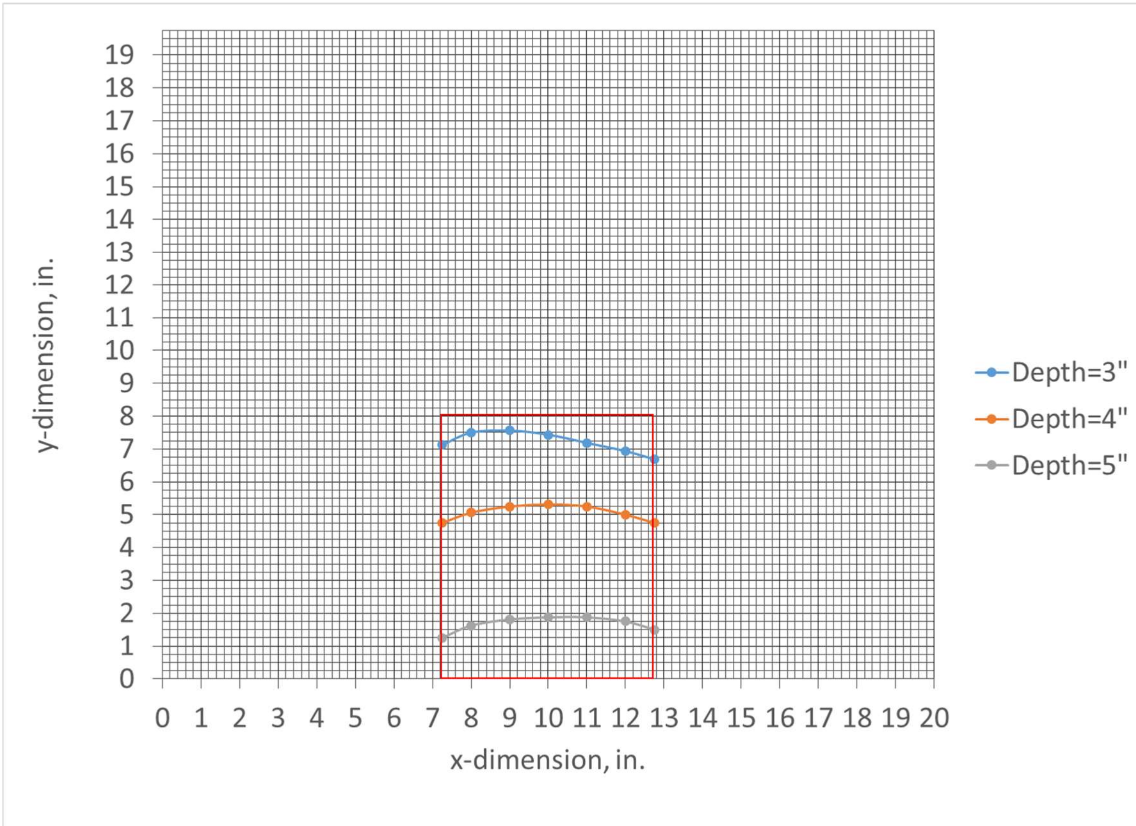

Figure 587: Failure Surface Contours of test PW8L5Lay

G.27 Failure Surface Contours of test PW8L5Lay2

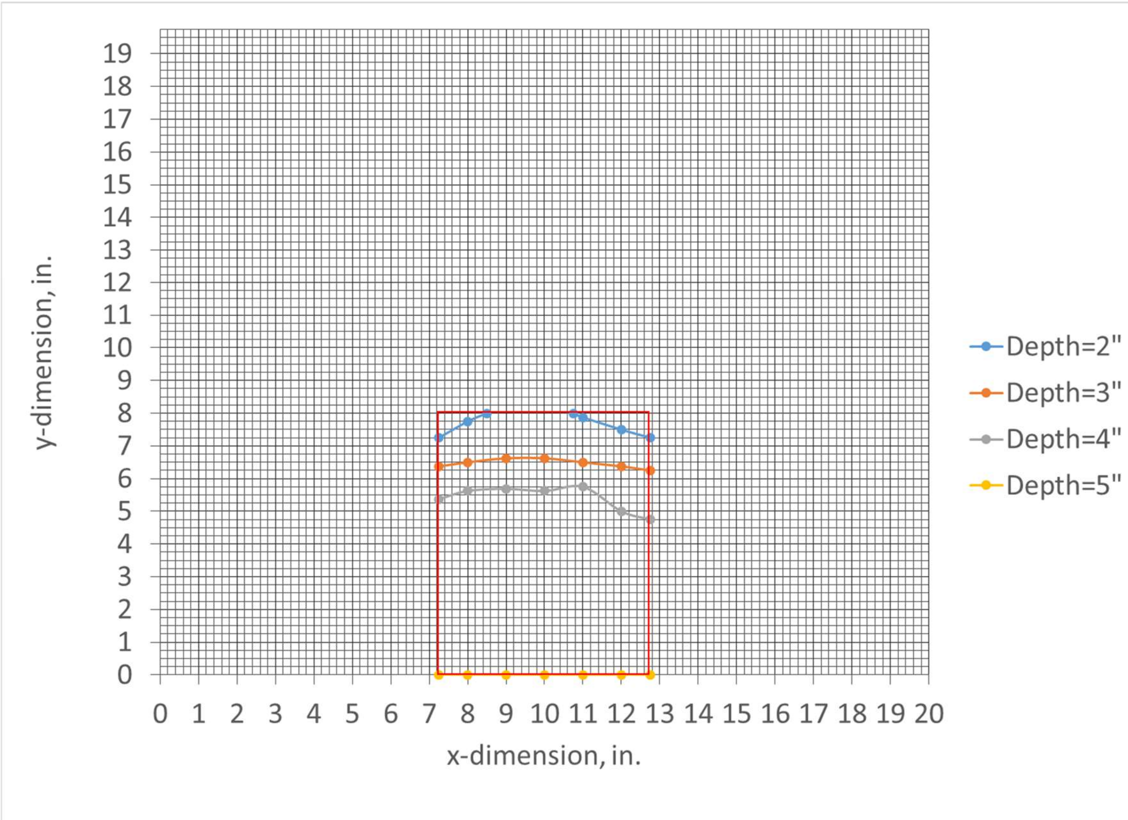

Figure 588: Failure Surface Contours of test PW8L5Lay2

G.28 Failure Surface Contours of test PW8L5Lay3

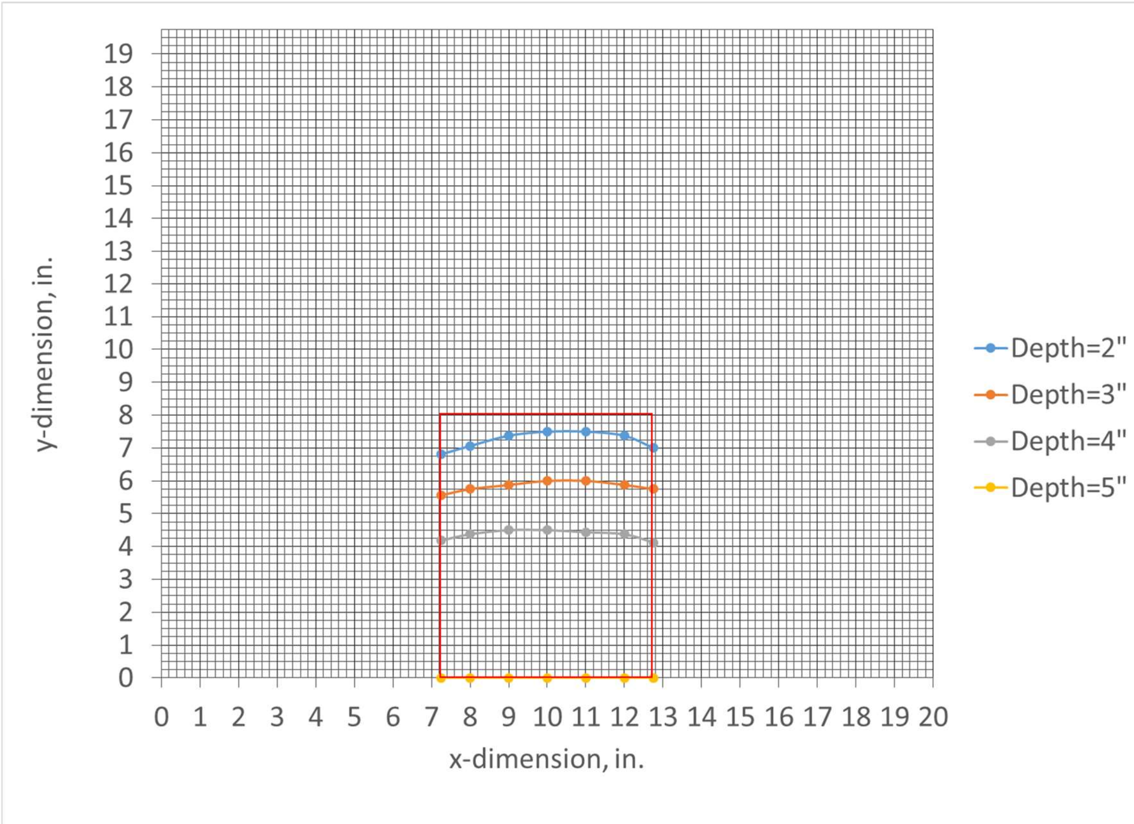

Figure 589: Failure Surface Contours of test PW8L5Lay3

G.29 Failure Surface Contours of test PW8L10Lay

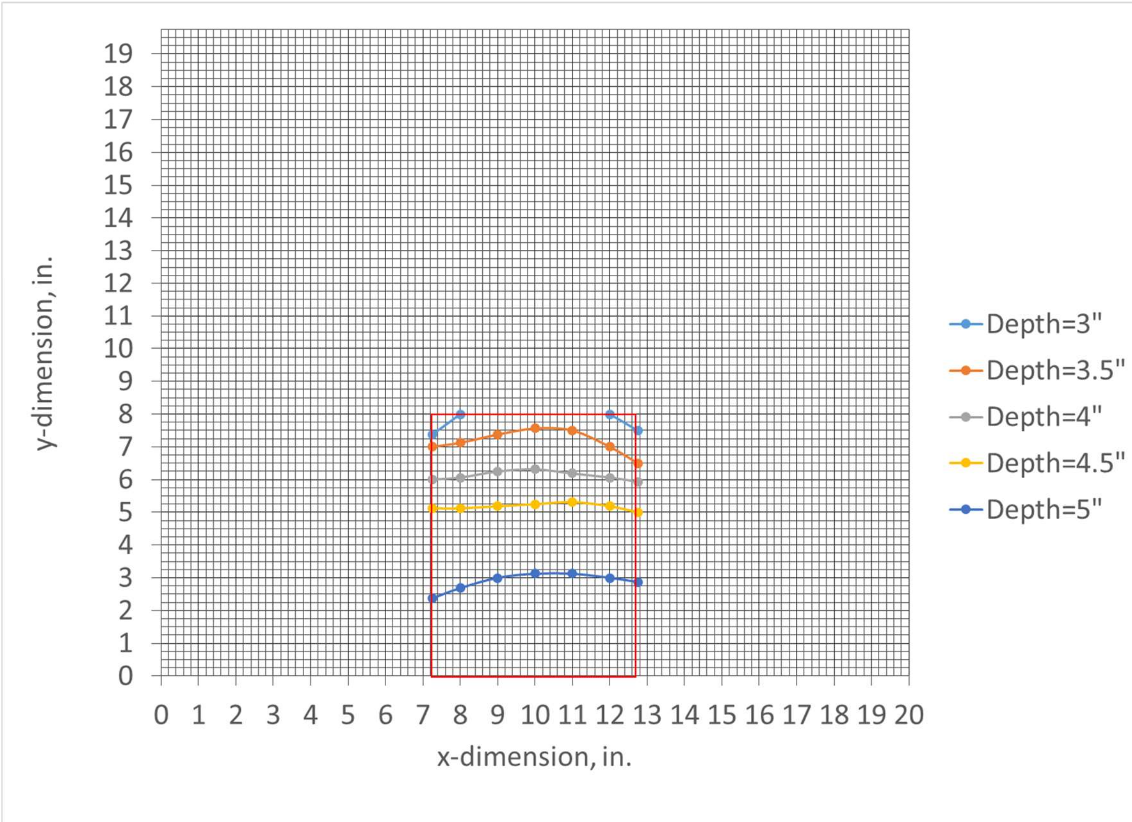

Figure 590: Failure Surface Contours of test PW8L10Lay

G.30 Failure Surface Contours of test PW8L10Lay2

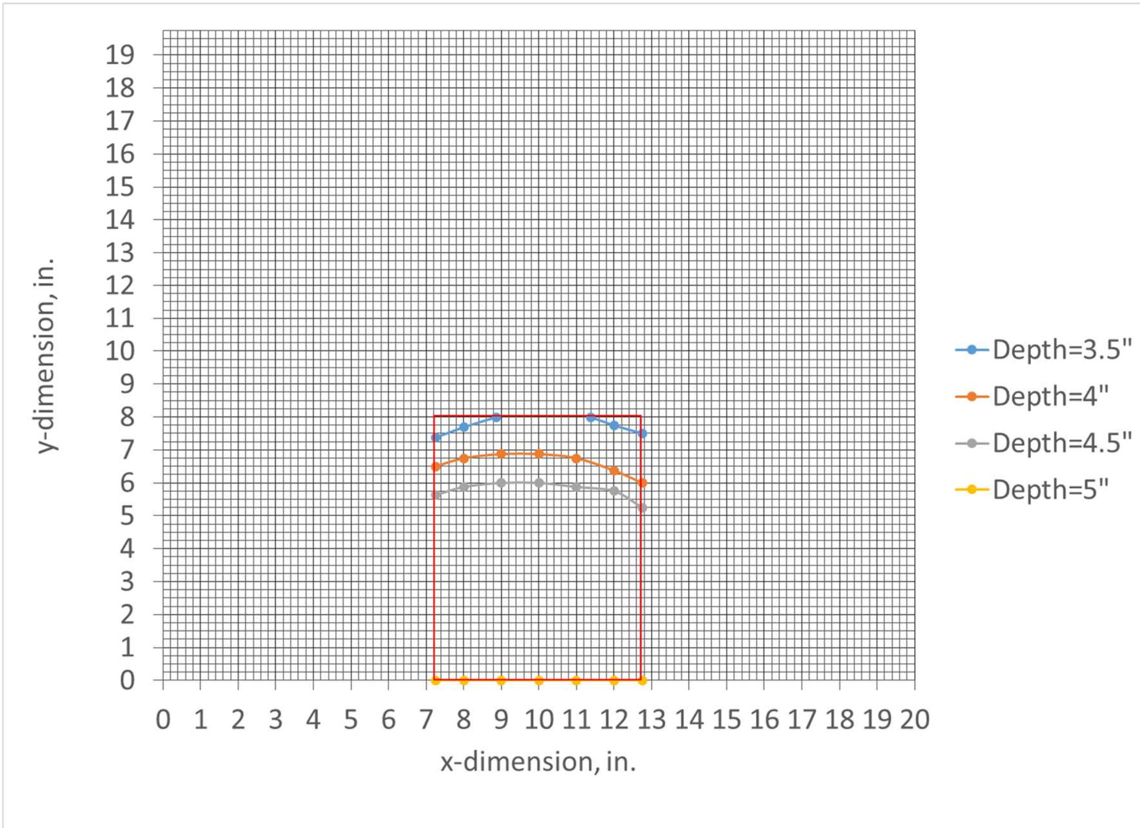

Figure 591: Failure Surface Contours of test PW8L10Lay2

G.31 Failure Surface Contours of test PW8L10Lay3

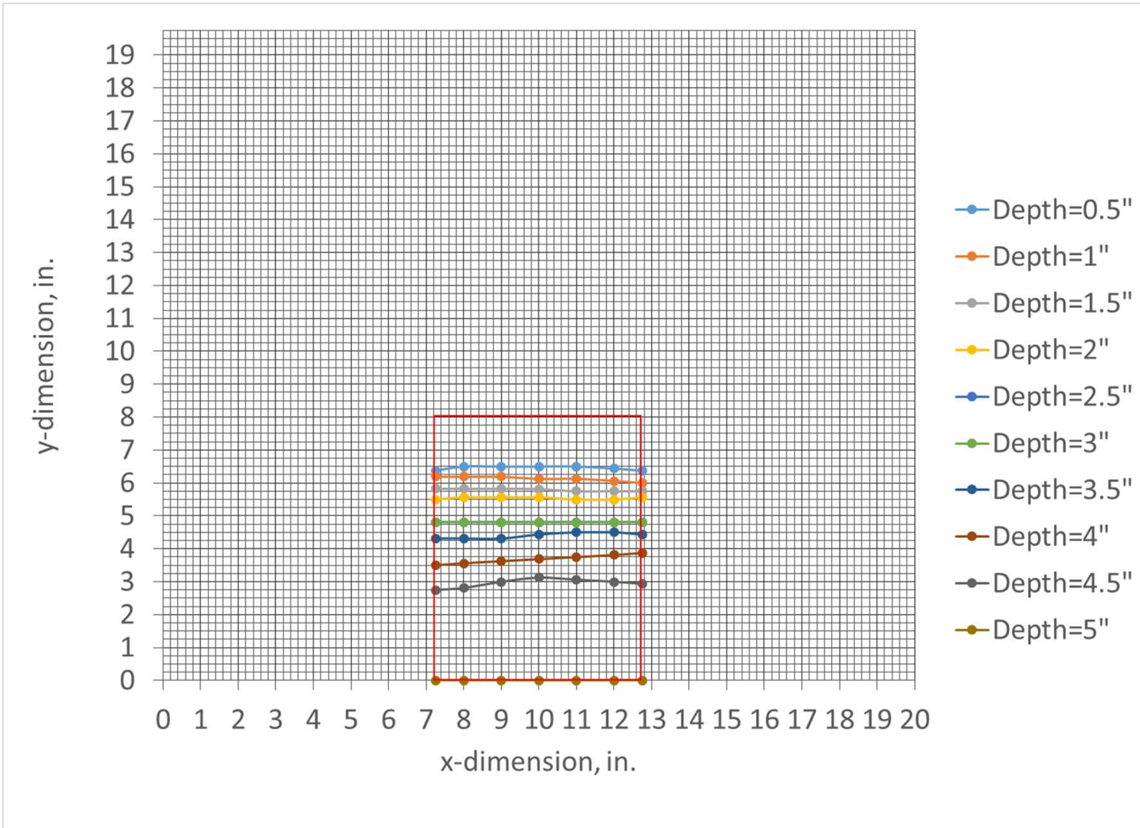

Figure 592: Failure Surface Contours of test PW8L10Lay3

G.32 Failure Surface Contours of test PW11L5Lay

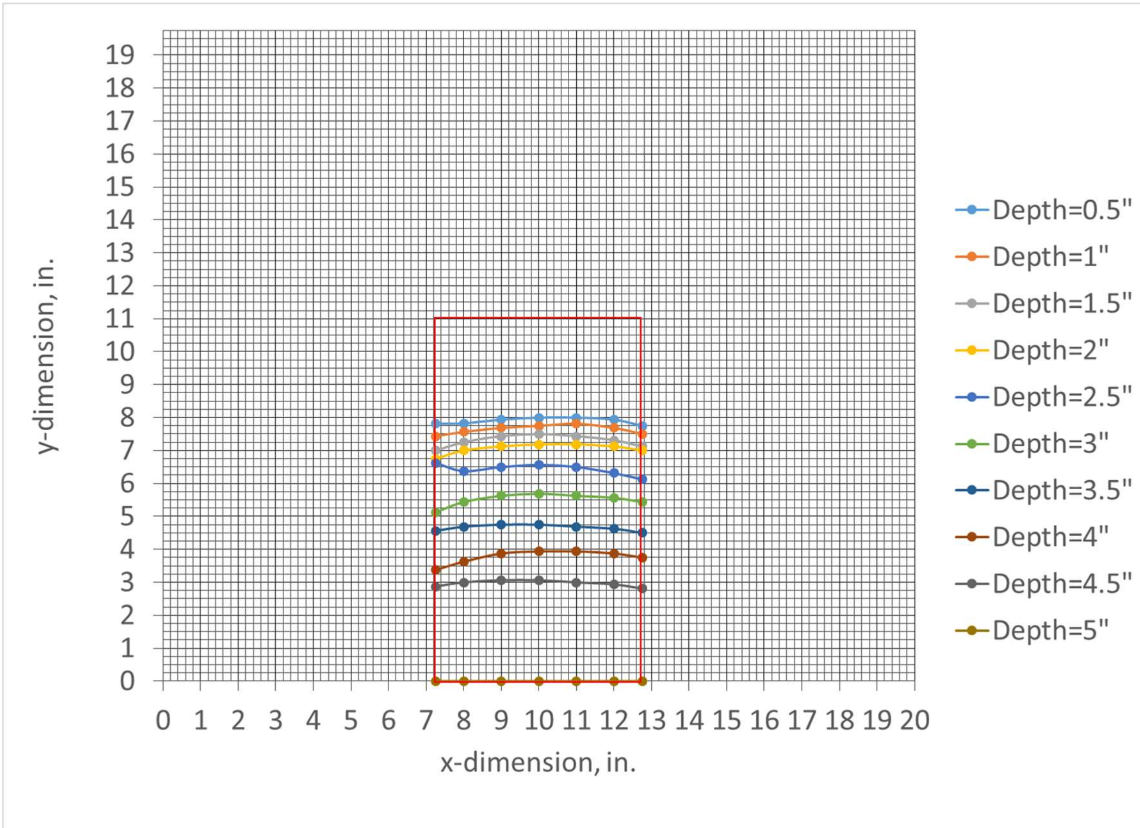

Figure 593: Failure Surface Contours of test PW11L5Lay

G.33 Failure Surface Contours of test PW11L5Lay2

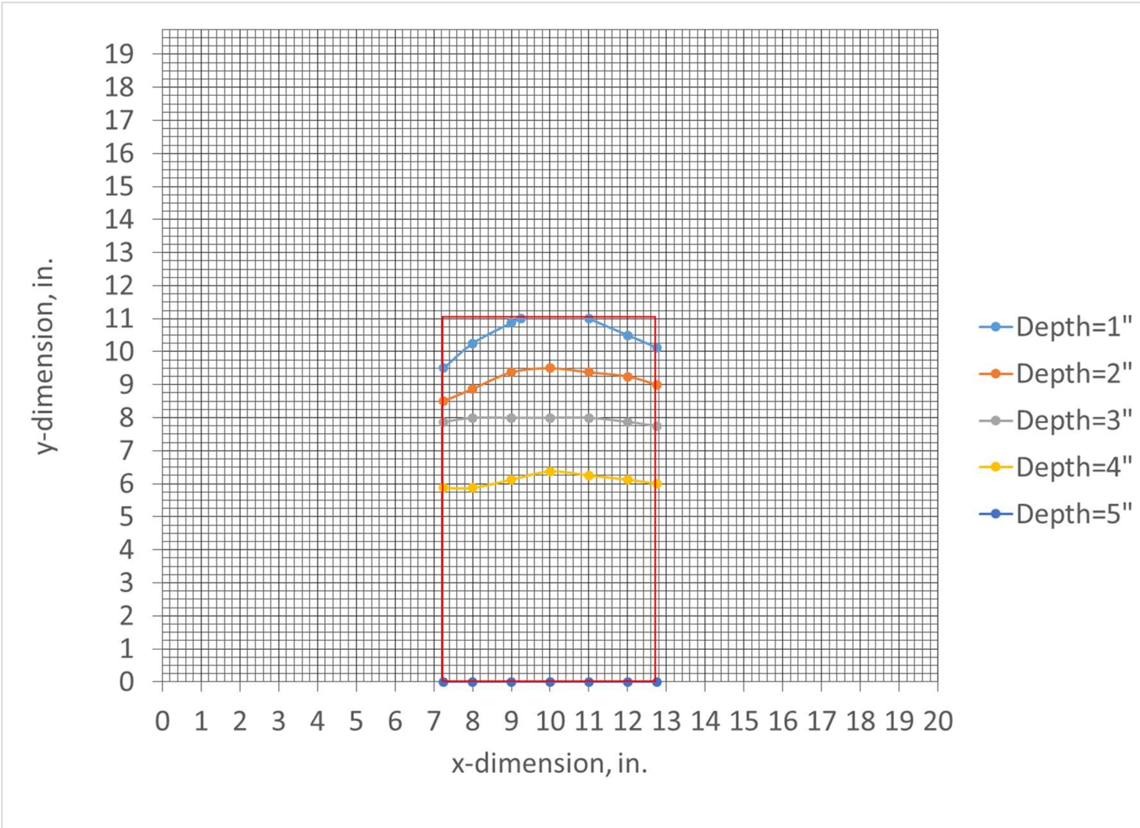

Figure 594: Failure Surface Contours of test PW11L5Lay2

G.34 Failure Surface Contours of test PW11L5Lay3

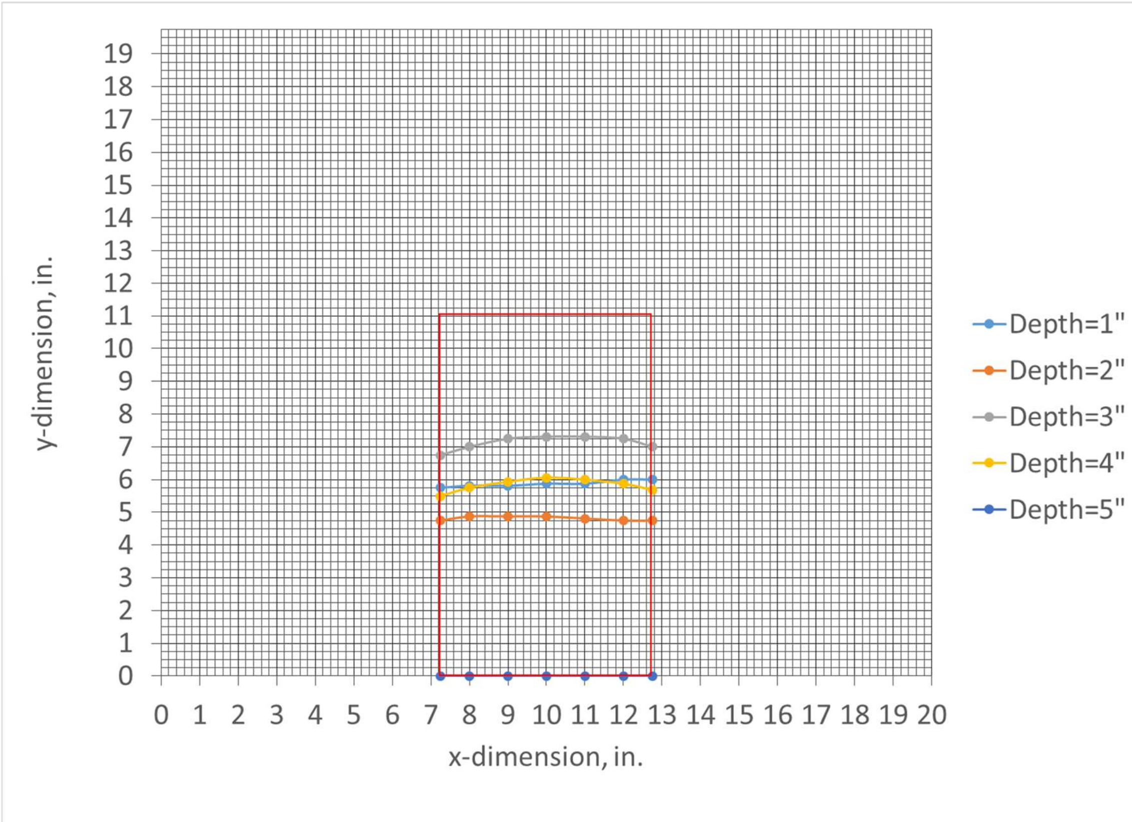

Figure 595: Failure Surface Contours of test PW11L5Lay3

G.35 Failure Surface Contours of test PW11L10Lay

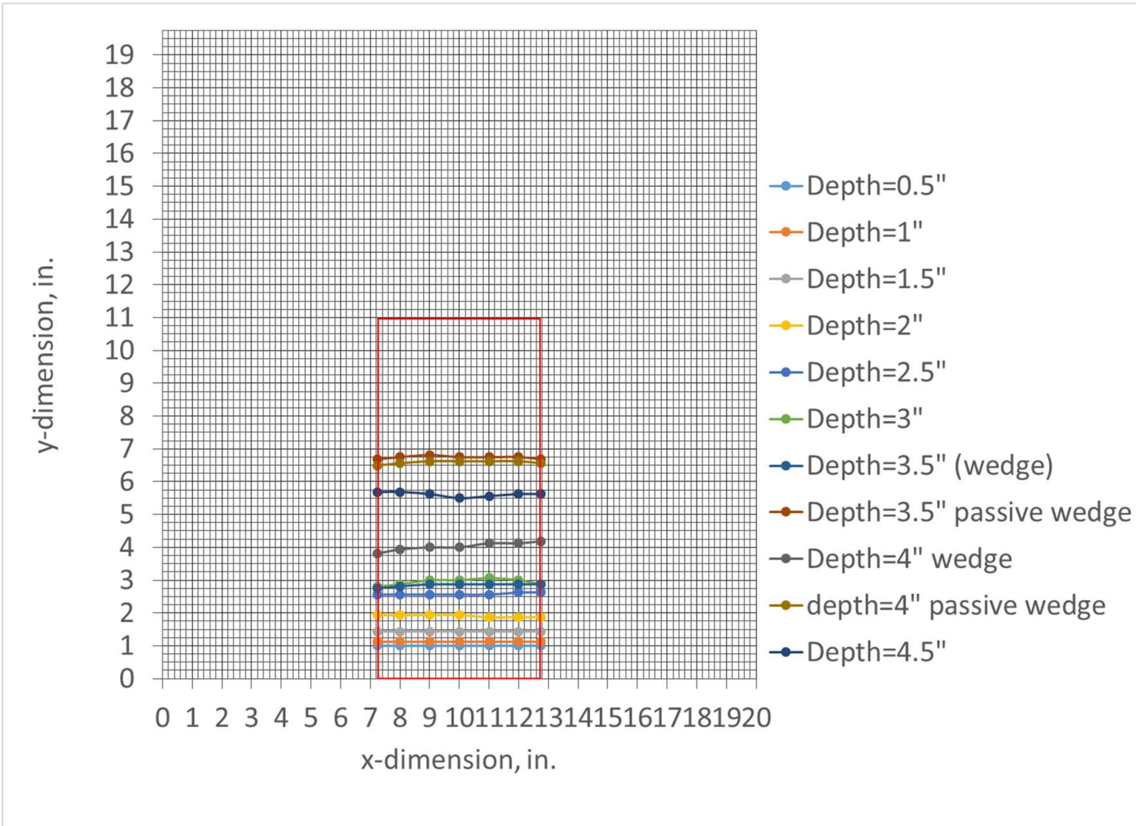

Figure 596: Failure Surface Contours of test PW11L10Lay

G.36 Failure Surface Contours of test PW11L10Lay2

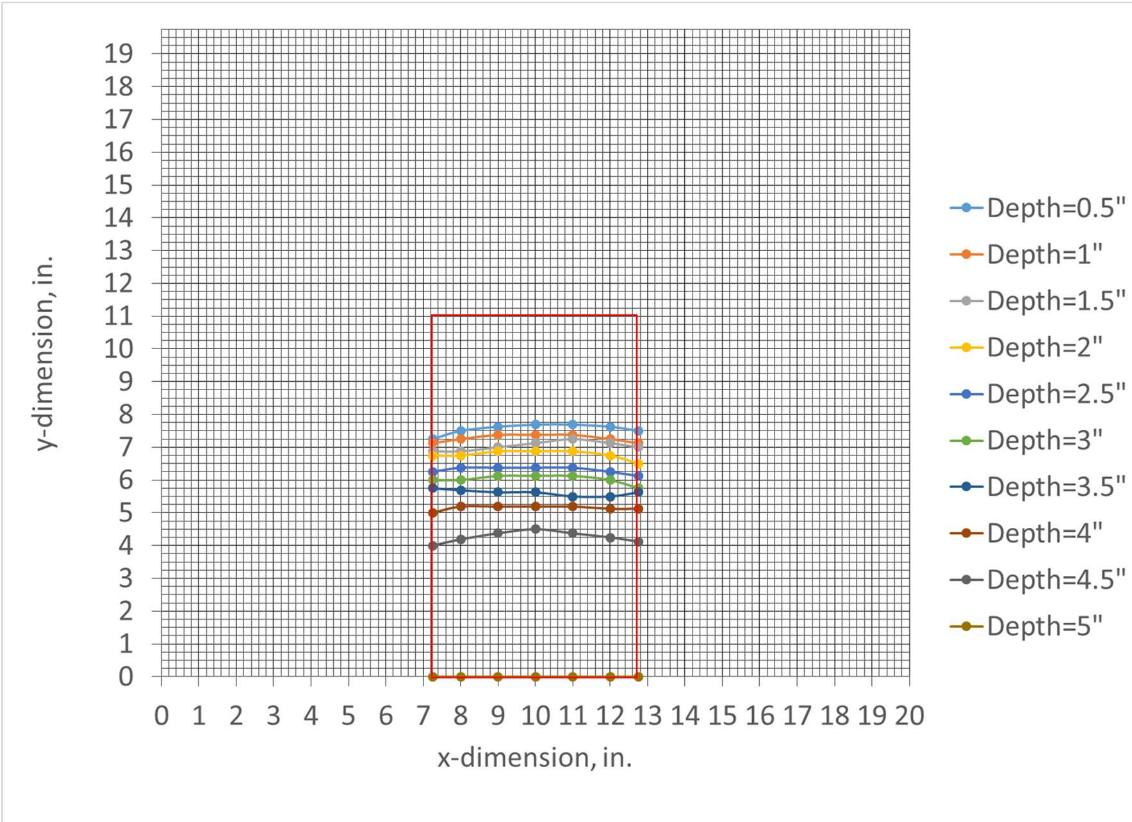

Figure 597: Failure Surface Contours of test PW11L10Lay2

G.37 Failure Surface Contours of test PW11L10Lay3

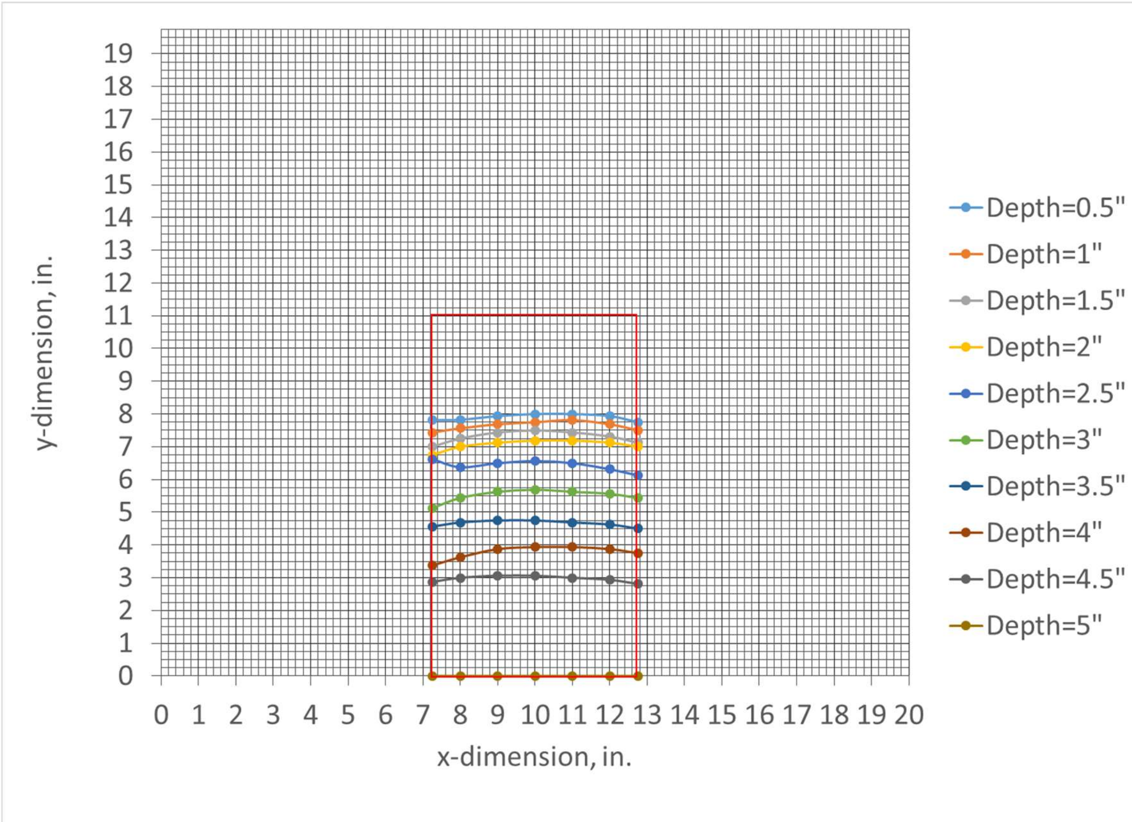

Figure 598: Failure Surface Contours of test PW11L10Lay3

G.38 Failure Surface Contours of test NR3 from painted layers

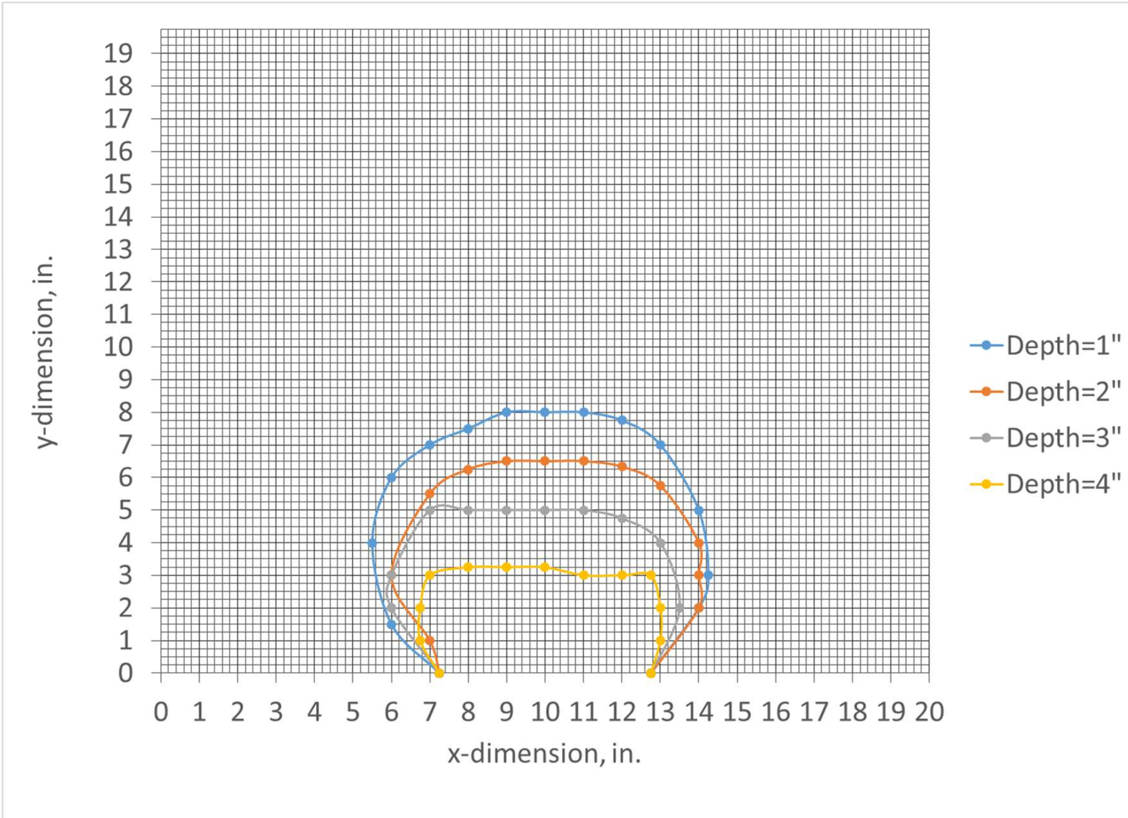

Figure 599: Failure Surface Contours of test NR3

G.39 Failure Surface Contours of test 8W8L5Lay3 from painted layers

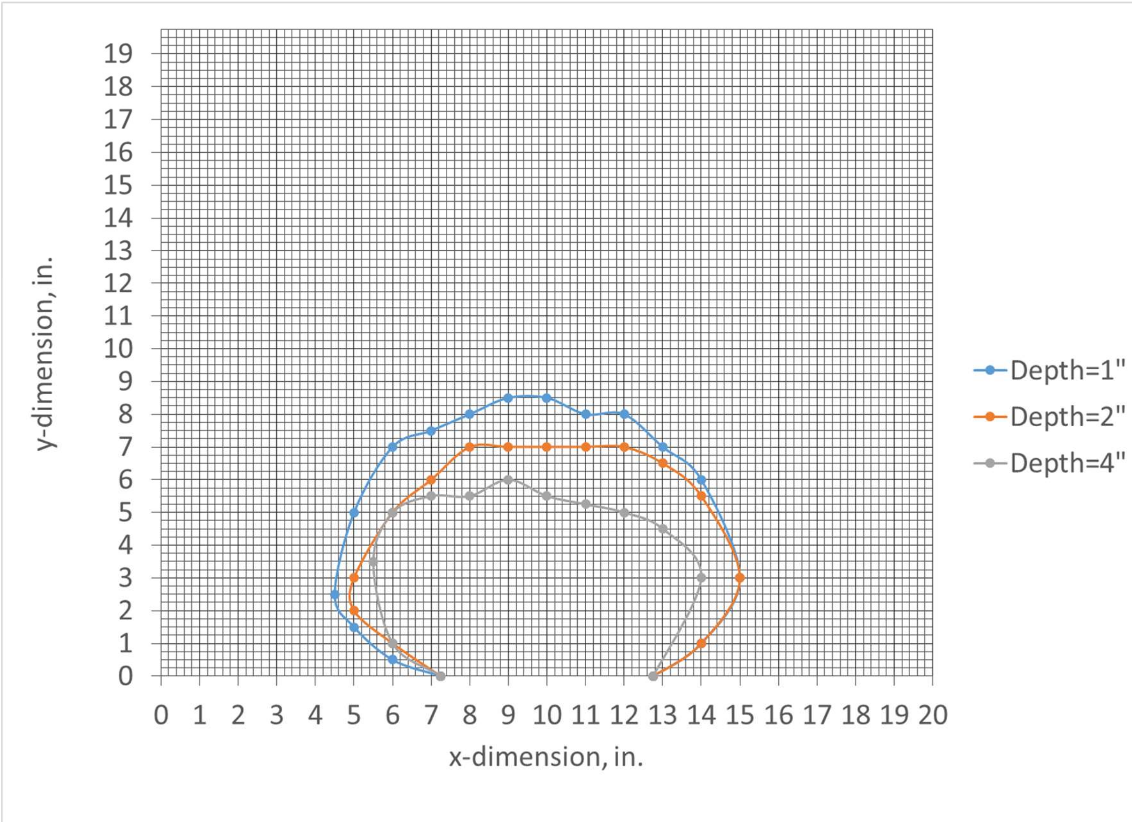

Figure 600: Failure Surface Contours of test 8W8L5Lay3

G.40 Failure Surface Contours of test 8W8L10Lay3 from painted layers

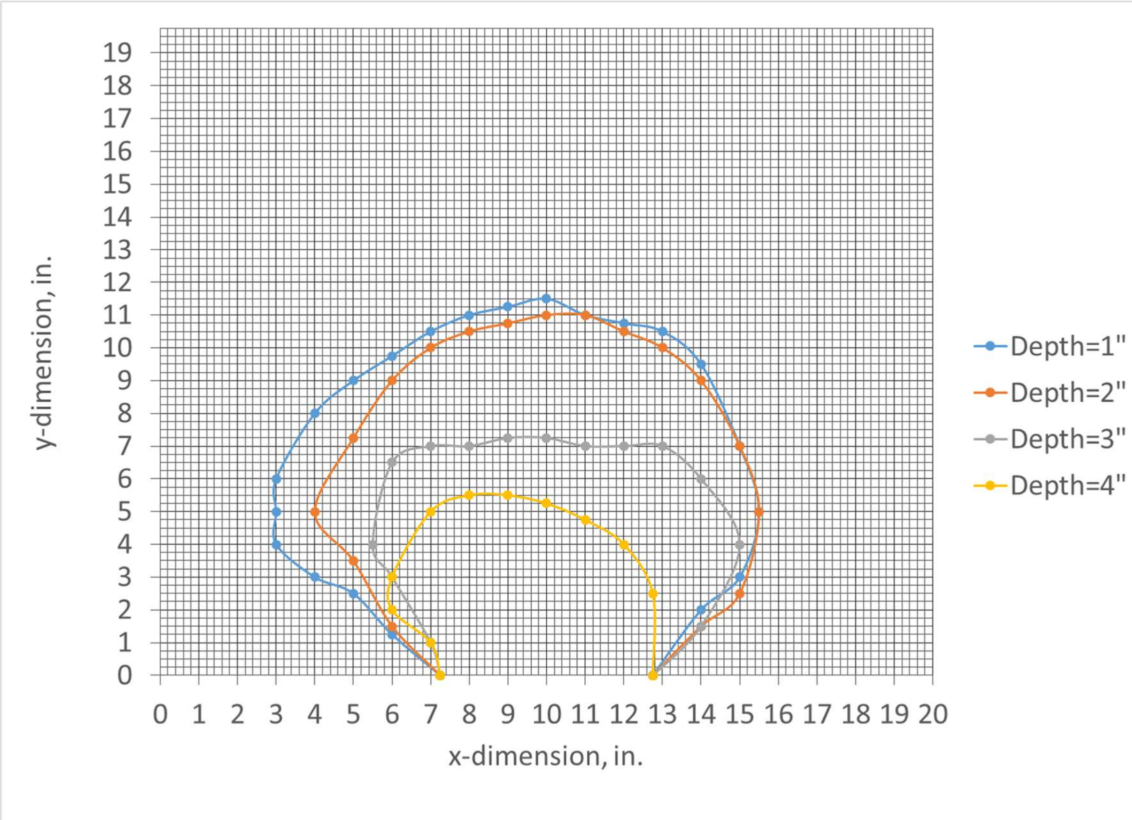

Figure 601: Failure Surface Contours of test 8W8L10Lay3

G.41 Failure Surface Contours of test 8W11L5Lay3 from painted layers

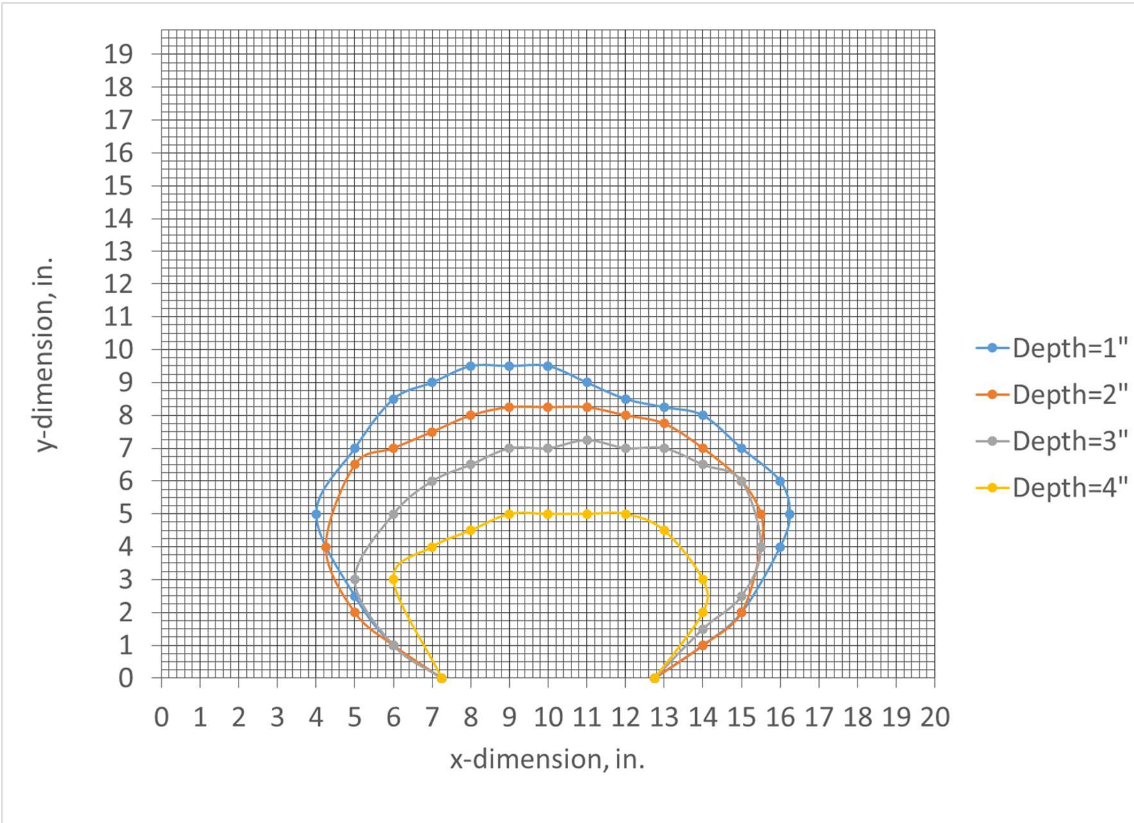

Figure 602: Failure Surface Contours of test 8W11L5Lay3

G.42 Failure Surface Contours of test 8W11L10Lay3 from painted layers

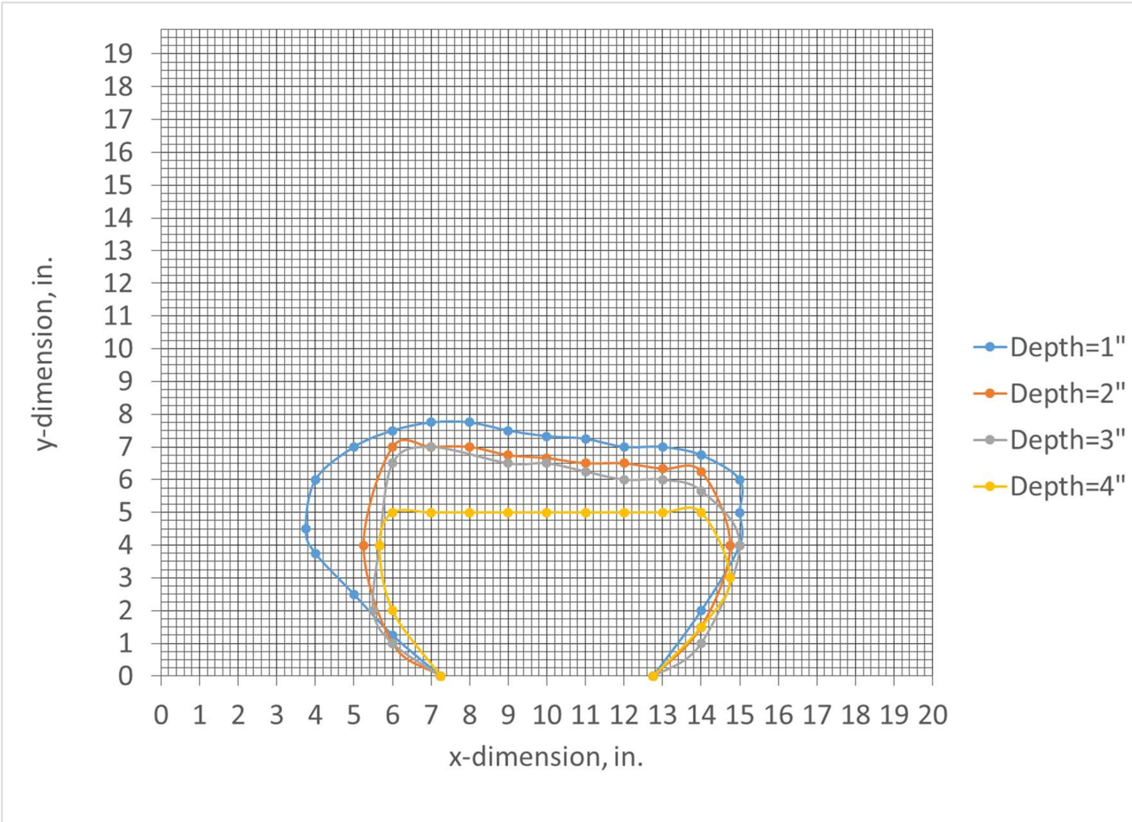

Figure 603: Failure Surface Contours of test 8W11L10Lay3

G.43 Failure Surface Contours of test 11W8L5Lay3 from painted layers

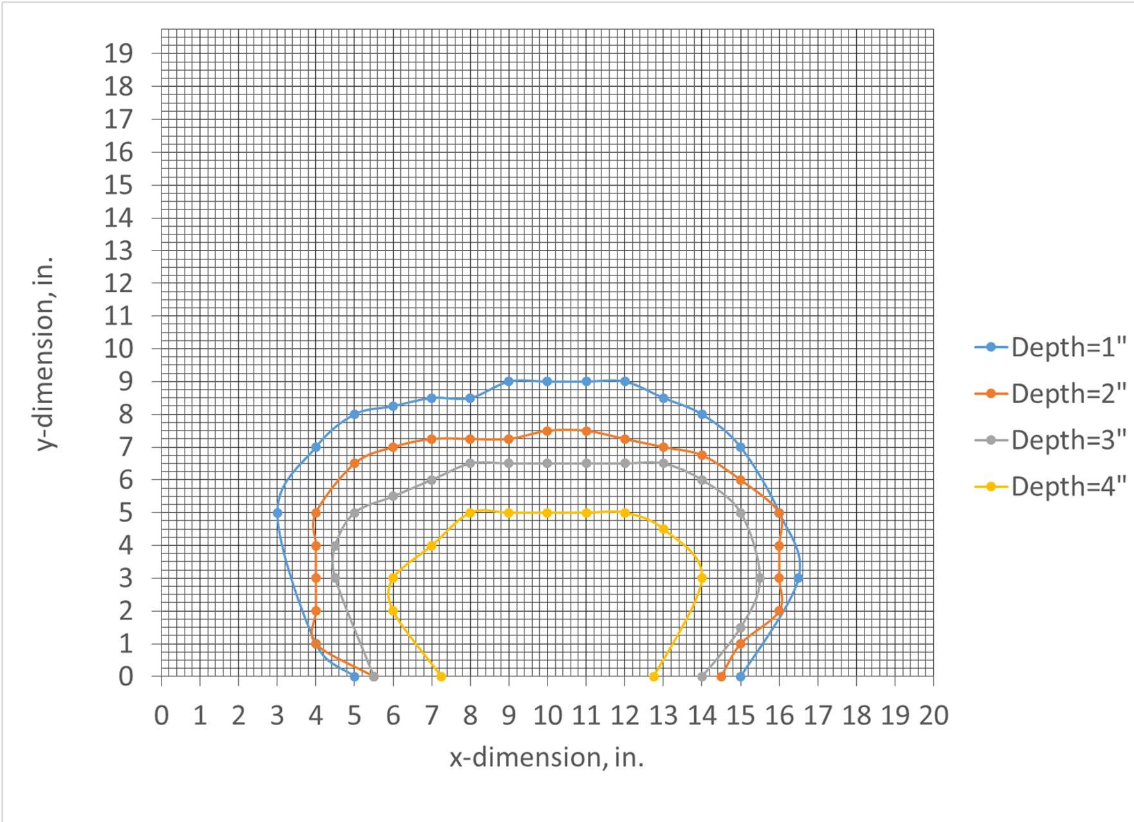

Figure 604: Failure Surface Contours of test 11W8L5Lay3

G.44 Failure Surface Contours of test 11W8L10Lay3 from painted layers

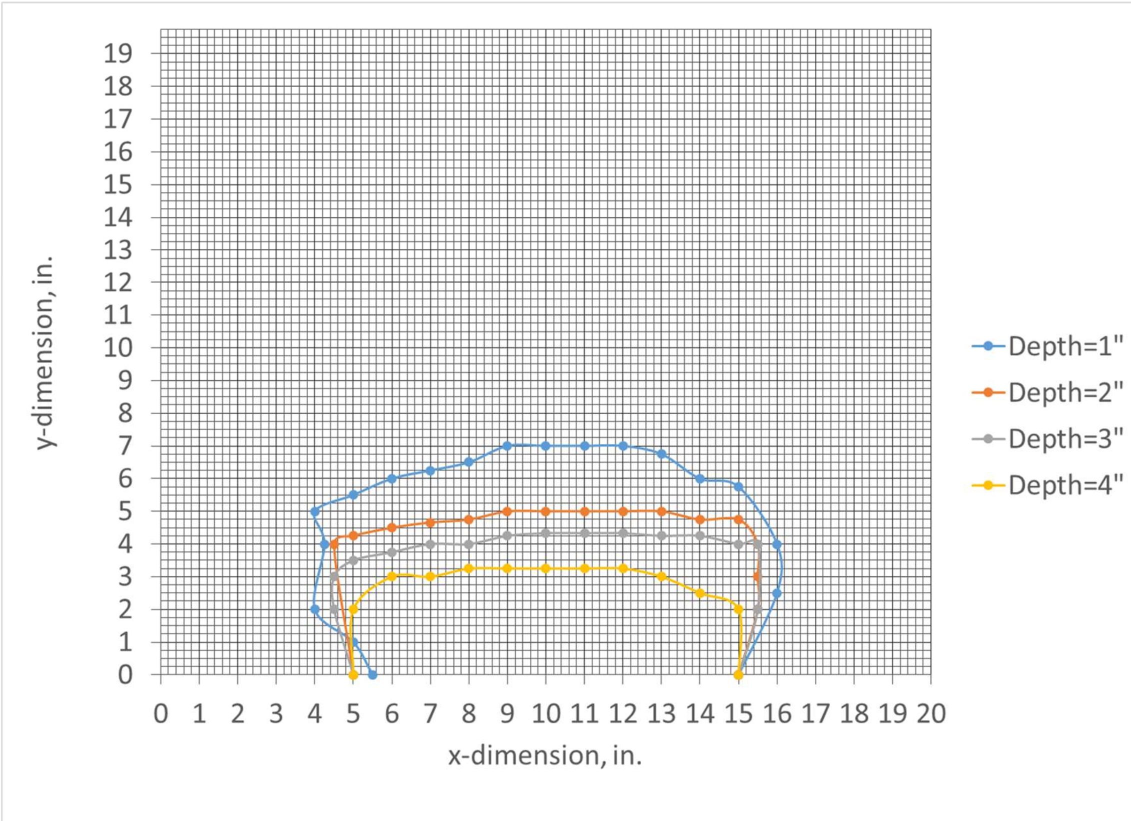

Figure 605: Failure Surface Contours of test 11W8L10Lay3

G.45 Failure Surface Contours of test 11W11L5Lay3 from painted layers

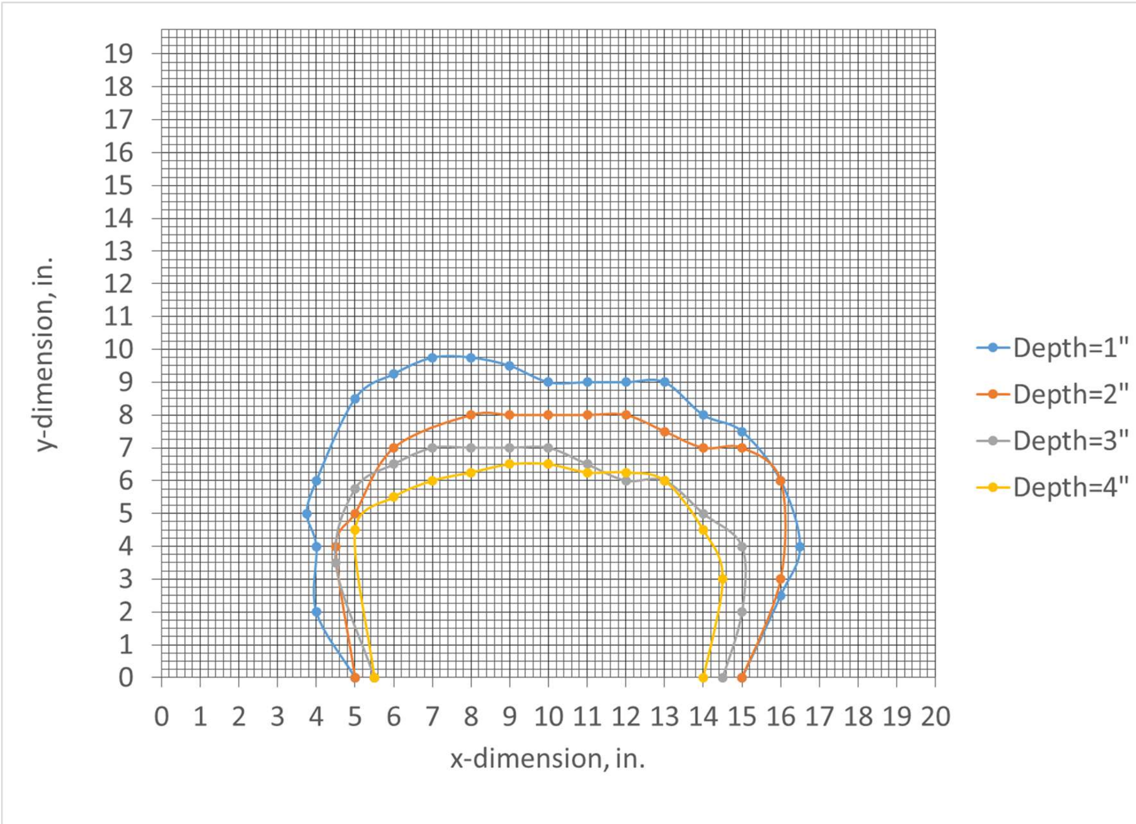

Figure 606: Failure Surface Contours of test 11W11L5Lay3

G.46 Failure Surface Contours of test 11W11L10Lay3 from painted layers

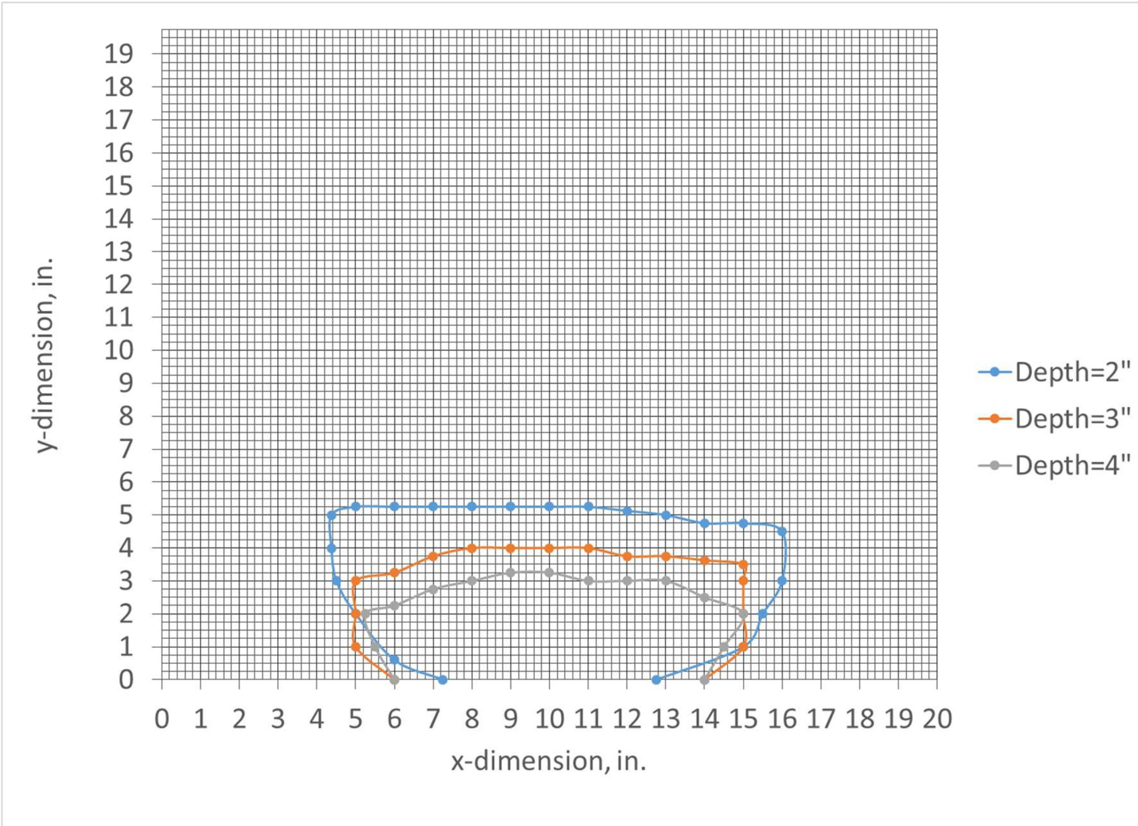

Figure 607: Failure Surface Contours of test 11W11L10Lay3

G.47 Failure Surface Contours of test PW8L5Lay3 from painted layers

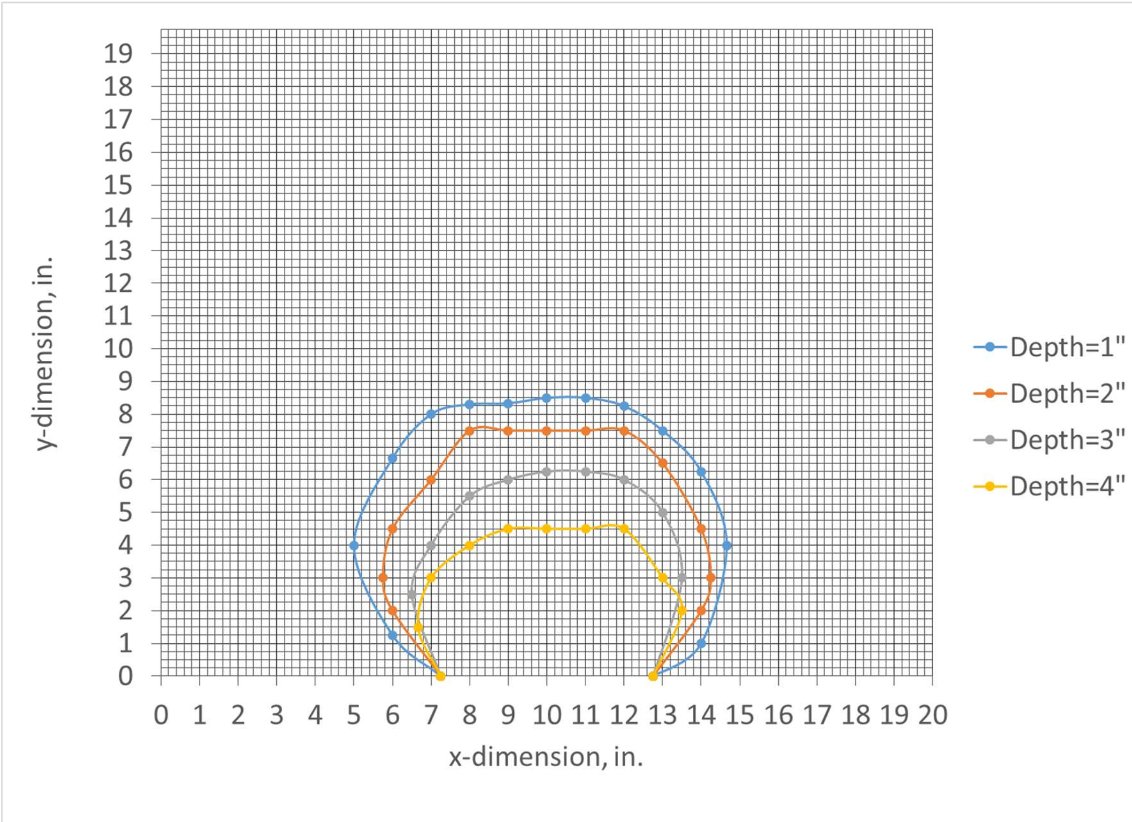

Figure 608: Failure Surface Contours of test PW8L5lay3

G.48 Failure Surface Contours of test PW8L10Lay3 from painted layers

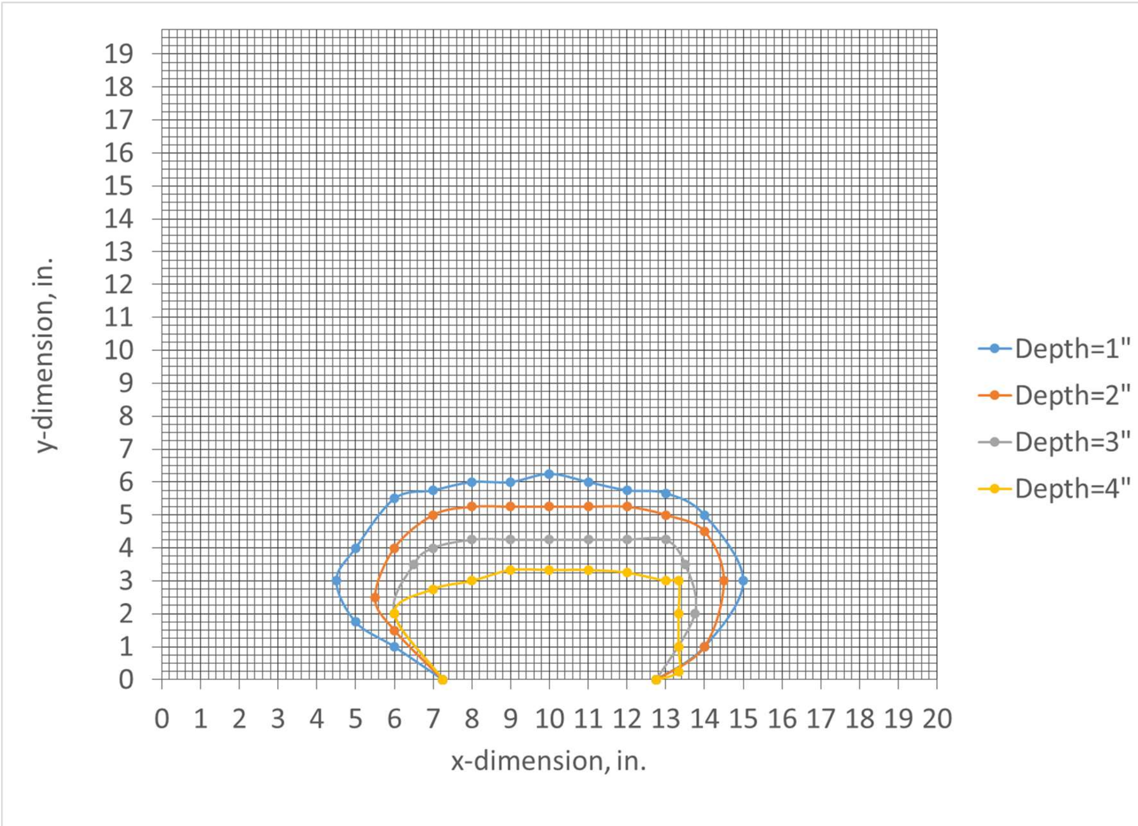

Figure 609: Failure Surface Contours of test PW8L10Lay3

G.49 Failure Surface Contours of test PW11L5Lay3 from painted layers

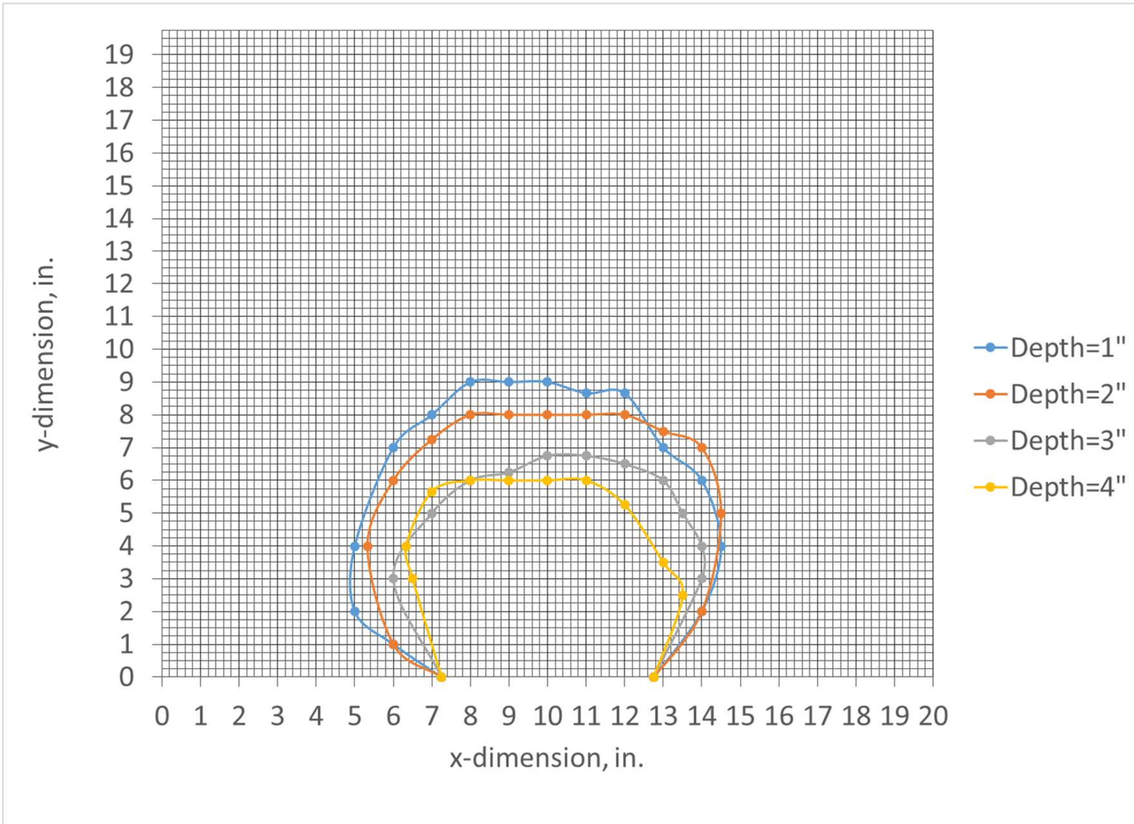

Figure 610: Failure Surface Contours of test PW11L5Lay3

G.50 Failure Surface Contours of test PW11L10Lay3 from painted layers

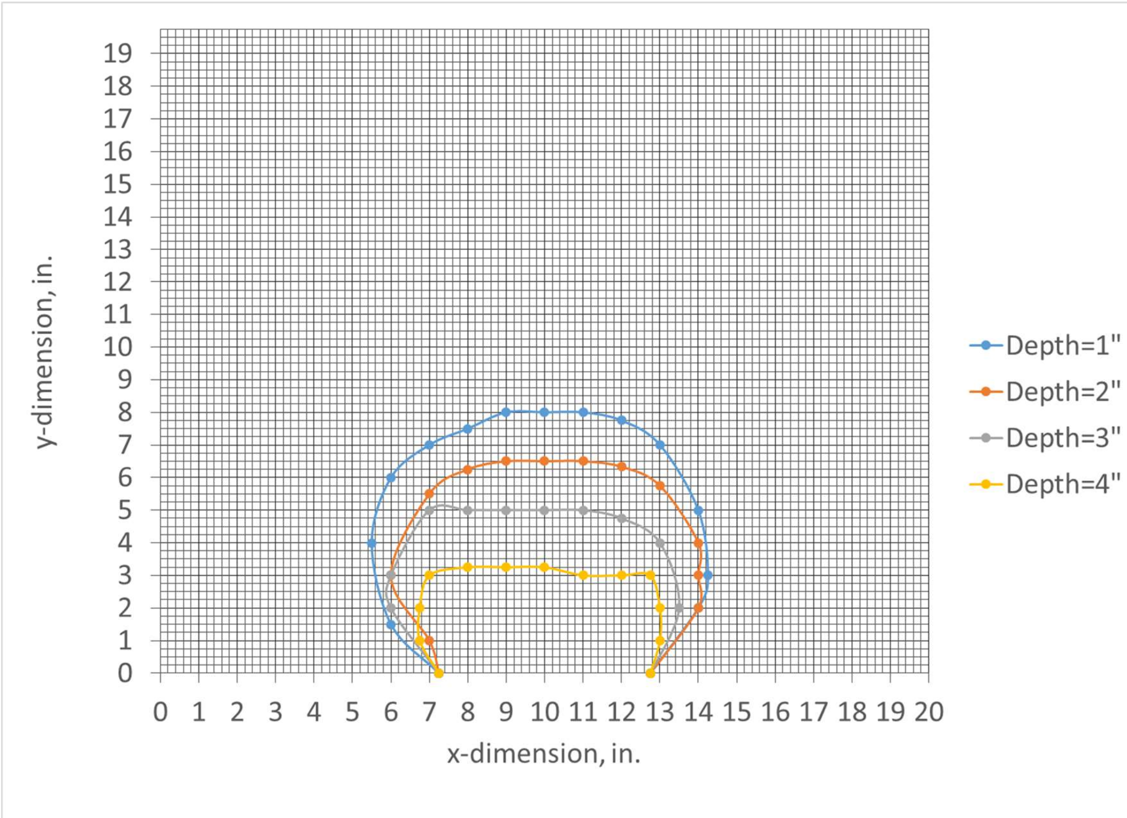

Figure 611: Failure Surface Contours of test PW11L10Lay3

APPENDIX H: MID-PLATE FAILURE SURFACE LOCATION

H.1 Introduction

In each test, the maximum y-dimension of the failure surface was observed at or near the x-direction midpoint of the pusher plate. To obtain a two dimensional passive failure surface "wedge," the failure surface points with x=10 (pusher plate midpoint) coordinates were plotted for each test and appear in this section.

H.2 Mid-Plate Failure Surface Location for Tests 8W8L5Lay, 8W8L5Lay2, and 8W8L5Lay3 from Reinforcement

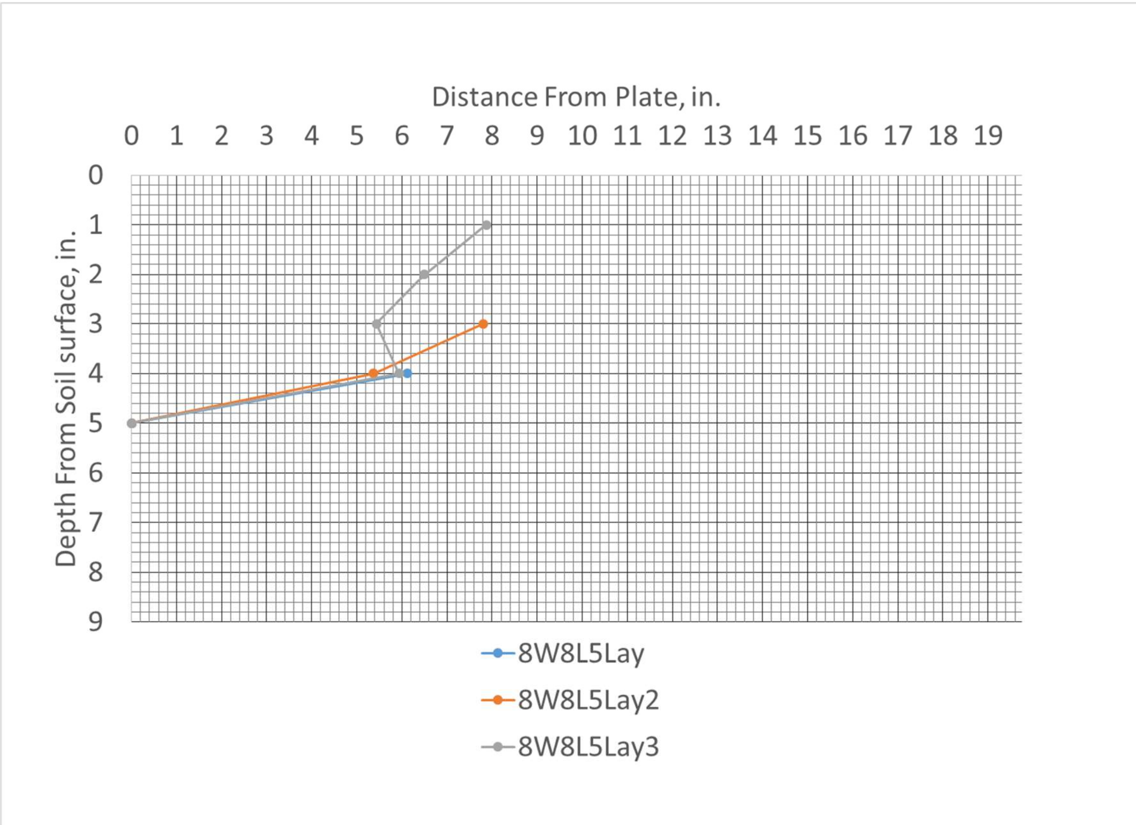

Figure 612: Mid-Plate Failure Surface Location for Tests 8W8L5Lay, 8W8L5Lay2, and 8W8L5Lay3 based on reinforcement deformation

H.3 Mid-Plate Failure Surface Location for Tests 8W8L10Lay, 8W8L10Lay2, and 8W8L10Lay3 from Reinforcement

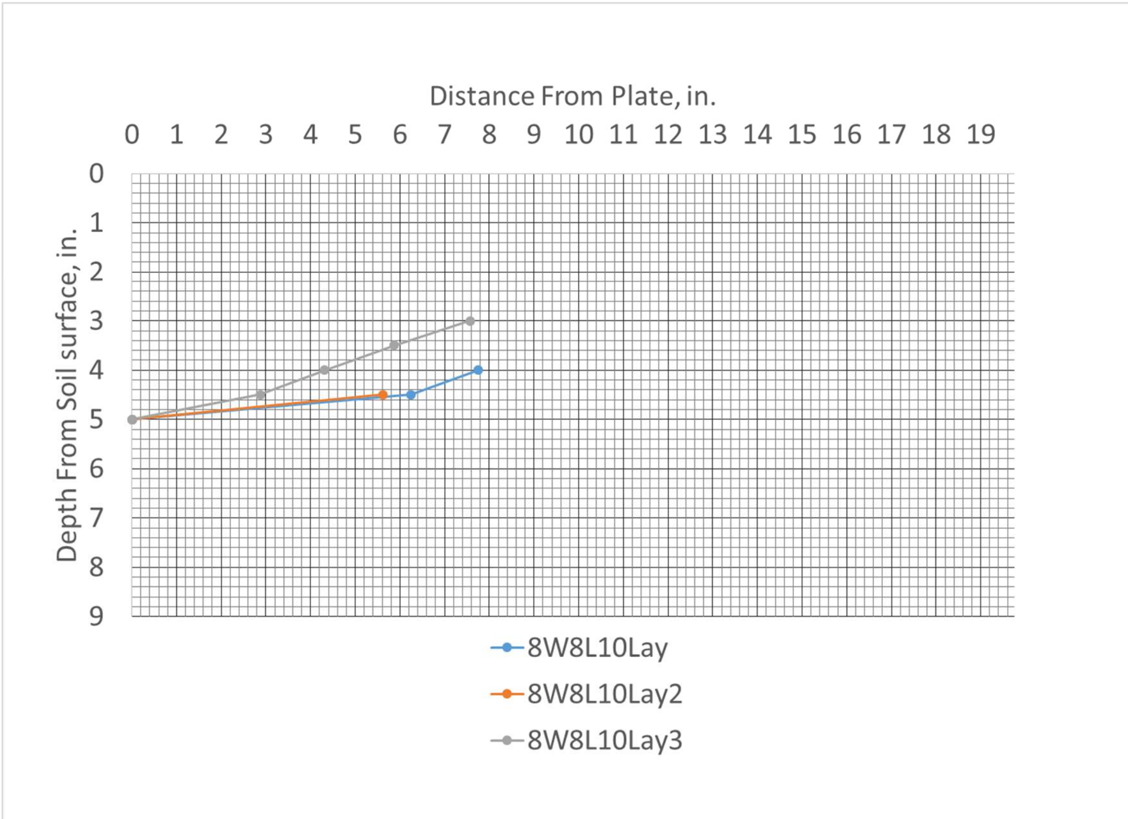

Figure 613: Mid-Plate Failure Surface Location for Tests 8W8L10Lay, 8W8L10Lay2, and 8W8L10Lay3 based on reinforcement deformation

H.4 Mid-Plate Failure Surface Location for Tests 8W11L5Lay, 8W11L5Lay2, and 8W11L5Lay3 from Reinforcement

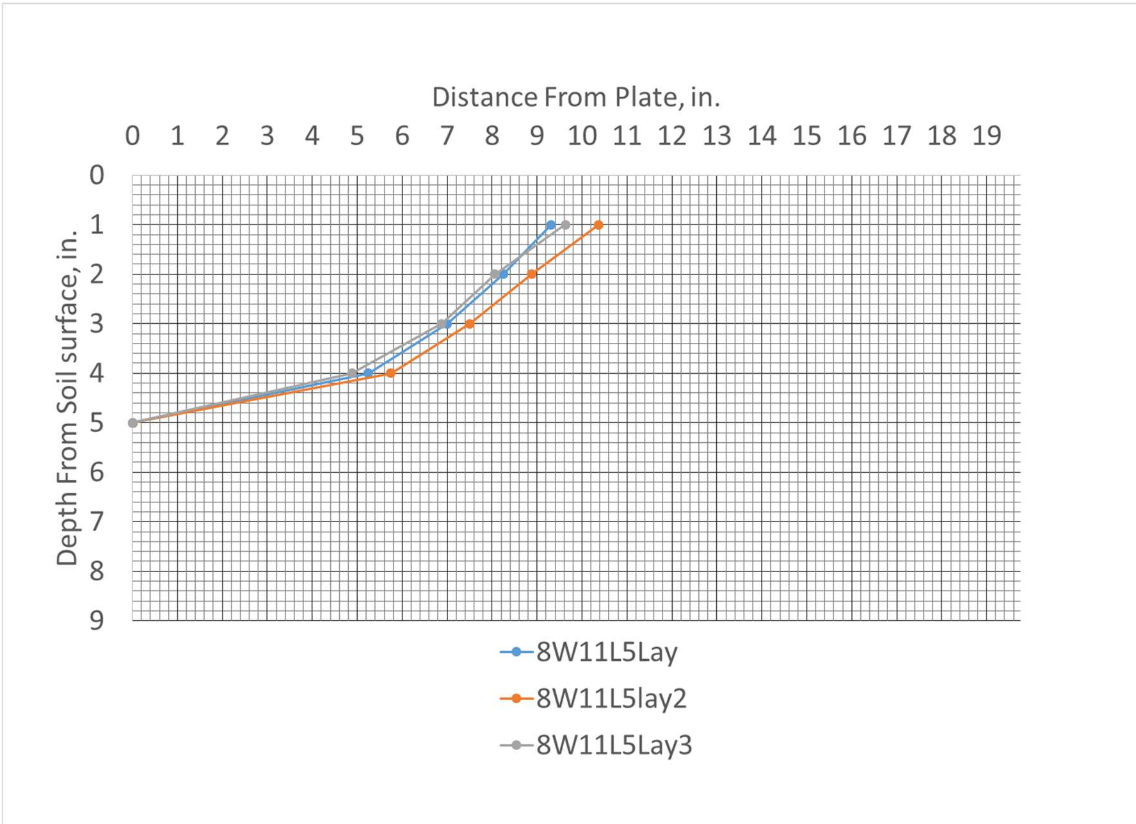

Figure 614: Mid-Plate Failure Surface Location for Tests 8W11L5Lay, 8W11L5Lay2, and 8W11L5Lay3 based on reinforcement deformation

H.5 Mid-Plate Failure Surface Location for Tests 8W11L10Lay, 8W11L10Lay2, and 8W11L10Lay3 from Reinforcement

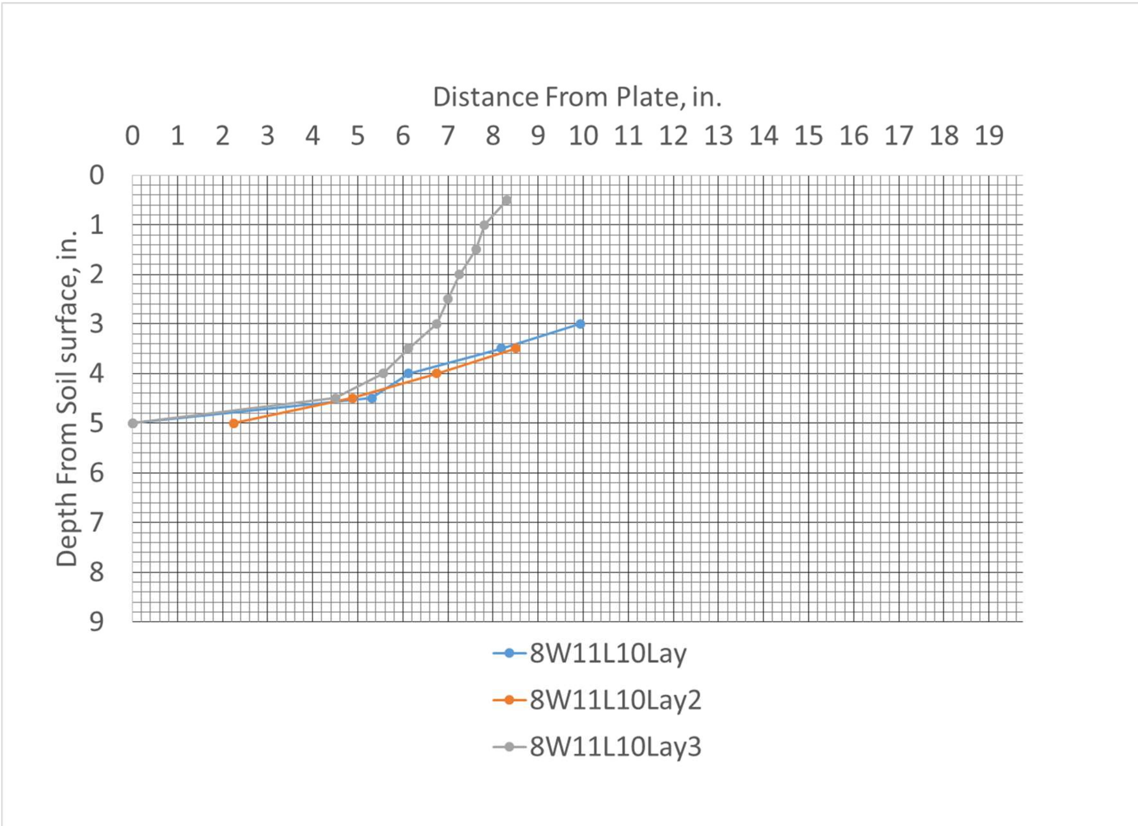

Figure 615: Mid-Plate Failure Surface Location for Tests 8W11L10Lay, 8W11L10Lay2, and 8W11L10Lay3 based on reinforcement deformation

H.6 Mid-Plate Failure Surface Location for Tests 11W8L5Lay, 11W8L5Lay2, and 11W8L5Lay3 from Reinforcement

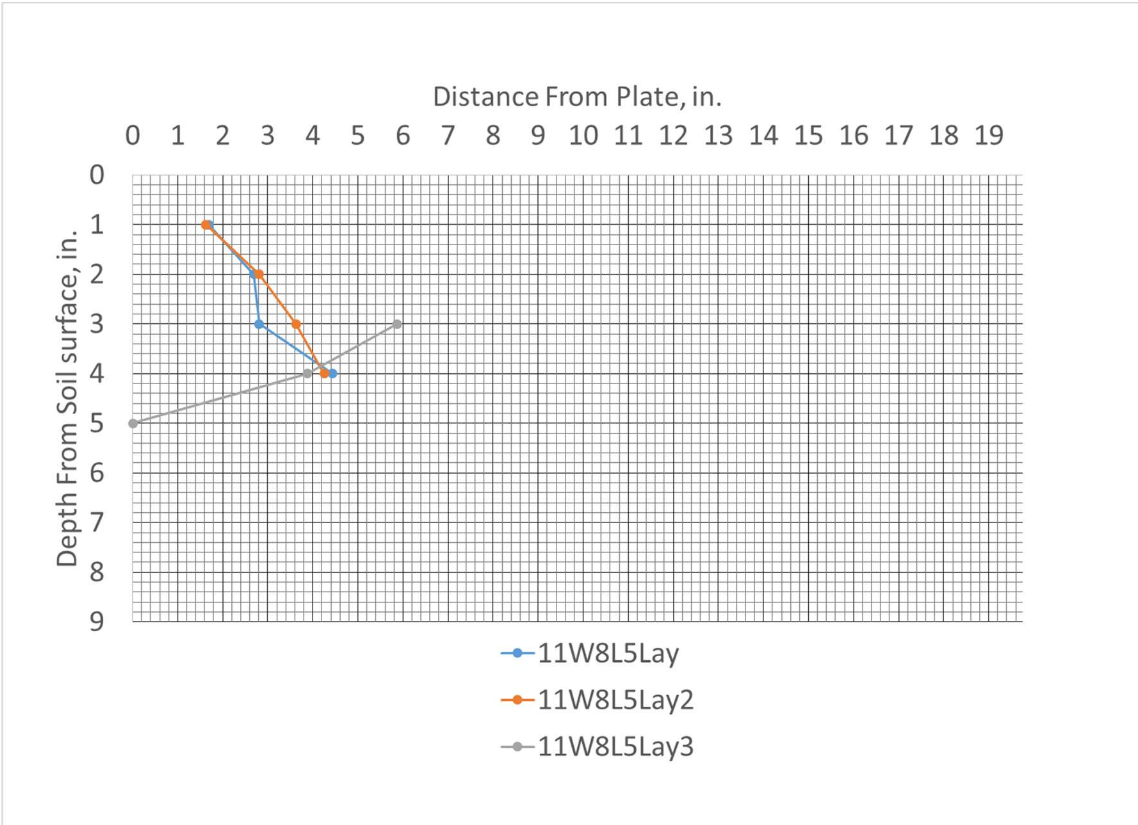

Figure 616: Mid-Plate Failure Surface Location for Tests 11W8L5Lay, 11W8L5Lay2, and 11W8L5Lay3 based on reinforcement deformation

H.7 Mid-Plate Failure Surface Location for Tests 11W8L10Lay, 11W8L10Lay2, and 11W8L10Lay3 from Reinforcement

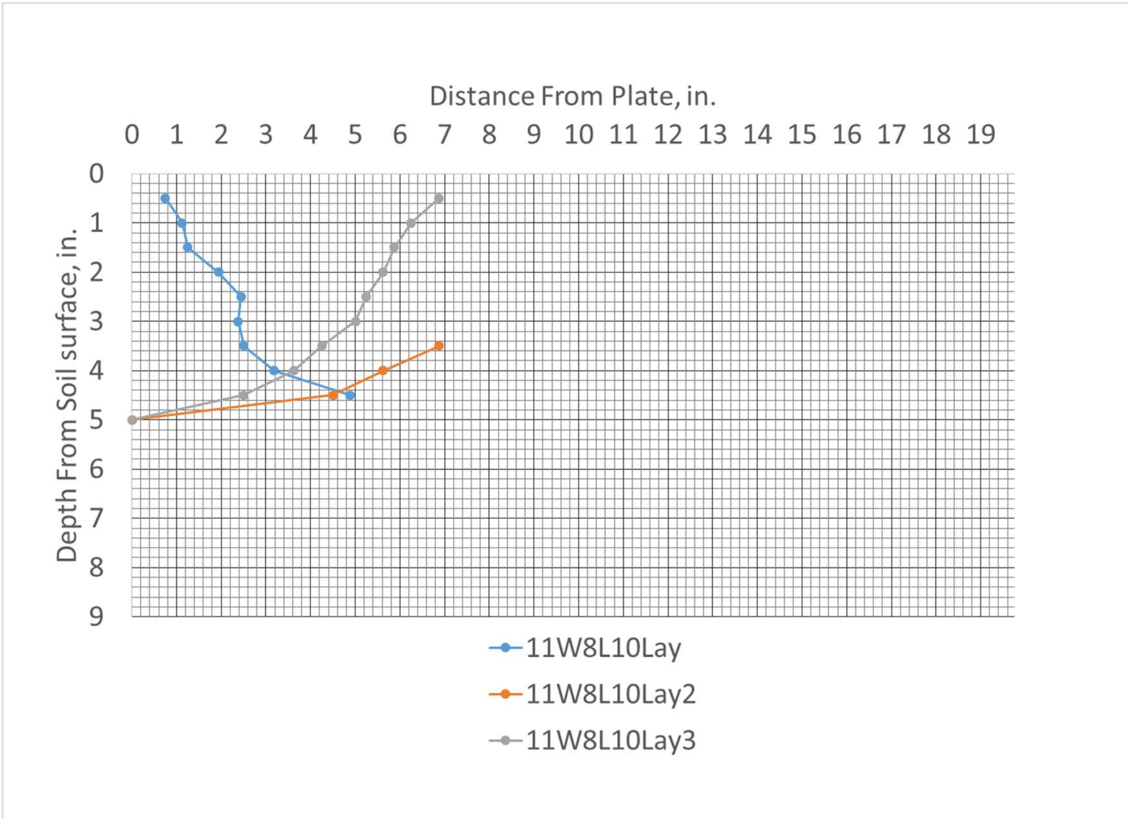

Figure 617: Mid-Plate Failure Surface Location for Tests 11W8L10Lay, 11W8L10Lay2, and 11W8L10Lay3 based on reinforcement deformation

H.8 Mid-Plate Failure Surface Location for Tests 11W11L5Lay, 11W11L5Lay2, and 11W11L5Lay3 from Reinforcement

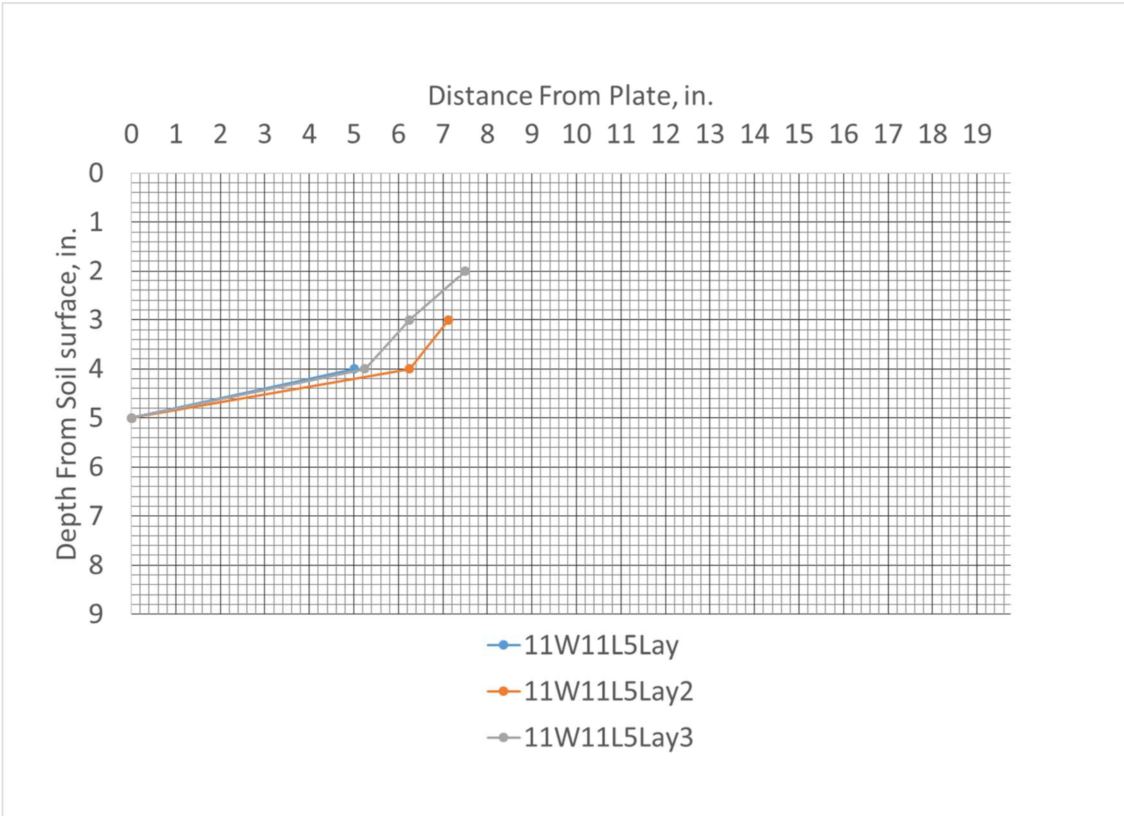

Figure 618: Mid-Plate Failure Surface Location for Tests 11W11L5Lay, 11W11L5Lay2, and 11W11L5Lay3 based on reinforcement deformation

H.9 Mid-Plate Failure Surface Location for Tests 11W11L10Lay, 11W11L10Lay2, and 11W11L10Lay3 from Reinforcement

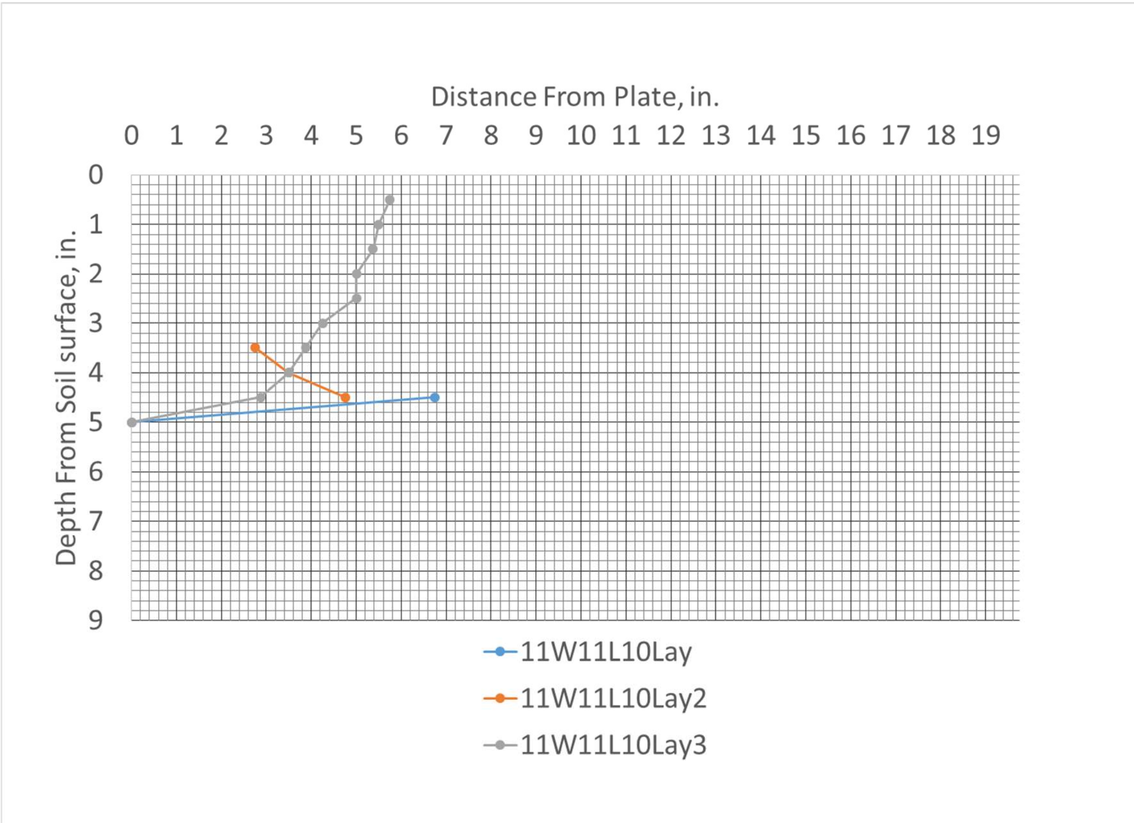

Figure 619: Mid-Plate Failure Surface Location for Tests 11W11L10Lay, 11W11L10Lay2, and 11W11L10Lay3 based on reinforcement deformation

H.10 Mid-Plate Failure Surface Location for Tests PW8L5Lay, PW8L5Lay2, and PW8L5Lay3 from Reinforcement

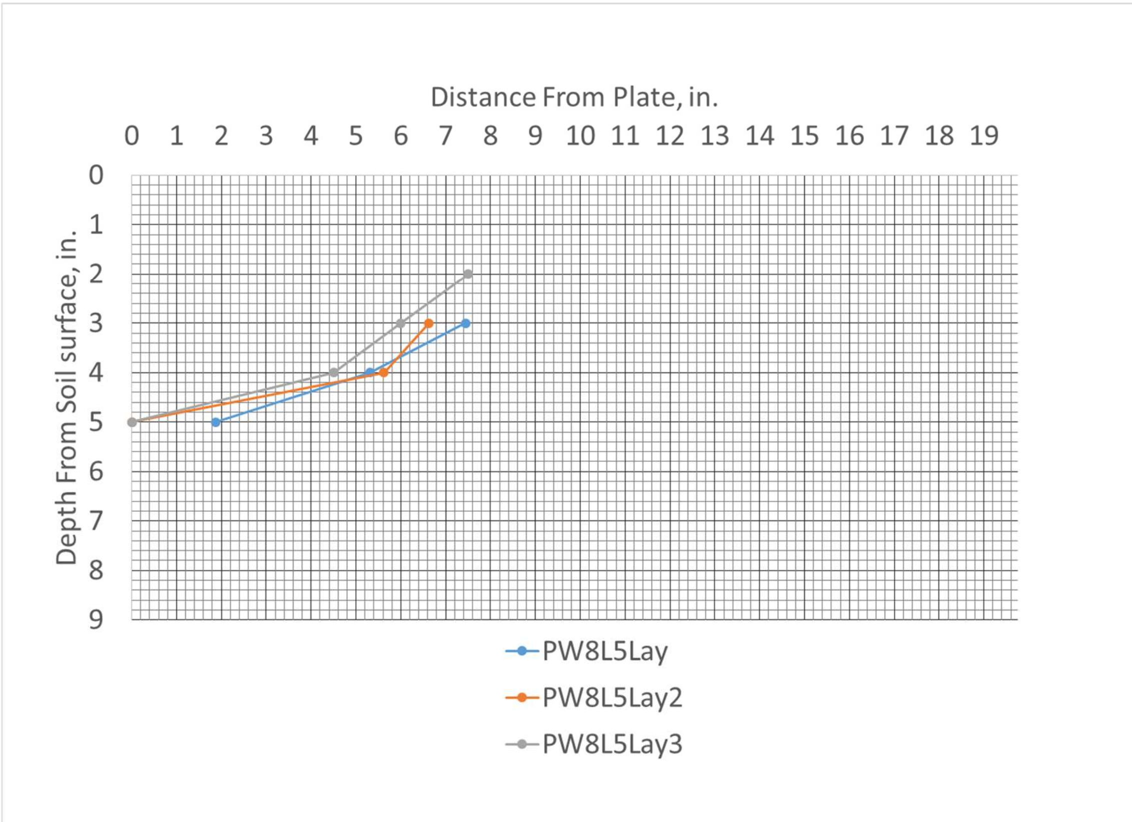

Figure 620: Mid-Plate Failure Surface Location for Tests PW8L5Lay, PW8L5Lay2, and PW8L5Lay3 based on reinforcement deformation

H.11 Mid-Plate Failure Surface Location for Tests PW8L10Lay, PW8L10Lay2, and PW8L10Lay3 from Reinforcement

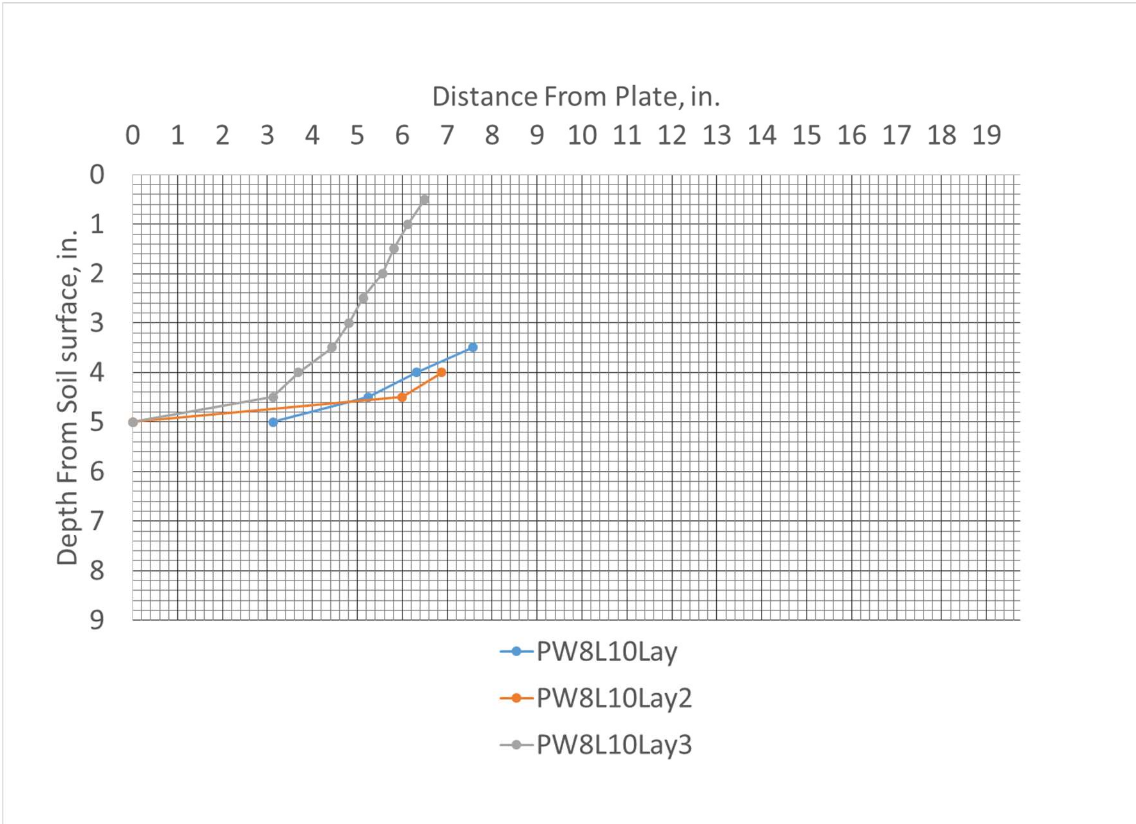

Figure 621: Mid-Plate Failure Surface Location for Tests PW8L10Lay, PW8L10Lay2, and PW8L10Lay3 based on reinforcement deformation

H.12 Mid-Plate Failure Surface Location for Tests PW11L5Lay, PW11L5Lay2, and PW11L5Lay3 from Reinforcement

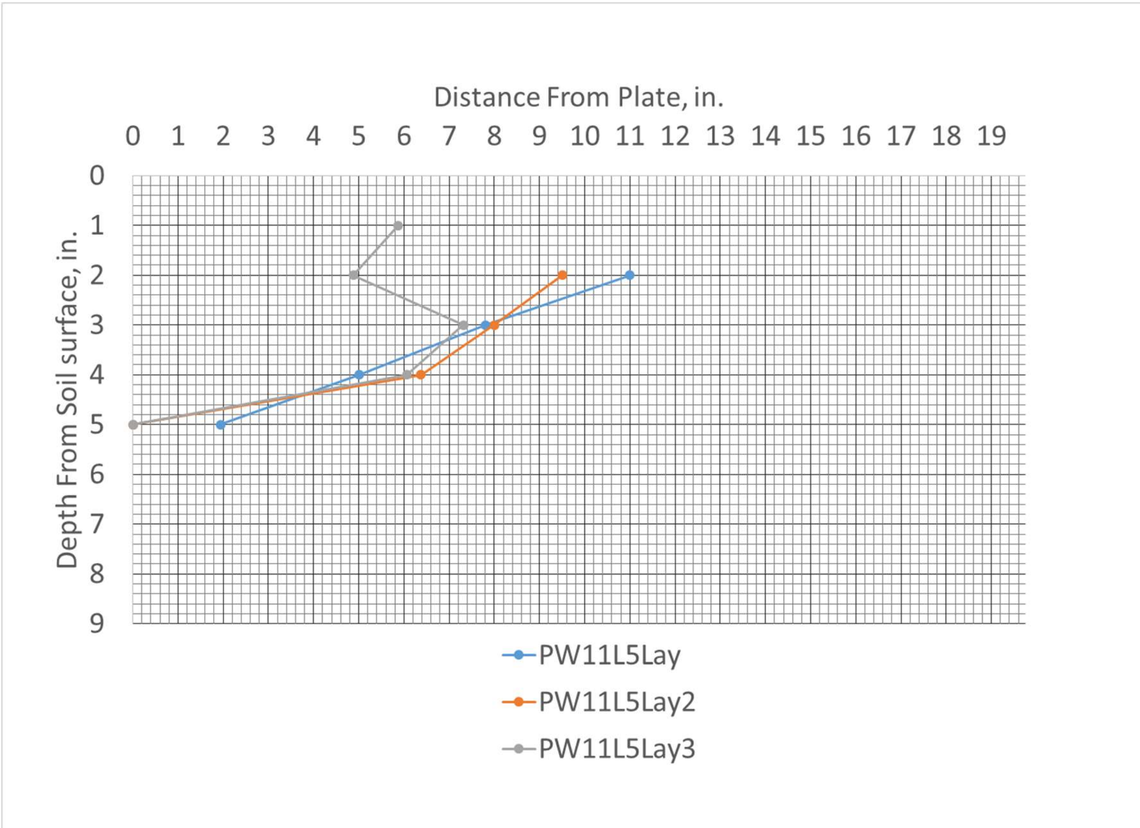

Figure 622: Mid-Plate Failure Surface Location for Tests PW11L5Lay, PW11L5Lay2, and PW11L5Lay3 based on reinforcement deformation

H.13 Mid-Plate Failure Surface Location for Tests PW11L10Lay, PW11L10Lay2, and PW11L10Lay3 from Reinforcement

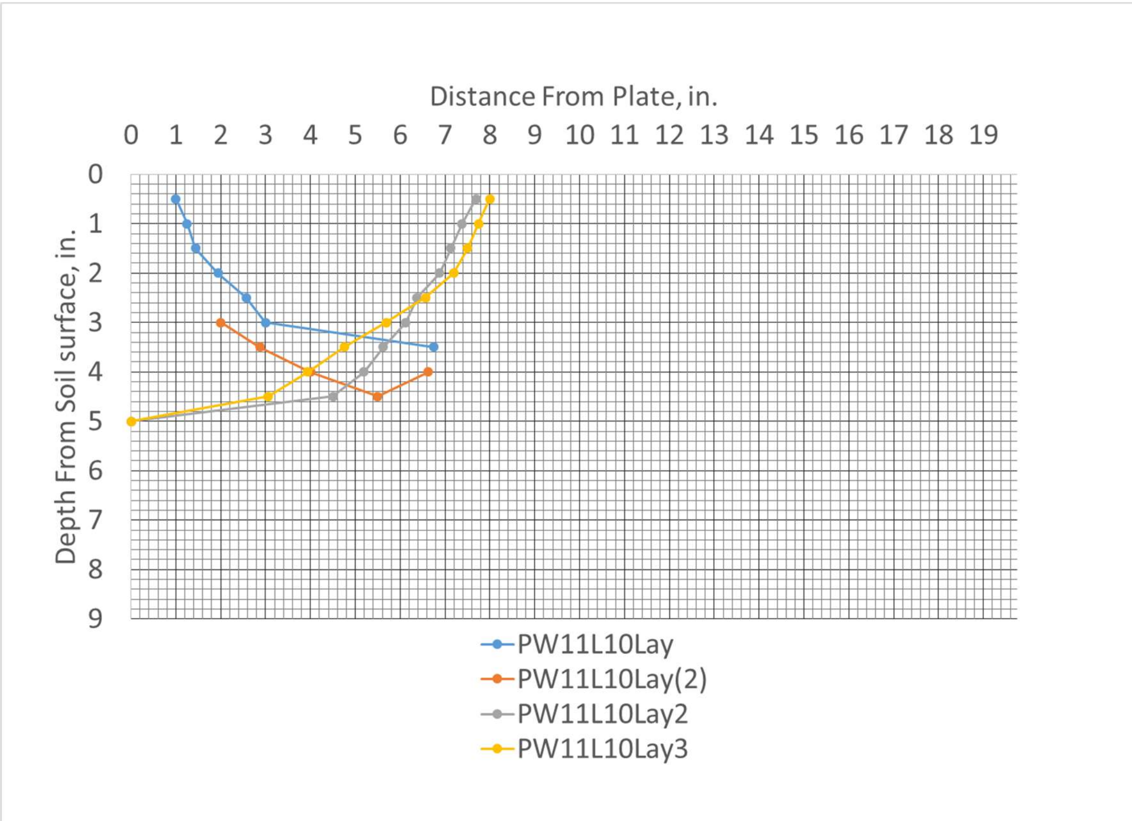

Figure 623: Mid-Plate Failure Surface Location for Tests PW11L10Lay, PW11L10Lay2, and PW11L10Lay3 based on reinforcement deformation

H.14 Mid-Plate Failure Surface Location for Test NR3 from layer paint

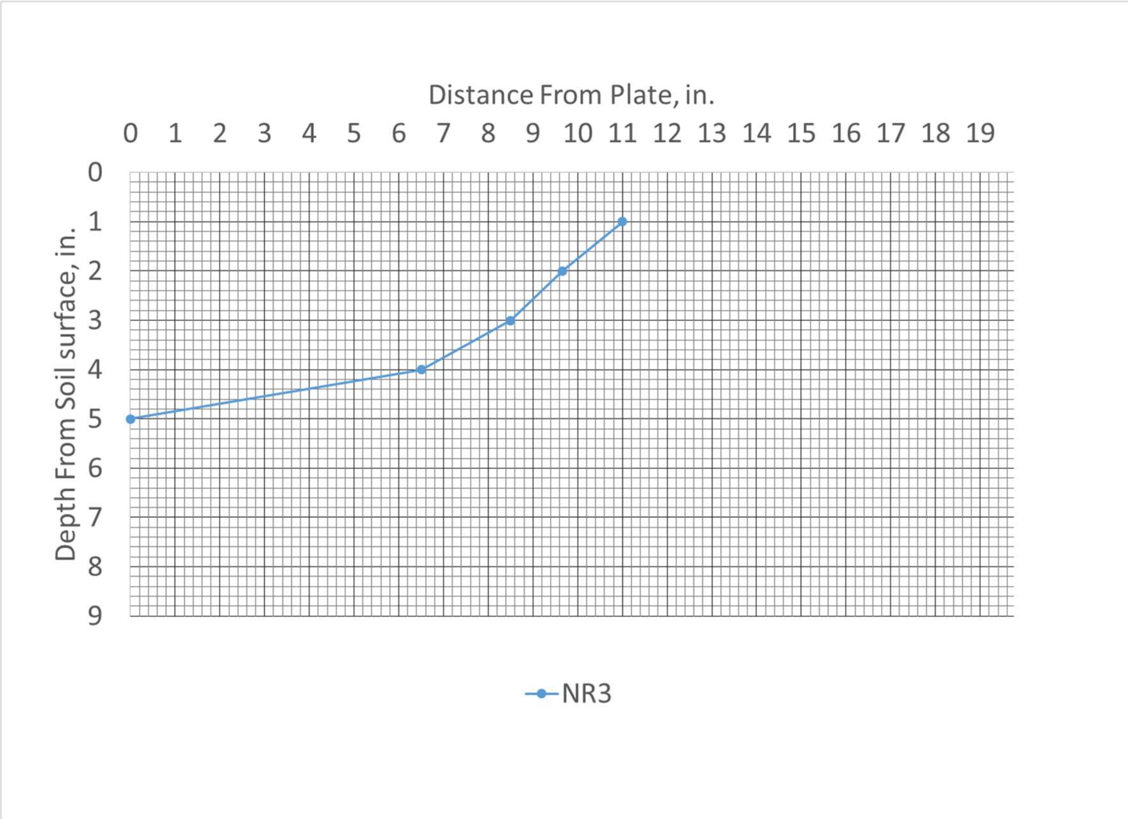

Figure 624: Mid-Plate Failure Surface Location for Test NR3 from layer paint

H.15 Mid-Plate Failure Surface Location for Test 8W8L5Lay3 from layer paint

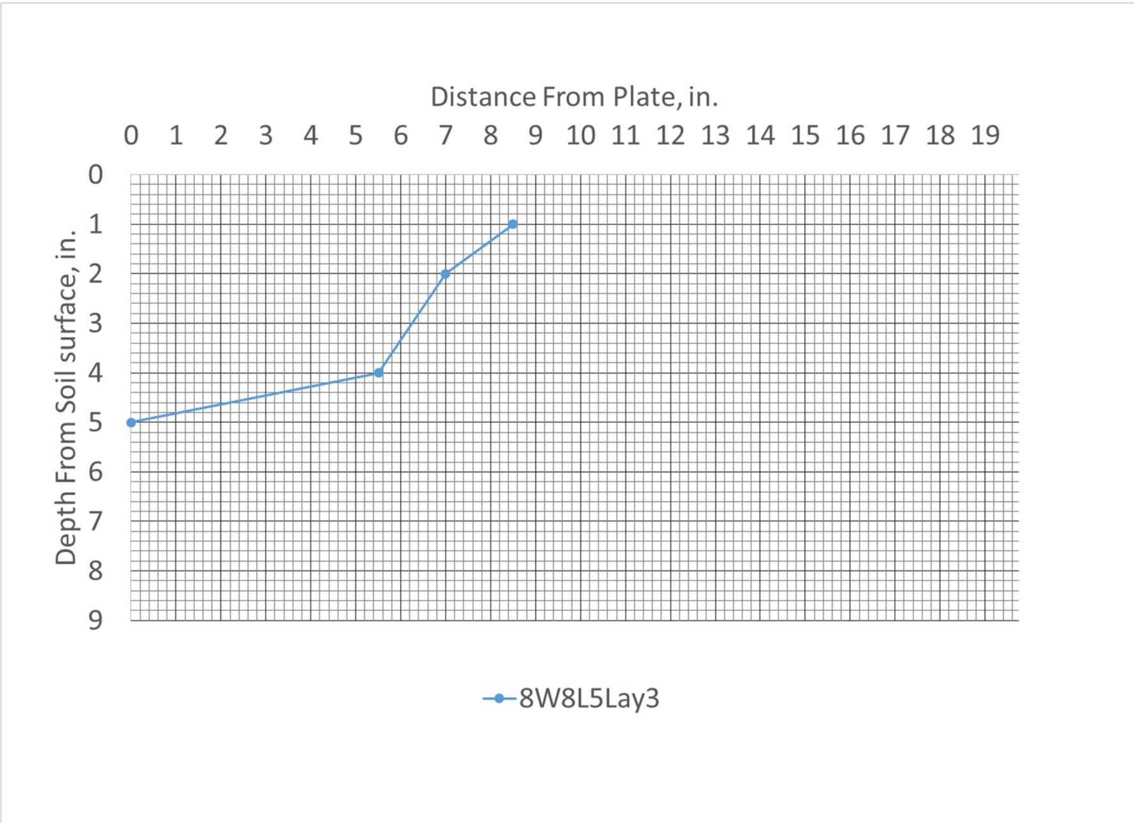

Figure 625: Mid-Plate Failure Surface Location for Test 8W8L5Lay3 from layer paint

H.16 Mid-Plate Failure Surface Location for Test 8W8L10Lay3 from layer paint

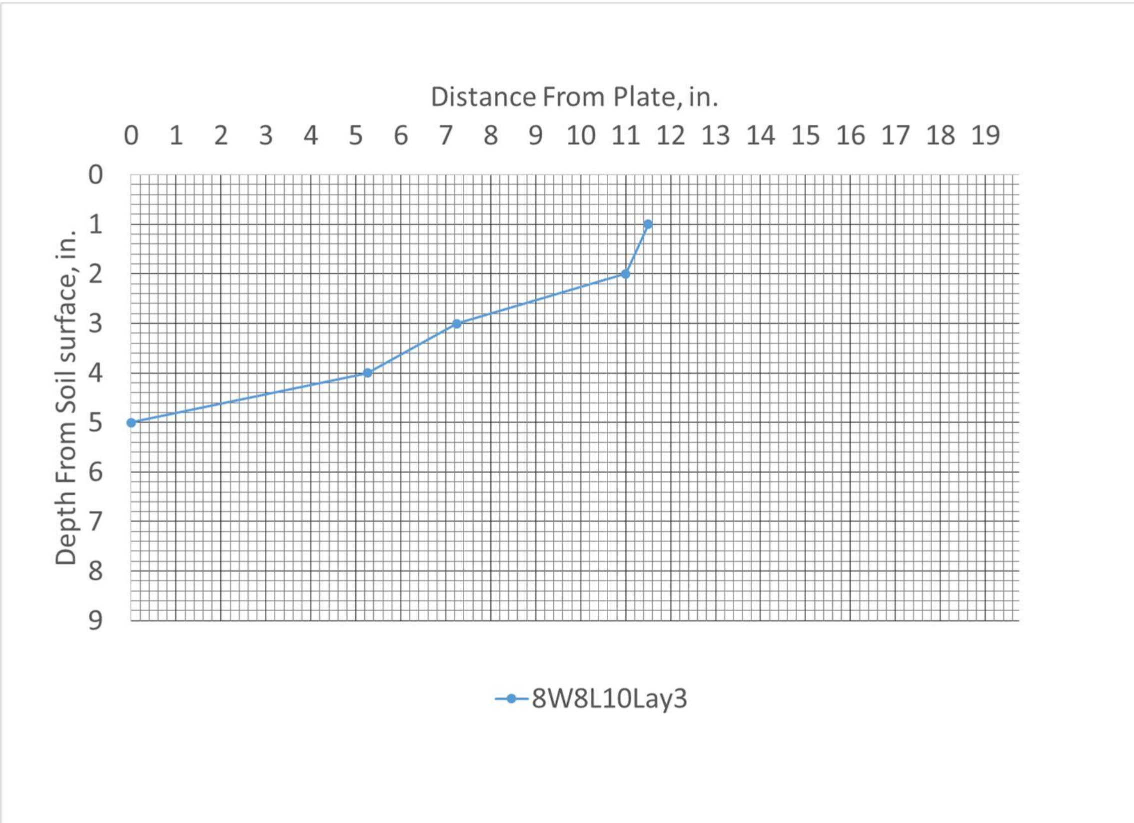

Figure 626: Mid-Plate Failure Surface Location for Test 8W8L10Lay3 from layer paint

H.17 Mid-Plate Failure Surface Location for Test 8W11L5Lay3 from layer paint

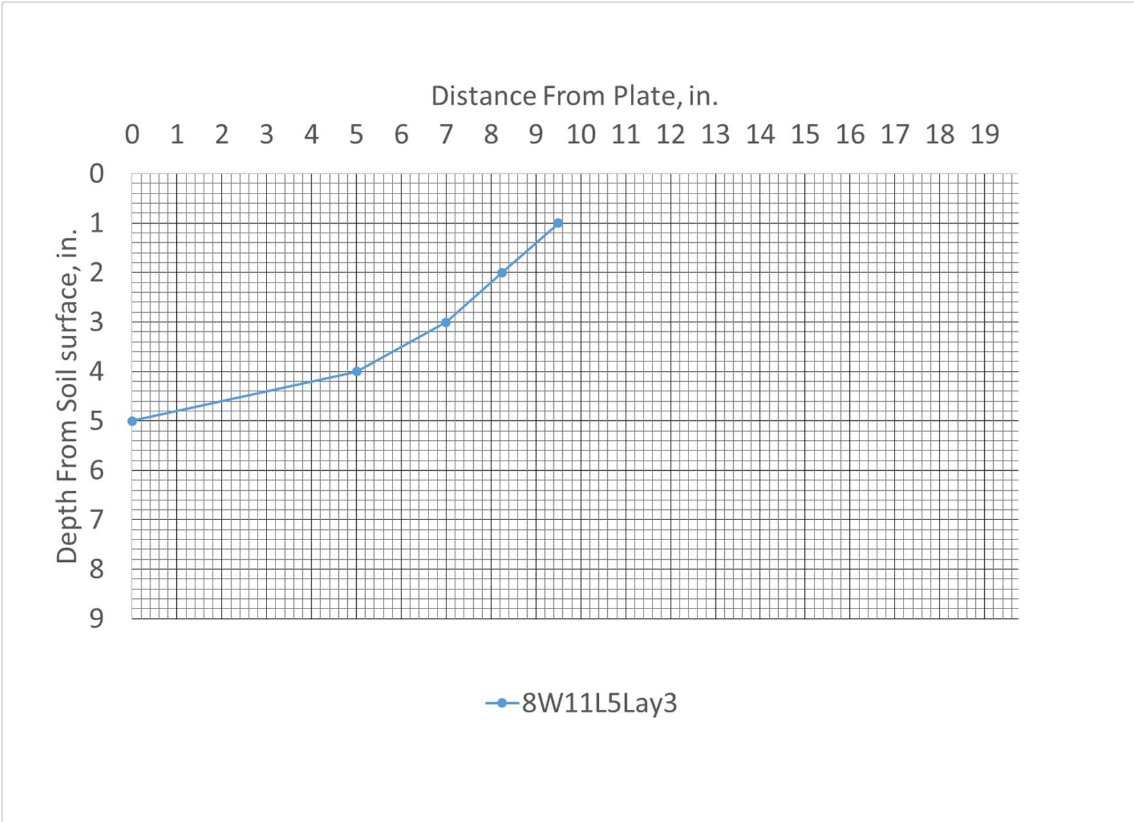

Figure 627: Mid-Plate Failure Surface Location for Test 8W11L5Lay3 from layer paint

H.18 Mid-Plate Failure Surface Location for Test 8W11L10Lay3 from layer paint

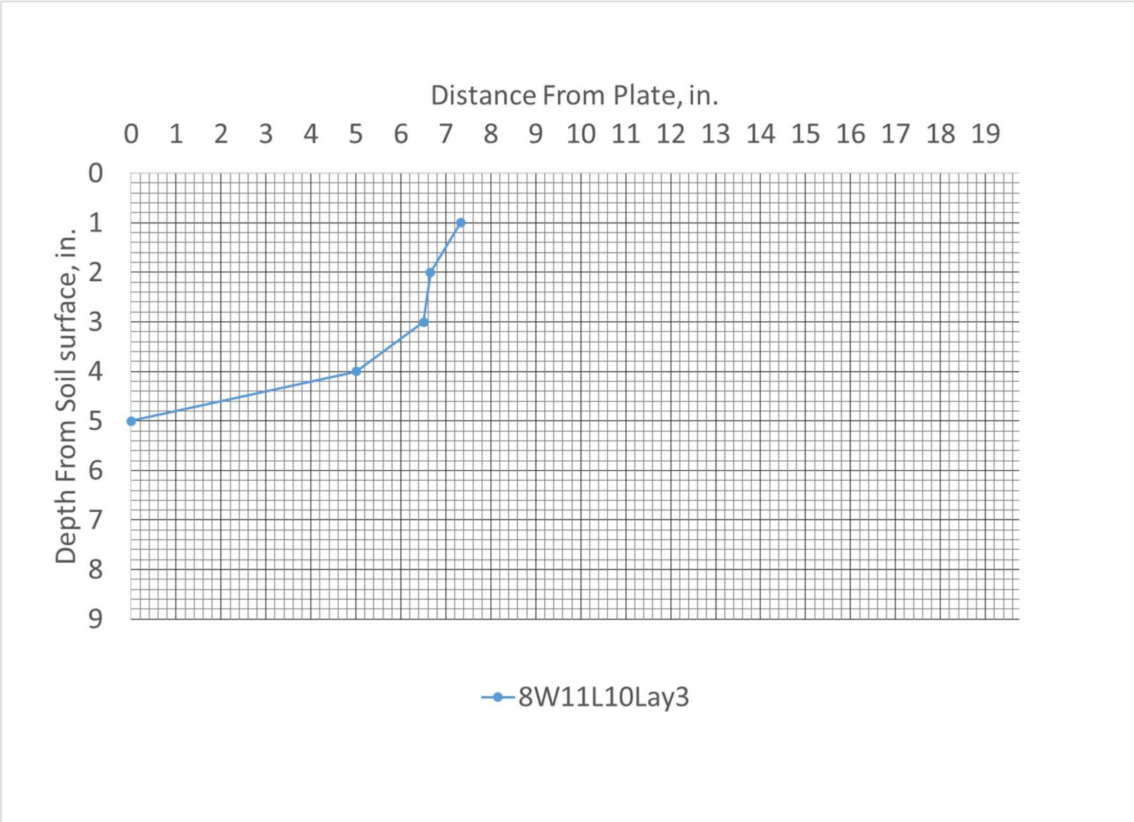

Figure 628: Mid-Plate Failure Surface Location for Test 8W11L10Lay3 from layer paint

H.19 Mid-Plate Failure Surface Location for Test 11W8L5Lay3 from layer paint

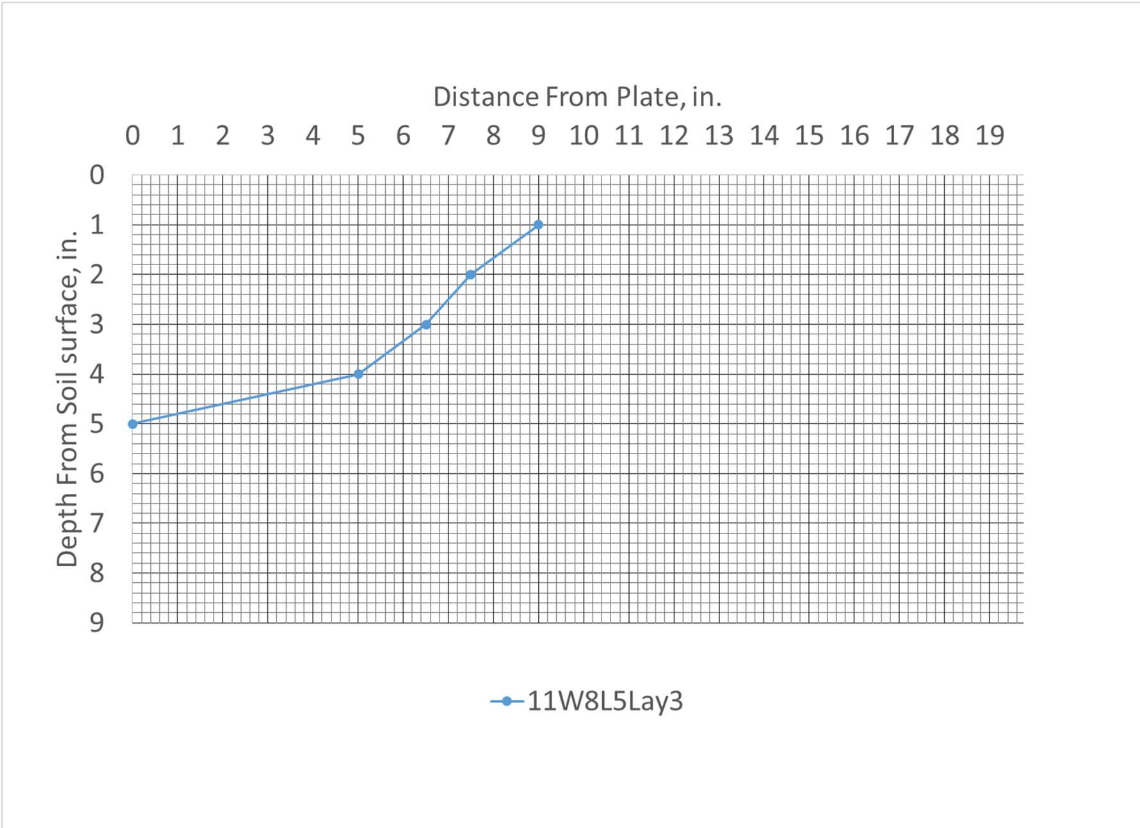

Figure 629: Mid-Plate Failure Surface Location for Test 11W8L5Lay3 from layer paint

H.20 Mid-Plate Failure Surface Location for Test 11W8L10Lay3 from layer paint

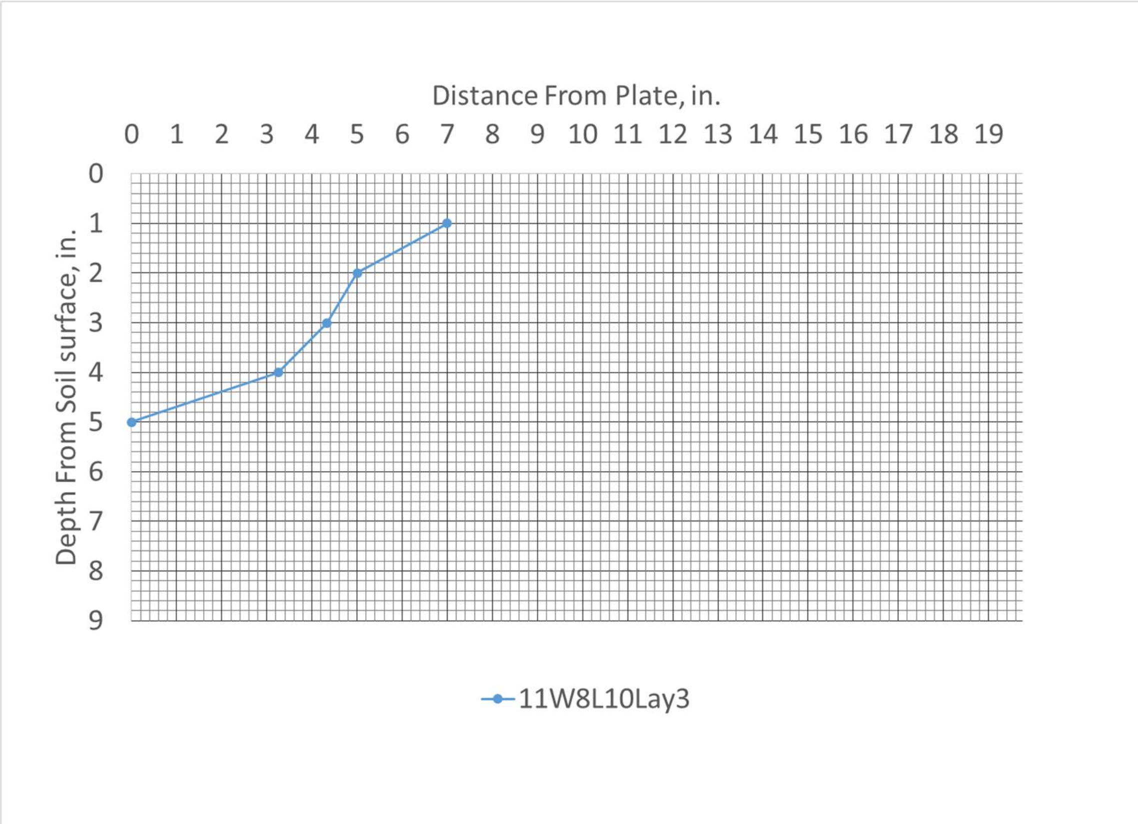

Figure 630: Mid-Plate Failure Surface Location for Test 11W8L10Lay3 from layer paint

H.21 Mid-Plate Failure Surface Location for Test 11W11L5Lay3 from layer paint

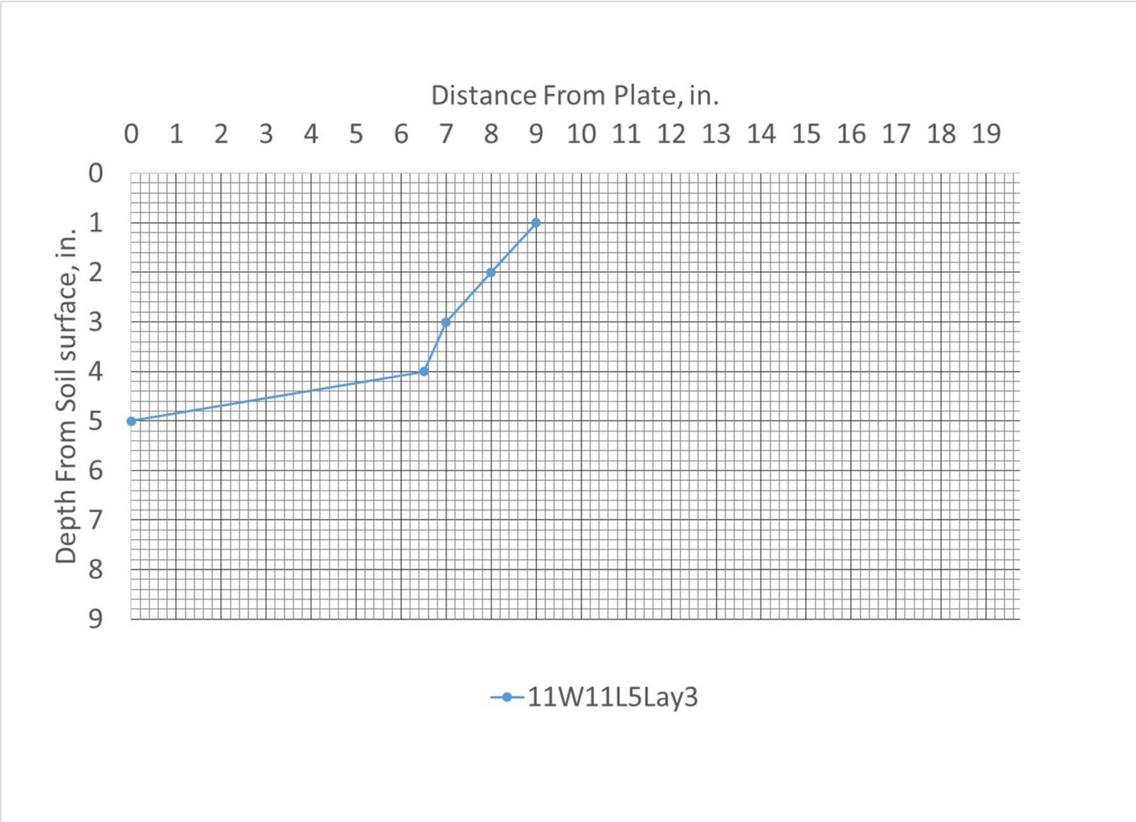

Figure 631: Mid-Plate Failure Surface Location for Test 11W11L5Lay3 from layer paint

H.22 Mid-Plate Failure Surface Location for Test 11W11L10Lay3 from layer paint

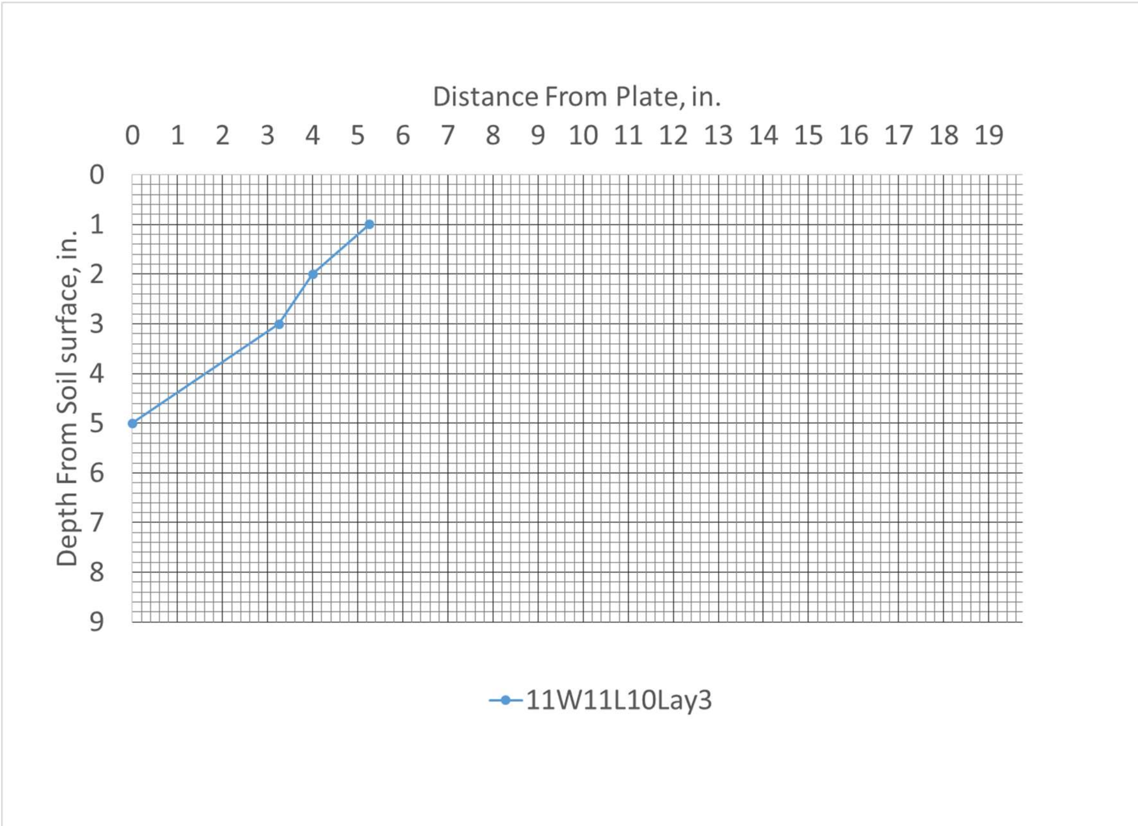

Figure 632: Mid-Plate Failure Surface Location for Test 11W11L10Lay3 from layer paint

H.23 Mid-Plate Failure Surface Location for Test PW8L5Lay3 from layer paint

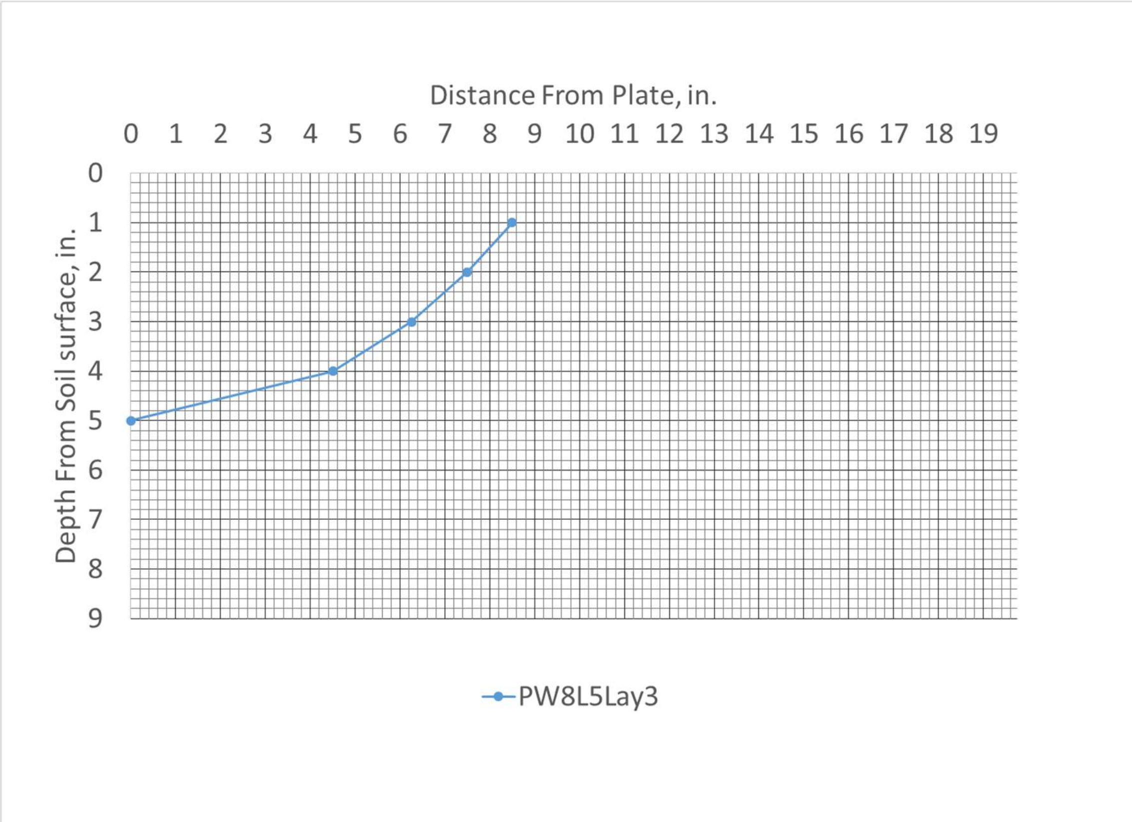

Figure 633: Mid-Plate Failure Surface Location for Test PW8L5Lay3 from layer paint

H.24 Mid-Plate Failure Surface Location for Test PW8L10Lay3 from layer paint

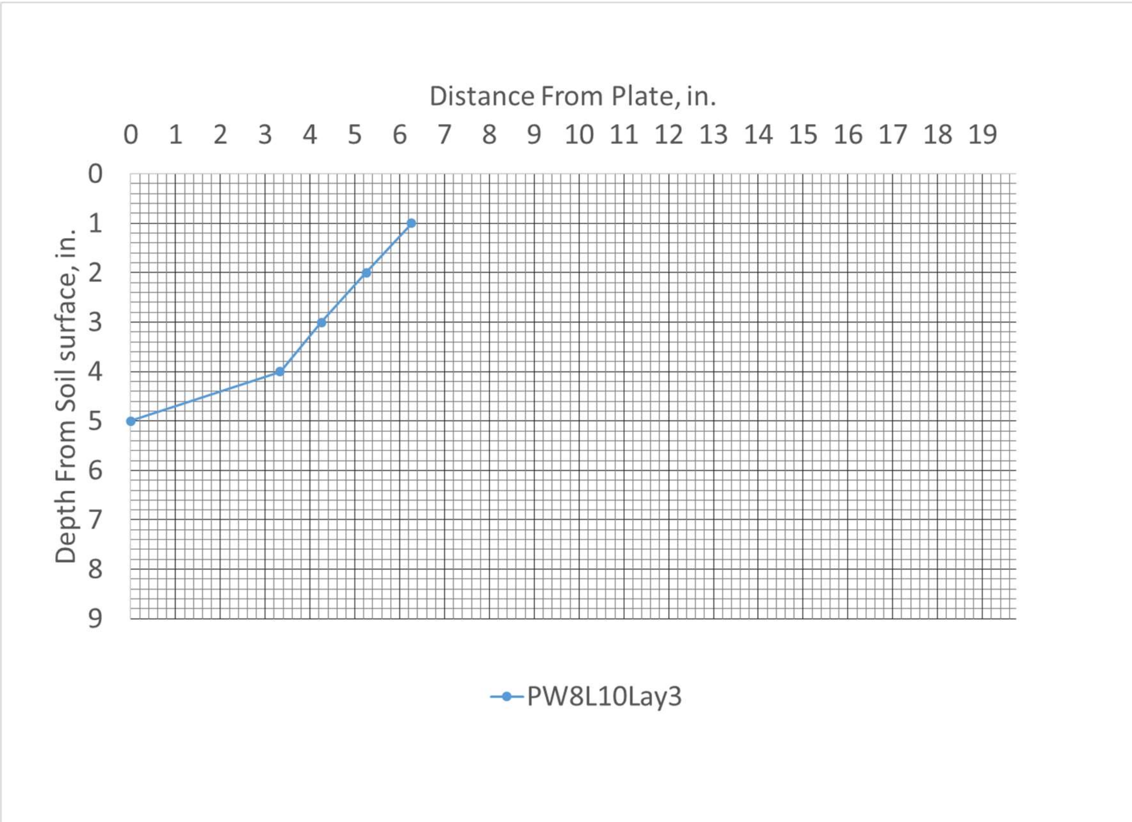

Figure 634: Mid-Plate Failure Surface Location for Test PW8L10Lay3 from layer paint

H.25 Mid-Plate Failure Surface Location for Test PW11L5Lay3 from layer paint

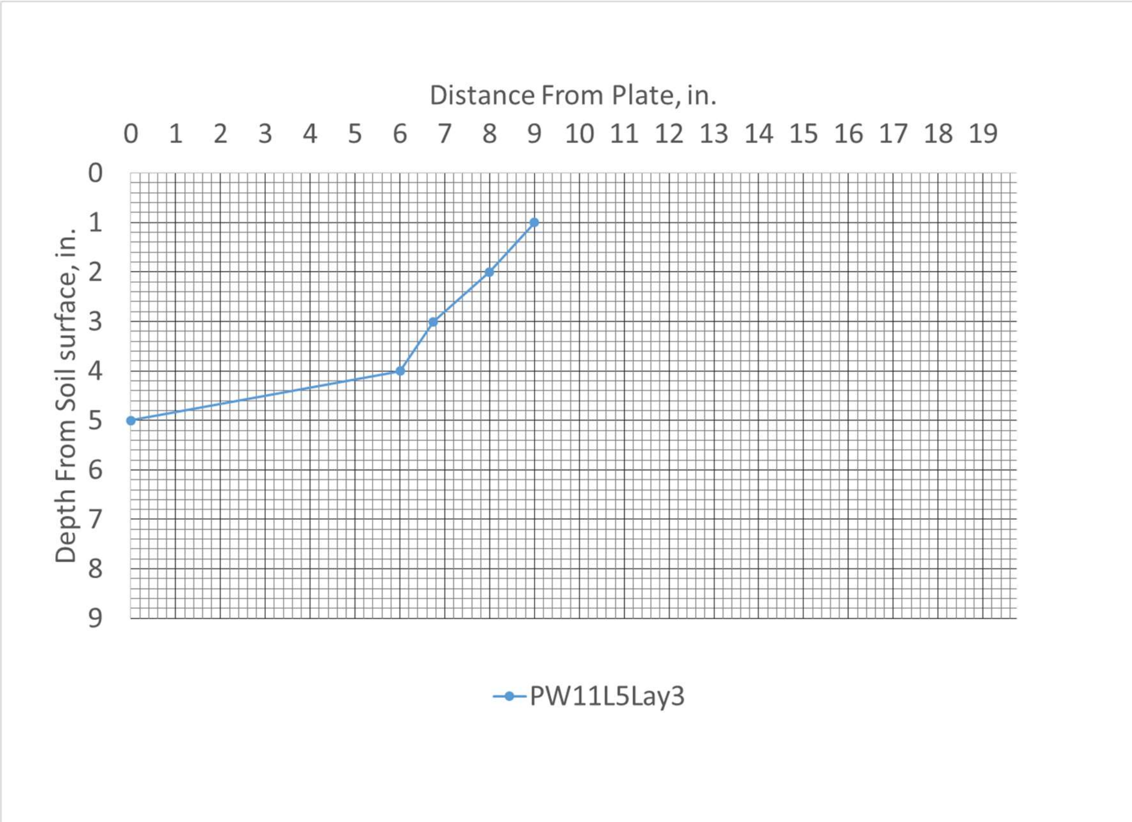

Figure 635: Mid-Plate Failure Surface Location for Test PW11L5Lay3 from layer paint

H.26 Mid-Plate Failure Surface Location for Test NR3 from layer paint

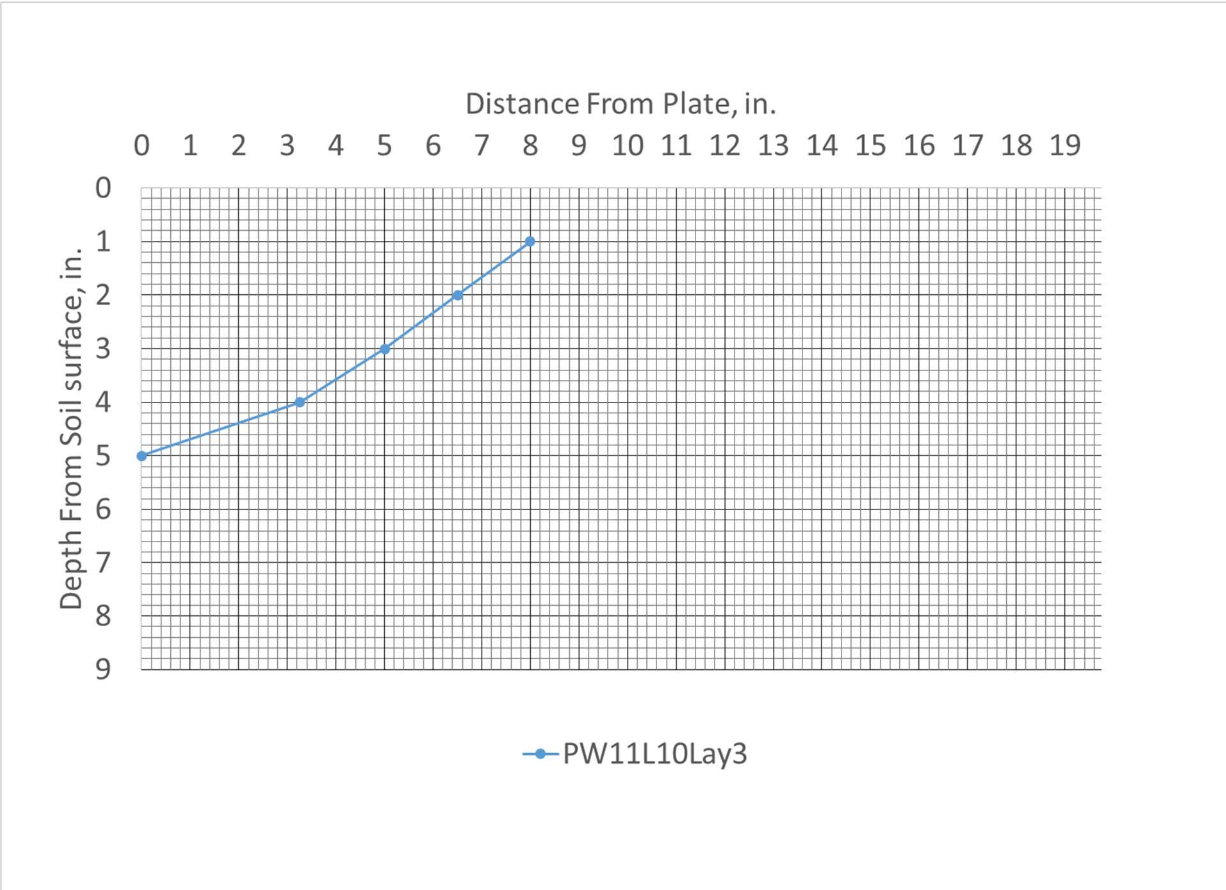

Figure 636: Mid-Plate Failure Surface Location for Test PW11L10Lay3 from layer paint

APPENDIX I: FLAC3D™ LOAD DISPLACEMENT PLOTS

I.1 Introduction

Load-displacement data were taken during FLAC3D™ simulation. These data were plotted using Microsoft Excel. Peak Force and the stiffness at 50% of the Peak Force were determined using each plot and are shown on the plot.

I.2 Load-Displacement Plot of Simulation 8W8L5Lay

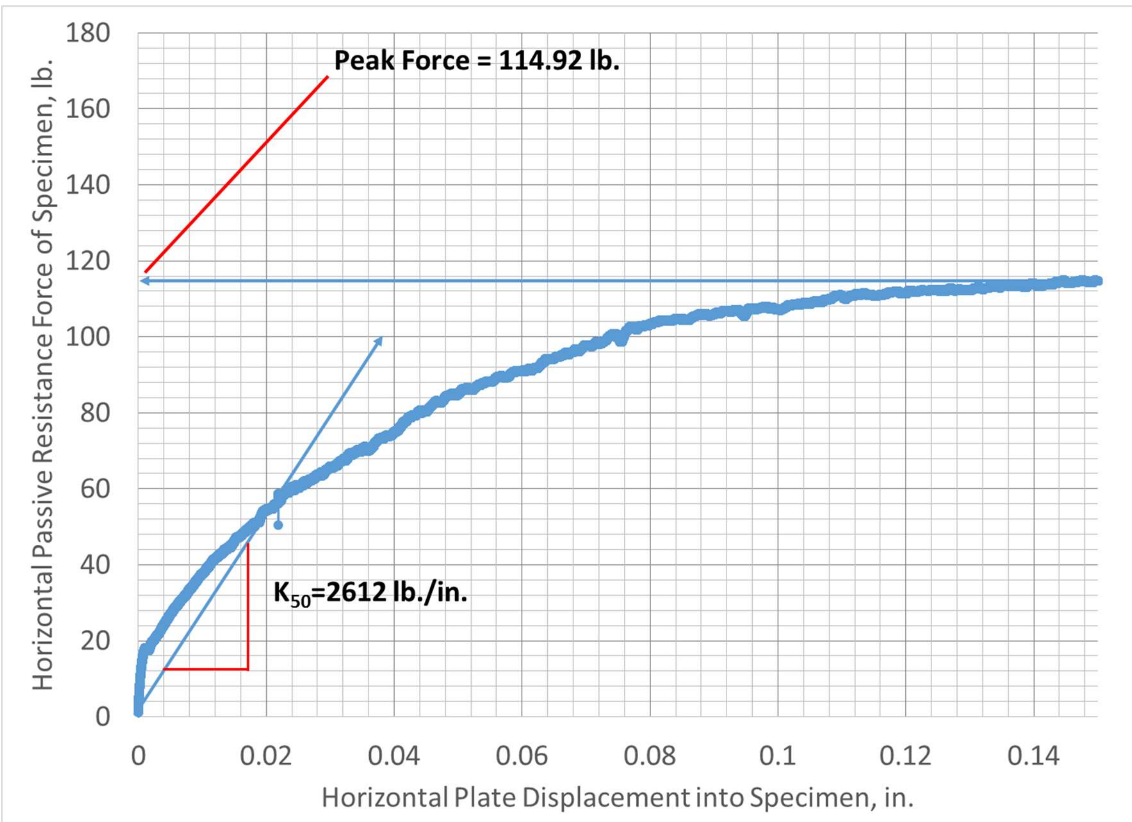

Figure 637: Load-displacement plot of simulation 8W8L5Lay

I.3 Load-Displacement Plot of Simulation 8W8L10Lay

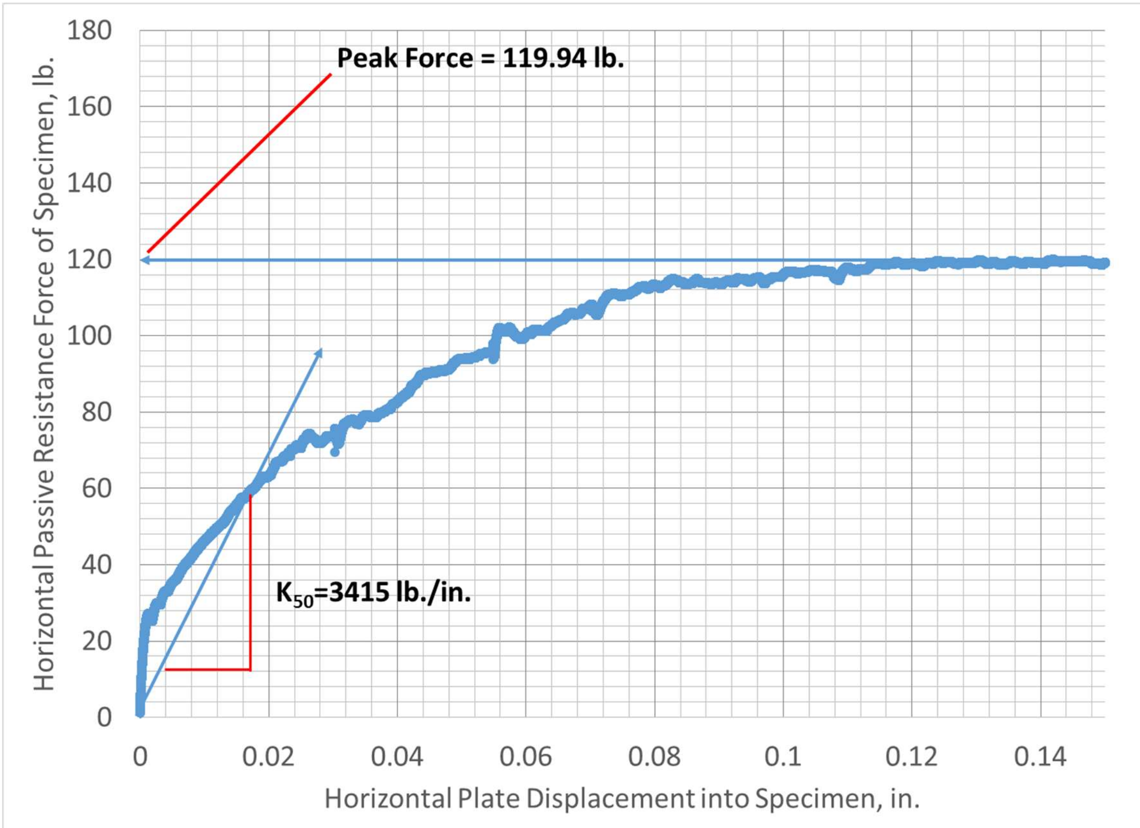

Figure 638: Load-displacement plot of simulation 8W8L10Lay

I.4 Load-Displacement Plot of Simulation 8W11L5Lay

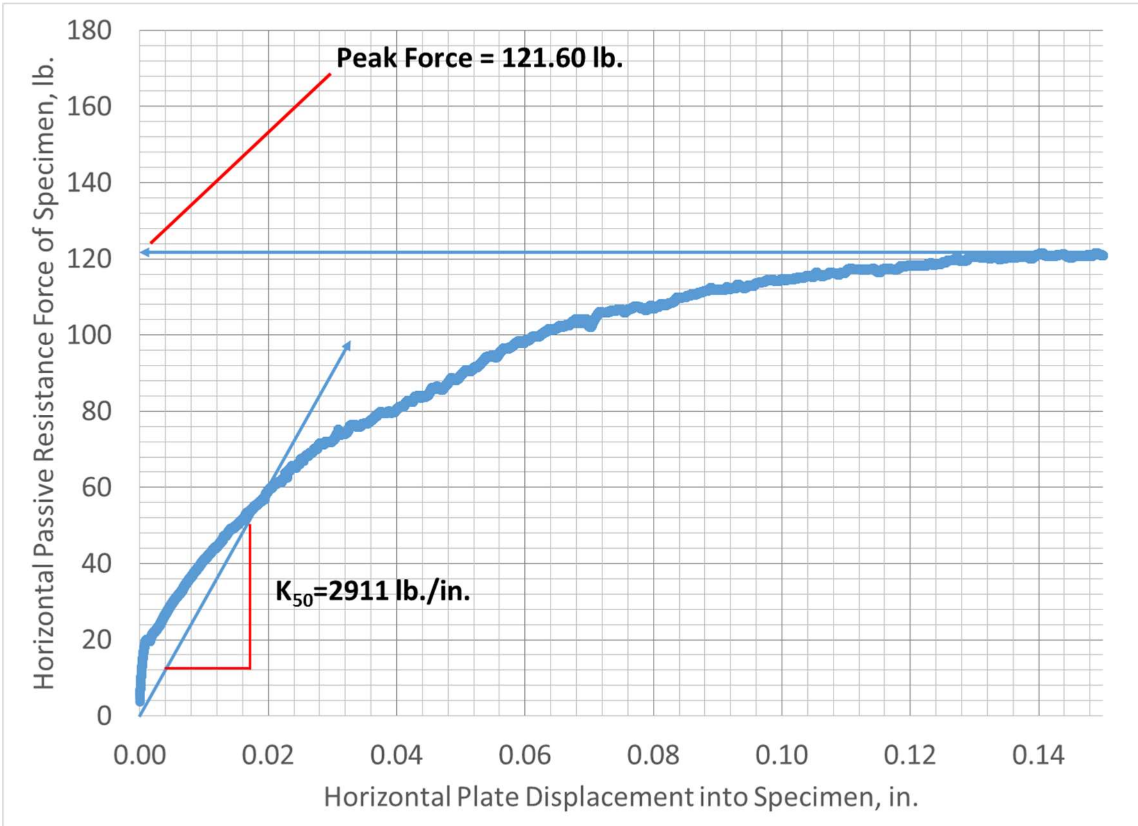

Figure 639: Load-displacement plot of simulation 8W11L5Lay

I.5 Load-Displacement Plot of Simulation 8W11L10Lay

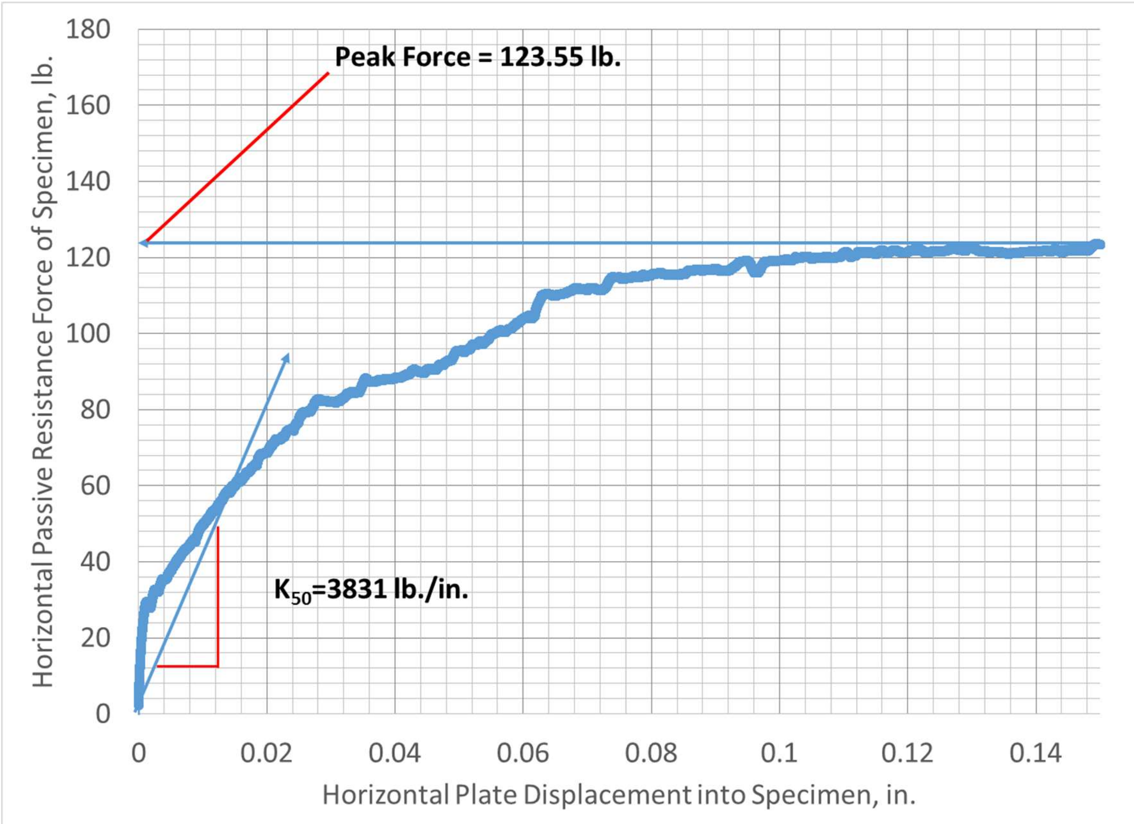

Figure 640: Load-displacement plot of simulation 8W11L10Lay

I.6 Load-Displacement Plot of Simulation 11W8L5Lay

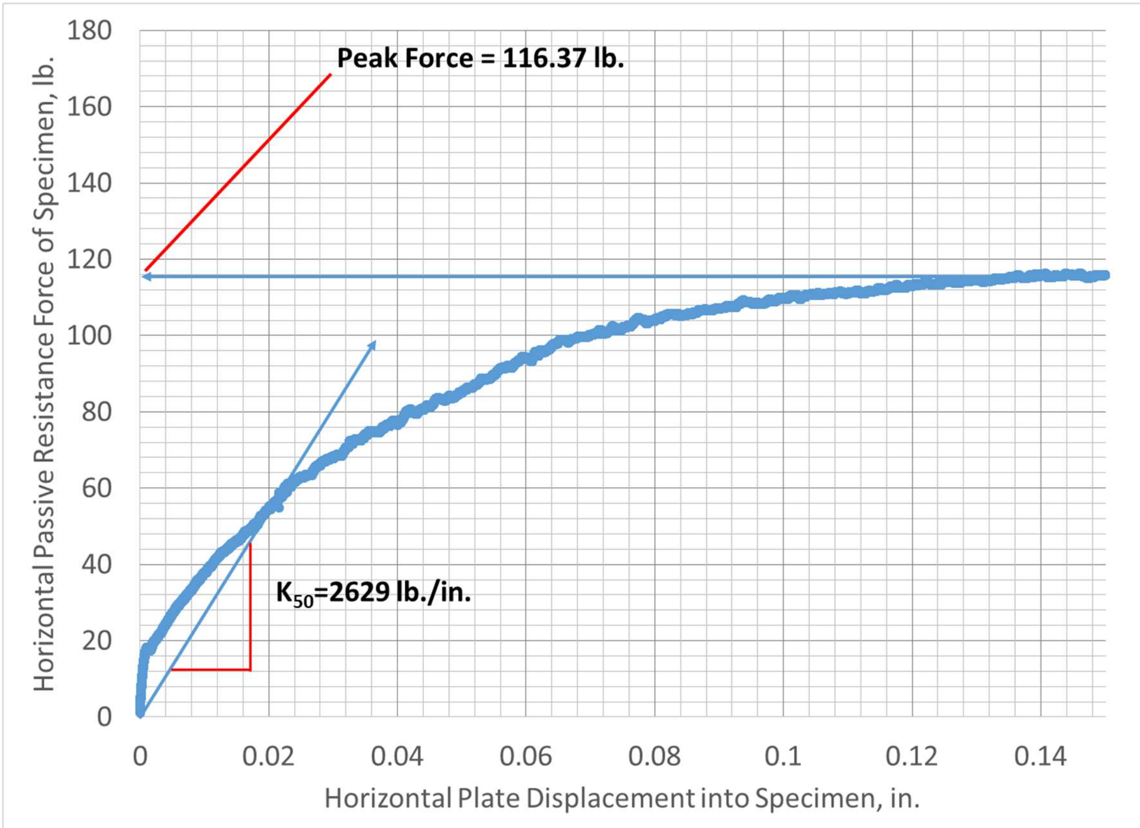

Figure 641: Load-displacement plot of simulation 11W8L5Lay

I.7 Load-Displacement Plot of Simulation 11W8L10Lay

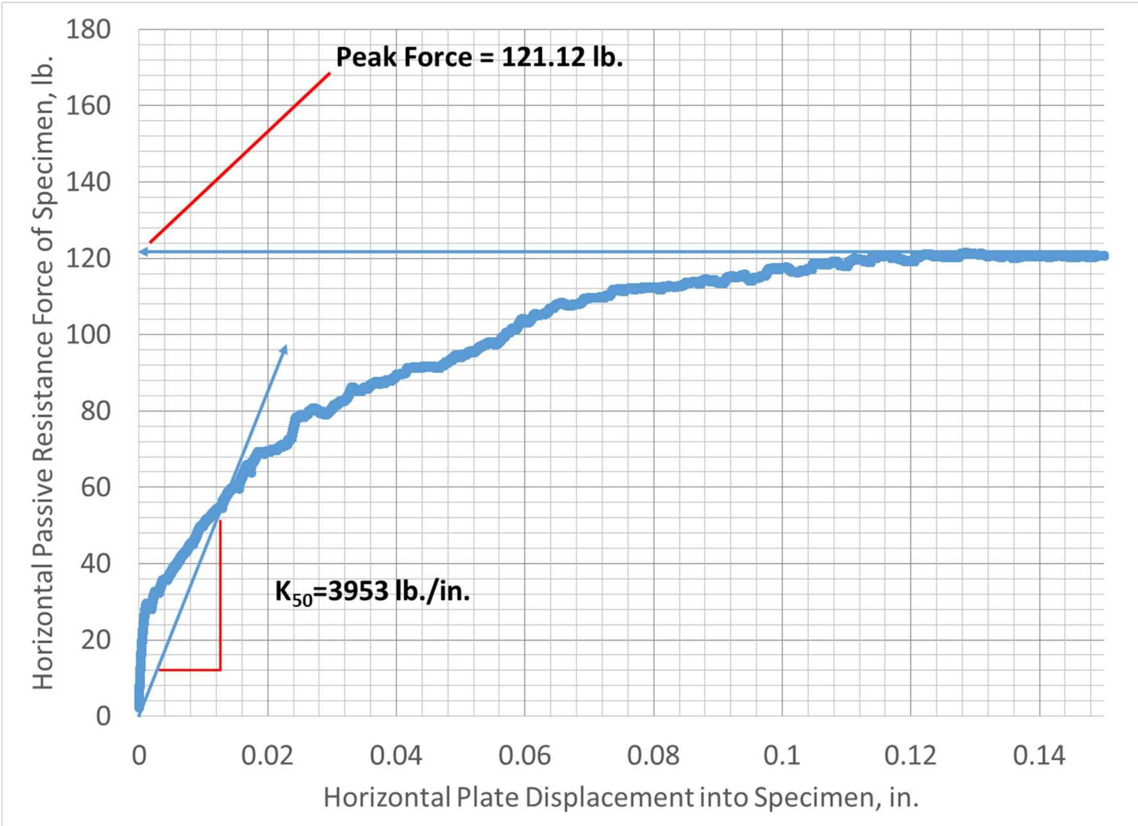

Figure 642: Load-displacement plot of simulation 11W8L10Lay

I.8 Load-Displacement Plot of Simulation 11W11L5Lay

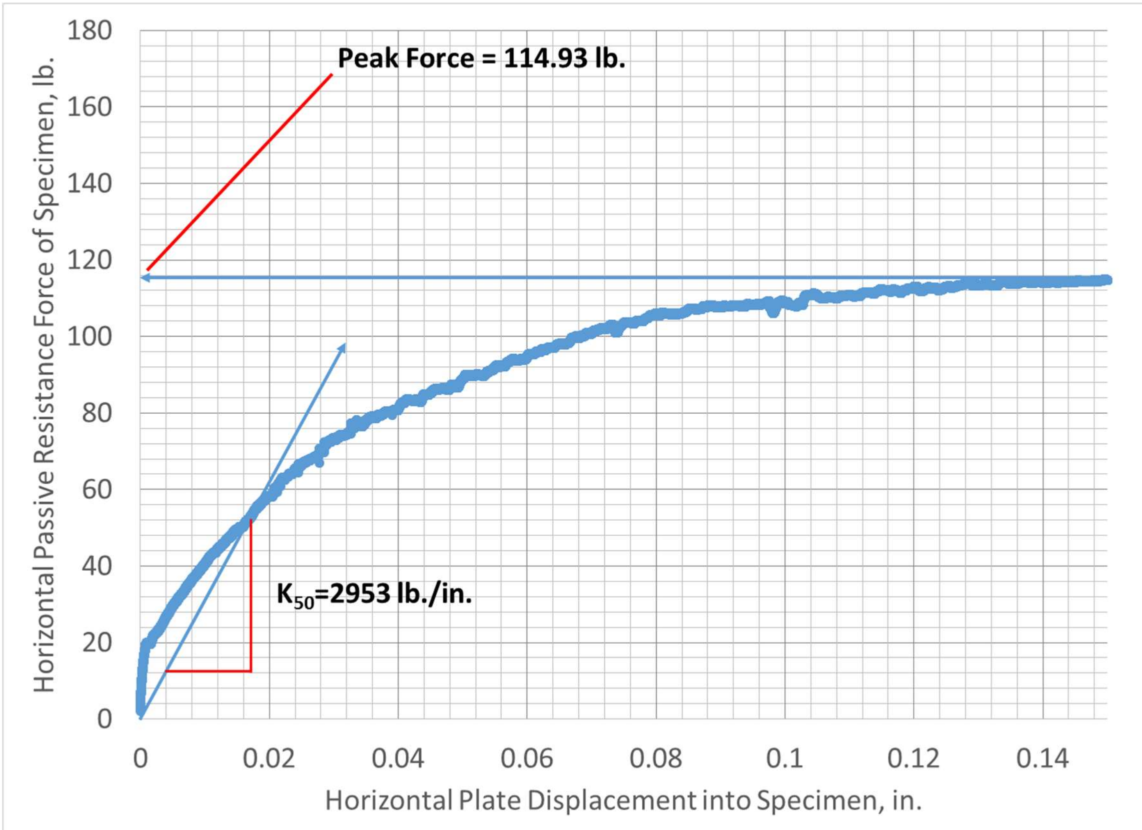

Figure 643: Load-displacement plot of simulation 11W11L5Lay

I.9 Load-Displacement Plot of Simulation 11W11L10Lay

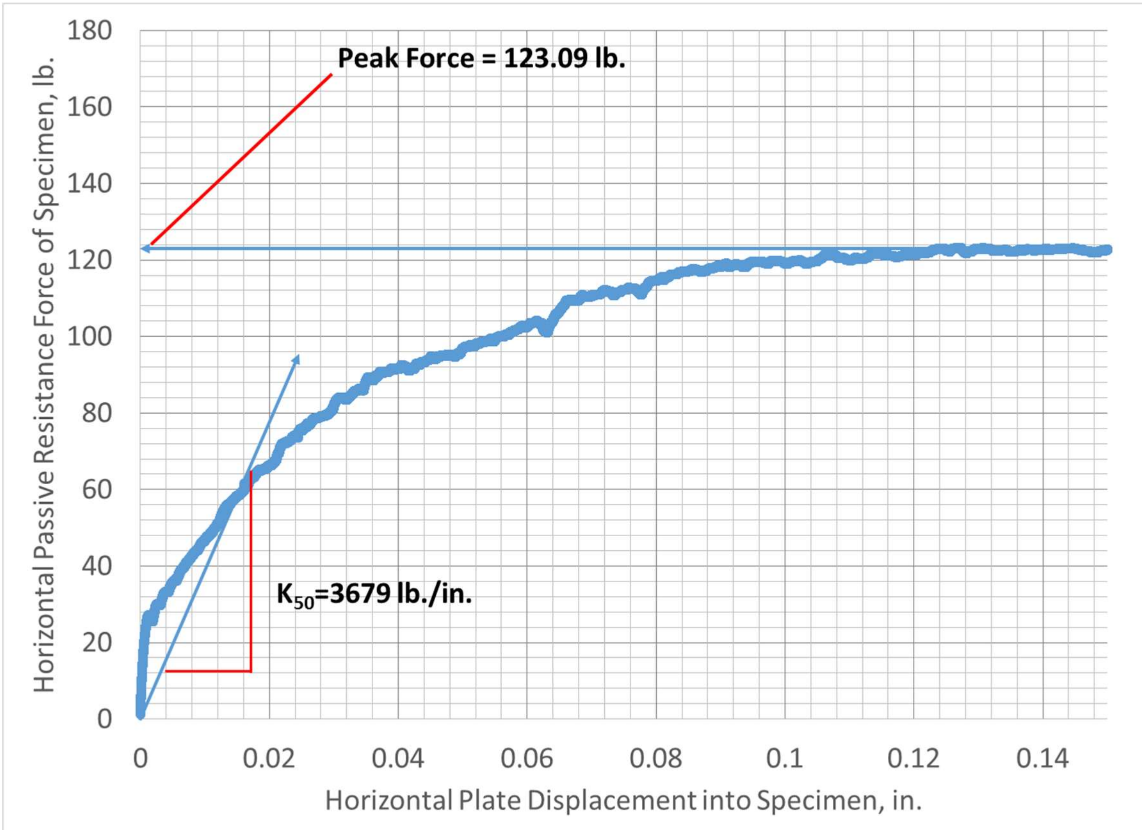

Figure 644: Load-displacement plot of simulation 11W11L10Lay

I.10 Load-Displacement Plot of Simulation PW8L5Lay

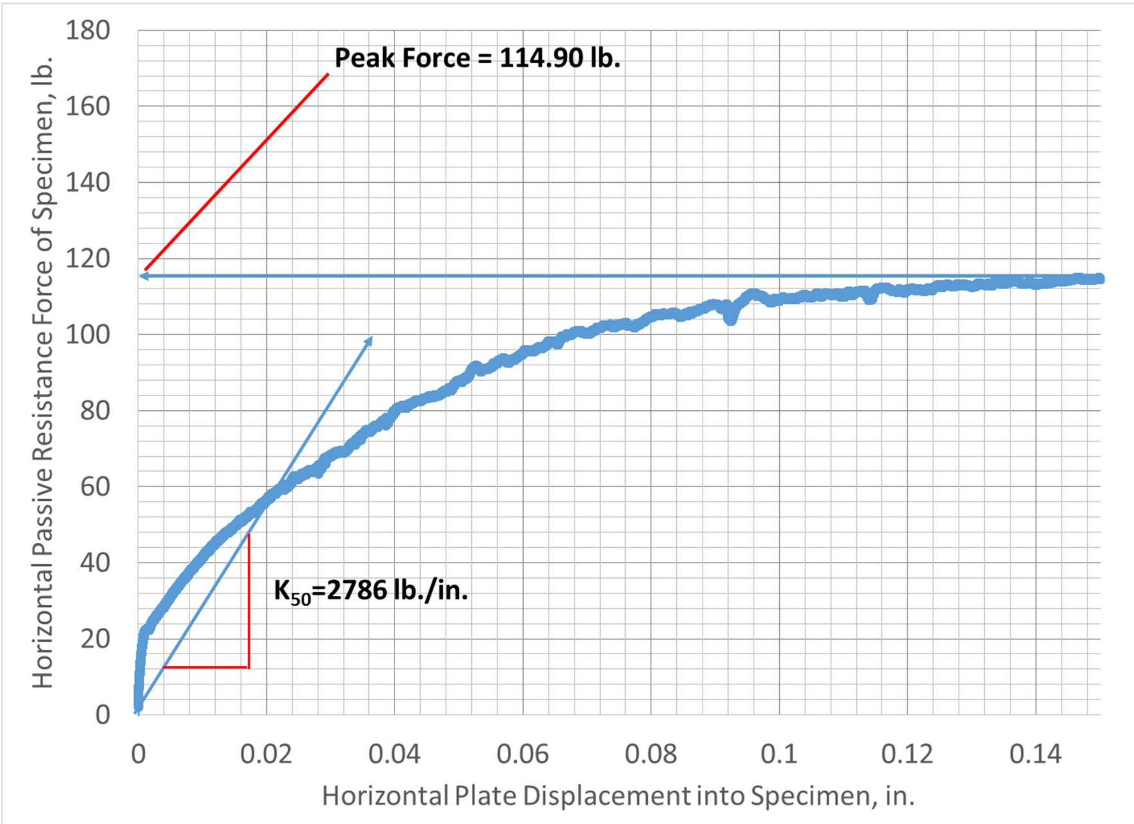

Figure 645: Load-displacement plot of simulation PW8L5Lay

I.11 Load-Displacement Plot of Simulation PW8L10Lay

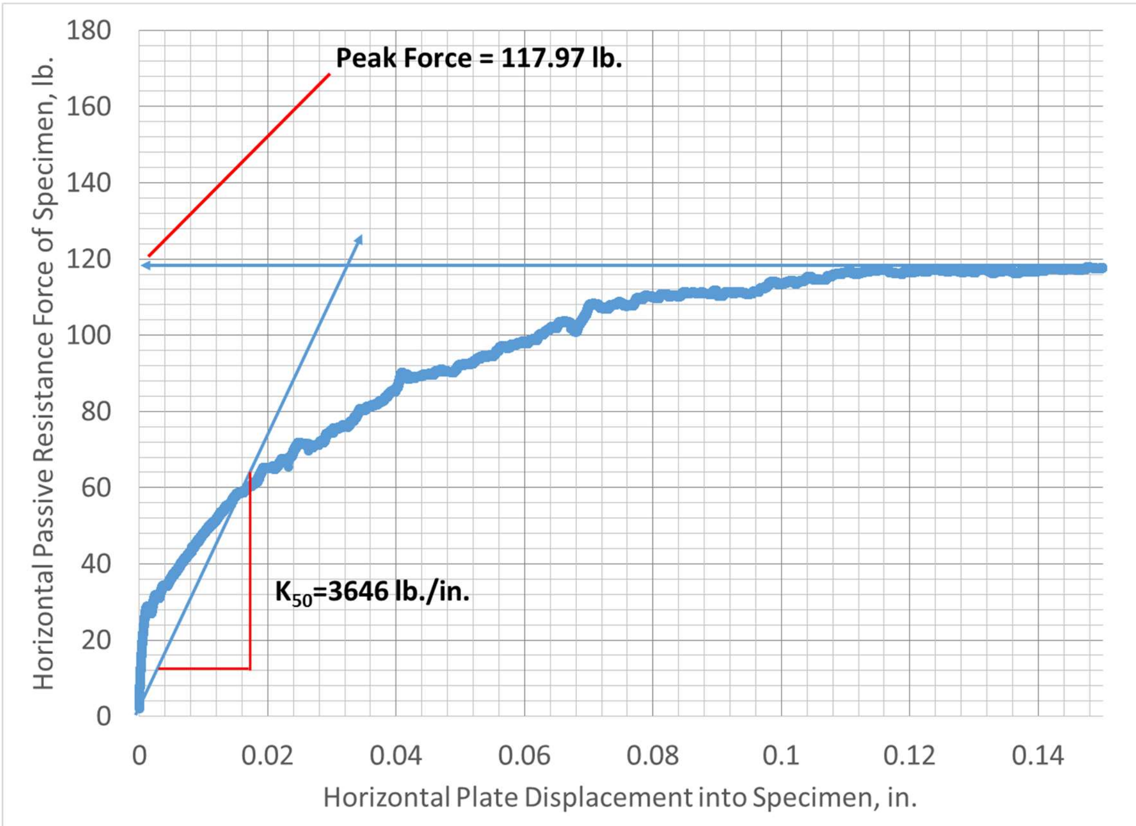

Figure 646: Load-displacement plot of simulation PW8L10Lay

I.12 Load-Displacement Plot of Simulation PW11L5Lay

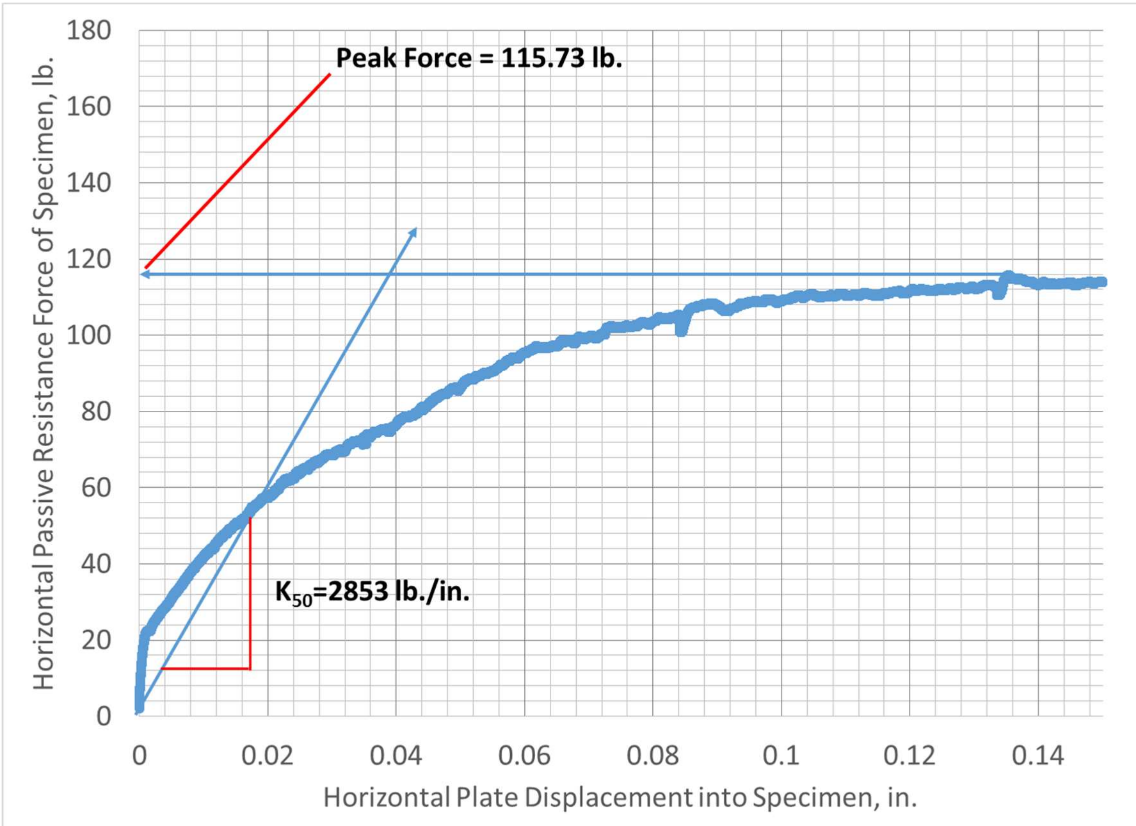

Figure 647: Load-displacement plot of simulation PW11L5Lay

I.13 Load-Displacement Plot of Simulation PW11L10Lay

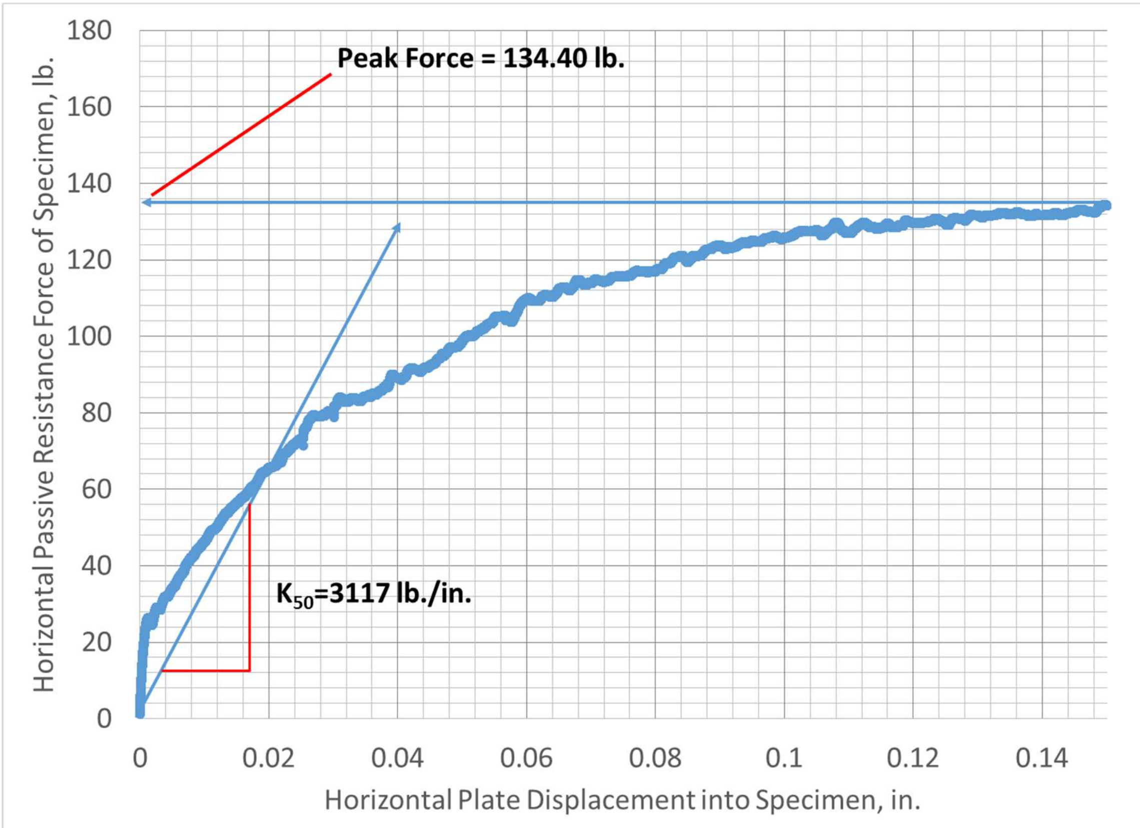

Figure 648: Load-displacement plot of simulation PW11L10Lay

I.14 Load-Displacement Plot of Simulation NR

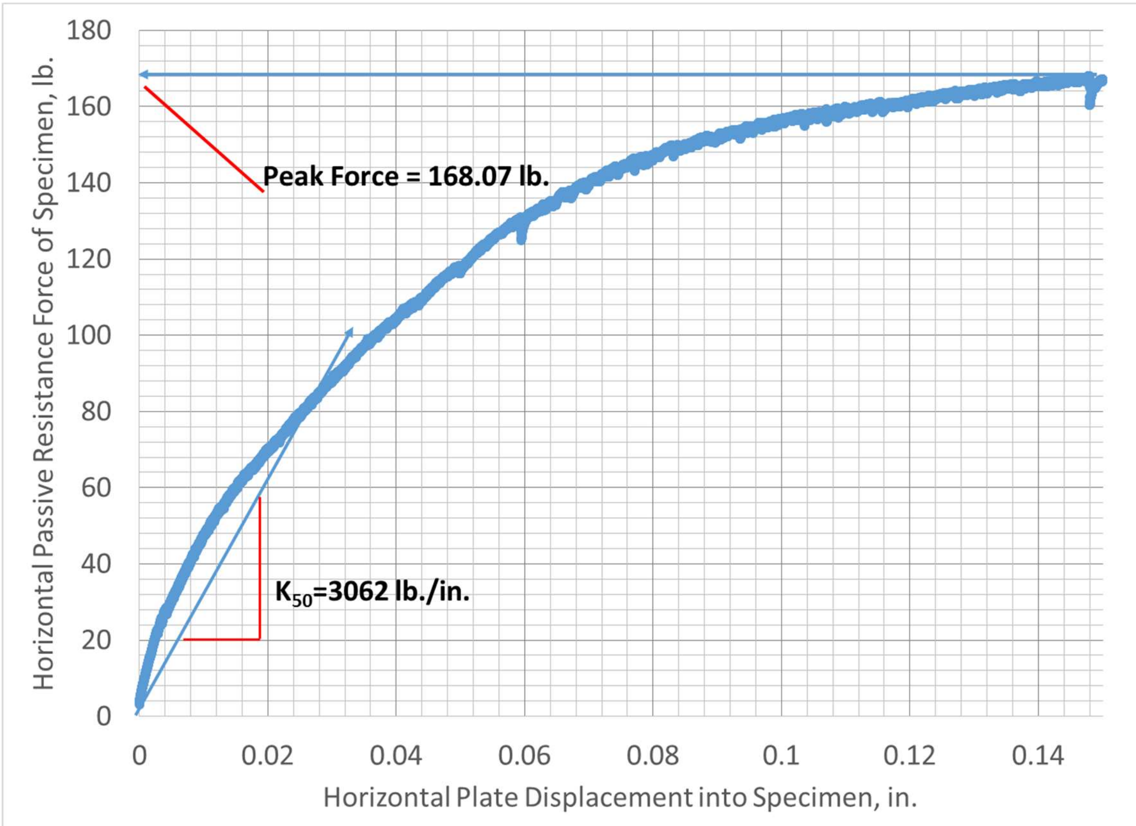

Figure 649: Load-displacement plot of simulation NR

APPENDIX J: FLAC3D™ SOIL PARAMETER CALIBRATION FROM TRIAXIAL TESTING

J.1 Introduction

Triaxial tests were performed at three different confining stresses for the test soil. The results of triaxial testing were used to calibrate the parameters E_{50}^{ref}, E_{ur}^{ref}, m, R_f, and ϕ to be used in the FLAC3D™ plastic hardening soil model.

J.2 Calibration of Friction Angle

From laboratory testing, the angle created by the Mohr-Coulomb failure envelope and the horizontal is the friction angle, ϕ. The friction angle was computed as 36.6 degrees, as shown in Figure 81.

J.3 Calibration of R_f, m, and E_{50}^{ref}

The first step in this calibration is to plot the curve of ε_1/q vs ε_1/q_f using the triaxial compression test lab data, as shown in Figure 650.

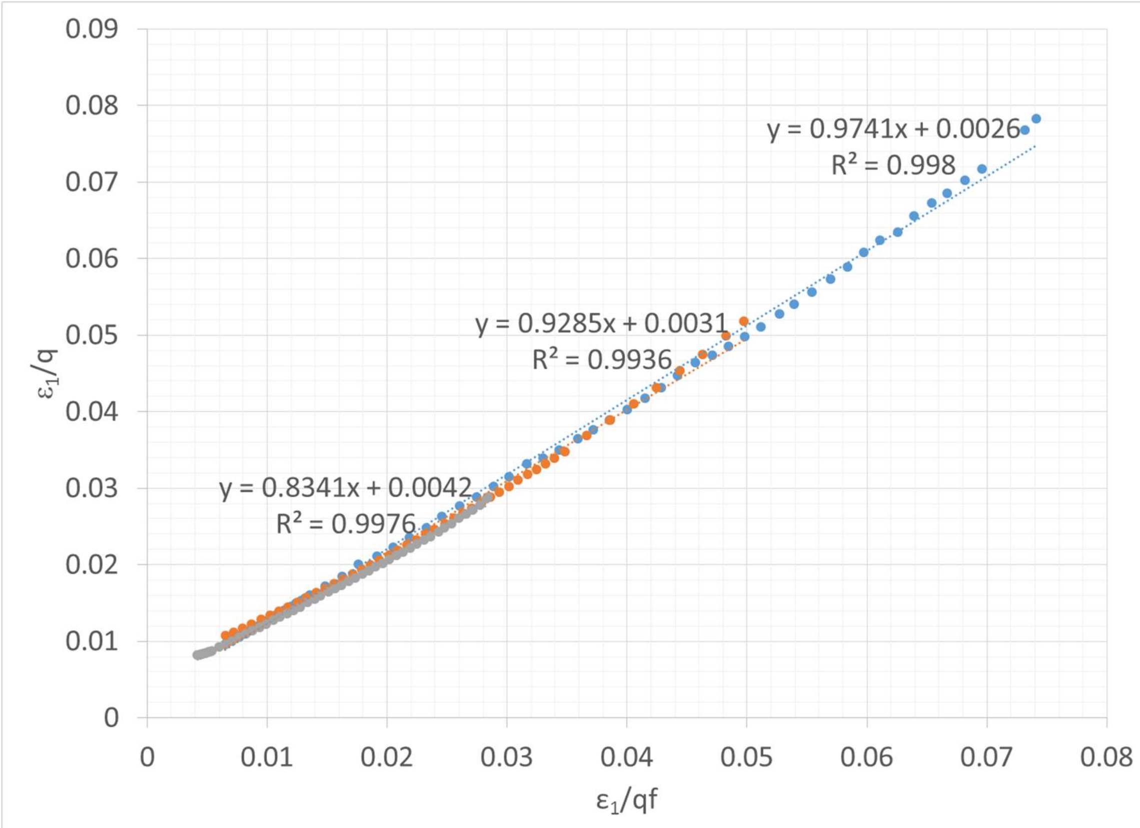

Figure 650: Determination of R_f and E_i from three sets of triaxial compression tests with three different confining stresses

R_f values are the slope of each linear trend line, while $1/E_i$ values are the y intercept of each linear trend line; see Table 75.

Table 75: Determination of R_f, m and E_{50}^{ref}

σ_3, psi	R_f	$1/E_i$	E_i	E_{50}	ln(E50)	$\ln(\sigma_3/p_{ref})$
15	0.9741	0.000026	38461.54	11020	9.307478	0.020202707
30	0.9285	0.000031	32258.06	7716.5	8.951121	0.713349888
45	0.8341	0.000042	23809.52	9253.1	9.132713	1.118814996

Plotting $\ln(E_{50})$ vs $\ln(\sigma_3/p_{ref})$ allows E_{50}^{ref} to be computed as the intercept of the trend line with the y-axis, Figure 651. The location of the triaxial compression curve for the 15 psi test was somewhat abnormal as the stress-strain curve indicated a more brittle material than the other two confining pressures. Due to this, a higher than likely E_{50} for the 15 psi confining pressure test was computed. Due to this, the 15 psi confining pressure triaxial test was not used in the calculation of E_{50}^{ref}.

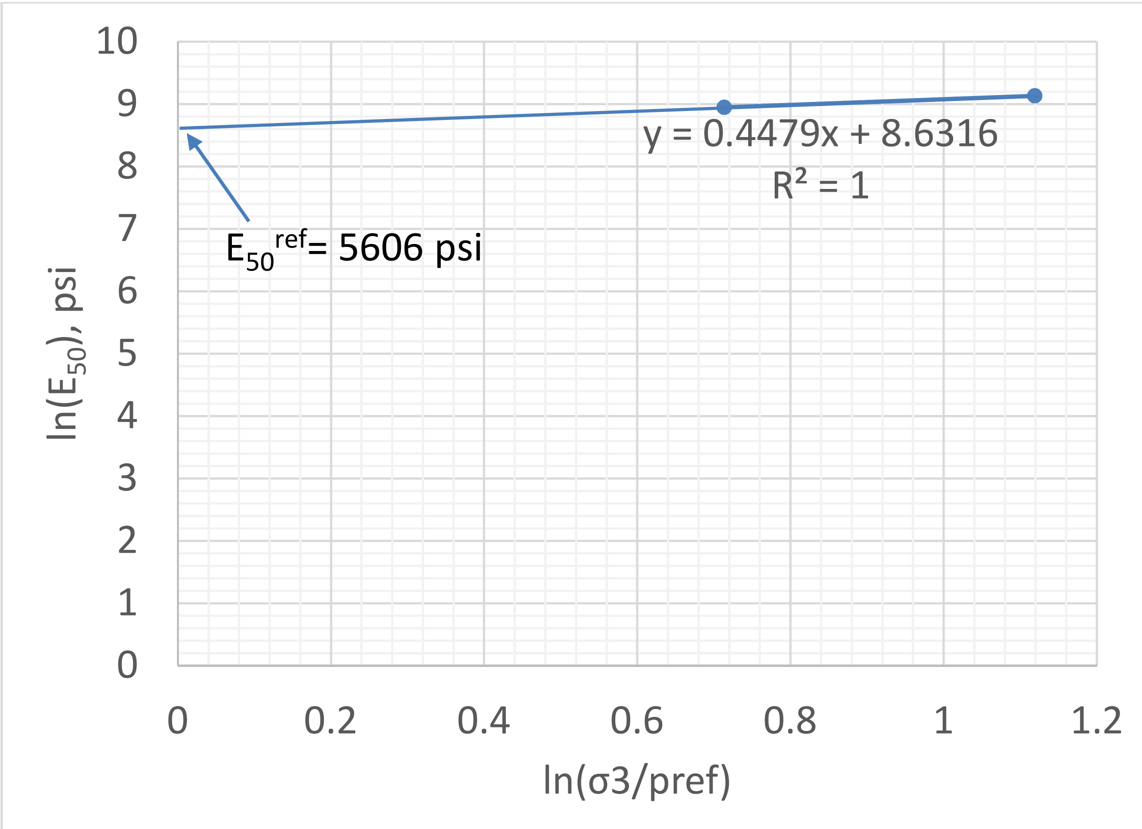

Figure 651: Determination of m and E_{50}^{ref} from two sets of triaxial compression tests with two different confining stresses.

The calibrated R_f value is the average of the R_f values presented in Table 55 and is 0.912. Parameter m is the slope of the trend line in Figure 651 and is 0.4479. The natural log of E_{50}^{ref} is the y-intercept of the trend line in Figure 651 and is 8.6316. E_{50}^{ref} is computed from this number and is 5606 psi.

J.4 Calibration of E_{ur}^{ref}

E_{ur}^{ref} was not calibrated due to unavailability of unload-reload data. Using suggestion from Cheng (2015), the E_{ur}^{ref} value (28030 psi) was taken as 5 times the E_{50}^{ref} value of 5606 psi.

APPENDIX K: SCALING OF BENCHTOP MODEL

K.1 Introduction

The benchtop test was designed to provide mechanical similarity between the benchtop test and full size MSE structures. To do this, physical properties of test geometry, soil, and reinforcement were scaled appropriately.

K.2. Test Geometry

There is no standard MSE structure. Reinforcement length, width and vertical spacing all vary considerably based on project requirements.

1. Length

A common starting point for reinforcement length is 0.7 multiplied by the structure's height. The reinforced structure height of the laboratory test was 5 in. and 0.7 times this height is 3.5 in. In this research, the lengths used were 8 in. and 11 in. which were intentionally much longer than 3.5 in. with the intent to augment the effect of reinforcement.

2. Width

Width of reinforcement varies with project requirements on full size MSE structures. The widths used in this research were 5.5 in., 8 in., and 11 in. These were chosen to reinforce the soil directly behind the pusher plate as well as two widths that were wider than the pusher plate to determine the effect of reinforcement width.

3. Vertical Spacing

There is no standard MSE structure spacing. However, 8 in vertical spacing is commonly used in GRS-IBS design as the facing units are 8" in depth. The benchtop test used both 0.5 in. and 1 in. vertical spacings. As 8" is common for GRS-IBS, the closer spacing of 0.5 in. was equated to this 8" spacing. From this, a geometric length scale of 16 in. full size MSE structure = 1 in. benchtop test was used to scale other geometric quantities of the benchtop test.

K.3 Soil

Soil gradation, unit weight, and strength parameters were considered for scaling.

1. Gradation

There is no standard for soils used in full size MSE structures. Soils may range from sands to much larger diameter gravels and stones depending on project requirements. However, a commonly used material for full size MSE structures is AASHTO #57 stone. To ensure the test soil behaved similarly to #57 stone in a full size MSE structure, a sand was chosen that approximately scaled geometrically using the 16:1 length scale factor and also had a gradation approximately parallel to #57 stone. The AASHTO #57 stone gradation range, Test Soil, and the gradation of a soil scaled 16X the test soil are shown in Figure 652. While not exactly within the range of the AASHTO #57 soil, the test soil is appropriately scaled.

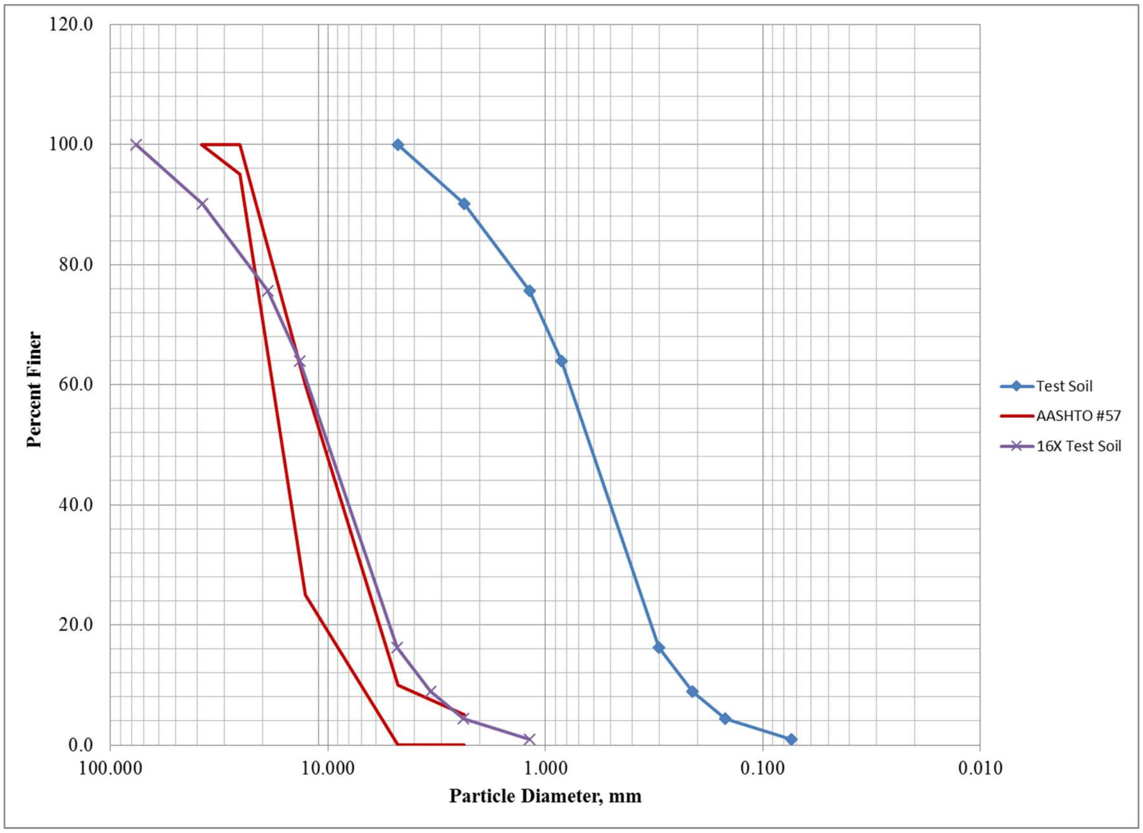

Figure 652: Gradations of Test soil, AASHTO 57 Range, and 16X Test Soil

2. Unit weight

The unit weight of the soil was scaled with a scale factor of 1:1. Unit weight exerts pressures based on the soil's geometry and strength characteristics. Scaling the geometry effectively scaled unit weight.

3. Strength parameters

The strength parameters were determined for the Test Soil through triaxial testing. Cohesion was determined to be zero and the angle of internal friction was determined to be 36.6°. These values were scaled with a scale factor of 1:1 as they are properties carried by the soil regardless of the size of the soil structure. The angle of internal friction is similar to that of materials used in full scale MSE structures.

4. Particle Shape

While not scaled or considered for scale, it should be noted that the particle shape of the test soil is approximately cubic, similar to many open graded aggregates used in full scale MSE structures.

K.4 Reinforcement Properties

Reinforcement interface friction with the test soil, tensile strength, and flexural rigidity were considered for scaling.

1. Interface Friction

Interface friction angles of geosynthetics are highly variable due to the wide variety of polymer types and geosynthetic types. The interface friction of the reinforcement with the test soil was 25°. The interface friction value was scaled with a scale factor of 1:1. The reinforcement interface friction angle is consistent regardless of the size of the reinforcement or the amount of soil present.

2. Tensile Strength

The tensile strength of the reinforcement was not scaled as the reinforcement was not expected to break during testing.

3. Flexural Rigidity

The flexural rigidity of a fabric is a function of its bending length (when tested using a cantilever test apparatus) and mass per unit area. Geosynthetics have highly variable flexural rigidities due to varying fabric structures and materials. For example, two woven geotextiles were tested in flexural rigidity in this research. While both were woven, the polyester geotextile had a stiffness of 2.11×10^{13} μJ/m and the high density polyethylene geotextile had a stiffness of 7.62×10^{13} μJ/m, approximately 3.6 times higher. While not tested due to testing limitations of the equipment and method used, it is very likely that certain geogrids and geomembranes have flexural rigidities that are orders of magnitude greater than the two woven geotextiles tested in this research. It is also likely that geogrids and geomembranes exist that have flexural rigidites similar to the woven geotextiles tested in this research. The flexural rigidities of geosynthetic reinforcements are highly variable, inferring that there are also a wide variety of flexural rigidities suitable for scale test reinforcement. Whereas the benchtop test geometry is approximately one order of magnitude smaller than a full size MSE structure as well as a wide variety of flexural rigidities that would be suitable for scale test reinforcement, it is reasonable to use a scale test reinforcement that has a flexural rigidity approximately one order of magnitude smaller than a known geotextile. The flexural rigidity of the paper used as test reinforcement was 2.88×10^{12} μJ/m, which is approximately an order of magnitude smaller than the polyethylene and polyester woven geotextiles tested in this research.